πN NEWSLETTER

No. 16 **March 2002**

Editors: D. Drechsel, G. Höhler, W. Kluge, H. Leutwyler, B. M. K. Nefkens, and H.-M. Staudenmaier

MENU 2001

Proceedings of the 9th International Symposium on Meson-Nucleon Physics and the Structure of the Nucleon

The George Washington University, Washington, D.C., U.S.A.
26–31 July 2001

Edited by H. Haberzettl and W. J. Briscoe

CNS Center for Nuclear Studies

The George Washington University WASHINGTON DC

The Department of Energy's Jefferson Lab THOMAS JEFFERSON NATIONAL ACCELERATOR FACILITY

NATIONAL SCIENCE FOUNDATION

BROOKHAVEN NATIONAL LABORATORY

πN NEWSLETTER

No. 16 **March 2002**

Editors:

D. Drechsel
Institut für Kernphysik
Universität Mainz
Postfach 3980
D-55099 Mainz
Germany
drechsel@kph.uni-mainz.de
Fax: (+49) 6131-39-25474

G. Höhler
Institut für Theoretische Teilchenphysik
Universität Karlsruhe
Postfach 6980
D-76128 Karlsruhe
Germany
gerhard.hoehler@physik.uni-karlsruhe.de
Fax: (+49) 721-608-8369

W. Kluge
Institut für Experimentelle Kernphysik
Universität Karlsruhe
Postfach 3640
D-76021 Karlsruhe
Germany
wolfgang.kluge@physik.uni-karlsruhe.de
Fax: (+49) 7247-82-3414

H. Leutwyler
Institut für Theoretische Physik
Universität Bern
Sidlerstr. 5
CH-3012 Bern
Switzerland
leutwyle@itp.unibe.ch
Fax: (+41) 31-631-3821

B. M. K. Nefkens
Department of Physics
University of California, Los Angeles
405 Hilgard Ave.
Los Angeles, CA 90024
U. S. A.
nefkens@physics.ucla.edu
Fax: (+1) 310-206-4397

H.-M. Staudenmaier
Institut für Theoretische Teilchenphysik
Universität Karlsruhe
Postfach 6980
D-76128 Karlsruhe
Germany
hans.staudenmaier@physik.uni-karlsruhe.de
Fax: (+49) 721-608-8369

Note from the Editors

The purpose of the πN Newsletter is to improve the exchange of information between physicists working in πN scattering and related fields such as nucleon structure, $\pi N \to \pi\pi N$, $\pi^- p \to \eta n$, $\gamma\pi \to \pi N$, $\pi\pi \to \pi\pi$, and electromagnetic form factors of pions and nucleons. The Newsletters will give results of new experiments, plans for experiments in the near future, analyses of experimental data, and related theoretical developments.

Since our first Newsletter appeared, subjects that have come under the limelight are for instance: the 'experimental' value of the πN σ-term and other quantities related to the strange quark content of the nucleon, the origin of the spin of the nucleon, applications of the Skyrme model and the pole structure of πN and $\pi\pi$ resonances in different sheets. There continues to be an interest in various quark and bag models of nucleon resonances, the existence of clusters of nucleon resonances, and so forth.

Requests for copies, or other inquiries, should be sent to W. Kluge (for Europe, Africa, and Western Asia) or to B. M. K. Nefkens (for the Americas, Australia, and Eastern Asia) at the addresses given at the left.

ISSN 0942-4148

Production and distribution of this issue:
Center for Nuclear Studies
The George Washington University
Washington, DC 20052, U.S.A.

MENU 2001

Proceedings of the
9th International Symposium on Meson-Nucleon Physics and the Structure of the Nucleon

The George Washington University, Washington, D.C., U.S.A.
26–31 July 2001

Editors
H. Haberzettl and W. J. Briscoe

Sponsors
Center for Nuclear Studies
The George Washington University
National Science Foundation
Thomas Jefferson National Accelerator Facility
Brookhaven National Laboratory

Institute of High Energy Physics,

The Chinese Academy of Sciences, Beijing, China

MENU2003 Announcement

The

Tenth International Symposium on Meson-Nucleon Physics and the Structure of the Nucleon (MENU2003)

will be organized by the Institute of High Energy Physics (IHEP), Beijing, China, around **August 25–30, 2003**. It is in a series held previously in Karlsruhe (1983), Los Alamos (1987), Gatchina/Leningrad (1989), Bad Honnef (1991), Boulder (1993), Blaubeuren (1995), Vancouver (1997), Zuoz (1999), and Washington, DC (2001).

Scientific topics will cover experimental and theoretical developments in meson-nucleon physics, baryon spectroscopy, photo- and electro-production of mesons, dibaryons, structure of the nucleon, chiral symmetry-based effective field theories, and QCD-inspired quark models of hadrons, etc.

The symposium is planned to be held at the Media Center which is a large multifunctional construction of Sino-Japanese joint venture, located near scenic Yuyuantan, very close to the Chinese Millenium Altar, CCTV, Military Museum. It is about 20 minutes to the Tian-An-Men Square at east and 10 minutes to IHEP at west by subway. The present price for a standard three-star double room is about US$60 per day. The URL for the Media Center is `http://mediacenter.com.cn`.

Beijing has a long history. Some 690 000 years ago, Peking Man lived at Zhoukodian, 48 kilometers southwest of Beijing. A small town appeared on the present site of southwestern Beijing in 1045 B.C. In the Liao Dynasty, it became the second capital. From then on, the city had been the capital of the Jin, Yuan, Ming and Qing dynasties until 1911. The People's Republic of China was founded with Beijing as its capital in 1949. There are many spectacular historic and scenic spots to see, e.g., the Great Wall, Forbidden City, Summer Palace, Temple of Heaven, etc.

In late August the weather in Beijing can usually be counted on to be sunny and pleasant, with temperatures typically in the mid- to upper twenties (Celsius).

A web site has been set up for the conference and will be regularly updated with detailed information as it becomes available. The URL is

`http://www.ihep.ac.cn/menu03/index.html`

Any suggestions and inquiries about the conference can be sent to

Bing-song Zou or Huan-ching Chiang / Professors of Physics
P.O. Box 918(4)
Beijing 100039, China
Phone: +86-10-68236162
Fax: +86-10-68218318
E-mail: `zoubs@mail.ihep.ac.cn` or `chiang@mail.ihep.ac.cn`

MENU 2001

Preface

The *9th International Symposium on Meson-Nucleon Physics and the Structure of the Nucleon (MENU2001)* was held at The George Washington University in Washington, DC, July 26–31, 2001.

These Symposia were initiated by Professors G. Höhler and B. M. K. Nefkens in 1983, with the first workshop taking place at the University of Karlsruhe in Germany. The main purpose then was to gain insights into the resonance structure of the nucleon by studying the production of mesons from the nucleon in hadronic processes. Soon, with the coming of Jefferson Lab, MENU began placing more emphasis on meson production in electromagnetically induced processes. Properties of the baryon resonances and the search for missing resonances were main issues in subsequent workshops.

The scope of the present conference, and the fact that we had about 130 registered participants from around the world, provides ample evidence that the meson-nucleon problem is still as interesting and viable as it was eighteen years ago. This year's workshop had a slightly more expanded scope as is reflected in the agenda. We invited again more speakers working in the area of electromagnetic interactions and in addition included more speakers whose expertise includes the study of hyperons and hyperon resonances. For the first time, significant representation was seen from Asia and in fact Beijing was selected as the site of MENU2003.

We expect that the MENU series will continue to influence the work of the Nuclear Physics community and we hope to see many of you in Beijing to continue the journey.

Last but not least, it is a pleasure to thank GW's Center for Nuclear Studies, the National Science Foundation, the Thomas Jefferson National Accelerator Facility, and the Brookhaven National Laboratory for their generous financial support. We also gratefully acknowledge the help and support of the administration of The George Washington University for allowing us to use the University's facilities free of charge. We particularly would like to thank the staff of the GW Conference Management Services and the staff of the GW Media and Public Affairs Building for their untiring efforts in helping run the conference as smoothly as possible.

William J. Briscoe and Helmut Haberzettl

Dedication to Professor Gerhard Höhler

The Proceedings of the *9th International Symposium on Meson-Nucleon Physics and the Structure of the Nucleon (MENU2001)* are dedicated to Professor Gerhard Höhler (Universität Karlsruhe), on the occasion of the 80th anniversary of his birthday in September 2001, in recognition of his important contributions to the field. The Proceedings are published as the present volume 16 of the πN NEWSLETTER, which was co-founded by Professor Höhler many years ago.

In the concluding session of MENU2001, on July 31, 2001, the participants joined in wishing Professor Höhler a most splendid 80th birthday. The participants recognize Professor Höhler's lifelong dedication and great contributions to the pion-nucleon problem, which is so fundamental to our understanding of hadronic dynamics. These wishes were conveyed to Professor Höhler in a letter sent by the organizers on behalf of all participants.

The papers of the present Proceedings are available for downloading at
http://menu2001.phys.gwu.edu/menu2001/proceedings.htm

πN NEWSLETTER

No. 16, March 2002

Contents

Plenary talks

Parallel talks

Progress in meson-nucleon physics: Status and perspectives

Ulf-G. Meißner

Forschungszentrum Jülich, Institut für Kernphysik (Th), D-52425 Jülich, Germany

(Received: 15 August 2001)

In this opening talk I will address some issues that exemplify the theoretical progress that has been made and is to be expected in the field of meson-nucleon physics. My emphasis will be on performing precision calculations to test aspects of QCD, including also electroweak probes. In addition, I discuss the problems and opportunities related to the strange quark sector.

1 Introduction: Precision and symmetries

The field of meson-nucleon physics is a very rich one, a few typical examples of processes to be discussed at this conference are shown in fig. 1, also listed are some (but by far not all) of the pertinent physics issues. The aim of this field is ambitious — one tries to understand QCD in the non-perturbative regime where the strong coupling constant is large. Therefore, one also speaks of *strong QCD*. This challenging theory can ultimately only be understood through precise and systematic calculations matched by equally accurate data. I will address here some of the theoretical developments that have been taken place over the last years, concentrating on the use of symmetries. For low energy processes, we have a consistent calculational scheme based on the QCD symmetries and their realizations, chiral perturbation theory (CHPT). It is based on a systematic expansion of S-matrix elements and transition currents in terms of small parameters. These are external momenta and quark masses with respect to the typical hadronic scale of about 1 GeV. The relevant degrees of freedom are not quarks and gluons but rather pions (Goldstone bosons) chirally coupled to nucleons (matter fields). As an example of a precise and systematic investigation I will consider isospin violation in πN scattering in section 2. Of course, CHPT does not allow to incorporate resonances and bound states systematically, for that, one has to perform a non-perturbative resummation. This can, however, be done in a fashion that preserves the low-energy structure as demanded by CHPT, see section 3, with applications to πN and $\bar{K}$N scattering. In the last section, I mention some outstanding problems which require some theoretical attention. Lastly, let me note that space forbids to discuss models, which can be quite useful or even indespensable, like e.g. in a systematic investigation of the baryon spectrum. This is left to other speakers.

2 Isospin violation in the pion-nucleon system

We now want to apply CHPT to one of the most studied processes, elastic pion-nucleon scattering. More precisely, we will consider systematically effects of isospin violation ($\not{I}$) due to the light quark mass difference, $m_u \neq m_d$, and electromagnetism, $q_u \neq q_d$. Before discussing in some detail isospin

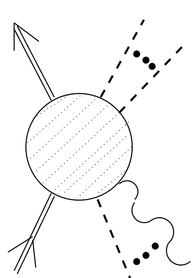

Figure 1: A typical diagram showing the many facets of pion-nucleon (meson-baryon) physics. Here, solid, dashed and wiggly lines denote nucleons (baryons), pions (Goldstone bosons) and photons (electroweak probes), in order. Pertinent processes are $\pi N \to \pi N$, $\pi N \to \pi\pi N$, $\gamma^{(\star)} N \to \pi N$, $\gamma^{(\star)} N \to \pi\pi N$, $\gamma^{(\star)} N \to \gamma N$, $KN \to KN$, and many others. The physics encoded in these reactions covers chiral QCD dynamics, the structure of the nucleon and of resonances, bound state dynamics, spin and polarization phenomena, electroweak interactions, and so on.

violation in πN scattering, a few general remarks are in order. In QCD plus QED, we have *two* sources of isospin violation. In QCD, the light quark mass difference leads to isovector terms, as reflected in the quark mass term (for two flavors)

$$\mathcal{H}_{\rm QCD}^{\rm mass} = m_u \bar{u}u + m_d \bar{d}d = \frac{1}{2}(m_u + m_d)(\bar{u}u + \bar{d}d) + \frac{1}{2}(m_u - m_d)(\bar{u}u - \bar{d}d) \ , \tag{1}$$

where the last term on the right hand side is clearly of isovector nature leading to strong $\not{I}$. Naively, one could expect huge $\not{I}$ effects since $|(m_u - m_d)/(m_u + m_d)| \simeq 1/3$. However, the scale one should compare to is the hadronic one, so that one indeed anticipates very small effects, $(m_u - m_d)/\Lambda_\chi < 1\%$. Only in processes involving neutral pions one can expect much bigger effects [1]. The other source of $\not{I}$ is electromagnetism (em). Hadron mass shifts due to virtual photon exchange between quarks can be estimated as $\delta m \simeq \alpha_{\rm em} \cdot \Lambda_{\rm QCD} \cdot \mathcal{O}(1) \sim$ few MeV. In fact, typical electromagnetic mass splittings in meson and baryon multiplets are of this order. Therefore, these two types of $\not{I}$ have to be considered *consistently*. This can be done by including virtual photons in the chiral effective Lagrangian of pions and nucleons, treating the electric charge e as another small parameter. The machinery to do such calculations has been developed over the last years [2]. To get a better idea about the size of the $\not{I}$ in πN scattering, let us a perform a lowest order tree level analysis comparing elastic $\pi^-\pi^+$, $\pi^- K^+$ and $\pi^- p$ scattering. The first two processes can be taken from the literature [3, 4],

$$\begin{aligned} a(\pi^-\pi^+ \to \pi^-\pi^+) &= \frac{M_{\pi^\pm}^2}{16\pi F_\pi^2} \left\{ 1 + \frac{M_{\pi^\pm}^2 - M_{\pi^0}^2}{M_{\pi^\pm}^2} \right\} = a_{\pi\pi}^{(\rm LO)} \left\{ 1 + 0.064 \right\} \ , \\ a(\pi^- K^+ \to \pi^- K^+) &= \frac{M_{\pi^\pm} M_{K^\pm}}{8\pi F_\pi^2 (M_{\pi^\pm} + M_{K^\pm})} \left\{ 1 + \frac{M_{\pi^\pm}^2 - M_{\pi^0}^2}{M_{\pi^\pm} M_{K^\pm}} \right\} = a_{\pi K}^{(\rm LO)} \left\{ 1 + 0.018 \right\} \ , \end{aligned} \tag{2}$$

where $a^{(\rm LO)}$ denotes the leading order isosymmetric S-wave scattering length. Note that the different normalization of the $\pi\pi$ and πK scattering amplitudes has historic roots. The relative suppression in the kaon case is due to the mass factor $M_\pi/M_K \simeq 0.28$. Therefore, in complete analogy one gets for the pion-nucleon case

$$a(\pi^- p \to \pi^- p) = \frac{M_{\pi^\pm} m_p}{8\pi F_\pi^2 (M_{\pi^\pm} + m_p)} \left\{ 1 + 0.018 \frac{M_{K^\pm}}{m_p} \right\} = a_{\pi p}^{(\rm LO)} \left\{ 1 + 0.01 \right\} \ , \tag{3}$$

so that we can expect $\not{I}$ effects of the order of one percent. Before considering that system, I point out again that it is mandatory to consider *all* possible $\not{I}$ effects at a given order, i.e. that one can get very misleading results if one considers only one particular "dominant" effect. A nice example are the QCD contributions to $\not{I}$ in $\pi^+ K^- \to \pi^0 K^0$ [4, 5], which are of relevance for the πK atom lifetime measurements at CERN [6],

$$a^{\rm strong\,\not{I}}(\pi^+ K^- \to \pi^0 K^0) \propto \frac{\epsilon}{\sqrt{3}} = \frac{\epsilon}{\sqrt{3}} \left\{ \underbrace{1 - \frac{M_K}{M_\pi}}_{\rm kinematical} + \underbrace{\frac{M_K^2 + M_\pi^2}{2 M_K M_\pi}}_{\pi^0\eta-{\rm mixing}} + \underbrace{\frac{M_K^2 - M_\pi^2}{2 M_K M_\pi}}_{\rm quark\ mass} \right\} , \tag{4}$$

having distinguished "kinematical" effects (due to meson mass splittings), "$\pi^0\eta$ mixing" effects which modify the isospin symmetric amplitude by factors of $\sin\epsilon$ or $\cos\epsilon$, with ϵ the standard mixing angle $\sim$ arctan$[(m_d - m_u)/(m_s - \hat{m})]$, and "quark mass insertions" for the four-meson vertex. It is obvious from the above that for the strong isospin violating contributions, individual "effects" are much larger (and can even be of opposite sign) than the total sum. Thus, for a reliable determination of the size of isospin breaking in the strong interactions, it is primordial to describe

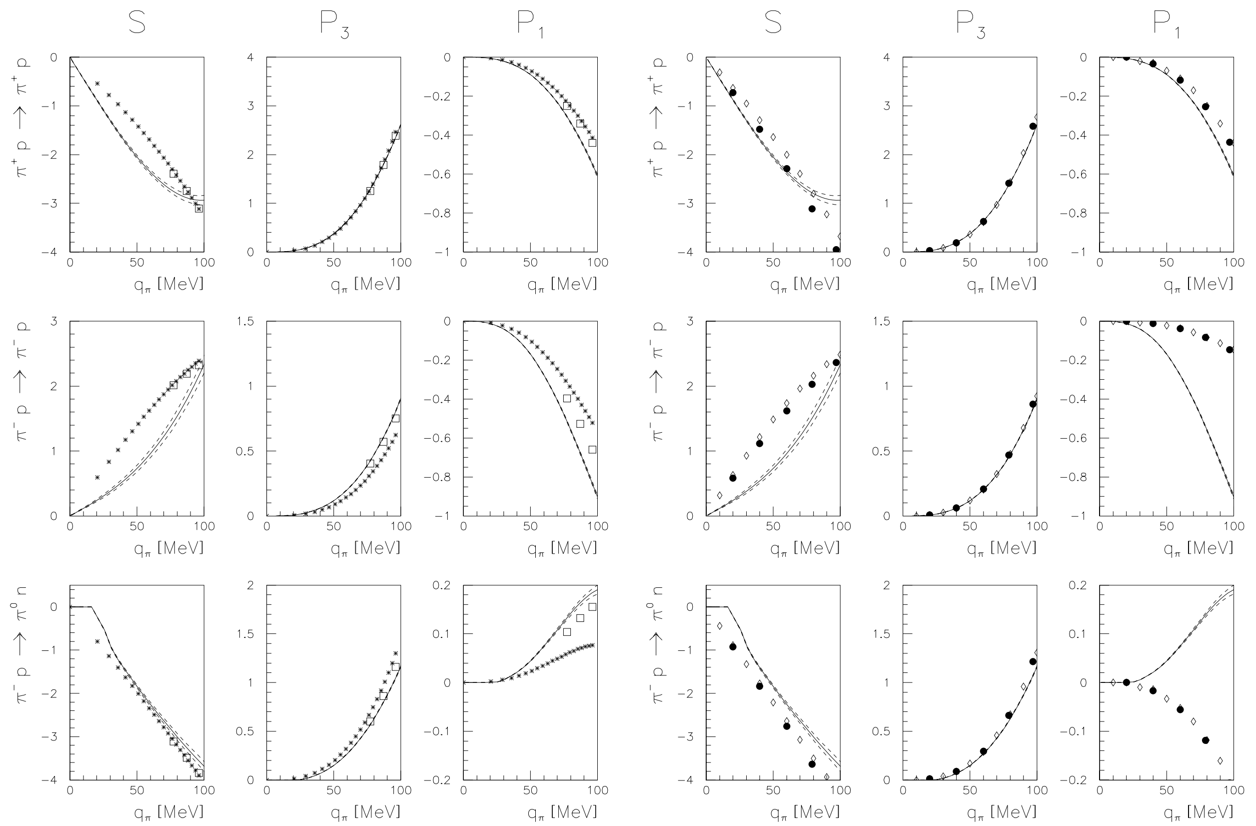

Figure 2: Strong pion-nucleon phase shifts as a function of the pion laboratory momentum q_π for the three measured channels. Shown are the S-wave and the $j = 1/2$, $3/2$ P-waves. The solid line corresponds to the CHPT solution [7], the dashed one to the one-sigma uncertainty range. Left panel: Comparison to the EM98 [10] (stars) and the EM00 [12] (open squares) phases. Right panel: Comparison to the KA85 [9] (full dots) and the SP98 [11] (open diamonds) phases.

electromagnetic and strong contributions consistently and to include all possible effects to the order one is working. This was achieved for the case of pion-nucleon scattering in the framework of chiral perturbation theory to third order in ref. [7], leading to a new phase shift analysis (for pion lab momenta below 100 MeV as deduced from the isospin symmetric fourth order calculation [8]). The resulting S- and P-wave phases for the three measured physical channels $\pi^\pm p \to \pi^\pm p$ and $\pi^- p \to \pi^0 n$ (charge exchange) are shown in fig. 2. CHPT does not leave any doubt about the correct definition of the *hadronic* masses of pions and nucleons (which are not the same for the pions as well as for the nucleons as often assumed), and allows to extract the strong part of the scattering amplitude in a unique way. At this order, there is only one strong $\not{I}$ violating operator whose strength can be fixed from the np mass difference. The em corrections are a bit more subtle. First, there are one- and two-photon exchanges, the latter amount to a few percent correction for the kinematics pertinent to the existing data. More precisely, for pion lab momenta $\vec{q}_\pi$, two-photon exchange is suppressed compared to one-photon exchange by a factor $e^2 M_\pi/(32|\vec{q}_\pi|) \leq 0.04$ for $|\vec{q}_\pi| \geq 10\,\mathrm{MeV}$. Then there are soft photon contributions in terms of loops and external leg radiation. Only the sum of these is IR finite and their contribution depends of course on the detector resolution. We have used $\Delta E_\gamma = 10\,\mathrm{MeV}$. In addition, there are hard photon contributions encoded in contact terms with undetermined low energy constants (LECs). After determining the unknown LECs by a fit to experimental data, one can switch off all electromagnetic interactions and describe QCD with unequal up- and down-quark masses and $e^2 = 0$. The so-determined strong phase shifts (mostly) agree with those of previous works [9–12] in the P-waves, but one finds a sizeably different behavior in the S-waves (in particular for $\pi^- p$ elastic scattering), compare fig. 2. This difference can be traced back to the inclusion (in CHPT) or omission (in other approaches) of *non-linear* photon-pion-nucleon couplings, i.e. vertices of the type $\bar{N}N\pi\pi\gamma$. Such vertices are a consequence of chiral symmetry and thus must be included. Of course, these results need to be checked further, in particular, one also has to extract the pertinent scattering lengths. In any case, it also should be investigated how such non-linear couplings can be included in the often used dispersion theoretical approaches to em corrections [13]. Given the hadronic amplitudes constructed in [7], one can address the question of isospin violation by studying the usual triangle relation involving elastic $\pi^\pm p$ scattering and the charge exchange reaction (for a general discussion of such triangle ratios, see [14] and references therein). An important advantage of the CHPT calculation lies in the fact that one can easily separate dynamical from static isospin breaking, the latter are due to hadron mass differences. Dynamical isospin breaking only occurs in the S-wave and is very small, $\sim 0.75\%$, in agreement with the estimate given in eq. (3). Static effects do not increase the size of isospin violation in the S-wave significantly; by no means can one account for the reported 7 % isospin breaking [15, 16]. These are presumably due to a mismatch between the models for the strong and the em interactions used in these works. Note also that one finds large error bars on the parameter values in the CHPT analysis. In order to improve this situation, one would like to fit to more experimental data. However, a third order CHPT calculation allows to describe scattering data for pion laboratory momenta not much higher than 100 MeV, a region where the data situation is not yet as good as one would hope. A fourth order calculation would certainly allow to fit to data higher in energy, but, on the other hand, would also introduce many more unknown coupling constants. Since isospin breaking effects are expected to be most prominent in the low energy region, one might question the usefulness of extending the analysis to full one-loop (fourth) order. Additional data for pion-nucleon scattering at very low energies would be very helpful in this respect. Also a combined fit to several reactions involving nucleons, pions, and photons, e.g. pion electro- and photoproduction, as well as $\pi N \to \pi\pi N$, would help in pinning down the fundamental low-energy constants more precisely.

3 Expanding the borders: Higher energies, resonances and all that

Going to higher energies, one has to implement unitarity constraints (imaginary parts become more important with increasing energy) as well as coupled channel dynamics. In addition, resonances appear, which might be genuine quark model states or be dynamically generated by strong final state interactions. Furthermore, relativistic effects become more important with increasing energies. Therefore, one needs a non-perturbative resummation scheme since in a perturbative theory like CHPT, one can never generate a bound state or a resonance. There exist many such approaches, but it is possible and mandatory to link such a scheme tightly to the chiral QCD dynamics. I follow here the approach pioneered by Oller and Oset [17] for meson interactions and demonstrate how this can be improved and extended for pion-nucleon [18] and $\bar{K}$N scattering [19]. To be specific, let us consider πN scattering. The starting point is the T-matrix for any partial wave, which can be represented in closed form if one neglects for the moment the crossed channel (left-hand) cuts (for more explicit details, see [18])

$$T = \left[\tilde{T}(W) + g(s)\right]^{-1} , \tag{5}$$

with $W = \sqrt{s}$ the cm energy (as noted in [18], the analytical structure is much simpler when using W instead of s). $\tilde{T}$ collects all local terms and poles (which can be most easily interpreted

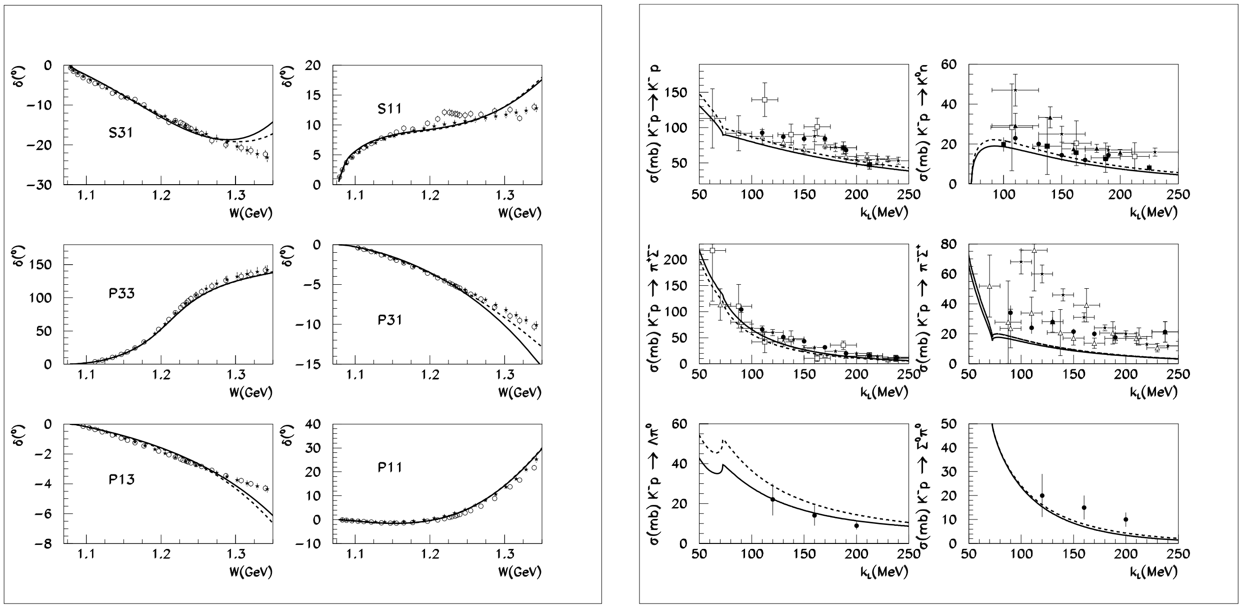

Figure 3: Left panel: Fit to the low (S,P) πN partial waves. The solid (dashed) lines refer to (un)constrained fits as explained in [18]. Right panel: Fit to various cross sections coupling to the $\bar{K}$N channel. Solid lines: best fit, dashed lines: natural values for the parameters, see [19].

in the large N_c world) and $g(s)$ is the meson-baryon loop function (the fundamental bubble) that is resummed by e.g. dispersion relations in a way to exactly recover the right-hand (unitarity) cut contributions. The function $g(s)$ needs regularization, this can be best done in terms of a subtracted dispersion relation and using dimensional regularization (for details, see [18]). It is important to ensure that in the low-energy region, the so constructed T-matrix agrees with the one of CHPT. In addition, one has to recover the contributions from the left-hand cut. This can be achieved by a hierarchy of matching conditions, e.g. for the πN system one has

$$\begin{aligned}
\mathcal{O}(p) &: \tilde{T}_1(W) = T_1^\chi(W) \ , \\
\mathcal{O}(p^2) &: \tilde{T}_1(W) + \tilde{T}_2(W) = T_1^\chi(W) + T_2^\chi(W) \ , \\
\mathcal{O}(p^3) &: \tilde{T}_1(W) + \tilde{T}_2(W) + \tilde{T}_3(W) = T_1^\chi(W) + T_2^\chi(W) + T_3^\chi(W) + \tilde{T}_1(W)\, g(s)\, \tilde{T}_1(W) \ , \quad (6)
\end{aligned}$$

and so on. Here, T_n^χ is the T-matrix calculated within CHPT to $\mathcal{O}(q^n)$. Of course, one has to avoid double counting as soon as one includes pion loops, this is achieved by the last term in the third equation (loops only start at third order in this case). In addition, one can also include resonance fields by saturating the local contact terms in the effective Lagrangian through explicit meson and baryon resonances (for details, see [18]). In particular, in this framework one can cleanly separate genuine quark resonances from dynamically generated resonance-like states. The former require the inclusion of an explicit field in the underlying Lagrangian, whereas in the latter case the fit will arrange itself so that the couplings to such an explicit field will vanish (see e.g. the discussion of the ρ as a genuine resonance versus the σ as a dynamically generated state in [20]). This method was applied to πN scattering below the inelastic thresholds in [18] by matching to the third order heavy baryon CHPT results and including the $\Delta(1232)$, $N^\star(1440)$, $\rho(770)$ and a scalar resonance. Instead of the CHPT low-energy constants (LECs), one now fits resonance parameters, of course, to a given order one can only determine as many (combinations) thereof as there are LECs A typical fit to the low partial waves is shown in the left panel of fig. 3. The threshold parameters are found to be in good agreement with values obtained from phase shift analyses (for an updated table, see e.g. [21])

and the Δ is found in the complex-W plane at (1210-i53) MeV, in good agreement with earlier findings [22]. It is also important to point out that the scalar exchange can be well represented by contact terms, i.e. no need for a light sigma meson arises. These considerations were extended to S-wave, strangeness $S = -1$ $\bar{K}$N scattering in [19]. In this case, one has to consider the coupling to the whole set of SU(3) coupled channels, these are $\bar{K}$N, $\Lambda\pi$, $\Sigma\pi$, $\Sigma\eta$ and ΞK (for earlier related work, see e.g. [23]). The lowest order (dimension one) effective Lagrangian was used, it depends on three parameters, which are the average baryon octet mass and the pion decay constant in the chiral limit and the subtraction constant appearing in the dispersion relation for $g(s)$. Their values can be estimated from simple considerations leading to the so-called "natural values". One finds a good description of the scattering data and the threshold ratios, see the dashed lines in the right panel of fig. 3. Leaving these parameters free, one obtains the best fit (solid lines). It is worth to stress that the values of the parameters of the best fit differ at most by 15% from their natural values. We have also investigated the pole structure of the S-wave $\bar{K}$N system in the unphysical Riemann sheets. In addition to the $I = 0$ pole close to the $\bar{K}$N threshold that can be identified with the $\Lambda(1405)$ resonance, one finds another pole with $I = 0$ close to the $\Sigma\pi$ threshold and another one with $I = 1$ close to the $\bar{K}$N channel opening (which is threefold degenerate in the isospin limit). Thus one can speculate about a nonet of $J = 1/2$ meson-baryon resonances with strangeness $S = -1$. Still, one has to investigate the $I = 1/2$ channel with $S = 0, -2$ in this energy interval to strengthen this conjecture. Also, one should include the next-to-leading order terms and constrain the fit by πN data in this energy region (for related studies, see e.g. [24,25]). Note also that one can use the results of ref. [19] to study the S-wave $\Lambda\pi$ phase shift at the Ξ mass which is of relevance for CP violation studies in the decay $\Xi \to \Lambda\pi \to p\pi\pi$ [26], see also [27] (for first experimental results, see [28]).

4 Summary and outlook

Here, I will address some open issues which should be at the center of theoretical investigations in the (near) future (or are already being looked at). This list is, of course, highly subjective but I try to cover as much ground as possible. Consider first the sector of the *non-strange* light quarks:

- In the threshold region a precision machinery exists, which allows in particular to investigate the dual effects of strong and electromagnetic isospin violation. Much more work is needed to really pin down these subtle effects in various reactions. Neutral pion scattering off protons should be measured, either via photoproduction [29] or multiple scattering in pp collisions [30].

- The results of ref. [7] for the em corrections to pion-nucleon scattering differ drastically from what has been available so far, see e.g. [13] or the recent work by the ZuAC Collaboration [31]. This deserves further study.

- To incorporate also data from higher energies, as particularly stressed by Höhler, the dispersion relation machinery should be married with chiral constraints, like e.g. using Roy-Steiner like equations, see e.g. [32], which has been proven fruitful in the analysis of $\pi\pi$ and πK scattering.

- Clearly, the bound state effective field theory calculations for pionic hydrogen and deuterium have to be finished/started to deduce the precise S-wave scattering lengths from the accurate PSI data, see Rusetsky's talk at this Conference.

- The status of sigma term is still unsatisfactory. The present value say from the GWU group (see Pavan's talk) is uncomfortably large. A fresh look at strangeness in the proton might be useful.

- Accurate photo/electroproduction data have shed much light on the chiral dynamics of QCD, see the talks by Beck and Merkel. However, the new neutral pion electroproduction data from MAMI-II (at photon virtuality $Q^2 = 0.05\,\mathrm{GeV}^2$) pose a serious challenge to theory. This needs to be resolved fast.

- The inclusion of resonances is still an open problem with the exception of the delta, which can be included systematically if one counts the nucleon-delta mass splitting as an additional free parameter (see the pioneering work in [33] and the systematization in [34]).

I conclude that we are testing various aspects of strong QCD and need to sharpen these investigations. In the *strange* quark sector, we are facing even more open problems, from which I mention a few:

- Clearly, more calculations based on the chiral unitary approach are needed, in particular the extension to photo-nuclear reactions (for some first attempt, see [35]) and matching to higher order CHPT amplitudes than done so far. Obviously, one has to determine more parameters than in SU(2), but this should not be considered a barrier but rather an opportunity to gain a better understanding of e.g. SU(3) flavor breaking.

- More accurate kaon photo/electroproduction data are needed to further test chiral baryon dynamics. A first analysis of the pioneering SAPHIR data from Bonn [41] on kaon photoproduction off protons showed that this is feasible [42].

- Such production studies will also shed more light of the questions surrounding the nature of states like the $\Lambda(1405)$. The bound-state versus resonance scenario might e.g. be settled by measuring transition form factors, see e.g. [36].

- Since $m_s \sim \Lambda_{\rm QCD}$, the question remains whether one should consider the strange quark light or heavy? This can be further studied by making use e.g. of heavy kaon CHPT, see [37]. This allows to establish true SU(2) results within SU(3).

- Very interesting is the question concerning the flavor dependence of chiral symmetry breaking. More specifically, does QCD have a complicated phase structure with $F_\pi^2 \neq 0$ and $\langle 0|\bar q q|0\rangle^{N_f=2}$ large (as indicated by the recent K_{e4} data from BNL E865 [38], see [39]) for two flavors but a small condensate for the SU(3) case, $\langle 0|\bar q q|0\rangle^{N_f=3} \simeq 0$ (which would neatly explain OZI violation in the scalar sector, see [40])?

In summary, it is important to perform systematic and precise calculations using as much as possible symmetry principles and quantum field theoretical methods. Combining these with dispersion theory, we can expect further progress in the field provided that there is also progress in the experimental situation for many processes involving pions, nucleons, photons and so on.

Acknowledgments: It is a pleasure to thank Nadia Fettes, José Antonio Oller and Bastian Kubis for many enjoyable collaborations. Bill Briscoe, Helmut Haberzettl and their staff deserve praise for a well organized meeting. I gratefully acknowledge financial support by the GW Center for Nuclear Studies.

References

[1] S. Weinberg, Trans. N.Y. Acad. of Sci. **38**, 185 (1977); Ulf-G. Meißner and S. Steininger, Phys. Lett. **B419**, 403 (1998); N. Fettes, Ulf-G. Meißner, and S. Steininger, Phys. Lett. **B451**, 233 (1999).

[2] R. Urech, Nucl. Phys. **B433**, 234 (1995); H. Neufeld and H. Rupertsberger, Z. Phys. **C71**, 131 (1996); Ulf-G. Meißner, G. Müller, and S. Steininger, Phys. Lett. **B406**, 154 (1997); G. Müller and Ulf-G. Meißner, Nucl. Phys. **B556**, 265 (1999); M. Knecht et al., Eur. Phys. J. **C12**, 469 (2000).
[3] M. Knecht and R. Urech, Nucl. Phys. **B519**, 329 (1998).
[4] B. Kubis and Ulf-G. Meißner, [hep-ph/0107199].
[5] A. Nehme and P. Talavera, [hep-ph/0107299]
[6] B. Adeva et al., CERN-SPSC-2000-032, CERN-SPS-P-284-ADD-1, Aug. 2000.
[7] N. Fettes and Ulf-G. Meißner, Nucl. Phys. **A693**, 693 (2001) [hep-ph/0101030].
[8] N. Fettes and Ulf-G. Meißner, Nucl. Phys. **A676**, 311 (2000).
[9] R. Koch, Nucl. Phys. **A448** (1986) 707.
[10] E. Matsinos, [hep-ph/9807395]; E. Matsinos, private communication.
[11] SAID on-line program, R.A. Arndt et al., see website http://gwdac.phys.gwu.edu/.
[12] A. Gashi et al., [hep-ph/0009081].
[13] J. Hamilton, B. Tromberg, and I. Øverbrø, Nucl. Phys. **B60**, 443 (1973); B. Tromberg and J. Hamilton, Nucl. Phys. **B76**, 483 (1974); B. Tromberg, S. Waldenstrøm, and I. Øverbrø, Phys. Rev. D**15**, 725 (1977).
[14] N. Fettes and Ulf-G. Meißner, Phys. Rev. C**63**, 045201 (2001).
[15] W.R. Gibbs, Li Ai, and W.B. Kaufmann, Phys. Rev. Lett. **74** (1995) 3740.
[16] E. Matsinos, Phys. Rev. C**56** (1997) 3014.
[17] J.A. Oller and E. Oset, Phys. Rev. D**60**, 074023 (1999).
[18] Ulf-G. Meißner and J.A. Oller, Nucl. Phys. **A673**, 311 (2000).
[19] Ulf-G. Meißner and J.A. Oller, Phys. Lett. **B500**, 263 (2001).
[20] J.A. Oller, [hep-ph/0007349].
[21] J.A. Oller and Ulf-G. Meißner, in Proceedings of $N^\star$-2001, to be published.
[22] G. Höhler, in: Landolt-Börnstein, Vol. 9b2, H. Schopper (ed.), Springer Verlag, Berlin, 1983; O. Hanstein, D. Drechsel and L. Tiator, Phys. Lett. **B385**, 45 (1996).
[23] N. Kaiser, P.B. Siegel and W. Weise, Nucl. Phys. **A594**, 325 (1995); E. Oset and A. Ramos, Nucl. Phys. **A635**, 99 (1998).
[24] M.F.M. Lutz and E.E. Kolomeitsev, [nucl-th/0004021].
[25] N. Kaiser, [nucl-th/0107006].
[26] Ulf-G. Meißner and J.A. Oller, Phys. Rev. D**64**, 014006 (2001).
[27] Jusak Tandean, A.W. Thomas and G. Valencia, Phys. Rev. D**64**, 014005 (2001).
[28] E756 Collaboration (K.B. Luk et al.). Phys. Rev. Lett. **85**, 4860 (2000).
[29] A.M. Bernstein, Phys. Lett. **B442**, 20 (1998).
[30] R. Meier, *this conference*, based on ideas of S. Kullander.
[31] A. Gashi et al, Nucl.Phys. **A686**, 447, 463 (2001).
[32] T. Becher and H. Leutwyler, JHEP **0106**, 017 (2001); P. Büttiker, private communication.
[33] E. Jenkins and A.V. Manohar, Phys. Lett. **259**, 353 (1991).
[34] T.R. Hemmert, B.R. Holstein and J. Kambor, J. Phys. G. **24**, 1831 (1998).
[35] N. Kaiser et al., Nucl. Phys. **A612**, 297 (1997); Nucl. Phys. **A672**, 249 (2000).
[36] L. Frankfurt et al., Phys. Rev. C**60**, 055202 (1999).
[37] A. Roessl, Nucl. Phys. **B555**, 507 (1999) 507; S.M. Oullette, [hep-ph/0101055].
[38] M. Zeller (for the BNL E865 Collaboration), "New Measurement of the Properties of K_{e4}^+ Decays", talk given at April Meeting of the American Physical Society, Washington, D.C., April 28 – May 1, 2001.
[39] G. Colangelo, J. Gasser and H. Leutwyler, Phys. Rev. Lett. **86**, 5008 (2001).
[40] S. Descotes, L. Girlanda, and J. Stern, JHEP **0001**, 041 (2000); S. Descotes and J. Stern, Phys. Lett. **B488**, 274 (2000); S. Descotes, JHEP **0103**, 002 (2001); B. Moussallam, Eur. Phys. J. **C14**, 111 (2000); B. Moussallam, JHEP **0008**, 005 (2000).
[41] M. Bockhorst et al., Z. Phys. **C63**, 3 (1994); The SAPHIR-Collaboration (M. Q. Tran et al.), Phys. Lett. **B445**, 20 (1998); The SAPHIR-Collaboration (S. Goers et al.), Phys. Lett. **B464**, 331 (1999).
[42] S. Steininger and Ulf-G. Meißner, Phys. Lett. **B391**, 446 (1997).

Status report on the light baryonic states

B.M.K. Nefkens and J.W. Price

UCLA, Los Angeles, CA 90095, U.S.A.

(Received: 19 October 2001)

The regularities in the spectrum of the light baryon resonances are reviewed and compared with those of the light mesons. We discuss the occurrence of parity doublets and clusters, and note the trends in the values of the masses, widths, spins, and parities. The importance of SU(3) flavor is illustrated and the status of quark model calculations of the baryonic spectrum is reviewed. The absence of evidence for baryonic hybrids is particularly interesting. We propose to use better symbols for the baryon resonances which do not conflict with the simple quark structure of QCD. We shall comment also on fine tuning the Star System for the hadronic states. The importance of greater support for the construction and operation of secondary beams of π, K, $\bar{p}$, $\vec{n}$ and $\vec{\gamma}$ up to 5 GeV/c for the future of non-perturbative QCD is emphasized.

1 Introduction

An important purpose of the biannual Symposium on "Meson-Nucleon Physics and the Structure of the Nucleon" (MENU) is to review the status of the light baryonic states. MENU provides a public forum for discussing the occurrence of regularities in the hadrons, and for evaluating the success of various hadron models, particularly of the light baryons which are made up of u, d, and s quarks.

2 Patterns in the widths of baryons

The width, Γ, of all light baryon resonances as listed in the Review of Particle Physics [1] is shown in Fig. 1.

Γ increases with the mass of the resonance and the magnitude depends on the strangeness number of the family (which is directly related to the number of u and d quarks.) The value of the average Γ for each family is given on the abscissa of Fig. 1. The relation between the widths is the following:

$$\Gamma(N^*) = \Gamma(\Delta^*) \simeq \frac{9}{4}\Gamma(\Lambda^*) = \frac{9}{4}\Gamma(\Sigma^*) \simeq 9\Gamma(\Xi^*) \ . \tag{1}$$

Riska [2] has noted that these ratios correspond to $[\#(u+d)]^2$, where $\#(u+d)$ is the number of up and down quarks. Note that the Ξ^* states are sufficiently narrow that they may be fruitfully explored in production experiments such as $\gamma p \to \Xi^- K^+ K^+$; this provides a practical way for discovering many of the missing Ξ^* resonances.

3 Patterns in baryon masses, spins and parities

Shown in Fig. 2 is a parity-pairing plot, which displays by rectangular boxes the real part of the pole of every known N^* state in eight vertical bands, one for each spin: 1/2, 3/2, $\cdots$ 15/2. Every band has two columns; the left for the negative parity states and the right for the positive ones. The star ranking of each state is indicated by the shading: four stars (darkest shade) are awarded to well-established states and one star (lightest shade) to the iffy ones.

There are clearly 3 mass regions in Fig. 2: 4 states have $m < 1600$ MeV, where m is the pole value of the state. None of these has a parity partner; we shall call them *bachelor* states. There are 16 states with $1600 < m < 2200$ MeV which form 8 parity doublets, and make two clusters. The

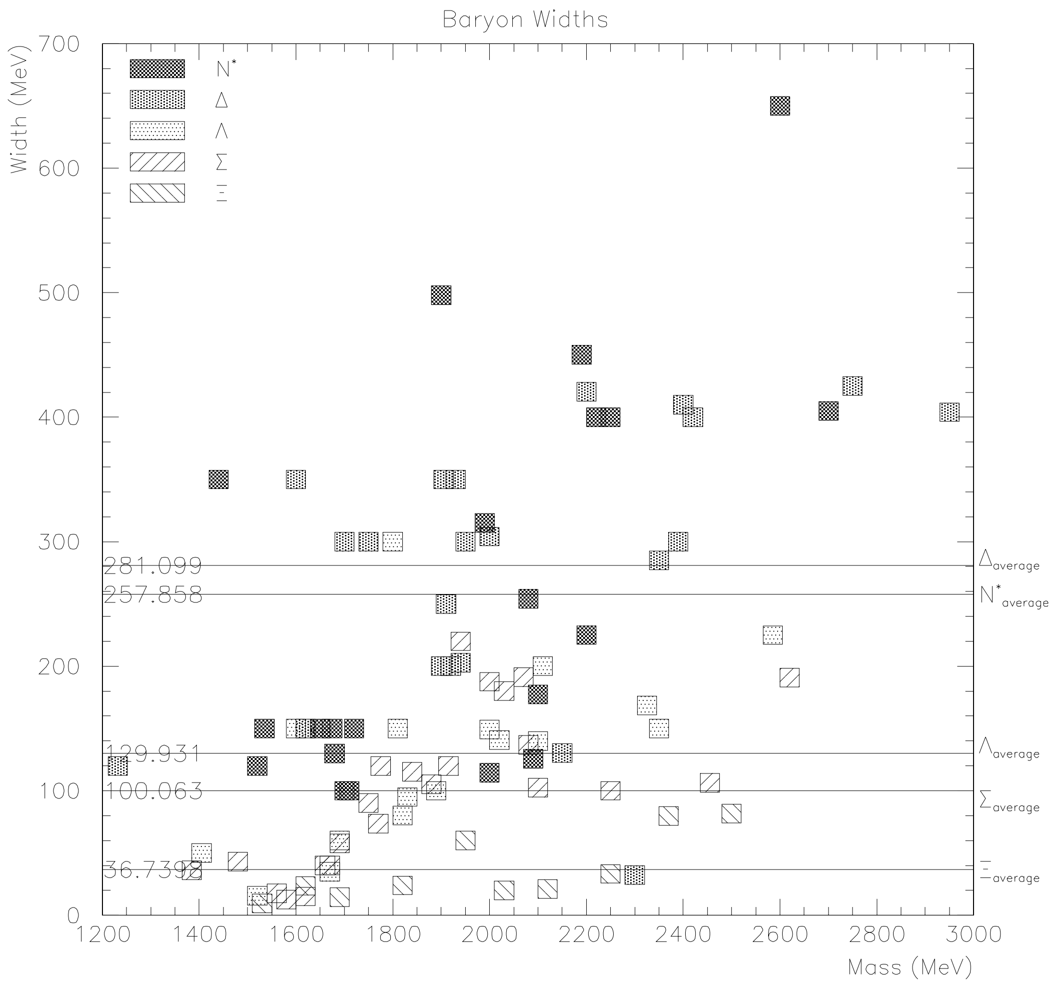

Figure 1: The width of all known light baryons. The horizontal lines are the average value for each family.

2 remaining states at $m > 2500$ MeV are single states; however, the searches for other states have been far from exhaustive. A similar pattern of parity doublet states is found in the Δ family. For the case of the Λ and Σ states there are not sufficient data for drawing a firm conclusion about the similar occurance of parity doublets.

The situation for the mesons is fundamentally different. Fig. 3 shows the parity pairing plot for the strange meson family. There is no evidence for parity doubling. The isosinglet and isotriplet meson families support this.

We conclude that parity doubling is a feature of the baryons which is *not seen* in the mesons. Possible reasons for this could be a diquark substructure [3] or some hitherto overlooked symmetry in the wave function.

4 The flavor symmetry of QCD

The Lagrangian of QCD, $\mathcal{L}_{QCD}$, is given by the following compact expression [1]:

$$\mathcal{L}_{QCD} = -\frac{1}{4} F^{(a)}_{\mu\nu} F^{(a)\mu\nu} + i \sum_q \bar{\psi}^i_q \gamma^\mu (D_\mu)_{ij} \psi^j_q - \sum_q m_q \bar{\psi}^i_q \psi_{qi} \ , \tag{2}$$

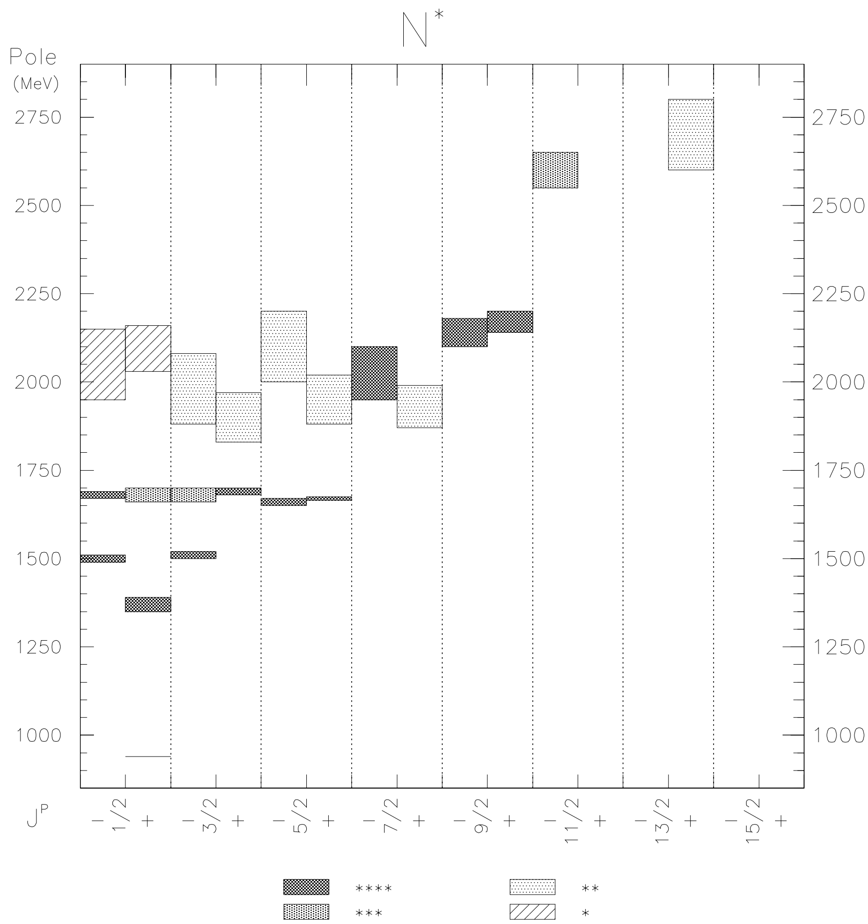

Figure 2: Parity pairing of the N^* states. Each resonance is plotted by its pole value in 8 columns for spin $\frac{1}{2}$ to $\frac{13}{2}$ negative parity states are on the left side and positive on the right. The darkest shade of gray is for 4 star states. The lightest is for one star.

with

$$
\begin{aligned}
F^{(a)}_{\mu\nu} &= \partial_\mu A^a_\nu - \partial_\nu A^a_\mu + g_s f_{abc} A^b_\mu A^c_\nu \ , \\
(D_\mu)_{ij} &= \delta_{ij}\partial_\mu - i g_s \sum_a \frac{\lambda^a_{i,j}}{2} A^a_\mu \ .
\end{aligned}
$$

ψ is the quark field, A is the gluon field and m_q is the mass of quark q. Eq. 2 may be arranged as follows:

$$\mathcal{L}_{QCD} = \mathcal{L}_0 + \mathcal{L}_m \ . \tag{3}$$

$\mathcal{L}_0$ consists of the first two terms of Eq. 2 and $\mathcal{L}_m$ is the third term. $\mathcal{L}_0$ depends only on the fields; it is the same for all 6 quarks and 8 gluons. This is the famous flavor symmetry of QCD, which is a manifestation of the universality of the strong interaction; it is broken by the mass term,

$$\mathcal{L}_m = -\sum_q \ \bar{\psi}_q m_q \psi_q \ .$$

The success of the SU(3) symmetry for systems of u, d and s quarks is indicative of $\mathcal{L}_0 >> \mathcal{L}_m$. $\mathcal{L}_m$ produces a change of about 15% in the mass of the hyperons.

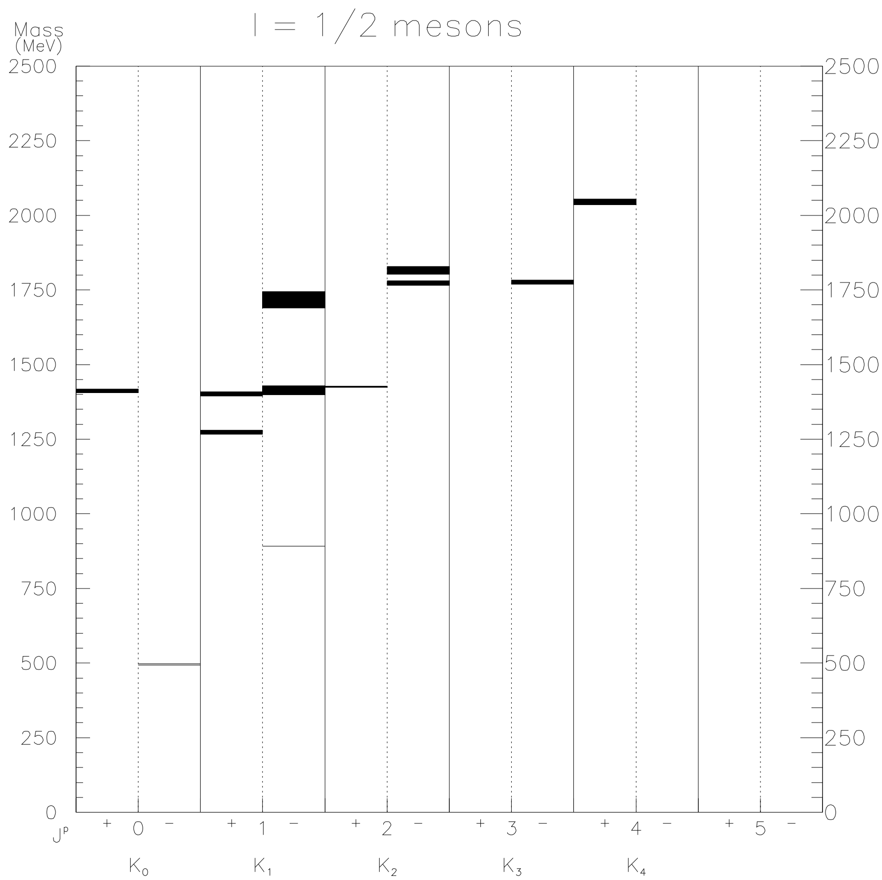

Figure 3: Lack of parity pairing of the light strange mesons.

Flavor symmetry explains the stunning similarity between the features of threshold $\pi^- \; p \to \eta \; n$ production and $K^- p \to \eta n$ as well as the amazing analogy between the Dalitz plots of $\pi^- \; p \to \pi^0 \pi^0 n$ and $K^- p \to \pi^0 \pi^0 \Lambda$ and the dissimilarity with $K^- p \to \pi^0 \pi^0 \; \Sigma^0$ [4].

5 Baryon mass calculations

The experimental masses [1] of the ground states of the four light baryon-octet families, the N, Λ, Σ and Ξ, are displayed in Fig. 4 by thick horizontal lines. Shown also are the masses of the ground states of the four decuplet families, the $\Delta(1232)$, $\Sigma(1385)$, $\Xi(1530)$ and $\Omega^-(1672)$. We shall compare these mass spectra with three very different model calculations which are representative of the large variety of calculations in this field.

1. Lattice-gauge, L-G, results obtained by the CP-PACS group [5] for a quenched QCD calculations are indicated in Fig. 4 by the stars. The L-G calculations used as input the masses of the π^0, ρ and ϕ mesons, they also set $m_u = m_d$. The agreement of this L-G calculation with the experimental masses is at the several percent level. For example, m_p(L-G) $= 878 \pm 25$ MeV, while m_p(exp) $= 938$ MeV. One should not be carried away by the level of agreement for the 8 baryon ground states of this and other calculations; this could give an undeserved sense of accomplishment. Note that the masses of the four decuplet states (which have a symmetric flavor state function) simply differ by the $s - d$ quark mass difference. Well before the birth of QCD, the resulting equal mass spacings were known as the Gell-Mann decuplet mass splitting relation. L-G and all quark models display this decuplet relation to the level

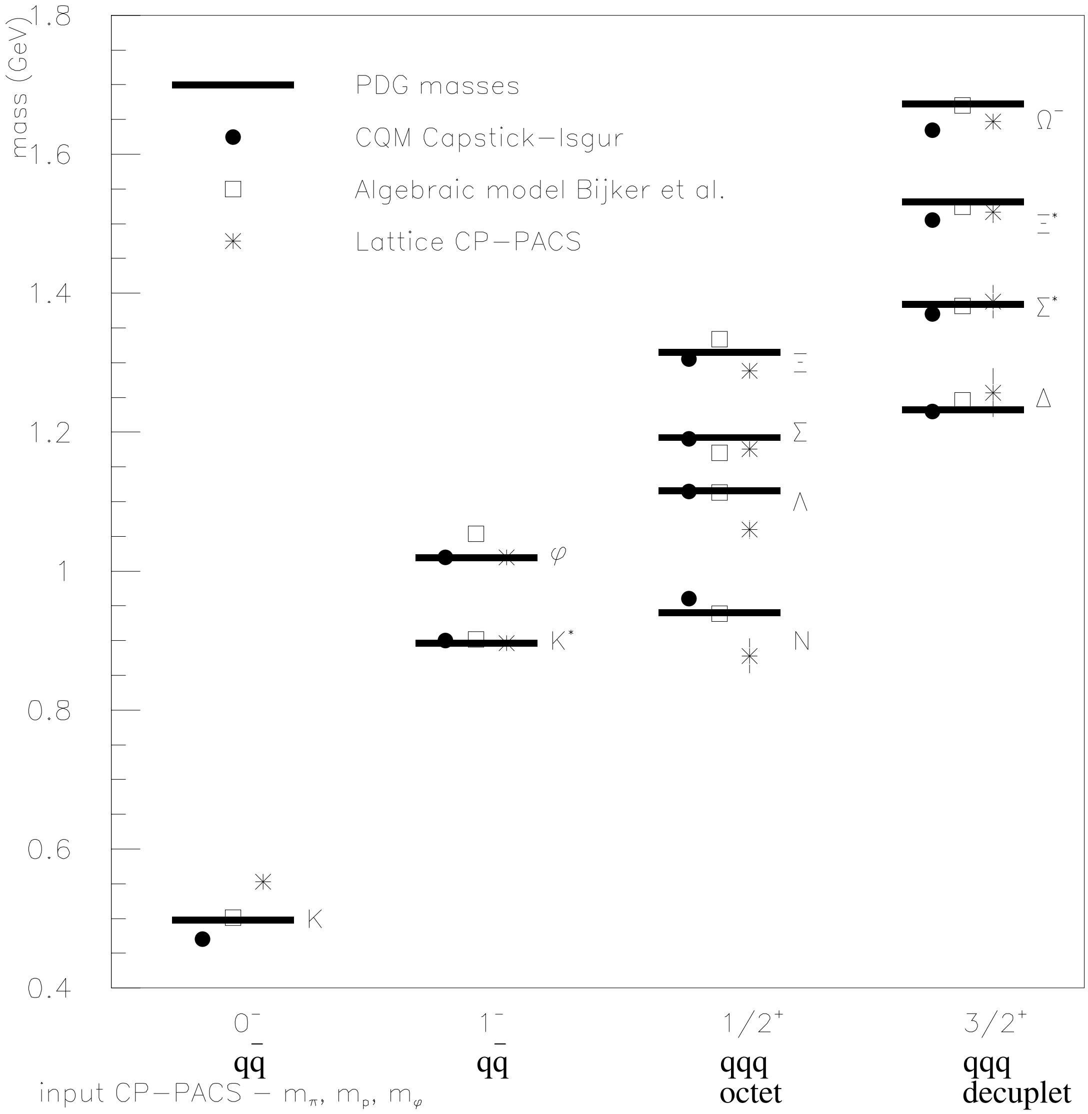

Figure 4: Masses of light baryons. The first column shows the K-meson, the second column the K^* and ϕ. the third column the baryon octet ground states, and the fourth column the baryon decuplet ground states. Solid lines are experimental data; black dots are for Capstick-Isgur [6]; open squares Bijker et al. [7]; stars CP-PACS [5].

of 1 MeV, however, experimentally it only holds to the level of 17 MeV. A similar relation applies to the octet ground-state masses, they obey the Gell-Mann-Okubo mass relation. This is different from the decuplet relation because the octets have mixed flavor symmetry. Thus, instead of 8 separate mass values there are actually only 4 independent numbers: the mass of the proton and the $p-\Delta$, $\Lambda-\Sigma$, and the $p-\Lambda$ mass differences.

2. The results of the relativized quark model calculations by Capstick and Isgur [6] are shown in Fig. 4 by black dots. The agreement with experiment is slightly better than the L-G model.

3. The algebraic model calculations by Bijker et al. [7], are shown by the open squares in Fig. 4. Again, the agreement with experiment is excellent which in part originates in the use of a larger input data set.

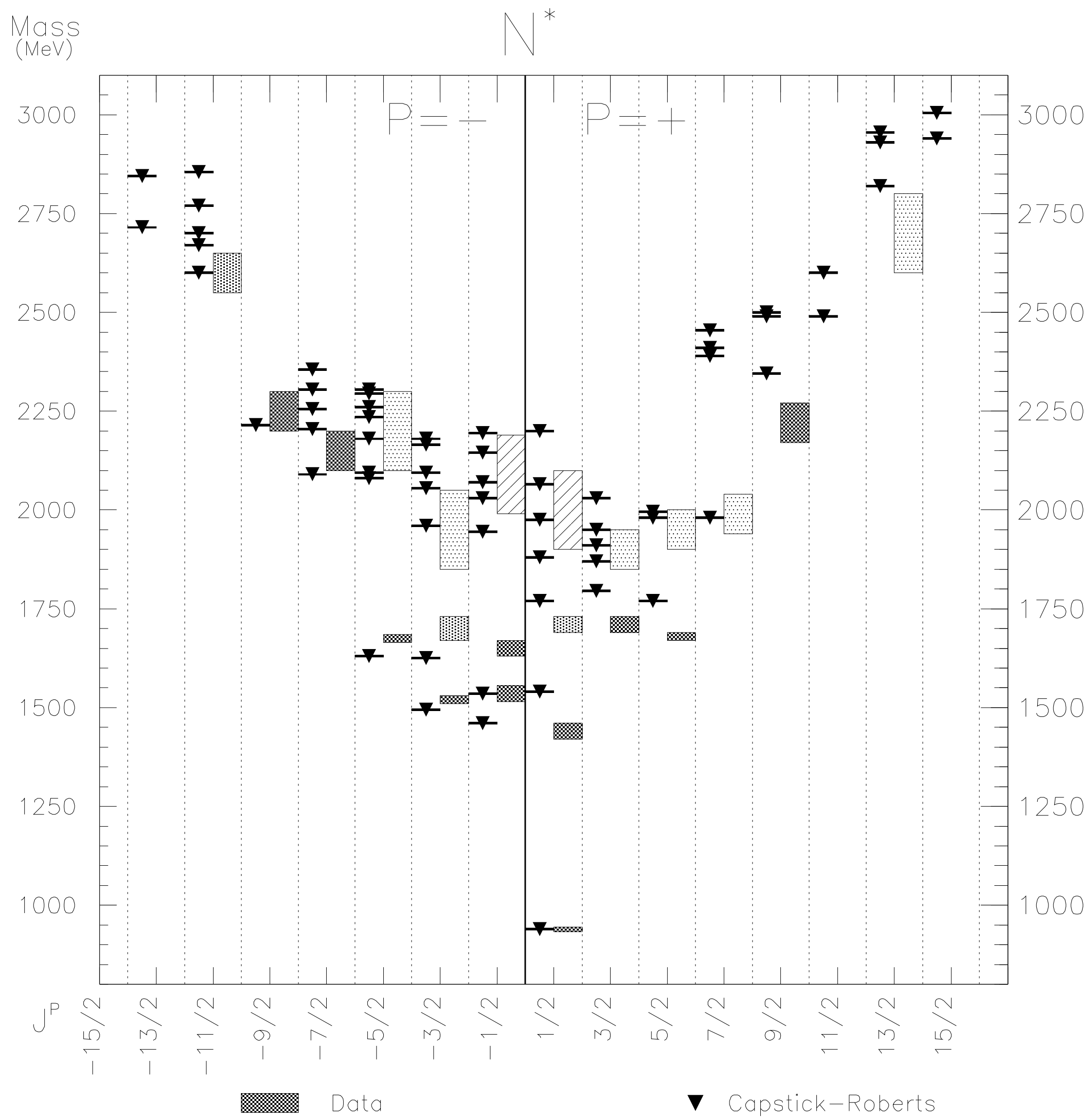

Figure 5: N^*-mass spectrum. The left side is for negative parity states. The right for positive. The experimental masses are given by the boxes. The lines with the triangle in the middle are the calculation by Capstick and Roberts [8].

The above calculations are less satisfactory when it comes to obtaining the mases of the baryonic excited states. The limitations inherent in using a quenched QCD calculations of the present L-G models makes them not useful in their current form for the calculation of the excited states. We hope that this will change in the not too distant future.

Among the available quark model calculations we chose the Capstick-Roberts [8] work which comes from the same school as [6]. Shown in Fig. 5 are the masses of all listed [1] N^* states. We use different shades of gray to indicate the number of stars given to each resonance. The predictions by Capstick and Roberts are shown by horizontal lines with a triangle in the middle. Qualitatively, the spectrum of the experimental masses below 2000 MeV is reproduced by most quark models. A close inspection reveals several nagging discrepancies:

1. The lowest established excited N^* state is the Roper resonance, which has positive parity and spin $\frac{1}{2}$, like the nucleon which is the ground state. In the quark model of [8] the lowest two states have negative parity and spin $\frac{1}{2}$ and $\frac{3}{2}$. This ordering is difficult to rectify except by a major modification such as the direct participation of Goldstone bosons in the quark-quark interaction [9].

2. The calculated masses of the positive parity states are all too high by some 80 MeV compared to the data, while all negative parity resonances are calculated to be too low by some 40 MeV. It is interesting that a similar quark model calculation [10] of the mesons agrees very well with the data.

3. Less than a quarter of the predicted states above 2000 MeV have been observed experimentally. The reason which is usually advanced for not seeing the "missing resonances" is their small coupling to the πN channel used for the identification by the πN partial wave analyses. A small coupling is indeed a feature of several quark models which use an independent channel calculation of the πN branching ratio. In reality there is a non-negligible coupling between various channels such as the πN and ηN channel. In these cases the πN final state is enhanced because it has the larger phase space.

Experimentally it will be hard to identify the plethora of missing N^* states with a mass > 2000 MeV. According to Fig. 1 we expect these states to have a width > 300 MeV. In the region 2000–2300 MeV the quark model predicts 30 states, all overlapping and broad. We propose that the mystery of the missing baryonic resonances be settled by a detailed investigation of the excited Ξ because all N^* states are related by flavor symmetry, discussed in section 4, to Ξ states that have the same spin and parity and a $\sim$450 MeV larger mass. However, they have a narrow width of $\sim$ 40 MeV. The Ξ^* states are readily accesible in production experiments such as $K^- p \to K^+ \Xi^*$ and $\gamma p \to K^+ K^+ \Xi^*$.

6 Where are the hybrid baryons?

There is no argument known which is based on QCD or on our understanding of confinement for limiting the baryons to 3 quark states, $|B\rangle = |qqq\rangle$. We expect also $|B\rangle = |qqqg\rangle$, $|B\rangle = |qqqgg\rangle$, etc. The latter two are called the hybrid baryons. They do not follow the simple SU(3)-flavor symmetry relations between the different light-quark baryon families. Thus, we do not expect that an N^* hybrid will have a flavor partner in the Λ family and vice versa. Shown in Fig. 6 by boxes are the various known Λ states using gray shading to indicate their star rating. We also show by the horizontal lines with crosses the SU(3) flavor prediction based on the experimentally observed N^* states and a simple expression to adjust for the flavor breaking due to the $s - d$ quark mass difference [4]. From this figure we can conclude that:

1. The Roper resonance, the $N(1440)\frac{1}{2}^+$, which has long been regarded as a hybrid candidate is not a hybrid because of the existence of the SU(3) flavor partner the $\Lambda(1600)\frac{1}{2}^+$.

2. There are no unaccounted-for Λ^* states, hence, there are no Λ hybrid candidates.

7 Nomenclature

To identify a specific baryonic resonance many authors use an outdated nomenclature which can be rather misleading. In this outdated system the proton is labelled a P_{11} state implying one unit of angular momentum of the constituents. This label dates back to the meson period in the history

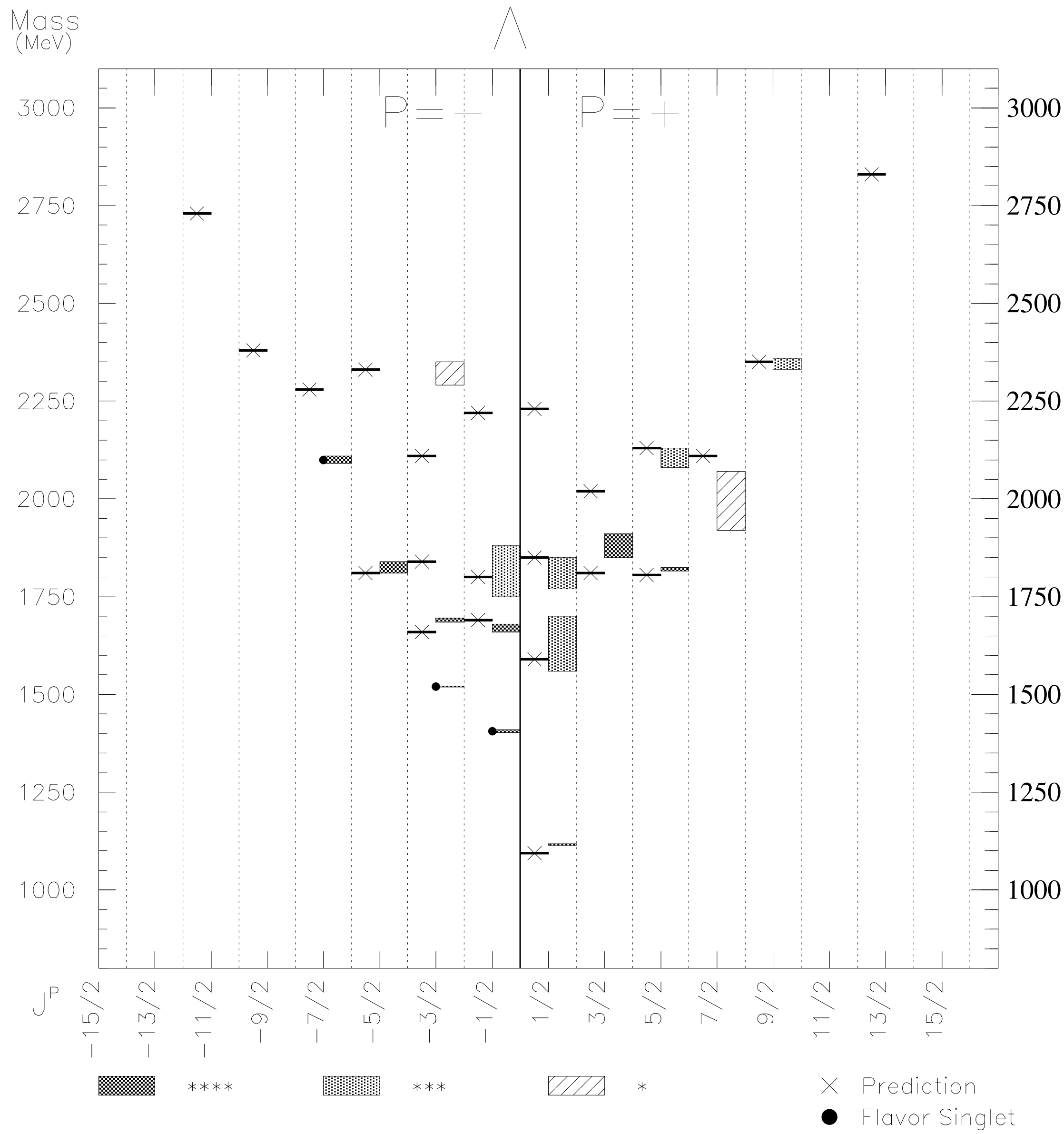

Figure 6: Λ^*-mass spectrum. The left side is for negative parity states, the right for positive. The experimental Λ^* masses are given by the boxes. The crosses are the theoretical predictions based on the known N^*mass values [4] and flavor symmetry.

of nuclear physics when the nucleon was considered to have a Dirac core surrounded by a P-wave pion cloud. The latter ingredient was needed to account for the observed magnetic dipole moments of the nucleons, $\mu_p = +2.79\mu_B$ and $\mu_n = -1.93\mu_B$.

In the quark era, with the success of QCD, it is hard to support the notion that the proton, which is the ground state of the N^* family and has a life time (into certain channels) in excess of 10^{32} years, is a P-state. We can rectify the situation by dropping the misleading nomenclature of L_{2I2J} and replace it by a simple system that uses measured parameters only. The first part is a capital or greek letter for the unique identification of the six light baryon families, the $N, \Delta, \Lambda, \Sigma, \Xi$, and Ω. This is followed by the mass in brackets and by the spin and parity. Thus, the proton's new symbol is $N(938)\frac{1}{2}^+$, the Roper is $N(1440)\frac{1}{2}^+$, the D_{13} is $N(1520)\frac{3}{2}^-$, and the S_{11} is $N(1535)\frac{1}{2}^-$. Similar conventions are used for the other families, e.g. the Λ ground state is $\Lambda(1116)\frac{1}{2}^+$, the lambda-Roper is $\Lambda(1600)\frac{1}{2}^+$, etc.

8 The star system

A practical system for quality assessment based on awarding a number of stars — as done by a well known restaurant guide — has been in use in baryon spectroscopy for many years. Every baryon resonance listed in the Review of Particle Physics [1] is awarded 1 to 4 stars. The meaning of the number of stars is the following.

**** Existence is certain, and properties are at least fairly well established.

*** Existence ranges from very likely to certain, but further confirmation is desirable and/or quantum numbers, branching fractions, etc. are not well determined.

** Evidence of existence is only fair.

* Evidence of existence is poor.

This system works well for the N and Δ families where all states have been investigated in several full, energy dependent and independent, πN partial wave analyses (PWA). The 3 and 4 star Λ and Σ states are in good shape as they come mainly from $\bar{K}N$ PWAs. However, there are several unsavory 1 and 2 star Σ candidates, which represent some questionable bumps in a few production experiments into inelastic channels. A major problem occurs in the case of the heavy baryons where all states have been discovered in production experiments. None of the new heavy baryons have an experimental determination of their spin and parity; instead, they are assigned a value based on the predictions of some popular quark models. We have seen in Sect. 5 how even the most extensive and widely used quark model does a poor job in the mass ordering of the lowest excited states. Furthermore, the actual mass calculation especially of the positive parity states is inaccurate by up to 80 MeV. Yet, the heavy baryon states have been given 3 and a few even 4 stars. The spin and parity are the vital characteristics of any resonance and a state does not warrant 3 or 4 stars when their is no experimental data on its spin and parity. We should fine tune the definition of 3 stars with this in mind.

Mark Manley [11] is floating the idea that we should establish a new class of 5 star states which is reserved for the "golden" resonances about whose existence and basic quantum numbers and properties there is no question. This idea has merits and deserves careful consideration by our community. In the meantime all physicists should be aware that the spin and parity of all heavy baryons are assigned based on the quark model without experimental verification.

9 Summary and conclusions

A large body of detailed information on the properties of the light baryons [1] has been accumulated. However, our knowledge is still very incomplete; it is insufficient to allow drawing reliable conclusions about the occurance of significant regularities such as parity doublets and clusters. Investigating the occurance of regularities is needed to make progress on the problem of quark confinement in QCD. There is currently no evidence for the existence of hybrids but we cannot exclude them either. The lack of any clear manifestations of the gluon degree of freedom in any baryonic system is unsettling. It points to hitherto unexpected aspects of QCD in the non-perturbative regime.

New data on the properties of the many expected, but undiscovered $\Lambda^*, \Sigma^*, \Xi^*$ and Ω^* states are urgently needed so we can establish the dependence of the $s-d$ quark mass difference on the energy and spin/parity of the confined 3 quark system. A convenient way to handle this is by investigating the validity of the Gell-Mann decuplet and the Gell-Mann-Okubo octet mass relations for high mass states with large spin and for the positive as well as negative parity states. This is needed for progress in the area of the "Origin of Mass", one of the areas of importance in our field. A coordinated effort is needed on the existence of N^* and Δ^* resonances with $m > 2000$ MeV. Required for this are sophisticated detectors and secondary beams of $\pi^{\pm}, K^{\pm}, \bar{p}, \vec{n}$, and $\vec{\gamma}$ up to 5 GeV. It is the responsibility of this community to raise the awareness of our colleagues to the importance of the physics we are engaged in and to the experimental tools, especially the secondary beams, required to get our jobs done.

References

[1] D.E. Groom et al., Eur. Phys. J. **C15**, 1 (2000).

[2] D.O. Riska, private communications (2000).

[3] F. Iachello, Phys. Rev. Lett. **62**, 2440 (1989).

[4] B.M.K. Nefkens, proc. NSTAR 2001 Conference D. Drechsel et al., editors, World Scientific, in press.

[5] S. Aoki et al. (CP-PACS), Phys. Rev. Lett. **84**, 238 (2000).

[6] S. Capstick and N. Isgur, Phys. Rev. D **34**, 2809 (1986)

[7] R. Bijker, F. Iachello, and A. Leviatan Ann. Phys. (NY) **236**, 69 (1994).

[8] S. Capstick and W. Roberts, Phys. Rev.**D49**, 4570 (1992).

[9] L. Glozman, D. O. Riska, Physics Reports **268** 263 (1996).

[10] S. Godfrey, N. Isgur, Phys. Rev. D **32** (1985), 189.

[11] M. Manley, private communication.

Low-energy pion-proton scattering at TRIUMF and PSI

R. Meier

Physikalisches Institut, Universität Tübingen
Auf der Morgenstelle 14, 72076 Tübingen, Germany

(Received: 30 October 2001)

Present discrepancies in extractions of the pion-proton sigma-term and the size of isospin breaking from pion-proton scattering are at least partly due to inconsistent and missing experimental information. To overcome these problems, a number of experiments on low energy pion-proton scattering have recently been done at TRIUMF and PSI. Elastic scattering cross sections and $\pi^- p$ analyzing powers have been measured by the CHAOS collaboration at TRIUMF, $\pi^+ p$ analyzing powers by the LEPS collaboration at PSI. An experiment on total single charge exchange cross sections at PSI has just started taking data. Results and/or status of these experiments are discussed. Finally, the feasibility of a π^0p elastic scattering measurement is explored.

1 Introduction

From πp observables, important quantities of the strong interaction can be extracted: the πNN coupling constant, the sigma-term of the proton and the size of isospin breaking.

Presently, there is no agreement on the value of any of these quantities [1]. For the sigma-term, values of recent extractions from elastic pion-proton scattering vary by up to a factor of 2. Some of the results lead to a strangeness content of the nucleon of up to 25% when compared to extractions of the sigma-term from baryon masses.

The size of isospin breaking in the pion-proton system has been investigated by using three experimentally accessible reactions: elastic scattering $\pi^\pm p \rightarrow \pi^\pm p$ and single charge exchange $\pi^- p \rightarrow \pi^0 n$. If isospin is conserved, the amplitudes for these reactions are connected by a triangle relation. The violation of this relation for s-waves at low energies has been tested by several groups, leading to contradictory results. While analyses by Gibbs *et al.* [2] and Matsinos [3] showed large isospin violation of about 7%, recent work by Fettes and Meißner lead to only 0.7% [4].

These discrepancies are partly due to the status of the πp data base, in particular at low energies. There are regions where information is still missing, and there are regions where the available experimental data are contradictory. New measurements of πp observables at low energies are aimed at providing additional information and resolving the discrepancies. While elastic scattering data are primarily needed for the extraction of the sigma-term (section 2), more information

On the single charge exchange (SCX) reaction π^-p$\rightarrow \pi^\circ$n should lead to a better determination of the size of isospin violation (section 3). The experiments which are discussed have been carried out at the PSI (Villigen, Switzerland) and TRIUMF (Vancouver, Canada) meson factories.

Isospin symmetry can in principle be studied in various ways in the πp system [4]. Presently, only the triangle identity involving the amplitudes of $\pi^\pm$p elastic scattering and the SCX reaction is experimentally accessible. Isospin violation is predicted to yield large effects when elastic scattering of neutral pions is considered [4]. In an outlook, the feasibility of a direct measurement of π°p elastic scattering at the CELSIUS/WASA facility (Uppsala, Sweden) is explored (section 4).

2 Elastic scattering: $\pi^\pm p \rightarrow \pi^\pm p$

For the extraction of the sigma-term, πp elastic scattering amplitudes have to be determined from data in the experimentally accessible region. These are then extrapolated to the Cheng-Dashen point below threshold. Besides measurements on pionic hydrogen, scattering cross sections at low energies, particularly in the angular region of the Coulomb-nuclear interference (CNI), are crucial for the accuracy of this extrapolation. Providing this information is the goal of the CNI experiment at TRIUMF [5].

Polarization observables provide additional constraints for phase shift analyses and can also be used to identify incorrect cross section data sets. Below $\approx$ 100 MeV, only one data set of analyzing powers at one energy has been available so far [6]. This situation is about to be improved considerably by two experiments: measurements in the π^-p elastic channel at TRIUMF [7], and in the π^+p elastic channel at PSI [8].

2.1 Differential cross section measurements at TRIUMF

The CNI experiment at TRIUMF has measured $\pi^\pm$p differential cross sections at 8 energies between 15 and 67 MeV, in an angular range from 8° to 180°. The data were taken using the CHAOS detector [9]. CHAOS is a 360° spectrometer, consisting of 4 concentric cylindrical wire chambers for particle tracking. The chambers are surrounded by blocks of scintillation- and Cerenkov-detectors for particle identification and triggering purposes. The spectrometer is located inside a dipole magnet providing a vertical magnetic field of up to 1.6 T. The incoming pion beam enters in the plane of the chambers and curves in toward the center where targets can be introduced through a hole in the upper pole tip of the magnet. In the CNI experiment, a planar liquid hydrogen target was used. For each event, the incoming particle and the outgoing reaction products were detected. At large scattering angles, both the elastically scattered pion as well as the backscattered proton were tracked. At forward scattering angles the recoil energy was too low for the protons to leave the target, therefore only the pion was detected. For normalization purposes, elastic scattering of muons was measured simultaneously using muons originating from a point close to the production target which could be separated from pions by the time of flight through the secondary beam line.

A major difficulty for measurements in the Coulomb-nuclear interference region at low scattering angles was overwhelming muon background from pion decay close to the hydrogen target. These decay muons could only partly be separated from scattered pions by kinematical constraints. Therefore a muon-pion identification detector was built for this experiment and included in the CHAOS data acquisition [10].

A total of over 3 TB of data were taken in 1999 and 2000, they are presently being analyzed [11]. Final results may be expected for the next MENU conference 2003.

2.2 Analyzing power measurements at TRIUMF

πp analyzing powers have been measured using the CHAOS spectrometer and a dynamically polarized butanol target with quantization axis perpendicular to the scattering plane. The analyzing power A_y is derived from relative scattering cross sections σ^+ and σ^- for opposite polarizations with absolute value p:

$$A_y = \frac{1}{p} \times \frac{\sigma^+ - \sigma^-}{\sigma^+ + \sigma^-} \ .$$

The polarized target setup was specially designed to match the CHAOS requirements. Polarization in the butanol sample was induced by microwave irradiation in the homogenous field of a superconducting solenoid outside the spectrometer. The target was moved to its position in the center of the detector in frozen spin mode while built-in superconducting coils were providing the necessary holding field. Once the target reached the data taking position inside CHAOS, the spectrometer magnet provided the holding field.

Analyzing power data taken for $\pi^\pm$p elastic scattering at energies across the Δ-resonance were published earlier [12]. A major difficulty in measuring analyzing powers at low energies is caused by the unavoidable presence of nuclei besides protons in a dynamically polarized target. The target sample itself contains carbon and oxygen, the cooling liquid helium and the target cell copper or iron. On these nuclei, reactions take place which cause background to pion-proton scattering. In the CHAOS experiment this difficulty was overcome by requiring the detection of the scattered pion and the backscattered proton in coincidence. Of course this limited the accessible angular region at low energies to backward pion scattering angles as only here the protons had enough energy to leave the target. For π^-p scattering, which was measured with this setup at energies from 140 MeV down to 57 MeV, this is the interesting region with large expected changes of the analyzing power with energy.

The analysis of the low energy data has been finished recently [13]. Results are shown in Fig. 1, compared to previous data from Sevior *et al.* [14] and KH80 [15] (dashed line) and GWU SM01 [16] (solid line) phase shift predictions. Good agreement is found with previous data and the phase shift predictions at higher energies. At 67 and 57 MeV however, significant deviations of the data from both phase shift analyses are found.

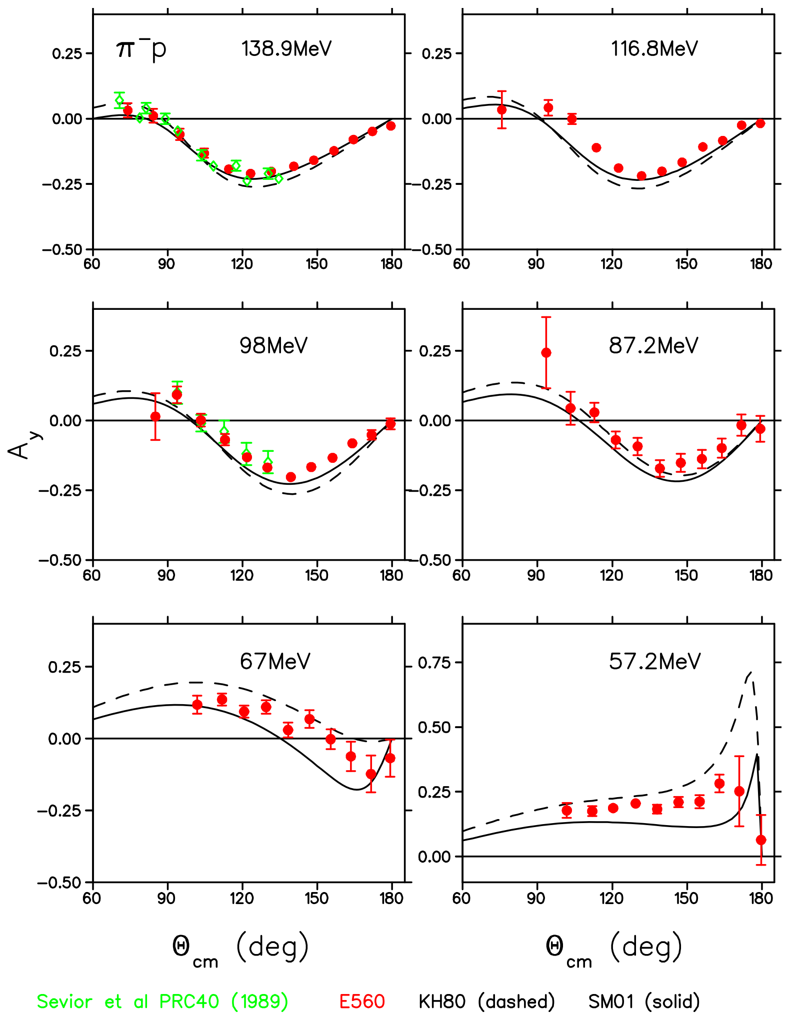

Figure 1: Analyzing powers for $\pi^- p$ elastic scattering. Solid points are from the TRIUMF/CHAOS experiment [13], open symbols from Sevior *et al.* [14]. Predictions of the KH80 [15] (dashed line) and the GWU SM01 [16] (solid line) phase shift analyses are shown.

2.3 *Analyzing power measurements at PSI*

For π^+p scattering, large variations of the analyzing power with energy are predicted at forward angles. There the coincidence method used in the CHAOS experiment to suppress background is not applicable. Instead, the LEPS spectrometer and a newly developed active polarized target [17] were used at PSI. The polarized scintillator target was a very efficient tool for background suppression and allowed measurements of the π^+p analyzing power at 87, 77, 67, 57, 51 and 45 MeV. Details of the experimental setup and procedure are given in a contribution to this conference [18], the analysis is in progress. Preliminary results show a similar pattern as the CHAOS π^-p data. At higher energies good agreement with previous data and phase shift analyses is found, while significant deviations from the phase shift analyses are seen at lower energies.

3 Single charge exchange: $\pi^- p \to \pi^0 n$

More single charge exchange data are needed to sufficiently restrict the analyses investigating isospin violation. If there was 7% isospin breaking in s-wave at low energies, as has been claimed [2, 3], significant effects are expected in total and differential cross sections as well as polarization observables.

Differential cross sections are being measured by the Crystal Ball collaboration at BNL [19]. Measurements of analyzing powers are planned at PSI [20]. As the accepted proposal is based on the use of the NMS spectrometer which is currently in operation at BNL, it is uncertain if and when these measurements can be done. Total SCX cross sections are presently being measured at PSI.

The expected effect for the total SCX cross section is illustrated in Fig. 2. Total cross section data [21, 22] are shown in comparison to the GWU SM01 [16] phase shift solution at low energies. Existing data do not have the accuracy to distinguish between the phase shift prediction and the curves with the s-wave contribution changed by $\pm 7\%$. Also shown are dummy data with an error of 2%, which is the proposed accuracy of a new total cross section measurement which has started taking data at PSI [23].

This experiment uses a transmission technique to measure the total SCX cross section. A small 4π box detector consisting of thin plastic scintillators has been constructed. Incoming negative pions are counted in three small beam defining counters and hit a polyethylene target of very well known dimensions and chemical properties. The measured quantity is the *disappearance* of incoming charged beam particles in the detector, i. e. the probability for a final state consisting of neutral particles only. The total cross section for the reaction $\pi^- p \to \pi^0 n$ is then derived from the transmissions of the polyethylene target, a carbon background target and empty target. Different

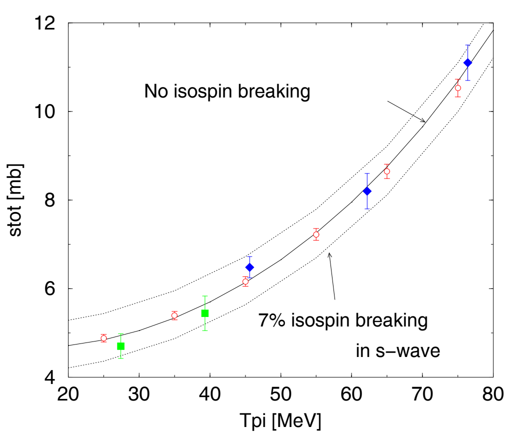

Figure 2: Low energy total cross section for the charge exchange reaction. The data are from Salomon *et al.* [21] (rectangles) and Bagheri *et al.* [22] (diamonds). The open points are dummy data and show the planned accuracy of the PSI total cross section experiment. The solid line is a phase shift prediction from the GWU SM01 analysis, the dotted lines show the variation if the size of the s-wave contribution is varied by $\pm 7\%$.

target thicknesses are used. An automatic target changing system allows a frequent variation of the target type. All detector ADCs and TDCs are being read out for every beam event at rates of up to 20kHz. Corrections have to be applied for the detection of neutrals in the detector, the π^0 Dalitz decay, pion decay and radiative pion capture. The total size of the corrections is about 7%.

In a first beam time, data have been taken at energies between $T_{\pi^-} = 60$ and 250 MeV. In a second beam time lower energies will be measured. The proposed accuracy of 2% is illustrated by the dummy data points shown in Fig. 2. Clearly it should allow the identification of isospin breaking on the level of 7% in s-wave.

4 Elastic scattering: $\pi^0 p \to \pi^0 p$

Considering all reaction channels in the pion-nucleon system, isospin symmetry can be tested in various ways. Besides the triangle relation between the amplitudes of $\pi^\pm p$ elastic scattering and $\pi^- p$ charge exchange, 5 other relations are known [4]. Of particular interest is a relation connecting $\pi^\pm p$ elastic scattering to $\pi^0 p$ elastic scattering. Here, Fettes and Meißner [4] find up to 40% violation of the relation in s-wave.

Recently, a possibility for measuring $\pi^0 p$ scattering has been put forward by S. Kullander [24]. He suggests to use the WASA detector at the proton beam of the CELSIUS synchrotron. With the WASA hydrogen pellet target, which produces a stream of solid hydrogen pellets of about 30 μm diameter, a luminosity of $10^{32}/\text{cm}^2\text{s}$ can be reached. Production of neutral pions in proton-proton collisions inside the hydrogen pellets at this luminosity occurs at high rates, for example at a proton kinetic energy of 650 MeV at a rate of about $4{*}10^5/\text{s}$. These neutral pions typically travel about 50 nm in their mean lifetime, so there is a finite probability for them to scatter from another proton in the hydrogen target. The reaction could be identified in a kinematically overconstrained way by detecting the two protons from the π^0 production, the backscattered proton from the $\pi^0 p$ scattering, and the two photons from the π^0 decay. Fig. 3 shows the statistical accuracy which could be reached in a measurement of the total $\pi^0 p$ elastic scattering cross section after 10^6s of beam at $T_p = 650$ MeV (assuming three body phase space for the kinetic energy distribution of the produced neutral pions, a total $\pi^0 p$ cross section derived from the GWU SM00 [16] phase shift analysis and 100% detector acceptance). Of course the time estimate is not realistic due to the finite detector acceptance, but a measurement of $\pi^0 p$ scattering appears feasible.

As even isospin breaking as large as 40% in s-wave gives only a small change of the total $\pi^0 p$ cross section, which is strongly p-wave dominated even at low energies due to its amplitude structure (cancellation of S31 and S11 contributions), isospin breaking at low energy should not be an initial goal for such a measurement. Instead, it could be done for an improved determination of the π^0 lifetime, which is presently known with a sizable uncertainty of 8%. The lifetime is connected

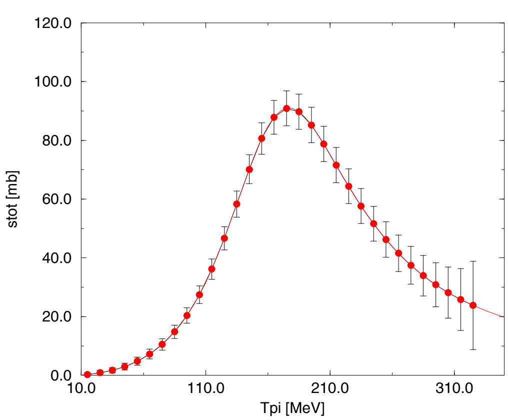

Figure 3: Simulated accuracy of π^0p total cross section data after 10^6s of $T_p = 650$ MeV beam at the CELSIUS synchrotron assuming 100% detector efficiency.

to the chiral anomaly, which is calculable as *'the most accurate prediction in QCD, which depends only on the number of colors'* [25]. Using $\pi^0 p$ scattering to determine the π^0 lifetime would be a method completely different from the measurement using the Primakoff effect which is proposed at JLAB [25].

Acknowledgments: The work discussed here has received support from the National Science and Engineering Research Council of Canada, the Instituto Nazionale di Fisica Nucleare, Italy, the Australian Research Council, the California State University Sacramento Foundation, the German Federal Minister of Education and Research (BMBF, 06TÜ987I), and the Deutsche Forschungsgemeinschaft.

References

[1] M. E. Sainio, p. 156; U. G. Meißner, p. 127; M. Knecht, p. 108, πN Newsletter **15** (1999).
[2] W. Gibbs *et al.*, Phys. Rev. Lett. **74**, 3740 (1995);
[3] E. Matsinos, Phys. Re. C **56**, 3014 (1997).
[4] N. Fettes, U. G. Meißner, Phys. Rev. C **63**, 045201 (2001); hep-ph/0101030.
[5] G. Smith *et al.*, TRIUMF proposal E778 (1996).
[6] R. Wieser *et al.*, Phys. Rev. C **54**, 1930 (1996).
[7] G. Smith *et al.*, TRIUMF proposal E560 (1992).
[8] R. Meier *et al.*, PSI proposal R97-01 (1998).
[9] G. R. Smith *et al.*, Nuclear Instruments and Methods A **362**, 349 (1995).
[10] E. Fragiacomo *et al.*, Nuclear Instruments and Methods A **439**, 45 (2000).
[11] H. Denz, *πp Cross Sections in the Coulomb-Nuclear Interference Region*, contribution to MENU 2001.
[12] G. J. Hofman *et al.*, Phys. Rev. C **58**, 3484 (1998).
[13] J. Patterson, PhD thesis, University of Colorado, Boulder (2001).
[14] M. E. Sevior *et al.*, Phys. Rev. C **40**, 2780 (1989).
[15] R. Koch, E. Pietarinen, Nucl. Phys. A **336**, 331 (1980).
[16] R. A. Arndt *et al.*, Phys. Rev. C **52** 2120 (1995).
[17] B. van den Brandt *et al.*, Nuclear Instruments and Methods A (2000).
[18] M. Cröni *et al.*, *Measurement of analyzing powers in πp scattering*, contribution to MENU 2001.
[19] M. Sadler, contribution to MENU2001.
[20] J. Comfort *et al.*, PSI proposal R99-02 (1999).
[21] M. Salomon *et al.*, Nucl. Phys. A **414**, 493 (1984).
[22] A. Bagheri *et al.*, Phys. Rev. C **38**, 885 (1988).
[23] E. Friedman *et al.*, PSI proposal R00-01 (2000).
[24] S. Kullander at the WASA physics jamboree, Uppsala (2000).
[25] A. Gasparian *et al.*, *A Precision Measurement of the Neutral Pion Lifetime via the Primakoff Effect* TJNAF Proposal E99-014 (1999).

Pion electroproduction at threshold

Harald Merkel
for the A1 Collaboration
Institut für Kernphysik, Johannes Gutenberg-Universtät Mainz, 55099 Mainz, Germany

(Received: 31 October 2001)

In this talk, our latest data set on $H(e, e'p)\pi^0$ at threshold at a four-momentum transfer of $Q^2 = 0.05\,\mathrm{GeV}^2/\mathrm{c}^2$ is presented. From threshold up to 4 MeV above threshold the full center of mass solid angle was covered. By measuring at three different values of the virtual photon polarization a longitudinal-transverse separation was performed. While threshold pion photoproduction is in very good agreement with theoretical calculations in the framework of Heavy Baryon Chiral Perturbation Theory, this data set reveals large discrepancies for the electroproduction case.

1 Introduction

The electromagnetic production of neutral pions very close to threshold is a well known testing ground for predictions in the framework of Heavy Baryon Chiral Perturbation Theory (HBChPT [1], see e.g. [2] for an current overview of the field or [3] for a textbook). In these experiments, the theoretical interest of directly producing the Goldstone Bosons of Chiral Symmetry is combined with the experimental precision made possible by the high quality electron beams of the existing continuous wave electron accelerators.

First generation experiments with real photons [4–6] showed the necessity to abandon the old Low Energy Theorems [7] in favor of higher order calculations in the systematic approach of HBChPT [8, 9], which was in impressive agreement with the experiment.

Recent photoproduction measurements [10] are close to the complete separation of all multipole amplitudes at threshold, and are still in good agreement with theory. First experiments to extend this success to electroproduction reactions were done at NIKHEF [11, 12] at a four momentum transfer of $Q^2 = 0.1\,\mathrm{GeV}^2/\mathrm{c}^2$. These experiments were extended by a complete Rosenbluth separation at MAMI [13] at the same Q^2. Although this four-momentum transfer was expected to be a little bit to high for the convergence of HBChPT, a qualitative agreement of the separated multipoles with calculations [9, 14] was claimed.

This talk presents an experiment [15] at a four-momentum transfer of $Q^2 = 0.05\,\mathrm{GeV}^2/\mathrm{c}^2$, i.e. half way between the photon point and the existing electro production data, with the surprising result, that HBChPT calculations seem not to agree anymore.

2 Experiment

The experiment took place at the three spectrometer setup of the A1 collaboration at the Mainz Microtron MAMI (see [16] for a detailed description of the setup). For the electron detection, spectrometer B with a solid angle of 5.4 msr was used for the forward angles, while for the Rosenbluth separation also a detection with the large solid angle of spectrometer C (28 msr) at backward angles was necessary.

The recoil proton was detected with spectrometer A. By detecting the recoil particle, the kinematical focusing of the Lorentz boost enabled us to cover the full center of mass solid angle up to a center of mass energy of $\Delta W = 4\,\mathrm{MeV}$ above threshold within each setting.

To perform a Rosenbluth separation, data were taken at three values of the virtual photon polarization $\epsilon = 0.49, 0.72, 0.93$. From the dependence on the azimuthal pion production angle ϕ, the cross section could be separated in $\sigma_0(\theta) = \sigma_T(\theta) + \epsilon\sigma_L(\theta)$ and $\sigma_{TL}(\theta)$. The transverse-transverse interference σ_{TT} was to small to be separated. Further experimental details are described in [15].

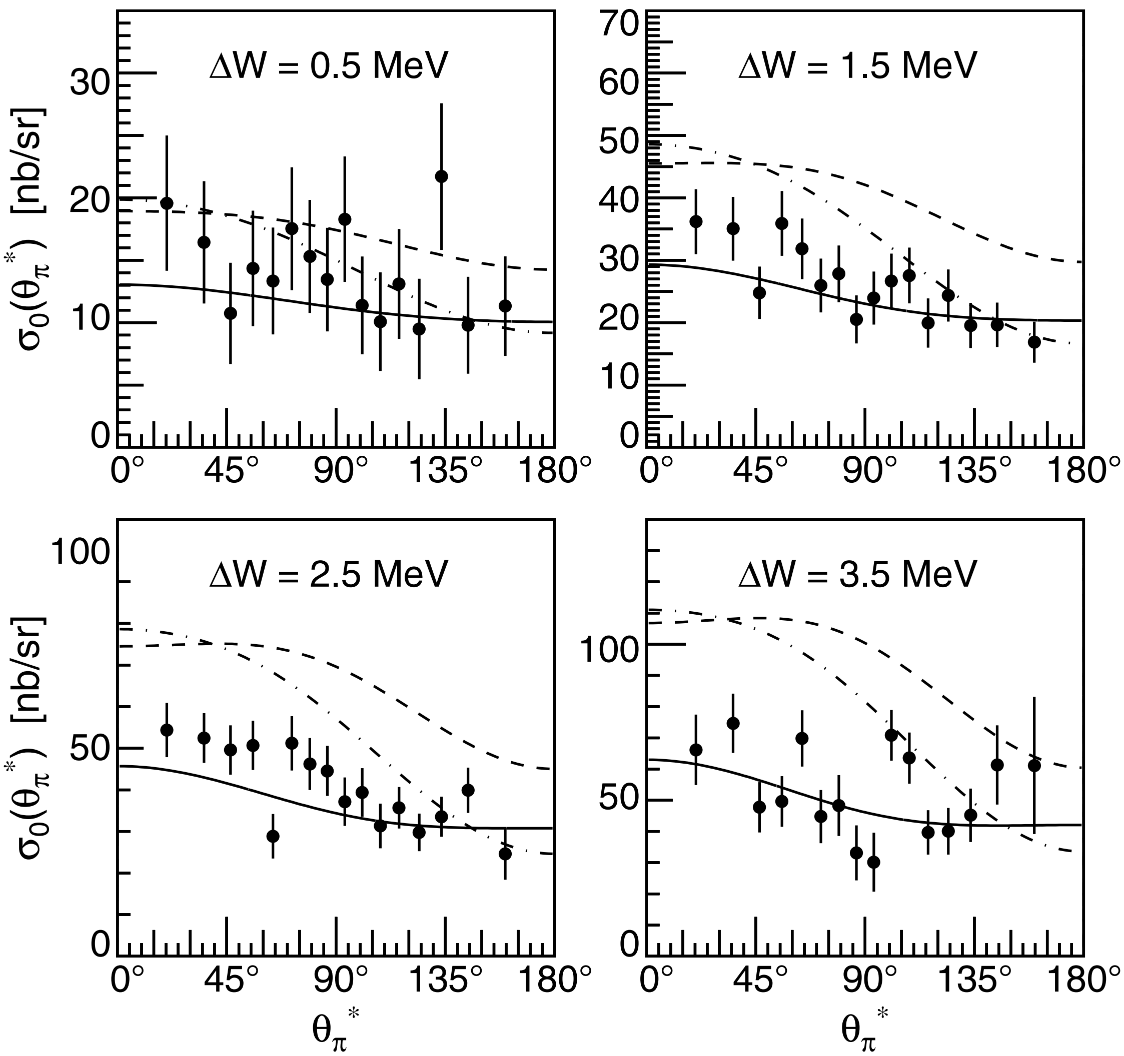

Figure 1: The differential cross section for the first four energy bins above threshold at $\epsilon = 0.72$. The solid line is a fit with the assumption of only s and p waves contributing to the cross section. The dashed line is the prediction of HBChPT [9], the dash-dotted line is the prediction of MAID [17].

3 Results

Figure 1 shows the differential cross section at the middle epsilon point. Figure 2 shows the transverse-longitudinal interference cross section. In both figures, the dashed line shows the prediction of HBChPT. As can be seen, HBChPT overestimates the cross section nearly by a factor of two. For comparison, we included the phenomenological model of the MAID group [17] (dash-dotted line), which also overestimates the data.

To further illustrate this discrepancy, it is useful to perform a simple fit (solid line) to the data with the assumption of only s and p waves contributing to the cross section. The cross section is decomposed, as usual, in angular coefficients

$$
\begin{aligned}
\sigma_T(\theta_\pi^*) &= (p_\pi^*/k_\gamma^*)\left(A + B\cos\theta_\pi^* + C\cos^2\theta_\pi^*\right), \\
\sigma_L(\theta_\pi^*) &= (p_\pi^*/k_\gamma^*)\left(A' + B'\cos\theta_\pi^* + C'\cos^2\theta_\pi^*\right),
\end{aligned}
$$

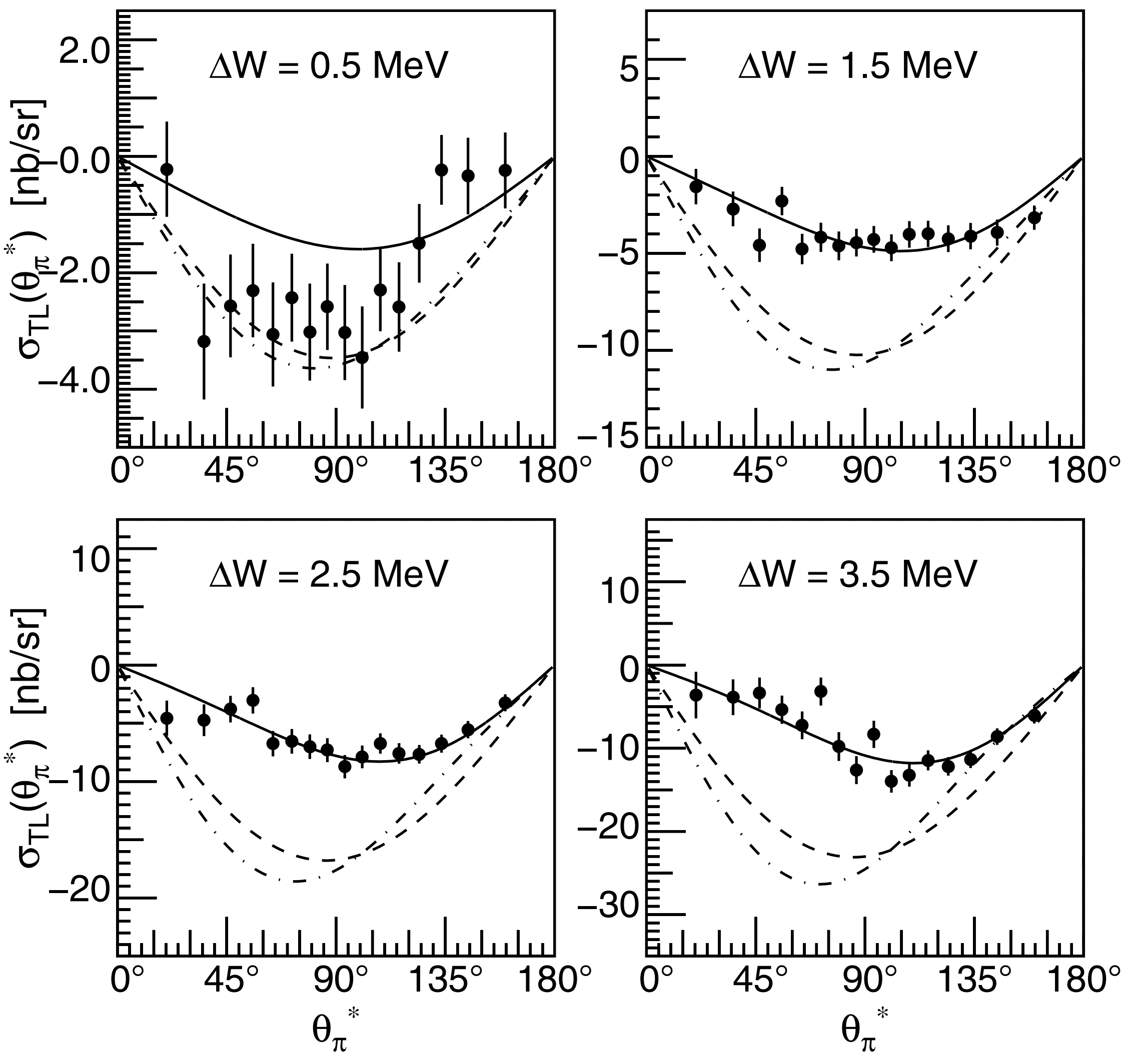

Figure 2: The transverse-longitudinal interference. Lines as in fig. 1.

$$
\begin{aligned}
\sigma_{TL}(\theta^*_\pi) &= (p^*_\pi/k^*_\gamma)\,(D\sin\theta^*_\pi + E\sin\theta^*_\pi\cos\theta^*_\pi)\,,\\
\sigma_{TT}(\theta^*_\pi) &= (p^*_\pi/k^*_\gamma)\left(F\sin^2\theta^*_\pi\right), \qquad (1)
\end{aligned}
$$

with the coefficients given by the multipole decomposition

$$
\begin{aligned}
A &= |E_{0+}|^2 + \frac{1}{2}\left(|P_2|^2 + |P_3|^2\right),\\
B &= 2\mathrm{Re}\,(E_{0+}P_1^*)\,,\\
C &= |P_1|^2 - \frac{1}{2}\left(|P_2|^2 + |P_3|^2\right),\\
D &= -\mathrm{Re}\,(E_{0+}P_5^* + L_{0+}P_2^*)\,,\\
E &= -\mathrm{Re}\,(P_1P_5^* + P_4P_2^*)\,,\\
F &= \frac{1}{2}\left(|P_2|^2 - |P_3|^2\right),\\
A' &= |L_{0+}|^2 + |P_5|^2,
\end{aligned}
$$

$$
\begin{aligned}
B' &= 2\mathrm{Re}\,(L_{0+}P_4^*)\,, \\
C' &= \left(|P_4|^2 - |P_5|^2\right).
\end{aligned}
\tag{2}
$$

At threshold, we assumed constant and real s wave amplitudes and p wave amplitudes proportional to the pion center of mass momentum, i.e. $P_i = \hat{P}_i\, p_\pi^{CMS}$ with $\hat{P}_i$ real and constant in energy. Since the cross section σ_{TT} is to small to be extracted from this experiment, the coefficient F was not determined and the p wave combination $P_{23}^2 = \frac{1}{2}(|P_2|^2 + |P_3|^2)$ was used as fit parameter.

Table 1 shows the extracted multipole amplitudes in comparison with the existing experiments and theoretical predictions. One has to note, that the multipole amplitudes of the old data sets deviated from the quoted amplitudes in the references, since they were re-fitted with the same assumptions mentioned above to get a comparable result.

The most striking result of this fit procedure is, that a much smaller value for $\hat{P}_{23}^2$ is extracted from this experiment than expected. This is a serious disagreement with the calculations of

Table 1: Extracted multipole amplitudes in comparison with the threshold values of HBChPT [9] and MAID [17]. The AmPS [11] value for $|L_{0+}|$ was extracted from their value for $a_0 \approx \epsilon_L |L_{0+}|^2$. For the AmPS [12] fit L_{0+} was fixed, since no Rosenbluth separation was performed.

	E_{0+}	L_{0+}	$\hat{P}_{23}^{\,2}$	$\hat{P}_1$	$\hat{P}_4$	$\hat{P}_5$
	$(10^{-3} m_\pi^{-1})$		$(10^{-6} m_\pi^{-4})$		$(10^{-3} m_\pi^{-2})$	
			$Q^2 = 0.05\,\mathrm{GeV}^2/\mathrm{c}^2$			
Fit	0.57	−1.29	100	12.0	0.29	−1.9
Error	±0.11	±0.02	±3	±0.3	±0.33	±0.3
AmPS [11]		(−)1.57				
		±0.96				
ChPT	0.27	−1.55	353	16.5	−0.72	−0.2
MAID	0.76	−1.4	250	15.0	−1.75	1.9
			photon point $Q^2 = 0\,\mathrm{GeV}^2/\mathrm{c}^2$			
MAMI [10]	−1.33		111	9.5		
ChPT	−1.14	−1.70	105	9.3	−0.6	−0.2
MAID	−1.16	−1.29	95	9.3	−3.0	2.2
			$Q^2 = 0.1\,\mathrm{GeV}^2/\mathrm{c}^2$			
MAMI [13]	0.58	−1.38	573	15.1	−2.3	0.1
	±0.18	±0.01	±11	±0.8	±0.2	±0.3
AmPS [12]	1.99	−1.33	526	16.4	−1.0	−1.0
	±0.3	fixed	±7	±0.6	±0.4	±0.4
ChPT	1.42	−1.33	571	20.1	−0.6	−0.1
MAID	2.2	−1.12	315	17.1	−1.1	1.4

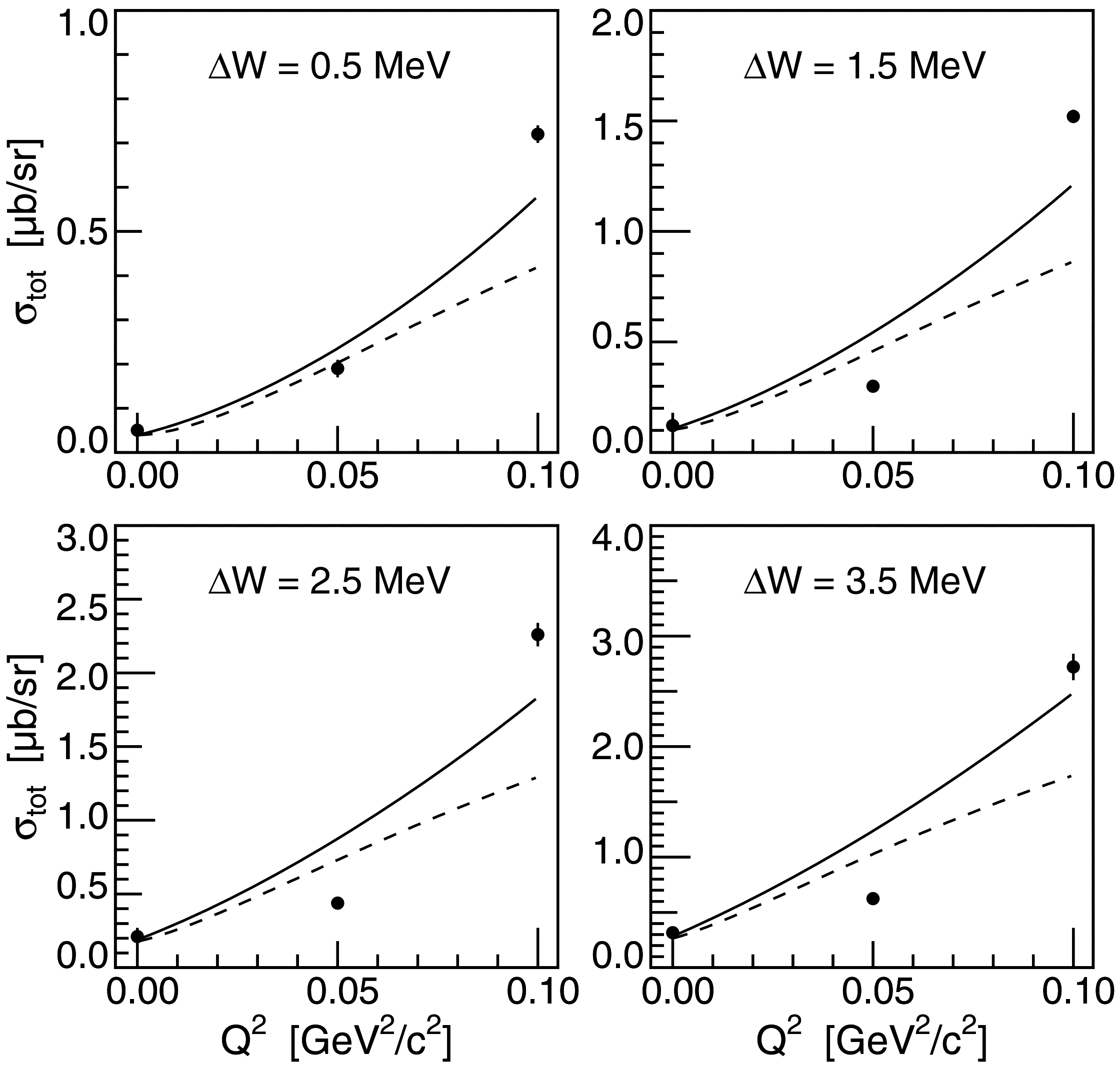

Figure 3: The total cross section vs. the four-momentum transfer. The data points are from [10], [13], and [15]. The solid line shows the prediction of HBChPT, the solid line the prediction of MAID.

HBChPT, since this combination does not contain further free parameters, which might be fitted, but is completely fixed by the photoproduction data.

The assumptions of the performed fit are, of course, questionable. E.g. with explicit energy dependence of the s waves strength can be shifted between s and p waves. Further, the cross section is dominated in the lower energy bins by the systematic error, leading to large systematic errors to the extracted multipoles. To illustrate the discrepancy in a completely model independent manner, in fig. 3 the total cross section was plotted against the four-momentum transfer.

In this figure, one might be surprised by the deviation of the $Q^2 = 0.1\,\mathrm{GeV}^2/\mathrm{c}^2$ data set, which was described as consistent with theory by different authors. This discrepancy was covered somehow by the way to extract and compare only multipoles and differential cross sections, and is even more surprising since both, HBChPT and MAID, include this data points in their fit.

On summary this Q^2 dependence of the total cross section indicates, that theory might need higher order calculations to describe the increased curvature in Q^2 in the cross section. The fit with s and p wave seems to indicate, that especially the description of the p waves have to be revised.

Since this result is somewhat surprising, it appears useful to repeat the measurement in an independent experiment. Such experiments are currently planned at Jefferson Lab [18] and MAMI with emphasis on the Q^2 dependence of the cross section.

References

[1] S. Weinberg, Physica **A96**, 327 (1979).

[2] A. M. Bernstein, J. L. Goity, and U.-G. Meißner, eds., *Chiral Dynamics: Theory and Experiment III* (World Scientific, Singapore, 2001).

[3] A. W. Thomas and W. Weise, *The Structure of the Nucleon* (WILEY-VCH, Berlin, 2001).

[4] R. Beck *et al.*, Phys. Rev. Lett. **65**, 1841 (1990).

[5] J. C. Bergstrom, Phys. Rev. **C44**, 1768 (1991).

[6] J. C. Bergstrom *et al.*, Phys. Rev. **C53**, 1052 (1996).

[7] H. Naus, Phys. Rev. **C 43**, R365 (1991).

[8] V. Bernard, N. Kaiser, and U.-G. Meißner, Nucl. Phys. **B383**, 442 (1992).

[9] V. Bernard, N. Kaiser, and U.-G. Meißner, Nucl. Phys. **A607**, 379 (1996), `hep-ph/9601267`.

[10] A. Schmidt *et al.*, (2001), `nucl-ex/0105010`.

[11] T. P. Welch *et al.*, Phys. Rev. Lett. **69**, 2761 (1992).

[12] H. B. van den Brink *et al.*, Phys. Rev. Lett. **74**, 3561 (1995).

[13] M. O. Distler *et al.*, Phys. Rev. Lett. **80**, 2294 (1998).

[14] V. Bernard, N. Kaiser, and U.-G. Meißner, Nucl. Phys. A **633**, 695 (1998).

[15] H. Merkel *et al.* (2001), `nucl-ex/0108020`.

[16] K. I. Blomqvist *et al.*, Nucl. Instr. and Meth. A **403**, 263 (1998).

[17] D. Drechsel *et al.*, Nucl. Phys. **A645**, 145 (1999), `nucl-th/9807001`.

[18] R. Lindgren *et al.*, Proposal E-01-014, TJNAF (2001).

Scrying new physics with the Crystal Ball

J.R. Comfort
for the Crystal Ball Collaboration

Department of Physics & Astronomy,
Arizona State University, Tempe, AZ 85287-1504,U.S.A.

(Received: 26 October 2001)

A program in baryon spectroscopy and meson decays with the Crystal Ball Detector is underway at the Brookhaven National Laboratory. A vast amount of high-quality data are being obtained on the formation and decays of N^*, Δ, Λ, and Σ resonances. Threshold η production patterns are very similar in $\pi^- p$ and $K^- p$ interactions. Comprehensive $2\pi^0$ data are best described by sequential decays through intermediate resonances. Precision studies of eta-meson decays are setting stringent challenges to theoretical descriptions.

1 Introduction

The concept of a Crystal Ball goes back to the days of Nostradamus. He would take a bowl of water, place it on a stand and stare at the reflection of some light from its surface. After some time, he would utter a rhyme, understood to be either about an upcoming event or an interpretation of a past event. With many of them deemed to be valid or successful, he won great fame for his ability to discern ("scry") the future. Through a comprehensive program in studying the formation and decays of baryon resonances and precision measurements of meson decays, the Crystal Ball Collaboration[1] is also seeking to *discern* new understandings of subatomic structure and interactions.

The SLAC Crystal Ball (CB) spectrometer was moved to Brookhaven National Laboratory (BNL) in 1995. After an engineering run in 1997, extensive data were obtained over four months of running in 1998 for a wide variety of reactions and decays. Some of the reaction channels and decays are listed in Table I. Neutral channels, whose end result is a neutron plus one or more photons, are produced. In this regard, the CB program complements the studies at the Jefferson Laboratory and elsewhere, at which charged channels are studied.

Table I. Decay Channels.

$\pi^- p$	$\to$	$\gamma\, n$
		$\pi^0\, n$
		$\pi^0\, \pi^0\, n$
		$\eta\, n$
$K^- p$	$\to$	$\pi^0\, \Lambda$
		$\pi^0\, \pi^0\, \Lambda$
		$\eta\, \Lambda$
		$\pi^0\, \Sigma^0$
		$\pi^0\, \pi^0\, \Sigma^0$
π^0	$\to$	$\gamma\, \gamma$
η	$\to$	$\gamma\, \gamma$
Λ	$\to$	$\pi^0\, n$
Σ	$\to$	$\gamma\, \Lambda$

Several results have already been published [1–5], and many more are yet to come. Some of these will be discussed below. The others are described briefly here.

- Prior to our experiments, very little information was known previously about the interaction of neutrons in our energy range with NaI(Tl). By using kinematic constraints of the two-body $\pi^- p \to \pi^0 n$ reaction, we were able to map out the response as a function of energy. Detection efficiencies reach as much as 35-40%. Special tuning of the Monte Carlo GEANT321 code was necessary to reproduce the behavior [3].

- Some data were obtained for $2\pi^0$ production from nuclear targets. Interest in this process was stimulated by results from the CHAOS group at TRIUMF for the $(\pi^+, \pi^-\pi^+)$ reaction which

[1] The Crystal Ball Collaboration consists of members from Abilene Christian University, Argonne National Laboratory, Arizona State University, University of California Los Angeles, University of Colorado, The George Washington University, Universität Karlsruhe, Kent State University, University of Maryland, Pertersburg Nuclear Physics Institute, University of Regina, Rudjer Bošković Institute, and Valparaiso University.

were interpreted that "nuclear matter strongly modifies the $\pi\pi$ interaction in the $J=I=0$ channel" [6]. Our results for an analogue $2\pi^0$ channel do not have a sharp peak near the 2π threshold as seen in the CHAOS data [2]. While there appears to be a shift of the invariant $2\pi^0$ mass distribution towards threshold with increasing nuclear mass, recent analyses suggest that it actually results from a supression of strength at high invariant mass due to increasing absorption of the $\Delta(1232)$ with higher nuclear mass.

A review of the N^* and Δ resonances [7] reveals substantial uncertainties in their listed properties. Considering the 4-star resonances alone, the masses are often specified only within 50 MeV and are sometimes uncertain by as much as 100 MeV. Similarly, the widths are typically poorly known and are often uncertain by as much as 150-200 MeV. The decay widths to particular channels are even less well known. The situation is worse for the hyperons. Some properties of Λ and Σ resonances are listed in Table II. Most of the data are quite old and typically of poor statistics.

Table II: Properties of Λ and Σ resonances.

Resonance	$2J^{\pi}$	PDG	P_{K^-} (MeV/c)	Mass (MeV)	Width (MeV)
$\Lambda(1405)$	1^-	****	——	1406±4	50±2
$\Lambda(1520)$	3^-	****	390	1520±1	16±1
$\Lambda(1600)$	1^+	***	580	1560-1700	50-250
$\Lambda(1670)$	1^-	****	740	1660-1680	25-50
$\Lambda(1690)$	3^-	****	780	1685-1695	50-70
$\Sigma(1385)$	3^+	****	——	1384±1	36±5
$\Sigma(1480)$	??	*	280	~1480	~50
$\Sigma(1560)$	??	**	490	~1560	~50
$\Sigma(1580)$	3^-	**	540	~1580	~15
$\Sigma(1620)$	1^-	**	630	~1620	20-85
$\Sigma(1660)$	1^+	***	720	1630-1690	40-200
$\Sigma(1670)$	3^-	****	740	1665-1685	40-80
$\Sigma(1690)$	??	**	780	~1690	30-150

2 K^-p reactions

Our CB program in experiment E914 is already providing new data with much improved precision for the first time in 20 years. A nice feature of the CB program is the ability to select states of pure isospin, as shown in Table III. I will describe and illustrate only a small portion of the data that we have.

Table III. K^-p selectivity.

$K^-p \to \eta\Lambda$, $K^-p \to \pi^0\Sigma^0$	Pure $I=0$	Selects Λ^*
$K^-p \to \pi^0\Lambda$	Pure $I=1$	Selects Σ^*
$K^-p \to \overline{K^0}n$	Mixed $I=0$, 1	

2.1 $K^-p \to \eta\Lambda$

Eta mesons are cleanly identified in the CB through their $\gamma\gamma$ and other decay channels. The total and differential cross sections for the $K^-p \to \eta\Lambda$ reaction near threshold are dominated by formation of the $\Lambda(1670)\frac{1}{2}^-$ resonance. There are many similarities between this reaction and the $\pi^-p \to \eta n$ reaction near threshold, which is dominated by the $N(1535)\frac{1}{2}^-$ resonance. These include a steep rise in the total cross section with similar values of the dependence on η momentum, peaking slightly above the threshold (see Fig. 1). The angular distributions are consistent with S-wave dominance, but with a small D-wave contribution that provides a slight bowl shape. The data support the view that the $N(1535)$ and $\Lambda(1670)$ states belong to the same SU(3) octet. A full paper on this reaction has been published [5]. A description of a unitary, multichannel analysis for data in the region of the $\Lambda(1670)$ state is given elsewhere in these proceedings [8].

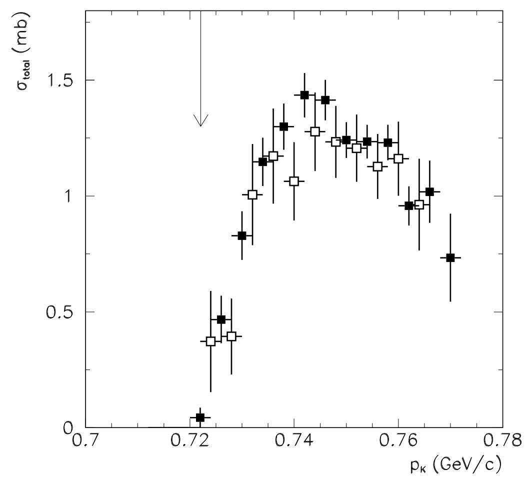

Figure 1: Total cross sections for the $K^-p \to \eta\Lambda$ reaction. The solid (open) squares are for the $\eta \to \gamma\gamma$ $(3\pi^0)$ decay mode. The arrow marks the threshold.

2.2 Other K^-p reactions

Differential cross sections and Λ polarizations were obtained at 18 momenta for the $K^-p \to \pi^0\Lambda$, $K^-p \to \overline{K^0}n$ and $K^-p \to \pi^0\Sigma$ reactions in the momentum range between 492 and 761 MeV/c [9]. Some of the data for 640 MeV/c are shown in Fig. 2. The coefficients A_n/A_0 for expansion in Legendre polynomials

$$\frac{d\sigma}{d\Omega} = \lambda^2 \sum_{n=0}^{n_{\max}} A_n P_n(\cos\theta) \tag{1}$$

were also obtained. Terms through $n = 3$ are needed, while the $n = 4$ terms are typically consistent with zero. From the polarization $P(\theta)$ data, the coefficients B_n/B_0 of the expansion

$$P(\theta) \cdot \frac{d\sigma}{d\Omega} = \lambda^2 \sum_{n=0}^{n_{\max}} B_n P_n^1(\cos\theta) \;, \tag{2}$$

where P_n^1 are the associated Legendre polynomials, could also be obtained. They are typically small, although the B_2/B_0 coefficients tend to become slightly negative at the higher momenta.

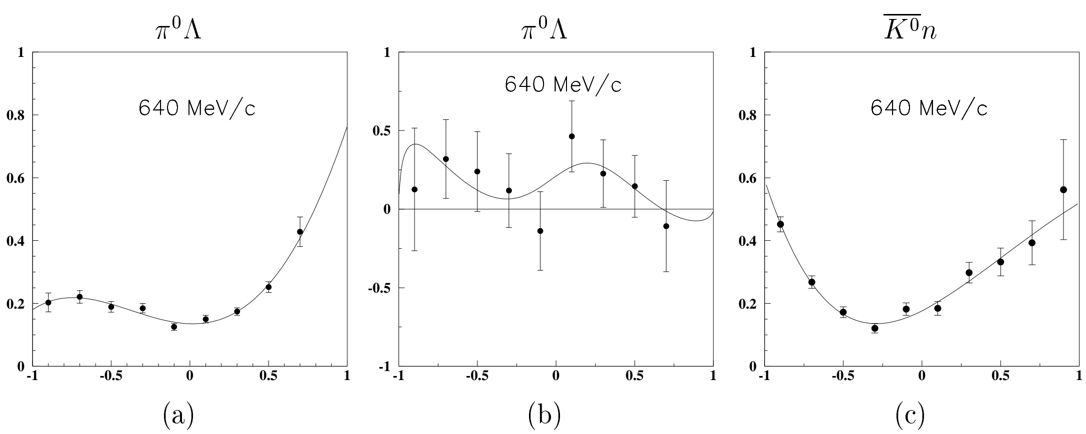

Figure 2: Cross sections (mb/sr) or polarizations for $K^-p \to \pi^0\Lambda$ reaction (left two figures), and $K^-p \to \overline{K^0}n$ reaction (right figure). The curves were obtained from fits with Eqs. (1) and (2).

As noted in Table II, the existence of the $\Sigma(1580)$ resonance is doubtful. Because quark models are unable to produce such a state at low energies, confirmation of the resonance would be a major challenge to them. The results of our analysis suggest that the $\Sigma(1580)$ is probably not needed. A full partial-wave analysis, including the new CB data, will be done to examine this issue in more detail.

3 Double π^0 production

Considerable attention has been given to a study of the $\pi^- p \to \pi^0\pi^0 n$ reaction. We are interested in the mechanism for $2\pi^0$ production as well as resonance structures in the $\pi^0\pi^0$ and $\pi^0 n$ invariant masses. An important question is the degree to which the two π^0's are formed as a correlated pair (*e.g.*, the elusive and controversial $f_0(400-1200)$ or "σ" particle), as distinguished from sequential π^0 decay through intermediate resonances (*e.g.*, $N^* \to \Delta(1232)\pi^0 \to n\pi^0\pi^0$). If formed by the (virtual) process $\pi_v^+\pi^- \to \pi^0\pi^0$, one can obtain important information on the isoscalar $\pi\pi$ scattering length a_0^0. A clearly evident resonance structure would give strong support to the existence of the σ particle. Recent photo-production data have provided evidence for a strong sequential process from the $D_{13}(1520)$ resonance through the $\Delta(1232)$ [10,11]. On the other hand, a broad peak with the characteristics of a σ particle has been reported from the $\pi^- p \to \pi^0\pi^0 n$ reaction at 9 GeV [12].

Data were obtained for 19 beam momenta in the range 0.30–0.75 GeV/c. This study is the most thorough ever of $2\pi^0$ production in $\pi^- p$ interactions. The Dalitz plots (at least above 0.350 GeV/c) do not have phase-space distributions, but rather show strong enhancements of the yields at high $2\pi^0$ invariant mass, typically also with a small peak at low invariant mass. See Fig. 3. In the $\pi^0 n$ projection, the enhancements are also near the mass of the $\Delta(1232)$.

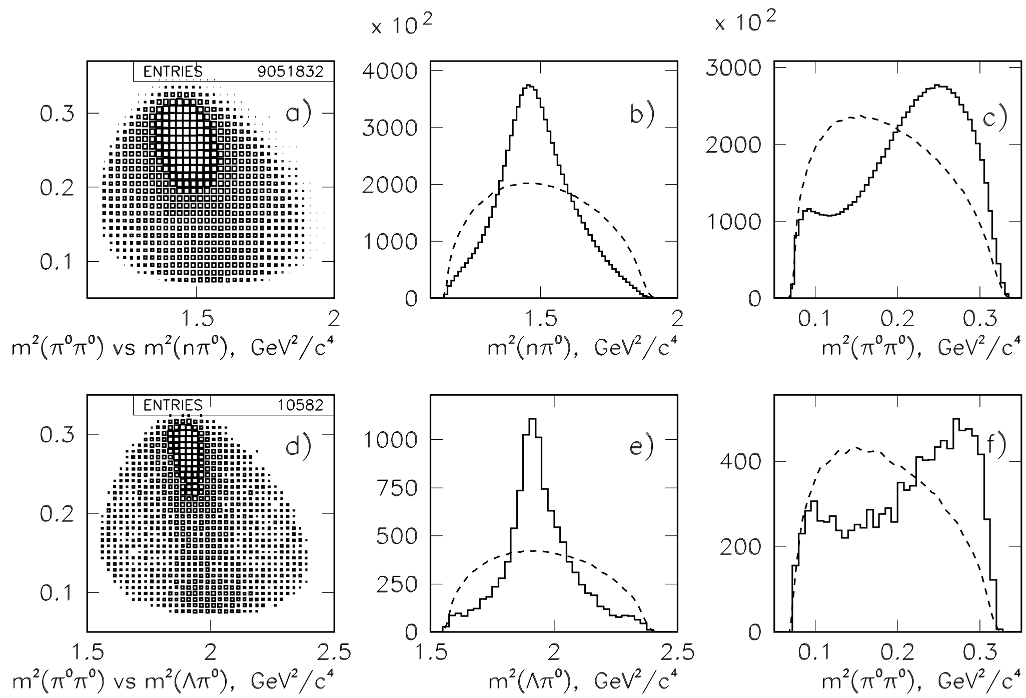

Figure 3: Dalitz plot and projections for the $\pi^- p \to \pi^0\pi^0 n$ reaction at 720 MeV/c (upper row), and the $K^- p \to \pi^0\pi^0\Lambda$ reaction at 750 MeV/c (lower row). The phase-space distributions (dashed lines) are shown on the projections.

The enhancement at high $m^2(\pi^0\pi^0)$ is in the region expected for the σ meson, which is cut off by our kinematics. On the other hand, the enhancement in $m^2(\pi^0 n)$ is near the location of the $\Delta(1232)$

(more accurately, the maximum of the $\pi^- p$ total cross section). One of the signatures for the σ is that the decay into two π^0's must be isotropic in its rest frame. As shown in the upper half of Fig. 4, neither the θ nor the ϕ distribution, in the Gottfried-Jackson (G-J) frame, is isotropic. (The ϕ angle here is also known as the Treiman-Yang angle [14].) We can also examine the hypothesis that the σ is formed via one-pion exchange (OPE). In that case, the four-momentum transfer is expected to peak near $-t \sim 1 \cdot m_\pi^2$ [13,14]. We find in the lower part of Fig. 4 that $-t$ actually peaks near 0.32 $(\mathrm{GeV}/c)^2$, or about $20 m_\pi^2$. The implications are that OPE contributes very weakly to these data, and that there is very little if any production of the σ.

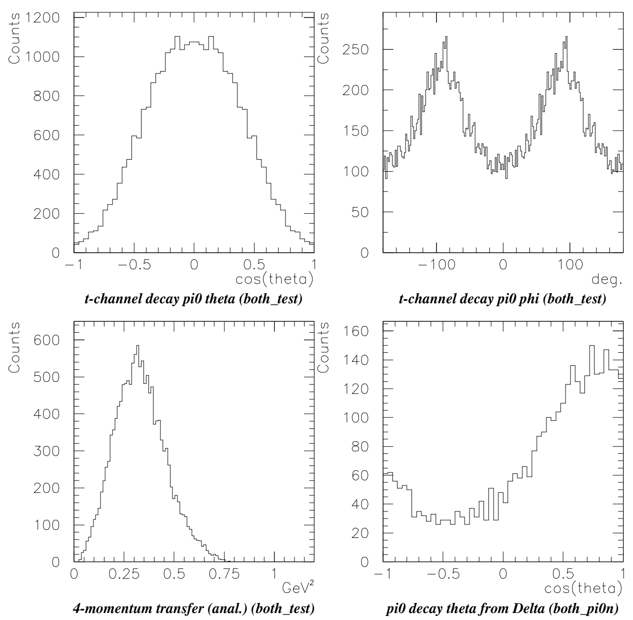

Figure 4: Distributions of double-π^0 production and decay. $\cos\theta$ (upper left) and ϕ (upper right) distributions in the double π^0 rest frame; t distribution of double-π^0 production (lower left); θ distribution of π^0 from a Δ^0.

The Dalitz plots and the projections show a very stable and consistent pattern as a function of energy. For momenta below about 650 MeV/c, the peak of the $m^2(\pi^0 n)$ distributions shifts to lower values, moving down to about 1.2 $(\mathrm{GeV}/c)^2$. For the $m^2(\pi^0\pi^0)$ distributions, the small peak at low m^2 vanishs below about 0.55 $(\mathrm{GeV}/c)^2$. We understand these behaviors as resulting from kinematics: as the incident momentum decreases, there is less energy for decays through the upper side of the Δ resonance. The data are thus consistent with the sequential π^0 decay of a nucleon resonance through the $\Delta(1232)$ over the entire momentum range of this experiment. The main resonances in this region are the $N(1440)\frac{1}{2}^+$ and $N(1520)\frac{3}{2}^-$, and so this reaction will help to map out the Roper.

The data were also examined for the reaction $\pi^- p \to \Delta\pi^0$, followed by π^0 decay of the Δ (which is not kinematically distinguishable from the sequential decay of a resonance). Events were selected by requiring that one π^0 and a neutron have an invariant mass within ± 60 MeV of the $\Delta(1232)$, while that for the other combination was more than 60 MeV away. The θ distribution of the π^0 decay of the Δ, which is the angular correlation of the two π^0's from the reaction, is shown in the last portion of Fig. 4. A Monte Carlo simulation of the sequential process, with an empirically determined angular correlation very similar to that in Fig. 4, produced a Dalitz plot almost indistinguishable from that shown in Fig. 3. Analysis of data for the $K^- p \to \pi^0\pi^0\Lambda$ reaction reveals very similar patterns to those of the $\pi^- p$ reaction, as shown in the lower part of Fig. 3. In this case, the decay $\Lambda^* \to \Sigma(1385)\pi^0 \to \Lambda(1116)\pi^0\pi^0$ is flavor symmetric with the N^* decay process. The $\Lambda(1600)\frac{1}{2}^+$ then has a role analogous to that of the $N(1440)\frac{1}{2}^+$. It appears that σ production from baryon resonances is quite small.

4 Decays of the η meson

The decays of the η meson are especially interesting because they allow us to explore the limits of basic symmetries such as C and CP invariance, as well as tests of chiral-perturbation (χPT) expansions and other models. I shall briefly describe some results, where full details are in recent publications [1,4]. Analyses of several other decay modes, including $\eta \to \pi^0\gamma\gamma$, $3\pi^0\gamma$, and 3γ, are nearing completion.

- The first determination was made of the upper limit for the branching ratio of the CP-forbidden decay $\eta \to 4\pi^0$. At the 90% confidence level, we obtained $\mathcal{B} \leq 6.9 \times 10^{-7}$. After making some theoretical adjustments for the very small available phase space, we estimate that this value provides about a 2% limit on CP violation in quark-family-conserving interactions.

- A precision determination was made for the quadratic slope parameter for the $\eta \to 3\pi^0$ decay. Calculations in Chiral Perturbation Theory to order $\mathcal{O}(p^2)$ and $\mathcal{O}(p^4)$, which contain terms proportional to $m_u - m_d$, give values for the decay width $\Gamma(\eta \to \pi^+\pi^-\pi^0)$ that are significantly below the experimental value. A quadratic dependence arises at $\mathcal{O}(p^6)$. Parameterizing the decay amplitude as $|A|^2 \sim 1 + 2\alpha z$, where z is a measure of the distance from the center of the $3\pi^0$ Dalitz plot, we find $\alpha = -0.031 \pm 0.004$. This value is about 2–5 times theoretical estimates [15] and provides a challenge to all the theoretical descriptions.

5 Summary and outlook

The Crystal Ball program is providing a wealth of high-quality data on a variety of topics in baryon spectroscopy and meson decays. We find strong evidence for flavor symmetry in the threshold behavior of $\pi^- p \to \eta n$ and $K^- p \to \eta\Lambda$ reactions, as well as in $2\pi^0$ production reactions. Production of a σ meson is very small. Data for the decays of the η meson are providing strong constraints on the understanding of basic symmetries, and tests of χPT expansions.

The CB Collaboration is preparing for several new experiments at BNL. These include: (1) extended studies of hyperon resonances through $K^- p$ reactions; (2) precision measurements of the $\pi^- p \to \pi^0 n$ reaction at low energies, to explore issues in isospin symmetry and possibly to get new constraints on the $m_u - m_d$ quark mass difference; and (3) a precision determination of the $K^+ \to \pi^0 e^+ \nu$ (K_{e3}) decay rate to obtain an improved value of the CKM matrix element V_{us}, for a test of CKM unitarity.

Acknowledgments: This work has been supported in part by the U.S. Department of Energy, the National Science Foundation, the Natural Sciences and Engineering Research Council of Canada, and the Russian Ministry of Science and Technology.

References

[1] S. Prakhov *et al.*, Phys. Rev. Lett. **84**, 4802 (2000).
[2] A. Starostin *et al.*, Phys. Rev. Lett. **85**, 5539 (2000).
[3] T.D.S. Stanislaus *et al.*, Nucl. Instrum. Methods A **462**, 463 (2001).
[4] W. B. Tippens *et al.*, Phys. Rev. Lett. **87**, 192001 (2001).
[5] A. Starostin *et al.*, Phys. Rev. C **64**, 055205 (2001).
[6] F. Bonutti *et al.*, Phys. Rev. Lett. **77**, 603 (1996); Phys. Rev. C **60**, 018201 (1999).
[7] Particle Data Group, Eur. Phys. J. C **15**, 1 (2000).
[8] D. M. Manley, these proceedings.
[9] J. Olmsted, Ph.D. dissertation, Kent State University (2001).
[10] F. Härter *et al.*, Phys. Lett. B **401**, 229 (1997).
[11] M. Wolf *et al.*, Eur. Phys. J A **9**, 5 (2000).
[12] K. Takamatsu, Nucl. Phys. A **675**, 312C (2000).
[13] B. R. Martin, D. Morgan, and G. Shaw, *Pion-Pion Interactions in Particle Physics*, (Academic, New York, 1976).
[14] S. B. Treiman and C. N. Yang, Phys. Rev. Lett. **8**, 140 (1962).
[15] J. Kambor, C. Wiesendanger, and D. Wyler, Nucl. Phys. **B465**, 215 (1996).

Chiral dynamics in the low-lying excited $S = -1$ baryons

E. Oset[a], A. Ramos[b], and C. Bennhold[c]

[a]Departamento de Física Teórica and IFIC, Centro Mixto Universidad de Valencia-CSIC, Institutos de Investigación de Paterna, Aptd. 22085, 46071 Valencia, Spain
[b]Departament d'Estructura i Constituents de la Matèria, Universitat de Barcelona, Diagonal 647, 08028 Barcelona, Spain
[c]Center for Nuclear Studies, Department of Physics, The George Washington University, Washington, DC 20052, U.S.A.

(Received: 9 November 2001)

The K^-N interaction is described using a multichannel Bethe-Salpeter equation with the lowest-order chiral Lagrangian and dimensional regularization for the loop function. Besides the well-known $\Lambda(1405)$ singlet, the method dynamically generates the s-wave octet states $\Lambda(1670)$ and the $\Sigma(1620)$. The size of the couplings allow classifying the $\Lambda(1405)$ and $\Lambda(1670)$ as quasibound $\bar{K}N$ and $K\Xi$ states, respectively.

1 Introduction

Low energy K^-N scattering and the coupling to inelastic channels demonstrates an example for a successful application of chiral dynamics in the baryon sector [1]. The studies of ref. [2] showed that an excellent description of the low-energy data can be obtained by starting from chiral Lagrangians and using a multichannel Lippman-Schwinger equation to account for multiple scattering and unitarity. By including all open channels above threshold and fitting a few chiral parameters of the second-order Lagrangian ref. [2] obtained good agreement with low-energy data. Expanding on this work, ref. [3] demonstrated that, by using the Bethe-Salpeter equation (BSE) with *all* coupled channels (above and below threshold) from the octet of pseudoscalar Goldstone bosons and ground-state baryons along with one cut-off to regularize the intermediate meson-baryon loops, the lowest-order chiral Lagrangian is sufficient to achieve a good description of all low-energy data. Further analysis came in in ref. [4] by regularizing the loop function using dimensional regularization, rather than a cut-off, and by introducing the N/D method and dispersion relations, which leads formally to the same algebraic equations found in [3].

One of the common findings shared by all the theoretical approaches is the dynamical generation of the $\Lambda(1405)$ resonance which appears with the proper width at the correct position, with the choice of a cut-off of natural size. This natural generation from the interaction of the meson-baryon system with the lowest-order Lagrangian allows us to identify that state as a quasibound meson-baryon state. This would explain why constituent quark models have had so many problems explaining this resonance [6].

In ordinary quark models the $\Lambda(1405)$ resonance would mostly be a SU(3) singlet of $J^P = 1/2^-$ and there would be an associated octet of s-wave excited $J^P = 1/2^-$ baryons that would include the N*(1535), the $\Lambda(1670)$, the $\Sigma(1620)$ and a Ξ^* state. In the chiral approach one would also expect the appearance of such a nonet of resonances. In fact, it appears naturally in the approach of ref. [3], with a degenerate octet, when setting all the masses of the octet of stable baryons equal on one side and the masses of the octet of pseudoscalar mesons equal on the other side. Yet, to obtain this result it is essential that the coupled-channels approach not omit any of the channels that can be constructed from the octet of pseudoscalar mesons and ground-state baryons. Here we extend the approach of ref. [3] to higher energies, using the methods developed in ref. [4].

2 Formalism and results

The lowest-order Lagrangian involving the octet of pseudoscalar mesons and the $1/2^+$ baryons is given in [7] and one has

$$L_1^{(B)} = \langle \bar{B} i\gamma^\mu \nabla_\mu B\rangle - M_B \langle \bar{B}B\rangle + \tfrac{1}{2} D \langle \bar{B}\gamma^\mu \gamma_5 \{u_\mu, B\}\rangle + \tfrac{1}{2} F \langle \bar{B}\gamma^\mu \gamma_5 [u_\mu, B]\rangle \ , \tag{1}$$

where the symbol $\langle\ \rangle$ denotes the trace of SU(3) matrices. The covariant derivative, u_μ and the matrices B and Φ involving the baryon and meson fields are defined in [3].

We include the $K^- p$ state and all channels that couple to it within chiral SU(3). These states are $\bar{K}^0 n$, $\pi^0\Lambda$, $\pi^0\Sigma^0$, $\pi^+\Sigma^-$, $\pi^-\Sigma^+$, $\eta\Lambda$, $\eta\Sigma^0$, $K^0\Xi^0$, $K^+\Xi^-$, leading to coupled-channels problem with ten final states.

The lowest-order amplitudes for these channels are easily evaluated from Eq. (1) and are given by

$$V_{ij} = -C_{ij} \frac{1}{4f^2} \bar{u}(p_i)\gamma^\mu u(p_j)(k_{j\mu} + k_{i\mu}) \ , \tag{2}$$

where $p_j, p_i (k_j, k_i)$ are the initial, final momenta of the baryons (mesons) and the matrix C_{ij}, which is symmetric, is given in [3].

In the present work the amplitudes are studied using the isospin formalism for which one must use average masses for the K (K^0, K^+), $\bar{K}$ $(K^-, \bar{K}^0)$, N (p, n), π (π^+, π^0, π^-), Σ $(\Sigma^+, \Sigma^0, \Sigma^-)$ and Ξ (Ξ^-, Ξ^0) states, where again the isospin states are given in [3].

We have four $I = 0$ channels, $\bar{K}N, \pi\Sigma$, $\eta\Lambda$ and $K\Xi$, while there are five $I = 1$ channels, $\bar{K}N, \pi\Sigma, \pi\Lambda, \eta\Sigma$ and $K\Xi$. The transition matrix elements in isospin formalism read like Eq. (2) substituting the C_{ij} coefficients by D_{ij} for $I = 0$ and by F_{ij} for $I = 1$, with the D_{ij} and F_{ij} coefficients given in [3].

In [4], using the N/D method of [5] for this particular case it was proved that, since the potential factorized with its on-shell value in the loop functions, the scattering amplitude could be written by means of the algebraic matrix equation

$$T = [1 - V\,G]^{-1}\,V \ , \tag{3}$$

with V the matrix of Eq. (2) evaluated on shell, with G a diagonal matrix involving the loop function of a meson and a baryon propagators which depends on $p^0 + k^0 = \sqrt{s}$.

One can see that Eq. (3), multiplying both members by $[1 - V\,G]$, is just the Bethe Salpeter equation but with the V matrix factorized on shell.

The analytical expression for G_l can be obtained from [4] using dimensional regularization,

$$\begin{aligned} G_l &= i2M_l \int \frac{d^4q}{(2\pi)^4} \frac{1}{(P-q)^2 - M_l^2 + i\epsilon} \frac{1}{q^2 - m_l^2 + i\epsilon} \\ &= \frac{2M_l}{16\pi^2} \Big\{ a_l(\mu) + \ln \frac{M_l^2}{\mu^2} + \frac{m_l^2 - M_l^2 + s}{2s} \ln \frac{m_l^2}{M_l^2} \\ &\quad + \frac{\bar{q}_l}{\sqrt{s}} \Big[\ln\big(s - (M_l^2 - m_l^2) + 2\bar{q}_l\sqrt{s}\big) + \ln\big(s + (M_l^2 - m_l^2) + 2\bar{q}_l\sqrt{s}\big) \\ &\quad - \ln\big(-s + (M_l^2 - m_l^2) + 2\bar{q}_l\sqrt{s}\big) - \ln\big(-s - (M_l^2 - m_l^2) + 2\bar{q}_l\sqrt{s}\big) \Big] \Big\} \ , \end{aligned} \tag{4}$$

which has been rewritten in a convenient way to show how the imaginary part of G_l is generated and how one can go to the unphysical Riemann sheets in order to identify the poles.

A coupled set of Eqs. (3) were solved in [3], using a cut off in the momentum of the loop integrals of 630 MeV. Changes in the cut off can be accommodated here in terms of changes in μ, the regularization scale in the dimensional regularization formula for G_l, or in the subtraction constant a_i. In order to obtain the same results as in [3] at low energies, we set μ equal to the cut off momentum of 630 MeV and then find the values of the subtraction constants such as to have G_l with the same value with the dimensional regularization formula and the cut off formula at the $\bar{K}N$ threshold. This determines the values

$$\begin{array}{lll} a_{\bar{K}N} = -1.84 \ , & a_{\pi\Sigma} = -2.00 \ , & a_{\pi\Lambda} = -1.83 \ , \\ a_{\eta\Lambda} = -2.25 \ , & a_{\eta\Sigma} = -2.38 \ , & a_{K\Xi} = -2.52 \ . \end{array} \tag{5}$$

This method guarantees that we reproduce the results of [3] at low energies. Then we extend the results to higher energies, searching for the possible appearance of new resonances.

In [8] we show the results for the real and imaginary parts of the $I = 0$ amplitudes for $\bar{K}N \to \bar{K}N$ and $\bar{K}N \to \pi\Sigma$, respectively. Both channels clearly display the signal from the $\Lambda(1670)$ resonance, although large background contributions are present in the amplitudes as well. To compare with experiment, [9], the speed plot method [10] is used and we find a qualitative agreement with the data. Here instead we show the results of a different analysis where the amplitudes are investigated in the second Riemann sheet searching for complex poles and the couplings of the resonance to the different decay channels.

In [8] we also studied the $I = 1$ channel and we find only rough agreement with the data in the $\bar{K}N \to \bar{K}N$ and $\bar{K}N \to \pi\Sigma$ amplitudes, but, just like the data, we find no evidence of a resonance signal that would allow us to identify the $\Sigma(1620)$ resonance. However, the absence of such a resonance would be somewhat surprising since we expect to get an octet of meson-baryon resonances and so far only a singlet and the $I = 0$ part of the octet (eventually mixed between themselves) have appeared. Since we do not see this state in the amplitudes at real energies we look for a pole in the complex plane. We go directly to the second Riemann sheet, which we take in our case as the one where the momenta of the channels which are open at energy W, with $\mathrm{Re}(z) = W$, are taken negative in G_l.

Near the poles the amplitudes that we are analyzing behave as

$$T_{ij} \simeq \frac{g_i g_j}{z - z_R} \ . \tag{6}$$

Thus, the residues of the T_{ij} matrix give the product of the coupling of the resonance to the i, j channels.

In the $I = 0$ amplitudes, and with $a_{K\Xi} = -2.52$ from Eq. (5), the search for poles leads us to the values $M_R = 1708 + i21$ MeV, $\Gamma = 42$ MeV, $B_{\bar{K}N} = 47\%$, $B_{\eta\Lambda} = 47\%$, and $B_{\pi\Sigma} = 6\%$, in remarkable agreement with the values obtained from the speed plot. By slightly changing the value of $a_{K\Xi}$ we can shift the pole position without affecting the agreement found at low energies. For $a_{K\Xi} = -2.67$, we obtain $M_R = 1680 + i20$ MeV, $\Gamma = 40$ MeV, $B_{\bar{K}N} = 54\%$, $B_{\eta\Lambda} = 38\%$, and $B_{\pi\Sigma} = 8\%$.

Consequently, the couplings obtained for the $\Lambda(1670)$ resonance, using $a_{K\Xi} = -2.67$, are

$$| g_{\bar{K}N} | = 0.61 \ , \qquad | g_{\pi\Sigma} | = 0.073 \ , \qquad | g_{\eta\Lambda} | = 1.1 \ , \qquad | g_{K\Xi} | = 12 \ . \tag{7}$$

Searching the complex plane for the $\Lambda(1405)$ resonance, we find

$$M_R = (1426 + i16) \text{ MeV} \qquad (\Gamma = 32 \text{ MeV}) \ ,$$

$$| g_{\bar{K}N} | = 7.4 \ , \qquad | g_{\pi\Sigma} | = 2.3 \ , \qquad | g_{\eta\Lambda} | = 2.0 \ , \qquad | g_{K\Xi} | = 0.12 \ ,$$

with only the $\pi\Sigma$ channel open for the decay.

We have also performed a search in the $I = 1$ channel and we indeed find a pole at

$$M_R = (1579 + i264)\ \text{MeV} \qquad (\Gamma \sim 528\ \text{MeV})\ ,$$

from the model with $a_{K\Xi} = -2.67$. The couplings obtained are

$$\mid g_{\bar{K}N} \mid = 2.6\ , \qquad \mid g_{\pi\Sigma} \mid = 7.2\ , \qquad \mid g_{\pi\Lambda} \mid = 4.2\ , \qquad \mid g_{\eta\Sigma} \mid = 3.5\ , \qquad \mid g_{K\Xi} \mid = 12\ .$$

The analysis of the above couplings reveals the nature of these resonances. In the case of the $\Lambda(1405)$ state the coupling to the $\bar{K}N$ channel is found to be very large, while the coupling to the other channels is small. This allows us to identify this resonance as a quasibound $\bar{K}N$ state in the present approach. Similarly, we find that the $\Lambda(1670)$ resonance has a large coupling to the $K\Xi$ channel and unusually small couplings to the other final states. This is the reason for the small width of the resonance in spite of the large phase space available for decay into the different channels. The large coupling to the $K\Xi$ channel allows identifying this state as a $K\Xi$ quasibound state. By contrast, the $\Sigma(1620)$ resonance has couplings of standard size to all channels, and, given the large phase space available, it has a sizeable decay width into all of the above channels and hence a considerably larger total width.

In summary, we have demonstrated that the chiral approach to $\bar{k}n$ and the other coupled channels, which proved so successful at low energies, extrapolates smoothly to higher energies and provides the basic features of the scattering amplitudes, generating the resonances which would complete the states of the nonet of the $j^p = 1/2^-$ excited states. the qualitative description of the data without adjusting any parameters is telling us that the basic information on the dynamics of these processes is contained in the chiral lagrangians. the analysis of the poles and the couplings of the resonances to the different channels lead us to identify the strong coupling of the $\lambda(1405)$ resonance to the $\bar{k}n$ state and the large coupling of the $\lambda(1670)$ resonance to the $k\xi$ state, allowing us to classify these resonances as quasibound $\bar{k}n$ and $k\xi$ states, respectively.

Acknowledgments: This work is also partly supported by DGICYT contract numbers BFM2000-1326, PB98-1247, by the EU TMR network Eurodaphne, contract no. ERBFMRX-CT98-0169, and by the US-DOE grant DE-FG02-95ER-40907.

References

[1] J. Gasser and H. Leutwyler, Nucl. Phys. **B250** (1985) 465.

[2] N. Kaiser, P. B. Siegel and W. Weise, Nucl. Phys. **A594** (1995) 325; N. Kaiser, T. Waas and W. Weise, Nucl. Phys. **A612** (1997) 297.

[3] E. Oset and A. Ramos, Nucl. Phys. **A635** (1998) 99.

[4] J.A. Oller and U.G. Meissner, Phys. Lett. **B500** (2001) 263.

[5] J.A. Oller and E. Oset, Phys. Rev. **D60** (1999) 074023.

[6] N. Isgur and G. Karl, Phys. Rev. **D18** (1978) 4187; *ibid.* **D20** (1979) 1191; S. Capstick and W. Roberts, Phys. Rev. **D49** (1994) 4570.

[7] A. Pich, Rep. Prog. Phys. **58** (1995) 563.

[8] E. Oset, A. Ramos and C. Bennhold, nucl-th/0109006.

[9] G. P. Gopal *et al.* Nucl. Phys. **B119** (1977) 362.

[10] G. Höhler, πN-Newsletter **9** (1993) 1.

Recent progress in pion photo- and electroproduction analysis

L. Tiator[a], D. Drechsel[a], S. Kamalov[b] and S. N. Yang[c]

[a]*Institut für Kernphysik, Universität Mainz, 55099 Mainz, Germany*
[b]*Laboratory of Theoretical Physics, JINR, 141980 Dubna, Russia*
[c]*Department of Physics, National Taiwan University, Taipei, Taiwan*

(Received: 31 October 2001)

Pion photo- and electroproduction has been studied at threshold and in the resonance region below $W < 2$ GeV. At threshold π^0 production can be very well explained within a dynamical model derived from an effective chiral Lagrangian. The final state interaction is nearly saturated by single charge exchange rescattering. In the resonance region new electroproduction data at $Q^2 = 1$ GeV^2 has been analyzed with $MAID$ and longitudinal and transverse photon helicity amplitudes have been determined for different resonances. A detailed study of the E/M and S/M ratios of the $N \to \Delta$ transition shows a zero crossing of R_{EM} near $Q^2 = 4$ GeV^2, whereas the R_{SM} becomes increasingly negative at large Q^2.

1 Introduction

The unitary isobar model $MAID$ is a model for single pion photo- and electroproduction off protons and neutrons [1]. It is based on a non-resonant background described by Born terms and vector meson exchange contributions and nucleon resonance excitations modeled by Breit-Wigner functions

$$t_{\gamma\pi}^{\alpha} = t_{\gamma\pi}^{B,\alpha} + t_{\gamma\pi}^{R,\alpha} \ . \tag{1}$$

Both parts, background and resonance are separately unitarized. This has been achieved by a K-matrix unitarization in the case of the background

$$t_{\gamma\pi}^{B,\alpha}(MAID) = \exp{(i\delta_\alpha)}\, \cos\delta_\alpha v_{\gamma\pi}^{B,\alpha}(W,Q^2) \ , \tag{2}$$

and by introducing a unitary phase ϕ_R for the resonance excitations

$$t_{\gamma\pi}^{R,\alpha}(W,Q^2) \ = \ \bar{\mathcal{A}}_{\alpha}^{R}(Q^2)\, \frac{f_{\gamma R}(W)\Gamma_R\, M_R\, f_{\pi R}(W)}{M_R^2 - W^2 - iM_R\Gamma_R}\, e^{i\phi_R} \ . \tag{3}$$

The phases δ_α are the elastic pion-nucleon scattering phases in a particular channel $\alpha = \{l, j, t\}$ below the inelastic threshold of two-pion production. In order to take account of inelastic effects, the factor $\exp{(i\delta_\alpha)}\cos\delta_\alpha$ is replaced by $\frac{1}{2}[\eta_\alpha \exp{(2i\delta_\alpha)} + 1]$ with the inelasticity parameters η_α at higher energies. Additional background terms are included to account for S- and P-wave pion loop effects.

In the case of the Dynamical Model (DMT) [2], the background contribution is given by

$$t_{\gamma\pi}^{B,\alpha}(DMT) = e^{i\delta_\alpha}\cos\delta_\alpha \left[v_{\gamma\pi}^{B,\alpha} + P\int_0^\infty dq' \frac{q'^2\, R_{\pi N}^{(\alpha)}(q,q')\, v_{\gamma\pi}^{B,\alpha}(q')}{W - E_{\pi N}(q')} \right] \ , \tag{4}$$

with the full πN scattering reaction matrix $R_{\pi N}^{(\alpha)}$. In this case the pion loop effects that are especially important near threshold are generated dynamically and show up as a principal value integral over the reaction matrix.

Presently, we have included 8 nucleon resonances, 3 Deltas: $P_{33}(1232)$, $S_{31}(1620)$ and $D_{33}(1700)$ and 5 N^*s: $P_{11}(1440)$, $D_{13}(1520)$, $S_{11}(1535)$, $S_{11}(1650)$ and $F_{15}(1680)$. All of them are included with longitudinal and transverse electromagnetic couplings. The corresponding helicity amplitudes $A_{1/2}$, $A_{3/2}$ and $S_{1/2}$ can be fitted to experimental data and can be freely changed in the $MAID$ program.

We will show results obtained with the Dynamical Model for the threshold region and present some recent fits to newer electroproduction data with $MAID$ for the resonance region with a discussion of the Q^2 evolution of the E/M and S/M ratios of the $N \to \Delta(1232)$ transition.

2 Results in the threshold region

For π^0 photoproduction, we first calculate the multipole E_{0+} near threshold by solving the coupled channels equation within a basis with physical pion and nucleon masses. The coupled channels equation leads to the following expression for the pion photoproduction t-matrix in the $\pi^0 p$ channel:

$$\begin{aligned} t_{\gamma\pi^0}(W) \;&=\; v_{\gamma\pi^0}(W) + v_{\gamma\pi^0}(W)\, g_{\pi^0 p}(W)\, t_{\pi^0 p\to\pi^0 p}(W) \\ &\qquad + v_{\gamma\pi^+}(W)\, g_{\pi^+ n}(W)\, t_{\pi^+ n\to\pi^0 p}(W)\ , \end{aligned} \tag{5}$$

where $t_{\pi^0 p\to\pi^0 p}$ and $t_{\pi^+ n\to\pi^0 p}$ are the πN t-matrices in the elastic and charge exchange channels, respectively. They are obtained by solving the coupled channels equation for πN scattering using the meson-exchange model of Ref. [3]. Our results for $Re\, E_{0+}$ show that practically all of the final state interaction effects originate from the $\pi^+ n$ channel and mainly stems from the principal value integral of Eq. (5). In this approach the $t_{\pi N}$ matrix contains the effect of πN rescattering to all orders. However, we have indeed found that only the first order rescattering contribution, i.e. the one-loop diagram, is important. This indicates that the one-loop calculation in ChPT is a reliable approximation for π^0 production in the threshold region.

If the FSI effects are evaluated with the assumption of isospin symmetry (IS), i.e., with averaged masses in the free pion-nucleon propagator, the energy dependence in $Re\, E_{0+}$ in the threshold region is very smooth. Below π^+ threshold the strong energy dependence (cusp effect) [4] only appears because of the pion mass difference and, as we have seen above, is related to the coupling with the $\pi^+ n$ channel. In most calculations, the effects from the pion mass difference below the π^+ production channel are taken into account by using the K-matrix approach [5],

$$Re\, E_{0+}^{\gamma\pi^0} = Re\, E_{0+}^{\gamma\pi^0}(IS) - a_{\pi N}\, \omega_c\, Re\, E_{0+}^{\gamma\pi^+}(IS)\sqrt{1-\frac{\omega^2}{\omega_c^2}}\ , \tag{6}$$

where ω and ω_c are the π^0 and π^+ c.m. energies corresponding to $W = E_p + \omega_\gamma$ and $m_n + m_{\pi^+}$, respectively, and $a_{\pi N} = 0.124/m_{\pi^+}$ is the pion charge exchange threshold amplitude. $E_{0+}^{\gamma\pi^{0,+}}(IS)$ is the $\pi^{0,+}$ photoproduction amplitude obtained with the assumption of isospin symmetry (IS), i.e., without the pion mass difference in Eq. (4). Such an approximation is often used in the data analysis in order to parametrize the E_{0+} multipole below $\pi^+ n$ threshold in the form of $E_{0+}(E) = a + b\sqrt{1-(\omega/\omega_c)^2}$. Numerically this approximation is very precise and differs only by 10% at the π^0 threshold and becomes indistinguishable above the π^+ threshold. In Fig. 1 the results obtained within this approximation scheme are represented by the solid curve and compared to the ChPT calculation (dash-dotted curve) [6]. Over the whole energy range the difference is rather small and within the experimental uncertainties. Huge effects, however, arise if the cusp would be neglected or obviously if the FSI effects would be totally ignored (dotted curve).

In Fig. 1 we also compare the predictions of our model for the differential cross section with recent photoproduction data from Mainz [8,9]. The dotted and solid curves are obtained without and with FSI effects, respectively. It is seen that both off-shell pion rescattering and cusp effect substantially improve the agreement with the data. This indicates that our model gives reliable predictions also for the threshold behaviour of the P-waves without any additional arbitrary parameters.

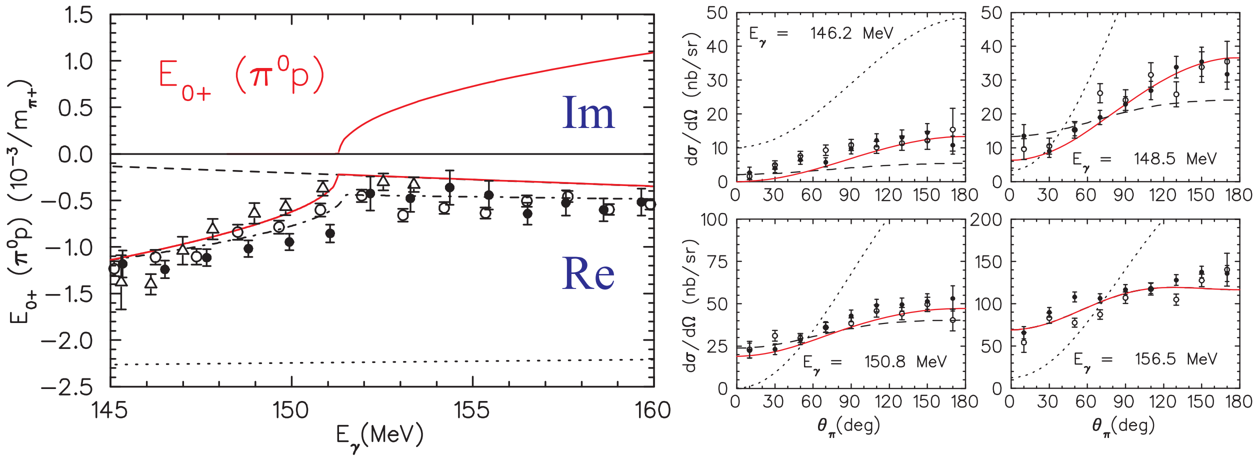

Figure 1: Real and imaginary parts of the E_{0+} multipole and differential cross sections below and above π^+ threshold for $\gamma p \to \pi^0 p$. The solid and dashed curves obtained with and without the cusp effect, respectively. The dotted curve is without FSI. The dash-dotted curve is the result of ChPT [5]. Data points for E_{0+} from Mainz [8]($\triangle$), [9]($\circ$) and Saskatoon [10]($\bullet$), and for $d\sigma$ from Mainz [8]($\bullet$), [9]($\circ$).

Pion electroproduction provides us with information on the $Q^2 = -k^2$ dependence of the transverse E_{0+} and longitudinal L_{0+} multipoles in the threshold region. The "cusp" effects in the L_{0+} multipole is taken into account in a similar way as in the case of E_{0+},

$$Re\, L_{0+}^{\gamma\pi^0} = Re\, L_{0+}^{\gamma\pi^0}(IS) - a_{\pi N}\, \omega_c\, Re\, L_{0+}^{\gamma\pi^+}(IS) \sqrt{1 - \frac{\omega^2}{\omega_c^2}}\ , \tag{7}$$

where all the multipoles are functions of total c.m. energy W and virtual photon four-momentum squared Q^2. It is known that at threshold, the Q^2 dependence is given mainly by the Born plus vector meson contributions in $v^B_{\gamma\pi}$, as described in Ref. [1]. Similar to pion photoproduction, the K-matrix approximation and full calculation agree with each other within a few percent. In Fig. 2 we show our results for the cusp and FSI effects in the E_{0+} and L_{0+} multipoles for π^0 electroproduction at $Q^2 = 0.1$ (GeV/c)^2, along with the results of the multipole analysis from NIKHEF [11] and Mainz [12]. Note that results of both groups were obtained using the P-wave predictions given by ChPT. However, there exist substantial differences between the $P-$wave predictions of ChPT and our model at finite Q^2. To understand the consequence of these differences, we have made a new analysis of the Mainz data [12] for the differential cross sections, using our DMT prediction for the P-wave multipoles instead. The S-wave multipoles extracted this way are also shown in Fig. 2 by solid circles. We see that the results of such a new analysis gives E_{0+} multipoles closer to the NIKHEF data and in better agreement with our dynamical model prediction. However, the results of our new analysis for the longitudinal L_{0+} multipoles stay practically unchanged from the values found in the previous analyses. Note that the dynamical model prediction for L_{0+} again agrees much better with the NIKHEF data. Further details are given in Ref. [13]

In contrast to DMT, in $MAID$ the FSI effects are taken into account using the K-matrix approximation, namely without the inclusion of off-shell pion rescattering contributions (principal value integral) in Eq. (4). As a result, the S-, P-, D- and F-waves of the background contributions are defined as

$$t^B_\alpha(MAID) = \exp\,(i\delta_\alpha)\,\cos\delta_\alpha\, v^B_\alpha(q_E, k)\ . \tag{8}$$

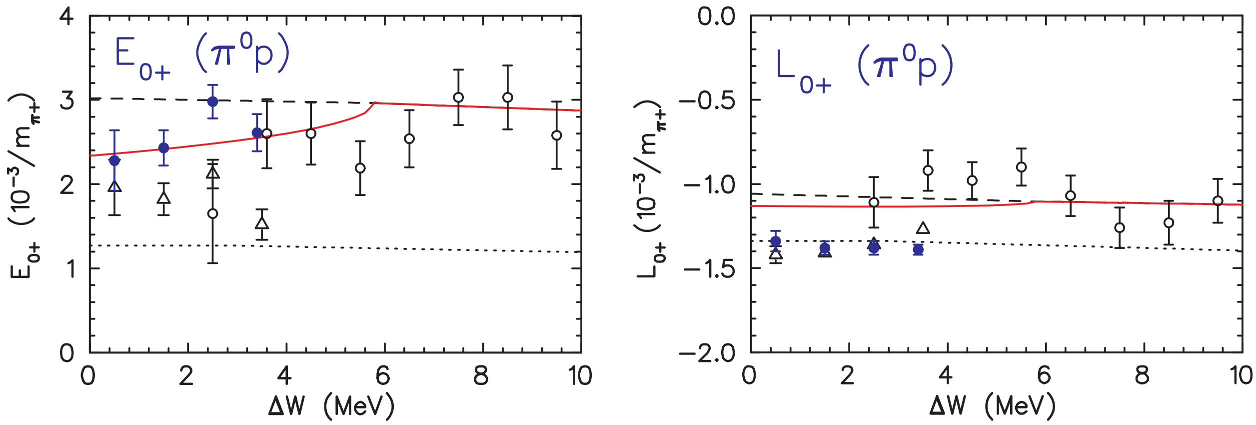

Figure 2: Real parts of E_{0+} and L_{0+} for $ep \to e'\pi^0 p$ at Q^2=0.1 (GeV/c)^2. Notations are the same as in Fig. 1. Data points from NIKHEF [11]($\circ$) and Mainz [12]($\triangle$). The results of the present work obtained by using the P-waves of our model are given by ($\bullet$).

However, as we have found above, dynamical model calculations show that pion off-shell rescattering is very important at low pion energies. The prediction of $MAID$ for $E_{0+}(\pi^0 p)$ at threshold, represented by the dotted curves in Fig. 1 lies substantially below the data. It turns out that it is possible to improve $MAID$, in the case of π^0 production at low energies, by introducing a phenomenological term and including the cusp effect of Eq. (6). In this extended version of $MAID2000$, we write the $E_{0+}(\pi^0 p)$ multipole as

$$Re\, E_{0+}^{\gamma\pi^0} = Re\, E_{0+}^{\gamma\pi^0}(MAID98) + E_{cusp}(W,Q^2) + E_{corr}(W,Q^2)\ , \tag{9}$$

where

$$E_{cusp}(W,Q^2) = -a_{\pi N}\,\omega_c\, Re\, E_{0+}^{\gamma\pi^+}(MAID98)\sqrt{1-\frac{\omega^2}{\omega_c^2}}\ . \tag{10}$$

The phenomenological term E_{corr} which emulates the pion off-shell rescattering corrections (or pion-loop contribution in ChPT) can be parameterized in the form

$$E_{corr}(W,Q^2) = \frac{A}{(1+B^2 q_\pi^2)^2}\,F_D(Q^2)\ , \tag{11}$$

where F_D is the standard nucleon dipole form factor. The parameters A and B are obtained by fitting to the low energy π^0 photoproduction data: $A = 2.01\times 10^{-3}/m_{\pi^+}$ and $B = 0.71\,fm$.

3 Results in the resonance region

For pion photoproduction in the resonance region we have recently performed a fit of $MAID$ for both the low-energy Δ region and the medium-energy resonance region up to $W = 1700$ MeV, where resonance parameters have been obtained as a part of the BRAG[1] partial wave benchmark analysis [14]. In fig. 3 we present a new fit of preliminary results on electroproduction, $p(e,e'p)\pi^0$, measured by the JLab Hall A collaboration [15]. The data has been taken at backward angles at $Q^2 = 1.0$ GeV^2 in the c.m. energy range from 0.95 GeV to 2.0 GeV. With a dataset of 363 data points in 3 observables, $d\sigma = d\sigma_T + \epsilon d\sigma_L, d\sigma_{LT}$ and $d\sigma_{TT}$ and pion angles of $146, 151$ and 167 degrees we performed a data analysis with $MAID$.

[1]Baryon Resonance Analysis Group, `http://cnr2.kent.edu/~manley/BRAG.html`

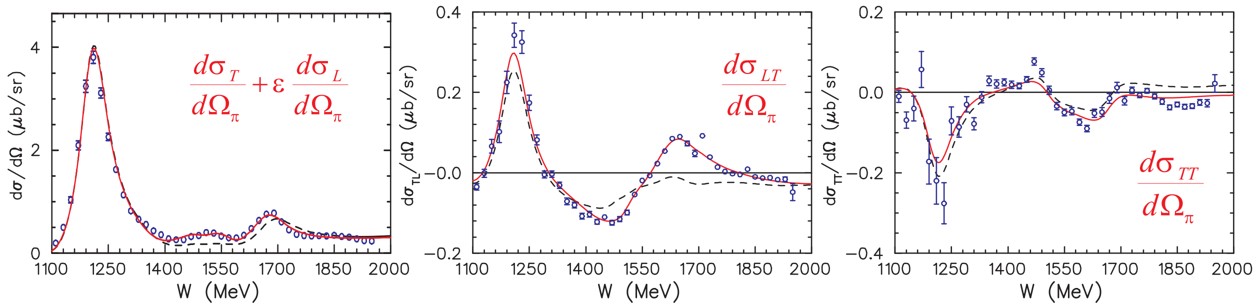

Figure 3: Preliminary experimental results from the JLab Hall A collaboration [15] at $Q^2 = 1.0$ GeV^2, $\theta_\pi = 167^0$ and $\epsilon = 0.9$ as functions of the c.m. energy W. The dashed lines show the standard $MAID2000$ calculations and the solid curves are the results of the fit to the data.

From the 20 possible resonance parameters we have varied 18 by fixing E_{2-} and S_{2-} of the $D_{13}(1520)$ because we did not find enough sensitivity in the data which are only taken at backward angles. In table 1 we give the result of our fit both for the multipole and the helicity amplitudes. The multipole amplitudes are compared to the default values of $MAID$. For the $\Delta(1232)$ resonance we give in addition the E/M and the S/M ratios. Both are consistent with the previous $MAID$ fits to photo- and electroproduction [16]. The R_{SM} ratio is very well determined by the $d\sigma_{LT}$ data and shows the tendency to larger negative values for increasing Q^2, while the R_{EM} ratio is much more uncertain and also the model uncertainties are larger than for the S/M ratio. From $d\sigma_{LT}$ we also find a large sensitivity to the S_{0+} amplitude of the $S_{11}(1535)$ resonance in the minimum around $W = 1500$ MeV as well as for the S_{2-} amplitude of the $D_{33}(1700)$ resonance in the second

N^*		$MAID$ defaults	$MAID$ fit results		helicity amplitudes
$P_{33}(1232)$	$\tilde{E}^{3/2}_{1+}$	-0.44	-0.38± 0.17	$A_{1/2}$	-72± 3
	$\tilde{M}^{3/2}_{1+}$	20.1	19.0± 0.4	$A_{3/2}$	-135± 3
	$\tilde{S}^{3/2}_{1+}$	-1.31	-1.55± 0.05	$S_{1/2}$	18± 1
	R_{EM}	-2.2	-2.0± 0.9		
	R_{SM}	-6.5	-8.1± 0.2		
$P_{11}(1440)$	$\tilde{M}^{1/2}_{1-}$	1.87	2.2± 0.2	$A_{1/2}$	-59± 9
	$\tilde{S}^{1/2}_{1-}$	1.26	0.6± 0.1	$S_{1/2}$	-11± 4
$D_{13}(1520)$	$\tilde{E}^{1/2}_{2-}$	-0.05	-0.05	$A_{1/2}$	-47± 6
	$\tilde{M}^{1/2}_{2-}$	1.71	1.2± 0.2	$A_{3/2}$	26± 4
	$\tilde{S}^{1/2}_{2-}$	0	0	$S_{1/2}$	0
$S_{11}(1535)$	$\tilde{E}^{1/2}_{0+}$	4.37	3.5± 0.8	$A_{1/2}$	61± 14
	$\tilde{S}^{1/2}_{0+}$	0.1	-1.2± 0.1	$S_{1/2}$	-15± 2
$S_{31}(1620)$	$\tilde{E}^{3/2}_{0+}$	0.21	3.4± 0.3	$A_{1/2}$	-50±5
	$\tilde{S}^{3/2}_{0+}$	0.89	1.7± 0.5	$S_{1/2}$	-18± 7
$S_{11}(1650)$	$\tilde{E}^{1/2}_{0+}$	2.8	3.0± 0.4	$A_{1/2}$	43± 6
	$\tilde{S}^{1/2}_{0+}$	0	-1.2± 0.6	$S_{1/2}$	-12± 6
$F_{15}(1680)$	$\tilde{E}^{1/2}_{3-}$	0.32	-0.06± 0.03	$A_{1/2}$	-52± 9
	$\tilde{M}^{1/2}_{3-}$	0.83	0.80± 0.05	$A_{3/2}$	33± 9
	$\tilde{S}^{1/2}_{3-}$	0	-0.10± 0.03	$S_{1/2}$	-7± 2
$D_{33}(1700)$	$\tilde{E}^{3/2}_{2-}$	-0.85	-1.0± 0.2	$A_{1/2}$	104±12
	$\tilde{M}^{3/2}_{2-}$	0.30	1.1± 0.1	$A_{3/2}$	-4±12
	$\tilde{S}^{3/2}_{2-}$	0	0.2± 0.1	$S_{1/2}$	-14± 7
PV-PS mixing:	Λ_m	450	350 ± 35		

Table 1: Proton resonance multipoles ($\tilde{A} \equiv \mathrm{Im}A(W = M_r)$ in $10^{-3}/m_\pi$), helicity amplitudes (in 10^{-3} GeV$^{-1/2}$) and values of the PV-PS mixing parameter Λ_m (in MeV) as in $MAID2000$ and obtained in our fit at $Q^2 = 1.0$ GeV^2. The $D_{13}(1520)$ $\tilde{E}_{2-}$ and $\tilde{S}_{2-}$ amplitudes were fixed. The E/M and S/M ratios of the $\Delta(1232)$ are given in percentage.

maximum around $W = 1650$ MeV. Furthermore most of the structure in $d\sigma$ and in $d\sigma_{TT}$ above $W = 1700$ MeV is explained by the M_{2-} amplitude of the $D_{33}(1700)$ resonance. However, the $MAID$ model does not include higher resonances so far.

In order to get information on resonance properties a careful analysis has to be taken. First of all, a partial wave decomposition in terms of multipoles is necessary to get information on quantum numbers as angular momentum, spin, parity and isospin. Second, a background separation is needed, as especially in pion production a large background is produced by the strong pion nucleon coupling. However, nucleon Born terms and vector meson exchange contributions are not the only source of background. Loop effects can give very large contributions especially for S- and P-waves, the most famous example is the E_{0+} in π^0 photoproduction at threshold. Our resonance extraction is based on the imaginary parts of the full multipoles in a specific spin-isospin channel at the resonance position. This minimizes the model dependence since resonance positions are mostly well known and this method can be applied to any given partial wave analysis. It is very similar to the method that has been applied for the $\Delta(1232)$, however, as Watson's theorem is no longer fulfilled for higher resonances, some uncertainties have to be accepted. The helicity amplitudes extracted by this way are "dressed" amplitudes and contain contributions from vertex corrections. They could be undressed by subtracting background contributions and unitarization corrections. By such a procedure they could be directly related to the Breit-Wigner couplings $\bar{\mathcal{A}}_\alpha^R(Q^2)$ of Eq. (3), however, such a method will always be model dependent.

The helicity amplitudes $A_{1/2}, A_{3/2}$ and $S_{1/2}$ are determined from the pion electroproduction multipoles at the resonance position

$$A_{1/2}^{\ell+} = -\frac{1}{2ac_I}[(\ell+2)\tilde{E}_{\ell+} + \ell\tilde{M}_{\ell+}] \; , \tag{12}$$

$$A_{1/2}^{(\ell+1)-} = +\frac{1}{2ac_I}[(\ell+2)\tilde{M}_{(\ell+1)-} - \ell\tilde{E}_{(\ell+1)-}] \; , \tag{13}$$

$$A_{3/2}^{\ell+} = +\frac{1}{2ac_I}\sqrt{\ell(\ell+2)}[\tilde{E}_{\ell+} - \tilde{M}_{\ell+}] \; , \tag{14}$$

$$A_{3/2}^{(\ell+1)-} = -\frac{1}{2ac_I}\sqrt{\ell(\ell+2)}[\tilde{E}_{(\ell+1)-} + \tilde{M}_{(\ell+1)-}] \; , \tag{15}$$

$$S_{1/2}^{\ell+} = -\frac{1}{\sqrt{2}ac_I}(\ell+1)\tilde{S}_{\ell+} \; , \tag{16}$$

$$S_{1/2}^{(\ell+1)-} = -\frac{1}{\sqrt{2}ac_I}(\ell+1)\tilde{S}_{(\ell+1)-} \; , \tag{17}$$

$$\text{with} \quad a = \sqrt{\frac{1}{\pi}\frac{k_W^R}{q_\pi^R}\frac{1}{2J+1}\frac{m_N}{M_R}\frac{\Gamma_\pi}{\Gamma_{tot}^2}} \quad \text{and} \quad c_I = \begin{cases} -\sqrt{1/3} & : \; I = 1/2 \\ \sqrt{3/2} & : \; I = 3/2 \end{cases} \; . \tag{18}$$

The equivalent photon energy k_W^R and the pion momentum q_π^R are given in the c.m. frame and evaluated at the resonance position, where also the pion electroproduction multipoles are obtained, $\tilde{A} \equiv \mathrm{Im}A(W = M_R)$ for $A = E, M, S$. For the transverse amplitudes these formulas agree with PDG and Ref. [17]. For longitudinal amplitudes we found different definitions in the literature, here we use a definition consistent with notations used in DIS [18].

In Fig. 4 we show our extracted values for the magnetic form factor $G_M^*/3G_D$ and the ratios R_{EM} and R_{SM} together with other data determined in different ways in recent experiments and data analyses on a semi-log scale. For photoproduction the Mainz results [21] are shown, around 0.125 GeV^2 the values of the Bates analysis and the result of the Mainz measurement with recoil polarization, in the medium Q^2 range the preliminary data of Bonn [20] and at high Q^2 our analysis of the JLab Hall C data [19] with $MAID$ and the DMT. The main difference between our results

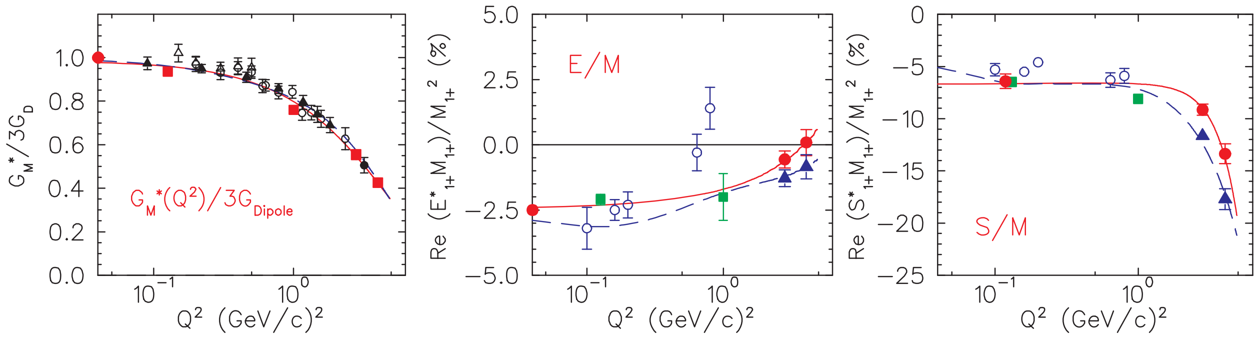

Figure 4: The Q^2 dependence of the magnetic G_M^* form factor and the E/M and S/M ratios at $W = 1232$ MeV. The solid and dashed curves are the $MAID$ and dynamical model results, respectively. JLab results discussed here are shown at $Q^2 = 1$ (GeV/c)^2, Bates results at 0.126 (squares), the Mainz double polarization result of S/M at 0.12 (full circle), data at 2.8 and 4.0 from Ref. [19] (squares) and preliminary results of the ratios in the range of 0.1 - 0.8 are from Bonn [20] (open circles). Results of our analysis for the ratios at 2.8 and 4.0 are obtained using $MAID$ (full circles) and the dynamical models (triangles). In the case of G_M^* they fully agree with Ref. [19]. For older data of G_M^* see Ref. [16]. The photoproduction results of Mainz [21] are placed at the lowest Q^2 value. All numbers are given in units of (GeV/c)^2.

and those of Ref. [19] is that our values of R_{EM} show a clear tendency to cross zero and change sign as Q^2 increases. This is in contrast with the results obtained in the original analysis [19] of the data which concluded that R_{EM} would stay negative and tend toward more negative values with increasing Q^2. Furthermore, we find that the absolute value of R_{SM} is strongly increasing.

4 Summary

With the unitary isobar model $MAID$ and the dynamical model DMT we have two very good tools available to analyze data of pion photo- and electroproduction and to plan new experiments with increased sensitivity to specific questions. While DMT includes pion loop contributions that are especially important for low partial waves (S and P), $MAID$ originally was constructed only from tree diagrams, resonance excitations and K-matrix unitarization contributions. Therefore, to get better agreement for S-waves, $MAID$ has been extended phenomenologically by low-energy corrections and the unitary cusp effect. At higher energies the PS-PV mixing of $MAID$ that was already introduced from the beginning, also serves for this purpose to effectively taking into account of loop contributions.

With all parameters already fixed by πN scattering and pion photoproduction in the resonance region, DMT describes pion photoproduction at threshold very well, similar to the calculations in ChPT or with dispersion relations. For electroproduction at threshold we also find good agreement with the experiment at $Q^2 = 0.1$ GeV^2, however, we also have problems describing the recent Mainz data at $Q^2 = 0.05$ GeV^2 as it also appears in ChPT calculations. In the resonance region both models DMT and $MAID$ can equally well describe photo- and electroproduction data up to $W = 1700$ MeV by fitting the photon helicity amplitudes $A_{1/2}, A_{3/2}$ and $S_{1/2}$ of the individual resonances. Here, we have demonstrated this with the preliminary Hall A data of JLab at $Q^2 = 1.0$ GeV^2. Even with a dataset limited to backward pion angles we are able to determine quite a few resonance parameters in satisfactory precision and can also give longitudinal couplings where previous information practically did not exist. For the E/M and S/M ratios of the Delta resonance we combine our previous fits of Mainz, Bates and JLab Hall C data with our new analysis and find a consistent Q^2 evolution of these ratios with a slowly rising R_{EM} that crosses zero around $Q^2 = 4$ GeV^2, and for the longitudinal coupling a R_{SM} that significantly increases to larger negative values at high Q^2. If expectations from pQCD will be fulfilled, a sharp rise in the E/M ratio towards 100% should be seen in the next generation of experiments above $Q^2 = 5$ GeV^2 and a leveling of the S/M ratio to a constant value.

Acknowledgments: We gratefully acknowledge financial support of this work in parts by the National Science Council of ROC under Grant No. NSC89-2112-M002-078, by Deutsche Forschungsgemeinschaft (SFB 443), and by a joint project NSC/DFG TAI-113/10/0.

References

[1] D. Drechsel, O. Hanstein, S.S. Kamalov and L. Tiator, Nucl. Phys. **A645**, 145 (1999); in the internet at `http://www.kph.uni-mainz.de/MAID/`.

[2] S.S. Kamalov and S.N. Yang, Phys. Rev. Lett. **83**, 4494 (1999); S.N. Yang, J. Phys. G **11**, L205 (1985).

[3] C.T. Hung, S. N. Yang, and T.-S.H. Lee, J. Phys. G **20**, 1531 (1994); Phys. Rev. C **64**, 034309 (2001).

[4] A. M. Bernstein, Phys. Lett. B **442**, 20 (1998).

[5] V. Bernard, N. Kaiser, and Ulf-G. Meißner, Z. Phys. C **70** (1996) 483; Nucl. Phys. A **607**, 379 (1996); and references contained therein.

[6] V. Bernard, J. Gasser, N. Kaiser, and Ulf-G. Meißner, Phys. Lett. B **268**, 291 (1991).

[7] J. M. Laget, Phys. Rep. **69**, 1 (1981).

[8] M. Fuchs *et al.*, Phys. Lett. B **368**, 20 (1996).

[9] A. Schmidt *et al.*, `nucl-exp/0105010`, Phys. Rev. Lett. (2001) in print.

[10] J. C. Bergstrom *et al.*, Phys. Rev. C **53**, R1052 (1996); C **55**, 2016 (1997).

[11] H. B. van den Brink *et al.*, Phys. Rev. Lett. **74**, 3561 (1995); Nucl. Phys. A **612**, 391 (1997).

[12] M. O. Distler *et al.*, Phys. Rev. Lett. **80**, 2294 (1998).

[13] S.S. Kamalov, G.-Y. Chen, S.N. Yang, D. Drechsel and L. Tiator, `nucl-th/0107017`, Phys. Lett. B in print.

[14] R.A. Arndt, I. Aznauryan, R.M. Davidson, D. Drechsel, O. Hanstein, S.S. Kamalov, A.S. Omelaenko, I. Strakovsky, L. Tiator, R.L. Workman, SA.N. Yang, Proc. of NSTAR2001, Mainz, World Scientific 2001, p 467.

[15] G. Laveissiere *et al.*, Proc. of NSTAR2001, Mainz, World Scientific 2001, p 271.

[16] S.S. Kamalov, S.N. Yang, D. Drechsel, O. Hanstein, and L. Tiator, Phys. Rev. C **64**, 032201 (2001).

[17] R.A. Arndt et al, Phys. Rev. C **42**, 1864 (1990).

[18] K. Abe *et al.*, Phys. Rev. D **58**, 112003 (1998).

[19] V.V. Frolov *et al.*, Phys. Rev. Lett. **82**, 45 (1999).

[20] R.W. Gothe, Prog. Part. Nucl. Phys. **44**, 185 (2000).

[21] R. Beck *et al.*, Phys. Rev. Lett. **78**, 606 (1997).

Two-pion production on the nucleon

S. Krewald, S. Schneider, and J. Speth

Institut für Kernphysik, Forschungszentrum, D-52425 Jülich, Germany

(Received: 31 October 2001)

A tree-level meson-exchange model for the production of two pions on the nucleon in the vicinity of the threshold is presented as a first step towards a theoretical understanding of the one- and two-meson decay of baryonic resonances. The present model includes both baryonic and mesonic resonances as intermediate states. The Roper resonance has been found to be generated dynamically by meson-baryon dynamics in a recent coupled channel model for the meson-nucleon reaction. In the present approach, we represent the Roper by an elementary resonance, but use coupling constants which reproduce the results of the coupled channel model. We partially unitarize the model at the two-body level. The experimental total cross sections and angular correlations near threshold are reproduced.

1 Introduction

Recent experimental progress has provided high quality data concerning the one- and two-meson production on the nucleon, both near threshold and in the resonance region. This new data may help to constrain theoretical models of the resonances. In particular, one would like to test models which predict a significant deviation from a three-valence quark structure for some resonances, such as the Roper resonance [1].

Near threshold, chiral perturbation theory has been applied to describe systematically the two-pion production data available. A lowest order calculation turned out to be insufficient [2]. At higher orders in chiral perturbation theory, the so-called low energy constants c_i have to be considered which are determined from a comparison with the data. It was found that after consideration of the low energy constants, the data near threshold can be reproduced already at tree level [3, 4]. Moreover, a quantitative interpretation of the low energy constants via resonance saturation has been proposed [3, 5]. The question arises whether one can replace the low energy constants by diagrams which contain explicit resonances and simultaneously keep the good agreement with the data achieved by chiral perturbation theory. At the tree level, such an approach has already been performed by Oset and collaborators many years ago [6]. The first step of our work program therefore is to collect all possible tree level diagrams with intermediate resonances. The next step is to unitarize the tree level model. In the present communication, we show some results where a two-body unitarization of the resonances has been imposed. Therefore the present calculations are limited to the vicinity of the two-pion production threshold.

2 The model

In Fig. 1, some of the tree-level diagrams considered are shown. We start from a πN initial state and consider processes with intermediate bosonic and fermionic resonances. In the energy range of interest, the bosonic resonances are the rho-meson and the sigma-meson. Both resonances are unitarized at the two-body level by mixing a bare meson with two-pion states carrying the same quantum numbers. The T-matrix for pion-pion scattering is worked out, and the experimental phase shifts near threshold are reproduced. The fermionic resonances considered in the present version of the model are the nucleon, the $\Delta-$resonance, and the Roper resonance. The $\Delta-$resonance is unitarized by solving a simplified T-matrix equation in the K-matrix approximation. In the present version of the model, the Roper resonance is parameterized by a simple Feynman pole diagram; the corresponding masses and coupling constants are chosen such as to reproduce the T-matrices of our coupled channel reaction model [1].

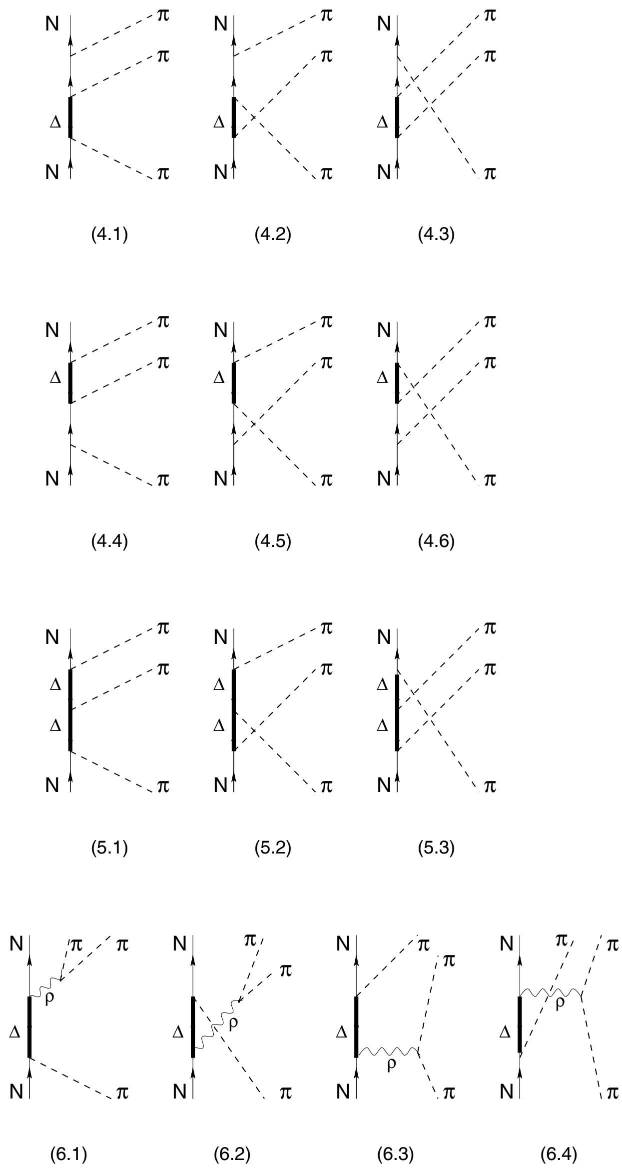

Figure 1: Some typical tree-level Feynman diagrams considered in the present calculation.

3 Results

In Fig. 2, we show the total cross sections obtained for the total cross sections of the five reactions $\pi^+p \to \pi^+\pi^+n$, $\pi^+p \to \pi^+\pi^0p$, $\pi^-p \to \pi^0\pi^-p$, $\pi^-p \to \pi^+\pi^-n$, $\pi^-p \to \pi^0\pi^0n$ as functions of the kinetic energy of the incoming pion. As expected from the isospin of the final state, the reaction $\pi^+p \to \pi^+\pi^+n$ is dominated by the diagrams involving intermediate Δ resonances. The overall agreement with the total cross sections is good with the exception of the reaction $\pi^+p \to \pi^+\pi^0p$. If one ignores the unitarization at the two-body level, the theoretical curve starts to overestimate the data for energies larger than $T_\pi = 250MeV$, as can be seen from Refs. [3, 4] and as we have confirmed in a previous non-unitarized version of our model. The present calculation is based on a unitarization of the resonant pion-nucleon partial wave only. This leads to an improvement as compared to a pure tree-level calculation, but of course, a unitarization of the non-resonant partial waves needs to be incorporated next.

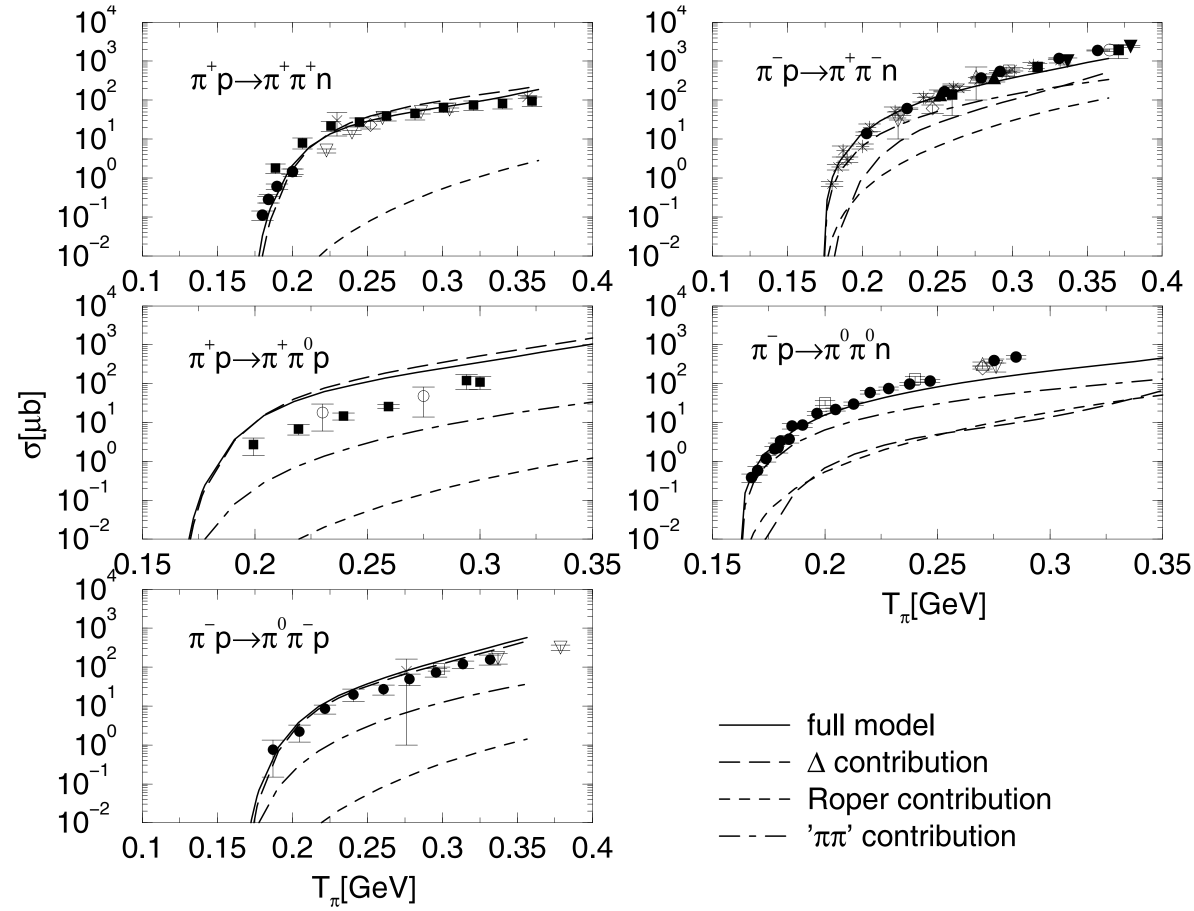

Figure 2: Total cross sections for the reactions $\pi N \to \pi\pi N$ near threshold are shown as functions of the kinetic energy of the incoming pion in the LAB frame. The solid lines refer to the full model. The contributions of diagrams with intermediate Δ's are given by the long-dashed line, while diagrams with an intermediate Roper resonance are represented by the short-dashed lines. Contributions from intermediate correlated two-pion states are given by the dashed-dotted lines.

The cross sections for the reactions $\pi^- p \to \pi^+\pi^- n$ and $\pi^- p \to \pi^0\pi^0 n$ are dominated by the diagrams with resonant intermediate two-pion states, which we loosely call "sigma" and "rho"(see dashed-dotted lines). In the case of these diagrams, the unitarization at the two-body level is essential: a pure tree-level calculation fails beyond $T_\pi = 250MeV$.

As expected, the influence of the Roper resonance in the threshold region is negligible (short dashed line). The maximum of the Roper resonance corresponds to $T_\pi = 480MeV$, which is a moderate extension of the energy range presently considered. The overall agreement of our model with the data suggests that we are on the right track and can next try to implement three-body unitarity at the K-matrix level. Now we discuss how well our model reproduces more exclusive data.

The differential cross sections are shown as a function of the invariant two-pion mass in Fig. 3. The data [7] show a noticeable deviation from the phase space distribution. The position of the maxima of the experimental differential cross sections is reproduced by our model, but we underestimate the magnitude for large values of the kinetic energy of the incident pionT_π. The two cases $T_\pi = 220MeV$ and $T_\pi = 240MeV$ have been investigated in Ref. [4]; our theoretical results are similar to the ones of Ref. [4].

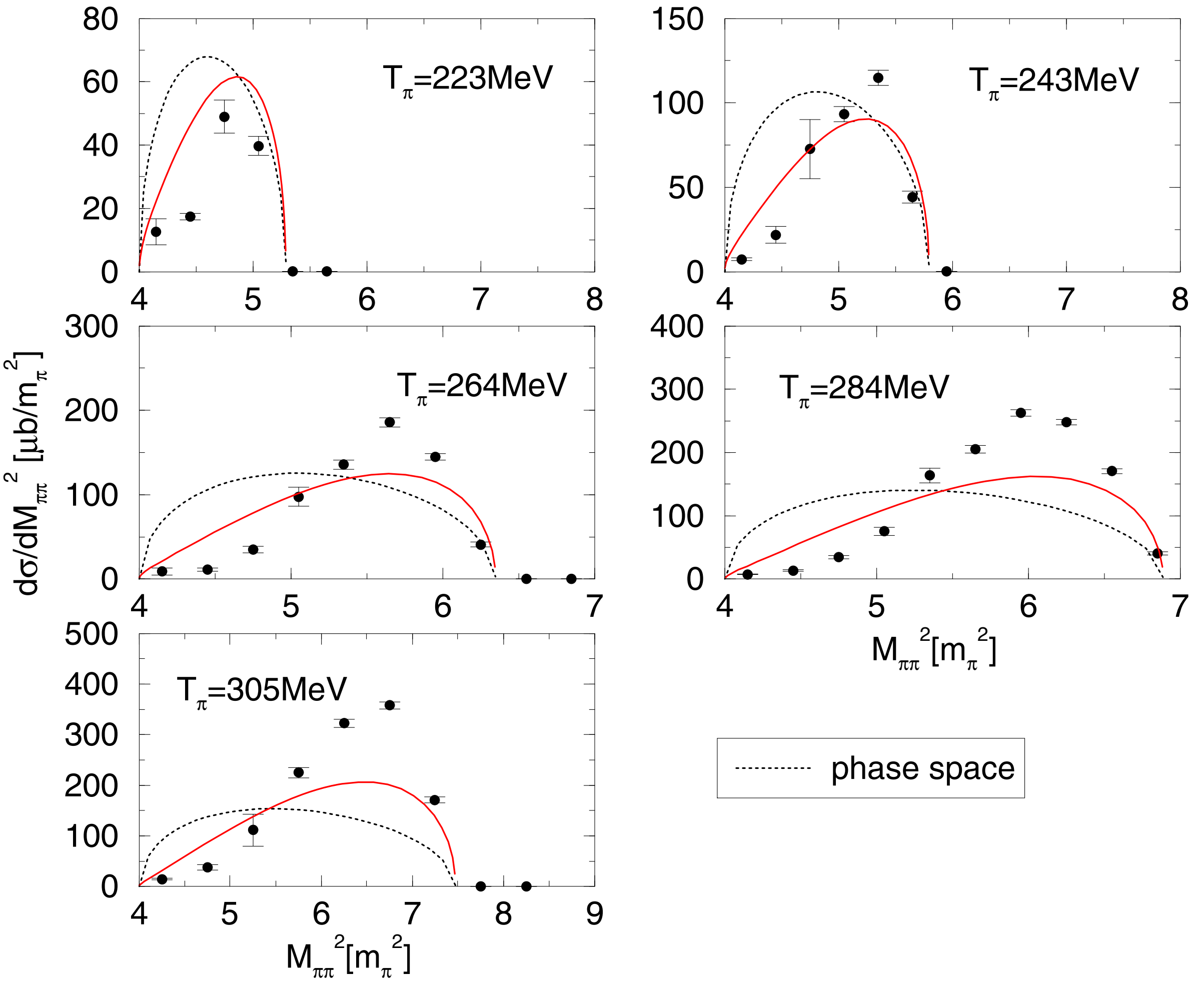

Figure 3: Differential cross sections for the reaction $\pi^- p \to \pi^+ \pi^- n$, as functions of the invariant two-pion mass. The dotted line refers to the phase space.

Ideally, one would like to analyse Dalitz plots. What is experimentally available at present, are angular correlation functions. The angular correlation function W is defined as the following ratio between triple and double differential cross sections:

$$W(\Theta_1, \Phi_1) = 4\pi \frac{\frac{d^3\sigma}{d\Omega_1 d\Omega_2 dT_2}}{\frac{d^2\sigma}{d\Omega_2 dT_2}} \ . \tag{1}$$

In ref. [8], experimental angular correlation functions are shown for the reaction $\pi^- p \to \pi^+ \pi^- n$ at a center-of-mass energy $\sqrt{s} = 1.301 GeV$. These data are compared with our model in Fig. 4. We find an overall agreement which is satisfactory. In Ref. [4], a problem was found in connection with the angular correlations functions: in third order of chiral perturbation theory, the data of Ref. [8] are overestimated at the angle $\Phi_{\pi^-} = 180^o$ for $\Theta_{\pi^-} \geq 90^o$, but are underestimated at $\Phi_{\pi^-} = 180^o$ for $\Theta_{\pi^-} \leq 90^o$. The present model does not have such a problem. We feel that this is not a problem of chiral perturbation theory as such, but rather it is a practical problem how to choose the optimal low energy constants.

The explicit inclusion of meson resonances in our model allows to understand the shape of the distributions qualitatively: for a fixed angle Θ_{π^-}, the angular correlation is maximal for the

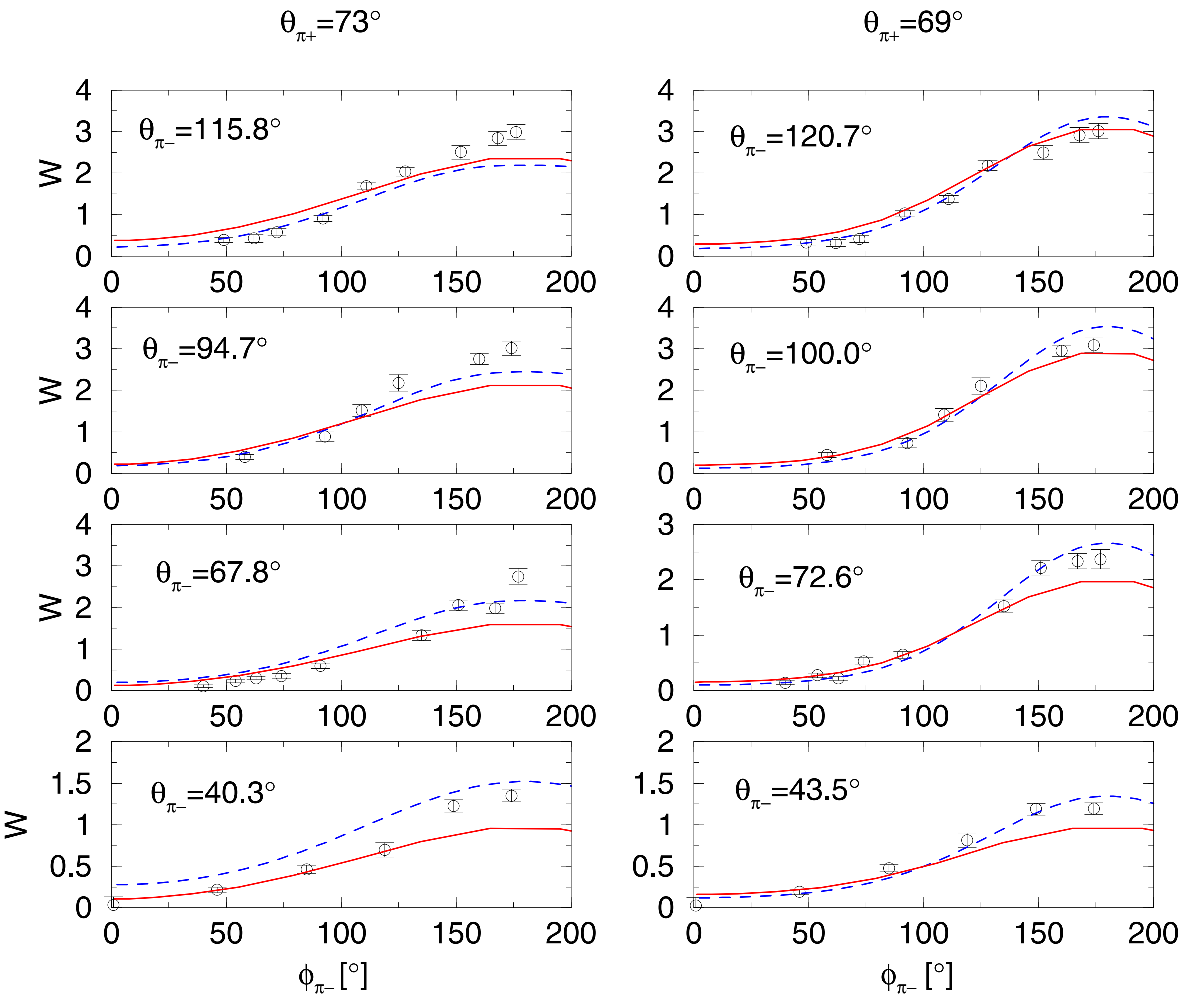

Figure 4: Angular correlation functions for the reaction $\pi^- p \to \pi^+\pi^- n$ are shown as a function of the angle Φ_{π^-} for different angles Θ_{π^-}. The full model is represented by the solid line, while the dashed line includes only those diagrams with intermediate meson resonances.

angle $\Phi_{\pi^-} = 180^o$. The coordinate system is chosen such that $\Phi_{\pi^+} = 0^o$. This means that the two produced pions tend to separate predominantly back-to-back in the $xy-$plane. We can interpret this finding as follows. Close to threshold, the intermediate meson-resonances ρ and σ are almost at rest in the center-of-mass frame. Therefore the produced pions are indeed expected to be emitted back-to-back. We can test this interpretation by simply including only those diagrams with intermediate meson resonances. The contribution of only these diagrams (dashed line) indeed reproduces most of the experimental cross section. There is some deviation between the dashed line and the full model because the data of ref. [8] were taken for a kinetic energy of the incident pion of $T_{\pi^-} = 0.284 GeV$ which is large enough to excite the Δ noticeably.

4 Conclusions

The model presented here is an intermediate step in the attempt to develop a microscopic model for the one- and two-pion decay of the resonances of the nucleon. The basic idea is to keep the formalism as simple as possible. We show that a tree-level model with partial unitarization at the two-body level can give a reasonable agreement with existing data in the vicinity of the threshold. It was found important to employ two-body t-matrices for the intermediate $\pi\pi$ and for the πN scattering which reproduce the known two-body data.

We feel encouraged to implement a simple treatment of three-body unitarity in order to be able to investigate the actual resonance region.

Acknowledgments: We gratefully acknowledge valuable discussions with T. Barnes, U.-G. Meißner and H.P. Morsch.

References

[1] O. Krehl, C. Hanhart, S. Krewald and J. Speth, Phys. Rev. **C**62, 025207 (2000).

[2] J. Beringer, πN Newsletter **7**, 33 (1992).

[3] V. Bernard, N. Kaiser and U.-G. Meißner, Nucl. Phys. **A**619, 261 (1997).

[4] N. Fettes, V. Bernard and U.-G. Meißner, Nucl. Phys. **A**669, 269 (2000).

[5] G. Ecker et al., Nucl. Phys. **B**321, 311 (1989).

[6] E. Oset and M.J. Vicente-Vacas, Nucl. Phys. **A**446, 584 (1985).

[7] M. Kermani et al., Phys. Rev. **C**58, 3419 (1998).

[8] R. Mueller et al., Phys. Rev. **C**48, 981 (1993).

Investigation of the photoinduced meson production by CB-ELSA

J. Langheinrich, for the CB-ELSA collaboration

Physikalisches Institut, Universität Bonn, Bonn, Germany

(Received: 31 October 2001)

The CB detector is designed to measure photons from neutral meson decay with a large acceptance and high energy and spacial resolution. The first CB-ELSA production campaign on a tagged real photon beam has been accomplished. In the preliminary evaluation the π^0, η, η', $\pi^0\pi^0$ and $\eta\pi^0$ production channels at the proton have been separated, clear evidence for the Σ^+K^0 channel have been found. Dalitz plots show a strong preference for an intermediate Δ-state in the $\pi^0\pi^0$ as well as in the $\eta\pi^0$ data.

1 Experimental setup and physics motivation

The Crystal-Barrel detector (CB) is already well known by a large number of publications concerning meson production in proton-antiproton reactions at the LEAR-facility (CERN) [1,2]. CB is designed as spherical modular calorimeter and comprises 1380 CsI(Tl) crystals covering 98% of the whole solid angle of 4π. The high granularity, density and signal/noise ratio makes it particularly suitable for the measurement of decay photons.

CB has been moved to the ELSA electron accelerator facility in Bonn. An embedded experimental setup has been designed for the measurement of photoinduced meson production in a liquid hydrogen target. Additional components in this setup are a tagging system for real photons, an inner detector with thin scintillating fibers to discriminate charge particles and a time-of-flight wall with high spatial resolution to detect scattered protons in the forward direction.

In the nonperturbative region of QCD the use of phenomenological QCD inspired models are very useful to describe the excitation of the nucleon. They are able to describe most of the production processes, but very often predictions derived from such models do not match the experimental situation. Especially the situation of nucleon resonances in the region between 1 and 2.5 GeV is today still unclear. A large number of resonances has been predicted but not verified. There are various approaches which provide a chance to get experiment and theory in agreement. One possibility is that the effective number of degrees of freedom is restricted [3]. Alternatively, there is the possibility that these states simply have not been observed so far. The reason might be that nearly all the existing data on non-strange baryon production result from πN scattering experiments. Therefore only these resonances could be discovered that couple to πN [4].

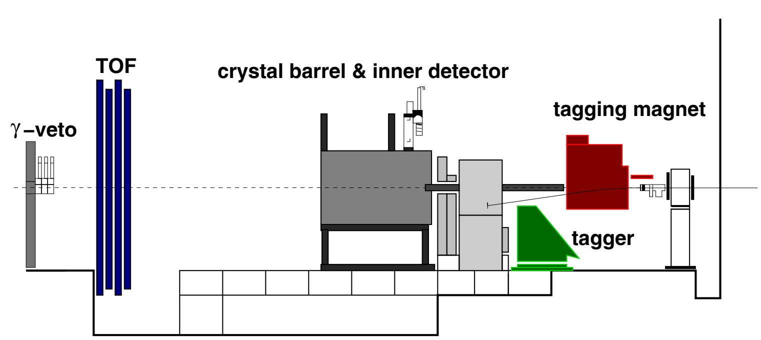

Figure 1: The setup of the CB-ELSA experiment.

One of the first experimental goals of the CB experiment is the search for resonances which decay into $\pi^0\Delta^+$ and $\eta\Delta^+$. The evaluation of the neutral decay channels provides a number of advantages compared with the $\pi^+\pi^-$ dominated charged channels, such as avoiding a high background rate by diffractive ρ-production.

2 First data from experiment

In the first production period we obtained approximately 10^8 events for each initial electron beam energy 1.4, 2.6 and 3.2 GeV. The tagging system is able to tag photons between 25% and 92% of the electron energy. For the first analysis, less than 30% of the statistics available for 3.2 GeV has been used. After subdividing the events according to the number of particle hits in the CB detector, and after applying some kinematic cuts, the meson production channels can be separated. The results for the reaction $\gamma p \to p\gamma\gamma$ are shown in fig. 2. The signal to background ratio is 1000:1 for the π^0 and 100:1 for the η peak. The ω meson has no decay mode into two photons, but missing one low energy photon from the three photon decay results in an asymmetric ω contribution to the two photon invariant mass spectrum. Even if the η' branching ratio into the two photon decay is only 2%, a clear η' peak is visible.

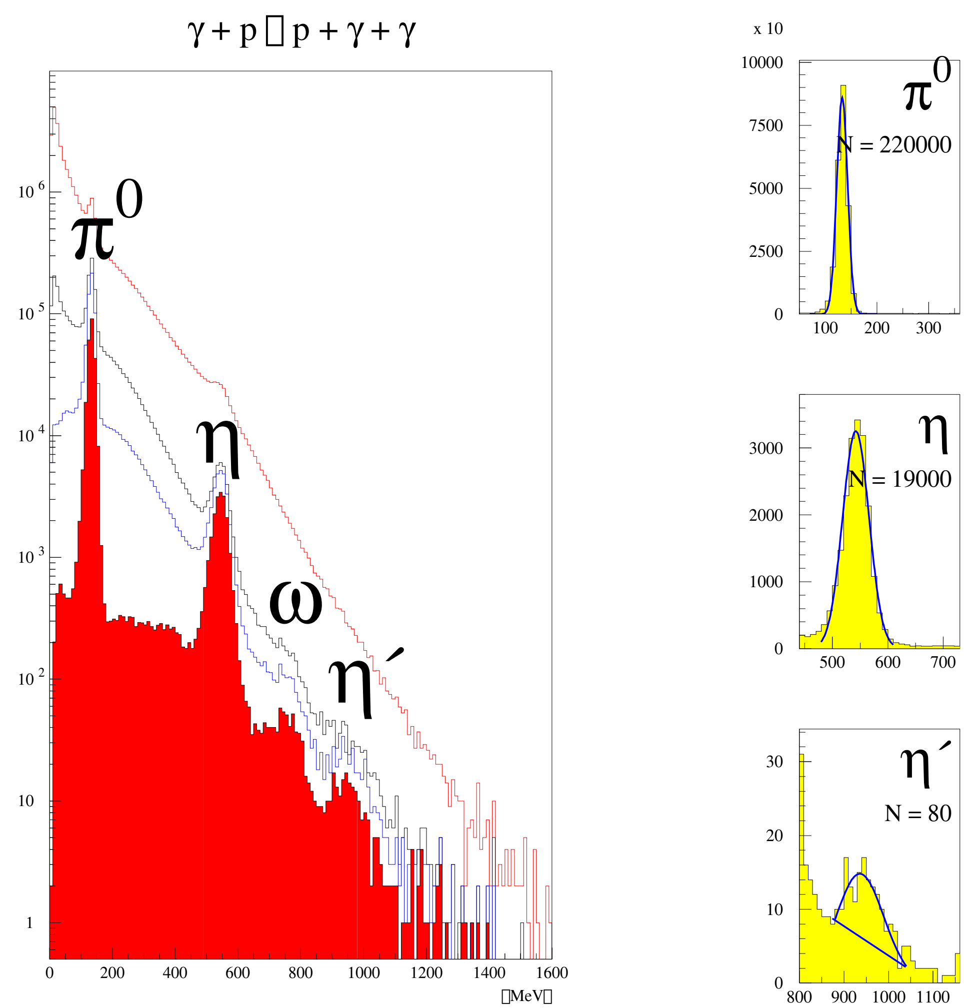

Figure 2: Invariant $\gamma\gamma$ mass the $\gamma p \to p\gamma\gamma$ reaction. To suppress background some kinematic cuts have been applied.

For $\gamma p \to p\gamma\gamma\gamma\gamma$ events the invariant mass of each $\gamma\gamma$ pair is plotted against the invariant mass of the other pair (fig. 3). Despite of some combinatorial background, the signal to background ratio for the $\pi^0\pi^0$ channel is 300:1. This channel is the subject of further investigation. Dalitz plots show a strong preference of the Δ-resonance as intermediate state, hints for other intermediate states as $D_{13}(1520)$ are visible. Another interesting channel is the $\pi^0\eta$ production. Fig. 3 (right part) shows the $p\pi^0\eta$ invariant mass and the Dalitz plot. Even in this channel a strong evidence for an intermediate Δ-state is visible.

Most of the events with 6 photons detected in the CB come from the $\eta \to \pi^0\pi^0\pi^0$ decay, the signal to background ratio for this channel is as high as for the $\gamma\gamma$ decay. To reconstruct the meson and compare the η yield from the two available channels after applying acceptance correction and the well known branching ratio will be a good test for systematic errors.

There are still events containing three π^0 not coming from the η decay. Plotting combinations of $p\pi^0$ invariant mass against $\pi^0\pi^0$ (fig. 4) reveal their origin: the Σ^+K^0 production. However, these particles have a non-negligible lifetime. Assuming the target as the origin of their tracks leads to a smearing of the peak.

Looking for the $\pi^0\pi^0\eta$-production and calculating the three meson invariant mass, a clear signature of the η' is visible. However for this channel background subtraction becomes more difficult. Other evaluation techniques such as kinematic fitting are currently under development and provide a refinement of this channel.

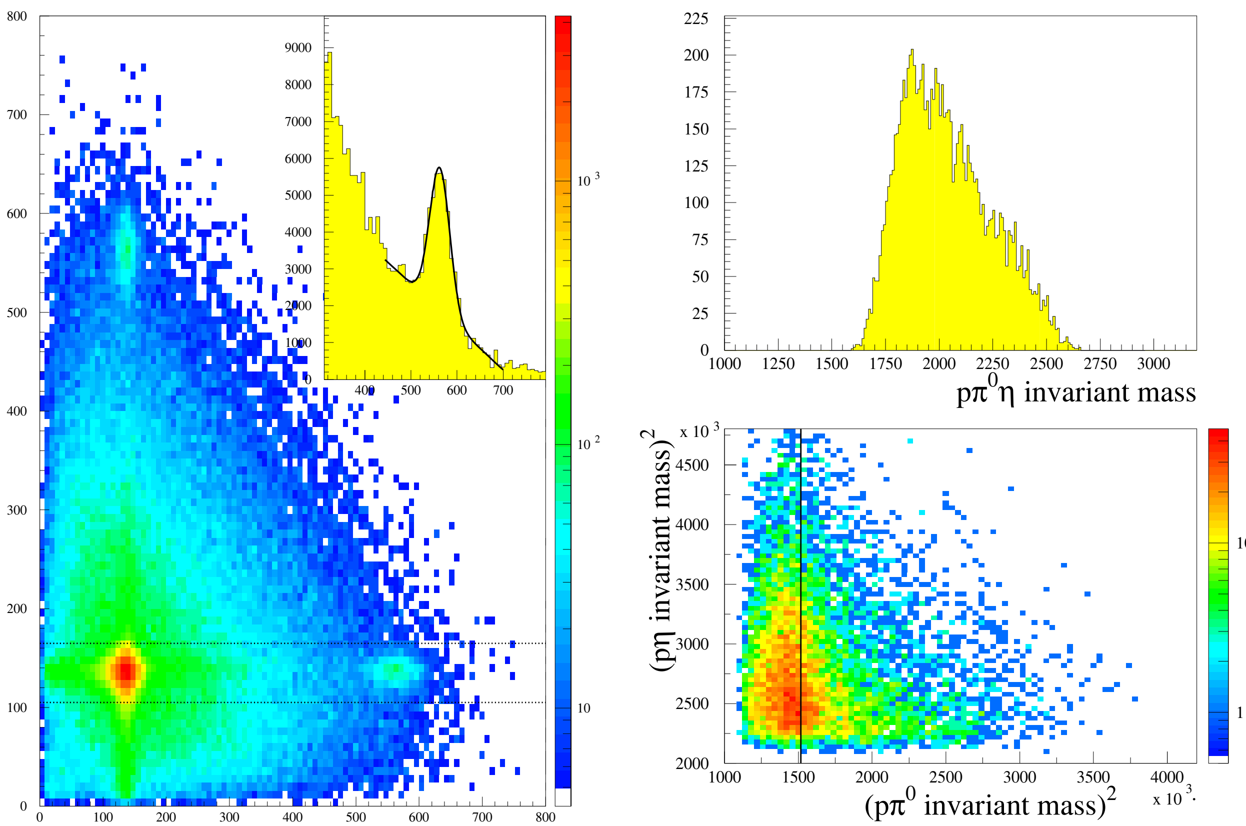

Figure 3: Left: the invariant mass in units of MeV of combinations of photon pairs in the $\gamma p \to p\gamma\gamma\gamma\gamma$ reaction. The one dimensional clipping shows the $\pi 0\eta$ region. Right, up: the $p\pi^0\eta$ invariant mass. Down: the Dalitz-plot. The solid line marks the delta resonance.

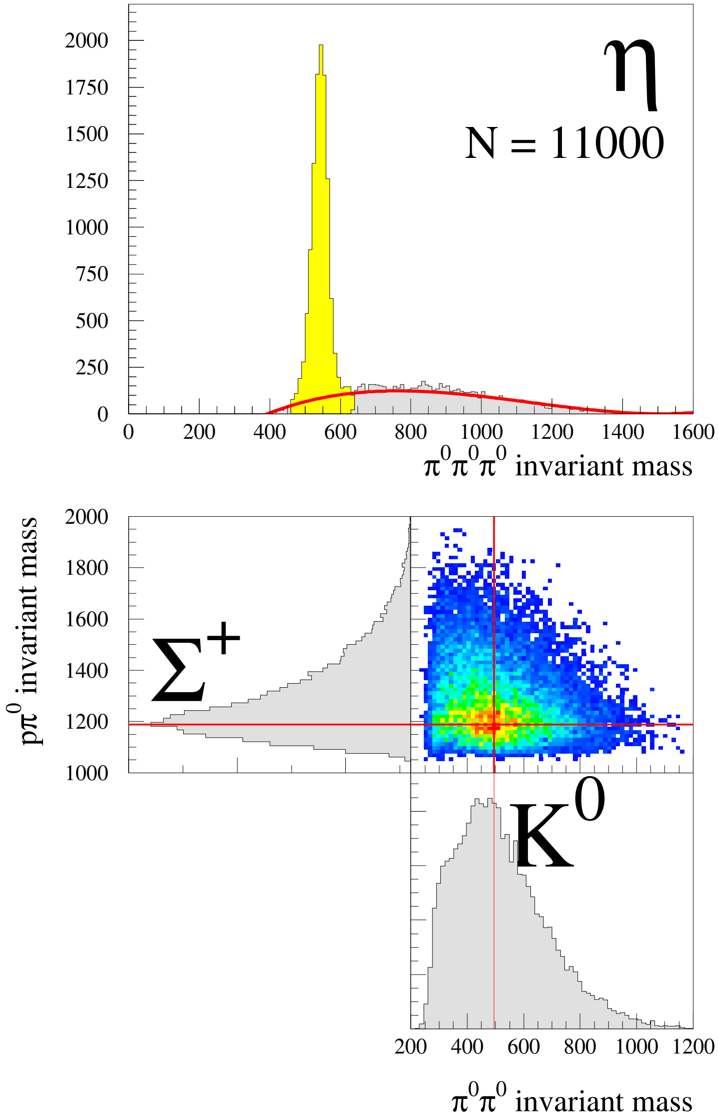

Figure 4: Top: The 3 π^0 invariant mass in units of MeV. Bottom: The invariant mass of a $p\pi^0$ combination plotted against the $\pi^0\pi^0$ invariant mass for events not within the η peak.

3 Future plans

To get an even better resolution in forward direction and a higher trigger rate, the TAPS detector will be added to the current experimental setup. The barrel will be modified by removing the first three rows of crystals in forward direction. The tagging system also must be modified - to enable higher tagging rates the wire chambers will be replace by scintillating fibers.

The next production run will start in November 2001. Encouraged by the first results we expect access to additional neutral production channels as well as the determination of cross sections with a high precision as result of further going analysis.

References

[1] The Crystal Barrel Collaboration (A. Abele *et al.*), Nucl. Phys. **B514**, 45 (1998).

[2] The Crystal Barrel Collaboration (A. Abele *et al.*), Nucl. Phys. **A679**, 563 (2001).

[3] D.B. Lichtenberg, Phys. Rev. **178**, 2197 (1969).

[4] R. Koniuk, N. Isgur, Phys. Rev. **D21**, 1868 (1980).

η electroproduction with CLAS

James A. Mueller

Department of Physics and Astronomy, University of Pittsburgh, Pittsburgh, PA 15260, USA
Email: mueller+@pitt.edu

(Received: 1 November 2001)

A series of measurements on η electroproduction have been done with the CEBAF Large Acceptance Spectrometer (CLAS) at Jefferson Laboratory. Our first result accurately measured the shape of the Q^2 dependence of $A_{\frac{1}{2}}$ between $0.25 < Q^2 < 1.5$ GeV^2, and revealed interesting new structure in the region around $W = 1.7$ GeV. Now we have data that have more than quadrupled the statistics and doubled the Q^2 coverage. This experiment produces precise measurements over the range $0.13 < Q^2 < 3.2$ GeV^2 and W from threshold up to 2.2 GeV with electron beam energy ranging from 1.5 to 4.2 GeV. We present preliminary measurements of the differential cross section for η electroproduction as a function of the hadronic center-of-mass angles to extract information on the response functions $R_T + \epsilon R_L$, R_{LT}, and R_{TT}. These are compared with the results from previously published data from CLAS, previous experiments, and predictions of models.

1 Introduction

Photo and electroproduction experiments on the nucleon provide a clean probe of nucleon structure since Quantum Electrodynamics is well understood. The reaction $ep \to ep\eta$ is an especially clean reaction for studying excited states of the proton, since it selects out isospin = 1/2 N^* resonances. The cross section for this reaction appears to be dominated by the $S_{11}(1535)$ resonance, which has quantum numbers $IJ^P = \frac{1}{2}\frac{1}{2}^-$, and is reached from the nucleon through an electric dipole transition. This is the only baryon resonance known to have a branching ratio into ηp larger than a few percent [1]. Past experiments [2,3] have established that the photocoupling amplitude ($A_{1/2}$) for the $S_{11}(1535)$ has a slower falloff with Q^2, indicating a more compact object than other N^* resonances. In this paper, I describe new measurements of η electroproduction with nearly complete angular coverage. These data are used to look for additional contributions to this reaction beyond the $S_{11}(1535)$ and to extract new values for $A_{1/2}$ of the S_{11}.

2 Results from first data run

This experiment was done using the CEBAF Large Acceptance Spectrometer (CLAS) [4] at the Thomas Jefferson National Accelerator Facility (TJNAF), nee CEBAF. In early 1998, the newly commissioned CLAS took its first production data with an electron beam on a hydrogen target. These results [5] were the basis of the thesis of Richard Thompson, and have been published in Physical Review Letters

2.1 The CLAS Detector and event selection

Toroidal magnet coils separate CLAS into 6 largely identical sectors, each covering 54° in ϕ. Tracking chambers (DC) in CLAS measure angles and momenta of charged particles for lab polar angles in the range $8° < \theta < 142°$. Outside the DC, scintillation counters (SC) provide time-of-flight measurements with which we can separate the charged hadrons into pions, kaons, and protons. For lab angles $\theta < 48°$, threshold Cerenkov detectors (CC) and Electromagnetic Calorimeters (EC) distinguish electrons from charged hadrons with high accuracy. A coincidence of the EC (with energy above $\sim$ 300 MeV) and the CC was required in the trigger for the data presented here.

For this analysis, events were selected with an identified electron and proton. A fiducial cut on

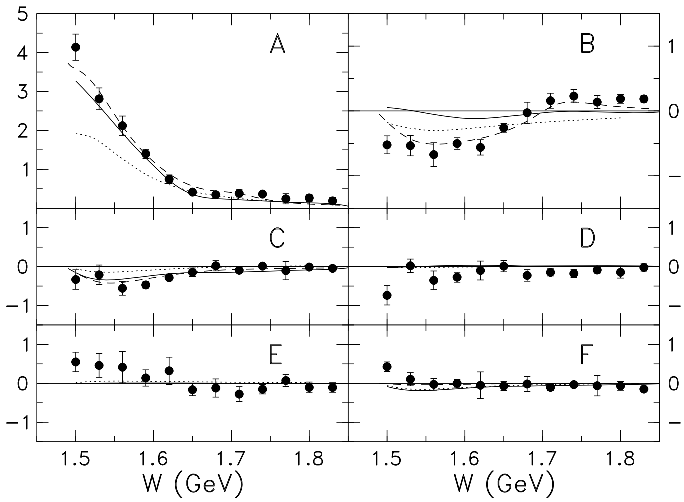

Figure 1: The results of the fit to the differential cross section using Equation 1. The dotted curve is from the old prediction of the Mainz Group [6]. The solid curve is derived from the new calculations of the ETA-MAID program [8]. The dashed curve is the result of a five-resonance fit using relativistic Breit-Wigner amplitudes with energy dependent widths.

these particles was applied to avoid the complicated regions near the magnetic coils and the edges of the CC. The momentum of the electron was required to be above 500 MeV in order to be well above the trigger threshold.

2.2 Differential cross sections

Events were then binned according Q^2, W, and the center-of-mass angles of the putative η ($\cos\theta^*_\eta$ and ϕ^*_η). The η yield was determined by fitting the distribution of missing mass recoiling against the *e-p* system. The fit is the sum of a peak at the η mass with a radiative tail plus a simple background function modified by the geometric acceptance for this reaction. The rms resolution for the missing mass peak is about 6 MeV. Acceptance for this reaction was calculated using a GEANT-based Monte Carlo simulation. The event generator included radiative effects using the peaking approximation, and the cross sections have been corrected for radiation. The acceptance varied from bin to bin with a high of 54%. Bins with acceptance less than 5% were not used in this analysis.

For each W and Q^2 bin, the differential cross sections were fit to a form that comes from an expansion of the response functions in terms of orthogonal polynomials.

$$\begin{aligned} \frac{d^2\sigma}{d\Omega^*_\eta} &= \frac{|p^*_\eta|}{K}\left[R_T + \epsilon R_L + \sqrt{2\epsilon(1+\epsilon)}R_{TL}\cos\phi^*_\eta + \epsilon R_{TT}\cos 2\phi^*_\eta\right] \qquad (1) \\ &\approx \frac{|p^*_\eta|}{K}\Big[A + B\cdot\cos\theta^*_\eta + C\cdot P_2(\cos\theta^*_\eta) \\ &\quad + \left(D\cdot\sin\theta^*_\eta + E\cdot\sin\theta^*_\eta\cos\theta^*_\eta\right)\cos\phi^*_\eta + F\cdot\sin^2\theta^*_\eta\cos 2\phi^*_\eta\Big] \ . \end{aligned}$$

Under the assumption that the cross section is dominated by the S_{11} partial wave, the A parameter represents the S-wave contribution, B and D come from S/P-wave interference, and C, D, and F are due to S/D-wave interference. Thus, nonzero values for B-F are evidence for non-resonant mechanisms or other N^* resonances. The results of these fits are shown in Figure 1. The terms representing R_{LT} and R_{TT} are small and in agreement with theoretical expectations [6]. A is the largest contribution and has, at low W, the expected Breit-Wigner shape due to an S-wave resonance close to threshold. C is slightly negative for low W, as is also seen in photoproduction, where it is due to the $D_{13}(1520)$. The most striking feature not seen in previous data is that the B parameter starts out negative at low W, but changes sign around 1.7 GeV. This could indicate variation of the relative phase between the S and P wave, or perhaps multiple canceling contributions whose relative magnitudes are changing. This feature is also seen [7] by the GRAAL experiment but was not reproduced by the earlier predictions [6] of the Mainz group. We attempted a simple resonance fit to our data. We included 5 resonances in the fit. The $S_{11}(1535)$, $S_{11}(1650)$, $P_{11}(1710)$, and $D_{13}(1520)$ were required to reproduce our data. We also included the $P_{11}(1440)$ in order to model the observed P-wave strength below the 1710, although this could also be non-resonant. Resonance masses and widths were fixed to their PDG values [1], with only the amplitudes of the Breit-Wigners allowed to float. The results of this fit is also shown in Figure 1.

Since these data were published, a new model [8], based on the MAID formalism has been developed for η electro and photoproduction. They fit the photoproduction data and the Q^2 dependence of the total electroproduction cross section in the $S_{11}(1535)$ region. Their fit yields large contributions to η production from the $S_{11}(1535)$, $S_{11}(1650)$, $P_{11}(1710)$, and $D_{15}(1675)$. If this is the case, and the D_{15} strength persists to moderate Q^2, then the B parameter could have significant contributions from P/D interference as well as S/P. The results of their new calculation are included in Figure 1. There is now much better agreement with our A and C parameters, but even worse agreement on B.

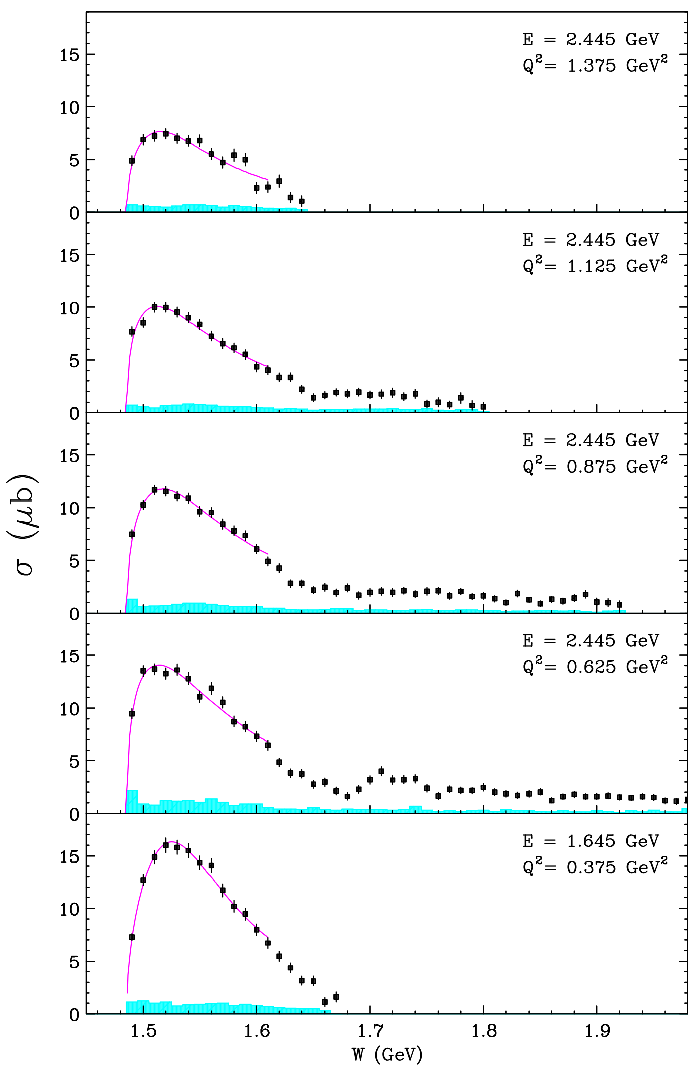

Figure 2: The integrated cross section measured for this experiment. The error bars on the points are statistical only. The size of the systematic uncertainty is indicated by the histogram at bottom of each plot. The curves are fits to a single Breit-Wigner with an energy dependent width.

2.3 *Integrated cross sections*

By summing events over $\cos\theta^*_\eta$ and ϕ^*_η, adequate statistics are available to bin the events finer in both W and Q^2. These cross sections are presented in Figure 2. The prominent peak at $W \sim 1.5$ GeV is the $S_{11}(1535)$, as seen in the isotropic part of the angular distributions. Fits to a relativistic Breit-Wigner with an energy-dependent width describe the low W region well, but there are deviations for $W > 1.65$ GeV. It is interesting to note that this is the same energy region where the B parameter derived from the angular distributions shows a strong variation. Saghai and Li [9] have interpreted a peak observed in the total photoproduction cross section as evidence for a third S_{11} resonance. Since this would be a state beyond what is predicted by the constituent quark model, this would be of great interest. We look forward to comparing their predictions to our data, both in the total and differential cross sections.

For each Q^2 bin, the peak cross section extracted from the fit can be used to extract $A_{1/2}$ with the assumption that $S_{1/2}$ is small. Consistent with PDG [1] and Armstrong, *et al.* [3], a value of the full width of 150 MeV and an $S_{11} \to \eta N$ branching fraction of 0.55 were used. The results of this measurement of $A_{1/2}$ are shown in Figure 4 along with some previous results converted to be consistent with our choice of Γ and b_η.

3 Preliminary results from the second data run

There have been additional runs of this experiment since the published data were collected. The second running period occurred in February and March of 1999. We are now analyzing those data. This will be the basis of the thesis of Haluk Denizli. With these new data we are able to measure $A_{1/2}$ for $0.13 < Q^2 < 3.2$ GeV^2. Higher energy data already taken, and yet to be taken, will allow this to be extended to even higher Q^2. As an indication of the improvement expected, the results from the first data run were based on only 60K η events. In the data samples we are analyzing from the second run, we have in excess of 600K η events. Preliminary results from our fits to angular

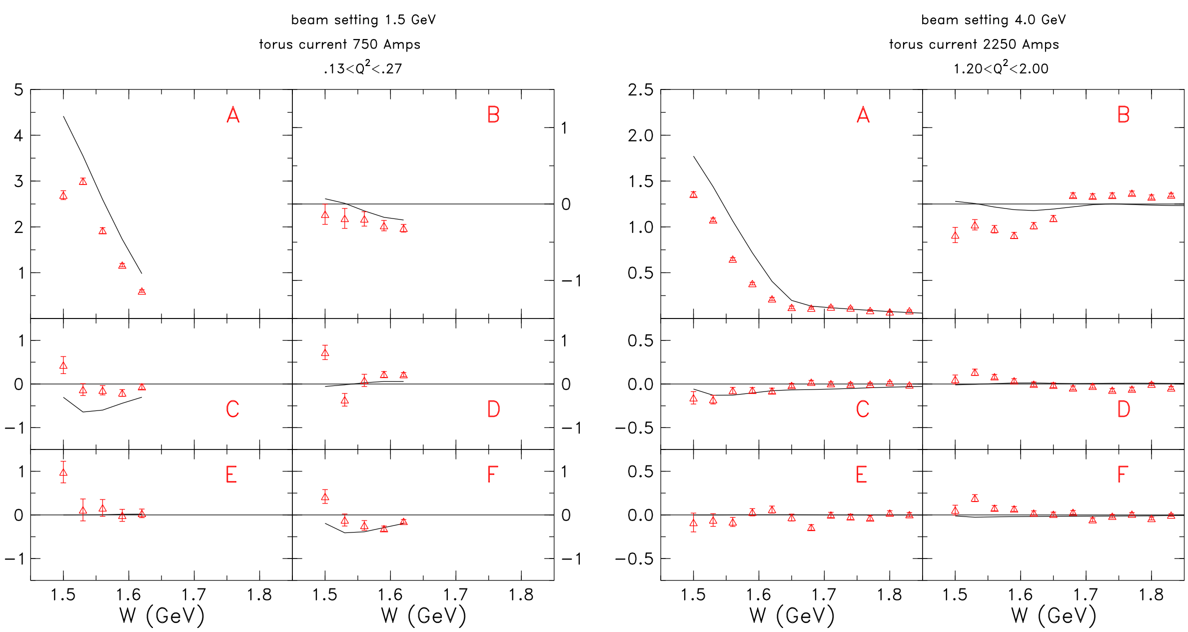

Figure 3: The results of the fit to the differential cross section using Equation 1. The plots on the left are for $Q^2 = 0.2$ GeV^2. Only statistical errors are shown and the data have not been corrected for radiative effects. The solid curve is derived from the new calculations of the ETA-MAID program [8].

Figure 4: Values of the photon coupling amplitude, $A_{1/2}$ obtained from the integrated cross sections compared to previous experiments and selected calculations. The "New CLAS data" include statistical errors only. The previous results have been converted to use consistent choices for the full width of the $S_{11}(1535)$ and the partial width into η. Four theoretical predictions are shown as well.

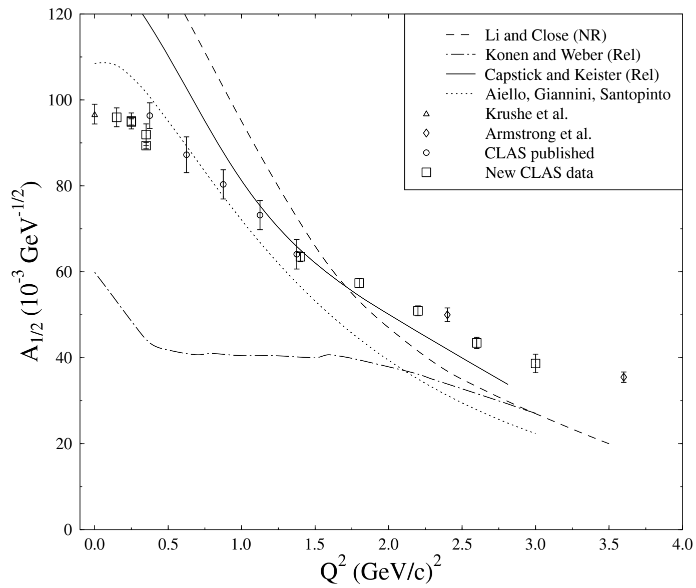

distributions are shown in Figure 3. Although these results only include statistical errors and have not yet been corrected for radiative effects, one can already see some interesting features. The data at $Q^2 = 1.6$ GeV^2 show trends similar to what we had already observed at $Q^2 = 0.75$ GeV^2. In particular, the rapid change from backward to forward peaking shown by the B parameter is still evident at this higher Q^2, and is not reproduced well by the ETA-MAID calculation [8]. For our lowest Q^2 bin ($Q^2 = .2$ GeV^2), the agreement with ETA-MAID is more reasonable. This is not surprising, since this model was tuned on the existing photoproduction measurements, while only the Q^2 evolution of $A_{1/2}$ for the $S_{11}(1535)$ was adjusted to match the electroproduction experiments. When we complete the analysis of these data, it will be interesting to see models can be readjusted to match the data more closely. It is also interesting to note that in this low Q^2, ETA-MAID predicts a measurable value for R_{TT}, in agreement with our measurement for the parameter F.

As was done in the published analysis, we bin the data more finely in Q^2 and extract values of $A_{1/2}$ for the $S_{11}(1535)$ from the total cross section. These are shown in Figure 4 along with values extracted from previous data. The data give a consistent picture, confirm our previous results and connect well to both the data of Armstrong *et al.* [3], and Krusche *et al.* [10]. It is clear that after this current data is analyzed, the experimental part of determining $A_{1/2}$ for the $S_{11}(1535)$ will be well under control for $Q^2 < 3$ GeV^2. The exact normalization of $A_{1/2}$ depends on the choice of parameters for the contributing resonances, however the *shape* is much less model dependent and is well determined. More detailed theoretical calculations are required to better determine absolute values of $A_{1/2}$ and estimate the model dependence of those values.

Four theoretical calculations [11,12] within the Constituent Quark Model are superimposed on the plot. Two of these are nonrelativistic, while the other two include features of relativity in the photon absorption and the 3-quark wave function. These are not the only theoretical predictions for $A_{1/2}$, but they give some indication of the range of models. The prediction of Aiello, Giannini, and Santopinto [12], gives the best agreement with our data, although even it falls off more rapidly with Q^2 than the data.

4 Conclusions

New preliminary results on η electroproduction from CLAS confirm our earlier published results. Structure seen above the $S_{11}(1535)$ both in the total cross section, and in the term in the partial wave analysis of the published work, is evident in the higher Q^2 regions of the more recent data. New measurements of $A_{1/2}$ for the $S_{11}(1525)$ agree with our previous work [5]. They also agree with the photoproduction experiments [10] and the high Q^2 data of Armstrong *et al.* [3] when analyzed with consistent assumptions. We hope to have final results based on this data by spring 2002.

References

[1] D.E. Groom *et al.*, Eur. Phys. J. **C15**, 1 (2000).

[2] F. Brasse *et al.*, Z. Phys. C**22**, 33 (1984). H. Breuker *et al.*, Phys. Lett **74B**, 409 (1978). F. Brasse *et al.*, Nucl. Phys. **B139**, 37 (1978). P. Kummer *et al.*, Phys. Rev. Lett. **30**, 873 (1973). U. Beck *et al.*, Phys. Lett **51B**, 103 (1974). J. Alder *et al.*, Nucl. Phys. **B91**, 386 (1975).

[3] C. S. Armstrong *et al.*, Phys. Rev. D**60**, 052004 (1999).

[4] W. Brooks, Nucl. Phys. **A663-664**, 1077 (2000).

[5] R. Thompson *et al.* Phys. Rev. Lett. **86**, 1702 (2001).

[6] G. Knochlein, D. Drechsel and L. Tiator, Z. Phys. **A352**, 327 (1995); L. Tiator, C. Bennhold, and S.S. Kamalov, Nucl. Phys. **A580**, 455 (1994).

[7] R. Renard *et al.* arXiv:hep-ex/0011098 (2000).

[8] W-T.Chiang *et al.*, arXiv:nucl-th/0110034 (2001)..

[9] B. Saghai, Z.-P. Li, Eur. Phys. J. **A11**, 217 (2001).

[10] B. Krusche *et al.*, Phys. Rev. Lett. **74**, 3736 (1995).

[11] Z. Li and F. Close, Phys. Rev. D**42**, 2207 (1990). W. Konen and H. J. Weber, Phys. Rev. D**41**, 2201 (1990). S .Capstick and B. D. Keister, Phys. Rev. D**51**, 3598 (1995).

[12] M. Aiello, M.M. Giannini, and E. Santopinto, J. Phys. G **24**, 753 (1998).

Pion-nucleon charge exchange measurements at low energy

M. E. Sadler, for the Crystal Ball Collaboration[1]

Department of Physics, Abilene Christian University, Abilene, TX 79699 U.S.A.

(Received: 31 October 2001)

An update is presented of measurements of pion-nucleon charge-exchange scattering taken with the Crystal Ball detector at Brookhaven National Laboratory. The present data are absolute differential cross sections at 150–350 MeV/c. A planned experiment will extend the measurements to even lower momenta.

1 Introduction

The differential cross section results reported here for $\pi^- p \to \pi^0 n$ were taken in 1998 by the new Crystal Ball Collaboration[1] at the Alternating Gradient Synchrotron (AGS) at Brookhaven National Laboratory. These data will complement differential-cross-section data for $\pi^\pm p \to \pi^\pm p$ and analyzing-power data for all three reactions 1) to investigate isospin invariance in the πN system, 2) to determine better the isospin-odd s-wave scattering length, 3) to extrapolate scattering amplitudes to the non-physical region (e.g., for determinations of the πN σ term), and 4) to perform more accurate evaluations of the πNN coupling constant, the mass splitting of the $P_{33}(1232)$ resonance and the up-down quark mass difference.

2 Discussion

A description of the Crystal Ball, the other experimental apparatus, and the analysis procedures is included in previous MENU proceedings [1, 2]. The new charge exchange data from 150 to 350 MeV/c will approximately equal the number of published data points in quantity and be of superior quality. A full angular distribution is measured simultaneously, decreasing the systematic errors involved in utilizing a small-acceptance neutral meson spectrometer at various positions. Measurement of the energy and direction of the photons from π^0 decay eliminates the need for neutron detectors used by most previous experiments. Accurate determination of the absolute neutron detection efficiency has been a problem in these measurements.

Recent attention has been devoted to evaluating the systematic errors that affect our results. The acceptance for detecting a π^0 at a given angle is obtained from a GEANT Monte Carlo simulation of the $\pi^- p \to \pi^0 n$ reaction. The photons from π^0 decay are propagated through the liquid hydrogen target, target walls and supports, beam pipe, veto barrel scintillator, and into the Crystal Ball. The photon may convert in any of these materials and may result in sufficient energy being deposited into the veto system to reject the event. Evaluation of this effect requires an accurate determination of the threshold energy in the veto counters that were utilized to reject

[1]The new Crystal Ball Collaboration consists of A. Barker, C. Bircher, B. Draper, C. Carter, M. Daugherity, S. Hayden, J. Huddleston, D. Isenhower, J. Qualls, C. Robinson and M. Sadler,*Abilene Christian University*, C. Allgower, R. Cadman and H. Spinka, *Argonne National Laboratory*, J. Comfort, K. Craig and A. Ramirez, *Arizona State University*, T. Kycia (deceased), *Brookhaven National Laboratory*, M. Clajus, A. Marusic, S. McDonald, B. M. K. Nefkens, N. Phaisangittisakul, S. Prakhov, J. Price, A. Starostin and W. B. Tippens, *University of California at Los Angeles*, J. Peterson, *University of Colorado*, W. Briscoe, A. Shafi and I. Strakovsky *George Washington University*, H. Staudenmaier, *Universität Karlsruhe*, D. M. Manley and J. Olmsted, *Kent State University*, D. Peaslee, *University of Maryland*, V. Abaev, V. Bekrenev, N. Kozlenko, S. Kruglov, A. Kulbardis, and I. Lopatin, *Petersburg Nuclear Physics Institute*, N. Knecht, G. Lolos and Z. Papandreou, *University of Regina*, I. Supek, *Rudjer Boskovic Institute* and A. Gibson, D. Grosnick, D. D. Koetke, R. Manweiler and S. Stanislaus, *Valparaiso University*, H. Calen, A. Kupse, T. Johanson and U. Wiedner, *Uppsala University*.

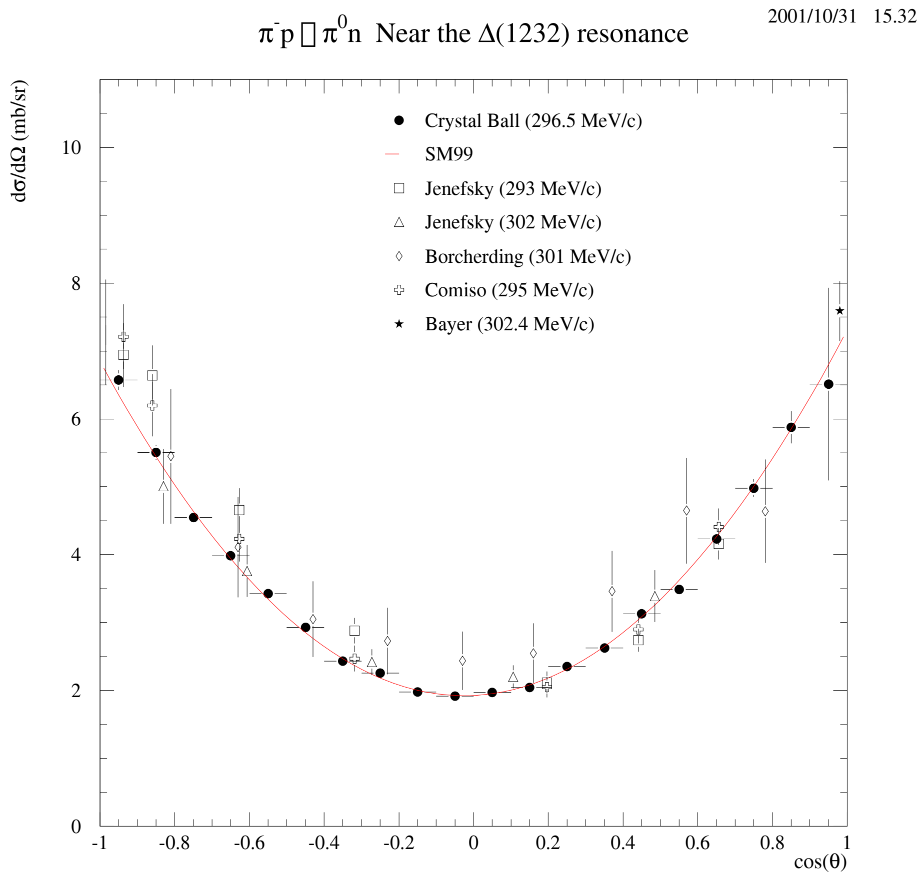

Figure 1: Preliminary results at 296.5 MeV/c compared with existing data at nearby momenta. Only statistical errors are included for the Crystal Ball data.

charged-particle events.

Other significant effects at low momenta are the decay, energy loss, and multiple scattering of the π^- beam. A beam Monte Carlo program has been developed to evaluate such effects as 1) pion decay into a muon that may pass time-of-flight cuts used for determining the pion fraction at the target (a few percent effect), 2) the actual average beam momentum at the center of the target, and 3) the fraction of the beam that satisfies the trajectory criteria through the beam counters but misses the target due to multiple scattering in air and the beam elements.

A systematic calibration of the beam momentum was also done, made possible by the excellent energy resolution of the Crystal Ball. An overall gain factor was adjusted for both data and Monte Carlo events to obtain the correct invariant mass for the π^0. The central beam momentum for the data was then adjusted to produce the same neutron missing mass as in the Monte Carlo. This procedure resulted in lowering the previously reported momenta, typically by about 2 MeV/c.

Preliminary data at 296.5 MeV/c are shown in Figure 1. The GWU SM99 [3] phase shift solution agrees very well with these data over the full angular range, as expected at this momentum since the scattering amplitude is dominated by the well-known $\Delta(1232)$ resonance. Also shown are previous data [4–7] at nearby momenta. Preliminary reults at five momenta below and one momentum above the $\Delta(1232)$ are shown in Figure 2.

A thinner target is needed to extend these measurements to lower momenta. Other modifications are also desired, such as placing the final beam counter closer to the target to reduce beam

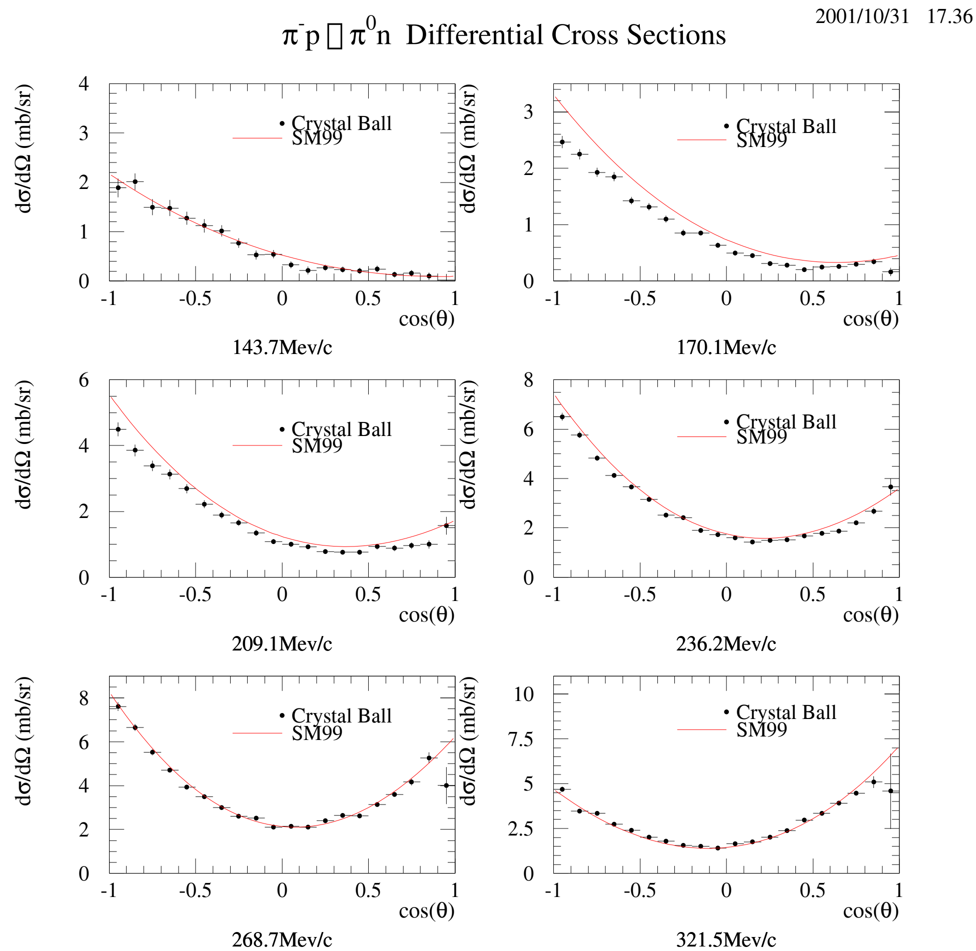

Figure 2: Preliminary results at momenta below and above the Δ resonance.

losses due to multiple scattering. An experiment [8] has been approved at the BNL AGS to make these measurements.

Acknowledgments: This work supported in part by US DOE, NSF, NSERC, Russian Ministry of Sciences and Volkswagen Stiftung.

References

[1] M.E. Sadler, Proc. of the Seventh Int. Conf. on Meson-Nucleon Physics and the Structure of the Nucleon, πN Newsletter **13**, 123 (1997).

[2] M.E. Sadler, Proc. of the Eighth Int. Conf. on Meson-Nucleon Physics and the Structure of the Nucleon, πN Newsletter **15**, 25 (1999).

[3] R.A. Arndt, *et al.*, Phys. Rev. **C52**, 2120 (1985). The PWA solutions presented were obtained from http://gwdac.phys.gwu.edu/.

[4] R.F. Jenefsky, *et al.*, Nucl. Phys. **A290**, 407 (1977).

[5] F.O. Borcherding, UCLA Thesis (1982).

[6] J.C. Comiso, *et al.*, Phys. Rev. **D12**, 738 (1973).

[7] W. Bayer, *et al.*, Nucl. Inst. and Meth. **134**, 449 (1976).

[8] AGS Experiment 958, J. Comfort and M. Sadler, cospokespersons, 20 October 2000.

Short-range contributions to eta-meson production near threshold

D. O. Riska[a] and M. T. Peña[b]

[a]*Helsinki Institute of Physics, POB 64, 00014 University of Helsinki, Finland,*
[b]*Departamento de Física and CFIF, IST-Instituto Superior Técnico, 1096 Lisboa, Portugal*

(Received: 3 September 2001)

The two-nucleon amplitudes, which are associated with the short range components of the nucleon-nucleon interaction contribute significantly to the cross section for the reaction $pp \to pp\eta$ near threshold. This result is analogous to the corresponding situation in the reaction $pp \to pp\pi^0$. The magnitude of the short range contributions is as large as that due to the conventional meson exchange mechanisms, which involve excitation of intermediate $N(1535)$ resonances. The most important of the short range contributions may be described as a renormalization of the axial charge operator of the nucleon in the two-nucleon system.

1 The $pp\eta$ coupling constant

The recent precision measurements of the cross section for $pp \to pp\eta$ near threshold, where S-wave production dominates [1, 2], should provide the necessary information on the two-nucleon mechanisms that govern the reaction. A key parameter in reaction amplitude is the $pp\eta$ coupling constant, which is still very poorly known.

The combination of spontaneously broken chiral symmetry and SU(3) flavor symmetry suggests that the coupling of the nucleons to the octet of light pseudoscalar mesons have the form

$$\mathcal{L}_{NNM} = i\frac{g_A}{2f_M}\bar{\psi}\gamma_5\gamma_\mu\partial_\mu M_a\lambda_a\psi \ , \tag{1}$$

where m_a is the octet (π, K, η) meson field and f_M is the decay constant. Empirically $f_\pi = 93$ MeV and f_η =112 MeV, so SU(3) flavor symmetry is a fairly good approximation for the decay constants.

The extended Goldberger-Treiman relation then gives the effective pseudovector coupling constants as

$$f_{\pi NN} = \frac{m_\pi}{2f_\pi}g_A \simeq 0.95 \ , \tag{2}$$

$$f_{\eta NN} = \sqrt{3}\frac{m_\eta}{2f_\eta}g_A \simeq 1.8 \ , \tag{3}$$

with $g_A = 1.267$. The corresponding pseudoscalar coupling constants are then

$$g_{\pi NN} = \frac{2m_N}{m_\pi}f_{\pi NN} = 12.8 \ , \tag{4}$$

$$g_{\eta NN} = \frac{2m_N}{m_\eta}f_{\eta NN} = 6.2 \ . \tag{5}$$

The value (5) is not much different from the value $g_{\pi NN}/\sqrt{3} = 7.4$, which would obtain with naive pseudoscalar coupling. The value for $f_{\pi NN}$ (2) is close to that (0.97) found with potential model fits to restricted phase shift analysis [3].

While the uncertainty in the value of the πNN coupling constant is small, that in the value of the ηNN coupling constant is very large. Comprehensive analyses of the data on η photoproduction on the nucleon indicates e.g., that the pseudoscalar coupling constant cannot exceed the value

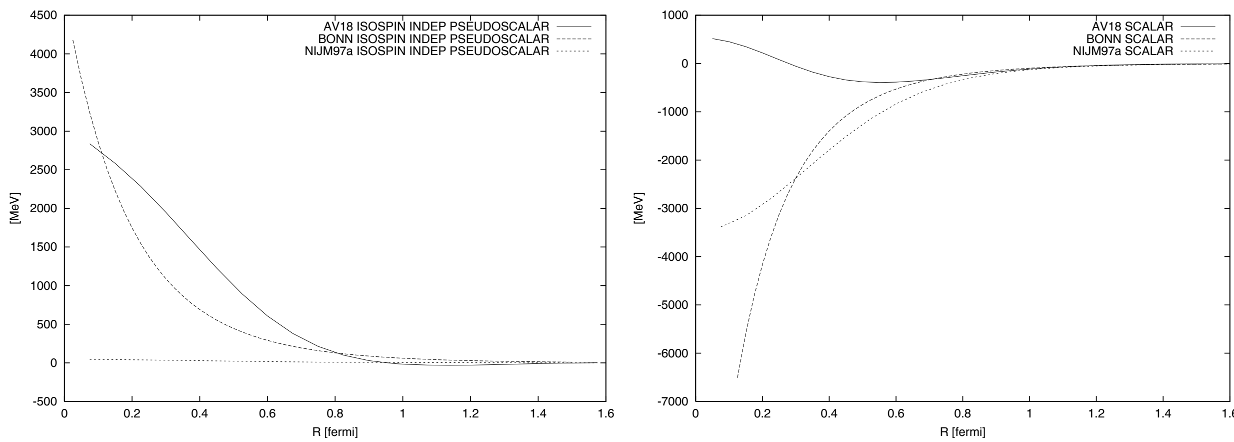

Figure 1: The isospin independent pseudoscalar (left) and scalar (right) components of the V18 [7], Bonn boson exchange [8] and Nijmegen 97a [9] potentials.

$g_{\eta NN} = 2.2$ by any appreciable amount [5]. This limiting value in fact coincides with the value used in the calculation based on the scattering length approximation for the ηN rescattering amplitude in Ref. [6].

All realistic phenomenological interaction nucleon-nucleon interaction models contain an isospin independent pseudoscalar exchange component, which may be interpreted as arising from η–meson exchange and shorter range exchange mechanisms with the quantum numbers of the η–meson. This components may be calculated approximately from the conventional isospin-independent interaction components as

$$v_P(r) = \frac{1}{4}v_C(r) - \frac{1}{2}m^2\int_r^\infty dr'r'v_{LS}(r') + 12m^2\int_r^\infty dr'r'\int_{r'}^\infty dr''\frac{v_T(r'')}{r''} - \frac{1}{4}v_{SS}(r). \qquad (6)$$

Here v_C, v_{LS}, v_T and $v_{SS}(r)$ are the central, spin-orbit, tensor and spin-spin interaction components respectively.

This potential component is shown in Fig. 1 for the V18 [7], Bonn boson exchange [8] and Nijmegen 97a [9] interaction models. The Paris potential [10] is similar in strength to the Bonn and V18 potentials. The volume integrals of these interactions provide a measure of the strength of their $\eta-$exchange component. If this is equated to $g^2_{\eta NN}/m^2$, the "effective" value of $g_{\eta NN}$ comes out as 7.4 for both the V18 and the Bonn boson exchange potentials but only as 1.8 for the Nijmegen 97a interaction. The former values equal that of pseudoscalar coupling, and is close to the value (5), whereas the latter is in line with what is required by η–meson photoproduction.

2 Rescattering mechanisms in $pp \to pp\eta$

With reasonably small values for $g_{\eta NN}$ the single nucleon production amplitude leads to very small values for the cross section for the reaction $pp \to pp\eta$, which fall far below the empirical values. The calculation of the matrix element requires knowledge of the initial $^3P_0$ scattering state above the energy range, where quantitative potential models apply. A simple ansatz for ths state is to use a distorted plane wave approximation extrapolated to the relevant energy range [11].

The conventional model for describing the cross section for η–meson production near threshold involves excitation of intermediate N(1535) resonances, which couple strongly to the ηN system [Fig. 2(a)]. This may either be based on an explicit resonance model or on phenomenological fits to the $\pi N \to \eta N$ amplitude. A recent calculation of the π and η rescattering amplitude based on the

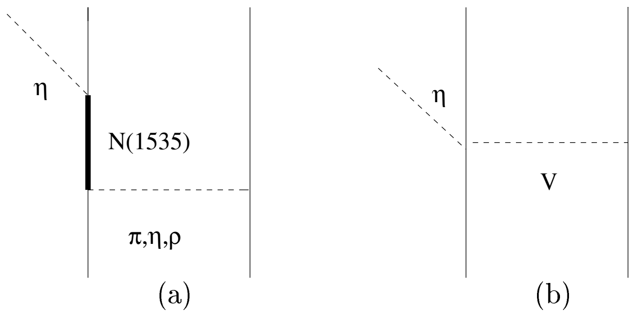

Figure 2: (a) Rescattering mechanisms involving the N(1535) resonance, (b) short range exchange mechanisms associated with the NN interaction.

latter method, with input from Refs. [12] leads to a cross section for the reaction $pp \to pp\eta$ [13] that falls more than an order of magnitude below the empirical values. Inclusion of ρ–meson exchange, with the $\rho NN(1535)$ coupling given by the quark model [14] increases the calculated cross section for $pp \to pp\eta$ by a factor ~ 3, although it remains far below the empirical values. The ρ–meson exchange mechanism is more important than pion exchange, and by itself is favored by the empirical ratio of the cross sections for $pp \to pp\eta$ and $pn \to pn\eta$ [15].

3 Short range exchange mechanisms in $pp \to pp\eta$

The contributions to the axial exchange charge operator that is associated with the short-range components of the nucleon-nucleon interaction have been derived in Refs. [16, 17]. These contributions are derived as the nonrelativistic limit of the nonsingular part of the axial current 5-point function with external leg couplings. In the case of non-derivative couplings such terms only arise from the negative energy poles in the nucleon propagator and are therefore commonly illustrated by the nucleon-antinucleon "pair currents" Feynman diagrams [Fig. 2(b), where the rescattering vertex has an intermediate negative energy state].

Because of the derivative pseudovector coupling for both the π and the η, no such two-nucleon operators contribute to the η production operator in the reaction $pp \to pp\eta$, which would be directly associated with the π- and η- exchange components of the nucleon-nucleon interaction. The isospin independent effective scalar and vector exchange components of the nucleon-nucleon interaction do however give rise to two-nucleon meson production operators. A key point is that these operators are completely determined by the interaction model, and involve no parameters that are not already present in the NN interaction, besides the overall η-nucleon coupling.

The isospin independent scalar exchange contribution to the two-nucleon η-production amplitude may moreover be derived directly, without reference to the 5-point function, in the following way. Consider the isospin independent scalar exchange component of the nucleon-nucleon interaction, which is proportional to the scalar Fermi invariant "S". To second order in v/c, this interaction takes the form

$$v_S^+(r)S = v_S^+(r)\left(1 - \frac{\vec{p}^{\,2}}{m_N^2}\right) - \frac{1}{2m_N^2}\frac{\partial v_S^+}{r\partial r}\vec{S}\cdot\vec{L}\ , \tag{7}$$

where $v_S^+(r)$ is a scalar function. To lowest order in v/c this function may be expressed in terms of the conventional potential components as [cf. (6)]

$$\begin{aligned} v_S^+(r) = {} & \frac{3}{4}v_C(r) + \frac{m^2}{2}\int_r^\infty dr r' v_{LS}(r') + \frac{1}{4}\left[3\int_r^\infty dr' \frac{v_T(r')}{r'} - v_T(r')\right] \\ & + \frac{1}{4}v_{SS}(r) + \frac{m^2}{4}\left[3\int_r^\infty dr' r' v_{LS2}(r') - r^2 v_{LS2}(r)\right]. \end{aligned} \tag{8}$$

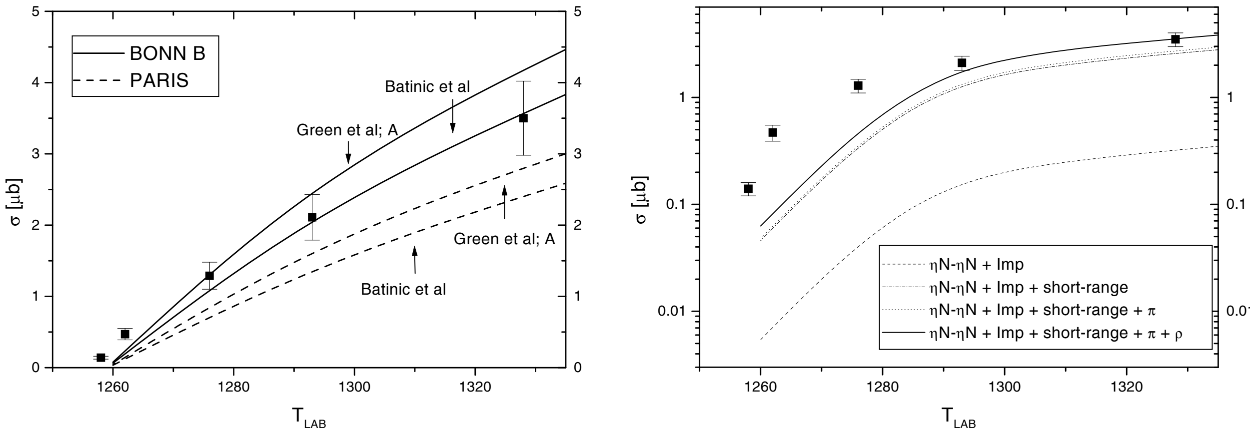

Figure 3: The cross section of the reaction $pp \to pp\eta$ near threshold. The data points are from Ref. [1]. Left: Calculations with the Bonn [18] (straight lines) and Paris [10] (dashed lines) potentials. The curves Batinic *et al.* and Green *et al.* refer to the models for the amplitude $\eta N \to \eta N$ given in Refs. [11] and [20], respectively. Right: Contributions of the short range mechanisms to the cross section using the Bonn B interaction. The effect of including the π– and ρ–meson exchange contributions are shown explicitly. From Ref. [13].

The $\vec{p}^{\,2}/m^2$ term in the spin-independent part of the interaction (7) may be combined with the kinetic energy term in the nuclear Hamiltonian, by replacing the nucleon mass by the effective "mass operator"

$$m^*(r) = m_N \left[1 + \frac{v_S^+(r)}{m_N}\right] \ . \tag{9}$$

The form of the scalar potential $v_S^+(r)$ is shown in Fig. 1 as obtained from the same phenomenological potential models as $v_P(r)$.

To first order in $v_S^+(r)$, the scalar component of the nucleon-nucleon interaction therefore implies the following two-body "correction" to the single nucleon η production operator:

$$T = \frac{v_S^+(r)}{m_N} T_1(S) + (1 \to 2) \ . \tag{10}$$

Here the spin-operator in $T_1(S)$ is implicitly assumed to be that of nucleon 1 of the interacting pair of nucleons. This operator coincides in form with the scalar exchange operator derived in Ref. [16]. The corresponding momentum space expression is

$$T(S) = -i f_{\eta NN} \frac{\omega_\eta}{m_\eta} \frac{v_S^+(\vec{k}_2)}{m_N} \vec{\sigma}^1 \cdot \vec{v}_1 + (1 \leftrightarrow 2) \ . \tag{11}$$

Here $v_S^+(k)$ is the Fourier transform of the scalar potential $v_S^+(r)$ and $\vec{v}_1 = (\vec{p}_1 + \vec{p}_1^{\,\prime})/2m_N$. This operator is completely determined by the nucleon-nucleon interaction model. Note that because the volume integral of the scalar exchange interaction is negative in all realistic nucleon-nucleon potentials, this exchange current contribution implies an enhancement of the cross section over the value given by the single nucleon pion production mechanism.

The expressions for the isospin-independent and isospin dependent vector exchange contributions to the axial charge operator as derived from the 5-point function are more complicated and have been given in Ref. [16].

In Fig. 3 the calculated cross section for the reaction $pp \to pp\eta$ near theshold is shown as obtained in Ref. [13] with inclusion of the short range exchange contribution based on the "Bonn B" nucleon-nucleon interaction model [18]. The result of adding the $\pi-$ and ρ–meson exchange contributions are also shown. In the figure the results are shown as obtained both with the Bonn [18] and Paris [10] potential models. In addition the sensitivity to the model for the ηN rescattering amplitude is shown, by giving the results for the different models in refs. [11, 20].

These results demonstrate the relative importance of the short range contribution to the meson production mechanism. It is analogous to that found to be of crucial importance for the near threshold cross section for the reaction $pp \to pp\pi^0$ [17]. They also show that the contribution from the short range mechanisms is as large as the conventionally considered rescattering mechanisms that involve intermediate nucleon resonances (see also [21]).

4 The effective axial charge operator

The production of $S-$wave pseudoscalar mesons is governed by the axial charge operator of the target system. This operator obtains a substantial two-nucleon pion exchange contribution, with the isospin structure $\vec{\tau}^1 \times \vec{\tau}^2$ [22]. Because of this isospin dependence this operator does not contribute to the reaction $pp \to pp\eta$ nor to $pp \to pp\pi^0$. As a consequence the short range contribution to the two-nucleon mechanism, considered above, is of dominant significance. This short range term also provides part of the explanation for the large enhancement of the axial charge of the nucleon seen in first forbidden $\beta-$transitions in heavy nuclei [23]. It also has an interesting analogy in heavy quark systems, where the scalar confining interaction replaces the attractive scalar field between nucleons in nuclei [24].

Acknowledgments: Research supported in part by the Academy of Finland through grant No. 43982, and by the Foundation for Science and Technology in Portugal through grants PRAXIS/P/FIS/10031/1998, CERN/P/FIS/40135/2000.

References

[1] H. Calén *et al.*, Phys. Lett. **B366**, 30 (1996).
[2] J. Smyrski *et al.*, Phys. Lett. **B474**, 182 (2000).
[3] V.G.J. Stoks, R. Timmermans and J.J. de Swart, Phys. Rev. C **47**, 512 (1993).
[4] L. Tiator, C. Bennhold and S.S. Kamalov, "Physics with GeV-Particle Beams", H. Machner and K. Sistemich, eds., p. 112 (World Scientific, Singapore, 1995).
[5] L. Tiator, C. Bennhold and S.S. Kamalov, Nucl. Phys. **A580**, 455 (1994).
[6] V. Bernard, N. Kaiser and U.-G. Meissner, Eur. J.Phys. **A4**, 259 (1999).
[7] R.B. Wiringa, V.G.J. Stoks and R. Schiavilla, Phys. Rev. C **51**. 38 (1995).
[8] R. Machleidt, K. Holinde and Ch. Elster, Phys. Rept. **149**, 1 (1987).
[9] V.G.J. Stoks and T.A. Rijken, Phys. Rev. C **59**, 3009 (1999).
[10] M. Lacombe *et al.*, Phys. Rev. C **21**, 861 (1980).
[11] M. Batinić, A. Švarc and T.-S.H. Lee, Physica Scripta **56**, 321 (1997).
[12] H. Garcilazo and M.T. Peña, Phys. Rev. C **61**, 064010 (2000); H. Garcilazo and M.T. Peña, Phys. Rev. C **C59**, 2389 (1999).
[13] M.T. Peña, H. Garcilazo, D.O. Riska, Nucl. Phys.**A683**, 322 (2001).
[14] D.O. Riska and G.E. Brown, Nucl. Phys. **A679**, 577 (2001).
[15] G. Fäldt and C. Wilkin, nucl-th/0104081.
[16] M. Kirchbach, D.O. Riska and K. Tsushima, Nucl. Phys. **A542**, 616 (1992).
[17] T.-S.H. Lee and D.O. Riska, Phys. Rev. Lett. **70**, 2237 (1993).

[18] R. Machleidt, Adv. Nucl. and Part. Phys., **19**, 189 (1989).
[19] M. Batinić *et al.*, Phys. Rev. **C51**, 2310 (1995).
[20] A.M. Green and S. Wycech, Phys. Rev. **C55**, R2167 (1997) Phys. Rev. **C60**, 035208 (1999).
[21] M.T. Peña, D.O. Riska and A. Stadler, Phys. Rev. **C60**, 045201 (1999).
[22] K. Kubodera, J. Delorme and M. Rho, Phys. Rev. Lett. **40**, 755 (1978).
[23] E.K. Warburton, Phys. Rev. Lett. **66**, 233 (1991).
[24] K.O.E. Henriksson, T.A. Lähde, C.J. Nyfält and D. Riska, Nucl. Phys. **A686**, 355 (2001).

Multichannel analyses of $\overline{K}N$ scattering

D. Mark Manley

Center for Nuclear Research, Department of Physics,
Kent State University, Kent, OH 44242-0001, U.S.A

(Received: 12 September 2001)

The first multichannel analyses of $\overline{K}N$ scattering were carried out in the early 1970s at c.m. energies below about 1900 MeV where data were available from bubble-chamber experiments. In 1998, precise data on several $\overline{K}N$ reactions including $K^-p \to \pi^0\Lambda$, $K^-p \to \pi^0\Sigma^0$, and $K^-p \to \eta\Lambda$ were measured at the BNL AGS by the Crystal Ball Collaboration. It is therefore timely to consider a new multichannel partial-wave analysis incorporating these new data. Incipient work along these lines is described.

1 Introduction

Data for πN scattering and pion photoproduction have been analyzed extensively by the method of partial-wave analyses (PWAs). These analyses have provided accurate amplitudes from which the properties of many N^* resonances have been deduced. It is likewise important to obtain reliable amplitudes for $\overline{K}N$ scattering in order to identify the full spectrum of Y^* resonances, and to deduce the properties of these resonances to test quark-model predictions. Although useful information about resonances in the $\overline{K}N$ system was determined by early single-channel analyses, the focus of this article is the full coupled-channel problem.

The first multichannel analyses [1–3] were carried out in the early 1970s and mainly incorporated data obtained from bubble-chamber experiments. In 1971, Kim *et al.* [1] carried out an energy-dependent PWA using effective-range expansions to fit data over seven intervals in the center-of-mass (c.m.) energy range 1430 to 1890 MeV. The solutions obtained in this analysis suffered from unphysical cusplike behavior. In 1972, Langbein and Wagner [2] performed an energy-independent PWA of data in the c.m. energy range 1540 to 1900 MeV using a traditional K-matrix approach. Their single-energy solutions did not vary smoothly with energy. In 1973, Lea *et al.* used a traditional K-matrix approach to perform an energy-dependent PWA over the c.m. energy range 1540 to 1880 MeV. They made several simplifying assumptions, including taking the partial widths for $\overline{K}N$, $\pi\Lambda$, and $\pi\Sigma$ to be constants. Their solution was later found to be incompatible with the precise data for $K^-p \to \overline{K^0}n$ measured in 1977 by Alston-Garnjost *et al.* [4].

In 1977, Gopal *et al.* [5] obtained energy-dependent solutions for $\overline{K}N$, $\pi\Lambda$, and $\pi\Sigma$ in the c.m. range 1480 to 2170 MeV by first fitting the three channels in parallel and then considering them together to find solutions with consistent parameters (masses and widths) for the resonances in each channel. In this analysis, the pure-isospin T-matrix amplitudes were assumed to have the form $T = T_{\rm B} + T_{\rm R}$, where the first and second terms describe background and resonant contributions, respectively. Such a form generally violates unitarity. These authors also parametrized the angular momentum barriers inconsistently for different partial waves. Nevertheless, their solution was generally in reasonable agreement with the precise data for $K^-p \to \overline{K^0}n$ measured by Alston-Garnjost *et al.* [4].

Another energy-dependent PWA published in 1977 was that of Martin and Pidcock [6], who used a conventional K-matrix approach to analyze $\overline{K}N$, $\pi\Lambda$, and $\pi\Sigma$ over the c.m. energy range 1540 to 2000 MeV. Their analysis used an improved treatment of the $\eta\Lambda$ and $\eta\Sigma$ thresholds compared with prior analyses. In this analysis, all channels other than $\overline{K}N$, $\pi\Lambda$, and $\pi\Sigma$ were represented, except for S waves, by a single super channel for a given partial wave.

2 Recent measurements and analyses

In 1998, precise data on several $\overline{K}N$ reactions including $K^-p \to \pi^0\Lambda$, $K^-p \to \pi^0\Sigma^0$, and $K^-p \to \eta\Lambda$ were measured at the Brookhaven National Laboratory AGS by the Crystal Ball Collaboration.[1] A new AGS experiment to study specific Y^* resonances with higher precision has been approved [7]. To take advantage of these data, it is timely to begin a new multichannel partial-wave analysis of $\overline{K}N$ reactions. As a first step along these lines, a coupled-channel analysis of S-wave scattering was recently completed over the c.m. energy range 1500 to 1900 MeV [8]. This analysis extracted resonance parameters for the $\Lambda(1670)\frac{1}{2}^-$ using, in part, the near-threshold data for $\sigma_{\rm tot}(K^-p \to \eta\Lambda)$ recently measured by the Crystal Ball Collaboration [9]. Results were obtained using a generalization of the well-known multichannel Breit-Wigner representation for T-matrix amplitudes. Our parametrization, described briefly below, has been applied successfully to describe πN elastic and inelastic scattering, including pion photoproduction [10].

2.1 *The Kent State multichannel parametrization*

The partial-wave S-matrix and T-matrix are related by $S = I + 2{\rm i}T = B^{\rm T}R\,B$, where R is unitary and symmetric, and B is unitary. We can write $T = B^{\rm T}\mathcal{T}B + \mathcal{T}_B$, where $\mathcal{T}_B = (B^TB - I)/2{\rm i}$ and $\mathcal{T} = (R - I)/2{\rm i}$. We constructed $\mathcal{T}$ from a K-matrix, $\mathcal{T} = K(I - {\rm i}K)^{-1}$, where

$$K_{ij} = \sum_{\alpha=1}^{N} \tan\delta_\alpha \; f_{i\alpha} f_{j\alpha} \; . \tag{1}$$

The phases δ_α depend on the total c.m. energy W, and N is the number of resonances included in the fit. Here

$$f_{i\alpha} = \frac{g_{i\alpha}}{\sqrt{\Gamma_\alpha(W)}} \qquad ; \qquad (g_{i\alpha})^2 = \Gamma_{i\alpha} \; , \tag{2}$$

where $\Gamma_{i\alpha}$ is the ith partial width for resonance α:

$$\Gamma_\alpha(W) = \sum_i \Gamma_{i\alpha}(W) \qquad \Longrightarrow \qquad \sum_i (f_{i\alpha})^2 = 1 \; . \tag{3}$$

The corresponding resonant T-matrix has matrix elements of the form,

$$\mathcal{T}_{ij} = \sum_{\alpha=1}^{N}\sum_{\beta=1}^{N} f_{i\alpha}\,[\mathcal{D}^{-1}]_{\alpha\beta}\; f_{j\beta} \; . \tag{4}$$

The energy-dependence of the phases δ_α was constructed such that

$$[\mathcal{D}^{-1}(W)]_{\alpha\beta} \propto \prod_{\alpha=1}^{N} \left(M_\alpha - W - {\rm i}\Gamma_\alpha(W)/2\right)^{-1} \; . \tag{5}$$

[1] The Crystal Ball Collaboration consists of: D. Isenhower, M. Sadler (*Abilene Christian University*); C.E. Allgower, H. Spinka (*Argonne National Laboratory*); J.R. Comfort, K. Craig, A.F. Ramirez (*Arizona State University*); M. Clajus, A. Marušić, S. McDonald, B.M.K. Nefkens, N. Phaisangittisakul, S. Prakhov, J.W. Price, A. Starostin, W.B. Tippens (*University of California Los Angeles*); J. Peterson (*University of Colorado*); W.J. Briscoe, A. Shafi, I.I. Strakovsky (*The George Washington University*); H.M. Staudenmaier (*Universität Karlsruhe*); D.M. Manley, J. Olmsted (*Kent State University*); D.C. Peaslee (*University of Maryland*); V.V. Abaev, V. Bekrenev, A.A. Kulbardis, N.G. Kozlenko, S. Kruglov, I.V. Lopatin (*Petersburg Nuclear Physics Institute*); N. Knecht, G. Lolos, Z. Papandreou (*University of Regina*); I. Supek (Rudjer Bošković Institute); D. Grosnick, D.D. Koetke, R. Manweiler, T.D.S. Stanislaus (*Valparaiso University*).

Poles occur at complex energies $W = W_\alpha$ where $M_\alpha - W - \mathrm{i}\Gamma_\alpha(W)/2 = 0$. Here, M_α and $\Gamma_\alpha(M_\alpha)$ are conventional Breit-Wigner parameters. As a special case, if $\alpha = N = 1$, we obtain the well-known result for a single resonance:

$$\mathcal{T}_{ij} = (\mathrm{e}^{\mathrm{i}\delta_\alpha} \sin \delta_\alpha)\ f_{i\alpha} f_{j\alpha} \ . \tag{6}$$

Then

$$[\mathcal{D}^{-1}(W)]_{\alpha\alpha} = \mathrm{e}^{\mathrm{i}\delta_\alpha} \sin \delta_\alpha = \frac{1}{\cot \delta_\alpha - \mathrm{i}} \ . \tag{7}$$

One common choice is

$$\cot \delta_\alpha(W) = \frac{M_\alpha - W}{\Gamma_\alpha(W)/2} \ . \tag{8}$$

The background matrix B was constructed from a product of unitary S matrices, each of which has a form that, when squared, is similar to the multichannel Breit-Wigner representation, but with unphysical pole positions. For attractive (repulsive) backgrounds, the real and imaginary parts of the pole position were taken to be positive (negative). Our background parametrization is unitary, easily allows couplings to be introduced for each channel, maintains proper threshold behavior, and provides a smooth energy dependence (away from thresholds) for real c.m. energies.

2.2 Results for $\Lambda(1670)\frac{1}{2}^-$

As an application of our unitary parametrization, we carried out a multichannel fit over the c.m. energy range 1500 to 1900 MeV. Our fit included near-threshold data obtained with the Crystal Ball at BNL for $\sigma_{\text{tot}}(K^-p \to \eta\Lambda)$. Older, less precise data for σ_{tot} were not included in the fit. We made the reasonable assumption that only the S-wave amplitude makes a significant contribution to σ_{tot} in the near-threshold region. Prior PWAs show that the $\overline{K}N \to \overline{K}N$ and $\overline{K}N \to \pi\Sigma$ S_{01} amplitudes require a large nonresonant background in the vicinity of $\Lambda(1670)$. Most analyses also require a broad $\Lambda(1800)$ to fit data up to 1900 MeV. To accommodate these structures and constrain the $\overline{K}N \to \eta\Lambda$ amplitude, the $\overline{K}N \to \overline{K}N$ and $\overline{K}N \to \pi\Sigma$ S_{01} amplitudes from the

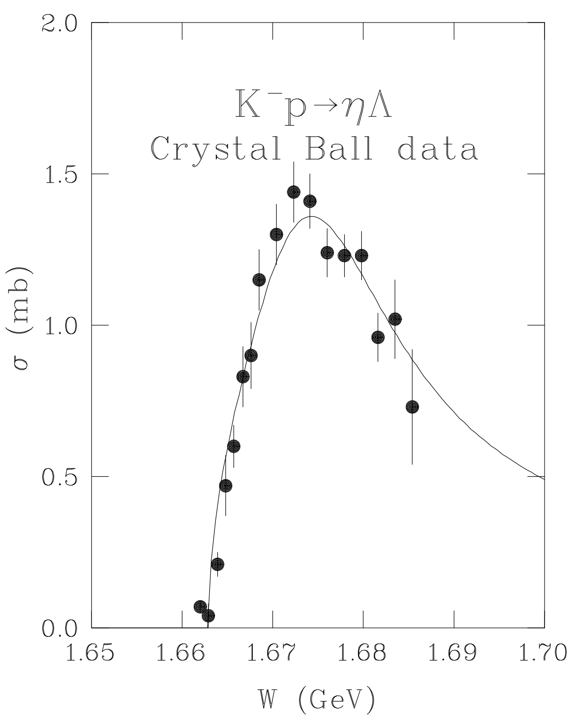

Figure 1: Total cross section for $K^-p \to \eta\Lambda$ as measured by the Crystal Ball Collaboration. The curve shows the result of our multichannel fit.

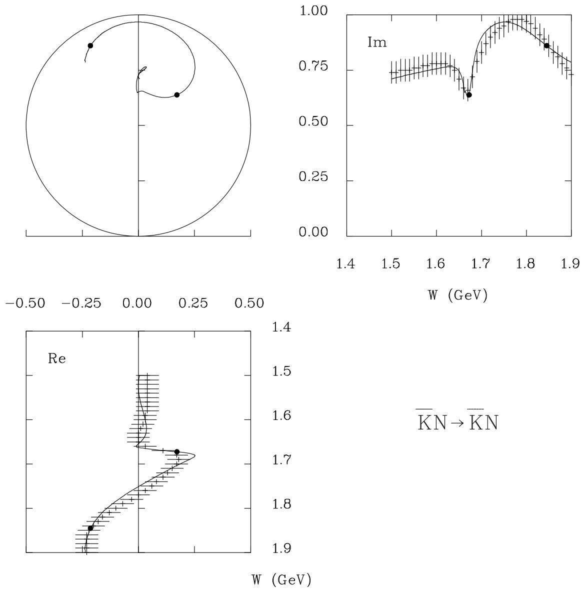

Figure 2: Argand amplitude for the $\overline{K}N \to \overline{K}N$ S_{01} partial wave. The curve shows the result of our multichannel fit. Solid dots mark the energies for the $\Lambda(1670)$ and $\Lambda(1800)$. The data are from the Gopal 77 analysis.

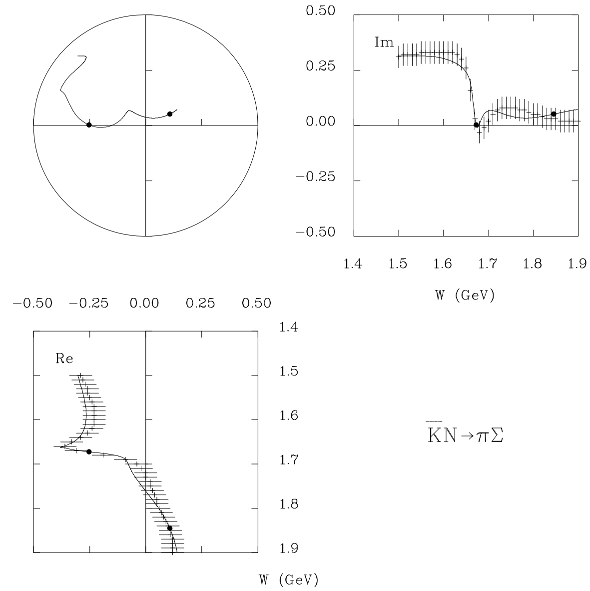

Figure 3: Argand amplitude for the $\overline{K}N \to \pi\Sigma$ S_{01} partial wave. The curve shows the result of our multichannel fit. Solid dots mark the energies for the $\Lambda(1670)$ and $\Lambda(1800)$. The data are from the Gopal 77 analysis.

Gopal 77 solution were included in our fit. We also included the $\overline{K}N \to \pi\Sigma(1385)$ $SD01$ amplitude from the Cameron 78 PWA [11]. Two additional channels were included to satisfy unitarity and account for flux into all other final states. The two added channels were a quasi-two-body $(\pi\pi)_{\mathrm{S}}\Lambda$ channel and a quasi-two-body $(\pi\pi)_{\mathrm{P}}\Sigma$ channel. An uncertainty of ± 0.05 was assigned to the real and imaginary parts of the input amplitudes. Nonresonant background was included in all six channels.

Our best fit has χ^2 per degree of freedom of 1.2 and included the broad $\Lambda(1800)$. The $\Lambda(1405)$, which has $\Gamma \approx 50$ MeV, was outside the energy range of our fit. Figures 1, 2, and 3 show some of the results of our six-channel fit. The corresponding resonance parameters for $\Lambda(1670)$ are summarized in Table 1. In the columns, Γ_i is the partial width for the i-th decay channel evaluated at the resonance energy, x_i is the corresponding branching fraction, $x = 0.37 \pm 0.07$ is the elasticity, and t is the amplitude at resonance excluding contributions from nonresonant background. The fitted Breit-Wigner mass and total width have the values $M = 1673 \pm 2$ MeV and $\Gamma = 23 \pm 6$ MeV, respectively. The corresponding pole position is $(1671 - \mathrm{i}11)$ MeV.

Channel	Γ_i (MeV)	$x_i = \Gamma_i/\Gamma$ (%)	$t = \sqrt{xx_i}$
$\overline{K}N$	8.5 ± 2.6	37.3 ± 6.8	0.37 ± 0.07
$\eta\Lambda$	3.6 ± 1.4	15.7 ± 5.5	0.24 ± 0.04
$\pi\Sigma$	8.8 ± 3.2	38.6 ± 7.9	-0.38 ± 0.03
$\pi\Sigma(1385)$	1.7 ± 1.5	7.6 ± 6.0	-0.17 ± 0.06
$\pi\pi\Lambda$	< 1	< 4	0.05 ± 0.11
$\pi\pi\Sigma$	< 1	< 1	0.00 ± 0.06

Table 1: Resonance parameters for the $\Lambda(1670)$ as determined from our multichannel fit.

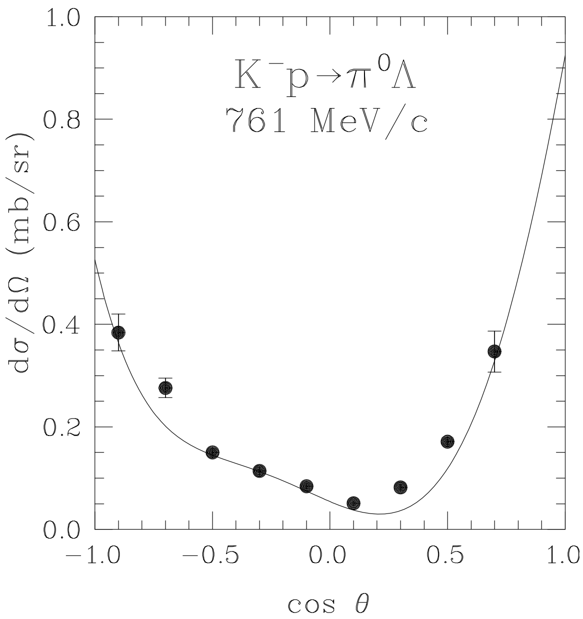

Figure 4: Preliminary results by the Crystal Ball Collaboration for the $K^- p \to \pi^0 \Lambda$ differential cross section at $P_{K^-} = 761$ MeV/c, or $W = 1681$ MeV. The curve is the prediction of the Gopal 77 partial-wave analysis.

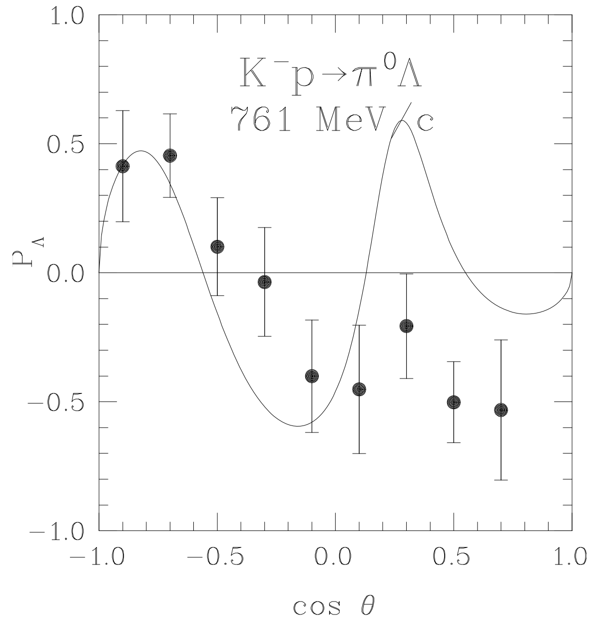

Figure 5: Preliminary results by the Crystal Ball Collaboration for the Λ polarization in $K^- p \to \pi^0 \Lambda$ at $P_{K^-} = 761$ MeV/c, or $W = 1681$ MeV. The curve is the prediction of the Gopal 77 partial-wave analysis.

3 Plans for future work

Plans are underway to begin a full-scale PWA of the world data for $\overline{K}N$ reactions using the Kent State multichannel parametrization. Results of the new PWA are anticipated to improve significantly our knowledge of the light hyperon resonances. Old PWAs of the $\overline{K}N \to \pi\Lambda$ reaction in the momentum range of the new Crystal Ball data were based mainly on bubble-chamber data measured in 1970 by Armenteros *et al.* [12]. Because our differential cross section ($d\sigma/d\Omega$) data for $K^- p \to \pi^0 \Lambda$ generally agree with the older, less precise data of Armenteros *et al.*, it was anticipated that the predictions of previous PWAs should also agree reasonably with our data. On the other hand, the Λ polarization (P_Λ) data of Armenteros *et al.* were of such low precision that we not *apriori* expect to find good agreement of PWA predictions with the polarization data measured by the Crystal Ball Collaboration. In order to check these expectations, we generated predictions for $d\sigma/d\Omega$ and P_Λ using the partial-wave solution of the 1977 PWA of Gopal *et al.* [5]. Figure 4 shows preliminary Crystal Ball results of $d\sigma/d\Omega$ for $K^- p \to \pi^0 \Lambda$ at a lab momentum of 761 MeV/c. The solid curve in the figure is the prediction of the Gopal 77 PWA. As expected, the agreement is generally quite good. Figure 5 shows the corresponding preliminary Crystal Ball results for the Λ polarization compared with the prediction of the Gopal 77 PWA. In this case, we see fairly good agreement at backward angles, but the prediction has the wrong sign at forward angles. Based on comparisons such as these, it is clear that the new polarization data from the Crystal Ball Collaboration will make a large impact on extracting partial-wave amplitudes. In particular, in the momentum range of the Crystal Ball measurements, the polarization data should help improve the determination of the P- and D-wave amplitudes. An improved determination of the P-wave amplitudes is especially of interest because these are needed to extract the properties of the Λ and Σ analogs of the controversial Roper resonance.

Acknowledgments: The author would like to thank the the GW Center for Nuclear Studies, and the organizers of MENU 2001, for their financial support and hospitality while he was in Washington, D.C. Partial financial support was provided by the U.S. Department of Energy. The author also thanks Kent State graduate students John Olmsted and John Tulpan for their helpful contributions to the data analysis. The Crystal Ball Collaboration contributed a major part of the data presented in this article.

References

[1] J.K. Kim, Phys. Rev. Lett. **27**, 357 (1971).
[2] W. Langbein and F. Wagner, Nucl. Phys. **B47**, 477 (1972).
[3] A.T. Lea *et al.*, Nucl. Phys. **B56**, 77 (1973).
[4] M. Alston-Garnjost *et al.*, Phys. Rev. Lett. **38**, 1003 (1977).
[5] G.P. Gopal *et al.*, Nucl. Phys. **B119**, 362 (1977).
[6] B.R. Martin and M.K. Pidcock, Nucl. Phys. **B126**, 266 (1977); *ibid.* 285 (1977); *ibid.* 349 (1977).
[7] AGS Experiment E953, D.M. Manley, B.M.K. Nefkens, and H. Spinka, co-spokespersons.
[8] D.M. Manley *et al.*, Phys. Rev. Lett. (submitted for publication).
[9] A. Starostin *et al.*, Phys. Rev. C (in press).
[10] D.M. Manley, Few-Body Syst. Suppl. **11**, 104 (1999), and unpublished.
[11] W. Cameron *et al.*, Nucl. Phys. **B143**, 189 (1978).
[12] R. Armenteros *et al.*, Nucl. Phys. **B21**, 15 (1970).

Hyperon photo- and electroproduction at CLAS

S. P. Barrow[a], representing the CLAS collaboration

[a] *Florida State University, Tallahassee, Florida, 32306, U. S. A.*

(Received: 12 October 2001)

The large acceptance and high multiplicity capabilities of the CLAS detector make it possible to study a wide range of previously unmeasured strange baryon production processes. Studies of the decay angular distributions of electroproduced strange baryons have yielded several interesting new results. The $\Lambda(1520)$ electroproduction decay angular distributions shed light on the spin projections of the $\Lambda(1520)$. Analysis of the decay angular distributions of the weakly decaying $\Lambda(1116)$ have revealed the induced baryon polarization due to unpolarized incident electron beams. In addition to these topics, other features of the CLAS strange baryon program, such as photoproduction and virtual photon L-T decompositions, are also briefly summarized.

1 Introduction

The hyperon physics program at CLAS uses polarized and unpolarized electron beams, with incident energies ranging from 2.4 to 6.0 GeV, to study hyperon photo- and electroproduction. A complete list of all approved analysis projects currently underway is summarized in Table 1. These experiments measure such aspects of hyperon production as the production cross sections and the corresponding response functions, the hyperon decay angular distributions, and the radiative decay strengths of the light hyperons.

The large acceptance of the CLAS detector makes it possible to study hyperon production over a wide kinematic regime. In addition, its high multiplicity capabilities enable the study of sequential processes such as decay angular distributions of electroproduced hyperons. Due to time constraints, the remainder of this talk will focus on the results of measurements of $\Lambda(1520)$ decay angular distributions (E89-043), as well as $\Lambda(1116)$ decay using unpolarized (E89-043) electron beams. The kinematic regimes presented here have not been studied in any previous measurements.

2 $\Lambda(1520)$ decay angular distributions

The CLAS event reconstruction is based on the missing mass technique to identify the mass of neutral hyperons and undetected particles. A study of electroproduction decay angular distributions requires detecting the scattered electron and at least two hadrons, and the $\Lambda(1520) \to p - K^-$ decay mode of the $\Lambda(1520)$ is the one best suited for study with CLAS. Figure 1 shows the relevant missing mass plots for $\Lambda(1520)$ electroproduction data taken as part of the 1998 and 1999 E1 run

Experiment	Title	Spokesperson(s)
E89-004	Hyperon photoproduction	R. Schumacher
E89-024	Radiative decays of light hyperons	G. Mutchler
E89-043	$\Lambda(1116)$, $\Lambda(1520)$ and $f_0(980)$ electroproduction	L. Dennis, H. Funsten
E93-030	Structure functions for kaon electroproduction	K. Hicks, M. Mestayer
E95-003	K° electroproduction	R. Schumacher, K. Dhuga
E99-006	Polarization observables in $p(\vec{e}, e'K^+)\Lambda$	D. Carman, K. Joo, L. Kramer, B. Raue
CAA-2000-1	K^* electroproduction	K. Hicks

Table 1: The strange baryon production experiments at CLAS.

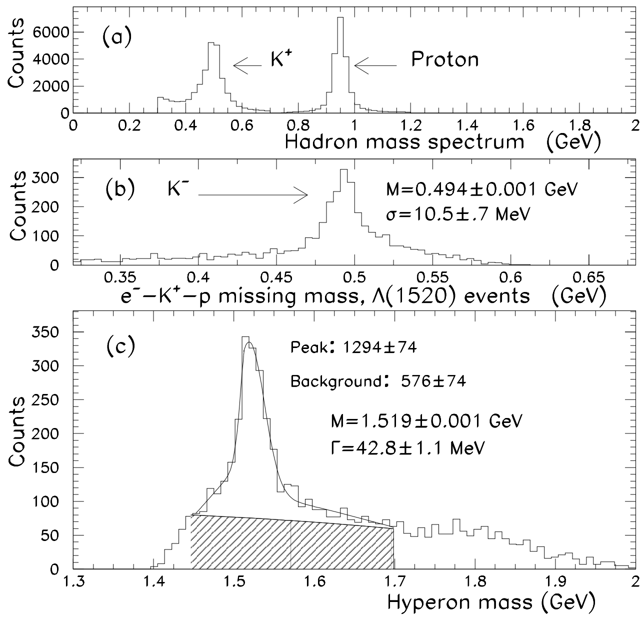

Figure 1: (a) The hadron mass spectrum for events that contain a proton track and a K^+ candidate. (b) The K^- missing mass spectrum for events in which the e$^-$-K^+ missing mass is consistent with the $\Lambda(1520)$ mass. (c) The hyperon mass spectrum for the e$^-$-K^+-K^--p final state. A cut on the K^- missing mass from 0.455 to 0.530 GeV was used to generate this hyperon spectrum.

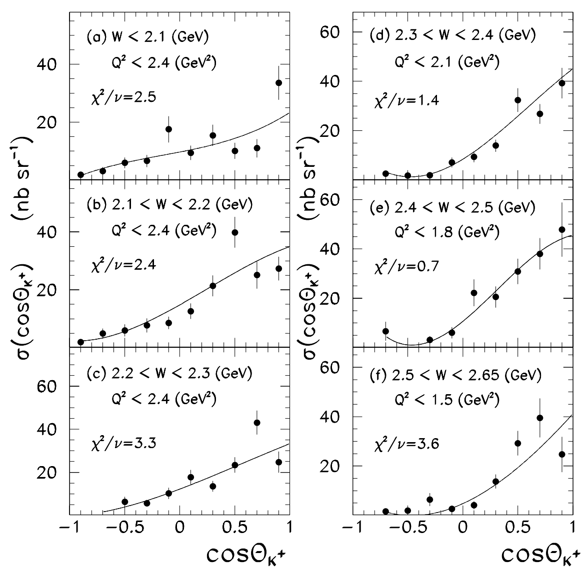

Figure 2: The $\Lambda(1520)$ $\cos\Theta_{K^+}$ differential cross section distributions for six regions of W. The error bars are statistical uncertainties only. The solid lines are the results of Legendre polynomial fits to the data. The lower limit $Q^2 = 0.9$ GeV^2 is used for all six distributions.

periods with beam energies of 4.05, 4.25, and 4.45 GeV. Reactions that produce other hyperons, such as the $\Lambda(1405)$, $\Sigma(1480)$, and $\Lambda(1600)$, account for the majority of the background under the $\Lambda(1520)$ peak, but the relative contributions from the individual processes are currently unknown. A complete listing of the hyperons whose mass and width have some overlap with the $\Lambda(1520)$ peak is presented in Ref. [1].

A measurement done at Daresbury of $\Lambda(1520)$ photoproduction [2] used incident photons with energies ranging from 2.8 to 4.8 GeV (total center-of-mass energy W from 2.5 to 3.1 GeV), and reports an exponential t-dependence dominated by t-channel exchange of the $K^*(892)$ meson, and not the lighter $K(494)$ meson. A thorough understanding of the reasons $\Lambda(1520)$ photoproduction proceeds mainly through the exchange of a heavier vector meson requires theoretical studies of the competition between vector and pseudoscalar meson exchange, and will not be addressed in this report. However, with CLAS it is possible to determine if $\Lambda(1520)$ electroproduction also proceeds mainly by t-channel vector meson exchange. This measurement complements the existing photoproduction one, and should greatly facilitate a theoretical understanding of $\Lambda(1520)$ production. The CLAS electroproduction center-of-mass angular distributions shown in Fig. 2 are consistent with t-channel dominance.

The $\Lambda(1520)$ is a $\mathrm{J}^\pi = \frac{3}{2}^-$ baryon, and its $p - K^-$ decay is a parity conserving strong decay mode. For an $m_z = \pm\frac{3}{2}$ projection the decay is characterized by a $\sin^2\Theta_{K^-}$ distribution, while an $m_z = \pm\frac{1}{2}$ projection has a $\frac{1}{3}+\cos^2\Theta_{K^-}$ distribution, where Θ_{K^-} is the polar angle of the outgoing K^- decay fragment relative to the incident target proton. The t-channel helicity frame $\cos\Theta_{K^-}$ decay angular distributions for four regions of Q^2 are shown in Fig. 3. The photoproduction angular

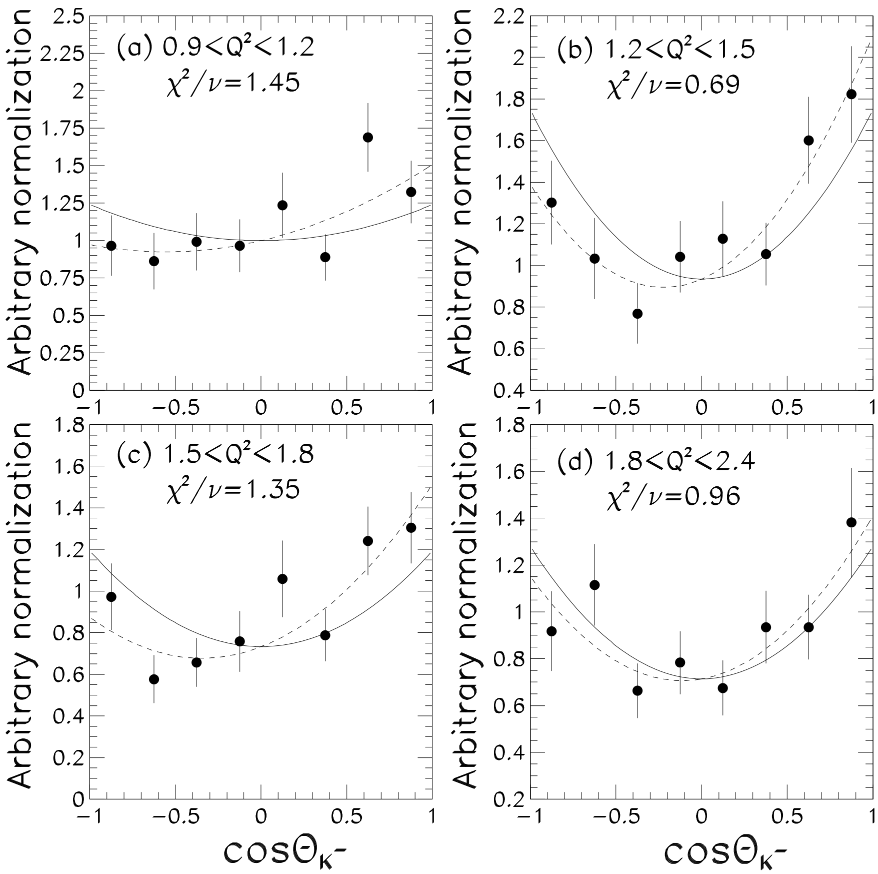

Figure 3: The $\Lambda(1520)$ $\cos\Theta_{K^-}$ decay angular distribution for four regions of Q^2. These distributions are averaged over the region of W from threshold to 2.43 GeV. The error bars are statistical uncertainties only. The solid line in each plot is the fitted contribution from the two spin projection terms of the $\Lambda(1520)$, and the dashed line is a fit that also includes a parameterization of the interference between the $\Lambda(1520)$ and other hyperons.

distribution [2] possesses a greatly enhanced $m_z = \pm\frac{3}{2}$ parentage relative to the electroproduction results presented here. All four of the distributions shown in Fig. 3 demonstrate a large $\frac{1}{3}+\cos^2\Theta_{K^-}$ contribution, which indicates the electroproduced $\Lambda(1520)$ hyperons are primarily populating the $m_z = \pm\frac{1}{2}$ spin projection.

If $\Lambda(1520)$ electroproduction proceeds exclusively through t-channel exchange of a spinless kaon, the $\Lambda(1520)$ spin projection is always $m_z = \pm\frac{1}{2}$, and the ratio of the $m_z = \pm\frac{3}{2}$ to $m_z = \pm\frac{1}{2}$ populations is zero. On the other hand, if the reaction proceeds exclusively through the transverse exchange of a J=1 K^* vector meson, the ratio of the $m_z = \pm\frac{3}{2}$ to $m_z = \pm\frac{1}{2}$ spin projections, if solely determined by Clebsch-Gordon coefficients, is 3 to 1. Therefore the electroproduction distributions shown in Fig. 3, and summarized in Table 2, could be evidence for a roughly equal mixture of $K^*(892)$ and $K(494)$ contributions, which is a significant departure from what was reported in the photoproduction measurement [2]. This analysis has recently been published in Phys. Rev. C [3].

Q^2 range (GeV^2)	ratio $(m_z = \pm\frac{3}{2})/(m_z = \pm\frac{1}{2})$
0.9-1.2	.806±.125
1.2-1.5	.534±.148
1.5-1.8	.614±.108
1.8-2.4	.558±.108

Table 2: The ratios of the $\Lambda(1520)$ electroproduction spin projection parentages for the four regions of Q^2 presented in Fig. 3. A complete discussion of these results is presented in Ref. [3].

3 $\Lambda(1116)$ distributions, unpolarized electron beam

In contrast to the $\Lambda(1520)$, the $\Lambda(1116)$ is a $J^{\pi} = \frac{1}{2}^{+}$ baryon. The $\Lambda(1116)$ decays weakly, and it is therefore possible to deduce the polarization of the $\Lambda(1116)$ by studying the asymmetry in its decay angular distribution. This provides a unique opportunity to study induced baryon polarization in hyperon production. Due to parity constraints on the strong interaction, such polarization is only permitted in the direction normal to the $\Lambda(1116)$ center-of-mass production plane. The decay angular distribution in the rest frame of the $\Lambda(1116)$ is of the form $\sigma(Cos\Theta_p) = A(1+\alpha{\cdot}PCos\Theta_p)$, where Θ_p is the polar angle of the outgoing proton. The polarization of the $\Lambda(1116)$ is deduced from the slope of the $Cos\Theta_p$ dependence. The relevant hadron spectra are shown in Fig. 4, and two examples of the acceptance corrected yields that are used to derive the $\Lambda(1116)$ polarization are shown in Fig. 5.

The induced polarization as a function of the center-of-mass quantity $\cos\Theta_{K^+}$ for two regions of W are shown in Fig. 6 [4]. Also shown are the results of a photoproduction measurement done at SAPHIR [5] of $\Lambda(1116)$ induced polarization over the same region of W studied with CLAS. The photo- and electroproduction measurements both indicate that for low W, close to threshold, the induced polarization of the $\Lambda(1116)$ is fairly small, while at higher W the $\Lambda(1116)$ polarization is larger and negative, especially for $Cos\Theta_{K^+} > 0.0$. The photo- and electroproduction data also suggest there might be no significant Q^2 dependence to the induced $\Lambda(1116)$ polarization. One obvious implication of this result is that the $\Lambda(1116)$ polarization is not very sensitive to the L-T decomposition of the (real or virtual) photon. Once this analysis is complete, it will be interesting to compare the W dependence of the $\Lambda(1116)$ induced polarization presented here with the polarization obtained with a nonlepton beam such as a pion or kaon beam.

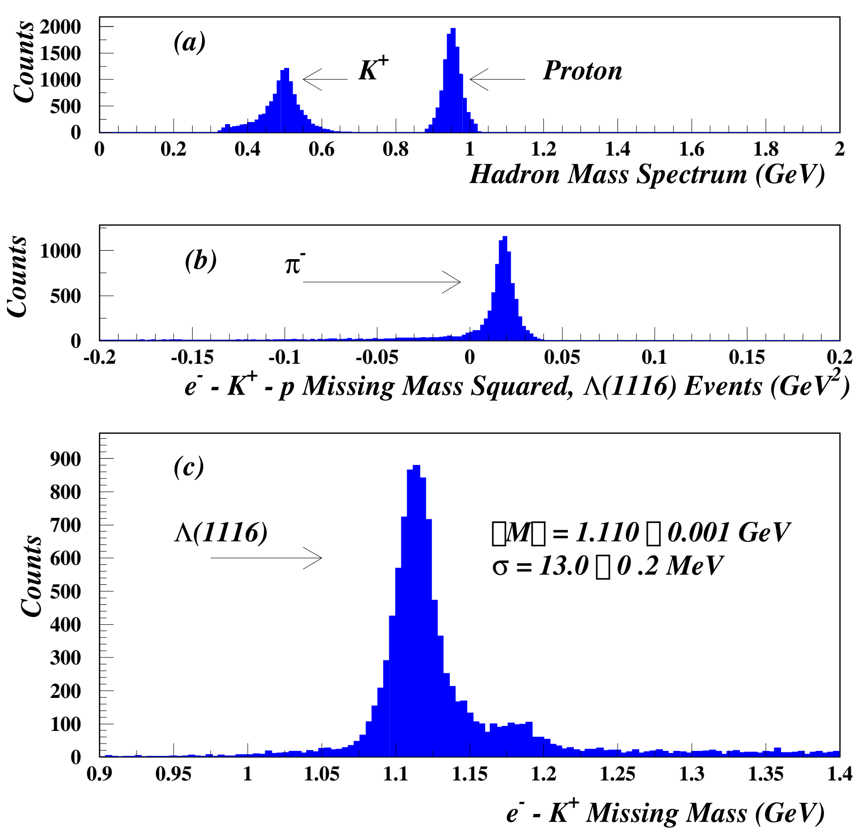

Figure 4: (a) The hadron mass spectrum for events that contain a proton track and a K^+ candidate, for $\Lambda(1116)$ events. (b) The π^- missing mass spectrum for events in which the e^--K^+ missing mass is consistent with the $\Lambda(1116)$ mass. (c) The hyperon mass spectrum for the e^--K^+-π^--p final state.

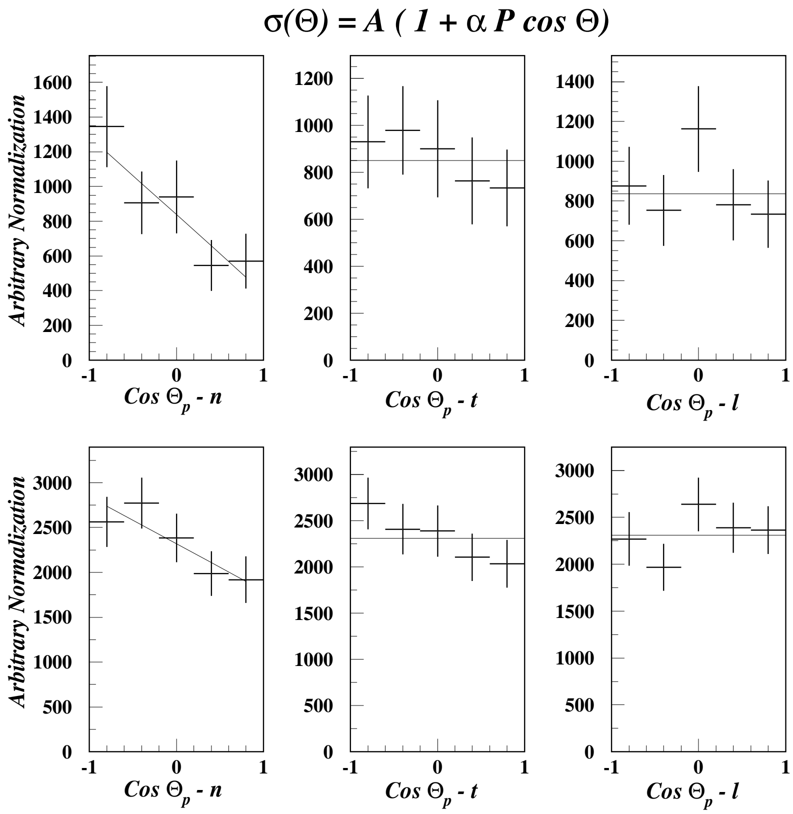

Figure 5: Two examples of $\Lambda(1116)$ decay angular distributions for three orthogonal projections. The upper trio is for $1.8 < W < 2.0$ GeV and $0.0 < Cos\Theta_p < 0.5$, while the lower trio is for the same range of W but $0.5 < Cos\Theta_p < 1.0$. For an unpolarized incident electron beam, only the "n" projection, which is normal to the hyperon production plane, is allowed to have a slope to its distribution. The "t" and "l" projections are in the center-of-mass production plane, and should be flat.

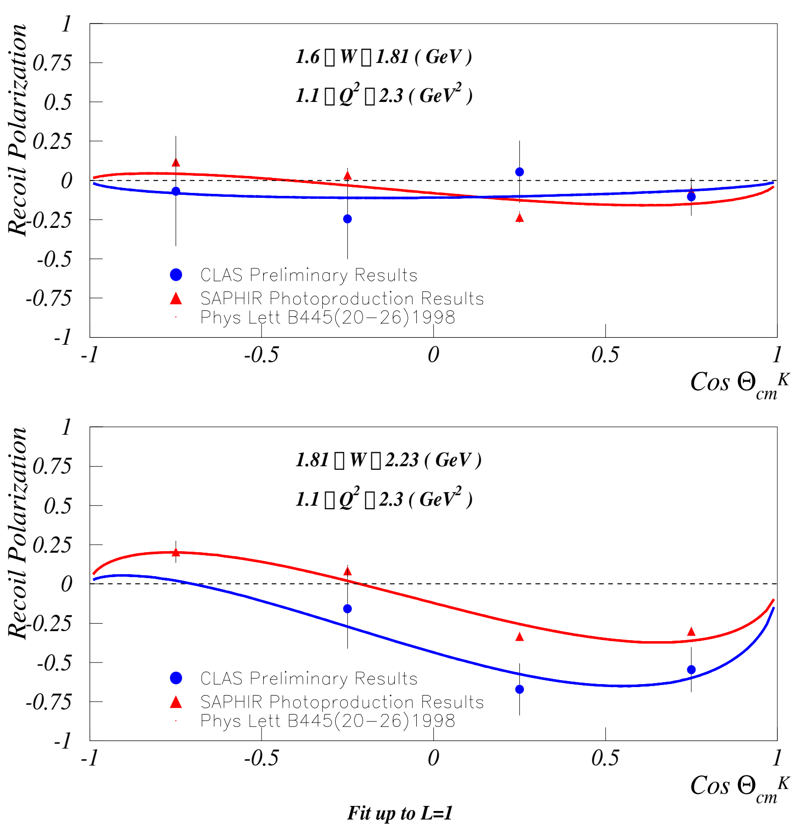

Figure 6: Preliminary CLAS results for the induced $\Lambda(1116)$ polarization from an unpolarized incident electron beam for two regions of W, and for $1.1 < Q^2 < 2.3$ GeV^2. Also shown in these plots are the results of a photoproduction measurement [5].

4 Conclusions

The detailed studies of the decay angular distributions of electroproduced hyperons presented here represent a significant addition to existing measurements of hyperon production. These measurements also provide excellent illustrations of the capabilities of the CLAS detector. Nonetheless, these results represent a small fraction of the total studies of hyperon production currently underway on data taken at CLAS. Combined with the other approved analysis activities summarized in Table 1, a much clearer understanding of the strange baryon production processes is emerging.

Acknowledgments: The CLAS collaboration is supported by the U.S. Department of Energy and the National Science Foundation, the French Commissariat à l'Energie Atomique, the Italian Istituto Nazionale di Fisica Nucleare, and the Korea Science and Engineering Foundation.

References

[1] D. Groom *et al.*, The European Physical Journal C **15**, 1 (2000).
[2] D. Barber *et al.*, Z. Physik C **7**, 17 (1980).
[3] S.P. Barrow *et al.*, Phys. Rev. C **64**, 044601 (2001), hep-ex/0105029.
[4] Data analysis results from S. McAleer (2001).
[5] M. Q. Tran *et al.*, Phys. Lett. B **445**, 20 (1998).

An isobar model for photo- and electroproduction of kaons on the nucleon

T. Mart[a], C. Bennhold[b], and H. Haberzettl[b]

[a] *Jurusan Fisika, FMIPA, Universitas Indonesia, Depok 16424, Indonesia*
[b] *Center for Nuclear Studies, Department of Physics,*
The George Washington University, Washington, DC 20052, U.S.A.

(Received: 20 November 2001)

An isobar model for kaon photoproduction on the nucleon has been constructed by using an effective Lagrangian technique. The model is constrained by applying SU(3) coupling constants in the Born terms and gauge invariance in the amplitude. A good agreement with available experimental data is obtained. The model is then extended to describe kaon electroproduction data by including the appropriate longitudinal terms.

1 Introduction

Since the discovery of strangeness by Gell-Mann and Nishijima almost five decades ago, the interest in its degrees of freedom has remained alive in nuclear physics, with the corresponding investigations nowadays spanning the range from quarks to nuclei. For nuclei, in particular, strangeness has given experimentalists a new tool for probing all nuclear levels while avoiding Pauli blocking, which is an inherent problem for conventional nuclei. Hypernuclear systems, therefore, appear as very promising subjects of study in nuclear physics and there have been considerable efforts by theory and experiment alike to uncover the behavior of nuclei 'doped' with one or several hyperons. From a theoretical point of view, the study of how to probe hypernuclear systems with photons requires knowledge of the elementary process of hyperon and kaon photoproduction on individual nucleons. At this elementary level, the investigation is most effectively performed in the framework of an isobar approach. The corresponding operator can then easily be implemented in the nuclear calculation.

2 The photoproduction model

In this section, we briefly review our isobar model. A more detailed discussion can be found, e.g., in Ref. [1]. Here, we only take the $p(\gamma, K^+)\Lambda$ channel as an example; other isospin channels will employ the same formalism, with only minor changes of the coupling constants and the resonance structure [2]. We start with appropriate Feynman diagrams for the s, u, and t-channel background terms and a number of resonances to derive the Lorentz-covariant transition amplitude. It is well known that certain diagrams of the background terms are not independently gauge invariant, but—for pointlike hadronic vertices—the sum of all diagrams is gauge invariant. Pointlike hadronic vertices, however, completely ignore the extended nature of an interacting system of baryons and mesons and, in our opinion, are not well justified. To account for the hadronic structures of the vertices, we therefore introduce form factors. In general, this considerably improves the description of experimental data and it suppresses the otherwise divergent behavior at higher energies. However, the mismatch of the functional behavior of the form factors in the various diagrams destroys gauge invariance. Thus, a prescription is required to restore it.

2.1 Gauge invariance and crossing symmetry

Recently, several methods have been put forward to overcome the problem of gauge invariance. Two of them have been compared in a model for kaon photoproduction on the nucleon [3]. The method proposed in Ref. [4] has been found to be superior since it leads to a much more reasonable description of experimental data allowing, in particular, the values of the leading coupling constants

$g_{K\Lambda N}$ and $g_{K\Sigma N}$ to be chosen in agreement with SU(3) predictions. The improvement over previous prescriptions is found to be mostly due to a suppression of the electric part of the Born terms (which is sometimes called the A_2 term) through a form factor denoted by $\widehat{F}$, which enters the description via the gauge-invariance-preserving current contribution introduced in Refs. [3, 4]. As far as gauge invariance is concerned, this function $\widehat{F}$ is largely arbitrary. For simplicity, in Refs. [3] it was chosen in the "democratic" form

$$\widehat{F}(s,t,u) = a_1 F_1(s) + a_2 F_2(u) + a_3 F_3(t) \ , \tag{1}$$

where $F_i(x) = [1 + (x - m_i^2)^2/\Lambda^4]^{-1}$ and the a_i are normalized distribution constants, $\sum_i \ a_i = 1$. Utilizing this choice of $\widehat{F}$, several recent isobar models [1,5,6] have reported significant improvement compared with the point-particle approximation. Similar results were obtained in coupled-channel analyses [7, 8].

The particular choice (1) implies kinematic singularities for the gauge-invariance-preserving current that has no immediate consequence for the calculation of (on-shell) amplitudes. Recently, Davidson and Workman [9] argued that this singularity should be avoided since it may adversely affect the calculation of quantities determined by analytic continuation of on-shell data. They suggest instead to use the form

$$\widehat{F}(s,t) = F_1(s) + F_3(t) - F_1(s)F_3(t) \tag{2}$$

as a simple way of removing that singularity. A more general form that also satisfies certain aspects of crossing symmetry is given by

$$\widehat{F}(s,t,u) = F_1(s) + F_1(u) + F_3(t) - F_1(s)F_1(u) - F_1(s)F_3(t) - F_1(u)F_3(t) + F_1(s)F_1(u)F_3(t) \ . \tag{3}$$

While Davidson and Workman's criticism is well taken, one should note that the main point of Refs. [3, 4] was not to suggest the choice (1) as the 'ultimate' recipe for preserving gauge invariance, but to emphasize that *gauge invariance can be preserved relatively simply while one still has the freedom of choosing a function* $\widehat{F}$. The particular choice for $\widehat{F}$ then depends on how sophisticated one's needs are. The simple choice of Eq. (1) in general has the advantage of still having two free fit parameters, whereas Eqs. (2) and (3) clearly are more sophisticated functional forms that address certain analyticity concerns.

Using Eqs. (1)–(3) we fitted the isobar model in Ref. [10] to all $p(\gamma, K^+)\Lambda$ data and the results are summarized in Table 1. To arrive at these results we fixed the leading coupling constants to the values predicted by SU(3) symmetry, and since SU(3) is broken these values are clearly not unique.

Table 1: The $\widehat{F}$ cut-offs for background ($\Lambda_{\rm b}$) and resonance ($\Lambda_{\rm r}$) terms and the χ^2/N obtained from fits to $p(\gamma, K^+)\Lambda$ data by fixing the Born couplings to the SU(3) values $g_{K\Lambda N}/\sqrt{4\pi} = -3.8$ and $g_{K\Sigma N}/\sqrt{4\pi} = 1.2$. The upper and lower limit for cut-offs are 2.00 GeV and 0.1 GeV, respectively. The form factor models HH, DW, and DWCS refer to Eqs. (1), (2), and (3), respectively.

	no polarization data ($N = 284$)			with polarization data ($N = 319$)		
$\widehat{F}$	HH	DW	DWCS	HH	DW	DWCS
$\Lambda_{\rm b}$	0.68	0.40	0.49	0.69	0.68	0.69
$\Lambda_{\widehat{F}}$	-	-	-	0.10	0.10	0.40
$\Lambda_{\rm r}$	1.03	1.06	1.02	1.00	0.97	2.00
χ^2/N	2.17	2.04	2.04	2.65	2.67	2.25

We find that the values for the cut-off Λ are quite sensitive to the choice of those coupling constants, i.e., decreasing the coupling constants will significantly increase the cut-off values. From Table 1 we see that the three choices do not produce significantly different χ^2 values unless we include the polarization data. It seems, therefore, that polarization data may allow one to discriminate between the models.

As seen from Table 1, in our model we allow different cut-off values for the background and resonance terms. Initially, the $\widehat{F}$ cut-off was the same as for the background terms and the values found correspond to rather "soft" form factors which strongly suppress contributions from background parts of the process. To understand the origin of this suppression, we further separated the $\widehat{F}$ cut-off from $\Lambda_{\rm b}$ and $\Lambda_{\rm r}$, and we obtained $\Lambda_{\widehat{F}} \approx 0.1$, much smaller than the other two cut-offs, which shows that the A_2 contribution would be dominant if we used a similar cut-off in the model. Reference [11] argued that such a result tends to be artificial, while a more desired cut-off greater than 1.5 GeV can be obtained by including two more hyperon resonances $\Lambda(1800)$ and $\Lambda(1810)$ in the model. We will show here that such argument is irrelevant in the present discussion.

First of all, the model in Ref. [11] has been only fitted to SAPHIR data by varying the leading coupling constants $-3.0 \leq g_{K\Lambda N}/\sqrt{4\pi} \leq 4.2$ and $0.9 \leq g_{K\Sigma N}/\sqrt{4\pi} \leq 1.3$. Using such constraints and including hyperon resonances, the model yields $\Lambda = 1.5$ GeV for the best cut-off with $\chi^2/N = 2.89$. We confirm this result with $\chi^2/N = 2.45$. However, we find that our minimization procedure does not stop at this point. Our best fit for this case yields $\chi^2/N = 2.09$ and therefore we are led to the suggestion that the fit performed in Ref. [11] may not have reached its absolute minimum. *Without* the two hyperon resonances, our model is able to fit *all* $p(\gamma, K^+)\Lambda$ data with $\chi^2/N = 3.14$, $\Lambda_{\rm b} = 1.5$ GeV, $\Lambda_{\rm r} = 2.0$ GeV, and (as a consequence, as we pointed out before) the Born coupling constants reach their allowed lower bounds.

Secondly, the hadronic form factors are unmeasurable quantities and only their products with

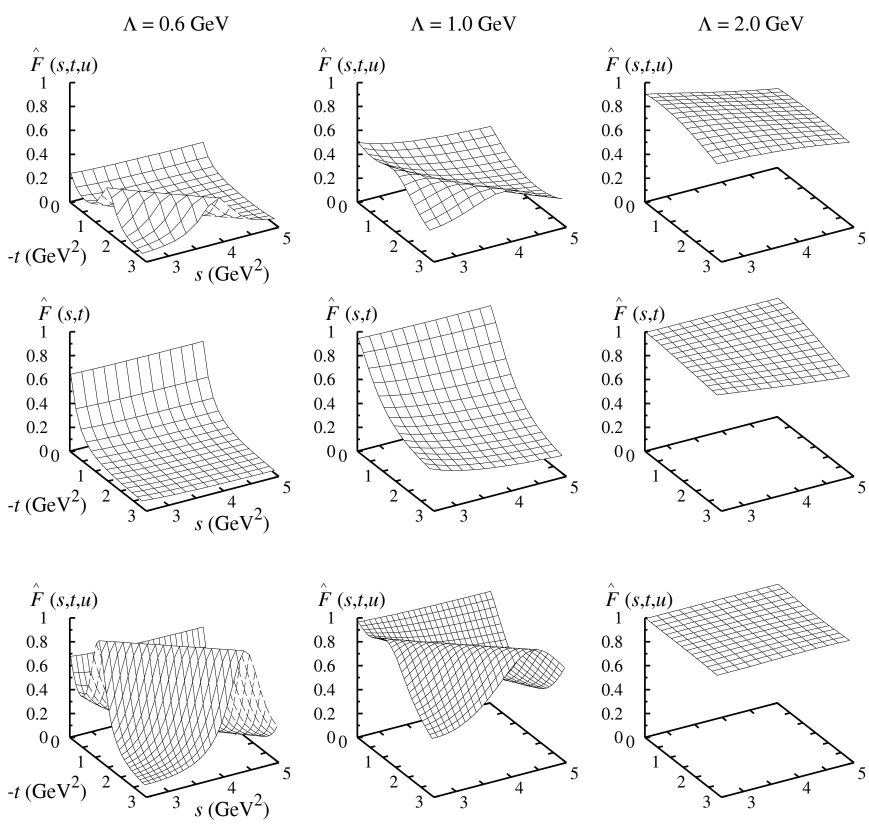

Figure 1: The gauge form factor $\widehat{F}(s,t,u)$ given by Eq. (1) with $a_1 = a_2 = a_3 = 1/3$ (top), $\widehat{F}(s,t)$ obtained from Eq. (2) (middle), and $\widehat{F}(s,t,u)$ given by Eq. (3) (bottom) plotted in the physical s and $-t$ region for different values of cut-off Λ.

coupling constants enter the model. Therefore, any attempt to extract the form factor cut-offs and coupling constants separately through an isobar model is theoretically impossible. Furthermore, as shown in Fig. 1, a relatively large cut-off ($\approx$ 2 GeV) essentially corresponds to a point-particle approximation in the physical region, thus effectively removing the influence of hadronic form factors from the model altogether.

A closer examination of Table 1 reveals that polarization data prefer the crossing symmetric form factor, Eq. (3), rather than any of the other recipes. This finding can be understood from Fig. 1, where we compare all forms of $\widehat{F}$ with different Λ. Clearly, it shows that a better agreement between the model and polarization data can be achieved only with a more structured $\widehat{F}$ which might be related to the more pronounced structure in angular distributions of recoil polarization.

In Fig. 2, we compare the models with different $\widehat{F}$ given in the last three columns of Table 1. All three prescriptions of $\widehat{F}$ exhibit very similar cross sections, except for the second peak that is slightly suppressed in the model with crossing symmetric $\widehat{F}$ due to the broadening of the $D_{13}(1895)$ width. By contrast, larger differences are seen in recoil polarizations, a result which is expected already from Table 1, where the χ^2/N also show sizeable differences. The differences between the models increase with W; and at the highest W, even the shapes of the polarizations are quite dissimilar. This finding is related to the observation that, at large s for $\Lambda = 0.6\,\mathrm{GeV}$, the $\widehat{F}$'s as shown in Fig. 1 also show quite dissimilar functional behavior. Although the generally sinusoidal shape of the recoil polarization can be nicely reproduced, we would like to wait for more precise data before drawing any further conclusions, since the polarization data shown in Fig. 2 have been averaged in relatively large θ and energy bins. We mention that we also found large differences between the three models in the photon and target asymmetry observables Σ and T.

2.2 Is there really a missing resonance in $p(\gamma, K^+)\Lambda$?

In Ref. [10] we have pointed out that the second peak in the total cross section shown in Fig. 2 could be a sign for a missing resonance, in the sense that the resonance "exists" in the quark model predictions but is absent in the πN channel analyses. For that purpose we took a constituent quark model [12] which predicts several possible states that have relatively large branching ratios to the $K\Lambda$ channel. We have performed fits for each of these states, allowing the fit to determine the mass, width and coupling constants of the resonance. We found that all appropriate states can reproduce the structure at W around 1900 MeV, but only for the $D_{13}(1895)$ state we found a remarkable

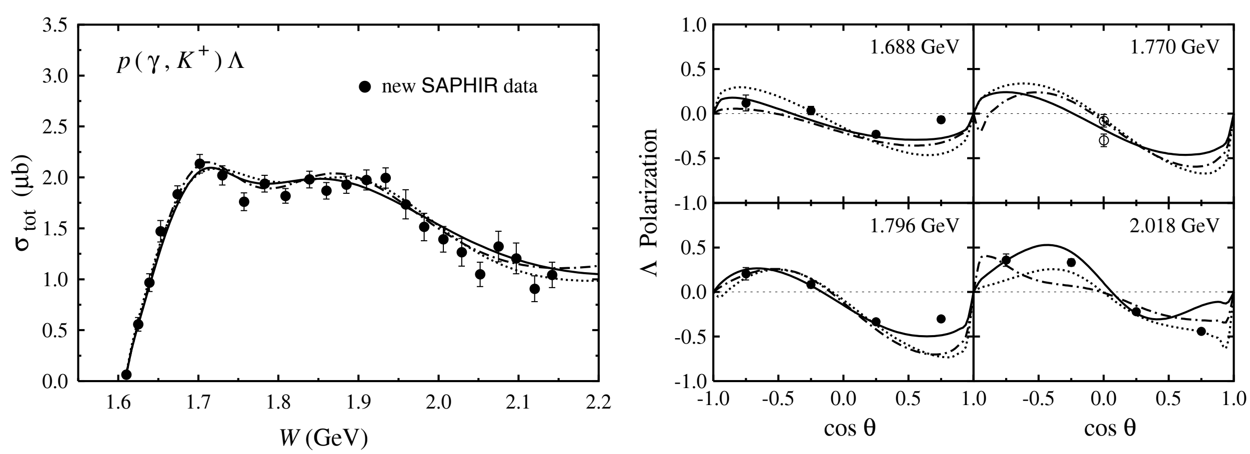

Figure 2: Total cross section (left) and recoil polarization (right) for the $p(\gamma, K^+)\Lambda$ process. Solid lines show the model with Eq. (3) in the A_2 amplitude, whereas dash-dotted and dotted lines are obtained with Eq. (1) and Eq. (2), respectively. Experimental data are taken from Ref. [13].

agreement between the predicted and extracted photocouplings, while for other states the result from our fit overestimate the quark model significantly. At the end of our report [10] we also pointed out that such analysis must be supported by a more rigorous coupled channel calculation as well as with more data in a photon asymmetry measurement.

Since then, several analyses have addressed the same question but ended up with different conclusions. Reference [14], e.g., stated that by using some "known" spin 3/2 and 5/2 nucleon resonances it is also possible to produce the second peak in Fig. 2. To our knowledge this is not surprising, since almost 30 years ago, by using a series of resonances with spin up to 5/2, Ref. [15] (see Fig. 4 therein)) has shown a second peak in the cross section at E_γ around 1.5 GeV (corresponding to $W \approx 1.9$ GeV). However, none of these high spin resonances has been reported either by PDG or other analyses to have a significantly large photocoupling to the $K\Lambda$ channel.

To conclude this section, we emphasize once more that the finding in Ref. [10] is intended as an alternative description for the structure found in $p(\gamma, K^+)\Lambda$ cross section with some support from quark models. Clearly, what is required are further rigorous analyses, such as, for example, a coupled channel calculation.

3 The electroproduction model

The photoproduction model discussed in the previous section can be easily extended to the case of electroproduction, by including the longitudinal terms in the transition matrix. For the Born terms this procedure is part of the gauge-invariance recipe [16]. For resonance terms we follow Ref. [17], i.e. for nucleon and delta resonances with parity ($\pm$) and spin 1/2 we used the following electromagnetic vertex:

$$\Gamma_\mu^{(\pm)} = \left[\frac{\kappa_{N^*}}{m_{N^*} + m_N} \, i\sigma_{\mu\nu} k^\nu \, F_2(k^2) + (\gamma_\mu k^2 - k_\mu \not{k}) \, \frac{F_3(k^2)}{k^2} \right] P^{(\pm)} \ ,$$

where $P^{(+)} = 1$ and $P^{(-)} = \gamma_5$, while for spin 3/2 the electromagnetic coupling reads

$$\Gamma_{\mu\nu}^{(\pm)} = \left[\left(g_{\mu\nu} - \frac{k_\mu \gamma_\nu}{m_{N^*} \pm m_N} \right) G_1(k^2) + \frac{k_\mu p_\nu - k \cdot p \, g_{\mu\nu}}{(m_{N^*} \pm m_N)^2} \, G_2(k^2) + \frac{k_\mu k_\nu - k^2 g_{\mu\nu}}{(m_{N^*} \pm m_N)^2} \, G_3(k^2) \right] P^{(\mp)} \ ,$$

with k and p denoting the (virtual) photon and baryon momenta, respectively. Since the electromagnetic vertices are extended in this case, we introduce a dipole-like form factor in every baryon resonance vertex and a monopole-like one in the case of meson resonances. For the background terms the form factors are relatively well known.

Using the hadronic coupling constants extracted from the photoproduction process we fit the electroproduction data by leaving the electromagnetic form factor cut-offs of resonances as free parameters. The result is shown in Fig. 3, where we compare all three models considered in Fig. 2 for the photoproduction. Although the χ^2 fit to electroproduction data seems to favor a crossing symmetric form factor, the quality of the present data is insufficient to clearly discriminate between the three models. It is very unfortunate that no data are available in the region where the models start to show large discrepancies, such as at small photon momentum transfer depicted in the right panel of Fig. 3. Interestingly, the two models with $\widehat{F}$ suggested in Ref. [9] exhibit minima in the transverse cross section at small k^2, where the longitudinal one reaches its maximum, and at $k^2 \approx -1.5$ GeV^2. By separating the contribution of individual resonance we found that, except for the K_1 intermediate state, all terms yield a decreasing cross section as a function of k^2. However, the contribution of K_1 is very small at small k^2, thus a bump is produced at $k^2 \approx -0.5$ GeV^2. We expect that experimental data for separated $d\sigma_L/d\Omega$ and $d\sigma_T/d\Omega$ with 10% accuracy at these kinematics will be sufficient to resolve this issue.

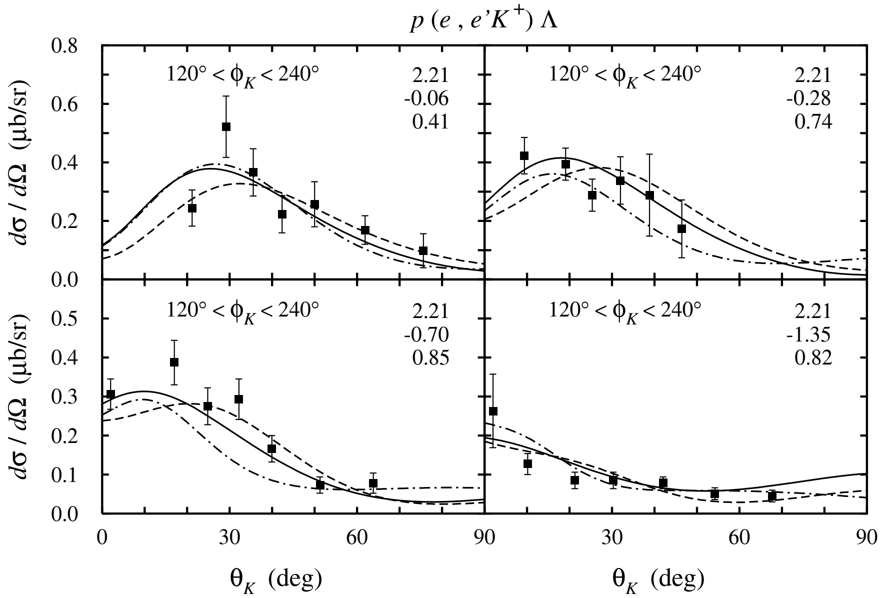

Figure 3: Differential cross section for the $p(e,e'K^+)\Lambda$ process. Notation for the curves is as in Fig. 2. The three numbers at the top-right side of every panel denote the total c.m. energy W, the square of the virtual photon momentum k^2, and the transverse polarization of the virtual photon ϵ, respectively. Experimental data are taken from [18].

Our final analysis including the other isospin channels will be reported in the near future [16].

Acknowledgments: This work was supported in part by the QUE project (TM) and by the U.S. Department of Energy Grant No. DE-FG02-95ER-40907.

References

[1] F. X. Lee, T. Mart, C. Bennhold, H. Haberzettl and L. E. Wright, Nucl. Phys. **A695**, 237 (2001).
[2] T. Mart, C. Bennhold and C. E. Hyde-Wright, Phys. Rev. C **51**, 1074 (1995).
[3] H. Haberzettl, C. Bennhold, T. Mart and T. Feuster, Phys. Rev. C **58**, 40 (1998).
[4] H. Haberzettl, Phys. Rev. C **56**, 2041 (1997).
[5] S. Janssen, *et al.*, Eur. Phys. J. A **11**, 105 (2001).
[6] B. S. Han, M. K. Cheoun, K. S. Kim and I. Cheon, Nucl. Phys. **A691**, 713 (2001).
[7] T. Feuster and U. Mosel, Phys. Rev. C **59**, 460 (1999)
[8] C. Bennhold, A. Waluyo, H. Haberzettl, T. Mart, G. Penner and U. Mosel, nucl-th/0008024.
[9] R. M. Davidson and R. Workman, Phys. Rev. C **63**, 025210 (2001).
[10] T. Mart and C. Bennhold, Phys. Rev. C **61**, 012201 (2000).
[11] S. Janssen, J. Ryckebusch, D. Debruyne and T. Van Cauteren, nucl-th/0107028.
[12] S. Capstick and W. Roberts, Phys. Rev. D **49**, 4570 (1994).
[13] M. Q. Tran *et al.* [SAPHIR Collaboration], Phys. Lett. B **445**, 20 (1998).
[14] B. Saghai, in the *Proceedings of the Workshop on Hypernuclear Physics with Electromagnetic Probes (HJLAB99)*, Hampton, Virginia, Dec. 1999, edited by L. Tang and O. Hashimoto, p. 24.
[15] Y. Renard, Nucl. Phys. **B40**, 499 (1972).
[16] H. Haberzettl, C. Bennhold, T. Mart, in preparation.
[17] J. M. Laget, Nucl. Phys. **A481**, 765 (1988).
[18] P. Brauel *et al.*, Z. Phys. C **3**, 101 (1979).

Pion-nucleon scattering in a Bethe-Salpeter approach

A. D. Lahiff [a] and I. R. Afnan [b]

[a] *TRIUMF, 4004 Wesbrook Mall, Vancouver, B.C., Canada V6T 2A3*
[b] *School of Chemistry, Physics and Earth Sciences,*
The Flinders University of South Australia, GPO Box 2100, Adelaide 5001, Australia

(Received: 18 September 2001)

A covariant model of elastic pion-nucleon scattering based on the Bethe-Salpeter equation is presented. We obtain a good description of the S- and P-wave phase shifts up to 360 MeV laboratory energy. We also compare results from the K-matrix approach and several 3-dimensional quasipotential equations to the Bethe-Salpeter equation.

1 Introduction

Over the past decade many dynamical models of pion-nucleon (πN) scattering based on meson-exchange have been developed. These models invariably begin with an effective hadronic Lagrangian describing the couplings between the various mesons and baryons. The tree-level diagrams obtained from this Lagrangian are then unitarized using an approximation to the Bethe-Salpeter equation (BSE) [1], such as the K-matrix approach or a 3-dimensional (3-D) quasipotential equation. The 3-D reduction procedure is ambiguous because there are an infinite number of different quasipotential equations [2, 3], each having different off-shell behaviour [4]. There is no overwhelming reason to choose one quasipotential equation over another. Sometimes quasipotential equations have been devised so as to have the correct one-body limit, however this argument has been shown to be not applicable to πN scattering [5]. Furthermore, many of the commonly used quasipotential equations violate charge-conjugation symmetry [6]. Here we avoid these problems by constructing a covariant model of elastic πN scattering [7] based on the BSE, which we solve without making any approximations to the relative-energy dependence of the kernel.

2 The model

The BSE for the $\pi N \to \pi N$ amplitude T is

$$T(q', q; P) = V(q', q; P) - \frac{i}{(2\pi)^4} \int d^4q'' V(q', q''; P) G_{\pi N}(q''; P) T(q'', q; P) \ , \tag{1}$$

where $G_{\pi N}$ is the 2-body πN propagator. In principle, both the π and N propagators should be fully dressed, but for only 2-body unitarity to be maintained, $G_{\pi N}$ has the simple form

$$G_{\pi N}(q; P) = \frac{1}{(\mu_\pi P - q)^2 - m_\pi^2 + i\epsilon} \frac{\mu_N \not{P} + \not{q} + m_N}{(\mu_N P + q)^2 - m_N^2 + i\epsilon} \ , \tag{2}$$

where μ_N and μ_π are functions of $s = P^2$ such that $\mu_N + \mu_\pi = 1$. The solution of the BSE does not depend on the choice of $\mu_N(s)$ and $\mu_\pi(s)$, so we use the simplest possibility: $\mu_N = \mu_\pi = 1/2$. The interaction kernel V is truncated to include only the 2nd order $\pi N \to \pi N$ diagrams obtained from the following interaction Lagrangian:

$$\begin{aligned} \mathcal{L}_{\text{int}} \quad &= \quad \frac{f_{\pi NN}}{m_\pi} \bar{N} \gamma_5 \gamma^\mu \boldsymbol{\tau} N \cdot \partial_\mu \boldsymbol{\pi} + \mathcal{L}_{\pi N \Delta} + g_{\sigma NN} \bar{N} N \sigma + \frac{g_{\sigma\pi\pi}}{2m_\pi} \sigma \, \partial_\mu \boldsymbol{\pi} \cdot \partial^\mu \boldsymbol{\pi} \\ &\quad + g_{\rho NN} \bar{N} \tfrac{1}{2} \boldsymbol{\tau} \cdot \left(\gamma_\mu \boldsymbol{\rho}^\mu + \frac{\kappa_\rho}{2m_N} \sigma_{\mu\nu} \partial^\mu \boldsymbol{\rho}^\nu \right) N + g_{\rho\pi\pi} \boldsymbol{\rho}^\mu \cdot (\boldsymbol{\pi} \times \partial_\mu \boldsymbol{\pi}) \ . \end{aligned} \tag{3}$$

Due to the ambiguity in the description of spin-3/2 particles, we consider two different possibilities for the $\pi N\Delta$ vertex:

$$\mathcal{L}^{\rm conv}_{\pi N\Delta} = \frac{f_{\pi N\Delta}}{m_\pi}\,\bar{\Delta}^\mu\,(g_{\mu\nu}+x_\Delta\gamma_\mu\gamma_\nu)\,\mathbf{T}N\cdot\partial^\nu\boldsymbol{\pi}+\text{h.c.}\,, \tag{4}$$

$$\mathcal{L}^{\rm Pas}_{\pi N\Delta} = \frac{f_{\pi N\Delta}}{m_\pi m_\Delta}\,\epsilon^{\mu\nu\alpha\beta}(\partial_\mu\bar{\Delta}_\nu)\gamma_5\gamma_\alpha\mathbf{T}N\cdot\partial_\beta\boldsymbol{\pi}+\text{h.c.} \tag{5}$$

Here $\mathcal{L}^{\rm conv}_{\pi N\Delta}$ is the conventional $\pi N\Delta$ vertex which contains the so-called off-mass-shell parameter x_Δ, while $\mathcal{L}^{\rm Pas}_{\pi N\Delta}$ is the Pascalutsa vertex [8]. For the Δ propagator we use the standard Rarita-Schwinger (RS) form [9]. It is well known that the RS spin-3/2 propagator contains off-mass-shell spin-1/2 components. The use of the Pascalutsa $\pi N\Delta$ vertex, together with the RS Δ propagator, ensures that the s- and u-channel Δ poles present in V are free of any contributions from the spin-1/2 components of the RS Δ propagator.

Regularization is achieved by the introduction of form factors. We consider two different parameterizations: in model I we associate a cutoff function with each vertex, where this cutoff function is taken as the product of form factors that depend on the 4-momentum squared of each particle present at the vertex. In model II, we associate a form factor only with the pion propagator. In both models, each form factor is chosen to have the form:

$$f(q_a^2) = \left(\frac{\Lambda_a^2-m_a^2}{\Lambda_a^2-q_a^2}\right)^{n_a}\;. \tag{6}$$

This form factor fulfils the requirement of only having poles along the real axis. In this work we use $n_{\rm all}=1$ for model I, and $n_\pi=8$ for model II.

We solve the BSE by first expanding the nucleon propagator in the πN intermediate states into positive and negative energy components, and then sandwiching the resulting equation between Dirac spinors. This gives two coupled 4-D integral equations which are reduced to 2-D integral equations after partial wave decomposition. A Wick rotation [10] is performed in order to obtain

	conventional		Pascalutsa	
	model I	model II	model I	model II
$g^2_{\pi NN}/4\pi$	13.5	13.5	13.5	13.5
$g^{(0)2}_{\pi NN}/4\pi$	1.80	4.68	12.1	6.64
$f^2_{\pi N\Delta}/4\pi$	**0.365**	**0.365**	**0.741**	**0.63**
$f^{(0)2}_{\pi N\Delta}/4\pi$	**0.37**	**0.20**	**0.193**	**0.1**
x_Δ	**-0.11**	**-0.24**	—	—
$g_{\rho\pi\pi}g_{\rho NN}/4\pi$	**2.88**	**2.63**	**2.73**	**2.25**
κ_ρ	**2.66**	**2.03**	**4.11**	**4.97**
$g_{\sigma\pi\pi}g_{\sigma NN}/4\pi$	**-0.41**	**0.39**	**-3.80**	**-4.65**
$m^{(0)}_N$	1.34	1.14	1.72	1.18
$m^{(0)}_\Delta$	**2.305**	**1.492**	**2.60**	**1.498**
m_σ	**0.65**	**0.62**	**0.69**	**1.12**
Λ_N	**3.17**	—	**4.90**	—
Λ_Δ	**4.56**	—	**3.20**	—
Λ_π	**1.77**	**1.85**	**1.76**	**2.08**
Λ_ρ	**3.67**	—	**3.06**	—
Λ_σ	**1.30**	—	**4.26**	—

Table 1: The coupling constants and particle masses resulting from fits to the πN data using the two different form factor parameterizations (denoted as model I and model II), and the two different $\pi N\Delta$ vertices. The quantities in boldface were varied in the fits. All masses are in GeV.

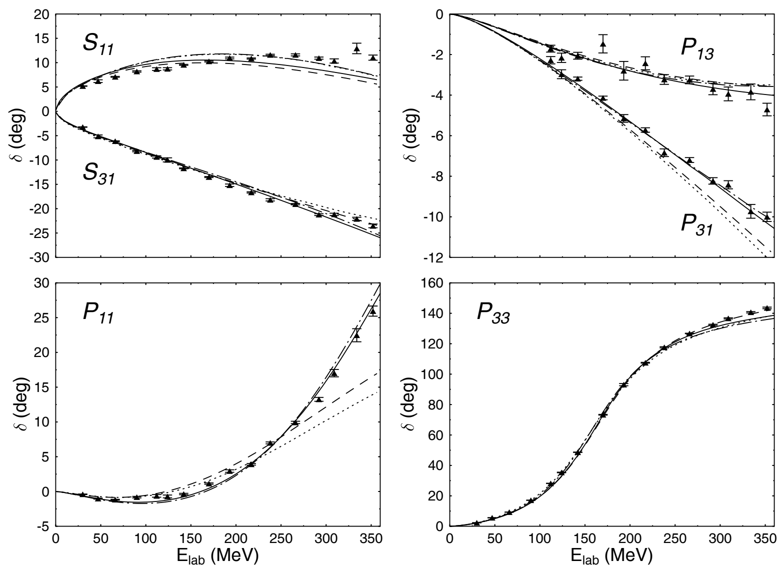

Figure 1: Phase shifts obtained from the BSE using the conventional $\pi N \Delta$ vertex [model I (solid line), model II (dot-dashed line)], and the Pascalutsa $\pi N \Delta$ vertex [model I (dashed line), model II (dotted line)]. The data points are from the SM95 partial wave analysis [11].

equations suitable for numerical solution. This means that all amplitudes are analytically continued in the relative-energy variables from the real axis to the imaginary axis, thereby avoiding the singularities of the kernel. Form factors with poles only along the real axis do not interfere with the Wick rotation provided the cutoff masses are large enough [7].

3 Numerical results

The free parameters are determined in χ^2 fits to the S- and P-wave phase shifts up to 360 MeV pion laboratory energy from the SM95 partial wave analysis [11]. The parameters obtained are shown in Table 1. Note that $g_{\pi NN}$ was fixed at $g_{\pi NN}^2/4\pi = 13.5$, while $g_{\pi NN}^{(0)}$ and $m_N^{(0)}$ were determined by the nucleon renormalization procedure [7]. This ensures that in the P_{11} partial wave the dressed s-channel nucleon pole diagram has a pole at the physical nucleon mass with a residue related to the physical πNN coupling constant.

The resulting phase shifts are shown in Figure 1. When the conventional $\pi N \Delta$ vertex is used, we obtain very good agreement with the partial wave analysis. There is some disagreement in the P_{11} partial wave when the the Pascalutsa $\pi N \Delta$ vertex is used, which suggests that the spin-1/2 components of the RS Δ propagator are necessary in order to obtain a good fit to the πN data. Note that the model II results are very close to the model I results, even though model II has four less free parameters. Therefore in our framework the use of a different cutoff mass for each particle results in unnecessary free parameters. The scattering lengths and volumes are shown in Table 2, where it is seen that we obtain reasonable agreement with the partial wave analyses.

Our coupling constants are consistent with the commonly accepted values in the literature,

$\ell_{2I\,2j}$	BSE (conv)	BSE (Pas)	SM95	KH80
S_{11}	0.177	0.172	0.175	0.173
S_{31}	-0.101	-0.105	-0.087	-0.101
P_{11}	-0.083	-0.058	-0.068	-0.081
P_{13}	-0.032	-0.031	-0.022	-0.030
P_{31}	-0.041	-0.041	-0.039	-0.045
P_{33}	0.178	0.187	0.209	0.214

Table 2: Scattering lengths and volumes obtained from the BSE in units of $m_\pi^{-(2\ell+1)}$, compared to results from the SM95 [11] and KH80 [12] πN partial wave analyses. The model I form factor parameterization was used.

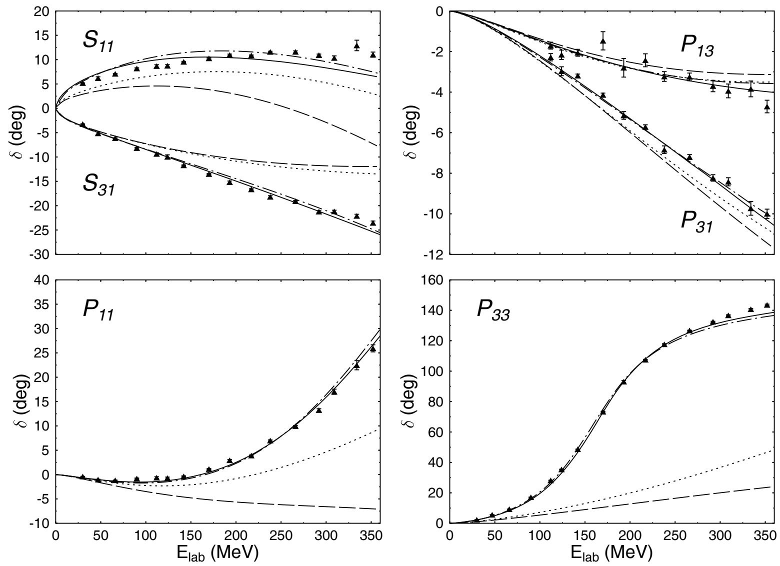

Figure 2: Comparison between the BSE [model I (solid line), model II (dot-dashed line)], and the K-matrix approximation [model I (dashed line), model II (dotted line)]. The conventional $\pi N\Delta$ vertex was used.

with the exception of $f_{\pi N\Delta}$ when the Pascalutsa $\pi N\Delta$ vertex is used. In this case, the $\pi N\Delta$ coupling constant is around twice as large as the so-called "empirical" value obtained from the decay $\Delta \to \pi + N$, i.e., $f^2_{\pi N\Delta}/4\pi = 0.36$. Notice in Table 1 that the choice of form factor parameterization does not have a significant effect on the values of the ρ and σ coupling constants. However, the choice of the $\pi N\Delta$ vertex does make a difference to κ_ρ and $g_{\sigma\pi\pi}g_{\sigma NN}$. It has been shown that Δ pole diagrams constructed using the conventional and Pascalutsa $\pi N\Delta$ vertices differ by a contact term [13]; in our models it appears that this contact term is partially being mimicked by the ρ and σ exchange diagrams.

4 Approximations to the Bethe-Salpeter equation

The BSE has not often been used in meson-exchange models to describe meson-baryon or baryon-baryon scattering processes. Due to the relative-energy integration, the BSE is usually regarded as being too hard to solve, so it has been much more common to use various approximations to the BSE. The K-matrix approach is the simplest method, where a unitary T matrix is found directly from the on-shell potential via

$$T = V - i\,\mathrm{Im}[G_{\pi N}]\,V \ . \tag{7}$$

This is obtained from the BSE when the principle-value parts of all loop diagrams are neglected. In Figure 2 we compare the K-matrix approach to the BSE, with the parameters obtained from the BSE fits used in the K-matrix approach calculations. For P_{13} and P_{31} the K-matrix results agree fairly well with the BSE. The results for the remaining partial waves illustrate the importance of dressing and multiple scattering: the K-matrix results deviate significantly from the BSE results. Note that for the model II form factors the K-matrix approach does slightly better than for model I, i.e., dressing and multiple scattering are more important in model I than in model II. This is due to the large size of the cutoff masses in the model I fit as compared to the cutoff mass in the model II fit (see Table 1).

Another approach is to approximate the relative-energy integration in the BSE in some way, resulting in a 3-D quasipotential equation. Note that many quasipotential equations depend on the choice of μ_N and μ_π [as defined in Eq. (2)] due to the violation of Lorentz-invariance. Here we consider the usual choice

$$\mu_N(s) = \frac{s + m_N^2 - m_\pi^2}{2s} \ , \qquad \mu_\pi(s) = \frac{s + m_\pi^2 - m_N^2}{2s} \ . \tag{8}$$

In the Cohen equation [14] it is assumed that the T matrix is independent of the relative-energy, and so the relative-energy integration can be performed explicitly over V and $G_{\pi N}$, resulting in a 3-D equation. In Salpeter's instantaneous equation [15], it is assumed that the interaction kernel is independent of the relative-energy, hence allowing the relative-energy integration to be performed explicitly over just $G_{\pi N}$. There are an infinite number of possible 3-D equations which are obtained from the BSE by replacing $G_{\pi N}$ by an approximate 2-body propagator which generates the πN unitarity cut, but contains a δ-function on the relative-energy. The Blankenbecler-Sugar (BbS) equation [16] uses the following propagator:

$$G_{\pi N}^{\rm BbS}(q;P) = 2\pi i \int_{s_{th}}^{\infty} \frac{ds' f(s',s)}{s' - s - i\epsilon} [\mu_N \not{P}' + \not{q} + m_N] \delta^{(+)}[(\mu_N P' + q)^2 - m_N^2] \delta^{(+)}[(\mu_\pi P' - q)^2 - m_\pi^2] \ , \tag{9}$$

where $s_{th} = (m_N + m_\pi)^2$, and the function $f(s',s)$ is taken as unity. We note that the choice of f is in fact arbitrary, provided $f(s,s) = 1$, hence allowing for the possibility of an infinity of different equations. Different choices for μ_N and μ_π also result in different equations. The Cooper-Jennings (CJ) equation [17] makes use of the propagator

$$G_{\pi N}^{\rm CJ}(q;P) = 2\pi i [\mu_N \not{P} + \not{q} + m_N] \int_{s_{th}}^{\infty} \frac{ds' f(s',s)}{s' - s - i\epsilon} \delta^{(+)}[(\mu_N P' + q)^2 - m_N^2] \delta^{(+)}[(\mu_\pi P' - q)^2 - m_\pi^2] \ , \tag{10}$$

where f is chosen such that $G_{\pi N}^{\rm CJ}$ can be rewritten as

$$G_{\pi N}^{\rm CJ}(q;P) = 2\pi i \, \frac{\delta(2P \cdot q)}{q^2 - k^2} \, [\mu_N \not{P} + \not{q} + m_N] \ , \tag{11}$$

with $k^2 = m_N^2 - s\mu_N^2(s)$.

Using the parameters obtained in the BSE fits to the πN partial wave analysis, we calculate phase shifts using the four different quasipotential equations and compare the results to the BSE.

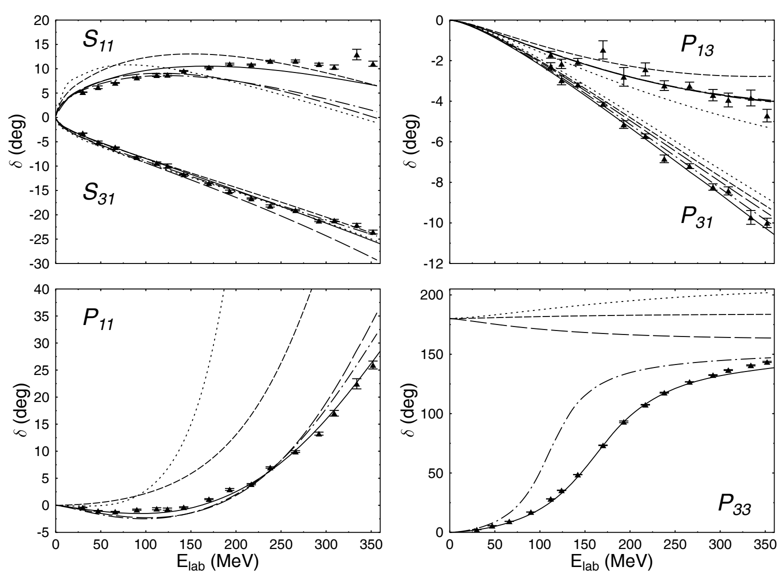

Figure 3: Comparison between the Bethe-Salpeter (solid line), Cohen (dot-dashed line), Salpeter (long-dashed line), Blankenbecler-Sugar (short-dashed line), and Cooper-Jennings (dotted line) equations. The conventional $\pi N \Delta$ vertex was used, with the model I form factor parameterization.

In Figure 3 we see that all four of the considered 3-D equations agree reasonably well with the BSE in the S_{31}, P_{13} and P_{31} partial waves. In the P_{11} partial wave, the Cohen and instantaneous equations agree well with the BSE results, but the Blankenbecler-Sugar and Cooper-Jennings equations generate far too much attraction. For P_{33} only the Cohen equation gives phase shifts with the same shape as the BSE results. The other three equations produce so much attraction that the $\Delta(1232)$ resonance has become a bound state, therefore causing the phase shifts at the πN threshold to be 180°, rather than 0°.

The agreement between the Cohen equation and the BSE is not surprising, and has been found before in $\phi\phi$ scattering [18]. The relative-energy integration over $VG_{\pi N}$ produces 4-body as well as 2-body thresholds. Consequently, the T matrix obtained from the Cohen equation contains more of the analytic structure generated by the BSE as compared to the other quasipotential equations considered here, which only contain the 2-body threshold.

5 Concluding remarks

In summary, we have presented a relativistic description of πN scattering based on the Bethe-Salpeter equation, which we have compared to some approximations schemes, including the K-matrix approach and four different 3-D quasipotential equations. In some partial waves large differences were found between the BSE and the other approaches.

The present model could be extended to higher energies by including resonances into the interaction kernel and couplings to inelastic channels, or extended to include the photon so as to give a covariant model of pion photoproduction including final-state interactions. Work in both these directions is in progress.

Acknowledgments: This work was supported by the Australian Research Council. We also acknowledge the South Australian Centre for Parallel Computing for access to their computing facilities.

References

[1] E. E. Salpeter and H. A. Bethe, Phys. Rev. **84**, 1232 (1951).
[2] R. J. Yaes, Phys. Rev. D **3**, 3086 (1971).
[3] A. Klein and T.-S. H. Lee, Phys. Rev. D **10**, 4308 (1974).
[4] C. Hung, S. N. Yang and T.-S. H. Lee, Phys. Rev. C **64**, 034309 (2001).
[5] V. Pascalutsa and J. A. Tjon, Phys. Rev. C **60**, 034005 (1999).
[6] V. Pascalutsa and J. A. Tjon, Phys. Lett. B **435**, 245 (1998).
[7] A. D. Lahiff and I. R. Afnan, Phys. Rev. C **60**, 024608 (1999).
[8] V. Pascalutsa, Phys. Rev. D **58**, 096002 (1998).
[9] W. Rarita and J. Schwinger, Phys. Rev. **60**, 61 (1941).
[10] G. C. Wick, Phys. Rev. **96**, 1124 (1954).
[11] R. A. Arndt, I. I. Strakovsky, R. L. Workman and M. M. Pavan, Phys. Rev. C **52**, 2120 (1995).
[12] R. Koch and E. Pietarinen, Nucl. Phys. A **336**, 331 (1980).
[13] V. Pascalutsa, Phys. Lett. B **503**, 85 (2001).
[14] H. Cohen, Phys. Rev. D **2**, 1738 (1970).
[15] E. E. Salpeter, Phys. Rev. **87**, 328 (1952).
[16] R. Blankenbecler and R. Sugar, Phys. Rev. **142**, 1051 (1966).
[17] E. D. Cooper and B. K. Jennings, Nucl. Phys. A **500**, 553 (1989).
[18] R. M. Woloshyn and A. D. Jackson, Nucl. Phys. B **64**, 269 (1973).

A relativistic meson-exchange model of pion-nucleon scattering

Shin Nan Yang[a], Guan-Yeu Chen[a], C. T. Hung[b], and T.-S. H. Lee[c]

[a]*Department of Physics, National Taiwan University, Taipei, Taiwan 10617, ROC*
[b]*Chung-Hua Institute of Technology, Taipei, Taiwan 11571, ROC*
[c]*Argonne National Laboratory, Argonne, Illinois 60439, U.S.A.*

(Received: 31 October 2001)

The pion-nucleon scattering is investigated by using several three-dimensional reduction schemes of the Bethe-Salpeter equation for a model Lagrangian involving π, N, Δ, ρ, and σ fields. It is found that all of the resulting meson-exchange models can give similar good descriptions of the πN scattering data up to 400 MeV. However they have significant differences in describing the πN off-shell t-matrix elements. The effect of the difference in the off-shell behaviors is explored in threshold π^0 photoproduction.

1 Introduction

Pion-nucleon interaction is one of the fundamental building blocks in the description of nuclear reactions involving pions. Most of the existing theoretical studies of intermediate energy nuclear reactions have been carried out with simple phenomenological πN models which are often parameterized as separable forms. Since the meson-exchange models [1] have been very successful in describing NN scattering, it is reasonable to expect that the πN dynamics at low and intermediate energies can also be described by the same approach. Several attempts [2–8] have been made recently to construct πN models within the field-theoretic meson-exchange picture. In this talk I will report the recent progress [9] we have made in improving the πN model which was previously developed by us in [2, 5]. Our immediate objective is to obtain an accurate meson-exchange πN model, which is needed within the Hamiltonian formulation of pion photoproduction developed in Ref. [10]. The importance of a reliable description of πN off-shell behaviors in the study of (γ, π) reaction on nucleon has been demonstrated in [2]. We show here that, with a proper choice of πN off-shell behavior, it is possible to give a good description, comparable to that provided by the chiral perturbation theory calculation, of the threshold π^0 photoproduction from proton, in addition to other pion photoproduction data at higher energies up to resonance region [11].

2 The model

We start with the Bethe-Salpeter (BS) equation for the πN scattering

$$T_{\pi N} = B_{\pi N} + B_{\pi N} G_0 T_{\pi N} \ , \tag{1}$$

where $B_{\pi N}$ is the sum of all irreducible two-particle Feynman amplitudes and G_0 is the relativistic free pion-nucleon propagator.

Eq. (1) is a four-dimensional integral equation. Since we are interested in constructing a πN model to be embedded within the conventional nuclear theoretical framework, which is three-dimensional, we will employ three-dimensional reduction scheme of Eq. (1) to proceed. This can be done by replacing the propagator G_0 of Eq. (1) with an approximate propagator $\hat{G}_0(k; P)$ which would reduce Eq. (1) to a three-dimensional integral equation. In order to maintain the two-body unitarity, one often chooses a $\hat{G}_0$ which can reproduce the πN elastic cut. It is well known that the choice of such a $\hat{G}_0$ is rather arbitrary. In this work, we focus on a class of three-dimensional equations which can be obtained by choosing the following form

$$\hat{G}_0(k;P) = \frac{1}{(2\pi)^3}\int \frac{ds'}{s-s'} f(s,s')\left[\alpha(s,s')\not{P}+\not{k}+m_N\right]$$
$$\times\, \delta^{(+)}\left([\eta_N(s')P'+k]^2-m_N^2\right)\delta^{(+)}\left([\eta_\pi(s')P'-k]^2-m_\pi^2\right)\ , \qquad (2)$$

where $P' = \sqrt{s'/s}P$, and $P = p+q$ and $k = \eta_\pi(P^2)p - \eta_N(P^2)q$ are the total and relative 4-momentum, respectively; f, α, η_N and η_π are the dimensionless degree of freedom of reduction constrained by the conditions $\eta_N+\eta_\pi = 1$, $f(s,s) = 1$ and $\alpha(s,s) = \eta_N(s)$. The last two conditions ensure the reproduction of elastic cut. The superscript $(+)$ associated with δ-functions means that only the positive energy part is kept in defining the propagator. It is common to choose the following definition for the $\eta's$: $\eta_N(s) = \varepsilon_N(s)/(\varepsilon_N(s)+\varepsilon_\pi(s))$ and $\eta_\pi(s) = \varepsilon_\pi(s)/(\varepsilon_N(s)+\varepsilon_\pi(s))$, where $\varepsilon_N(s) = (s+m_N^2-m_\pi^2)/2\sqrt{s}$ and $\varepsilon_\pi(s) = (s-m_N^2+m_\pi^2)/2\sqrt{s}$ are the center of mass (CM) energies of nucleon and pion, respectively.

This class of propagators, where both particles are equally off mass shell such that the relative energy dependence in the interaction is removed, was first proposed by Blankenbecler and Sugar (BbS) [12] and Thompson (Thomp) [13] and used in the construction of Bonn NN potential. In this work, we consider two more reduction schemes of the same class in order to explore the scheme dependence of the results, namely, the one proposed by Cooper-Jennings (CJ) [14] and the other a modified version constructed by Kadyshevsky (Kady) [15]. CJ propagator was designed to remove as much short-range structure in the propagator as possible in order to preserve chiral symmetry, while the modified Kadyshevsky propagator has the advantage that the resulting three-dimensional integral equation is of the Lippmann-Schwinger equation type and the obtained potential is more readily to be used in many-body systems. The characteristics of these four propagators, namely, BbS, Kady, Thomp, and CJ are summarized in Table I.

The integral over s' in Eq. (2) can be carried out to give, in the CM frame,

$$\hat{G}_0(k;s) = \frac{1}{(2\pi)^3}\frac{\delta(k_0-\hat{\eta}(s_{\vec{k}},\vec{k}))}{\sqrt{s}-\sqrt{s_{\vec{k}}}}\frac{2\sqrt{s_{\vec{k}}}}{\sqrt{s}+\sqrt{s_{\vec{k}}}}f(s,s_{\vec{k}})\,\frac{\alpha(s,s_{\vec{k}})\gamma_0\sqrt{s}+\not{k}+m_N}{2E_N(\vec{k})2E_\pi(\vec{k})}\ , \qquad (3)$$

where $E_N(\vec{k})$ and $E_\pi(\vec{k})$ are the nucleon and pion energies with three-momentum $\vec{k}$ and $\sqrt{s_{\vec{k}}} = E_N(\vec{k})+E_\pi(\vec{k})$, $\hat{\eta}(s,\vec{k}) = E_N(\vec{k})-\eta_N(s)\sqrt{s}$. We then obtain a πN scattering equation which in the CM frame takes the following familiar form

$$t(\vec{k}',\vec{k};E) = v(\vec{k}',\vec{k};E) + \int d\vec{k}''\, v(\vec{k}',\vec{k}'';E)\, g_0(\vec{k}'';E)\, t(\vec{k}'',\vec{k};E)\ , \qquad (4)$$

	BbS	Kady	Thomp	CJ
$\alpha(s,s')$	$\eta_N(s')\sqrt{\frac{s'}{s}}$	$\eta_N(s')\sqrt{\frac{s'}{s}}$	$\eta_N(s)$	$\eta_N(s)$
$f(s,s')$	1	$\frac{\sqrt{s}+\sqrt{s'}}{2\sqrt{s'}}$	$\frac{\sqrt{s}+\sqrt{s'}}{2\sqrt{s}}$	$\frac{4\sqrt{ss'}\,\varepsilon_N(s')\,\varepsilon_\pi(s')}{ss'-(m_N^2-m_\pi^2)^2}$

Table I: The functions $\alpha(s,s')$ and $f(s,s')$ of Eq. (2), chosen for the four considered reduction schemes, i.e., Blankenbecler and Sugar (*BbS*) [12], modified Kadyshevsky (*Kady*) [15], Thompson (*Thomp*) [13], and Cooper and Jennings (*CJ*) [14].

where E is the total energy in the CM frame. Explicitly, the relations between (t, v, g_0) and $(T, B, \hat{G}_0)$ are $t(\vec{k}', \vec{k}; E) = \int dk'_0 dk_0\, \delta(k'_0 - \hat{\eta}')T(k', k; E)\delta(k_0 - \hat{\eta}), v(\vec{k}', \vec{k}; E) = \int dk'_0 dk_0\, \delta(k'_0 - \hat{\eta}')B(k', k; E)\delta(k_0 - \hat{\eta})$, and $g_0(\vec{k}; E) = \int dk_0 \hat{G}_0(k; E)$, where $\hat{\eta}' = \hat{\eta}(s_{\vec{k}'}, \vec{k}')$ and $\hat{\eta} = \hat{\eta}(s_{\vec{k}}, \vec{k})$.

To proceed, we further approximate the $\hat{B}(k', k; E)$ in Eq. (1) by the tree approximation of the the following interaction Lagrangian

$$\begin{aligned} \mathcal{L}_I \quad = \quad & \frac{f^{(0)}_{\pi NN}}{m_\pi} \bar{N}\gamma_5\gamma_\mu \vec{\tau} \cdot \partial^\mu \vec{\pi} N - g^{(s)}_{\sigma\pi\pi} m_\pi \sigma(\vec{\pi} \cdot \vec{\pi}) - \frac{g^{(v)}_{\sigma\pi\pi}}{2m_\pi} \sigma \partial^\mu \vec{\pi} \cdot \partial_\mu \vec{\pi} \\ & - g_{\sigma NN} \bar{N}\sigma N - g_{\rho NN} \bar{N} \left\{ \gamma_\mu \vec{\rho}^{\,\mu} + \frac{\kappa^\rho_V}{4m_N} \sigma_{\mu\nu} \left(\partial^\mu \vec{\rho}^{\,\nu} - \partial^\nu \vec{\rho}^{\,\mu}\right) \right\} \cdot \tfrac{1}{2}\vec{\tau} N \\ & - g_{\rho\pi\pi} \vec{\rho}^{\,\mu} \cdot (\vec{\pi} \times \partial_\mu \vec{\pi}) - \frac{g_{\rho\pi\pi}}{4m^2_\rho}(\delta - 1)(\partial^\mu \vec{\rho}^{\,\nu} - \partial^\nu \vec{\rho}^{\,\mu}) \cdot (\partial_\mu \vec{\pi} \times \partial_\nu \vec{\pi}) \\ & + \left\{ \frac{g^{(0)}_{\pi N\Delta}}{m_\pi} \bar{\Delta}_\mu \left[g^{\mu\nu} - \left(Z + \tfrac{1}{2}\right) \gamma^\mu \gamma^\nu \right] \vec{T}_{\Delta N} N \cdot \partial_\nu \vec{\pi} + h.c. \right\} . \end{aligned} \tag{5}$$

The notations of Bjorken-Drell are used in Eq. (5) to describe the interactions involving the field operators for the nucleon N, the pion $\vec{\pi}$, the rho meson $\vec{\rho}$, and a fictitious scalar meson σ. Δ_μ is the Rarita-Schwinger field operator for the Δ, and $\vec{T}_{\Delta N}$ is the isospin transition operator between a nucleon and a Δ. The resulting driving term consists of the direct and crossed N and Δ terms, and the t-channel σ- and ρ-exchange terms. The corresponding potential matrix elements can be found in Ref. [9]. The admixture of vector and scalar $\sigma\pi\pi$ couplings in Eq. (5) is designed to simulate the broad width observed experimentally in the S-wave correlated $\pi\pi$ pair [5].

Because of the appearance of one-particle intermediate state in the driving term corresponding to direct nucleon Born diagram, renormalization of the nucleon mass and the πNN coupling constant is needed. We follow the procedure of Afnan and his collaborators [16] to constrain the fit of P_{11} phase shifts by imposing the nucleon pole condition. This leads to a proper treatment of the renormalization of nucleon mass and the πNN coupling constant. It also yields the needed cancellation between the contributions from the repulsive nucleon pole and the attractive background, such that a reasonable fit to the πN phase shifts in P_{11} channel can be achieved.

To complete the model we need to introduce form factors to regularize the potential matrix elements $v(\vec{k}, \vec{k}')$. In this work we follow Pearce and Jennings [3] and associate each external leg of the potential matrix elements with a form factor of the form

$$F(\Lambda, p) = \left[\frac{n\Lambda^4}{n\Lambda^4 + (p^2 - m^2)^2} \right]^n , \tag{6}$$

where $p = (p_0, \vec{p})$ with $p_0 = (m^2_N + p^2_E)^{1/2}$ defined by the on-shell momentum p_E of the incident energy. Note that as $n \to \infty$, $F(\Lambda, p)$ approaches to a Gaussian form.

The parameters which are allowed to vary in fitting the empirical phase shifts are: $(g_{\sigma NN} g^{(s)}_{\sigma\pi\pi})$, $(g_{\sigma NN} g^{(v)}_{\sigma\pi\pi})$, $(g_{\rho NN} g_{\rho\pi\pi})$, and δ for the t-channel σ and ρ exchanges, $m^{(0)}_\Delta$, $g^{(0)}_{\pi N\Delta}$, Z for the Δ mechanisms, and the cut-off parameters Λ's of the form factors of Eq. (6). In the crossed N diagram, the physical πNN coupling constant is used. For the crossed Δ diagram, the situation is not so clear since the determination of the "physical" $\pi N\Delta$ coupling constant depends on the nonresonant contribution in the P_{33} channel. In principle, it can be determined by carrying out a renormalization procedure similar to that used for the nucleon. However, it is a much more difficult numerical task because the Δ pole is complex. As in Ref. [3–5], such a renormalization for the Δ is not carried out in this work and we simply allow the coupling constant used in the crossed Δ diagram to also vary in the fit to the data. This coupling constant is denoted as $g_{\pi N\Delta}$.

3 Results and discussions

We present here only the results for models with rank $n = 10$ form factor defined by Eq. (6). The constructed models are called $C10$, $B10$, $T10$, and $K10$ for the Cooper-Jennings, Blankenbecler-Sugar, Thompson, and modified Kadyshevsky reduction schemes, respectively. For each model, we adjust the parameters described in the previous section to fit the data of πN scattering phase shifts [17]. The results for the $K10$ model is shown in Fig. 1. We see that the data can be described very well except in the P_{11} channel, where our predictions lie below the data at energy higher than 1300 MeV. The difficulty in getting the same quality fit to this channel is mainly due to the nucleon renormalization conditions for the nucleon mass and πNN coupling constant. This difficulty is well known in the literature. The results of other three models are very similar.

The resulting parameters of the constructed four models are listed in Table II. We first notice that the bare πNN coupling constant $g^{(0)}_{\pi NN} = (2m_N/m_\pi)f^{(0)}_{\pi NN}$ is considerably smaller than the physical value $g_{\pi NN}$ in all models. This large vertex renormalization is closely related to an about

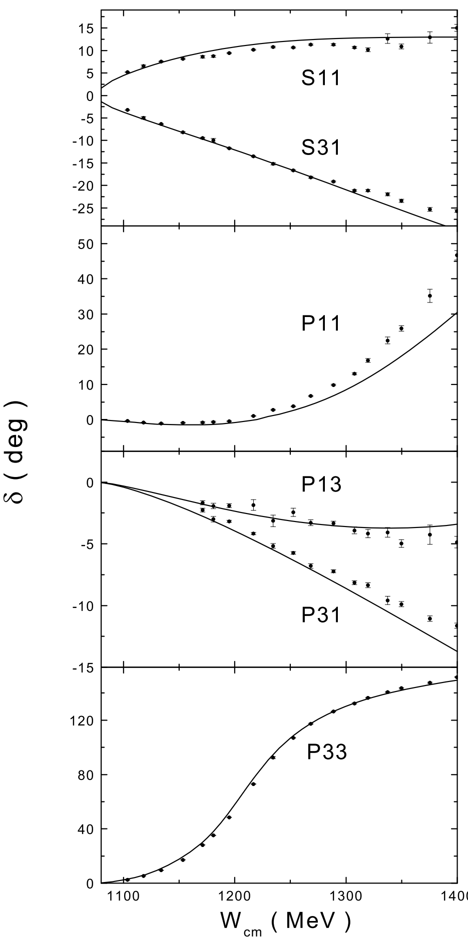

Figure 1: Our model predictions for πN phase shifts in S- and P-waves obtained within modified Kadyshevsky reduction scheme and with the use of a $n = 10$ form factor of Eq. (6). The data are from [17].

Parameter	C10	B10	T10	K10
m_N	939	939	939	939
$m_N^{(0)}$	1093	1059	1065	1073
m_π	137	137	137	137
m_Δ	1232	1232	1232	1232
$m_\Delta^{(0)}$	1428	1404	1407	1420
m_ρ	770	770	770	770
m_σ	654	662	654	654
$g^2_{\pi NN}/4\pi$	14.3	14.3	14.3	14.3
$g^{(0)^2}_{\pi NN}/4\pi$	4.41	6.46	5.77	6.82
$g_{\sigma NN}g^{(s)}_{\sigma\pi\pi}/4\pi$	0	0	-0.49	-0.39
$g_{\sigma NN}g^{(v)}_{\sigma\pi\pi}/4\pi$	144	228	-1.52	-1.43
$g_{\rho NN}g_{\rho\pi\pi}/4\pi$	3.13	2.90	3.05	2.68
δ	1	1	0.65	1.26
$g^2_{\pi N\Delta}/4\pi$	0.36	0.36	0.29	0.33
$g^{(0)^2}_{\pi N\Delta}/4\pi$	0.17	0.17	0.17	0.18
Z	-0.38	-0.092	-0.13	-0.065
κ^ρ_V	2.25	1.44	1.45	1.41
Λ_N	1117	1384	1300	1373
Λ_σ	512	500	653	400
Λ_ρ	1214	1545	1431	2272
Λ_Δ	1035	1390	1522	1507
Λ_π	700	700	682	767

Table II. The parameters of the constructed meson-exchange models are compared. The form factor Eq. (6) with $n = 10$ is used. The models are constructed by using the three-dimensional reduction schemes of C10, B10, T10, and K10.

150 MeV mass shift between the bare mass $m_N^{(0)}$ and m_N, as seen in the first two rows of Table 2. The determined physical coupling constant $g_{\pi N\Delta}$ for the crossed Δ term, is also significantly larger than the bare coupling constant $g_{\pi N\Delta}^{(0)}$. The large difference between the bare mass $m_\Delta^{(0)} \sim 1400$ MeV and the resonance position $m_\Delta = 1232$ MeV seems to be a common feature of the constructed models.

The parameters associated with the ρ-exchange are comparable to that of other meson-exchange πN models. The $\sigma-$exchange turns out to be not important in the fit. If we set the coupling constant $g_{\sigma NN} g_{\sigma\pi\pi}^{(v)}$ of all models to zero, the resulting phase shifts are not changed much. It is also interesting to note that the fit to the data seems to favor a soft πNN form factor with $\Lambda_\pi \leq 750$ MeV for all models considered.

We have also investigated how the models depend on the parameterization of the form factors. If form factors defined by Eq. (6) with $n = 2$ are used, we find that a fit comparable to that shown in Fig. 1 can be obtained as well as shown in [9]. There are some significant, though not very large, changes in the resulting parameters.

4 Threshold π^0 photoproduction

The constructed four models can be considered approximately phase-shift equivalent. We therefore can examine how the resulting πN off-shell dynamics depends on the chosen three-dimensional reduction. The πN off-shell amplitudes are needed to study nuclear dynamics involving pions. To be specific, let us focus here on how the constructed models can be used to investigate the near threshold π^0 photoproduction where considerable progress has been made in the last few years [18].

In the dynamical model for pion photoproduction [10, 11], the physical multipoles in channel $\alpha = \{l, j\}$, is given by

$$t_\alpha(q_E, k) = \exp(i\delta_\alpha)\, \cos\delta_\alpha \left[v_\alpha(q_E, k) + P\int_0 dq' \, \frac{R_{\pi N}^{(\alpha)}(q_E, q')\, v_\alpha(q', k)}{E(q_E) - E(q')} \right] , \tag{7}$$

where δ_α and R_α are the πN phase shift and reaction matrix, in channel α, respectively, q_E is the pion on-shell momentum and $k = \mid \mathbf{k} \mid$ the photon momentum. The second term on the r.h.s. of Eq. (7) correspond to the off-shell rescattering effects after the pion is first produced by transition potential $v_{\gamma\pi}$. We see that it explicitly depends on the off-shell behaviors of $R_{\pi N}^{(\alpha)}$.

In Fig. 2, we show our dynamical model prediction for the E_{0+} multipole for $\gamma p \to \pi^0 p$ near threshold, obtained from Eq. (7) with $R_{\pi N}^{(\alpha)}$ given by the four πN models constructed above, as

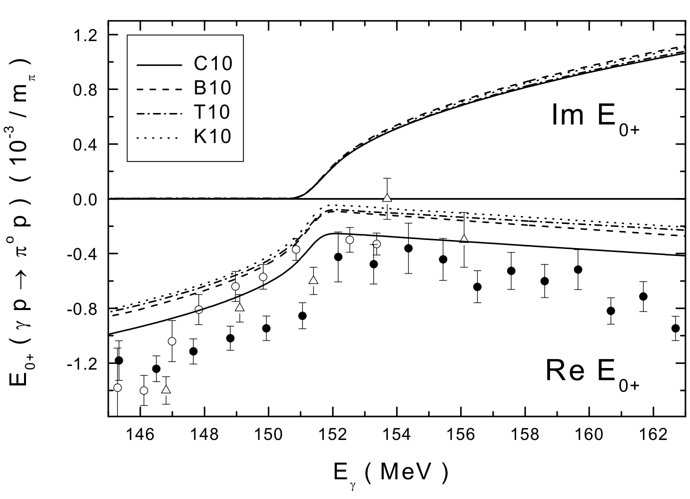

Figure 2: Our dynamical model predictions for the real (lower panel) and imaginary (upper panel) parts of the E_{0+} multipole for threshold π^0 photoproduction obtained from Eq. (7) with final state πN interaction given by the C10, B10, T10, and K10 models. Data points from Ref. [19].

compared with recent precise measurements [19]. It is seen that indeed the predictions for E_{0+} obtained with four different πN models constructed with different three-dimensional reduction schemes, namely, C10, B10, T10, and K10, show some varaitions, even though they all exhibit similar energy dependence. It is interesting to see that only the prediction obtained with C10 agrees well with the data. This is likely related to the fact that Cooper-Jennings propagator was designed to restore chiral symmetry and the threshold π^0 photoproduction is mostly dictated by chiral symmetry and gauge invariance. It is very assuring that the same model has been found to give excellent agreement with the data at higher energies [11]. Our dynamical model predictions for the π^0 electroproduction can also describe well the experiment [20].

5 Summary

In summary, we have shown that the πN scattering data up to 400 MeV can be equally well described by four reduction schemes of Bethe-Salpeter equation. The resulting meson-exchange models yield rather different off-shell dynamics. We show that the π^0 threshold photoproduction is indeed quite sensitive to the πN off-shell dynamics. We find that, within a dynamical model for pion photoproduction, only the predictions calculated with the off-shell behaviors obtained with Cooper-Jennings' propagator can agree with the experiments.

Acknowledgments: This work is supported in part by the National Science Council of ROC under grant No. NSC89-2112-M002-078 and the U.S. Department of Energy, Nuclear Physics Division, under contract No.W-31-109-ENG-38 and also in part by the U.S.-Taiwan National Science Council Cooperative Science Program grant No. INT-9021617.

References

[1] R. Machleidt, K. Holinde and Ch. Elster, Phys. Reports, **149**, 1 (1987); M. Lacombe *et al.*, Phys. Rev. **C21**, 861 (1980).

[2] C.C. Lee, S.N. Yang, and T.-S.H. Lee, J. Phys. **G17,** L131 (1991); S.N. Yang, Chin. J. Phys. **29,** 485 (1991).

[3] B.C. Pearce and B. Jennings, Nucl. Phys. **A528,** 655 (1991).

[4] F. Gross and Y. Surya, Phys. Rev. **C47**, 703 (1993).

[5] C.T. Hung, S.N. Yang and T.-S.H. Lee, J. Phys. **G20,** 1531 (1994).

[6] T. Sato and T.-S. H. Lee, Phys. Rev. **C54**, 2660 (1996).

[7] A.D. Lahiff and I.R. Afnan, Phys. Rev. **C60**, 024608 (1999).

[8] V. Pascalutsa and J.A. Tjon, Phys. Rev. **C61**, 054003 (2000).

[9] C.T. Hung, S.N. Yang and T.-S.H. Lee, Phys. Rec. **C64,** 034309 (2001).

[10] S.N. Yang, J. Phys. **G11**, L205 (1985).

[11] S.S. Kamalov and S.N. Yang, Phys. Rev. Lett. **83** 4494 (1999).

[12] R. Blankenbecler and R. Sugar, Phys. Rev. **142**, 1051 (1966).

[13] R.H. Thompson, Phys. Rev. **D1**, 110 (1970).

[14] M. Cooper and B. Jennings, Nucl. Phys. **A500**, 553 (1989).

[15] V.G. Kadyshevsky, Nucl. Phys. **B6**, 125 (1968).

[16] S. Morioka and I.R. Afnan, Phys. Rev. **C26**, 1148 (1982).

[17] R.A. Arndt, I.I. Strakovsky and R.L. Workman, Phys. Rev. **C53**, 430 (1996).

[18] "Chiral Dynamics: Theory and Experiment", Eds. A.M. Bernstein *et. al.*, Springer, New York, 1997.

[19] M. Fuchs *et al.*, Phys. Lett. **B368**, 20 (1996); J.C. Bergstrom *et al.*, Phys. Rev. **C53**, R1052 (1996) ; **C55** 2016 (1997); A. Schmidt *et al.*, nucl-exp/0105010.

[20] S.S. Kamalov, G.Y. Chen, S.N. Yang, D. Drechsel, and L. Tiator, to appear in Phys. Lett. **B**, 2001.

Recent results of coupled-channel analyses and an overview of BRAG

S.A. Dytman

Department of Physics and Astronomy, University of Pittsburgh, Pittsburgh, PA 15260, U.S.A.

(Received: 31 October 2001)

A brief review of the status of coupled channel analyses for extraction of baryon resonance properties. This is the main link between the large body of experiments and the microscopic studies of baryon structure. Recent results on the parameters and their model dependence are reported.

1 Introduction

This is a time when the knowledge about baryon resonances can grow rapidly. Many dedicated experiments are underway, most of which have reports at this conference. The quality of data is unprecedented for this subject. Many reactions are being measured with vast statistics and high polarization of the beam and/or target. The complexity of the final state has also grown. It is appropriate that the analysis methods used to extract their properties be reexamined and improved where possible. The Baryon Resonance Analysis Group (BRAG) has been formed for this purpose.

2 Formalism

Models are always used to extract baryon properties because there is no objective theory for the scattering process. Thus, it is important to understand the advantages and disadvantages of each model. It is dangerous to use a model where it is not valid. Definition of a model dependent error would be an ambitious step beyond that.

A simple, traditional way to analyze data for resonance properties is with the Breit-Wigner shape, the isobar models. This models the energy (s is the invariant square of the energy) dependence with the right relationship between the real and imaginary parts of the T matrix. The real part goes through a zero, the imaginary part peaks at the resonance mass, and there is a peak in the cross section when s is equal to the resonance mass squared. However, this expression in not analytic, i.e. the T-matrix is not defined for imaginary s, and there is no prescribed way to generalize the one channel case to the multichannel case. The Mainz group [1] has developed an ad hoc prescription that satisfies unitarity to simultaneously analyze πN elastic scattering and pion photoproduction data.

A traditional way to generalize to multiple channels satisfying unitarity is the K-matrix [2, 3]. Each resonance is represented by a matrix in channel space that has coupling parameters to each channel. The full K matrix is a sum of the resonance and nonresonance contributions. The resonance terms have Breit-Wigner energy dependence and the nonresonant terms are calculated from diagrams such as the Born terms for photoproduction. This has the disadvantage of not being naturally analytic. Although it can be converted to a T-matrix, the Riemann structure is not secure.

Another multichannel method to fit data uses a T-matrix. The CMB model [4] is intrinsically analytic and unitary. It can incorporate any 2-body or quasi-2-body channel for which there are PWA inputs. While the common K-matrix model assumes all rescattering in the intermediate state is on-shell, the CMB model uses a Dyson-Schwinger equation to fully model rescattering. Although the Pitt-ANL model [5] has included Born diagrams for pion and eta photoproduction, the major disadvantage of this model as presently constructed is the use of distant poles in place of πN nonresonant interaction diagrams.

The work of Meissner, Oset, and collaborators [6] has a somewhat different starting point. They assume reactions according to a Chiral Lagrangian and fit its parameters to the data. Form factors are avoided through proper renormalization techniques. They introduce rescattering in a T-matrix through loop effects for each meson-baryon combination. Limitations on the loops and the orbital angular momentum that can be handled reduces the region of energy that can be studied. They presently include no *explicit* resonant mechanisms and still fit data.

3 Role of poles

A resonance can be found as a peak in a cross section, a rotation in the Argand plot (a Breit-Wigner amplitude) [2, 3, 7], or as a pole in the T-matrix [4–6]. The first is simple to implement, but it is difficult to assess the validity. The other two methods have a more solid basis, but still can be sensitive to the choice of nonresonant mechanisms and form factors. Pole positions are felt to be less model dependent and have always been an important part of the PDG summary.

The Pitt-ANL T-matrix amplitude analysis [5] differs from the work of Meissner, Oset, and collaborators. Although each finds poles, an amplitude analysis can only insert resonances and determine whether the fit prefers states under study or not. On the other hand, the chiral Lagrangian doesn't make assumptions about reaction mechanisms. Resonances are not explicitly introduced, but can be created through strong meson-baryon interactions. Poles must then be studied to learn whether they are resonances or not.

The T-matrix amplitude is characterized in the complex s plane by Riemann sheets. Above πN threshold, there are 2 sheets because the ambiguity in taking square roots of complex numbers. They are joined at the $\Re e\, s$ axis along the unitary or 'right hand' branch cut. Each kinematic threshold causes a new branch cut and each sheet splits into two more sheets. Thus, a two-channel problem (e.g. πN and ηN) has 4 sheets. The standard way to label the sheets is in terms of the sign of the imaginary part of the channel momentum which involves square roots of energy in any formalism. See Ref. [8] and its references for a more complete discussion. Every physical pole has an associated 'bare' pole that is on the real axis or at infinity. This 'bare' pole has an important role in understanding the phyisical or 'dressed' pole. We can think of a resonance as dressed by the coupling to the asymptotic channels, also called final state interactions.

Poles that have the largest effect on observables are found in the lower part (negative imaginary part) and can be found on any Riemann sheet except the first. The primary pole is always the pole that is closest to the real axis. In the two channel case, that is the third sheet. (See Ref. [9] for a discussion of this case.) These poles can have either resonant or nonresonant sources and have differences in behavior as a result.

If the pole is a resonance, it never has poles on every sheet. In the two-channel case it will have the primary pole on the third and secondary poles on the second or fourth sheets. These two pole positions will likely be at similar energies with $\Re e\, s$ at about the Breit-Wigner mass and $\Im m\, s$ at approximately half of the Breit-Wigner width. Most importantly, the 'bare' pole location can be determined from gradually turning off the 'dressing'. Each resonance pole will move to the real axis above threshold, e.g. $s > (m_\pi + m_p)^2$. The poles on different sheets due to the same resonance will move to the same bare pole.

The other main possibility is that the pole comes from large coupling constants in a t-channel mechanism, e.g. pion or rho exchange. This nonresonant mechanism can produce 'dressed' poles on any sheet. There can be poles on every sheet and they are unlikely to be close to each other in energy because they are not associated with a bare pole above πN threshold. They come from bare poles at $s < -(m_\pi + m_p)^2$ (commonly called the left hand cut) or at infinity. Tracking each pole by turning off the interactions will show its genealogy. A common behavior for so-called coupled channel (CC) poles is to switch sheets [8], further complicating interpretation.

Thus, an objective potential has the best possibilities to find the true analytic structure of the amplitude and the true provenance of each physical pole comes from finding its bare pole. A model should provide s-channel (resonant) and t-channel (nonresonant) mechanisms and let the data decide which is preferred. The CMB model introduces only bare poles that correspond to resonances. Simpler models unfortunately don't have bare poles.

4 Results

The results of fits for the D_{13} and S_{11} partial waves will be presented here. Each has well-established resonances at low mass, moderately well-established resonances at higher energy, and poorly understood resonances at the highest energies.

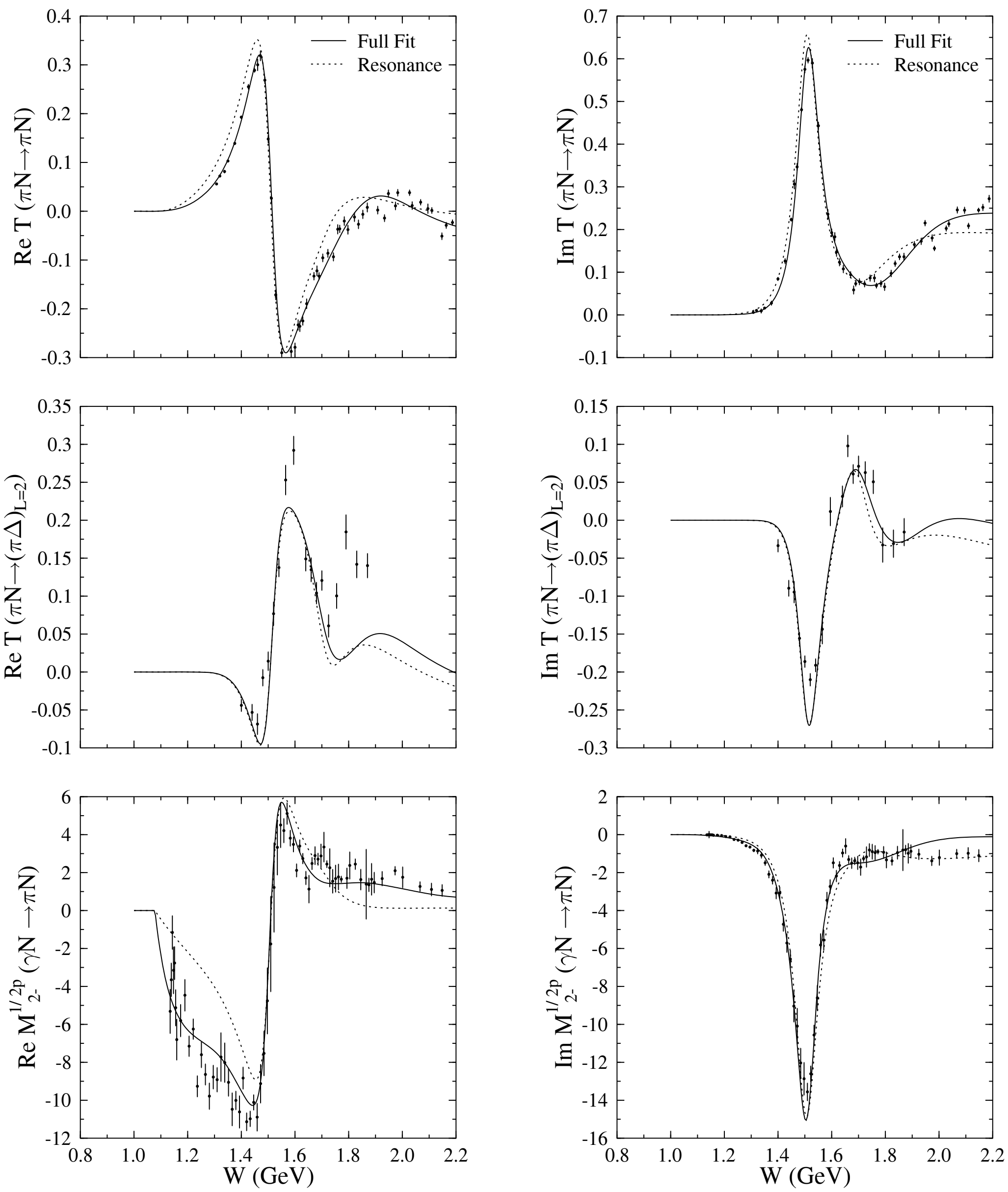

Figure 1: Sample fit results for D_{13}. Solid lines represent the fit to the D_{13} partial wave amplitudes and the dotted lines show the contributions due to resonances only.

Fits using the CMB model [5] for the D_{13} partial wave are shown in Fig. 1 for three reactions. The $D_{13}(1520)$ is prominent in all three reactions, a PDG 4* state [10]. The next state, $D_{13}(1700)$ is a 3* state, yet is barely seen in πN elastic and pion photoproduction T-matrices. It is seen most prominently in the $\pi N \to \pi\Delta$ partial wave. Does it deserve its 3* rating? PDG lists a 2* state at 2100 MeV. Only πN elastic scattering data exists for such high energies, but there is no sign of structure there. The fit is equally good with and without this state. Does it deserve to be listing by PDG?

Table 1 lists the properties of the two lower energy states to show the consistency of recent fit results [3, 5, 7] with each other and with PDG [10]. Other aspects of the analysis of this partial wave are discussed by Bennhold *et al.* [11]. In the table, we see that the 1520 state is uniformly described except for the GWU-Giessen analysis which has a poor fit to the data. The Breit-Wigner parameters of the 1700 MeV state vary from fit to fit because the $\pi N \to \pi\Delta$ reaction and associated backgrounds are modeled differently. The photocoupling amplitudes for the 1700 MeV state are poorly determined because the signal for this state is particularly weak in pion photoproduction.

The S_{11} partial wave has gathered a lot of interest in the last few years. Data in the region of the lowest state $S_{11}(1535)$ is fit with models assuming it is a resonance and assuming it is not a resonance. However, the PDG lists this state as a 4* resonance while giving broad ranges of values for its properties. The third state $S_{11}(2100)$ is a PDG 1* state of large mass and width (poorly determined). This state has been reported [12] at roughly 1700 MeV based on analysis of new eta photoproduction data from GRAAL [13]. Since the quark model has the robust prediction of two S_{11} states, this would be a significant finding.

The first S_{11} has a weak signal in πN elastic scattering and pion photoproduction, but very prominent peaks in the energy distribution of $\pi^- p \to \eta n$ and eta photo- and electroproduction. Those peaks can be fit with single-channel Breit-Wigner shapes [14] obtaining a large full width and large photocoupling for the state. On the other hand, analyses that fit only the pion observables either get widths and photocoupling amplitudes ($A^p_{1/2}$) about half as large [1]. It should be noted that there is considerable dependence on the W range used for the single channel fits. However, an assumption is made ignoring nonresonant contributions and interference with the overlapping state $S_{11}(1650)$. The pion analyses don't make these assumptions, but don't have the leverage in the data to separate resonant from nonresonant mechanisms. Large scale coupled channels analyses fit all data allowing for resonant and nonresonant interactions and multiple resonances, therefore getting a better picture of all aspects of this problem. We find strong interference between the first two states and much stronger nonresonant contributions than the pion analyses; each effect makes

Table 1: Model dependence for the $D_{13}(1520)$ (upper section) and $D_{13}(1700)$ (lower section). See text for details.

Model	Mass	Γ_{full}	$\mathrm{bf}_{\pi N}$	$A^p_{1/2}$	$A^p_{3/2}$
	MeV	MeV	%	$[\mathrm{GeV}]^{-1/2} * 10^{-3}$	
PDG	1515-30	110-135	50-60	-24(9)	166(5)
Pitt-ANL	1520(7)	118(8)	61(3)	-25(6)	171(7)
GWU-Giessen	1506	84	59	2	134
KSU	1521(1)	120(4)	56(2)	-18(5)	207(13)
PDG	1650-1750	50-100	5-15	-18(13)	-2(24)
Pitt-ANL	1730(26)	175(133)	4(2)	-47(9)	74(7)
GWU-Giessen	1690	202	0	3	42
KSU	1662(1)	509(30)	<1	-121(45)	-458(59)

the peak in the data much wider than the underlying $S_{11}(1535)$ peak. It shouldn't be a surprise that this global analysis gets results intermediate to the extremes mentioned above.

Using only published data, we have looked for evidence supporting the third S_{11}. The strongest structure is seen at ~1700-1800 MeV in our own $\pi^- p \to \eta n$ PWA [5]. However, the statistical significance is not strong. Fits with a third state have a χ^2 about the same as fits without it. The only difference is that the structure at ~1700-1800 MeV is fit much better when the third state is included. It is very interesting that the meager indication we have for the third S_{11} puts it at the close to the same energy found much more clearly in the new GRAAL and CLAS data.

Our last study was of the model dependence of the properties of the lower two S_{11} states. We did over 50 fits varying the input data and the model, using various reactions and using either the basic K-matrix [2] or the full CMB model. We find that using only pion data gives results consistent with Ref. [1] for either model. However, those results are sensitive to the handling of the strength that we know must be there for the data not fit. That is accounted for in the fit using the undesriable, but standard method of a dummy channel. In a broad range of fits, we find the full width, the partial width for πN and ηN, and the proton photocoupling amplitude of the 1535 MeV state are much better constrained than reported by PDG. Even some inadequate data sets get values comparable to those obtained with the best data sets. A full account of these results for the S_{11} partial wave can be found in our upcoming paper.

5 BRAG

The extraction of baryon resonance properties from data is a significant task because of the complexity of data and the lack of field theoretic models. The data is normally converted to partial wave amplitudes, then a model is used to determine the baryon properties. Each step has previously been done by individual groups, but the scope and importance of this work has led to the formation of a group of experimentalists and theorists called Baryon Resonance Analysis Group (BRAG).

BRAG membership is open to anyone at the web site `cnr2.kent.edu/~manley/BRAG.html`. The site has links to useful information and will be the repository for BRAG results. Although it is easy to join BRAG, we hope members will also contribute to its activities. There are presently 3 BRAG activities, but it is easy to define new ones and we hope that will happen.

- Model dependence of PWA: A recent study where a common database of pion photoproduction was analyzed by 11 separate programs for the E2/M1 ratio. The standard deviation of these results was 0.23% and can be thought of as part of a new *model dependence* contribution to the estimated error of this important quantity. This effort is continuing.

- Model dependence of baryon properties: A similar study of resonance properties began this summer. The same theme of different analyses of identical data sets will be employed. The group is starting with the D_{13} partial wave described above.

- Classification of baryon properties: We have recently begun a study of the ways baryons are rated and defined.

6 Conclusions

The study of baryon resonances is a broad subject involving many experiments and analyses. This work has attempted to show both the breadth and give a critical assessment of the present analyses. The advantages of coupled channel analyses and understanding the pole structure were emphasized.

The results for the D_{13} and S_{11} partial waves were discussed. The D_{13} suggests a way to assess and perhaps change the PDG star ratings. The lowest state (PDG 4*) has a very strong, solid signature and is well-understood in almost all analyses. The next state (PDG 3*) is seen predominantly in $\pi N \to \pi\Delta$ data which is not of high quality and the photocoupling amplitudes determined in various analyses have significant deviations from each other. This state might not deserve the high rating it gets. The third state (PDG 2*) is not definitively seen in any recent analysis and probably doesn't deserve to be included.

The S_{11} partial wave has many issues. The conflict between analyses of portions of data that resulted in a large error bar for reported PDG values was resolved by fitting all the data with a coupled channels code. The signs of a third S_{11} state at the PDG value of 2100 MeV were extremely weak. If the old data supports a state it is at 1700-1800 MeV. This is in interesting agreement with structure seen in the new GRAAL data. We report results of a model dependence study of the two lowest S_{11} states which finds values shifted and error bars smaller than the PDG listings.

Finally, we describe the interesting projects underway within the Baryon Resonance Analysis Group.

Acknowledgment: This work was supported by a grant from the National Science Foundation.

References

[1] D. Drechsel, O. Hanstein, S.S. Kamalov, L. Tiator, Nucl. Phys. **A645**, 145 (1999).

[2] R.G. Moorhouse, H. Oberlack, and A.H. Rosenfeld, Phys. Rev. D**9**, 1 (1974).

[3] T. Feuster and U. Mosel, Phys. Rev. C**58**, 457 (1998); C**59**, 461 (1999), A. Waluyo and C. Bennhold, private communication.

[4] R.E. Cutkosky, C.P. Forsyth, R.E. Hendrick, and R.L. Kelly, Phys. Rev. D**20**, 2839 (1979), R.E. Cutkosky, C.P. Forsyth, J.B. Babcock, R.L. Kelly, and R.E. Hendrick, in *Baryons 1980*, Proceedings of the IV-th International Conference on Baryon Resonances, ed. N. Isgur (University of Toronto, 1980), p. 19.

[5] T.P. Vrana, S.A. Dytman and T.-S. H. Lee, Physics Reports **328**, 181 (2000), to be published.

[6] E. Oset, U. Meissner, presentations at this conference.

[7] D.M. Manley and E.M. Saleski, Phys. Rev. D**45**, 4002 (1992), M. Manley, private communication.

[8] A.M. Badalyan, L.P. Kok, M.I. Polikarpov, and Yu.A. Siminov, Phys. Repts. **82**, 31 (1982).

[9] S. Dytman and C. Tanase, in Proceedings of the NSTAR2000 Conference, Feb., 2000, V.D. Burkert, L.Elouadrhiri, J.J. Kelly, and R.C. Minehart, eds., World Scientific, (Singapore, 2001) page 271.

[10] D.E. Groom, *et al.*, (Particle Physics Group), Review of Particle Physics, Eur. Phys. J. **C15**, 1 (2000).

[11] C. Bennhold, *et al.*, in Proceedings of the Workshop on the Physics of Excited Nucleons, Mainz, Germany, Feb. 2001, World Scientific (Singapore, 2001), page 109.

[12] Bijan Saghai and Zhen-Ping Li, Eur. Phys. J. **A11** 217 (2001). LANL preprint nucl-th/0104084.

[13] F. Renard, *et al.*(GRAAL collaboration), LANL preprint hep-ex/0011098, submitted to Phys. Lett., presentation at this conference.

[14] B. Krusche, N. Mukhopadhyay, J.F. Zhang, and M. Benmerrouche, Phys. Lett. **B397**, 171 (1997).

The pion-nucleon Σ term is definitely large: results from a GWU analysis of πN scattering data

M. M. Pavan,[a] R. A. Arndt,[b] I. I. Strakovsky,[b] and R. L. Workman[b]

[a]*University of Regina*
TRIUMF, Vancouver, B.C. V6T-2A3, Canada
[b]*Center for Nuclear Studies, Department of Physics,*
The George Washington University, Washington, DC 20052, U.S.A.

(Received: 31 October 2001)

A new result for the πN Σ term from a George Washington University/TRIUMF group analysis of πN data is presented. The value Σ=79±7 MeV was obtained, compared to the canonical value 64±8 MeV found by Koch. The difference is explained simply by the PSI pionic hydrogen value for $a_{\pi^- p}$, the latest results for the πNN coupling constant, and a narrower Δ resonance. Many systematic effects have been investigated, including Coulomb corrections, and database changes, and our results are found to be robust. In the standard interpretation, our value of Σ implies a nucleon strangeness fraction y/2~0.23. The implausibility of such a large strange component suggests that the relationship between Σ and nucleon strangeness ought to be re-examined.

1 Introduction

The πN sigma term Σ has long been a thorn in the side of low energy quantum chromodynamics (QCD) [1,2]. The canonical result Σ=64±8 MeV was obtained by Koch [3,4] based on an analysis of pre-1980 πp and $\pi\pi$ scattering data, KH80 [4,5]. Gasser, *et al.* [6] later developed an alternative method of extracting Σ which agreed perfectly with Koch when using the same KH80 solution. In the usual picture, the nucleon strangeness parameter is

$$y/2 = \frac{< N|\bar{s}s|N >}{< N|\bar{u}u + \bar{d}d|N >} \ . \tag{1}$$

The canonical Σ result yields $y = 0.11 \pm 0.07$, whereby the strange quarks would contribute ~110 MeV to the nucleon mass, an amount considered too large to be physical in light of results from *e.g.* neutrino scattering [7]. This "sigma term puzzle" spawned a whole generation of πN scattering experiments that have greatly increased the size and the quality of the scattering database.

A long-standing prejudice has been that new and better πN scattering data and an updated analysis ultimately would result in a smaller value for y. With the new generation of experiments almost all completed, our George Washington University/TRIUMF group has sought to extract the Σ term as part of our ongoing πN partial-wave and dispersion relation analysis program, which employs the most up-to-date πN scattering data in our SAID database [8]. Our main conclusion is that contrary to wishful expectation, a thorough analysis of the new data has yielded a *larger* value, $\Sigma = 79 \pm 7$ MeV, which can be understood simply in light of the new experimental information. The sigma term and our analysis will be summarized briefly. Details can be found *e.g.* in Refs. [4,6,9,10].

2 The pion-nucleon sigma term

The sigma term $\hat{\sigma}$ measures the nucleon mass shift away from the chiral ($m_u = m_d = 0$) limit, thereby parameterizing the explicit breaking of chiral symmetry in QCD due to the non-zero up and down quark masses. Models of nucleon structure are required to determine $\hat{\sigma}$. The canonical result $\hat{\sigma} = 35 \pm 5$ MeV is due to Gasser [11] based on SU(2) chiral perturbation theory plus meson

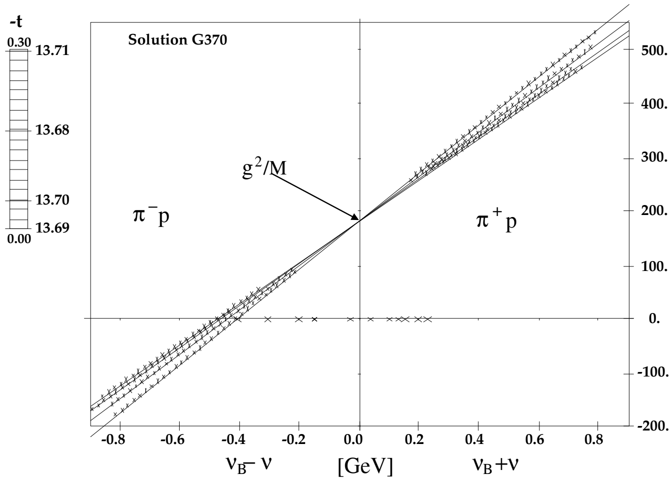

Figure 1: Determination of the πNN coupling constant from the Hüper dispersion relation. The y-intercept gives the coupling g^2/M, and the left (right)-hand side of the figure is dominated by π^-p (π^+p) data. This technique is well suited to determine the coupling constant since most systematic effects (*e.g.* Coulomb corrections) affect each side asymmetrically, "pivoting" the curves about the intercept, hence greatly reducing their effect on g^2.

loop corrections. One obtains the strangeness y from

$$\sigma(0) = \frac{\hat{\sigma}}{1-y} \ , \tag{2}$$

where the theorem of Brown, Pardee, and Peccei [12] relates $\sigma(0)$ to the isoscalar invariant πN scattering amplitude $D^+(\nu, t)$ at the "Cheng-Dashen" point [13], $\nu = 0, t = 2m_\pi^2$:

$$\begin{aligned} \Sigma &= F_\pi^2 \bar{D}^+(0, 2m_\pi^2) \\ &= \sigma(2m_\pi^2) + \Delta_R \ , \end{aligned} \tag{3}$$

where

$$\sigma(2m_\pi^2) = \sigma(0) + \Delta_\sigma \tag{4}$$

and F_π=92.4 MeV is the pion decay constant, ν is the crossing energy variable, and t is the four-momentum transfer. The "remainder term" Δ_R is small (<2 MeV [14]). The nucleon scalar form factor $\sigma(t)$ shifts by an amount Δ_σ=15 MeV from $t = 0$ to $t = 2m_\pi^2$, calculated from a $\pi\pi$ dispersion relation analysis [6] and recently confirmed by a chiral perturbation theory calculation [15]. The bar over $\bar{D}^+$ indicates that the pseudo-vector Born term has been subtracted.

The Cheng-Dashen point lies outside the physical πN scattering region, so the experimental $\bar{D}^+$ amplitude must be extrapolated to obtain Σ. The most reliable extrapolations are based on dispersion relation (DR) analyses of the scattering amplitudes [4]. The Koch result $\Sigma = 64 \pm 8$ MeV was based on hyperbolic dispersion relation calculations [3]. More recently, Gasser, *et al.*, (GLLS) [6] developed another dispersion theoretic approach based on forward subtracted πN dispersion relations. Expanding $D^+(t)$ as a power series in t, the experimental sigma term Σ can be expressed as

$$\begin{aligned} \Sigma &= F_\pi^2(\bar{d}_{00}^+ + 2m_\pi^2 \bar{d}_{01}^+ + \ldots) && (5) \\ &= F_\pi^2(\bar{d}_{00}^+ + 2m_\pi^2 \bar{d}_{01}^+) + \Delta_D && (6) \\ &= \Sigma_d + \Delta_D && (7) \end{aligned}$$

The GLLS, or truncated, sigma term Σ_d is obtained via the subthreshold coefficients $\bar{d}_{00}^+$ and $\bar{d}_{01}^+$, calculated from the forward subtracted $\bar{D}^+$ and "derivative" $\bar{E}^+$ dispersion relations, respectively. They can also be determined from the subtraction constants $D^+(0,t) = C^+(0,t)$ in the fixed-t dispersion relation $C^+(\nu, t)$. The intercept of the curve $D^+(0,t)$ yields d_{00}^+, whereas the slope at

$t = 0$ yields d^+_{01}. The "curvature correction" term $\Delta_D = 12 \pm 1$ MeV was determined from a $\pi\pi$ dispersion relation analysis [6]. The great advantage of this approach is that $\sigma(0)$ can be obtained simply from Σ_d via [6]

$$\sigma(0) = \Sigma_d - (3 \pm 3)\mathrm{MeV} \tag{8}$$

since the correction terms Δ_σ and Δ_D almost cancel, both having similar $\pi\pi$ amplitude input [6].

The analysis of Ref. [6] used the Karlsruhe KH80 [5] πN phases as input and fit just the low energy data. Their result was $\Sigma_d \sim$50 MeV, or $\Sigma \sim$62 MeV (with Δ_D=12 MeV), in agreement with Koch [3]. Questions regarding the accuracy of the E^+ dispersion relation integral, which is more sensitive to the smaller and more poorly known higher partial waves than other dispersion relations, were answered by the good agreement which demonstrated the reliability of the approach.

3 Analysis procedure

Solutions from our ongoing πN partial-wave and dispersion relation analysis are released when changes to the database and analysis method warrant [8]. Details of our analysis method can be found in Ref. [9, 10, 16]. An energy-dependent πN partial-wave analysis (PWA) is performed on the available data up to 2.1 GeV pion laboratory kinetic energy, applying constraints from forward $C^\pm(\omega)$ and $E^\pm(\omega)$ DRs, as well as fixed-t $B_\pm(\nu, t)$ (in the "Hüper" form [4]) and $C^\pm(\nu, t)$ DRs. These dispersion relations are constrained [1] to be satisfied to within <2% from 30 to 800 MeV for $-0.4 < t < 0.0$ GeV$^2/c^2$. The dispersion integrals use the Karlsruhe KH80 phases from 2.1 to 4.5 GeV and high energy parameterizations above that using forms found in Refs. [4, 17].

Dispersion relations depend on *a priori* unknown constants *e.g.* scattering lengths and g^2. Our analysis determines these constants by a best fit to the data and the dispersion relations. The coupling g^2, the $\pi^- p$ s-wave scattering length $a_{\pi^- p}$, and the p-wave scattering volume a^+_{1+} were fixed for each fit over a grid of values (for reasons of fit stability), where the combination with the lowest χ^2 yields the final solution. The fitting procedure automatically chooses the best-fit isovector scattering length a^-_{0+} and volume a^-_{1+}, and the subtraction constants $C^\pm(0, t)$. This method enables us to check their sensitivity to various systematic effects, *e.g.* database changes.

The low energy P_{13} partial wave is constrained to follow the expected partial wave dispersion relation behaviour in its Chew-Low approximation form [18], which our other p-waves satisfy without constraint. As well, the low energy F and higher partial waves, too small to be determined from the πN scattering data, are constrained to agree with those calculated by Koch [19] from partial wave projections of fixed-t dispersion relations, which are dominated by t-channel ($\pi\pi$) contributions. This ensures that our higher partial waves satisfy analyticity and unitarity requirements.

4 Results

Our main results are summarized in Figs. 1 and 2 and Table 1. We find for the πNN coupling constant $g^2/4\pi = 13.69 \pm 0.07$ (or $f^2 = 0.0757 \pm 0.0004$), stable in our solutions for many years (see [16]). Our coupling constant agrees with most other recent results, in particular the comprehensive NN and πN analyses of the Nijmegen group (see Ref. [20] and references cited therein). Note that this result is perfectly consistent with both the Goldberger-Treiman discrepancy [21, 22] and the Dashen-Weinstein sum rule [23], removing a long-standing inconsistency when using the older Karlsruhe value [5] 14.3±0.3.

For the s-wave scattering lengths we obtain $3a_{\pi^- p} = 0.261$ m$_\pi^{-1}$ and $3a^-_{0+} = 0.260$ m$_\pi^{-1}$, with 1-2% uncertainties. The $\pi^- p$ scattering length agrees with the PSI pionic hydrogen result $3a^{\mathrm{psi}}_{\pi^- p} =$

[1]This range has been increased from previous analyses, and in practice the dispersion relations are well satisfied somewhat beyond that range due to the energy dependent partial wave forms

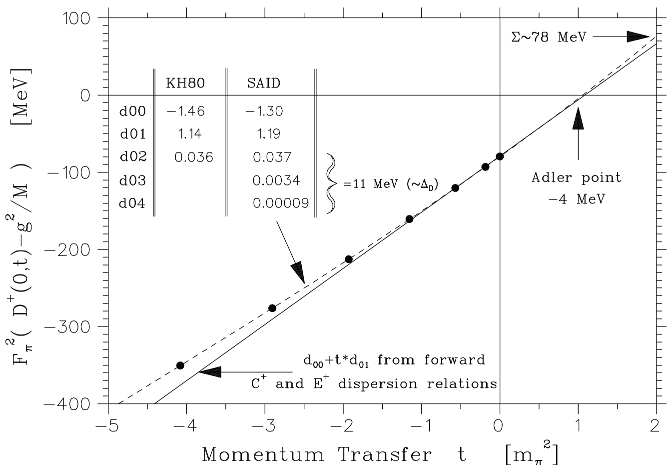

Figure 2: The amplitude $\overline{C}^+(0,t)$ (points) evaluated from fixed-t $C^+(\nu,t)$ dispersion relations. A fit (dashed line) yields the subthreshold coefficients in the table. The solid diagonal line is inferred from forward $C+$ and E^+ dispersion relations, and agrees perfectly with $\overline{d}_{00}$ and $\overline{d}_{01}$ in the table. The curvature terms ($\overline{d}_{0i}, i \geq 2$) imply Δ_D >11 MeV, consistent with the canonical result 12±1 MeV from Ref. [6]. The amplitude is very small as expected at $t = m_\pi^2$ ("Adler point"). The overall consistency tends to support our result for the sigma term, $\Sigma \sim 79 \pm 7$ MeV.

0.2649 ± 0.0024 m_π^{-1}, while the isovector scattering length satisfies the Goldberger-Miyazawa-Oehme (GMO) sum rule [21] when using our coupling constant and integral $J_{\rm gmo} = -1.08 \pm 0.03$ mb^{-1}. The p-wave scattering volume $a_{1+}^+ = 0.133$ m_π^{-3} is consistent with recent analyses of low energy data [25], as expected since the resonanct P_{33} partial wave dominates the low energy data and a_{1+}^+.

The dispersion relations are very well satisfied up to about 1 GeV, in general much better than KH80. From the forward $C^+(\omega)$ and $E^+(\omega)$ dispersion relations, we obtained the coefficients $\bar{d}_{00} = -1.30$ m_π^{-1} and $\bar{d}_{01} = 1.19$ m_π^{-3}, in perfect agreement with the results from the slope and intercept of the $C^+(0,t)$ subtraction constants at $t = 0$, shown in Fig. 2. The equivalent $\bar{d}_{01}$ result from the E^+ dispersion relation, with its $\sim l^3$ sensitivity to partial waves, and the $C^+(\nu,t)$ dispersion relation, with its $\sim l$ sensitivity, supports the reliability of our higher partial waves.

Figure 2 shows a polynomial fit to $C^+(0,t)$ near $t = 0$, from which $\bar{d}_{02}$, $\bar{d}_{03}$, and $\bar{d}_{04}$ were estimated. The $\bar{d}_{02}$ coefficient is in perfect agreement with the Karlsruhe result [4], while the sum of the higher order terms yield a curvature correction $\Delta_D > 11$ MeV, in agreement with the $\pi\pi$ dispersion relation result [6] 12 ± 1 MeV. Moreover, the curve extrapolates to about -4 MeV at the "Adler point" (t=m_π^2), consistent with expected corrections to the Adler Consistency Condition [26], where it would be identically 0 in the chiral limit. Compatibility with t-channel dispersion relations and chiral constraints gives us confidence in the reliability of our subthreshold coefficient results.

From the above subthreshold coefficients, and the curvature correction from Ref. [6], our result for the sigma term is Σ=79±7 MeV, compared to the Koch value 64±8 MeV [3]. Though surprising, the result is readily explained by the new experimental information. Table 1 shows the breakdown of Σ_d into its dispersion relation terms for both the KH80 solution and our own. With respect to KH80 result, the new PSI pionic hydrogen and deuterium scattering length [24] $a_{0+}^+ \sim 0.000$ m_π^{-1},

Solution	Σ_d [MeV] =	"a_{0+}^+ const.	Born	$\int$D$^+$	"a_{1+}^+" const.	Born	$\int$E$^+$
KH80	50 =	-7	+9	-91	+352	-142	-72
FA01	67 =	0	+9	-88	+351	-136	-69
difference	17 =	**+ 7**	**0**	**+3**	**−1**	**+6**	**+3**

Table 1: Comparison of Σ_d from the Karlsruhe solution KH80 [5] and our recent solution FA01. The change in the C^+ subtraction constant (a_{0+}^+) term, the E^+ Born term, and both integral terms are consistent with expectations from, respectively, pionic atom data [24], the coupling constant $g^2/4\pi \sim 13.7$ (see Ref. [20]), and a narrower Δ resonance width. Values are rounded. See text for details.

which we reproduce, causes a 7 MeV increase. With a πNN coupling constant $g^2/4\pi \sim 13.7$ [16,20], Σ_d increases by 6 MeV [2]. It is well known that the KH80 solution overshoots the data on the left wing of the Δ resonance. Our solution fits the available data much better than KH80, resulting in a narrower Δ width. This leads directly to the 3 MeV increases in each of the dispersion integrals shown in Table 1. Consequently there is sound experimental evidence to support our new Σ result.

4.1 Systematic checks

Perhaps the most important systematic check is the sensitivity of our results to the scattering database. Around the Δ resonance, there is a well known disagreement between the TRIUMF $\pi^\pm$ differential cross section [27] and PSI $\pi^\pm$ total cross section data [28] on the one hand, and the older CERN results [29] on the other. Only a small increase 0.07 and 4 MeV was observed in $g^2/4\pi$ and Σ_d, respectively, for the "CERN-only" database. In practice, both sets are included in the final fit[3]. We found that weeding out large χ^2 data sets had little effect on the result. Also, since the low energy data are consistent with the PSI pionic atom results [24], we conclude that there are no large systematic effects from reasonable changes to the current scattering database.

The hadronic amplitudes are corrected for Coulombic effects following the Nordita prescription [30], supplemented in this analysis at high energies by extended-source Coulomb barrier factors [31]. The current approach improved the agreement with the PSI pionic atom results over our previous Nordita+point-source barrier results; however, neither the coupling constant nor Σ_d varied outside the errors when using point- or extended-source barrier factors exclusively, or the Nordita corrections supplemented by either. Moreover, the isospin-violating Δ resonance is "split" defining "hadronic"="Δ^{++}", consistent with the Nordita definition, but find no difference to our previous approach with "hadronic"="$(\Delta^0 + \Delta^{++})/2$", or with no splitting at all. We conclude that there are also no large systematic uncertainties from our Coulomb correction scheme.

The implementation of our dispersion relation constraints was also checked. We found that every reasonable form for the high energy amplitudes (>2 GeV) yields virtually identical results. Agreement between the forward subtracted and fixed-t unsubtracted dispersion relations is good for reasonable constraints (*i.e.* typical experimental error $\sim$2%), but suffers if they become too tight, <0.5%. Constraining the low energy P_{13} partial wave to follow the Chew-Low form lowered Σ_d by 6 MeV, but once corrected, reasonable deviations caused changes much smaller than our error bar. We also had solutions where the low energy F and higher partial waves were not rigorously constrained to the Koch values [19], and no significant difference was found. Furthermore, Olsson [32], from a new dispersion relation sum rule, and Kaufmann and Hite [33], from an interior dispersion relation analysis, obtained values for Σ consistent with our own using an earlier SAID solution. Consequently, we are confident in the reliability of our dispersion relation analysis.

5 Summary

In summary, we have performed a comprehensive partial wave and dispersion relation analysis of the available πN scattering data up to 2.1 GeV that includes several improvements upon prior analyses [9,10]. For the pion nucleon coupling constant we obtained $g^2/4\pi = 13.69 \pm 0.07$, consistent with our previous determinations [9,16] and the Nijmegen results [20]. Our s-wave scattering lengths agree with the latest PSI pionic hydrogen and deuterium results [24]. Our πN sigma term result is $\Sigma_d = 67 \pm 6$ MeV, or $\Sigma = 79 \pm 7$ MeV, compared to the canonical result 64 ± 8MeV from Koch [3]. These results have proven robust with respect to the many systematic checks that we have performed. In light of the large nucleon strangeness content $y/2 \sim 0.23$ inferred in the standard

[2] The above increases were also noted in Ref. [24]

[3] The other low and Δ resonance energy data are fit somewhat better in "TRIUMF+PSI-only" solution

picture, we believe that alternate interpretations of a large sigma term ought to be examined carefully.

Acknowledgments: We gratefully acknowledge a contract from Jefferson Lab under which this work was done. The Thomas Jefferson National Accelerator Facility (Jefferson Lab) is operated by the Southeastern Universities Research Association (SURA) under DOE contract DE-AC05-84ER40150. We are grateful to W. Gibbs for the calculation of the extended source Coulomb barrier factors. M.M.P. thanks D. Bugg for the wine, and he and M. Sainio, G. Oades, W. Gibbs and B. Loiseau for fruitful discussions.

References

[1] E. Reya, Rev. Mod. Phys. **46**, 545 (1974).
[2] R. L. Jaffe, Phys. Rev. D**21**, 3215 (1980).
[3] R. Koch, Z. Phys. C**15** 161 (1982).
[4] G. Höhler, *Pion Nucleon Scattering*, Landolt-Börnstein, **9**B2, ed. H. Schopper (Springer) Berlin, 1983.
[5] R. Koch, E. Pietarinen, Nucl. Phys. A**336** 331 (1980).
[6] J. Gasser, H. Leutwyler, M.P. Locher, M.E. Sainio. Phys. Lett. **B213** 85 (1988) ; *ibid* , Phys. Lett. **B253** 252 (1991) ; *ibid* , Phys. Lett. **B253** 260 (1991)
[7] See Ref.19 in [2].
[8] The SAID πN database are available at "ssh said@said.phys.vt.edu", or http://gwdac.phys.gwu.edu/. Solutions are available also upon request.
[9] R.A. Arndt, I.I. Strakovsky, R.L. Workman, M.M. Pavan, Phys. Rev. C**52** 2120 (1995) ; R.A. Arndt, R.L. Workman, M.M. Pavan, Phys. Rev. C**49** 2729 (1994).
[10] M.M. Pavan, R.A. Arndt, I.I. Strakovsky, and R.L. Workman, πN Newsletter 15, 118 (1999) ; also an www.ArXiv.org electronic preprint nucl-th/9912034.
[11] J. Gasser, Ann. Phys. **136** 62 (1981).
[12] L.S. Brown, W.J. Pardee, and R.D. Peccei, Phys. Rev. D**4** 2801 (1971).
[13] T.P. Cheng and R. Dashen, Phys. Rev. Lett. **26** 594 (1971).
[14] V. Bernard, N. Kaiser, and Ulf-G. Meißner, Phys. Lett. B**389**, 144 (1996).
[15] T. Becher and H. Leutwyler, Eur. Phys. J. C**9**, 643 (1999).
[16] M.M. Pavan, R.A. Arndt, R.L. Workman, I.I. Strakovsky, Phys. Scripta T**87** 65 (2000).
[17] A.D. Martin and T.D. Spearman, ' *"Elementary Particle Theory"*, (North-Holland) 1970.
[18] J. Hamilton, *"Pion-Nucleon Interactions"* in High Energy Physics, ed. E.H.S. Burhop (Academic Press) New York, 1964.
[19] R. Koch, Nucl. Phys. A**448** 707 (1986).
[20] J.J. deSwart, M.C.M. Rentmeester, and R.G.E. Timmermans, πN Newsletter 13, 96 (1997).
[21] M.L. Goldberger and S.B. Treiman, Phys. Rev. **110** 1178 (1958).
[22] C. A. Dominguez, Riv. Nuovo Cim. **8**, 1 (1985).
[23] J.L. Goity, R. Lewis, M. Schvellinger, and L. Zhang, Phys. Lett. B**454**, 115 (1999).
[24] H.Ch. Schröder, *et al.*, Eur. Phys. J. C**21** 473 (2001).
[25] E. Matsinos, Phys. Rev. C**56** 3014 (1997) (E. Matsinos, private communication) ; A. Gashi, E. Matsinos, G.C. Oades, G. Rasche, and W.S. Woolcock, www.ArXiv.org electronic preprint hep-ph/009081.
[26] S.L. Adler, Phys. Rev. **137**, 1022 (1965).
[27] M.M. Pavan, *et al.*, www.ArXiv.org electronic preprint nucl-ex/0103006 ; J.T. Brack, *et al.*, Phys. Rev. C**34**, 1771 (1986) ; *ibid*, Phys. Rev. C**51**, 929 (1995).
[28] E. Pedroni, *et al.*, Nucl. Phys. A**300**, 321 (1978).
[29] P.J. Bussey, *et al.*, Nucl. Phys. B**58**, 363 (1973) ; A.A. Carter, *et al.*, Nucl. Phys. B**26**, 445 (1971).
[30] B. Tromborg, S. Waldenstrom, I. Overbo, Phys. Rev. D. **15** 725 (1977).
[31] The extended-source barrier factors were supplied by W. Gibbs, private communication, Sept. 2001.
[32] M.G. Olsson, Phys. Lett. B**482**, 50 (2000) ; and these proceedings.
[33] W.B. Kaufmann and G.E. Hite, Phys. Rev. C**60** 055204 (1999).

Calculation of πN partial waves from hyperbolic dispersion relations

J. Stahov

University of Tuzla, Tuzla, Bosnia and Herzegovina
and Abilene Christian University, Abilene, TX 79699, U.S.A.

(Received: 1 November 2001)

Partial wave relations that are obtained by a projection of the hyperbolic dispersion relations (HPWR) were used to calculate the low energy πN partial waves. Corresponding kernels, which are explicitly known, couple a given s-channel wave to imaginary parts of the s-channel partial waves and imaginary parts of the $\pi\pi N\bar{N}$ partial waves. The real parts of the isospin even and odd combinations of the πN partial waves were calculated from threshold to 500 MeV/c. Using the present input from the s-channel and the t-channel, the higher partial waves ($l \geq 2$) are well determined using the HPWR method.

1 Introduction and notation

The πN partial waves at low energies are of interest for various applications. Among these, the πN σ term is without doubt the hottest topic. Recent discussions concerning the "experimental value" of the πN σ term are strongly related to results for the low energy πN amplitudes. It is known that experiments alone cannot lead to a unique determination of the πN partial waves. From experimental data at low energies one cannot determine higher partial waves which are "too small to be determined and too large to be neglected." In all methods of calculations of the σ term one needs to perform extrapolation to the Cheng Dashen point ($\nu = 0$, $t = 2m_\pi^2$). Corresponding dispersion relations require input from outside of the physical region. For instance, in the fixed-t dispersion relations when $t > 0$ the path of integration lies completely outside of the physical region. Corresponding partial wave expansions of invariant amplitudes receive a significant contributions from the higher partial waves. For this reason contributions of higher partial waves can be an important part of information in resolving present dilemmas about the value of the σ term. We will apply partial wave relations obtained from the hyperbolic dispersion relations (HPWR) to calculate πN partial waves at low energies. This method is compared to another method — partial wave relations from the fixed-t dispersion relations (FTPWR). We will also consider so called reduced partial waves $F_l^{\pm}$ which are defined as:

$$F^I_{l\pm} = \frac{T^I_{l\pm}}{q^{2l+1}} \ , \qquad T^I_{l\pm} = \frac{\eta^{\pm}_{l\pm} e^{2i\delta^{\pm}_{l\pm}} - 1}{2i} \ ,$$

with parameters I: isospin ($I = 3/2, 1/2$); $l_\pm$: total angular momentum $J = l \pm 1/2$; $\eta^I_{l\pm}$: inelasticities; $\delta^I_{l\pm}$: phase shifts; q: momentum in the center of mass system. Isospin combinations of partial waves, even and odd, are defined by

$$F^{\pm}_{l\pm} = \frac{1}{3}\left[F^{1/2}_{l\pm} + \begin{pmatrix} 2 \\ -1 \end{pmatrix} F^{3/2}_{l\pm}\right] \ .$$

The analytic structure of the πN partial waves can be inferred from the analytic structure of the πN invariant amplitudes. For details we refer to [1]. Here we list the positions of the cuts and the nucleon pole:

- Right-hand cut: the s-channel cut $s > (m + m_\pi)^2$;
- t-channel circle cut $s = (m^2 - m_\pi^2)$;
- Nucleon exchange short cut;

• Nucleon pole at $s = m^2$ (only P_{11} wave);
• Left-hand cut (u-channel cut, t-channel cut, N-exchange cut).

Based on the analytic structure of invariant amplitudes and partial waves, two methods have been developed and used in the past in order to calculate πN partial waves. In partial wave dispersion relations approach (PWDR) one starts from known analytic structure of partial waves and writes corresponding partial wave dispersion relations [2]. Only parts of the left hand cut and the circle cut can be calculated, the rest is described by discrepancy function. Recent evaluation of PWDR [3] shows that the t-channel contributions are large and mostly dominant over the rest for the higher partial waves. Discrepancy function can be large, the choice of its parametrization is arbitrary and can cause problems in the numerical evaluation. The advantage of the PWDR method is that it can be used for any energy in the s-channel. This method is still important tool in calculation of the πN partial waves. Partial wave relations are obtained if one inserts the real parts of invariant amplitudes, expressed in terms of corresponding dispersion relations, into the partial wave projection formula. At the same time, the imaginary parts of invariant amplitudes under dispersion integral, are expressed in partial waves. In this way one obtains a real part of a particular partial wave in terms of imaginary parts of all others.

2 Partial wave relations from the fixed-t dispersion relations

Using the fixed-t dispersion relations, Baacke and Steiner [4] obtained partial wave relations for the s-channel partial waves, which for F^I_{l+} can be written in the form

$$F^I_{l+}(w) = (N^I_{FT})_{l+} + \frac{1}{\pi} \int\limits_{(m+m_\pi)^2}^{\infty} dw' \sum_{l'=0}^{\infty} \left[K^I_{ll'}(w,w') \, \mathrm{Im} F^I_{l'+}(w') + K^I_{ll'}(w,-w') \, \mathrm{Im} F^I_{(l'+1)-}(w') \right] \ ,$$

where w is total energy in c.m. frame, N_{FT} is the nucleon exchange contribution, and summation goes over imaginary parts of all partial waves in the s-channel. For details we refer to [4] and [5]. Kernels $K^{\prime}_{ll}$ appearing in FTPWR are explicitly known, there are no unknown contributions and everything looks promising. However, there are no t-channel contributions which are the leading contributions to higher partial waves. The system of partial wave relations for the πN partial waves, which does not include contributions from the t-channel, may not have approximate solution involving a reasonable number of partial waves. This is exactly what happens when applying the FTPWR — slow convergence of corresponding expansions. In order to improve convergence Koch derived modified FTPWR [5] using once subtracted dispersion relations for the amplitude $A^{(+)}$ (subtraction point $\nu = 0$). Koch included the t-channel contributions by using the fixed-ν dispersion relations for the subtraction function $A^+(0,t)$. Using this method, Koch obtained the πN partial waves up to $l = 3$.

3 Partial wave relations from the hyperbolic dispersion relations

The t-channel contributions can be taken into account explicitly by writing dispersion relations along curves passing through s- and t-channels and allowing a partial wave projection. Hite and Steiner [6] proposed such kind of dispersion relations for crossing even amplitudes along hyperbolas in the Mandelstam plane:

$$(s-u)(u-a) = b \ ,$$

where s and u are Mandelstam variables, a is an asymptote and b is a parameter.

The most important features of hyperbolic dispersion relations are:
• Dispersion relations receive contributions from all three channels.

• Knowledge of absorptive parts of amplitudes is required only in regions inside corresponding Lehmann ellipses where expansions in terms of imaginary parts of corresponding partial waves converge.

The resulting partial wave relations (HPWR) for $F^{\pm}_{l+}$ have the following form,

$$\begin{aligned}
\mathrm{Re}F^{\pm}_{l+}(w) &= (N^{\pm}_{Hyp})_{l\pm} + \frac{1}{\pi}\int\limits_{(m+m_\pi)}^{\infty} dw' \sum_{l'=0}^{\infty}\left[K^{\pm}_{ll'}(w,w')\,\mathrm{Im}F^{\pm}_{l'+}(w) + K^{\pm}_{ll'}(w,-w')\,\mathrm{Im}F^{\pm}_{(l'+1)-}(w')\right] \\
&+ \frac{1}{\pi}\int\limits_{4m_\pi^2}^{\infty} dt' \sum_{J=0}^{\infty}\left[G_{lJ}(w,t')\,\mathrm{Im}f^J_{+}(t') + H_{lJ}(w,t')\,\mathrm{Im}f^J_{-}(t')\right],
\end{aligned}$$

where N_{Hyp} is nucleon exchange contribution, $N_{Hyp} = N_{FT}$ $(l > 1)$. The main properties of HPWR are:

• The s-channel kernels K'_{ll}, and the t-channel kernels G_{lJ}, H_{lJ} are explicitly known. They reproduce all cuts present in the analytic structure of the πN partial waves. As a consequence, obtained partial waves have a correct analytic structure in any approximation involving a finite number of partial waves. This allows us to make a test to find whether a partial wave solution is compatible with the the following analytic structure which is required of all partial waves:

• Kernels K'_{ll} couple each πN partial wave to the imaginary parts of other s-channel partial waves.

• Kernels G_{lJ} and H_{lJ} couple each s-channel partial wave to the imaginary part of the t-channel partial waves $f^J_{\pm}$. Summation goes over even $J = 0, 2, \ldots$ for isospin even partial waves and over odd $J = 1, 3, \ldots$ for isospin odd partial waves. Contribution of the t-channel S-wave strongly dominates in case of isospin even partial waves, and P waves dominate in the case of isospin odd partial waves.

• In derivation of HPWR, absorptive parts of invariant amplitudes are expressed in terms of corresponding partial waves (in the s-channel and in the t-channel). Hyperbolas must not enter the double spectral regions or their mirrors in the Mandelstam plane. This implies that the HPWR are valid only in the region below some maximum energy $w_{\max} = 1.3$ GeV which corresponds to $k_{\max} = 500$ MeV/c for $a = -0.4$ GeV^2.

4 Estimation of the leading terms in the HPWR

In order to estimate the leading contributions to a given partial wave in HPWR one has to analyze behavior of corresponding kernels and of the nucleon exchange term. Analysis close to threshold shows general behavior of corresponding terms [7]. From the explicit formulas for the nucleon exchange contribution, and the t-channel kernels as well, it can be concluded:

• $F^{\pm}_{(l+1)-}$: the t-channel contributions are strongly dominant,

• F^{+}_{l+}: the t-channel contributions and the N-exchange contributions are comparable,

• F^{-}_{l+}: the nucleon exchange is dominant contribution for $l < 5$, for higher values of l the t-channel contributions again dominate.

• Numerical evaluations show that contribution of the P_{33} wave to higher partial waves is small.

Having estimated leading contributions from HPWR, it can be concluded that leading, t-channel, contributions to higher waves must be described in the FTPWR by contributions of higher partial waves and possibly by high energy contributions (both poorly known). Due to behavior of the t-channel kernels $(1/t^{l+1})$, contributions from higher values of t are strongly suppressed so that input from the t-channel available today makes it possible to obtain reliable predictions for the higher $(l > 3)$ πN partial waves from HPWR.

5 The input

The s-channel part of the input consists of the results of the existing partial wave solutions. We have used the Karlsruhe Ka84 solution and the GWU SP00 solution. Results from Ka84 are available up to a lab momentum of $k_{\max} = 6$ GeV/c. Results from Sp00 solution are available up to 2.2 GeV/c. In our calculations we use values of πN coupling constant as obtained in particular solutions: $f^2 = 0.079$ (Ka84) and $f^2 = 0.076$ (Sp00). Input from the t-channel consists of the $\pi\pi N\bar{N}$ helicity amplitudes $f^J_{\pm}$. The input exists for $4m_\pi^2 \leq t \leq 50m_\pi^2$, and $J = 0, 1, 2, 3$. We used results obtained by the Karlsruhe group given in [1]. We adjusted Karlsruhe solution for f^0_+ to results of Gasser *et al.* [8] in the region where the scattering length approximation is valid, taking their values for the S-wave scattering length and the effective range: $a_{00} = 0.20\pm0.01$, $b_{00} = 0.24\pm0.01$ (in n.u.).

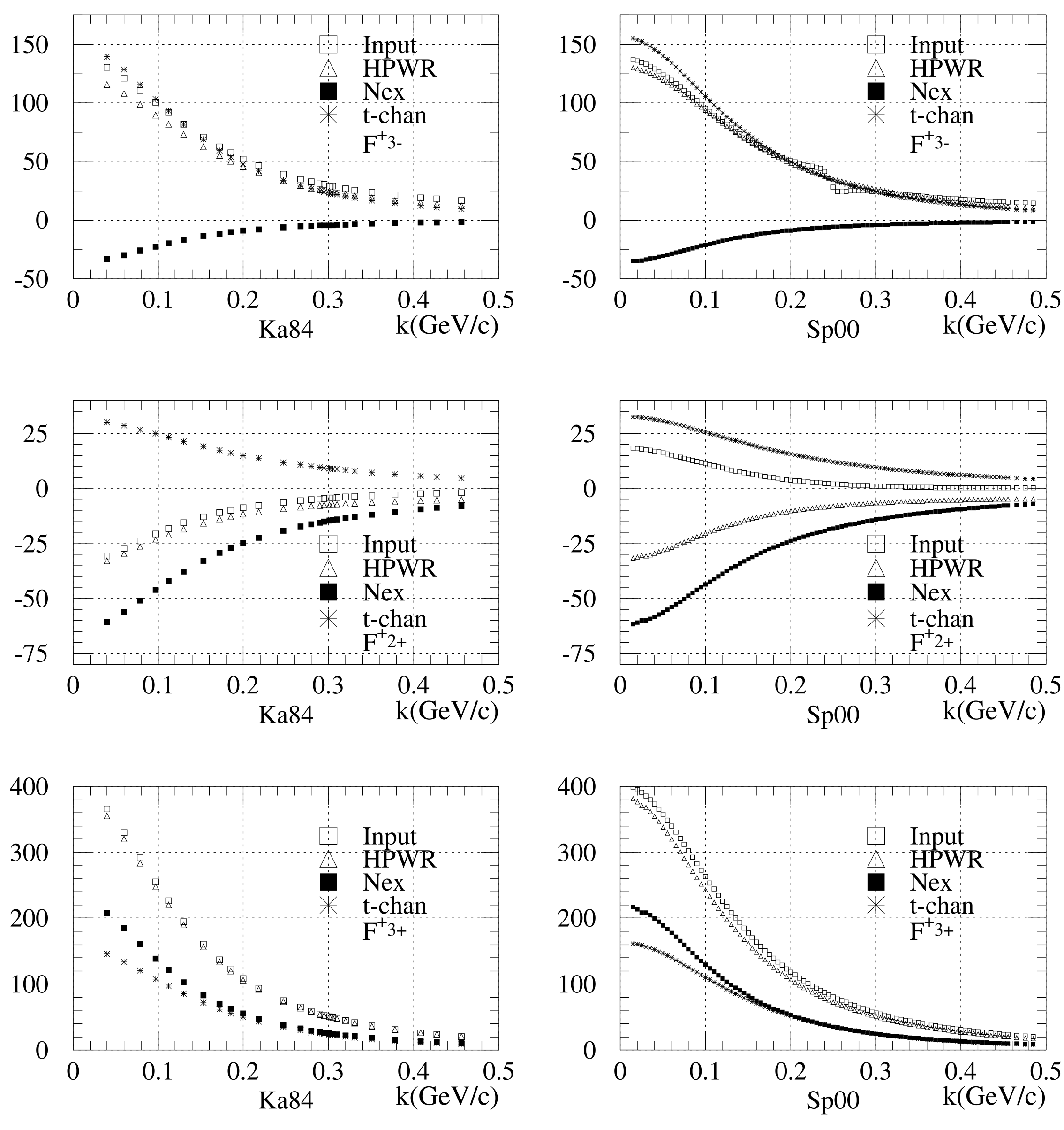

Figure 1: D and F waves obtained from HPWR.

6 Results

We have calculated the real parts of the isospin even and odd combinations up to $l = 10$. Our results for real parts of reduced partial waves will be satisfactory, if they agree on average with corresponding real parts from start solution. Contributions that have not been taken into account are in general slowly varying functions so we do expect a good prediction of the shape of partial waves as a function of energy. A variety of shapes is strong evidence that partial wave from start solution is not consistent with required analytic properties of partial waves and it is probably wrong. Some results are shown in figures and compared with values from starting partial wave solution. Only isospin even combinations of partial waves are shown because of their importance in calculation of the πN σ term. As can be seen from Figure 1, partial waves from the Ka84 solution are consistent with results obtained from HPWR. D-waves from Sp00 solution should be taken with caution. The partial wave F^{+}_{2+}, which is dominated by the nucleon exchange, is obviously wrong in Sp00 solution. It has the wrong sign. More figures are available upon request from the author.

7 Conclusions

The conclusions are:

• Leading contributions to πN partial waves in the framework of HPWR are analysed and understood.

• Higher πN partial waves at low energies can be obtained using HPWR. Satisfactory results can be obtained using presently available input.

• Lower partial waves can be obtained using a modified FTPWR.

• New results for the t-channel input would improve reliability of obtained results.

• When applying dispersion relations outside of the physical region, obtained values for invariant amplitudes can not be considered as reliable while higher partial waves in partial wave input are not well determined.

Acknowledgments: I wish to thank Prof. G. Höhler for his continuous encouragement and support and for many valuable discussions. This work was partly supported by DOE grant DE-FG03-94ER40860. I also would like to thank the Ministry of Education of Tuzla Kanton, Bosnia and Herzegovina and the Organizing Committee of MENU2001 for making my attendance at the Conference possible.

References

[1] G. Höhler, Landolt–Börnstein vol. **I/9b2**, *Pion-Nucleon Scattering* (Springer, Berlin, 1983).

[2] J. Hamilton, T.D. Spearman, Ann. Physics **12** (1961) 172; J. Hamilton *et al.*, Phys. Rev. **128** (1962) 1881.

[3] R. Koch, M. Hutt, Z. Phys. **C19** (1983) 119.

[4] J. Baacke, F. Steiner, Fortschr. Phys. **18** (1970) 67.

[5] R. Koch, Nucl. Phys. **A448** (1986) 707.

[6] G. Hyte and Steiner, Nuovo Cim. **18A** (1973) 237.

[7] J. Stahov, Thesis, University Zagreb, 1983.

[8] J. Gasser, H. Leutwyler, M. Sainio, Phys. Lett. **B253** (1991) 260.

Resurrecting the KH78/80 partial wave analysis

P. Piirola,[a] E. Pietarinen,[a,b] and M.E. Sainio[a,b]

[a] *Department of Physics,*
[b] *Helsinki Institute of Physics,*
P.O. Box 64, 00014 University of Helsinki, Finland

(Received: 11 October 2001)

Most of the data from the meson factories were available only after the πN partial wave analysis of Koch and Pietarinen [1] was published over 20 years ago. Since then, both the experimental precision and the theoretical framework have evolved a lot as well as the computing technology. Both the new and the earlier data are to be analysed by a highly modernised version of the earlier approach. Especially the propagation of the measurement errors in the analysis will be considered in detail, visualisation tools will be developed using the Python/Tkinter combination [2], and the huge data base of experiments will be handled by MySQL [3].

1 Introduction

About 20 years ago Koch and Pietarinen performed an energy-independent partial-wave analysis on pion-nucleon elastic and charge-exchange differential cross sections and elastic polarisations for laboratory momenta below 500 MeV/c incorporating the constraints from fixed-t dispersion relations as well as crossing and unitarity (the KH78 and KH80 analyses) [1]. Since then, however, new low-energy data have emerged in all charge channels: examples of recent high precision results for the differential cross sections are given in refs. [4–6], polarisation parameter in refs. [7–9] and the spin rotation parameter in ref. [10]. There are also some new measurements of integrated cross sections [11]. Especially the high precision measurements of the hadronic level shift and width on pionic hydrogen and deuterium [12], giving information of the pion-nucleon interaction just at the threshold, have opened a completely new chapter in the study of the low-energy pion-nucleon interaction. Another direction where significant advances have taken place is the theoretical framework where we study the low-energy pion-nucleon interaction. The tool, chiral perturbation theory (χPT), has been developed in the 80's and 90's and the work continues. The development of χPT motivates a new partial wave analysis from the theoretical point of view — on one hand strong interaction physics is becoming a precision science also in the low-energy region, on the other hand, there is need for πN phenomenology to fix some of the low-energy constants appearing in the meson-baryon lagrangian. See, for example, the talk of Meißner in these proceedings [13].

It is our goal to make use of the new data in an analysis which, in addition to the requirements of analyticity, crossing and unitarity, includes the constraints from chiral symmetry.

2 The old KH78/80 analysis

The aim of the KH analysis was to determine the amplitudes satisfying several conditions:

1. The amplitudes had to reproduce all the data which were available at that time, which means $\frac{d\sigma}{d\Omega}$, σ_{tot} and P within their associated errors.

2. The solution had to fulfil the isospin invariance.

3. All partial waves had to satisfy the unitarity condition.

4. The crossing symmetry was implicitly assumed, because Mandelstam variables were used.

5. The invariant amplitudes were going to have the correct analyticity properties in s at fixed-t.

6. The amplitudes at fixed-s were to be analytic in $\cos\theta$ in the small Lehman ellipse.

The experimental data is not enough to fix a unique partial wave solution, but further theoretical constraints are needed. The constraints from fixed-t analyticity and from the isospin invariance are strong enough to resolve the ambiguities [14].

3 Three stages of the analysis

3.1 Fixed-t analysis

The old KH analyses consist of three phases: fixed-t analysis, fixed-θ analysis and fixed-s analysis, which were iterated until the results agreed up to about 3 %. The fixed-t analysis was carried out at 40 t-values in the range from zero to -1.0 GeV^2. The analysis would be too complicated, if one were working with dispersion integrals, so the expansion [15, 16]

$$C(\nu,t) = C_N(\nu,t) + H(Z,t)\sum_{i=0}^{n} c_i Z^i \tag{1}$$

was used for t-values smaller than $-4m\mu$, $(\nu = (s-u)/4m)$. In the expansion the nucleon pole term $C_N(\nu,t)$ is treated separately, and the sum is multiplied by a factor $H(Z,t)$, which describes the expected asymptotic behaviour. The essence of the expansion is that the sum is written in terms of functions Z, which have the correct analytic behaviour, i.e. it is *not* a polynomial approximation, but a series presentation of an analytic function, which is just truncated at some reasonable point (ca. $n = 50$ or $n = 100$), because infinite accuracy is impossible. The condition of smoothness and the compatibility with the data constrain the terms with large index i to be negligible [15, 16].

The expansion coefficients c_i are determined by minimising

$$\chi^2 = \chi^2_{\text{data}} + \chi^2_{\text{pw}} + \chi^2_{\text{penalty}}\ . \tag{2}$$

Here χ^2_{data} comes from the experimental errors, χ^2_{pw} belongs to the deviation from the fixed-s partial wave solution and the last term is used to suppress large values of the higher coefficients of the expansion. In practice, the analyticity constraints cannot be used without smoothing the data. The aim is, of course, to smooth out the statistical fluctuations without distorting the physically relevant structures.

3.2 Fixed-θ analysis

The fixed-t constraint is often used only for t values from zero to about -0.5 GeV^2, because the partial wave expansions for the imaginary parts of the invariant amplitudes do not converge for large $|t|$. In the range $t \in (-0.5, -1.5]$ GeV^2 the truncated partial wave expansions can still be reasonable approximations, but for t values below ca. -1 or -1.5 GeV^2 the fixed-t analyticity cannot be applied anymore. So another analyticity constraint is used to cover the rest of the angular range at intermediate and at high energies. The calculation was made at 18 angles between $\cos\theta = -0.9 \ldots 0.8$. Analysing methods are the same as in the fixed-t analysis: the expansion method is used and the coefficients are fixed by minimising χ^2, i.e. by fitting to the data and to the fixed-t solution.

3.3 Fixed-s analysis

The third stage, the fixed-s analysis, is a standard phase shift analysis in the sense that the partial waves are fitted to the data. On the other hand, it is not the usual one, because the partial waves are fitted also to the fixed-t and to the fixed-θ amplitudes. Now 92 momentum values were selected from the energy range $0 \ldots 200$ GeV/c, 6 of the momenta were above 6 GeV/c. Again, the coefficients were fixed by minimising χ^2 which now included also a term suitable to enforce unitarity.

4 Treatment of the data

The electromagnetic corrections proposed by Tromborg et al. at momentum values below 0.65 GeV/c [17], were applied to the data. At higher momentum, only the one-photon exchange correction was applied, taking into account the Coulomb phase. In all three different analyses, the data were shifted to the selected energy bins (i.e. the selected values of s, t or θ) using the previous solution of the iteration to calculate the correction. Some data points requiring too large a momentum shift were omitted. The normalisation of some data sets had to be corrected to guarantee a smooth extrapolation to the forward direction, and to the input for the forward amplitude.

5 Life after KH80

The latest KH phase shift analysis was finished in 1980. After that there has been very accurate measurements of pionic hydrogen level shift and width, $\frac{d\sigma}{d\Omega}$ has been measured with good accuracy, many spin rotation parameter measurements has been done as well as polarisation parameter measurements. Also, some integrated cross section measurements have been performed. The newer data has never been analysed by the methods of Koch and Pietarinen, and for example the results of Pavan et al. [4] are not compatible with the results of the old analyses. So, an updated version of the analysis is certainly needed.

6 The code of Pietarinen

The original code was made for the NDP Fortran compiler, which runs under MS-DOS. The code needs to be ported to UNIX. We have tested the code in an old MS-DOS machine, and most of the main tasks seem to be working correctly. What is still needed, is a modification of the s-plane conformal mapping. This has effects on all routines, which are related to the fixed-t analysis. Also some modifications are needed to be able to study the isospin analysis.

The code base is divided into several parts:

- There is a program for comparing the partial wave solution to existing data. It simply plots the data and the solution in the same picture, and allows the comparison of different data sets to the solution.
- The second part is for shifting the experimental data points into the fixed-t bins. The earlier solution is used for interpolation, and those data points which are to be shifted too much are rejected.
- The next part is for making a starting value for the fixed-t expansion.
- One program is for the iteration to adjust the fixed-t amplitude to the experimental data and to the current solution.
- The main part of the program makes the actual partial wave analysis and adjusts the solution simultaneously to the data and to the fixed-t amplitudes.

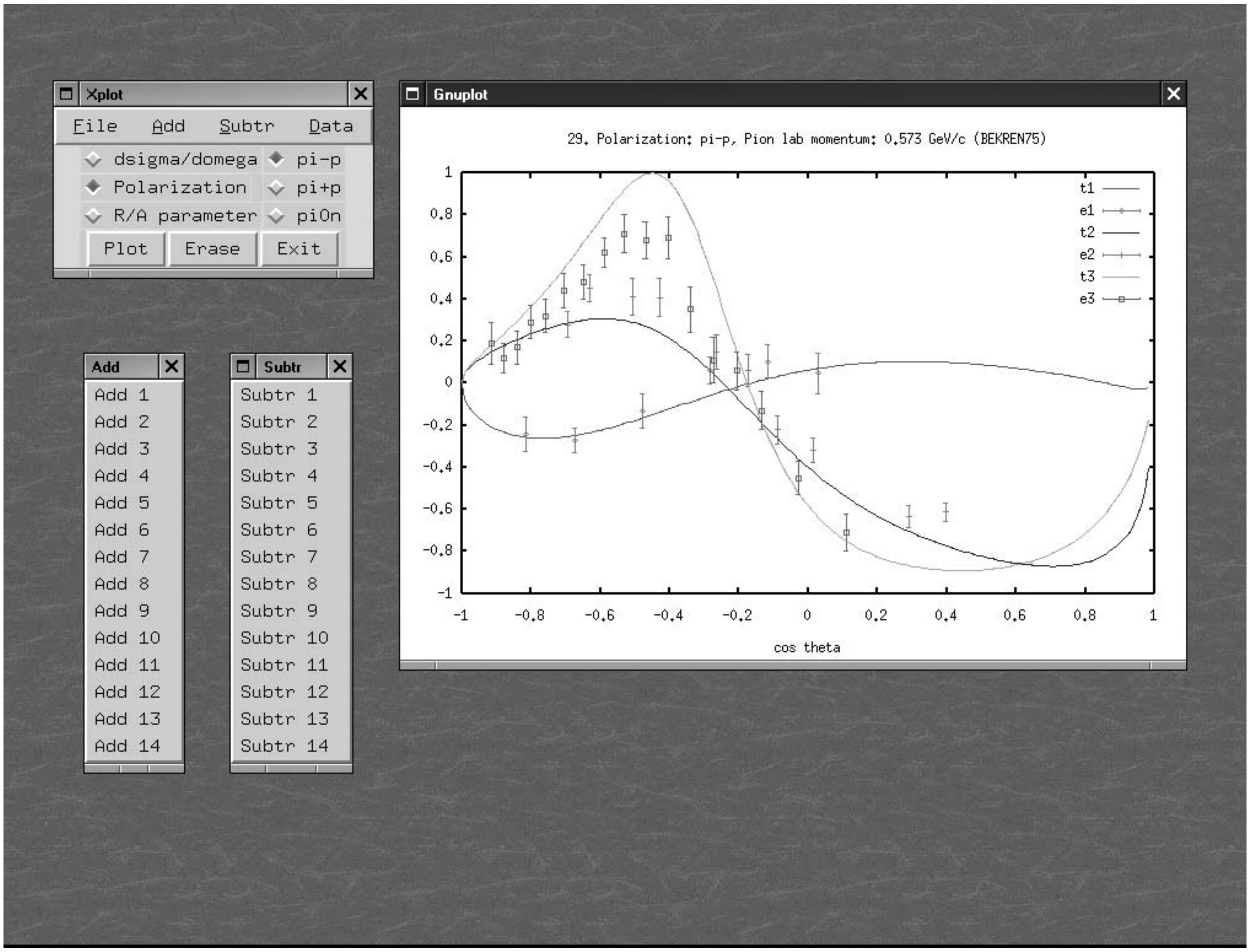

Figure 1: Screen shot of the plotting program. In the plot there are three different measurements at different momentum values (0.192 GeV/c, 0.425 GeV/c and 0.573 GeV/c) [18–20], and the corresponding partial wave solutions — so it is possible to compare the goodness of the different data sets by the "eye ball" method. The scattered particles and the reaction can be chosen by the radiobutton widgets. The different data sets are selected by the same method as in the original code of Pietarinen, i.e. by moving up or down in the data base with `Add` or `Sub` buttons. The method is quite crude, and it is going to change when the data base is converted to MySQL format.

7 The current status

7.1 Porting the code

During the porting process the most extensive work is needed for writing the graphical user interface, the data base engine and the plotting routines. The graphics routines of the original code were impossible to get working under UNIX, so we decided to use the Python/Tkinter combination for the GUI, and the Python/Gnuplot combination for plotting routines. The old code was reused as much as possible, but many parts still needed almost complete rewriting. We decided to write all the new code in Fortran 95, so, at the moment, most of the calculation engine is written in Fortran 77 and some parts in Fortran 95. All routines of the old code were modified to take almost all input from the stdin and to write output to stdout, so it should now be possible to change the whole GUI with a reasonable amount of work, whenever it becomes necessary.

7.2 *The current status*

At present, the plotting program, the interpolation program and the program calculating the starting value of the fixed-t analysis are ported to UNIX, and all the functionality of the original versions is implemented (fig. 1). The part, which iterates to adjust the fixed-t amplitudes, the partial wave solution, and the experimental data, compiles OK but the GUI is still under construction. The heart of the whole program, the part making the actual analysis, is still in a completely untested stage.

7.3 *Comparison of the numerics*

We have compiled the code with different compilers running on different operating systems in order to check the stability of the mathematical subroutines[1]. Comparing the results of the routines compiled by different compilers showed that the routines are *not* currently stable enough for production use.

For illustration, the interpolator part of the program calculates 173670 interpolated data points. When comparing the results of routines compiled by GNU Fortran to those calculated by NDP Fortran, one notices that 96% of the new data points agree up to 0.01%, but in some cases there are significant discrepancies: namely 73 data points of the 173670 differ by more than 1%, and in the worst case the difference is 28%. The cause of these discrepancies is unknown when writing this.

8 The next phase

After chasing the bugs and finding the reasons for the numerical unstabilities, we are hoping to find a better way to handle the propagation of the experimental errors than that used in the old KH analysis.

Because of the size of the data base, and because of the discrepancies in the different data sets, the visualisation of the data and the partial wave solutions is essential. Also, during the analysis, the program is used a lot, so the graphical user interface has to be easy and efficient to use. For making the choice of the data sets as easy as possible, we have plans to convert our text file data bases to MySQL format.

We intend to get the first preliminary results by the end of the year.

Acknowledgments: We wish to thank A.M. Green for useful comments on the manuscript. We gratefully acknowledge financial support by the Academy of Finland grant 47678, the TMR EC-contract CT980169, and the Magnus Ehrnrooth Foundation.

References

[1] R. Koch and E. Pietarinen, Nucl. Phys. **A336**, 331 (1980).
[2] G. van Rossum et al., `http://www.python.org/` (1990-2001).
[3] M. Widenius et al., `http://www.mysql.com/`.
[4] M.M. Pavan et al., nucl-ex/0103006 (2001).
[5] E. Frlež et al., Phys. Rev. **C57**, 3144 (1998), hep-ex/9712024.
[6] M. Janousch et al, Phys. Lett. **B414**, 237 (1997).
[7] C.V. Gaulard et al., Phys. Rev. **C60**, 024604 (1999).
[8] G.J. Hofman et al., Phys. Rev. **C58**, 3484 (1998).

[1] We have tried the old NDP Fortran compiler for MS-DOS, the Compaq Fortran in Digital UNIX, the Lahey/Fujitsu Fortran for Linux, and different versions of the GNU/Linux Fortran.

[9] R. Wieser et al., Phys. Rev. **C54**, 1930 (1996).
[10] I. Supek et al., Phys.Rev. **D47**, 1762 (1993).
[11] B.J. Kriss et al., Phys. Rev. **C59**, 1480 (1999).
[12] H.C. Schröder at al., Phys. Lett. **B469**, 25 (1999).
[13] Ulf-G. Meißner, these proceedings, hep-ph/0108133 (2001).
[14] G. Höhler, in: *Landolt-Börnstein* Vol. 9b2 (1983).
[15] E. Pietarinen, Nucl. Phys. **B107**, 21 (1976).
[16] E. Pietarinen, Physica Scripta **14**, 11 (1976).
[17] B. Tromborg, S. Waldenstrøm, and I. Øverbø, Phys.Rev. **D15**, 725 (1977).
[18] J.C. Alder et al., Phys. Rev. **D27**, 1040 (1983).
[19] J.C. Alder et al., Lett. Nuovo Cim. **23**, 381 (1978).
[20] V.S. Bekrenev et al., Sov. J. Nucl. Phys. **24**, 45 (1976).

Electromagnetic and strong isospin breaking in hadronic amplitudes

A. Rusetsky

Institute for Theoretical Physics, University of Bern, Sidlerstrasse 5, 3012 Bern, Switzerland, and HEPI, Tbilisi State University, University St. 9, 380086 Tbilisi, Georgia

(Received: 19 October 2001)

The general procedure for extracting the isospin-symmetric quantities from the experimental data on low-energy hadronic processes and observables of hadronic atoms is discussed. This implies the consistent definition - in the context of ChPT - of the idealized pure QCD world by switching off effects caused by electromagnetic corrections and quark mass differences in full QCD+QED. We further address the application of the general approach based on the non-relativistic effective Lagrangians and ChPT, to the calculation of the isospin-breaking characteristics in hadronic atoms, and matching of the short-range hadronic potentials to ChPT.

1 Introduction

The energy spectrum and decays of hadronic atoms have recently been measured by several experimental collaborations. In particular, the measurement of the $\pi^+\pi^-$ atom decay width by DIRAC collaboration at CERN [1] which will result in the determination of the difference $a_0 - a_2$ of the S-wave $\pi\pi$ scattering lengths at a $5\,\%$ precision, would allow one to directly test the large/small condensate scenario of chiral symmetry breaking in QCD with two flavors. Further, the Pionic Hydrogen collaboration at PSI intends to extract the S-wave πN scattering lengths from the ongoing measurement of the pionic hydrogen at a $1\,\%$ accuracy [2]. This will yield a more precise value of the πNN coupling constant and of the πN σ-term. Finally, the DEAR collaboration [3] at the DAΦNE facility plans to measure the energy level shift and lifetime of the $1s$ state in K^-p and K^-d atoms, and it is expected [3] that this will result in an accurate determination of the $I = 0, 1$ S-wave scattering lengths. It will be a challenge for theorists to extract from this new information a more precise value of e.g. the KN σ-term and of the strangeness content of the nucleon.

In order to fully exploit the high-precision experimental data, it is imperative to design the theoretical framework for the analysis of these data which would describe hadronic atoms in the accuracy that matches the experimental precision. In practice, this means the following. The Deser-type formulae which are used to extract the strong scattering lengths from the measured values of the strong energy shift in the ground state ΔE_{str}, and the partial decay width into the hadronic channel Γ_{c0}, are given by

$$\Delta E_{str} \sim \Psi_0^2 \,\mathrm{Re}\, a_{cc}\,(1+\delta_\epsilon)\ , \qquad \Gamma_{c0} \sim (\text{phase space})\,\Psi_0^2\,|a_{c0}|^2\,(1+\delta_\Gamma)\ , \tag{1}$$

where Ψ_0 denotes the value of the Coulomb wave function at the origin, a_{cc} and a_{c0} are particular isospin combinations of the "purely strong" hadronic scattering lengths, and δ_ϵ, δ_Γ stand for the isospin-breaking corrections which depend on the fine structure constant α and the up and down quark mass difference $m_d - m_u$. To proceed further, the following fundamental questions should be answered.

i) The scattering lengths a_{cc}, a_{c0} are calculated in pure QCD. How this limit is consistently defined from QCD+QED? (Under QCD+QED we mean QCD+photons. We do not consider leptons explicitly.). Note that, in the view of the announced accuracy $0.3\,\%$ in the future measurement of the energy shift of the π^-p atom by Pionic Hydrogen collaboration at PSI, the question of the precise definition of the pure QCD limit is not only academic.

ii) Once it is clear what a_{cc} and a_{c0} are, how one calculates isospin-breaking corrections δ_ϵ, δ_Γ?

iii) Historically, the isospin-breaking corrections were first calculated in the framework of the potential scattering theory approach [4, 5]. The predictions do not always agree with the predictions obtained by using ChPT, that have emerged later. For this reason, the status of the calculations based on the potential model, should be clarified. This implies the derivation of the short-range hadronic potentials which are consistent with ChPT.

In this work, the above questions will be addressed.

The issue of "purification" of the experimental data with respect to strong and electromagnetic isospin-breaking corrections arises in the closely related problem of the the low-energy hadronic scattering. For this reason, the discussion below is relevant also for the scattering problem.

2 Pure QCD limit of QCD+QED [6]

The problem of definition of the pure QCD limit can be put as follows. We start with QCD+QED. The parameters of the theory are the strong running constant $\bar{g}(\mu)$, fine structure constant α, and the up and down quark masses $\bar{m}_u(\mu)$, $\bar{m}_d(\mu)$, where μ stands for the running scale. These 4 parameters, in principle, can be determined by fitting 4 independent hadron masses, e.g. M_{π^+}, M_{π^0}, m_p and m_n. Switching off electromagnetic interactions, one arrives at the theory with 3 parameters: strong coupling constant and the quark masses. Assuming further that quark masses are equal, we get the theory with two parameters $g(\mu)$ and $\hat{m} = m_u(\mu) = m_d(\mu)$, which is referred to as pure QCD. One has to answer the question, how the parameters $g(\mu)$ and $\hat{m}$ are related to the original parameters in QCD+QED, and to the physical observables.

One should emphasize, that at present the only available method to tackle the non-perturbative QCD dynamics at low energy is provided by ChPT. For this reason, we shall discuss the splitting of electromagnetic and strong interactions at the level of the low-energy effective theory. Below, we shall provide three consecutive definitions of pure QCD.

2.1 *Definition 1*

The running parameters in QCD+QED obey the following RG equations (We choose the $\overline{\mathrm{MS}}$ renormalization scheme)

$$\begin{aligned}
\mu\frac{d}{d\mu}\bar{g} &= \beta(\bar{g},\bar{e}) = \beta_0(\bar{g}) + \bar{e}^2\beta_1(\bar{g}) + O(\bar{e}^4)\ , \\
\mu\frac{d}{d\mu}\bar{e} &= \varepsilon(\bar{g},\bar{e}) = \bar{e}^3\varepsilon_1(\bar{g}) + O(\bar{e}^5)\ , \\
\mu\frac{d}{d\mu}\bar{m}_q &= \gamma(\bar{g},\bar{e})\bar{m}_q = \left[\gamma_0(\bar{g}) + \bar{e}^2\gamma_1^{(q)}(\bar{g}) + O(\bar{e}^4)\right]\bar{m}_q\ , \qquad q = u, d
\end{aligned} \tag{2}$$

The parameters of pure QCD run according to

$$\begin{aligned}
\mu\frac{d}{d\mu}g &= \beta_0(g)\ , \\
\mu\frac{d}{d\mu}\hat{m} &= \gamma_0(g)\hat{m}\ .
\end{aligned} \tag{3}$$

One may match the running parameters of pure QCD to QCD+QED at a some scale μ_1

$$g(\mu_1) = \bar{g}(\mu_1)\ , \qquad \hat{m}(\mu_1) = \frac{1}{2}\left(\bar{m}_u(\mu_1) + \bar{m}_d(\mu_1)\right)\ . \tag{4}$$

Further, any physical quantity in QCD+QED can be expanded in the isospin-breaking parameters α and $\Delta \doteq \bar{m}_d(\mu_1) - \bar{m}_u(\mu_1)$. The first term in this expansion which does not contain these parameters, corresponds to the pure QCD limit of QCD+QED. It is important to note that the "purely strong" quantities calculated in this limit, depend on the choice of the matching scale μ_1. The chiral expansion is performed in the quark mass $\hat{m}(\mu_1)$, and the coefficients of this expansion depend only of $g(\mu_1)$.

The above definition of the pure QCD limit is unique once the matching scale μ_1 is fixed. From the point of view of implementation of this prescription into the framework of ChPT, it is, however, not the most convenient one. In particular, the hadron masses M_π and m_N in pure QCD are not directly related to the measured masses of hadrons.

2.2 Definition 2

We shall change the definition of the pure QCD limit and adjust the parameter $\hat{m} \to \hat{m}'$ so that the pion mass M_π in the effective theory of pure QCD coincides, by convention, with the charged pion mass in the effective theory of QCD+QED. The expansion of the pion mass squared in these two theories is given by

$$\begin{aligned}
\text{QCD+QED:} \qquad & M_{\pi^+}^2 = 2\hat{m}B + a_1(\hat{m}B)^2 \ln\frac{\hat{m}B}{\mu_E} + a_2(\mu_E)(\hat{m}B)^2 + a_3\alpha + a_4 B^2\Delta^2 + \cdots \,, \\
\text{pure QCD:} \qquad & M_\pi^2 = 2\hat{m}'B + a_1(\hat{m}'B)^2 \ln\frac{\hat{m}'B}{\mu_E} + a_2(\mu_E)(\hat{m}'B)^2 + \cdots \,,
\end{aligned} \tag{5}$$

where μ_E denotes the scale of the effective theory (ChPT). The QCD scale which is implicitly present, is taken equal to the matching scale μ_1 - for this reason, the expansion coefficients B, a_1, $a_2(\mu_E)$ which depend only on $g(\mu_1)$, are the same in both theories. With this prescription, one may evaluate the corrections to the pure QCD limit in any physical quantity, given the chiral expansion of this quantity in QCD+QED - the charged pion mass then serves as a reference mass for the pure QCD limit. The drawback of the above definition is that the nucleon mass in pure QCD is not directly related to the physical baryon masses, so in the calculations one has to always resort to the chiral expansion of the former.

2.3 Definition 3

In order to fit the nucleon mass in pure QCD to the particular value, one has to adjust $g(\mu_1)$. Then, the coefficients in the chiral expansion - low-energy constants (LECs) - which depend on $g(\mu_1)$, will also change in the pure QCD limit. We may estimate the magnitude of this change, considering the chiral expansion of the nucleon mass

$$\begin{aligned}
\text{QCD+QED:} \qquad & m_p = \overset{0}{m} - 8c_1\hat{m}B + 2Bc_5\Delta - 2\pi\alpha F^2(f_1+f_2+f_3) \,, \\
\text{pure QCD:} \qquad & m_N = \overset{0}{m} - 8c_1\hat{m}'B \,,
\end{aligned} \tag{6}$$

where $\overset{0}{m}$ and F denote the nucleon mass and the pion decay constant in the chiral limit, and c_1, c_5, f_1, f_2, f_3 stand for the strong and electromagnetic LECs, respectively [8]. Using the estimates for these LECs leads to $(m_p - m_N)/m_p \simeq 4 \cdot 10^{-3}$. In other words, in order to adjust the nucleon mass in pure QCD to the proton mass, Λ_{QCD} should change only by 0.4 %. The change in LECs is expected to be tiny as well. At this accuracy, we arrive at the following definition of the pure QCD limit of QCD+QED which is the most convenient one in the context of the effective field theory:

In the pure QCD limit of QCD+QED, the quark mass and strong coupling constant are fixed from the requirement that the pion and nucleon masses are equal, by convention, to the charged *pion and proton masses, respectively. In the effective theory of QCD+QED, the values of the strong LECs stay put in the pure QCD limit.*

We would like to mention that since now the systematic error in the calculation of isospin breaking corrections within ChPT by far exceeds 0.4 %, for the time being one may safely stick to the definition 3.

3 Calculation of isospin-breaking corrections

Once the pure QCD limit where the hadronic scattering lengths a_{cc}, a_{c0} are calculated, is unambiguously defined, one can systematically calculate the isospin-breaking corrections δ_ϵ δ_Γ in the Deser-type formulae (1). Since this problem has been addressed in detail in our previous publications [9–12], we give here only the brief description of the approach and quote the results. The method employed is based on the merger of the non-relativistic effective Lagrangian approach to the bound states and ChPT.

i) At the first step, one constructs the most general effective Lagrangian from the non-relativistic hadron fields and the photon field. The Lagrangian consists of an infinite tower of operators with an increasing mass dimension, allowed by the symmetries. In the calculations at a given order in α only few operators with the lowest mass dimension are relevant.

ii) The couplings in the non-relativistic Lagrangian are matched at physical threshold to the relativistic amplitudes calculated in QCD+QED. In the matching, there is no need to resort to the chiral expansion of the relativistic amplitudes.

iii) At a next step, one calculates the bound state observables - energy shift and decay width - in the non-relativistic theory in terms of the couplings of the non-relativistic Lagrangian. Through the matching procedure, these observables are expressed via the relativistic amplitudes, so that all reference to the non-relativistic theory disappears in the final expressions.

iv) At the last step, we evaluate the isospin-breaking corrections in the amplitudes, invoking ChPT. Using the relations between the amplitudes and the observables of hadronic atoms, it is straightforward to obtain the expressions for δ_ϵ, δ_Γ.

The application of the above-mentioned general procedure to the particular bound systems yields:

3.1 *Decay of the $\pi^+\pi^-$ atom*

Assumption about the standard scenario of chiral symmetry breaking in QCD leads to a very rigid prescription for the $\pi^+\pi^-$ atom lifetime [12]

$$\tau = (2.9 \pm 0.1) \cdot 10^{-15}\ \mathrm{s}\,, \tag{7}$$

where bulk of the uncertainty comes from the error in the value of $a_0 - a_2$ evaluated in ChPT [13]. For a fixed value of $a_0 - a_2$, the accuracy in the lifetime equals 1.2 % [12]. Any discrepancy between the measured value of the lifetime and the above prediction would mean that the chiral symmetry breaking in QCD proceeds differently from the standard picture.

3.2 *Energy shift of the π^-p atom*

With the use of the non-relativistic effective Lagrangian technique, the general expression for the strong energy level shift of the π^-p atom was obtained in the first non-leading order in the isospin-breaking parameters α and $m_d - m_u$, and (formally) in all orders in the chiral expansion. The order-of-magnitude estimate of the isospin-breaking correction in the elastic scattering amplitude at chiral order p^2 yields the following value for the correction to the energy shift [11]

$$\delta_\epsilon = (4.8 \pm 2.0) \cdot 10^{-2} \ , \tag{8}$$

where the large uncertainty is caused by the poor knowledge of some $O(p^2)$ LECs in the pion-nucleon Lagrangian. (For the quark-model estimates of these couplings, see Ref. [14]).

Full calculation of the $O(p^3)$ isospin-breaking correction to the elastic scattering amplitude has been recently performed [15], and will be published elsewhere.

Application of the above approach for the description of other hadronic bound states is foreseen.

4 Universality and the construction of hadronic potentials

As was mentioned in the introduction, the predictions for the isospin-breaking corrections in the characteristics of hadronic atoms made on the basis of the potential scattering approach, generally differ from those obtained in ChPT. The reason for this difference is that the potentials in these calculations have not been matched to ChPT and therefore do not contain a full content of isospin breaking effects in QCD+QED. In order to bring these two approaches into conformity, it is necessary to provide a constructive algorithm for matching the hadronic potentials to ChPT *in the isospin-breaking phase*. This question was considered in detail in our recent publication [16]. Below, we give a brief outline of the procedure.

i) The conventional short-range potentials are considered as a mere regularization of the singular pointlike interactions which describe low-energy interactions of hadrons in the field theory. For this reason, the shape of the potential does not bear a physical information. Couplings in the potential are determined from matching of the scattering amplitudes in the potential approach and in the underlying field theory, both expended in powers of the CM momentum squared $\mathbf{p}^2$. Performing the matching at higher order in $\mathbf{p}^2$, one arrives at a more accurate description of both the scattering amplitudes and bound-state observables in the potential approach. Apart from the above matching condition, no further restriction is imposed on the potentials.

ii) The derivation of the potential for the description of bound states is based on the universality, which states that the properties of bound states are the same in the potential scattering approach and field theory, once the threshold scattering amplitudes are the same. Due to the universality, one may carry out the matching in the scattering sector, where the perturbation expansion in α works.

iii) The reason why the results of calculations for the observables of hadronic atoms carried out within the potential approach [4, 5] generally differ from those obtained in ChPT, is now crystal clear. In order to agree with the latter, the potentials should be matched to QCD in the isospin-breaking phase. The matching, in general, generates a nonzero isospin-breaking part of the short-range hadronic potential. Furthermore, it may turn out that the prediction for the isospin-breaking corrections to the atom observables in the potential approach is close to that of ChPT. This means that the isospin-breaking part of the short-range potential (only in this particular hadronic channel) constructed through the matching procedure, is very small.

5 Conclusions

i) In this work, a definition of the pure QCD limit of QCD+QED was discussed in detail. In particular, it was demonstrated that the convention where the pion and nucleon masses are set to be equal the charged pion mass and the proton mass, respectively, is the most convenient one in the applications. If one performs calculations within ChPT, the systematic error introduced by use of this convention in the pure QCD quantities, is of order of 0.4 %.

i) The general approach based on the non-relativistic effective Lagrangians and ChPT, has been successfully applied to the calculation of the isospin-breaking corrections in the decay width of the $\pi^+\pi^-$ atom ad the strong energy shift of the π^-p atom.

iii) Constructive algorithm based on the universality conjecture is provided, that allows one to match the potential used in the calculations of the hadronic atom characteristics to ChPT.

Acknowledgments: I am grateful to J. Gasser and H. Leutwyler for interesting discussions. This work was supported in part by the Swiss National Science Foundation, and by TMR, BBW-Contract No. 97.0131 and EC-Contract No. ERBFMRX-CT980169 (EURODAΦNE), and by SCOPES Project No. 7UZPJ65677.

References

[1] B. Adeva *et al.*, CERN proposal CERN/SPSLC 95-1 (1995).

[2] H.-Ch. Schröder *et al.*, Phys. Lett. **B469** (1999) 25; D. Gotta, πN Newslett. **15**, 276 (1999).

[3] "DAΦNE exotic atom research: the DEAR proposal", DEAR collaboration (R. Baldini et al.), Preprint LNF-95-055-IR, (1995).

[4] G. Rasche and W.S. Woolcock, Nucl. Phys. **A381**, 405 (1982); U. Moor, G. Rasche, and W.S. Woolcock, Nucl. Phys. **A587**, 747 (1995); A. Gashi, G.C. Oades, G. Rasche, and W.S. Woolcock, Nucl. Phys. **A628**, 101 (1998); A. Gashi, G.C. Oades, G. Rasche, and W.S. Woolcock, Preprint hep-ph/0108116.

[5] D. Sigg, A. Badertscher, P.F.A. Goudsmit, H.J. Leisi, and G.C. Oades, Nucl. Phys. **A609**, 310 (1996).

[6] The material presented in this section is based on unpublished notes by H. Leutwyler, and on work done in collaboration with J. Gasser [7].

[7] J. Gasser and A. Rusetsky, to be published.

[8] N. Fettes, U.-G. Meissner and S. Steininger, Nucl. Phys. **A640**, 199 (1998); U.-G. Meißner and G. Müller, Nucl. Phys. **B556** (1999) 265.

[9] A. Gall, J. Gasser, V.E. Lyubovitskij, and A. Rusetsky, Phys. Lett. **B462**, 335 (1999).

[10] J. Gasser, V.E. Lyubovitskij, and A. Rusetsky, Phys. Lett. **B471**, 244 (1999).

[11] V.E. Lyubovitskij and A. Rusetsky, Phys. Lett. **B494**, 9 (2000).

[12] A. Gall, J. Gasser, V.E. Lyubovitskij, and A. Rusetsky, Phys. Rev. **D64**, 016008 (2001).

[13] G. Colangelo, J. Gasser and H. Leutwyler, Phys. Lett. **B488**, 261 (2000); Nucl. Phys. **B603**, 125 (2001).

[14] V.E. Lyubovitskij, T. Gutsche, A. Faessler, and R. Vinh Mau, Preprint hep-ph/0109213.

[15] J. Gasser, M.A. Ivanov, E. Lipartia, M. Mojžis, and A. Rusetsky, in preparation.

[16] E. Lipartia, V.E. Lyubovitskij and A. Rusetsky, Preprint hep-ph/0110186.

Threshold and subthreshold πN scattering amplitudes; comparison with chiral perturbation theory predictions

B.R. Martin[a] and G.C. Oades[b]

[a]*Department of Physics, University College London, Gower Street, London WC1E 6BT, England*
[b]*Institute of Physics and Astronomy, Aarhus University, DK-8000 Aarhus C, Denmark*

(Received: 31 October 2001)

We make use of a conformal mapping representation to impose fixed-t analyticity on the invariant amplitudes obtained from various sets of πN phase shifts. Values of these amplitudes are examined at threshold and at the symmetry point $\nu = 0$.

Dedication

Last Autumn one of the founding fathers of our field, Jim Hamilton, died at the age of 82. We dedicate this report to his memory.

Mea culpa

At the last MENU Symposium in Zuoz I presented values for the subthreshold expansion parameters calculated using the finite contour dispersion relations [1].

$$Re\overline{X}(\nu,t) = \nu^2 \frac{P}{\pi} \int_{\nu_{th}}^{\nu_1} \frac{Im\overline{X}(\nu',t)}{\nu'^2\,(\nu'^2-\nu^2)} d\nu' + \overline{X}_{FC}(\nu^2,t) \ .$$

The results given for the amplitudes $\overline{D}^{(\pm)}$ were unfortunately in error due to partial confusion with the $\overline{C}^{(\pm)}$ amplitudes. I appologize for this error. The corrected tables for the $\overline{D}^{(\pm)}$ amplitudes are given in Table 1.

$\overline{D}^+$	KH80	SM95	SP98	SM99	Stahov [2]
d^+_{00}	−1.46±0.04	−1.34±0.02	−1.29±0.02	−1.26±0.02	−1.30±0.01
d^+_{01}	1.15±0.11	1.19±0.04	1.23±0.04	1.24±0.04	1.17±0.02
d^+_{02}	0.02±0.06	0.02±0.02	0.03±0.02	0.03±0.02	0.02±0.01
d^+_{10}	1.14±0.04	1.11±0.02	1.11±0.02	1.11±0.02	1.13±0.01
d^+_{11}	0.17±0.09	0.18±0.04	0.18±0.04	0.18±0.04	0.21±0.01
d^+_{20}	0.20±0.01	0.20±0.01	0.20±0.01	0.20±0.01	0.23±0.02

$\frac{D^-}{\nu}$	KH80	SM95	SP98	SM99	Stahov [2]
d^-_{00}	1.55±0.02	1.45±0.01	1.46±0.01	1.43±0.01	1.47±0.01
d^-_{01}	−0.12±0.06	−0.13±0.02	−0.11±0.02	−0.13±0.02	−0.14±0.01
d^-_{02}	0.02±0.03	0.01±0.01	0.02±0.01	0.01±0.01	0.01±0.01
d^-_{10}	−0.20±0.01	−0.16±0.01	−0.16±0.01	−0.16±0.01	−0.17±0.01
d^-_{11}	−0.06±0.02	−0.04±0.01	−0.04±0.01	−0.04±0.01	−0.04±0.01
d^-_{20}	−0.04±0.01	−0.04±0.01	−0.04±0.01	−0.04±0.01	−0.04±0.01

Table 1: Corrected values for the subthreshold expansion parameters for the amplitudes $\overline{D}^{(+)}$ and $\overline{D}^{(-)}/\nu$.

1 Conformal mapping method

In this report, we use a modified version of the finite contour method using a conformal mapping representation

$$\overline{X}(\nu,t) = \sum_{n=1}^{n=N_L} c_n(t) z^n + \sum_{n=0}^{n=N_H} d_n(t) z_H^n \ ,$$

where

$$z(\nu) = \frac{\nu_H \left[v_{th}^2 - \nu^2\right]^{1/2} - \nu_{th} \left[v_H^2 - \nu^2\right]^{1/2}}{\nu_H \left[v_{th}^2 - \nu^2\right]^{1/2} + \nu_{th} \left[v_H^2 - \nu^2\right]^{1/2}} \ , \tag{1}$$

$$z_h(\nu) = \frac{\nu_H - \left[v_H^2 - \nu^2\right]^{1/2}}{\nu_H + \left[v_H^2 - \nu^2\right]^{1/2}} \ . \tag{2}$$

As usual,

$$\nu = \frac{s-u}{4M} \ .$$

ν_{th} is the threshold value and ν_H is the highest value where we use phase shifts to reconstruct the invariant amplitudes (in practice, 2.2 GeV/c). $\overline{X}$ is one of the Born stripped amplitudes $\overline{B}^{(+)}/\nu$, $\overline{B}^{(-)}$, $\overline{D}^{(+)}$ or $\overline{D}^{(-)}/\nu$.

Making use of this representation instead of the usual dispersion relations has two advantages. Both the real and imaginary parts of the amplitudes are smoothed instead of only the real parts and the representation can be used to fit over the whole phase shift region instead of only the low energy region. Using various sets of phase shifts (KH80, KA84, SM95, SP98, SM99, SM01 [3]), we make fits to the invariant amplitudes at a grid of fixed-t values (0.0, -0.25, -0.50, -0.75, -1.00, -1.25, -1.50, -1.75, -2.00) (units with $m_\pi = 1$ are used throughout).

We use the Pietarinen penalty function technique when making our fits and use $N_L = 110$ and $N_H = 30$. The χ^2 values indicate that the point to point statistical errors on the amplitudes are of the order of 5% for the earlier sets of phase shifts and of the order of 2% for the later sets. For the two Karlsruhe sets we use a coupling constant corresponding to $G^2/4\pi = 14.28$ and for all the other sets we use $G^2/4\pi = 13.72$. From these fits we can then evaluate the invariant amplitudes at $\nu = \nu_{th}$ and at $\nu = 0$ (or at other ν values).

2 Threshold values

We first look at the threshold values which are related to the usual scattering lengths (see the book of Höhler A3.5.2, equation A.3.66 [4]) but which are maybe more interesting when we compare with the predictions of chiral perturbation theory.

In the case of the amplitudes $D^{(\pm)}$ including terms up to $l = 2$ gives

$$ReD^{(\pm)}(\nu_{th},t) = D_0^{(\pm)} + D_1^{(\pm)} t + D_2^{(\pm)} t^2 + D_3^{(\pm)} t^3$$

while for $B^{(\pm)}$ terms up to $l = 2$ give

$$ReB^{(\pm)}(\nu_{th},t) = B_0^{(\pm)} + B_1^{(\pm)} t + B_2^{\pm} t^2$$

In both cases the last terms are very small and we do not show them here. The other values are shown in Tables 2 and 3.

Year	$D_0^{(+)}$	$D_1^{(+)}$	$D_2^{(+)}$	$B_0^{(+)}$	$B_1^{(+)}$
1980	-0.11	1.63	-0.02	-32.10	1.36
1984	-0.10	1.62	-0.02	-31.81	1.40
1995	-0.01	1.63	-0.05	-30.65	1.34
1998	0.04	1.66	-0.05	-30.66	1.34
1999	0.07	1.68	-0.04	-30.67	1.33
2001	0.06	1.63	-0.06	-30.64	1.34
Koch [5]	-0.12	1.52	-0.01	-31.77	1.20
χPT [6]	-0.14	1.56	-0.02	-33.08	1.03
χPT [7]	0.04	1.70	-0.01	-32.28	1.11
Errors	~ 0.18	~ 0.40	~ 0.20	~ 0.08	~ 0.06

Table 2: Values for the expansion coefficients in t at threshold for the $+$ amplitudes.

Year	$D_0^{(-)}$	$D_1^{(-)}$	$D_2^{(-)}$	$B_0^{(-)}$	$B_1^{(-)}$
1980	1.27	-1.32	0.07	11.31	-1.26
1984	1.32	-1.31	0.07	12.06	-1.13
1995	1.28	-1.28	0.06	12.10	-1.02
1998	1.28	-1.27	0.06	12.05	-1.03
1999	1.25	-1.28	0.06	12.04	-1.04
2001	1.27	-1.29	0.06	11.97	-1.03
Koch [5]	1.33	-1.26	0.06	11.91	-0.90
χPT [6]	1.35	-1.31	0.05	12.26	-0.90
χPT [7]	1.26	-1.25	0.05	12.21	-0.86
Errors	~ 0.02	~ 0.04	~ 0.02	~ 0.16	~ 0.16

Table 3: Values for the expansion coefficients in t at threshold for the $-$ amplitudes.

The value of the $\pi^- p$ s-wave scattering length is particularly interesting in view of the very accurate measurement of the energy shift of pionic hydrogen [8]. Using

$$a_{\pi^- p} = \frac{M}{4\pi(M+m)}\left(D_0^{(+)} + D_0^{(-)}\right)$$

gives the values shown in Table 4. Note that already in 1963 using the data available at that time, Hamilton and Woolcock obtained a remarkably good value for this scattering length using the newly developed dispersion relation techniques.

3 Values for $\nu = 0$

We now turn to the values along the line $\nu = 0$. These are usually expanded about $t = 0$ in the form

$$\overline{X}(0,t) = x_{00} + x_{01}t + x_{02}t^2 + ...$$

Similarly, if we expand about $\nu = 0$ for fixed t, the usual notation is

$$\overline{X}(\nu,0) = x_{00} + x_{10}\nu^2 + x_{20}\nu^4 + ...$$

Tables of these coefficients are available on request but they add little new to the values given at Zuoz. Instead, we concentrate on the t dependence of the amplitudes $\overline{D}^{(\pm)}(0,t)$ along the line $\nu = 0$ and their extrapolation to the on mass shell Cheng-Dashen point, $\nu = 0, t = 2$.

Year	$a_{\pi^- p}$
1963 (Hamilton and Woolcock [9])	0.085 ± 0.005
1980	0.080
1984	0.085
1995	0.088
1998	0.091
1999	0.091
2001	0.092
Koch [5]	0.084
χPT [6]	0.084
χPT [7]	0.090
pionic hydrogen [8]	0.088

Table 4: Values for the $\pi^- p$ s-wave scattering length.

Consider a twice subtracted fixed-ν dispersion relation for $\overline{D}^{(+)}$. This has the form

$$\begin{aligned}\overline{D}^{(+)}(0,t) &= \frac{(t_0-t)}{t_0}\overline{D}^{(+)}(0,0) + \frac{t}{t_0}\overline{D}^{(+)}(0,t_0) \\ &+ \frac{t(t-t_0)}{\pi}\int_4^{\infty}\frac{ImD^{(+)}(0,t')}{t'(t'-t_0)(t'-t)}dt' + \\ &+ \frac{t(t-t_0)}{\pi}\int_{-\infty}^{-26}\frac{ImD^{(+)}(0,t')}{t'(t'-t_0)(t'-t)}dt'\end{aligned}$$

Ignoring the distant left hand singularity and evaluating at the Cheng-Dashen point, choosing $t_0 = -2$, then gives

$$\begin{aligned}\overline{D}^{(+)}(0,2) &= 2\overline{D}^{(+)}(0,0) - \overline{D}^{(+)}(0,-2) + \\ &+ \frac{8}{\pi}\int_4^{\infty}\frac{Im\overline{D}^{(+)}(0,t')}{t'(t'+2)(t'-2)}dt'\end{aligned}$$

For $Im\overline{D}^{(+)}(0,t)$ we use the Höhler values of the $J=0$ $\pi\pi \to N\overline{N}$ helicity amplitude [10]

$$Im\overline{D}^{(+)}(0,t) = \frac{4\pi}{M^2}Imf_+^0(t)$$

and truncate the integral at $t' = 40$. The values of $\overline{D}^{(+)}(0,2)$ obtained in this way as well as the corresponding values for the on mass shell Σ are shown in Table 5. In this table we also show the values of the on mass shell Σ obtained by simple linear extrapolation together with a curvature correction of 12 MeV.

It would be nice to compare the individual expansion coefficients with predictions from χPT. Various predictions have been made by Meissner et al. in a series of papers [7] but, unfortunately,

Year	$\overline{D}^{(+)}(0,2)$	Σ (MeV)	$d_{00}^{(+)}$	$d_{01}^{(+)}$	"Σ_{lin}"
1980	1.10	68	-1.36	1.10	64
1984	1.08	67	-1.34	1.06	78
1995	1.34	83	-1.23	1.09	71
1998	1.45	90	-1.18	1.14	80
1999	1.45	93	-1.14	1.16	85
2001	1.44	89	-1.16	1.09	75

Table 5: $\overline{D}^{(+)}$ at the Cheng-Dashen point.

Year	$d_{00}^{(-)}$	$d_{01}^{(-)}$	$d_{00}^{(-)}+2d_{01}^{(-)}$
1980	1.47	−0.13	1.21
1984	1.51	−0.12	1.27
1995	1.46	−0.14	1.18
1998	1.46	−0.13	1.20
1999	1.43	−0.14	1.15
2001	1.44	−0.14	1.16
Ref. [12]			1.19

Table 6: $\overline{D}^{(-)}/\nu$ at the Cheng-Dashen point.

these values are not very satisfactory. The problem is that the variables ν and t are not very suitable expansion variables for normal heavy baryon χPT [11]. This problem does not arise in the Lorentz invariant approach and in a new paper by Becher and Leutwyler [12] detailed studies are made of the low energy πN system. As an example we consider their predictions for the amplitude $\overline{D}^{(-)}/\nu$ at the Cheng-Dashen point which we compare with the predictions of a simple linear extrapolation in Table 6.

References

[1] G.C. Oades, πN Newsletter **15**, 307 (1999).

[2] J. Stahov, πN Newsletter **15**, 13 (1999).

[3] The references to the various sets of phase shifts are as follows: KH80: R. Koch and E. Pietarinen, Nucl. Phys. **A336**, 331 (1980) and R. Koch, Z. Phys. **C15**, 161 (1982). KA84: R. Koch, Z. Phys. **C29**, 597 (1985). SM95:R.A. Arndt, I.I. Strakovsky, R.L. Workman and M.M. Pavan, Phys. Rev. **C52**, 2120 (1995). SP98, SM99, SM01: I am grateful to R. A. Arndt and M.M. Pavan for providing details of these updates of the SAID phase shifts. For details see the SAID web-page http://gwdac.phys.gwu.edu.

[4] G. Höhler, Landolt-Börnstein vol. **I/9b2**, Pion-Nucleon Scattering, Springer, Berlin, 1983.

[5] R. Koch, Nucl. Phys. **A448**, 707 (1986).

[6] M. Mojžiš, Euro. Phys. J. C**2**, 181 (1998).

[7] N. Fettes and U. Meissner, Nucl. Phys. A**676**, 311 (2000) and references therein.

[8] H. Ch. Schröder et al., Phys. Lett. B469 25 (1999).

[9] J. Hamilton and W.S. Woolcock, Rev. Mod. Phys. **35**, 737 (1963).

[10] G. Höhler, see Table 2.4.6.1 of Ref. [4].

[11] E-mail from Nadia Fettes:
"The subthreshold parameters are the expansion parameters of the standard invariant pion–nucleon amplitudes. Since these amplitudes are not the "natural" ones for a HBχPT calculation, and neither are ν and t the natural kinematical variables, the calculation of the pion–nucleon amplitudes to order q^n will only give us the subthreshold parameters to order q^{n-1}.
So, what happens is that in the 98–paper, I calculated the amplitude up to 3rd order, which effectively means that I will get the subthreshold parameters only up to 2nd order. The problem you talk about exactly appears in the part of the amplitude I am not able to pin down by a third–order calculation, since the fourth–order amplitude will influence this part.
So, in this respect both papers hep-ph/9803266 v2 and hep-ph/9611253 v2 go beyond the accuracy they should actually go, and this can lead to problems such as you found now. Sorry for this."

[12] T. Becher and H. Leutwyler, J. High Energy Phys. **06**, 017 (2001).

Pion-nucleon sigma-term — a review

M.E. Sainio

Helsinki Institute of Physics, and
Department of Physics, University of Helsinki, P.O. Box 64, 00014 Helsinki, Finland

(Received: 31 October 2001)

A brief review of the pion-nucleon sigma-term is given. Aspects of both chiral perturbation theory and phenomenology are discussed.

1 Introduction

The pion-nucleon sigma-term is defined as

$$\sigma = \frac{\hat{m}}{2m_p}\langle p|\bar{u}u + \bar{d}d|p\rangle \ , \qquad \hat{m} = \frac{1}{2}(m_u + m_d) \ ,$$

i.e. as the proton matrix element of the u- and d- quark mass term of the QCD hamiltonian (m_p is the mass of the proton). More generally, sigma-terms are proportional to the scalar quark currents

$$\langle A|m_q\bar{q}q|A\rangle \ ; \qquad q = u, d, s \ ; \qquad A = \pi, K, N \ .$$

These are of interest, because they are related to the hadron mass spectrum, to the scattering amplitudes through Ward identities, to the strangeness content of A, to the quark mass ratios and to the question of dark matter. For an early review of the topic, see ref. [1].

The pion-nucleon sigma-term is the $t = 0$ value of the scalar form factor

$$\bar{u}'\sigma(t)u = \hat{m}\,\langle p'|\bar{u}u + \bar{d}d|p\rangle \ , \qquad t = (p' - p)^2 \ ,$$

i.e. $\sigma = \sigma(t = 0)$. The strangeness content of the proton can then be defined as

$$y = \frac{2\,\langle p|\bar{s}s|p\rangle}{\langle p|\bar{u}u + \bar{d}d|p\rangle}$$

(the OZI rule would imply y=0).

Algebraically the σ can be written in the form

$$\sigma = \frac{\hat{m}}{2m_p}\frac{\langle p|\bar{u}u + \bar{d}d - 2\bar{s}s|p\rangle}{1 - y} \ ,$$

where the numerator is proportional to the octet breaking piece in the hamiltonian. To first order in SU(3) breaking we have now

$$\sigma \simeq \frac{\hat{m}}{m_s - \hat{m}}\frac{m_\Xi + m_\Sigma - 2m_N}{1 - y} \simeq \frac{26\ \text{MeV}}{1 - y} \ ,$$

where the quark mass ratio

$$\frac{m_s}{\hat{m}} = 2\,\frac{M_K^2}{M_\pi^2} - 1 \simeq 25$$

has been used.

Chiral perturbation theory (ChPT) allows for the determination of the combination

$$\hat{\sigma} = \sigma(1 - y)$$

from the baryon spectrum. Therefore, if the sigma-term can be determined from data, the strangeness content y can be estimated.

Section 2 will be dealing with the ChPT aspects of the sigma. The phenomenological discussion will follow in section 3. A brief summary is given is section 4 together with reference to recent developments in the lattice frontier.

2 The σ-term

ChPT gives in leading order

$$\hat{\sigma} \simeq 26 \text{ MeV}$$

as indicated above. The $\mathcal{O}(m_q^{3/2})$ calculation of Gasser and Leutwyler [2, 3] yields

$$\hat{\sigma} = 35 \pm 5 \text{ MeV} \ .$$

Borasoy and Meißner [4] have made the calculation in the heavy baryon framework of ChPT to order $\mathcal{O}(m_q^2)$ with the result

$$\hat{\sigma} = 36 \pm 7 \text{ MeV}.$$

2.1 Scalar form factor

Contact to pion-nucleon scattering can be made at the unphysical Cheng-Dashen point ($s = u = m_N^2$, $t = 2M_\pi^2$) and, therefore, it is of interest to determine the difference of the scalar form factor

$$\Delta_\sigma \equiv \sigma(2M_\pi^2) - \sigma(0) \ .$$

In leading order we have [3, 5]

$$\Delta_\sigma = \frac{3g_A^2 M_\pi^3}{64\pi F_\pi^2} + \mathcal{O}(M_\pi^4 \ln M_\pi^2) \ ,$$

which is numerically about 7 MeV. ChPT to one loop yields $\Delta_\sigma \simeq 5$ MeV [6]. In heavy baryon ChPT (HBChPT) including the $\mathcal{O}(p^4)$ pieces due to the low-lying spin-3/2 baryons the result $\Delta_\sigma \simeq 15$ MeV is obtained [7]. A dispersion analysis where particular emphasis was on the treatment of the $\pi\pi$ interaction dominating the curvature of the $\sigma(t)$ yields [8]

$$\Delta_\sigma = 15.2 \pm 0.4 \text{ MeV} \ .$$

More recently, Becher and Leutwyler have calculated [9] the scalar form factor to order p^4 in a formulation of the baryon ChPT which keeps the Lorentz and chiral invariance explicit at all stages. The result for Δ_σ is

$$\Delta_\sigma = 14.0 \text{ MeV} + 2M^4 \bar{e}_2 \ ,$$

where M is the leading order result for M_π ($M^2 = 2\hat{m}B$) and $\bar{e}_2$ is a renormalized coupling constant due to the $\mathcal{L}_N^{(4)}$ lagrangian. Comparison with the result of the dispersive calculation shows that the piece proportional to $\bar{e}_2$ is small as it should be.

The value of the form factor at $t = 0$, i.e. the σ, can be calculated from the quark mass expansion of the nucleon mass by making use of the Feynman-Hellmann theorem

$$\sigma = \hat{m}\frac{\partial m_N}{\partial \hat{m}}$$

or equivalently

$$\sigma = M^2\frac{\partial m_N}{\partial M^2} \ .$$

The physical mass of the nucleon to order p^4 is [9,10]

$$m_N = m_0 + k_1 M^2 + k_2 M^3 + k_3 M^4 \ln\frac{M^2}{m_0^2} + k_4 M^4 + \mathcal{O}(M^5) \ ,$$

where m_0 is the nucleon mass in the chiral limit and the factors k_i contain the low-energy constants. This yields for σ

$$\sigma = k_1 M^2 + \frac{3}{2}k_2 M^3 + k_3 M^4\{2\ln\frac{M^2}{m_0^2} + 1\} + 2k_4 M^4 + \mathcal{O}(M^5)$$

and numerically

$$\sigma = (75 - 23 - 7 + 0)\ \mathrm{MeV} = 45\ \mathrm{MeV} \ ,$$

where the leading term, 75 MeV, is fixed by requiring the result $\sigma = 45$ MeV for the sigma-term [13]. Also, the term $k_4 M^4$ is put equal to 0, because it is expected to be very small.

A $\mathcal{O}(p^3)$ calculation in HBChPT, where the low-energy constants are fixed inside the Mandelstam triangle, gives [14] the value $\sigma = 40$ MeV, if Karlsruhe phase shifts (KA84) are used as input. The VPI input (SP99) would yield $\sigma \simeq 200$ MeV.

2.2 Cheng-Dashen point

As mentioned earlier, contact to the pion-nucleon interaction can be made at the Cheng-Dashen point: A low-energy theorem of chiral symmetry states

$$\Sigma \equiv F_\pi^2 \bar{D}^+(\nu = 0, t = 2M_\pi^2) = \sigma(2M_\pi^2) + \Delta_R \ ,$$

where $\nu = (s-u)/4m_N$, $\bar{D}^+$ is the isoscalar D-amplitude with the pseudovector Born term subtracted and Δ_R is the remainder. The quantity Δ_R is formally of the order M_π^4, and the one-loop result [a $\mathcal{O}(p^3)$ value] is $\Delta_R = 0.35$ MeV [6]. In HBChPT it has been shown that no logarithmic contribution to order M_π^4 appears [11]. This result is verified in the $\mathcal{O}(p^4)$ calculation of the pion-nucleon amplitude [12]. Numerically, with the low-energy constants estimated with the resonance exchange saturation, the result is $\Delta_R \simeq 2$ MeV [11] which is considered to be the upper limit for Δ_R. Therefore, it can well be approximated as

$$\Sigma \simeq \sigma(2M_\pi^2) \ .$$

One may, of course, ask how this result would change, if the fact $m_u - m_d \neq 0$ would be taken into account.

3 Σ phenomenology

The standard expression for the πN amplitude is

$$T_{\pi N} = \bar{u}'[A(\nu,t) + \frac{1}{2}\gamma^\mu(q+q')_\mu B(\nu,t)]u \ ,$$

where q and q' are the initial and final pion momentum respectively. The D-amplitude is

$$D(\nu,t) = A(\nu,t) + \nu B(\nu,t)$$

and, through the optical theorem,

$$\mathrm{Im}\, D(\omega, t=0) = k_{\mathrm{lab}}\, \sigma \ .$$

Its imaginary part in the forward direction is directly fixed by the cross section data (ω is the initial pion laboratory energy). The isospin components are simply related to the amplitudes in the particle basis

$$D^{\pm} = \frac{1}{2}(D_{\pi^- p} \pm D_{\pi^+ p}) \ .$$

The relevant combination for the Σ -term discussion is the isoscalar piece, D^+, at the Cheng-Dashen point.

The standard value with the Karlsruhe input has been the result [15]

$$\Sigma = 64 \pm 8 \text{ MeV}$$

based on hyperbolic dispersion relations. The error reflects the internal consistency of the method. An attempt to include an estimate of the error in Σ generated by the errors of the low-energy data was published in ref. [13]. The numerical result there was $\Sigma \simeq 60$ MeV with the Karlsruhe input.

The Σ can also be related to the threshold parameters [16]

$$\Sigma = F_\pi^2[L(a^+_{l\pm}, \tau) + (1 + \frac{M_\pi}{m_N})\tau J^+] + \delta^{ChPT} \ ,$$

where L is a linear combination of the threshold parameters and τ is a free parameter, J^+ is the integral over the total cross section

$$J^+ = \frac{2M_\pi^2}{\pi} \int_0^\infty \frac{\sigma^+(k')}{\omega(k')^2}\, dk'$$

and δ^{ChPT} is the remainder from ChPT, see also ref. [17], where references to earlier work in a similar spirit can be found. In such a formulation the contribution from a^+_{1+} to Σ may vary from -150 MeV to 250 MeV for $\tau \in [-1, 1]$. Olsson has recently [18] written a sum rule for Σ which includes an expansion in terms of threshold parameters. With the Karlsruhe input the consistent result, $\Sigma = 55 \pm 6$ MeV, follows. With input from ref. [19] the value $\Sigma = 71 \pm 9$ MeV is obtained.

3.1 *Low-energy analysis*

At low energy the pion-nucleon interaction is dominated by six partial waves, 2 s-waves and 4 p-waves. Therefore, six relations are needed to pin down the six partial waves. Such relations can be obtained by writing six dispersion relations for the $D^\pm$, $B^\pm$ and $E^\pm$ where

$$E^{\pm} = \frac{\partial}{\partial t}(A^\pm + \omega B^\pm)|_{t=0} \ .$$

There are two subtraction constants in the 6 dispersion relations, one for D^+ and E^+ ($x = M_\pi/m_N$):

$$\begin{aligned}\bar{D}^+(\mu) &= 4\pi(1+x)a^+_{0+} + \frac{g^2x^3}{M_\pi(4-x^2)} \ , \\ \bar{E}^+(\mu) &= 6\pi(1+x)a^+_{1+} - \frac{g^2x^2}{M^3_\pi(2-x)^2} \ .\end{aligned}$$

As described in ref. [13] the six dispersion relations can be solved iteratively with input for the invariant amplitudes from high energy (here $k_{lab} \geq 185$ MeV/c) and for the high partial waves at low energy. The method allows for fixing two of the constants in the subthreshold expansion for $\bar{D}^+$ in powers of ν^2 and t

$$\bar{D}^+ = d^+_{00} + d^+_{10}\nu^2 + d^+_{01}t + d^+_{20}\nu^4 + d^+_{11}\nu^2 t + \dots \ ,$$

where

$$d^+_{00} = \bar{D}^+(0) \ , \qquad d^+_{01} = \bar{E}^+(0) \ .$$

The curvature term Δ_D is defined by

$$\Sigma = F^2_\pi(d^+_{00} + 2M^2_\pi d^+_{01}) + \Delta_D \equiv \Sigma_d + \Delta_D \ ,$$

where Δ_D is dominated by the $\pi\pi$ cut giving [8]

$$\Delta_D = 11.9 \pm 0.6 \text{ MeV} \ .$$

Σ_d is a sensitive quantity as is demonstrated by the numerical values for the two solutions, A and B, of ref. [13], where $\Sigma_d = 48 - 50$ MeV with an error of about 10 MeV. Now the question is how the value for Σ would change, if amplitudes based on modern meson factory data would be used as input instead of the Karlsruhe amplitudes where input mostly consisted of data before the meson factory era. With the VPI/GWU input (SM99 and SM01) [20] results typically in the range

$$\Sigma_d = ([-80. \text{ to } -77.] + [146. \text{ to } 157.]) \text{ MeV} = 65. \text{ to } 80. \text{ MeV}$$

follow, i.e. a considerably larger value than the Karlsruhe input would give. The corresponding π^-p scattering length

$$a_{\pi^-p} = 0.0857 - 0.0899 \ M_\pi^{-1}$$

is to be compared with the experimental value $0.0883 \pm 0.0008 \ M_\pi^{-1}$ [21].

4 Summary

In a lattice calculation the value for σ can be obtained from the quark mass expansion of the nucleon mass by making use of the Feynman-Hellmann theorem as given above. A new development has recently been the inclusion of dynamical quarks [22] giving $\sigma = 18 \pm 5$ MeV. In general, there is, however, the problem that the value for m_q is still quite large and the extrapolation to small quark mass values is uncertain.

The nucleon mass in full (two-flavour) QCD as a function of the pion mass has been calculated by UKQCD [23] and CP-PACS [24] collaborations. The values so found have been fitted with a ChPT-inspired expression [25]

$$m_N = \alpha + \beta M^2_\pi + \sigma_{NN}(M_\pi, \Lambda) + \sigma_{N\Delta}(M_\pi, \Lambda)$$

for the quark mass dependence of the nucleon mass leading to the result $\sigma = 45 - 55$ MeV. The functions σ_{NN} and $\sigma_{\Delta N}$ are due to the nucleon self-energy diagrams with an intermediate nucleon and delta respectively.

Promising steps have been made in the lattice frontier, but still more work is needed. For the phenomenological part questions remain. It turns out that Σ is a quite sensitive quantity and, therefore, requirements of consistency of the low-energy data and analysis are of particular importance. E.g., Σ_d is sensitive to the high partial waves at low energy. An additional problem is the question of electromagnetic corrections close to the physical threshold, see [26, 27].

Acknowledgments: I wish to thank A.M. Green for useful remarks on the manuscript. Financial support of the Academy of Finland grant 47678, the TMR EC-contract CT980169 and the Magnus Ehrnrooth Foundation is gratefully acknowledged.

References

[1] E. Reya, Rev. Mod. Phys. **46**, 545 (1974).
[2] J. Gasser, Ann. Phys. (N.Y.) **136**, 62 (1981).
[3] J. Gasser and H. Leutwyler, Phys. Rep. **87**, 77 (1982).
[4] B. Borasoy and U.-G. Meißner, Ann. Phys. (N.Y.) **254**, 192 (1997).
[5] H. Pagels and W.J. Pardee, Phys. Rev. **D4**, 3335 (1971).
[6] J. Gasser, M.E. Sainio, and A. Švarc, Nuc. Phys. **B307**, 779 (1988).
[7] V. Bernard, N. Kaiser, and U.-G. Meißner, Z. Phys. **C60**, 111 (1993).
[8] J. Gasser, H. Leutwyler, and M.E. Sainio, Phys. Lett. **B253**, 260 (1991).
[9] T. Becher and H. Leutwyler, Eur. Phys. J. **C9**, 643 (1999).
[10] H. Leutwyler, πN Newsletter **15**, 1 (1999).
[11] V. Bernard, N. Kaiser, and U.-G. Meißner, Phys. Lett. **B389**, 144 (1996).
[12] T. Becher and H. Leutwyler, JHEP **06**, 017 (2001).
[13] J. Gasser, H. Leutwyler, and M.E. Sainio, Phys. Lett. **B253**, 252 (1991).
[14] P. Büttiker and U.-G. Meißner, Nucl. Phys. **A668**, 97 (2000).
[15] R. Koch, Z. Phys. **C15**, 161 (1982).
[16] J. Gasser, Proc. 2nd International Workshop on πN Physics, Los Alamos, Report LA-11184-C, 266 (1987).
[17] M.P. Locher and M.E. Sainio, Nucl. Phys. **A518**, 201 (1990).
[18] M.G. Olsson, Phys. Lett. **B482**, 50 (2000).
[19] A. Gashi *et al.*, hep-ph/9902207 (1999).
[20] R.A. Arndt, private communication.
[21] H.-Ch. Schröder *et al.*, Phys. Lett. **B469**, 25 (1999).
[22] S. Güsken *et al.*, Phys. Rev. **D59**, 054504 (1999).
[23] C.R. Allton *et al.*, Phys. Rev. **D60**, 034507 (1999).
[24] S. Aoki *et al.*, Phys. Rev. **D60**, 114508 (1999).
[25] D.B. Leinweber, A.W. Thomas, and S.V. Wright, Phys. Lett. **B482**, 109 (2000).
[26] V.E. Lyubovitskij and A. Rusetsky, Phys. Lett. **B494**, 9 (2000).
[27] N. Fettes and U.-G. Meißner, Nucl. Phys. **A693**, 693 (2001).

Pion-nucleon scattering in the energy region 300–2000 MeV

S. P. Kruglov

Petersburg Nuclear Physics Institute, Gatchina,
Leningrad district, 188350, Russia

(Received: 18 October 2001)

Differential cross sections of $\pi^- p$ charge exchange scattering are measured in region from 456 to 725 MeV/c. The experiment is carried out at the pion channel of the PNPI synchrocyclotron in Gatchina by detecting the recoil neutron in coincidence with one gamma from the decay $\pi^0 \to 2\gamma$. Results obtained for the backward scattering are presented in comparison with the prediction of different phase shift analyses. Also we tested isospin bounds and showed that the new charge exchange DCS are within allowed region showing no isospin violation. Measurements of the spin rotation parameters in $\pi^+ p$ elastic scattering are performed in joint (PNPI–ITEP) experiment at the pion channel of the ITEP (Moscow) synchrotron at the incident pions momenta of 1430 and 1620 MeV/c. Obtained values of these parameters agree with the predictions of the phase shift analysis VPI and contradict obviously to the analyses KH-80 and CMB.

1 Introduction

The program "Baryon spectroscopy with π-mesons in the energy range from 300 to 2000 MeV" is under way at PNPI and ITEP. In the period after 1989 investigations at PNPI are carried out in collaboration with groups from UCLA (USA) and ACU (USA).

At PNPI, the differential cross sections (DCS) and the polarization parameters P, R, A were measured for $\pi^\pm p$ elastic scattering at many energies of incident pions in the range from 300 to 640 MeV. In total, about 450 experimental points were obtained as a result of these experiments, these points formed a main part of the data-base in a phase shift analysis (PSA) PNPI–94 [1]. Very interesting result obtained in PSA PNPI–94 is an observation of charge splitting in the P_{33} phase shifts; quantitatively this effect can be characterized by the difference $\delta_{33}^{++} - \delta_{33}^{0}$. This difference depends on energy and varies from +2 degrees at $T_\pi = 200$ MeV to –2 degrees at $T_\pi = 450$ MeV. Following values for the masses (M) and widths (Γ) of the P_{33} resonances were obtained:

$$M^0 = 1233.1 \pm 0.3 \text{ MeV} , \qquad M^{++} = 1230.5 \pm 0.2 \text{ MeV} ,$$
$$M^0 - M^{++} = 2.6 \pm 0.4 \text{ MeV} , \qquad \Gamma^0 - \Gamma^{++} = 5.1 \pm 1.0 \text{ MeV} .$$

2 Study of reaction $\pi^- p \to \pi^0 n$ in the region of low-lying πN resonances

At present, the accuracy in determining the characteristics of πN resonances is limited mostly by a lack of high-quality experimental data on $\pi^- p$ charge exchange. To improve the situation and fill the gap in the data-base, measurements of DCS for the reaction $\pi^- p \to \pi^0 n$ are now underway at PNPI in the energy range from 337 to 600 MeV (corresponding values of momenta are 456 to 725 MeV/c). In this experiment, we detect the recoil neutron in coincidence with one of gammas from the decay $\pi^0 \to 2\gamma$.

A schematic view of the experimental setup is shown in Fig. 1. Neutron detectors were designed and manufactured at UCLA. The detector consists of three contiguous scintillator blocks each block being viewed by two photomultiplier tubes connected in coincidence. The energy of the neutrons is measured using the time-of-flight technique, with a 5 m base. Gamma detectors were placed at angles kinematically conjugated with the neutron detectors. Two different types of total absorption electromagnetic calorimeters are used in the experiment. The first detector is the Čerenkov spectrometer made of eight lead glass SF-5 blocks arranged in a 4×2 array, and the second one

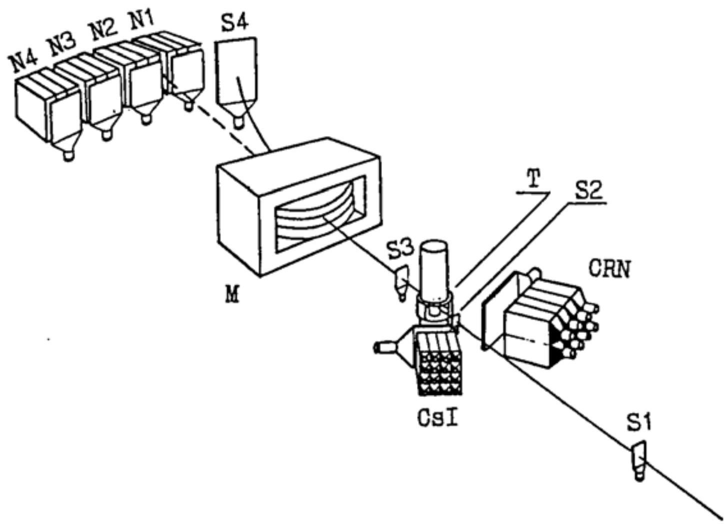

Figure 1: Schematic drawing of the setup for measurements of cross sections of $\pi^- p$ charge exchange scattering. S1, S2: monitor counters; S3, S4: beam veto counters; N1–N4: neutron detectors; M: magnet deflecting incident pion beam; T: liquid hydrogen target; CsI: gamma-detector consisting of 16 crystals CsI(Na); CRN: gamma-detector consisting of 8 Čerenkov lead glass blocks.

consists of sixteen (4×4 array) CsI(Na) crystals. A special hodoscope of beam counters (not shown in Fig. 1), which was placed in the dispersive part of the pion channel, provides the possibility of dividing the total momentum acceptance (6% FWHM) into several narrower momentum bins.

Till now, measurements were performed for backward scattering angles ($\Theta^{cm} = 175°, 166°, 157°$) at nine momenta in the range from 456 to 725 MeV/c [2]. To eliminate the contribution due to charge exchange scattering of the incident pions on the scintillator of the monitor counter S_2 and on elements of the target construction, at every energy measurements were made using both a hydrogen-filled and an empty target. Then a channel-by-channel subtraction of corresponding neutron time-of-flight spectra is performed subsequently after a normalization to one incident pion.

The results obtained are presented in Fig. 2. Statistical errors are within circles. Systematic errors are at a level of 5–10% for most of momenta; and only at 490 MeV/c and 573 MeV/c, where the contribution of the radiative capture $\pi^- p \to \gamma n$ becomes essential, the systematic errors reach 13–16%. The quoted systematic errors were obtained by quadrature summing following components: uncertainties in evaluating the above mentioned contribution of the radiative capture, errors of measuring the liquid hydrogen density, errors in measuring the efficiency of neutron detectors, uncertainties in determining contaminations of electrons and muons in the beam, errors in an angular alignment of the gamma and neutron detectors.

For the angle $\Theta^{cm} = 175°$ two sets of data are presented: one was obtained using Čerenkov lead glass blocks as gamma-detector and another – with CsI(Na) crystals. As one can see in Fig. 1, neutron detectors N1 and N2 conjugated with these two gamma-detectors are located at equal angles symmetrically to the beam line. It means that combinations N1 + CsI and N2 + CRN measure DCS for one and the same scattering angle (which is defined by the disposition of the neutron detector) using two various types of gamma detectors and at different geometry of the experiment. A comparison of DCS values obtained for these two cases will allow to estimate a level of additional systematic errors which were not taken into account above. The analysis of data obtained shows that in most cases the difference between two sets of DCS does not exceed 10%.

Shown by curves in Fig. 2 are the predictions of PSAs KH–80 [3], PNPI–94 [1] and VPI (SM-95 solution) [4]. Our experimental results agree satisfactorily with the SM-95 PSA and seem to contradict to the predictions of KH-80 PSA. It can be considered as an indication that results of KH-80 PSA may be incorrect in some energy ranges and need to be revised.

To illustrate the contribution that our new results give to the world data-base, in Fig. 3 values

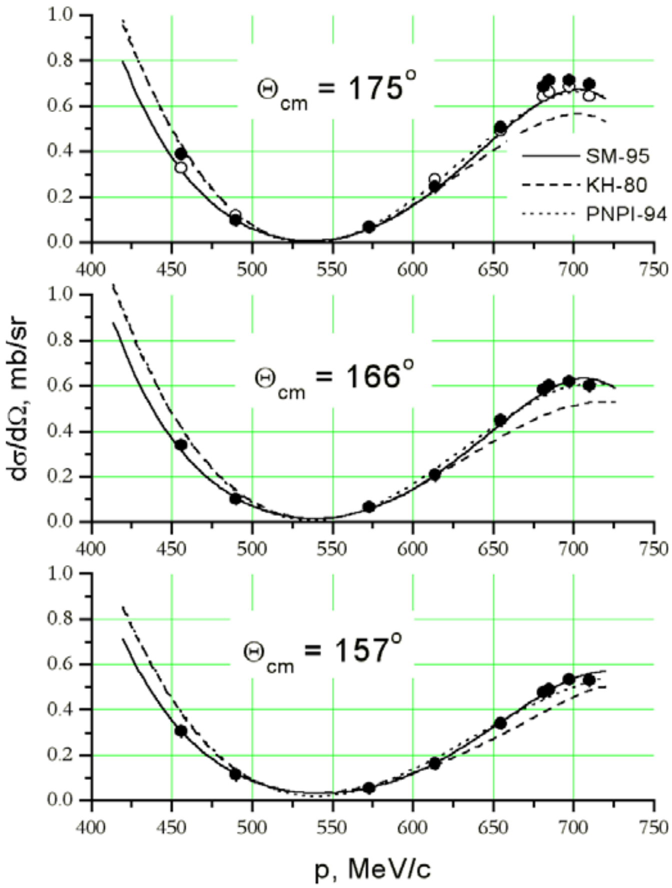

Figure 2: Results of measuring differential cross sections of $\pi^- p$ charge exchange scattering to backward angles. Data obtained with Čerenkov spectrometers are shown by solid circles, those obtained with CsI(Na) crystals – by open circles. Shown by curves are the predictions of phase shift analyses SM–95 (solid lines), KH–80 (dashed lines) and PNPI–94 (dotted lines).

of DCS for $\Theta^{cm} = 166^\circ$ obtained in this work are shown in comparison with results of previous experiments. One can see that below 600 MeV/c there was no data at all prior to our measurements. At higher momenta there exists only one set of systematic data, which agree satisfactorily with our results. All other results shown in Fig. 3 are very scarce and contradictory, they have big errors.

Thus, PNPI results for backward scattering angles excels all previous experiment in accuracy. Moreover, our new data cast doubts on the most of obtained earlier results which were used till now in phase shift analyses.

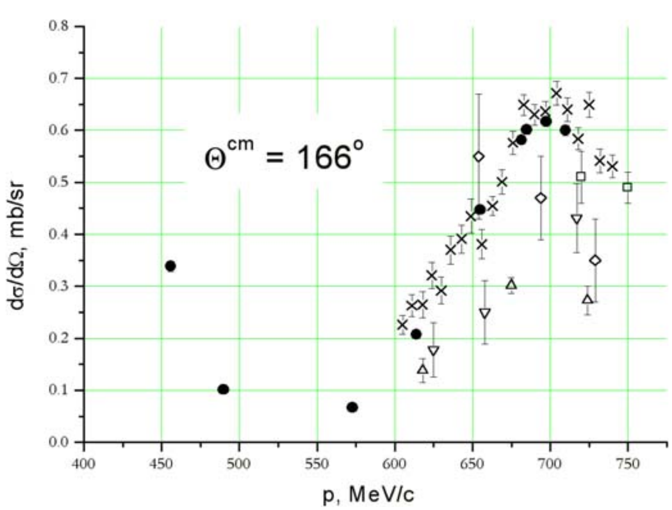

Figure 3: Differential cross sections of the reaction $\pi^- p \to \pi^0 n$ for the angle $\Theta^{cm} = 166^\circ$ measured in this work (solid circles) are shown in comparison with results of other experiments: ∇ – C.B. Chiu *et al.*, Phys. Rev. **156**, 1415 (1967); $\Box$ – E. Hyman *et al.*, Phys. Rev. **165**, 1437 (1968); $\Diamond$ – F. Bulos *et al.*, Phys. Rev. **187**, 1827 (1969); $\times$ – N.C. Debenham *et al.*, Phys. Rev. D **12**, 2545 (1975); Δ – R.M. Brown *et al.*, Nucl. Phys. B **117**, 12 (1976).

In reactions for which one can measure three charge channels (such as $\pi^+p \to \pi^+p$, $\pi^-p \to \pi^-p$, $\pi^-p \to \pi^0n$) but which, through isospin invariance, are described by only two isospin amplitudes, there exist constraints and, in particular, inequalities which the data must satisfy:

$$\left[\sqrt{\frac{d\sigma^+}{d\Omega}} - \sqrt{\frac{d\sigma^-}{d\Omega}}\right]^2 \leq 2\,\frac{d\sigma^0}{d\Omega} \leq \left[\sqrt{\frac{d\sigma^+}{d\Omega}} + \sqrt{\frac{d\sigma^-}{d\Omega}}\right]^2 . \qquad (1)$$

Since differential cross sections of $\pi^\pm p$ elastic scattering were measured at PNPI earlier [5], we calculated on the base of elastic scattering data bounds for DCS of π^-p charge exchange scattering and compared these bounds with new experimental results. Such comparison for $\Theta^{cm} = 175°$ is presented in Fig. 4. It should be stressed here that measurements for all three charge channels ($\pi^+p \to \pi^+p$, $\pi^-p \to \pi^-p$, $\pi^-p \to \pi^0n$) were made at one and the same pion channel that allowed to exclude systematic errors due to possible small (at a level of $\pm 0.5\%$) incorrectness in the momentum calibration of the pion channel. One can see that the charge exchange data are within allowed region showing no isospin violation. Moreover, these data tend to lie close to the lower bound. It confirms so called near-saturation of isospin bounds – the phenomenon which was extensively discussed about 25 years ago. Different theoretical models were proposed then for explaining this puzzle, but none of them could give quantitative description of the phenomenon.

We plan to continue measurements of the differential cross sections of the reaction $\pi^-p \to \pi^0n$ for smaller scattering angles. For forward angles we will use a new device – an $\eta(\pi^0)$-spectrometer – which was recently created at PNPI. The PNPI $\eta(\pi^0)$-spectrometer consists of two total absorption electromagnetic calorimeter for detecting both γ-quanta from the decay $\eta \to 2\gamma$ or $\pi^0 \to 2\gamma$. Each calorimeter is a 6×4 array of CsI(Na) crystals with an individual size of $6 \times 6 \times 30$ cm^3; the last figure is a thickness, it corresponds to 16.2 X_0.

3 Measurement of the spin rotation parameters for π^+p elastic scattering in the second resonance region

The most of πN resonances have masses more than 1750 MeV that corresponds to T_π >1000 MeV. Our knowledge about characteristics of these resonances comes from phase shift analyses of experimental πN data. And till now this knowledge is very poor – even for the well established resonances. There exist essential discrepancies between values of the resonance mass and width given by the three global PSAs: KH, CMB and VPI. In some cases the πN resonances obtained in the analyses KH and CMB were not found in the analysis VPI. For example, N^* reso-

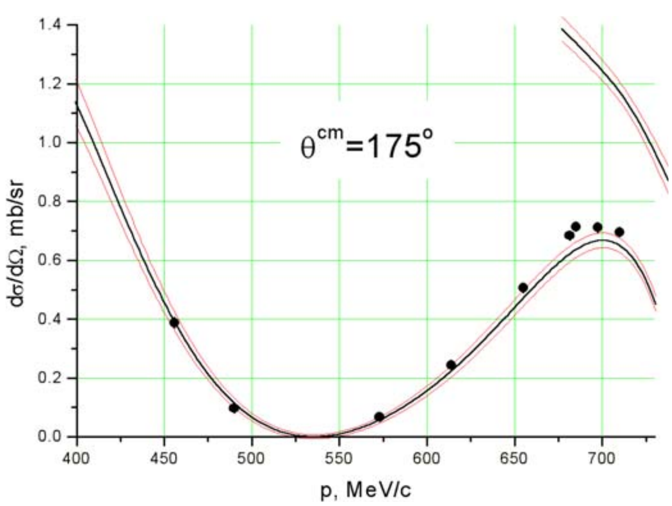

Figure 4: Differential cross sections of the reaction $\pi^-p \to \pi^0n$ for the angle $\Theta^{cm} = 175°$ obtained in this work (solid circles) are given in comparison with the isospin bounds calculated using the equation (1) and results of our previous experiments [5] in which DCS of π^-p and π^+p elastic scattering were measured.

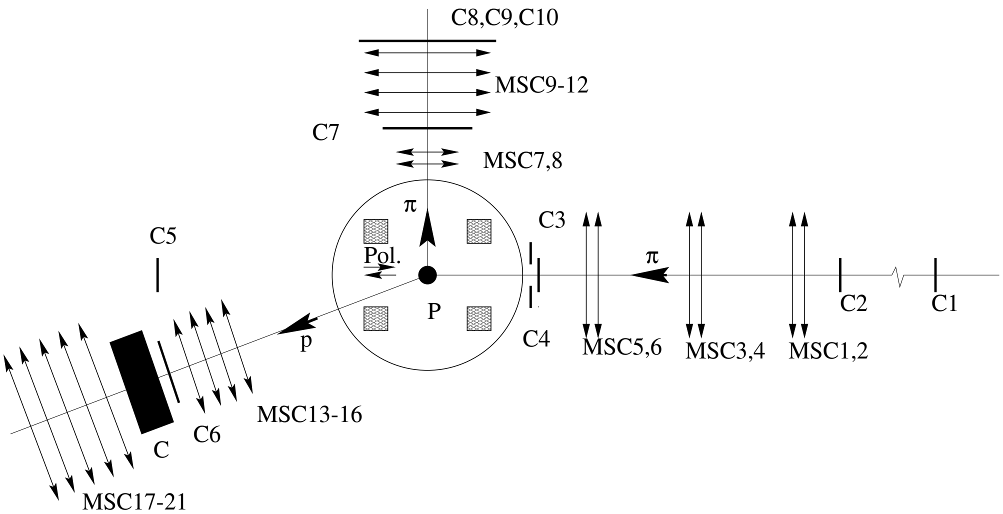

Figure 5: The experimental layout. P: polarized proton target; C: carbon filter; MSC1–MSC21: multiwire magnetostrictive spark chambers to detect the incident pion (MSC1–MSC6), the scattered pion (MSC7–MSC12) and the recoiled proton before (MSC13–MSC16) and after (MSC17–MSC21) the second scattering; C1–C10: scintillation counters for forming the trigger and identifying the positive pions in the beam by the time-of-flight technique.

nances $D_{13}(1700)$, $F_{17}(1990)$, $D_{13}(2080)$ and the Δ-resonances $S_{31}(1900)$, $P_{33}(1920)$ are absent in PSA VPI, although, for example, the resonance $D_{13}(1700)$ has the very high rating (***) in another two PSAs.

The only way to remove such ambiguities is to measure the spin rotation parameters A and R. Such measurements were performed recently by the PNPI–ITEP collaboration. The experiment was carried out at the pion channel of the ITEP accelerator at the incident pions momenta of 1430 and 1620 MeV/c [6]. This experiment is rather complicated since it requires a polarized proton target of special type – with the polarization vector lying in the horizontal plane. To extract the spin rotation parameters, it is necessary to measure an asymmetry of the secondary scattering of the recoil protons on nuclei with the known analyzing power (usually, carbon).

The experimental setup is shown in Fig. 5. Its basis elements are: a polarized proton target; a proton polarimeter; sets of multiwire spark chambers to detect the incident and scattered pions. Two different types of proton polarimeter were used in the experiment. One was a multi-plate polarimeter made of optical spark chambers with graphite electrodes; a special television system was developed for filmless read-out in this case. Another type of polarimeter consists of one thick graphite block with two sets of spark chambers (in front and behind of this block) to detect the recoil proton before and after the secondary scattering; the analyzing power of this polarimeter was determined experimentally [7] using the beam of polarized protons available at ITEP. Just the latter type of polarimeter is shown in Fig. 5.

Obtained results are shown in Fig. 6 in comparison with the predictions of different PSAs. One can see that experimental data confirm the predictions of the analysis VPI (solution SM–95) and contradict obviously to the predictions of the analyses KH and CMB. This result is very important since all characteristics of πN resonances presented in Listings of the Review of Particle Physics are based just on the PSAs KH and CMB. The fact that the experimental data do not confirm the predictions of these analyses leads to the conclusion that these Listings need to be revised.

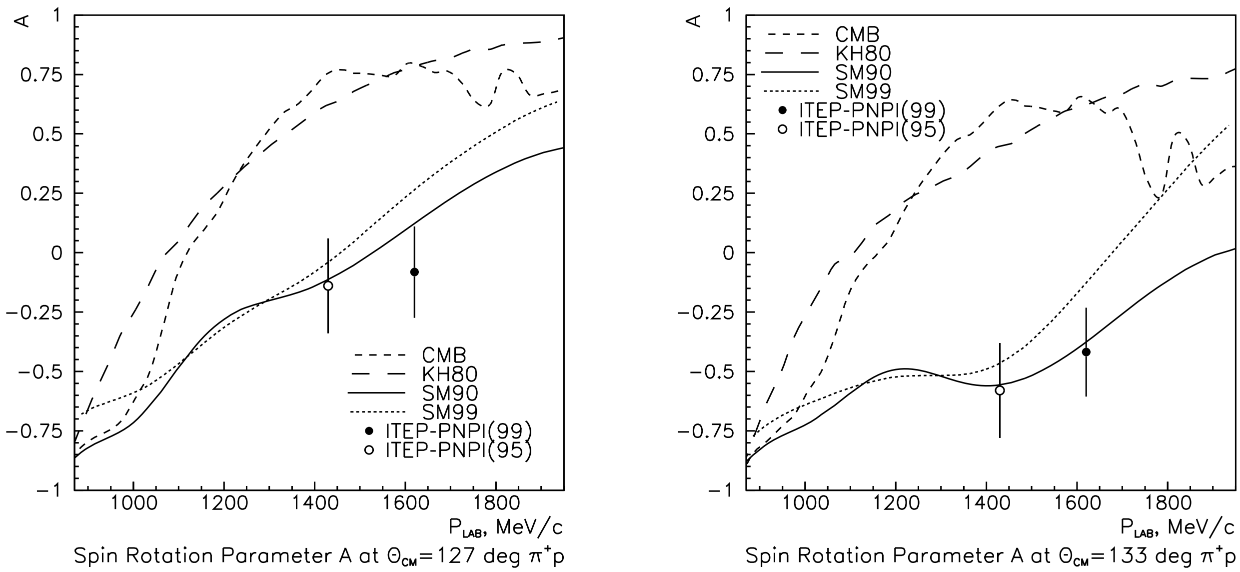

Figure 6: Results of measuring the spin rotation parameter A in π^+p elastic scattering. Shown by curves are the predictions of different phase shift analyses.

Acknowledgments: This work was supported by the Russian State Scientific-Technical Program "Fundamental Nuclear Physics" and by the Russian Foundation for Basic Research.

References

[1] V.V. Abaev and S.P. Kruglov, Z. Phys. A**352**, 85 (1995).

[2] I.V. Lopatin, *et al.*, Preprint PNPI–2363, Gatchina, 32p. (2000).

[3] G. Höhler, *"Pion-Nucleon Scattering"*, Landolt-Börnstein, vol. 9b (Springer-Verlag, 1980).

[4] R.A. Arndt, *et al.*, Phys. Rev. C **52**, 2120 (1995).

[5] V.A. Gordeev, *et al.*, Nucl. Phys. A**364**, 408 (1981).

[6] I.G. Alekseev, *et al.*, Phys. Lett. B**351**, 585 (1995); Phys. Lett. B**485**, 32 (2000).

[7] I.G. Alekseev, *et al.*, Nucl. Instr. Meth. A**434**, 254 (1999).

Analysis of pion electroproduction data

R. A. Arndt, I. I. Strakovsky, and R. L. Workman

Center for Nuclear Studies, Department of Physics,
The George Washington University, Washington, DC 20052, U.S.A.

(Received: 7 September 2001)

A fit to the existing pion electroproduction data is presented. This work builds upon our previous analyses of pion photoproduction and elastic pion-nucleon scattering over the Delta resonance region. We comment on the extraction of $E_{1+}^{3/2}/M_{1+}^{3/2}$ (E2/M1) and $S_{1+}^{3/2}/M_{1+}^{3/2}$ (S2/M1) ratios, and note that the E2/M1 ratio approaches, and possibly crosses, zero below a Q^2 of 5 $(\mathrm{GeV}/c)^2$.

1 Introduction

Over the last several years, we have assembled a database containing the existing pion electroproduction data [1] and have made a number of trial fits to this set, exploring possible extensions to the methods we have applied to pion photoproduction [2]. These efforts have intensified now that a flood of new and precise data is becoming available from measurements performed at Jefferson Lab, Mainz and Bonn. Preliminary CLAS data (unpolarized and beam polarization π^0 and π^+ [3] and double polarization π^+ [4]) will soon increase the database size from approximately 10K to 30K points. These new data were taken at CM energies covering mainly the Delta region, and a number of new single-Q^2 [5–7] and Q^2-dependent [8, 9] fits have been carried out, in the hope that a better determination of $\Delta(1232)$ properties might now be possible.

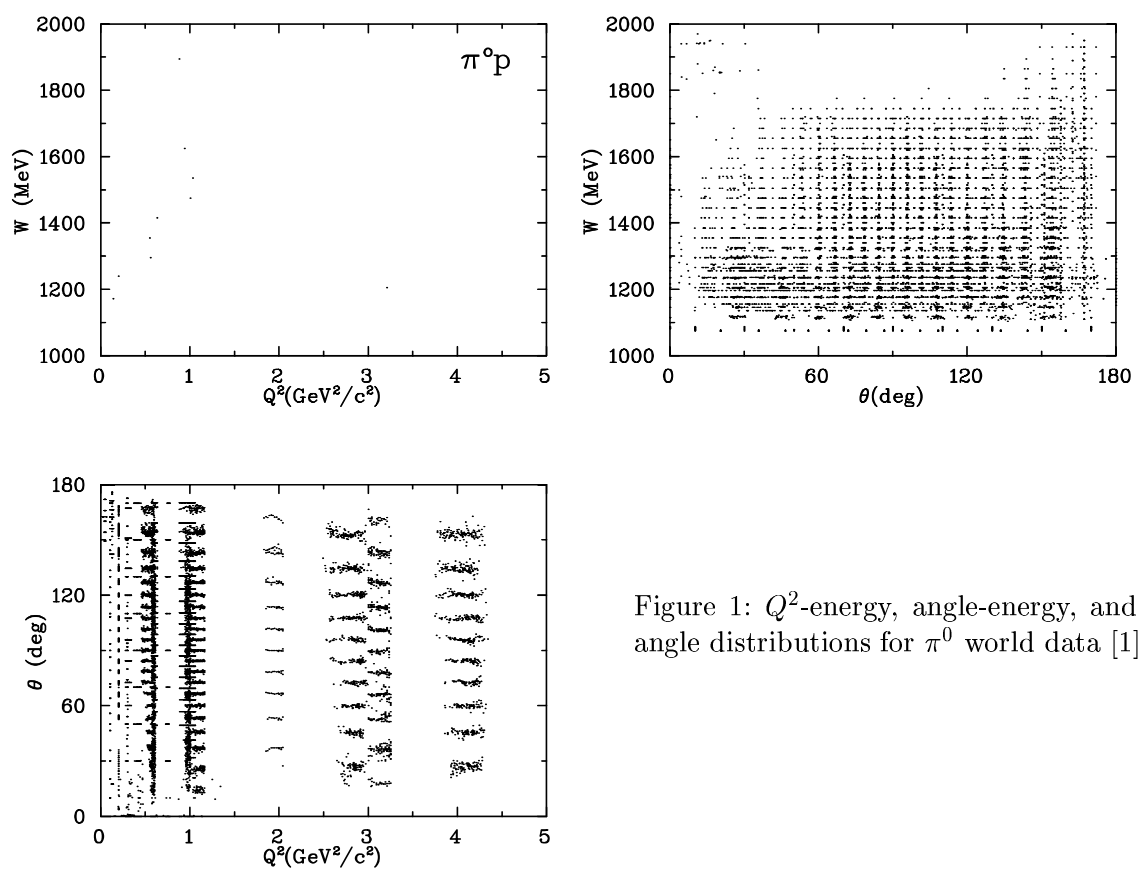

Figure 1: Q^2-energy, angle-energy, and Q^2-angle distributions for π^0 world data [1].

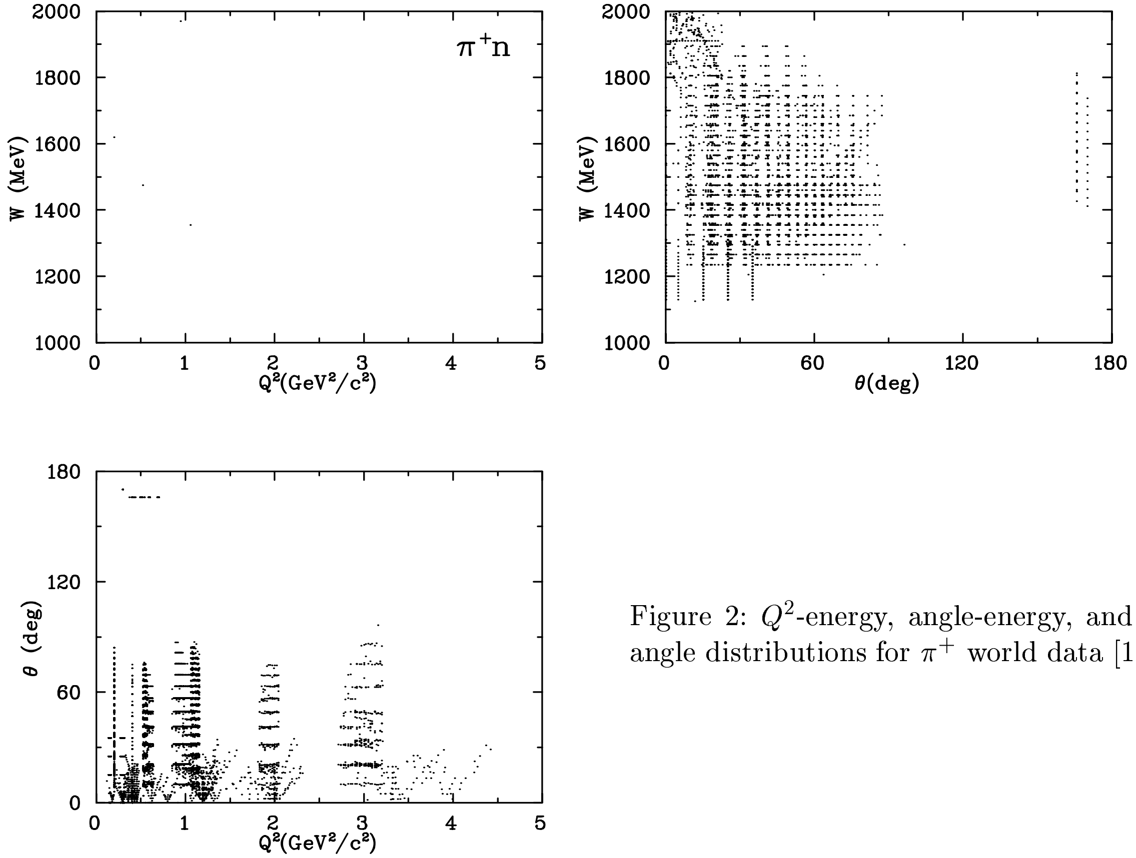

Figure 2: Q^2-energy, angle-energy, and Q^2-angle distributions for π^+ world data [1].

These recent determinations have generally confirmed that the E2/M1 ratio remains "small" (compared to the PQCD limit of 100%) at moderate values of Q^2. However, while some fits [8] find a cross-over to positive values, below 5 $(\mathrm{GeV}/c)^2$, others do not [5,9]. For this reason, we have made a number of fits, both Q^2-dependent and single$-Q^2$, in order to see if a clear trend emerges.

In the following section, we will give an overview of the existing data, and indicate where the abovementioned Jefferson Lab measurements will be added. We will then briefly outline the methods used in our fits. Results for the E2/M1 and S2/M1 ratios will be compared to other recent determinations. Finally, we will attempt to draw some conclusions from this exercise.

2 The Database

It is somewhat more involved to show the data-distribution in electroproduction (a function of W, Q^2, θ, ϕ, ϵ) than photoproduction (a function of W, θ). In Figs. 1 and 2, we have given 3 projections (with a sum over all ϵ and ϕ values) for both the π^0 and π^+ datasets. This serves to show much of the database is limited to Q^2 values below about 1 $(\mathrm{GeV}/c)^2$, and how little is measured for π^+ electroproduction at backward angles (θ). The preliminary CLAS data are similarly concentrated below 2 $(\mathrm{GeV}/c)^2$, but have much better angular coverage in the π^+ channel.

3 Fitting Strategy

The method we have used to fit electroproduction data is a direct modification of our photoproduction formalism. As in the photoproduction case, correct threshold behavior and Watson's theorem are built in. Multipoles are parameterized using the form

$$M = (\mathrm{Born} + \alpha_B)(1 + iT_{\pi N}) + \alpha_R T_{\pi N} + (\mathrm{Im}T - T^2)(\alpha_r^H + i\alpha_i^H) \ , \tag{1}$$

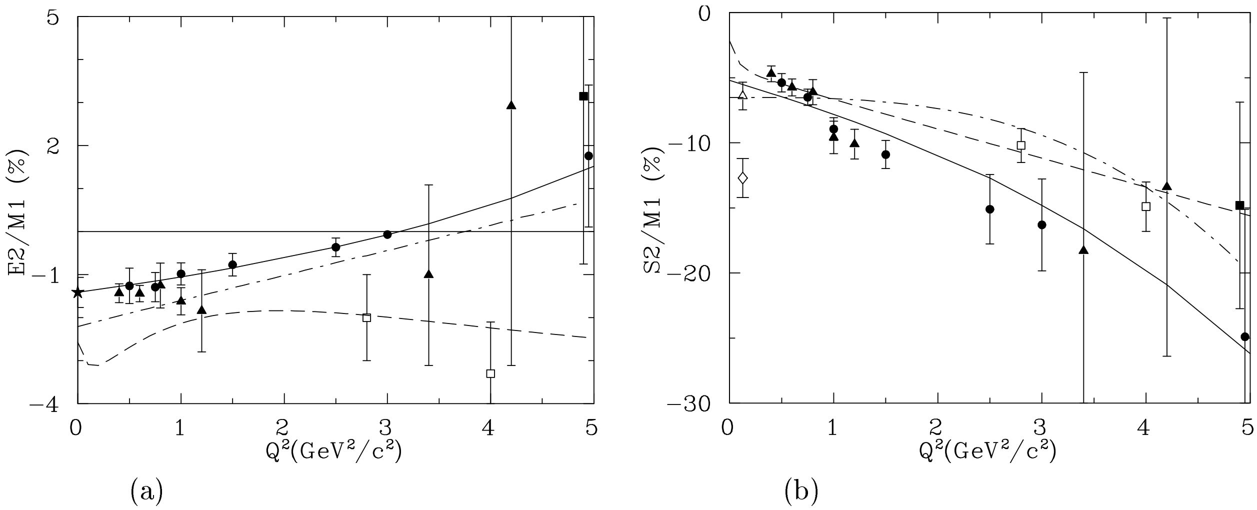

Figure 3: (a) E2/M1 and (b) S2/M1 ratios vs Q^2. Values were extracted from our QDF (filled circles) using world and preliminary CLAS data (filled square: world data only) and SQS (filled triangle) solutions. Results from Ref. [5] (open squares) are given in both (a) and (b). In addition, in (a), our pion photoproduction result ($Q^2 = 0$) [2] (filled asterisk), and in (b), the data of Refs. [6] (open triangle) and [7] (open diamond) are shown. The solid curves give best-fit results vs the set of QDF solutions. Dash-dotted and dashed curves are from Refs. [8] and [9], respectively.

wherein $T_{\pi N}$ is the πN elastic T-matrix [10] for the πN partial wave connected to a particular multipole, the Born term contains pion and vector-meson exchanges, and α_B, α_R, α_r^H, and α_i^H are phenomenological structure functions. At $Q^2 = 0$, this is the form used in photoproduction. Thus, our present photoproduction analysis is used to anchor the fit at this point. At non-zero Q^2, the Born terms have built-in Q^2 dependence. Other terms were initially modified by a factor

$$f(Q^2) = \frac{k}{k(Q^2=0)} \frac{1}{(1+Q^2/0.71)^2} e^{-\Lambda Q^2} (1 + \alpha Q^2) \ , \tag{2}$$

where k is the photon CM momentum, Λ is a universal cutoff factor, and α is searched for each multipole. The fit was significantly improved if further variability was allowed in the energy dependence. As a result, an additional parameter was searched (constrained to zero at the resonant point W_R)

$$\alpha Q^2 \to Q^2 \left(\alpha + \beta \left[\frac{W}{W_R} - 1 \right] \right) \ , \tag{3}$$

W being the CM energy.

As in our photoproduction analysis, we have performed energy/Q^2 dependent fits over the full kinematic range. We have also fitted data clustered around particular Q^2 values. This allows us to look for trends or problems in the global fit.

4 Comparisons and Conclusions

Our results for Q^2-dependent (QDF) and single-Q^2 (SQS) fits are summarized in Table 1, for cases including (CLAS) and excluding (NoCLAS) a set of preliminary CLAS data. Results for the E2/M1 and S2/M1 ratios, as functions of Q^2, are also displayed in Fig. 3. As is evident from Table 1, and Figs. 1 and 2, the database is very sparse above a Q^2 of about 1 (GeV/c)^2. The single-Q^2 points in this region have correspondingly large uncertainties.

QDF solutions:

$Q^2_{\min} - Q^2_{\max}$ $(\mathrm{GeV}/c)^2$	χ^2/data	Data
0.0−5.0	18713/10713	NoCLAS
0.0−0.5	14647/9304	CLAS
0.0−0.8	32483/20734	CLAS
0.0−1.0	37610/24139	CLAS
0.0−1.5	48294/29820	CLAS
0.0−2.5	50013/31091	CLAS
0.0−3.0	51572/31837	CLAS
0.0−5.0	53828/33209	CLAS

SQS solutions:

$Q^2_{\min} - Q^2_{\max}$ $(\mathrm{GeV}/c)^2$	χ^2/data	Data
0.2−0.4	10808/6733	CLAS
0.4−0.6	17163/11020	CLAS
0.6−0.8	9882/7497	CLAS
0.8−1.0	4393/3274	CLAS
1.0−1.2	8393/4529	CLAS
2.8−3.4	1318/948	CLAS
3.8−4.2	831/697	CLAS

Table 1: Comparison of Q^2-dependent (QDF) and single-Q^2 (SQS) solutions.

Most fits were carried out including preliminary CLAS data. A single fit over the full range, excluding the CLAS data, is given for comparison. In Fig. 3, all variants of the fit are included, along with the fits of Refs. [5–7] and the analyses of Refs. [8,9]. Our global fit tends to follow more closely the result of Ref. [8]. Our single-Q^2 fits, though confirming the trend seen in the global fits, have such large uncertainties that they actually overlap with the ratios extracted in Ref. [5]. An improvement will require a more complete coverage of measurements above 1−2 $(\mathrm{GeV}/c)^2$.

Acknowledgments: This work was supported in part by a U.S. Department of Energy Grant No. DE-FG02-99ER41110. We also acknowledge a contract from Jefferson Lab under which part of this work was done. Jefferson Lab is operated by the Southeastern Universities Research Association under DOE contract DE-AC05-84ER40150.

References

[1] The available electroproduction database and a few representative fits are available via SAID. Both Internet [http://gwdac.phys.gwu.edu] and Telnet/ssh [gwdac.phys.gwu.edu, user:SAID] access are available.

[2] R. A. Arndt, I. I. Strakovsky, and R. L. Workman, Phys. Rev. C **53**, 430 (1996).

[3] V. Burkert, private communications.

[4] R. De Vita, these proceedings.

[5] V. V. Frolov *et al.*, Phys. Rev. Lett. **82**, 45 (1999).

[6] Th. Pospischil *et al.*, Phys. Rev. Lett. **86**, 2959 (2001).

[7] F. Kalleicher *et al.*, Z. Phys. **A359**, 201 (1997).

[8] The Mainz fits are available at the MAID website [http://www.kph.uni-mainz.de/MAID/]. See also S. S. Kamalov, S. N. Yang, D. Drechsel, O. Hanstein, and L. Tiator, Phys. Rev. C **64**, 032201 (2001).

[9] T. Sato and T. S. H. Lee, Phys. Rev. C **63**, 055201 (2001).

[10] R. A. Arndt, I. I. Strakovsky, R. L. Workman, and M. M. Pavan, Phys. Rev. C **52**, 2120 (1995).

Single π^+ electroproduction experiments using CLAS

Hovanes Egiyan[a], for the CLAS Collaboration

[a]*Department of Physics, The College of William and Mary, Williamsburg, VA 23187, U.S.A.*

(Received: 29 October 2001)

The study of single pion electroproduction processes provides valuable information on the structure of the nucleon and its excited states. Although these reactions have been studied for decades, there has never been a set of data containing both $p\pi^0$ and $n\pi^+$ channels with a nearly full coverage of the reaction phase space. The CEBAF Large Acceptance Spectrometer (CLAS) located in Hall B of Jefferson Lab is an experimental device well suited for conducting these experiments. The CLAS data were taken using the CEBAF electron beam, incident on a liquid H_2 target. The large phase space coverage of CLAS and the high statistical accuracy of the data will allow us to perform a combined analysis of single pion electroproduction cross sections in both $p\pi^0$ and $n\pi^+$ channels.

1 Introduction

One of the best ways to investigate the structure of the nucleon and the excited states is to study the single pion electroproduction, because many of the states with masses below 1.7 GeV favor the pion-nucleon decay modes. The first resonance region is dominated by the $P_{33}(1232)$ state with a pion-nucleon branching ratio $\Gamma_\pi/\Gamma > 99\%$. For this resonance the quantities of greatest interest are the ratios of the electric and scalar quadrupole amplitudes to that of the magnetic dipole: $R_{EM} \equiv \frac{E_{1+}}{M_{1+}}$, $R_{SM} \equiv \frac{S_{1+}}{M_{1+}}$. The Constituent Quark Model (CQM) [1], which is considered valid for large distances, predicts very small values for these ratios at small Q^2. On the other hand, at very small distances corresponding to large momentum transfers, using helicity conservation arguments, perturbative QCD (pQCD) predicts that the ratio R_{EM} should be unity [2]. Therefore, a transition from $R_{EM} \approx 0$ to $R_{EM} = 1$ is expected at some intermediate values of the four-momentum transfer. The value of Q^2 at which this transition occurs will help to determine at which distances perturbative QCD begins to work. The R_{SM} ratio is predicted by pQCD to be constant at very high Q^2 [2].

The second resonance region is dominated by three isospin $I = 1/2$ resonances: $P_{11}(1440)$, $D_{13}(1520)$ and $S_{11}(1535)$. The structure of the $P_{11}(1440)$ "Roper" resonance is currently not well understood. In CQM it is identified as a radially excited 3-quark state, but the mass of this state is difficult to explain within the CQM framework. One of the possible explanations of the "Roper" resonance is that it is a hybrid state [3]. Although these two kinds of states have the same quantum numbers, their predicted internal structures are entirely different. It was shown that the photo-coupling amplitudes $A_{1/2}$ and $S_{1/2}$ have different Q^2 dependence for the three-quark and hybrid states of the $P_{11}(1440)$ [3]. The existing experimental data on pion electroproduction does not allow us to draw definite conclusions about the nature of the "Roper" resonance. The $S_{11}(1535)$ and $D_{13}(1520)$ resonances in the second resonance region are relatively better understood. But the values for the $A_{1/2}$ photon coupling amplitude for $S_{11}(1535)$ at $Q^2 = 0$ obtained from the η and π photoproduction channels are in significant disagreement. Because there is no adequate amount of pion electroproduction data, such a comparison is not possible at non-zero Q^2 values. For the $D_{13}(1520)$ the transverse photon asymmetry $A_1 \equiv \frac{|A_{1/2}|^2-|A_{3/2}|^2}{|A_{1/2}|^2+|A_{3/2}|^2}$ is expected to proceed through a transition from $A_1 = -1$ at $Q^2 = 0$ to $A_1 = +1$ at very large values of Q^2 by both CQM and pQCD [4]. More experimental data on single pion electroproduction are needed to understand the

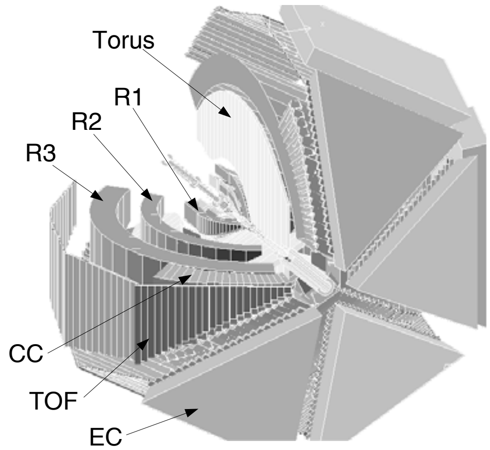

Figure 1: Three-dimensional schematic view of the CLAS detector.

structure of these states. Due to the isospin $I = 1/2$ nature of these resonances the study of $\pi^+ n$ final state in electroproduction on the proton is more appropriate than the $\pi^0 p$ channel.

One of the main goals of the CLAS collaboration is to significantly increase the data set which can be used to improve our knowledge of the baryon spectrum and the structure of the corresponding states. Many experiments are planned and conducted to measure the differential cross sections and the polarization observables. The present experiment measures the unpolarized cross section of the single π^+ electroproduction on a proton target. The 4π CLAS detector allows us for the first time to cover nearly the full angular range for this reaction in the hadronic rest frame with very high statistical accuracy.

2 Experiment

The data were taken using the CLAS detector located in Hall B at Jefferson Lab in Newport News, Virginia. A three dimensional schematic view of the detector is shown in Fig. 1. The toroidal magnetic field of the spectrometer is generated by the six superconducting magnetic coils symmetrically arranged around the beam axis. The six identical detector packages fill the space between the cryostats of the magnet. Each sector of the detector consists of three regions of drift chambers (R1, R2, R3) for tracking of charged particles [5], gas Čerenkov counters (CC) for electron identification [6], scintillator counters of the time-of-flight system (TOF) for charged particle identification [7], and sampling calorimeters (EC) [8] to detect showers from electrons and photons. The CEBAF electron beam with 1.515 GeV energy was delivered onto a 5 cm long liquid hydrogen target at an average current of 3 nA. Scattered electrons were detected and reconstructed in the angular range from $20° - 55°$ with an average momentum resolution of $\approx 0.7\%$. The coincident positive pions were reconstructed from $8° - 140°$ in the laboratory frame and were identified using the time-of-flight system of CLAS. A cut on the neutron missing mass was used to select the single pion production events. In order to reduce the fraction of events where π^+ decays in flight, a vertex cut $\mid z_\pi - z_e \mid < 2$ cm was applied. The corresponding coverage for this reaction in Q^2, W and the two center-of-mass angles θ^* and ϕ^* is shown in Fig. 2.

The geometrical acceptance, the efficiency and the resolution of the detector were simulated using a GEANT-based computer model of CLAS. The event generator used the Mainz Unitary Isobar Model[1] [9] to calculate the single pion electroproduction cross section. It also incorporated radiative effects [10] to account for the loss of events due to the neutron missing mass cut. The

[1]In this analysis all cross sections and structure functions calculated using the MAID model include only partial waves up to $l \leq 5$.

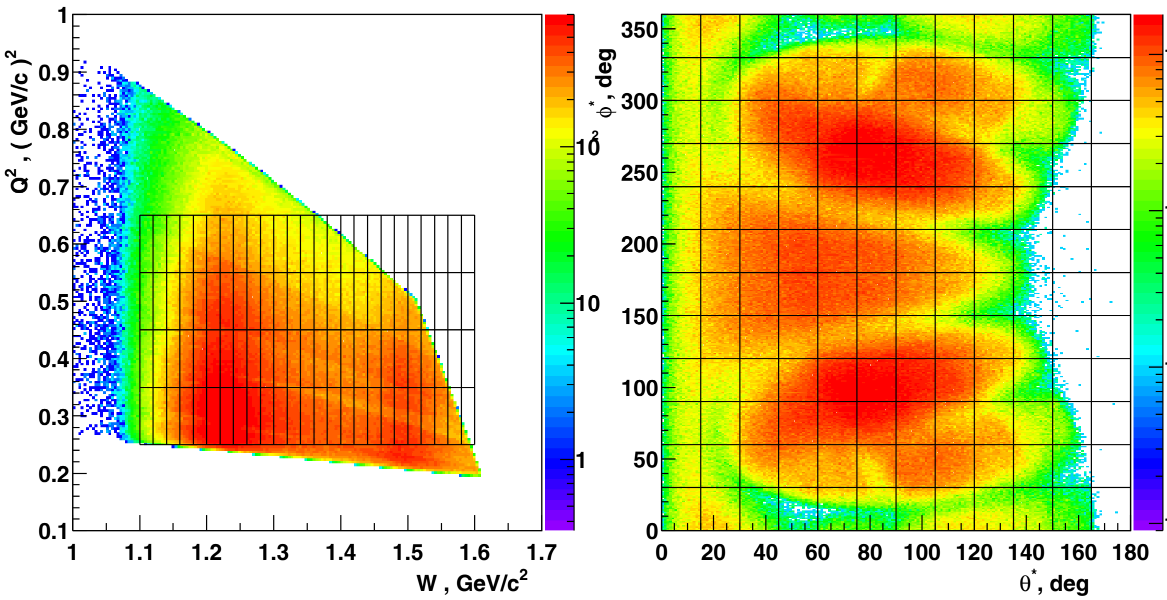

Figure 2: The kinematic coverage of the data and the binning used in the analysis.

detector simulation program used the magnetic field map, surveyed positions of the detector components, known malfunctioning wires and phototubes. The effects of π^+ decays in the detector are also reproduced in the simulations. Software fiducial cuts were applied to define the geometrical regions where the detector response was reliably reproduced by the simulation. The radiative corrections were done using the Mo and Tsai formalism [11] with modifications for exclusive electroproduction processes [10]. The binning of the data is illustrated in Fig. 2 and is shown in Table 1.

3 Preliminary results

The cross section of single π^+ electroproduction with unpolarized beam and target can be written [12] as:

$$\frac{\partial^5 \sigma}{\partial E' \partial \Omega_e \partial \Omega^*_\pi} = \Gamma \cdot \frac{d\sigma}{d\Omega^*_\pi} \, , \tag{1}$$

$$\frac{d\sigma}{d\Omega^*_\pi} = \sigma_T + \epsilon\sigma_L + \epsilon\sigma_{TT}\cos 2\phi^* + \sqrt{2\epsilon(1+\epsilon)}\sigma_{TL}\cos\phi^* \, , \tag{2}$$

where Γ is the virtual photon flux, ϵ is the photon polarization parameter, and $\frac{d\sigma}{d\Omega^*_\pi}$ is the virtual photoproduction cross section. σ_T, σ_L, σ_{TT} and σ_{TL} are the unpolarized structure functions dependent on Q^2, W and θ^*. By fitting the ϕ^*-dependence of the experimental cross section we obtain σ_{TT}, σ_{TL} and the linear combination $\sigma_T + \epsilon\sigma_L$.

Variable	# of bins	Lower limit	Upper limit	Width
Q^2	4	0.25 GeV^2	0.65 GeV^2	0.10 GeV^2
W	25	1.1 GeV	1.6 GeV	20 MeV
θ^*	12	0°	180°	15°
ϕ^*	12	0°	360°	30°

Table 1: The number and the sizes of data bins. Values for the limits indicate the upper and lower edges of the bins, rather than the bin centers.

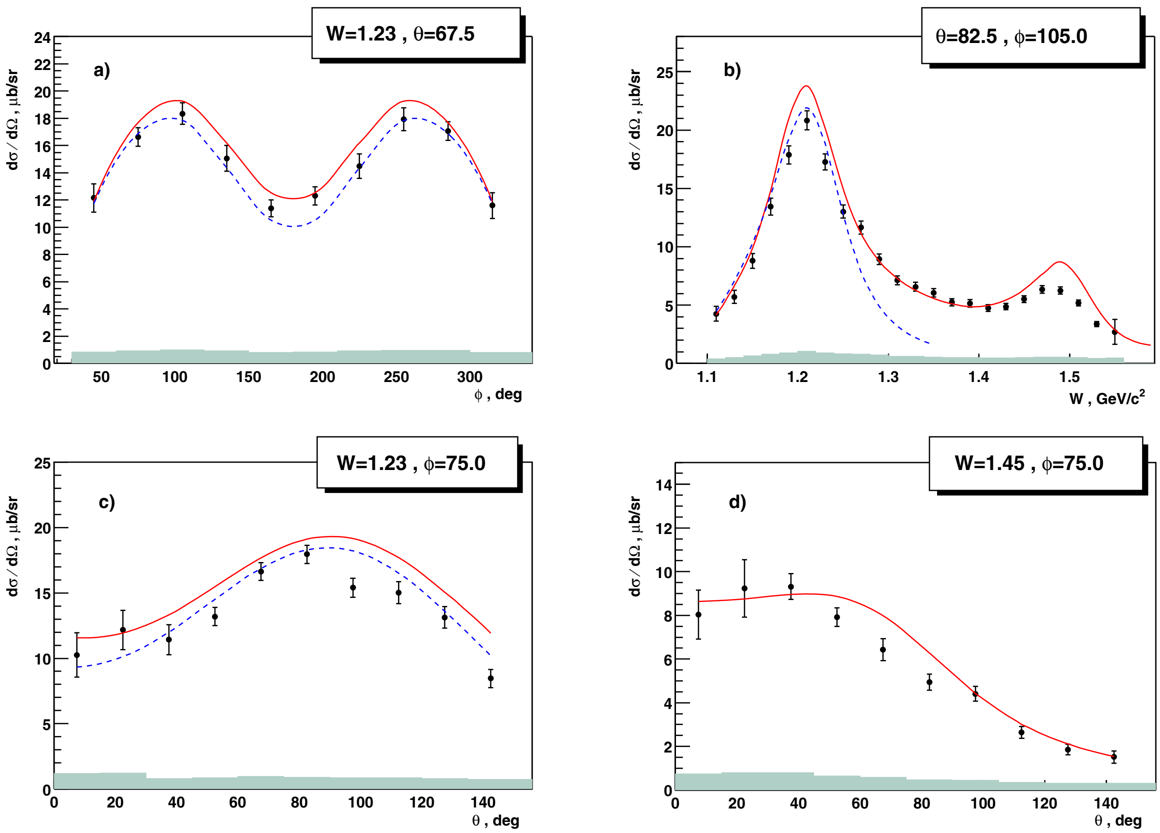

Figure 3: Preliminary virtual photoproduction cross sections $d\sigma/d\Omega^*$ at $Q^2 = 0.4$ GeV^2 from the CLAS experiment, compared with MAID2000 [9] (solid curves) and Sato-Lee model [13] (dashed curves): a) ϕ^* dependence of the cross section at $W = 1.23$ GeV; b) W dependence at $\theta^* = 82.5^o$ and $\phi^* = 105^o$; c) and d) θ^* dependence at $\phi^* = 75^o$ and $W = 1.23$ GeV and $W = 1.45$ GeV.

Sample plots of the preliminary results for the virtual photoproduction cross sections $\frac{d\sigma}{d\Omega^*_\pi}$ compared with the MAID2000 [9] and Sato-Lee [13] models are shown in Fig. 3. The error bars indicate the statistical errors, while the shaded areas underneath show the estimated systematic uncertainties. The average combined relative error for the cross sections is $\frac{\delta\sigma}{\sigma} \approx 8\% - 9\%$. The ϕ^*-dependence of the cross sections is consistent with Eq. 2, while the W-dependence shows two distinct peaks in the first and second resonance regions. The behavior of the cross sections versus θ^* angle is consistent with a combination of s-channel resonance production and t-channel pion exchange.

Fig. 4 and Fig. 5 show the preliminary results for the σ_{TT}, σ_{TL} and the linear combination $\sigma_T + \epsilon\sigma_L$ of the structure functions versus W and θ^*, obtained by fitting the ϕ^*-distributions of the cross sections for single π^+ electroproduction. From Figs. 3, 4, 5 one can see that overall the MAID2000 and Sato-Lee models describe the CLAS π^+ data reasonably well. But in the $\Delta(1232)$ region these models overestimate the cross sections and the $\sigma_T + \epsilon\sigma_L$ linear combination. A comparison for σ_{TT} term indicates better agreement between the experimental data and the model calculations for the $\Delta(1232)$ region. Therefore, one can conclude that the resonant amplitudes for $P_{33}(1232)$ are well known, mostly from analyses of π^0 channel, while the background processes, which make significant contributions to the longitudinal terms, are relatively poorly understood for the π^+ channel. The

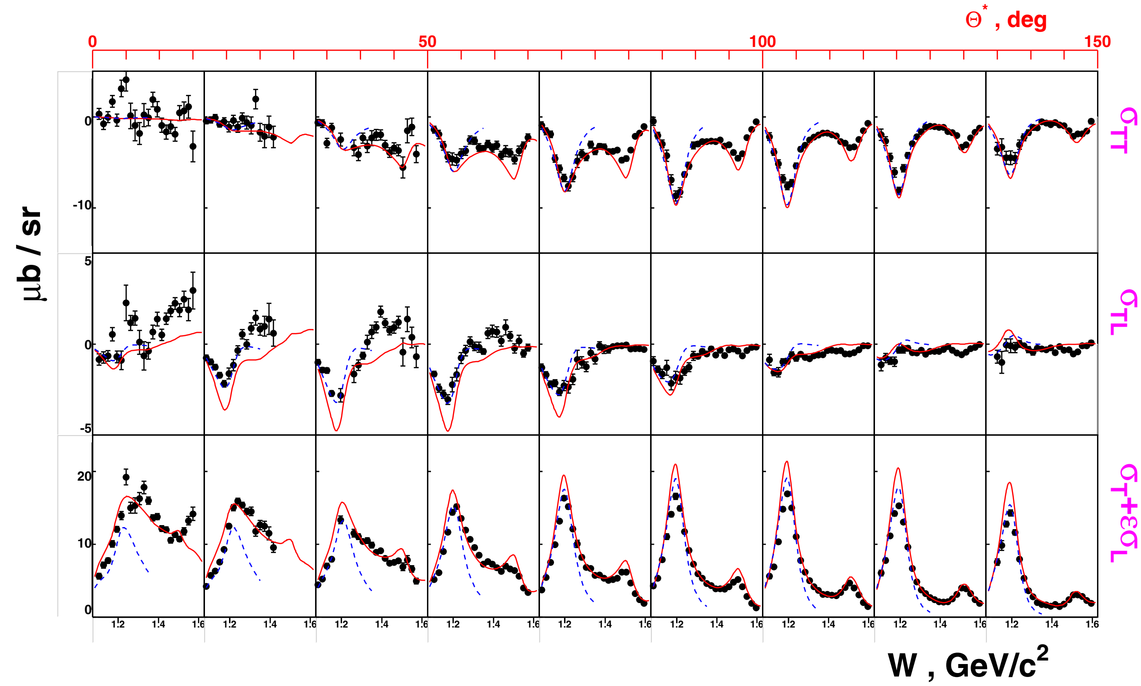

Figure 4: Preliminary results for the structure functions σ_{TT}, σ_{TL} and the linear combination $\sigma_T + \epsilon\sigma_L$ vs. W at $Q^2 = 0.3$ GeV^2 for different values of θ^*, compared with MAID2000 [9] (solid curves) and Sato-Lee model [13] (dashed curves).

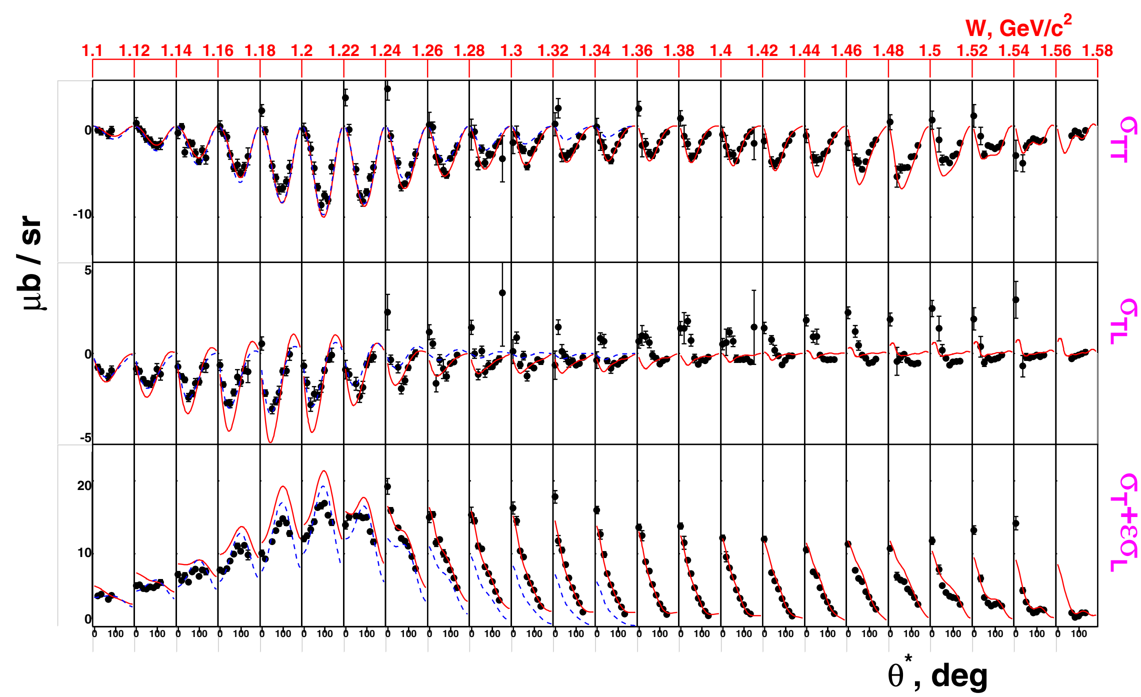

Figure 5: Preliminary results for the structure functions σ_{TT}, σ_{TL} and the linear combination $\sigma_T + \epsilon\sigma_L$ vs. θ^* at $Q^2 = 0.3$ GeV^2 for different values of W, compared with MAID2000 [9] (solid curves) and Sato-Lee model [13] (dashed curves).

MAID2000 model overestimates both the $\sigma_T + \epsilon\sigma_L$ and σ_{TT} terms at the second resonance peak[2]. In addition, there is disagreement for the σ_{TL} structure function between MAID2000 and the data in the "Roper" resonance region of 1.36 GeV $< W <$ 1.48 GeV. Therefore, future analyses of these cross sections can help better constrain the resonant and background amplitudes for single π^+ electroproduction.

This experiment provides us with the best data set on single π^+ electroproduction in the resonance region, covering nearly full angular range in the center-of-mass frame of the hadronic system. In addition to the $\pi^+ n$ channel, there are CLAS data on single π^0 electroproduction cross sections. A combined analysis of these data sets will allow us to separate $I = 1/2$ and $I = 3/2$ isospin components of the electroproduction amplitudes. It is expected that the beam asymmetry is sensitive to $A_{1/2}$ and $S_{1/2}$ photon coupling amplitudes for the $P_{11}(1440)$ [14, 15]. The single and double spin asymmetries from CLAS will also be available for both $\pi^+ n$ and $\pi^0 p$ channels. The future analysis of the combined data set will significantly improve our knowledge of the resonant amplitudes for the states in the first and second resonant regions.

Acknowledgments: This analysis work was supported by the DOE grant DE-FG02-96ER41003. Many thanks to Volker Burkert, Keith Griffioen and Stepan Stepanyan for their help in the analysis of the data, and to the JLab/Hall B staff and CLAS collaboration for their hard work in conducting this experiment.

References

[1] N. Isgur, "Nuclear physics from the quark model with chromodynamics", Acta Austriaca, Suppl. XXVII, 177 (1985).

[2] C.E. Carlson, Phys. Rev. D **34**, 2704 (1986).

[3] Zh. Li, V. Burkert, Zh. Li, Phys. Rev. D **46**, 70 (1992).

[4] V. Burkert, "Leptonic Production of Baryon Resonances", Perspective in the Structure of Hadronic Systems, Edited by M.N. Harakeh, *et al.*, Plenum Press, New York, (1994).

[5] M.D. Mestayer, *et al.*, Nucl. Inst. and Meth. **A449**, 81 (2000).

[6] G. Adams, *et al.*, Nucl. Inst. and Meth. **A465**, 414 (2001).

[7] E.S. Smith, *et al.*, Nucl. Inst. and Meth. **A432**, 265 (1999).

[8] M. Amarian, *et al.*, Nucl. Inst. and Meth. **A460**, 239 (2001).

[9] D. Drechsel, O. Hanstein, S.S. Kamalov, L. Tiator , Nucl. Phys. **A645**, 145 (1999).

[10] R. Minehart, C. Smith, AAO_RAD program; Private communications.

[11] L.W. Mo, Y.S. Tsai, Rev. Mod. Phys. **41**, 205 (1969).

[12] F. Foster, and G. Hughes, "Electroproduction of nucleon resonances", Rep. Prog. Phys. **46**, 1445 (1983).

[13] T. Sato and T.-S.H. Lee, Phys. Rev. C **54**, 2660 (1996).

[14] Kyungseon Joo, Private Communications.

[15] Inna Aznaurian, Private Communications.

[2]The Sato-Lee model [13] only incorporates the $\Delta(1232)$ resonance, and therefore is not expected to describe the data above the first resonance region.

Meson photoproduction at GRAAL

V. Kouznetsov[a,b,*], representing the GRAAL Collaboration:
O. Bartalini[a,c], V. Bellini[d], J.-P.Bocquet[e], M. Castoldi[f], A. D'Angelo[a], J.-P. Didelez[h], R. Di Salvo[a], A. Fantini[a], G. Gervino[g], F. Ghio[i], B. Girolami[i], M. Guidal[h], E. Hourany[h], R. Kunne[h], A. Lapik[b], P. Levi Sandri[j], A. Lleres[e], D. Moricciani[a], V. Nedorezov[b], L. Nicoletti[e], D. Rebreyend[e], F. Renard[e], N. Roudnev[k], C. Schaerf[a], M.L. Sperduto[d], M.C. Sutera[d], A. Turinge[l], A. Zabrodin[b], A. Zucchiatti[f]

[a]*University "Tor Vergata" and INFN Sezione di RomaII, I-00133 Rome, Italy*
[b]*Institute for Nuclear Research, 117312 Moscow, Russia*
[c]*University of Trento, I-38100 Trento, Italy*
[d]*INFN, Laboratori Nazionali del Sud, I-95123 Catania, Italy*
[e]*Institut des Sciences Nucléaires, 38026 Grenoble, Frnace*
[f]*INFN, Sezione di Genova, I-16146 Genoa, Italy*
[h]*Institut de Physique Nucléaire, 91406 Orsay, France*
[g]*INFN, Sezione di Torino and University of Turin, I-10125 Turin, Italy*
[i]*Instituto Superiore di Sanita and INFN Sezione di RomaI, I-00161 Rome, Italy*
[j]*INFN, Laboratori Nazionali di Frascati, I-00044 Frascati, Italy*
[k]*Institute of Theoretical and Experimental Physics, 117259 Moscow, Russia*
[l]*Kurchatov Institute of Atomic Energy, 123182 Moscow, Russia*
[*]*Email:* `slava@roma2.infn.it`, `slava@cpc.inr.ac.ru`

(Received: 2 November 2001)

The highly polarized and tagged photon beam and the almost 4π detector of the GRAAL Collaboration make it possible to produce high quality photoproduction data. Recent results on beam polarization asymmetries Σ for π^+ and η photoproduction, measured over wide angular and energy ranges, are presented. Data of high precision provide important constraints for partial wave analysis.

1 Introduction

Probing the nucleon with polarized photons provides important information regarding the spectrum of nucleon excited states. Over past years, the photoproduction of mesons has demonstrated its potential [1–5] as a tool to explore N^*, complementary to the πN scattering. Precise data from modern photon factories essentially impact theoretical studies of nucleon resonances.

Properties of resonances are extracted from the photoproduction data by means of the partial wave analysis and the multipole decomposition in the framework of different approaches [1–5]. The comparison of calculated observables to experimental data constraints theoretical models and determines the role and properties of the included resonances. The extraction of resonances parameters requires both unpolarized cross section data and polarization observables [6]. While the cross section is a source of information on dominating components of the scattering amplitude, the polarization observables are much more sensitive to the non-dominant contributions. For pseudoscalar meson photoproduction, this is well illustrated in terms of four helicity amplitudes H_i corresponding to four possible helicity states of the target and recoil nucleon,

$$\begin{aligned}
\frac{d\sigma}{d\Omega} &\sim \mid H_1 \mid^2 + \mid H_2 \mid^2 + \mid H_3 \mid^2 + \mid H_4 \mid^2 \ , \\
\Sigma &\sim \mathrm{Re}(H_1 H_4^* - H_2 H_3^*) \ , \\
T &\sim \mathrm{Im}(H_1 H_2^* + H_3 H_4^*) \ , \\
R &\sim \mathrm{Im}(H_1 H_3^* + H_2 H_4^*) \ ,
\end{aligned}$$

where the three single-polarization observables Σ, T, R are the beam, target and recoil asymmetries, i.e. the measures of anisotropy of a reaction yield in respect to the polarization of the incoming photon, target and recoil nucleons.

The novel GRAAL facility [7] was designed to measure the polarization observables, in particular, the Σ beam asymmetry, in photon-induced reactions. During last years, experimental data have been collected for various channels of the photon-nucleon interaction. The recent progress in the analyses of π^+ and η photoproduction is presented in this report.

2 The GRAAL setup

A polarized and tagged photon beam (Fig. 1) at GRAAL is produced by backscattering of laser light on 6.04 GeV electrons which circulate in the storage ring of the ESRF (Grenoble, France). Through the use of green 514 nm laser light, the tagged spectrum covers an energy range of 0.55−1.1 GeV. Alternately, the UV line can be employed, resulting in an energy range of 0.8−1.5 GeV. The linear beam polarization varies from ~0.45 at the lower energy limits to 0.98 at the upper limits. The tagger provides an energy resolution of 16 MeV(FWHM) which is limited by the emittance and energy spread of the electron beam. The γ tagging rate is 2×10^6 photons per second for the integrated spectrum. The detection system (Fig. 1) includes three main parts:

- At forward angles $\theta_{lab} \leq 25°$ there are two planar wire chambers, a thin time-of-flight (TOF) hodoscope made up of 26 horizontal and 26 vertical plastic scintillator strips, each 3 cm thick, and a TOF shower wall [8]. The latter is an assembly of 16 modules, each being a sandwich of four converter-plus-scintillator layers.
- At central angles from 25° to 155°, the target is surrounded by two cylindrical wire chambers, a 5 mm thick scintillator ΔE barrel, and a BGO ball made up of 480 crystals, each of 21 radiation lengths [9].
- At backward angles $\theta_{lab} \geq 155°$ there are two plastic scintillator disks separated by a 1 cm lead converter.

The apparatus provides the detection and identification of all types of final state particles in an almost 4π solid angle.

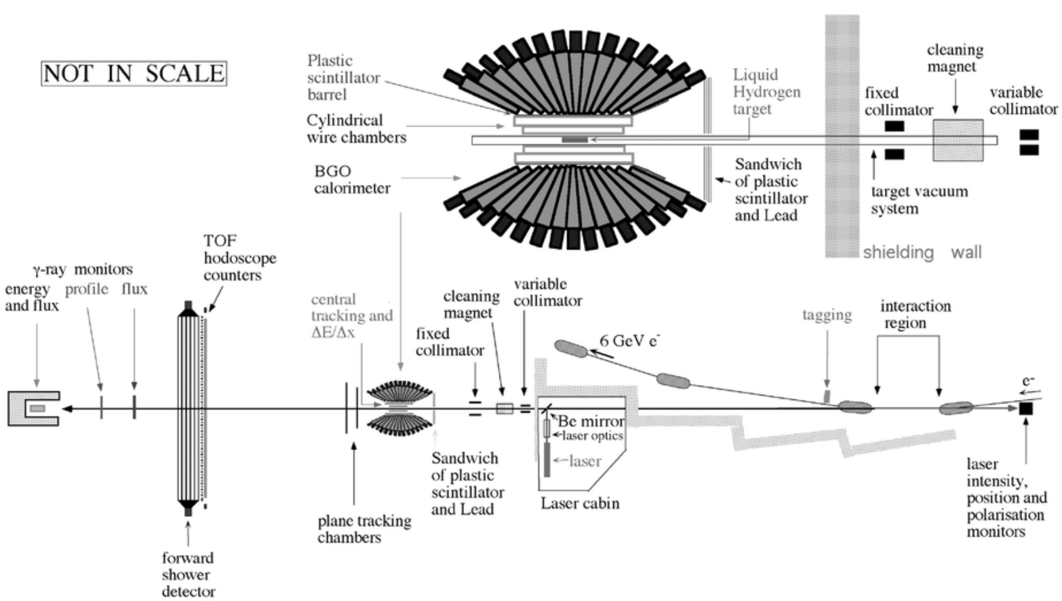

Figure 1: The GRAAL setup.

The azimuthal symmetry of the GRAAL detector makes it suitable for measurements of the Σ beam asymmetry. For photons linearly polarized in the vertical plane with a polarization degree P, the cross section of the reaction under study can be written as

$$\left(\frac{d\sigma}{d\Omega}\right)_{pol}(\phi) = \left(\frac{d\sigma}{d\Omega}\right)_{unpol}\Big[1 + P\,\Sigma\,\cos(2\phi)\Big]\ ,$$

where ϕ is the angle between the reaction plane and the beam polarization, Σ is the beam asymmetry. By switching the beam polarization alternatively between horizontal and vertical states, two independent sets of data can be collected. The sum of two yields normalized by the respective fluxes provides the unpolarized cross section and the possibility to correct the small azimuthal anisotropies in the detector response. The Σ beam asymmetry can be extracted from the fit to the ϕ distributions of selected events as

$$\frac{\left(\frac{d\sigma}{d\Omega}\right)_{pol}(\phi)}{\left(\frac{d\sigma}{d\Omega}\right)_{unpol}} = 1 + P\,\Sigma\,\cos(2\phi) = \frac{2F_{ver}(\phi)}{F_{ver}(\phi) + \alpha F_{hor}(\phi)}\ ;$$

F_{ver} and F_{hor} are measured azimuthal distributions of selected events for the vertical and horizontal beam polarizations, α is the ratio of the beam fluxes for each polarization state.

3 π^+N photoproduction

Initially, 92 beam asymmetry data for positive pion photoproduction have been measured from 0.6 to 1.05 GeV using the green laser [10]. These data, shown in Fig. 2 together with the most accurate previous results [11–13], are in good agreement with the other experiments. Data points cover an almost unmeasured region of backward angles.

Recently, new data have been obtained at higher energies of 0.8-1.5 GeV using the UV laser [14]. The new data set (Fig. 3) includes 237 beam asymmetries, measured over an angular range of 40-160°. 136 data points were produced in an almost unexplored domain above 1.05 GeV, where only

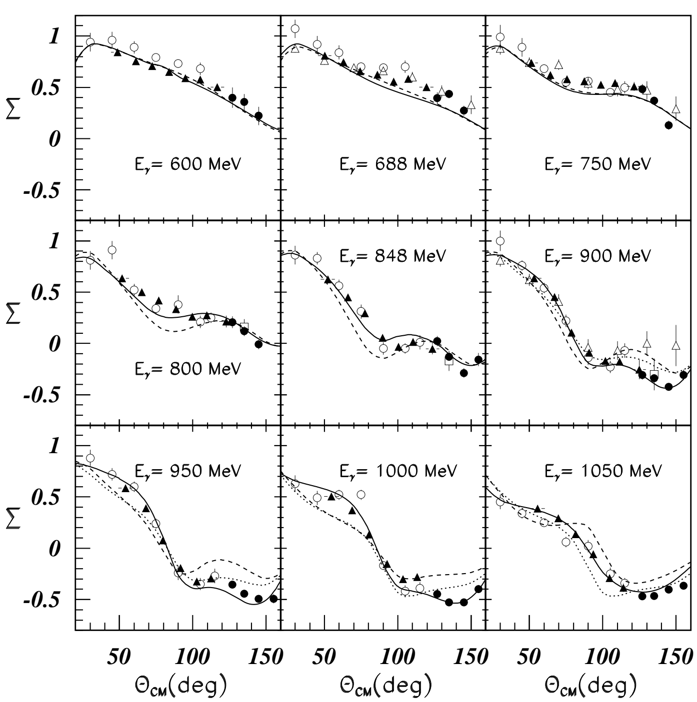

Figure 2: Σ beam asymmetry for π^+n photoproduction. Black circles and triangles indicate the GRAAL results [10], measured with the green laser; open circles indicate the results of the Daresbury group [11]; open triangles and squares indicate the results from SLAC [12, 13]. Solid lines are the FA01 solution of the SAID partial wave analysis; dashed lines are the predictions of MAID2000 [3]; dotted lines are the results from [15] after fitting the benchmark data base [16].

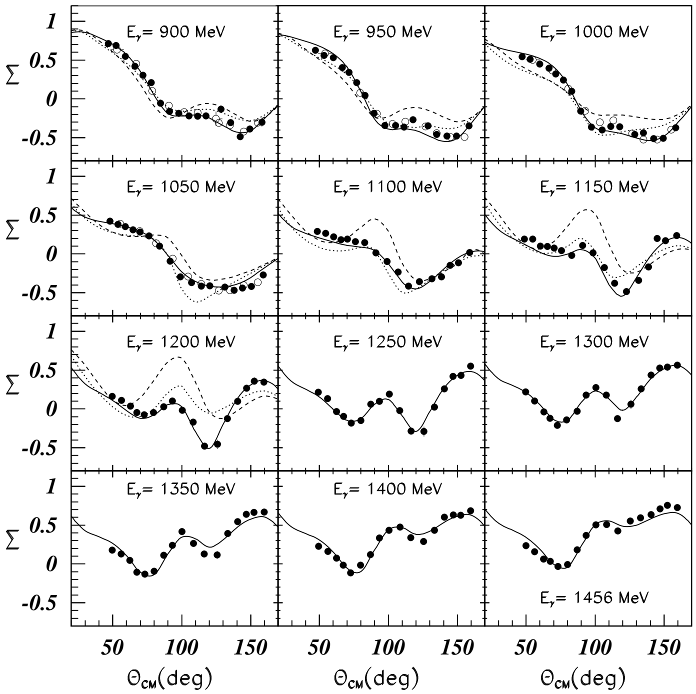

Figure 3: Σ beam asymmetry for π^+n photoproduction. Black circles indicate the new GRAAL results (preliminary), measured with the UV laser; open circles indicate the previous GRAAL results from [10]. Solid lines are the FA01 solution of the SAID partial wave analysis; dashed lines are the predictions of MAID2000 [3]; dotted lines are the results from [15] after fitting the benchmark data base [16].

45 old data of lower accuracy were available. New results also cover backward angles above 120° where no previous measurements exist. Through the use of the wire chambers in order to determine the pion trajectories, the improved resolution in the determination of the scattering angle Θ_{cm} of about 3° have been achieved. This feature has made it possible to produce the data points with narrow angular bins of 6-10°, in order to reveal a complicate angular variation of Σ.

In Fig. 3, both sets of data are compared at overlapping energies. The data have been obtained using either green or UV lasers, which produce different beam spectra and different polarizations for each beam energy [7]. Given these differences, the reproducibility of our results is excellent and supports the quality of both data sets.

We have compared our results with the predictions of a unitary isobar model MAID2000 [3]. At the energies below 0.95 GeV, this model reasonably reproduces our data. At higher energies the difference becomes more pronounced. The latest version of these calculations [15], which includes resonance parameters derived from a fit to the restricted data base [16], exhibits an improvement. Nevertheless, the discrepancy still remains above 1 GeV.

The new FA01 solution of the partial wave analysis of the Data Analysis Center of The George Washington University (SAID) have been developed after adding our data to the data base [2]. This solution reproduces our data reasonably well, with χ^2/data of 555/237.

4 η photoproduction

Fig. 4 shows beam asymmetries for η photoproduction on the proton, measured at GRAAL three years ago [17]. No other results were available. The measurement have been performed using the green laser from the threshold to 1.1 GeV. The results have been produced in two ways: analyzing events, when two or six photons, originating from the ($\eta \to 2\gamma$) and ($\eta \to 3\pi^0 \to 6\gamma$) decay channels are detected in the BGO ball; and with the detection of one photon from the ($\eta \to 2\gamma$) decay in the forward shower wall and the other in the BGO. Both analyses have provided statistically independent sets of data, which have confirmed each the other. The results have shown the large forward values of the asymmetry Σ near 1.05 GeV, not predicted by old models.

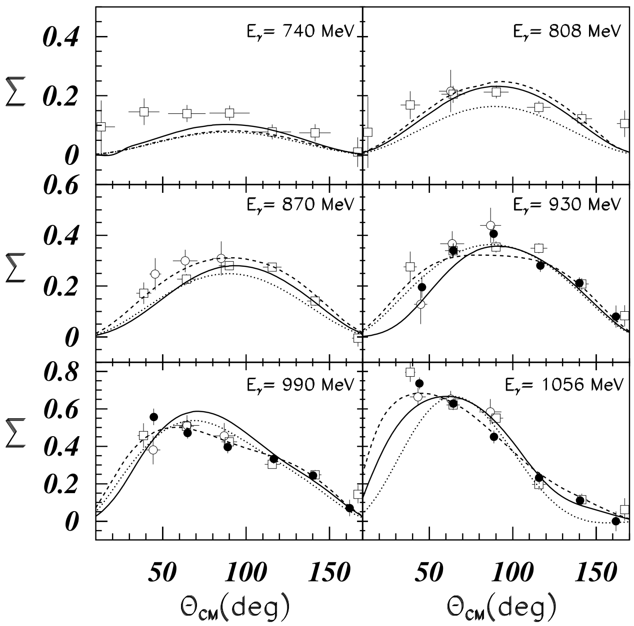

Figure 4: Σ beam asymmetry, corresponding to the η photoproduction on the proton. Open squares and circles indicate the results from [17] measured using the green laser: the squares correspond to the detection of 2 or 6γ's in the BGO ball; circles correspond to 1γ in the forward shower wall, and 1γ in the BGO. Black circles are our preliminary results, measured with the UV laser. Solid curves are predictions of the eta-MAID [5]; dashed curves denote the BO12 solution of the SAID analysis [18]; dotted curves are predictions of the quark model of B. Saghai and Z. Li [4].

The analysis of new data, collected with the UV laser at higher energies, aims to reveal more details in the variation of Σ at forward angles. One important advantage is the use of the wire chambers to reconstruct the tracks of recoil protons, in order to achieve the best angular resolution in the determination of the scattering angle Θ_{cm}. Both type of events (2 or 6 γ's in the BGO and 1γ in the forward wall and 1γ in the BGO) are considered together. The latter essentially increases the overall statistics at forward angles. These features make it possible to reduce the widths in the angular binning as compared with the previous data.

In Fig. 4, preliminary results of the new analysis are shown together with the published data using the similar angular bins. As in the case of $\pi^+ n$ data, the reproducibilty of our results is quite good. The main set of the new results is shown in Fig. 5. The data exhibit a peak near $\sim 50°$ at

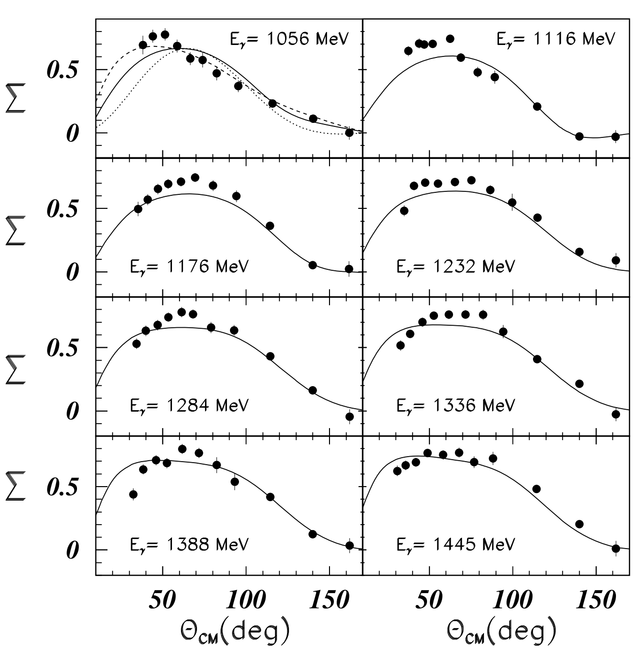

Figure 5: Preliminary results for the Σ beam asymmetry observable for the η photoproduction on the proton measured using the UV laser. Solid curves are predictions of the eta-MAID [5]; dashed curves denote the BO12 solution of the SAID analysis [18]; dotted curves are predictions of the quark model of B. Saghai and Z. Li [4].

the photon energy of 1.05 GeV, which was not clear evidenced in the previous results. At higher energies, the peak becomes more spread, showing large values of Σ at the angles from 40 to 90°.

Our results are compared with the predictions of several models: the BO12 solution of the SAID partial wave analysis [18]; the quark model of B. Saghai and Z. Li [4]; and the eta-MAID [5]. All the models are rather close to the data below 1.05 GeV. However, neither of them well reproduces the observed peculiarity near 50° at 1.05 GeV. At higher energies, the predictions of the eta-MAID model, only available, are in reasonable agreement with our data.

5 Conclusions

Over last several years, the GRAAL Collaboration produces polarized photoproduction data of high precision. The recent progress in the study of π^+ and η photoproduction is reported. New constraints are placed upon partial wave analyses.

Acknowledgments: We are grateful to all theoreticians who were interested in our data. We wish to thank I. Strakovsky, R. Workman, S. Kamalov, B. Saghai, L. Tiator, and W.-T. Chiang for their close co-operation with GRAAL. We acknowledge the machine operation group of the ESRF for providing the stable beam operation, and the staffs of the contributing Institutes for their assistance in the development and maintenance of the apparatus.

References

[1] R. M. Davidson, N. C. Mukhopadhyay, M. S. Pierce, R. A. Arndt, I. I. Strakovsky, and R. L. Workman, Phys. Rev. C **59**, 1059 (1999); L. Tiator, D. Drechsel, G. Knöchlein, and C. Bennhold, Phys. Rev. C **60**, 035210 (1999); R. L. Workman, R. A. Arndt, and I. I. Strakovsky, Phys. Rev. C **62**, 048201 (2000); T. Mart and C. Bennhold, Phys. Rev. C **61**, 012201 (2000); T. Feuster and U. Mosel, Phys. Rev. C **59**, 460 (1999).

[2] R. Arndt, I. Strakovsky, and R. Workman, Phys. Rev. C **53**, 430 (1996). The SAID solutions and the single-pion photoproduction data base are available via telnet/ssh to gwdac.phys.gwu.edu, user: said.

[3] D. Drechsel, O. Hanstein, S. Kamalov, and L. Tiator, Nucl. Phys. **A645**, 145 (1999); Predictions are available at http://www.kph.uni-mainz.de/MAID.

[4] B. Saghai and Z. Li, Eur. Phys. J. A **11**, 217 (2001).

[5] W.-T. Chiang, S.N. Yang, L. Tiator, and D. Drechsel, E-print Nucl-th/0110034. Predictions are available at http://www.kph.uni-mainz.de/MAID.

[6] W.-T. Chiang and F. Tabakin, Phys. Rev. C **55**, 2054 (1997); R. Workman, Few Body Syst. Suppl. **11**, 94 (1999).

[7] J. P. Bocquet *et al.*, Nucl. Phys. **A622**, 125 (1997).

[8] V. Kouznetsov *et al.*, to be published in Nucl. Instr. and Meth.

[9] F. Ghio *et al.*, Nucl. Instr. and Meth. **A404**, 71 (1998);

[10] J. Ajaka *et al.*, Phys. Lett. **B475**, 372 (2000).

[11] P. J. Bussey *et al.*, Nucl. Phys. **B154**, 205 (1979).

[12] G. Knies *et al.*, Phys. Rev. D **10**, 2778 (1974).

[13] R. Zdarko and E. Dolly, Nuovo Cimento **A10**, 10 (1972).

[14] Publication in preparation.

[15] S. Kamalov, private communication; S. Kamalov *et al.*, E-print nucl-th/0106045.

[16] R. A. Arndt *et al.*, "Multipole Analysis of Benchmark Dataset for Pion Photoproduction", to appear in the Proceedings of the Workshop on the Physics of Excited Nucleons (NSTAR 2001), Mainz, Germany, 7-10 March 2001, Eprint nucl-th/0106059.

[17] J. Ajaka *et al.*, Phys. Rev. Lett. **81**, 1797 (1998).

[18] R. Arndt, I. Strakovsky, and R. Workman, Bull. Am. Phys. Soc. **45**, 34 (2000).

New results and future plans with real photons at MAMI

R. Beck, R. Leukel, and A. Schmidt

Institut für Kernphysik, Johannes Gutenberg Universität Mainz, Johann–Joachim–Becher–Weg 45, 55099 Mainz, Germany

(Received: 31 October 2001)

The photon asymmetry in the reaction $p(\vec{\gamma},\pi^0)p$ has been measured with the photon spectrometer TAPS using linearly polarized photons from the tagged–photon facility at the Mainz Microtron MAMI close to the pion threshold and in the $\Delta(1232)$–resonance region. The total and differential cross sections were also measured simultaneously with the photon asymmetry. This allowed determination of the S–wave and all three P-wave amplitudes. The results in the threshold region are compared to the predictions of ChPT. With the photon spectrometer TAPS the full polar angular range of the pion could be covered and from the new results in the $\Delta(1232)$ region a $E2/M1$–ratio of $-(2.4\pm0.16_{stat}\pm0.24_{sys})$ is extracted.

1 Pion photoproduction in the threshold region

The photoproduction of pions near threshold has been a topic of considerable experimental and theoretical activities over the past years, ever since the results of the experiments, performed in Saclay [1], Mainz ([2] [3]) and Saskatoon [4], were at variance with the prediction of a low energy theorem (LET), which was derived in the early 70's [5, 6]. Being based on fundamental principles, this LET predicted the value of the S–wave threshold amplitude E_{0+} in a power series in $\mu = m_\pi/m_N$, the ratio of the masses of the pion and nucleon.

The discrepancy could be explained by a calculation in the framework of heavy–baryon chiral perturbation theory (ChPT) [7], which showed that additional contributions due to pion loops in μ^2 have to be added to the old LET. Refined calculations within heavy–baryon ChPT [8] led to descriptions of the four relevant amplitudes at threshold by well–defined expansions up to order p^4 in the S–wave amplitude E_{0+} and p^3 in the P–wave combinations P_1, P_2 and P_3, where p denotes any small momentum or pion mass, the expansion parameters in heavy–baryon ChPT. To that order, three low–energy constants (LEC) due to the renormalization counter terms appear, two in the expansion of E_{0+} and an additional LEC b_P for P_3, which have to be fitted to the data or estimated by resonance saturation.

However, two combinations of the P–wave amplitudes, P_1 and P_2, are free of low–energy constants. Their expansions in μ converge rather well leading to new LETs for these combinations. Therefore, the P–wave LETs offer a significant test of heavy–baryon ChPT. However, for this test the S–wave amplitude E_{0+} and the three P–wave combinations P_1, P_2 and P_3 have to be separated. This separation can be achieved by measuring the photon asymmetry using linearly polarized photons, in addition to the measurement of the total and differential cross sections.

The differential cross sections can be expressed in terms of the S– and P–wave multipoles, assuming that close to threshold neutral pions are only produced with angular momenta l_π of zero and one. Due to parity and angular momentum conservation only the S–wave amplitude E_{0+} ($l_\pi = 0$) and the P–wave amplitudes M_{1+}, M_{1-} and E_{1+} ($l_\pi = 1$) can contribute and it is convenient to write the differential cross section and the photon asymmetry in terms of the three P–wave combinations $P_1 = 3E_{1+} + M_{1+} - M_{1-}$, $P_2 = 3E_{1+} - M_{1+} + M_{1-}$ and $P_3 = 2M_{1+} + M_{1-}$. The c.m. differential cross section is

$$\frac{d\sigma(\theta)}{d\Omega} = \frac{q}{k}\left(A + B\ cos(\theta) + C\ cos^2(\theta)\right)\ , \tag{1}$$

where θ is the c.m. polar angle of the pion with respect to the beam direction and q and k denote the c.m. momenta of pion and photon, respectively. The coefficients $A = |E_{0+}|^2 + |P_{23}|^2$, $B = 2Re(E_{0+}P_1^*)$ and $C = |P_1|^2 - |P_{23}|^2$ are functions of the multipole amplitudes with $P_{23}^2 = \frac{1}{2}(P_2^2 + P_3^2)$. Earlier measurements of the total and differential cross sections already allowed determination of E_{0+}, P_1 and the combination P_{23}.

In order to obtain E_{0+} and all three P–waves separately and to test the new LETs of ChPT, it is necessary to measure, in addition to the cross sections, the photon asymmetry Σ,

$$\Sigma = \frac{d\sigma_\perp - d\sigma_\parallel}{d\sigma_\perp + d\sigma_\parallel}\ , \tag{2}$$

where $d\sigma_\perp$ and $d\sigma_\parallel$ are the differential cross sections for photon polarizations perpendicular and parallel to the reaction plane defined by the pion and proton. The asymmetry is proportional to the difference of the squares of P_3 and P_2:

$$\Sigma(\theta) = \frac{q}{2k}(P_3^2 - P_2^2) \cdot sin^2(\theta) / \frac{d\sigma(\theta)}{d\Omega}\ . \tag{3}$$

1.1 New experimental results in the threshold region

A measurement of the reaction $p(\vec{\gamma},\pi^0)p$ [9] was performed at the Mainz Microtron MAMI [10] using the Glasgow/Mainz tagged photon facility [11, 12] and the photon spectrometer TAPS [13]. The MAMI accelerator delivered a continuous wave beam of 405–MeV electrons. Linearly polarized photons were produced via coherent bremsstrahlung in a 100–μm–thick diamond radiator [14, 15] with degrees of polarization of up to 50%. The neutral pion decay photons were detected in TAPS [16], an array of 504 BaF_2–detectors, which was built up around a liquid hydrogen target. The total and differential cross sections were measured over the energy range from π^0–threshold to 168 MeV. Fig. 1 shows the results for the total cross section in comparison to Ref. [4] and [3].

The results for the photon asymmetry are shown in Fig. 2 in comparison to the values of ChPT [8] and to a prediction of a dispersion theoretical calculation (DR) by Hanstein, Drechsel and Tiator [17]. The photon asymmetry was determined from all the data between threshold and 166 MeV for which the mean energy was 159.5 MeV. The theoretical predictions are shown for the same energy. The values for the real and imaginary part of E_{0+} and the three P–wave combinations were

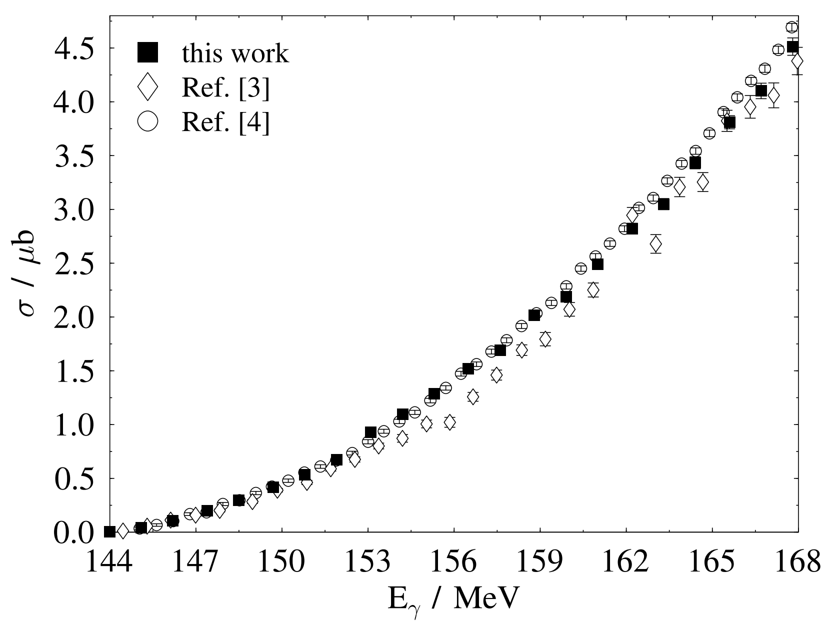

Figure 1: Total cross sections for π^0 photoproduction close to threshold with statistical errors (without systematic error of 5%) as function of incident photon energy (solid squares, this work Ref. [18], open circles, Ref. [4], open diamonds Ref. [3]).

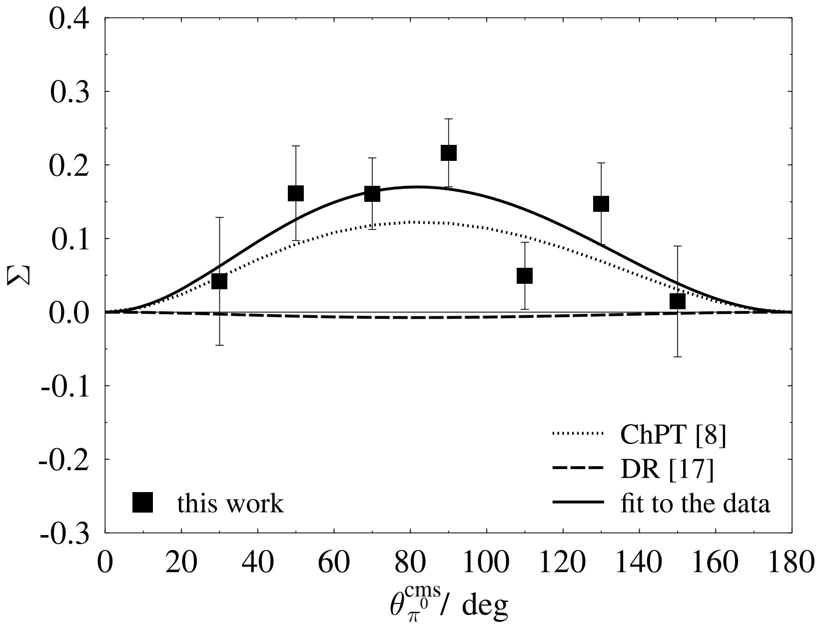

Figure 2: Photon asymmetry Σ for π^0 photoproduction at 159.5 MeV photon energy with statistical errors (without systematic error of 3%) as a function of the polar angle θ (solid line: fit to the data) in comparison to ChPT [8] (dotted line) and DR [17] (dashed line).

extracted via two multipole fits to the cross sections and the photon asymmetry simultaneously. The two multipole fits differ in the energy dependence of the real parts of the P–wave combinations. For the first fit the usual assumption of a behaviour proportional to the product of q and k was adopted (qk–fit, $\chi^2/dof = 1.28$). The assumption made for the second fit is an energy dependence of the P–wave amplitudes proportional to q (q–fit, $\chi^2/dof = 1.29$). This is the dependence which ChPT predicts for the P–wave amplitudes in the near–threshold region, but at higher energies the prediction is in between the q and qk energy dependence. The results of both multipole fits for ReE_{0+} as a function of the incident photon energy are shown in Fig. 3 and compared with the predictions of ChPT and of DR. The results for the threshold values of ReE_{0+} (at the π^0– and π^+–threshold), for the parameter β of ImE_{0+} and for the values of the threshold slopes of the three P–wave combinations of the qk–fit and the q–fit are summarized in Table 1, for more details see [18].

For both fits the low–energy theorems of ChPT ($\mathcal{O}(p^3)$) for P_1 and P_2 agree with the measured

	this work		ChPT	DR[a]
	qk–fit[a]	q–fit		
$E_{0+}(E_{thr}^{p\pi^0})$	$-1.23 \pm 0.08 \pm 0.03$	$-1.33 \pm 0.08 \pm 0.03$	-1.16	-1.22
$E_{0+}(E_{thr}^{n\pi^+})$	$-0.45 \pm 0.07 \pm 0.02$	$-0.45 \pm 0.06 \pm 0.02$	-0.43	-0.56
β	$2.43 \pm 0.28 \pm 1.0$	$5.2 \pm 0.2 \pm 1.0$	2.78	3.6
P_1	$9.46 \pm 0.05 \pm 0.28$	$9.47 \pm 0.08 \pm 0.29$	9.14 ± 0.5	9.55
P_2	$-9.5 \pm 0.09 \pm 0.28$	$-9.46 \pm 0.1 \pm 0.29$	-9.7 ± 0.5	-10.37
P_3	$11.32 \pm 0.11 \pm 0.34$	$11.48 \pm 0.06 \pm 0.35$	10.36	9.27
P_{23}	10.45 ± 0.07	10.52 ± 0.06	11.07	9.84

Table 1: Results of both fits (qk–fit and q–fit) for ReE_{0+} at the π^0– and π^+–threshold (unit: $10^{-3}/m_{\pi^+}$), for the parameter β of ImE_{0+} (unit: $10^{-3}/m_{\pi^+}^2$) and for the three combinations of the P–wave amplitudes (unit: $q \cdot 10^{-3}/m_{\pi^+}^2$) with statistical and systematic errors in comparison to the predictions of ChPT [8,19] ($\mathcal{O}(p^3)$) and of a dispersion theoretical approach (DR, [17]). ([a] Values of the P–wave combinations converted into the unit $q \cdot 10^{-3}/m_{\pi^+}^2$.)

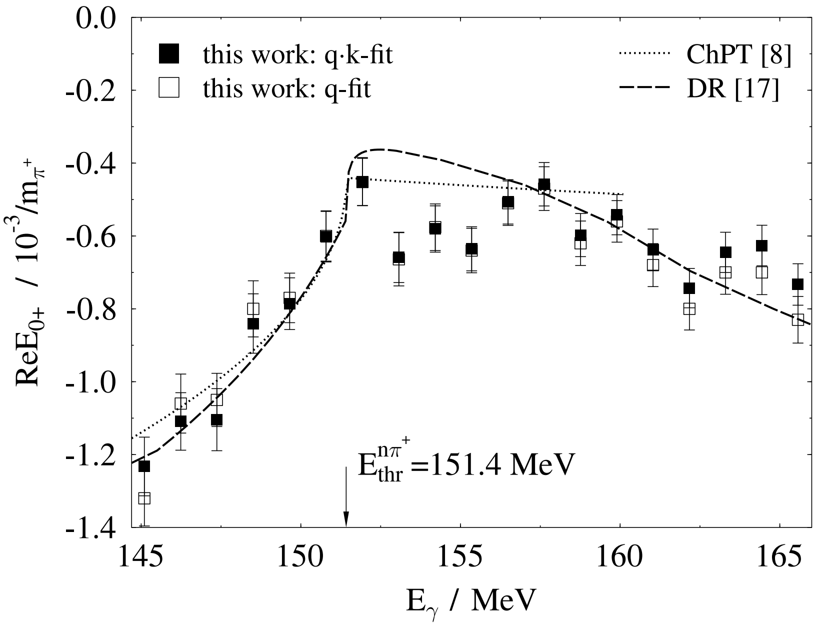

Figure 3: Results for ReE_{0+} with statistical errors as a function of incident photon energy E_γ for an assumed energy dependence of the P–wave amplitudes proportional to $q \cdot k$ (solid squares) and q (open squares) in comparison to ChPT [8] (dotted line) and DR [17] (dashed line).

experimental results within their systematic and statistical errors. The experimental value for P_3 is higher than the value of ChPT, which can be explained by the smaller total and differential cross sections of Ref. [3], used by ChPT to determine the dominant low–energy constant b_P for this multipole [19]. A new fourth–order calculation in heavy–baryon ChPT by Bernard *et al.*, introduced in [20] and compared to the new MAMI data presented in this letter, shows, that the potentially large Δ–isobar contributions are cancelled by the fourth–order loop corrections to the P–wave low–energy theorems. This gives confidence in the third–order LET predictions for P_1 and P_2, which are in agreement with the present MAMI data. With the new value of b_P [20], fitted to the present MAMI data, the ChPT calculation is in agreement with the measured photon asymmetry.

2 The $\gamma N \to \Delta(1232)$ transition and the E2/M1 ratio

Low energy electromagnetic properties of baryons, such as mass, charge radius, magnetic and quadrupole moments are important observables for any model of the nucleon structure. In various constituent–quark models a tensor force in the inter–quark hyperfine interaction, introduced first by de Rujula, Georgi and Glashow [21], leads to a d–state admixture in the baryon ground–state wave–function. As a result the tensor force induces a small violation of the Becchi–Morpurgo selection rule [22], that the $\gamma N \to \Delta(1232)$ excitation is a pure $M1$ (magnetic dipole) transition, by introducing a non–vanishing $E2$ (electric quadrupole) amplitude. For chiral quark models or in the Skyrmion picture of the nucleon, the main contribution to the $E2$ strength stems from tensor correlations between the pion cloud and the quark bag, or meson exchange currents between the quarks. To observe a static deformation (d–state admixture) a target with a spin of at least 3/2 (e.g. Δ matter) is required. The only realistic alternative is to measure the transition $E2$ moment in the $\gamma N \to \Delta$ transition at resonance, or equivalently the $E_{1+}^{3/2}$ partial wave amplitude in the $\Delta \to N\pi$ decay. The experimental quantity of interest to compare with the different nucleon models is the ratio $R_{EM} = E2/M1 = E_{1+}^{3/2}/M_{1+}^{3/2}$ of the electric quadrupole $E2$ to the magnetic dipole $M1$ amplitude in the region of the $\Delta(1232)$ resonance. In quark models with $SU(6)$ symmetry, for example the MIT bag model, $R_{EM} = 0$ is predicted. Depending on the size of the hyperfine interaction and the bag radius, broken $SU(6)$ symmetry leads to $-2\% < R_{EM} < 0$ [23–26]. Larger negative values in the range $-6\% < R_{EM} < -2.5\%$ have been predicted by Skyrme models [27] while results from chiral bag models [28] give values in the range -2% to -3%. The first Lattice QCD result is $R_{EM} = (+3\pm9)\%$ [29] and a quark model with exchange currents yields values of about -3.5% [30].

The determination of the quadrupole strength $E2$ in the region of the $\Delta(1232)$ resonance has been the aim of a considerable number of experiments and theoretical activities in the last few years. Experimental results have been published for the differential cross section and photon asymmetry of pion photoproduction off the proton from the Mainz Microtron MAMI and the laser backscattering facility LEGS at Brookhaven National Laboratory, with the results $R_{EM} = -(2.5\pm0.2_{stat}\pm0.2_{sys})\%$ from the Mainz group [31] and $R_{EM} = -(3.0 \pm 0.3_{stat+sys} \pm 0.2_{mod})\%$ from the LEGS group [32]. These new R_{EM} results have started intense discussions about the correct way to extract the $E2/M1$ ratio from the new experimental data. In particular the large variation in the R_{EM} values obtained in theoretical analyses of these data at RPI [33] ($R_{EM} = -(3.2 \pm 0.25)\%$), VPI [34] ($R_{EM} = -(1.5 \pm 0.5)\%$) and Mainz [35] ($R_{EM} = -(2.5 \pm 0.1)\%$) was quite unsatisfactory. Since small differences in the differential cross section occur in the mentioned MAMI/DAPHNE and LEGS experiments, a new experiment on neutral pion photoproduction off the proton has been performed at the Mainz Microtron covering the full polar angle range of the pion. The new enlarged set of experimental results should allow a determination of R_{EM} more accurately.

2.1 New Experimental Results for $\gamma N \to \Delta(1232)$

Figure 4 shows the new results for the photon asymmetry for six different energies in the Δ–resonance region. For the first time this new experiment delivers data in the full polar angle range. The new results are in good agreement with the experimental data of MAMI/DAPHNE and LEGS. In addition, the photon asymmetries of all three experiments are compared to the dispersion theoretical analysis of Hanstein [35,36] and good agreement is found.

The unpolarized differential cross sections for the same six photon energies in the Δ–resonance region are shown in Figure 5. The new results are in agreement with the MAMI/DAPHNE, the LEGS data differ not only in the absolute values of the differential cross section but show as well a different angular distribution. In addition, the results of the Hanstein analysis for the MAMI/TAPS data are shown. In the angular momentum expansion of the neutral pion photoproduction it is sufficient to take into account s– and p–waves, i.e. $l_\pi = 0$ or 1 only. The angular distributions for the unpolarized cross section $d\sigma_0/d\Omega$, the parallel part $d\sigma_{||}/d\Omega$ (pion detected in the plane defined by the photon polarization and the photon momentum vector), and perpendicular part $d\sigma_\perp/d\Omega$ can be expressed in the s– and p–wave approximation by the parametrization

$$\frac{d\sigma_j(\theta)}{d\Omega} = \frac{q}{k}\left(A_j \; + \; B_j cos(\theta) \; + \; C_j cos^2(\theta)\right) \;, \tag{4}$$

where q and k denote the center of mass momenta of the pion and the photon, respectively, and j indicates the parallel ($||$), perpendicular ($\perp$) and unpolarized (0) components. The coefficients A_j, B_j and C_j are quadratic or bilinear functions of the s– and p–wave amplitudes. In particular, $d\sigma_{||}/d\Omega$ is sensitive to the E_{1+} amplitude, because of interference with M_{1+} in the terms

$$A_{||} \;=\; \mid E_{0+} \mid^2 + \mid 3E_{1+} - M_{1+} + M_{1-} \mid^2 \;, \tag{5}$$

$$B_{||} \;=\; 2\mathrm{Re}[E_{0+}(3E_{1+} + M_{1+} - M_{1-})^*] \;, \tag{6}$$

$$C_{||} \;=\; 12\mathrm{Re}[E_{1+}(M_{1+} - M_{1-})^*] \;. \tag{7}$$

Furthermore, the ratio

$$R = \frac{1}{12}\frac{C_{||}}{A_{||}} = \frac{\mathrm{Re}(E_{1+}(M_{1+} - M_{1-})^*)}{\mid E_{0+} \mid^2 + \mid 3E_{1+} + M_{1+} - M_{1-} \mid^2} \tag{8}$$

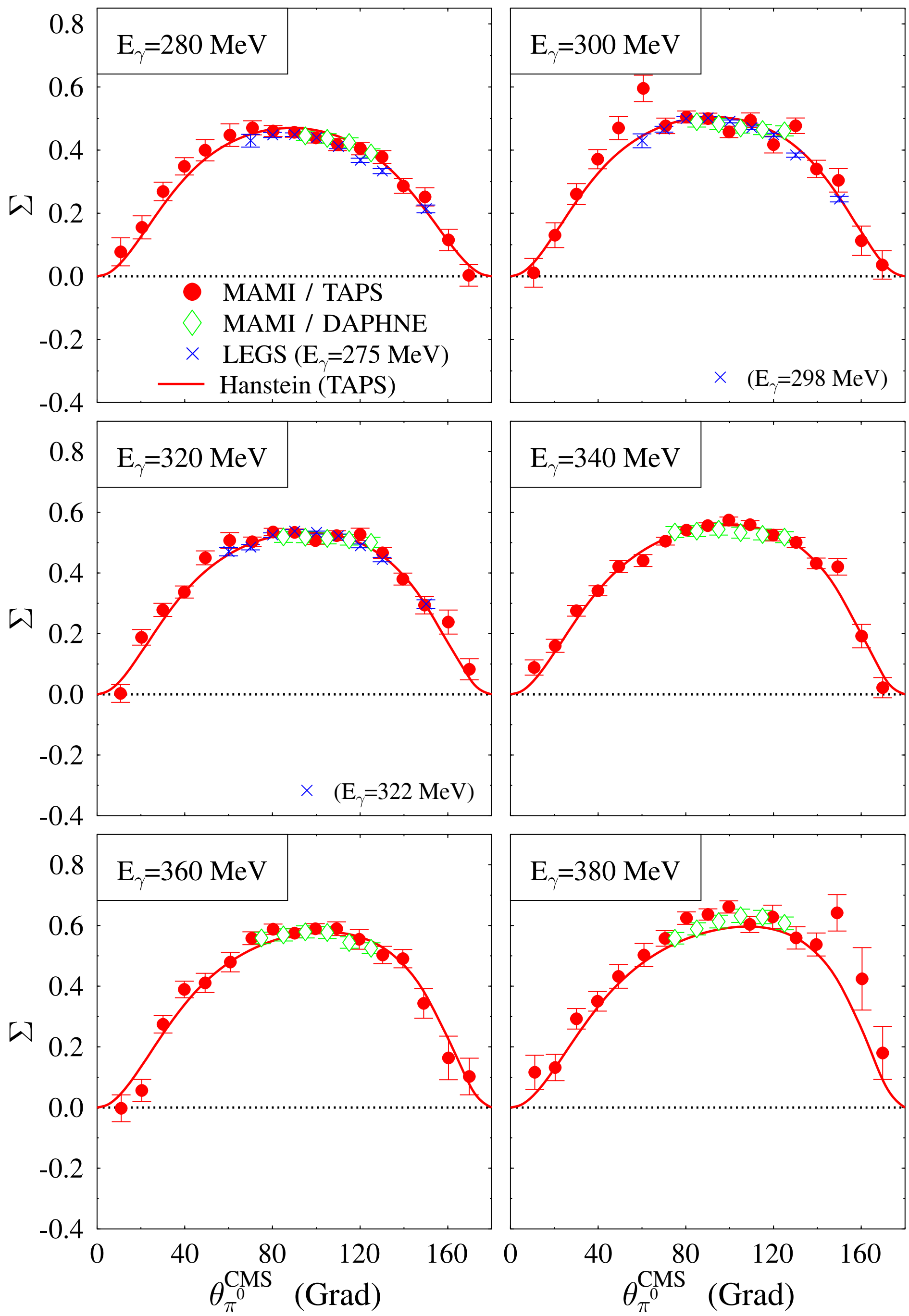

Figure 4: Photon asymmetries Σ in the Δ–resonance region (solid circles, this work Ref. [38], open diamonds Ref. [31] and crosses Ref. [32]).

can be identified with the ratio $R_{EM} = E_{1+}^{3/2}/M_{1+}^{3/2}$ at the $\Delta(1232)$ resonance ($\delta_{33} = 90°$)

$$R \simeq R_{EM} = \left.\frac{\mathrm{Im}E_{1+}^{3/2}}{\mathrm{Im}M_{1+}^{3/2}}\right|_{W=M_\Delta} . \tag{9}$$

This is the crucial point of our analysis [37]. This method offers the advantage of being independent of absolute normalization and insensitive to many systematic errors, because R_{EM} is extracted from

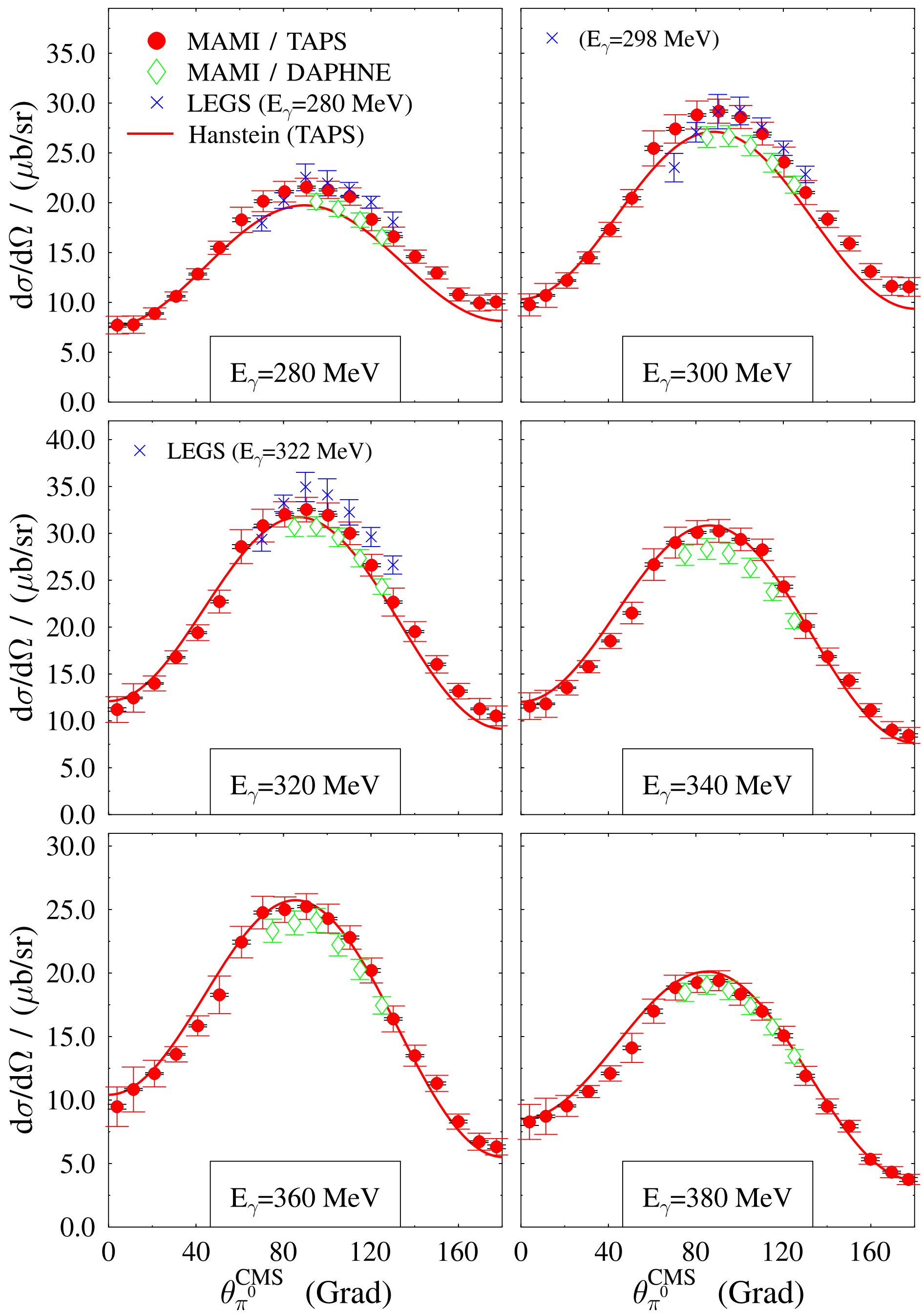

Figure 5: Differential cross sections in the Δ–resonance region. MAMI/TAPS results are shown with statistical (1-2 %) and systematic errors (solid circles, this work Ref. [38], open diamonds Ref. [31] and crosses Ref. [32]).

the ratio of the coefficients $C_{||}$ and $A_{||}$ fitted to the angular distribution of $d\sigma_{||}/d\Omega$. Further, the following indentity can be derived [38]:

$$R = \frac{1}{12}\frac{C_{||}}{A_{||}} = \frac{1}{12}\frac{\frac{C}{A} + \Sigma(\theta = 90^\circ)}{1 - \Sigma(\theta = 90^\circ)} \approx R_{EM} \;, \tag{10}$$

which depends only on the shape (C/A) of the differential cross section $d\sigma/d\Omega$ and the photon asymmetry Σ at $\theta^{CMS} = 90°$. Using Equation 10, a value for the ratio R_{EM} can be extracted [38]:

$$R_{EM} = (-2.4 \pm 0.16_{stat.} \pm 0.24_{sys})\% \; . \tag{11}$$

Acknowledgment: This work is supported by Deutsche Forschungsgemeinschaft (SFB 201 and SFB 443).

References

[1] E. Mazzucato *et al.*, Phys. Rev. Lett. **57**, 3144 (1986).
[2] R. Beck *et al.*, Phys. Rev. Lett. **65**, 1841 (1990).
[3] M. Fuchs *et al.*, Phys. Lett. **B368**, 20 (1996).
[4] J. C. Bergstrom *et al.*, Phys. Rev. **C53**, R1052 (1996); Phys. Rev. **C55**, 2016 (1997).
[5] P. de Baenst, Nucl. Phys. **B24**, 633 (1970).
[6] I. A. Vainshtein and V. I. Zakharov, Nucl. Phys. **B36**, 589 (1972).
[7] V. Bernard, J. Gasser, N. Kaiser, and U.–G. Meißner, Phys. Lett. **B268**, 291 (1991).
[8] V. Bernard, N. Kaiser, and U.–G. Meißner, Z. Phys. **C70**, 483 (1996).
[9] A. Schmidt, Ph.D. thesis, University Mainz (2001), nucl-ex/0105010 (2001) to be published in Phys. Rev. Lett.
[10] H. Herminghaus, K.H. Kaiser, and H. Euteneuer, Nucl. Instr. and Meth. A **138** 1 (1976).
[11] I. Anthony *et al.*, Nucl. Instrum. Meth. A **301** 230 (1991).
[12] S. J. Hall *et al.*, Nucl. Instrum. Meth. A **368**, 698 (1996).
[13] R. Novotny, IEEE Trans. Nucl. Sci **38**, 379 (1991)
[14] D. Lohmann, and J. Peise *et al.*, Nucl. Instr. and Meth. **A343**, 494 (1994)
[15] A. Schmidt, Diplomarbeit, University Mainz (1995).
[16] R. Novotny, IEEE Trans. Nucl. Sci **43**, 1260 (1996).
[17] O. Hanstein, D. Drechsel, and L. Tiator, Phys. Lett. **B399**, 13 (1997).
[18] A. Schmidt, Phys. Rev. Lett. in print and nucl-ex/0105010.
[19] V. Bernard, N. Kaiser, and U.–G. Meißner, Phys. Lett. **B378**, 337 (1996).
[20] V. Bernard, N. Kaiser, and U.–G. Meißner, Eur. Phys. J. **A11**, 209 (2001).
[21] A. Rujula, H. Georgi and S.L. Glashow, Phys. Rev. **D12**, 147 (1975).
[22] C. Becchi and G. Morpurgo, Phys. Lett. **17**, 352 (1965).
[23] R. Koniuk and N. Isgur, Phys. Rev. **D21**, 1868 (1980).
[24] S.S. Gershteyn *et al.*, Sov. J. Nucl. Phys. **34**, 870 (1981).
[25] D. Drechsel and M.M. Giannini, Phys. Lett. **B143**, 329 (1984).
[26] S. Capstick, Phys. Rev. **D46**, 2864 (1992).
[27] A. Wirzba and W. Weise, Phys. Lett. **B188**, 6 (1987).
[28] K. Bermuth *et al.*, Phys. Rev. **D37**, 89 (1988).
[29] D.B. Leinweber, Proc. Int. Conf. "Baryons92" page 29 (1992).
[30] A. Buchmann *et al.*, Phys. Rev. **C55**, 448 (1997).
[31] R. Beck and H.-P. Krahn *et al.*, Phys. Rev. Lett **78**, 606 (1997).
[32] G. S. Blanpied *et al.*, Phys. Rev. Lett. **79**, 4337 (1997).
[33] R.M. Davidson and N.C. Mukhopadhyay, Phys. Rev. Lett **79**, 4509 (1997).
[34] G. Keaton and R.L. Workman, Phys. Rev. Lett **79**, 4511 (1997).
[35] O. Hanstein *et al.*, Phys. Lett. **B385**, 45 (1996).
[36] O. Hanstein *et al.*, Nucl. Phys. **A632**, 561 (1998).
[37] R. Beck *et al.*, Phys. Rev. **C 61**, 035204 (2000).
[38] R. Leukel, Ph.D. thesis, University Mainz, 2001.

Baryon spectroscopy at the Beijing Electron Positron Collider

B.S. Zou, X.B. Ji, and H.X. Yang, representing the BES Collaboration

Institute of High Energy Physics, CAS, P.O. Box 918 (4), Beijing 100039, P.R. China

(Received: 27 October 2001)

The BES Collaboration has collected 58 million J/ψ events at the Beijing Electron-Positron Collider (BEPC). J/ψ decays provide an excellent place for studying excited nucleons and hyperons—N^*, Λ^*, Σ^* and Ξ^* resonances. Physics motivation, data status, partial wave analyses and future prospects are presented for the baryon resonance program at BES.

1 Physics motivation

Baryons are the basic building blocks of our world. If we cut any piece of object smaller and smaller, we will finally reach the nucleons, *i.e.*, the lightest baryons, and we cannot cut them smaller any further. So without mention any theory, we know that the study of baryon structure is at the forefront of exploring microscopic structure of matter. From theoretical point of view, since baryons represent the simplest system in which the three colors of QCD neutralize into colorless objects and the essential non-Abelian character of QCD is manifest, understanding the baryon structure is absolutely necessary before we claim that we really understand QCD.

Spectroscopy has long proved to be a powerful tool for exploring internal structures and basic interactions of microscopic world. Ninety years ago detailed studies of atomic spectroscopy resulted in the great discovery of Niels Bohr's atomic quantum theory [1]. Forty to sixty years later, still detailed studies of nuclear spectroscopy resulted in Nobel Prize winning discoveries of nuclear shell model [2] and collective motion model [3] by Aage Bohr *et al.* Comparing with the atomic and nuclear spectroscopy at those times, our present baryon spectroscopy is still in its infancy [4]. Many fundamental issues in baryon spectroscopy are still not well understood [5]. The possibility of new, as yet unappreciated, symmetries could be addressed with accumulation of more data. The new symmetries may not have obvious relation with QCD, just like nuclear shell model and collective motion model.

Joining the new effort on studying the excited nucleons, N^* baryons, at new facilities such as CEBAF at JLab, ELSA at Bonn, GRAAL at Grenoble and SPRING8 at JASRI, we also started a baryon resonance program at BES [6], at the Beijing Electron-Positron Collider (BEPC). The J/ψ and ψ' experiments at BES provide an excellent place for studying excited nucleons and hyperons—N^*, Λ^*, Σ^* and Ξ^* resonances [7]. The corresponding Feynman graph for the production of these excited nucleons and hyperons is shown in Fig. 1 where Ψ represents either J/ψ or ψ'.

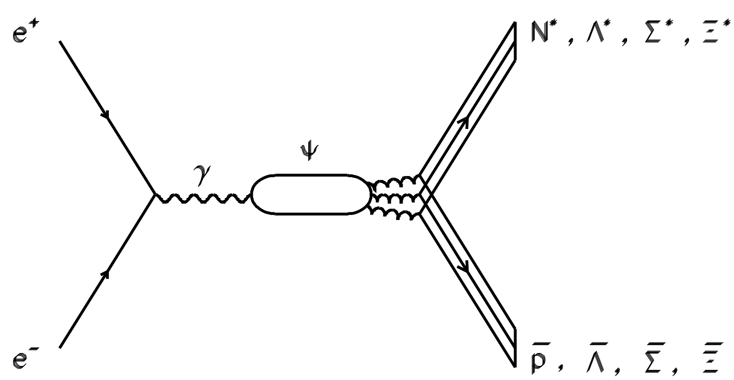

Figure 1: $\bar{p}N^*$, $\bar{\Lambda}\Lambda^*$, $\bar{\Sigma}\Sigma^*$ and $\bar{\Xi}\Xi^*$ production from e^+e^- collision through the Ψ meson.

Comparing with other facilities, our baryon program has advantages in at least three obvious aspects:

(1) We have pure isospin 1/2 πN and $\pi\pi N$ systems from $J/\psi \to \bar{N}N\pi$ and $\bar{N}N\pi\pi$ processes due to isospin conservation, while πN and $\pi\pi N$ systems from πN and γN experiments are mixture of isospin 1/2 and 3/2, and suffer difficulty on the isospin decomposition;

(2) ψ mesons decay to baryon-antibaryon pairs through three or more gluons. It is a favorable place for producing hybrid (qqqg) baryons, and for looking for some "missing" N^* resonances which have weak coupling to both πN and γN, but stronger coupling to g^3N;

(3) Not only N^*, Λ^*, Σ^* baryons, but also Ξ^* baryons with two strange quarks can be studied. Many QCD-inspired models [8, 9] are expected to be more reliable for baryons with two strange quarks due to their heavier quark mass. More than thirty Ξ^* resonances are predicted where only two such states are well established by experiments. The theory is totally not challenged due to lack of data.

2 Data status

The BEijing Spectrometer (BES) is a conventional solenoidal magnet detector that is described in detail in Ref. [10]. A four-layer central drift chamber (CDC) surrounding the beampipe provides trigger information. A forty-layer cylindrical main drift chamber (MDC), located radially outside the CDC, provides trajectory and energy loss (dE/dX) information for charged tracks over 85% of the total solid angle. An array of 48 scintillation counters surrounding the MDC measures the time-of-flight (TOF) of charged tracks. Radially outside of TOF system is a 12 radiation length thick, lead-gas barrel shower counter (BSC) operating in the limited streamer mode. This device covers $\sim$ 80% of the total solid angle and measures the energies of electrons and photons.

BES started data-taking in 1989 and was upgraded in 1998. The upgraded BES is named BESII while the previous one is called BESI. BESI collected 7.8 million J/ψ events and 3.7 million ψ' events. BESII has collected 50 million J/ψ events.

Based on 7.8 million J/ψ events collected at BESI before 1996, the events for $J/\Psi \to \bar{p}p\pi^0$ and

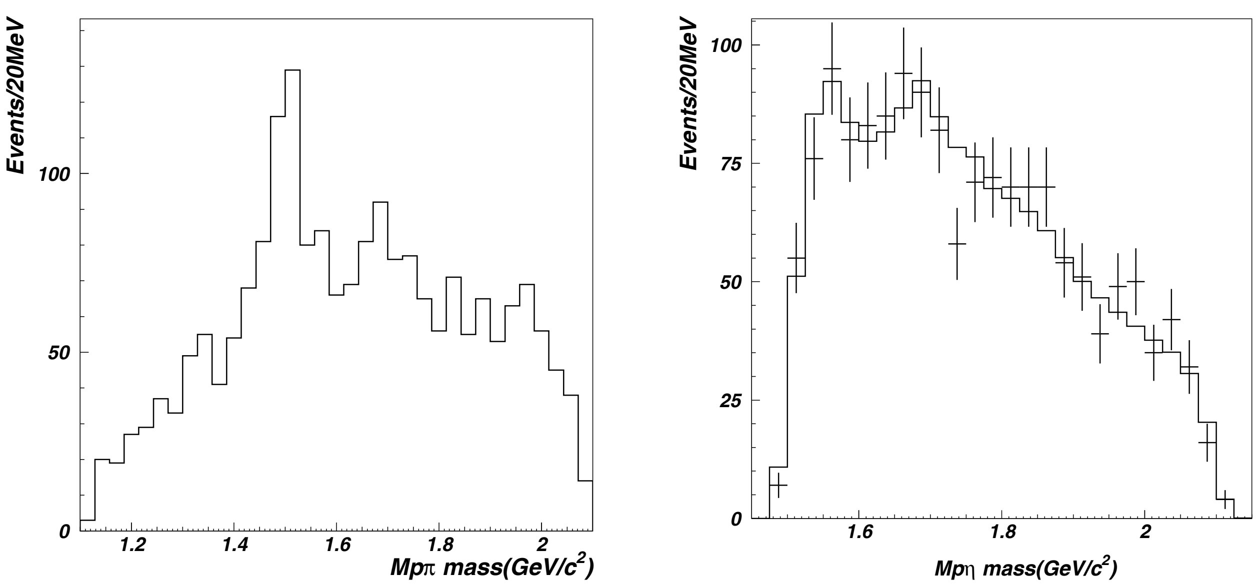

Figure 2: Left: $p\pi^0$ invariant mass spectrum for $J/\psi \to \bar{p}p\pi^0$; right: $p\eta$ invariant mass spectrum for $J/\psi \to \bar{p}p\eta$. BESI data

$\bar{p}p\eta$ have been selected and reconstructed with π^0 and η detected in their $\gamma\gamma$ decay mode [6]. The corresponding $p\pi^0$ and $p\eta$ invariant mass spectra are shown in Fig. 2 with clear peaks around 1500 and 1670 MeV for $p\pi^0$ and clear enhancement around the $p\eta$ threshold, peaks at 1540 and 1650 MeV for $p\eta$.

With 50 million new J/ψ events collected by BESII of improved detecting efficiency, we expect to have one order of magnitude more reconstructed events for each channel. We show in Figs.3 and 4 preliminary results for $J/\psi \to p\bar{n}\pi^-$ [11] and $J/\psi \to pK^-\bar{\Lambda} + h.c.$ [12] channels, respectively. For $J/\psi \to p\bar{n}\pi^-$ channel, proton and π^- are detected. With some cuts of backgrounds, the missing mass spectrum shows a very clean peak for the missing antineutron with negligible backgrounds; The $N\pi$ invariant mass spectrum of 28,904 reconstructed events from half BESII data looks similar to the $p\pi$ invariant mass spectrum for $J/\psi \to p\bar{p}\pi^0$ as in Fig. 2, but with much higher statistics. For $J/\psi \to pK^-\bar{\Lambda}$ and $\bar{p}K^+\Lambda$ channels, there are clear Λ^* peaks at 1.52 GeV, 1.69 GeV and 1.8 GeV in pK invariant mass spectrum, and N^* peaks near $K\Lambda$ threshold and 1.9 GeV for $K\Lambda$ invariant mass spectrum.

We are also reconstructing $J/\psi \to \bar{p}p\omega$, $\bar{p}p\pi^+\pi^-$ and other channels. The $\bar{p}p\omega$ channel suffers larger background and the $\bar{p}p\pi^+\pi^-$ suffers the complication of $\pi\pi$ S-wave interaction [4,13].

3 Partial wave analyses

In order to get more useful information about properties of the baryon resonances, such as their J^{PC} quantum numbers, mass, width, production and decay rates, etc., partial wave analyses (PWA) are necessary.

The basic procedure for our partial wave analyses is the standard maximum likelihood method:
(1) construct amplitudes A_i for each i-th possible partial waves;
(2) from linear combination of these partial wave amplitudes, get the total transition probability for each event as $w = |\sum_i c_i A_i|^2$ with c_i as free parameters to be determined by fitting data;
(3) maximize the following likelihood function $\mathcal{L}$ to get c_i parameters as well as mass and width

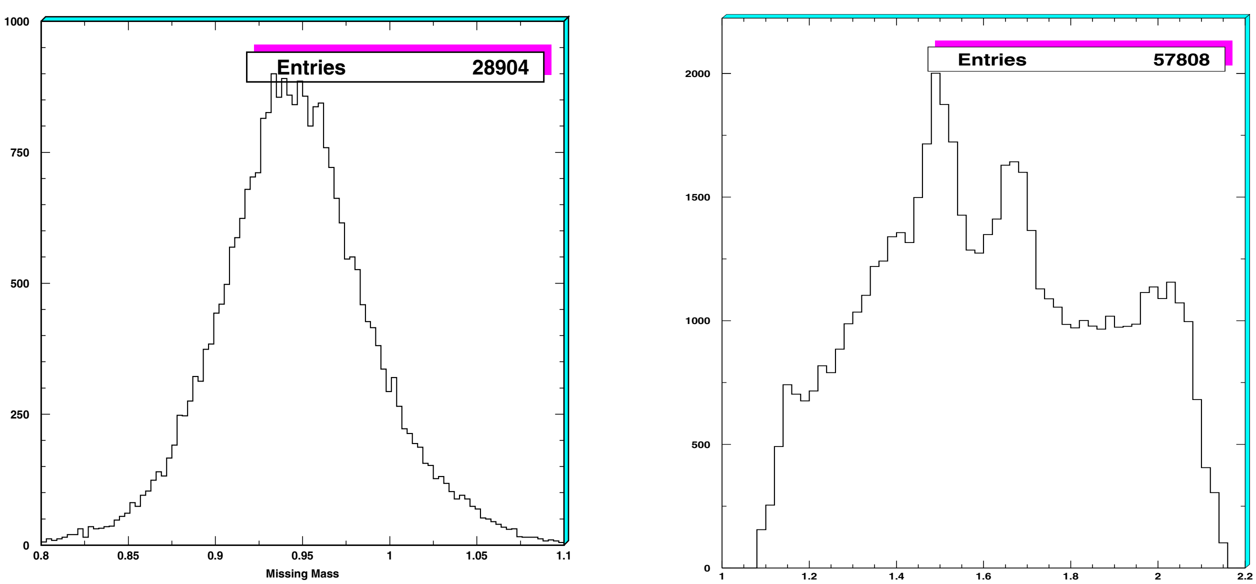

Figure 3: Left: missing mass spectrum against $p\pi^-$ for $J/\psi \to \bar{n}p\pi^-$; right: $p\pi^-$&$\bar{n}\pi^-$ invariant mass spectrum for $J/\psi \to \bar{n}p\pi^-$. Preliminary BESII data.

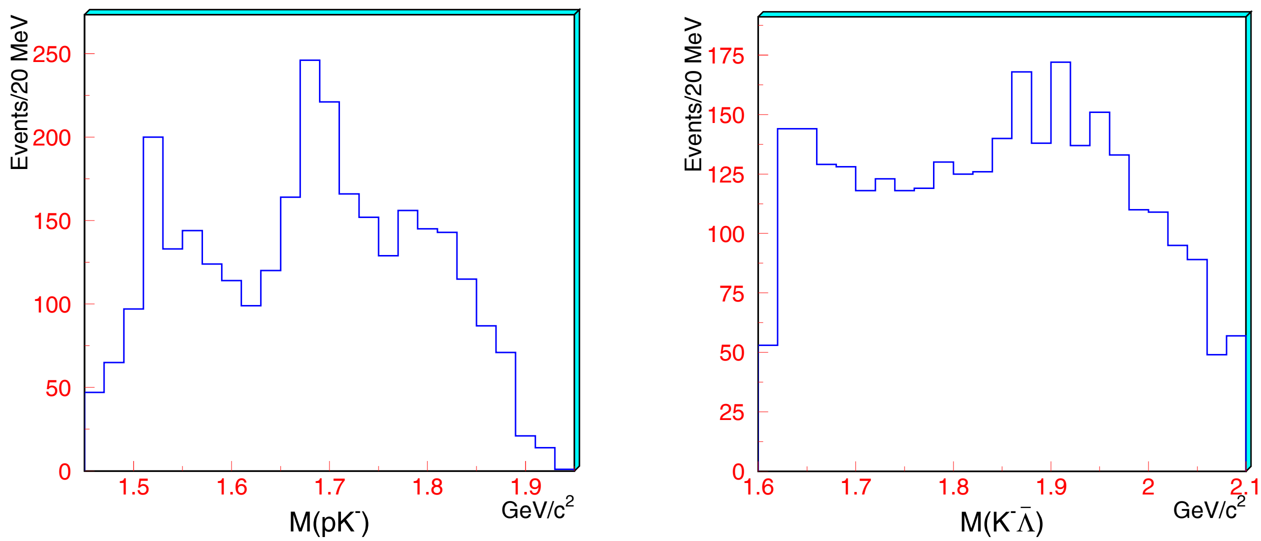

Figure 4: Left: pK invariant mass spectrum for $J/\psi \to pK\Lambda$; right: $K\Lambda$ invariant mass spectrum for $J/\psi \to pK\Lambda$. Preliminary BESII data.

parameters for the resonances,

$$\mathcal{L} = \prod_{n=1}^{N} \frac{w_{data}}{\int w_{MC}} \ ,$$

where N is the number of reconstructed data events and w_{data}, w_{MC} are evaluated for data and Monte Carlo events, respectively.

For the construction of partial wave amplitudes, we assume the effective Lagrangian approach [14,15] with Rarita-Schwinger formalism [16–18]. In this approach, there are three basic elements for constructing amplitudes: particle spin wave functions, propagators and effective vertex couplings; the amplitude can be written out by Feynman rules for tree diagrams.

For example, for $J/\psi \to \bar{N}N^*(3/2+) \to \bar{N}(k_1,s_1)N(k_2,s_2)\eta(k_3)$, the amplitude can be constructed as

$$A_{3/2+} = \bar{u}(k_2,s_2)k_{2\mu}P^{\mu\nu}_{3/2}\big(c_1 g_{\nu\lambda} + c_2 k_{1\nu}\gamma_\lambda + c_3 k_{1\nu}k_{1\lambda}\big)\gamma_5 v(k_1,s_1)\psi^\lambda \ ,$$

where $u(k_2,s_2)$ and $v(k_1,s_1)$ are 1/2-spinor wave functions for N and $\bar{N}$, respectively; ψ^λ the spin-1 wave function, *i.e.*, polarization vector, for J/ψ. The c_1, c_2 and c_3 terms correspond to three possible couplings for the $J/\psi \to \bar{N}N^*(3/2+)$ vertex. The c_1, c_2 and c_3 can be taken as constant parameters or with some smooth vertex form factors in them if necessary. The spin 3/2 propagator $P^{\mu\nu}_{3/2}$ for $N^*(3/2+)$ is

$$P^{\mu\nu}_{3/2} = \frac{\gamma\cdot p + M_{N*}}{M^2_{N*} - p^2 - iM_{N*}\Gamma_{N*}}\left[g^{\mu\nu} - \frac{1}{3}\gamma^\mu\gamma^\nu - \frac{2p^\mu p^\nu}{3M^2_{N*}} + \frac{p^\mu\gamma^\nu - p^\nu\gamma^\mu}{3M_{N*}}\right] \ ,$$

with $p = k_2 + k_3$.

Other partial wave amplitudes can be constructed similarly [19]. Programming these amplitudes and maximum likelihood method to fit the data is straightforward, but very tedious. Now we are extending the automatic Feynman Diagram Calculation (FDC) package [20] to work for our partial wave analyses of baryon resonance channels. Using the extended FDC package, we have performed a partial wave analysis of the $\bar{p}p\eta$ channel [6] of BESI data and are now working on more channels.

For the $\bar{p}p\eta$ channel, there is a definite requirement for a $J^P = \frac{1}{2}^-$ component at $M = 1530 \pm 10$ MeV with $\Gamma = 95 \pm 25$ MeV near the ηN threshold. In addition, there is an obvious resonance around 1650 MeV with $J^P = \frac{1}{2}^-$ preferred, $M = 1647 \pm 20$ MeV and $\Gamma = 145^{+80}_{-45}$ MeV. These two N^* resonances are believed to be the two well established states, $S_{11}(1535)$ and $S_{11}(1650)$, respectively. In the higher $p\eta(\bar{p}\eta)$ mass region, there is a evidence for a structure around 1800 MeV; with BESI statistics we cannot determine its quantum numbers.

For the $S_{11}(1535)$ propagator, we tried both constant and energy-dependent width. The Breit-Wigner mass is not sensitive at all to these two choices. The Breit-Wigner width differs by 10 MeV for these two choices: $\Gamma = 90 \pm 20$ MeV for the case of a constant width and $\Gamma = 100 \pm 20$ MeV for the case of an energy-dependent width assuming 50% to ηN and 50% to πN. The pole position $(M, \Gamma/2)$ is $(1530, 45)$ MeV and $(1512, 46)$ MeV for assuming constant width and the energy-dependent width, respectively.

Preliminary partial wave analysis [11] of BESII data on $\bar{n}p\pi^-$ channel gives a similar result on $N^*(1535)$ with much smaller error bars. The outstanding narrow peak around 1.5 GeV in the πN invariant mass spectrum demands $N^*(1535)$ to be narrow (width definitely less than 120 MeV) rather model independently, while PDG gives a width of $100 \sim 250$ MeV.

4 Future prospects

BESII just finished data-taking for the 50 million J/ψ events in last May. We are now working on partial wave analyses of $J/\psi \to p\bar{n}\pi^-$, $p\bar{p}\omega$ channels to study N^* resonances, and $pK^-\bar{\Lambda}$, $\bar{p}K^+\Lambda$ channels to study Λ^* resonances as well as $N^* \to \Lambda K$. As next step, we are going to investigate $\Lambda\bar{\Sigma}^-\pi^+$, $pK^-\bar{\Sigma}^0$ channels to study Σ^* resonances; and $K^-\Lambda\bar{\Xi}^+$, $K^+\bar{\Lambda}\Xi^-$ channels to study Ξ^* resonances. These channels are relative easy to be reconstructed by BES. For example, for $K^-\Lambda\bar{\Xi}^+$, we can select events containing K^- and Λ with $\Lambda \to p\pi^-$, then from missing mass spectrum of $K^-\Lambda$ we should be able to identify the very narrow $\bar{\Xi}^+$ peak. We will investigate more complicated channels when we get more experienced and more manpower. Meanwhile more theoretical efforts are needed for better partial wave analyses and extraction of physics from our experimental results [21].

A major upgrade of the collider to BEPC2 is planned to be finished in about 4 years. A further two order of magnitude more statistics is expected to be achieved. Such statistics will enable us to perform partial wave analyses of plenty important channels from not only J/Ψ but also Ψ' decays which will allow us to study heavier baryon resonances, *e.g.*, for mass up to 2.36 GeV for Ξ^* resonances. We expect BEPC2 to play a very important unique role in studying excited nucleons and hyperons, i.e., N^*, Λ^*, Σ^* and Ξ^* resonances, and make important discoveries for understanding microscopic structure of matter.

Acknowledgments: We would like to thank Profs. Bill Briscoe and Helmut Haberzettl for their kind invitation and financial support for our participation of this very interesting and successful conference. This work is partly supported by National Science Foundation of China under contract Nos. 19991487 and 19905011.

References

[1] N. Bohr, Phil. Mag. **26**, 1-25, 471-502, 857-875 (1913).

[2] M. Mayer and J. Jensen, *Elementary Theory of Nuclear Shell Structure*, John Wiley and Sons, Inc., New York (1955).

[3] A. Bohr and B. Mottelson, *Nuclear Structure Vol. I, Single-Particle Motion* (1969) and *Vol. II, Nuclear Deformations* (1975), W.A. Benjamin, Inc., Reading, Massachusetts.

[4] Particle Data Group, Euro. Phys. J. **C15**, 1 (2000).

[5] S. Capstick *et al.*, hep-ph/0012238.

[6] BES Collaboration, J.Z. Bai *et al.*, Phys. Lett. **B510**, 75 (2001); BES Collaboration, H.B. Li et al., Nucl. Phys. **A675**, 189c (2000); BES Collaboration, B.S. Zou *et al.*, *Excited Nucleons and Hadronic Structure, Proc. of NSTAR2000 Conf. at JLab, Feb 2000.* Eds. V. Burkert *et al.*, World Scientific (2001) p. 155.

[7] B.S. Zou, Nucl. Phys. **A684**, 330 (2001).

[8] S. Capstick and N. Isgur, Phys. Rev. **D34**, 2809 (1986).

[9] L. Glozman, W. Plessas, K. Varga and R. Wagenbrunn, Phys. Rev. **D58**, 094030 (1998).

[10] BES Collaboration, Nucl. Instr. Methods, **A344**, 319 (1994); *ibid.*, **A458**, 627 (2001).

[11] X.B. Ji (BES Collaboration), Ph.D. thesis of Shandong University, (2001).

[12] H.X. Yang (BES Collaboration), Ph.D. thesis of IHEP, (2001); Y.C. Zhu (BES Collaboration), Nucl. Phys. **691**, 381 (2001).

[13] B.S. Zou and D.V. Bugg, Phys. Rev. **D48**, 3948 (1993); Phys. Rev. **D50**, 591 (1994).

[14] M. Benmerrouche, N.C. Mukhopadhyay and J.F. Zhang, Phys. Rev. Lett. **77**, 4716 (1996); Phys. Rev. **D51**, 3237 (1995).

[15] M.G. Olsson and E.T. Osypowski, Nucl. Phys. **B87**, 399 (1975); Phys. Rev. **D17**, 174 (1978); M.G. Olsson *et al.*, *ibid.* **17**, 2938 (1978).

[16] W. Rarita and J. Schwinger, Phys. Rev. **60**, 61 (1941).

[17] C. Fronsdal, Nuovo Cimento Suppl. **9**, 416 (1958); R.E. Behrends and C. Fronsdal, Phys. Rev. **106**, 345 (1957).

[18] S.U. Chung, *Spin Formalisms*, CERN Yellow Report 71-8 (1971); Phys. Rev. **D48**, 1225 (1993); J.J. Zhu and T.N. Ruan, Commun. Theor. Phys. **32**, 293, 435 (1999).

[19] W.H. Liang, P.N. Shen, J.X. Wang and B.S. Zou, in preparation.

[20] J.X. Wang, Comput. Phys. Commun. **77**, 263 (1993).

[21] H.Q. Jiang, talk given at this conference; B.S. Zou *et al.*, Euro. Phys. J. **A11**, 341 (2001).

Theoretical study of N^* from J/Ψ decays

H.Q. Jiang[a-d], B.S. Zou[a-d], P.N. Shen[a-d], R.G. Ping[b], G.X. Peng[a,b], and W.H. Liang[b]

[a]*CCAST (World Lab.), P.O. Box 8730, Beijing 100080*
[b]*Institute of High Energy Physics, The Chinese Academy of Sciences, Beijing 100039*
[c]*Institute of Theoretical Physics, The Chinese Academy of Sciences, Beijing 100039*
[d]*Center of Theoretical Nuclear Physics, National Laboratory of Heavy Ion Accelerator, Lanzhou 730000, P.R. China*

(Received: 18 October 2001)

J/ψ decay processes have multi-advantages in studying the structure of baryons. In this paper we discuss the study of the structure of excited nucleons by using the J/ψ hadronic decay processes. Various decay amplitudes for various intermediate resonant states are discussed in the framework of the relativistic covariant formalism. Considering the lowest-order quark diagrams for baryon-antibaryon pair productions from the J/ψ decays we calculated the baryon-antibaryon angular distributions. We find that the process $J/\psi \to \bar{p}N^*$ or $p\bar{N}^*$ provides a new way to probe the internal structure of the N* resonances. A quark model calculation for $J/\psi \to \bar{p}p$, $N^*(1440)\bar{p}$ and $N^*\bar{N}^*$ are presented. The implication for the internal structure of $N^*(1440)$ is discussed.

1 Introduction

The information sources of excited states of the nucleon mainly come from the formation and production experiments induced by pions and photons [1]. The conventional masses, pole positions, widths, and elasticities of the N^* resonances come largely from partial-wave analysis of pion-nucleon total, elastic, and charge-exchange scattering data [2]. Partial-wave analysis have also been performed on much smaller data set to get $N\eta$, ΛK, and ΣK branching fractions. Other branching fractions come from isobar-model analysis of $\pi N \to \pi\pi N$ data. All electromagnetic properties of the N^* resonances are $N\gamma$ couplings,which are obtained in the partial-wave analysis of the single-pion photo-production, η photo-production, and the Compton scattering. Most photo-production analysis has taken the existence, masses, and widths of the resonances from the $\pi N \to \pi N$ analysis, and has only determined the $N\gamma$ couplings.

However, there are some problems in the study of N^* resonances. Some masses of excited nucleons can not be theoretically reproduced and much more baryons are predicted than the observed states [3]. Besides, the experimental uncertainties for the masses and widths are large. On the other hand, QCD is a fundamental theory for strong interactions. However, from theoretical point of view, one faces non-perturbation QCD problem here. One has to make models for the structure of the nucleon. Therefore, the calculated results are model dependent. According to the standard quark-model, baryons are made of three quarks. What are the excitation modes? Spin-orbital excitation, unstable meson-nucleon bound states or quark-diquark structure? Many fundamental issues are still not well understood. For example, the special place in the spectrum for the Roper resonance is a well-known long-standing problem. It has therefore been suggested [4] that the Roper resonance is a gluonic excitation state of the nucleon, i.e., a "hybrid baryon". A new generation of experiments on N^* physics with electromagnetic probes has recently been started at new facilities such as CEBAF at JLAB, ELSA at Bonn, GRAAL at Grenoble. The main goal of modern N^* experiments is to determine the full spectrum of excited states.

In the analysis of the pion and photon induced reactions, one of the difficulties is the decomposition of isospin 1/2 and 3/2 resonances, which causes large uncertainty. Recently, it has been pointed out that the data of J/Ψ decays collected at the Beijing Electron-Positron Collider (BEPC) can

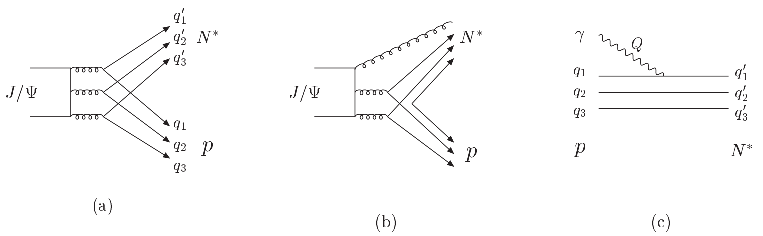

Figure 1: Diagram for N^* production from J/Ψ decays for (a) 3-quarks (qqq) N^* and (b) hybrid (qqqg) N^*, and from (c) γN reaction.

also be used to study the properties of light baryon resonances with the following advantages [7].

1) Because the isospins of J/Ψ and $\bar{p}$ are 0 and $\frac{1}{2}$, respectively, the isospin of N^* in $J/\Psi \to \bar{p}N^*$ can only be $\frac{1}{2}$. The simplest isospin structure makes the analysis much easier.

2) J/Ψ decay is a gluon-rich process. A typical picture of the process $J/\Psi \to \bar{p}N^*$ or $p\bar{N}^*$ is plotted in Fig. 1(a). Meanwhile J/Ψ is also possible to decay into $\bar{p}$ and a hybrid baryon, shown in Fig. 1(b). Therefore, J/Ψ decay enables us to study the "normal" N^* and the hybrid N^* simultaneously. It should be noted that this process can also be utilized to study excited hyperon (Y^*) spectra since gluon is flavor-blind.

3) Comparing to the photo-production process, Fig. 1(c), one finds that in the J/Ψ decay case, shown in Fig. 1(a), three created quarks are more symmetric, while in the $\gamma p \to N^*$ process, presented in Fig. 1(c), the photon coupled quark is in the asymmetric status to the rest two quarks. Therefore the processes $J/\Psi \to \bar{p}N^*$ and $\gamma p \to N^*$ should be able to probe different aspects of the quark distributions inside baryons. This may help us to distinguish various quark models.

4) The annihilation cross section of e^+e^- through J/Ψ is about two order of magnitude larger than that without going through J/Ψ. The branching ratios for the channels we are interested in are large [2]. The Beijing Spectrometer (BES) at BEPC just collected 50 million J/Ψ events. The plentiful data make the N^* study possible.

2 Partial wave analysis of J/Ψ decay

In this section we briefly discuss the partial wave analysis of J/Ψ decays. Partial wave analysis (PWA) is an effective method for analyzing experimental data. There are two type of PWA, one is based on the helicity amplitude and another is in the covariant tensor formalism. The helicity of J/Ψ produced in e^+e^- annihilation is $\lambda = \pm 1$. Here we analyze J/Ψ decays in the framework of the relativistic covariant formalism. In order to write out the partial wave amplitudes, we need to know the wave functions of particles with various spins, propagators of intermediate particles and the effective vertices.

The process of $J/\Psi \to p\bar{p}\eta$ has been discussed in ref. [8]. Here we take the process $J/\Psi \to p\bar{p}\omega$ as an example to show different characters of the decay from different intermediate resonances. The Feynman diagrams for $J/\Psi \to p\bar{p}\omega$ are shown in Figure 2.

The spin of N^* can be any half integer due to spin-orbit couplings. The total amplitude is a sum of contributions from various intermediate resonances.

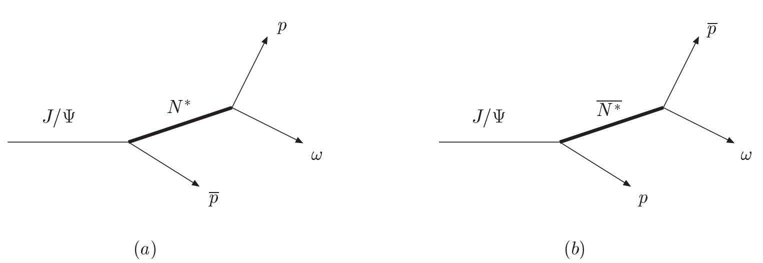

Figure 2: Feynman diagram of process $J/\Psi \to p\bar{p}\omega$ with N^* and $\bar{N}^*$ being intermediate states.

The spin-$\frac{1}{2}$ wave function is the standard Dirac spinor, which satisfies the Dirac equation. The wave function of spin-1 particle is the polarization four-vector $\epsilon^\mu(\vec{p},\lambda)$, where $\lambda = 0, \pm 1$ is the helicity of the particle. In terms of the C-G coefficient, one can write the wave function of the particle with higher spins.

We construct the propagator for the intermediate resonance with half-integer spin by a product of the projection operator of the resonance and the corresponding Breit-Wigner factor.

Constructing the effective vertices is an important step in the PWA. Generally, it is not necessary to consider the contributions of loop graphs in PWA, since these contributions have been included in the effective vertices. The effective vertices are constructed from the symmetry consideration.

The total amplitude is the superposition of various partial wave amplitudes

$$\mathcal{A} = \sum_i c_i A_i \ , \tag{1}$$

where A_i refers to a specific partial wave amplitude and the coefficient c_i is a complex free parameter which contains the information of the coupling constant and is to be determined by fitting the experimental data. Then, the differential cross-section can be written as

$$d\sigma \propto |\sum_i c_i A_i|^2 d\Phi_3(P; p_1, p_2, p_3) \ , \tag{2}$$

where $d\Phi_3$ is the Lorentz-invariant 3-body phase space.

Alternatively, Eq. (2) can be written in the following forms

$$\frac{d\sigma}{d(\cos\beta)} \propto |\sum_i c_i A_i|^2 dE_1 dE_3 d\alpha d\gamma \ , \tag{3}$$

$$\frac{d\sigma}{dm_{13}} \propto |\sum_i c_i A_i|^2 |\vec{p}_1^{\,*}||\vec{p}_2| d\Omega_1^* d\Omega_2 \ , \tag{4}$$

and

$$\frac{d\sigma}{dm_{13}^2 dm_{23}^2} \propto |\sum_i c_i A_i|^2 d\alpha d(\cos\beta) d\gamma \ , \tag{5}$$

where (α, β, γ) are three Euler angles that specify the orientation of the system of decay products relative to the decaying particle, $(|\vec{p}_2|, \Omega_2)$ is the momentum of $\bar{p}$ in the rest frame of J/Ψ, $(|\vec{p}_1^{\,*}|, \Omega_1^*)$ is the momentum of p in the rest frame of p and ω, and $m_{jk}(j,k = 1,2,3)$ is the invariant mass of particle j and particle k with $m_{jk}^2 = (p_j + p_k)^2$.

According to above equations one can calculate the angular distribution, invariant mass spectrum and the Dalitz plot for $J/\Psi \to p\bar{p}\omega$. Fitting the experimental data of the angular distribution, invariant mass spectra and the Dalitz plot by adjusting c_i's, one can extract the information of the properties of N^* resonances.

Here we only present a Monte-Carlo simulation for the invariant mass spectra of $p\omega$, the angular distributions of $\bar{p}$ and the Dalitz plots for some typical decay modes in the Fig. 3. Different interaction modes and resonances give different angular distributions, Dalitz plots and the invariant mass distributions [6]. By comparing with the data we can determine the spin of the intermediate resonance. The data analysis for $J/\Psi \to p\bar{p}\omega$ from BES is in progress.

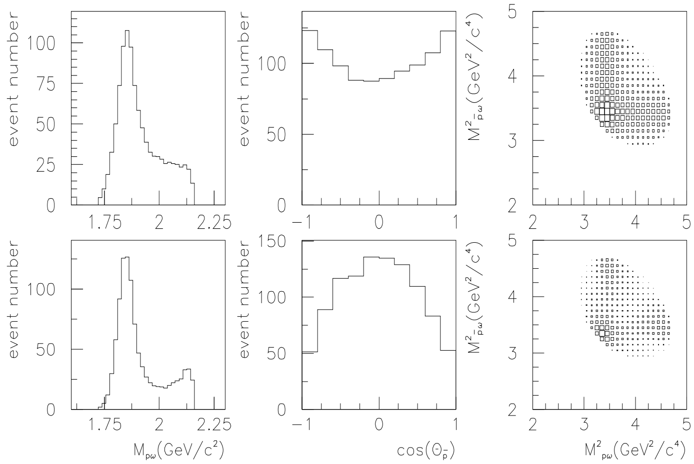

Figure 3: The upper part corresponds to the N^* resonance with $J^P_{N^*} = \frac{1}{2}^-$. The lower part corresponds to the N^* resonance with $J^P_{N^*} = \frac{3}{2}^+$.

3 The structure of N^* from J/Ψ decays

From the naive quark model, baryons are made of three quarks. The diagram for a decay of the J/Ψ into two baryons is depicted in Fig. 1(a). The basic amplitude corresponding to Fig. 1(a) can be written as

$$\begin{aligned}
&\langle q_i, s_i, q'_i, s'_i, i=1,2,3|\hat{T}|J/\Psi^{(\Lambda)}\rangle \\
&\quad = C_0 \delta^4\Big(P_\Psi - \sum_{i=1}^{3} q_i - \sum_{i=1}^{3} q'_i\Big) \cdot \epsilon_\Psi^{(\Lambda)\lambda} \cdot \frac{g_{\mu\lambda}g_{\nu\rho} + g_{\nu\lambda}g_{\mu\rho} + g_{\rho\lambda}g_{\mu\nu}}{(q_1+q'_1)^2(q_2+q'_2)^2(q_3+q'_3)^2} \\
&\quad \cdot \bar{u}(q'_1, s'_1)\gamma^\mu v(q_1, s_1)\bar{u}(q'_2, s'_2)\gamma^\nu v(q_2, s_2)\bar{u}(q'_3, s'_3)\gamma^\rho v(q_3, s_3) , \qquad (6)
\end{aligned}$$

where $\epsilon_\Psi^{(\Lambda)}$ is the polarization four-vector of J/Ψ with the helicity value Λ, P_Ψ is the four-vector momentum of J/Ψ, $q'_i, s'_i (q_i, s_i)$ are the four-vector momenta and spin z-projection of quarks (anti-quarks), respectively. We have put all color matrix elements, QCD strong coupling constants, J/Ψ decay constants, etc., into a single overall constant C_0.

The relation between the $J/\Psi \to \bar{p}N'$ amplitude and the basic quark diagram amplitude Eq. (6) is

$$\begin{aligned}
\mathcal{M}^{(\Lambda)}_{s_z, s'_z} &\equiv \langle \Psi_{\bar{p}}(q, s_z)\Psi_{N'}(q', s'_z)|\hat{T}|J/\Psi^{(\Lambda)}\rangle \\
&= \sum_{s_i, s'_i} \int \prod_{i=1}^{3} \frac{d\vec{q}_i}{(2\pi)^3 2q_i^0} \frac{d\vec{q}'_i}{(2\pi)^3 2q_i'^0} \langle \Psi_{\bar{p}}(q, s_z)\Psi_{N'}(q', s'_z)|q_i, s_i, q'_i, s'_i, i=1,2,3\rangle \\
&\quad \cdot \langle q_i, s_i, q'_i, s'_i, i=1,2,3|\hat{T}|J/\Psi^{(\Lambda)}\rangle \ . \qquad (7)
\end{aligned}$$

Here $\langle \Psi_{\bar{p}}(q, s_z)\Psi_{N'}(q', s'_z)|q_i, s_i, q'_i, s'_i, i=1,2,3\rangle$ is the product of quark model wave functions of $\bar{p}$ and N' in momentum space, with constraints $\delta^4(q - q_1 - q_2 - q_3) \cdot \delta^4(q' - q'_1 - q'_2 - q'_3)$.

The only difference between quark wave functions of the proton and $N^*(1440)$ is their spatial parts. From these amplitudes $\mathcal{M}^{(\Lambda)}_{s_z, s'_z}$, we can get the decay cross section for $J/\Psi^{(\Lambda)} \to \bar{p}N'$ as

$$d\Gamma(J/\Psi^{(\Lambda)} \to \bar{p}N') = \frac{1}{32\pi^2}\left\{\left|\mathcal{M}^{(\Lambda)}_{\frac{1}{2},\frac{1}{2}}\right|^2 + \left|\mathcal{M}^{(\Lambda)}_{\frac{1}{2},-\frac{1}{2}}\right|^2 + \left|\mathcal{M}^{(\Lambda)}_{-\frac{1}{2},\frac{1}{2}}\right|^2 + \left|\mathcal{M}^{(\Lambda)}_{-\frac{1}{2},-\frac{1}{2}}\right|^2\right\} \frac{|\vec{q}|}{M_\Psi^2} d\Omega \ , \qquad (8)$$

with Ω as the solid angle of $\vec{q}$. The calculation of $J/\Psi \to \bar{N}^*N^*$ is similar, just replacing the quark radial wave function of the anti-proton by that of the $\bar{N}^*(1440)$. With formulas above, the calculation of the decay cross sections is straightforward though tedious.

The ingredients of our quark model calculation are the spatial wave functions for the proton, anti-proton, $N^*(1440)$ and $\bar{N}^*$ and an overall normalization factor C_0. If the H. O. form is used, there are two parameters to be fixed, the constituent quark mass m_q and the harmonic-oscillator parameter α. In most quark model calculations [3, 10–13], the quark mass m_q has been chosen in the range of 220 $\sim$ 340 MeV, and α in the range of $0.06 \sim 0.22 GeV^2$ which corresponds to the nucleon radius in the range of 0.42 $\sim$ 0.8 fm. In the following, we limit our parameters in these ranges. In the J/Ψ at rest system, the two baryon clusters are moving in opposite directions with relativistic speeds, each becoming very flat. Their spatial quark wave functions in their c.m. system are related to those in this system by a Lorentz transformation [10].

The J/Ψ decay cross sections for $\bar{p}p$, $\bar{p}N^*$ and $\bar{N}^*N^{*+}$ can be expressed as

$$\frac{d\Gamma(J/\Psi^{(\pm)} \to \bar{p}p)}{d\Omega} = N_{\bar{p}p}(1 + \alpha_p cos^2\theta) \ , \tag{9}$$

$$\frac{d\Gamma(J/\Psi^{(\pm)} \to \bar{p}N^*)}{d\Omega} = R_* N_{\bar{p}p}(1 + \alpha_* cos^2\theta) \ , \tag{10}$$

$$\frac{d\Gamma(J/\Psi^{(\pm)} \to \bar{N}^*N^{*+})}{d\Omega} = R_{**} N_{\bar{p}p}(1 + \alpha_{**} cos^2\theta) \ . \tag{11}$$

Here $N_{\bar{p}p}$ is a constant direct related to the experimental branching ratio of $J/\Psi \to \bar{p}p$ and can be used to fix the overall normalization constant C_0. The experimental value for α_p is (0.62 ± 0.11) [15] and can be used to put further limit on the range of parameters α and m_q. The shaded area in Fig. 4 shows the range allowed by one standard deviation of the experimental α_p value.

In order to investigate the importance of the Lorentz contraction effect, we have also performed the calculation by ignoring this effect, *i.e.*, assuming $\vec{k}_\rho = \vec{q}_\rho$ and $\vec{k}_\lambda = \vec{q}_\lambda$. The resulted ($\alpha$, m_q) area allowed by one standard deviation of the experimental α_p value is shown in Fig. 4 by the area surrounded by the solid line. One can see that the Lorentz contraction effect is very large and cannot be ignored [14].

With (α, m_q) values in the shaded area of Fig. 4, our quark model calculation predicts $\alpha_* = 0.36 \pm 0.08$, $\alpha_{**} = 0.08 \pm 0.05$, $R_* = 2.1 \sim 4.8$ and $R_{**} = 2.0 \sim 24.0$. Mixing between the ground

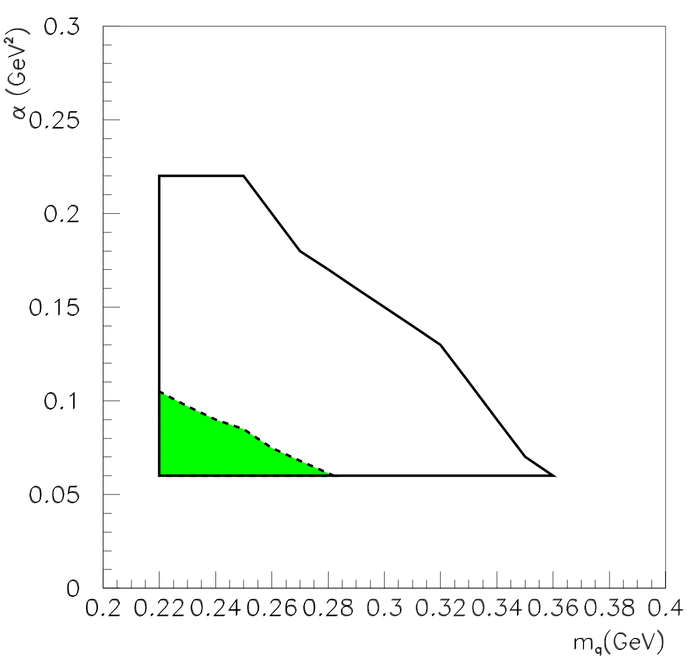

Figure 4: The constrained area for parameters (α, m_q) from experimental data $\alpha_p = 0.62 \pm 0.11$ [15]. The shaded area is the result with the Lorentz contraction effect; the area surrounded by the solid line is the result ignoring the Lorentz contraction effect.

state and the radially excited states [12] will not change our result much due to the relative negative sign of mixing for the proton and $N^*(1440)$.

There are no experimental data on $\bar{p}N^*$ and $\bar{N}^*N^*$ channels yet. However from both BESI [8] and MARKII [16] experiments, there is a clear peak around 1.5 GeV in the πN invariant mass in $J/\psi \to \bar{p}N\pi$ processes, although no partial wave analyses were performed. Very recently BESII has finished data-taking for 50 million more J/ψ events, which is about two order of magnitude more statistics than MARKII data and one order of magnitude more statistics than BESI data. With such statistics, partial wave analyses of relevant channels are possible. New experimental results on $J/\Psi \to \bar{p}p$, $J/\Psi \to \bar{p}N^*$ and $J/\Psi \to \bar{N}^*N^*$ will help us to narrow down the quark model (α, m_q) parameters and study the nature of N^*. If the $J/\Psi \to \bar{p}N^*$ production rate is significantly larger than our quark model prediction, it may indicate that the N^* is a hybrid [9]; if $J/\Psi \to \bar{p}N^*$ production rate is significantly smaller than our prediction, then it may indicate that the N^* contains a large component of πN in its internal structure [13]. For a more quantitative statement, concrete theoretical calculations for hybrid and molecule baryon production are needed. A calculation for a hybrid-baryon configuration of $N^*(1440)$ depicted in diagram 1(b) is in progress.

Acknowledgments: We thank D.V. Bugg, L. Kisslinger, H.B. Li, Y.W. Yu and Z.Y. Zhang for useful discussions and comments. This work is partly supported by the National Science Foundation of China under contract Nos. 19975053,10075057, 19991487 and 19905011.

References

[1] V.Burkert, Proceedings, *Perspectives in the structure of hadronic systems*, ed. by M.N. Harakeh *et al.*, Plenum Press, New York, 1994.

[2] Particle Data Group, Euro. Phys. J. C**15**,1 (2000) .

[3] N. Isgur and G. Karl, Phys. Rev. D**18**, 4187 (1978); *ibid.* **19**, 2653(1979); S. Capstick and N. Isgur, Phys. Rev. D **34**, 2809 (1986); L. Glozman *et al.*, Phys. Rev. D **58**, 094930 (1998); R. Bijker, F. Iachello and A. Leviatan, Ann. Phys. (N.Y.) **236**, 69 (1994); K.F. Liu and C.W. Wong, Phys. Rev. D **28**, 170 (1983).

[4] T. Barnes and F.E. Close, Phys. Lett. B**123**, 89 (1983); E. Golowich, E. Haqq and G. Karl, Phys. Rev. D **28**, 160 (1983); L. Kisslinger and Z.P. Li, Phys. Rev. D **51**, R5986 (1995).

[5] R. Workman, Few Body Syst. Suppl. **11**, 943 (1999).

[6] W.H. Liang *et al.*, Preprint.

[7] B.S. Zou, Nucl. Phys. A**675**, 167 (2000); Nucl. Phys. A**684**, 330 (2001).

[8] BES Collaboration, H.B. Li *et al.*, Nucl. Phys. A**675**, 189c (2000).

[9] S. Capstick and P. Page, Phys. Rev. D **60**, 111501 (1999).

[10] S. Capstick and B.D. Keister, Phys. Rev. D **51**, 3598 (1995).

[11] F. Foster and G. Hughs, Z. Phys. C**14**, 123 (1982); C. Hayne and N. Isgur, Phys. Rev. D **25**, 1944 (1982); Z.Y. Zhang *et al.*, Nucl. Phys. A**625**, 59 (1997).

[12] S. Capstick, Phys. Rev. D **46**, 1965 (1992).

[13] Y.B. Dong *et. al.*, Phys. Rev. C **60**, 035203 (1999).

[14] B.S. Zou *et al.*, to appear in Euro. Phys. J. A.

[15] DM2 Collaboration, Nucl. Phys. B**292**, 653 (1987).

[16] M.W. Eaton *et al.*, Phys. Rev. D **29**, 804 (1984).

Helicity structure of the γN interaction and the GDH sum rule

P. Pedroni, for the GDH and A2 collaborations

INFN-Sezione di Pavia, via Bassi 6, Pavia, Italy

(Received: 17 October 2001)

First measurements of pion photoproduction using circularly polarized photons on longitudinally polarized protons were carried out at MAMI (Mainz) in the energy range E_γ=200-800 MeV. Results of the helicity dependence of the total inclusive photoabsorption cross section and of the double pion photoproduction channels will be presented. These data provide new input for multipole analyses and determine the main contribution to the Gerasimov-Drell-Hearn (GDH) integral and the forward spin polarizability γ_0.

1 Introduction

The helicity dependent total cross section for the absorption of real photons on nucleons, $\sigma_{3/2}$ and $\sigma_{1/2}$, corresponding to the two parallel or antiparallel relative spin configurations, respectively, are related to the anomalous magnetic moment κ of the nucleon via the Gerasimov-Drell-Hearn (GDH) sum rule [1]:

$$\int_0^\infty (\sigma_{3/2} - \sigma_{1/2}) \, \frac{d\nu}{\nu} = \frac{2\pi\alpha}{m^2}\kappa^2 \ . \tag{1}$$

In a similar way, the forward spin polarizability γ_0, a structure constant of the nucleon still unmeasured, can be obtained as:

$$\gamma_0 = -\frac{1}{4\pi^2} \int_0^\infty (\sigma_{3/2} - \sigma_{1/2}) \, \frac{d\nu}{\nu^3} \ . \tag{2}$$

Both equations connect the static properties of the nucleon (m, e, κ, γ_0) with the dynamics of the excitation spectrum.

The GDH sum rule is based on very general physics principles (low-energy theorems, optical theorem, unsubtracted dispersion relation) applied to the Compton forward amplitude and gives important constraints for the models of the nucleon. Due to its fundamental character this prediction, formulated in the 1960's, deserves a verification which has been awaiting technical developments that only recently have taken place.

In the past years, some estimates of the GDH sum rule have been made using multipole analyses of the existing pion photoproduction data (mainly from unpolarized experiments) and a simple model for the contribution of double pion photoproduction processes [2]. These estimates were incompatible with the GDH sum rule prediction, giving significantly higher values for the proton but much lower for the neutron [2–6]. A couple of more recent phenomenological approaches, that use a Regge type model to evaluate an additional high-energy multihadron contribution, give an estimated value much closer to the expected one [7, 8].

However, the present lack of direct experimental data on the double polarization observables prevents to draw any definitive conclusions about any violation of the GDH sum rule.

Apart from the GDH sum rule, another important motivation to study the helicity structure of single and double pion photoproduction lies in the fact that it provides completely new and up to now inaccessible information on partial wave amplitudes. The inclusion of this new observable into multipole analyses will allow to access small resonant amplitudes and help to separate them from the dominating ones and from the non-resonant background.

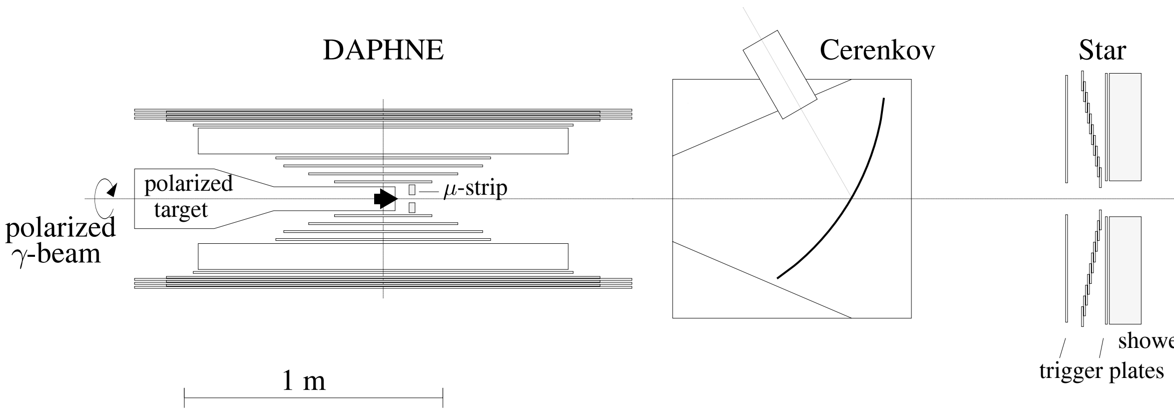

Figure 1: Schematic side view of the experimental setup of the GDH experiment in Mainz.

The aim of the GDH collaboration[1] is to provide an extensive data set of helicity dependent cross sections for all the partial and the total reaction channels both on the proton and on the neutron with a combined use of the MAMI (Mainz) ($m_\pi \leq$ E$_\gamma \leq$ 800 MeV) and ELSA (Bonn) (600 MeV $\leq$ E$_\gamma \leq$ 3 GeV) accelerators.

In the following, results taken at Mainz on the total inclusive and double pion production processes will be presented. Other results about the helicity depence of single pion photoproduction processes and of the higher energy part of the measurement can be found in [9, 10].

2 Experimental setup

The experiment was carried out at the tagged photon facility of the MAMI accelerator in Mainz. Circularly polarized electrons were produced by bremsstrahlung of longitudinally polarized electrons. The source of polarized electrons, based on the photoeffect on strained GaAs crystals, delivered routinely electrons with a degree of polarization of about 75% or higher [11]. The degree of polarization was continuously measured throughout the experiment by Möller scattering in a magnetized vacoflux foil. Both electrons were detected in coincidence in the tagging spectrometer.

Polarized nucleons were available in the frozen spin target [12] that was built and operated by the Bonn, Bochum and Nagoya groups. The system consisted of a horizontal dilution refrigerator and a superconducting polarization magnet, which was used in the polarization phase together with a microwave system for dynamical nuclear polarization (DNP). The polarization was maintained during the measurement in the "frozen spin" mode at temperatures of about 50 mK by an internal superconducting coil (B $\simeq$ 0.4 T) which is integrated into the dilution refrigerator. The target material was butanol (C_4H_9OH). At 2.5 T maximum polarization values close to 90% were obtained for the protons with a typical relaxation time in the "frozen spin" mode of about 200 hours. The holding field was homogeneous enough to allow for continuous NMR monitoring of the target polarization during the experiment.

The photon induced reaction products were registered by means of the detector DAPHNE [13], made by CEA Saclay and INFN - Sezione di Pavia, which is complemented by forward detectors to increase the solid angle acceptance (see fig. 1). DAPHNE is essentially a charged particle tracking detector having a cylindrical symmetry. It consists of 3 coaxial layers of multi-wire proportional chambers, surrounded by a segmented $\Delta E - E - \Delta E$ plastic scintillator telescope and by a double scintillator-absorber sandwich which allows the detection of neutral pions with a useful efficiency.

[1]This collaboration is formed by researchers from the Universities of Mainz, Bonn, Bochum, Erlangen, Göttingen, Lund, Nagoya, Tübingen and from INFN-Sezione di Pavia, RUG Gent, CEA Saclay, INR Moscow.

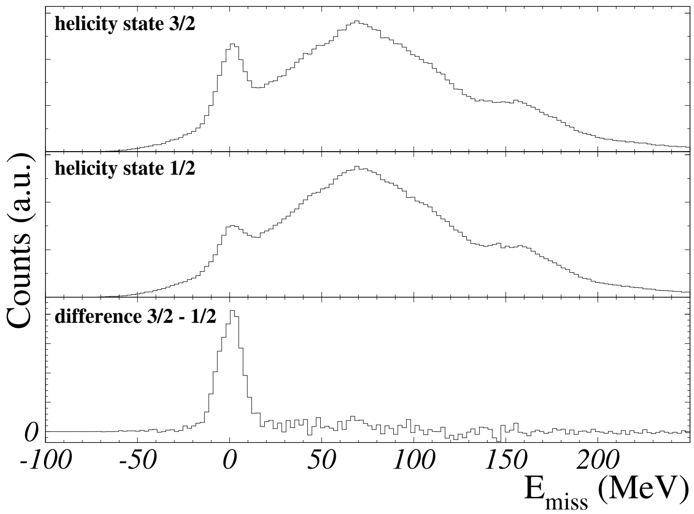

Figure 2: Missing energy spectra for the reaction $\vec{\gamma}\vec{p} \to p\pi^0$ under the assumption that the proton originated from a reaction on a free proton. The spectra are shown for both helicity states and their difference.

The additional forward detectors are the silicon microstrip device MIDAS [14], a Cerenkov counter for online suppression of electrons and positrons, the annular ring detector STAR [15] and a forward sandwich counter.

3 Data analysis

In the following, data recorded by the DAPHNE detector only will be presented. The forward detectors information will be used in a second step of the analysis.

In the analysis of the data from the polarized butanol target, the background contribution from the reactions produced on the unpolarized C and O nuclei of the target could not be fully separated from the polarized H contribution [16]. However this background, coming from spinless nuclei, is not polarization dependent and cancels when the difference between events in the 3/2 and 1/2 helicity states is taken. As an example, Fig. 2 shows this difference in E_{miss} (missing energy) obtained from events with a photoemission proton in the Δ region. E_{miss} is the difference between the measured proton kinetic energy and the proton kinetic energy evaluated (using E_γ and the polar emission angle) under the assumption that the proton originated from a π^0 production process on hydrogen. Missing energy distributions are shown for both helicity states and for their difference. The region outside the peak at $E_{miss} = 0$ corresponds to quasi-free reactions on C and O nuclei and has a yield consistent with zero in the difference spectrum.

3.1 Total inclusive cross section

An inclusive method of data analysis has been developed to determine the total absorption cross section. Its characteristics are fully described in [17, 18] and it is based on the following main features:

- the detection of charged hadrons allow a direct measure of the main part (70-80%) of the hadronic events;
- most of the remaining part (15-20%) can be accessed by detecting events having only neutral pions inside the DAPHNE acceptance while an additional small contribution ($\sim 5\%$) can be evaluated from experimental charged particle spectra or using models.

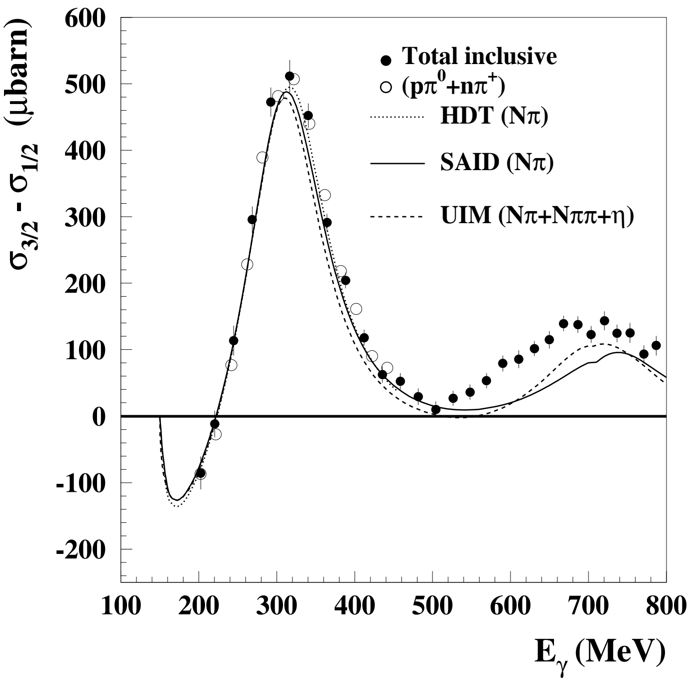

Figure 3: The helicity difference ($\sigma_{3/2} - \sigma_{1/2}$) of the total photoabsorption cross section on the proton [18] (full circles) is compared to the sum of the single pion channels in the Δ region (open circles) [16] and to the model predictions.

3.2 Exclusive measurements

The DAPHNE detector has a wide angular and momentum acceptance for both charged ($p, \pi^{\pm}$) and neutral particles (n, π^0). The identification and the energy determination of the charged particles is performed, with high efficiency ($\geq 80\%$) by the maximum likelihood method described in [19] while neutrons and π^0s can only be identified (without any energy determination) with an efficiency of $10-20\%$. These combined features allow the separation of all the single and double photoproduction channels up to 800 MeV.

3.3 Systematic errors

The dominant contribution to the systematic error stems from uncertainties in photon flux, target density and beam and target polarizations; their sum in quadrature is about 4% of $\Delta\sigma$. The remaining sources of systematic errors are due to uncertainties in wire chamber efficiency (1%), extrapolation (a few % at maximum) and π^0 detection efficiency (4%). This leads to a total systematic error of about 6% on the measured helicity differences.

4 Results and Discussion

4.1 Total inclusive cross section

The analysis procedure as briefly outlined above results in the total cross section difference ($\sigma_{3/2} - \sigma_{1/2}$) depicted in Fig. 3 [18]. It is compared with the sum of our previously published helicity differences for the $n\pi^+$ and $p\pi^0$ channels in the Δ region [16]. The good agreement found between the different analyses gives us confidence in their reliability.

In the same figure, our data are also compared to the HDT [20] (up to 450 MeV), SAID [21], and UIM [22] analyses. In the Δ resonance region, there is a good agreement between experiment and theories. In the second resonance region, a significant contribution from double pion photoproduction is clearly visible. This feature is not completely reproduced by the UIM model. The measured value of the GDH integral between 200 and 800 MeV amounts to 226 ± 5 $(stat) \pm 12$ (sys) μb.

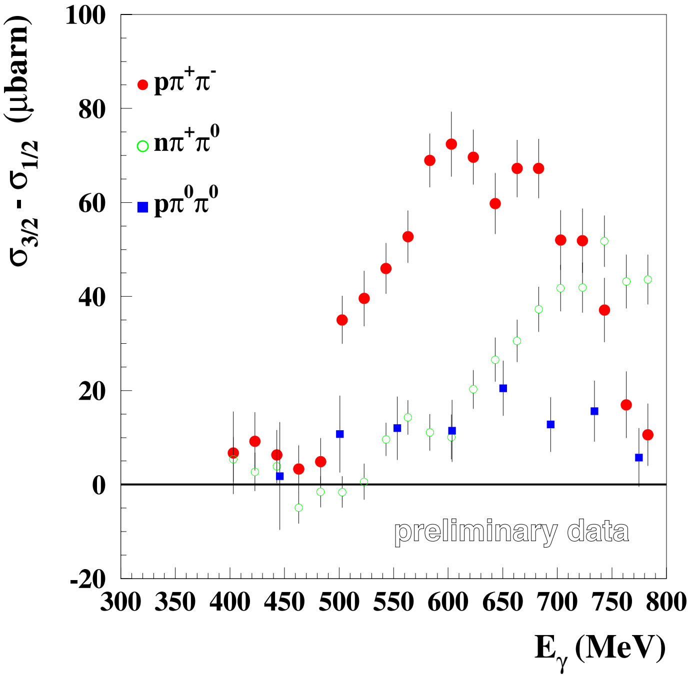

Figure 4: Preliminary results for the helicity $(\sigma_{3/2} - \sigma_{1/2})$ of all 3 pion photoproduction channels on the proton.

Due to the ν^{-3} weighting, the γ_0 integral is almost saturated by $E_\gamma = 800$ MeV. The value of the γ_0 integral between 200 and 800 MeV amounts to $[-187 \pm 8\ (stat) \pm 10\ (sys)] \cdot 10^{-6}$ fm^4.

Although the measured photon energy interval is too narrow to draw any definitive conclusion, a reasonable estimate of the GDH sum rule value can be deduced if we use the existing models for the evaluation of the missing contributions. The UIM model [22] gives a contribution of -30μb for $E_\gamma < 200$ MeV and $+40\mu$b for $800 < E_\gamma < 1650$ MeV. For $E_\gamma > 1650$ MeV, Ref. [7] gives a contribution of -26 μb. The combination of our experimental result with these predictions yields an estimate (210 μb) which within the experimental errors is consistent with the GDH sum rule value (1). It should be kept in mind that, especially above $E_\gamma = 800$ MeV, none of the models has yet been validated experimentally and only a measurement in this energy region can lead to a definitive conclusion about the high energy contribution to the GDH-integral. Our collaboration is performing such a measurement at ELSA (Bonn) up to $E_\gamma \simeq 3$ GeV [10], and extensions to higher energies are under way or in preparation at Jefferson Lab and SLAC.

In case of the γ_0-integral (2) the contribution from $E_\gamma < 200$ MeV is important, the UIM prediction being $+104 \cdot 10^{-6}$ fm^4. The missing high energy contribution, according to UIM and Ref. [7], is $-3 \cdot 10^{-6}$ fm^4 only. The combination with our experimental result gives an estimate of $-86 \cdot 10^{-6}$ fm^4 for γ_0 .

Several predictions, based on dispersion relations [23,24] and chiral perturbation theory [25–29], have been made for γ_0 in the last few years. They range from (-390 to $+460$) $\cdot 10^{-6}$ fm^4. Our result is close to the range of γ_0 values predicted by dispersion theories.

4.2 Exclusive measurements

In Fig. 4 [30] the preliminary results for the helicity difference $(\sigma_{3/2} - \sigma_{1/2})$ of all double pion photoproduction channels on the proton are shown.

According to the existing models [31], the large positive $(\sigma_{3/2} - \sigma_{1/2})$ values for the $p\pi^+\pi^-$ channel, are mainly due to an intermediate excitation of a $\Delta\pi$ state, with the D_{13} resonance playing a minor role. On the contrary, the intermediate excitation of the D_{13} should give the dominant contribution to the $n\pi^+\pi^0$ channel, through the $D_{13} \to n\rho$ decay mode.

The intermediate D_{13} excitation is expected to play a major role also for the $p\pi^0\pi^0$ channel (through the $D_{13} \to \Delta\pi$ decay mode) but the small quantity of data analysed up to now for this reaction (about 1/4 of the total statistics) prevents any clear experimental conclusion.

5 Summary and outlook

First data on the helicity dependence of the photon-nucleon reactions in the energy range from 200 to 800 MeV are now available from MAMI. The helicity difference of the total cross section gives valuable information on the nucleon spin structure and allows a test of the GDH sum rule together with a measurement of the forward spin polarizability γ_0. In addition, new input for multipole analyses is also available from the data on the single and double pion production channels.

References

[1] S.B. Gerasimov, Sov. J. Nucl. Phys. **2**, 430 (1966) S.D. Drell and A.C. Hearn, Phys. Rev. Lett. **16**, 430 (1966).

[2] I. Karliner, Phys. Rev. D **7**, 2717 (1973).

[3] R.Workman and R. Arndt, Phys. Rev. D **45**, 1789 (1992).

[4] V. Burkert and Z. Li, Phys. Rev. D **47**, 46 (1993).

[5] A. Sandorfi *et al.*, Phys. Rev. D **50**, 11 (1994).

[6] D. Drechsel and G. Krein Phys. Rev. D **58**, 116009 (1998).

[7] N. Bianchi and T. Thomas, Phys. Lett. **B 450**, 439 (1999).

[8] S. Simula *et al.*, e-print hep-ph/0107036.

[9] I. Preobrajenski, Proceedings of this Conference.

[10] G. Zeitler, Proceedings of this Conference.

[11] K. Aulenbacher *et al.*, Nucl. Instrum. Methods Phys. Res. Sect. A **391**, 498 (1997).

[12] C. Bradtke *et al.* Nucl. Instrum. Methods Phys. Res. Sect. A **436**, 430 (1999).

[13] G. Audit *et al.*, Nucl. Instrum. Methods Phys. Res. Sect. A **301**, 473 (1991.)

[14] S. Altieri *et al.*, Nucl. Instrum. Methods Phys. Res. Sect. A **452**, 185 (2000).

[15] M. Sauer *et al.* Nucl. Instrum. Methods Phys. Res. Sect. A **378**, 143 (1996).

[16] J. Ahrens *et al.*, Phys. Rev. Lett. **84**, 26 (2000).

[17] M. MacCormick *et al.*, Phys. Rev. C **53**, 41 (1998).

[18] J. Ahrens *et al.*, Phys. Rev. Lett. **87**, 02203 (2001).

[19] A. Braghieri *et al.*, Nucl. Instrum. Methods Phys. Res. Sect. A **343**, 623 (1996).

[20] O. Hanstein *et al.*, Nucl. Phys. **A 632**, 561 (1998).

[21] R.A. Arndt *et al.*, Phys. Rev. C **53**, 430 (1996), solution SP01.

[22] D. Drechsel *et al.*, Nucl. Phys. **A 645**, 145 (1999).

[23] D. Babusci *et al.*, Phys. Rev. C **58**, 1013 (1998).

[24] D. Drechsel *et al.*, Phys. Rev. C **61**, 015204 (2000).

[25] V. Bernard *et al.*, Int. J. Mod. Phys. **E4**, 193 (1995).

[26] T.R. Hemmert *et al.*, Phys. Rev. D **57**, 5746 (1998).

[27] X. Ji *et al.*, Phys. Lett. **B 472**, 1 (2000).

[28] K.B. Vijaya Kumar *et al.*, Phys. Lett. **B 479**, 167 (2000).

[29] G.C. Gellas *et al.*, Phys. Rev. Lett. **85**, 14 (2000).

[30] H.Holvoet, PhD thesis, University of Gent, 2001: M. Lang, PhD thesis, University of Mainz, in preparation; F. Zapadtka, PhD thesis, University of Göettingen, in preparation.

[31] J.C. Nacher and E. Oset, e-print nucl-th/0106005.

The spin of the nucleon in effective models

H. Weigel

Institute of Theoretical Physics, Tübingen University
Auf der Morgenstelle 14, D–72076 Tübingen, Germany

(Received: 17 October 2001)

The three flavor soliton approach for baryons is utilized to discuss effects of flavor symmetry breaking in the baryon wave–functions on axial current matrix elements. The flavor content of the singlet axial current matrix elements, that parameterizes the quark spin contribution to the total angular momentum, is disentangled and studied as a function of the effective flavor symmetry breaking. Here the nucleon and the Λ–hyperon are considered.

1 Introduction

Even though the fundamental theory for the strong interaction processes of hadrons, Quantum Chromodynamics (QCD), is well established, hadron properties can unfortunately not be computed directly. However, QCD contains a hidden expansion parameter, the number (N_C) of color degrees of freedom, that is beneficial for model building. For arbitrarily large N_C, QCD becomes equivalent to a theory of weakly interacting mesons [1]. That is, the meson interaction strengths scale like $1/N_C$ while baryon masses and radii scale like N_C and N_C^0, respectively [2]. Meson Lagrangians may possess localized solutions to the field equations with finite field energy: solitons. Their energies scale inversely with the meson coupling and their extensions approach constants as the coupling increases. These analogies lead to the conjecture that baryons emerge as solitons in the effective meson theory that is equivalent to QCD [2, 3]. Although this meson theory cannot be derived from QCD, low–energy meson phenomenology provides sufficient constraints to build sensible models. Especially chiral symmetry and its breaking in the vacuum introduce non–linear interactions for the pions, the (would–be) Goldstone bosons of chiral symmetry. Then effective Lagrangians are constructed from the chiral field $U = \exp\left(i\vec{\tau}\cdot\vec{\pi}/f\right)$ that are invariant under global chiral transformations $U \to LUR^\dagger$. As $U^\dagger U = 1$, at least two derivatives are required

$$\mathcal{L}_0 = \frac{f^2}{4}\mathrm{tr}\left(\partial_\mu U \partial^\mu U^\dagger\right) . \tag{1}$$

Extracting the axial current $A_\mu^a = f\partial_\mu \pi^a + \mathcal{O}(\vec{\pi}^3)$ from $\mathcal{L}_0$ provides the electroweak coupling and determines the pion decay constant $f = f_\pi = 93\mathrm{MeV}$. Having established a chiral model, a finite energy soliton solution must be obtained and quantized to describe baryon states. I will outline this approach in section 2. In section 3 I will consider three flavor extensions thereof with special emphasis on the role of flavor symmetry breaking [4]. I will employ these methods to compute axial current matrix elements of baryons in section 4. These matrix elements are major ingredients for the description of the nucleon spin structure [5] as they reflect its various quark flavor contributions [6] and they parameterize hyperon beta–decay. The effects of flavor symmetry breaking will be essential to discuss the strange quark contribution. Section 5 contains some concluding remarks.

2 Baryons as chiral solitons

Scaling considerations show that the model (1) does not contain stable soliton solutions. Therefore Skyrme added a stabilizing term [3]

$$\mathcal{L} = \frac{f_\pi^2}{4}\mathrm{tr}\left[\partial_\mu U \partial^\mu U^\dagger\right] + \frac{1}{32e^2}\mathrm{tr}\left(\left[U^\dagger\partial_\mu U, U^\dagger\partial_\nu U\right]\left[U^\dagger\partial^\mu U, U^\dagger\partial^\nu U\right]\right) , \tag{2}$$

that is of fourth order in the derivatives. There are other stabilizing extensions of $\mathcal{L}_0$, as *e.g.* including vector mesons [7,8]. Although such extensions appear physically more motivated, I will stick to the Skyrme model for pedagogical reasons when explaining the soliton picture for baryons.

The soliton solution to (2) assumes the famous hedgehog shape

$$U_{\rm H}(\vec{r}) = \exp\left(i\vec{\tau}\cdot\hat{r}F(r)\right) . \tag{3}$$

The equations of motion become an ordinary second order differential equation for the chiral angle $F(r)$ that are obtained by extremizing the classical energy

$$E_{\rm cl} = E_{\rm cl}[F] = \int d^3r \left\{\frac{f_\pi^2}{2}\left(r^2F'^2 + 2\sin^2F\right) + \frac{\sin^2F}{2e^2}\left(2F'^2 + \frac{\sin^2F}{r^2}\right)\right\} . \tag{4}$$

It can be argued [9] that the baryon number equals the winding number of the mapping (3), *i.e.* $B = [F(\infty) - F(0)]/\pi$. Hence the boundary conditions $F(0) = -\pi$ and $F(\infty) = 0$ corresponding to unit baryon number determine the chiral angle uniquely. This soliton does not yet describe states of good spin and/or flavor as the *ansatz* (3) does not possess the corresponding symmetries. Such states are generated by restoring these symmetries through collective coordinates $A(t)$,

$$U(\vec{r},t) \;=\; A(t)\, U_{\rm H}(\vec{r})\, A^\dagger(t) , \tag{5}$$

and subsequent canonical quantization thereof [10]. This introduces right and left generators $[A, R_i] = A\tau_i/2$ and $[A, L_i] = \tau_i A/2$, respectively. While the isospin interpretation $I_i = L_i$ is general, the identity $J_i = -R_i$ for the spin is due to the hedgehog structure (3), as is the relation $|\vec{I}| = |\vec{J}|$. Quantizing the collective coordinates yields a Hamiltonian in terms of spin (isospin) operators

$$H_{\rm coll} \;=\; E_{\rm cl} + \frac{\vec{J}^{\,2}}{2\alpha^2} \;=\; E_{\rm cl} + \frac{\vec{I}^{\,2}}{2\alpha^2} . \tag{6}$$

The moment of inertia is also a functional of the above determined chiral angle

$$\alpha^2[F] = \frac{2}{3}\int d^3r \sin^2F\left[f_\pi^2 + \frac{1}{e^2}\left(F'^2 + \frac{\sin^2F}{r^2}\right)\right] . \tag{7}$$

Matching the mass difference $M_\Delta - M_{\rm N} = \frac{3}{2\alpha^2} \sim 300{\rm MeV}$ fixes the undetermined parameter $e \approx 4.0$.

3 Extension to three flavors

The generalization to three flavors is carried out straightforwardly by taking $A(t) \in SU(3)$ with the hedgehog (3) embedded in the isospin subgroup. However, the Lagrangian acquires two essential extensions. The first one is the Wess–Zumino–Witten term [9]. Gauging it for local $U_V(1)$ shows that indeed the winding number current equals the baryonic current. Furthermore it constrains A to be quantized as a fermion (for N_C odd). The second extension originates from flavor symmetry breaking that is reflected by different masses and decay constants of the pseudoscalar mesons

$$\mathcal{L}_{\rm SB} = \frac{f_\pi^2 m_\pi^2 - f_K^2 m_K^2}{2\sqrt{3}}{\rm tr}\left\{\lambda_8\left(U + U^\dagger\right)\right\} + \frac{f_K^2 - f_\pi^2}{4\sqrt{3}}{\rm tr}\left\{\lambda_8\left(\partial_\mu U\partial^\mu U^\dagger U + {\rm h.c.}\right)\right\} . \tag{8}$$

The explicit form of $\mathcal{L}_{\rm SB}$ is model dependent, however, the techniques to study its effects on baryon properties are general. The $SU(3)$ collective coordinates are parameterized by eight "Euler–angles"

$$A = D_2(\hat{I})\, {\rm e}^{-i\nu\lambda_4} D_2(\hat{R})\, {\rm e}^{-i(\rho/\sqrt{3})\lambda_8} , \tag{9}$$

where D_2 denote rotation matrices of three Euler–angles for each, rotations in isospace ($\hat{I}$) and coordinate–space ($\hat{R}$). Substituting the *ansatz* (5) into $\mathcal{L} + \mathcal{L}_{\rm SB}$ and canonical quantization of the collective coordinates A yields

$$H = H_{\rm s} + \tfrac{3}{4}\,\gamma\,\sin^2\nu\ . \tag{10}$$

The symmetric piece of this Hamiltonian only contains Casimir operators that may be expressed in terms of the $SU(3)$–right generators R_a ($a = 1, \ldots, 8$):

$$H_{\rm s} = E_{\rm cl} + \frac{1}{2\alpha^2}\sum_{i=1}^{3} R_i^2 + \frac{1}{2\beta^2}\sum_{\alpha=4}^{7} R_\alpha^2\ . \tag{11}$$

While β^2 is a moment of inertia similar to α^2 in eq (7), γ originates from symmetry breaking

$$\gamma = \gamma[F] = \frac{2\pi}{3}\int d^3r\ \left[\left(f_K^2 m_K^2 - f_\pi^2 m_\pi^2\right)(1-{\rm cos}F) + \frac{f_K^2 - f_\pi^2}{2}{\rm cos}F\left(F'^2 r^2 + 2{\rm sin}^2 F\right)\right]\ .$$

The generators R_a can be expressed in terms of derivatives with respect to the 'Euler–angles'. The eigenvalue problem $H\Psi = \epsilon\Psi$ reduces to sets of ordinary second order differential equations for isoscalar functions which only depend on the strangeness changing angle ν [11]. Only the product $\omega^2 = \frac{3}{2}\gamma\beta^2$ appears in these differential equations that are integrated numerically. Thus ω^2 is interpreted as the effective strength of the flavor symmetry breaking. A value in the range $5 \lesssim \omega^2 \lesssim 8$ is required to obtain reasonable agreement with the empirical mass differences for the $\frac{1}{2}^+$ and $\frac{3}{2}^+$ baryons [4]. The eigenstates of the symmetric piece (11) are members of definite $SU(3)$ representations, *e.g.* the octet (**8**) for the low–lying $\frac{1}{2}^+$ baryons. Upon flavor symmetry breaking, states of different representations are mixed. At $\omega^2 = 6$ the nucleon amplitude contains a 23% contamination of the state with nucleon quantum numbers in the $\overline{\mathbf{10}}$ representation. This must be interpreted as a strong deviation from flavor covariant wave–functions.

4 Axial current matrix elements

The effect of the derivative type symmetry breaking terms is mainly indirect. They provide the splitting between the various decay constants and thus increase γ because of $f_K^2 m_K^2 - f_\pi^2 m_\pi^2 \approx 1.5 f_\pi^2 (m_K^2 - m_\pi^2)$. Otherwise the $(f_K^2 - f_\pi^2)$–terms may be omitted. Whence there are no symmetry breaking terms in current operators and the non–singlet axial charge operator is parameterized as

$$\int d^3r\ A_i^{(a)} = c_1 D_{ai} - c_2 D_{a8} R_i + c_3 \sum_{\alpha,\beta=4}^{7} d_{i\alpha\beta} D_{a\alpha} R_\beta\ , \qquad c_i = c_i[F]\ , \tag{12}$$

where $D_{ab} = \frac{1}{2}{\rm tr}\left(\lambda_a A \lambda_b A^\dagger\right)$, $a = 1, \ldots, 8$ and $i = 1, 2, 3$. When integrating out *strange* degrees of freedom, $\omega^2 \to \infty$ the strangeness contribution to the nucleon axial charge should vanish. The eigenstates of (10) parametrically depend on ω^2 and for $\omega^2 \to \infty$ the singlet current

$$\int d^3r\ A_i^{(0)} = -2\sqrt{3} c_2 R_i\ , \qquad i = 1, 2, 3\ . \tag{13}$$

	$n \to p$	$\Lambda \to p$	$\Sigma \to n$	$\Xi \to \Lambda$	$\Xi \to \Sigma$	$\Sigma \to \Lambda$
emp.	1.267 ± 0.004	0.718 ± 0.015	0.340 ± 0.017	0.25 ± 0.05	1.287 ± 0.158	0.61 ± 0.02
$F\&D$	$1.26 = g_A$	0.725 ± 0.009	0.339 ± 0.026	0.19 ± 0.02	$1.26 = g_A$	0.65 ± 0.01

Table 1: The empirical values for the g_A/g_V ratios of hyperon beta–decays [12]. For $\Sigma \to \Lambda$ only g_A is given. Also the flavor symmetric predictions are presented using the values for $F\&D$ of Ref. [13].

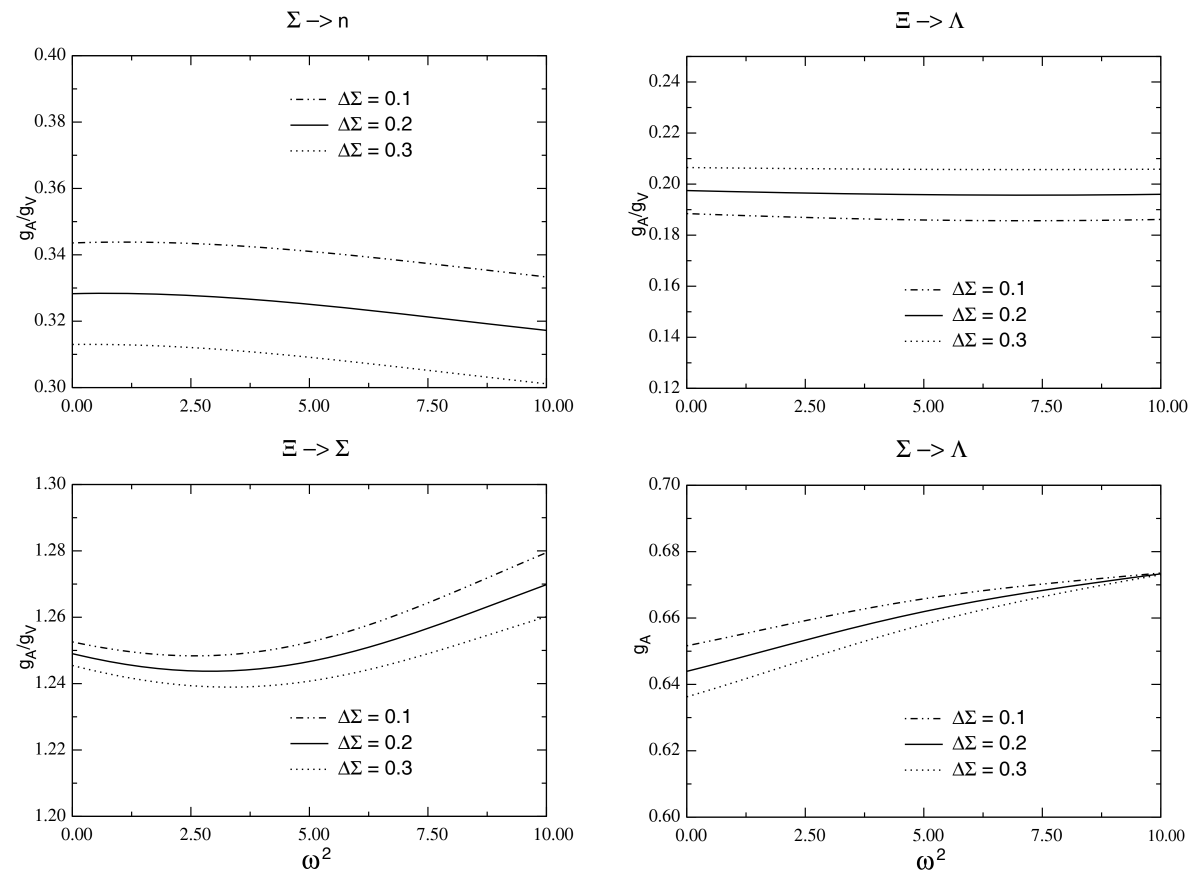

Figure 1: The predicted decay parameters for the hyperon beta–decays using $\omega_{\rm fix}^2 = 6.0$. The errors originating from those in $\Delta\Sigma_N$ are indicated.

yields a vanishing nucleon matrix element of the strangeness projection, $A_i^{(s)} = (A_i^{(0)} - 2\sqrt{3}A_i^{(8)})/3$. The identity of c_2 in eqs (12) and (13) goes beyond group theoretical arguments. Actually all model calculations in the literature [14, 15] are consistent with (13). To completely describe the hyperon beta–decays I demand matrix elements of the vector charges that are obtained from the operator

$$\int d^3r\, V_0^{(a)} = \sum_{b=1}^{8} D_{ab} R_b = L_a \ . \tag{14}$$

The values for g_A and g_V (only g_A for $\Sigma^+ \to \Lambda e^+ \nu_e$) are obtained from the matrix elements of respectively the operators in eqs (12) and (14), sandwiched between the eigenstates of the full Hamiltonian (10). I choose c_2 according to $\langle N\uparrow| \int d^3r\, A_3^{(0)} |N\uparrow\rangle = \sqrt{3}c_2 = \Delta\Sigma = 0.2 \pm 0.1$ [6] and subsequently determine c_1 and c_3 at $\omega_{\rm fix}^2 = 6.0$ such that the empirical values for the nucleon axial charge, g_A and the g_A/g_V ratio for $\Lambda \to p e^- \bar{\nu}_e$ are reproduced*. This predicts the other decay parameters and describes their variation with symmetry breaking as shown in figure 1. The dependence on flavor symmetry breaking is very moderate† and the results can be viewed as reasonably agreeing with the empirical data, *cf.* table 1. The two transitions, $n \to p$ and $\Lambda \to p$, which are not shown in figure 1, exhibit a similar negligible dependence on ω^2. Hence these

*Here the problem of the too small model prediction for g_A will not be addressed but rather the empirical value $g_A = 1.26$ will be used as an input to fix the c_n.

†However, the individual matrix elements entering the ratios g_A/g_V vary strongly with ω^2 [16].

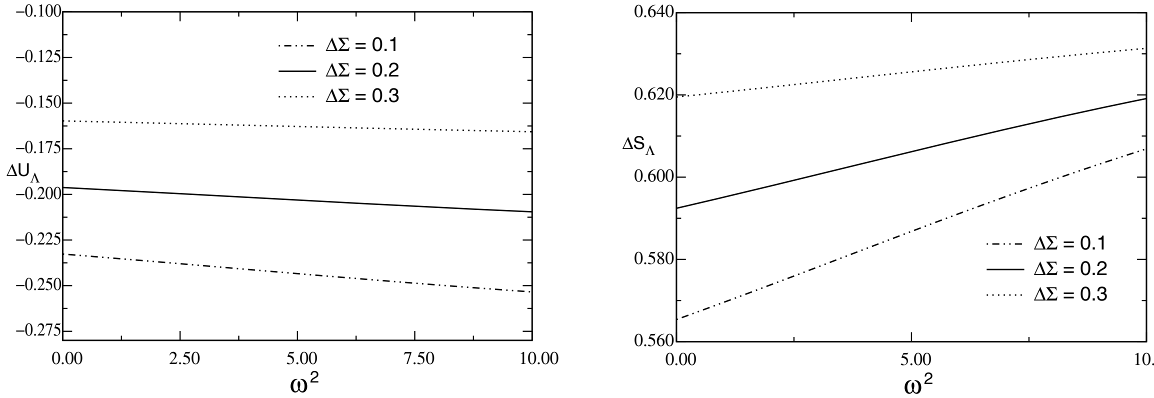

Figure 2: The contributions of the *non–strange* (left panel) and *strange* (right panel) degrees of freedom to the axial charge of the Λ. Again $\omega^2_{\rm fix} = 6.0$ was assumed.

predictions are not sensitive to the choice of $\omega^2_{\rm fix}$. Comparing the results in figure 1 with the data in table 1 shows that the calculation using the strongly distorted wave–functions agrees equally well with the empirical data as the established [13] flavor symmetric $F\&D$ fit.

Figure 2 shows the flavor components of the axial charge of the Λ hyperon. Again, the various contributions to the axial charge of the Λ exhibit only moderate dependencies on ω^2. The *non–strange* component, $\Delta U_\Lambda = \Delta D_\Lambda$ slightly increases in magnitude. The *strange* quark piece, ΔS_Λ grows with symmetry breaking since $\Delta\Sigma_\Lambda$ is kept fixed. These results nicely agree with an $SU(3)$ analysis applied to the data [17].

The observed independence on ω^2 does not occur for all matrix elements of the axial current. A prominent exemption is the *strange* quark component in the nucleon, ΔS_N. For $\Delta\Sigma = 0.2$, say, it is significant at zero symmetry breaking, $\Delta S_N = -0.131$ while it decreases (in magnitude) to $\Delta S_N = -0.085$ at $\omega^2 = 6.0$.

This far I have only considered the general sturcture of the current operators without computing the constants c_i from a model soliton, though I had the Skyrme model in mind. However, this model is too simple to be realistic. For example, it improperly predicts $\Delta\Sigma = 0$ [4]. More complicted models must be utilized, as *e.g.* the vector meson model that has been established for two flavors in ref [7]. Later it has been generalized to three flavors and been shown to fairly describe hyperon beta–decay [14]. To account for different masses and decay constants a minimal set of symmetry breaking terms is included [18] that add symmetry breaking pieces to the axial charge operator,

$$\delta A_i^{(a)} = c_4 D_{a8} D_{8i} + c_5 \sum_{\alpha,\beta=4}^{7} d_{i\alpha\beta} D_{a\alpha} D_{8\beta} + c_6 D_{ai}(D_{88} - 1) \ , \qquad \delta A_i^{(0)} = 2\sqrt{3}\, c_4 D_{8i} \ .$$

The coefficients $c_1, \ldots, c_6$ are functionals of the soliton and can be computed once the soliton is constructed [16]. As the model parameters cannot be completely determined in the meson sector [7] I use the small remaining freedom to accommodate baryon properties in three different ways, see table 2. The set denoted by 'masses' refers to a best fit to the baryon mass differences. It predicts the axial charge somewhat on the low side, $g_A = 0.88$. The set named 'mag.mom.' refers to parameters that yield magnetic moments of the $\frac{1}{2}^+$ baryons close to the respective empirical data (with $g_A = 0.98$) and finally the set labeled 'g_A' reproduces [14] the axial charge of the nucleon as well as the hyperon beta–decay data. As presented in table 2, the predictions for the axial properties of the Λ are insensitive to the model parameters. The singlet matrix element of the Λ hyperon is smaller than that of the nucleon. Sizable polarizations of the *up* and *down* quarks in the Λ are again

	Λ			N			
"fits"	$\Delta U = \Delta D$	ΔS	$\Delta\Sigma$	ΔU	ΔD	ΔS	$\Delta\Sigma$
masses	-0.155	0.567	0.256	0.603	-0.279	-0.034	0.291
mag. mom.	-0.166	0.570	0.238	0.636	-0.341	-0.030	0.265
g_A	-0.164	0.562	0.233	0.748	-0.476	-0.016	0.256

Table 2: Spin content of the Λ in the realistic vector meson model. For comparison the nucleon results are also given. Three sets of model parameters are considered, see text.

predicted. They are slightly smaller in magnitude but nevertheless comparable to those obtained from the $SU(3)$ symmetric analyses [17].

5 Conclusions

In this talk I utilized the picture that baryons emerge as solitons in an effective meson theory to compute various baryon matrix elements. Here I focused on the effects of flavor symmetry breaking in the baryon wave–functions and showed that despite of strong deviations from flavor covariant wave–functions the empirical parameters for hyperon beta–decay are reproduced. Effective symmetry breaking is treated as a parameter and consistency with the the two–flavor limit (infinitely heavy strange quarks) relates singlet and octet axial currents beyond group theory. With this I showed that chiral soliton models explain the proton spin puzzle, *i.e.* the smallness of the observed axial singlet current matrix element. Furthermore flavor symmetry breaking in the nucleon wave–function significantly reduces the polarization of the strange quarks inside the nucleon.

Acknowledgment: This work has been supported by the Deutsche Forschungsgemeinschaft with Heisenberg–Fellowship We 1254/3-1 and under research contract We 1254/4-2.'

References

[1] G. t' Hooft, Nucl. Phys. **B72** (1974) 461; **B75** (1975) 461.
[2] E. Witten, Nucl. Phys. **B160** (1979) 57.
[3] T. H. R. Skyrme, Proc. Roy. Soc. Lond. **A260** (1961) 127.
[4] H. Weigel, Int. J. Mod. Phys. **A11** (1996) 2419, J. Schechter and H. Weigel, arXiv:hep-ph/9907554.
[5] R. L. Jaffe, arXiv:hep-ph/9602236.
[6] J. R. Ellis and M. Karliner, arXiv:hep-ph/9601280.
[7] P. Jain *et al.*, Phys. Rev. **D37** (1988) 3252; Ulf–G. Meißner *et al.*, Phys. Rev. **D39** (1989) 1956.
[8] Ö. Kaymakcalan, S. Rajeev, and J. Schechter, Phys. Rev. **D30** (1984) 594.
[9] E. Witten, Nucl. Phys. **B223** (1983) 422, Nucl. Phys. **B223** (1983) 433.
[10] G. S. Adkins, C. R. Nappi, and E. Witten, Nucl. Phys. **B228** (1983) 552.
[11] H. Yabu and K. Ando, Nucl. Phys. **B301** (1988) 601.
[12] C. Caso *et al.*, (Particle Data Group), Eur. Phys. J. **C3** (1998) 1; M. Bourquin *et al.*, Z. Phys. **C12** (1982) 307; **C21** (1983) 1.
[13] R. Flores–Mendieta, E. Jenkins, and A. V. Manohar, Phys. Rev. **D58** (1998) 094028.
[14] N. W. Park and H. Weigel, Nucl. Phys. **A541** (1992) 453.
[15] A. Blotz, M. Praszałowicz, and K. Goeke, Phys. Lett. **B317** (1993) 195.
[16] H. Weigel, Nucl. Phys. **A690** (2001) 595.
[17] R. L. Jaffe, Phys. Rev. **D54** (1996) 6581
[18] P. Jain *et al.*, Phys. Rev. **D40** (1989) 855.

Muon capture in hydrogen

S. Ando, F. Myhrer and K. Kubodera

Department of Physics & Astronomy,
University of South Carolina, Columbia, SC 29208, U.S.A.

(Received: 31 October 2001)

Theoretical difficulties in reconciling the measured rates for ordinary and radiative muon capture are discussed, based on heavy-baryon chiral perturbation theory. We also examine ambiguity in our analysis due to the formation of $p\mu p$ molecules in the liquid hydrogen target.

1 Introduction

Ordinary and radiative muon captures (OMC and RMC) on a proton, $\mu^- p \to n\nu_\mu$ and $\mu^- p \to n\nu_\mu\gamma$, are fundamental weak-interaction processes in nuclear physics and constitute primary sources of information on g_P, the induced pseudoscalar coupling constant of the weak nucleon current [1]. The most accurate existing measurements of the OMC and RMC rates have been carried out using a liquid hydrogen target. The experimental OMC rate in liquid hydrogen obtained by Bardin *et al.* [2] is

$$\Lambda_{liq}^{exp} = 460 \pm 20 \quad [\mathrm{s}^{-1}] \qquad (\mathrm{OMC}). \tag{1}$$

As for RMC, Jonkmans *et al.* [3] measured the absolute photon spectrum for $E_\gamma \geq 60$ MeV and deduced therefrom the partial RMC branching ratio, R_γ, which is the number of RMC events (per stopped muon) producing a photon with $E_\gamma \geq 60$ MeV. The measured value of R_γ is [3,4]

$$R_\gamma^{exp} = (2.10 \pm 0.22) \times 10^{-8} \quad (\mathrm{RMC}). \tag{2}$$

Surprisingly, the value of g_P deduced in [3,4] from the RMC data is $\sim$1.5 times larger than the PCAC prediction, g_P^{PCAC} [5]. By contrast, the value of g_P deduced in [2] from the OMC data is in good agreement with the PCAC prediction. Heavy-baryon chiral perturbation theory (HBChPT), a low-energy effective theory of QCD, allows us to go beyond the PCAC approach, but the results of detailed HBChPT calculations up to next-to-next-to-leading order [6] essentially agree with those obtained in the PCAC approach. Thus the theoretical framework for estimating g_P appears to be robust. What then can be the origin of the apparent conflict between the g_P values determined from OMC and RMC ? In this talk we wish to address a number of issues relevant to this question.

The OMC process is described by the standard electroweak theory. The lepton current, j_α^{lepton}, interact with the very heavy W boson ($m_W \simeq 80$ GeV) which propagates and interacts with the hadronic current, J_β^{hadron}. Since the maximal momentum transfer between the two currents, $q_{max} \simeq m_\mu \ll m_W$, we can for all practical purposes replace the W boson propagator with a constant. Then the interaction between the lepton and hadron currents reduces to:

$$\sim \frac{G_F}{\sqrt{2}} j_\alpha^{lepton} J_\alpha^{hadron} \ . \tag{3}$$

where G_F is the effective Fermi constant. Since the leptons are considered point particles, the lepton current is given by the incoming muon and outgoing neutrino spinors: $j_\alpha^{lepton} = \bar{u}_\nu \gamma_\alpha (1-\gamma_5) u_\mu$. The hadronic current however is less well known due to the structure of the nucleons. We write $J_\beta^{hadron} = V_\beta - A_\beta$, where the vector current, V_β, and the axial current, A_β, can be written as (based on symmetry considerations and neglecting second-class currents):

$$V_\beta = \bar{u}_n \left[g_V(q^2)\gamma_\beta + i\, \frac{g_M(q^2)}{2m_N}\, \sigma_{\beta\delta} q^\delta \right] u_p \ , \tag{4}$$

$$A_\beta = \bar{u}_n \left[g_A(q^2)\gamma_\beta\gamma_5 + \frac{g_P(q^2)}{m_\mu}\; q_\beta\gamma_5 \right] u_p \ , \tag{5}$$

where u_n and u_p are the outgoing neutron and incoming proton spinors; and q is the momentum transferred to the nucleon. The four form factors, $g_V(q^2)$, $g_M(q^2)$, $g_A(q^2)$ and $g_P(q^2)$, in Eqs.(4) and (5) are, at low momentum transfers relevant to the OMC and RMC reactions, given by known parameters:

$$g_V(q^2) \;=\; 1 + \frac{1}{6} <r^2> q^2 + \cdots \ ; \qquad g_M(q^2) = \kappa_p - \kappa_n + \cdots \ ; \tag{6}$$

$$g_A(q^2) \;=\; g_A\left(1 + \frac{1}{6} < r_A^2 > q^2 + \cdots\right) \ ; \tag{7}$$

$$g_P(q^2) \;=\; \frac{2m_\mu f_\pi g_{\pi NN}}{m_\pi^2 - q^2} - \frac{1}{3} g_A m_\mu m_N <r_A^2> + \cdots \ . \tag{8}$$

Here $<r^2> \simeq 0.585$ fm^2 is the square of the isovector nucleon radius, $<r_A^2> \simeq 0.42$ fm^2 is the axial radius squared, and κ_p and κ_n are the proton and neutron anomalous magnetic moments, respectively. In the induced pseudoscalar form factor, $g_P(q^2)$, the form of the dominant "pion-pole" term is dictated by the PCAC hypothesis.

In OMC the momentum transfer is $q^2{=}(m_\mu - E_\nu)^2 - E_\nu^2 = -0.88m_\mu^2$ and, traditionally, the pseudoscalar coupling "constant", g_P, is defined as $g_P \equiv g_P(q^2 = -0.88m_\mu^2)$, and thus the PCAC value is $g_P^{PCAC} = 6.77 g_A(0)$ [7]. We remark that the contribution of the $g_P(q^2)$ term to OMC is suppressed due to the fact that $q^2{=}-0.88m_\mu^2$ is far from the pion pole. The rationale for using RMC to determine g_P is that the three-body kinematics in the final state allows q^2 to approach the pion pole, enhancing thereby the contribution of the pseudoscalar term. With the photon energy denoted by E_γ, we have $q^2 \simeq (2m_\mu E_\gamma - m_\mu^2)$, which is positive for sufficiently large values of E_γ, and which can reach the maximal value $\simeq m_\mu^2$. In [3,4], the RMC process is measured for $E_\gamma >$ 60 MeV. Meanwhile, a great challenge in observing RMC is its very low branching ratio ($\sim 10^{-3}$ compared to OMC), and it was quite a feat that the TRIUMF group succeeded in measuring R_γ. It should also be mentioned that the absolute photon spectrum (for $E_\gamma \geq 60$ MeV) measured in [3,4] gives information on the q^2 dependence of $g_P(q^2)$. The afore-mentioned surprising conclusion that, to fit the TRIUMF RMC data, one needs to adopt $g_P \sim 1.5\ g_P^{PCAC}$ has triggered re-examination of the foundation of the theoretical framework used for the analysis. In particular, it motivated detailed systematic calculations based on HBChPT for RMC as well as OMC [8–12].

2 Chiral perturbation theory and the atomic capture rates

Chiral perturbation theory (ChPT) is an effective field theory of QCD tailored for describing low-energy hadronic interactions. Since the physical degrees of freedom here are hadrons, not quarks or gluons, we "integrate out" the quark and gluon fields to obtain an effective lagrangian, $\mathcal{L}_{eff}$, pertinent to the hadronic degrees of freedom. $\mathcal{L}_{eff}$ should inherit all the symmetry properties of QCD (and the patterns of their breaking, if any), including chiral symmetry. For our purposes, it is sufficient to consider only two flavors (u and d); correspondingly, $\mathcal{L}_{eff}$ contains only the nucleon and pion fields. If chiral symmetry is an exact symmetry of $\mathcal{L}_{eff}$, then the right- and left-handed nucleon fields decouple, and the left- and right-handed Noether currents are separately conserved: $\partial_\alpha\, j^\alpha_{left} = 0$ and $\partial_\alpha\, j^\alpha_{right} = 0$. The QCD vacuum state, however, does not respect chiral symmetry, i.e. chiral symmetry is spontaneously broken. Then, according to the Goldstone theorem, there appear massless pseudoscalar Goldstone fields, which can be identified with (massless) pions. In reality, $\mathcal{L}_{QCD}$ contains a tiny quark mass term ($m_{quark} \simeq$10 MeV) that violates chiral symmetry and that gives rise to a finite pion mass. A consequence of the non-zero mass is that the axial current is no longer conserved. Since $m_{quark} \ll \Lambda_{chiral} \simeq 1$ GeV, this explicit chiral symmetry breaking can be treated as a small perturbation, and ChPT consists in expanding $\mathcal{L}_{eff}$ and transition amplitudes in terms of Q/Λ_{chiral} and $m_{pion}/\Lambda_{chiral}$, where Q is a typical scale of external momenta: $Q \sim |\vec{p}_{pion}| \sim |\vec{p}_{nucleon}|$. A version of ChPT that is particularly useful for our present purposes is HBChPT, wherein the nucleon is treated as a heavy particle for which a Foldy-Wouthuysen-like non-relativistic expansion can be used. In HBChPT we have an expansion

$$\mathcal{L}_{eff} \;=\; \sum \mathcal{L}_\beta = \mathcal{L}_1 + \mathcal{L}_2 + \cdots \;. \tag{9}$$

Here the "chiral index" β is given by $\beta = d + n/2 - 1$, where n is the number of nucleon fields involved in a given vertex and d the number of derivatives or powers of m_π involved. For example, the lowest chiral order lagrangian is given as

$$\mathcal{L}_1 \;=\; \bar{N}\left[i\,\frac{\partial}{\partial t} + \frac{g_A}{2f_\pi}\,\boldsymbol{\tau}\cdot(\vec{\sigma}\cdot\vec{\nabla}\boldsymbol{\pi})\right]N + \frac{1}{2}\left(\partial_\beta\boldsymbol{\pi}\cdot\partial^\beta\boldsymbol{\pi}\right) - \frac{1}{2}m_\pi^2\boldsymbol{\pi}^2 + \cdots \;, \tag{10}$$

while the next order Lagrangian is given by

$$\mathcal{L}_2 \;=\; \bar{N}\left[\frac{\vec{\nabla}^2}{2m_N} + \cdots\right]N + \cdots \;. \tag{11}$$

It is to be noted that in HBChPT the Schroedinger operator $\vec{\nabla}^2/(2m_N)$ for the nucleon kinetic energy is treated as a "recoil" correction to $\mathcal{L}_1$. In muon capture (both OMC and RMC), $Q \sim m_\mu$=105.7 MeV or $Q/\Lambda_\chi \sim 0.1$ and hence the chiral expansion is expected to converge rapidly. The explicit calculations in HBChPT [9, 12] corroborates this expectation.

For OMC, leading-order (LO) contributions in chiral counting come from two tree diagrams of order $(Q/\Lambda_{chiral})^0$. Next-to-leading order (NLO) contributions are again given by two tree diagrams which however are of order $(Q/\Lambda_{chiral})^1$. These NLO diagrams arising from $\mathcal{L}_2$ define the nucleon-weak current (or pion) vertices which include the nucleon recoil correction of order $\sim m_N^{-1}$. To next-to-next-to-leading order (NNLO), $(Q/\Lambda_{chiral})^2$, we have both tree and one-pion-loop diagrams. The tree diagrams here involve vertices coming from $\mathcal{L}_3$, which contains three low energy constants (LEC). Two of them can be determined from $< r^2 >$ and $< r_A^2 >$, while the third LEC can be constrained by the Goldberger-Treiman discrepancy. The one-pion-loop diagrams effectively introduce a form factor at the nucleon-pion vertex. It should be stressed that there are *no* free parameters in this ChPT calculation; all the LEC's are given by g_A, $\kappa_p - \kappa_n$, $f_\pi \simeq 93$ MeV, $g_{\pi N}$, $<r^2>$, $<r_A^2>$, and the Goldberger-Treiman discrepancy Δ_π defined by $m_N g_A = f_\pi g_{\pi N}(1-\Delta_\pi)$. Bernard *et al.* [11] have shown the very rapid convergence of these ChPT calculations for the spin-averaged OMC rate: $\Lambda = (247 - 62 - 4 + \cdots)\mathrm{s}^{-1}$, where the the first, second and third terms correspond to the LO, NLO and NNLO contributions, respectively. We can see that the NLO term is ~25% of the LO term and that the NNLO term is ~1.6% of the LO term. Meanwhile, the OMC rate from the μ-p singlet atomic state exhibits a more subtle convergence behavior, indicating that a systematic calculation based on well-defined chiral expansion is indeed needed to get accurate predictions:

$$\Lambda_s(\mathrm{s}^{-1}) = 957 - \frac{245\mathrm{GeV}}{m_N} + \left[\frac{30.4\mathrm{GeV}^2}{m_N^2} - 43.17\right] + \cdots \simeq 687\mathrm{s}^{-1} \;. \tag{12}$$

The second term in this expression is the nucleon recoil correction. Of the two terms in the square brackets representing the NNLO corrections, the first represents the m_N^{-2} correction term while the second term originates from the q^2-dependence in the hadronic form factors given by the ChPT terms of one-loop order. It is noteworthy that these two terms cancel each other to a significant

	BHM (NLO)	AMK (NLO)	BHM (NNLO)	AMK (NNLO)
Λ_s^{OMC}	711	722	687	695
Λ_t^{OMC}	14	12	13	12

Table 1: Comparison of calculated atomic OMC rates. Λ_s (Λ_t) is the atomic capture rate (in sec^{-1}) calculated for the initial singlet (triplet) hyperfine state including terms up to NLO or NNLO, as indicated. The entries for the columns labeled "BHM" and "AMK" are taken from [11] and [10], respectively. The "AMK" results have been obtained with the use of $g_A = 1.267$ and $g_{\pi N} = 13.4$. Apart from small chiral corrections, the numerical results of the classic works by Primakoff and Opat would be close to those of AMK(NNLO), if the updated value of $g_A = 1.267$ is adopted; Primakoff and Opat used $g_A = 1.24$ and $g_A = 1.22$, respectively.

degree, a feature that cannot be studied reliably without a systematic expansion scheme such as ChPT. We compare in Table 1 the OMC rates obtained in two independent ChPT calculations, BHM [11] and AMK [10]. The variance in the results of BHM and AMK are ascribable to the slight differences in the approaches used.

The RMC atomic capture rates have been calculated with the same $\mathcal{L}_{eff}$. The use of $\mathcal{L}_{eff}$ ensures that the photon coupling in our RMC calculation automatically satisfies gauge invariance. The leading order (LO) diagram representing the emission of a photon by a muon gives a dominant contribution. In LO we also have Feynman diagrams of the following types: (i) a photon couples to an intermediate pion propagator; (ii) a photon couples to a pion-nucleon vertex; (iii) a photon couples to a W^--pion vertex. In the Coulomb gauge, there are five LO Feynman diagrams, ten NLO diagrams, and more than twenty NNLO diagrams including pion-loop diagrams [9].

It has been pointed out [14] that, with the use of the atomic RMC rates calculated model-independently with the use of HBChPT, it is extremely difficult to reproduce R_γ^{exp} obtained in the TRIUMF experiment. We describe below some salient features of this difficulty.

3 Muonic states in liquid hydrogen

To make a comparison between theory and experiment, one needs to relate the theoretically calculated atomic OMC and RMC rates to the capture rates measured in a liquid H_2 target, Λ_{liq} and R_γ, respectively. It is also important to know the temporal behavior of each of the various μ-capture components (capture from the atomic states and capture from p-μ-p molecular states). Fig. 1 schematically depicts various competing atomic and molecular processes in liquid H_2. A muon stopped in liquid hydrogen quickly forms a muonic atom (μ-p) in the lowest Bohr state. The atomic hyperfine-triplet state (S=1) decays extremely rapidly to the singlet state (S=0), with a transition rate $\lambda_{10} \simeq 1.7 \times 10^{10}$ s^{-1}. In the liquid hydrogen target a muonic atom and a hydrogen molecule collide with each other to form a p-μ-p molecule with the molecule predominantly in its ortho state. The transition rate from the atomic singlet state to the ortho p-μ-p molecular state, $\lambda_{pp\mu}$, has an averaged value $\lambda_{pp\mu} \sim 2.5 \times 10^6$ s^{-1}, which is comparable to the muon decay rate, $\lambda_0 = 0.455 \times 10^6$ s^{-1}. The ortho p-μ-p state further decays to the para p-μ-p molecular state with a rate $\lambda_{op} \sim (4-7) \times 10^4$ s^{-1}.

We now discuss very briefly the time structure relevant to the OMC experiment [2]. We denote by $N_s(t)$, $N_{om}(t)$ and $N_{pm}(t)$ the numbers of muons at time t in the atomic singlet, ortho-molecular, and para-molecular states, respectively. They satisfy coupled differential equations (the kinetic equations), see Eq. (54a) in Ref. [13]. For illustration purposes, let us consider a case in which there is one muon in the atomic singlet state at $t = 0$; *i.e.*, $N_s(0) = 1$ and $N_{om}(0) = N_{pm}(0) = 0$. $N_s(t)$, $N_{om}(t)$ and $N_{pm}(t)$ corresponding to this case are plotted in Fig. 2. It turns out to be crucially

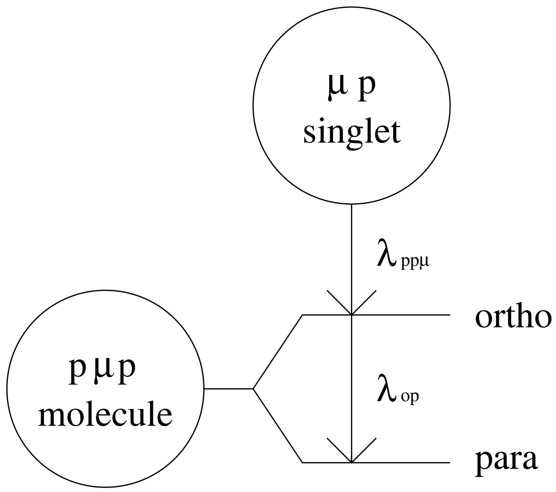

Figure 1: Atomic and molecular states relevant to muon capture in liquid hydrogen; $\lambda_{pp\mu}$ is the transition rate from the atomic singlet state to the ortho p-μ-p molecular state, and λ_{op} is that from the ortho to para molecular state.

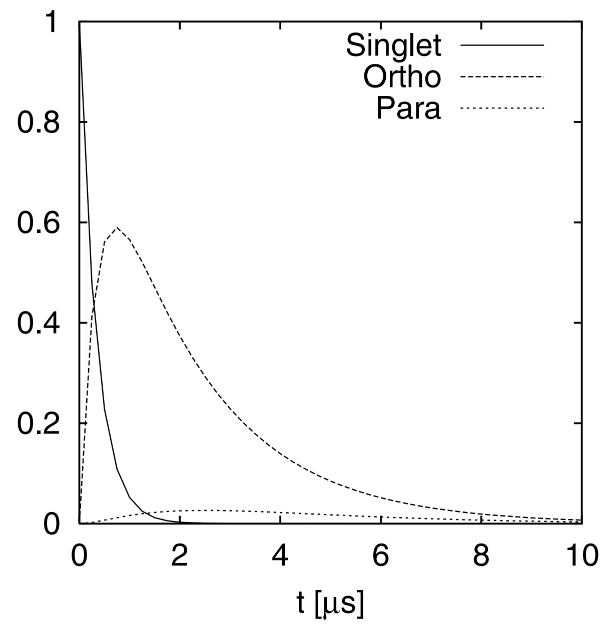

Figure 2: Number of muons at time t in each state in liquid hydrogen.

important to take proper account of the t-dependence of these populations in analyzing the OMC data in [2], since data taking in Ref. [2] starts at $t \neq 0$.

In the OMC experiment (see Fig. 4 in Ref. [2]), μ^- beams arrive at the target in a (on the average) 3 μs-long burst with repetition rate 3000 Hz. The data collection typically starts 1 μs after the end of the 3 μs-long beam burst, and the measurement lasts until 306 μs after the end of the beam burst. To proceed, we assume that the quoted average time intervals represent the actual values (ignoring fluctuations). Then, provided all the muons arrive at the same time, we can choose with no ambiguity that arrival time as the origin of time ($t = 0$) and let $t = t_i$, the starting time for data collection, refer to that origin. However, the finite duration (3 μs) of the beam burst causes uncertainty in the value of $t = t_i$; t_i can be anywhere between 1.0 μs and 4.0μs. We choose here to average over the muon burst duration time for deducing Λ_{liq}, see Ref. [14] for details.

For the RMC experiment [3,4], the muons essentially arrive one by one and data taking begins at $t_i = 365$ ns. We therefore can neglect the beam burst duration time in calculating R_γ, see Ref. [14].

4 Discussion

The value of Λ_{liq} obtained with the use of the atomic OMC rates calculated in HBChPT up to NNLO is $\Lambda_{liq} \simeq 459$ s^{-1} [10,14]. This value is in good agreement with Λ_{liq}^{exp}. By contrast, it is not possible to reproduce R_γ^{exp} in Eq.(1) in the existing theoretical framework and with the use of the standard set of input parameters, see Ref. [14] for a more detailed discussion.

The important question is: Have we exhausted all possibile ways for reconciling the measured OMC and RMC rates? One thing worth studying as a speculative possibility [14] is the sensitivity of Λ_{liq} and R_γ to a so-far neglected possible change in the value of the molecular mixing parameter ξ. As first discussed by Weinberg [15], ξ parametrizes a possible mixing of the spin-3/2 and spin-1/2 states in the p-μ-p molecule, and this mixing changes the molecular capture rate to

$$\Lambda'_{om} = \xi \Lambda_{om}(1/2) + (1-\xi)\Lambda_{om}(3/2) \ , \tag{13}$$

where $\Lambda_{om}(1/2) = \Lambda_{om}$ and $\Lambda_{om}(3/2) = 2\gamma_O\Lambda_t$ for both OMC and RMC; $\Lambda_{om} = 2\gamma_O(0.75\Lambda_s + 0.25\Lambda_t)$ and $2\gamma_O = 1.009$ [13]. Although the existing theoretical estimate suggests $\xi \simeq 1$ [13], we treat ξ, as we did in Ref. [10], as a parameter to fit the data. Our study [14] demonstrates that, even with this extra adjustable parameter, it is impossible to fit the OMC and the RMC data simultaneously. In Ref. [14] we have also found that both the OMC and RMC capture rates are sensitive to the value of λ_{op}. Obviously, the results of a more precise measurement of λ_{op} at TRIUMF [17] will be very important for both OMC and RMC. Note that since HBChPT constrains the value of g_P with high accuracy, there is not much room for adjusting the value of g_P.

Our findings reported in [14] and briefly summarized in this talk are mostly the reconfirmation of the conclusions stated in one way or another in the literature, but we hope that the coherent treatment of OMC and RMC in liquid hydrogen as described in Ref. [14] would be useful. Although we have presented examples of simulation of the experimental conditions, they are only meant to serve illustrative purposes. Definitive analyses can be done only by the people who carried out the relevant experiments. Finally, we remark that a precise measurement of the OMC rate in hydrogen gas is planned at PSI [16]. This experiment will allow us to avoid the molecular complexity discussed above and directly test the HBChPT prediction [10, 11].

Acknowledgments: We are grateful to Peter Kammel, Tim Gorringe and Harold Fearing for useful comments. This work is supported in part by NSF grant PHY-9900756.

References

[1] See, *e.g.,* M. Morita, *Beta decay and muon capture*, W. A. Benjamin, Inc. (1973).

[2] G. Bardin *et al.*, Phys. Lett. **B 104** (1981) 320; Nucl. Phys. **A 352** (1981) 365.

[3] G. Jonkmans *et al.*, Phys. Rev. Lett. **77** (1996) 4512.

[4] D. H. Wright *et al.*, Phys. Rev. **C 57** (1998) 373.

[5] See, *e.g.*, S.L. Adler and Y. Dothan, Phys.Rev. 151,1267 (1966).

[6] V. Bernard, N. Kaiser and U.-G. Meißner, Phys. Rev. **D50**, 6899 (1994); V. Bernard, H.W. Fearing, T.R. Hemmert and U.-G. Meißner, Nucl. Phys. **A 635**, 121 (1998); *ibid* **A 642**, 563 (1998).

[7] H. W. Fearing, Phys. Rev. **C 21** (1980) 1951.

[8] T. Meissner, F. Myhrer and K. Kubodera, Phys. Lett. **B416** (1998) 36.

[9] S. Ando and D.-P. Min, Phys. Lett. **B 417** (1998) 177.

[10] S. Ando, F. Myhrer and K. Kubodera, Phys. Rev. **C 63** 015203 (2001).

[11] V. Bernard, T. Hemmert and U.-G. Meißner, Nucl. Phys. **A 686**, 290 (2001)

[12] H. W. Fearing, R. Lewis, N. Mobed and S. Scherer, Phys. Rev. **D 56** (1997) 1783; Nucl. Phys. **A 631** (1998) 735c; V. Bernard, H. W. Fearing, T. R. Hemmert and U.-G. Meißner, Nucl. Phys. **A 635** (1198) 121; **A 642** (1998) 563.

[13] D. D. Bakalov, M. P. Faifman, L. I. Ponomarev, and S. I. Vinitsky, Nucl. Phys. **A 384** (1982) 302.

[14] S. Ando, F. Myhrer and K. Kubodera, USC report USC(NT)-01-06, nucl-th/0109068 (2001).

[15] S. Weinberg, Phys. Rev. Lett. **4**, 575 (1960).

[16] D. V. Bailin *et al.*, PSI proposal R-97-05.1 (Dec. 1996); P. Kammel, priv. comm. and talk at the Intern. Riken Conference, MCF01, Shimoda, Japan (April 2001) to appear in Hyperfine Interactions.

[17] D. Armstrong *et al.*, TRIUMF proposal E766 (June 1997).

Modern Dyson-Schwinger equation studies

M.B. Hecht and C.D. Roberts

Physics Division, Argonne National Laboratory
Argonne, IL 60439, USA

(Received: 23 October 2001)

The dichotomy of the pion as QCD's Goldstone mode and a bound state of massive constituents is easily understood using the Dyson-Schwinger equations. That provides the foundation for an efficacious phenomenology, which correlates the pion's charge radius and electromagnetic form factor with its valence quark distribution function; and simultaneously provides a Poincaré covariant description of the nucleon, its form factors and, more recently, meson photoproduction processes. This well-constrained framework can also be used to eliminate candidates for an extension of the Standard Model by providing the relation between current-quark electric dipole moments and that of the neutron.
— A summary of two presentations, one by each author.

1 Introduction

A focus of contemporary studies in QCD is the development of an intuitive understanding of the spectrum and interactions of hadrons in terms of QCD's elementary excitations; i.e., quarks and gluons. Progress can be made by applying a single framework to the calculation of many observables. This facilitates a verification of necessary model assumptions, and the identification of robust correlations between a theory's keystones and hadron properties. Non-hadronic electroweak interactions provide the obvious test bed for any such approach because the electroweak probes are well understood and hence a given experiment yields immediate access to properties of the hadron target. Thus constrained the framework can be used reliably to make predictions for other phenomena, even those far removed from the domain on which it was constrained; e.g., the properties of QCD at nonzero temperature and baryon density.

Herein we supply a brief description of recent progress with the Dyson-Schwinger equations (DSEs) [1] in these applications. A familiar DSE is the gap equation that describes pairing and condensation in low temperature superconductors; another is the Bethe-Salpeter equation, whose solution provides the mass and "wave function" of a bound state in quantum field theory. These are subjects in which the nonperturbative character of DSEs is paramount, to which we will return. However, at their simplest, the DSEs are a generating tool for perturbation theory: the weak coupling expansion of any particular DSE yields all the well-known Feynman diagrams. This is of immense help in studying QCD because it means there is little or no model dependence in the ultraviolet behaviour of calculated quantities. The key model-dependence is limited to the infrared domain, a property that can be exploited to probe the dynamics underlying confinement and dynamical chiral symmetry breaking (DCSB), which are QCD's signature nonperturbative phenomena. The recent successes and current challenges in this application are documented in Refs. [2, 3].

2 Dynamical chiral symmetry breaking

While the dynamical breaking of chiral symmetry in QCD is fundamental to the success of chiral perturbation theory: it is only owing to DCSB that $m_\pi = 0$ in the chiral limit and the scale of f_π is set by the constituent-quark mass, understanding the origin of this phenomenon is outside the scope of the theory. This is where QCD's *gap equation*, depicted in Fig. 1, finds immediate

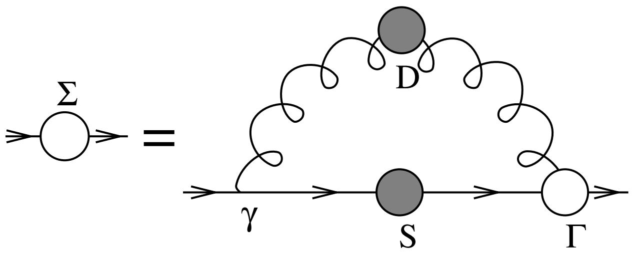

Figure 1: QCD Gap Equation or Dyson-Schwinger equation for the quark self energy, Σ. Here: D is the dressed-gluon propagator; Γ, the dressed-quark-gluon vertex; and $S = 1/[i\gamma\cdot p + m + \Sigma(p)]$, the dressed-quark propagator.

application [4]. The solution provides the dressed-quark propagator in terms of the self-energy, Σ:

$$S(p) \;=\; 1/[i\gamma\cdot p + m + \Sigma(p)]\,, \qquad \Sigma(p) = i\gamma\cdot p\,[A(p^2)-1] + B(p^2)\,, \tag{1}$$

where m is the current-quark mass, and the functions $A(p^2)$, $B(p^2)$ are completely determined by the nature of the force between quarks.

Employing a weak coupling expansion yields the perturbative results: $A(p^2) \approx 1$ and

$$B(p^2) = m\left(1 - \frac{3\alpha_s}{4\pi}\ln[p^2/m^2] + \ldots\right)\,, \tag{2}$$

where the ellipsis indicates that, like the zeroth and first order contributions, every higher-order term in the perturbative evaluation of $B(p^2)$ is proportional to the current-quark mass. Hence at every finite order in perturbation theory the scalar piece of the quark's self-energy, $B(p^2)$, vanishes in the chiral limit, $m = 0$. Therefore dynamical mass generation, and hence DCSB, is impossible in perturbation theory.

Now the essentially nonperturbative character of DSEs becomes important. The self-energy appears in the denominator of the r.h.s. in Fig. 1 but in the numerator on the l.h.s. This makes the equation nonlinear and hence its self-consistent solution can exhibit properties inaccessible in perturbation theory. Using simple models of the equation's kernel one can unambiguously establish that $B(p^2) \neq 0$ is the favoured solution in the chiral limit if, and only if, the integrand provides sufficient support on the domain $k^2 \in [0,2]\,\mathrm{GeV}^2$; i.e., if the effective coupling in the infrared is *strong enough* [4,5]. A realistic, one-parameter model of the effective interaction [6] yields the mass function depicted in Fig. 2. It is important to remember that the existence of a nonzero solution in the chiral limit is a purely nonperturbative effect. Hence the domain on which the chiral limit solution and the u-quark solution are nearly indistinguishable is that on which nonperturbative dynamics is dominant in QCD: where they separate marks the beginning of the perturbative domain and this point is characterised by a length-scale of $\sim 0.15\,\mathrm{fm}$.

The quark condensate is a fundamental fitting parameter in chiral perturbation theory. In DSE studies it is a calculated quantity that can simply be read-off from the large-p^2 behaviour of the dressed-quark mass function. In Landau gauge

$$M(p^2) \stackrel{\text{large}-p^2}{=} \frac{2\pi^2\gamma_m}{3}\,\frac{\left(-\langle\bar{q}q\rangle^0\right)}{p^2\left(\frac{1}{2}\ln\left[\frac{p^2}{\Lambda^2_{\rm QCD}}\right]\right)^{1-\gamma_m}}\,, \tag{3}$$

where $\gamma_m = 12/(33-2N_f)$, $N_f = 4$, is the anomalous mass dimension, and $\langle\bar{q}q\rangle^0$ is the gauge-invariant and renormalisation-point-independent vacuum quark condensate, which is easily evolved to the mass-scale $\sim 1\,\mathrm{GeV}$ relevant to chiral perturbation theory. The one-parameter model of Ref. [6] yields

$$-\langle\bar{q}q\rangle^0_{1\,\mathrm{GeV}} = (0.241\,\mathrm{GeV})^3\,, \tag{4}$$

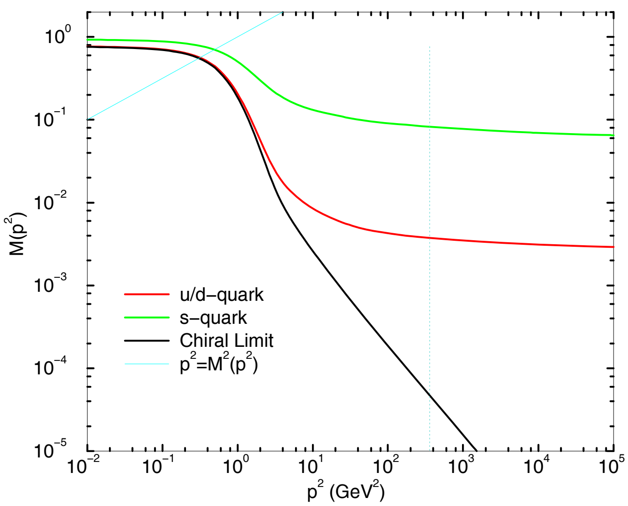

Figure 2: Quark mass function: $M(p^2) = B(p^2)/A(p^2)$, in the chiral limit, and for the u-quark (isospin symmetry is assumed): $m_u^{1\,\mathrm{GeV}} = 5.5\,\mathrm{MeV}$, and the s-quark: $m_s^{1\,\mathrm{GeV}} = 130\,\mathrm{MeV}$. The intersection of the line $p^2 = M^2(p^2)$ with a given curve gives the Euclidean constituent-quark mass [6].

a value consistent with recent lattice simulations [7]. The condensate's value is a QCD analogue of the Cooper pair density in a BCS superconductor, and the value in Eq. (4) corresponds to a density of $1.8\,\mathrm{fm}^{-3}$. Each sphere in a close-packed sea with this density would have a radius $r_{\langle\bar{q}q\rangle} = 0.76\,\mathrm{fm}$, which is just 15% larger than the pion's charge radius and 13% less that the proton's. This comparison underscores the importance of a proper description of DCSB in any attempt to explain low-energy phenomena.

3 Mesons

An aim of contemporary experiments is to explore the transition between the nonperturbative and perturbative domains in QCD. That requires momentum transfers at which a theoretical description of the reactions must be Poincaré covariant. For mesons this means employing an homogeneous Bethe-Salpeter equation (BSE) to calculate the mass, and the amplitude that will be used in evaluating necessary matrix elements. (While QCD's gap equation is a DSE for the dressed-quark 2-point function, a propagator, the BSE is a DSE for a 3-point function; i.e., a vertex.) There is a direct connection between the Bethe-Salpeter bound state equation and the vertices that appear in the Ward-Takahashi identities that are a true field theoretical representation of current conservation. The simplest of these identities relate the vertices to the dressed-quark propagator and therefore their fulfillment is only possible if there is a tight connection between the kernel in QCD's gap equation and that in the Bethe-Salpeter equations.

It is a feature of quantum field theory that the Bethe-Salpeter kernel cannot be written in a closed form and hence all concrete calculations must employ a truncation. This is also true of the gap equation's kernel. It is commonplace to find calculations that ignore the constraints applied by the Ward-Takahashi identities, and employ kernels in the the gap equation and the BSE that are incompatible. Such studies necessarily violate the chiral symmetry constraints which the success of chiral perturbation theory has shown to be so important in low-energy QCD. It need not be thus.

3.1 A mass formula

There is at least one practical, systematic, symmetry preserving truncation of the DSEs [8]. It has been used [9] to prove Goldstone's theorem in QCD, to obtain quark-level Goldberger-Treiman relations that relate the scalar functions in the pion's Bethe-Salpeter amplitude to those in the dressed-quark propagator, and to derive a mass-formula for flavour nonsinglet pseudoscalar mesons:

$$f_H^2\, m_H^2 = -\langle\bar{q}q\rangle_\zeta^H\, \mathcal{M}_\zeta^H \ . \tag{5}$$

In this equation: $\mathcal{M}_\zeta^H = m_\zeta^{q_1} + m_\zeta^{q_2}$ is the sum of the current-quark masses of the meson's constituents, with ζ the renormalisation point; the electroweak decay constant is obtained from

$$f_H \, P_\mu = Z_2(\zeta,\Lambda) \int^\Lambda \frac{d^4 q}{(2\pi)^4} \, \mathrm{tr} \left[\left(\tfrac{1}{2} T^H\right)^{\mathrm{t}} \gamma_5 \gamma_\mu \mathcal{S}(q_+) \Gamma^H(q;P) \mathcal{S}(q_-) \right] \,, \tag{6}$$

with $Z_2(\zeta,\Lambda)$ the quark wavefunction renormalisation, Λ the mass-scale in a translationally invariant regularisation of the integral, $q_\pm = q \pm P/2$ (P_μ is the meson's momentum and Γ^H is its bound state amplitude), and, e.g., $T^{\pi^+} = (\lambda^1 + i\lambda^2)/2$, where $\{\lambda^j, j = 1, \ldots, 8\}$ are the Gell-Mann matrices, and $(\cdot)^{\mathrm{t}}$ denotes matrix transpose; and the in-hadron condensate is

$$i\langle \bar{q} q \rangle_\zeta^H = f_H \, Z_4(\zeta,\Lambda) \int^\Lambda \frac{d^4 q}{(2\pi)^4} \, \mathrm{tr} \left[\left(\tfrac{1}{2} T^H\right)^{\mathrm{t}} \gamma_5 \mathcal{S}(q_+) \Gamma^H(q;P) \mathcal{S}(q_-) \right] \,. \tag{7}$$

The Z_2 on the r.h.s. of Eq. (6) ensures that f_H is gauge invariant, and cutoff and renormalisation-point independent; i.e., that it is observable. (Equation. (6) is the field theoretical expression for the pseudovector projection of the pion's wavefunction at the origin in configuration space.) Furthermore, the quark-level Goldberger-Treiman relations and Eq. (6) make plain that in the presence of DCSB the magnitude of the pion's leptonic decay constant is set by the constituent-quark mass. The same is true for $\langle \bar{q} q \rangle_\zeta^H$, which, in the chiral limit, is identical to the vacuum quark condensate [9]. The factor Z_4 ensures that the in-hadron condensate is gauge and cutoff independent, and that its renormalisation-point dependence is precisely that required to ensure $\langle \bar{q} q \rangle_\zeta^H \mathcal{M}_\zeta$ is renormalisation-point *in*-dependent.

Equation (5) is written suggestively: it has the appearance of the Gell-Mann–Oakes–Renner relation, and it can be shown [9] that for small current-quark masses it does indeed coincide with that formula. The new aspect of the equation is that it is valid *independent* of the current-quark mass of the constituents: the DSE derivation assumes nothing about the size of $m_\zeta^{q_1,q_2}$. It has consequently been used to prove that the mass of a heavy pseudoscalar meson rises linearly with the mass of its heaviest constituent [10]. Equation (5) is a single mass formula that unifies the light- and heavy-quark domains. It also provides [11] an understanding of recent lattice-QCD data on the current-quark mass-dependence of pseudoscalar meson masses.

The truncation scheme of Ref. [8] is the foundation for a phenomenological model that has been used to very good effect in describing light-quark mesons [6, 12]. That model is the only one to predict [13] a behaviour for the pion's electromagnetic form factor that agrees with the results of a recent Hall C experiment [14]. The large-Q^2 behaviour of the form factor can be obtained algebraically and one finds [15] $Q^2 F_\pi(Q^2) = $ const., up to logarithmic corrections, in agreement with the perturbative-QCD expectation. This result relies on the presence of pseudovector components in the pion's Bethe-Salpeter amplitude, which is guaranteed by the quark-level Goldberger-Treiman relations proved in Ref. [9].

3.2 Pion's valence quark distribution function

The DSEs provide a chiral-symmetry preserving, dynamical approach to QCD, which easily captures the dichotomous nature of the pion as: 1) QCD's Goldstone mode; and 2) a bound state of quarks with large constituent-masses, and unifies the low- and high-Q^2 domains. They are therefore well-suited to a study of the pion's valence-quark distribution function, $u_V^\pi(x)$. (This is a measurable expression of the pion's quark-gluon substructure but it cannot be calculated in perturbation theory.) Since π targets are scarce other means must be employed to measure $u_V^\pi(x)$ and one approach is to infer it from πN Drell-Yan [16], which yields $u_V^\pi(x) \propto (1-x)$ for $x \simeq 1$. However, a DSE calculation predicts [17]: $u_V^\pi(x) \overset{x\sim 1}{\propto} (1-x)^2$, at a resolving scale of $\mu^2 \simeq 1\,\mathrm{GeV}^2$,

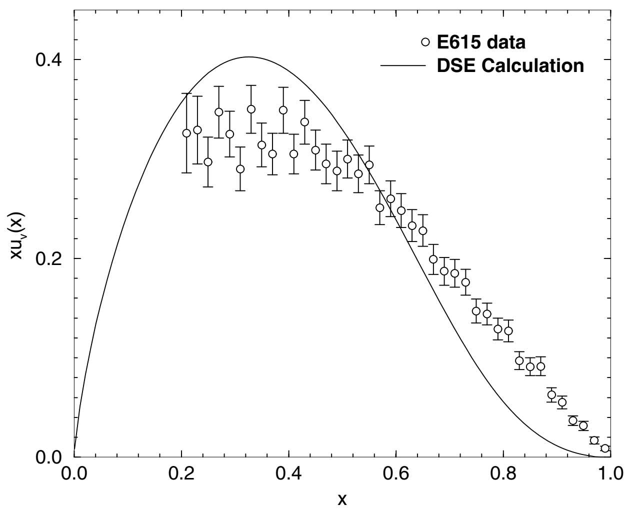

Figure 3: DSE result for $x\, u_V^\pi(x)$ [17], evolved to $\mu^2 = 16\,\mathrm{GeV}^2$ using the first-order, nonsinglet renormalisation group equation, for direct comparison with the Drell-Yan data [16].

and while this conflicts with the extant experimental result, as apparent in Fig. 3, it is consistent with the perturbative-QCD expectation [18]. The discrepancy is very disturbing because a verification of the experimental result would present a profound threat to QCD, even challenging the assumed vector-exchange nature of the interaction. The DSE study [17] has refocused attention on this disagreement, and is the catalyst for a resurgence of interest in $u_V^\pi(x)$ and proposals for its remeasurement [19].

4 Baryons

A direct analogy to treating mesons via the Bethe-Salpeter equation is to describe baryons using a Poincaré covariant Fadde'ev equation. Of course, that equation also involves a kernel about which assumptions must be made in order to arrive at a tractable problem. Here the truncation scheme of Ref. [8] provides, *a posteriori*, a basis for treating baryons as quark-diquark composites using a Fadde'ev equation of the type proposed in Ref. [20]. Therein two quarks are always correlated as a colour-antitriplet diquark quasiparticle (because ladder-like gluon exchange is attractive in the $\bar{3}_c$ quark-quark scattering channel) and binding in the nucleon is effected by the iterated exchange of roles between the dormant and diquark-participant quarks. A first numerical study of this Fadde'ev equation was reported in Ref. [21], and following that there have been numerous more extensive analyses and applications; e.g., Refs. [22,23], which are reviewed in Ref. [24].

4.1 Fadde'ev amplitude Ansatz

In developing an efficacious phenomenology it is possible to bypass solving the Fadde'ev equation, which can be a numerically intensive process, and employ a product *Ansatz* for the nucleon's bound state amplitude; an approach kindred to that which is still employed fruitfully in the study of meson properties, e.g., Ref. [25]. The simplest *Ansatz* retains only a scalar (0^+) diquark correlation and models the nucleon's amplitude as [26]:

$$\psi(p_i,\alpha_i,\tau_i) \propto \varepsilon_{c_1c_2c_3}\, [\Gamma^{0^+}(\tfrac{1}{2}(p_1-p_2);K)]^{\tau_1\tau_2}_{\alpha_1\alpha_2}\ \Delta^{0^+}(K)\ [\mathcal{S}(\ell;P)u(P)]^{\tau_3}_{\alpha_3}\ , \tag{8}$$

where: (p_i,α_i,τ_i) are the momenta, spin and isospin labels of the quarks comprising the nucleon; $\varepsilon_{c_1c_2c_3}$ is the Levi-Cività symbol that gives the colour singlet factor; $P = p_1+p_2+p_3$, $K = p_1+p_2$ and $\ell = (-p_1-p_2+2p_3)/3$; $\Delta^{0^+}(K)$ is a pseudoparticle propagator for the scalar diquark formed from quarks 1 and 2, and Γ^{0^+} is a Bethe-Salpeter-like amplitude describing their relative momentum

	Obs.	Calc.
$(r_p)^2$ (fm^2)	$(0.87)^2$	$(0.78)^2$
$(r_n)^2$ (fm^2)	$-(0.34)^2$	$-(0.40)^2$
μ_p (μ_N)	2.79	2.85
μ_n (μ_N)	-1.91	-1.61
$g_{\pi NN}$	13.4	13.9
$\langle r^2_{\pi NN}\rangle$ (fm^2)	$(0.93\text{-}1.06)^2$	$(0.63)^2$
g_A	1.26	0.98
$\langle r^2_A\rangle$ (fm^2)	$(0.68 \pm 0.12)^2$	$(0.83)^2$
$g_{\rho NN}$	6.4	5.61
$g_{\omega NN}$	7–10.5	10.0

Table 1: Calculated values of a range of physical observables obtained [26] using the Fadde'ev *Ansatz* parameters in Eq. (11). The "Obs." column reports experimental values [27] or values employed in a typical meson exchange model [28].

correlation; $\mathcal{S}$, a 4×4 Dirac matrix, describes the relative quark-diquark momentum correlation; and $u(P)$ is a free-nucleon spinor. The unknown functions are parametrised as ($\mathcal{F}(x) = (1-\mathrm{e}^{-x})/x$):

$$\Delta^{0^+}(K) = \frac{1}{m^2_{0^+}}\,\mathcal{F}(K^2/\omega^2_{0^+})\,,\; \Gamma^{0^+}(k;K) = \frac{1}{\mathcal{N}^{0^+}}\,Ci\gamma_5\, i\tau_2\,\mathcal{F}(k^2/\omega^2_{0^+})\,, \tag{9}$$

$$\mathcal{S}(\ell;P) = \frac{1}{\mathcal{N}^{\psi}}\,\mathcal{F}(\ell^2/\omega^2_{\psi})\left[I_{\rm D} - \frac{\rm R}{M}\left(i\gamma\cdot\ell - \ell\cdot\hat{P}\,I_{\rm D}\right)\right]\,, \tag{10}$$

where: $C = \gamma_2\gamma_4$ is the charge conjugation matrix; $\mathcal{N}^{0^+}$ is a calculated normalisation factor that guarantees an electric charge of 1/3 for the scalar diquark; $\mathcal{N}^{\psi}$ is a similar factor that ensures the proton has unit charge; and $\rm R = 0.5$ measures the ratio of lower to upper component in the nucleon's spinor in the rest frame, which is taken from Fadde'ev equation studies [11]. The model has three parameters: m_0^+, the diquark's mass; and ω_{0^+} and ω_ψ. They have physical intepretations: $d_{0^+} = 1/m_{0^+}$ is the distance over which a scalar diquark correlation can propagate inside the nucleon; $l_{0^+} = 1/\omega_{0^+}$ is a measure of the mean separation between the quarks in the scalar diquark; and $l_\psi = 1/\omega_\psi$ measures the mean separation between the dormant quark and the diquark.

In the many applications of this *Ansatz* the parameters are typically determined by requiring a least-squares fit to the proton's electromagnetic form factor, as described in Ref. [26]. The procedure yields (in GeV or fm, as appropriate)

$$\begin{array}{ccc|ccc} m_{0^+} & \omega_{0^+} & \omega_\psi & 1/m_{0^+} & 1/\omega_{0^+} & 1/\omega_\psi \\ \hline 0.62 & 0.79 & 0.23 & 0.32 & 0.25 & 0.86 \end{array} \tag{11}$$

and it is plain that these values provide an internally consistent picture: $l_{0^+} < l_\psi$, which means that the dormant quark is spatially separated from the diquark; and $d_{0^+} < r_p$, the proton's charge radius, so that the diquark doesn't propagate outside the nucleon. The subsequent calculated results are then predictions and tests of the model's fidelity, which can be gauged from Table 1.

4.2 Meson photoproduction

The same *Ansatz* is being used to study photoproduction of mesons from the nucleon. These processes are important for developing an understanding of the structure of nucleon resonances and in searching for "missing" resonances; i.e., those states predicted by constituent quark models that are hitherto unobserved. The aim of these calculations is to provide and constrain the input to meson exchange models, which are the tool that makes possible a comparison with data by subsequently incorporating details of the reaction mechanism. First results for ω photoproduction were presented in Ref. [29] and, while only the t-channel π-exchange mechanism was described, the results at forward angles, where this process must dominate, demonstrate the approach's promise. A calculation of the contributions to the cross-section from the s- and u-channel processes is almost complete.

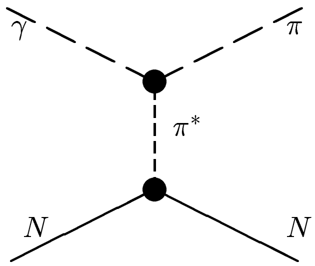

Figure 4: t-channel π-exchange contribution to the π-photoproduction amplitude. In meson exchange models the $\gamma\pi^*\pi$ vertex is usually considered momentum-independent.

Meanwhile the analogous contribution to pion photoproduction, illustrated in Fig. 4, has been calculated and the parameter-free results are depicted in Fig. 5. The solid curve is the Born approximation calculated using an efficacious meson exchange model [31]. That model neglects the necessary momentum dependence of the $\gamma\pi^*\pi$ vertex, for which the DSEs make a prediction. Including the calculated vertex yields the short-dashed curve in Fig. 5, which is not materially different. *A posteriori*, this justifies the meson exchange model expedient of neglecting quark-gluon substructure for these vertices. Of course, with the new DSE predictions, quantitative improvements are now possible. The dashed and dot-dashed curves in Fig. 5 were obtained using the calculated dipole width for the πNN vertex: $F_{\pi NN}(t_\pi)$, which is larger ($\lesssim 2$) than that fitted to data in Ref. [31]. The effect is significant in this case. However, there are preliminary indications that the particularly soft form factor used in the meson exchange model is implicitly also accounting for off-nucleon-mass-shell suppression in the form factor. It is a known property (see, e.g., Ref. [25]) that vertices describing the interaction of three composite objects provide suppression when any one of the attached legs is off-shell. The DSE prediction for the strength of this effect will facilitate the qualitative improvement of meson exchange models by making possible the explicit representation of this phenomenon.

4.3 Neutron's electric dipole moment

A well-founded description of the nucleon makes many applications possible, even constraining extensions of the Standard Model, which is an important focus of contemporary nuclear and particle physics. It has long been known that the possession of an electric dipole moment (EDM) by a spin-1/2 particle would signal the violation of time-reversal invariance. Any such effect is likely small, given the observed magnitude of CP and T violation in the neutral kaon system, and this makes neutral particles the obvious subject for experiments: the existence of an electric monopole charge would overwhelm most signals of the dipole strength. It is therefore natural to focus on the neutron, which is the simplest spin-$\frac{1}{2}$ neutral system in nature. Attempts to measure the neutron's EDM, d_n, have a long history and currently [32]

$$|d_n| < 6.3 \times 10^{-26}\, e\,\mathrm{cm}\ (90\%\ \mathrm{C.L.})\ . \tag{12}$$

(NB. $e/(2M_n) = 1.0 \times 10^{-14}\, e\,\mathrm{cm}$. Therefore, writing $d_n = eh_n/(2M)$, where M is the neutron's mass and h_n is its "gyroelectric ratio," Eq. (12) corresponds to $|h_n| < 6.0 \times 10^{-12}$.)

This experimental constraint on d_n has been very effective in ruling out candidates for theories that enlarge the Standard Model. That is true because in the Standard Model the first nonzero contribution to a free quark's EDM appears at third order and involves a gluon radiative correction (i.e., $\mathrm{O}(\alpha_s\, G_F^2)$, for the same reason that flavour-changing neutral currents are suppressed: the GIM mechanism) so that [26]

$$d_n^{\mathrm{SM}} \lesssim 10^{-34}\, e\,\mathrm{cm}\ . \tag{13}$$

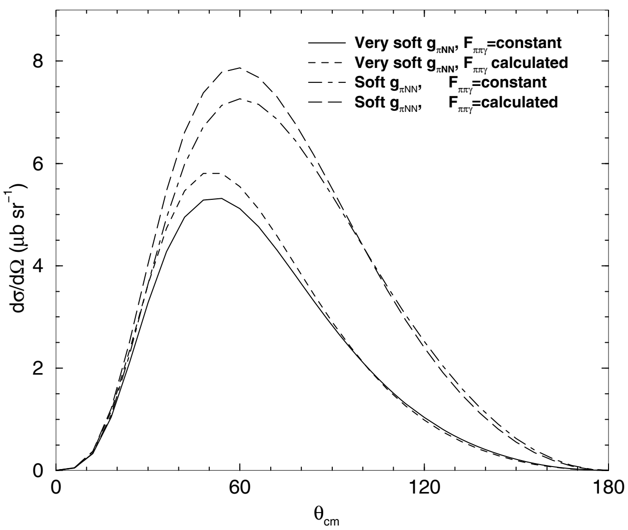

Figure 5: $\gamma N \to \pi N$ differential cross-section at $E_\gamma = 0.34\,\mathrm{GeV}$ as obtained solely from the Born diagram in Fig. 4. The solid line is the Born cross-section obtained [30] using the meson exchange model of Ref. [31] whose parameters were fitted to data in a full T-matrix calculation. The remaining curves, discussed in the text, are calculated using DSE input.

This is seven orders-of-magnitude less than the experimental upper bound. However, the Standard Model is peculiar in this regard and candidates for its extension typically contain many more possibilities for CP and T violation, which are not *a priori* constrained to be small. Hence Eq. (12) is an important and direct constraint on these extensions because Eq. (13) indicates that the Standard Model contribution to d_n cannot interfere at a level that could currently cause confusion.

Extensions of the Standard Model are typically used to predict current-quark EDMs, and to proceed from these to a result for d_n one must have an understanding of the relation between current-quarks and constituent-quarks, and a reliable model of the neutron. The DSEs give both: the first from the gap equation, and the second from the Fadde'ev equation studies and their phenomenological application. Putting these elements together one arrives [26] at a quantitative relation between the current-quark's gyroelectric ratio and that of the neutron: $h_n \approx -91\, h_d$. Here the very large magnifying factor: 91, owes its appearance to DCSB, which turns the current-quark into the constituent-quark, and it means that Eq. (12) applies the following bound:

$$|h_d| < 7.4 \times 10^{-14}\,. \tag{14}$$

(NB. Most extensions of the Standard Model predict $h_u \ll h_d$.) This DCSB-tightened bound very much threatens the viability of a popular three-Higgs-boson model of spontaneous CP violation [33]. Furthermore, and importantly, the result in Eq. (14) is independent of the model used to calculate h_d and hence can be applied directly to constrain any extension of the Standard Model.

5 Epilogue

Owing to dynamical chiral symmetry breaking in QCD the pion appears as both a Goldstone mode and a bound state of massive constituents. The existence of at least one systematic, symmetry preserving truncation scheme makes a detailed understanding and explanation of this phenomenon possible using the Dyson-Schwinger equations (DSEs). This is the starting point for a successful phenomenology of strong interaction phenomena, which quantitatively and qualitatively unifies the low- and high-energy regimes. Since the DSEs maintain contact with perturbation theory, the model-dependence is restricted to a statement about the infrared behaviour of the quark-quark interaction; i.e., the unknown nature of the long-range force in QCD. This remaining model-dependence is a virtue because it makes possible the correlation of observables via a parametrisation of this infrared behaviour and hence the use of experiments as a probe of the confining force.

Acknowledgment: This work was supported by the US Department of Energy, Nuclear Physics Division, under contract no. W-31-109-ENG-38.

References

[1] C.D. Roberts and A.G. Williams, Prog. Part. Nucl. Phys. **33**, 477 (1994).
[2] C.D. Roberts and S.M. Schmidt, Prog. Part. Nucl. Phys. **45**, S1 (2000).
[3] R. Alkofer and L. v. Smekal, Phys. Rept. **353**, 281 (2001).
[4] For a pedagogical introduction see: C.D. Roberts, "Nonperturbative QCD with Modern Tools," in *Frontiers in Nuclear Physics*, edited by S. Kuyucak (World Scientific, Singapore, 1999) pp. 212-261.
[5] C.D. Roberts, "Continuum strong QCD: Confinement and dynamical chiral symmetry breaking," nucl-th/0007054.
[6] P. Maris and C.D. Roberts, Phys. Rev. C **56**, 3369 (1997).
[7] P.C. Tandy, "Soft QCD modeling of meson electromagnetic form factors," nucl-th/0106031.
[8] A. Bender, C.D. Roberts and L. v. Smekal, Phys. Lett. **B 380**, 7 (1996).
[9] P. Maris, C.D. Roberts and P.C. Tandy, Phys. Lett. **B 420**, 267 (1998).
[10] M.A. Ivanov, Yu.L. Kalinovsky and C.D. Roberts, Phys. Rev. **D 60**, 034018 (1999).
[11] M.B. Hecht, C.D. Roberts and S.M. Schmidt, "Contemporary applications of Dyson-Schwinger equations," nucl-th/0010024.
[12] P. Maris, these proceedings.
[13] P. Maris and P.C. Tandy, Phys. Rev. C **61**, 045202 (2000).
[14] J. Volmer *et al.* [The Jefferson Lab F_π Collaboration], Phys. Rev. Lett. **86**, 1713 (2001).
[15] P. Maris and C.D. Roberts, Phys. Rev. C **58**, 3659 (1998).
[16] J.S. Conway *et al.*, Phys. Rev. D **39**, 92 (1989).
[17] M.B. Hecht, C.D. Roberts and S.M. Schmidt, Phys. Rev. C **63**, 025213 (2001).
[18] S.J. Brodsky, M. Burkardt and I. Schmidt, Nucl. Phys. B **441**, 197 (1995).
[19] R.J. Holt and P.E. Reimer, "Structure of the Goldstone bosons," nucl-ex/0010004; K. Wijesooriya, *et al.*, "The $H(e,e'n)X$ Reaction and the Pion Structure Function," proposal no. JLab PR01-110.
[20] R.T. Cahill, C.D. Roberts and J. Praschifka, Austral. J. Phys. **42**, 129 (1989).
[21] C.J. Burden, R.T. Cahill and J. Praschifka, Austral. J. Phys. **42**, 147 (1989).
[22] H. Asami, N. Ishii, W. Bentz and K. Yazaki, Phys. Rev. C **51**, 3388 (1995); H. Mineo, W. Bentz and K. Yazaki, *ibid.* **60**, 065201 (1999).
[23] M. Oettel, M.A. Pichowsky and L. von Smekal, Eur. Phys. J. A **8**, 251 (2000); M. Oettel, R. Alkofer and L. von Smekal, Eur. Phys. J. A **8**, 553 (2000).
[24] M.A. Pichowsky, these proceedings.
[25] M.A. Pichowsky, S. Walawalkar and S. Capstick, Phys. Rev. D **60**, 054030 (1999).
[26] M.B. Hecht, C.D. Roberts and S.M. Schmidt, Phys. Rev. C **64**, 025204 (2001).
[27] K.L. Miller *et al.*, Phys. Rev. **D 26**, 537 (1982); T. Kitagaki *et al.*, Phys. Rev. D **28**, 436 (1983); S. Kopecky, P. Riehs, J.A. Harvey and N.W. Hill, Phys. Rev. Lett. **74**, 2427 (1995); S.G. Karshenboim, Can. J. Phys. **77**, 241 (1999); D.E. Groom *et al.*, Eur. Phys. J. **C 15**, 1 (2000).
[28] T. Sato and T.S. Lee, Phys. Rev. C **54**, 2660 (1996).
[29] M.B. Hecht, C.D. Roberts and S.M. Schmidt, "The character of Goldstone bosons," nucl-th/0106011.
[30] T.-S.H. Lee, private communication.
[31] T. Sato and T.-S.H. Lee, Phys. Rev. C **54**, 2660 (1996).
[32] P.G. Harris, *et al.*, Phys. Rev. Lett. **82**, 904 (1999).
[33] S. Weinberg, Phys. Rev. Lett. **37**, 657 (1976).

Electromagnetic, weak, and strong interactions of light mesons

P. Maris

Dept. of Physics, North Carolina State University, Raleigh, NC 27695-8202, U.S.A.

(Received: 30 October 2001)

The ladder-rainbow truncation of the set of Dyson–Schwinger equations is used to study a variety of electroweak and strong processes involving light mesons. The parameters in the effective interaction are constrained by the chiral condensate and f_π; the current quark masses are fitted to m_π and m_K. The obtained electromagnetic form factors are in good agreement with the data. Also the weak K_{l3} decay and the radiative and strong decays of the vector mesons agree reasonably well with the data. Finally, we indicate how processes such as π-π scattering can be described within this framework as well.

1 Introduction

Our goal is to describe the hadrons and their interactions in terms of their constituents, quarks and gluons, using the underlying theory, QCD. The set of Dyson–Schwinger equations [DSEs] form a useful tool for this purpose [1]. In rainbow-ladder truncation, they have been successfully applied to calculate the masses and decay constants of light pseudoscalar and vector mesons [2,3]. The dressed-quark propagator, as obtained from its DSE, together with the meson Bethe–Salpeter amplitude [BSA], form the necessary elements for calculations of strong interactions in impulse approximation, such as the $\rho \to \pi\pi$ decay. For electroweak processes, such as the electromagnetic form factors, radiative decays, and semileptonic decays, one also needs the $q\bar{q}\gamma$ and $q\bar{q}W$ vertices.

1.1 *Dyson–Schwinger equations*

The DSE for the renormalized quark propagator in Euclidean space is

$$S(p)^{-1} = i\, Z_2\, \not p + Z_4\, m(\mu) + Z_1 \int \frac{d^4q}{(2\pi)^4}\, g^2 D_{\mu\nu}(p-q)\, \tfrac{\lambda^i}{2}\gamma_\mu\, S(q)\, \Gamma^i_\nu(q,p) \;, \tag{1}$$

where $D_{\mu\nu}(k)$ is the dressed-gluon propagator and $\Gamma^i_\nu(q;p)$ the dressed-quark-gluon vertex. The most general solution of Eq. (1) has the form $S(p)^{-1} = i\not p A(p^2) + B(p^2)$ and is renormalized at spacelike μ^2 according to $A(\mu^2) = 1$ and $B(\mu^2) = m(\mu)$ with $m(\mu)$ the current quark mass.

Mesons are described by solutions of the homogeneous BSE

$$\Gamma_H(p_+,p_-;Q) = \int \frac{d^4q}{(2\pi)^4}\, K(p,q;Q)\; S(q_+)\, \Gamma_H(q_+,q_-;Q)\, S(q_-) \;, \tag{2}$$

at discrete values of $Q^2 = -m_H^2$, where m_H is the meson mass. In this equation, $p_+ = p + \eta Q$ and $p_- = p - (1-\eta)Q$ are the outgoing and incoming quark momenta respectively, and similarly for $q_\pm$. The kernel K is the renormalized, amputated $q\bar{q}$ scattering kernel that is irreducible with respect to a pair of $q\bar{q}$ lines. Together with the canonical normalization condition for $q\bar{q}$ bound states, Eq. (2) completely determines the bound state BSA Γ_H. Different types of mesons, such as (pseudo-)scalar, (axial-)vector, and tensor mesons, are characterized by different Dirac structures.

The dressed $q\bar{q}\gamma$ and $q\bar{q}W$ vertices satisfy an inhomogeneous BSE: e.g. the quark-photon vertex $\Gamma_\mu(p_+,p_-;Q)$, with Q the photon momentum and $p_\pm$ the quark momenta, satisfies [4]

$$\Gamma_\mu(p_+,p_-;Q) = Z_2\, \gamma_\mu + \int \frac{d^4q}{(2\pi)^4}\, K(p,q;Q)\; S(q_+)\, \Gamma_\mu(q_+,q_-;Q)\, S(q_-) \;. \tag{3}$$

Solutions of the homogeneous version of Eq. (3) define vector meson bound states at timelike photon momenta $Q^2 = -m_V^2$. It follows that $\Gamma_\mu(p_+,p_-)$ has poles at those locations [5].

Table 1: Overview of results for the light pseudoscalar and vector meson masses and leptonic decay constants, all in GeV. Experimental data are from Ref. [6].

	m_π	f_π	m_K	f_K	m_ρ	f_ρ	m_{K^*}	f_{K^*}	m_ϕ	f_ϕ
calc.	0.138	0.131	0.497	0.155	0.742	0.207	0.936	0.241	1.072	0.259
expt.	0.138	0.131	0.496	0.160	0.770	0.216	0.892	0.225	1.020	0.236

1.2 Model truncation

To solve the BSE, we use a ladder truncation,

$$K(p,q;P) \to -\mathcal{G}\big((p-q)^2\big)\, D_{\mu\nu}^{\rm free}(p-q)\tfrac{\lambda^i}{2}\gamma_\mu \otimes \tfrac{\lambda^i}{2}\gamma_\nu \;, \tag{4}$$

in conjunction with the rainbow truncation for the quark DSE: $\Gamma^i_\nu(q,p) \to \gamma_\nu\lambda^i/2$ together with $Z_1 g^2 D_{\mu\nu}(k) \to \mathcal{G}(k^2) D_{\mu\nu}^{\rm free}(k)$ in Eq. (1). This truncation preserves, independent of the details of the effective interaction $\mathcal{G}(k^2)$, both the vector Ward–Takahashi identity [WTI] for the $q\bar{q}\gamma$ vertex and the axial-vector WTI. The latter ensures the existence of massless pseudoscalar mesons connected with dynamical chiral symmetry breaking [2]. In combination with impulse approximation, the former ensures electromagnetic current conservation [5].

For the effective quark-antiquark interaction, we employ the Ansatz given in Ref. [3]. The ultraviolet behavior of this effective interaction is chosen to be that of the QCD running coupling $\alpha(k^2)$; the ladder-rainbow truncation then generates the correct perturbative QCD structure of the DSE-BSE system of equations. In the infrared region, the interaction is sufficiently strong to produce a realistic value for the chiral condensate of about $(240\,\mathrm{GeV})^3$. With this model, we can solve the BSE for pseudoscalar and vector mesons, and calculate the meson masses and leptonic decay constants. The model parameters, along with the quark masses, are fitted to give a good description of the chiral condensate, $m_{\pi/K}$ and f_π. The results of our model calculations [3] are shown in Table 1 and are in reasonable agreement with the data.

2 Meson interactions

In impulse approximation, processes such as electromagnetic scattering, the weak K_{l3} decay, radiative and strong decays of vector mesons, can all be described by the same generic loop integral

$$I^{abc}(P,Q,K) = N_c \int \frac{d^4q}{(2\pi)^4}\,\mathrm{Tr}\big[S^a(q)\,\Gamma^{a\bar{b}}(q,q';P) S^b(q')\,\Gamma^{b\bar{c}}(q',q'';Q)\,S^c(q'')\,\Gamma^{c\bar{a}}(q'',q;K)\big] \;, \tag{5}$$

where $q-q'=P$, $q'-q''=Q$, $q''-q=K$, and momentum conservation dictates $P+Q+K=0$. In Eq. (5), S^i is the dressed quark propagator with flavor index i, and $\Gamma^{i\bar{j}}(k,k';P)$ stands for a generic vertex function with incoming quark flavor j and momentum k', and outgoing quark flavor i and momentum k. Depending on the specific process under consideration, this vertex function could be a meson BSA, a $q\bar{q}\gamma$ vertex, or, in case of weak processes, a $q\bar{q}W$ vertex. In the calculations discussed below, the propagators, the meson BSAs, and the $q\bar{q}\gamma$ and $q\bar{q}W$ vertices are all obtained as solutions of their respective DSE in rainbow-ladder truncation, without adjusting any of the model parameters.

2.1 Electromagnetic form factors

Meson electromagnetic form factors in impulse approximation are described by two diagrams, with the photon coupled to the quark and to the antiquark respectively. Each diagram corresponds

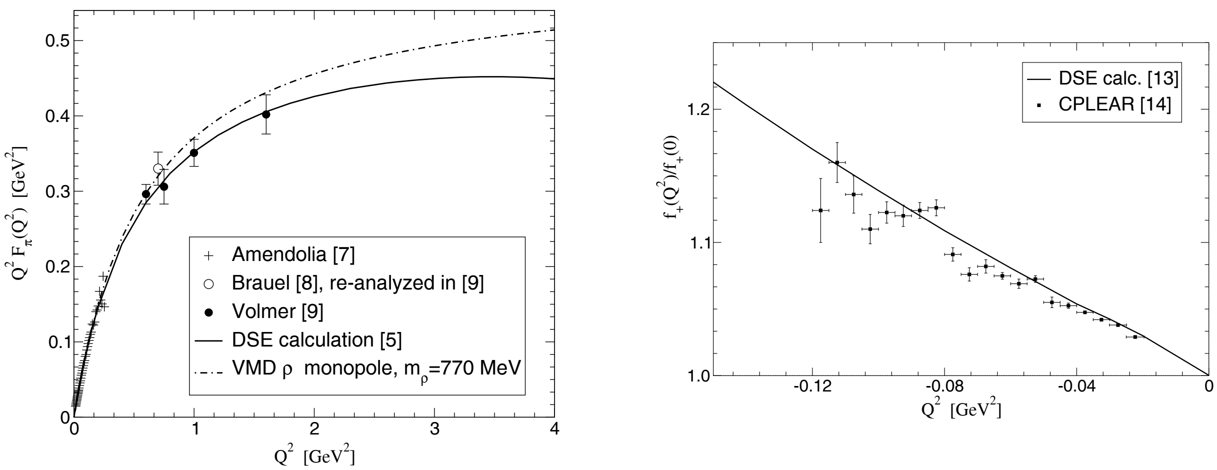

Figure 1: On the left, our result for $Q^2F_\pi(Q^2)$, and right, our curve for the K_{l3} form factor $f_+(Q^2)$.

to an integral like Eq. (5) with two meson BSAs and one $q\bar{q}\gamma$-vertex. With Q being the photon momentum, and the incoming and outgoing pseudoscalar mesons having momentum $P \mp Q/2$, we can define a form factor for each of these diagrams [5]

$$2\,P_\nu\,F_{a\bar{b}\bar{b}}(Q^2) \;\;=\;\; I_\nu^{abb}(P-Q/2,Q,-(P+Q/2))\,. \tag{6}$$

We work in the isospin symmetry limit, and thus $F_\pi(Q^2) = F_{u\bar{u}u}(Q^2)$. The K^+ and K^0 form factors are given by $F_{K^+} = \frac{2}{3}F_{u\bar{s}u} + \frac{1}{3}F_{u\bar{s}\bar{s}}$ and $F_{K^0} = -\frac{1}{3}F_{d\bar{s}d} + \frac{1}{3}F_{d\bar{s}\bar{s}}$ respectively.

Our result for Q^2F_π is shown in Fig. 1, together with experimental data from Refs. [7–9]; the corresponding charge radius, together with the neutral and charged kaon charge radii, are given in Table 2. The obtained charge radii agree quite well with the experimental data [7, 10, 11], as do our form factors. Up to about $Q^2 = 2\,\mathrm{GeV}^2$, our result for F_π can be described very well by a monopole with mass scale given by our calculated m_ρ, $m = 742\,\mathrm{MeV}$. Above this value, our curve starts to deviate more and more from this naive VMD monopole. Our results for F_K are given in Ref. [5] and can be fitted quite well up to about $Q^2 = 2 \sim 3\,\mathrm{GeV}^2$ by a monopole with mass scale slightly larger than the ρ mass. Asymptotically, these form factors behave like $Q^2F(Q^2) \to c$ up to logarithmic corrections [12]. However, numerical limitations prevent us from accurately determining the constants c.

2.2 Weak interactions

The matrix element $\langle\pi^-(P+Q/2)|\bar{s}\gamma_\mu u|K^0(P-Q/2)\rangle$ describing the semileptonic decay of neutral kaons via a W-boson with momentum Q can be characterized by two form factors

$$I_\mu^{dsu}(P-Q/2,Q,-(P+Q/2)) \;\;=\;\; 2\,P_\mu\,f_+(Q^2) + Q_\mu\,f_-(Q^2)\,. \tag{7}$$

Table 2: Calculated charge radii in fm^2, with expt. data [7,10,11], and K_{l3} observables. The double entries for the expt. K_{l3} data [6] correspond to the neutral and charged K_{l3} decays respectively.

	r_π^2	$r_{K^+}^2$	$r_{K^0}^2$	λ_+	λ_0	$-\xi$	$\Gamma(K_{e3})$	$\Gamma(K_{\mu3})$
calc.	0.45	0.38	-0.086	0.027	0.018	0.11	$7.38{\cdot}10^6 s^{-1}$	$4.90{\cdot}10^6 s^{-1}$
expt.	0.44	0.34	-0.054	.0276, .0288	.006, .025	0.31, 0.11	7.50, 3.89	5.26, 2.57

The form factors $f_\pm$ for the K^0 decay are essentially the same as those for K^+; in the isospin limit, the only difference between the matrix elements for the K^0 and the K^+ decay is a factor of $\sqrt{2}$, the π^0 being $(u\bar{u} - d\bar{d})/\sqrt{2}$, which results in a factor of 2 difference in the partial decay width.

In the right panel of Fig. 1 we show our result for $f_+(t)$ [13], together with the experimental data for this form factor [14]. Experiments are often characterized in terms of the transverse, f_+, and the scalar form factor f_0, rather than f_-, which is defined by

$$f_0(Q^2) \;=\; \frac{Q_\mu\, I^{dsu}_\mu\big(P - Q/2, Q, -(P+Q/2)\big)}{m_K^2 - m_\pi^2} = f_+(Q^2) - \frac{Q^2}{m_K^2 - m_\pi^2} f_-(Q^2)\,. \tag{8}$$

The dimensionless slope parameter λ for these form factors is defined as $\lambda = -m_\pi^2 f'(0)/f(0)$; ξ is defined as $f_-(0)/f_+(0)$. The partial decay width can be obtained by integrating the decay rate, which depends on the lepton masses. Both the shape and the magnitude we obtain for these form factors agree well with experiments, as can be seen from Table 2.

2.3 Radiative decay of vector mesons

We can describe the radiative decay of the vector mesons using the same loop integral, Eq. (5), this time with one vector meson BSA, one pseudoscalar BSA, and one $q\bar{q}\gamma$-vertex [18] . The on-shell value gives us the coupling constant, which can be used to calculate the partial decay width. For virtual photons, we can define a form factor $F_{VP\gamma}(Q^2)$, normalized to 1 at $Q^2 = 0$, which can be used in estimating meson-exchange contributions to hadronic processes [15–17].

In the isospin limit, the $\rho^0\,\pi^0\,\gamma$ and $\rho^\pm\,\pi^\pm\,\gamma$ vertices are identical, and are given by

$$\frac{1}{3}\, I^{uuu}_{\mu\nu}(P, Q, -(P+Q)) \;=\; \frac{g_{\rho\pi\gamma}}{m_\rho}\, \epsilon_{\mu\nu\alpha\beta} P_\alpha Q_\beta\, F_{\rho\pi\gamma}(Q^2)\,, \tag{9}$$

where P is the ρ momentum. The $\omega\,\pi\,\gamma$ vertex is a factor of 3 larger, due to the difference in isospin factors. For the $K^\star \to K\gamma$ decay, we have to add two terms: one with the photon coupled to the $\bar{s}$-quark and one with the photon coupled to the u- or d-quark, corresponding to the charged or neutral $K^\star$ decay respectively.

As Eq. (9) shows, it is $g_{VP\gamma}/m_V$ that is the natural outcome of our calculations; therefore, it is this combination that we report in Table 3, together with the corresponding decay widths [18]. The agreement between theory and experiment for $g_{VP\gamma}/m_V$ is within about 10%, except for the discrepancy in the charged $K^\star \to K\gamma$ decay for which we have no explanation. Likewise the large difference between the neutral and charged ρ decay width is beyond the reach of the isospin symmetric impulse approximation. Note that part of the difference between the experimental and calculated decay width comes from the phase space factor because our calculated vector meson masses deviate up to 5% from the physical masses.

2.4 Strong decays of vector mesons

If we continue the calculation of the electromagnetic form factors into the timelike region, we find a pole at the mass of the vector meson bound states. Using the behavior of the electromagnetic form

Table 3: Vector meson radiative decays: coupling g/m in GeV^{-1} and partial decay width in keV.

	g/m	$\Gamma_{\rho^\pm\pi^\pm\gamma}$	$\Gamma_{\rho^0\pi^0\gamma}$	g/m	$\Gamma_{\omega\pi\gamma}$	g/m	$\Gamma_{K^{\star\pm}K^\pm\gamma}$	g/m	$\Gamma_{K^{\star 0}K^0\gamma}$
calc.	0.69	53	(53)	2.07	479	0.99	90	1.19	130
expt.	0.74	68	(102)	2.31	717	0.83	50.3	1.28	116

Table 4: Overview of our results for vector meson strong decays (left): dimensionless coupling constants and partial decay width in MeV, and right, π-π scattering lengths, compared to leading order chiral perturbation theory, $a_0^0 = 7m_\pi^2/(8\pi f_\pi^2)$ and $a_0^2 = -m_\pi^2/(4\pi f_\pi^2)$ [20] (Weinberg's limit).

	$g_{\rho\pi\pi}$	$\Gamma_{\rho\pi\pi}$	$g_{\phi KK}$	$\Gamma_{\phi KK}$	$g_{K^\star K\pi}$	$\Gamma_{K^\star K\pi}$
calc.	5.4	115	4.3	6.7	4.0	31
expt.	6.02	151	4.64	2.2	4.60	50

	a_0^0	a_0^2
calc.	0.170	0.045
Ref. [20]	0.156	0.045

factors $F_{u\bar{u}u}$ and $F_{u\bar{s}\bar{s}}$ around this pole, we can extract the coupling constants $g_{\rho\pi^+\pi^-}$ and $g_{\phi K^+K^-}$ respectively [18] , which govern the strong decays $\rho \to \pi\pi$ and $\phi \to KK$. The results from this analysis are given in Table 4, and are reasonably close to the experimental data. Similarly, the two form factors f_+ and f_0 describing the weak K_{l3} decay exhibit poles at $Q^2 = -m_{K^\star}^2$ and $Q^2 = -m_\kappa^2$ respectively, due to vector and scalar $u\bar{s}$ bound states [13]. From the behavior close to the pole we can extract the coupling constant for the strong decay $K^\star \to K\pi$ as well. A direct calculation of the strong vector meson decays, using on-shell meson BSAs but different numerical techniques [19], agrees reasonably well with these results extracted from the electroweak form factors. Note that the factor of three difference between the experimental and our calculated decay width for the ϕ is due to the phase factor $(1 - 4m_K^2/m_\phi^2)^{3/2}$: with our calculated masses, this factor is 0.051, whereas with the actual physical masses this factor is 0.015. The dimensionless coupling constants agree within 10% to 15% with the experimental data.

3 π-π scattering

Although impulse approximation seems to work remarkably well for a variety of interactions involving three external particles, one has to go beyond impulse approximation in order to describe processes with four (or more) external particles. As an example, consider π-π scattering at threshold. The generic loop integral for π-π scattering in impulse approximation is

$$A \;=\; N_c \int \frac{d^4q}{(2\pi)^4} \mathrm{Tr}\big[S(q)\,\Gamma_\pi(q,q')\,S(q')\,\Gamma_\pi(q',q'')\,S(q'')\,\Gamma_\pi(q'',q''')\,S(q''')\,\Gamma_\pi(q''',q)\big]\,. \quad (10)$$

At threshold in the chiral limit, $\Gamma_\pi(k + P/2, k - P/2) \to i\gamma_5 B(k^2)/f_\pi$, and thus

$$A \;\to\; 4\,N_c \int \frac{d^4k}{(2\pi)^4} \frac{B^4(k)/f_\pi^4}{(k^2A^2(k) + B^2(k))^2}\,, \quad (11)$$

which is nonzero. On the other hand, chiral symmetry dictates that the threshold scattering amplitudes vanish in the chiral limit like m_π^2/f_π^2 [20]. Clearly, impulse approximation is insufficient to describe π-π scattering.

In order to properly describe π-π scattering in the rainbow-ladder truncation, all possible diagrams with one or more insertions of the ladder kernel K across two pion BSAs should be added to the impulse contribution [21], as indicated in Fig. 2. If we include these sets of ladder diagrams, we can show numerically that the threshold π-π scattering amplitudes indeed vanish like m_π^2/f_π^2, using the same model as in the previous section. The corresponding scattering lengths are given in Table 4. We expect that in particular a_0^0 will receive significant corrections from pion loop effects, which we have not included in our calculation: in chiral perturbation theory, higher order corrections (i.e. pion loops) change the leading order result to $a_0^0 = 0.220$ and $a_0^2 = 0.0444$ [22].

So far, we have only considered π-π scattering, but also in other hadronic 4-particle processes one should consider the contributions from these infinite sums of ladder terms, in addition to

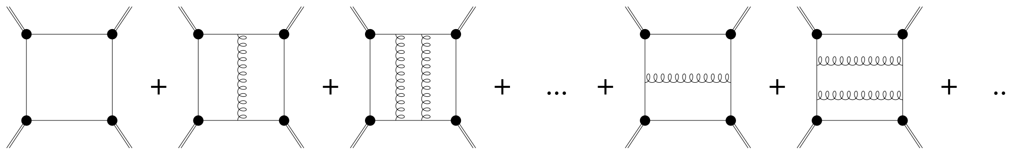

Figure 2: Diagrams needed to correctly describe π-π scattering in rainbow-ladder truncation [21].

the impulse term. In general, we expect the role of these summed ladder contributions to be less important than in π-π scattering, except for processes that receive significant contributions from resonances. By adding these ladder diagrams one can unambiguously incorporate $q\bar{q}$ bound state effects, and we expect that this approach can provide a fundamental underpinning to many processes described by effective meson lagrangians.

Acknowledgments: I would like to thank Peter Tandy for our collaboration on the electromagnetic form factors; the work on π-π scattering was done in collaboration with Pedro Bicudo, Steve Cotanch, Felipe Llanes-Estrada, Emilio Ribiero, and Adam Szczepaniak; I would also like to thank Dennis Jarecke, Chueng-Ryong Ji, and Craig Roberts for useful discussions. This work was funded by DOE under grants No. DE-FG02-96ER40947 and DE-FG02-97ER41048, and by NSF under grant No. INT-9807009, and benefitted from the resources of the National Energy Research Scientific Computing Center.

References

[1] C. D. Roberts and S. M. Schmidt, Prog. Part. Nucl. Phys. **45S1**, 1 (2000); R. Alkofer and L. von Smekal, Phys. Rept. **353**, 281 (2001); see also M.B. Hecht and C.D. Roberts, arXiv:nucl-th/0110058, these proceedings.
[2] P. Maris and C. D. Roberts, Phys. Rev. C **56**, 3369 (1997).
[3] P. Maris and P. C. Tandy, Phys. Rev. C **60**, 055214 (1999).
[4] P. Maris and P. C. Tandy, Phys. Rev. C **61**, 045202 (2000).
[5] P. Maris and P. C. Tandy, Phys. Rev. C **62**, 055204 (2000).
[6] Particle Data Group, C. Caso *et al.*, Eur. Phys. J. **C3**, 1 (1998).
[7] S. R. Amendolia *et al.* [NA7 Collaboration], Nucl. Phys. B **277**, 168 (1986).
[8] P. Brauel *et al.*, Z. Phys. C **3**, 101 (1979).
[9] J. Volmer *et al.* [The Jefferson Lab F(pi) Collaboration], Phys. Rev. Lett. **86**, 1713 (2001).
[10] S. R. Amendolia *et al.*, Phys. Lett. B **178**, 435 (1986).
[11] W. R. Molzon *et al.*, Phys. Rev. Lett. **41**, 1213 (1978) [Erratum-ibid. **41**, 1523 (1978)].
[12] P. Maris and C. D. Roberts, Phys. Rev. C **58**, 3659 (1998).
[13] C. Ji and P. Maris, Phys. Rev. D **64**, 014032 (2001).
[14] A. Apostolakis *et al.*, Phys. Lett. **B473**, 186 (2000).
[15] P. C. Tandy, Prog. Part. Nucl. Phys. **39**, 117 (1997).
[16] J. W. Van Orden, N. Devine and F. Gross, Phys. Rev. Lett. **75**, 4369 (1995).
[17] M. B. Hecht, C. D. Roberts and S. M. Schmidt, arXive:nucl-th/0106011.
[18] P. Maris and P. C. Tandy, arXiv:nucl-th/0109035.
[19] D. Jarecke, P. Maris, and P.C. Tandy, in preparation.
[20] S. Weinberg, Phys. Rev. Lett. **17**, 616 (1966).
[21] P. Bicudo, arXiv:nucl-th/0110052; P. Bicudo, S. Cotanch, F. Llanes-Estrada, P. Maris, E. Ribeiro, and A. Szczepaniak, in preparation.
[22] G. Colangelo, J. Gasser and H. Leutwyler, Phys. Lett. B **488**, 261 (2000).

Dyson-Schwinger studies of baryons

M. A. Pichowsky

Department of Physics, Kent State University, Kent, OH 44240, U.S.A.

(Received: 30 October 2001)

Studies of the Dyson-Schwinger equations of QCD have made impressive advances in recent years. While the early studies were successful in helping to understand the properties of the pion, and elucidate its role as both Goldstone boson and quark-antiquark bound state, more recent studies have explored far-reaching phenomena such as the spectra and decay properties of the light-quark mesons, heavy-quark mesons, as well as quark and gluon dynamics at finite temperatures and densities. Even from the beginning, there has been interest in applying these same methods to three-quark bound states, the baryons. Such studies have been limited by the difficulties in obtaining solutions to realistic models of three-body bound states within quantum field theory. Still, contemporary Dyson-Schwinger studies of baryons continue to make significant advances which promise to provide new insights into the non-perturbative dynamics of quarks and gluons. The basic ideas and principles underlying these studies and some results are presented here.

1 Introduction

Dyson-Schwinger studies focus on exploring the phenomena of hadrons and nuclei in terms of the non-perturbative dynamics of quarks and gluons. This quantum field theoretic approach takes its name from the Dyson-Schwinger Equations (DSEs) of QCD which are used as an organizational framework. The DSEs are an infinite set of coupled integral equations, directly derived from the QCD Lagrangian, that relate all the fully-dressed Green functions of QCD to each other. These Greens functions represent dynamical quantities like the quark and gluon propagators, as well as quark-antiquark scattering amplitudes, three-quark scattering amplitudes and many others. One might say that upon obtaining all of these Green functions, one would have a complete solution of QCD, in that the resulting Green functions could be used to calculate any hadron observable. Of course, the fact that there are an infinite number of such relations ensures that the complete solution is not forthcoming. In practice, one approximates QCD by using what is known as a *truncation* of the DSEs. These lead to a finite and closed set of DSEs which can then be solved exactly. The determination of truncations that provide realistic and useful approximations to QCD is of central importance to the Dyson-Schwinger approach.

A great deal about the utility of a particular DSE truncation can be learned from phenomenological applications to hadron observables. It should be no surprise that there have been many such studies of hadron phenomena. One important aspect of the Dyson-Schwinger framework is that it provides a straight-forward understanding how the non-perturbative dynamics of quark and gluons lead to the unique role of the pion in nature, as both a Goldstone boson of QCD and quark-antiquark bound state. A short account may be found in Ref. [1]. In the past twenty years or so, there has been considerable effort in exploring the light-quark and heavy-quark meson spectra, decays and electromagnetic properties, and more recently to understand aspects of finite-temperature and non-equilibrium QCD that are central to RHIC physics.

In most of the aforementioned topics, the focus of research has been on the meson sector. However, there remains a wealth of information contained within the baryon sector that has yet to be fully tapped within Dyson-Schwinger studies. Baryons represent a new domain which may be more sensitive to particular aspects of QCD that are less constrained by conventional studies of meson phenomena.

Even in the earliest days of the Dyson-Schwinger framework, the importance of studying baryons was clear. Some of the earliest studies were carried out in Ref. [2]. Later, studies [3] included additional degrees of freedom necessary to describe both the nucleon and the low-lying $\Delta(1232)$ resonance (with πN decay quantum numbers $L_{2I,2J} = P_{33}$). Such studies typically employed point-like diquark degrees of freedom owing to the lack of the computational power necessary to carry out more realistic calculations using non-local two-quark correlations. Hence the baryons were viewed as a two-body bound state of a quark and a diquark. This simplification was necessary to avoid the difficulties inherent in solving the fully covariant three-quark bound-state problem. Interest in this problem has continued to grow. Recently, studies have begun to use more realistic degrees of freedom and in particular, finite-sized diquark correlations. The use of finite-sized correlators is far more realistic for a description of two-quark propagation, but requires the introduction of additional (and more complicated) interactions in order to maintain the electromagnetic gauge invariance of the theory [4, 5].

Even so, with all of the effort made towards improving our understanding of the three-quark bound-state problem in QCD [6, 7, 8], there is no doubt that Dyson-Schwinger studies of baryon phenomena will provide a new window into the non-perturbative dynamics of QCD. Perhaps such studies will resolve some of the questions that have remained unanswered by studies of the meson sector. Studies of baryons represent a new and important frontier for the Dyson-Schwinger framework.

The goal of the present article is to provide an introduction to some of the ideas that form the basis for Dyson-Schwinger studies of baryons rather than details of particular numerical studies. Only the most basic features of the nucleon solutions obtained from such studies will be discussed. Those readers interested in a deeper understanding of current research are directed to the articles provided in the references.

2 Three-quark bound states and diquarks

The starting point for a model calculation of baryons is the presumption that, at its core, the baryon is a three-quark bound state. The quarks in the baryon must then interact via the three-quark scattering kernel an infinite number of times in order to form a bound state. The DSEs that describe the three-quark bound state can be reorganized into the well-known Faddeev equations. These can be separated into a complicated, coupled-set of two-body and three-body scattering equations. A formal derivation of these equations and their practical solution within relativistic quantum mechanics is discussed in Ref. [9]. Basically, the approach involves separating out pieces of the three-quark propagator in which two of the quarks interact with each other while the third quark acts as a spectator. The integral equations for such terms are solved first, yielding the two-quark correlations g_1, g_2 and g_3. A Feynman diagram depicting such an integral equation for g_1 is shown in Figure 1. The solutions for these two-quark propagators g_i are then reinserted into other integral equations, which ultimately yield the fully-dressed three-quark scattering Green function and baryon bound-state amplitudes $\Psi(p_1, p; P)$. Such bound-state amplitudes can then be used to calculate desired observables, such as electromagnetic form factors, decay constants, and scattering or photoproduction cross sections. This approach is well-defined and leads to the solution of the Faddeev problem, although it may be rather involved and cumbersome to carry out in practice.

A practical simplification is often made in which the two-quark correlation $g_1(p, q; P)$, depicted in Figure 1, is assumed to be well-described in terms of sums of *separable* correlations,

$$g_1(p, q; P) \;=\; \chi(p; P)\; D(P)\; \bar{\chi}(q; P) \;+\; \chi_\mu(p; P)\; D_{\mu\nu}(P)\; \bar{\chi}_\nu(q; P) \;+\; \cdots \;, \tag{1}$$

where P is the total momentum of the two incoming quarks, p and q are their relative momenta, $\chi(p; P)$ and $\chi_\mu(p; P)$ are referred to as the scalar and axial-vector *diquark* Bethe-Salpeter amplitudes

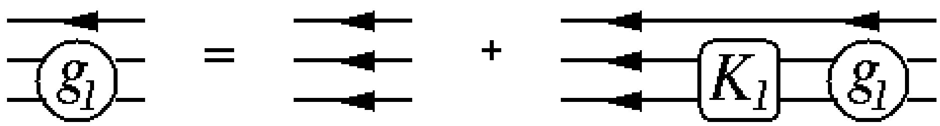

Figure 1: Diagram depicting an integral equation giving a contribution to the three-quark propagator that arises from the fully-dressed two-quark propagator g_1. Two of the quarks interact via the kernel K_1 while the remaining quark acts like a spectator. The assumption that g_1 is a *separable* function leads to the realization of the baryon as a bound state of a quark and a *diquark*.

(their adjoints are denoted $\bar{\chi}(p;P)$ and $\bar{\chi}_\mu(p;P)$) and $D(P)$ and $D_{\mu\nu}(P)$ are the scalar and axial-vector diquark propagators. In principle, there are additional contributions to g_1 but in Eq. (1) only the two most significant are included explicitly. Phenomenological studies suggest that the scalar diquarks contribute to up to 70% of the nucleon bound-state amplitude $\Psi(p_1, p; P)$ and axial-vector diquarks contribute up to 30% [7]. Of course, these percentages will differ in other baryons.

Let us consider the role of diquarks for a moment. If a scalar diquark really existed and could be observed as an asymptotic state with a well-defined mass M_{0+}, there would be a pole at $P^2 = -M_{0+}^2$ in the two-quark Green function $g_1(p, q; P)$ and $D(P) \to (P^2 + M_{0+}^2)^{-1}$. Of course, colored diquarks have never been observed in nature and so one does not expect the Green function $D(P)$ to have poles for any real value of P^2. Then, the obvious question arises as to whether Eq. (1) is a reasonable form to assume for a two-quark correlator $g_1(q, p; P)$.

Surprisingly, quenched calculations of QCD on a lattice may suggest that some diquark channels are well-represented by the form in Eq. (1). Using the method of maximum entropy, the authors of Ref. [10], evaluate the correlators for various quark-antiquark and two-quark sources. Their results for the pseudoscalar (π-meson) and vector (ρ-meson) quark-antiquark correlators are shown for various hopping parameters κ (corresponding to quark masses from 30 to 250 MeV) in the two left-most plots in Figure 2. Although, it is clear that the pion mass pole has not yet settled down to the accepted value of $m_\pi = 140$ MeV, the ρ-meson peak is quite near its accepted value of $m_\rho =$ 770 MeV. The important observation is that even though the ρ-meson is unstable (and therefore can not be directly observed) its important role in nuclear physics arises from the fact that its spectral representation (middle plot in Figure 2) clearly shows an obvious well-defined peak at the accepted value of the ρ-meson mass. This suggests that quark-antiquark correlations in the vector channel near the ρ-meson resonance may behave like a separable contribution (analogous to the form in Eq. (1)) with correlation length $1/m_\rho$.

In the final plot of Figure 2, the correlations of the scalar and axial-vector diquark correlators

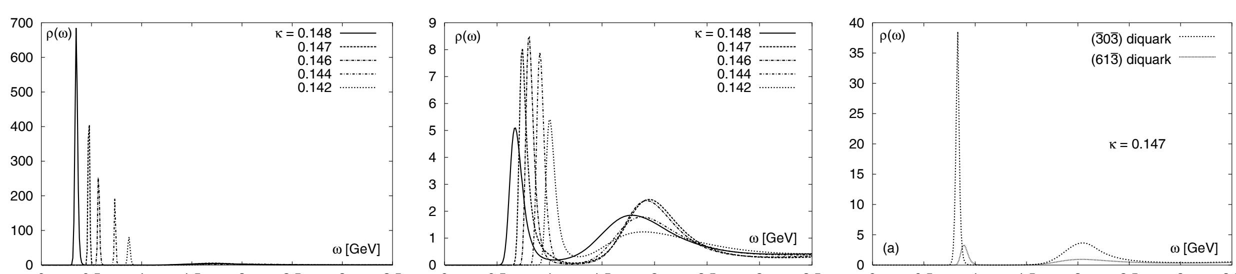

Figure 2: Spectral representations calculated by quenched-lattice QCD for π meson (left) and ρ meson (center) and scalar and axial-vector diquark (right) correlations. Figure adapted from Ref. [10].

are shown. What is truly surprising is the appearance of a rather well-defined peak, suggesting that although diquarks may not be observable particles, they might still be well modelled in terms of quasi-particles with well-defined mass scales. Such a conclusion would be suggestive of a form for the two-quark correlator $g_1(p,q;P)$ as in Eq. (1).

One way in which a diquark correlation might be realized within Dyson-Schwinger calculations is through the use of a confined-diquark propagator modelled in terms of an *entire* function,

$$D(P) = \frac{1}{M_{0^+}^2} \frac{1-e^{-P^2/\omega_{0^+}^2}}{P^2/\omega_{0^+}^2} \,, \tag{2}$$

where ω_{0^+} and M_{0^+} are model parameters [4, 6]. Such a function is called entire because it has no singularities anywhere in the complex plane and therefore has no Lehman representation and describes the propagation of a confined quasi-particle[1]. Although confined and having no well-defined mass, this form of diquark propagator $D(P)$ does have a well-defined correlation length given by $1/M_{0^+}$. Another possibility occurs when the confined propagators have only pairs of complex-conjugate poles,

$$D(P) = \frac{Z(P^2)}{P^2+\mathcal{M}^2} + \frac{Z^*(P^2)}{P^2+\mathcal{M}^{2*}} \,. \tag{3}$$

Here, $Z(P^2)$ is an analytic function, $\mathcal{M}^2 = M_{0^+}^2 + i\mu^2$, and M_{0^+} and μ are real mass scales. Such forms are suggestive of results from numerical studies of the DSEs, will not lead to production thresholds, and so are confining. More importantly, Dyson-Schwinger calculations of kaon photoproduction off the nucleon seem to prefer quark and diquark propagators that have complex-conjugate poles rather than being entire [8].

By assuming a separable form for the diquark correlators and quark propagators either modelled or obtained from numerical studies, one can solve the quark-diquark Bethe-Salpeter equation,

$$\Psi(p;P) = \int \frac{d^4k}{(2\pi)^4}\, K(p,k;P)\, D(\frac{1}{2}P+k)S(\frac{1}{2}P-k)\,\Psi(k;P) \,, \tag{4}$$

to determine the nucleon Bethe-Salpeter amplitude $\Psi(p;P)$. The key element required to solve Eq. (4) is the kernel $K(p,k;P)$ which not only contains the interaction between the quark and diquark, but also contains the quark-quark interaction within the diquark. Thus, the three-body nature of the problem is hidden within the kernel of Eq. (4). Also, the kernel contains a quark-exchange contribution necessary to implement Fermi-exchange antisymmetry at the level of the three quarks. By providing an interaction that swaps one of the quarks within the diquark with the spectator quark outside the diquark, it ensures that each of the three quarks has the opportunity to be part of the diquark.

The Bethe-Salpeter equation (4) is a linear integral equation which can be solved in a straightforward manner once the form of the kernel is known. Examples of this are carried out using finite-sized diquarks in Refs. [5] and [7]. The numerical solution yields both the mass of the nucleon and its Bethe-Salpeter amplitude $\Psi(p;P)$, knowledge of which allows one to compute observables such as electromagnetic form factors.

2.1 *Electromagnetic properties of the nucleon*

One of the first observables to calculate with obtained nucleon Bethe-Salpeter amplitudes is the nucleon electric and magnetic form factors $G_E(q^2)$ and $G_M(q^2)$. In the impulse approximation, the

[1]It is important to point out that although the use of an entire function for a model diquark propagator is certainly not necessary, such forms have been found to be very useful in phenomenological studies of hadron observables [1].

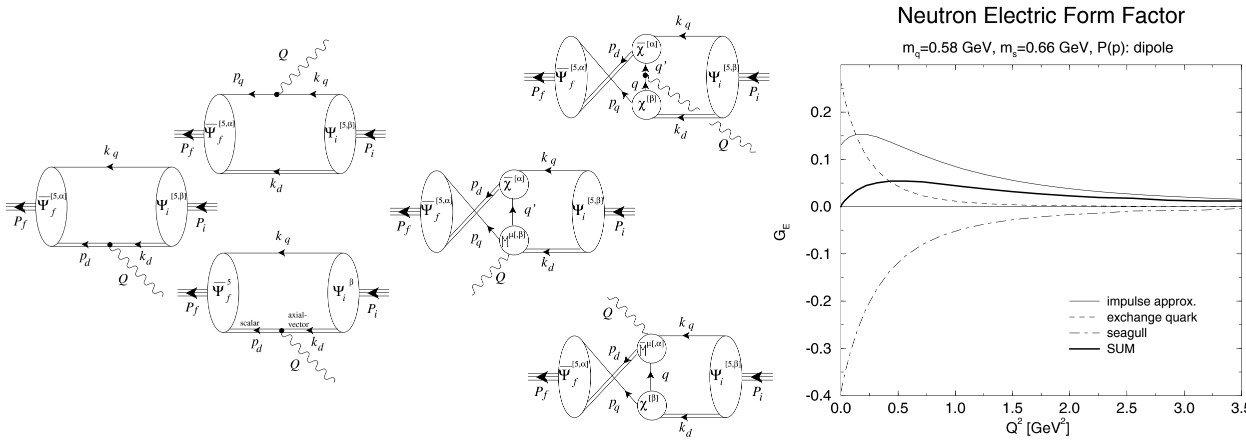

Figure 3: The three diagrams comprising the impulse approximation (left), and three diagrams necessary when quark-exchange kernel is used with finite-sized diquarks (center). At right, the relative contributions of impulse and beyond impulse to the neutron electric form factor as calculated with scalar diquarks only in Ref. [5].

electromagnetic properties of the nucleon are given by the sum of three contributions shown by the left-most diagrams in Figure 3. These contributions describe the case in which a photon strikes either the quark or diquark inside the nucleon bound state. The third diagram corresponds to the situation in which the diquark is struck by the photon causing a transition from one type of diquark to another, in this case a transition between axial and scalar diquarks.

It is shown in Ref. [5] that by themselves, the impulse-approximate diagrams are insufficient to describe the conserved electromagnetic current of the nucleon. That is, if these were the only contributions included, one obtains a neutron form factor given by the *thin*, solid curve in the plot of Figure 3. Clearly, in the static limit $q^2 = 0$, the neutron is not neutral. The problem is that the kernel $K(q,p;P)$ contains terms that depend on the total momentum P, and so gauge invariance requires that the photon be allowed to couple to these terms. This includes both the quark being exchanged in the quark-exchange kernel (shown by top center diagram) as well as the Bethe-Salpeter amplitudes $\chi(p;P)$ of the diquarks (shown by bottom, center two diagrams in Figure 3). It is always necessary to go beyond the impulse approximation to include additional diagrams when the diquark has finite spatial extent. When these diagrams are added the resulting neutron form factor is given by the heavy, solid curve in Figure 3. The various contributions are also provided in this plot and from their relative magnitude, one finds that for the neutron, such contributions are not at all negligible. It is clear that some observables, like the neutron form factors, are particularly sensitive to the three-quark nature of the nucleon. (In contrast, more than 75% of the proton electric form factor comes from the impulse diagrams alone [5].) The conclusion is that the nucleon is fundamentally a three-quark problem and as such, three-quark contributions, such as those appearing beyond the impulse approximation, are not negligible. Hence, the implementation of finite-size diquark amplitudes and quark-exchange kernels are critical since they reintroduce much of the three-body dynamics into the nucleon Bethe-Salpeter equation (4).

The results of the calculations of Ref. [7] with scalar and axial-vector diquarks are provided in Figure 4. Here, two sets of model parameters were explored. In model I (II) the diquark masses are taken to be $M_{0^+} = 0.625$ (0.588) MeV and $M_{1^-} = 0.684$ (0.831) MeV. One interesting result was that the q^2 dependence of the normalized ratio of the proton electric and magnetic form factors $\mu_p G_E(q^2)/G_M(q^2)$ provides an upper limit of 30% for the amount of axial-vector diquark components in the nucleon. This serves as an example of how phenomenological studies continue

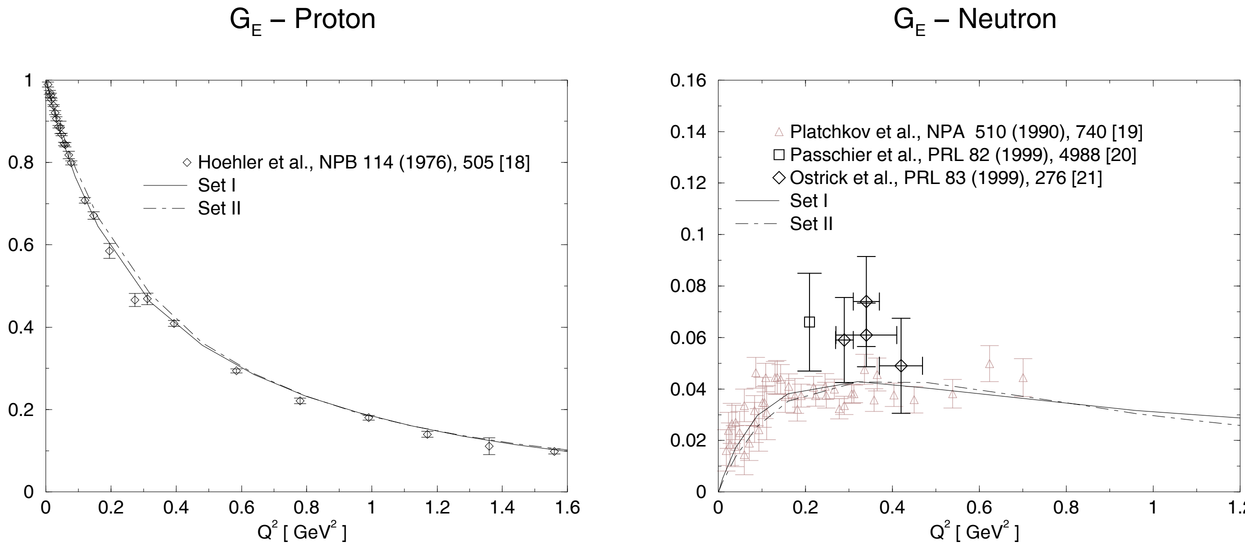

Figure 4: Electric form factors obtained using finite-sized scalar and axial-vector diquarks. Figure adapted from Ref. [7].

to provide important insights into the QCD dynamics of quark and two-quark correlations within baryons.

3 Future prospects

Much work remains to be done in order to bring our level of understanding for the baryon bound states up to par with the current level of understanding in the meson sector. Success will require further studies of the three-quark bound-state problem from different directions in order to get a more complete picture of the dynamics involved in baryon structure. Nonetheless, current results are providing some of these insights and promise to provide many more in the future.

Acknowledgments: The author gratefully acknowledges support received from the U.S. Department of Energy under contract DE-FG02-87ER40365 and the National Science Foundation under contracts PHY0070368, and PHY0071361.

References

[1] See M.B. Hecht and C.D. Roberts, these proceedings and references therein.
[2] R.T. Cahill, C.D. Roberts and J. Praschifka, Austral. J. Phys. **42**, 129 (1989); C.J. Burden, R.T. Cahill and J. Prashifka, Austal. J. Phys. **42**, 147 (1989).
[3] H. Asami, N. Ishii, W. Bentz and K. Yazaki, Phys. Rev. C **51**, 3388 (1995); H. Mineo, W. Bentz and K. Yazaki, Phys. Rev. C **60**, 065201 (1999); V. Keiner, Phys. Rev. C **54**, 3232 (1996); V. Keiner, Z. Phys. A **354**, 87 (1996).
[4] J.C.R. Bloch, C.D. Roberts, S.M. Schmidt, A. Bender and M.R. Frank, Phys. Rev. C **60**, 062201 (1999).
[5] M. Oettel, M. A. Pichowsky and L. von Smekal, Euro. Phys. J. A **8**, 251 (2000).
[6] M.B. Hecht, C.D. Roberts and S.M. Schmidt, Phys. Rev. C **64** 025204 (2001).
[7] M. Oettel, R. Alkofer and L. von Smekal, Euro. Phys. J. A **8**, 553 (2000).
[8] S. Ahlig, *et al.*, Phys. Rev. D **64** 014004 (2001).
[9] See A. Gårdestig, these proceedings and references therein.
[10] I. Wetzorke and F. Karsch, lat-ph/00080008, 2000.

A relativistic quark model of baryons

Bernard Metsch and Ulrich Löring

Institut für Theoretische Kernphysik, Universität Bonn,
Nußallee 14-16, D 53115 Bonn, Germany

(Received: 31 October 2001)

On the basis of the three-particle Bethe-Salpeter equation we formulated a relativistic quark model for baryons. Assuming the propagators to be given by their free form with constituent quark masses and the interaction kernel by an instantaneous potential, which contains a string-like parameterization of confinement and a flavor dependent interaction motivated by instanton effects we can account for the major features in the baryon spectrum, such as the low position of the Roper resonance and the occurrence of approximate parity doublets apparent in the N- and Λ-spectra.

1 Introduction

Still the most successful description of the baryonic excitation spectrum is the non-relativistic constituent quark model (NRCQM). It essentially assumes that baryon resonances are q^3-bound states, coupled weakly to meson fields. This certainly can be questioned: The decay widths of hadronic resonances are in general appreciable. The assumption should be understood to state that the coupling to strong decay channels does not influence the *relative* positions of resonances at the level of, say, 50 MeV. Thus the major mass splittings are supposed to reflect the excitation of the degrees of freedom of three constituent quarks, which have an effective constituent quark mass, carry flavor and color in the fundamental representations of the corresponding groups, are described by Pauli-spinors and thus obey the Pauli-principle. In its simplest form, assuming the interaction to be given by harmonic forces, these ingredients provides a natural explanation of the ground state flavor octet and decuplet, the lowest orbital excitations ("1-$\hbar\omega$-states") and the rough position of the lowest state of each spin. A comparison with the experimental spectrum, however, also reveals some conspicuous shortcomings: there is no natural explanation of the position of the lowest scalar/isoscalar excitations, such as the Roper-resonance, nor of the low position of some radial/orbital Δ-resonances at 1.9 GeV. In addition to these phenomenological considerations there are also some more fundamental objections: even with constituent quark masses of a few hundred MeV, quarks in hadrons are not really slow — the expectation value of p/m_q being roughly of order unity — processes at larger momentum transfer intrinsically require a relativistically covariant treatment of boosts, and in particular for the ground state mesons there are binding effects which are large compared to the masses of the constituents.

These considerations led us to the formulation of a relativistically covariant quark model for mesons on the basis of the instantaneous Bethe-Salpeter equation, see e.g. [1, 2] and references therein, while at the same time retaining all the successful features of the NRCQM.

2 The covariant q^3 Bethe Salpeter equation

In momentum space the Bethe-Salpeter equation for the Bethe-Salpeter amplitude $\chi_{\bar{P}}(x_1, x_2, x_3) = \langle 0 \mid T\Psi(x_1)\Psi(x_2)\Psi(x_3) \mid \bar{P}\rangle$ of a bound state with $\bar{P}^2 = M^2$ reads

$$\chi_{\bar{P}}(p_\xi, p_\eta) = S_1^F(\tfrac{1}{3}\bar{P} + p_\xi + \tfrac{1}{2}p_\eta) \otimes S_2^F(\tfrac{1}{3}\bar{P} - p_\xi + \tfrac{1}{2}p_\eta) \otimes S_3^F(\tfrac{1}{3}\bar{P} - p_\eta) \times (-i) \int \frac{d^4p'_\xi}{(2\pi)^4} \frac{d^4p'_\eta}{(2\pi)^4} K(\bar{P}, p_\xi, p_\eta, p'_\xi, p'_\eta) \chi_{\bar{P}}(p'_\xi, p'_\eta) , \qquad (1)$$

where $\bar{P}=\sum_{i=1}^{3} p_i$ is the total 4-momentum and $p_\xi=\frac{1}{2}(p_1-p_2)$, $p_\eta=\frac{1}{3}(p_1+p_2-2p_3)$ are Jacobi momenta. S^F denotes the full quark propagator and $K=K^{(3)}+\bar{K}^{(2)}$ is the integral kernel which contains both irreducible three-body $K^{(3)}$ and two-body forces $\bar{K}^{(2)}$. Both S^F and K are unknown functions for strongly interacting particles and thus have to be modeled. We start by making the assumption, that the full quark propagator can be approximated by its free form

$$S_i^F(p) \approx i\,[\gamma(p)-m_i\ +\ i\epsilon]^{-1}\ ,$$

where m_i is the effective constituent quark mass, which thus is a free parameter in our model. We furthermore assume, that the irreducible kernel can be suitably written as

$$K^{(3)}(p_\xi,p_\eta;p'_\xi,p'_\eta)\big|_{\bar{P}=(M,\vec{0})}=V^{(3)}(p_{\xi\perp},p_{\eta\perp};p'_{\xi\perp},p'_{\eta\perp})\ ,\quad K^{(2)}(p_\xi,p'_\xi)\big|_{\bar{P}=(M,\vec{0})}=V^{(2)}(p_{\xi\perp},p'_{\xi\perp})\ , \quad (2)$$

where $p_\perp \equiv p-\frac{\bar{P}p}{\bar{P}^2}\ \bar{P}$. In a frame where $\bar{P}=(M,\vec{0})$ the kernel then depends on the spatial components of the relative momenta only and thus reflects an instantaneous potential in the rest frame of the baryon. Both assumptions are in fact borrowed from the NRCQM, which accounts for confinement by assuming a string-like three body potential for constituent quarks. In fact the instantaneous approach is somewhat problematic for two particle interactions. For the moment we will assume that retardation effects of the propagation of the spectator quark can be parametrized by construction of an effective 3-body kernel through $\langle G_0\rangle V_{ij}^{eff}\langle G_0\rangle := \langle G_0 K_{ij}^{(2)} G_0\rangle$, where $G_0 := S_1^F\otimes S_2^F\otimes S_3^F$ is the free 3-quark propagator and $\langle G_0\rangle := \int \frac{dp_\xi^0}{2\pi}\frac{dp_\eta^0}{2\pi}G_0$. With these assumptions one can integrate out the p_ξ^0, p_η^0 dependence in Eq.(1) and derive the Salpeter equation:

$$\Phi=-i\langle G_0\rangle\big(V^{(3)}+V_{\rm eff}\big)\Phi \quad (3)$$

for the Salpeter amplitude $\Phi := \int \frac{dp_\xi^0}{2\pi}\frac{dp_\eta^0}{2\pi}\chi$, with $V_{\rm eff}=\sum_{i<j}V_{ij}^{\rm eff}$. The normalization of Φ follows from the normalization of the Bethe-Salpeter amplitude and reads

$$\sum_{\alpha\beta\gamma}\int \frac{d^3p_\xi d^3p_\eta}{(2\pi)^6}\Phi^*_{M\alpha\beta\gamma}(\vec{p}_\xi,\vec{p}_\eta)\ \Phi_{M\alpha\beta\gamma}(\vec{p}_\xi,\vec{p}_\eta)=2M\ . \quad (4)$$

This allows to reformulate Eq.(3) as an eigenvalue problem $\mathcal{H}\,\Phi = M\,\Phi$ with the Salpeter Hamiltonian

$$\begin{aligned}(\mathcal{H}\Phi_M)(\vec{p}_\xi,\vec{p}_\eta) = \sum_{i=1}^{3} H_i(\vec{p}_i)\Phi_M(\vec{p}_\xi,\vec{p}_\eta) + \Big[\Lambda_1^+(\vec{p}_1)\otimes\Lambda_2^+(\vec{p}_2)\otimes\Lambda_3^+(\vec{p}_3) \qquad (5)\\ +\Lambda_1^-(\vec{p}_1)\otimes\Lambda_2^-(\vec{p}_2)\otimes\Lambda_3^-(\vec{p}_3)\Big]\ \gamma^0\otimes\gamma^0\otimes\gamma^0\int\frac{d^3p'_\xi}{(2\pi)^3}\ \frac{d^3p'_\eta}{(2\pi)^3}\ \big(V^{(3)}+V_{\rm eff}\big)(\vec{p}_\xi,\vec{p}_\eta,\vec{p}'_\xi,\vec{p}'_\eta)\ \Phi_M(\vec{p}'_\xi,\vec{p}'_\eta)\end{aligned}$$

with the Dirac Hamiltonian H_i and $\Lambda_i^\pm$ being projectors on states of positive (+) and negative (−) energy spinors. Note that with the present instantaneous approximation we get the same number of states as in the NRCQM, nevertheless our approach goes beyond a simple "relativization" by explicitly taking into account the coupling to negative energy components. In this formulation we can determine masses and Salpeter amplitudes for baryons by diagonalizing the Hamiltonian of Eq.(5) in an appropriate large, but finite basis. In order to calculate electroweak observables in the framework of the Mandelstam formalism we need the full Bethe-Salpeter amplitude. This can be found in the rest frame through the Bethe Salpeter equation

$$\chi_M=-iG_0\big(V^{(3)}_{\rm conf}+V^{\rm eff}\big)\Phi\ ,$$

and, because of formal covariance, can be calculated for any on-shell momentum $\bar{P}$ with $\bar{P}^2=M^2$.

3 A covariant quark model for light-flavored baryons

In order to calculate the spectrum of baryons with light flavors we have to specify the interaction kernels $K^{(3)} = V^{(3)}$ and $K^{(2)} = V^{(2)}$ in instantaneous approximation. We parameterize a three-body confinement kernel by a potential $V^{(3)}_{\text{conf}}$ which rises linearly with inter-quark distances. The gross features of the baryon resonances seem to indicate that the dominating confinement forces should be spin-independent, at least in the non-relativistic limit; moreover, too large spin-orbit effects should be suppressed. To realize both properties we assume the Dirac structure given by a specific combination of spin-independent scalar and time-like vector[1] Dirac structures:

$$\begin{aligned} V^{(3)}_{\text{conf}}(\mathbf{x}_1,\mathbf{x}_2,\mathbf{x}_3) &= 3\,a\;\frac{1}{4}\left[\mathbb{1}\otimes\mathbb{1}\otimes\mathbb{1}+\gamma^0\otimes\gamma^0\otimes\mathbb{1}+\text{cycl. perm.}\right] \\ &\quad +\; b\sum_{i<j}|\mathbf{x}_i-\mathbf{x}_j|\;\frac{1}{2}\left[-\mathbb{1}\otimes\mathbb{1}\otimes\mathbb{1}+\gamma^0\otimes\gamma^0\otimes\mathbb{1}+\text{cycl. perm.}\right]\;. \end{aligned} \tag{6}$$

Here, the offset a and the slope b enter as free parameters in our model.

In order to describe spin-dependent splittings, such as that of the ground-state octet and decuplet, we adopt the explicitly flavor-dependent 2-quark interaction[2], derived by 't Hooft from instanton effects:

$$V^{(2)}_{\text{'t Hooft}}(\mathbf{x}) = \frac{-4}{\lambda^3\pi^{\frac{3}{2}}}\,e^{-\frac{|\mathbf{x}|^2}{\lambda^2}}\left[\mathbb{1}\otimes\mathbb{1}+\gamma^5\otimes\gamma^5\right]\mathcal{P}^{\mathcal{D}}_{S_{12}=0}\otimes\left(g_{nn}\mathcal{P}^{\mathcal{F}}_{\mathcal{A}}(nn)+g_{ns}\mathcal{P}^{\mathcal{F}}_{\mathcal{A}}(ns)\right)\;. \tag{7}$$

Here, the four-fermion contact interaction has been smeared out by a Gaussian function with effective range λ; the operator $\mathcal{P}^{\mathcal{D}}_{S_{12}=0}$ in Dirac space projects on anti-symmetric spin-singlet states, $\mathcal{P}^{\mathcal{F}}_{\mathcal{A}}(nn)$ and $\mathcal{P}^{\mathcal{F}}_{\mathcal{A}}(ns)$ denote the projectors on flavor-antisymmetric non-strange and non-strange–strange quark pairs. Although the constituent quark masses m_n, m_s as well as the 't Hooft couplings g_{nn}, g_{ns} and the range λ can be related to standard QCD-parameters by instanton theory, we determine these parameters by a fit to the experimental baryon spectrum; for the values of the seven free parameters and a consistency check of the QCD-relations we refer to Refs. [4, 5].

As 't Hooft's interaction affects flavor antisymmetric qq-pairs only this interaction does not act on flavor symmetric states, such as the Δ-resonances, which are thus determined by the dynamics of the confinement potential alone. Accordingly, the constituent quark masses and the confinement parameters were determined by a fit to the spectrum in this sector without any influence of the residual interaction. In this manner a reasonable description of the complete Δ-spectrum including the linear Regge trajectory ($M^2 \sim J$) up to highest orbital excitations $J = \frac{15}{2}$ can be obtained, see the upper part of Fig. 1. However, the suspicious low position of the three negative-parity "$3\hbar\omega$" states quoted by the PDG [6] around 1900 MeV as well as that of the $\Delta\frac{3}{2}^+(1600)$ is not accounted for (as in several other quark models). Since in our opinion the experimental evidence of these negative parity states from π–N-scattering is rather weak, a confirmation by complementary (electro-/photo-production) experiments, such as the CLAS experiment at CEBAF (JLab) or the Crystal Barrel experiment at ELSA (Bonn), seems of great importance. The instanton-induced interaction does act on particular flavor octet (and singlet) states.

The 't Hooft coupling g_{nn} is adjusted to the ground-state N-Δ–splitting (and correspondingly g_{ns} to the Ξ^*-Ξ– and Σ^*-Σ-Λ–splittings in the strange sector); then all other states of the nucleon-

[1] The appearance of $\gamma^0\otimes\gamma^0$ is allowed because the potential is defined in the rest-frame of the baryon.

[2] This interaction is usually used in connection with the solution of the $U_A(1)$-problem. In the framework of calculations for mesons [1] we have indeed shown that it yields the correct splitting of the lowest meson nonet and in general of all low-lying meson states. Moreover, we found [4] that the alternative QCD-based residual interaction – the one-gluon exchange – can be discarded on phenomenological grounds.

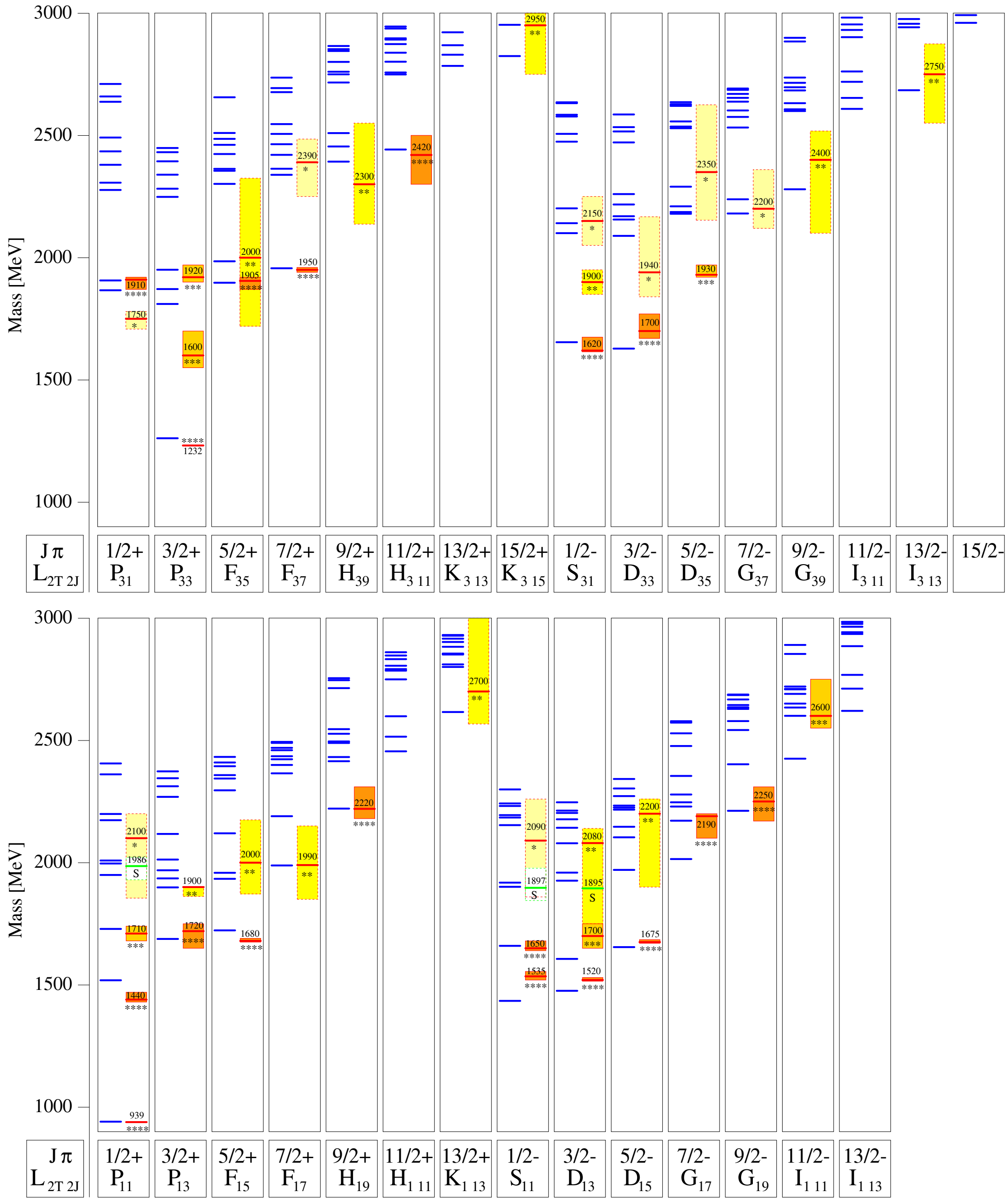

Figure 1: The complete Δ- (top) and nucleon spectrum (bottom): Our calculation in the left part of each column is compared to the experimental spectrum [6] in the right part of each column. Resonances are classified by total spin and parity J^π. The experimental position is indicated by a bar, the corresponding uncertainty by the shaded box which is darker for better established resonances; the status of each resonance is additionally indicated by stars.

(and the Λ-, Σ-, Ξ-) spectrum are real parameter-free predictions. The lower part of Fig. 1 shows as an example our predictions for the complete N-spectrum. As can be seen from this figure, our predictions can nicely reproduce several features at least in qualitative but mostly even in completely quantitative agreement with the experimental findings.

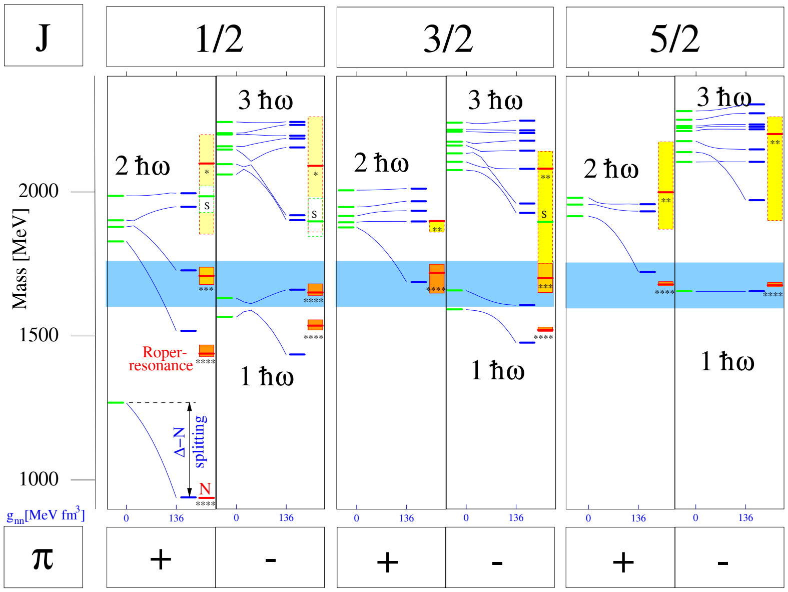

Figure 2: [Left] Instanton-induced effects in the nucleon spectrum. The curves illustrate the change of the spectrum with increasing 't Hooft coupling g_{nn} which finally is fixed to reproduce the correct N-Δ–splitting.

Figure 3: [Below] Parity doublets for higher lying nucleon resonances. See also caption to Fig. 2 .

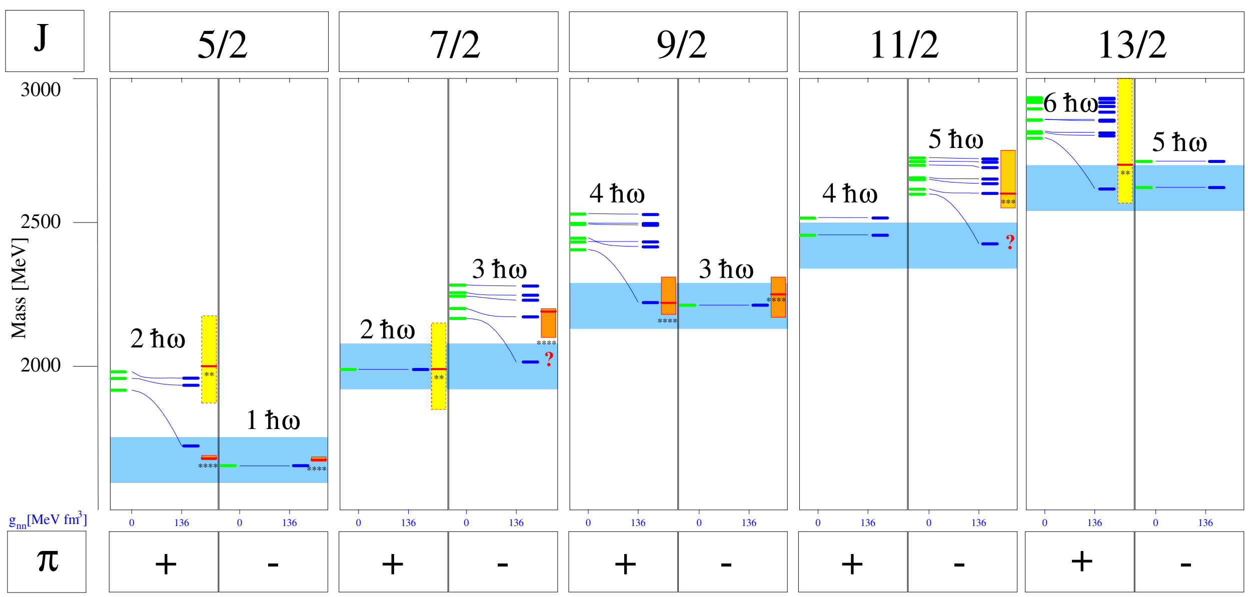

It is instructive to analyze the consequences of instanton effects for the shape of the spectrum in some more detail. Figure 2 illustrates the effect of 't Hooft's force on the lowest nucleon states. We find a selective lowering of some particular states and once the coupling is fixed to reproduce the experimental N–ground-state position we can automatically account very well for the major spin-dependent mass splittings observed in the experimental spectrum. For instance in the "$2\hbar\omega$" band exactly four states are lowered relative to the other states such as required by the experimental findings. In particular one finds that in this manner the extremely low position of the prominent Roper resonance can be accounted for quite naturally. We should remark here that the specific interplay of 't Hooft's force, the relativistic effects and the particular choice for the Dirac structure of the confinement potential are essential to describe these effects quantitatively.

A very interesting feature of our relativistic quark model with instanton induced forces is that it gives a natural dynamical explanation of the so-called *parity doublets*: A glance at the experimental

N- and Λ-spectrum reveals a conspicuous degeneracy of some states with the same spin and opposite parity. Prominent, well-established, examples are $N\frac{5}{2}^+(1680)$–$N\frac{5}{2}^-(1675)$, $N\frac{9}{2}^+(2220)$–$N\frac{9}{2}^-(2250)$, $\Lambda\frac{5}{2}^+(1820)$–$\Lambda\frac{5}{2}^-(1830)$. In the Σ–spectrum no clear indications of parity doublets is found. In the literature these observations have been related to a phase transition from the Nambu–Goldstone mode of chiral symmetry to the Wigner–Weyl mode in the upper part of the baryon spectrum [7–9] . In the present model also this feature can be understood as an instanton-induced effect: In general 't Hooft's force lowers those sub-states of a major oscillator shell[3] which contain so-called scalar diquarks, i.e. quark pairs with trivial spin and angular momentum. This is found in particular for the high spin states in a given $N\hbar\omega$ oscillator shell, see Fig. 3. For given $N\hbar\omega$ the maximum total angular momentum for a state containing such a scalar diquark is $J = (L_{\max} = N) + \frac{1}{2}$. 't Hooft's force lowers this state enough to become almost degenerate with the unaffected spin-quartet state of the adjacent oscillator shell with $N-1$, which has opposite parity but the same total angular momentum: $J = (L_{\max} = N-1) + \frac{3}{2}$. In this way patterns of approximate parity doublets for *all* lowest excitations in the sectors $J = \frac{5}{2}$ to $J = \frac{13}{2}$ are formed *systematically.* In the $N\frac{5}{2}^\pm$ and $N\frac{9}{2}^\pm$ sectors this scenario is nicely confirmed experimentally by the well-established parity doublets mentioned above: $N\frac{5}{2}^+(1680)$–$N\frac{5}{2}^-(1675)$ and $N\frac{9}{2}^+(2220)$–$N\frac{9}{2}^-(2250)$. In the $N\frac{7}{2}$ sector, however, the present experimental findings seem to deviate from such a parity doubling structure due to the rather high position of the $N\frac{7}{2}^-(2190)$. Although this state is given a four-star rating [6] an investigation of this sector with the new experimental facilities would be highly desirable. The same mechanism explains approximate parity doublet structures also for states with lower angular momentum as *e.g.* the N^* doublets in the second resonance region around ~ 1700 MeV with spins $J^\pi = \frac{1}{2}^\pm$, $\frac{3}{2}^\pm$, and $\frac{5}{2}^\pm$ (see Fig. 2). Observable consequences of this parity doubling scenario should manifest in a different shape of electromagnetic $\gamma^* p \to N^*$ transition form factors of both members of a doublet due to their significantly different internal structures: That member of the doublet, which is affected by 't Hooft's force (e.g. $N\frac{5}{2}^+$), exhibits a rather strong scalar diquark correlation and thus its structure should be more compact compared to its unaffected doublet partner (e.g. $N\frac{5}{2}^-$) whose structure is expected to be rather soft. Consequently, the transition form factor to the latter resonance decreases faster than that to its doublet partner with the scalar diquark contribution (see Fig. 3 of Ref. [10] for an example). Finally, we should mention that in the strange sector (see Ref. [5]) 't Hooft's force accounts in a similar way for the prominent doublets of the Λ-spectrum. At the same time instanton-induced effects are found to be significantly weaker in the Σ-spectrum, thus explaining the fact that no clear experimental indications of parity doublets are observed in this sector.

The investigations presented here have been restricted to the spectra of baryons alone, which poses of course only a first (successful) test of our model. Strong and electroweak decays as well as formfactors pose additional stringent tests. In the present covariant framework formfactors were already computed in the Mandelstam formalism [11]; indeed we found that we can reliably calculate such observables up to high momentum transfers. Work on the perturbative calculation of strong decays is more difficult but in progress; first results are very promising, e.g. a *parameter-free* (!) prediction [12] of $\Delta\frac{3}{2}^+(1232) \to N\pi$ yields a decay width $\Gamma = 109$ MeV in very good agreement with the experimental value $\Gamma = 119 \pm 5$ MeV.

Acknowledgments: We would like to acknowledge the contributions of K. Kretzschmar, D. Merten and H.-R. Petry. We thank the Deutsche Forschungsgemeinschaft (DFG) for financial support.

[3]Note that despite of the linear confinement adopted here, the assignment of states to oscillator shells still provides an adequate classification of states with confinement alone.

References

[1] M. Koll, R. Ricken, D. Merten, B.C. Metsch, H.R. Petry, Eur. Phys. J. A **9**, 73 (2000).

[2] R. Ricken, M. Koll, D. Merten, B.C. Metsch, H.R. Petry, Eur. Phys. J. A **9**, 221 (2000).

[3] U. Löring, K. Kretzschmar, B.Ch. Metsch, H.R. Petry, Eur. Phys. J. A **10**, 309 (2001).

[4] U. Löring, B.Ch. Metsch, H.R. Petry, Eur. Phys. J. A **10**, 395 (2001).

[5] U. Löring, B.Ch. Metsch, H.R. Petry, Eur. Phys. J. A **10**, 447 (2001).

[6] Particle Data Group, *'Review of Particle Physics'*, Eur. Phys. J. **C15**, 1-878 (2000).

[7] L. Y. Glozman, Phys. Lett. B **475**, 329 (2000).

[8] T. D. Cohen and L. Y. Glozman, hep-ph/0102206 (2001).

[9] M. Kirchbach, Nucl. Phys. A **689**, 157 (2001).

[10] U. Löring, B.Ch. Metsch, *Parity doublets from a relativistic quark model*, Proceedings of the *Workshop on The Physics of Excited Nucleons (NSTAR 2001)*, World Scientific (2001), p. 221.

[11] K. Kretzschmar, U. Löring, B.Ch. Metsch, *Elektroweak form factors of the nucleon in a relativistic quark model of baryons*, in progress.

[12] D. Merten, private communication (2001).

New positive-parity baryons, and baryon-meson loop effects

Simon Capstick and Danielle Morel

Department of Physics, Florida State University, Tallahassee, FL 32306-4350, U.S.A.

(Received: 16 November 2001)

Several positive-parity non-strange baryons with masses below about 2200 MeV are predicted by quark models to exist, but are not present in analyses of pion-nucleon elastic scattering data. This may be because such states do not couple strongly to the pion-nucleon channel. Analyses which include other channels and new data should find such states if they exist. Model predictions are complicated by the presence of light positive-parity baryons with excited gluonic degrees of freedom (hybrids) with similar quantum numbers and masses. The prospects for discovery of new positive-parity states is discussed in the context of models. An important ingredient missing in many models is the correction of the masses and wavefunctions of the states from higher Fock-space components like $qqq(q\bar{q})$, which can be described by a sum of baryon-meson intermediate states. Existing models of these corrections will be described, along with a calculation currently underway which significantly extends the basis of intermediate states.

1 Missing states

Models of baryon structure differ in their picture of the important effective degrees of freedom. Popular models include: potential models [1], which describe baryons as bound states of constituent quarks with effective masses and strong and electromagnetic form factors; flux-tube model enhancements of the potential model, which describe (hybrid) baryon states with excited glue [2]; algebra-based models [3], where excited states are viewed as collective excitations of string-like objects; and bag models, where light quarks move in a bag with pions coupled to the surface [4]. These models differ in their predictions for the number of excited states in a given mass region. For example, there is a larger density of excited states in the flux-tube and algebra-based models since they also describe excitations of the degrees of freedom responsible for confinement. An extreme picture is the quark-diquark model [5], which has fewer degrees of freedom at energies too low to excite the diquark relative coordinate. Such a model cannot be conclusively ruled out without the discovery of states present in more popular models which treat the quarks symmetrically.

More states appear in such symmetric models than are currently present in analyses of elastic and inelastic data for scattering from nucleons. Such states are commonly called *missing* states. Ignoring for the moment the degrees of freedom associated with confinement and details of the (residual) quark-quark interactions left over after accounting for confinement, potential models are useful for gaining a rough idea of the type of excitation present in a given mass range. The first group of states above the ground states N and $\Delta(1232)$ are negative-parity orbital excitations, with seven non-strange states with spins up to 5/2. Good evidence for the existence of all of these states exists in pion-nucleon elastic scattering data.

In such models the next group of states in the spectrum has positive parity, with either two orbital excitations (not necessarily in the same vector relative coordinate) or radial excitations. Note that there are positive-parity states present in analyses which are lower in mass than the negative-parity states, for example the Roper resonance $N1/2^+(1440)$. Although this state turns out lighter than other positive-parity excitations [1,6,7] in models with various residual interactions between the quarks, its nature remains controversial [8].

It is likely that several of these positive-parity states are missing because, until recently, experiments which involved excited baryons had the $N\pi$ channel as the initial or final state, or both. States which do not couple strongly to this channel are unlikely to be seen in such experiments.

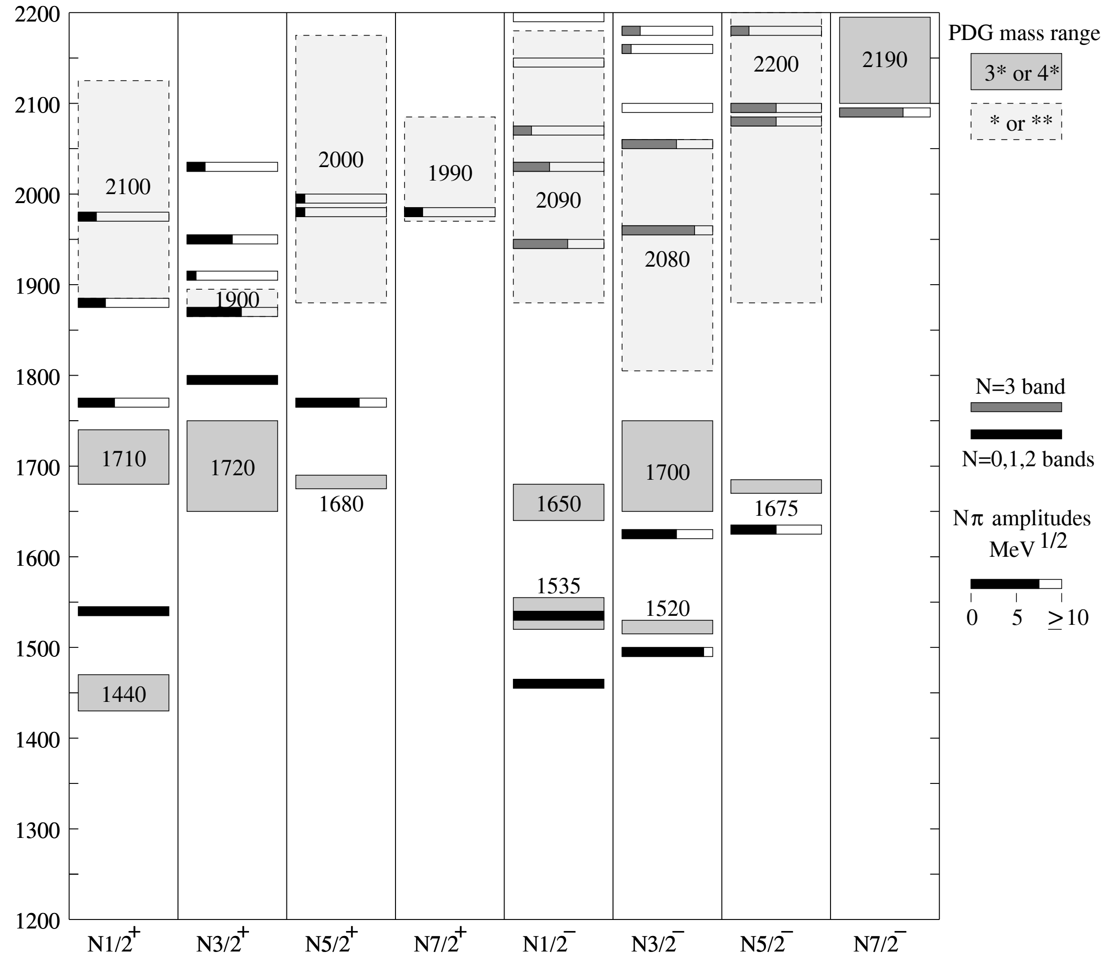

Figure 1: Model masses (bars) and predicted $N\pi$ amplitudes (solid regions within bars) for nucleon states with masses below 2200 MeV, compared with the results of analyses [12].

This is reinforced by the calculation within potential models of baryon $N\pi$ decays [9–11], which show that states with substantial couplings to the $N\pi$ channel correspond in number and roughly in mass to those seen in analyses. An example of the results of such a calculation [6,10] for nucleon states is illustrated in Fig. 1. This spectrum [6] is generated using a one-gluon-exchange interaction between the quarks, with a strength fit to the Δ-N splitting, and includes the associated Coulomb, tensor, and spin-orbit interactions. In the nonrelativistic limit the relative sizes of these interactions are as prescribed by the one-gluon-exchange interaction between a pair of free quarks; the potentials are taken to be momentum dependent, and their strengths away from this limit are parameterized. Strong-decay couplings are calculated [10] using the resulting wavefunctions and a pair-creation model, where the quark-antiquark pair are created with the quantum numbers of the vacuum, $^3P_0$.

The resulting couplings to the πN channel, for example, are illustrated in Fig. 1 by the length of the solid region inside the bar representing a given state's mass prediction. It can be seen that in most cases the states which have been seen in the analyses [12] correspond to the states with a given set of quantum numbers which have the largest $N\pi$ couplings [11]. Calculations of the strong decay amplitudes to other channels [13] of all states predicted by the model allow prediction of which channels are favorable to discover missing states. A comprehensive program is underway to take data in these channels, and, just as importantly, to analyse the data [14] from all of these channels at the same time in a multi-channel analysis. Their discovery should tightly constrain models of the interactions between quarks and their strong decays.

2 Hybrid baryons

This process is likely to be complicated by the presence of excited states of the gluon degrees of freedom confining the quarks, which show up as additional positive-parity excited states. In the case of mesons, where non-relativistic bound states of a quark and antiquark with $\mathbf{J} = \mathbf{L} + \mathbf{S}$ have quantum numbers

$$P = (-1)^{L+1} , \qquad C = (-1)^{L+(S+1)+1} = (-1)^{L+S} , \tag{1}$$

where the charge conjugation parity C is defined only for self-conjugate mesons, certain quantum numbers are excluded. If the glue binding the quarks is excited these 'exotic' quantum numbers can be attained. In the case of baryons, however, all possible quantum numbers can be attained by three quarks moving in a potential.

This potential can be pictured as an adiabatic surface given by the minimum length, for a given set of quark positions, of a Y-shaped string joining the quarks, such as arises in the strong-coupling limit of lattice QCD. The string is required to have this shape in order to maintain global color gauge invariance. In lattice QCD the plaquette operator from the lattice action moves the tubes in a direction transverse to their original orientation, and it can also move the junction. In a flux-tube model of the confining degrees of freedom based on this strong-coupling limit, the flux-tubes and the junction are discretized using beads. Their equilibrium positions are given by the minimum length string configuration, which defines the usual confining potential

$$V_{\text{conf}}(\mathbf{r}_1, \mathbf{r}_2, \mathbf{r}_3) = \sigma(l_1 + l_2 + l_3) = \sigma L_{\min} , \tag{2}$$

where σ is the meson string tension. Note that this confining potential is linear at large quark-junction separations.

To find the masses and quantum numbers of conventional and hybrid baryons in this flux-tube picture [2], the quarks positions are fixed and the junction is allowed to move relative to its equilibrium position. At the same time the strings are allowed to move transverse to their equilibrium positions, see Fig. 2. The energy of the ground state of the string, for every set of quark positions $\{\mathbf{r}_i\}$, defines the adiabatic potential $V_B(\mathbf{r}_1, \mathbf{r}_2, \mathbf{r}_3)$ which differs from V_{conf} by the addition of zero-point motion of the string. The masses and quantum numbers of conventional baryon states can be found by solving for the energies of three quarks moving in the confining potential V_B, with additional (residual) interactions between the quarks. The first excited state of the string defines a new adiabatic potential $V_H(\mathbf{r}_1, \mathbf{r}_2, \mathbf{r}_3)$, and hybrid baryon masses and quantum numbers can be found by solving for the motion of three quarks in this modified potential. Numerical calculations find, with the addition of a one-gluon exchange interaction between the quarks at short distance, that the lightest hybrids are quark-spin $S = 1/2$ N states at 1870 MeV and $S = 3/2$ Δ states

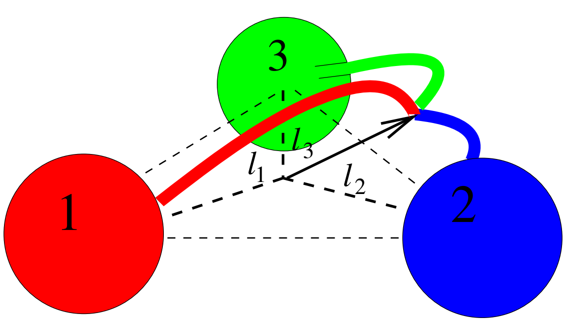

Figure 2: Motion of the junction and strings relative to their minimum energy configuration in a hybrid baryon.

at 2075 MeV, with a model error of ±100 MeV on the mean mass of these states. These states have the quark orbital quantum numbers $L^P_{qqq} = 0^+$ and string quantum numbers $l^\pi = 1^+$, leading to overall $L^P = 1^+$. If these orbital quantum numbers are combined with the quark spin and the either totally symmetric or antisymmetric exchange symmetry of the flux-tube state, there arise light non-strange hybrids with quantum numbers

$$(N,\Delta)^{2S+1}J^P = N^2 1/2^+,\ N^2 3/2^+,\ \Delta^4 1/2^+,\ \Delta^4 3/2^+,\ \Delta^4 5/2^+ \ . \tag{3}$$

These are the same light-hybrid quantum numbers as those found in bag-models with constituent gluon $(qqq)_8 g$ hybrids [15], with the exception of the flavor of the $J^P = 5/2^+$ state, which is a nucleon in the bag model. These calculations describe hybrids by using the transverse-electric lowest-energy eigenmode of a single vector 'constituent' gluon in a spherical cavity, with quarks also moving in the bag and interacting via perturbative one-gluon exchange with themselves and the constituent gluon. The masses of the lightest hybrid states in this model are, however, considerably lighter than those predicted by the flux-tube model. For example, the lightest bag-model hybrid state is a $N1/2^+$ state predicted to lie between the Roper resonance and the state $N1/2^+(1710)$ seen in analyses. If there are hybrids at these low masses, we should expect to have seen a surfeit of low-lying $N1/2^+$ states relative to qqq predictions. Although the mass, photocouplings, and even qqq nature of the Roper resonance are controversial, there is so far no evidence for a third light P_{11} resonance in this region. Obviously, careful analysis of existing and new data in many channels is required to rule out one or the other of these pictures and find these exciting new states of baryonic matter.

3 Unquenching the quark model

In QCD there are $qqq(q\bar{q})$ configurations possible in baryons, and these must have an effect on the constituent quark model, similar to the effect of unquenching lattice QCD calculations. These effects can be modeled by allowing baryons to include baryon-meson (BM) intermediate states, which lead to baryon self energies and mixings of baryons of the same quantum numbers. A calculation of these effects requires a model of baryon-baryon-meson (BB′M) vertices and their momentum dependence. It is also necessary to have a model of the spectrum and structure of baryon states, including states not seen in analyses of experimental data, in order to provide wavefunctions for calculating the vertices, and to know the thresholds associated with intermediate states containing missing baryons.

Baryon self energies due to BM intermediate states and BM decay widths can be found from the real and imaginary parts of loop diagrams. The size of such self energies can be expected to be comparable to baryon widths. For this reason, such self energies cannot be ignored when comparing the predictions of any quark model with the results of analyses of experiments. Since the splittings between states which result from differences in self energies can be expected to be comparable to those that arise from the residual interactions between the quarks, a complete calculation of the spectrum needs to adjust the residual interactions, and with them the wavefunctions of the states used to calculate the BB′M vertices, to account for these additional splittings.

This procedure can best be illustrated by examining the effects of baryon-meson intermediate states on the Δ-N mass splitting, traditionally used to set the strength of the spin-dependent contact interactions between the quarks. If these spin-dependent interactions are turned off, it is still possible that these states have self energies from BM loops which are different and so cause a splitting between the states. Assume for now that there are only ground-state baryons and mesons, made up of u, d, and s quarks with the same mass, and that there are no residual interactions between the quarks. All baryons will have the same masses and wavefunctions, and the same is true of mesons. In this limit all of the intermediate states $\mathrm{B}'\mathrm{M}$ used to calculate self energies have the same mass $M_{\mathrm{B}'}+m_{\mathrm{M}}$, and the energy-dependent self energies calculated in the center-of-momentum frame of ground-state baryon B

$$\Sigma_{\mathrm{B}}(E) = \sum_{\mathrm{BM}} \int d\mathbf{k} \frac{\mathcal{M}^{\dagger}_{\mathrm{BB'M}}(k)\mathcal{M}_{\mathrm{BB'M}}(k)}{E - \sqrt{M_{\mathrm{B}}^2 + k^2} - \sqrt{m_{\mathrm{M}}^2 + k^2}} \tag{4}$$

differ only because of the flavor and spin structure of the strong decay matrix element $\mathcal{M}_{BB'M}(k)$. It should be true that in this limit all baryon self energies are the same, and this has been demonstrated to be true by Zenczykowski [16], *if* the set of intermediate states includes all allowed combinations of the ground state octet and decuplet baryons and ground state pseudoscalar and vector mesons. This implies that calculations of self energies which do not include vector mesons, for example, do not start at this limit and so cannot be expected to produce physically meaningful results away from it.

A calculation [17] of the Δ-N splitting where the intermediate states are restricted to the set of states $\mathrm{B}'\pi$, with baryon states B' chosen from a set of excited N and Δ states, converges only when excited states from the $N = 0$ (ground), $N = 1$ (lowest-lying negative-parity excited), $N = 2$ (positive-parity excited), *and* $N = 3$ (highly-excited negative-parity) states are included. Similar results for the convergence properties of the ρ and ω meson self energies are found in a calculation of the effects of meson-meson intermediate states [18]. This suggests that calculations which restrict the intermediate baryons to (spatial) ground states cannot be expected to have converged.[1]

A calculation of the self energies of N and Δ has been carried out [19] using a ${}^3P_0$ pair-creation model to calculate the momentum-dependent vertices $\mathcal{M}^{\dagger}_{BB'M}(k)$, using wavefunctions calculated using a relativized model [6] with a variable-strength spin-dependent (one-gluon exchange) contact interaction between the quarks. This calculation takes into account intermediate states $\mathrm{B}'\mathrm{M}$ with

$$\mathrm{M} \in \{\pi, K, \eta, \eta', \rho, \omega, K^*\} \ , \qquad \mathrm{B}' \in \{N, \Delta, \Lambda, \Sigma, \Sigma^*\} \ , \tag{5}$$

including all excitations of the baryon states up to and including the $N = 3$ band states. Note that ϕ mesons couple weakly to non-strange baryon states (such decays are OZI suppressed) and so they are ignored.

The usual version of the ${}^3P_0$ model gives vertices that are too hard, and the loop integrals required to evaluate the self energies get large contributions from high momenta. These vertices are modified by adopting a pair-creation operator used by Geiger and Isgur and Silvestre-Brac and Gignoux, with a form factor $\exp(-f^2[\mathbf{p}_q - \mathbf{p}_{\bar{q}}]^2)$, with $f^2 = 2.8$ GeV^2 which gives the quark-pair-creation vertex a size of around 0.35 fm. As the self energies due to a given intermediate state depend crucially on the masses adopted for the intermediate hadrons, these are taken to be the physical masses, where known, and model masses [6] otherwise. The 'bare' masses required to reproduce the known physical masses of the N and Δ are found by solving the uncoupled self-consistent equations

$$E_N + \Sigma_N(E_N) = M_N \ , \qquad E_\Delta + \Sigma_N(E_\Delta) = M_\Delta \tag{6}$$

for the 'bare' masses E_N^0 and E_Δ^0. Note that the self energies tend to be large and negative, but only differences in the self energies are observables.

When wavefunctions with no residual interactions between the quarks are used, this results in bare masses which satisfy $E_\Delta^0 - E_N^0 \simeq 140$ MeV. This agrees well with the expectation from other

[1]It is expected that since orbital and radial excitations of mesons tend to be significantly more massive than their corresponding ground states, it may be possible to ignore their excited states in the set of intermediate states, but this needs to be confirmed.

models that about half of the Δ-N splitting comes from quark-quark residual interactions, but in this picture the rest of the splitting arises from a source very different from one-pseudoscalar-boson-exchange (OBE) or similar mechanisms between the quarks. Of course OBE, as well as quark self-energies due to mesons, are included as certain time orderings and limits in a calculation which evaluates self energies due to all B$'$M intermediate states. The introduction of residual interactions which can accomodate the rest of the observed Δ-N splitting affects the wavefunctions and so the vertices, but does not significantly affect the difference in the bare energies.

This calculation is currently being extended to the self energies of negative-parity excited states. In this case there are two $N1/2^-$ and two $N3/2^-$ states close in mass which can be expected to mix due to off-diagonal terms in their self energies. The same is true of the ground state nucleon and Roper resonance. Previous calculations limited to ground state intermediate baryons which ignore this mixing [20] have found splittings which resemble spin-orbit splittings in these negative-parity states. It is likely that a much deeper understanding of the baryon spectrum and of the residual interactions between the quarks will result from understanding the extent of splittings in the spectrum due to these self energies.

Acknowledgments: The authors would like to gratefully acknowledge discussions of this work with Winston Roberts, Nathan Isgur, Michael Pichowsky, and Jorge Piekarewicz. This work is supported by the U.S. Department of Energy under contract DE-FG02-86ER40273.

References

[1] N. Isgur and G. Karl, Phys. Rev. D **18**, 4187 (1978); D **19**, 2653 (1979).
[2] S. Capstick and P. R. Page, Phys. Rev. D **60**, 111501 (1999).
[3] R. Bijker, F. Iachello and A. Leviatan, Ann. Phys. **236**, 69 (1994); **284**, 89 (2000).
[4] T. DeGrand, R.L. Jaffe, K. Johnson and J. Kiskis, Phys. Rev. D **12**, 2060 (1975); T.A. DeGrand and R.L. Jaffe, Ann. Phys. **100**, 425 (1976); S. Théberge, A.W. Thomas and G.A. Miller, Phys. Rev. D **22**, 2838 (1980).
[5] G. R. Goldstein, TUFTS-TH-G88-5, Presented at *Workshop on Diquarks*, Turin, Italy, Oct 24-26, 1988.
[6] S. Capstick and N. Isgur, Phys. Rev. D **34**, 2809 (1986).
[7] L.Y. Glozman and D.O. Riska, Phys. Rept. **268**, 263 (1996).
[8] J. Speth, O. Krehl, S. Krewald and C. Hanhart, Nucl. Phys. A **680**, 328 (2000).
[9] F. Stancu and P. Stassart, Phys. Rev. D **38**, 233 (1988).
[10] S. Capstick and W. Roberts, Phys. Rev. D **47**, 1994 (1993).
[11] R. Koniuk and N. Isgur, Phys. Rev. D **21**, 1868 (1980).
[12] D. E. Groom *et. al.* (Particle Data Group), Eur. Phys. J. C **15**, 1 (2000).
[13] P. Stassart and F. Stancu, Phys. Rev. D **42**, 1521 (1990); D **47**, 2140 (1993); Z. Phys. A **351**, 77 (1995); R. Koniuk, Nucl. Phys. **B195**, 452 (1982); S. Capstick and W. Roberts, Phys. Rev. D **49** 4570 (1994); D **57**, 4301 (1998); D **58**, 074011 (1998)
[14] D. M. Manley and E. M. Saleski, Phys. Rev. D **45**, 4002 (1992); T. P. Vrana, S. A. Dytman and T. S. Lee, Phys. Rept. **328**, 181 (2000).
[15] T. Barnes and F. E. Close, Phys. Lett. **B123**, 89 (1983); E. Golowich, E. Haqq and G. Karl, Phys. Rev. D **28**, 160 (1983); C. E. Carlson, T. H. Hansson and C. Peterson, *ibid.* D **27**, 1556 (1983).
[16] P. Zenczykowski, Ann. Phys. (NY) **169**, 453 (1986).
[17] M. Brack and R. K. Bhaduri, Phys. Rev. D **35**, 3541 (1987).
[18] P. Geiger and N. Isgur, Phys. Rev. Lett. **67**, 1066 (1991).
[19] PhD thesis of Danielle Morel (FSU).
[20] B. Silvestre-Brac and C. Gignoux, Phys. Rev. D **43**, 3699 (1991); W. Blask, M.G. Huber, B. Metsch, Z. Phys. **A326**, 143 (1987).

The CELSIUS/WASA 4π detector project

H. Calén[b], C. Bargholtz[o], D. Bogoslawsky[d], A. Bondar[f], H. Clement[c], L. Demirörs[m], C. Ekström[b], K. Fransson[a], M. Gornov[n], J. Greiff[a], V. Grebenev[n], Y. Gurov[n], L. Gustafsson[a], B. Höistad[a], G. Ivanov[d], M. Jacewicz[a], E. Jiganov[d], A. Johansson[a], T. Johansson[a], S. Keleta[a], K. Kilian[g], N. Kimura[k], I. Koch[a], S. Kullander[a], A. Kupść[b], L. Kurdadze[f], A. Kuzmin[f], A. Kuznetsov[d], P. Marciniewski[a], B. Morosov[d], B.M.K. Nefkens[l], W. Oelert[g], S. Oreshkin[f], C. Pauly[m], Y. Petukhov[d], A. Povtorejko[d], J. Pätzold[c], R.J.M.Y. Ruber[b], V. Sandukovsky[d], W. Scobel[m], T. Sefzick[g], R. Shafigullin[n], V. Sidorov[f], B. Shwartz[f], V. Sopov[j], J. Stepaniak[e], A. Sukhanov[f], V. Tchernychev[j], P-E. Tegnér[o], P. Thörngren Engblom[a], V. Tikhomirov[d], A. Turowiecki[i], G. Wagner[c], U. Wiedner[a], K. Wilhelmsen[o], Z. Wilhelmi[i], A. Yamamoto[k], H. Yamaoka[k], J. Zabierowski[h], and J. Zlomańczuk[a]

[a]*ISV, Uppsala, Sweden;* [b]*TSL, Uppsala, Sweden;* [c]*Tübingen University, Germany;* [d]*JINR, Dubna, Russia;* [e]*INS, Warsaw, Poland;* [f]*BINP, Novosibirsk, Russia;* [g]*IKP, Forschungszentrum, Jülich, Germany;* [h]*INS, Lodz, Poland;* [i]*Inst. of Exp. Phys., Warsaw Univ., Poland;* [j]*ITEP, Moscow, Russia;* [k]*KEK, Tsukuba, Japan;* [l]*UCLA, Los Angeles, USA;* [m]*Hamburg University, Germany;* [n]*Mephi, Moscow, Russia;* [o]*Stockholm University, Sweden*

(Received: 31 October 2001)

A new experimental facility for light-ion physics has been prepared at the CELSIUS accelerator and storage ring of the The Svedberg Laboratory in Uppsala. The main motivation for the facility is investigations of rare processes, in particular some rare eta decays (e.g. decay into an electron-positron pair with predicted branching ratio around 10^{-9}). In addition, a wide range of meson production reactions will be accessible and studied with high accuracy. The necessary high luminosity of around $10^{32}\mathrm{cm}^{-1}\mathrm{s}^{-1}$ will be achieved by using small frozen hydrogen pellets as internal targets in CELSIUS. The detector installation is essentially completed. The pellet target system and the readout electronics are being tuned for high luminosity conditions. After some initial problems the pellet target has operated reliably during the last year and provided possibilities for regular commissioning runs.

1 Introduction

The CELSIUS/WASA, a facility for medium energy light-ion physics at the The Svedberg Laboratory in Uppsala, is now coming into operation. The experiment is designed to study some rare processes with cross sections in the picobarn region. A newly developed target system provides small frozen hydrogen spheres (pellets) as internal targets in the CELSIUS accelerator. At present the maximum energy for protons is 1360 MeV and after a planned upgrade it will be increased to 1900 MeV. The main parameters of the CELSIUS proton beams are listed in table 1.

Proton beam parameters:	uncooled	cooled
Maximum kinetic energy	1360 MeV	550 MeV
Beam diameter	7 mm	1 mm
Relative momentum spread	2×10^{-3}	2×10^{-4}
Number of stored protons	5×10^{10}	1×10^{10}
Beam current	27 mA	4.5 mA

Table 1: Some parameters of the CELSIUS storage ring.

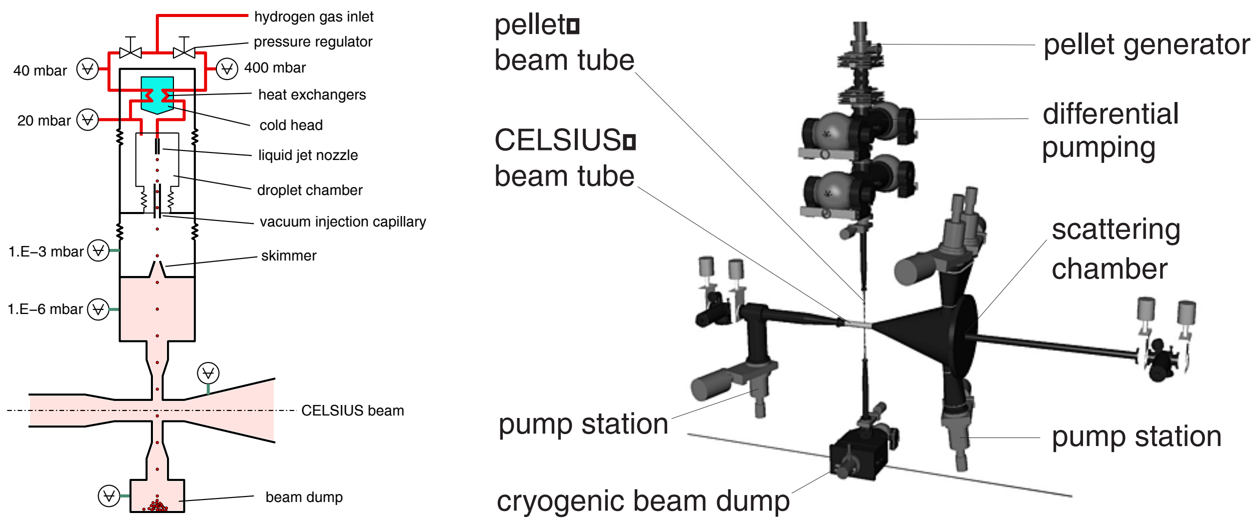

Figure 1: Schematic view of the pellet target system.

2 Pellet target system

The layout of the pellet target system is shown in figure 1. A jet of liquid hydrogen is broken up into droplets by a vibrating nozzle. The droplets freeze by evaporation in the droplet chamber and form pellets that are injected into vacuum. After collimation, the pellets are directed through a thin long tube into the scattering chamber. This arrangement provides the necessary space to put a 4π detection system around the interaction region. The pellet target thickness of up to $5 \cdot 10^{15}$ atoms/cm^2 gives acceptable half-lives of the circulating ion beam as well as acceptable vacuum conditions. Some design parameters of the pellet target are listed in table 2. The small size of the pellets ensures that the probability of secondary interactions inside the target is low. The pellet system was developed in Uppsala [1] and was successfully tested earlier at CELSIUS with hydrogen and deuterium pellets [2]. At present the system provides pellets with a diameter of about 50 μm and with a frequency of a few kHz. This has made possible the running in and tuning of the detector system. For the anticipated high luminosity runs, further development of the pellet system is needed, in order to have the smaller pellets and higher frequency.

Pellet target parameters:	
pellet diameter	25 μm
pellet frequency	20 kHz
pellet stream divergence	0.04°
effective target thickness	$10^{15} - 10^{16}$ atoms/cm^2
beam diameter	$2 - 4$ mm

Table 2: Some design parameters of the pellet target system.

3 Overview of the WASA 4π detector

The detector consists of three main parts: a central detector, a forward detector and a zero-degree spectrometer. A cross section of the central and the forward detectors is presented in figure 2.

The forward detector covers scattering angles from 3° to 18°. Its purpose is the measurement of charged target recoil particles and scattered projectiles. The central detector is optimized for meson decay products like electrons, photons and charged pions. It consists of a cylindrical drift

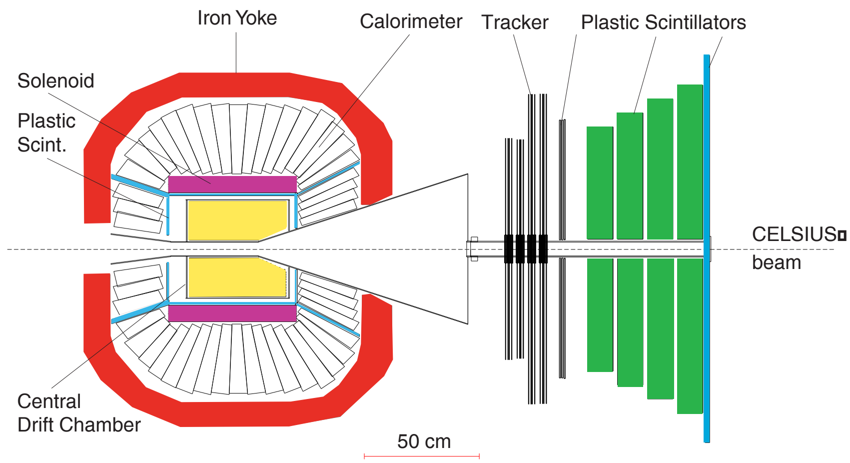

Figure 2: Cross section in the plane of the CELSIUS beam of the WASA 4π detector.

chamber, placed inside of a superconducting solenoid, and of an electromagnetic calorimeter of CsI crystals. Fast signals for trigger purposes are provided by a plastic scintillator barrel enclosing the drift chamber. The zero-degree spectrometer is positioned in the accelerator quadrant downstream of the pellet target and used for measurement of deutrons, ^{3}He and ^{4}He particles scattered at angles below 1° (table 3).

The forward detector, described in detail in [3], consists of several planes of plastic scintillators. Four layers, 11cm thick each, are used to measure the energy of charged particles. The other plastic detectors are used for trigger and for particle identification. Charged particles tracking is provided by several layers of thin walled straw tubes. The main parameters are listed in table 4.

In the central detector, charged particles tracks are measured by 17 layers of individual thin drift tubes (1738 in total). This central drift chamber covers scattering angles from 24° to 159°. The momentum resolution with a magnetic field of 1 Tesla for different particles is given in table 5. The superconducting solenoid has to have walls as thin as possible in order to minimize disturbance on the particle energy determination in the electromagnetic calorimeter. The wall thickness corresponds to 0.18 radiation lengths only, a record for this kind of magnets. The plastic scintillator barrel provides ΔE information for charged particle identification.

Sensitive Material	CsI and high purity germanium
Range of scattering angle	0°-0.85°
Rigidity range (Zp/p_{beam})	0.3–0.95

Table 3: Parameters of the Zero-degree spectrometer.

Scattering angle resolution	$< 0.2°$ (FWHM)
Energy resolution Δ E/E	3 % (FWHM)
Thickness	$1X_0 \sim 50$ g/cm^2
Maximum kinetic energy for stopping	
charged pions	170 MeV
protons	300 MeV
deuterons	400 MeV
alpha particles	900 MeV

Table 4: Parameters and typical performance of the Forward Detector.

Maximum kinetic energy for stopping:	
charged pion	190 MeV
proton	400 MeV
deuteron	450 MeV
Energy resolution for:	
100 MeV photon	10 % (FWHM)
stopped charged particles	3 % (FWHM)
Momentum resolution for:	
electrons (20 – 600 MeV/c)	1 % (FWHM)
$\pi^{\pm}$ and μ (100 – 600 MeV/c)	4 % (FWHM)
protons (200 – 800 MeV/c)	5 % (FWHM)

Table 5: Parameters and typical performance of the Central Detector.

The electromagnetic calorimeter covers scattering angles from 20° to 169° (96% of 4π steradians). Its primary purpose is to detect and measure photons, electrons and positrons with energies up to 600 MeV. The calorimeter consists of 1012 sodium-doped CsI scintillating crystals. The crystals are shaped as truncated pyramids and supported on the back end only. They are placed in 24 layers along the beam. A layer in the central part consists of 48 identical crystals. The length of the crystals vary from 30 cm (16.2 X_0) in the central part to 25 cm in the forward and 20 cm in the backward part. Each crystal is optically coupled by light guides to a photomultiplier placed outside of the iron yoke and supplied with an optical fiber providing light pulser signals for monitoring and calibration purposes. The use of photomultipliers provides a clear advantage in terms of energy resolution and timing.

4 Initial physics programme

The forward detector and 112 crystals of the calorimeter were used previously during six years for experiments at the CELSIUS cluster-jet target. Studies of near threshold π^0 and η meson production in nucleon-nucleon collisions as well as $\pi^+\pi^-$ pair production have been made [4]– [8]. Some of the

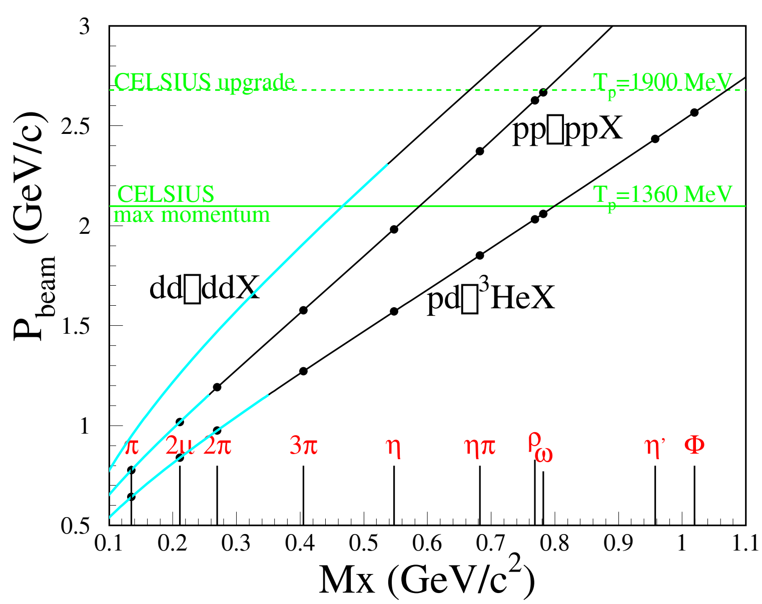

Figure 3: Some particles that can be studied at CELSIUS/WASA.

Reaction	$pp \to pp\eta$		$pd \to {}^3\mathrm{He}\eta$
T_p[MeV]	1360	1500	895
Cross section	5 μb	25 μb	0.5μb
Useful rate (ηs/day)	2×10^7	1×10^8	2×10^6
Tagging resolution (FWHM)	5 MeV	10 MeV	<1 MeV

Table 6: Production reactions for the η decay programme. Rates are estimated for a luminosity of 10^{32} cm^{-2}s^{-1}.

reaction channels were measured for the first time. Other items of interest were bremsstrahlung, deuteron break-up mechanism, and searches for dibaryon states.

The studies of light mesons production from pp and pd interactions will be continued with high acceptance conditions that allow for efficient identification of meson production events over a large kinematical range. By comparing different decay modes of the mesons, the control of systematic errors can be improved. For example the η meson could be identified by its decay into two photons as well as by its decay into three pions.

Figure 3 shows some mesonic final states that could be studied at CELSIUS in pp, pd and dd interactions. The solid horizontal line represent the present momentum limit of CELSIUS and the dashed line the limit after the planned upgrade. The upgrade will open new physics possibilities, like η' and ϕ meson production studies.

The collaboration has an extended programme for studies of rare decays of the η meson. The aim is to search for violations of fundamental symmetries and to provide crucial tests of Chiral Perturbation Theory. The most important production reactions of the eta meson for the decay programme are summarized in table 6. Eta mesons for the precise measurements of the not so rare $\eta \to 3\pi$ or $\eta \to \pi^0\gamma\gamma$ decays can be produced in $pd \to^3$ Heη reaction close to the threshold where ^{3}He is measured in the zero-degree spectrometer. For the very rare decays with branching ratios of 10^{-8} the reaction $pp \to pp\eta$ at 1360 MeV must be used. During runs in the Spring 2001, the proper detector performance for η production tagging by the measurement of protons in this reaction was verified. In a short test run with 895 MeV protons and deuterium pellets, η meson production events with a ^{3}He measured in the zero-degree spectrometer were detected.

References

[1] B. Trostell, Nucl. Instr. and Meth. **A362**, 41 (1995).

[2] C. Ekström et al., Nucl. Instr. and Meth. **A371**, 572 (1996).

[3] H. Calén *et al.,* Nucl. Instr. and Meth. **A379**, 57 (1996).

[4] A. Bondar *et al.,* Phys. Lett. **B356**, 8 (1995).

[5] H. Calén *et al.,* Phys. Lett. **B366**, 39 (1996).

[6] H. Calén *et al.,* Phys. Rev. Lett. **79**, 2642 (1997),

[7] H. Calén *et al.,* Phys. Rev. **C80**, 2667 (1998).

[8] J. Złomańczuk *et al.,* Phys. Lett. **B436**, 251 (1998).

[9] H. Calén *et al.,* Phys. Lett. **B458**, 190 (1999).

Meson production in $p + d$ reactions

H. Machner[a]
representing the GEM Collaboration
M. Betigeri[i], J. Bojowald[a], A. Budzanowski[d], A. Chatterjee[i], J. Ernst[g], L. Freindl[d], D. Frekers[h], W. Garske[h], K. Grewer[h], A. Hamacher[a], J. Ilieva[a,e], L. Jarczyk[c], K. Kilian[a], S. Kliczewski[d], W. Klimala[a,c], D. Kolev[f], T. Kutsarova[e], J. Lieb[k], A. Magiera[a,c], H. Nann[j], L. Pentchev[e], H. S. Plendl[k], D. Protić[a], B. Razen[a], P. von Rossen[a], B. J. Roy[i], R. Siudak[d], A. Strzałkowski[c], R. Tsenov[f], K. Zwoll[b]

[a]*Institut für Kernphysik, Forschungszentrum Jülich, Jülich, Germany*
[b]*Zentrallabor für Elektronik, Forschungszentrum Jülich, Jülich, Germany*
[c]*Institute of Physics, Jagellonian University, Krakow, Poland*
[d]*Institute of Nuclear Physics, Krakow, Poland*
[e]*Institute of Nuclear Physics and Nuclear Energy, Sofia, Bulgaria*
[f]*Physics Faculty, University of Sofia, Sofia, Bulgaria*
[g]*Institut für Strahlen- und Kernphysik der Universität Bonn, Bonn, Germany*
[h]*Institut für Kernphysik, Universität Münster, Münster, Germany*
[i]*Nuclear Physics Division, BARC, Bombay, India*
[j]*IUCF and Physics Department, Indiana University, Bloomington, Indiana, USA*
[k]*Physics Department, George Mason University, Fairfax, Virginia, USA*

(Received: 4 October 2001)

Total and differential cross sections for the reactions $p + d \to {}^3He + m^0$ with $m = \pi, \eta$ and $p + d \to {}^3H + \pi^+$ were measured with the GEM detector at COSY. For both reactions a strong forward–backward asymmetry is found. The differential cross sections for the pion production show a dramatic variation in the angular distribution. The total cross sections for all reactions studied show the strong influence of nucleon resonances. The data are compared with model calculations.

1 Introduction

The deuteron is a loosely bound system with a large distance between the two nucleons. It seems therefore a good testing ground for the impulse approximation. In addition, its wave function as well as those of the produced light nuclei are believed to be well known from electron scattering and one can hope that a theoretical treatment in the three-nucleon sector might be possible.

In the vicinity of the threshold the baryonic systems are emitted at rather small laboratory angles. Hence it is sufficient to have a geometrically small detector for the detection of the heavy recoiling nuclei. Energy and emission-direction measurement together with particle identification allow the reconstruction of the properties of the unobserved meson with the help of conservation laws. However, this method requires good track reconstruction to distinguish good events from experimental and/or physical background. This is achieved in the present experiment with the GEM setup [1]. It makes use of a solid state telescope with high precision resolution, a very thin target cell with extremely thin walls and a beam with small emittance.

All three reactions studied can proceed through a resonance: the $\Delta(1232)$ in the case of pion production and the $N^*(1535)$ in the case of eta production. We will discuss the influence of the resonances on the cross sections later.

In the reactions of interest one is dealing with large momentum transfers. This is shown in Fig. 1 for the reactions with the neutral mesons. While the momentum transfer for the $p + d \to {}^3He + \eta$ decreases strongly with increasing beam momentum, the dependence of q in the case of

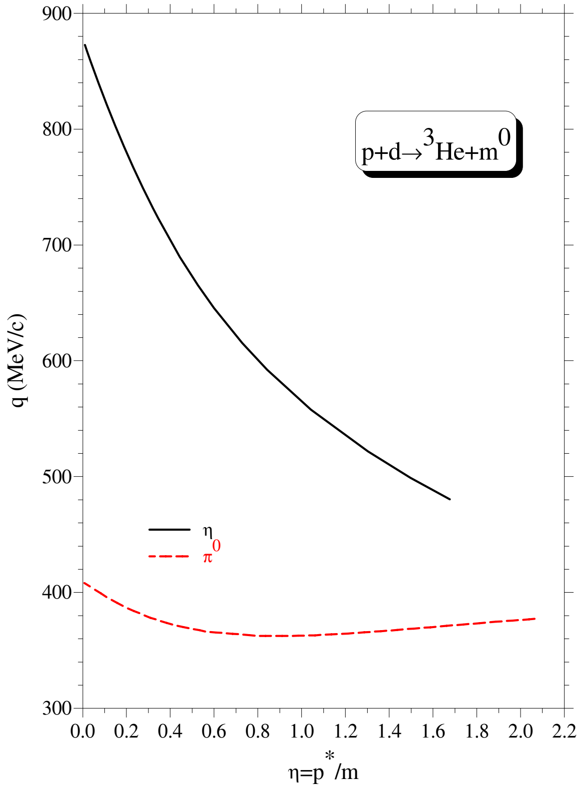

Figure 1: [Left] The momentum transfer q as function of the meson relative center of mass momentum η, i.e. the meson center of mass momentum divided by the corresponding mass.

Figure 2: [Below] The Germanium Wall. The response of the Quirl detector to a two hit event is shown. To the left and right there are two luminosity monitors, consisting of two scintillator paddles each. Each pair acts in coincidence and is denoted by L_R and L_L, respectively.

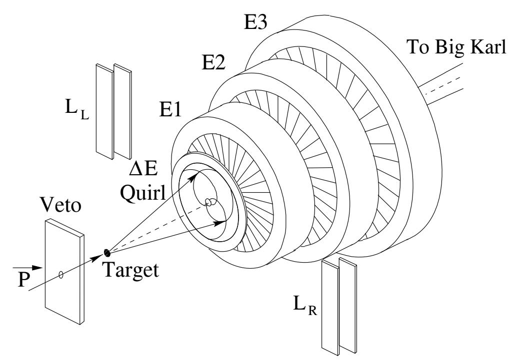

$p + d \rightarrow {}^3He + \pi^0$ reaction is rather weak. From the numbers involved one can estimate that pion production can occur on one target nucleon, whereas the large momentum transfer in the case of η– production makes such a mechanism unlikely. Both target nucleons have to participate making two-step processes very likely.

The theoretical studies in $p + d \rightarrow (A = 3) + meson$ have not been particularly successful although a lot of effort was devoted to this subject over the years [2].

2 Experiments

The proton beams were extracted from the cooler–synchrotron COSY in Jülich. Although the beam was not cooled it typically had an emittance of 2.5 π mm mrad in all directions. The detector used is a stack of diodes made from high purity Germanium. The diodes have structures on the front side as well as on the rear side allowing track reconstruction, energy measurement and particle identification. With this detector, called Germanium Wall [1] (see Fig. 2), we measured the heavy $A = 3$ recoils. It permits measurement of the particle type, the energy of the recoil and its direction. Thus the four momentum vector of the reaction product can be constructed. Then, by making use of conservation laws, the four momentum vectors of the unobserved mesons could be extracted. Recoils emitted at zero degree in the laboratory were measured with the magnetic spectrograph BIG KARL. Both detector elements together form the GEM detector.

3 Results

In Fig. 3 the missing mass spectrum for charged pions from the $pd \rightarrow {}^3H\pi^+$ reaction at 850 MeV/c is shown. Two things are worth mentioning: the high statistics in the experiment and the small background. In case of the η production the background is larger due to multi–pion production.

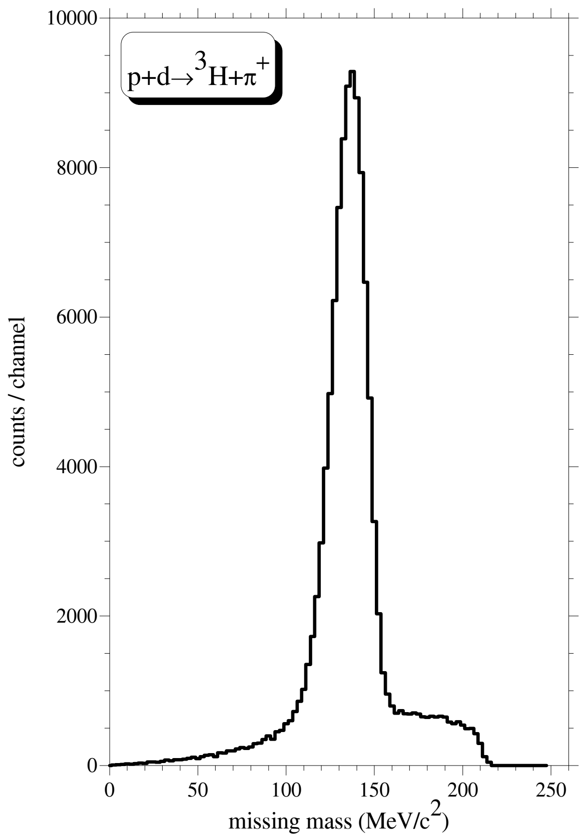

Figure 3: Deduced missing mass for the charged pion from the kinematically complete measurement of the triton. The small background was subtracted for each angular bin.

The background was subtracted by fitting a smooth curve to it. The resulting counting rate was converted to cross sections and the emission angle in the laboratory into those in the center of mass system.

3.1 π production

As an example we show in Fig. 4 the angular distributions for recoiling ^3He from the $pp \to {}^3He\pi^0$ reaction in the center of mass system. The data are for beam momenta from 750 MeV/c up to 1050 MeV/c in steps of 50 MeV/c. The data up to 850 MeV/c are published [3]. The other data are at present still preliminary.

The distributions are strongly non-isotropic with a much higher yield at backward angles corresponding to the smaller momenta of the recoiling ion. For the lowest beam momentum of 750 MeV/c measured by us, the angular distribution shows an almost exponential slope, while the distribution is isotropic at threshold [4]. For the higher beam momenta measured by us, an isotropic component in addition to the exponential shows up with increasing importance. This points to a change in the reaction mechanism and it will be interesting to compare the present data with models in order to see wether existing models can reproduce this feature of the data. In Ref. [3] the low energy data were compared with different models. This comparison was not too successful with respect to the shape and the absolute height of the model calculations. Here we will concentrate on model comparisons with the approach of Locher and Weber [5]. This model makes use of the differential cross sections for the $pp \to d\pi^+$ cross sections together with form factors to yield the $pd \to (A = 3)\pi$ cross section. In case of the ^3He production we approximate the $pn \to d\pi^0$ cross section by the isospin related $pp \to d\pi^+$ cross section. The differential cross section in this model

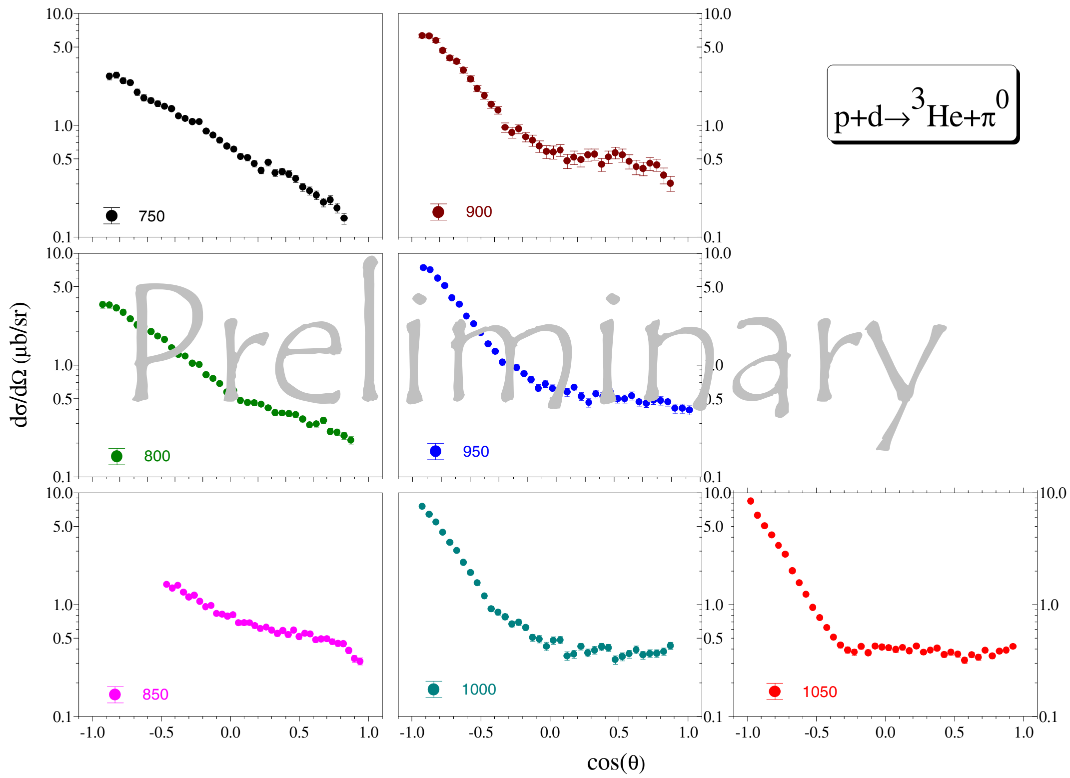

Figure 4: Angular distributions for the recoiling ^3He ions from $pd \to {}^3He\pi^0$ reaction for beam momenta indicated in the figure. All quantities are given in the center of mass system.

is given by

$$\frac{d\sigma(pd \to t\pi^+)}{d\Omega} = S\ K\,|F_D(q) - F_E(q)|^2\,\frac{d\sigma}{d\Omega}(pp \to d\pi^+) \tag{1}$$

with S, a spin factor, K a kinematical factor, and F_D, the direct form factor and F_E, the exchange form factor, i.e. an elastic πd scattering after pion emission from the incident proton. It should be stressed that further graphs are included in the calculation via antisymmetrization. The graph corresponding to $F_D(q)$ is treated in most calculations. The form factors were evaluated with emphasis on the short-range components of the deuteron and the triton. This is achieved by fitting the free parameters in a Hulthén function to the deuteron–charge form factor and similarly for ^3He. In this case several different functional dependencies were tested including Eckart function, 3-pole function, Gaussian, and exponential. All calculations require normalization factors when compared to the data. Best results were obtained for the Eckart wave function and an exponential. In the case of the Eckart function an overall normalization factor of 1.5 was applied to all data. We made the following additional assumptions which are different from the original Locher–Weber approach. The emission angle, i.e. the angle between the beam and the meson, is assumed to be the same for the present reaction and the underlying $pN \to d\pi$ reaction. Similarly, we assume the same eta-value for both reactions. In Figs. 5 and 6 data are compared to calculations. The calculations assumed an Eckart type wave function for ^3He. The contributions from the direct term and the exchange term are shown separately. Also shown is the coherent sum. The exchange term is found to be almost negligible at the smaller beam momentum. The forward angle of the ^3He, i.e. the part with the larger momentum transfer can not be described by the model. At higher beam momenta the agreement between data and calculation is much more satisfactory.

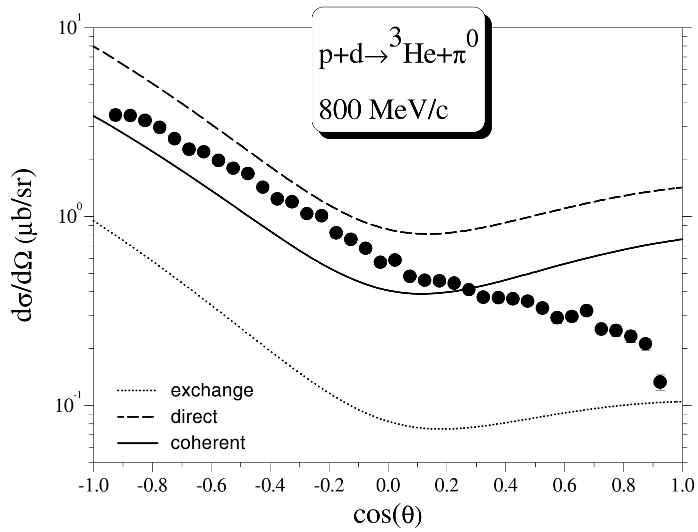

Figure 5: Angular distribution of ^3He ions from the reaction $pd \rightarrow {}^3H\pi^+$ at a beam momentum of 800 MeV/c. Calculations within the model discussed in the text are shown as curves. For the ^3He wave function an Eckart form was assumed. An overall normalization factor of 1.5 was applied. The dashed curve is the contribution from the direct term, the dotted the one from the exchange term, and the solid curve the coherent sum of both.

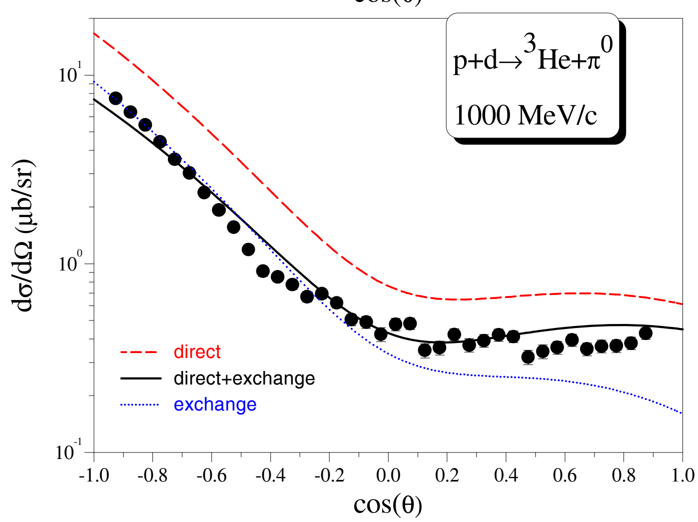

Figure 6: Same, but for a beam momentum of 1000 MeV/c. These data are preliminary.

3.2 η production

For η-production we obtained an angular distribution [6] which is dominated by p-wave in contrast to near threshold, where the angular distributions are s-wave dominated. A Legendre polynomial of second order was found to account for the data. From this fit a total cross section of $\sigma = 573 \pm 83\ (stat.) \pm 69\ (syst.)\ nb$ was deduced. This result is close to the one obtained by Banaigs et al. [7] at a slightly higher energy. The present result is compared with earlier measurements in Fig. 7. All cross sections from threshold up to $T_p \approx 1500\ MeV$ could be nicely accounted for by a simple calculation, also plotted in Fig. 7. This energy region corresponds to the center of the N^* S_{11} resonance ($\Gamma \sim 200$ MeV) known to couple strongly to the η–N channel [9]. One may therefore attempt to describe the cross section by an intermediate $N^*(1535)$ resonance excitation:

$$\sigma(E) = \frac{p_\eta}{p_p}|M(E)|^2 \tag{2}$$

with E the excitation energy and M the matrix element which is calculated as in photoproduction on the proton [10] as a Breit–Wigner form with an energy dependent width. All parameters were taken from Refs. [9] and [10]. The only free parameter is the strength fitted to the present data point. The trend of the data is reproduced, which may be taken as an indication that production of the $N^*(1535)$ resonance is the dominant reaction mechanism and that the product of kinematics

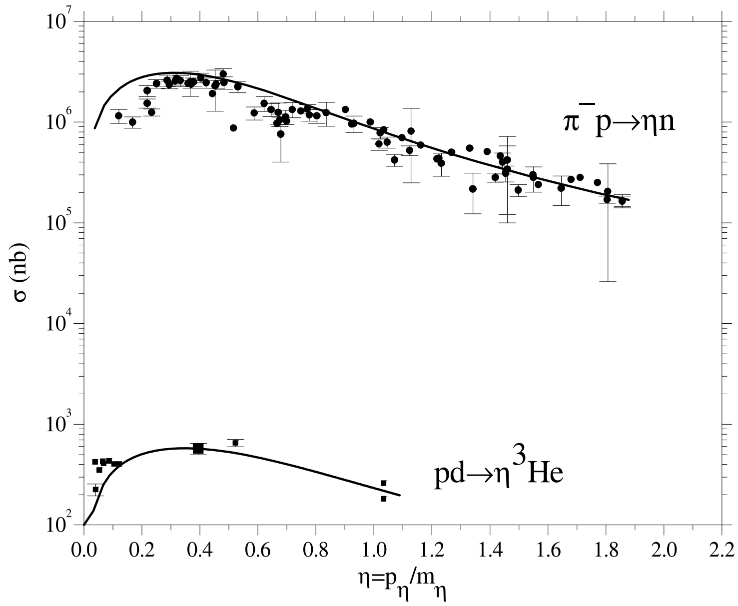

Figure 7: Excitation functions of η production in different reactions as function of $\eta = p_\eta{}^*/m_\eta$. The upper band is the data from $\pi^- p \to n\eta$ reactions, the middle band from $pp \to pp\eta$ reactions and the lowest one from $pd \to {}^3He\eta$ reactions. The solid curves are predictions assuming the matrix element from photoproduction of η mesons off the proton assuming only resonance production of the $N^*(1535)$. For the $pp \to pp\eta$ reaction an additional resonance at 1740 MeV/c was assumed (dashed curve).

and form factor changes very little over the present energy range. Deviations occur near threshold which might be an indication of strong final-state interactions (see Fig. 7).

References

[1] M. Bettigeri *et al.*, Nucl. Instrum. Methods Phys. Res. **A421**, 447 (1999).

[2] L. Canton, G. Cattapan, G. Pisent, W. Schadow, J. P. Svenne, Phys. Rev. **C 57** (1998) 1588; L. Canton and W. Schadow, Phys. Rev. **C 56** (1997) 1231.

[3] M. Bettigeri *et al.*, Nucl. Phys. **A 690**, 473 (2001).

[4] V. N. Nikulin *et al.*, Phys. Rev. **C 54**, 1732 (1996).

[5] M. P. Locher and H. J. Weber, Nucl. Phys. **B76**, 400 (1974).

[6] M. Bettigeri *et al.*, Phys. Lett. **B472**, 267 (2000).

[7] J. Banaigs *et al.*, Phys. Lett. **B45**, 394 (1973).

[8] P. Berthet *et al.*, Nucl. Phys. **C443**, 589 (1985).

[9] Particle Data Group (C. Caso *et al.*), The European Phys. J. **3**, 1 (1999).

[10] B. Krusche, Acta Phys. Polonica **27B**, 3147 (1996).

Charge symmetry breaking in np $\rightarrow$ dπ^0

S. D. Reitzner

Department of Physics and Astronomy, Ohio University, Athens, OH 45701, U.S.A.

(Received: 5 November 2001)

The charge-symmetry breaking (CSB) experiment using the SASP spectrometer at TRIUMF aims to measure the forward-backward scattering asymmetry (A_{fb}) for the np $\rightarrow$ dπ^0 reaction at a neutron beam energy of 279.5 MeV. A_{fb} can be non-zero only if charge-symmetry is violated. The dominant contributions to CSB in np $\rightarrow$ dπ^0, which are not present in elastic scattering, are due to $\eta - \pi^0$ and $\eta' - \pi^0$ mixing and the u - d quark mass difference in pion-nucleon scattering. With a predicted value ranging from $(-35$ to $+70)\times10^{-4}$near 280 MeV for A_{fb}, the measurement has an estimated statistical uncertainty of $\pm5\times10^{-4}$ and systematic uncertainties that are no greater than $\pm7\times10^{-4}$. The observable will be obtained from a χ^2 minimization procedure which compares data with a simulation in four dimensions.

1 Introduction

Contributions to the nuclear potential which are dependent on the difference between the u and d quark masses manifest as charge dependent effects and are very small when compared the charge independent contributions. Thus, these charge dependent contributions to the nuclear potential are difficult to study and hence are less well known. By investigating nuclear reactions which differentiate protons from neutrons, the charge symmetry breaking (CSB) contributions to the nuclear force can be studied.

Comparisons of pp to nn systems are complicated by the presence of the Coulomb potential for which a large correction must be applied to extract out the CSB signal. In contrast, np scattering lacks any Coulomb interaction between the interacting nucleons. The electromagnetic interaction is reduced relative to the strong interaction making np scattering a clean venue in which to investigate CSB. Previous experiments of CSB in the np system studied elastic processes. To complement these measurements, CSB in the np $\rightarrow$ dπ^0 inelastic process is being studied as it has CSB contributions that are not present in the elastic scattering experiments.

Two models which describe CSB in np $\rightarrow$ dπ^0 have contributions which are an order of magnitude greater than those found for elastic scattering. A pion production model developed by Niskanen [2] describes the dominant contribution to CSB as arising from $\eta - \pi^0$ and $\eta' - \pi^0$ mixing. The contributions due to $\eta - \pi^0$ and $\eta' - \pi^0$ mixing are linearly dependent on the ηNN coupling constant and the $\eta - \pi$, $\eta' - \pi$ mixing amplitudes. The mixing amplitudes are well known from the analysis of η and η' decay [1] however, the ηNN coupling constant is not well determined with measured values ranging from $g^2_{\eta NN}/4\pi = 0.2$ to 6.2 [2,3]. If CSB contributions exist in the np $\rightarrow$ dπ^0 reaction originating from $\eta - \pi^0$ mixing, then there exists an opportunity to constrain the ηNN coupling constant.

An effective field theory model developed by van Kolck [4] has CSB contributions which are dependent on the u-d quark mass difference in π^0N scattering. These contributions to CSB are dependent on the values of δm_N (the proton-neutron mass difference attributed to the quark mass difference) and $\bar{\delta} m_N$ (the proton-neutron mass difference attributed to electromagnetic effects). The values for δm_N and $\bar{\delta} m_N$ are not very well constrained [4]. As such, the measurement of CSB in np $\rightarrow$ dπ^0 has the potential to place tighter constraints on the values for δm_N and $\bar{\delta} m_N$.

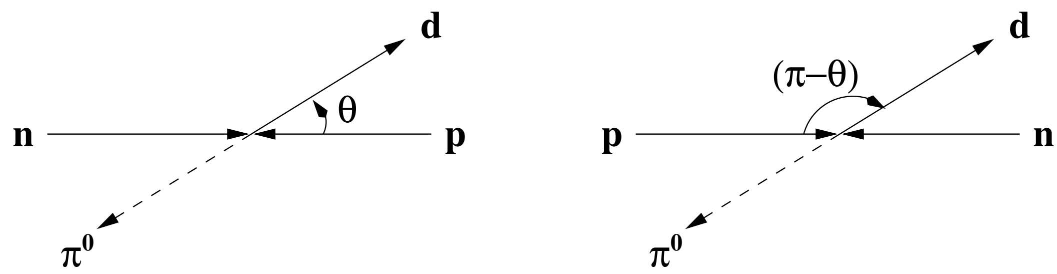

Figure 1: The np $\rightarrow$ dπ^0 reaction in the centre of mass frame before and after the charge symmetry operator is applied.

The charge symmetry operator is defined to be:

$$P_{CS} \equiv e^{i\pi \vec{T}_2} \ , \tag{1}$$

and operates on a wave function, rotating T_3 to $-T_3$ while leaving the magnitude of $\vec{T}$ unchanged. For the nucleon system, P_{CS} rotates neutrons into protons and vice versa. In figure 1, the diagram on the left shows the np $\rightarrow$ dπ^0 system, in the centre of mass (CM) frame, before the application of the CS operator. The diagram on the right shows the same system after the application of the CS operator. While the neutron and proton change positions, the pion and deuteron remain unchanged as their third components of isospin are zero. The overall effect of the CS operator on the np $\rightarrow$ dπ^0 system is to change forward going deuterons into backward going deuterons.

The cross-section for the np $\rightarrow$ dπ^0 reaction in the centre of mass frame can be parameterized as:

$$\frac{d\sigma}{d\Omega} = A_0 + A_1 P_1\big(\cos(\theta)\big) + A_2 P_2(\cos(\theta)\big) \ , \tag{2}$$

where P_i are Legendre polynomials, θ is the centre of mass scattering angle, and A_0, A_1, and A_2 are parameters [5]. Odd powers of $\cos(\theta)$ in the angular distribution produce an asymmetry in the CM cross-sections between the forward and backward scattered deuterons. The A_1 term reflects the size of the charge symmetry breaking effects as it is multiplied to the odd term in $\cos\theta$. If charge symmetry is conserved then $A_1 = 0$. The observable for this asymmetry is what is called the forward-backward scattering asymmetry or A_{fb}. In the centre of mass system $A_{fb}(\theta)$ is as:

$$A_{fb}(\theta) \equiv \frac{\sigma(\theta) - \sigma(\pi - \theta)}{\sigma(\theta) + \sigma(\pi - \theta)} \ , \tag{3}$$

where $\sigma(\theta)$ is the cross-section for the deuteron to scatter at an angle θ. The total integrated A_{fb}, for the np $\rightarrow$ dπ^0 system, is defined as:

$$A_{fb} \equiv \frac{\int_0^{\pi/2} [\sigma(\theta) - \sigma(\pi - \theta)] \sin(\theta) d\theta}{\int_0^{\pi} \sigma(\theta) \sin(\theta) d\theta} \ . \tag{4}$$

Using equation 2 in equation 4, A_{fb} can be related A_1 through the relation:

$$A_{fb} = \frac{1}{2} A_1 / A_0 \ . \tag{5}$$

Thus by determining the value of A_1 from the data, A_{fb} will be determined. Figure 2 shows the size of the contributions to A_{fb} at the energy of interest.

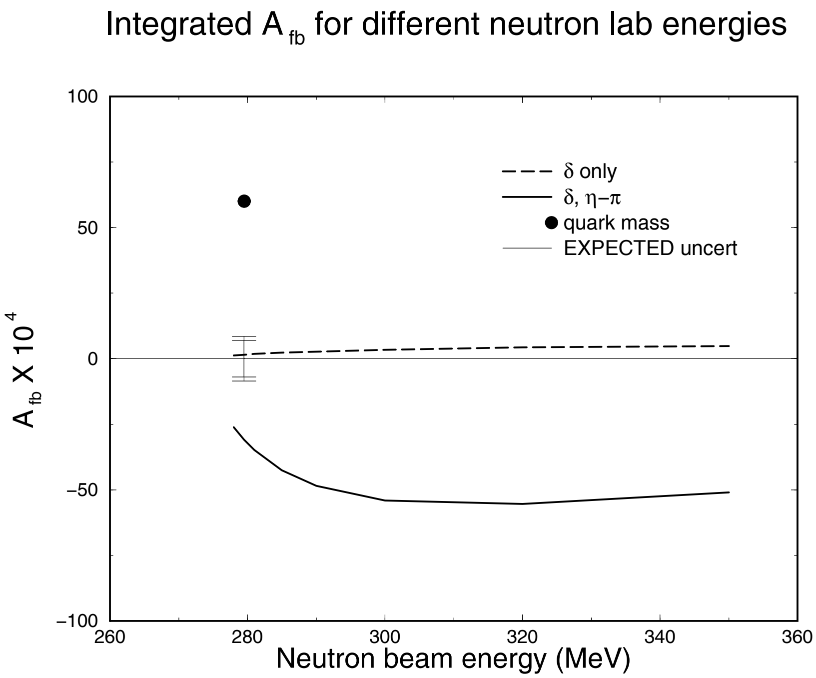

Figure 2: Contributions to A_{fb} near threshold. The dashed line represents the contributions from the neutron-proton mass difference from pion production. The solid line shows the inclusion of $\eta - \pi$ mixing. The solid dot is the contribution from the u-d quark mass difference in π^0N scattering only. The inner error bars indicate the expected statistical uncertainty and the outer error bars indicate the quadratic sum of the statistical and systematic uncertainties.

2 Experimental apparatus

The measurement of np $\rightarrow$ dπ^0 uses a 279.5 MeV secondary neutron beam to produce deuterons in a 2 cm liquid hydrogeng3 (LH_2) target. The secondary neutron beam is produced in a charge exchange reaction between the primary proton beam and a ^{7}Li target. Three multi-wire proportional counters positioned downstream of the LH_2 target are used to measure the deuteron trajectory as it leaves the target. The SASP [6], a QQD clamshell spectrometer, immediately downstream of the multi-wire proportional counters, momentum analyses the particles. Two vertical drift chambers (VDCs) are set downstream of the exit of the dipole to reconstruct the particle tracks from which the particles' momentum can be deduced. A focal plane beam blocker, mounted immediately upstream of the upstream VDC, is a tungsten-alloy block thick enough to stop 300 MeV protons. The blocker prevents protons from reaching the focal plane detectors. This blocker can be moved along the focal plane as required for special measurements.

Two sets of paddle hodoscopes are placed downstream from the VDCs. The energy deposited in the paddles, along with the time of flight information, provide particle identification. A single monolithic scintillator above the paddle plane is used for a top end trigger. A pair of CH2 scintillators, immediately downstream from the target acts as a trigger. A second pair of CH2 scintillators upstream of the target act as veto counters for any charge particles which are present in the secondary neutron beam [7].

3 Extraction

The combined effects of energy loss, multiple scattering and a finite beam energy width effectively blur the boundary between the forward and backward scattered deuterons. Furthermore, the effects

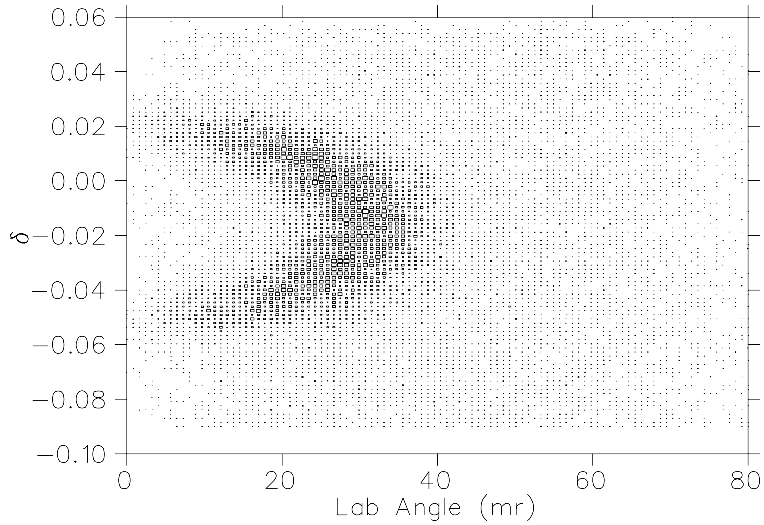

Figure 3: The locus extracted from the np $\rightarrow$ dπ^0 data.

of energy dependent hadronic losses and the spectrometer acceptance are folded into the data making it next to impossible to extract A_{fb} directly from the data. To overcome these obstacles in extracting A_{fb}, a simulation of the experiment is used to determine the value for the CM cross-section parameter A_1 for the np $\rightarrow$ dπ^0 reaction. The GEANT detector and simulation package [8] is used for the simulation and can generate simulated data for the reactions: np $\rightarrow$ dπ^0, and np elastic scattering.

Elastic np scattering and a simulation of that reaction was used to test the viability of the np $\rightarrow$ dπ^0 GEANT model. The cross-section for np-elastic scattering is well know and slowly varies at the energy of interest. Furthermore, the beam used for the np elastic studies is the same used in np $\rightarrow$ dπ^0 so the same spectrometer acceptance space is probed. Measurement of np-elastic scattering was done with the SASP magnetic fields held constant and the incident beam energy changed to produce protons with momentum which match the momentum mean and extremes of the deuteron momentum. This results of the np-elastic studies allows for the acceptance space to be mapped from which a common acceptance space, which is momentum independent in both the simulation and the data, can be selected. As the field map used to describe the SASP dipole field in the simulation is taken at a different field strength than that used for the experiment, the field map can not account for the magnetic field saturation effects on the data. Corrections for these and off-axis aberrative effects were extracted from the np elastic studies and applied to both the simulation and the data.

The value for A_{fb} is determined by comparing the deuteron locus extracted from the simulation to the locus extracted from the data. This deuteron locus has the measured deuteron momentum (δ) plotted against the deuteron lab scattering angle as seen in figure 3. A set of input parameters for the simulation are found that best fit the data locus. This set of parameters is at the global minimum of a four dimensional χ^2 surface where each dimension represents one of four parameters including A_1/A_0. The global minimum is determined from a fit of a four dimensional second order Taylor expansion to the χ^2 surface. Each point on the χ^2 surface is calculated by comparing the data to the simulation in which the four input parameters are varied. Thus, for a four dimensional grid with three points per axis, a total of $3^4 = 81$ loci must be generated, each with a differing combination of the input parameters of interest.

To discourage any bias on the quality of the model, based on the expected result of A_{fb}, an unknown offset has been applied to the parameter A_1/A_0 in the simulation. This offset is chosen to be within -5 to $+5$ % which is a wide but plausible range for the expected value for A_1/A_0 and was selected by a member of the collaboration not involved in the simulation development.

Due to the limit on the amount time available to create a multi-parameter χ^2 surface, it is necessary to determine which set of parameters will have the strongest effect on the final outcome on the value of A_1/A_0. Those parameters for which the contributions to the systematic uncertainty is less than or equal to 0.05% can be held fixed. The sensitivity of A_1/A_0 to a parameter P_i is extracted from a χ^2 surface generated from the χ^2 fit of a simulation versus simulation comparison. The simulated locus designated as the standard locus is generated with all parameters set to their nominal values. The simulated loci that are to be fit to the standard locus are generated as a two dimensional grid where each axis on the grid represents one of the two varied parameters: A_1/A_0, and P_i. With three points per axis, a set of nine loci are generated by GEANT. The grid step size for a parameter P_i is three times the size of the uncertainty in P_i and $\pm 3.5\%$ for A_1/A_0. The sensitivity of A_1/A_0 to parameter P_i is defined as how much A_1/A_0 changes ($\Delta A_i/A_0$) when P_i is offset from its best estimated value by ΔP_i. If A_1/A_0 is the dependent coordinate then the sensitivity can be extracted from the partial derivative of the χ^2 surface at the global minimum. The product of the sensitivity and the uncertainty in P_i will give the systematic uncertainty in A_1/A_0 attributed to the uncertainty in P_i. The parameters which A_1/A_0 has the largest sensitivities to are the LH_2 target thickness, the central momentum setting of SASP and the beam energy. These three parameters, along with A_1/A_0 were varied in the main grid. The uncertainties in these parameters, when extracted from the main grid, will be smaller than those found through conventional methods thus making the measurement of A_{fb} meaningful.

To test the credibility of the GEANT model of the data, the simulation must obtain a statistically equivalent value of A_1/A_0 from differing regions of target space. The output for GEANT produces separate sets of loci, corresponding to the region of target space selected to test the model viability. The target cuts can be broken down into two sub-sets of cuts: spacial cuts on vertical position (X_i), horizontal position (Y_i), and angular cuts based on the deuteron horizontal scattering (ϕ_i).

4 Status

The generation of the main grid is complete and A_1/A_0 has been extracted from the standard acceptance space and the acceptance sub-spaces. For the majority of the acceptance sub-spaces, the best value for A_1/A_0 was found to be within error of the result with the full acceptance, as seen in table 1. Only the sub-spaces corresponding to the top ($X_i = -2$ to 0 cm) and bottom ($X_i = 0$ to 2 cm) regions of the target diverged significantly from the value of A_1/A_0 extracted from the standard acceptance space. This indicates a flaw in the model which does not accurately describe the differences experienced by the deuterons as they pass through upper or lower regions of the target.

The results for the value of the LH_2 target thickness reported that the bottom target space required a thicker target than the top target space. Deuteron yields did not reveal any LH_2 target thickness difference between the top and bottom portions of the target. Looking into measurements for the thickness of the front end trigger (FET) scintillator revealed that the lower portion of the FET was thicker than the top. The main grid was regenerated using the modified FET thickness. The results from the top and bottom target sub-spaces now have a better agreement for the target thickness but still report a difference in A_1/A_0.

As mentioned above, the off-axis aberration corrections were obtained from np elastic scattering; these may not be applicable for deuterons moving through the spectrometer off-axis so similar

Acceptance X_iY_i	Angular	$\Delta(A_1/A_0)$ $\times 10^{-4}$
std: ± 2 cm	std ϕ_i	0
std	8 mr tighter	-1 ± 14
$r < 2$ cm	std	-2 ± 14
$r < 1$ cm	std	-19 ± 23
± 1 cm	std	-19 ± 20
± 0.66 cm	std	17 ± 31
X_i -2 - 0 cm std: Y_i	std	82 ± 18
X_i 0 - 2 cm std: Y_i	std	-86 ± 19
Y_i -2 - 0 cm std: X_i	std	6 ± 19
Y_i 0 - 2 cm std: X_i	std	-9 ± 18

Table 1: The difference between the best value for A_1/A_0 for the various acceptance sub-space as compared to A_1/A_0 extracted from the standard acceptance space. X_i and Y_i represent the vertical and horizontal cuts in target space respectively, r represents the radius of a circle, and ϕ_i represents the horizontal scattering angle out of the target.

corrections were obtained from the np $\rightarrow$ dπ^0 data itself. These corrections to the data brought the vertical vertex position dependence of the momentum into agreement with that of the simulation. This correction was applied to the data as the data can be quickly replayed within an hour while applying the correction to the simulation would require the generation of a new grid and take up to three weeks. The comparison of the model to the corrected data does not show any improvement in the disagreement of the value of A_1/A_0 for the top and bottom sub-spaces of the target. With this disagreement still present after applying the vertex position correction, the unknown offset to A_1/A_0 in the simulation will not be revealed.

References

[1] S.A. Coon *et al.*, Phys. Rev. C**34**, 2784 (1986).

[2] J.A. Niskanen., Few-Body Systems **26**, 241 (1999).

[3] M. Benmerrouche, N.C. Mukhopadhyay, J.F. Zhang, Phys. Rev. D **51**, 3237 (1995).

[4] U. van Kolck, J.A. Niskanen, and G.A. Miller, Phys. Lett. **B493**, 65 (2000).

[5] D.A. Hutcheon *et al.*, Nucl. Phys. **A535**, 618 (1991).

[6] P.L. Walden *et al.*, Nucl. Instr. and Meth. **A421**, 142 (1999).

[7] D.A. Hutcheon *et al.*, Nucl. Instr. Meth. **A459**, 448 (2001).

[8] GEANT, Detector Description and Simulation Tool, (1993).

Spin physics in the resonance region with CLAS

R. De Vita[a]
for the CLAS Collaboration
[a]*Istituto Nazionale di Fisica Nucleare, via Dodecaneso 33, 16146 Genova, Italy*

(Received: 31 October 2001)

Spin structure functions in the deep inelastic region have been measured extensively over the past two decades. Much less is known in the region of the nucleon resonances and at low to intermediate Q^2. A large experimental program is in progress in Hall B at Jefferson Lab with the CLAS detector to study this kinematic region, employing polarized electrons impinging on polarized proton and deuteron targets. Among the experimental goals of this program are the study of spin structure functions and asymmetries in inclusive and exclusive reactions. Preliminary results on the spin structure funtions g_1 and on its first moment on the proton and the deuteron are presented. In addition, spin asymmetries in single pion electroproduction are discussed.

1 Physics motivation

Experiments with polarized lepton beams and polarized targets in deep inelastic scattering (DIS) have been a fundamental source of information on the spin structure of the nucleon for more than two decades. These measurements give direct access to the nucleon spin structure function g_1, which, in the parton model, describes the polarization of the quarks and anti-quarks inside the nucleon. It can be expressed as

$$g_1(x) = \frac{1}{2}\left(\frac{4}{9}\Big[\Delta u(x) + \Delta\bar{u}(x)\Big] + \frac{1}{9}\Big[\Delta d(x) + \Delta\bar{d}(x) + \Delta s(x) + \Delta\bar{s}(x)\Big]\right) \ . \tag{1}$$

A surprising outcome of these studies was the result of the EMC experiment [1], which found that at small distances the quarks carry only a fraction of the nucleon spin. Since that time, the spin structure of the nucleon has been of central interest both for experimental and theoretical research, and several measurement were completed. In the high Q^2 region, the general interest was focused on the study of spin structure functions and on fundamental sum rules such as the Bjorken sum rule [2]. This sum rules relates the first moment of the spin structure function $\Gamma_1 = \int_0^1 g_1(x)dx$ to the axial coupling constant g_A,

$$\Gamma_1^p - \Gamma_1^n = \frac{1}{6}g_A \ , \tag{2}$$

and is based on very general principles. This sum rule has been evolved at finite Q^2 by pQCD techniques, and is now verified experimentally at the 5% level.

At the opposite extreme of the kinematic range, $Q^2 = 0$, the Gerasimov-Drell Hearn (GDH) sum rule [3, 4] relates the energy integral of the helicity difference of the total photo-absorption cross section to a static property of the nucleon, its anomalous magnetic moment κ,

$$\int_{thr}^{\infty} \frac{\sigma_{1/2} - \sigma_{3/2}}{\nu} d\nu = -\frac{2\pi^2\alpha}{M^2}\kappa^2 \ . \tag{3}$$

The GDH sum rule is based on unsubtracted dispersion relations, on the forward Compton scattering amplitude, and on the Optical and Low Energy Theorems, i.e. very general assumptions. The sum rule has been recently studied at MAMI up to photon energies of 850 MeV [5], and is presently under investigation at ELSA [6]. The analysis of the MAMI data showed that the GDH sum rule for the proton is reasonably statisfied.

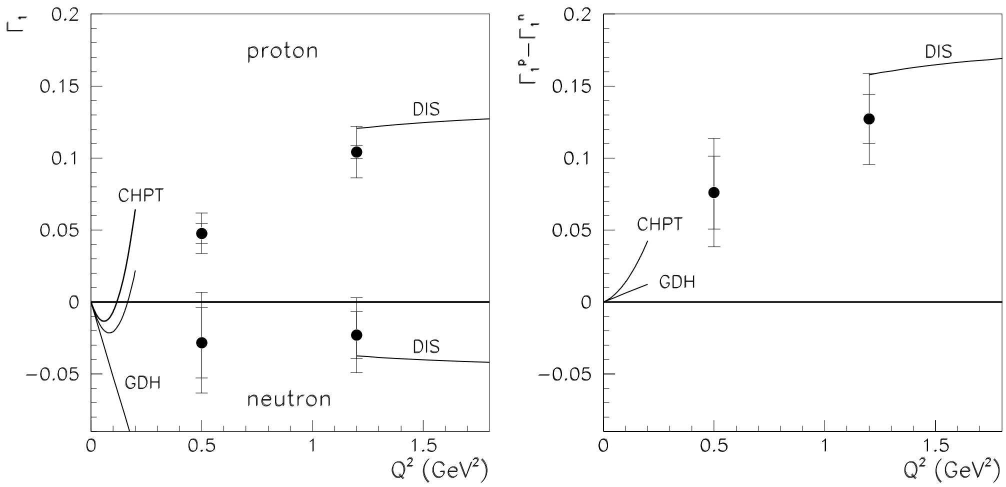

Figure 1: First moment of the spin structure function g_1 for the proton and neutron (left) and for the proton-neutron difference. Data points are from SLAC [7]. The DIS slope at large Q^2 is shown. The $Q^2 = 0$ slope predicted by the GDH sum rule is indicated as well as chiral perturbation theory calculation from ref. [13].

In the limit of small Q^2, the GDH sum rule defines the slope of $\Gamma_1(Q^2)$, the first moment of the structure function g_1,

$$\Gamma_1(Q^2) \to \frac{Q^2}{16\pi^2\alpha}\int_{thr}^{\infty}\frac{\sigma_{1/2}-\sigma_{3/2}}{\nu}d\nu = -\frac{Q^2}{8M^2}\kappa^2. \tag{4}$$

This relation defines a connection between the $Q^2 = 0$ and $Q^2 \to \infty$ limits. This implies that for $Q^2 \to 0$, Γ_1 should be negative, in contrast with the positive values observed in the DIS region. Consequentely, a dramatic change in the nucleon spin structure must occur somewhere in the intermediate Q^2 region. As shown in Fig. 1, this regime is lacking both of experimental data and theoretical predictions. Starting from the high Q^2 limit, pQCD predictions have been extended down to $Q^2 = 1$ GeV^2, while Chiral Perturbation theory has been used to evolve the GDH sum rule up to $Q^2 = 0.1$ GeV^2. However a gap in between still remains. This region is expected to be dominated by higher twist effects and resonance contribution. Measurements of spin structure function in this range are therefore very important to understand at what distance scale perturbative QCD will break down and to identify the relevant non-perturbative mechanisms. In addition, since the resonance helicity structure is expected to vary with the distance scale, such measurement would provide fundamendal constraints for baryon structure models. For this purpose, measurements of spin observables in exclusive channels are of great importance, since these reactions are spin and isospin filters for the excitation of baryon resonances.

The main goal of the spin physics program in Hall B at Jefferson Laboratory is to perform a detailed study of spin structure functions in inclusive and exclusive reactions. The first experiments on polarized hydrogen (NH_3) and deuteron (ND_3) have been completed.

2 Experimental setup

The CLAS detector [8] in Hall B at Jefferson Lab was used to study double polarization observables on proton and deuteron targets. A longitudinally polarized electron beam with energies of 2.5 and 4.3 GeV was incident on polarized NH_3 and ND_3 targets. The beam polarization, measured routinely with a Møller polarimeter was typically $\sim 70\%$ and was reversed in a pseudo-random sequence at a frequency of 1 Hz to reduce systematic effects. The beam current was typically in the range 1-4 nA, corresponding to a luminosity of $4 - 16 \cdot 10^{33}$ cm^{-2}s^{-1}.

The target consisted of NH_3 and ND_3 pellets in a 1 cm thick cell immersed in liquid helium at a temperature of 1 K. A superconducting Helmholtz magnet produced a 5 Tesla field oriented along the beam direction. Nuclear polarization was induced by DNP technique [9] driven by a microwave field at 140 GHz. The NH_3 and ND_3 polarization were respectively 50-70% and 15-25%.

CLAS is a magnetic spectrometer based on a six-coil torus magnet whose field is primarily oriented along the azimuthal direction. The particle detection system includes drift chambers for track reconstruction, scintillation counters for the time of flight measurement, Cerenkov counters for electron-pion discrimination, and electromagnetic calorimeters to identify electrons and neutrals. Thanks to the large acceptance, it can simultaneously detect the scattered electron and hadrons in the final state, allowing the measurement both of inclusive and exclusive reaction in a wide Q^2 and W range. A first data taking period was completed in the Fall of 1998 for a total of 3 billions triggers. A second run was performed in 2000-2001. The results presented in this paper are based on the analysis of the 1998 data.

3 Data analysis and results

The extraction of the spin structure functions from the data is performed by measuring the double spin asymmetry

$$A_{exp} = \frac{1}{P_b P_t f} \frac{N(+-) - N(++)}{N(+-) + N(++)} , \tag{5}$$

where N indicates the event yield, the signs in parenthesis represent the beam and target helicities, P_b and P_t are respectively the beam and target polarization and f is the dilution factor, i.e. the fraction of events from free nucleons in the NH_3 or ND_3 target. In inclusive scattering, this experimental asymmetry can be expressed in terms of virtual-photon asymmetries as [10]

$$A_{exp} = \sqrt{1-\epsilon^2} \cos\theta_\gamma \frac{A_1 + \eta A_2}{1 + \epsilon R} , \tag{6}$$

where ϵ is the virtual photon polarization, θ_γ is the angle between the target spin and the virtual-photon momentum direction, $\eta = \tan\theta_\gamma \sqrt{2\epsilon/(1+\epsilon)}$, and R is the longitudinal-transverse cross section ratio σ_L/σ_T. The structure function A_1 is the virtual photon helicity asymmetry,

$$A_1 = \frac{|A_{1/2}|^2 - |A_{3/2}|^2}{|A_{1/2}|^2 + |A_{3/2}|^2} , \tag{7}$$

while A_2 is a longitudinal-transverse interference term. The asymmetries A_1 and A_2 are related to the spin structure function g_1 by

$$g_1(x, Q^2) = \frac{\tau}{1+\tau} \left[A_1(x, Q^2) + \frac{1}{\sqrt{\tau}} A_2(x, Q^2) \right] F_1(x, Q^2) , \tag{8}$$

where F_1 is the usual unpolarized structure function.

The formalism of eq. 6 is valid also for exclusive reactions. However in that case the photon asymmetries A_1 and A_2 will depend also on the pion center-of-mass polar angle [11]. Figure 2 shows the asymmetry $A_1 + \eta A_2$ for the proton (left) and the deuteron (right). For both targets, the asymmetry shows a strong W dependence which reflects the resonance structure. The photon helicity asymmetry A_1 is in fact extremely sensitive to the structure of the excited state. In the excitation of the $P_{33}(1232)$, $A_{3/2} \sim \sqrt{3} A_{1/2}$ and therefore $A_1 \sim= -0.5$, in contrast with spin-1/2 states, as the $P_{11}(1440)$ or the $S_{11}(1535)$, for which $A_{3/2} = 0$, and $A_1 = 1$.

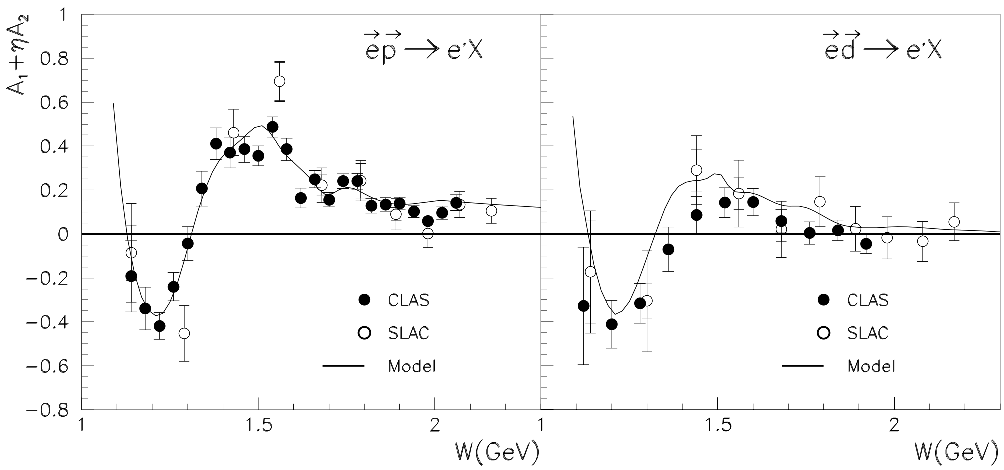

Figure 2: Asymmetry $A_1 + \eta A_2$ for the proton (left) and the deuteron (right) for $Q^2 = 0.4 - 0.6$ GeV^2. The CLAS data are shown in comparison with previous measurements from SLAC. The solid curve is a parameterization that was used for radiative corrections and to extrapolate at $x \to 0$ for the evaluation of Γ_1.

Using a parameterization of the world data on F_1 and A_2, $g_1(x, Q^2)$ was extracted from eq. 8. Examples of $g_1(x, Q^2)$ are shown in fig. 3. At low Q^2 (upper plot), g_1 is dominated by the negative contribution of the $P_{33}(1232)$ state, while at higher Q^2 (lower plot) the more positive values reflects the contribution of higher mass states as the $S_{11}(1535)$ and $D_{13}(1520)$. The dashed line is a phenomenological parameterization of the structure function based on previous data [12], while the solid line represents a model of $g_1(x, Q^2)$, which has beed used to extrapolate to $x \to 0$ for the Γ_1 integral evaluation. The results for $\Gamma_1^p(Q^2)$ are shown in fig. 4. The slope at $Q^2 = 0$ predicted by the GDH sum rule and the chiral perturbation theory calculation of Ji. et al. [13] are shown. The DIS slope at large Q^2 is also indicated, as well as calculation from ref. [14] and [15]. The expected sign reversal of Γ_1 is observed at $Q^2 = 0.3$ GeV^2.

The double spin asymmetry in exclusive channels has been evaluated for $\vec{p}(\vec{e}, e'p)\pi^0$, $\vec{p}(\vec{e}, e'\pi^+)n$, $\vec{n}(\vec{e}, e'\pi^-)p$. The Q^2 dependence of the asymmetry $(A_1 + \eta A_2)/(1 + \epsilon R)$ of the $\vec{p}(\vec{e}, e'\pi^+)n$ channel

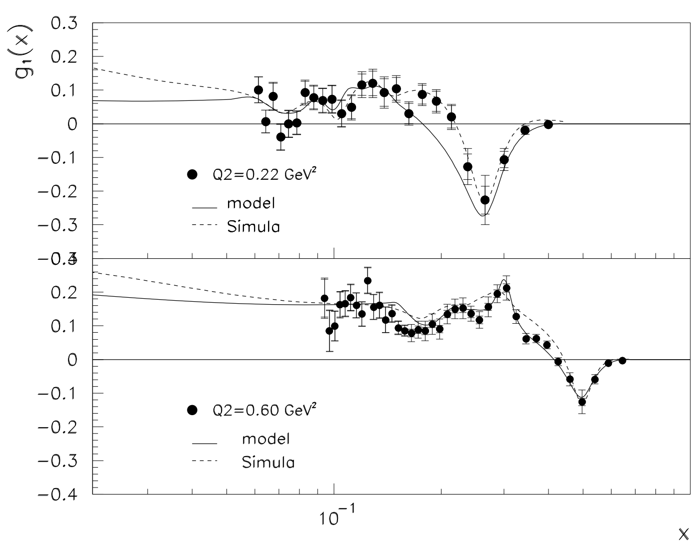

Figure 3: Spin structure funtion g_1 for the proton. The solid curve is a parameterization that was used for radiative corrections and to extrapolate at $x \to 0$ for the evaluation of Γ_1.

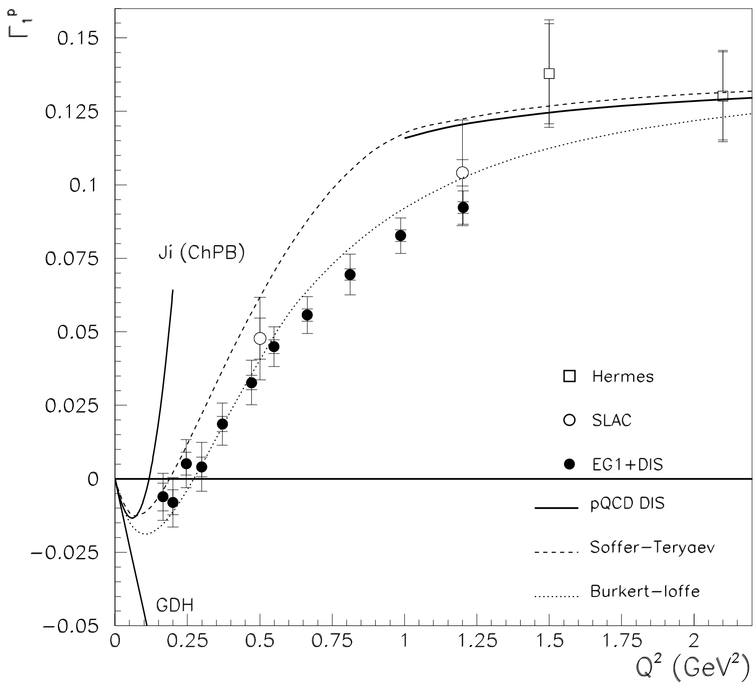

Figure 4: First moment of the structure function g_1. The CLAS data are shown in comparison with previous measurements from SLAC and HERMES.

is shown in fig. 5 for four W ranges, integrated over $\cos\theta_\pi^*$. The dotted curve represents the pure resonance contribution as predicted by the AO model [16], while the solid and dashed lines are, respectively, the AO and MAID2000 [17] calculations including non-resonant amplitudes. In the low W region, the asymmetry is strongly affected by non-resonant processes, leading to positive values in spite of the negative asymmetry expected for the $P_{33}(1232)$ state. For $W > 1.48$ GeV, the resonance contribution becomes dominant and the asymmetry is positive, indicating that the reaction is dominated by the helicity-1/2 amplitude.

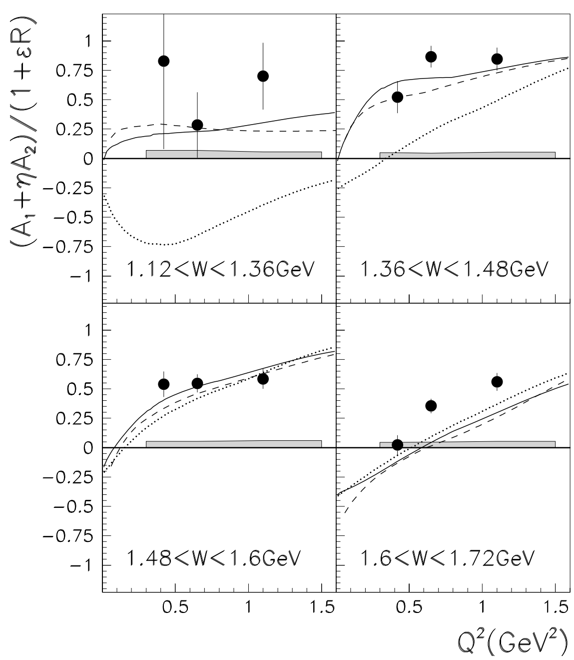

Figure 5: Q^2 dependence of the double spin asymmetry $(A_1 + \eta A_2)/(1 + \epsilon R)$. The error bars show the statistical error while the shaded bands represent the systematic uncertainty. The data are compared with the pure resonance contribution (dotted line) predicted by the AO model [16], with the MAID [17](dashed line) and AO (solid line) full calculations.

4 Conclusion and outlook

The CLAS data on the proton and the deuteron provide the first detailed look at the spin structure of the nucleon in the resonance region at low and moderate Q^2. The measured asymmetries show strong contribution from resonance excitation with rapidly changing helicity structure. The first moment of the structure function $g_1(x,Q^2)$ has been extracted, and shows a dramatic change with Q^2 with a sign change at $Q^2 = 0.3$ GeV^2. The double spin asymmetry in single pion electroproduction has been measured for the first time. The large and positive asymmetry indicates the dominance of helicity-1/2 transitions.

New data have been taken in 2000-2001 both on proton and deuteron targets, covering an energy range from 1.5 to 5.7 GeV. This data will allow to extend the measured Q^2 range from 0.05 to 2.5 GeV^2, with significant improvement in the measurement accuracy.

References

[1] EMC, J. Ashman *et al.*, Phys. Lett. **B206**, 364 (1988), and Nucl. Phys. **B328**, 1 (1989).

[2] J. D. Bjorken, Phys. Rev. **148**, 1467 (1966).

[3] S. B. Gerasimov, Sov. J. Nucl. Phys. **2**, 430 (1966).

[4] S. D. Drell and A. C. Hearn, Phys. Rev. Lett. **16**, 908 (1966).

[5] J. Ahrens *et al.*, Phys. Rev. Lett. **87**, 022003 (2001).

[6] G. Anton, in Few Body Systems, Springer, pg. 177 (1998), Proceedings of the Workshop on N* Physics and Non-perturbative QCD, eds. S. Simula, B. Saghai, N. Mukhopadhhyay, V. Burkert, Trento, Italy.

[7] K. Abe *et al.*, Phys. Rev. **D58**, 112003 (1998).

[8] W. Brooks, Nucl. Phys. **A663**, 1077c (2000).

[9] A. Abragam, *The principle of nuclear magnetism*, Oxford Clarendon Press (1961).

[10] R.G. Roberts, *The structure of the Proton*, Cambridge University Press, (1990).

[11] A. Bartl and W. Majerotto, Nucl. Phys. **B62**, 267 (1973).

[12] S. Simula *et al.*, hep-ph/0107036.

[13] X. D. Ji *et al.*, Phys. Lett. **B472**, 1 (2000).

[14] J. Soffer and O. V. Teryaev, Phys. Rev. Lett. **70**, 3372 (1993), Phys. Rev. **D51**, 25 (1995).

[15] V. D. Burkert and B. L. Ioffe, Phys. Lett. **B296**, 223 (1992); J. Exp. Theor. Phys. **78**, 619 (1994).

[16] V. Burkert and Z. Li, Phys. Rev. **D47**, 46 (1993).

[17] D. Drechsel *et al.*, Nucl. Phys **A645**, 145 (1999).

Photoproduction of vector mesons on the proton at large momentum transfer

Marco Battaglieri[a]
(for the CLAS collaboration)

[a]*Istituto Nazionale di Fisica Nucleare,*
Via Dodecaneso 33, 16146 Genova, Italy

(Received: 18 October 2001)

The differential cross section $d\sigma/dt$ for vector mesons photoproduction above the resonance region ($2.6 < W < 2.9$ GeV) was measured at Jefferson Laboratory up to a momentum transfer $-t = 5\,\mathrm{GeV}^2$. The measurement of the differential cross section down to 100 pb/GeV^2 as well as the full kinematic coverage, was possible for the first time thanks to the combination of the 100% duty cycle of CEBAF and the large acceptance of the CLAS detector. High momentum transfer selects small transverse size components of both photon and hadron. In this situation, hard processes (gluon and quark exchange) and other mechanisms like quark correlations may play a dominant role. It is expected that the combined measurement of ϕ and ρ meson over a wide range of t will allow the different contributions to be disentangled and better understood.

1 Introduction

Vector mesons (ρ, ω and ϕ) have the same quantum numbers as the photon ($J^{PC} = 1^{--}$) therefore, in certain conditions, a photon beam can be considered as a beam of $quark - antiquark$ pairs. The hadronic structure of the photon arises from fluctuation of the virtual photon in a ($q\bar{q}$) state of mass M_V during a formation time τ given by the indetermination principle of Heisenberg,

$$\tau = \frac{2\nu}{(Q^2 + M_V^2)} , \tag{1}$$

where Q^2 is the squared mass and ν is the energy of the virtual photon.

In photoproduction experiments ($Q^2 = 0$), if the energy is high enough ($\nu > 2\,\mathrm{GeV}$), $\tau \sim 1.5$ fm is comparable with the target diameter and therefore the interaction is similar to the interaction of hadrons. In this condition, we can distinguish two well defined dynamical regimes depending on the momentum transfer $-t$. The low $-t$ ($-t < 1\,\mathrm{GeV}^2$) shows a diffractive behavior interpreted in the frame of the Vector Meson Dominance (VMD) model [1] as the elastic scattering of vector mesons off the proton target. In a more recent approach, this process is also described by the t-channel exchange of the Pomeron and some other Regge trajectories (π, σ-meson, $f_2(1270)$, etc.) [2]. Fig. 1 shows the main reaction mechanisms and the good agreement in a wide W range for the total cross section dominated by the low $-t$ dynamics. At high $-t$ ($-t > 1\,\mathrm{GeV}^2$), where the cross section is sensitive to the microscopic details of the interaction, the underlying physics can be described using parton degrees of freedom. In a QCD-inspired framework, the small impact parameter ($\approx 1/\sqrt{-t}$) prevents the constituent gluons (quarks) of the exchange from interacting and forming a Pomeron (Reggeon). Within certain models [3,4] this means that the constituents can be resolved into two-gluon (two-quark) structures (Fig. 2-a).

Moreover, small transverse sizes select configurations where each gluon couples to different quarks both in the vector meson and the nucleon, giving access to the correlation function in the proton (Fig. 2-b) [2]. Due to the dominant $s\bar{s}$ component of the ϕ, and to the extent that the strangeness of the proton is small, the ϕ photoproduction at large $-t$ is a good tool to resolve the Pomeron into its simplest 2-gluon component. In the ρ case, its light quark composition also allows valence quarks to be exchanged between the baryon and the meson states (Fig. 2-c) [2]. The

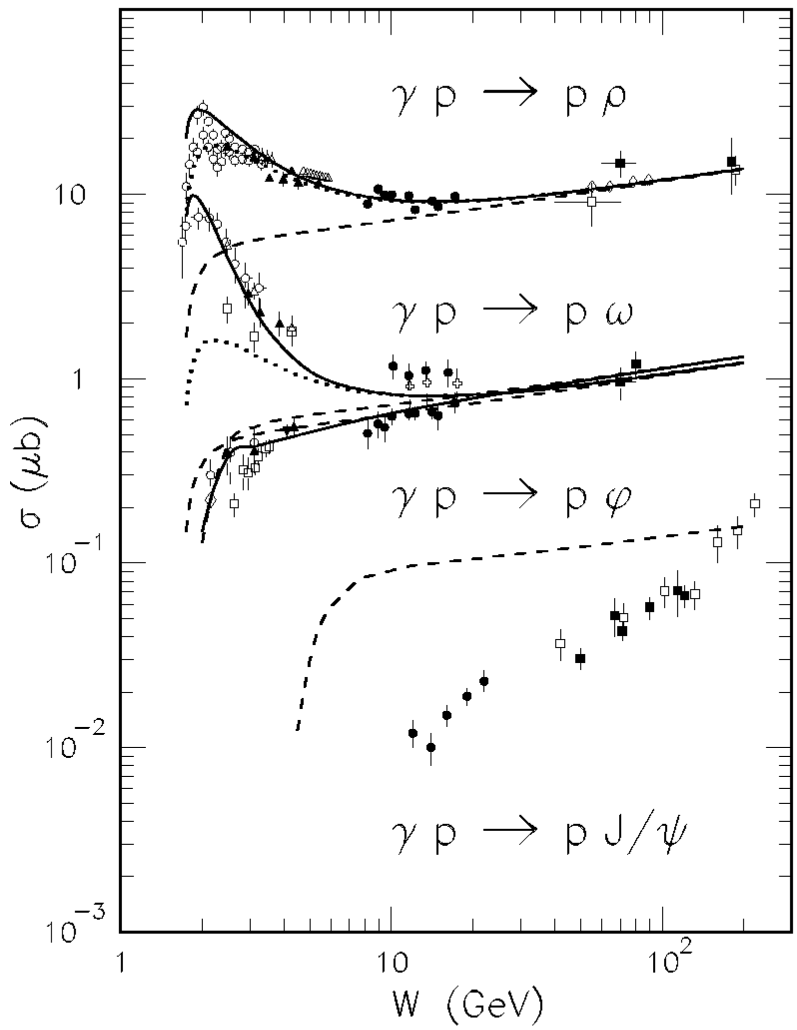

Figure 1: Total cross section of vector meson photoproduction. Dashed lines: Pomeron exchange. Dotted lines include also f_2 meson exchange. Full lines include in addition π and σ exchange.

comparison between the two channels puts stringent constraints on our understanding of reaction mechanisms.

Vector mesons photoproduction at Jefferson Laboratory above the resonance region ($3 < \nu < 4\,\mathrm{GeV}$), covering the whole momentum transfer (up to $-t = 5\,\mathrm{GeV}^2$), have been partially completed [5,6], giving the first physical outputs in this dynamical regime.

2 Experimental setup

The data were obtained with the CEBAF Large Acceptance Spectrometer (CLAS) in Hall B of the Thomas Jefferson National Accelerator Facility. CLAS is a nearly 4π spectrometer based on a toroidal magnetic field generated by 6 superconducting coils. Three drift chambers regions allowed tracking of charged particles; time of flight scintillators were used for hadron identification. Momentum resolution of the electron and hadron is of the order of 1% while detector efficiencies, referred to the full solid angle, range from 50% for electron to about 70% for protons and pions. The experiment was performed using a bremsstrahlung photon beam, tagged in the E_γ range 3–4 GeV. The high intensity flux ($6.10^6\,\gamma/s$) was measured with a pair spectrometer calibrated using a total absorption counter in dedicated low intensity runs. The coincidences between the photon tagger and the CLAS detector (TOFs) triggered the recording of hadronic interactions.

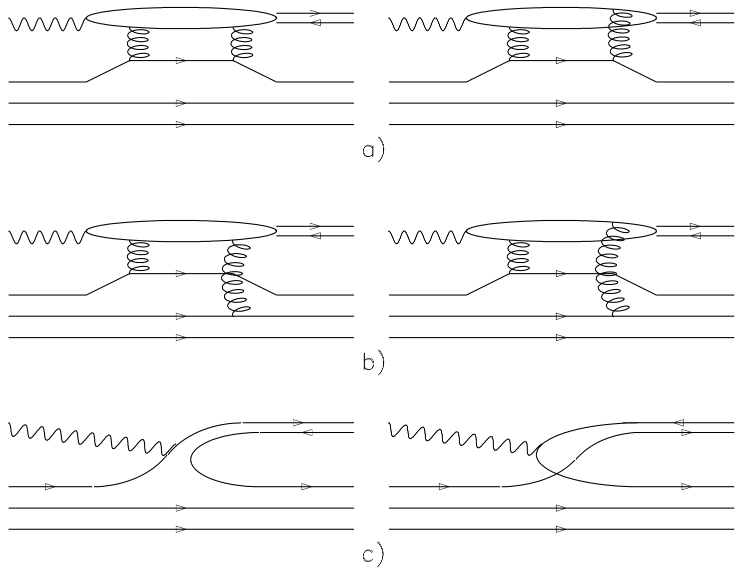

Figure 2: The Feynman diagrams corresponding to a) two-gluon exchange from a single quark, b) two-gluon exchange taking into account quark correlations in the nucleon, and c) quark exchange.

3 Data analysis

The reaction $\gamma p \to p\phi$ has been measured via proton and k^+ detection and missing (k^-) mass technique. Due to the good CLAS resolution, a clear peak in the k^- mass region is visible and allows the identification the two kaons final state. In each t bin of the invariant (k^+k^-) mass, the non resonant background under the ϕ peak was subtracted in different ways (fitting the shape of the data and using a simple model). In this approach an evaluation of the systematic error related to the ϕ separation was obtained. The CLAS efficiency and its geometrical acceptance was determined using a realistic event generator (improved using the measured distribution and iterating the procedure) and a GEANT-based description of the detector. The small width of the ϕ allowed to bin the efficiency as a function of the a quasi-two-body reaction variables without introducing any model dependence.

The reaction $\gamma p \to p\rho^0$ with $\rho^0 \to \pi^+\pi^-$ has been measured detecting all possible final configurations containing at least two hadrons and using the missing mass technique when necessary. The large width of the rho meson ($\sim$ 150 MeV) required a carefully evaluation of the detector efficiency as a function of the six kinematical variables (corresponding to the three hadrons in the final state) to avoid any model dependency. For each (E_γ,Q^2,$-t$) bin, a simultaneous fit of both the invariant mass $(p\pi^+)$ and $(\pi^+\pi^-)$ was performed using an extension of the model of ref. [7] in order to separate the ρ production from the other channels ($\Delta^0\pi^+$,$\Delta^{++}\pi^-$,phase space, $f_2(1270)$) contributing to the $p\pi^+\pi^-$ final state.

The reaction $\gamma p \to p\omega$ was detected via the main decay channel $\omega \to \pi^+\pi^-\pi^0$ using a combination of the procedures described above: missing mass technique, sideband subtraction, GEANT-based efficiency evaluation, etc. In this analysis a great benefit was represented by the sizable production cross section ($\sim 5\mu$barn) and the good peak-background ratio (the ω mass width is $\sim$ 8 MeV). Since the analysis of this channel is still in progress, no results will be presented for this reaction.

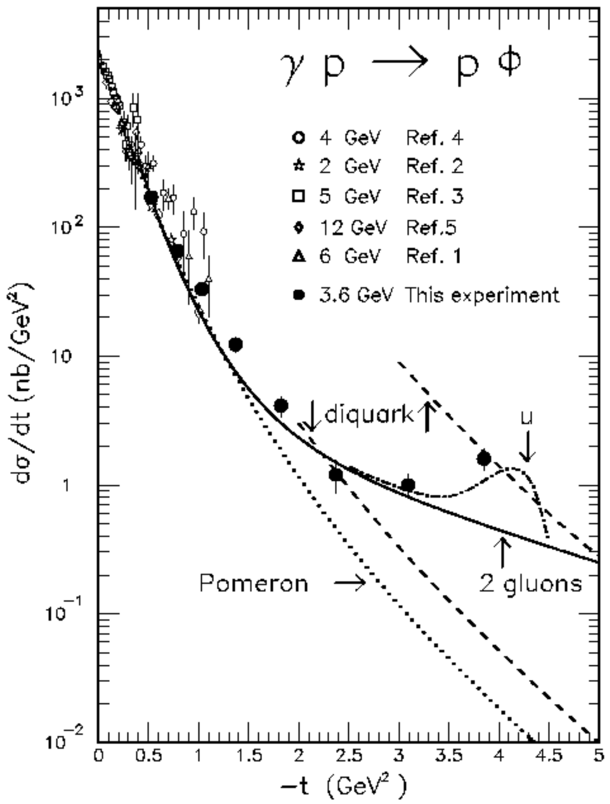

Figure 3: The differential cross section of the reaction $\gamma p \to p\phi$. See text for explanation.

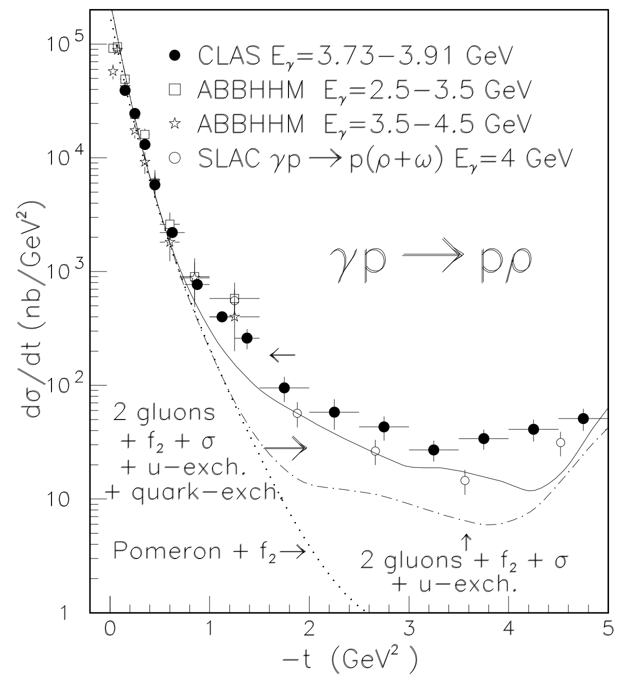

Figure 4: The differential cross section of the reaction $\gamma p \to p\rho^0$. See text for explanation.

4 Results

The measured $d\sigma/dt$ for elastic ϕ photoproduction on the proton [5], up to $-t = 4\,\mathrm{GeV}^2$ is shown in fig. 3. At low momentum transfer the two-gluon exchange model of J.M. Laget and R. Mendez-Galain [2,4] (solid line) coincides with the well known diffractive behavior (dotted line). For $-t > 2\,\mathrm{GeV}^2$ the data rule out the diffractive Pomeron exchange and strongly favor its two-gluon realization. In the calculation the gluons can couple to any quarks in the baryon (see fig. 2-a,b) and quark correlations in the proton are taken into account assuming the simplest form of its wave function with three valence quarks equally sharing the proton longitudinal momentum. Close to the kinematic limit t_{max}, the good agreement with data is obtained adding the baryon exchange in the u-channel. In the same plot two perturbative QCD calculations are also shown (dashed lines). Both of them are not able to describe the data demonstrating that the asymptotic regime is not yet reached.

The obtained $d\sigma/dt$ for elastic ρ photoproduction on the proton [6], up to $-t = 5\,\mathrm{GeV}^2$ has been plotted in fig. 4. The comparison with a model similar to ref. [2] is also shown (dot dashed line). The parameters of the two-gluon exchange mechanism are fixed from the analysis of the ϕ channel. The low momentum transfer region is well reproduced when the two Regge trajectories (f_2 and σ) are included while the model underestimates the large $-t$ region, indicating that other reaction mechanisms are needed. The good agreement with data is obtained (solid line) when quark-exchange processes (see fig. 2-c) are added. As explained in Refs. [8] these hard-scattering mechanisms can be incorporated in an effective way by using the so called "saturated" trajectory. Regge trajectories are usually linear in t but are expected to "saturate", i.e. be t-independent, at

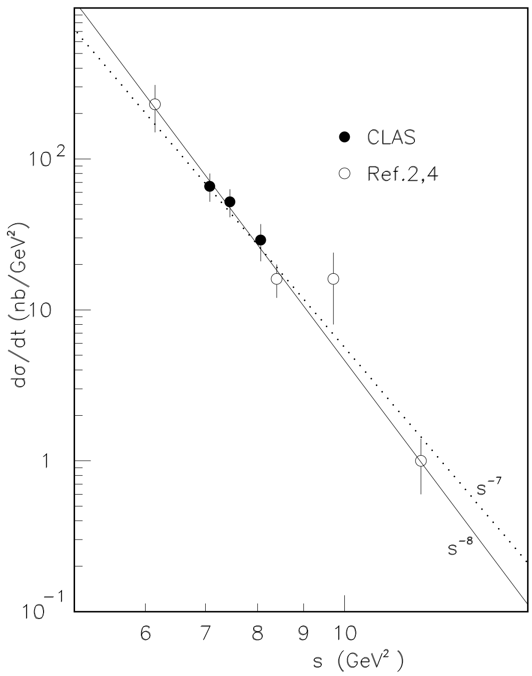

Figure 5: The $\theta_{cm} = 90°$ cross section as function of the CMS energy of the reaction $\gamma p \to p\rho^0$.

large momentum transfer. The trajectory has been chosen as $\alpha(t) = -1$ when $-t > 3\,\mathrm{GeV}^2$ [2] to be compatible with quark counting rules [9]. The solid line in fig. 4 shows the full calculation, including such saturating trajectory. Quark exchange increases the cross section at large $-t$ by a factor two.

The ρ^0 cross section at $\theta_{cm} = 90°$ is shown in Fig. 5 where we plot our data for three W bins together with the existing data from SLAC. The power law s^{-C} fit to $d\sigma/dt$ at 90° in the center of mass is performed using the old SLAC data and the new CLAS points. The fit yields $C = 7.9 \pm 0.3$ ($\chi^2 = 0.6$) showing a good agreement with s^{-8} behavior. The quark exchange diagrams of Fig. 2-c-left (point-like interaction) and 2-c-right (hadronic component of the photon) have a s^{-7} and s^{-8} power-law behavior respectively, both by dimensional counting [9] and by recent models [10]. Note that also the saturated σ Regge trajectory behaves like s^{-8}. Like the differential cross section at fixed energy, the s dependence suggests the presence of quark interchange hard mechanisms in addition to the two-gluon exchange process.

5 Conclusion

Vector meson photoproduction at large momentum transfer is a unique tool to study and understand the quark-gluon structure of hadronic matter. Precise measurements and full kinematic coverage are necessary in order to disentangle the different mechanisms competing at intermediate energies. The Hall B of Jefferson Lab completed a set of dedicated experiments with photons tagged in the 4–5 GeV range covering the interested $-t$ region. Data were collected during the 1998 and the 1999 data taking and first physics outputs are coming up. Different channels were analysed in the same framework simultaneously. At large momentum transfer the ϕ data support a model where the Pomeron is resolved into its simplest component, two gluons, which may couple to any quark in the proton and in the vector meson. The ρ data indicate that other processes, such as quark interchange, are important to fully describe this channel. In conclusion, a consistent picture is emerging from ϕ and ρ photoproduction showing that this kinematical region can be described as a *non perturbative partonic regime* where microscopic degrees of freedom (gluons and quarks) mix together with lower energy hadrons picture (constituent quarks, dressed gluons).

References

[1] T.H. Bauer *et al.*, Rev. Mod. Phys. **50**, 261 (1978).
[2] J.M. Laget, Phys. Lett. **489B**, 313 (2000).
[3] A. Donnachie and P.V. Landshoff, Phys. Lett. **B185**, 403 (1987).
[4] J.M. Laget and R. Mendez-Galain, Nucl. Phys. **A581**, 397 (1995).
[5] E. Anciant *et al.*, Phys. Rev. Lett. **85**, 4682 (2000).
[6] M. Battaglieri *et al.*, Phys. Rev. Lett. **87**, 172002 (2001); M. Battaglieri, Nucl. Phys. **A680**, 286c (2001).
[7] M. Ripani *et al.*, Nucl. Phys. **A672**, 220 (2000).
[8] M. Guidal, J.M. Laget, and M. Vanderhaeghen, Nucl. Phys. **A627**, 645 (1997).
[9] S.J. Brodsky and G.R. Farrar, Phys. Rev. Lett. **31**, 1153 (1973).
[10] H.W Huang and P. Kroll, Eur. Phys. J. **C17**, 423 (2000).

Medium modifications of hadrons studied with photonuclear reactions

S. Schadmand, *for the TAPS and A2 collaborations*

II. Physikalisches Institut, Heinrich-Buff-Ring 16, D-35392 Giessen, Germany

(Received: 31 October 2001)

The experiments with the electromagnetic calorimeter TAPS using tagged photon beams focus on meson production from the free proton and from nucleons bound in nuclei. Results from the recent TAPS campaign at the tagged photon facility MAMI (Mainz) on double pion photoproduction are presented. The observations using a proton target provide direct evidence for a ρ strength in the decay of the D_{13} resonance. Furthermore, double pion production from nuclei is used as a tool to study in-medium modifications of the $\pi\pi$ interaction which might indicate a partial restoration of chiral symmetry.

1 Introduction

The TAPS research program with photon beams investigates the structure of the nucleon by studying the photoexcitation of nucleon resonances and their subsequent meson decay. The studies are performed on the free proton as well as on nucleons bound in nuclei.

The nucleon resonances accessible with MAMI beam energies cover the resonance mass region of M(N*) = 1400–1600 MeV, called the second resonance region. In single-pion production, the identification of the individual resonances is hindered by their large widths and strong overlap with each other. A separation of the resonances in the second resonance region is possible via the characteristic decay into two π and into η mesons. The left panel of figure 1 shows the decomposition of the total photoabsorption cross section on the proton into single and double meson production. A comparison of photoabsorption cross sections on the proton and on nuclei in the right panel figure 1 shows strong differences in the second resonance region [1]. The resonance structure is prominent in photoabsorption on the free nucleon and appears strongly suppressed for photoabsorption on nuclei. In this energy region, the $D_{13}(1520)$ resonance is dominantly excited in photoproduction and an in-medium broadening of this resonance could be the cause of the observations [2, 3]. The broadening would arise from coupling the resonance to the $N\rho$ final state since the ρ meson itself is appreciably broadened in the nuclear medium [4]. This scenario is based on a substantial ρ-decay

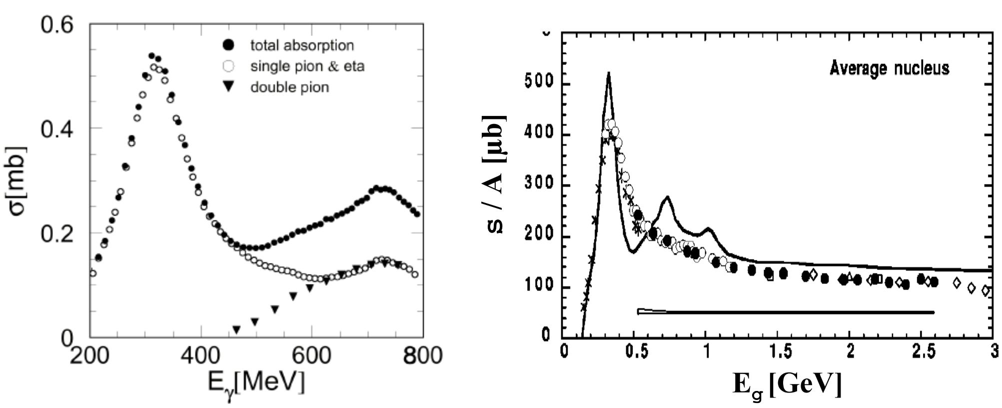

Figure 1: Left: Decomposition of the total photoabsorption cross section on the proton into single and double meson production reactions. Right: Comparison of photoabsorption cross sections on the proton (solid line) and nuclei, taken from [1].

width of the D_{13} resonance which should be observable on the free proton. The ρ-decay width of the free D_{13} resonance is quoted by the Particle Data Group [5] and Manley [6]. However, the parameters were extracted from coupled channel analyses of pion induced reactions and the decay channel was not directly observed. Indications for ρ strength in photoabsorption experiments have been deduced by the DAPHNE group in the $\gamma n \rightarrow \pi^- \pi^\circ p$ reaction on a deuteron target [7] by comparison to model calculations of Ochi *et al.* [8]. In the experimental analysis, effects stemming from the fact that the neutron is bound in the deuteron target had to be accounted for. In section 3, the TAPS results on the first direct observation of the ρ strength from the reaction $\gamma + p$ [9] are reported.

The study of double pion production is extended to nucleons embedded in nuclei in order to investigate in-medium modifications of the $\pi\pi$ interaction which might indicate a partial restoration of chiral symmetry [10–12]. The results of pion-induced experiments (π^+,$\pi^+\pi^-$) [13] and (π^-,$\pi^\circ\pi^\circ$) [14] could be interpreted in that sense. Photon-induced reactions can reach higher nuclear densities and should be more sensitive to in-medium effects. In section 4, the TAPS study of the reactions $\gamma + A \rightarrow \pi^\circ\pi^\circ + X$ with $A =$ p, D, C and Pb is discussed.

2 Experimental setup

The experiments were performed with the TAPS detector [15] in combination with the Glasgow tagged photon beam facility [16] at the MAMI accelerator in Mainz [17]. Six detector blocks consisting of 64 BaF_2-plastic telescopes, respectively, and a forward wall of 120 telescopes were arranged in a plane around the scattering chamber. The detection system provides time-of-flight, energy, and pulse shape information of the detected particles. In addition, neutral/charged particle identification can be derived from thin plastic scintillators in front of the BaF_2 crystals. In the experimental campaign, quasimonochromatic photons up to 850 MeV were employed. $\pi^\circ\pi^\circ$ and $\pi^+\pi^\circ$ data were simultaneously acquired using the same detection system and similar analysis. π° mesons were identified via their 2 photon decay using an invariant mass analysis and charged pions via time-of-flight.

3 Double pion photoproduction on the proton

Figure 2 shows the total cross section of the reaction $\gamma\, p \rightarrow \pi^+\pi^\circ\, n$ and $\gamma\, p \rightarrow \pi^\circ\pi^\circ\, p$ as a function of the incident photon energy. The TAPS results (filled and open circles) are compared to theoretical

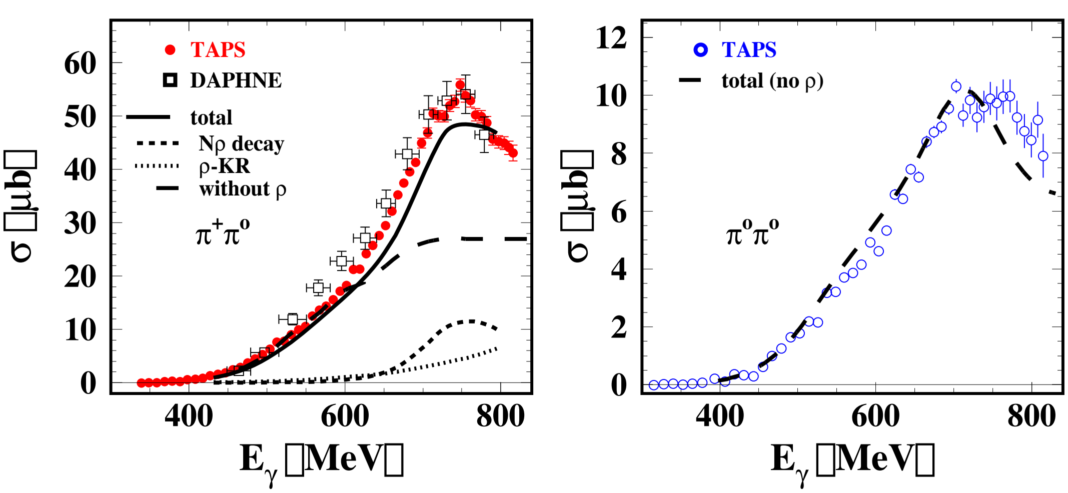

Figure 2: $\pi^+\pi^\circ$ (left) and $\pi^\circ\pi^\circ$ (right) total photoproduction cross section from the proton as a function of incident photon energy. (See text).

predictions of [18] (solid curve). In both panels of figure 2, dashed curves respresent the theoretical result without a ρ contribution [19]. The TAPS result is consistent with a previous measurement performed with the DAPHNE detector (open squares) [20] confirming the resonance structure at the $D_{13}(1520)$ resonance (E_γ = 760 MeV). The structure stems from the $D_{13} \to N\rho$-decay interfering with the ρ-Kroll-Rudermann contribution [18], both indicated separately (short-dashed and dotted curves). The statistics of the TAPS results allow to directly compare $\pi\pi$ invariant mass distributions from the reactions $\gamma p \to \pi^+\pi^\circ n$ and $\gamma p \to \pi^\circ\pi^\circ p$ [9]. The $\rho \to \pi\pi$ contribution can be observed in the $\pi^+\pi^\circ$ invariant mass distributions but the ρ-meson decay into $\pi^\circ\pi^\circ$ is forbidden due to isospin conservation in the strong interaction. Thus, deviations of $\pi^+\pi^\circ$ from $\pi^\circ\pi^\circ$ invariant mass distributions are regarded as a measure of the ρ contribution. Figure 3 shows $\pi\pi$ invariant mass distributions for the $\pi^\circ\pi^\circ$ and $\pi^+\pi^\circ$ reactions on the proton. At low excitation energies both experimental distributions agree within the error bars with phase space. It should be noted that $\pi\pi$ production proceeds to a large extent through the sequential decay of the $D_{13}(1520)$ ($E_\gamma = 760$ MeV) via the $\Delta(1232)$ resonance [21]. $N\pi$ invariant mass distributions from the present data set indicate that a sequential decay is also important in the $\pi^+\pi^\circ$ channel [9]. This is in accordance with the assumption of refs. [19, 22]. In the second resonance region the $\pi^+\pi^\circ$ system

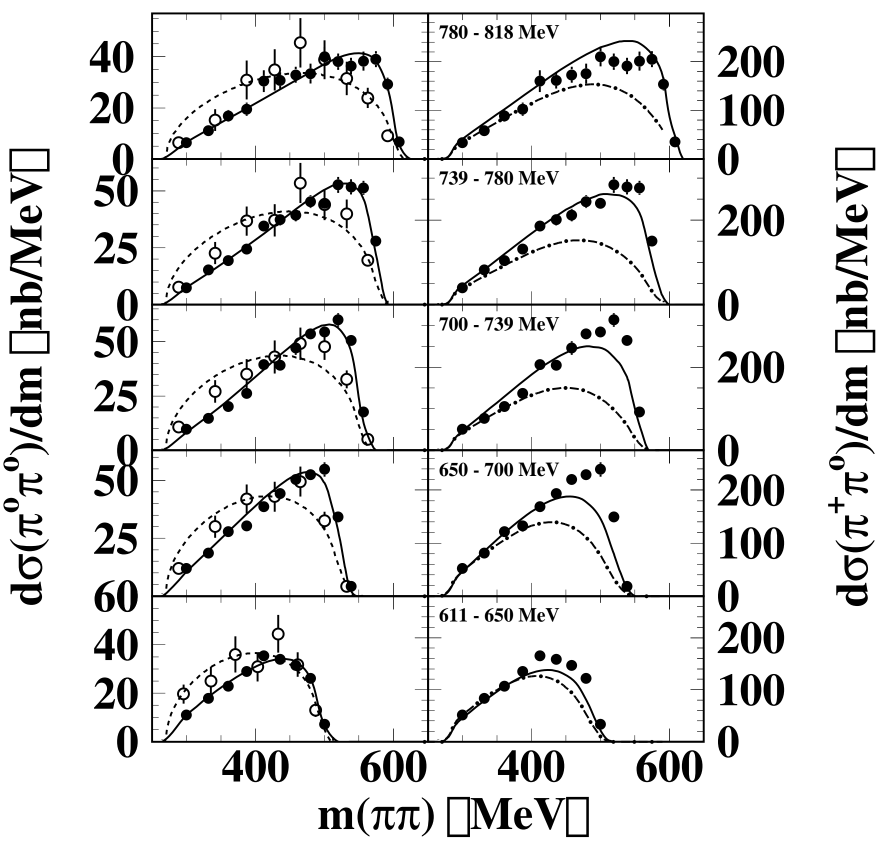

Figure 3: Invariant mass distributions of pion pairs from the proton for five bins of incident photon energy. Left column: Comparison of the shape of the distributions for $\gamma p \to \pi^+\pi^\circ n$ (solid circles) and $\gamma p \to \pi^\circ\pi^\circ p$ (open circles). Dashed curve: phase space expectation, full curve: fit to the $\pi^+\pi^\circ$ data [9]. The vertical scale corresponds to the $\pi^\circ\pi^\circ$ data, the $\pi^+\pi^\circ$ data and the curves are normalized to the same area. Right column: Comparison of the $\pi^+\pi^\circ$ distributions to the calculations with (solid line) [18] and without (dash-dotted line) [19] ρ contributions.

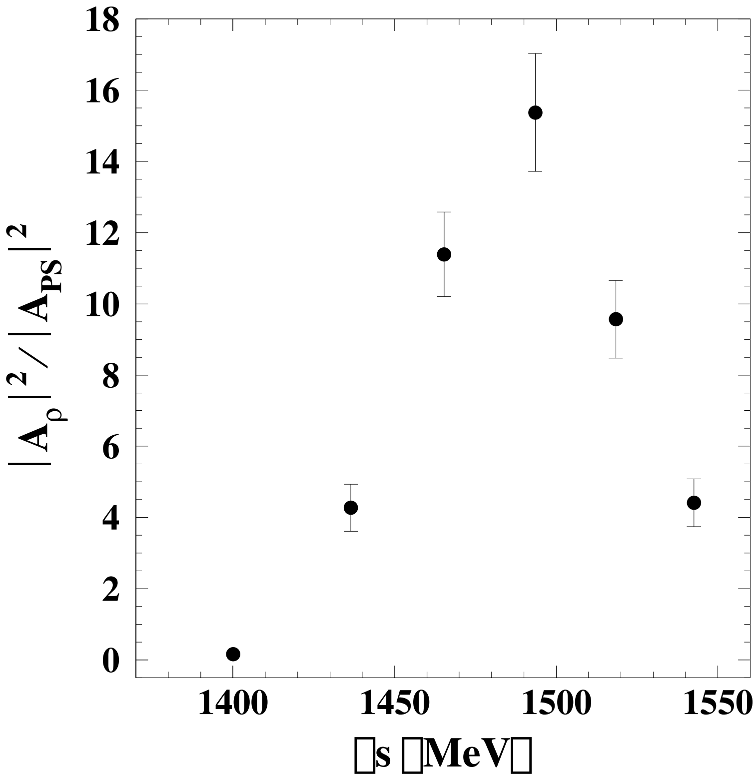

Figure 4: Ratio of squared ρ channel and phase space amplitudes deduced from the fit to the $\pi^+\pi^\circ$ data from the proton as in figure 3.

shows a pronounced shift to higher masses. As pointed out above, the decay of a ρ° meson cannot decay into $2\pi^\circ$. The deviation towards higher invariant masses in the charged channel is attributed to an intermediate ρ^+ meson. Here, the low energy tail of the broad ρ meson of mass 770 MeV and full width 150 MeV is populated. The right hand side of figure 3 shows a comparison of the mass distributions to the calculations with and without the inclusion of the $D_{13} \to N\rho$- and ρ-Kroll-Rudermann decays, using the PDG-values for masses and widths [5]. The deviations are assigned to a ρ branch of the $D_{13}(1520)$ resonance since this state is predominantly excited in the second resonance region and the $\pi^+\pi^\circ$ cross section in figure 2 shows a broad peak at the $D_{13}(1520)$ resonance ($E_\gamma = 760$ MeV, $\Gamma_{D_{13}} = 120$ MeV).

This conclusion is supported by a simplified fit to the data considering a phase space contribution (representing sequential decays in approximation) and a ρ contribution as in $\gamma p \to \rho^+ n \to \pi^+\pi^\circ n$. The fit is explained in more detail in [9]. The ratio of squared ρ channel and phase space amplitudes deduced from the fit to the $\pi^+\pi^\circ$ data is shown in figure 4. The ratio, plotted as a function of the center of mass energy $\sqrt{s}$, is a measure of ρ contributions and exhibits a resonance structure near the mass pole of the $D_{13}(1520)$ resonance. The result that the D_{13} resonance has a substantial ρ-decay branch is confirmed by the rigorous theoretical treatment of double pion photoproduction [18] which has been motivated by this experiment. Here, the cross section is reproduced for a branching ratio of 20% for the $D_{13} \to N\rho$ channel.

4 In-medium double pion photoproduction

The σ meson is assumed to be an isoscalar-scalar $\pi\pi$ state and is quoted to have a mass of 500–1200 MeV in the vacuum [5]. This meson is considered to be a tool to investigate chiral symmetry restoration as it has the same quantum numbers as the QCD vacuum. The σ meson ($J^P = 0^+$) and the π meson ($J^P = 0^-$) are chiral partners having equal spin and opposite parity but different vacuum masses, in accordance with spontaneous chiral symmetry breaking. Partial restoration of chiral symmetry is expected to be progressing with increasing baryon density or temperature. In this case, this would lead to a dropping of the σ mass, reaching the π mass in the extreme case of full chiral symmetry restoration.

The dropping of the σ mass should be observable via its decay into pion pairs. Here, the $\pi\pi$ invariant mass distributions should exhibit a shift towards the two-pion threshold with increasing baryon density [10–12]. This signature of partial chiral symmetry restoration is expected to set in already at normal nuclear density. The π meson, being a Goldstone boson, does not experience such drastic mass changes. However, the observed pions may experience final state interactions and appropriate care has to be taken in the interpretation of the results.

In the TAPS photoproduction experiments at MAMI the reactions $\gamma + A \to \pi^\circ\pi^\circ + X$ with $A =$ p, D, C and Pb were studied. The incident photon energy was chosen to be 400 MeV in order to keep the sum of the pion kinetic energies below 100 MeV, thereby minimizing pion final state interactions. From the proton to the carbon and to the lead target, the resulting $\pi^\circ\pi^\circ$ mass distributions exhibit a gradual mass shift towards small invariant masses, as expected from theoretical predictions of chiral symmetry restoration. For the carbon target, good agreement is found with the $\pi^\circ\pi^\circ$ data measured with the crystal ball using pion beams. The results are compared to $\pi^+\pi^\circ$ distributions in order to judge the influence of final state interactions. The $\pi^+\pi^\circ$ production channel, carrying isospin $I = 1$, cannot stem from the σ meson decay but the charged pions undergo final state interactions similar to neutral pions. The $\pi^+\pi^\circ$ distributions do not exhibit the same mass shift. It can be concluded that final state interactions of the produced pions play a minor role at these energies. The observed shift in the $\pi^+\pi^\circ$ mass distributions is consistent with the prediction of partial chiral symmetry resoration at normal nuclear density. This result confirms earlier measurements by the CHAOS collaboration with pion beams [13] which were hampered in their quantitative interpretation by acceptance issues.

5 Summary

The $\pi\pi$ photoproduction from the proton up to 820 MeV excitation energy has been measured. The $\pi^+\pi^\circ$ system has been compared to simultaneously measured $\pi^\circ\pi^\circ$ data.

For the proton the $\pi^+\pi^\circ$ invariant mass distributions are shifted towards higher masses. This behavior provides first experimental evidence for a contribution of an intermediate ρ^+ meson with a subsequent decay into two pions in the reaction $\gamma\, p \to \rho^+ n \to \pi^+\pi^\circ\, n$. Because of the resonant behavior this ρ strength is assigned to the decay of the $D_{13}(1520)$ resonance as also found in recent calculations by J.C. Nacher *et al.* [18]. The ρ-decay branch of the $D_{13}(1520)$ is of great interest for the understanding of medium modifications in nuclear reactions. A strong broadening of the ρ spectral function should have an impact on the decaying resonance and might play a role in the depletion of the nuclear photoabsorption cross section in the second resonance region.

The TAPS results on double pion photoproduction from nuclei are used as a tool to study a possible signature of partial chiral symmetry restoration. In contrast to previous pion-induced measurements, photon-induced reactions avoid absorption of the incident probe on the nuclear surface. The mass distributions show a shift in the $\pi^\circ\pi^\circ$ invariant mass distributions towards small invariant masses which is not observed in the $\pi^+\pi^\circ$ channel. The shift increases gradually as a function of target mass number. It is consistent with theoretical expectations of partial chiral symmetry restoration and the corresponding signature of a dropping σ mass.

Acknowledgments: This work was supported by Deutsche Forschungsgemeinschaft (SFB 201) and the U.K. Engineering and Physical Sciences Research Council.

References

[1] V. Muccifora *et al.*, Phys. Rev. C **60** (1999) 064616 and references therein.

[2] M. Effenberger *et al.*, Phys. Rev. **C60** (1999) 044614.

[3] U. Mosel *et al.*, Prog. Part. Nucl. Phys. **42** (1999) 163.

[4] F. Klingl *et al.*, Nucl. Phys. **A624** (1997) 527.

[5] C. Caso *et al.*, (Review of Particle Physics) Eur. Phys. J. **C3** (1998).

[6] D. M. Manley and E. M. Saleski, Phys. Rev. D **45** (1992) 4002.

[7] A. Zabrodin *et al.*, Phys. Rev. **C60** (1999) 055201.

[8] K. Ochi *et al.*, Phys. Rev. **C56** (1997) 1472; K. Ochi *et al.*, nucl-th/9711031.

[9] W. Langgärtner *et al.*, Phys. Rev. Lett. **87** (2001) 052001.

[10] T. Hatsuda *et al.*, Phys. Rev. Lett. 82 (1999) 2840.

[11] P. Schuck *et al.*, nucl-th/0002031.

[12] R. Rapp et al., Phys. Rev. C 59 (1999) 1237.

[13] F. Bonutti *et al.*, Phys. Rev. Lett. 77 (1996) 603.

[14] A. Starostin *et al.*, Phys. Rev. Lett. 85 (2000) 5539.

[15] R. Novotny, IEEE Trans. Nucl. Science **38** (1991) 379.

[16] I. Anthony *et al.*, Nucl. Inst. Meth. **A301** (1991) 230.

[17] Th. Walcher, Prog. Part. Nucl. Phys. **24** (1990) 189.

[18] J.C. Nacher *et al.*, nucl-th/0012065 and private communication.

[19] J.A. Gómez Tejedor, E. Oset, Nucl. Phys. **A600** (1996) 413.

[20] A. Braghieri *et al.*, Phys. Lett. **B363** (1995) 46.

[21] M. Wolf *et al.*, Eur. Phys. J. **A9** (2000) 5.

[22] L.Y. Murphy, J.M. Laget, DAPNIA/SPhN **96-10** (1996).

Meson and hyperon production with polarised protons of about 3 GeV

M. Maggiora[a], for the DISTO Collaboration*

[a]*Dipartimento di Fisica "A. Avogadro" and INFN, Torino, Italy*

(Received: 31 October 2001)

Recent data for K^- and η' production in proton-proton scattering at 3.67 GeV/c are reported together with preliminary results for the ρ production. The D_{yy} dependence on x_F for exclusive Λ production at 3.67 (preliminary) and 2.94 GeV/c is compared with existing inclusive data and with model predictions; A_y data are also reported.

1 Introduction

The DISTO spectrometer, described in details elsewhere [1], was set at the Laboratoire Saturne in Saclay. A polarised proton beam with a kinetic energy up to 2.9 GeV was hitting an unpolarised liquid hydrogen target, put in the center of a magnetic field.

All charged particles from several different production channels were detected simultaneously with a large coverage of the phase space, because of the wide angular and momentum acceptance of the spectrometer. As an example, pseudoscalar (η, η') and vector mesons (ω, ϕ and ρ) production in proton-proton scattering have been studied in parallel with the investigation of Λ and Σ^0 production.

2 Meson production

All the results reported herewith concern data collected at 3.67 GeV/c and meson production channels characterised by final states with four charged particles: $\vec{p}p \rightarrow ppK^-K^+$, $\vec{p}p \rightarrow pp\eta'$ ($\eta' \rightarrow \pi^+\pi^-\eta$) and $\vec{p}p \rightarrow pp\rho$ ($\rho \rightarrow \pi^+\pi^-$). Total cross sections and angular distributions have been determined for these channels.

The absolute normalisations were obtained from the total cross section of η production ($\vec{p}p \rightarrow pp\eta$), simultaneously measured in order to reduce the large systematic uncertainties associated with the absolute calibrations of both the beam intensity and the trigger efficiency. The value assumed for the η cross section ($\sigma_{pp\rightarrow pp\eta}(\sqrt{s} - \sqrt{s_0} = 0.554\ GeV) = (135 \pm 35)\ \mu b$) has been obtained by interpolation of the data available from the literature [2]. The acceptance corrections for the apparatus were obtained through Montecarlo simulations.

2.1 *The K^- meson production*

To investigate the K^- production we ask for events in which the proton-proton missing mass M^{pp}_{miss} is equal to the kaon-kaon invariant mass M^{KK}_{inv}. The peak in Fig. 1.a correspond to the signal, where $|M^{KK}_{inv} - M^{pp}_{miss}| \simeq 0$. It is superimposed on a small background resulting from imperfect $\pi - K$ separation in a fraction of the events of the type $pp \rightarrow pK^+\Lambda \rightarrow ppK^+\pi^-$ or $pp \rightarrow pp\pi^+\pi^-X$.

We present in Fig. 1.b the acceptance corrected cross sections. The dashed curve is an estimate of the non-resonant contribution; the global fit (solid line) is the sum of the non-resonant and the ϕ contribution. These two separate terms lead to the cross sections for the two contributions:

*F. Balestra, Y. Bedfer, R. Bertini, L.C. Bland, A. Brenschede, F. Brochard, M.P. Bussa, Seonho Choi, M. Colantoni, M. Debowski, M. Dzemidzic, J.-Cl. Faivre, I.V. Falomkin, L. Fava, A. Ferrero, L. Ferrero, J. Foryciarz, V. Frolov, R. Garfagnini, D. Gill, A. Grasso, E. Grosse, S. Heinz, V.V. Ivanov, W.W. Jacobs, W. Kühn, A. Maggiora, M. Maggiora, A. Manara, D. Panzieri, H.-W. Pfaff, G. Piragino, G.B. Pontecorvo, A. Popov, J. Ritman, P. Salabura, V. Tchalyshev, F. Tosello, S.E. Vigdor, and G. Zosi.

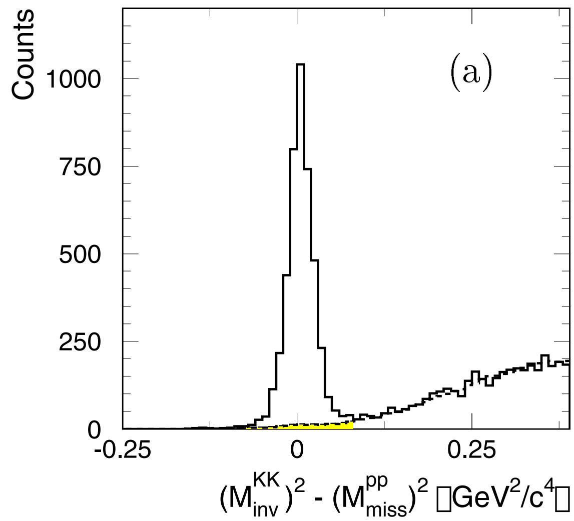

Figure 1: (a) K^- production shows up as a peak at $|M_{inv}^{KK} - M_{miss}^{pp}| \simeq 0$; background (dashed line) is estimated by scaling the inclusive distribution without any requirement for kaon identification. (b) Solid line accounts for the resonant ($\phi \to K^+K^-$) and for the non-resonant (dashed line) contributions to the acceptance corrected M_{inv}^{KK} distribution. (c) Our result is compared with data from the literature [3] and with calculations from Sibirtsev [4].

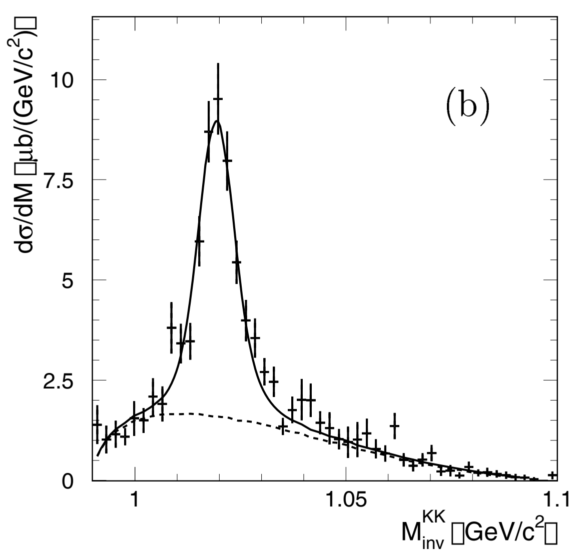

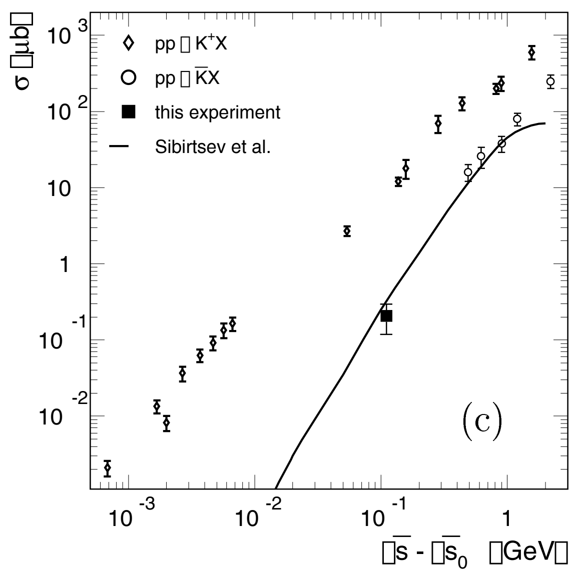

$\sigma_{non-res} = (110 \pm 9 \pm 46)\ nb$ and $\sigma_{\phi \to K^-K^+} = (90 \pm 7 \pm 40)\ nb$. The total K^- cross section, $\sigma_{pp \to ppK^-K^+} = (200 \pm 11 \pm 80)\ nb$, is plotted as the solid data point in Fig. 1.c, where it is compared with estimates of K^- inclusive production cross section at higher energies (open circle) taken from literature [3]. Our data point, measured in this experiment near the production threshold, agrees with the predictions from Sibirtsev [4] (solid curve) using a one meson exchange model including π, K and K^* mesons.

The total cross sections for inclusive K^+ production, shown as open diamonds in Fig. 1.c, are more than an order of magnitude larger then the corresponding K^- inclusive cross sections, at comparable distances above the K^+ threshold, in strong contrast to the nearly equal cross sections measured in sub-threshold heavy ion collisions at the same distance from the respective thresholds. Quantitative calculations [5] show that this cannot be due simply to a rescattering process. Model predictions suggest that this difference might arise from an in-medium effect, where the antikaon are subject to strongly attractive and kaons to slightly repulsive forces; the results of these effective potentials should be to reduce the antikaon production threshold in a dense nuclear medium, leading to the observed enhanced antikaon yields.

Data available before DISTO had either been deduced from $\bar{K}^0$ results, or summing contribu-

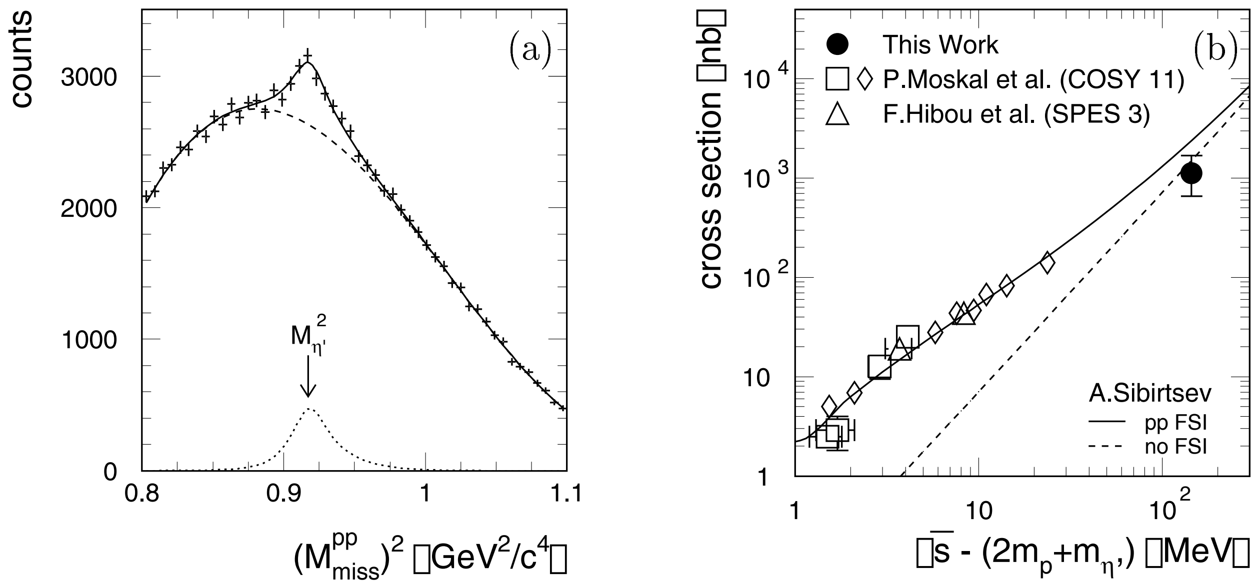

Figure 2: (a) Frame shows in the acceptance corrected M^{pp}_{miss} distribution the η' signal superimposed on a fourth degree polynomial background. (b) Our result is compared with data from literature [6] and with OBE calculations from Sibirtsev [7] including or not FSI.

tions from different exclusive channels with one or two pion in the final state; our results is the first available for inclusive[1] production near threshold.

2.2 The η' meson production

We have investigated η' production in the channel $\vec{p}p \to pp\eta'$ through the decay $\eta' \to \pi^+\pi^-\eta$ (BR = 43.8 %); since the η decays then mostly (BR = 71.5 %) in neutral particles, the final state is still composed of four charged particles, with an η going undetected; thus a first background rejection is performed asking for a four body missing mass compatible with the η mass. A further selection is performed making use of particle identification to discriminate between π^+ mesons and protons in the final state.

The contribution of the η' production (Fig. 2.a) shows up in the M^{pp}_{miss} distribution, in correspondence of the η' mass. The signal has been parametrised from Montecarlo simulation and rescaled to match data by a χ^2-minimization procedure: the background has been parametrised by a fourth degree polynomial, and is coming mostly from non-resonant $pp\eta\pi^+\pi^-$ production and from final states like $pp\pi^+\pi^-\pi\pi$ where two pions go undetected.

The value obtained from DISTO for the η' exclusive cross section $\sigma = (1.12 \pm 0.15 \pm^{+0.42}_{-0.31})\mu b$ shows systematic uncertainties dominated by the background subtraction and the relative (η versus η') acceptance corrections. Our result is compared (Fig. 2.b) with calculations from Sibirtsev [7] from a one-pion-exchange model including (solid line) or not (dashed line) final state interactions. The full calculation well accounts for data near threshold but predicts a cross section of about 2.3 μb at our energy, which is significantly above our measurement

The investigation on the origin of the η' mass goes through the evaluation of the η'-nucleon coupling constant. The attempt to determine this constant, making use of the data available before DISTO near the production threshold, has been complicated by the importance of the final state interactions. Our results is the first in a region in which the reaction mechanism is no more

[1]Our datum, although coming from an exclusive measurement, is also an inclusive production cross section, since no other final states are kinematically allowed.

dominated by final state interactions.

2.3 The ρ meson production

The exclusive ρ production ($pp \to pp\rho$) has been identified through its dominant $\pi^+\pi^-$ decay channel. Effective background rejection can be obtained asking for a 4-body missing mass compatible with zero, and for a M^{pp}_{miss} mass compatible with the di-pion invariant mass $M^{\pi\pi}_{inv}$. Particle identification has been used too in order to discriminate between pions and protons in the final state. A large part of the remaining background is related to Δ^{++} production, that is strongly reduced with appropriate kinematic cuts.

Fig. 3.a shows the acceptance corrected $M^{\pi\pi}_{inv}$ mass distribution for different values of $\cos(\theta_{CM})$, being θ_{CM} the ρ production angle in the center of mass: the $M^{\pi\pi}_{inv}$ distribution is non-resonant for $\cos(\theta_{CM}) < 0.4$ and isotropic; the ρ peak shows up only for $\cos(\theta_{CM}) > 0.5$. The energy and width of this peak, obtained with a fit including a Breit-Wigner and a third order polynomial, are consistent with those reported in Ref. [8].

There is very little knowledge about ρ production in proton-proton reactions for center of mass energies below 5 GeV; the only data available before DISTO came from early bubble chamber experiments, suffering of low statistic, and at higher proton energies.

In the OBE framework, the differential angular cross section has been proposed [9] as the best observable to distinguish between two main processes responsible for the vector meson production near threshold. Whereas a flat angular distribution should signal superiority of the mesonic current, a strong forward peaking at $\cos^2(\theta_{CM})$ should indicate a large nucleonic current. The total cross section, $\sigma \approx 20\ \mu b$, is still to be consider preliminary; it is significantly lower ($\sim$ 5 times) than that calculated in the resonance model of Ref. [10], and roughly a factor of two lower than that predicted by a one pion exchange model [11]. The angular dependence (Fig. 3.b) of the differential cross section indicates higher partial waves up to a $L = 2$ contribute to the ρ meson production, and might signal predominance of the nucleonic current in the meson production.

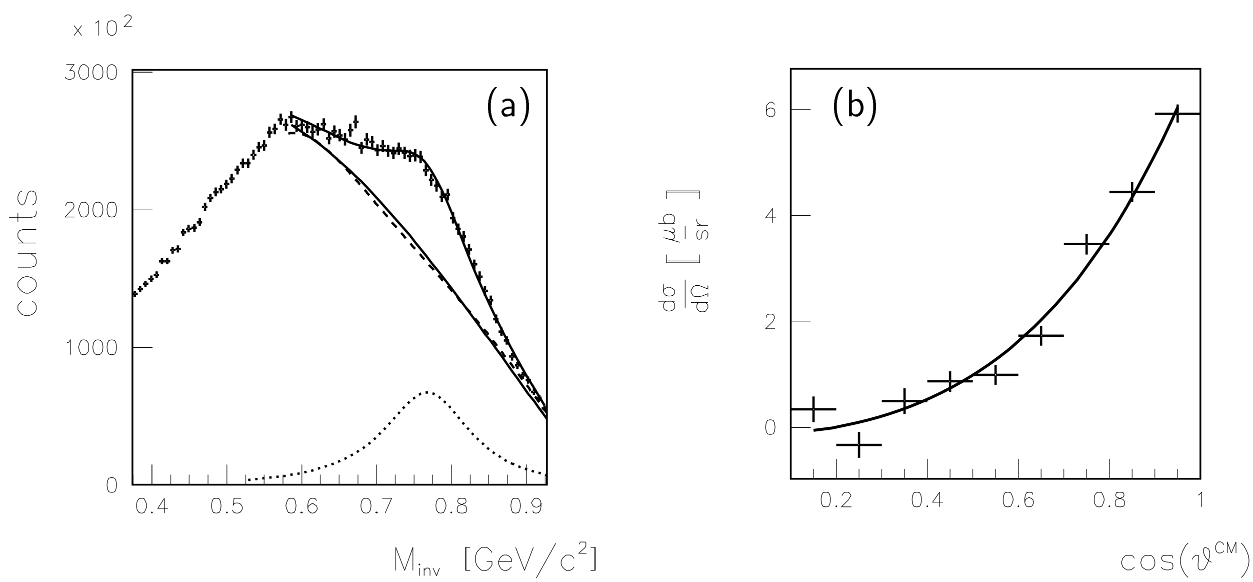

Figure 3: ρ production. (a) The acceptance corrected distribution of $M^{\pi\pi}_{inv}$ for $\cos(\theta_{CM}) > 0.5$ has been fitted with a Breit-Wigner function (dotted curve) and a third order polynomial to account for background (solid lines); the dashed line represents the $M^{\pi\pi}_{inv}$ distribution for $\cos(\theta_{CM}) < 0.4$, normalised to the same maximum. (b) Angular distribution of the differential cross section fitted with the first even Legendre polynomials.

3 Hyperon production

One of the main questions being addressed is the investigation of the hyperon production mechanism; in particular polarisation observables are key observables to perform this task. This section will focus on the spin observables for exclusive Λ production ($\vec{p}p \to pK^+\vec{\Lambda}$).

The Λ spin quantisation axis is defined as the normal to the Λ production plane (defined by the beam and Λ momenta as $\hat{n} = \frac{\vec{p}_B \times \vec{p}_\Lambda}{|\vec{p}_B \times \vec{p}_\Lambda|}$). The beam quantisation axis is fixed: the vertical axis normal to the horizontal plane, in the laboratory frame. The Λ polarisation is determined, as a fore-aft asymmetry in the angular distribution of the decay proton in the Λ rest frame, from the self-analysing weak decay $\Lambda \to p\pi^-$.

This article reports the results (some preliminary) concerning the spin transfer parameter D_{yy} and the analysing power A_y for the exclusive Λ production. The complete kinematic reconstruction allow to resolve the Λ's directly produced from those coming from the Σ^0 and other Y^* decays, making use of the proton-kaon missing mass spectrum ($M^{pK^+}_{miss}$) at the reaction vertex.

The beam polarisation P_B was reversed each spill, and evaluated on-line by the Saclay polarimeter; unfortunately this measurement was not compatible with the data taking. A more precise off-line determination of P_B can be achieved by mean of the data collected simultaneously for the proton-proton elastic scattering, making use of the A_y from the literature for this reaction. The polarisation is remarkably stable, and it has been evaluated precisely for data collected at 2.94 GeV/c, where more experimental A_Y data are available; at higher energies, the results concerning the Λ production are still preliminary, since they still rely on the on-line polarimeter analysis. Since P_B is stable, a new P_B value would lead simply to a rescaling of the Λ polarisation observables.

3.1 The D_{yy} spin transfer parameter in exclusive Λ production

Fig. 4.a shows the dependence on the Feymann parameter x_{F} of the D_{yy} obtained by our collaboration for the Λ's directly produced at 3.67 GeV/c: the D_{yy} is sizeable and negative in the whole kinematic range. Error bars include systematic uncertainties, dominated by the residual contamination in the exclusive Λ sample of Λ's coming from the decay of Σ^0 and from Y^* resonances.

Our results are the first available from exclusive measurements, and the first available for the region $x_{\mathrm{F}} < 0$. Our data are compared in Fig. 4.a with inclusive data from the literature [12]: at higher energies D_{yy} is positive for $x_{\mathrm{F}} > 0$; at intermediate energies, D_{yy} is consistent with zero. If we want to compare our results with the inclusive data from the literature, we must consider the filled triangles, showing our semi-inclusive data: the D_{yy} obtained considering not only the directly produced Λ's, but all the Λ's reconstructed by the DISTO spectrometer, i.e. also the Λ's coming from other channels. The inclusion in the Λ sample of the Λ's coming from the Σ^0 decay leads to a less negative D_{yy}. The different behaviour at low ($D_{yy} < 0$) and at higher energies ($D_{yy} > 0$) is an indication of a possible difference in the reaction mechanism.

In the framework of the boson exchange model, assuming the fragmentation model scheme, in the beam fragmentation region ($x_{\mathrm{F}} > 0$) the outgoing hyperon is preferentially correlated with the polarised proton from the beam. Spin and angular momenta conservation (see diagrams in Fig. 4) require a spin flip at the production vertex when a kaon is exchanged; the spin of the Λ and the spin of the incident proton must then be in opposite directions, leading to a negative D_{yy}. This is not the case if a pion is exchanged. In the target fragmentation region ($x_{\mathrm{F}} < 0$), where in fragmentation scheme the outgoing hyperon is preferentially correlated with the unpolarised proton from the beam, no polarisation transfer should occur from the beam to the hyperon.

Fig. 4.b-c compare the experimental data for D_{yy} for exclusive Λ production at 3.67 and 2.94 GeV/c with the predictions, folded with DISTO acceptance, of a model developed by J.M.Laget [13] according to the scheme described above. The effect of the Λ-proton final state interaction (FSI),

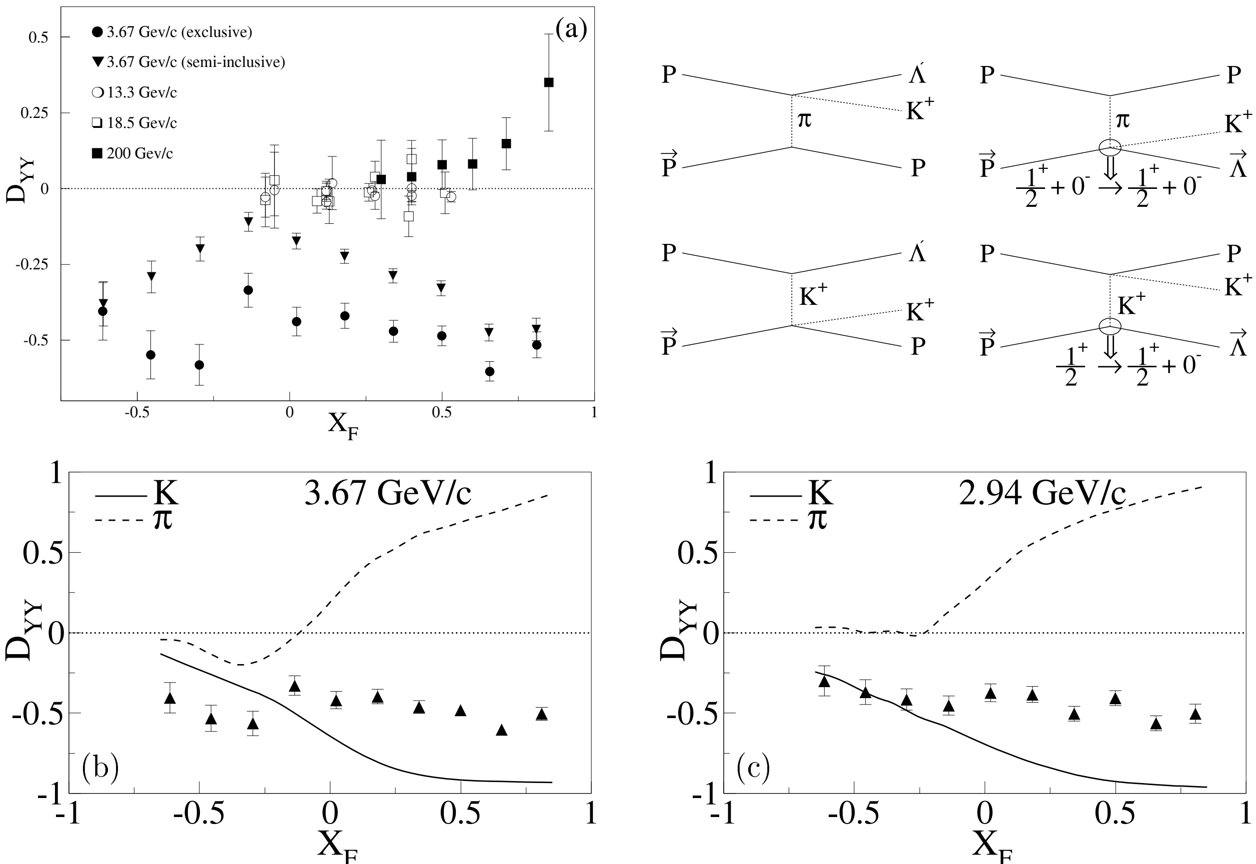

Figure 4: (a) D_{yy} vs. $x_{\rm F}$ for our *exclusive* $\vec{p}p \to pK^+\vec{\Lambda}$ data at 3.67 GeV/c and for *inclusive* production at higher energies [12]. Also shown our *semi*-inclusive results at the same energy. (b-c) Theoretical calculations [13] of D_{yy} for various *exclusive* Λ production mechanisms: kaon-exchange (solid curve) an pion-exchange (dashed), combined with a Λ-p final state interaction. The Feymann diagrams indicate the dominant exchange contributions for positive vs. negative $x_{\rm F}$ and spin structures at vertices.

included in the calculations, is to make the D_{yy} negative at $x_{\rm F} < 0$. We can see how, if we consider only the beam fragmentation region, our experimental data at both energies suggest the prevalence of the kaon exchange diagram. In the target fragmentation region, where without the intervention of FSI the D_{yy} for both the pion and the kaon exchange contributions should be compatible with zero, the sizeable and negative D_{yy} results have still to be understood. At 2.94 GeV/c, where FSI are more important, one can see that at $x_{\rm F} < 0$ kaon exchange predictions, folded with FSI, almost reproduce our data, while at 3.67 GeV/c, where FSI are less important, this is no more true.

The comparison of the results at 3.67 and 2.94 GeV/c shows as the D_{yy} energy dependence is rather smooth in the DISTO energy range; error bars include systematic uncertainties.

3.2 The A_y analysing power in exclusive Λ production

Fig. 5 reports, for two different incident momenta, the A_y dependence on $x_{\rm F}$ and on $\cos(\theta_{\Lambda,CM})$, being $\theta_{\Lambda,CM}$ the Λ production angle in CM frame. The A_y is less important than the D_{yy}, but still mostly negative; the energy dependence is rather smooth.

At the higher energy, A_y is more important (Fig. 5.b) when the Λ is produced backward in the CM frame ($\cos(\theta_{\Lambda,CM}) < 0$).

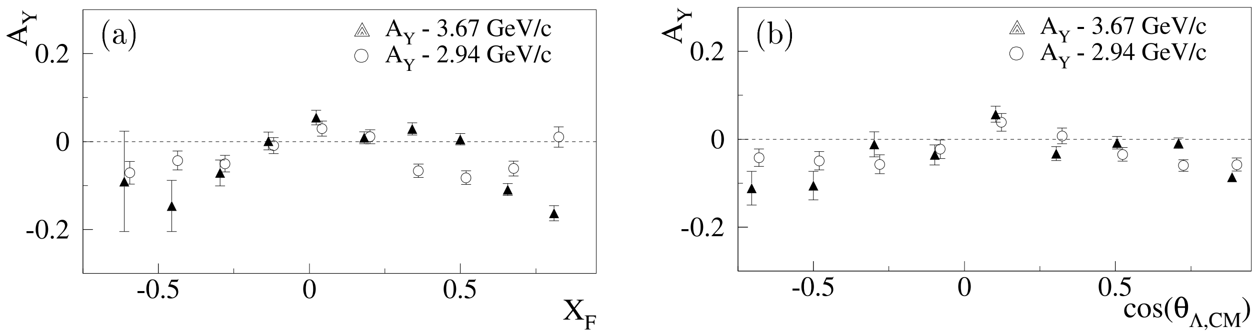

Figure 5: A_y results for $\vec{p}p \to pK^+\vec{\Lambda}$ at two beam momenta: (a) A_y vs. x_{F}; (b) A_y vs. $\cos(\theta_{\Lambda,CM})$.

4 Conclusions

The first available data for the cross section in K^- production near threshold has been provided. These data are essential for the interpretation of heavy ion data, and show an antikaon cross section lower of more than order of magnitude than the kaon production cross section at the same excess energy. The enhancement in heavy ion data has been explained, up to now, by an in-medium effect. The obtained cross section for η' production is the first available in an energy range where the reaction mechanism is no more dominated by final state interactions, and will be useful to determine the η'-nucleon coupling constant, an element needed to solve the puzzle of the origin of the η' mass. Preliminary results have been reported also on the exclusive ρ production total cross section, the first available near threshold. The differential cross section indicates higher partial waves contributions, and a possible predominance of the nucleon current in meson production.

The first data available for exclusive Λ production with polarised beams show a D_{yy} negative and sizeable. This suggest in the beam fragmentation region the predominance, in the framework of the boson exchange models, of the kaon exchange mechanism. The data that we present for the target fragmentation region are the first available. They cannot yet be interpreted, within the fragmentation model approach, by the quoted model. The A_y data are also negative, even if less sizeable than the D_{yy} data, and are more negative when the Λ's are produced backward in the center of mass.

References

[1] F. Balestra *et al.*, Nucl. Instr. Meth. **A426**, 385 (1999).

[2] F. Balestra *et al.*, Phys. Rew. **C93**, 24004 (2001).

[3] F. Balestra *et al.*, Phys. Lett. **B468**, 7 (1999) and references there in.

[4] A. Sibirtsev, W. Cassing, and C. M. Ko, Z. Phys. **A358**, 101 (1997).

[5] E. L. Bratkovskaya, W. Cassing, and U. Mosel, Nucl. Phys. **A622**, 593 (1997).

[6] F. Balestra *et al.*, Phys. Lett. **B491**, 29 (2000) and references there in.

[7] A. Sibirtsev, Eur. Phys. J. **A2**, 333 (1998).

[8] Particle Data Group, C. Caso *et al.*, Eur. Phys. J. **C3**, 364 (1998).

[9] K. Nakayama , Phys. Rev. **C57**, 1580 (1998).

[10] S.Teis *et al.*, Z. Phys. **A356**, 421 (1997); C. Ernst *et al.*, Phys. Rev. **C58**, 447 (1998); E. Bratkovskaya, Nucl. Phys. **A653**, 301 (1999).

[11] A. Sibirtsev, Nucl. Phys. **A604**, 445 (1996).

[12] B. E. Bonner *et al.*, Phys. Rev. Lett. **58**, 447 (1987); B. E. Bonner *et al.*, Phys. Rev. **D38**, 729 (1988); A. Bravar *et al.*, Phys. Rev. Lett. **78**, 4003 (1997).

[13] J. M. Laget, Phys. Lett. **B259**, 24 (1991).

Two-pion exchange in proton-proton scattering

W. R. Gibbs[a] and Benoît Loiseau[b]

[a]*Department of Physics, New Mexico State University, Las Cruces, NM 88003, U.S.A.*
[b]*LPNHE, Université P. & M. Curie, Paris 75230, France*

(Received: 15 August 2001)

We present calculations of the two-pion-exchange contribution to proton-proton scattering at 90° using form factors appropriate for representing the distribution of the constituent partons of the nucleon.

1 Introduction

The cross section and the spin-correlation observable, C_{NN}, measured in the region from 0 to 12 GeV/c P_{lab} at 90^o provide an excellent testing ground for our theories of hadronic interactions. These data have been the focus of a number of experimental [1] and theoretical studies [2]. There is an apparent simplification of the amplitude in the region from 4 GeV/c to 8 GeV/c. At 90° the spin-correlation observable C_{NN} has a constant value of about 0.07 which might indicate the dominance of a single mechanism. The simple quark exchange mechanism gives 1/3 for C_{NN}.

One pion exchange provides an important contribution below about 2 GeV/c. The exchange of two pions has been used as a basis for the NN interaction at low energies and it is reasonable to assume that it remains important at higher energies. We have calculated the box and crossed two-pion exchange Feynman graphs with nucleons as intermediate states. Even if this mechanism dominates one can not expect good quantitative agreement with the data due to the strong inelasticity of the NN interaction at these energies since distortion effects need to be considered. None the less, several questions can be raised and answered.

2 Two-pion exchange calculation

The full cross section is given by

$$\frac{d\sigma}{d\Omega} = \left(\frac{m^2}{4\pi E}\right)^2 |M|^2 ,$$

where, for pseudo-scalar coupling and box kinematics M is

$$M_{PS} = g^4 \frac{1}{(2\pi)^4} \int \frac{dq\, [\bar{u}(k')\gamma_5(\not{p}+m)\gamma_5 u(k)]_1\, [\bar{u}(-k')\gamma_5(\not{p}'+m)\gamma_5 u(-k)]_2}{(p^2-m^2+i\epsilon)(p'^2-m^2+i\epsilon)(q^2-\mu^2+i\epsilon)(q'^2-\mu^2+i\epsilon)} .$$

In this expression the minus sign on k and k' applies only to spatial components. Corresponding to the propagator for proton 1, we have

$$\begin{aligned}\bar{u}(k')\gamma_5(\not{p}+m)\gamma_5 u(k) &= \bar{u}(k')\gamma_5[(p_0-E_p)\gamma_0 + E_p\gamma_0 - \boldsymbol{\gamma}\cdot\mathbf{p} + m]\gamma_5 u(k) \\ &= -\bar{u}(k')(p_0-E_p)\gamma_0 u(k) + 2m\bar{u}(k')\gamma_5 \sum_r u_r(p)\bar{u}_r(p)\gamma_5 u(k) ,\end{aligned}$$

where the spinors $u_r(p)$ are on shell with energy $E_p \equiv \sqrt{\mathbf{p}^2+m^2}$.

The integral can be written as an operator in spin space in the form

$$M_{PS} = g^4 \frac{1}{(2\pi)^4} \int \frac{dq\Theta_1(p)\Theta_2(p')}{(p^2-m^2)(p'^2-m^2)(q^2-\mu^2)(q'^2-\mu^2)} ,$$

where

$$\Theta_1(p) = \frac{1}{2m}\left\{(E_p - p_0)\left(E + m + \frac{\boldsymbol{\sigma_1}\cdot\mathbf{k}'\boldsymbol{\sigma_1}\cdot\mathbf{k}}{E+m}\right)\right.$$
$$\left. + \frac{[(E+m)\boldsymbol{\sigma_1}\cdot\mathbf{p} - (E_p+m)\boldsymbol{\sigma_1}\cdot\mathbf{k}'][(E_p+m)\boldsymbol{\sigma_1}\cdot\mathbf{k} - (E+m)\boldsymbol{\sigma_1}\cdot\mathbf{p}]}{(E_p+m)(E+m)}\right\} .$$

In the case of pseudo-vector coupling the interaction is given by $\frac{f}{\mu}\bar{\psi}\gamma_\mu\gamma_5\boldsymbol{\tau}\cdot\partial^\mu\boldsymbol{\phi}_\pi\psi$ and the operator corresponding to the first proton propagator is

$$(p^2 - m^2)P_{PV} = -\frac{f^2}{\mu^2}\bar{u}(k')\not{q}'\gamma_5(\not{p}+m)\not{q}\gamma_5 u(k)$$
$$= \frac{f^2}{\mu^2}\bar{u}(k')\gamma_5(p^2-m^2)(\not{p}+3m)\gamma_5 u(k) + \frac{f^2 4m^2}{\mu^2}\bar{u}(k')\gamma_5(\not{p}+m)\gamma_5 u(k) .$$

The operator naturally separates into a term which corresponds to a contact term and one which is identical to the pseudo-scalar expression given before

$$P_{PV} = \frac{f^2}{\mu^2}\bar{u}(k')\gamma_5(\not{p}+3m)\gamma_5 u(k) + g^2\frac{\bar{u}(k')\gamma_5(\not{p}+m)\gamma_5 u(k)}{p^2-m^2} = P_C + P_{PS} .$$

Defining an operator analogous to $\Theta_1(p)$ for the contact term for the first proton

$$C_1(p) = \frac{E+m}{2m}\left[E_p - p_0 + 2m + (E_p - p_0 - 2m)\frac{\boldsymbol{\sigma_1}\cdot\mathbf{k}'\boldsymbol{\sigma_1}\cdot\mathbf{k}}{(E+m)^2}\right]$$
$$+ \frac{[(E+m)\boldsymbol{\sigma_1}\cdot\mathbf{p} - (E_p+m)\boldsymbol{\sigma_1}\cdot\mathbf{k}'][(E_p+m)\boldsymbol{\sigma_1}\cdot\mathbf{k} - (E+m)\boldsymbol{\sigma_1}\cdot\mathbf{p}]}{2m(E_p+m)(E+m)} ,$$

we can write

$$M_{PV} = \frac{g^4}{16m^4}\frac{1}{(2\pi)^4}\int dq\frac{C_1(p)C_2(p')}{(q_0^2-\omega^2)(q_0^2-\omega'^2)} + \frac{g^4}{4m^2}\frac{1}{(2\pi)^4}\int dq\frac{C_1(p)\Theta_2(p')}{(p'^2-m^2)(q_0^2-\omega^2)(q_0^2-\omega'^2)}$$
$$+ \frac{g^4}{4m^2}\frac{1}{(2\pi)^4}\int dq\frac{\Theta_1(p)C_2(p')}{(p^2-m^2)(q_0^2-\omega^2)(q_0^2-\omega'^2)} + M_{PS}.$$

3 Proton structure

The expressions in the previous section lack the form factors which are associated with each pion-nucleon vertex. We treat the two protons as particles with intrinsic size related to the distribution of (primarily) constituent quarks in the nucleon, assuming that the underlying interaction of the pions is with the partons. The form factor can be directly obtained as the Fourier transform of the density [3]. Such a derivation is inherently non-relativistic since it is not expressed in terms of Lorentz invariants.

An exponential parton density leads to the form, $(\alpha^2-\mu^2)^2/(\mathbf{q}^2+\alpha^2)^2$. A common relativistic generalization is

$$\frac{(\alpha^2-\mu^2)^2}{(q_0^2-\mathbf{q}^2-\alpha^2)^2} ,$$

but this procedure introduces an additional singularity in q_0 on the real axis.

A second generalization of $\mathbf{q}^2$ can be obtained by the following argument. The form factor must be a function of Lorentz scalars only. There are three four-vectors, the initial and final nucleon momenta (k,k') and the pion momentum (q) of which only two are independent. Choose one of the nucleon momenta (k) and the pion momentum (q). From these we can construct three scalars q^2, k^2, and $k \cdot q$. In order to be homogeneous in k and q, the only two invariants we can consider are $(k \cdot q)^2$ and $k^2 q^2$. The linear combination $(k \cdot q)^2 - k^2 q^2$ reduces to $m^2 \mathbf{q}^2$ if the nucleon is on shell at rest. We use the generalization

$$\mathbf{q}^2 \to Q^2(k,q) \equiv \frac{(k \cdot q)^2 - k^2 q^2}{m^2} ,$$

which has the property $Q^2(k \pm q, q) = Q^2(k,q)$. Either the initial or final nucleon momentum may be used. A number of authors have used a similar form in one way or another [4].

One can also be led to this expression by the requirement that $Q^2(k,q) = Q^2(k',q)$. Since $k' = k+q$ (for example) this condition is suggestive of the vector cross product. The four-dimensional cross product is defined by the use of a totally antisymmetric 4-component tensor, $\epsilon_{ijk\ell}$. Since we still have only two vectors (say a and b) the result is a tensor

$$T_{ij} = \sum_{k,\ell=0,1,2,3} \epsilon_{ijk\ell} a_k b_\ell ,$$

with 6 independent components. We can separate the components into two classes: one in which the zero index is free and one in which it is summed over

$$\begin{aligned} T_{0j} &= \sum_{k,\ell=1,2,3} \epsilon_{0jk\ell} a_k b_\ell = [\mathbf{a} \times \mathbf{b}]_j , \\ T_{ij} &= a_0 b_k - b_0 a_k = [a_0 \mathbf{b} - b_0 \mathbf{a}]_k, \quad i,j,k \ \text{ cyclic} \neq 0 . \end{aligned}$$

Contracting this tensor with the metric tensor we find

$$\frac{1}{2} \sum g_{ii'} g_{jj'} T_{ij} T_{i'j'} = \frac{1}{2} \sum g_{ii} g_{jj} T_{ij} T_{ij} = (a_0 \mathbf{b} - b_0 \mathbf{a})^2 - (\mathbf{a} \times \mathbf{b})^2 \equiv (a \cdot b)^2 - a^2 b^2 .$$

In general, two invariants are available, $(k \cdot q)^2/m^2$, which evaluates to q_0^2 in the rest frame of the nucleon and $[(k \cdot q)^2 - k^2 q^2]/m^2$, which evaluates to $|\mathbf{q}|^2$. We could choose any combination of $|\mathbf{q}|^2$ and q_0^2 for the variable in the rest frame. Only $[(k \cdot q)^2 - k^2 q^2]/m^2$ and q^2 are independent of which nucleon momentum (k or k') is used.

By choosing a function independent of q_0 in the nucleon rest frame, the interaction is instantaneous, perhaps a physically reasonable choice since the valence quarks are always present, hence they do not have a formation time. For the present calculation we can always choose the nucleon to be one of the external lines, and hence on shell. We use

$$f(k,q) = f(\mathbf{k}, q_0, \mathbf{q}) = \left[\frac{\Lambda^2}{(k \cdot q/m)^2 - q^2 + \Lambda^2} \right]^2 .$$

A product of four of these factors will appear, one for each vertex. For the box diagram we have

$$f(\mathbf{k}, q_0, \mathbf{q}) f(-\mathbf{k}, q_0, \mathbf{q}) f(\mathbf{k}', q_0, \mathbf{q}') f(-\mathbf{k}', q_0, \mathbf{q}') ,$$

while for the crossed diagram the factors are

$$f(\mathbf{k}, q_0, \mathbf{q}') f(-\mathbf{k}, q_0, \mathbf{q}) f(\mathbf{k}', q_0, \mathbf{q}) f(-\mathbf{k}', q_0, \mathbf{q}') .$$

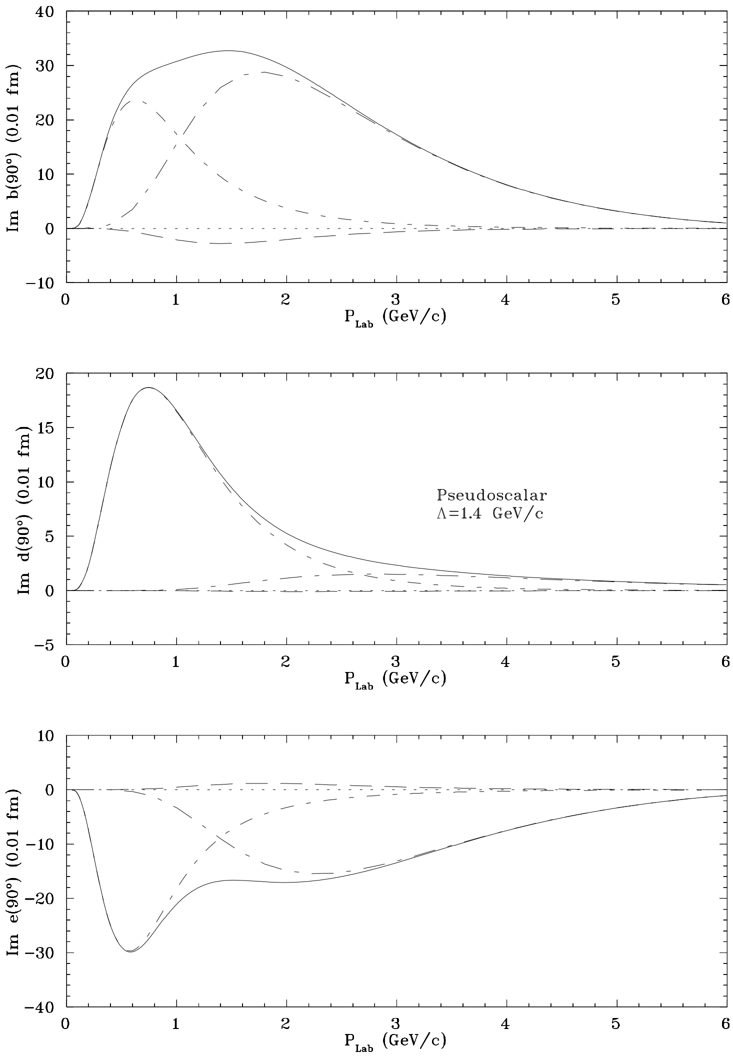

Figure 1: Contributions to the imaginary part of the b, d and e pseudo-scalar amplitudes. The short dash-dot line shows the result of placing the two nucleons on shell. The dashed and long dash-dot curves show the principal value parts from the box and cross diagrams respectively. The two-nucleons-on-shell contribution dominates at low energy but dies out at high energy where the amplitudes are dominated by the principal-value part of the crossed diagram.

The difference in the variables appearing in these expressions has important consequences for the behavior of the box and crossed graphs.

The off-shell range in the calculation, Λ, which corresponds to the extension of the proton distribution of partons can be evaluated from other sources. Coon and Scadron [5] found Λ between 0.8 and 1.0 GeV/c for a monopole form. To convert to an equivalent dipole form at low momentum transfer one can multiply by $\sqrt{2}$ giving a range from 1.13 to 1.41 GeV/c. In lattice QCD calculations Liu, Dong and Draper [6] find $\Lambda = 0.747$ GeV/c for a monopole form and $\Lambda = 1.32$ GeV/c for a dipole.

We use a dipole form and most of the calculations shown will be for $\Lambda = 1.4$ GeV/c.

4 Results

To describe nucleon-nucleon scattering we use the amplitudes defined by the Saclay group [7] given by the equation

$$M(\mathbf{k}_f, \mathbf{k}_i) = \frac{1}{2}\Big[(a+b) + (a-b)\boldsymbol{\sigma_1}\cdot\mathbf{n}\,\boldsymbol{\sigma_2}\cdot\mathbf{n} + (c+d)\boldsymbol{\sigma_1}\cdot\mathbf{m}\,\boldsymbol{\sigma_2}\cdot\mathbf{m} + (c-d)\boldsymbol{\sigma_1}\cdot\mathbf{l}\,\boldsymbol{\sigma_2}\cdot\mathbf{l}$$
$$+ e(\boldsymbol{\sigma_1}+\boldsymbol{\sigma_2})\cdot\mathbf{n}\Big]\,, \qquad \text{with} \quad \mathbf{l} = \frac{\mathbf{k}_f + \mathbf{k}_i}{|\mathbf{k}_f + \mathbf{k}_i|}, \quad \mathbf{m} = \frac{\mathbf{k}_f - \mathbf{k}_i}{|\mathbf{k}_f - \mathbf{k}_i|}, \quad \mathbf{n} = \frac{\mathbf{k}_i \times \mathbf{k}_f}{|\mathbf{k}_i \times \mathbf{k}_f|}\ .$$

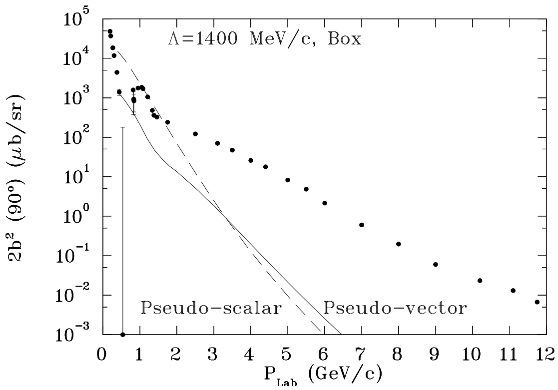

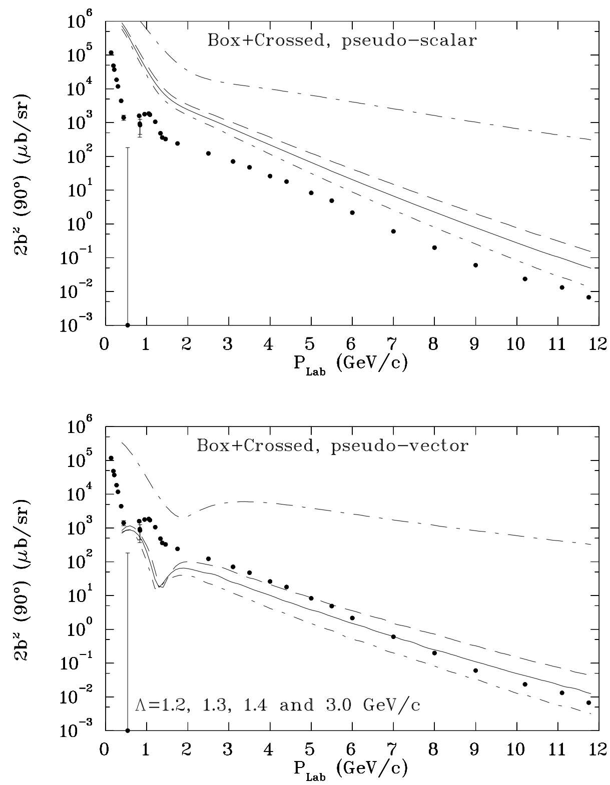

Figure 2: [Above] The calculation of $2|b|^2$ for the box diagram. The dashed line shows the result for the pseudo-scalar coupling and the solid line that of the pseudo-vector.

Figure 3: [Right] Dependence of $|b|^2$ on the value of Λ for pseudo-scalar (top) and pseudo-vector (bottom) couplings. The smaller values of the partial cross sections correspond to the smaller values of Λ in order.

With identical particle symmetry $a(90°) = 0$ and $c(90°) = -b(90°)$, so only 3 amplitudes are needed to describe the scattering. At 90°

$$\sigma = \frac{1}{2}(2|b|^2 + |d|^2 + |e|^2) \ ; \quad \sigma C_{NN} = \frac{1}{2}(-2|b|^2 + |d|^2 + |e|^2) \ ,$$

so from the data we can extract $2|b|^2$ and $|d|^2 + |e|^2$ directly.

Figure 1 shows the amplitudes coming from different types of contribution for pseudo-scalar coupling. The case of pseudo-vector coupling is similar. We see that the important contributors are different at high and low energies. Figure 2 shows the results of the box diagram for PS and PV coupling for the partial cross section $|b|^2$. While the contribution of this diagram falls rapidly, the crossed diagram falls much more slowly as one can see from Figure 3 which shows the sum for various values of Λ. Clearly the crossed diagram dominates at high energy. This difference can be traced to the difference in the variables in the form factors as mentioned above. We also see a very large sensitivity to the value of the off-shell range which is very natural since the fall-off of the cross section is given primarily by the form factor.

Figure 4 (left) shows the result of the sum of the box and crossed diagrams for the sum $d^2 + e^2$.

We see that each case there is a large difference between PS and PV coupling, as pointed out (at lower energies) by Robilotta *et al.* [8]. However, the PS and PV couplings can be mixed. Gross *et al.* [9] found 1/4 PS and 3/4 PV. Goudsmit *et al.* [10] found a small mixture of PS (about 3%).

Kondratyuk and Scholten [11] found a mixture which varied with momentum transfer, being dominated by PV at low values and about equal at higher values. This is expected since chiral symmetry imposes pseudo-vector coupling at low energy.

Figure 4 (right) shows a comparison with the spin correlation observable. We see that the PS and PV results bracket the data.

The underlying structure of the proton, represented here by the form factor, plays an essential

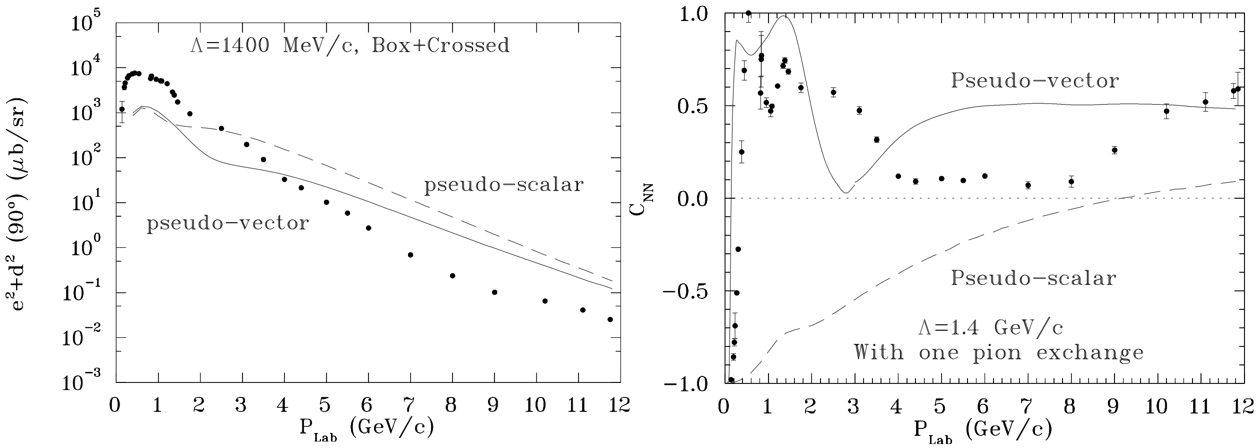

Figure 4: Left: Dependence of $|e|^2 + |d|^2$ on the type of coupling. Right: Comparison with the experimental values of C_{NN} for the different couplings.

role in the scattering in this energy range.

Our conclusions are: 1) two pion exchange gives a significant contribution to pp scattering in this energy region, 2) the crossed graph dominates over the box at high energies 3) the important contributions at high energies are different than at low energies and 4) there is a significant reduction of the cross section for PV coupling compared to PS coupling similar to that seen in low-energy pion-nucleon scattering.

Acknowledgments: The LPNHE is a Unité de Recherche des Universités Paris 6 et Paris 7, associée au CNRS. This work was supported by the U. S. Department of Energy and the National Science Foundation.

References

[1] G. R. Court *et al.*, Phys. Rev. Lett. **57**, 507 (1986); T. S. Bhatia *et al.*, Phys. Rev. Lett. **49**, 1135 (1982); E. A. Crosbie *et al.*, Phys. Rev. D**23**, 600 (1981); A. Lin *et al.*, Phys. Rev. Lett. **41**, 1257 (1978); D. G. Crabb *et al.*, Phys. Rev. Lett. **41**, 1257 (1978); J. R. O'Fallon *et al.*, Phys. Rev. Lett. **39**, 733 (1977).

[2] S. J. Brodsky, C. E. Carlson and H. Lipkin, Phys. Rev. D**20**, 2278 (1979); Glennys R. Farrar, Steven Gottlieb, Dennis Sivers and Gerald H. Thomas, Phys. Rev. D**20**, 202 (1979); Gordon P. Ramsey and Dennis Sivers, Phys. Rev. D**45**, 79 (1992), Phys. Rev. D**47**, 79 (1993).

[3] W. R. Gibbs and B. Loiseau, Phys. Rev. C**50**, 2742 (1994).

[4] G. Ramalho, A. Arriaga and M. T. Peña, Phys. Rev. C**60**, 047001 (1999); B. D. Keister and L. S. Kisslinger, Nucl. Phys. **A326**, 445 (1979); G. Wolf, Phys. Rev. **182**, 1538 (1969); H. P. Durr and H. P. Pilkuhn, Nuovo Cim. **40**, 899 (1965); J. Benecke and H. P. Durr, Nuovo Cim. **56**, 269 (1968).

[5] S. A. Coon and M. D. Scadron, Phys. Rev. C**42**, 2256 (1990); Phys. Rev. C**23**, 1150 (1981).

[6] K. F. Liu, S. J. Dong and T. Draper, Phys. Rev. Lett. **74**, 2172 (1995).

[7] J. Bystricky, F. Lehar, and P. Winternitz, J. Phys. **39**, 1 (1978).

[8] M. R. Robilotta and C. A. da Rocha, Nucl. Phys. **A615**, 391 (1997).

[9] F. Gross and Y. Surya, Phys. Rev. C**47**, 73 (1993).

[10] P. F. A. Goudsmit, H. J. Leisi, E. Matsinos, B. L. Birbrair and A. B. Gridnev, Nucl. Phys. **A575**, 673 (1994).

[11] S. Kondratyuk and O. Scholten, Phys. Rev. C**59**, 1070 (1999).

Fundamental quantities from doubly subtracted forward dispersion relations

W. R. Gibbs[a] and W. B. Kaufmann[b]

[a]*Department of Physics, New Mexico State University, Las Cruces, NM 88003, U.S.A.*
[b]*Department of Physics and Astronomy, Arizona State University, Tempe, AZ 85287, U.S.A.*

(Received: 24 August 2001)

We comment on the extraction the pion-nucleon coupling, the GMO integral $J^{(-)}$, and the isoscalar scattering length from doubly subtracted dispersion relations.

1 Introduction

The accurate determination of the pion-nucleon coupling constant (f) from pion-nucleon data is of the great importance. For example, much of the evidence that one-pion exchange is an important mechanism in the nucleon-nucleon interaction is based on the comparison of the values extracted from πN and NN scattering data. The determination of f^2 is (optimistically) approaching an accuracy of 1%. For this purpose the best tools are probably forward dispersion relations, because they express f^2 directly in terms of measurable quantities: the $\pi^{\pm}p$ total cross sections [1] and subtraction constants, used to improve convergence, which are usually chosen as the real parts of the forward scattering amplitude. The most accurate value of the latter is the π^- scattering length, recently obtained from from pionic atom measurements [2]. Real parts of scattering amplitudes have also been obtained from $\pi^{\pm}p$ elastic scattering data in the Coulomb interference region [3].

In forward dispersion relations for π^-p scattering, the coupling constant extracted will be for the π^-pn vertex. The hadronic mass differences can be accounted for in the sense that the short cut in the π^0n and π^-p thresholds may be taken into account and the Born pole taken at the neutron mass. Coulomb corrections to the data need to be made, however, and can lead to problems (see later).

2 GMO derivation

The GMO sum rule [4] derives from a forward dispersion relation for $H(\omega) \equiv [F_-(\omega) - F_+(\omega)]/\omega$, where ω is the total laboratory energy of the pion, and $F_{\pm}(\omega)$ are the (hadronic) forward elastic $\pi^{\pm}N$ scattering amplitudes in the laboratory frame. $H(\omega)$ is nonsingular at $\omega = 0$ because of the crossing relation $F_{\pm}(\omega) = F_{\mp}(-\omega)$. The resulting dispersion relation,

$$\mathrm{Re}[F_-(\omega) - F_+(\omega)] = \frac{4\omega f^2}{\omega^2 - \omega_N^2} + \frac{\omega}{2\pi^2}\int_{\mu}^{\infty} \frac{k'[\sigma_-(\omega') - \sigma_+(\omega')]d\omega'}{\omega'^2 - \omega^2} \ ,$$

evaluated at $\omega = \mu$ yields

$$-\tilde{b}_1 - \frac{2\mu f^2}{\mu^2 - \omega_N^2} = \frac{\mu}{4\pi^2}\int_0^{\infty} \frac{[\sigma_-(\omega') - \sigma_+(\omega')]dk'}{\omega'} \equiv \mu J^{(-)} \ ,$$

where $\tilde{b}_1 \equiv [F_+(\mu) - F_-(\mu)]/2$ is the isospin odd scattering length in the laboratory frame, and $\omega_N \equiv -\left(\mu^2 - m^2 + m_n^2\right)/2m \approx -\mu^2/2m$ corresponds to the neutron pole at $s = m_n^2$. In these expressions, μ is the charged pion mass, m is the proton mass, and m_n is the neutron mass. The sum rule relates f^2, $\tilde{b}_1$, and $J^{(-)}$. Conventionally, $J^{(-)}$ is determined by integration over the extensive experimental data base [1] supplemented by amplitudes reconstructed from phase shifts [5]. While $J^{(-)}$ is usually defined as the integral in the GMO sum rule, in the next section we will regard it

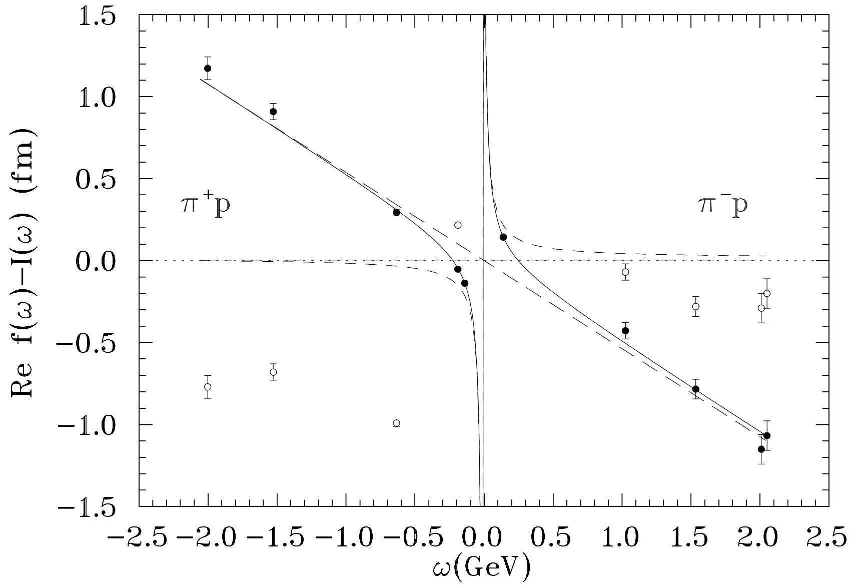

Figure 1: Comparison with the real parts of forward amplitudes. The open points show the experimental real amplitudes without subtraction of the integral $I(\omega)$. The long dashed curve shows the linear term, the short dashed curve the pole contribution, the dash-dot curve (almost identical to zero on this plot) $\tilde{b}_0$, and the solid curve represents the sum.

to be defined by the expression on the far left. The integral converges only if the π^+ and π^- total cross sections become equal at high energy. This seems to be the case, but they are also increasing so some question about the degree of convergence can be raised. Of perhaps greater concern is that the high energy data does not provide complete coverage and may be of less accuracy. For this reason an independent determination of $J^{(-)}$ is of value.

3 Doubly subtracted dispersion relation

We use a dispersion relation for the π^-p amplitude subtracted at points $\omega = \pm\mu$ [6],

$$\mathrm{Re}F_-(\omega) = \frac{2k^2 f^2}{(\mu^2-\omega_N^2)(\omega_N-\omega)} + \frac{\omega+\mu}{2\mu}\tilde{a}_- - \frac{\omega-\mu}{2\mu}\tilde{a}_+ + I(\omega)\ ,$$

$$\text{with}\quad I(\omega) \equiv \frac{k^2}{4\pi^2} P\int_\mu^\infty \frac{1}{k'}\left[\frac{\sigma_-(\omega')}{\omega'-\omega} + \frac{\sigma_+(\omega')}{\omega'+\omega}\right] d\omega'\ ,$$

or

$$\mathrm{Re}F_-(\omega) - I(\omega) = -\frac{2(\mu^2-\omega\omega_N)f^2}{(\mu^2-\omega_N^2)(\omega_N-\omega)} + \omega J^{(-)} + \tilde{b}_0\ ,$$

where the last line uses the second definition for $J^{(-)}$ given above and $\tilde{b}_0 = [F_+(\mu) + F_-(\mu)]/2$. Crossing symmetry has been used. It is instructive to look at the three terms on the right hand side of the above equation since the coefficient of each term has it own interest. The integral $I(\omega)$ is determined from total cross section data as in the previous section. Fig. 1 shows the prediction compared with the Baillon data set [3] and indicates the contributions of the various terms in the dispersion relation.

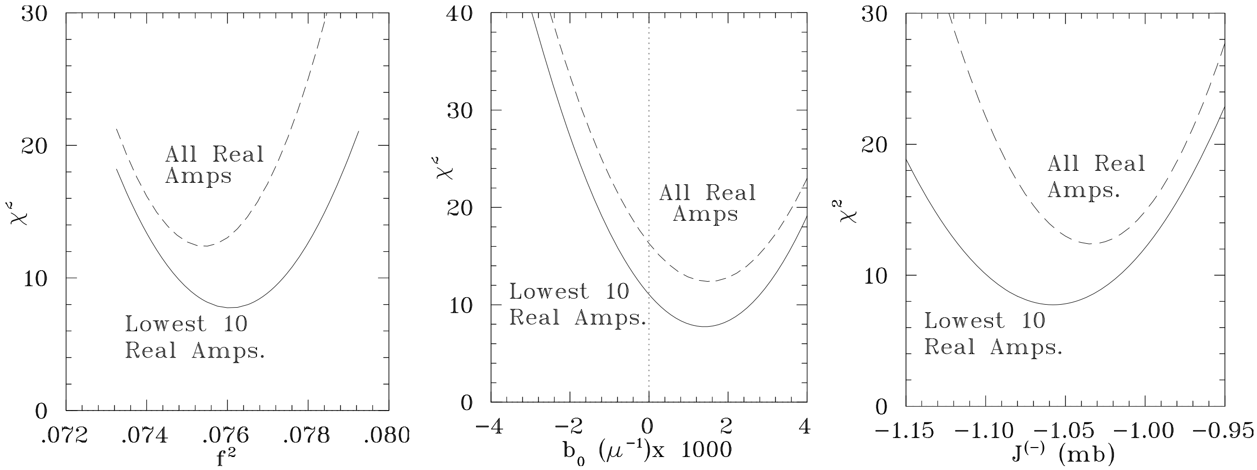

Figure 2: Comparison of the χ^2 from the fit to the parameters. The lowest 10 forward amplitudes are the two scattering lengths, one point from our previous analysis [7] at 50 MeV and the Baillon [3] data. The dashed curves include data up to 6 GeV/c from Ref. [8] to estimate the consistency with higher energy data.

To estimate the values of the parameters the dispersion relation for chosen values of f^2, $\tilde{b}_0$ and $J^{(-)}$ is used to generate a set of predictions for the real parts of the amplitudes. These predictions are used with the forward-scattering amplitude data and scattering lengths to calculate a value of χ^2. We have adopted the following scattering lengths:

$$\tilde{a}_- = 0.1434 \pm 0.0013 \text{ [Lab fm]} \sim 0.1248 \pm 0.0011 \text{ [CM fm]} \sim 0.0883 \pm 0.0008 \text{ [CM } \mu^{-1}] \ ,$$
$$\tilde{a}_+ = -0.1380 \pm 0.0024 \text{ [Lab fm]} \sim -0.1201 \pm 0.0021 \text{ [CM fm]} \sim -0.0850 \pm 0.0015 \text{ [CM } \mu^{-1}] \ ,$$

where $\tilde{a}_-$ is taken from the atomic data, and $\tilde{a}_+$ is taken from Ref. [7]. From the solid curves in Fig. 2 we find the values $f^2 = 0.0760 \pm 0.010$, $\tilde{b}_0 = 0.0014 \pm 0.0008$ and $J^{(-)} = -1.06 \pm 0.03$.

While this picture seems coherent there are questions regarding the extraction of the Coulomb effects (in particular from the total cross sections). One example is the transition from the Nordita corrections to the point Coulomb barriers in the VPI/GWU analysis.

Acknowledgment: This work was supported by the National Science Foundation.

References

[1] Total cross sections from the PDG, found at `http://pdg.lbl.gov/2000/contents_plots.html`.

[2] H.-Ch. Schröder *et al.*, Phys. Lett. **B469**, 25 (1999).

[3] P. Baillon, C. Bricman, M. Ferro-Luzzi, P. Jenni, J. M. Perreau, R. D. Tripp and T. Ypsilantis, Nucl. Phys. **B105**, 365 (1976).

[4] M. L. Goldberger, H. Miyazawa and R. Oehme, Phys. Rev. **99**, 986 (1955).

[5] VPI/GWU phase-shift analysis, available on the internet at `http://gwdac.phys.gwu.edu/`.

[6] For a derivation of this well-known relation see, for example, N. M. Queen and G. Violini, *Dispersion Theory in High-Energy Physics* (Halsted Press, 1974).

[7] W. R. Gibbs, Li Ai and W. B. Kaufmann, Phys. Rev. **C57**, 784 (1998).

[8] G. G. Vorob'ev, Sov. J. Nucl. Phys. **19**, 433 (1974). [The values of ReF were obtained by combining these (ReF)/(ImF) data with the ImF obtained from total cross sections.]

Meson-nucleon physics: Past, present and future

B. M. K. Nefkens

UCLA, Los Angeles, CA 90095, U.S.A.

(Received: 14 November 2001)

We will present some thoughts on the following topics:

1. Major highlights in the history of strong interactions such as isospin, the pion, SU(3), quarks, the color degree of freedom, QCD.

2. Topics of high current interest such as quark confinement, the origin of mass, the search for the gluon degrees of freedom, chiral symmetry, flavor symmetry, regularities in the properties of the light-baryon families (parity doublets, clusters) decay patterns, hadronization, chiral restoration, effective Lagrangians and their degrees of freedom.

3. The input parameters for QCD and for effective models.

4. Hadron physics as a necessary aspect of precision tests of the Standard Model and of the Search for New Physics.

1 Introduction

Some of the basic questions that have been discussed at MENU2001, our highly successful symposium which we are concluding this afternoon, are:

"Where are we in the study of Hadron Physics?"
"What has been accomplished recently in this field?"
"Which are the most interesting problems?"

I will endeavor to address these questions. In preparing this report I have been aided by the White Papers of two recent workshops, "Key Issues in Hadron Physics" [1], and the DNP meeting on Hadronic Physics [2], and two reports on the subject by James Bjorken [3,4].

We are at a momentous time in the short history of Hadronic Physics. There is a growing appreciation for the intellectual challenges presented by QCD in the non-perturbative regime, for the crucial role which it plays in precision tests of the Standard Model (SM), and in the search for New Physics beyond the SM. There is also a growing concern about the lack of a major laboratory for hadron physics with secondary beams. The practitioners of Hadron Physics are only loosely organized and they are seriously underfunded.

Our field of physics may be defined as follows [3]: "Hadron Physics is the physics of the hadronic structures and the strong - interacting vacuum". It is a subfield of quantum chromodynamics. QCD at short distance, $d \sim< 0.1$fm, is a perturbative theory of pointlike quarks and gluons. Its validity in this regime is well established, e.g. the strong coupling constant α_s has been determined in more than a dozen different ways [5] to an accuracy of a few percent; we also point to the very successful results coming from Z and W studies. At large distances such as > 2 fm, Hadron Physics is a theory of pions and nucleons and their strange counterparts. It is characterized by the spontaneous symmetry breaking of the approximate chiral symmetry of QCD. At intermediate distance occur a rich variety of phenomena including hadron resonances, Regge trajectories, soft diffractions and hadronization. Except for a few simple lattice - gauge calculations, the role of QCD is very limited; it mainly justifies the use of chiral symmetry, chiral perturbation theory, the N_c^{-1} expansion, and so forth. The real need for calculations of practical quantities is at intermediate energy. The mass of the proton and neutron have been measured to an accuracy of a few parts in 10^7. The best result of a recent lattice-gauge calculation [6] for the proton mass in 878±25 MeV. The hadronic corrections are now the main limitation to such interesting Standard-Model tests as the new muon anomalous magnetic moment or $g-2$ experiment [7], the measurement of CP violation in the $2\pi^0$ and $\pi^+\pi^-$ decay of K_L/K_S (the so called ϵ'/ϵ experiment) [8,9], the unitarity test of the CKM matrix [10] and precision determinations of α_s. At this MENU2001 symposium much of the full spectrum of non-perturbative QCD has been under the microscope.

2 Highlights from the rich history of hadron physics

It is all together appropriate to have a short recitation of major highlights of our field. They have led to the current models and effective Lagrangians of strong interaction physics, in particular, they led to the creation of our major theory, Quantum Chromodynamics, QCD.

a) One of the oldest concepts in nuclear physics is that of isospin. Its role in the development of the theory of strong interactions is hard to overstate. Isospin was an early attempt to formulate the universality of the strong interaction at a time when only the neutron and proton had been identified. Isospin paved the way for Yang-Mills fields and it helped to usher non-abelian theory into strong interaction physics. Isospin was one of the earliest cases of a broken symmetry. Now, at the beginning of the 21st century, we know the origin of isospin breaking: it is the difference in the masses and the electric charges of the up and down quarks. The study of isospin breaking occurring in the baryons and mesons of different spin and parity continues to be of great importance. It is the only way to determine the up-down quark mass difference in various hadronic environments [11]. Isospin violation leads to meson mixing for instance $\pi^0-\eta$ and $\rho-\omega$, also to baryon mixing such as $\Lambda-\Sigma^0$. The modern perspective is that isospin is a subgroup of a larger symmetry, the flavor symmetry of massless QCD.

b) The pion has had and still has a major impact on strong interaction physics, especially on phenomenological models for nucleon-nucleon scattering. The current viewpoint is that the pion is the lightest of the 3 Goldstone bosons that are associated with the spontaneous breaking of chiral symmetry of a massless QCD.

c) SU(3) symmetry was born out of the wealth of great baryon and meson spectroscopic data. Measurements of SU(3) breaking, for instance the mass difference of the baryon octet and decuplet ground states, are the sole way for obtaining the $s-d$ quark-mass difference. SU(3) breaking is responsible for multiplet impurity such as due to $\eta-\eta'$ mixing. SU(3) is a special subgroup of the (broken) flavor symmetry of QCD.

d) Perhaps the most astonishing discovery, which was prompted by abundant new spectroscopic data, was the quark being the ultimate hadronic building block. The quark has several spectacular properties such as a non-integral electric charge and baryon number. A single, free quark cannot be observed because it is captive to the asymptotic freedom condition of QCD.

e) The latest "quantum number" to be discovered is the color charge. Again it was the well established details of baryon spectroscopy, in this case the features of the Δ^{++} (1232) resonance, together with our faith in the validity of Fermi-Dirac statistics which brought this about.

f) QCD is now considered to be the theory of all strong interactions. It has many virtues but its major shortcoming is that it cannot be solved in the non-perturbative regime. Thus, it is helpless when one needs to calculate detailed properties of the proton, neutron and complex nuclei.

3 High-profile subjects

Problems and topics in hadron physics which are drawing considerable attention these days include the following.

a) What is the mechanism that is responsible for the confinement of the quarks? So far no one has succeeded in deriving the confinement conditions from QCD. This is a major theoretical challenge. Help could be provided by the determination of the regularities that characterize the confined quark systems. Parity doublets dominate the N^* spectra in the mass range 1600-2300 MeV [12]. Do they occur also for heavier masses? Parity doublets are also seen in in the Δ, Λ, Σ families. There is no evidence for parity doublets among the three light-quark meson families. Baryons above a certain mass appear to come in clusters as well. There is currently insufficient data to see if clusters extend to the N^* mass region above 2300 MeV.

An interesting analogy can be made to the confinement of the electron in the hydrogen atom. In this case confinement does not follow from Maxwell's equations which govern the electromagnetic interactions. Rather, confinement in the case of the hydrogen atom is the consequence of the quantization conditions from quantum mechanics. The major breakthrough to solving this historic confinement puzzle came from the interpretation of the experimentally discovered regularities in the frequencies of the spectral lines of the hydrogen atom known as the Rydberg formula. Maybe the spectra of the excited states of the light baryons could play the same role in helping to understand quark confinement.

b) What is the origin of the mass of the proton? Over 99% of the rest mass of everyone in this room and elsewhere is due to hadronic matter in the form of free and bound protons and neutrons The proton consists of two up and one down quark for the grand total of 18 MeV and similarly for the neutron. Where does the remaining 98% come from? The missing piece is called the quark condensate, it comes from the interaction of the quarks with the vacuum. This brings up the question: "What really is the vacuum?"

c) A fascinating subject is the proposed existence of new forms of matter: hybrids, glueballs, pentaquarks, bound states of mesons and baryons, molecular-type states, etc. There is a lot of speculation about this subject. Our main theory is QCD, the theory of interacting quarks and gluons, so we might expect that confined states have quark and gluon degrees of freedom. There is no example of a certified hybrid baryon, not even a single good candidate [12]. The established baryons all obey SU(3) flavor symmetry which implies that they are qqq states. There are a few candidates for a glueball and hybrid in the meson sector. Since there is no free meson target available a unique determination of the spin and parity of a candidate is hard to make and so far no polarized target data, which is very helpful, is available.

The many successes of the simple quark model (QM) are somewhat of a mystery. In the QM all baryons are qqq states and they can be classified in SU(3) multiplets. This implies one antisymmetric singlet state and two mixed octets with the same J^P, plus one related totally symmetric decuplet. All mesons are grouped in nonets with the same J^P; each one consists of one singlet and 8 octet states. The QM accounts for the main features, though not the details of the masses, widths, decay branching rations, magnetic dipole moments and strength of electromagnetic couplings of all established baryons and mesons. There is as yet no compelling evidence for a gluon degree of freedom. This leads us to the important question: "Where in hadron physics at low energy is the glue?"

Recently, a new large facility was put into operation for the important goal of discovering and subsequently determining the basic properties of the quark-gluon plasma. This new state of matter is high on the list of interests of many a nuclear theorist. It is important also to make the necessary investments to enable the measurements of the properties of hadronic matter at standard density and temperature. As a minimum we need to measure the mass, width, and branching ratios of the excited states of the 6 light baryon and 3 meson families, in particular of the Σ^*, Ξ^* and Ω^* states below 4 GeV.

d) Broken symmetries play a major role in the theory of the strong interactions. We think here of chiral symmetry, flavor symmetry with its sub areas of isospin and SU(3) symmetry and the U(1) symmetry. There has been considerable speculation on the occurrence of chiral restoration at intermediate energy [13] and some on U(1) restoration. Do there exist other symmetries which play a role in the structure of the baryons at ordinary density due to a diquark substructure of the baryons [14]? Are there other clues besides the occurrence of parity doublets? The parity doublets are seen in the baryon spectra above a certain mass which is 1600 MeV for the N^* family. By contrast they do not occur for the meson families. We recall the occurrence of the extraordinary S-wave η decays of the low lying $J^P = \frac{1}{2}^-$ octet baryons, the $N(1535)$, $\Lambda(1670)$ and $\Sigma(1750)$. It is of interest to see if this special η-decay feature occurs in the Ξ family as well. The above set of 3 states suggests the existence of a Ξ state with $J^P = \frac{1}{2}^-$ and a mass of approximately 1875 MeV.

The first excited state in the N^* family is the $N(1440)\frac{1}{2}^+$ and in the Λ^* it is the $\Lambda(1600)\frac{1}{2}^+$. They have the same spin/parity as the family's ground state and they are relatively broad. The same holds for the $\Delta(1600)\frac{3}{2}^+$, which is a decuplet state. We speculate that this phenomenon applies to the other baryon families as well and urge a search for a $\Sigma^*\ \frac{1}{2}^+$ octet state of mass ~ 1680 MeV as well as a $\Xi^*\ \frac{1}{2}^+$ octet state around 1800 MeV. Furthermore we anticipate a $\Sigma^*\ \frac{3}{2}^+$ decuplet state of mass ~ 1770 MeV, a $\Xi^*\ \frac{3}{2}^+$ decuplet state around ~ 1900 MeV and a $\Omega^*\ \frac{3}{2}^+$ at ~ 2050 MeV. All are expected to be relatively broad states.

e) Creation of matter out of energy is another important subject. The Einstein condition,

$$E^2 = p^2c^2 + m^2c^4 \ ,$$

which is incorporated in QCD does not say anything about changing energy into $q\bar{q}$ pairs and gluons. It would be quite useful to understand how the features of mass creation such as the simple reaction $\pi^- p \to \pi^0\pi^0 n$ come out of QCD. Chiral perturbation theory has been very successful in giving a detailed account of threshold π^0 photoproduction. The next step is the threshold production of the other two Goldstone bosons, the K and η. The creation of new particles at low energy is related to a process called hadronization in high energy physics. This is the creation of hadrons by a high energy quark or gluon in jet-type events.

It is desirable to make a systematic study of meson and baryon-antibaryon production using beams of $\pi^\pm, K^\pm, p, \bar{p},\ e^-$ and γ.

f) The development of effective models for the making of practical calculations of hadron-hadron scattering, resonance decay, and particle production is a mandatory aspect of our field. Which are the most suitable degrees of freedom to use? How complementary are the different models and how well does each model implement the symmetries of QCD? There is a large variety of strong interaction models to choose from: chiral perturbation theory, the N_c^{-1} expansion, Skyrmions, meson exchange, nuclear potentials, vector meson dominance, bag models, and so forth.

4 Input parameters to QCD and to effective Lagrangians.

QCD needs 3 types of input:

1. Λ_{QCD}, the fundamental strength scale; one can also choose the running coupling constant α_s. The experimental determination of this input is done using high energy experiments that operate in the perturbative regime of QCD. The present precision achieved is several percent. To go much beyond that one must first learn how to make the hadronic corrections which belong in the domain of non-perturbative QCD. The hadronic corrections are made using a suitable effective Lagrangian. Efforts are underway to use large computers and many new algorithms for lattice-gauge calculations; they still have a long way to go before becoming practical.

2. The masses of the six quarks. Since there are no free quarks the mass determinations are a joint endeavor of theory and experiment. What we know best is the ratio of quark mass differences.

3. The θ parameter of QCD. The upper limit on the electric dipole moment of the neutron provides an upper bound $\theta \leq 2 \times 10^{-10}$. It does not play a significant role in QCD at present.

The effective models needed for calculating strong interaction results in the non-perturbative regime of QCD require a large set of inputs. Many of these are discussed in detail at our MENU symposium and related workshops and conferences such as MESON 2001, Baryon 2001, NSTAR 2001 and PANIC. We mention a few inputs of the many needed:

- a) The meson decay constants: F_π, F_η, F_K, etc.
- b) The meson-nucleon coupling constants: $G_{\pi NN}$, $G_{\eta NN}$, etc.
- c) The meson-meson scattering lengths: $a_{\pi\pi}$, $a_{\eta\pi}$, etc.
- d) Various mixing angles such as the SU(3) singlet-octet mixing angles for the pseudoscalar and vector mesons etc.
- e) Hadron form factors for the proton, neutron and the light mesons.

5 Goals of Hadron Physics.

The meeting entitled "Key Issues in Hadronic Physics held in Duck, NC on Nov. 6–9 2001 provided the following useful formulation of the overall objectives of our field [1].

The primary goals of hadronic physics are to determine the relevant degrees of freedom that govern hadronic phenomena at all scales, to establish the connection of these degrees of freedom to the parameters and fundamental fields of QCD, and to use our understanding of QCD to quantitatively describe a wide array of hadronic phenomena, ranging from terrestrial nuclear physics to the behavior of matter in the early universe. We list below some very specific goals for the near future in our area.

1. The determination of the ratio of the difference and sum of the up and down current-quark masses,

$$R = \frac{m_d - m_u}{m_d + m_u} \ .$$

The ratio eliminates many of the conceptual problems arising from the fact that free quarks have never been observed, despite much searching, and are not expected to be seen as free particles. Experimentally, a nice, clean way to investigate the up-down quark mass difference is by a measurement of the absolute decay rate for the decay $\eta \to 3\pi$. Another good way is by an accurate measurement of the ratio

$$\frac{\Gamma(\eta \to \pi^+\pi^-\pi^0)}{\Gamma(\eta \to 3\pi^0)} \ .$$

Other ways include 2 special ratios of meson decay modes,

$$\frac{\Gamma(\eta' \to \eta\ 2\pi^0)}{\Gamma(\eta' \to 3\pi^0)} \ ,$$

and

$$\frac{\Gamma(\psi' \to \eta\psi)}{\Gamma(\psi' \to \pi^0\psi)} \ .$$

2. The determination of the ratio of quark-masses

$$\frac{m_s - m_u}{m_d + m_u}.$$

This requires careful measurements of SU(3) flavor breaking such as probed in the Gell-Mann-Okubo octet and Gell-Mann decuplet mass relations. This should be done for different spin/parity baryons.

3. It would be nice to have a full QCD calculation of the neutron-proton mass difference which is known experimentally to an accuracy of a few parts in 10^7.

4. It is time that we measured the magnetic dipole moment of other particles than the ground state octet and decuplet baryons.

5. The determination of $\pi^0 - \eta$ mixing in different nuclear environments.

6. Accurate measurements of the inputs to the various effective theories such as the meson-nucleon coupling constants, the meson-meson scattering lengths, the decay constants, and so forth.

6 The importance of Hadron Physics in testing the Standard Model.

The Standard Model (SM) of electroweak interactions has been subjected to many experimental tests and passed them all with flying colors. Yet, the SM is called a model and not a theory. It suffers from having 17 input parameters which must be extracted from many experiments and this does not include 3 or 6 possible neutrino masses and several mixing angles. The SM does not explain why there are three families of fundamental fermions; parity violation is inserted into the theory by choosing a left-handed doublet and a right-handed singlet of fermions in the input structure; the nature of the spontaneous symmetry breaking that generates the mass of the elementary fermions is unknown; these are just some of the shortcomings of the SM. New ideas, such as supersymmetry, are going beyond the classical SM. Experiments which explore the limits of the SM, euphemistically called "Searches for New Physics", are limited by the insufficiently known hadronic corrections. Since there is no analytic solution to QCD in the vast non-perturbative domain, one is forced to rely on effective Lagrangians and on models. Below are a few examples of recent precision measurements in the frontier of the SM, they involve real as well as virtual hadrons. The usefulness of the experiments is limited mainly by the uncertainties in the hadronic corrections.

1. The latest measurement of $g-2$, the anomalous g-value of the muon magnetic moment, made at BNL, is of sufficient precision to be sensitive to "New Physics" [7]. $g-2$ calculations have 3 components: a. the pure QED part, which is known to 0.025 *ppm*; b. the electroweak part known to 0.03 *ppm*; c. the hadronic corrections, which have an uncertainty of 0.57 *ppm*, originate in the higher order electromagnetic interactions of leptons arising from virtual hadronic contributions to the photon propagator. An important contribution comes from light-light scattering where the error is due mainly to the poorly known form factors of the intermediate π, η and η'. This can be improved if new measurements are made of single and particularly of double Dalitz decays such as $\eta \rightarrow e^+e^-\mu^+\mu^-$.

2. An important investigation into the nature of CP-violation is the determination of the ratio of the direct to indirect CP- violation parameters, ϵ to ϵ' [8,9]. This is done by measuring the ratio of K_L^0 and K_S^0 decay into $\pi^+\pi^-$ and $\pi^0\pi^0$ at the level 10^{-3} to 10^{-4}. It is immediately clear that at this level the hadronic corrections originating in the $s-d$ quark transition and the isospin breaking due to the $u-d$ quark mass difference are major, they greatly cloud the interpretation of the precision measurements.

3. CP violation has finally been seen outside the $K^0 - \bar{K}^0$ system namely in B decays at the $B/\bar{B}$ and Belle storage [15,16] rings. The data are subject to similar type corrections as in K-decays.

4. The Standard Model requires that the Kobayashi-Maskawa-Cabbibo (CKM) matrix is a unitary matrix. This has not been verified to any desirable precision. The CKM matrix provides a test in which supersymmetry could show up before the LHC turns on. This test requires only accurate values for V_{ud} and V_{us}; V_{ub} is very small and is known well enough for the purpose. V_{ud} is being measured in super-allowed beta decays, also in neutron decay. V_{us} must be obtained from a precision measurement of the decay rate and spectrum of K_{e3} decay, $K^+ \rightarrow \pi^0 e^+ v$. The limits are

due to the uncertainties in the handling of SU(3) breaking and isospin violation, if the latter is a surprise it is due to $\pi^0 - \eta$ mixing in the final state.

5. Another area where the hadronic corrections limit the accuracy of the results is the determination of the input parameters to QCD and the SM. The success of perturbative QCD may be illustrated compactly by the internal agreement on the average value of the strong coupling parameter α_s obtained in 12 different ways [5]. The average value quoted [5] is $\alpha_s(M_z) = 0.1181 \pm 0.002$. To do much better one needs to know the masses of the quarks for which one depends on non-perturbative QCD!

Our conclusion is that major advances in the frontier of particle and nuclear physics depend on the advances that are being made in the physics of the non-perturbative sector.

Acknowledgments

It is my pleasure to express the heartfelt appreciation of the participants for the dedicated efforts in organizing this very successful International Symposium MENU2001 made by Bill Briscoe and Helmut Haberzettl and their dedicated staff. Their countless hours of unheralded work on visitor matters, subsidies, program balance and all the organizational details have paid off handsomely. MENU2001 will be recorded in the annals of hadron-physics history as a four-star conference, the highest rating we can bestow.

References

[1] "Key Issues in Hadronic Physics", White Paper of Hadron Workshop, Duck, NC Nov. 6 – 9, 2000.

[2] Proceedings of the DNP Meeting on Hadronic Physics, JLab, Dec 16 – 4, (2000).

[3] "What's New in Hadron Physics", J. Bjorken, talk given at Intersections (2000).

[4] "Why Hadron Physics", J. Bjorken, to be published.

[5] "Review of Particle Physics", by the Particle Data Group, D.E. Groom et al., Eur. Phys. J. C **15**, 401 (2000).

[6] CP-PACS, S. Aoki et al., Phys. Rev. Lett. **84**, 238 (2000).

[7] Muon $(g-2)$ Collaboration, H.N. Brown et al., Phys. Rev. Lett. **86**, 2227 (2001).

[8] KTEV Collaboration, A. Alavi-Harati et al., Phys. Rev. Lett **83**, 22 (1999).

[9] NA48 Collaboration, V. Fanti et al., Phys. Lett. **B465**, 335 (1999).

[10] Crystal Ball Collaboration, AGS proposal #927, B. Nefkens et al., UCLA report.

[11] G. Miller, B. Nefkens and I. Slaus, Physics Reports **194**, p.1 (1990).

[12] B. Nefkens and J.W. Price, contribution to this conference.

[13] G.E. Brown, M. Buballa and M. Rho, Nucl. Phys. **A609,** 519 (1996).

[14] M. Anselmo and E. Predazzi, Rev. of Mod. Phys. **65,** 1199 (1993).

[15] Babar Collaboration, B. Aubert et al., Phys. Rev. Lett. **87,** 091801 (2001).

[16] Belle Collaboration, K. Abe et al., Phys. Rev. Lett. **87**, 091802 (2001).

Chiral dynamics and pion-nucleon scattering around the $N^*(1535)$ resonance

T. Inoue, J.C. Nacher, M.J. Vicente Vacas, and E. Oset

Departamento de Física Teórica and IFIC, Centro Mixto Universidad de Valencia-CSIC Institutos de Investigación de Paterna, Apdo. correos 22085, 46071, Valencia, Spain

(Received: 30 October 2001)

We study here the S-wave interaction of mesons with baryons in the strangeness $S = 0$ sector in a coupled channel unitary approach. See ref. [1] for details.

1 Introduction

The various meson-baryon scatterings are studied in a chiral unitary model with the Bethe-Salpeter equation, where the on-shell amplitudes are factorized and the BS equation is reduced to an algebraic equation [2–6]. The scattering matrix at the total center of mass energy $\sqrt{s}$, is given by

$$T(\sqrt{s}) = [1 - V(\sqrt{s})G(\sqrt{s})]^{-1}V(\sqrt{s}) \ , \tag{1}$$

where V is a transition potential matrix and G is a diagonal matrix representing the loop integral of a meson and a baryon. The matrix V is taken from the lowest order chiral Lagrangian involving mesons and baryons. For example, in the case of S-wave, V is written as

$$V_{ij}(\sqrt{s}) = -C_{ij}\frac{1}{4f^2}\bar{u}(p')\gamma^\mu u(p)(k_\mu + k'_\mu) \ , \tag{2}$$

with the meson weak decay constant f, and the initial(final) meson momentum k (k'). The coefficients C_{ij} which reflect the flavor symmetry of the problem, are obtained from the Lagrangian. The divergent loop integral G defined by

$$G_i(\sqrt{s}) = i\int\frac{d^4q}{(2\pi)^4}\,\frac{2M_i}{(P-q)^2 - M_i^2 + i\epsilon}\,\frac{1}{q^2 - m_i^2 + i\epsilon} \ , \tag{3}$$

with $P \equiv (\sqrt{s}, \vec{0})$ and the baryon(meson) mass $M_i(m_i)$, is done with some regularization. The finite contribution of the renormalization which appears in the real part of $G_i(\sqrt{s})$, is treated as an unknown parameter and determined through the fitting to the data. The imaginary part of $G_i(\sqrt{s})$ is proportional to the phase space and ensures unitarity. For example, with the dimensional regularization, the integral is calculated as

$$\begin{aligned}
\mathrm{G}_i(\sqrt{s}) = \frac{2M_i}{(4\pi)^2}\Bigg\{ & a_i(\mu) + \log\frac{m_i^2}{\mu^2} + \frac{M_i^2 - m_i^2 + s}{2s}\log\frac{M_i^2}{m_i^2} \\
& + \frac{Q_i(\sqrt{s})}{\sqrt{s}}\log\left(s - (M_i^2 - m_i^2) + 2\sqrt{s}Q_i(\sqrt{s})\right) + \frac{Q_i(\sqrt{s})}{\sqrt{s}}\log\left(s + (M_i^2 - m_i^2) + 2\sqrt{s}Q_i(\sqrt{s})\right) \\
& - \frac{Q_i(\sqrt{s})}{\sqrt{s}}\log\left(-s + (M_i^2 - m_i^2) + 2\sqrt{s}Q_i(\sqrt{s})\right) - \frac{Q_i(\sqrt{s})}{\sqrt{s}}\log\left(-s - (M_i^2 - m_i^2) + 2\sqrt{s}Q_i(\sqrt{s})\right)\Bigg\} ,
\end{aligned} \tag{4}$$

where $a_i(\mu)$ is the contribution of the higher order counter terms and $Q_i(\sqrt{s})$ is the on-shell center of mass momentum of i-th meson-baryon system [5].

To study the pion-nucleon scattering, the six coupled meson-baryon systems, { $\pi^- p$, $\pi^0 n$, ηn, $K^+\Sigma^-$, $K^0\Sigma^0$, and $K^0\Lambda$ }, are considered. It is found that qualitatively good S-wave scattering amplitudes are obtained with appropriate values of $a_i(\mu)$ [4]. However, in this simple model, quantitative agreement is not achieved, particularly in the isospin 3/2 sector. In this paper, we improve this model and try to reproduce the πN scattering in a wide energy range.

2 VMD inspired chiral coefficients and the $\pi\pi N$ channels

First, we recall that the S-wave meson-baryon amplitudes from the lowest order chiral Lagrangian are equivalent to the amplitudes of vector meson exchange in the t-channel, in the vector meson dominance(VMD) hypothesis. This indicates that the Lagrangian is the effective manifestation of the vector meson exchange mechanism. According to this consideration, we introduce the following correction to the chiral coefficient to account for the momentum transfer dependence of the vector meson propagator

$$C_{ij} \to C_{ij} \times \int \frac{d\hat{k}'}{4\pi} \frac{-m_v^2}{(k'-k)^2 - m_v^2} \qquad \text{at} \qquad \sqrt{s} > \sqrt{s_{ij}^0}\ , \tag{5}$$

where $\sqrt{s_{ij}^0}$ is the energy where the integral of (5) is unity, and which appears in between the thresholds of the two i, j channels. At low energies, this correction is negligible but this is not the case at the intermediate energies studied here. In fact the ρ meson tail, with $m_\rho = 770$ MeV, reduces the $\pi^- p \leftrightarrow \pi^- p$ element about 25% at energies around 1500 MeV.

Second, we extend our model to include the $\pi\pi N$ channels and $\pi N \leftrightarrow \pi\pi N$ transitions. We consider the BS equation (1) with the eight coupled channels including the six meson-baryon channels and two $\pi\pi N$ channels, $\pi^0\pi^- p$ and $\pi^+\pi^- n$. The $\pi^0\pi^0 n$ channel is not included because it does not couple to the S-wave πN. We treat the transition potentials of S-wave $\pi N \leftrightarrow \pi\pi N$ as free inputs and determine them so that they account for the data. We introduce a two loop integral $\tilde{G}(\sqrt{s})$ for the intermediate $\pi\pi N$ state

$$\tilde{G}(\sqrt{s}) = i^2 \int \frac{d^4 q_1}{(2\pi)^4} \int \frac{d^4 q_2}{(2\pi)^4} (\vec{q}_1 - \vec{q}_2)^2 \frac{2M_N}{(P - q_1 - q_2)^2 - M_N^2 + i\epsilon} \frac{1}{q_1^2 - m_\pi^2 + i\epsilon} \frac{1}{q_2^2 - m_\pi^2 + i\epsilon}\ , \tag{6}$$

which includes the vertex structure for the factorization. The real part of $\tilde{G}(\sqrt{s})$ in the renormalized model has several subtraction terms to be fixed by the data and we find it to be compatible with zero.

3 Results and discussions

By varying the input $\pi N \leftrightarrow \pi\pi N$ potential and the subtractions in the real part of loop integrals, we find a reasonable set of them which reproduce both the elastic πN scattering and the pion production cross sections simultaneously. The subtraction parameters $a_i(\mu)$ for the meson-baryon loop integrals which we obtain are

$$\mu = 1200 \text{ MeV}\ , \quad a_{\pi N}(\mu) = 2.0\ , \quad a_{\eta N}(\mu) = 0.1\ , \quad a_{K\Lambda}(\mu) = 1.5\ , \quad a_{K\Sigma}(\mu) = -2.8\ . \tag{7}$$

The determined S-wave $\pi N \leftrightarrow \pi\pi N$ amplitudes a_{11}(isospin 1/2) and a_{31} (isospin 3/2) are shown in Fig.1, where we compare the real part of them with two empirical ones [7,8]. The lower energy

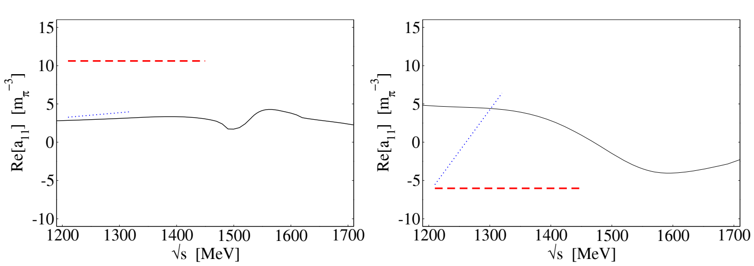

Figure 1: The S-wave $\pi N \leftrightarrow \pi\pi N$ amplitudes a_{11} and a_{31}. The solid lines are the real part obtained in the present model. The dashed and dotted lines are those of [7] and [8] respectively.

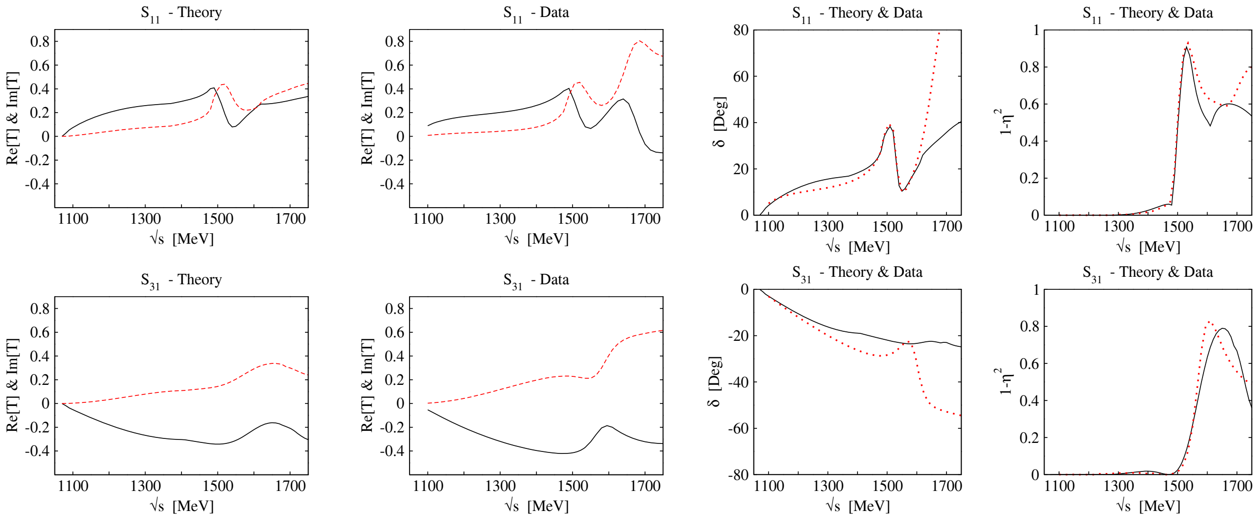

Figure 2: Scattering amplitudes, phase-shifts and inelasticities for the S_{11} and S_{31} πN partial waves. The solid (dashed) lines in amplitudes are the real (imaginary) parts. The dotted lines in the phase-shifts and inelasticities correspond to the data analysis of ref. [9].

part of the our $a_{11}(\sqrt{s})$ agrees with that of the paper [8] but it is quite different from the one of [7]. On the other hand our $a_{31}(\sqrt{s})$ amplitude is different from both [7] and [8]. While it is possible to reproduce the $\pi N \to \pi\pi N$ cross sections with the three set of amplitudes, a simultaneous description of the $\pi N \to \pi\pi N$ cross sections and the $\pi N \to \pi N$ scattering date is not possible with the amplitude of [7] and [8].

The resulting scattering amplitudes, phase-shifts and inelasticities for the S_{11} (isospin 1/2) and S_{31} (isospin 3/2) πN partial waves, are shown in Fig.2. One can see that results agree with the data in the energy range from threshold to 1600 MeV. We cannot obtain agreement in such a broad range without the correction of the chiral coefficient. It shows the importance of the correction. Another important thing to note is that, as seen in this figure, the inelasticities are well reproduced even at low energies in both S_{11} and S_{31}. These are provided by the $\pi\pi N$ channels. If $\pi\pi N$ channels are not included, the inelasticities of $S_{11}(S_{31})$ below 1487 (1690) MeV are zero and do not agree with data.

Acknowledgments: This work has been partly supported by the Spanish Ministry of Education in the program "Estancias de Doctores y Tecnólogos Extranjeros en España", by the DGICYT contract number BFM2000-1326 and by the EU TMR network Eurodaphne, contact no. ERBFMRX-CT98-0169.

References

[1] T. Inoue, M.J. Vicente Vacas and E. Oset, hep-ph/0110333

[2] N. Kaiser, T. Wass, W. Weise, Nucl. Phys. **A612**, 297 (1997)

[3] J.A. Oller, E. Oset and A. Ramos, Prog. Part. Nucl. Phys. **45**, 157 (2000).

[4] J.C. Nacher, *et al.* , Nucl. Phys. **A678**, 187 (2000).

[5] J.A. Oller and Ulf-G. Meissner, Phys. Lett. **B500**, 263 (2001).

[6] J. Nieves and E. Ruiz Arriola, hep-ph/0104307.

[7] D. Mark Manley, Phys. Rev. **D30**, 536 (1984).

[8] H. Bukhardt and J. Lowe, Phys. Rev. Lett. **67**, 2622 (1991).

[9] Center for Nuclear Studies, http://gwdac.phys.gwu.edu/.

An isobar model study of η photoproduction and electroproduction

Wen-Tai Chiang[a], Dieter Drechsel[b], Lothar Tiator[b], and Shin Nan Yang[a]

[a] *Department of Physics, National Taiwan University, Taipei 10617, Taiwan*
[b] *Institut für Kernphysik, Universität Mainz, 55099 Mainz, Germany*

(Received: 31 October 2001)

We study η photo- and electroproduction on the nucleon using an isobar model, and compare the results with recent data. The model contains contributions from Born terms, vector meson exchanges, and nucleon resonances. Besides the dominant $S_{11}(1535)$, we show that the second S_{11} resonance, $S_{11}(1650)$, is required in order to extract $S_{11}(1535)$ resonance parameters properly. For electroproduction, the Q^2 dependence of the photon helicity amplitude $A^p_{1/2}(Q^2)$ for $S_{11}(1535)$ extracted from this model is presented. This model (ETA-MAID) is implemented as a part of the MAID program.

Eta photo- and electroproduction on the nucleon, $\gamma^* N \to \eta N$, provide an alternative tool to study N^* besides πN scattering and pion photoproduction. There are fewer resonances involved since the ηN state couples to N^* with isospin $I = 1/2$ only. Therefore, this process is cleaner and more selective to distinguish certain resonances than other processes, e.g., pion photoproduction. This provides opportunities to access less studied resonances and possibly the "missing resonances".

The isobar model used in this work is closely related to the unitary isobar model (MAID) developed by Drechsel *et al.* [1]. The major difference from MAID is the lack of the unitarization procedure since the necessary information on ηN scattering is not available for η production. In this isobar model, the nonresonant background contains the usual Born terms and vector meson exchanges. It is obtained by evaluating the Feynman diagrams derived from an effective Lagrangian. In addition to the dominant $S_{11}(1535)$, we also consider N^* contributions from $D_{13}(1520)$, $S_{11}(1650)$, $D_{15}(1675)$, $F_{15}(1680)$, $D_{13}(1700)$, $P_{11}(1710)$, and $P_{13}(1720)$. For the relevant multipoles $\mathcal{M}_{\ell\pm}$ ($= E_{\ell\pm}$, $M_{\ell\pm}$, $S_{\ell\pm}$) of the resonance contributions, we assume a Breit-Wigner form

$$\mathcal{M}_{\ell\pm}(W,Q^2) = \tilde{\mathcal{M}}_{\ell\pm}(Q^2)\,\frac{W_R\Gamma_{\rm tot}(W)}{W_R^2 - W^2 - iW_R\Gamma_{\rm tot}(W)}\, f_{\eta N}(W)\, C_{\eta N}\ , \tag{1}$$

where $f_{\eta N}(W)$ is the usual Breit-Wigner factor describing the decay of the $N^* \to \eta N$, the isospin factor $C_{\eta N}$ is -1, and $\zeta_{\eta N} = \pm 1$ describes the relative sign between $N^* \to \eta N$ and $N^* \to \pi N$ couplings. The total width $\Gamma_{\rm tot}$ here is taken as the sum of $\Gamma_{\eta N} + \Gamma_{\pi N} + \Gamma_{\pi\pi N}$, and each partial decay width is given a proper energy dependence form. More details for our isobar model can be found in our recent paper [2].

Applying our isobar model, we have fitted recent photoproduction data including total and differential cross sections from TAPS (MAMI/Mainz) [3] and GRAAL [4], as well as the polarized beam asymmetry from GRAAL [5]. Our results for the total cross section are shown in Fig. 1, and compared with the TAPS and GRAAL data. They are in good agreement except for the bump observed in the GRAAL data in the region $E_\gamma^{\rm lab} = 1050$ to 1100 MeV that can not be reproduced in our model. However, note that the total cross section of the GRAAL data is obtained from integrating the differential cross sections, by use of a polynomial fit in $\cos\theta$ for extrapolation to the uncovered region. Therefore, the proper way to figure out the discrepancy is to compare the differential cross sections directly. In Fig. 2, we plot the differential cross sections at four different energies between $E_\gamma^{\rm lab} = 1050$ - 1100 MeV where the bump occurs. It is seen from these differential cross sections that there are no obvious differences, except for the forward angles, where the error bars are quite big. Therefore, we conclude that the discrepancy is due to the extrapolation of the GRAAL data to the forward angles and not heavily supported by the data themselves.

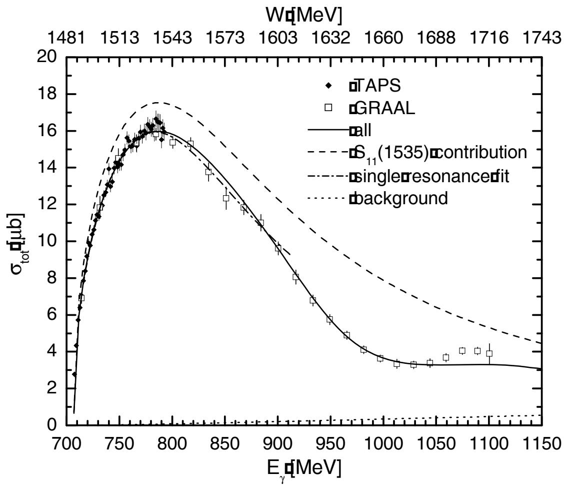

Figure 1: Total cross section for $\gamma p \to \eta p$. The data are from TAPS [3] and GRAAL [4].

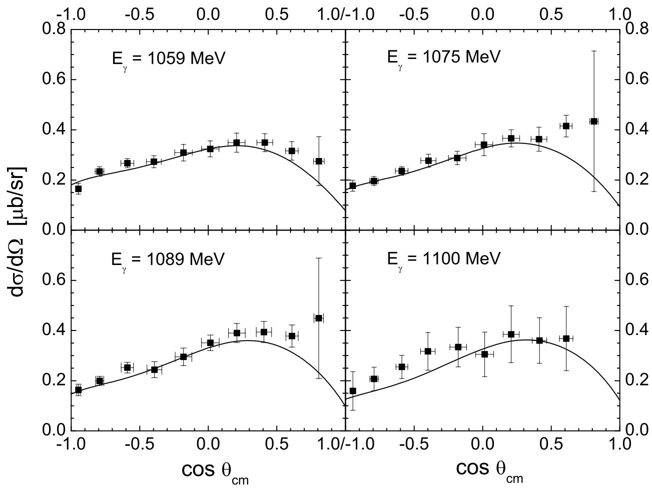

Figure 2: Differential cross section for $\gamma p \to \eta p$ at energies between $E_\gamma^{\rm lab}$ = 1050 - 1100 MeV. The data are from GRAAL [4].

Fig. 1 shows that the background contribution is very small, and the total cross section is dominated by the $S_{11}(1535)$ at low energy. However, the contribution from the second resonance, $S_{11}(1650)$, can not be neglected. Even though a single S_{11} resonance can fit the low energy data nicely up to $E_\gamma^{\rm lab} = 910$ MeV (the dash-dotted curve in Fig. 1), it can by no means describe the higher energy region. Moreover, the single resonance fit yields incorrect resonance parameters, as shown in Table 1. In fact, the decay width and photon coupling obtained in the single S_{11} resonance fit are significantly smaller than the full results when both S_{11} resonances are properly included.

In electroproduction, we assume the form for the Q^2 dependence of the $S_{11}(1535)$ resonance

$$A^p_{1/2}(Q^2) = A^p_{1/2}(0)\, \frac{1 + s_n\, Q^2}{1 + s_d\, Q^2}\, F_D(Q^2)\ , \tag{2}$$

where s_n and s_d are taken as parameters to be determined. For the other resonances considered in this study, we adopt the Q^2 dependence given by the single quark transition model [6] as used in MAID, and modify the $Q^2 \le 1$ (GeV/c)^2 region to comply our photoproduction ($Q = 0$) fit values. Therefore, we fit the electroproduction data with only two new parameters, s_n and s_d. The rest of the parameters are fixed from the photoproduction fit. There are two recent η electroproduction data sets from Jefferson Lab: Armstrong *et al.* [7] and Thompson *et al.* [8]. When fitting these electroproduction data, we fix all the parameters determined from the photoproduction data except for the Q^2 dependence of the helicity amplitudes $A^p_{1/2,\,3/2}(Q^2)$. The Q^2 dependence of the $S_{11}(1535)$ is described by the form of Eq. (2), and the parameters s_n and s_d are determined from

Table 1: Parameters of the $S_{11}(1535)$ resonance. The results of the single resonance fit are obtained by performing the fit to low energy data using only one S_{11} resonance. The second row is the our full result including two S_{11} resonances.

Fit	Mass [MeV]	Width [MeV]	$A^p_{1/2}$ [10^{-3} GeV$^{-1/2}$]	$\beta^{S_{11}(1535)}_{\eta N}$
Single S_{11} resonance fit	1536	159	103	50%
Double S_{11} resonance fit	1541	191	118	50%

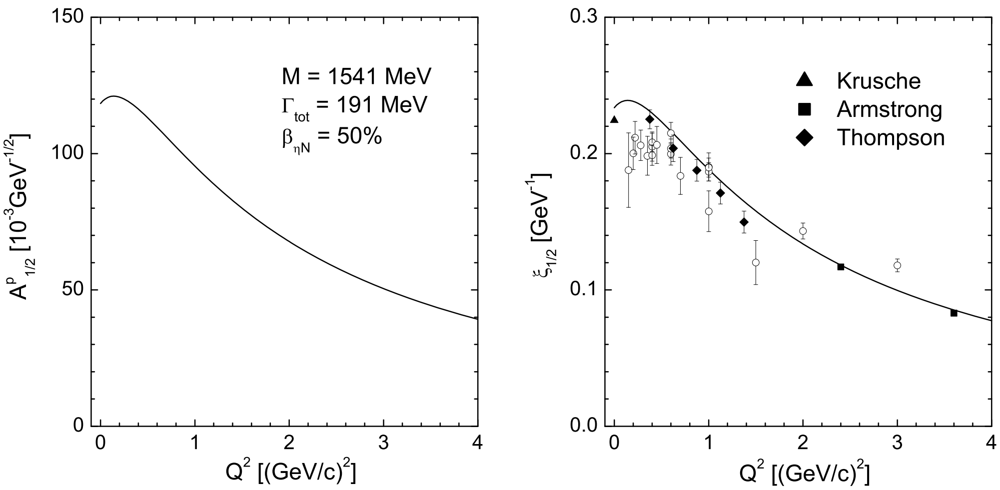

Figure 3: Left panel: Our results for the photon helicity amplitude $A^p_{1/2}(Q^2)$ for $S_{11}(1535) \to \gamma p$. Right panel: The result for the quantity $\xi_{1/2}$ compared with the values extracted from recent JLab data: Armstrong *et al.* [7] and Thompson *et al.* [8], and previous data from Ref. [10]. The photoproduction data point ($Q^2 = 0$) is from Krusche *et al.* [3].

electroproduction data. Fitting all the JLab data, we obtain the results: $s_n = 2.394$ (GeV/c)$^{-2}$ and $s_d = 0.085$ (GeV/c)$^{-2}$.

In Fig. 3 we show our result for the Q^2 dependence of the photon helicity amplitude $A^p_{1/2}(Q^2)$ for $S_{11}(1535) \to \gamma p$. In order to avoid large model uncertainties arising from different values of partial and total widths of the $S_{11}(1535)$ employed in different analyses, we choose not to compare with the helicity amplitudes $A^p_{1/2}(Q^2)$ extracted from other analyses directly. Instead, we compare the nearly model-independent quantity, $\xi_\lambda = A_\lambda \sqrt{m_N k_R \beta_{\eta N}/M_R q_R \Gamma_{\rm tot}}$, introduced by Benmerrouche *et al.* [9]. As opposed to the uncertainty from $\beta_{\eta N}$ and $\Gamma_{\rm tot}$ between different analyses, the quantity ξ_λ is almost independent of the extraction process. In Fig. 3 we compare our $\xi_{1/2}(Q^2)$ values for $S_{11}(1535)$ with the ones extracted from the recent JLab data [7, 8] and older data [10]. It is seen that overall good agreement is achieved up to $Q^2 = 4.0$ (GeV/c)^2.

Acknowledgments: This work was supported in parts by the National Science Council of ROC under Grant No. NSC89-2112-M002-078, by Deutsche Forschungsgemeinschaft (SFB 443), and by a joint project NSC/DFG TAI-113/10/0.

References

[1] D. Drechsel, O. Hanstein, S.S. Kamalov, and L. Tiator, Nucl. Phys. A645 (1999) 145.
[2] W.-T. Chiang, S.N. Yang, L. Tiator and D. Drechsel, arXiv: nucl-th/0110034.
[3] B. Krusche *et al.*, Phys. Rev. Lett. 74 (1995) 3736.
[4] F. Renard *et al.*, arXiv: hep-ex/0011098.
[5] J. Ajaka *et al.*, Phys. Rev. Lett. 81 (1998) 1797.
[6] V. Burkert and Zh. Li, Phys. Rev. D47 (1993) 46.
[7] C.S. Armstrong *et al.*, Phys. Rev. D60 (1999) 052004.
[8] R. Thompson *et al.*, Phys. Rev. Lett. 86 (2001) 1702.
[9] M. Benmerrouche, N.C. Mukhopadhyay and J.F. Zhang, Phys. Rev. D51 (1995) 3237.
[10] F.W. Brasse *et al.*, Nucl. Phys. B139 (1978) 37; F.W. Brasse *et al.*, Z. Phys. C22 (1984) 33; U. Beck *et al.*, Phys. Lett. B51 (1974) 103; H. Breuker *et al.*, Phys. Lett. B74 (1978) 409.

Pion-proton cross sections in the Coulomb-nuclear-interference region

Holger Denz
for the CHAOS collaboration

Physikalisches Institut, Universität Tübingen,
Auf der Morgenstelle 14, 72076 Tübingen, Germany

(Received: 31 October 2001)

Improved measurements of elastic πp-cross sections at low energies are crucial for a good determination of the value of the sigma-term. The CNI experiment at TRIUMF using the CHAOS spectrometer measured differential cross sections, with emphasis on small angles, at several energies between 15 and 67 MeV, covering a large angular range. The analysis of the data is in progress.

1 Motivation

The πp sigma-term is an important parameter in chiral perturbation theory and a measure of explicit chiral symmetry breaking:

$$\sigma_{\pi p} = \frac{m_u + m_d}{4M} \langle p | \bar{u}u + \bar{d}d | p \rangle \ ,$$

Its value can be extracted from πp scattering data. However, despite continuous efforts, it is still not well known, and published values vary widely [1,2].

An important reason for this are problems in the scattering database for low-energy πp-scattering. Inconsistencies and missing information in the existing data sets still impede a reliable extraction. To extract the sigma-term from πp scattering data, the scattering amplitudes have to be extrapolated to sub-threshold. Thus, a better knowledge of the low-energy region is crucial to overcome this problem. Additionally, measurements of elastic $\pi^{\pm}$p-scattering in the Coulomb-Nuclear interference (CNI) region at small angles, where the hadronic and the Coulomb scattering amplitude are of the same order of magnitude and interference effects between those 2 amplitudes play a role, allow a direct access to the isospin-even forward scattering amplitude [3] which is used in the determination of the πp sigma-term.

The CNI experiment [4,5] addresses these problems by measuring elastic $\pi^{\pm}$p differential cross sections at low energy and over a large angular range, including the CNI region down to about 6 degrees, with a statistical precision of better than two percent in one-degree angular bins. The goal is to provide a consistent set of low-energy scattering cross sections.

2 Experiment

The CNI experiment was carried out at the TRIUMF research facility in Vancouver, Canada, using the CHAOS spectrometer.

CHAOS is a magnetic spectrometer consisting of 4 concentric rings of wire chambers (WC1-4) to measure the tracks of charged particles, surrounded by plastic scintillator and leadglass detector blocks (CFT) for triggering purposes and particle identification. It has a large in-plane acceptance, the out-of-plane acceptance is ± 7 degrees. The magnetic field is oriented perpendicular to the scattering plane. Using the wire chamber information, the tracks of the incoming and scattered pion can be reconstructed, and the momentum of the scattered particle and the scattering angle can be determined.

For the CNI experiment, a liquid hydrogen target was inserted through a hole in the top magnet lid into the central region of the detector. The target cell contains 80 ccm of liquid hydrogen and has

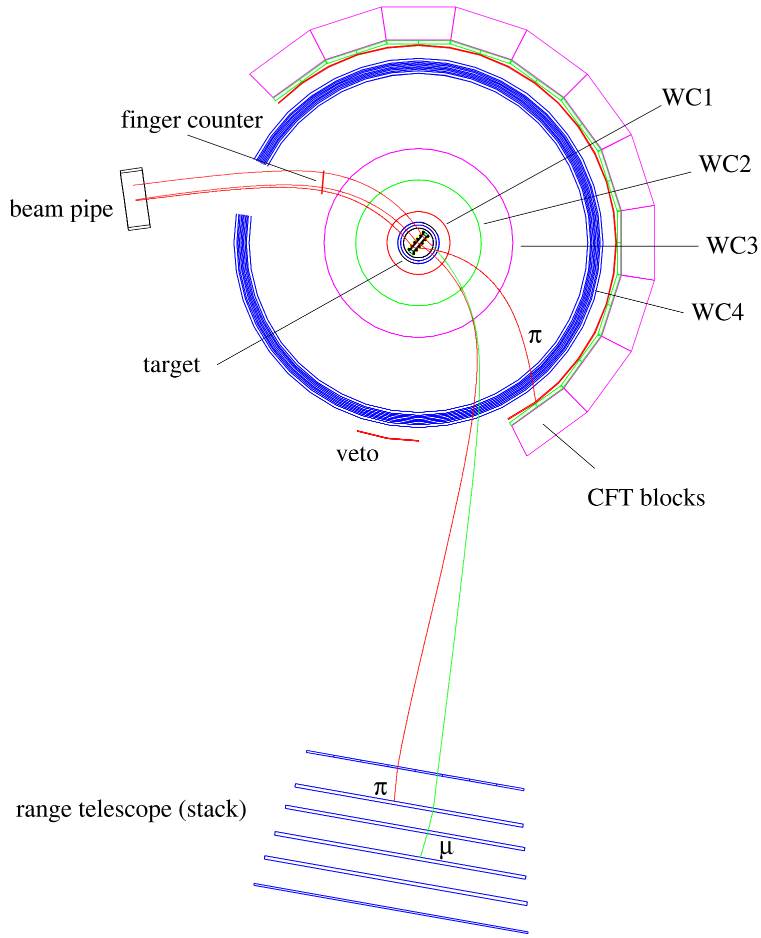

Figure 1: CHAOS in CNI setup

a flat geometry with a thickness of 12.5 mm. Background from surrounding material was subtracted by vertex reconstruction and, in the case of the innermost target windows, by subtracting empty target runs.

For normalisation purposes μp cross sections were measured simultanously. Beam particles were identified as $\pi/\mu/$e by their time of flight from the production target to the CHAOS detector.

A large source of background in this experiment was the decay of pions into muons in the detector. At low energies especially the forward angle region is heavily contaminated by decay muons. Because of the low energies of recoil protons a coincidence requirement cannot be used for background suppression.

Furthermore, muons from pion decays in the target region have a very similar signature to scattered pions. Only part of the muon decays can be identified by their kinematics. The remaining muons are identified with a range telescope installed in the forward angle region instead of the usual CFT blocks.

This range telescope consists of 6 layers of plastic scintillator with Aluminium absorbers of suitable thickness between the layers. The thickness of these absorbers can be varied to adjust the detector for different energies. Due to the slightly different energy loss pions and muons are stopped in different layers of the detector. The energy deposition in the single layers, the range in the detector and the time of flight to the first layer is used to identify the particles. To achieve a good particle identification, the decision is made by an appropriately trained neural network [6].

The first layer of the telescope is segmented into 8 paddles. This allows the prescaling of events at low angles, which is important due to the steep rise in the cross sections towards small angles.

Using this setup is a crucial ingredient to make a measurement in the Coulomb-Nuclear Interference region at small angles feasible.

3 Status

The experiment had a total of 10 months of beamtime from March 1999 to December 2000, we took data at 8 energies (15, 20, 26, 33, 40, 45, 57 and 67 MeV). In total, about 3.2 TB of data were taken. The skimming (generating a reduced data set) is finished, and the analysis of the data is in progress. Final results should be available in 2003.

Acknowledgments: We gratefully acknowledge financial support by the National Science and Engineering Research Council of Canada, The Instituto Nazionale di Fisica Nucleare, Italy, the Australian Research Council, the California State University Sacramento Foundation, the Bundesministerium für Bildung und Forschung (06 TU 987) and the Deutsche Forschungsgemeinschaft (European Graduate School Basel-Tübingen).

References

[1] M. Knecht, πN Newsletter **15**, 108 (1999).

[2] Papers by M. Pavan, M. Sainio, and M.G. Olsson, these Proceedings.

[3] Ch. Joram *et al.*, Phys. Rev. **C 51**, 2144 (1995).

[4] TRIUMF research proposal E778, G. Smith *et al.*, $\pi^{\pm}$p Differential Cross Sections in the Coulomb-Nuclear Interference Region (1996).

[5] G. R. Smith, πN Newsletter **15**, 19 (1999).

[6] E. Fragiacomo *et al.*, Nuclear Instruments and Methods in Physics Research **A 439**, 45 (2000).

Measurement of analyzing powers in πp scattering

M. Cröni[1], B. van den Brandt[2], R. Bilger[1], J. Breitschopf[1], H. Clement[1], J. Comfort[5], H. Denz[1], K. Föhl[4], E. Friedman[6], J. Gräter[1], P. Hautle[2], G. J. Hofman[3], P. Jesinger[1], J. A. Konter[2], S. Mango[2], R. Meier[1], M. Pavan[3], J. Pätzold[1], G. J. Wagner[1], and F. von Wrochem[1]

[1]*Physikalisches Institut, Universität Tübingen, 72076 Tübingen, Germany*
[2]*Paul Scherrer Institut, 5232 Villigen PSI, Switzerland*
[3]*TRIUMF, Vancouver BC, V6T 2A3, Canada*
[4]*Department of Physics and Astronomy, University of Edinburgh, UK*
[5]*Arizona State University, Tempe, AZ 85287, USA*
[6]*Racah Institute of Physics, The Hebrew University, Jerusalem 91904, Israel*

(Received: 6 November 2001)

This measurement is part of an experimental program [1] to improve the πN scattering database at low energies in order to allow a consistent extraction of important quantities of the strong interaction. One observable is the analyzing power in elastic π^+p scattering. It has been measured at PSI at several energies below 100 MeV. A polarized scintillator target was used. The experimental setup and some details of the data analysis are discussed.

1 Introduction

The πp system is the simplest directly experimentally accessible system to study hadronic interactions. Observables in πp scattering can be used in the evaluation of the πNN coupling constant [2], the isospin symmetry violation [3] and the sigma term of the proton [4].

There are known inconsistencies in the πp cross section data base at low energies. The analyzing power A_y as an independent observable provides new information for phase shift analyses and also allows the identification of inconsistent cross section data sets. This has been shown by Wieser *et al.* [5] who first published analyzing power data at an energy below 100 MeV. In our experiment, analyzing powers were measured for pion kinetic energies of 45, 51, 57, 68, 77 and 87 MeV in an angular range between 40 and 120 degrees.

2 Experimental setup

The measurement of the analyzing power A_y in elastic scattering $\pi^+p \to \pi^+p$ was performed at the Paul Scherrer Institut (PSI) using the **L**ow **E**nergy **P**ion **S**pectrometer (LEPS) and a polarized scintillator target which was developed at PSI [6].

Pions with well defined momentum were scattered from protons polarized perpendicular to the scattering plane. The pion detector LEPS measured relative cross sections depending on angle and polarization. The analyzing power can be extracted from two measurements with opposite target polarizations $p^\pm$ and the corresponding relative differential cross sections $\sigma^\pm$ at the scattering angle ϑ,

$$A_y(\vartheta) = \frac{1}{|p^\pm|} \times \frac{\sigma^+ - \sigma^-}{\sigma^+ + \sigma^-} \; .$$

A dynamically polarized target setup was used. The target sample was a plastic scintillator doped with paramagnetic centers for polarizability. It was placed in a target cell which simultaneously served as mixing chamber of a $^3He/^4He$ dilution refrigerator. The polarizing field was provided by a 2.5 T superconducting Helmholtz coil. Polarization was induced by microwave irradiation of the sample. Due to the construction of the target, a lot of nuclei other than protons were present in the

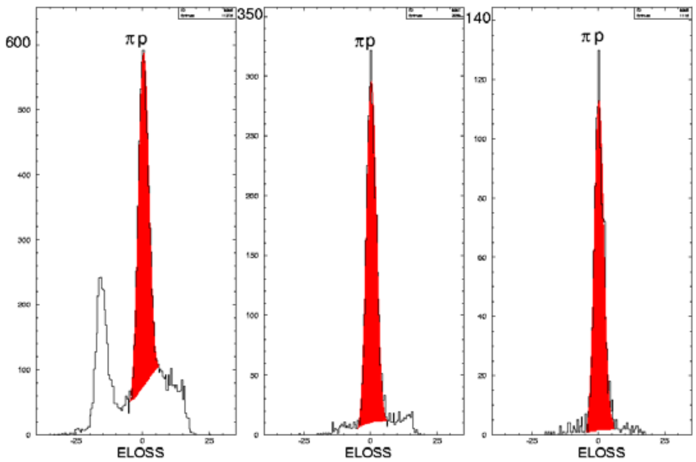

Figure 1: Focal plane spectra from LEPS with increasing cuts on the target ADC. The peak from πp elastic scattering is marked. In the left plot, the left peak is due to πC elastic scattering. The background is almost completely removed by requiring higher and higher thresholds on the target ADC (left to right).

beam interaction region. This gave rise to background for πp elastic scattering. This background was efficiently suppressed by using the active target light information. The light signal caused by a throughgoing particle depends on the particle type and energy, therefore it depends on the type of the reaction in the target. For example, the light output caused by a recoil proton is much higher than by a recoil carbon nucleus or a throughgoing pion. Because of the different light output it is possible to separate πp scattering events in the target from other reactions by applying cuts in the target ADC spectra.

This method is illustrated in Fig. 1. From left to right the threshold on the target ADC was increased, which removed the background almost completely.

3 Data analysis

For the calculation of the analyzing power, at minimum two independent runs at different polarizations are needed. If cuts on the target ADC are used for background reduction, a good ADC calibration is required to make sure that the cut in one run is at the same position as in the other run.

In a first step, the πC peak was used for the ADC calibration. The area under the (spin zero) carbon peak is known to be independent of polarization. The cut positions for different runs are

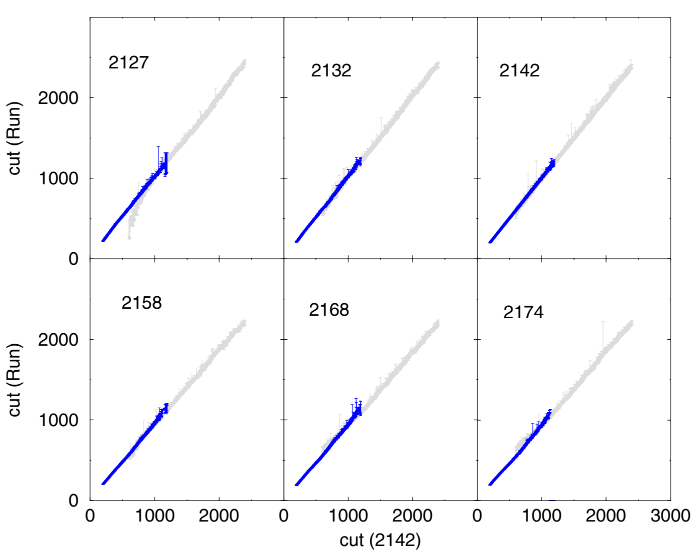

Figure 2: Calibration curves for six runs with different polarizations from one set. The lower (dark) part of the curve was evaluated from the πC peak and the upper (bright) part from the relative change of the πp peak. Plotted are equivalent cuts in one run over the cut in a reference run.

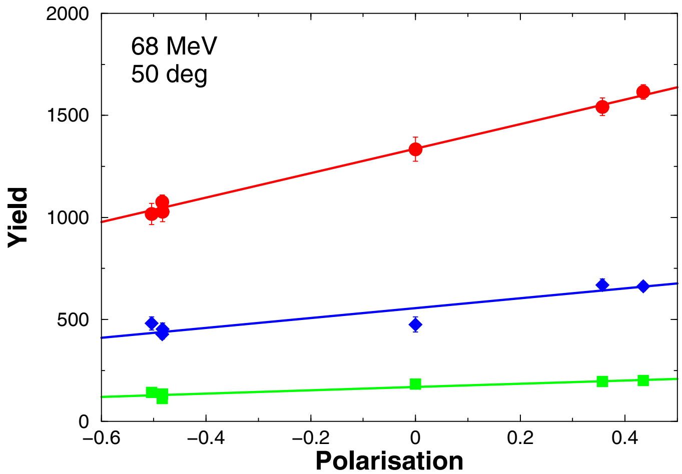

Figure 3: Example of the A_y determination from different ADC cuts on the same data set. A_y is determined from a straight line fit.

equivalent if the areas under the πC peak are identical. In a second step this method can be expanded to higher ADC values by using the relative change of the proton peak area (Fig. 2).

After the ADC calibration, analyzing powers are calculated from the measured relative cross sections using the relation

$$\sigma_p = \sigma_0(1 + p\mathrm{A_y}) \ .$$

The linear dependence of the relative cross section on the polarization can be used in a straight line fit in a σ-p-diagram as shown in Fig. 3. This figure illustrates the procedure for different cuts on the target ADC. If the ADC calibration is applied correctly, there is no correlation between analyzing powers and the cut position.

4 Results and outlook

The analysis is still in progress. Preliminary results for energies between 68 MeV and 87 MeV show good agreement with predictions from phase shift analyses [7, 8] and the previous data at 68 MeV [5]. For energies at or below 57 MeV however, there are significant differences between the preliminary analyzing power data and predictions from phase shift analyses.

Acknowledgments: The work was supported by the German Federal Minister of Education and Research (BMBF, 06TÜ9871) and the Deutsche Forschungsgemeinschaft.

References

[1] R. Meier, *Low energy Pion-Proton Scattering at TRIUMF and PSI*, contribution to MENU 2001

[2] M. E. Sainio, πN Newsletter **15**, 156, (1999).

[3] U. G. Meißner, πN Newsletter **15**, 127, (1999).

[4] M. Knecht, πN Newsletter **15**, 108, (1999).

[5] R. Wieser *et al.*, Phys. Rev. C **54**, 1930, (1996).

[6] B. van den Brandt *et al.*, Nuclear Instruments and Methods A **446**, 592-9, (2000).

[7] R. Koch, E. Pietarinen, Nucl. Phys. A **336**, 331, (1980).

[8] R. A. Arndt *et al.*, Phys. Rev. C **52**, 2120, (1995).

Helicity dependence of single-pion photoproduction: results from the GDH experiment at MAMI

I. Preobrajenski, for the A2- and GDH-Collaboration at MAMI

Institut für Kernphysik, Universität Mainz, J.-J.-Becher Weg 45, 55099 Mainz, Germany

(Received: 28 October 2001)

The helicity dependence of the $\gamma p \to n\pi^+$ and $\gamma p \to p\pi^0$ channels have been measured for incident photon energies from pion threshold to 800 MeV. We used the large acceptance detector DAPHNE with additional forward components, a newly developed frozen-spin target, and the tagged circularly polarized photon beam facility of the MAMI accelerator in Mainz. Results for the polarized total and differential cross sections are presented and compared with theoretical predictions.

1 Introduction

An important aspect of our knowledge about the nucleon structure is the understanding of its excitation spectrum. One method of investigating this is through experiments with real photons. Recent development of polarized beams and targets gives the opportunity to explore polarization degrees of freedom of the nucleon.

Special interest lies in the examination of single-pion photoproduction in the region of the first resonances. The decomposition of the total one-pion cross section into multipoles shows which multipoles can be accessed. For the unpolarized total cross section, since σ is the sum of the squares of the multipoles, only big multipoles play a role, and for the $p(\gamma,\pi^0)p$ it is mostly M_{1+}. The contribution of this multipole is fairly well known from neutral-pion photoproduction experiments in the Δ- region. In the case of the $p(\gamma,\pi^+)n$ channel, which has been investigated with photoproduction experiments near threshold, the nonresonant term E_{0+} carries a big part of the information about the total cross section.

Through double-polarization experiments one should be able to access the smaller multipoles. Using circularly polarized photons and longitudinally polarized protons the difference of the total cross sections with helicity states 3/2 and 1/2 can be measured. Here the interference term $(E^*_{1+}M_{1+})$ appears in addition to the sum of the squares of the multipoles. Since M_{1+} is large, the contribution of the term is also large and such a cross section difference becomes sensitive to the small multipole E_{1+}. The contributions of other small multipoles are negligible and the comparison of the polarized and unpolarized cross section can help to extract E_{1+}. Since the sensitivity to both M_{1+} and E_{1+} is present, the polarized cross sections will also assist to extract the EMR-ratio [1].

Polarization observables are also a powerful tool to investigate resonance parameters. As it is well-known, to carry out completely model-independent multipole analyses of pion photoproduction, nine single and double polarization observables have to be measured. As it was shown by Beck *et al.* [2], a combined measurement of unpolarized differential cross sections and beam asymmetries Σ allows one to extract the EMR-ratio in an almost model-independent way. As it is shown in Fig. 1, the differential cross section difference $(d\sigma/d\Omega)_{3/2} - (d\sigma/d\Omega)_{1/2}$ indicates a strong sensitivity to the $D_{13}(1520)$ resonance. The weak sensitivity to $S_{11}(1535)$ and almost negligible sensitivity to $P_{11}(1440)$ makes the helicity-dependent cross section an excellent probe for parameters of the D_{13}.

The helicity-dependent single-pion cross sections were measured in the frame of the GDH experiment at the tagged-photon facility of the MAMI accelerator in Mainz in the energy range $m_\pi < E_\gamma < 800\,\mathrm{MeV}$. The detailed setup of the GDH experiment can be found in [3]. We will present here the total and the differential cross section differences for energies up to 800 MeV.

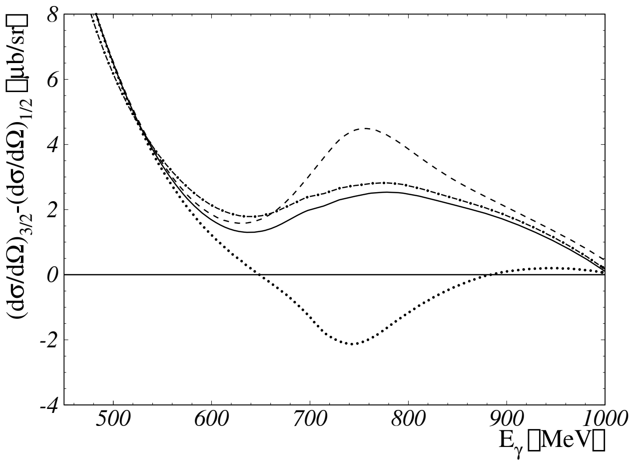

Figure 1: Sensitivity of the differential cross section difference (channel $\gamma p \to p\pi^0$) at $\theta_\pi^{CM} = 90°$ to the different resonances as described by the UIM [7]. For dotted, dashed and dashed-dotted curves the coupling constants of the $D_{13}(1520)$, $S_{11}(1535)$ and $P_{11}(1440)$ resonances respectively have been set to zero. Solid line is a standard UIM solution.

2 Results and Comments

The results of the analysis using the detector DAPHNE alone are presented here. The analysis methods are described in details in [1], [3] and [4].

Prior to the main experiment, data for detector calibration and for testing the analysis methods were taken with the same apparatus using an unpolarized pure liquid-hydrogen target. A good agreement found between old and present data strongly suggests that the detector response is well under control.

Fig. 2 shows the total cross section difference for both single-pion channels in comparison to theoretical predictions. Polarized differential cross sections also indicate a good agreement with results of partial-wave analyses in the region of Δ resonance (see [1]).

Because of double-pion background, our present analysis method does not allow for the extraction of the cross sections for the $\gamma p \to n\pi^+$ channel beyond the Δ-region. In contrast, the reaction channel $\gamma p \to p\pi^0$ could be analyzed up to a maximum photon energy of 800 MeV. Fig. 3 shows the differential cross section difference for the energy region between 550 and 790 MeV compared to predictions of SAID (solid) and UIM (dashed). One sees quite a good agreement at low energies. Starting with $\sim$ 660 MeV, a discrepancy between the theoretical curves and the data points be-

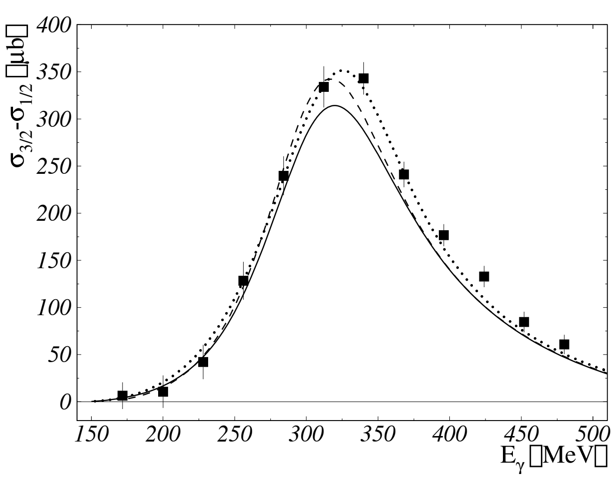

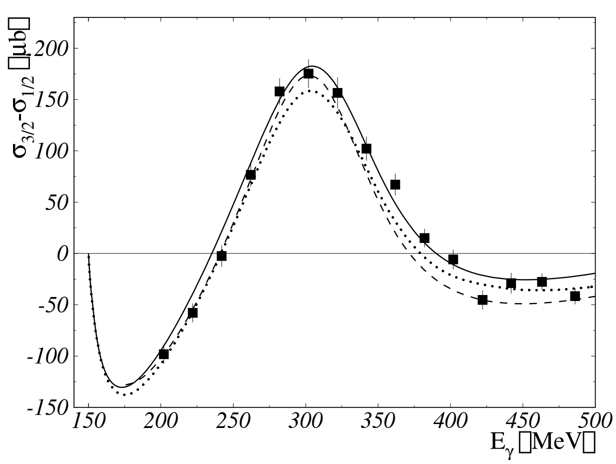

Figure 2: Total cross section difference for $\vec{\gamma}\vec{p} \to p\pi^0$ (left) and $\vec{\gamma}\vec{p} \to n\pi^+$ (right) compared to predictions of the multipole analyses HDT [5] (dotted), SAID [6] (solid), and UIM [7] (dashed).

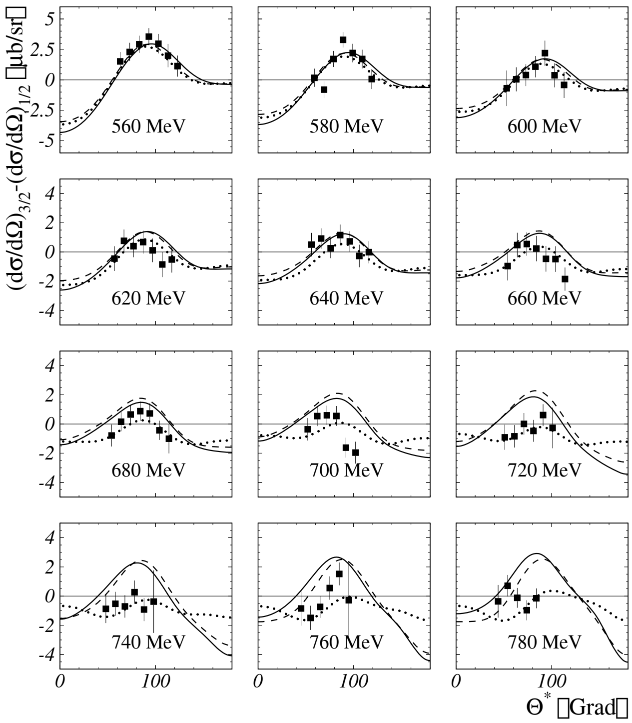

Figure 3: Differential cross section difference for $\gamma p \to p\pi^0$ in comparison to SAID (solid) and UIM (dashed) analysis. Dotted curve is the modified UIM solution. For the modification the $E_{2-}^{1/2}$ strength was decreased and $M_{2-}^{1/2}$ was increased by 30%, respectively.

comes visible. Keeping in mind the sensitivity of the cross section difference to the D_{13} resonance, we modified the strength of the coupling constant in order to get the theoretical curves closer to the data. A reduction of the $E_{2-}^{1/2}$ strength of -30% will alone solve the discrepancy for the polarized case. At the same time such a modification will decrease the unpolarized cross sections, where good agreement was found. In order to restore consistency, the $M_{2-}^{1/2}$ has to be increased. For the exercise we have chosen the same magnitude and have increased the magnetic multipole by 30%. The modified UIM solution is shown in Fig. 3 by the dotted curve. With this modification we are able to describe both polarized and unpolarized $p\pi^0$ cross section. The unpolarized cross section under backward angles is especially sensitive to this modification. Therefore, precise data in this angular and energy region are very important.

A significant result could be obtained including our data in a partial wave analysis. There are other observables which show a sensitivity to the parameters of the $D_{13}(1520)$ (for example, beam asymmetry Σ in $\gamma p \to n\pi^+$, see [8]), and a joint analysis of different observables and different channels will shed more light on the discrepancy between existing data and theoretical predictions. This work has already been started together with the UIM and SAID groups.

References

[1] I. Preobrajenski, Ph.D. Thesis, University of Mainz, 2001.

[2] R. Beck *et al.*, Phys. Rev. Lett. **78**, 78 (1997).

[3] J. Ahrens *et al.*, Phys. Rev. Lett. **84**, 5952 (2000).

[4] J. Ahrens *et al.*, Phys. Rev. Lett. **87**, 022003 (2001).

[5] O. Hanstein *et al.*, Nucl. Phys. A, **632**, 561, (1999).

[6] R.A. Arndt *et al.*, Phys. Rev. C **53**, 430 (1996), recent SAID (GWU) solution SM01, R.A. Arndt, I. Strakovsky and R. Workmann (to be published).

[7] D. Drechsel *et al.*, Nucl. Phys. **A645**, 145 (1999).

[8] R. Workmann *et al.*, Phys. Rev. C **62**, 048201 (2000).

First experimental check of the GDH sum rule at ELSA

Günter Zeitler, for the GDH-Collaboration

Physikalisches Institut IV, Universität Erlangen-Nürnberg,
Erwin-Rommel-Str. 1, 91058 Erlangen, Germany

(Received: 18 October 2001)

The GDH-Collaboration checks the very fundamental GDH sum rule experimentally for the first time. We measure the helicity dependent total photoabsorption cross section with circularly polarized real photons and longitudinally polarized nucleons in the photon energy range 0.14-3.1 GeV at tagged photon facilities at MAMI (Mainz) and ELSA (Bonn). Our new data taken at ELSA up to 1.9 GeV for the proton give access to the energy behavior of the GDH integrand and of the running GDH integral.

1 Introduction

The GDH sum rule was derived in 1966 by Gerasimov [1], and independently by Drell and Hearn [2]. It connects well known static properties (relative precision better than 10^{-6}) of the nucleon, like the anomalous magnetic moment κ and the mass m, to dynamic observables of the nucleon. As an observable of the dynamics of the excitation spectrum, the total cross section σ of circularly polarized real photons on longitudinally polarized nucleons is regarded in the helicity states 3/2 (spins parallel) and 1/2 (spins antiparallel). Its difference is weighted by the inverse of the photon energy ν and integrated up to infinity (α denotes the fine-structure constant):

$$\int_0^\infty d\nu \frac{\sigma_{3/2}(\nu) - \sigma_{1/2}(\nu)}{\nu} = \frac{2\pi^2\alpha}{m^2}\kappa^2 \ . \tag{1}$$

Its dispersion theoretic derivation is based on very fundamental physical principles: Lorentz and gauge invariance allow to express the Compton forward amplitude by a spin-dependent and a spin-independent amplitude. Unitarity of the scattering amplitude leads to the optical theorem, which relates the forward amplitude to the total photoabsorption cross section. Due to causality the Compton forward amplitude is analytic and by assuming that no subtraction is necessary (*no-subtraction-hypothesis*) one can derive a dispersion relation which can be Taylor expanded. Lorentz and gauge invariance are again the underlying principles of the Low-Theorem [3], which holds for very low photon energies. This theorem connects the spin-dependent scattering amplitude in first order with κ and m and in third order of energy with the spin polarizability γ_0. If one compares this expression in first order of energy with the Taylor expanded dispersion relation, also in first order of energy, one directly ends up with the GDH sum rule (Eq. (1)).

The experimental verification of the sum rule is most likely a validation of the *no-subtraction-hypothesis* since this is the only non-fundamental part of the derivation. Additionally, the energy dependence of the cross section in the two helicity states gives important constraints for multipole analyses in the resonance region on the one hand and makes restrictions about the validity of Regge models on the other hand.

2 Experimental setup at ELSA

The GDH-experiment is carried out at two accelerators to cover a wide photon energy range. At MAMI we measure in the resonance region from pion threshold to 0.8 GeV. Data taking on the proton was finished in 1998 and results have been published recently [4, 5]. The MAMI part is discussed in detail by P. Pedroni and I. Preobrajenski in these proceedings. The following will focus on the experimental setup at the electron stretcher accelerator facility ELSA in Bonn and on our new results obtained there in the energy range from 0.7-1.9 GeV.

2.1 Circularly polarized photon beam

Polarized electrons, which are produced by photo effect of a strained superlattice GaAs-crystal, are accelerated in ELSA up to 3.2 GeV and are finally extracted to the experiment with a duty cycle of up to 95%. Since ELSA is a circular accelerator, depolarizing resonances have to be overcome [6,7]. In addition, the vertically orientated electron spin has to be rotated in the external beam line to the longitudinal direction for the experiment. Thus, the polarization of the delivered electrons depends on energy and is typically 50-75 % at a maximum extracted beam current of 2 nA. The electron beam helicity is randomly reversed at the source every few seconds both to gain access to a measurement in the two helicity states and to avoid systematic errors.

Circularly polarized photons are produced by bremsstrahlung from longitudinally polarized electrons in a thin metal radiator foil. The helicity transfer depends only on the ratio of the energies of the emitted photon and of the primary electron [8]. The tagging system covers an energy range of 68-96% of the primary electron energy. Consequently more than 80% of the electron polarization is transferred to the photon and 5 primary electron energy settings (1.0, 1.4, 1.9, 2.4, 3.2 GeV) are used to cover the photon energy range at ELSA (0.7-3.1 GeV).

An active collimator system [9] in the photon beamline is necessary to eliminate low energy photon background produced by the collimation process and to determine the photon flux correctly even at a tagged bremsstrahlung rate of 1.3 MHz, which we use typically.

The electron polarization is permanently monitored by the GDH-Møller-Polarimeter situated in the primary electron beam behind the tagging system. The Møller-target consists of magnetized Vacoflux foils, which provide polarized electrons for the Møller scattering process. Both scattered electrons are momentum separated by a dipole magnet and are detected in coincidence in an arrangement of 14 leadglass detectors. This two-arm spectrometer has an acceptance of $\Theta_{CMS} = [65^o, 115^o]$ and allows a fast diagnostics of the electron beam polarization.

2.2 Longitudinally polarized target

The actively collimated photon beam impinges on the longitudinally polarized target nuclei which are provided within a horizontal ^{3}He/^{4}He dilution cryostat [11]. This cryostat is operated in the frozen-spin mode at about 60 mK. Beads of butanol ($H(CH_2)_4OH$) endowed with paramagnetic radicals are used as target material, which can be polarized by the dynamic nuclear polarization technique up to 85%. Since C and O nuclei are spinless particles, only the H is polarized. By using an internal superconducting holding coil with a magnetic field of 0.4 T we achieved decay times of 200 hours. In particular, this coil has the advantage of generating a low fringe field in the GDH-Detector. The target was repolarized approximately every two days. Usually the spin orientation was reversed on that occasion to allow for systematic studies. The target polarization is measured by an NMR-system before and after re-polarization. Due to its horizontal design the cryostat can be inserted into the GDH-Detector from upstream side, resulting in a minimal dead solid angle.

2.3 GDH-Detector

In the ELSA photon energy range, photoabsorption processes lead to multi particle final states which are hard to detect individually. In addition, some of these partial channels are even unknown. To avoid systematic uncertainties arising from unobserved final states, the total photoabsorption cross section is measured inclusively.

The concept of the GDH-Detector [10] is that at least one reaction product is detected from all possible hadronic final states with almost complete acceptance as far as solid angle and efficiency

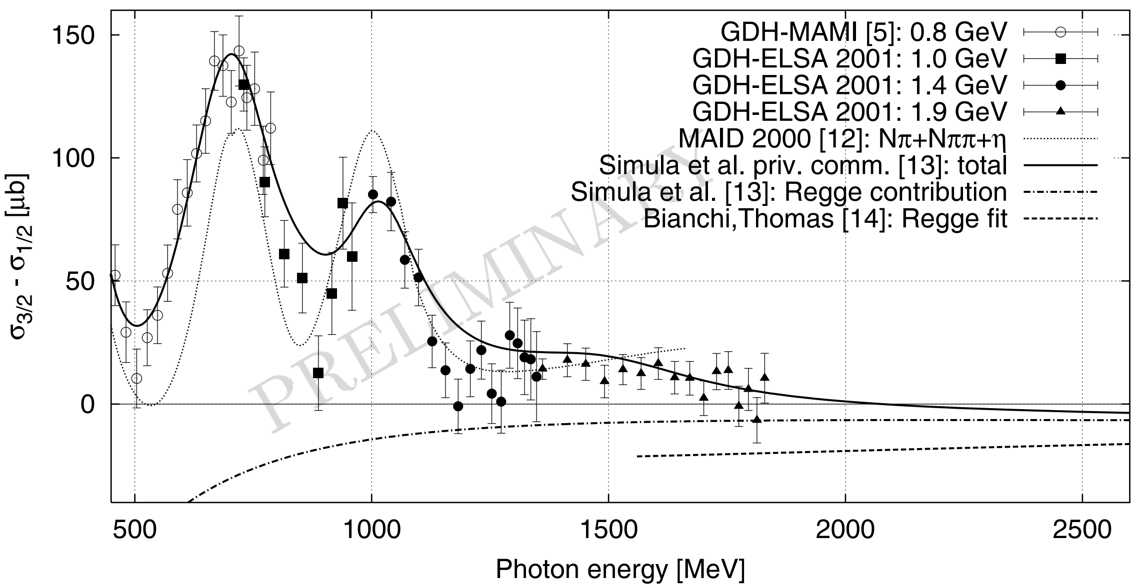

Figure 1: Doubly polarized total cross section difference off the proton compared to models.

are concerned. These conditions are fulfilled by an arrangement of 7 hadron detection modules, which surround the target with a solid angle of $99.6\% \cdot 4\pi$. Each module consists of a scintillator plate for detecting charged hadrons and a following lead-scintillator sandwich for detecting decay photons. The detection efficiency for the hadronic final states is higher than 99%.

An important part of the detector concept is the suppression of electromagnetic background caused by pair production in the field of nuclei and by Compton scattering off orbital electrons. Due to the Lorentzboost this background is strongly emitted into forward directions. With the help of a threshold CO_2-Čerenkov detector, which covers polar angles of $0^o \leq \theta \leq 15^o$, these particles can be detected and suppressed with an efficiency of $(99.990 \pm 0.003)\%$.

The complete setup has been tested extensively with unpolarized beam and nuclei. We obtained unprecedented data quality for solid state targets like Be and C. An important point was to prove that the GDH-Detector is able to measure cross section differences. From the measured cross section of a solid state $[CH_2]_n$-target we subtracted the C-cross section to determine the H-cross section. The excellent agreement with literature data shows the reliability of the whole setup and of the analysis procedure. In addition, we performed test measurements with polarized beam and polarized target to investigate possible sources of fake asymmetries. All results are compatible with zero.

3 Results

Fig. 1 shows our new preliminary results for the doubly polarized total cross section difference off the proton measured at ELSA at primary electron energies of 1.0, 1.4 and 1.9 GeV. The new data is plotted together with the already published MAMI data [5]. The data sets from the different accelerators and from various primary electron energy settings match very well. The 2^{nd} and 3^{rd} resonance are clearly visible and even more pronounced than in the unpolarized hydrogen cross section. The measured difference is positive up to 1.9 GeV, which may indicate that the $F_{35}(1905)$ and $F_{37}(1950)$ resonances significantly contribute. Our data is compared with two models. The parameterization of the unitary isobar model MAID [12] fails esp. in the 2^{nd} resonance. Simula et al. [13] performed a Regge-based fit to deep inelastic scattering data and extrapolated to $Q^2 = 0$. In addition, they took into account all 4-star-resonances up to $W = 2$ GeV. This model describes our data better, though this is mainly due to an adjustment of the width of the $P_{33}(1232)$ as well as

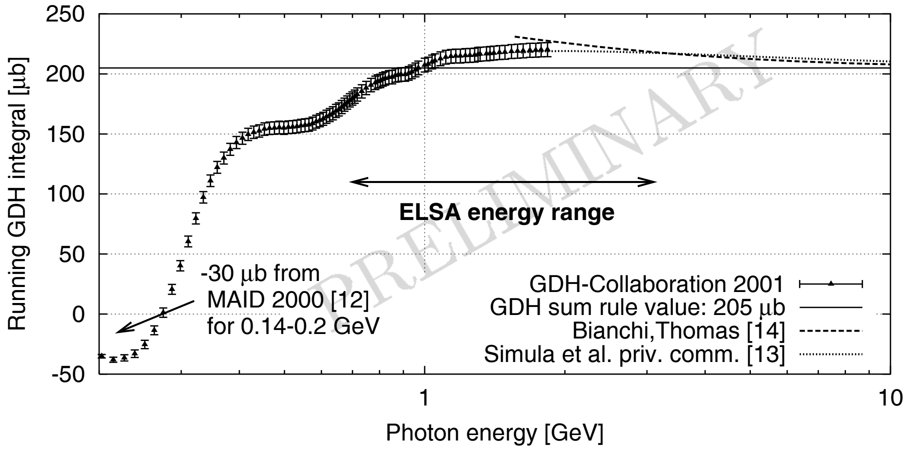

Figure 2: Running GDH integral up to 1.9 GeV. Error bars indicate statistical errors only.

of the strengths and the widths of the $D_{13}(1520)$ and $F_{15}(1680)$ resonances to our data. However, it is remarkable that this model predicts a sign change of $\sigma_{3/2} - \sigma_{1/2}$ at 2.1 GeV. Besides [13] there exists another Regge-inspired analysis of deep inelastic scattering data [14]. Their parameterization can be extrapolated to $Q^2 = 0$, which gives also a negative sign for $\sigma_{3/2} - \sigma_{1/2}$ in the Regge regime.

In Fig. 2 we used the measured data to calculate the GDH integral in dependence of the upper integration bound. This so called running GDH integral clearly overruns the sum rule value for the proton of 205 μb showing that the question of a sign change is of prime importance. Assuming that each Regge prediction [13,14] is valid and that the sum rule holds, one would expect a high energy development of the running GDH integral as denoted by the dashed lines in Fig. 2 indicating the convergence of the GDH integral. In this figure each predicted high-energy contribution is summed up in dependence of the lower integration bound. As a consequence, these negative contributions would improve the agreement between experimental data and GDH sum rule prediction.

Analysis of the data up to 3.1 GeV will clarify the validity of these Regge predictions in this energy regime and will give answer to the question whether the GDH sum rule holds or not. Moreover, we will continue the experiment with deuterated butanol at ELSA and MAMI.

References

[1] Gerasimov, S. B., Sov. J. Nucl. Phys. **2**, 430 (1966).
[2] Drell, S. D. and Hearn, A. C., Phys. Rev. Lett. **16**, 908 (1966).
[3] Low, F. E., Phys. Rev. **96**, 1428 (1954);
Gell-Mann, M. and Goldberger, M. L., Phys. Rev. **96**, 1433 (1954)
[4] GDH-Collaboration: Ahrens, J. *et al.*, Phys. Rev. Lett. **84**, 5950 (2000).
[5] GDH-Collaboration: Ahrens, J. *et al.*, Phys. Rev. Lett. **87**, 022003 (2001).
[6] Nakamura, S. *et al.*, Nucl. Inst. Meth. A **411**, 93 (1998).
[7] Hoffmann, M. *et al.*, SPIN 2000 - Proc. of the 14^{th} Int. Spin Physics Symp., Osaka, Japan, 756 (2001).
[8] Olsen, H. and Maximon, L. C., Phys. Rev. **114**, 887 (1959).
[9] Zeitler, G. *et al.*, Nucl. Inst. Meth. A **459**, 6 (2001).
[10] Helbing, K. *et al.*, accepted: Nucl. Inst. Meth. A, (2001).
[11] Bradtke, Ch. *et al.*, Nucl. Inst. Meth. A **436**, 430 (1999).
[12] Drechsel, D. *et al.*, Nucl. Phys. A **645**, 145 (1999); Drechsel, D. *et al.*, Phys. Rev. D **63**, 114010 (2001).
[13] Simula, S. *et al.*, Preprint RM3-TH/01-4 resp. hep-ph/0107036 and *private communication* (2001).
[14] Bianchi, N. and Thomas, E., Phys. Lett. B **450**, 439 (1999).

Precision measurements of electroproduction of π^0 near threshold: A test of chiral QCD dynamics

A commissioning experiment for the BigBite Spectrometer

R.A. Lindgren[a], D.W. Higinbotham[b], J.R.M. Annand[c], and V. Nelyubin[d]
for The BigBite Collaboration and The Hall-A Collaboration

[a]*University of Virginia, Charlottesville, VA 22903, USA*
[b]*Massachusetts Institute of Technology, Cambridge, MA 02139, USA*
[c]*University of Glasgow, Glasgow, Scotland, UK*
[d]*St. Petersburg Nuclear Physics Institute, Gatchina, Russia*

(Received: 12 November 2001)

We propose to make a high precision measurement of the reaction $p(e,e'p)\pi^0$ near threshold in a fine grid of Q^2 and ΔW in the range of 0.04 $[GeV/c]^2 \leq Q^2 \leq$ 0.14 $[GeV/c]^2$ and 0 $MeV \leq \Delta W \leq$ 20 MeV. The large acceptance of the BigBite spectrometer will enable us to make all measurements with the spectrometers at a single position, thereby minimizing systematic uncertainties. The results will provide a stringent experimental test of chiral QCD dynamics, a test made all the more critical by recent measurements showing disagreement with the predictions of Chiral Perturbation Theory.

1 Introduction

During the last several years significant progress has been made in the application of QCD in the non-perturbative regime via the use of Chiral Perturbation Theory (ChPT) [1]. Symmetry breaking effects are introduced via perturbative expansions in terms of static and dynamic variables such as m_π/M and Q^2/M, where m_π (M) is the mass of the pion (nucleon) and Q^2 is the four-momentum transferred to the π-N system. Since it involves the well understood electromagnetic interaction and small kinematic quantities, near-threshold electromagnetic production of pions (in particular, neutral pions due to the absence of the overshadowing Kroll-Ruderman term) from nucleons provides an ideal testing ground for ChPT. As ChPT is an "effective" field theory, the description of pion electroproduction contains parameters which must be fixed by measurement, the so-called Low Energy Constants or LEC's. However, once these are fixed it should be possible to predict consistently the evolution with Q^2 and W (center-of-mass energy of the π-N system) of all observables.

Considerable effort has gone into measurements of both the photo-production $p\left(\gamma,\pi^0\right)$ and electro-production $p(e,e'p)\pi^0$ of neutral pions near threshold. Measurements at Mainz [2] and Saskatoon [3] of the lowest contributing multipole (E_{0+}) to photoproduction are well reproduced by ChPT. The most recent high precision measurements of electroproduction were made at Mainz with four-momentum transfers of 0.10 $[GeV/c]^2$ [4] and 0.05 $[GeV/c]^2$ [5]. The former measurement yielded results consistent with the predictions of ChPT so it was surprising that the latter measurements disagreed significantly. Discrepancies were observed both at threshold (the limiting value of the L_{0+} multipole was observed to be twice the predicted value) and at higher values of W where the P–wave contributions are significant. If these discrepancies which, incidentally, are also inconsistent with the predictions of the SAID analysis and MAID model [6, 7], remain unresolved they will constitute a serious threat to the viability of ChPT as a useful theory of dynamical processes. Such a result would be problematical as ChPT is firmly grounded in the basic properties of QCD.

The goal of the proposed measurements is, therefore, to measure precisely the reaction $p(e,e'p)\pi^0$ from threshold to $\Delta\mathrm{W} = 20$ MeV above threshold for a range of momentum transfers encompassing those of the Mainz data and extending to both lower and higher values: 0.04 $[GeV/c]^2 \leq Q^2 \leq$

$0.14[GeV/c]^2$. The ϕ dependence of the cross section will be used to extract the structure functions $\sigma_T+\epsilon_L\sigma_L$, σ_{TL}, and σ_{TT}. The cross section data will also be used in a partial wave analysis to provide information on the non-resonant contribution.These data will enable us to a) either confirm or refute the existence of a significant discrepancy with the predictions of ChPT and b) depending upon the result of a) either investigate the source of the discrepancy or test the ability of ChPT to predict higher P–wave contributions.

2 Description of experiment

To study the $p(e, ep')\pi^0$ reaction at threshold in Hall A of Jefferson Lab, we plan to use the large acceptance BigBite spectrometer [8, 9] to detect the proton, the High Resolution Spectrometer (LHRS) with septum magnet (constructed for experiments [10–12]) to detect the electron, and the highly segmented lead glass calorimeter (constructed for experiment [13]) for calibration. The BigBite spectrometer's 96 msr solid angle acceptance and 80% momentum acceptance will allow new measurements to be made with high statistical precision (1% at peak cross sections). Systematic errors will be minimized since the BigBite spectrometer can measure the entire proton angular distribution within a single kinematic setting. This differs greatly from previous Mainz measurements, where several spectrometer positions were required to cover the necessary angular range. The septum magnet will allow the Hall-A spectrometers to reach small scattering angles (6 degrees) with high beam energies to maximize the cross section for a given Q^2. The high resolution of the electron spectrometer will allow a precise determination of the W and $\vec{q}$ quantities. The large acceptance of BigBite will permit a large fraction of the cone of forward-emitted protons along $\vec{q}$ to be detected. The Hall-A standard 15 cm long liquid hydrogen target will be replaced by a 10 cm version with thinner windows and walls. The RHRS will be used as a single arm electron detector to monitor the luminosity during the experiment. The lead-glass calorimeter, developed for the $p(\gamma,\gamma)$ experiment [13], will be used as an electron arm in coincidence with BigBite to calibrate the BigBite spectrometer's angular and momentum acceptances.

The measured momentum and the (θ,ϕ) angles of the proton will be used for the calculation of the missing mass and the angles of the pion in the pion-nucleon center of mass system. The missing mass distribution will be used to suppress background. Near threshold the data will be obtained in 1 MeV bins in ΔW from $\Delta W = 0 - 20$ MeV, and three 0.01 $(GeV/c)^2$ bins in Q^2 for each kinematic setting. The angular distribution for each ΔW and Q^2 bin will be presented in eighteen bins in θ and twelve bins in ϕ. Statistical uncertainties are expected to be on the level of 1-2% at angles where the cross section is maximum and 2.5% on the average. The kinematics and beam time estimates shown in Table 1 are based on the cross section calculations of MAID and SAID. The time shown in the table does not include energy changes, calibrations or tune up. A luminosity of 1×10^{37} Hz/cm^2 is assumed corresponding to a beam current of 5 uA and a target thickness of 0.7 gm/cm^2.

In Hall A, luminosities $10^{37} - 10^{38}$ Hz/cm^2 can be achieved and the total counting rate in the focal plane detection system will be correspondingly high. For the projected $p(e, ep')\pi^0$ experiment,

Table 1: Kinematics.

Setting Number	Beam Energy [MeV]	HRS Momentum [MeV]	HRS Angle [degrees]	W MeV	Q^2 $[\mathrm{GeV/c}]^2$	BigBite Momentum [MeV]	BigBite Angle [degrees]	Beam Time [hours]
1	2400	2222	6.0	1074	0.04 - 0.08	215 - 275	45 - 54	100
2	3200	2996	6.0	1074	0.07 - 0.14	270 - 340	50 - 57	100

protons will be ejected from the target at rates $> 10^6$ Hz, necessitating a new focal-plane detection system. It will be necessary to replace both the trigger plastic scintillators and the position sensing multi-wire drift chambers with a higher segmented system and with faster counting MWPC. In order to keep straggling and multiple scattering at a minimum particularly for the 20 - 30 MeV protons, a new scattering chamber, vacuum system, thin exit window, and helium bag will be used as part of the BigBite transport system.

3 Summary

We propose an experiment that is a precision test of ChPT. This experiment requires the upgrade and commissioning of the Hall-A BigBite spectrometer. Once commissioned, this spectrometer will be of general utility for future experiments, including a continuation of charged and neutral pion production experiments on the proton and deuteron.

References

[1] U.-G. Meissner, Chiral QCD: Baryon dynamics, in *Encyclopedia of Analytic QCD*, edited by M. Schifman, to be published by World Scientific (2000).

[2] M. Fuchs *et al.*, Phys. Lett. **B368**, 20 (1996).

[3] J.C. Bergstrom *et al.*, Phys. Rev. **C53**, R1052 (2996).

[4] M.O. Distler *et al.*, Phys. Rev. Lett. **80**, 2294 (1996).

[5] H. Merkel, Pion threshold electro- and photo- production, Talk for the Chiral Dynamics 2000 Workshop.

[6] R.A. Arndt, I.I. Strakovsky and R.L. Workman, Phys. Rev. **C53**, 430 (1996). The SAID web site is at `http://gwdac.phys.gwu.edu`.

[7] D. Drechsel, O. Hanstein, S.S. Kamalov and L. Tiator, Nucl. Phys. **A645**, 145 (1999).

[8] D.J.J. de Lange *et al.*, Nucl. Instr. and Meth. **A406**, 182 (1998).

[9] D.J.J. de Lange *et al.*, Nucl. Instr. and Meth. **A412**, 254 (1998).

[10] K. Kumar *et al.*, Constraining the nucleon strangeness radius in parity violating electron scattering, TJNAF Proposal E99-115.

[11] D. Armstrong *et al.*, Parity violation from ^4He at low Q^2: A clean measurement of ρ_s, TJNAF Proposal E00-114.

[12] R. Michaels, A clean measurement of the neutron skin of ^{208}Pb through parity violating electron scattering, TJNAF Proposal E00-003.

[13] C. Hyde-Wright *et al.*, Exclusive compton scattering on the proton, TJNAF Proposal E99-114.

Kaon photo- and electroproduction on the deuteron with hyperon recoil polarization

K. Miyagawa[a], T. Mart[b], C. Bennhold[c], and W. Glöckle[d]

[a]Department of Applied Physics, Okayama University of Science, 1-1 Ridai-cho, Okayama 700, Japan
[b]Jurusan Fisika, FMIPA, Universitas Indonesia, Depok 16424, Indonesia
[c]Center for Nuclear Studies, Department of Physics, The George Washington University, Washington, DC 20052, U.S.A.
[d]Institut für Theoretische Physik II, Ruhr-Universität Bochum, D-4478 Bochum, Germany

(Received: 31 October 2001)

Photo- and electroproduction processes of K^+ on the deuteron are investigated theoretically. Modern hyperon-nucleon forces as well as an updated kaon production operator on the nucleon are used. Sizable effects of the hyperon-nucleon final state interaction are seen in various observables.

1 Introduction

Electro- and photo-production processes of K^+ on light nuclei are the most promising candidates that allow us to study the YN interaction in continuum. They also allow for an access to the elementary cross sections on the neutron, such as $\gamma + n \to K^+ + \Sigma^-$, in kinematic regions where final-state interaction effects are small. An inclusive $d(e, e'K^+)YN$ experiment has already been performed, while the data for $d(\gamma, K^+Y)N$ and $^3\text{He}(\gamma, K^+Y)N$ are being analyzed at TJNAF.

We predict the inclusive and exclusive $\gamma + d \to K^+ + \Lambda(\Sigma) + N$ cross sections and various polarization observables [1]. These analyses incorporate the modern YN interactions of the Nijmegen group, NSC97f and NSC89, using an updated kaon production operator [2]. We also report the preliminary results of the $d(e, e'K^+)YN$ reaction.

2 Results

The predictions of the inclusive $d(\gamma, K^+)$ cross sections are given in Fig. 1, as a function of lab momentum P_K. The incident photon energy is 1.3 GeV, while the outgoing kaon angle is fixed to

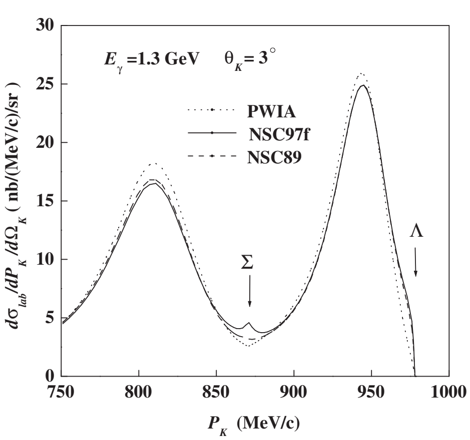

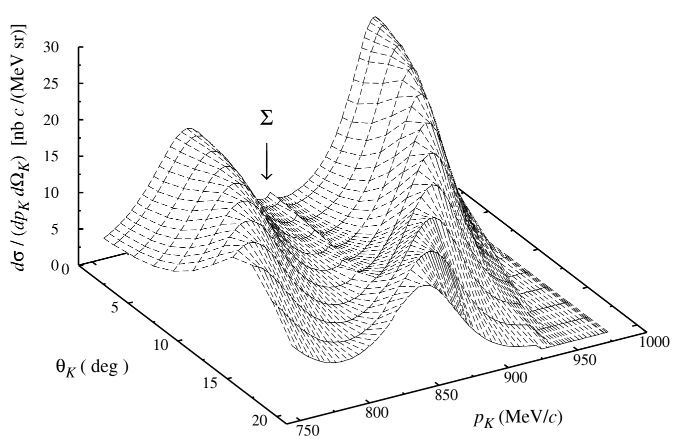

Figure 1: Inclusive $d(\gamma, K^+)$ cross section as a function of kaon lab momentum P_K (left). The same cross section for NSC97f plotted as a function of P_K and θ_K (right). The $K^+\Lambda N$ and $K^+\Sigma N$ thresholds are indicated by the arrows.

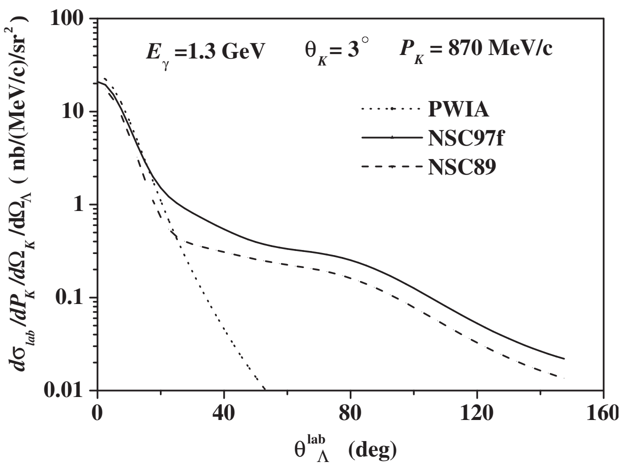

Figure 2: Exclusive $d(\gamma, K^+\Lambda)$ cross section for $\theta_K = 3°$, lab momentum $P_K = 870$ MeV/c, and photon lab energy $E_\gamma = 1.3$ GeV as a function of the lab Λ scattering angle.

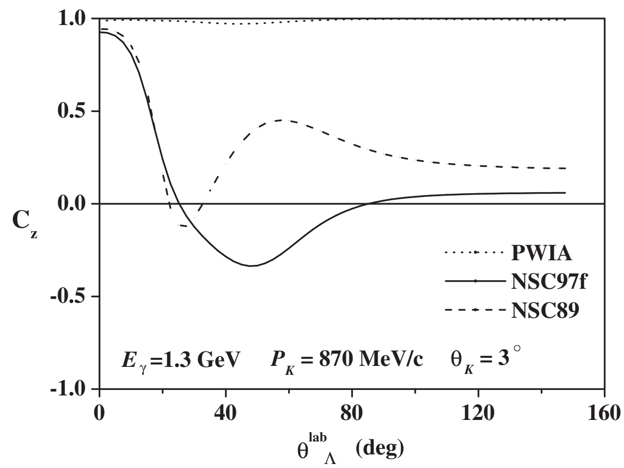

Figure 3: Double Polarization C_z for the same P_K, θ_K and E_γ as in Fig. 2.

$\theta_K = 3°$. The results with the final state interaction NSC97f are compared to the results with NSC89 and to the PWIA calculations. Sizable FSI effects are seen above the Λ threshold for both of the YN interactions. However, only NSC97f shows a prominent enhancement around the Σ threshold. The θ_K-evolution of this effect can be seen in the same figure, where we find FSI decreases and slowly disappears as a function of θ_K. Typical results of the exclusive $d(\gamma, K^+\Lambda)n$ cross sections and double polarization observables C_z are shown in Figs. 2 and 3. In C_z, FSI results show dramatic deviations from PWIA. In Figs. 4 and 5, the cross sections and the Λ recoil polarization P_y are depicted for a different kaon angle. The Λ polarizations are strongly influenced by FSI.

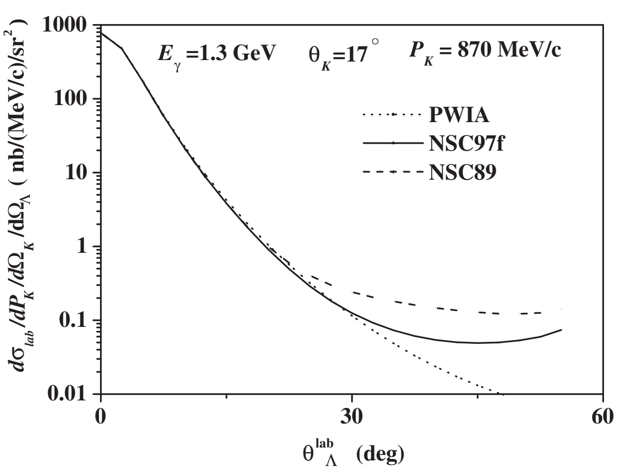

Figure 4: Exclusive $d(\gamma, K^+\Lambda)$ cross section for $\theta_K = 17°$, lab momentum $P_K = 870$ MeV/c, and photon lab energy $E_\gamma = 1.3$ GeV as a function of the lab Λ scattering angle.

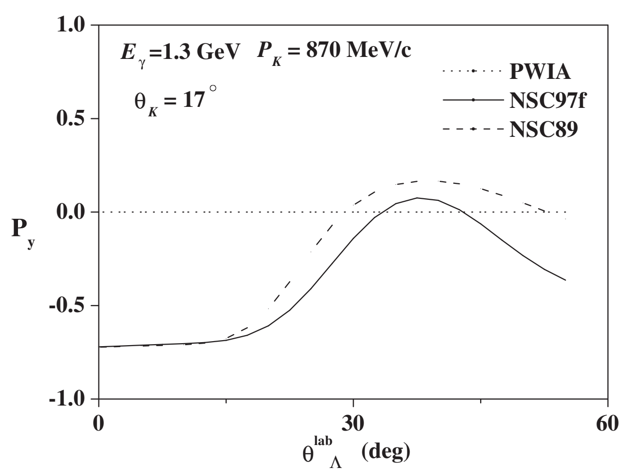

Figure 5: Λ recoil polarization P_y for the same P_K, θ_K and E_γ as in Fig. 4.

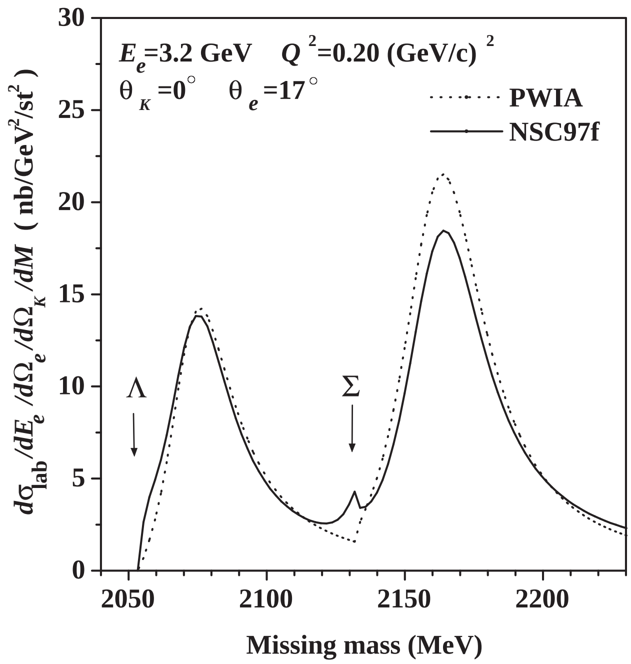

Figure 6: Missing mass spectrum for the reaction $d(e, e'K^+)$. The results with the YN final state interaction NSC97f are compared to the PWIA results. The Λ and Σ thresholds are indicated by the arrows.

We also present preliminary results for the electroproduction process $d(e, e'K^+)$ in Fig. 6. As in the case of the photoproduction, YN FSI effects are seen near both Λ and Σ thresholds.

References

[1] See also K. Miyagawa, H. Yamamura, T. Mart, C. Bennhold, H. Haberzettl, and W. Glöckle, Nucl. Phys. **A691**, 64 (2001); nucl-th/0011086.

[2] F.X. Lee, T. Mart, C. Bennhold, H. Haberzettl, and L.E. Wright, nucl-th/9907119; C. Bennhold, H. Haberzettl, and T. Mart, nucl-th/9909022.

Generalized multipole amplitudes for pion-delta photoproduction

S.C. Karppi, C. Bennhold, and A.B. Waluyo

Center for Nuclear Studies, Department of Physics,
The George Washington University, Washington, DC 20052, U.S.A.

(Received: 19 November 2001)

The formalism for the reactions $\pi N \to \pi\Delta$ and $\gamma N \to \pi\Delta$ is discussed in the framework of helicity and multipole amplitudes. After developing the general Dirac structure of the elementary amplitudes we introduce a set of eight generalized multipole amplitudes ($E^{l_N}_{l\pm\pm}$, $E^{l_N}_{l\pm}$, $M^{l_N}_{l\pm\pm}$, $M^{l_N}_{l\pm}$) that have the same physical meaning as the four conventional multipoles ($E_{l\pm}$, $M_{l\pm}$) of $\gamma N \to \pi N$. The relationship to the traditional πN amplitudes is pointed out.

Among the many final states nucleon resonances can decay into the $\pi\pi N$ state is among the more difficult to include properly. Rather than treat the full complexity of the three-body final state this channel is usually treated in the quasi two-body approximation. Here we discuss the excitation of intermediate-state baryon resonances in the reactions $\pi N \to \pi\Delta$ and $\gamma N \to \pi\Delta$ within the framework of a previously developed effective Lagrangian coupled-channels model [1]. This effort is part of a larger effort to rigorously model the reactions $\pi N \to \pi\pi N$ and $\gamma N \to \pi\pi N$. We treat $\pi\Delta$, ρN, $\pi P_{11}(1440)$, and σN explicitly as "asymptotic" final states, underlying the $\pi\pi N$ state. We have developed the formalism to express partial-wave amplitudes in terms of Feynman diagrams, for the reactions $\pi N \to \pi\Delta$ and $\gamma N \to \pi\Delta$. The overall approach is to express partial-wave amplitudes in terms of resonance parameters and coupling constants (contained in the Feynman diagrams), and to adjust the resonance parameters and constants using experimentally derived partial-wave amplitudes as model inputs. An important part of this effort is the use of the helicity formalism to treat arbitrary spin in the initial and final particle states. Among other things, for $\gamma N \to \pi\Delta$, we have developed partial-wave expansions and defined a set of eight generalized multipole amplitudes ($E^{l_N}_{l\pm\pm}$, $E^{l_N}_{l\pm}$, $M^{l_N}_{l\pm\pm}$, $M^{l_N}_{l\pm}$) that have the same physical meanings (though extended) as the four conventional multipoles ($E_{l\pm}$, $M_{l\pm}$) of $\gamma N \to \pi N$ [2,3]. Similarly, for $\pi N \to \pi\Delta$, we have developed partial-wave expansions in terms of the generalized partial-wave amplitudes that Manley *et al.* [4] originally defined for pion-induced reactions on the nucleon. As a key future goal, not to be presented in this paper, we intend to use this formalism, to extract the properties of resonances having relatively large branching ratios into the $\pi\Delta$ decay channel. We also intend, eventually, to make comparisons between the properties that we extract and the independent predictions made by constituent quark models and other theoretical approaches.

Using Lorenz covariance, time-reversal invariance and parity conservation leads to the following general Dirac-space parameterizations,

$$T = A + B(\not{q} + \not{q}') \ , \qquad \text{for} \quad \pi N \to \pi N \ , \tag{1}$$

$$T_\mu \gamma_5 = A_1 q_\mu + A_2 q'_\mu + (B_1 q_\mu + B_2 q'_\mu)(\not{q} + \not{q}') \ , \qquad \text{for} \quad \pi N \to \pi\Delta \ , \tag{2}$$

where for a reaction $\pi N \to \pi Baryon$ we use the momenta $qp \to q'p'$. These expressions, well-known for the $\pi N \to \pi N$ but to our knowledge not published elsewhere for $\pi N \to \pi\Delta$, contain unknown scalar functions A and B which depend on the above four momenta. Note that the T-matrix with a Δ in the final state contains a subscript μ to be contracted with the Δ Rarita-Schwinger spinor.

For photoproduction, the equivalent expressions are,

$$T\gamma_5 = A\not{\varepsilon}\not{k} + B(\not{k} q\cdot\varepsilon - \not{\varepsilon} q\cdot k) + C(\not{k} P\cdot\varepsilon - \not{\varepsilon} P\cdot k) + D(P\cdot k q\cdot\varepsilon - q\cdot k P\cdot\varepsilon) \ , \tag{3}$$

$$T_\mu = (A_1 k_\mu + A_2 q_\mu)\not\varepsilon\not k + (B_1 k_\mu + B_2 q_\mu)(\not k q\cdot\varepsilon - \not\varepsilon q\cdot k)$$
$$+ (C_1 k_\mu + C_2 q_\mu)(\not k P\cdot\varepsilon - \not\varepsilon P\cdot k) + (D_1 k_\mu + D_2 q_\mu)(P\cdot k q\cdot\varepsilon - q\cdot k P\cdot\varepsilon)\ . \qquad (4)$$

The first expression is the well-known form for $\gamma N \to \pi N$ (previously developed by Chew *et al.* [3]); the second one is for $\gamma N \to \pi\Delta$. For the momenta in the reaction $\gamma N \to \pi Baryon$ we use the notation $kp \to qp'$, and $P = (p+p')/2$. The above equations require gauge invariance to be used in addition to the constraints used in the hadronic reactions. The unknown functions (A, B, C, D, etc.) are functions of the above momentum four vectors.

As the next step we proceed with a partial-wave decomposition, invoking the helicity formalism. In his classic paper [2], Walker introduced four "helicity elements" A_{n+}, $A_{(n+1)-}$, B_{n+}, $B_{(n+1)-}$ for the reaction $\gamma N \to \pi N$. Analogously, we introduce eight generalized helicity amplitudes for the reaction $\gamma N \to \pi\Delta$, $A_{(n-1)++}$, A_{n+}, $A_{(n+1)-}$, $A_{(n+2)--}$ and $B_{(n-1)++}$, B_{n+}, $B_{(n+1)-}$, $B_{(n+2)--}$, defined through the equations,

$$_{\pi\Delta}\langle \pm\tfrac{1}{2}\,|T^J|\,\tfrac{1}{2}\rangle_{\gamma N} \equiv -\frac{1}{2}\sqrt{2}\Big\{\sqrt{3}A^J_{(n-1)++} \pm \frac{1}{\sqrt{3}}A^J_{n+} - \frac{1}{\sqrt{3}}A^J_{(n+1)-} \mp \sqrt{3}A^J_{(n+2)--}\Big\}\ , \qquad \text{for} \quad J \geq \frac{1}{2}\ , \qquad (5)$$

$$_{\pi\Delta}\langle \pm\tfrac{3}{2}\,|T^J|\,\tfrac{1}{2}\rangle_{\gamma N} \equiv -\frac{1}{2}\sqrt{2}\sqrt{(J-\tfrac{1}{2})(J+\tfrac{3}{2})}\Big\{\frac{1}{J-\frac{1}{2}}A^J_{(n-1)++} \pm \frac{1}{J-\frac{1}{2}}A^J_{n+} + \frac{1}{J+\frac{3}{2}}A^J_{(n+1)-} \pm \frac{1}{J+\frac{3}{2}}A^J_{(n+2)--}\Big\}\ , \qquad \text{for} \quad J \geq \frac{3}{2}\ , \qquad (6)$$

$$_{\pi\Delta}\langle \pm\tfrac{1}{2}\,|T^J|\,\tfrac{3}{2}\rangle_{\gamma N} \equiv \frac{1}{2}\frac{1}{\sqrt{2}}\sqrt{(J-\tfrac{1}{2})(J+\tfrac{3}{2})}\Big\{\sqrt{3}B^J_{(n-1)++} \pm \frac{1}{\sqrt{3}}B^J_{n+} - \frac{1}{\sqrt{3}}B^J_{(n+1)-} \mp \sqrt{3}B^J_{(n+2)--}\Big\}\ , \qquad \text{for} \quad J \geq \frac{1}{2}\ , \qquad (7)$$

$$_{\pi\Delta}\langle \pm\tfrac{3}{2}\,|T^J|\,\tfrac{3}{2}\rangle_{\gamma N} \equiv -\frac{1}{2}\frac{1}{\sqrt{2}}(J-\tfrac{1}{2})(J+\tfrac{3}{2})\Big\{-\frac{1}{J-\frac{1}{2}}B^J_{(n-1)++} \mp \frac{1}{J-\frac{1}{2}}B^J_{n+} - \frac{1}{J+\frac{3}{2}}B^J_{(n+1)-} \mp \frac{1}{J+\frac{3}{2}}B^J_{(n+2)--}\Big\}\ , \qquad \text{for} \quad J \geq \frac{3}{2}\ . \qquad (8)$$

In these equations, the "index" n is related to the total angular momentum J via the equation $n = J - 1/2$. Note that the helicity partial-wave amplitudes as written above are of mixed parity. Inverting the above equations and expressing them in the LS basis, rather than helicity bases, leads to amplitudes of good parity,

$$A^J_{(n+2)--} = \sqrt{2}\Big\{-\frac{\sqrt{(J+\frac{3}{2})(J-\frac{1}{2})}}{8\sqrt{3}(J+1)}\langle l_f = J+\tfrac{3}{2},\, s_f=\tfrac{3}{2}\,|T^J|\,l_i = J-\tfrac{1}{2},\, s_i=\tfrac{3}{2}\rangle + \frac{1}{2}\sqrt{\frac{J+\frac{3}{2}}{6(J+1)}}\langle l_f = J+\tfrac{3}{2},\, s_f=\tfrac{3}{2}\,|T^J|\,l_i = J-\tfrac{1}{2}, s_i=\tfrac{1}{2}\rangle + \frac{J+\frac{3}{2}}{8(J+1)}\langle l_f = J+\tfrac{3}{2},\, s_f=\tfrac{3}{2}\,|T^J|\,l_i = J+\tfrac{3}{2},\, s_i=\tfrac{3}{2}\rangle\Big\}\ , \qquad \text{for} \quad P = (-1)^{J+\frac{1}{2}}\ , \qquad (9)$$

Reaction	Multipole	Quantum numbers	Parity	Lowest orb. ang. mom. in final state	$l_{\pi N}$
$\gamma N \to \pi N$	$E_{l_{\pi N}+}$	$L - \frac{1}{2} = J = l_{\pi N} + \frac{1}{2}$	$(-1)^L$	0	
$\gamma N \to \pi N$	$E_{l_{\pi N}-}$	$L + \frac{1}{2} = J = l_{\pi N} - \frac{1}{2}$	$(-1)^L$	2	
$\gamma N \to \pi N$	$M_{l_{\pi N}+}$	$L + \frac{1}{2} = J = l_{\pi N} + \frac{1}{2}$	$(-1)^{L+1}$	1	
$\gamma N \to \pi N$	$M_{l_{\pi N}-}$	$L - \frac{1}{2} = J = l_{\pi N} - \frac{1}{2}$	$(-1)^{L+1}$	1	
$\gamma N \to \pi \Delta$	$E^{l_{\pi N}}_{l_{\pi\Delta}++}$	$L + \frac{1}{2} = J = l_{\pi\Delta} + \frac{3}{2}$	$(-1)^L$	0	$l_{\pi\Delta} + 2$
$\gamma N \to \pi \Delta$	$E^{l_{\pi N}}_{l_{\pi\Delta}+}$	$L - \frac{1}{2} = J = l_{\pi\Delta} + \frac{1}{2}$	$(-1)^L$	0	$l_{\pi\Delta}$
$\gamma N \to \pi \Delta$	$E^{l_{\pi N}}_{l_{\pi\Delta}-}$	$L + \frac{1}{2} = J = l_{\pi\Delta} - \frac{1}{2}$	$(-1)^L$	2	$l_{\pi\Delta}$
$\gamma N \to \pi \Delta$	$E^{l_{\pi N}}_{l_{\pi\Delta}--}$	$L - \frac{1}{2} = J = l_{\pi\Delta} - \frac{3}{2}$	$(-1)^L$	2	$l_{\pi\Delta} - 2$
$\gamma N \to \pi \Delta$	$M^{l_{\pi N}}_{l_{\pi\Delta}++}$	$L - \frac{1}{2} = J = l_{\pi\Delta} + \frac{3}{2}$	$(-1)^{L+1}$	0	$l_{\pi\Delta} + 2$
$\gamma N \to \pi \Delta$	$M^{l_{\pi N}}_{l_{\pi\Delta}+}$	$L + \frac{1}{2} = J = l_{\pi\Delta} + \frac{1}{2}$	$(-1)^{L+1}$	1	$l_{\pi\Delta}$
$\gamma N \to \pi \Delta$	$M^{l_{\pi N}}_{l_{\pi\Delta}-}$	$L - \frac{1}{2} = J = l_{\pi\Delta} - \frac{1}{2}$	$(-1)^{L+1}$	1	$l_{\pi\Delta}$
$\gamma N \to \pi \Delta$	$M^{l_{\pi N}}_{l_{\pi\Delta}--}$	$L + \frac{1}{2} = J = l_{\pi\Delta} - \frac{3}{2}$	$(-1)^{L+1}$	3	$l_{\pi\Delta} - 2$

Table 1: Generalized multipoles for $\gamma N \to \pi\Delta$, compared with $\gamma N \to \pi N$.

$$
\begin{aligned}
A^J_{(n+1)-} = \sqrt{2}\Bigg\{ & -\frac{\sqrt{3(J+\frac{3}{2})(J-\frac{1}{2})}}{8J}\left\langle l_f = J+\tfrac{1}{2},\, s_f = \tfrac{3}{2}\left|T^J\right| l_i = J - \tfrac{3}{2},\, s_i = \tfrac{3}{2}\right\rangle \\
& + \frac{J+\frac{3}{2}}{8J}\left\langle l_f = J+\tfrac{1}{2},\, s_f = \tfrac{3}{2}\left|T^J\right| l_i = J + \tfrac{1}{2},\, s_i = \tfrac{3}{2}\right\rangle \\
& + \frac{1}{2}\sqrt{\frac{J+\frac{3}{2}}{2J}}\left\langle l_f = J+\tfrac{1}{2},\, s_f = \tfrac{3}{2}\left|T^J\right| l_i = J + \tfrac{1}{2},\, s_i = \tfrac{1}{2}\right\rangle \Bigg\}\ , \\
& \text{for} \quad P = (-1)^{J-\frac{1}{2}}\ , \qquad (10)
\end{aligned}
$$

where we have given only two of the eight expressions as an example. Finally, as discussed by Walker [2], the helicity elements, $A_{l\pm}$ and $B_{l\pm}$, can be expressed in terms of the conventional electric and magnetic multipoles, $E_{l\pm}$ and $M_{l\pm}$, of $\gamma N \to \pi N$. The difference between these two sets comes from the angular momentum coupling in the initial photon-nucleon state. The helicity elements require coupling the spin of the photon with the spin of the nucleon to a total initial spin state which is then coupled with the photon-nucleon orbital angular momentum l_i to a total angular momentum J. The electric and magnetic multipoles, on the other hand, making use of the classical notation of electric and magnetic fields, require coupling the spin of the photon to the orbital angular momentum l_i, resulting in $L = l_i,\ l_i \pm 1$, which is then coupled to the spin of the nucleon to form the total angular momentum J. We introduce and define a set of eight generalized multipoles for the process $\gamma N \to \pi\Delta$ using the notation: $E^{l_N}_{l\pm\pm}$, $E^{l_N}_{l\pm}$, $M^{l_N}_{l\pm\pm}$, $M^{l_N}_{l\pm}$. The subscript l denotes the relative orbital momentum in the final state, $l_{\pi\Delta}$, while the superscript l_N is redundant and merely denotes what the πN orbital angular momentum would be. Other angular momentum properties are given in table 1.

Partial wave	Multipole $\gamma N \to \pi N$	Multipole $\gamma N \to \pi \Delta$
S_{11}	E_{0+}	E^0_{0+}, E^0_{2--}
P_{13}	E_{1+}, M_{1+}	E^1_{1+}, M^1_{1+}, E^1_{3--}, M^1_{3--}
D_{13}	E_{2-}, M_{2-}	E^2_{2-}, M^2_{2-}, E^2_{0++}, M^2_{0++}

Table 2: Comparison between conventional and generalized multipoles.

As an example, two of these multipoles are given below as a function of the partial-wave amplitudes in the LS basis,

$$E^{l_{\pi N}}_{l_{\pi\Delta}--} = \frac{\langle l_f = J+\frac{3}{2},\, s_f = \frac{3}{2} \left| T^J \right| l_i + s_\gamma = J + \frac{1}{2},\, s_N = \frac{1}{2} \rangle}{\sqrt{(J+\frac{1}{2})(J+\frac{3}{2})}} \,, \qquad \text{for} \quad P = (-1)^{J+\frac{1}{2}} \,, \tag{11}$$

$$E^{l_{\pi N}}_{l_{\pi\Delta}-} = \frac{\langle l_f = J+\frac{1}{2},\, s_f = \frac{3}{2} \left| T^J \right| l_i + s_\gamma = J - \frac{1}{2},\, s_N = \frac{1}{2} \rangle}{\sqrt{(J-\frac{1}{2})(J+\frac{1}{2})}} \,, \qquad \text{for} \quad P = (-1)^{J-\frac{1}{2}} \,. \tag{12}$$

In order to clarify the meaning of these generalized multipoles we present for a few cases in table 2 a comparison between standard πN partial waves, conventional $\gamma N \to \pi N$ multipoles and generalized $\gamma N \to \pi \Delta$ multipoles. For the purpose of identifying baryon resonances this illustrates that, e.g., just as the $S_{11}(1535)$ state shows up in the $N(\gamma,\pi)N$ multipole E_{0+} it contributes to the $N(\gamma,\pi)\Delta$ multipoles E^0_{0+} and E^0_{2--}. Similarly, the famous $P_{33}(1232)$ state which appears in the $N(\gamma,\pi)N$ multipoles E_{1+} and M_{1+} contributes to the generalized multipoles E^1_{1+}, M^1_{1+}, E^1_{3--}, and M^1_{3--}. Note that no isospin index has been attached to the generalized multipoles.

The next step will be to actually model these generalized multipoles which will be done in an effective Lagrangian coupled-channels framework. On the experimental side, performing a partial-wave multipole analysis and actually extracting these multipoles from cross section and polarization data obtained at Jlab and another facilities represents an arduous and challenging task in the years to come.

References

[1] T. Feuster and U. Mosel, Phys. Rev. C **59**, 460 (1999).

[2] R.L. Walker, Phys. Rev. **182**, 1729 (1969).

[3] G.F. Chew, M.L. Goldberger, F.E. Low, and Y. Nambu, Phys. Rev. **106**, 1345 (1957).

[4] D.M. Manley, R.A. Arndt, Y. Goradia, and V.L. Teplitz, Phys. Rev. D **30**, 904 (1984).

N^* masses from lattice QCD

Leming Zhou[a] and Frank X. Lee[a,b]

[a]*Center for Nuclear Studies, Department of Physics,*
The George Washington University, Washington, DC 20052, U.S.A.
[b]*Jefferson Lab, 12000 Jefferson Avenue, Newport News, VA 23606, USA*

(Received: 31 October 2001)

We report results on N^* masses in the spin 1/2 and 3/2 sectors using an anisotropic lattice and a highly-improved lattice QCD action. States with both positive and negative parity are isolated via parity projection methods. The need for spin project to isolate the spin 3/2 states is also demonstrated. Clear splittings from the nucleon ground state are observed. The basic pattern of the splittings is consistent with experiments at the quark masses explored.

Lattice QCD can play an important role in understanding the N^* spectrum. One can systematically study the spectrum sector by sector, with the ability to dial the quark masses, dissect the degrees of freedom, assess the systematic errors, all on the computer. The rich structure of the excited baryon spectrum, as tabulated by the particle data group [1], provides a fertile ground for exploring how the internal degrees of freedom in the nucleon are excited and how QCD works in a wider context. One outstanding example is the parity splitting pattern in the low-lying N^* spectrum which is a direct manifestation of spontaneous chiral symmetry breaking of QCD, because without it QCD predicts parity doubling in the baryon spectrum. The experimental effort on the excited baryons has intensified in recent years at JLab and other accelerators, generating renewed debate on how well these states are known. The star-rating system on the observed states is a reflection of the situation. Given that state-of-the-art lattice QCD simulations have produced a ground-state spectrum that is very close to the observed values [2], it is important to extend the success beyond the ground states. There exist already a number of lattice studies of N^* spectrum [3, 4, 5, 6], focusing mostly on the spin 1/2 sector. In this study, we explore the possibility of calculating the excited baryon states in the spin 3/2 sector. A complimentary study from the perspective of vacuum condensates is in [7].

We consider the following interpolating field with $I(J^P) = \frac{1}{2}\left(\frac{3}{2}^+\right)$ [8]

$$\chi_\mu = \epsilon^{abc}\left(u_a^T C\gamma_5\gamma_\rho d_b\right)\left(g^{\mu\rho} - \frac{1}{4}\gamma^\mu\gamma^\rho\right)\gamma_5 u_c \ . \tag{1}$$

Interpolating field for Σ and Ξ can be obtained with appropriate substitutions of quark fields. For the Λ we consider three types interpolating fields which we term as SU(3) octet (Λ_8), flavor singlet (Λ_s), and common (Λ_c) having the structure:

$$\chi_\mu^{\Lambda_8} = \frac{1}{\sqrt{6}}\epsilon_{abc}\{2(u_a^T\Gamma_1 d_b)\Gamma_2 s_c + (u_a^T\Gamma_1 s_b)\Gamma_2 d_c - (d_a^T\Gamma_1 s_b)\Gamma_2 u_c\} \ , \tag{2}$$

$$\chi_\mu^{\Lambda_s} = -2\epsilon_{abc}\{-(u_a^T\Gamma_1 d_b)\Gamma_2 s_c + (u_a^T\Gamma_1 s_b)\Gamma_2 d_c - (d_a^T\Gamma_1 s_b)\Gamma_2 u_c\} \ . \tag{3}$$

Here $\Gamma_1 = C\gamma_5\gamma_\rho$ and $\Gamma_2 = (g^{\mu\rho} - \frac{1}{4}\gamma^\mu\gamma^\rho)\gamma_5$ for spin-3/2 states. For spin-1/2 states, $\Gamma_1 = C\gamma_5$, $\Gamma_2 = 1$. The common $\chi_\mu^{\Lambda_c}$ consists of terms common to both $\chi_\mu^{\Lambda_8}$ and $\chi_\mu^{\Lambda_s}$. It does not impose any flavor symmetry on the quarks composing Λ.

Despite having an explicit parity by construction, these interpolating fields couple to both positive and negative parity states. A parity projection is needed to separate the two. In the large Euclidean time limit, the correlator with fixed boundary condition in the time direction and zero spatial momentum becomes

$$G_{\mu\nu}(t) = \sum_{\mathbf{x}} \langle 0 | \chi_\mu(x)\, \bar{\chi}_\nu(0) | 0 \rangle = f_{\mu\nu} \left[\lambda_+^2 \frac{\gamma_4 + 1}{2} e^{-M_+ t} + \lambda_-^2 \frac{-\gamma_4 + 1}{2} e^{-M_- t} \right] , \tag{4}$$

where $f_{\mu\nu}$ is some function common to both terms. The relative sign in front of γ_4 provides the solution: by taking the trace of $G_{\mu\nu}(t)$ with $(1 \pm \gamma_4)/4$, one can isolate M_+ and M_-, respectively.

It is well-known that a spin 3/2 interpolating field couples to both spin 3/2 and spin 1/2 states. A spin projection can be used to isolate the individual contributions in the correlation function $G_{\mu\nu}$. Using the spin-3/2 projection operator [9],

$$P^{3/2}_{\mu\nu} = g_{\mu\nu} - \frac{1}{3}\gamma_\mu \gamma_\nu - \frac{1}{3p^2}(\gamma \cdot p \gamma_\mu p_\nu + p_\mu \gamma_\nu \gamma \cdot p) , \tag{5}$$

the spin-3/2 and spin-1/2 can be projected out by

$$G^{3/2}_{\mu\nu}(t) = \sum_{\lambda=1}^{4} G_{\mu\lambda}(t) P^{3/2}_{\lambda\nu} , \qquad G^{1/2}_{\mu\nu}(t) = \sum_{\lambda=1}^{4} G_{\mu\lambda}(t)(1 - P^{3/2}_{\lambda\nu}) . \tag{6}$$

The details of the simulation parameters can be found in [4]. First we present in Figure 1 mass ratios for the spin 1/2 baryons to the ground-state nucleon as a function of $(\pi/\rho)^2$. Mass ratios have minimal dependence on the uncertainties in determining the scale and the quark masses, so that a more reliable comparison with experiment could be made.

Figure 2 shows the results for the 3/2+ N^* states. Spin projection reveals clearly two different exponentials due to the spin-3/2 and spin-1/2 parts, with the expected behavior of 3/2+ state heavier than the 1/2+ one. One would get a false signal for the spin-3/2 state from the dominant spin-1/2 state without spin projection. The large error bars indicate sensitive cancellations in the projection procedure. Figure 3 shows the similar plots for the 3/2− N^* states.

In conclusion, we have obtained clear signals for spin 3/2 N^* states on an anisotropic lattice. Both states of both negative and positive parity are isolated with a parity projection technique. The need for spin projection is further demonstrated. The basic pattern of the splittings is mostly consistent with experiment, but more study is needed to address the discretization errors. Of particular importance is the approach to the chiral limit, which can be studied with the overlap action which has exact chiral symmetry on the lattice [10].

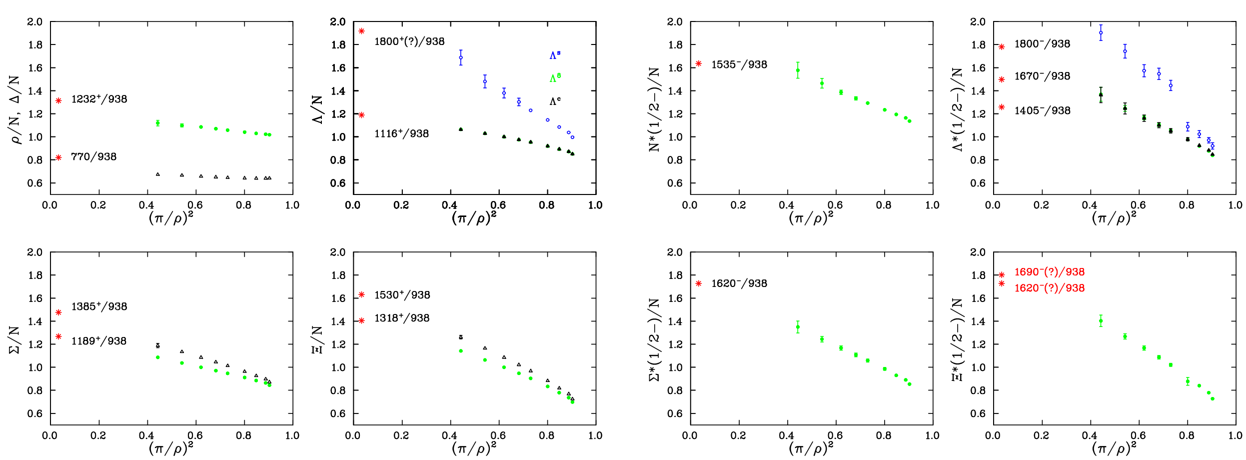

Figure 1: Left: mass ratios of ground state baryons. Right: mass ratios of 1/2− N^* states. Experimental points are indicated for reference.

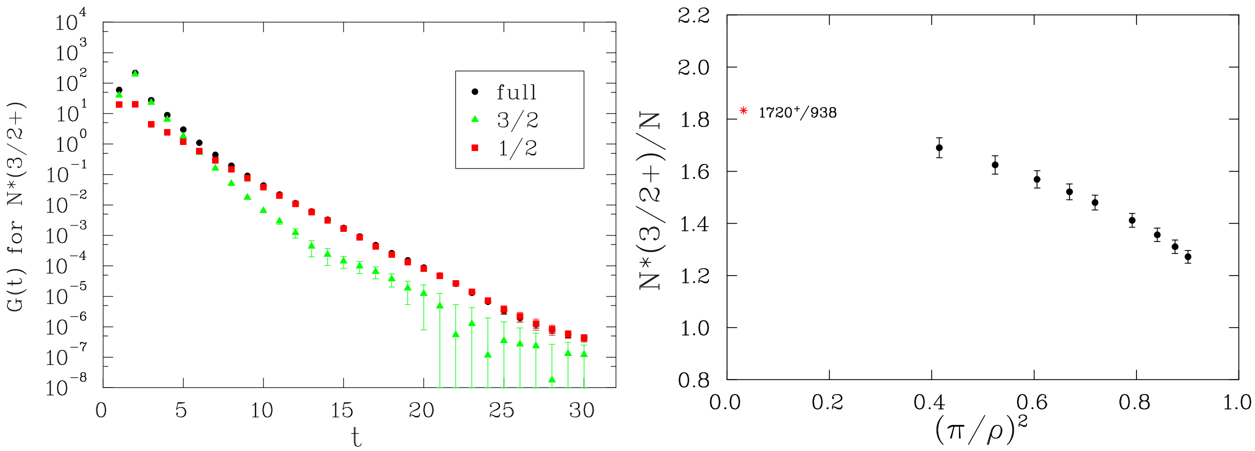

Figure 2: Left: correlation functions for positive-parity nucleon states at the smallest quark mass. Right: mass ratios for 3/2+ N^* states. Experimental points are indicated for reference.

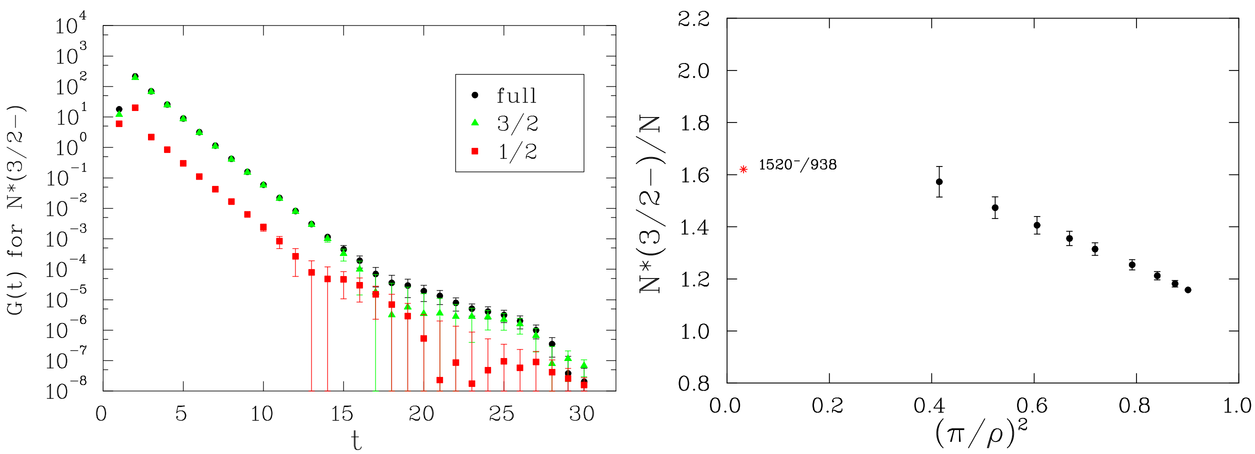

Figure 3: Similar to Figure 2, but for negative-parity states.

Acknowledgments: This work is supported in part by U. S. Department of Energy under grant DE-FG02-95ER40907, and is part of the effort by the Lattice Hadron Physics Collaboration [11]. The computing resources at NERSC and JLab have been used.

References

[1] Particle Data Group, Eur. Phys. J. C **15**, 1 (2000).
[2] S. Aoki, *et al.*, Phys. Rev. Lett. **84**, 238 (2000).
[3] D.B. Leinweber, Phys. Rev. D **51**, 6383 (1995).
[4] F.X. Lee, D.B. Leinweber, Nucl. Phys. B (Proc. Suppl.) **73**, 258 (1999); F.X. Lee, hep-lat/0011060.
[5] S. Sasaki, *et. al.*, hep-ph/0004252, hep-lat/0002019, hep-lat/0102010.
[6] D. Richards, Nucl. Phys. B (Proc. Suppl.) **94**, 269 (2001); hep-lat/0106022.
[7] X. Liu, F.X. Lee, these proceedings.
[8] Y. Chung, H. G. Dosch, M Kremer, and D. Schall, Nucl. Phys. B **197**, 55 (1982).
[9] D.B. Leinweber, T. Draper, and R.M. Woloshyn, Phys. Rev. D **46**, 3067 (1992).
[10] S.J. Dong, F.X. Lee, K.F. Liu, J.B. Zhang, Phys. Rev. Lett. **85**, 5051 (2000).
[11] Lattice Hadron Physics Collaboration, http://www.jlab.org/ dgr/lhpc/

N^* masses from QCD sum rules

Xinyu Liu[a] and Frank X. Lee[a,b]

[a] *Center for Nuclear Studies, Department of Physics, The George Washington University, Washington, DC 20052, U.S.A.*
[b] *Jefferson Lab, 12000 Jefferson Avenue, Newport News, VA 23606, USA*

(Received: 28 October 2001)

We report N^* masses in the spin-1/2 and spin-3/2 sectors using the method of QCD Sum Rules. They are based on three independent sets derived from generalized interpolating fields. The predictive ability of each sum rule is examined by a Monte-Carlo based analysis procedure in which all three phenomenological parameters (mass, coupling, threshold) are extracted simultaneously. A parity projection technique is also studied.

The QCD Sum Rule method [1] is a time-honored method that has proven useful in revealing a connection between hadron phenomenology and the non-perturbative nature of the QCD vacuum via only a few parameters (the vacuum condensates). It has been successfully applied to a variety of observables in hadron phenomenology, providing valuable insights from a unique, QCD-based perspective, and continues an active field (try a keyword search with 'QCD Sum Rule'). The method is analytical (no path integrals!), is physically transparent (one can trace back term by term which operators are responsible for what), and has minimal model dependence (Borel transform, and a continuum threshold). The accuracy of the approach is limited due to limitations inherent in the operator-product-expansion (OPE), but well understood.

Our goal is to explore the possibility of using the method to understand the N* spectrum. The calculation of baryon masses in the approach is not new [2, 3, 4, 5, 6]. Here we focus on the excited states and emphasize the predictive ability of the method for N* properties based on careful analysis, using a rigorous Monte Carlo-based [7] numerical analysis procedure that treats all three phenomenological parameters (mass, coupling, threshold) as free parameters and extracts them simultaneously with error bars. In particular, we study the low-lying states in the spin-1/2 and spin-3/2 sectors with both positive and negative parity. A similar analysis for the baryon decuplet has been done [8].

The starting point is the time-ordered, two-point correlation function in the QCD vacuum:

$$\Pi(p) = i \int d^4x \, e^{ip\cdot x} \langle 0 \,|\, T\{\, \eta(x)\, \bar{\eta}(0) \,\}\,|\, 0\rangle \ , \tag{1}$$

where η is the interpolating field that has the quantum numbers of the baryon under consideration. We consider the most general current for the nucleon with $I(J^P) = \frac{1}{2}\left(\frac{1}{2}^+\right)$,

$$\eta^N_{1/2}(x) = -2 \ \left[\epsilon_{abc} \left(u^{aT}(x) C\gamma_5 d^b(x) \right) u^c(x) + \beta \, \epsilon_{abc} \left(u^{aT}(x) C d^b(x) \right) \gamma_5 u^c(x) \right] \ . \tag{2}$$

Here C is the charge conjugation operator, the superscript T means transpose, and ϵ_{abc} makes it color-singlet. The real parameter β can be varied to achieve maximal overlap with the state in question. The choice advocated by Ioffe [2] and often used in QCD sum rules studies corresponds to $\beta = -1.0$. It is well-known that a baryon interpolating field couples to states of both parities, despite having an explicit parity by construction. The results below will show that β can be varied to saturate a sum rule with either positive or negative parity states. For states with $I(J^P) = \frac{1}{2}\left(\frac{3}{2}^+\right)$, we consider

$$\eta^N_{3/2,\mu}(x) = \epsilon_{abc} \left[\left(u^{aT}(x) C\sigma_{\rho\lambda} d^b(x) \right) \sigma^{\rho\lambda}\gamma_\mu u^c(x) - \left(u^{aT}(x) C\sigma_{\rho\lambda} u^b(x) \right) \sigma^{\rho\lambda}\gamma_\mu d^c(x) \right] \ . \tag{3}$$

The interpolating fields for Σ, Λ and Ξ can be obtained by appropriate substitutions of quark fields under SU(3) color symmetry or flavor symmetry.

With two kinds of interpolating fields, three possible correlation functions can be constructed: the correlator of generalized spin-1/2 currents $\eta_{1/2}$ and $\bar{\eta}_{1/2}$, the mixed correlator of generalized spin-1/2 current $\eta_{1/2,\mu} = \gamma_\mu \gamma_5 \eta_{1/2}$ and the spin-3/2 current $\bar{\eta}_{3/2,\nu}$, and the correlator of spin-3/2 currents $\eta_{3/2,\mu}$ and $\bar{\eta}_{3/2,\nu}$. From them, 11 independent sum rules emerge which can be used to study $1/2\pm$ and $3/2\pm$ states.

Table 1 shows the predictions for 1/2+ states from the chiral-odd sum rules at the tenser structure $\gamma_\mu p_\nu \hat{p}$, using the Monte-Carlo analysis. Sum rules fall into two categories: one with odd-dimension operators (chiral-odd) and the other with even-dimension operators (chiral-even). The predictions compare favorably with the observed values, with an accuracy of about 100 MeV. The couplings come as by-products which are useful in the calculation of matrix elements because they enter as normalization. Table 2 shows the predictions for 3/2− states.

Table 1: Predictions for 1/2+ states from the chiral-odd sum rules at the structure $\gamma_\mu p_\nu \hat{p}$.

Sum Rule	Region (GeV)	w (GeV)	$\tilde{\lambda}_{1/2}\tilde{\alpha}_{1/2}$ (GeV^6)	Mass (GeV)	Exp. (GeV)
$N_{\frac{1}{2}+}$ ($\beta = +1.0$)	1.06 to 1.46	1.31± .22	1.13± .53	1.06± .11	0.938
$\Sigma_{\frac{1}{2}+}$ ($\beta = +1.0$)	1.12 to 1.53	1.48± .23	1.62± 0.68	1.16 ± .12	1.193
$\Xi_{\frac{1}{2}+}$ ($\beta = +1.0$)	1.35 to 1.80	1.69± .27	2.61± 1.20	1.32± .14	1.318
$\Lambda_{\frac{1}{2}+}$ ($\beta = +1.0$)	1.28 to 1.72	1.53± .24	0.66± 0.28	1.23± .12	1.116

Table 2: Predictions for 3/2− states from the chiral-odd sum rules at the structure $g_{\mu\nu}$.

Sum Rule	Region (GeV)	w (GeV)	$\tilde{\lambda}^2_{3/2}$ (GeV^6)	Mass (GeV)	Exp. (GeV)
$N_{\frac{3}{2}-}$	0.95 to 1.17	1.65± .24	27.6± 11.8	1.44± .13	1.520
$\Sigma_{\frac{3}{2}-}$	1.29 to 1.36	1.91± .25	46.6± 20.1	1.69 ± .14	1.580
$\Xi_{\frac{3}{2}-}$	1.30 to 1.39	2.19± .27	84.8± 42.9	1.84± .16	1.820
$\Lambda_{\frac{3}{2}-}$	1.22 to 1.32	2.01± .25	19.8± 9.3	1.71± .15	1.690

Table 3: Predictions for 1/2− states from the new method where parity is exactly separated.

Sum Rule	Region (GeV)	w (GeV)	$\tilde{\lambda}^2_{3/2}$ (GeV^6)	Mass (GeV)	Exp. (GeV)
$N_{\frac{1}{2}-}$ ($\beta = +1.1$)	0.80 to 1.80	2.26±.08	4.58±.38	1.53±.05	1.535
$\Sigma_{\frac{1}{2}-}$ ($\beta = +1.1$)	0.80 to 1.90	2.35±.06	5.74±.69	1.63±.07	1.620
$\Xi_{\frac{1}{2}-}$ ($\beta = +1.1$)	0.80 to 1.80	2.38±.06	5.42±.68	1.61±.08	1.620
$\Lambda_{\frac{1}{2}-}$ ($\beta = +1.1$)	0.90 to 1.80	2.49±.04	7.06±.55	1.67±.05	1.670

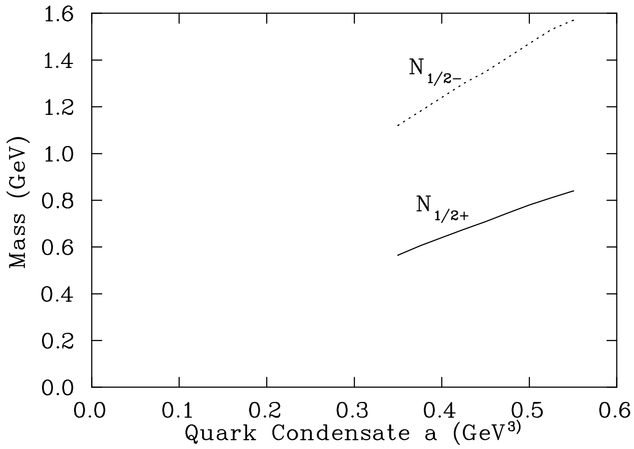

Figure 1: Mass splitting between $N^*_{\frac{1}{2}-}$ and $N_{\frac{1}{2}+}$ as a function of the quark condensate parameter $a = -(2\pi)^2 \langle \bar{q}q \rangle$. The physical point corresponds to $a = 0.52$ GeV^3.

One drawback in the conventional approach is that states with both parities contribute in the sum rules. Although sometimes one can saturate a sum rule with a certain parity by adjusting β, as done above, it is desirable to separate the two parities exactly. This can be achieved by replacing the time-ordering operator T in the correlation function in Eq. (1) with $x_0 > 0$, and constructing sum rules in the complex p_0-space in the rest frame ($\vec{p} = 0$) [9]. This is equivalent to a parity projection technique used in lattice QCD calculation of N* masses [10]. Table 3 shows the predictions for 1/2− states in this method. The results are much improved, as indicated by the smaller error bars and very wide Borel regions. The agreement with experiment is excellent. To further investigate the origin of splittings between parity partners, we show in Figure 1 the mass splittings between $N_{\frac{1}{2}-}$ and $N_{\frac{1}{2}+}$ as a function of the quark condensate (the order parameter of spontaneous chiral symmetry breaking). One can see a clear decrease in the splitting with decreasing quark condensate, in the range that the sum rule does not break down.

In conclusion, we demonstrated the predictive power of QCD sum rules for N* masses in the low-lying 1/2± and 3/2− sectors, with an accuracy on the order of 5 to 10%. The parity separation method is promising. We are extending it to the spin-3/2 sector. More analysis is under way to understand the details of the splitting patterns across particle channels and parities, in terms of explicit and dynamical chiral symmetry breaking.

Acknowledgment: This work is supported in part by U.S. Department of Energy under Grant DE-FG03-93DR-40774.

References

[1] M.A. Shifman, A.I. Vainshtein and Z.I. Zakharov, Nucl. Phys. **B147**, 385, 448 (1979).

[2] B.L. Ioffe, Nucl. Phys. B 188, 317 (1981); Nucl. Phys. B 191, 591(E) (1981); Z. Phys. C 18, 67, (1983)

[3] V.M. Belyaev and B.L. Ioffe, Sov. Phys. JETP **56**, 493 (1982); Sov. Phys. JETP **57**, 716 (1983).

[4] Y. Chung, H.G. Dosch, M. Kremer and D. Schall, Z. Phys. **C57**, 151 (1984).

[5] L.J. Reinders, H. Rubinstein and S. Yazaki, Phys. Rep. **127**, 1-97 (1985).

[6] D.B. Leinweber, Ann. of Phys. (N.Y.) **198**, 203 (1990).

[7] D.B. Leinweber, Ann. of Phys. (N.Y.) **254**, 328 (1997).

[8] F.X. Lee, Phys. Rev. C **D57**, 322 (1998).

[9] D. Jido, N. Kodama, and M. Oka, Phys. Rev. **D54**, 4532 (1996); hep-ph/9611322.

[10] L. Zhou, F.X. Lee, these proceedings.

Chiral behavior of quark distributions from lattice QCD

W. Detmold[a], W. Melnitchouk[b], and A.W. Thomas[a]

[a]*Special Research Centre for the Subatomic Structure of Matter and Department of Physics and Mathematical Physics, Adelaide University, Adelaide, SA 5005, Australia.*
[b]*Jefferson Lab, 12000 Jefferson Avenue, Newport News, VA 23606, U.S.A.*

(Received: 22 October 2001)

The current status of quark distributions within lattice QCD is reviewed. Lattice data on the low moments of the nonsinglet distribution $u-d$ are presented and a method for the extrapolation of these moments to physical quark masses is proposed. The extent to which the available moments determine the Björken x and quark mass dependence of the original distribution is also investigated.

1 Moments of quark distributions

Until recently, state of the art studies [1] of the moments of parton distributions within lattice QCD have led to large discrepancies with experimental data. Due to computational constraints, current lattice calculations are performed at quark masses much greater than those of the physical light quarks. Consequently, an extrapolation to the physical region must be made in order to compare with experiment. A naive linear extrapolation results in values for the first three non-trivial moments of the unpolarised $u-d$ distribution that are 50% above the phenomenological values [2]. However, this approach ignores important physics related to the chiral and heavy quark limits. The inclusion of these effects motivates an improved extrapolation procedure that provides a possible resolution of this discrepancy [3].

One knows on very general grounds that a linear extrapolation in m_q (or equivalently m_π^2 via the Gell-Mann–Oakes–Renner relation) must fail as it omits crucial nonanalytic structure associated with chiral symmetry breaking. Even at the lowest quark mass accessed on the lattice, the pion mass is over 300 MeV. Earlier studies of chiral extrapolations of lattice data for hadron masses, magnetic moments and charge radii (see Ref. [3] for details) have shown that for quark masses above 50–60 MeV, hadron properties behave very much as one would expect in a constituent quark model, with relatively slow, smooth behavior as a function of the quark mass. However, for $m_q < 50$ MeV one typically finds rapid, nonlinear variation due to the nonanalytic behavior of Goldstone boson loops. In particular, the leading nonanalytic (LNA) contribution to the n-th moment, $\langle x^n\rangle_q$, of a nonsinglet quark distribution behaves as [4] $\langle x^n\rangle_q \sim m_\pi^2 \log m_\pi^2$.

In addition, the quark distributions are known in the heavy quark limit; the proton consists of two up quarks and a down quark each carrying 1/3 of the momentum, so the distribution $u(x)-d(x) \overset{m_q\to\infty}{\longrightarrow} \delta(x-1/3)$. Consequently, the moments behave as $\langle x^n\rangle_{u-d} \overset{m_q\to\infty}{\longrightarrow} 1/3^n$. In order to fit the lattice data at larger m_π while preserving the correct chiral behavior of moments as $m_\pi \to 0$ and the correct heavy quark limit, the moments of $u-d$ are fitted with the form:

$$\langle x^n\rangle_{u-d} \;=\; a_n\left(1+c_{\rm LNA}m_\pi^2\log\frac{m_\pi^2}{m_\pi^2+\mu^2}\right) \;+\; b_n\frac{m_\pi^2}{m_\pi^2+m_{b,n}^2}\;, \qquad (1)$$

where the coefficient $c_{\rm LNA} = -(1+3g_A^2)/(4\pi f_\pi)^2$ is determined from chiral perturbation theory, and b_n is constrained by the heavy quark limit to $b_n = \frac{1}{3^n} - a_n\left(1-\mu^2 c_{\rm LNA}\right)$. The parameter $m_{b,n}$ controls the approach to the heavy quark limit and is fixed to 5 GeV in the results presented here. In Ref. [3], the m_π dependence of the moments was investigated in a meson cloud based model and found to be well parameterised by Eq. (1), providing further motivation for the use of this form. The parameter μ represents the scale above which pion loops become unimportant. Studies of the

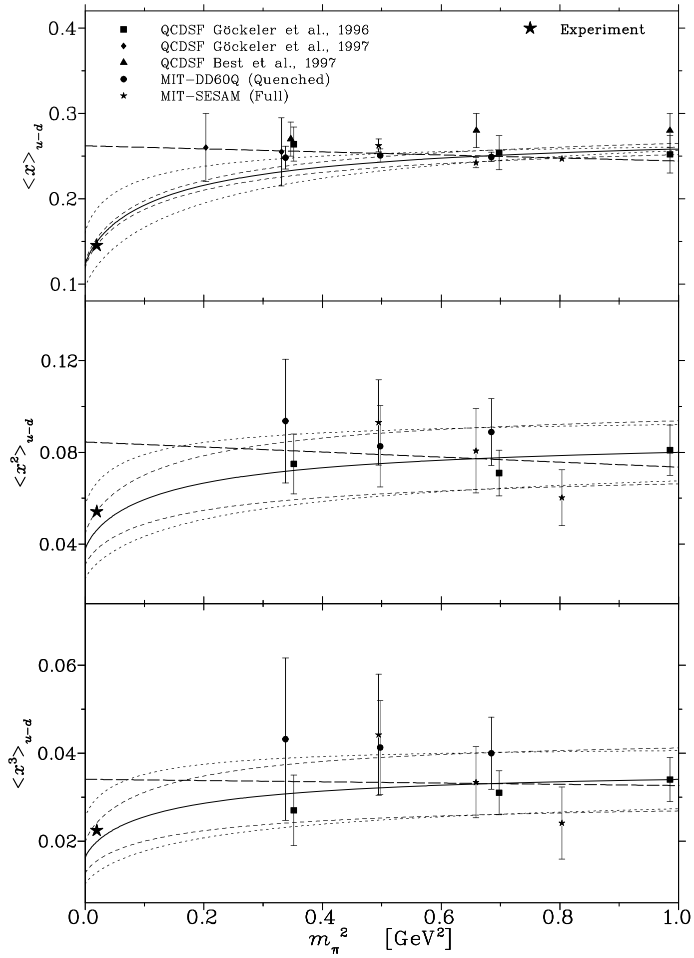

Figure 1: The three lowest, non-trivial moments of the $u-d$ quark distribution. The straight (long-dashed) lines are linear fits to the data, while the curves incorporate the LNA behavior in the chiral limit. For each moment, the best fit to the lattice data using Eq. (1) is shown by the solid curve (with μ = 550 MeV), while the inner envelope about this represents the statistical errors in the data. The effect of the uncertainty in the parameter μ is illustrated by the outer lower (upper) short-dashed curves, which correspond to μ = 400 (700) MeV. The star represents the phenomenological values [2]. The data are from Ref. [1].

m_π dependence of hadronic masses, magnetic moments and charge radii all suggest that pions begin to play an important role below $m_\pi \sim 500$ MeV.

Figure 1 shows the lattice data extrapolated on the basis of Eq. (1). Unfortunately, the lattice data are at too large quark masses for μ to be constrained reliably, however, with the choice μ = 550 MeV the agreement between the lattice data and the experimental values is clearly excellent. Accurate data at $m_\pi^2 \sim 0.05$ GeV^2 would allow μ to be determined from lattice calculations.

2 Björken x and mass dependence of quark distributions

One can also investigate to what extent the low moments can be used to determine the Björken x and quark mass dependence of the distribution $u_v(x) - d_v(x)$. One possible way to do this is to assume a functional form for the distribution and use the corresponding moment space expression to fit the extrapolated moments [5]. The resulting, reconstructed distribution is displayed in Fig. 2 along with the average parameterisation of Ref. [2], and the distribution that arises from the linearly extrapolated moments. Clearly, the agreement is good for the improved extrapolation, but the shape of the linearly extrapolated distribution is quite different.

Finally, having a formula that gives the first three moments at any value of m_π^2 allows an exploration of the mass dependence of the quark distribution. The distributions that result from fits to the moments for a variety of pion masses are shown in Fig. 3. As the mass increases, the

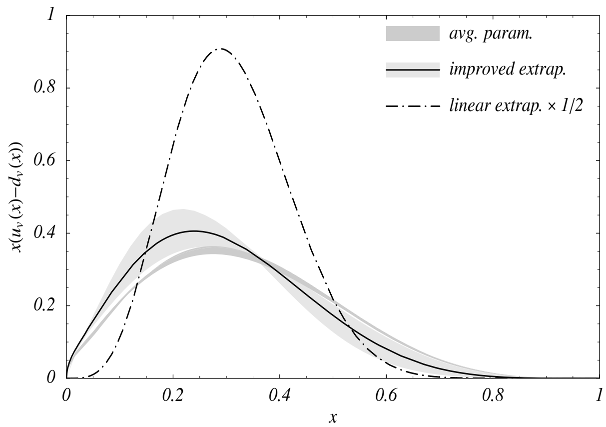

Figure 2: The physical valence $x(u_v(x) - d_v(x))$ distribution, extracted using the improved chiral extrapolation of the lattice moments (solid), and a linear extrapolation, scaled by a factor 1/2 (dot–dashed). The lighter shaded region indicates a 1σ variation of the fit parameters about the optimal values for the improved extrapolation, while the dark shaded region represents the spread between global parameterizations [2].

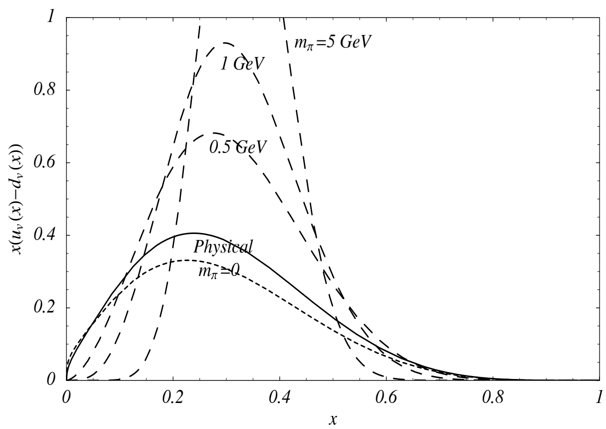

Figure 3: The nonsinglet valence distribution $x(u_v(x) - d_v(x))$ extracted from the improved extrapolation formula, Eq. (1), for various pion masses: $m_\pi = 0$ (short-dashed), $m_\pi = 0.139$ GeV (solid), $m_\pi = 0.5$, 1 and 5 GeV (long-dashed).

trend is clearly towards a heavy quark limit of a δ-function at $x = 1/3$. The similarity between the linearly extrapolated distribution of Fig. 2 and the heaviest pion mass distribution in Fig. 3 also supports, *a posteriori*, the inclusion of the heavy quark limit in the fitting form, Eq. (1).

In summary, we have shown that the correct chiral extrapolation of moments of nonsinglet parton distributions on the lattice resolves the long-standing discrepancy with experiment. Furthermore, we have demonstrated that the basic features of the x distribution can be reconstructed from just the lowest few moments calculated on the lattice.

Acknowledgments: We express our thanks both to our collaborators, J.W. Negele and D.B. Renner, and to the conference organisers. This work was supported by the Australian Research Council, the Physics Division of Argonne National Laboratory, and the DOE contract DE-AC05-84ER40150 under which the Southeastern Universities Research Association (SURA) operates the Thomas Jefferson National Accelerator Facility.

References

[1] M. Göckeler *et al.*, Phys. Rev. D **53**, 2317 (1996); M. Göckeler *et al.*, Nucl. Phys. Proc. Suppl. **53**, 81 (1997); C. Best *et al.*, hep-ph/9706502; D. Dolgov *et al.*, hep-lat/0011010.

[2] A.D. Martin, R.G. Roberts, W.J. Stirling and R.S. Thorne, Eur. Phys. J. C **14**, 133 (2000); H.L. Lai *et al.*, Eur. Phys. J. C **12**, 375 (2000); M. Glück, E. Reya and A. Vogt, Eur. Phys. J. C **5**, 461 (1998).

[3] W. Detmold *et al.*, Phys. Rev. Lett. 87, 172001 (2001).

[4] A.W. Thomas, W. Melnitchouk and F.M. Steffens, Phys. Rev. Lett. **85**, 2892 (2000).

[5] W. Detmold, W. Melnitchouk and A. W. Thomas, Eur. Phys. J Direct C **13**, 1 (2001).

The solar *hep* processes in effective field theory

Tae-Sun Park[a], Kuniharu Kubodera[a], Dong-Pil Min[b], and Mannque Rho[b,c,d]

[a] *Department of Physics and Astronomy, University of South Carolina, Columbia, SC 29208, USA*

[b] *School of Physics and Center for Theoretical Physics, Seoul National University, Seoul 151-742, Korea*

[c] *Service de Physique Théorique, CEA Saclay, 91191 Gif-sur-Yvette Cedex, France*

[d] *Institute of Physics and Applied Physics, Yonsei University, Seoul 120-749, Korea*

(Received: 31 October 2001)

By combining effective field theory with the standard nuclear physics approach (SNPA) we obtain a high-precision estimate of the S factor for the solar *hep* process. The accurate wave functions available in SNPA are used to evaluate the nuclear matrix elements for the transition operators that result from chiral perturbation theory (ChPT). All the contributions up to N^{3}LO in ChPT are included. The resulting parameter-free, error-controlled prediction is: $S(hep) = (8.6 \pm 1.3) \times 10^{-20}$ keV-b.

This brief report is based on the results of work done in collaboration with L.E. Marcucci, R. Schiavilla, M. Viviani, A. Kievsky and S. Rosati [2, 3]. A detailed exposition of the basic ideas underlying our approach can be found in [1].

1 Introduction

The *hep* process in the Sun,

$$^3\mathrm{He} + p \to {}^4\mathrm{He} + e^+ + \nu \ , \tag{1}$$

produces the highest energy solar neutrinos, $E_\nu^{\max}(hep) \simeq 20$ MeV. The *hep* neutrinos therefore can influence the interpretation of the results of a recent Super-Kamiokande experiment that have raised many important issues concerning the solar neutrino problem and neutrino oscillations [4,5]. It is to be noted that the reliable estimation of the *hep* cross section, indispensable for addressing these issues, is a long-standing challenge for nuclear physics [6]. This is mainly because the leading one-body contributions are highly suppressed and furthermore the chiral filter mechanism — which allows us to accurately estimate many-body corrections — is ineffective for this process. For a detailed discussion, see Ref. [2, 3].

The objective of our present work is to obtain a significantly improved estimate of the *hep* rate using effective field theory (EFT). To this end, we adopt a strategy that exploits the known merits of the standard nuclear physics approach (SNPA) and heavy-baryon chiral perturbation theory (HBChPT) simultaneously. HBChPT, a well established low-energy EFT of QCD, is used to calculate the transition operators; *all* the operators up to next-to-next-to-next-to-leading order (N^{3}LO) will be considered. The evaluation of the corresponding nuclear matrix elements requires highly accurate nuclear wave functions. Although it is, at least in principle, possible to derive from HBChPT nuclear wave functions to a specified chiral order, we choose not to do so. Instead, we use realistic wave functions obtained in SNPA. The power of the proposed scheme is the ability to correlate the beta decay processes in the $A = 2, 3, 4$ nuclei. Thus, as explained in more detail below, if the single unknown constant in our EFT is fixed using one of these processes, then we can make totally parameter-free predictions for the remaining processes.

2 Theory and results

The *hep* process is dominated by the Gamow-Teller (GT) transition, and hence the reliability of the *hep* rate estimate is essentially governed by precision with which one can calculate the GT amplitude. According to the chiral counting rule [9], the leading order contributions are due to the well-known one-body (1B) operators, and the first corrections arise from N^{3}LO two-body (2B) currents that are suppressed by $(Q/\Lambda_\chi)^3$ compared to the 1B. Here Q stands for the typical three-momentum scale and/or the pion mass, and $\Lambda_\chi \sim 1$ GeV is the chiral scale. As stated, we consider here *all* the contributions up to N^{3}LO. It is worth emphasizing that three-body currents, which are N^{4}LO, can be legitimately ignored in our N^{3}LO calculation.

The N^{3}LO 2B currents consist of the one-pion-exchange (OPE) and nucleon-nucleon contact-term (CT) parts, $\mathbf{A}_{2\mathrm{B}} = \mathbf{A}_{2\mathrm{B}}(\mathrm{OPE}) + \mathbf{A}_{2\mathrm{B}}(\mathrm{CT})$. With the low-energy constants fixed from πN data [13], the OPE part is completely determined. On the other hand, the CT part contains one parameter, $\hat{d}^R$, whose direct evaluation from QCD is not available at present. Fortunately, it turns out that tritium β-decay, μ-d capture and ν–d scattering are sensitive to the same parameter, $\hat{d}^R$, and that they do not depend on any additional parameters up to N^{3}LO. Thus, any of these processes can give the renormalization condition to fix the value of $\hat{d}^R$. Here we choose to use the tritium β-decay rate, Γ_β, which is accurately known experimentally [14]. Once $\hat{d}^R$ is fixed, our calculation involves no unknown parameters.

We calculate the matrix elements of the transition operators with state-of-the-art realistic nuclear wave functions. $A = 2, 3, 4$. We employ the correlated-hyperspherical-harmonics (CHH) wave functions, obtained with the Argonne v_{18} (Av18) potential (supplemented with the Urbana-IX three-nucleon potential for the $A \geq 3$ nuclei) [7]. To control short-range physics in a consistent manner, we apply the regulator

$$S_\Lambda(q^2) = \exp\left(-\frac{q^2}{2\Lambda^2}\right) \quad . \tag{2}$$

to all the nuclear systems in question. The cutoff parameter Λ characterizes the energy-momentum scale of our EFT.

The value of $\hat{d}^R$ determined from the experimental value of Γ_β is $\hat{d}^R = (1.00 \pm 0.07,\ 1.78 \pm 0.08,\ 3.90 \pm 0.10)$. Here and hereafter, parenthesized three numbers correspond to the three choices of Λ, $\Lambda = 500$, 600 and 800 MeV, in this order. To see the role of the $\hat{d}^R$-term, it is informative to look at $\delta_{2\mathrm{B}}$, the ratio of the 2B matrix element to that of 1B. With only the OPE part taken into account, we have $\delta_{2\mathrm{B}}^{\mathrm{OPE}} = (-1.1,\ -1.5,\ -2.0)$. The inclusion of the $\hat{d}^R$ term leads to $\delta_{2\mathrm{B}}^{\mathrm{N3LO}} = \delta_{2\mathrm{B}}^{\mathrm{OPE+CT}} = (-0.60,\ -0.64,\ -0.73)$. Thus the $\hat{d}^R$-term drastically reduces the Λ-dependence of the 2B contribution; we see only ~10 % variation for the entire range of Λ under study. The Λ-dependence in the total GT amplitude becomes more pronounced due to a strong cancellation between the 1B and 2B terms, but this amplified Λ-dependence still remains within acceptable levels.

In addition to the $^3S_1$ contributions governed by the GT amplitude, there are also tiny $^1S_0$ and sizable P-wave contributions. The latter have little Λ-dependence (< 2 %), and responsible for about one-third of the total S factor. Adding all the contributions, the S-factor at threshold reads

$$S(hep) = (8.6 \pm 1.3) \times 10^{-20} \text{ keV-b} \ , \tag{3}$$

where the "error" spans the range of the Λ-dependence for $\Lambda = 500$–800 MeV. This result is to be compared to the latest SNPA estimate in Ref. [7]: $S = 9.64 \times 10^{-20}$ keV-b.

3 Discussion

By determining the only parameter of the theory, $\hat{d}^R$, from the experimental data on triton beta decay, we have succeeded in estimating the *hep* S-factor in a parameter-free and error-controlled manner. Our HBChPT calculation (up to N^{3}LO) gives a much more accurate estimate than hitherto available. The EFT results turn out to give support to those obtained in the latest SNPA calculation [7].

To decrease the uncertainty in Eq.(3), we need to reduce the Λ-dependence in the two-body GT term. According to a general *tenet* of EFT, the Λ-dependence should diminish when higher order terms are included. A preliminary study indicates that it is indeed possible to reduce the Λ-dependence significantly by including N^{4}LO corrections. In this connection, we remark that the *hen* process, $^3\mathrm{He} + n \to {}^4\mathrm{He} + \gamma$, seems very interesting to look into. The *hen* process shares many features with the *hep* including the suppression of the 1B matrix element and the structure of the many-body currents. Accurate experimental data are available for the *hen* cross sections, but so far no theoretical calculations have succeeded in explaining the data quantitatively. Thus applying the same EFT technique to the *hen* process [15] is very interesting, and that will also provide a useful check of the formalism employed in our estimation of $S(hep)$.

References

[1] T.-S. Park, K. Kubodera, D.-P. Min and M. Rho, Nucl. Phys. A **684**, 101 (2001); G.E. Brown and M. Rho, Phys. Repts., in press, hep-ph/0101015

[2] T.-S. Park, L.E. Marcucci, R. Schiavilla, M. Viviani, A. Kievsky, S. Rosati, K. Kubodera, D.-P. Min and M. Rho, nucl-th/0106026; nucl-th/0107012.

[3] T.-S. Park, K. Kubodera, D.-P. Min and M. Rho, nucl-th/0108050.

[4] J.N. Bahcall, Phys. Repts. **333**, 47 (2000) and references therein.

[5] R. Escribano, J.-M. Frere, A. Gevaert and D. Monderen, Phys. Lett. B **444**, 397 (1998).

[6] J.N. Bahcall, hep-ex/0002018; J.N. Bahcall and P.I. Krastev, Phys. Lett. B **436**, 243 (1998).

[7] L.E. Marcucci *et al.*, Phys. Rev. C **63**, 015801 (2001).

[8] For a recent review, see J. Carlson and R. Schiavilla, Rev. Mod. Phys. **70**, 743 (1998).

[9] S. Weinberg, Phys. Lett. B **251**, 288 (1990); Nucl. Phys. B **363**, 3 (1991).

[10] T.-S. Park, K. Kubodera, D.-P. Min and M. Rho, Phys. Rev. Lett. **74**, 4153 (1995); Nucl. Phys. A **596**, 515 (1996).

[11] T.-S. Park, K. Kubodera, D.-P. Min and M. Rho, Phys. Lett. B **472**, 232 (2000).

[12] C.H. Hyun, T.-S. Park and D.-P. Min, Phys. Lett. B **516**, 321 (2001).

[13] V. Bernard, N. Kaiser and Ulf.-G. Meißner, Nucl. Phys. B **457**, 147 (1995).

[14] R. Schiavilla, V.G.J. Stoks, W. Glöckle, H. Kamada, A. Nogga, J. Carlson, R. Machleidt, V.R. Pandharipande, R.B. Wiringa, A. Kievsky, S. Rosati and M. Viviani, Phys. Rev. C **58**, 1263 (1998).

[15] Y.-H. Song *et. al.*, work in progress.

A method for calculating meson photoproduction from the nucleon

Michael G. Fuda and Hamoud Alharbi

Department of Physics, University at Buffalo-SUNY, Buffalo, NY 14260, U.S.A.

(Received: 10 August 2001)

The essential ingredient in the method is a mass operator which describes the coupling between meson-baryon, photo-baryon, and single-baryon channels. The various amplitudes are obtained from three-dimensional Lippmann-Schwinger equations. The S-matrix elements transform properly under inhomogeneous Lorentz transformations and moreover are gauge invariant. Within our framework we have derived the most general forms for the matrix elements describing the processes $\gamma + B \Longleftrightarrow B'$ and $\gamma + B \Longleftrightarrow \mu + B'$ where γ is a photon, B and B' are baryons, and μ is a meson. The various matrix elements can be derived from effective Lagrangians using Okubo's method.

1 Introduction

If the inhomogeneous Lorentz transformation $x' = ax + b$ is applied successively it leads to the multiplication law $(a', b') \circ (a, b) = (a'a, a'b + b')$. This is the law of combination for the Poincaré group. In relativistic quantum mechanics the state vectors must transform according to $|\psi'\rangle = U(a,b)|\psi\rangle$ where the unitary operators $U(a,b)$ provide a representation of the Poincaré group; in particular $U(a',b)\,U(a,b) = U(a'a, a'b+b')$. For proper inhomogeneous Lorentz transformations these operators can be parametrized in the form

$$U(a,b) = \exp\left(ib^{\mu}P_{\mu}\right)\exp\left(-\frac{i}{2}\omega^{\alpha\beta}J_{\alpha\beta}\right) \ , \quad \omega^{\alpha\beta} = -\omega^{\beta\alpha} \ , \quad J_{\alpha\beta} = -J_{\beta\alpha} \ , \tag{1}$$

where P is the four-momentum operator and J is the angular momentum tensor. The Poincaré algebra is obtained from $U(a',b)\,U(a,b) = U(a'a, a'b+b')$ by considering infinitesimal transformations and is given by the commutation rules

$$\begin{aligned} [P_{\mu}, P_{\nu}] &= 0 \ , \\ [J_{\mu\nu}, P_{\rho}] &= i\left(g_{\nu\rho}P_{\mu} - g_{\mu\rho}P_{\nu}\right) \ , \\ [J_{\mu\nu}, J_{\rho\lambda}] &= i\left(g_{\mu\lambda}J_{\nu\rho} + g_{\nu\rho}J_{\mu\lambda} - g_{\mu\rho}J_{\nu\lambda} - g_{\nu\lambda}J_{\mu\rho}\right) \ , \end{aligned} \tag{2}$$

where g is the metric tensor. In a Bakamjian-Thomas construction [1] of the generators, i.e., the components of P and J, it is convenient to define $P = \left(P^0, P^1, P^2, P^3\right) = (H, \mathbf{P})$, $\mathbf{K} = (J_{10}, J_{20}, J_{30})$, and $\mathbf{J} = (J_{23}, J_{31}, J_{12})$. Here H is the Hamiltonian, $\mathbf{P}$ is the three-momentum operator, $\mathbf{K}$ is the generator of rotationless boosts, and $\mathbf{J}$ is the angular momentum operator. The mass operator is defined by

$$M^2 = P^{\mu}P_{\mu} = H^2 - \mathbf{P}^2 \ , \tag{3}$$

which can be inverted to give the familiar formula

$$H = \left(\mathbf{P}^2 + M^2\right)^{1/2} \ . \tag{4}$$

By introducing the Newton-Wigner [2,3] position operator $\mathbf{X}$, a spin operator $\mathbf{S}$ can be defined through the relation

$$\mathbf{J} = \mathbf{X} \times \mathbf{P} + \mathbf{S} \ . \tag{5}$$

It can be shown [1,3] that the boost operator $\mathbf{K}$ can be expressed in the form

$$\mathbf{K} = -\frac{1}{2}\left(H\mathbf{X} + \mathbf{X}H\right) - \frac{\mathbf{P} \times \mathbf{S}}{M + H} \ . \tag{6}$$

According to (4)-(6), the 10 generators $\{H, \mathbf{P}, \mathbf{K}, \mathbf{J}\}$ have been expressed in terms of the set $\{M, \mathbf{P}, \mathbf{S}, \mathbf{X}\}$. The only non-zero commutators of this set are

$$\left[X^j, P^k\right] = i\delta_{jk} \ , \quad \left[S^j, S^k\right] = i\varepsilon_{jkl}S^l \ , \tag{7}$$

which are familiar from nonrelativistic quantum mechanics. If the members of the set $\{M, \mathbf{P}, \mathbf{S}, \mathbf{X}\}$ satisfy the correct commutation relations, then the generators defined by (4)-(6) satisfy the Poincaré algebra given by (2). In a Bakamjian-Thomas construction, we choose $\mathbf{P}$, $\mathbf{S}$, and $\mathbf{X}$ to be the same as the operators for the relevant system of non-interacting particles; then the only commutation rules of the set $\{M, \mathbf{P}, \mathbf{S}, \mathbf{X}\}$ that remain to be satisfied are $[\mathbf{P}, M] = 0$, $[\mathbf{X}, M] = 0$, $[\mathbf{S}, M] = 0$. We construct M according to $M = M_0 + U$, where M_0 is the mass operator for the non-interacting system, and U is an interaction. Then in order to ensure Poincaré invariance we must only impose the commutation rules

$$[\mathbf{P}, U] = 0 \ , \quad [\mathbf{X}, U] = 0 \ , \quad [\mathbf{S}, U] = 0 \ . \tag{8}$$

2 The model

For our model space we choose states of the type $|B\rangle, |\mu B\rangle, |\gamma B\rangle$, where B 's are baryon's, μ's are mesons, and γ is the photon. We encounter 5 types of interaction matrix elements; $\langle B| U |B\rangle$ is a mass renormaliztion constant, $\langle B'| U |\mu B\rangle$ and $\langle B'| U |\gamma B\rangle$ are vertex interactions, and $\langle \mu' B'| U |\mu B\rangle$ and $\langle \mu' B'| U |\gamma B\rangle$ are potentials. In the $|N\rangle - |\pi N\rangle$ sector, for example, the commutation rules (8) restrict these matrix elements to the forms

$$\begin{aligned}
\langle \mathbf{p}'_N \, i'm' | \, U \, |\mathbf{p}_N \, im\rangle &\backsim \delta^3\left(\mathbf{p}'_N - \mathbf{p}_N\right)\delta_{i'i}\delta_{m'm}U_{NN} \ , \\
\langle \mathbf{q}'\mathbf{p}'t' \, i'm' | \, U \, |\mathbf{p}_N \, im\rangle &\backsim \delta^3\left(\mathbf{p}' - \mathbf{p}_N\right)\langle t' \, i'm' | \, U_{\pi N,N}\left(\mathbf{q}'\right)|im\rangle \ , \\
\langle \mathbf{q}'\mathbf{p}'t' \, i'm' | \, U \, |\mathbf{q}\mathbf{p}tim\rangle &\backsim \delta^3\left(\mathbf{p}' - \mathbf{p}\right)\langle t' \, i'm' | \, U_{\pi N,\pi N}\left(\mathbf{q}', \mathbf{q}\right)|tim\rangle \ ,
\end{aligned} \tag{9}$$

where $\mathbf{q} = (\mathbf{p}_\pi)_{\text{cm}} = -(\mathbf{p}_N)_{\text{cm}}$, $\mathbf{p} = \mathbf{p}_\pi + \mathbf{p}_N$, the i's and $t's$ are 3-components of isospin, and the m's are 3-components of spin. The commutator $[\mathbf{P}, U] = 0$ leads to the Dirac delta functions in (9), while the commutator $[\mathbf{X}, U] = 0$ implies that $U_{NN}, U_{\pi N,N}(\mathbf{q}')$,and $U_{\pi N,\pi N}(\mathbf{q}', \mathbf{q})$ cannot depend on the *total* three-momentum of the states. In order for $[\mathbf{S}, U] = 0$ to be satisfied it is necessary that $U_{\pi N,N}(\mathbf{q}')$ and $U_{\pi N,\pi N}(\mathbf{q}', \mathbf{q})$ be rotationally invariant functions of $\mathbf{q}', \mathbf{q}$ and $\boldsymbol{\sigma}$. The structures such as (9) guarantee that the Poincaré algebra is satisfied. It can be shown that the Bakamjian-Thomas construction leads to $S-$matrix elements that transform properly in going from one inertial frame to another [4]. Transition probabilities are invariant.

In our model the strong interaction $T-$matrix elements are obtained by solving the Lippmann-Schwinger equations [5]

$$\begin{aligned}
T_{\mu' B',\mu B}\left(\mathbf{q}', \mathbf{q}; z\right) &= V_{\mu' B',\mu B}\left(\mathbf{q}', \mathbf{q}; z\right) + \sum_{\mu'' B''}\int \frac{V_{\mu' B',\mu'' B''}\left(\mathbf{q}', \mathbf{q}''; z\right) d^3q'' T_{\mu'' B'',\mu B}\left(\mathbf{q}'', \mathbf{q}; z\right)}{\Delta_{\mu'' B''}\left(\mathbf{q}''\right) 2W_{\mu'' B''}\left(\mathbf{q}''\right)\left[z - W_{\mu'' B''}\left(\mathbf{q}''\right)\right]} \ , \\
V_{\mu' B',\mu B}\left(\mathbf{q}', \mathbf{q}; z\right) &= U_{\mu' B',\mu B}\left(\mathbf{q}', \mathbf{q}\right) + \sum_{B''}\frac{U_{\mu' B',B''}\left(\mathbf{q}'\right) U_{B'',\mu B}\left(\mathbf{q}\right)}{2m_{B''}\left[z - m^{(0)}_{B''}\right]} \ , \\
W_{\mu B}\left(\mathbf{q}\right) &= \omega_\mu\left(\mathbf{q}\right) + \varepsilon_B\left(\mathbf{q}\right), \ \Delta_{\mu B}\left(\mathbf{q}\right) = (2\pi)^3 \, 2\omega_\mu\left(\mathbf{q}\right)\varepsilon_B\left(\mathbf{q}\right)/W_{\mu B}\left(\mathbf{q}\right) \ .
\end{aligned} \tag{10}$$

Here m_B is the physical mass of a baryon and $m^{(0)}_B$ is its bare mass. We have been able to show that the most general $B \Longleftrightarrow \gamma b$ vertex function and $\mu B \Longleftrightarrow \gamma b$ potential consistent with rotational invariance and gauge invariance are given by

$$U_{B,\gamma b}(\mathbf{q},\lambda) = \sum_{m_B nl} |s_B m_B\rangle\, U_{B,\gamma b}(q,n,l)\, \mathbf{Z}^{m_B \dagger}_{nls_b s_B}(\widehat{\mathbf{q}}) \cdot \boldsymbol{\varepsilon}(\mathbf{q},\lambda) \ , \tag{11}$$

$$U_{\mu B,\gamma b}\left(\mathbf{q}';\mathbf{q},\lambda\right) = \sum_{jm}\sum_{gLnl} Y^{m}_{(gs_\mu)Ls_Bj}\left(\widehat{\mathbf{q}}'\right) U^{(j)}_{\mu B,\gamma b}\left(q',g,L;q,n,l\right) \mathbf{Z}^{m\dagger}_{nls_bj}(\widehat{\mathbf{q}}) \cdot \boldsymbol{\varepsilon}(\mathbf{q},\lambda) \ , \tag{12}$$

where $|s_B m_B\rangle$ is a baryon spin vector, $\boldsymbol{\varepsilon}(\mathbf{q},\lambda)$ is a photon's polarization vector, and λ is its helicity. The angular momentum eigenstates that appear are defined by

$$\mathbf{Z}^{m}_{1lsj}(\widehat{\mathbf{q}}) = \frac{1}{\sqrt{l(l+1)}}\left(i\nabla_{\mathbf{q}} \times \mathbf{q}\right) \sum_{m_l m_s} Y^{m_l}_{l}(\widehat{\mathbf{q}})\, |sm_s\rangle \left\langle lsm_l m_s \right| jm\rangle \ , \tag{13}$$

$$\mathbf{Z}^{m}_{2lsj}(\widehat{\mathbf{q}}) = -i\widehat{\mathbf{q}} \times \mathbf{Z}^{m}_{1lsj}(\widehat{\mathbf{q}}) \ , \tag{14}$$

$$Y^{m}_{(gs_\mu)Ls_Bj}(\widehat{\mathbf{q}}) = \sum_{m_g m_\mu}\sum_{M_L m_B} Y^{m_g}_{g}(\widehat{\mathbf{q}})\, |s_\mu m_\mu\rangle \left\langle g s_\mu m_g m_\mu \right| LM_L\rangle\, |s_B m_B\rangle \left\langle L s_B M_L m_B \right| jm\rangle \ . \tag{15}$$

To first order in e the $\gamma + B \Longrightarrow \mu' + B'$ photoproduction amplitudes are given by

$$\begin{aligned} T_{\mu' B',\gamma B}\left(\mathbf{q}';\mathbf{q},\lambda;z\right) &= V_{\mu' B',\gamma B}\left(\mathbf{q}';\mathbf{q},\lambda;z\right) \\ &+ \sum_{\mu'' B''}\int \frac{T_{\mu' B',\mu'' B''}\left(\mathbf{q}',\mathbf{q}'';z\right) d^3q'' V_{\mu'' B'',\gamma B}\left(\mathbf{q}'';\mathbf{q},\lambda;z\right)}{\Delta_{\mu'' B''}\left(\mathbf{q}''\right) 2W_{\mu'' B''}\left(\mathbf{q}''\right)\left[z - W_{\mu'' B''}\left(\mathbf{q}''\right)\right]} \ , \end{aligned} \tag{16}$$

$$V_{\mu' B',\gamma B}\left(\mathbf{q}';\mathbf{q},\lambda;z\right) = U_{\mu' B',\gamma B}\left(\mathbf{q}';\mathbf{q},\lambda\right) + \sum_{B''} \frac{U_{\mu' B',B''}\left(\mathbf{q}'\right) U_{B'',\gamma B}(\mathbf{q},\lambda)}{2m_{B''}\left[z - m^{(0)}_{B''}\right]} \ . \tag{17}$$

We see that (16), (17), and (11)-(14) imply that $T_{\mu' B',\gamma B}\left(\mathbf{q}',\mathbf{q};z\right) \Longrightarrow T_{\mu' B',\gamma B}\left(\mathbf{q}',\mathbf{q};z\right)$ when $\boldsymbol{\varepsilon}(\mathbf{q},\lambda) \Longrightarrow \boldsymbol{\varepsilon}(\mathbf{q},\lambda) + const.\mathbf{q}$, so we have gauge invariance.

We have shown previously [5,6] that the Okubo method [7] can be used to obtain the vertex functions and potentials from effective Lagrangians.

References

[1] B. Bakamjian and L.H. Thomas, Phys. Rev. **92**, 1300 (1953).

[2] T.D. Newton and E.P. Wigner, Rev. Mod. Phys. **21**, 400 (1949).

[3] B.D. Keister and W.N. Polyzou, in Advances in Nuclear Physics, edited by J.W. Negele and E.W. Vogt (Plenum, New York, 1991), Vol. 20, p. 225.

[4] M.G. Fuda, Phys. Rev. C**64**, 027001 (2001).

[5] Y. Elmessiri and M.G. Fuda, Phys. Rev. C**60**, 044001 (1999).

[6] M.G. Fuda, Few-Body Systems **23**, 127 (1998).

[7] S. Okubo, Prog. Theor. Phys. **12**, 603 (1954).

Covariant description of hadron scattering processes

A. Gårdestig, M.A. Pichowsky, A. Szczepaniak, and J.T. Londergan

Nuclear Theory Center, Indiana University, Bloomington, IN 47408, U.S.A.

(Received: 21 September 2001)

A covariant formalism for multiple hadron scattering is developed and applied to the $\pi\pi$ system. The main features of the model are described and future extensions discussed.

1 Introduction

Although there are an enormous amount of data in the resonance region (e.g., from Hall B at TJNAF), their interpretation has met with difficulties. The main obstacle is the initial and final state interactions which obscure the dynamics of the bare hadronic states. In this paper we present a model [1,2] which gives a general and consistent description of multiple scattering and is constructed to provide a link between the bare states and the observed dynamics. The framework also includes the full effect of three-particle states, previously not considered in this field.

2 Overview of model

The Bakamjian-Thomas formulation [3] allows for a generalization of a non-covariant microscopic model (like the constituent quark model) to a Lorentz-covariant theory. Thus we could safely use the non-covariant Lippmann-Schwinger equation (LSE) $T = V + VGT$; a theorem tells us that the on-shell quantities (observables) will be covariant.

By restricting our attention to 1-, 2-, and 3-particle states the potential matrix V has the possible topologies shown in Fig. 1. The T-matrix and Green's function G are given by

$$T = \begin{pmatrix} T_{11} & T_{12} & T_{13} \\ T_{21} & T_{22} & T_{23} \\ T_{31} & T_{32} & T_{33} \end{pmatrix} , \qquad G = \begin{pmatrix} G_1 & 0 & 0 \\ 0 & G_2 & 0 \\ 0 & 0 & G_3 \end{pmatrix} , \tag{1}$$

where G is diagonal since the hadron states are eigenstates to the invariant mass operator. As a first step toward the solution of the LSE, we neglect V_{33} and the five-point interaction of V_{23} and V_{32}, which will keep the calculations fairly simple while still including the important dynamics. When solving by substitution, the quantity $V_{22} + V_{23}G_3V_{32}$ appears. It is separated into the two-body self-energy Σ, which contains all terms with an overall δ-function in the relative momentum, and the interaction kernel K, with no δ-function, both depicted in Fig. 2. They play a fundamental role in our framework and all other quantities are derived from them. Hence Σ turns up, e.g., in the integral equations for the dressed 1- and 2-body propagators and K in the equations for the dressed vertices. The solution for T_{22} could then be written as

$$T_{22} = G_2^{-1}\widetilde{G}_2(t^{(1)} + t^{(2)})\widetilde{G}_2G_2^{-1} + G_2^{-1}\widetilde{G}_2\Sigma , \tag{2}$$

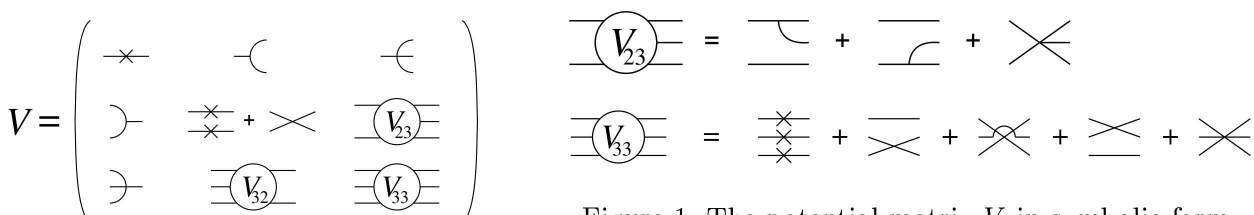

Figure 1: The potential matrix V in symbolic form.

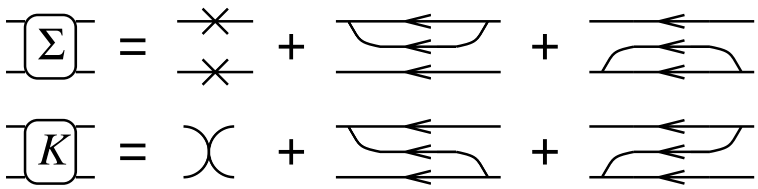

Figure 2: The definitions of Σ and K.

where $t^{(1)}$ contains all terms that proceed through one-body states and $t^{(2)}$ all terms that do not have any one-body singularities.

If the full 3-body equation system is considered, there will be 2 new terms in Σ and 14 new terms in K. The five-point interaction in V_{23} and V_{32} gives yet another 25 terms for K. This separation of the Σ and K terms in the complete system of integral equations leads to the Faddeev equations. Solving them results in four independent integral equations which could be solved simultaneously and need as input the results of three other consecutive integrations [2]. However, it might be enough to include only part of this solution, since the important three-body state $N\pi\pi$ is generally assumed to be dominated by $\pi\pi$ interactions with a spectator nucleon, rather than πN interactions with a spectator pion.

3 Test example: $\pi\pi$ scattering

The $\pi\pi$ system allow for some simplifications: spin relations are trivial, we put $V_{13} = V_{31} = V_{33} = 0$, assume less than four particles, and restrict to energies less than 1400 MeV.

Our Hilbert space: In the *two-body channel* we assume that $\pi\pi$, $K\bar{K}$ and their coupling provide the only relevant dynamics. The *one-body space* consists of π, K, ρ, K^*, and $f_0(1350)$. The scalar-isoscalar $f_0(980)$ meson is in our model a $K\bar{K}$ bound state, while three f_0's above 1300 MeV are bunched together to a broad $f_0(1350)$. The *three-body states* are $|\pi\pi\rho\rangle$, $|\pi\pi f_0\rangle$, $|K\bar{K}\rho\rangle$, $|K\bar{K}f_0\rangle$, $|\pi\bar{K}K^*\rangle$, and $|\pi KK^*\rangle$.

The vertices are finite-sized and given by form factors $V_{21}^i = a_i e^{-q^2/\Lambda_i^2}$, where the vector couplings are put equal, $a_{\pi\pi\rho} = a_{K\bar{K}\rho} = a_{\pi KK^*}$, and fitted to give the $\rho \to \pi\pi$ width at $E = m_\rho =$ 770 MeV.

We use two direct interactions: a 4-point kernel which mimics dynamical chiral symmetry breaking $K^{4\pi J} \propto (qp)^J e^{-q^2/\Lambda^2} e^{-p^2/\Lambda^2}$, $K^{4K} = 0$ and a short-range scalar meson attraction through $|\pi\pi X\rangle$ and $|K\bar{K}X\rangle$. This scalar meson X is never on-shell since its mass is 1500 MeV.

4 Results and discussion

The results (Fig. 3) show that there is a weak attractive effective $\pi\pi$ potential, with a rapid rise due to the crossing of the $K\bar{K}$ threshold and the nearby narrow bound $K\bar{K}$ state $f_0(980)$. If the $\pi\pi \leftrightarrow K\bar{K}$ mixing is decreased the phase shift will look more and more like a step function. The rapid rise is thus a consequence of the *weakness* of the $\pi\pi \leftrightarrow K\bar{K}$ coupling. The linear behavior at low energy is due to chiral symmetry breaking, but is in our approach modeled, since quantum mechanics does not automatically provide chiral symmetry. Since $\eta_{\pi\pi} = 1$ up to the $K\bar{K}$ threshold, with no clear indication of a flux drain to a 4π state, our neglect of four-body states is justified.

An important aspect of our model is that most of the strength of the $\pi\pi$ potential is caused by the scalar mesons. They provide a strong interaction for all energies below 1400 MeV and they are the dominant contribution to the $\pi\pi \leftrightarrow K\bar{K}$ mixing. In contrast to other models (e.g., the Jülich model where the vector meson exchange is strong and attractive), our vector meson exchange is very weak and repulsive.

The numerical accuracy was tested by calculating the total cross section and compare it with the forward scattering amplitude according to the optical theorem. It is found that, even though

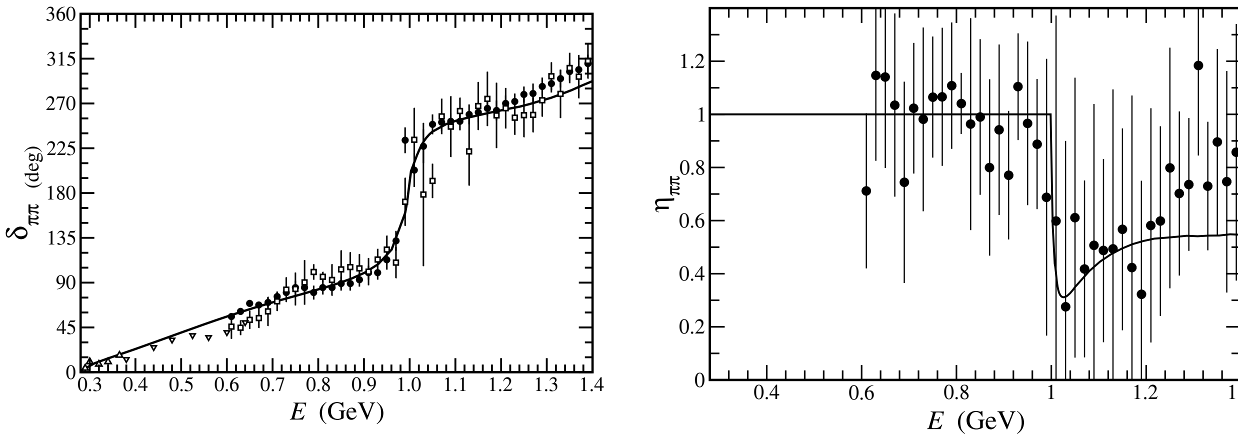

Figure 3: The fitted $\pi\pi$ phase shift $\delta_{\pi\pi}$ and inelasticity $\eta_{\pi\pi}$ together with data from [4].

unitarity is broken by an explicitly time-dependent exponential factor, the exponent could for all practical purposes be made small enough that the violation is of the order of 10^{-6}. The model is hence regarded to be effectively unitary.

5 Conclusion

The model presented here provide a relativistic description of hadron scattering, which allows for a connection between basic hadron features deduced from, e.g., quark models and observed hadron dynamics. For the first time a complete treatment of the three-body states has been developed, which will be needed to understand important hadron processes like the $\pi N \to \pi\pi N$ inelasticity in the P_{11} channel and the nature of the $N^*(1440)\frac{1}{2}^+$ state.

We are currently working on extending the model to this more challenging and interesting set of problems.

References

[1] M.A. Pichowsky, A. Szczepaniak, and J.T. Londergan, Phys. Rev. D**64**, 036009 (2001).

[2] M.A. Pichowsky, A. Gårdestig, A. Szczepaniak, and J.T. Londergan (in preparation).

[3] B. Bakamjian and L.H. Thomas, Phys. Rev. **92**, 1300 (1953); see also M.G. Fuda and H. Alharbi, these proceedings.

[4] R. Kaminski, L. Lesniak, and K. Rybicki, Acta. Phys. Polon. **B31**, 895 (2000); G. Grayer, *et al.*, Nucl. Phys. **B75**, 189 (1974); L. Rosselet, *et al.*, Phys. Rev. D**15**, 574 (1977); V. Shrinivasan *et al.*, Phys. Rev. D**12**, 681 (1975).

QED radiative corrections to the cross section and beam asymmetry in exclusive pion electroproduction

A. Afanasev[a,b], I. Akushevich[a,b], V. Burkert[a], and K. Joo[a]

[a] *TJNAF, Newport News, VA 23606, U.S.A.*
[b] *North Carolina Central University, Durham, NC 27707, U.S.A.*

(Received: 10 October 2001)

The explicit formulae for the lowest order QED radiative correction to cross section and beam spin asymmetry in the exclusive pion electroproduction are obtained. A Fortran code EXCLURAD is developed based on the exact and leading log formulae. Several analytical and numerical tests are performed.

1 Introduction

New measurements using CLAS at Jefferson Lab/Hall B are being carried out to vastly improve the systematic and statistical precision of single pion electroproduction and cover a wide kinematic range in four momentum transfer Q^2 and invariant mass W, as well as to measure the full angular range of the resonance decay into the nucleon-pion final state:

$$\begin{aligned} e(k_1) + N(p) &\longrightarrow e'(k_2) + \pi^+(p_h) + n(p_u) \ , \\ e(k_1) + N(p) &\longrightarrow e'(k_2) + p(p_h) + \pi^0(p_u) \ . \end{aligned}$$

A correct calculation of radiative corrections (RC) becomes more important in interpreting the measured experimental data such as unpolarized cross section and polarization observables. In this report, we present new results on a covariant calculation of radiative corrections to polarized exclusive pion electroproduction (Fig. 1).

2 Radiative corrections and code EXCLURAD

The calculation is based on the approach known as the Bardin-Shumeiko method of covariant extraction of infrared divergence [1] (see also review [2]). We follow the paper [3] where this approach was developed for exclusive electroproduction processes. In contrast to the treatment developed by Mo and Tsai [4], this approach has the advantages that it is exact and does not include any artificial parameters like Δ. At the first stage, the identity transformation of the bremsstrahlung (Figs. 1b and 1c) cross section is used to separate out the infrared divergence (IR) term:

$$\sigma_R = \sigma_R - \sigma_{IR} + \sigma_{IR} = \sigma_F + \sigma_{IR} \ .$$

The IR terms from σ_{IR} cancel exactly with corresponding terms in the vertex function (Fig. 1d).

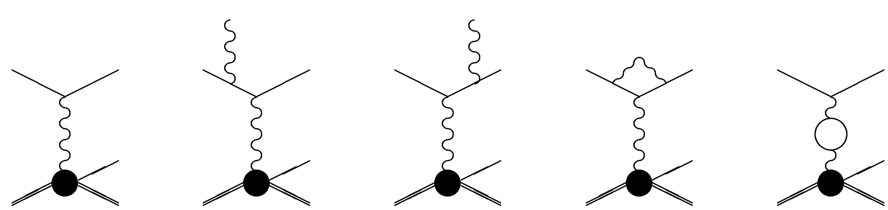

a) b) c) d) e)

Figure 1: Feynman diagrams contributing to the Born and the radiative correction cross sections.

Another important ingredient of the calculation is the covariant hadronic tensor. In general, it includes five structure functions $\mathcal{H}_i$, related to the photo-absorption structure functions σ_T, σ_L, σ_{TT}, σ_{LT} and σ'_{LT}, which have to be calculated within a specific model. The result for RC can be presented in the following form

$$\delta = \frac{\sigma_{obs}}{\sigma_0} = \exp(\delta_{inf})(1 + \delta_{vr} + \delta_{vac}) + \frac{\sigma_{hard}}{\sigma_0} \ .$$

Here, σ_{obs} and σ_0 are the four-fold observed cross section and Born (Fig. 1a) cross section, respectively. δ_{vr} and δ_{inf} are results of IR cancellation of the vertex function (Fig. 1d) and soft photon radiation ($S' = 2p_2k_1$, $X' = 2p_2k_2$). They depend only on kinematic variables

$$\delta_{inf} = \frac{\alpha}{\pi}\left(\log\frac{Q^2}{m^2} - 1\right)\log\frac{v_{max}^2}{S'X'} \ , \quad \delta_{VR} = \frac{\alpha}{\pi}\left(\frac{3}{2}\log\frac{Q^2}{m^2} - 2 - \frac{1}{2}\log^2\frac{X'}{S'} + \mathrm{Li}_2\frac{S'X' - Q^2M^2}{S'X'} - \frac{\pi^2}{6}\right) .$$

The exponent is the result of the so-called procedure of exponentiation of multiple soft-photon contributions. The correction $\delta_{vac} = \delta_{vac}^{lept} + \delta_{vac}^{hadr}$ is a contribution of the vacuum polarization by leptons and hadrons (Fig. 1e). The cross section σ_F has a form of a three dimensional integral over the photonic phase space:

$$\sigma_F = \frac{-\alpha^3}{2^9\pi^4 S^2 W^2}\int d\Omega_k \frac{dv}{f}\sum_i \left[\frac{\sqrt{\lambda_W}}{\tilde{Q}^4}\theta_i \mathcal{H}_i(\tilde{Q}^2, \tilde{W}^2, \tilde{t}) - \frac{4F_{IR}\sqrt{\lambda_W^0}}{Q^4}\theta_i^0 \mathcal{H}_i(Q^2, W^2, t)\right] \ ,$$

where f, θ_i, F_{IR}, λ_W, θ_i^0 and λ_W^0 are kinematic functions. Tilde arguments of structure functions are defined with photon momentum:

$$\tilde{Q}^2 = -(q-k)^2 \ , \quad \tilde{W}^2 = (p_1 + q - k)^2 \ , \quad \tilde{t} = (q - k - p_h)^2 \ .$$

Integration over v is conducted up to v_{max}. This maximal inelasticity is defined by kinematics or cuts used in the analysis.

There are two important cross-checks provided. First one is the extraction of leading log contribution. The contribution extracted from exact formulae was compared with the one obtained by direct calculation using leading log methods [5]. We also tested the inclusive formulae for radiative correction obtained by integrating over hadron angles. It is possible to show analytically that inclusive formulae are reproduced in this case.

A computer code was written using the exact and leading log formulae to compute the RC calculation for the unpolarized cross section and beam spin asymmetry of exclusive pion electroproduction. Three models are used for the photo-absorption structure functions: MAID98 and MAID2000 [6], the model developed by Sato and Lee [7] and the AO model [8]. The calculation can be done with or without a cut on inelasticity. There are options for calculating of inelasticity v distribution with and without RC.

3 Numerical analysis

Typical plots demonstrating the RC to cross sections and beam spin asymmetries are presented in Figs.2 and 3. Fig.2 also shows the model dependence of the corrections. We note that these results are obtained without any inelasticity cuts. If such a cut is used the results for RC to cross section are defined by the factorized corrections only, and $\sigma_F \to 0$. As a result, the correction to cross section approaches a value around $\delta = 0.8$, while RC to the asymmetry tends to zero.

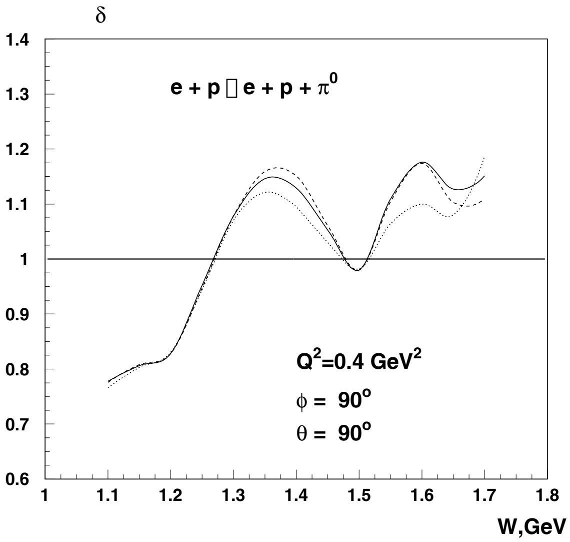

Figure 2: W-dependence of RC to the cross section. Dotted, dashed and solid lines correspond to AO, MAID98 and MAID2000.

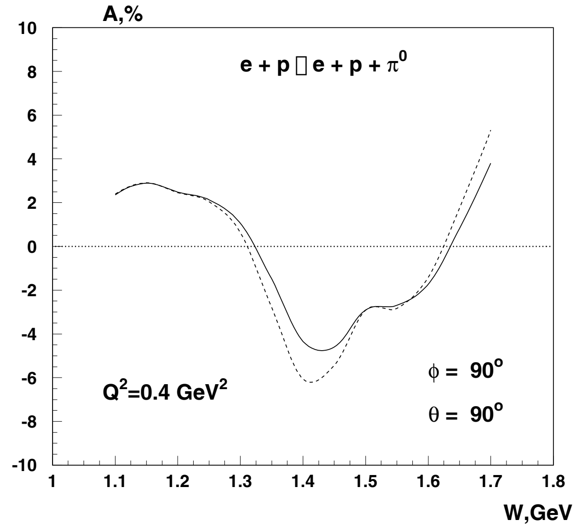

Figure 3: Born (dashed) and observed (solid) beam asymmetry vs W calculated using MAID2000.

Numerical analysis carried out for the kinematic conditions at Jefferson Lab allows us to make the following conclusions. Radiative correction to the cross section is very sensitive to the cut on inelasticity. Using a harder cut leads to smaller corrections. A hard cut can also suppress corrections to the beam spin asymmetry. Correction to cross section can be several tens %. A model dependence of the correction has been studied. An iterative procedure may be required for the regions where the model dependence is large. The correction has a non-trivial angular dependence in $\cos\theta$ and ϕ. This angular dependence in RC is quite important in performing partial wave analysis.

Acknowledgments: This work was supported by DOE grant DE-AC05-84ER40150. AA acknowledges additional support through NSF grant PHY-0098642.

References

[1] D. Y. Bardin and N. M. Shumeiko, Nucl. Phys. **B127**, 242 (1977).

[2] A. Akhundov, D. Bardin, L. Kalinovskaya and T. Riemann, Fortsch. Phys. **44**, 373 (1996).

[3] I. Akushevich, Eur. Phys. J. **C8**, 457 (1999).

[4] L. W. Mo and Y. Tsai, Rev. Mod. Phys. **41**, 205 (1969).

[5] A. De Rujula, R. Petronzio and A. Savoy-Navarro, Nucl. Phys. **B154**, 394 (1979).

[6] D. Drechsel, O. Hanstein, S.S. Kamalov, L. Tiator, Nucl. Phys. **A645**, 145 (1999).

[7] T. Sato and T.-S.H. Lee, Phys. Rev. C **63**, 055201 (2001).

[8] V.Burkert, private conversation.

The χ-BS(3) approach

M.F.M. Lutz[a] and E.E. Kolomeitsev[b]

[a] *Gesellschaft für Schwerionenforschung (GSI), Planck Str. 1, D-64291 Darmstadt, Germany*
[b] *ECT*, Villa Tambosi, I-38050 Villazzano (Trento) and INFN, G.C. Trento, Italy*

(Received: 18 October 2001)

We present the results of the χ-BS(3) approach demonstrating that a combined chiral and $1/N_c$ expansion of the Bethe-Salpeter interaction kernel leads to a good description of the kaon-nucleon, antikaon-nucleon and pion-nucleon scattering data typically up to laboratory momenta of $p_{\rm lab} \simeq 500$ MeV. We solve the covariant on-shell reduced coupled channel Bethe-Salpeter equation with the interaction kernel truncated to chiral order Q^3 and to the leading order in the $1/N_c$ expansion

The main features and crucial arguments of our recent work on meson-baryon scattering [1] are briefly summarized. Within the χ-BS(3) approach we consider the number of colors (N_c) in QCD as a large parameter relying on a systematic expansion of the interaction kernel in powers of $1/N_c$. The coupled-channel Bethe-Salpeter kernel is evaluated in a combined chiral and $1/N_c$ expansion including terms of chiral order Q^3.

We expect all baryon resonances, with the important exception of those resonances which belong to the large N_c baryon ground states, to be generated by coupled channel dynamics. This conjecture is based on the observation that unitary (reducible) loop diagrams are typically enhanced by a factor of 2π close to threshold relatively to irreducible diagrams. That factor invalidates the perturbative evaluation of the scattering amplitudes and leads necessarily to a non-perturbative scheme with reducible diagrams summed to all orders. In our present scheme we consider an explicit s-channel baryon nonet term with $J^P = \frac{3}{2}^-$ in the interaction kernel as a reminiscence of further inelastic channels not included like for example the $K\,\Delta_\mu$ or $K_\mu\,N$ channel.

The scattering amplitudes for the meson-baryon scattering processes are obtained from the solution of the coupled channel Bethe-Salpeter scattering equation. Approximate crossing symmetry of the amplitudes is guaranteed by a renormalization program which leads to the matching of subthreshold amplitudes. A further important ingredient of our scheme is a systematic and covariant on-shell reduction of the Bethe-Salpeter equation. We point out that an on-shell reduction is mandatory as to avoid an unphysical and uncontrolled dependence on the choice of chiral coordinates or the choice of interpolating fields. In other words given our scheme the on-shell scattering amplitude will not change if we used a different representation of the chiral Lagrangian. In the χ-BS(3) scheme the on-shell reduction is implied unambiguously by the existence of a unique and covariant projector algebra which solves the Bethe-Salpeter equation for any choice of quasi-local interaction terms.

At subleading order Q^2 the chiral $SU(3)$ Lagrangian predicts the relevance of 12 basically unknown parameters, which all need to be adjusted to the empirical scattering data. It is important to realize that chiral symmetry is largely predictive in the $SU(3)$ sector in the sense that it reduces the number of parameters beyond the static $SU(3)$ symmetry. For example one should compare the six tensors which result from decomposing $8 \otimes 8 = 1 \oplus 8_S \oplus 8_A \oplus 10 \oplus \overline{10} \oplus 27$ into its irreducible components with the subset of SU(3) structures selected by chiral symmetry in a given partial wave. Thus static $SU(3)$ symmetry alone would predict 18 independent terms for the s-wave and two p-wave channels rather than the 12 chiral Q^2 background parameters. In our work the number of parameters was further reduced significantly by insisting on the large N_c sum rules for the symmetry conserving quasi-local two body interaction terms leaving only 5 parameters. All parameters are

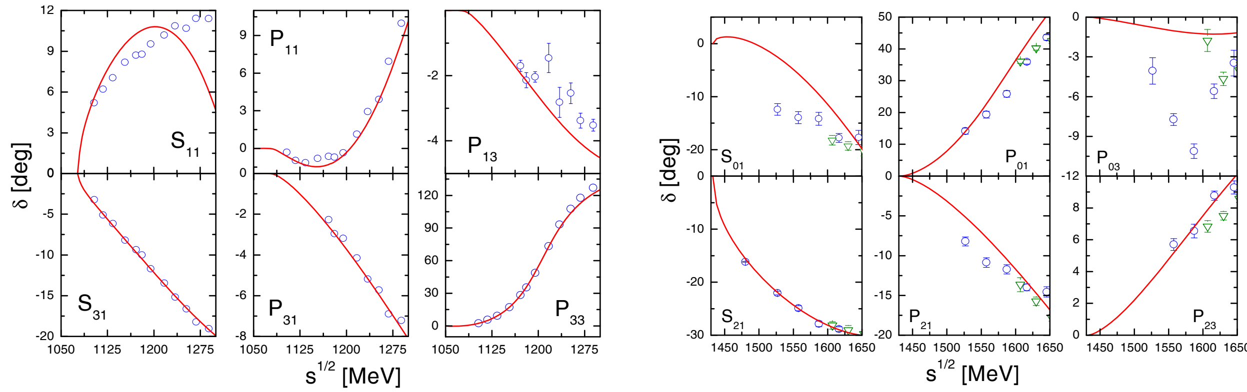

Figure 1: Left panel: S- and p-wave pion-nucleon phase shifts. The single energy phase shifts are taken from [2]. Right panel: S- and p-wave K^+-nucleon phase shifts. The solid lines represent the results of the χ-BS(3) approach. The open circles are from the Hyslop analysis [3] and the open triangles from the Hashimoto analysis [4]

found to have natural size.

At chiral order Q^3 the number of parameters increases significantly unless further constraints from QCD are imposed. A systematic expansion of the interaction kernel in powers of $1/N_c$ leads to a much reduced parameter set. For example the $1/N_c$ expansion leads to only four further parameters describing the refined symmetry-conserving two-body interaction vertices. This is to be compared with the ten parameters we established to be relevant at order Q^3 if large N_c sum rules are not imposed. Note that at order Q^3 there are no symmetry-breaking 2-body interaction vertices. To that order the only symmetry-breaking effects result from the refined 3-point vertices. Here a particularly rich picture emerges. At order Q^3 we established 23 parameters describing symmetry-breaking effects in the 3-point meson-baryon vertices. For instance, to that order the baryon-octet states may couple to the pseudo-scalar mesons also via pseudo-scalar vertices rather than only via the leading axial-vector vertices. Out of those 23 parameters 16 contribute at the same time to matrix elements of the axial-vector current. Thus in order to control the symmetry breaking effects, it is mandatory to include constraints from the weak decay widths of the baryon octet states also. A detailed analysis of the 3-point vertices in the $1/N_c$ expansion of QCD reveals that in fact only ten parameters, rather than the 23 parameters, are needed at leading order in that expansion. Since the leading parameters together with the symmetry-breaking parameters describe at the same time the weak decay widths of the baryon octet and decuplet ground states, the number of free parameters does not increase significantly at the Q^3 level if the large N_c limit is applied.

In the left panel of Fig. 1 we confront the result of our global fit with the empirical πN phase shifts. All s- and p-wave phase shifts are well reproduced up to $\sqrt{s} \simeq 1300$ MeV with the exception of the S_{11} phase for which our result agrees with the partial-wave analysis less accurately. We emphasize that one should not expect quantitative agreement for $\sqrt{s} > m_N + 2\, m_\pi \simeq 1215$ MeV where the inelastic pion production process, not included in this work, starts. The missing higher order range terms in the S_{11} phase are expected to be induced by additional inelastic channels or by the nucleon resonances $N(1520)$ and $N(1650)$. We confirm the findings of [6, 7] that the coupled $SU(3)$ channels, if truncated at the Weinberg-Tomozawa level, predict considerable strength in the S_{11} channel around $\sqrt{s} \simeq 1500$ MeV where the phase shift shows a resonance-like structure. Note, however that it is expected that the nucleon resonances $N(1520)$ and $N(1650)$ couple strongly to each other and therefore one should not expect a quantitative description of the S_{11} phase too far away from threshold. Similarly we observe considerable strength in the P_{11} channel leading to a

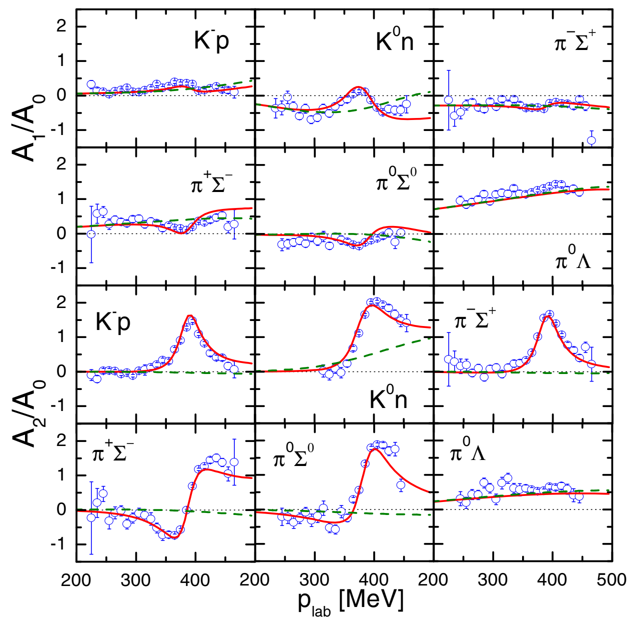

Figure 2: Coefficients A_1 and A_2 for the $K^-p \to \pi^0\Lambda$, $K^-p \to \pi^\mp\Sigma^\pm$ and $K^-p \to \pi^0\Sigma$ differential cross sections, where $\frac{d\sigma(\sqrt{s},\cos\theta)}{d\cos\theta} = \sum_{n=0}^{\infty} A_n(\sqrt{s})\, P_n(\cos\theta)$. The data are taken from [5]. The solid lines are the result of the χ-BS(3) approach with inclusion of the d-wave resonances. The dashed lines show the effect of switching off d-wave contributions.

resonance-like structure around $\sqrt{s} \simeq 1500$ MeV. We interpret this phenomenon as a precursor effect of the p-wave $N(1440)$ resonance. We stress that our approach differs significantly from the recent work [7] in which the coupled SU(3) channels are applied to pion induced η and kaon production which require much larger energies $\sqrt{s} \simeq m_\eta + m_N \simeq 1486$ MeV or $\sqrt{s} \simeq m_K + m_\Sigma \simeq 1695$ MeV. We believe that such high energies can be accessed reliably only by including more inelastic channels. It may be worth mentioning that the inclusion of the inelastic channels as required by the $SU(3)$ symmetry leaves the πN phase shifts basically unchanged for $\sqrt{s} < 1200$ MeV.

In the right panel of Fig. 1 we confront our s- and p-wave K^+-nucleon phase shifts with the most recent analyses by Hyslop et al. [3] and Hashimoto [4]. We find that our partial-wave phase shifts are reasonably close to the single energy phase shifts of [3] and [4] except the P_{03} phase for which we obtain much smaller strength. Note however, that at higher energies we smoothly reach the single energy phase shifts of Hashimoto [4].

In Fig. 2 we compare the empirical ratios A_1/A_0 and A_2/A_0 of the inelastic K^-p scattering with the results of the χ-BS(3) approach. Note that for $p_{\rm lab} < 300$ MeV the empirical ratios with $n \geq 3$ are compatible with zero within their given errors. A large A_1/A_0 ratio is found only in the $K^-p \to \pi^0\Lambda$ channel demonstrating the importance of p-wave effects in the isospin one channel. The dashed lines of Fig. 2, which are obtained when switching off d-wave contributions, confirm the importance of this resonance for the angular distributions in the isospin zero channel.

References

[1] M.F.M. Lutz and E.E. Kolomeitsev, Nucl. Phys. A, in print, nucl-th/0105042.

[2] R.A. Arndt et al., Phys. Rev. C**52**, 2120 (1995).

[3] J.S. Hyslop et al., Phys. Rev. C**46**, 961 (1992).

[4] K. Hashimoto, Phys. Rev. C**29**, 1377 (1984).

[5] T.S. Mast et al., Phys. Rev. D**11**, 3078 (1975); R.O. Bangerter et al., Phys. Rev. D**23**, 1484 (1981).

[6] N. Kaiser, T. Waas and W. Weise, Nucl. Phys. A**612**, 297 (1997).

[7] J.S. Caro Ramon et al., Nucl. Phys. A**672**, 249 (2000).

Application of Roy's equations to analysis of $\pi\pi$ experimental data

B. Loiseau[a], R. Kamiński[b] and L. Leśniak[b]

[a]*LPNHE, Univ. P. & M. Curie, Paris, France*
[b]*Henryk Niewodniczański Institute of Nuclear Physics, Kraków, Poland*

(Received: 2 October 2001)

The scalar-isoscalar, scalar-isotensor and vector-isovector $\pi - \pi$ partial wave amplitudes are analyzed. Preliminary results indicate that only the scalar-isoscalar amplitude fitted to the "down-flat" data satisfies Roy's equations and consequently crossing symmetry.

1 Motivations and theoretical constraints

Pions are produced in many reactions. A good experimental and theoretical information on low, medium and high-energy pion-pion interactions should give us a better understanding of non-perturbative QCD and of the chiral perturbation theory. It allows a better insight into $q\bar{q}$ vacuum condensate and then into the mechanism of spontaneous breaking of chiral symmetry. It should also give a better knowledge of the meson spectrum in particular of the σ-meson and glueballs.

Recently Kamiński *et al.* [1], using not only pion-exchange but also a_1-exchange, have reanalyzed the data obtained in the seventies on the $\pi^- p \to \pi^+\pi^- n$ reaction at 17.2 GeV/c without and with a polarized target. Essentially, for $m_{\pi\pi}$ between 600 and 980 MeV, two solutions "up-flat" and "down-flat" (hereafter called *up* and *down*) were found for the pion-pion isoscalar S-wave.

Besides unitarity and analyticity, crossing symmetry plays a very important role in the $\pi\pi$ interactions as in each channel the same particles interact. Projection on partial waves of the twice subtracted fixed-t dispersion relations leads to Roy's equations for the scattering amplitude of isospin I, viz.

$$\mathrm{Re} f_\ell^I(s) = \begin{pmatrix} a_0^0 \\ 0 \\ a_0^2 \end{pmatrix} \delta_{\ell 0} + (2a_0^0 - 5a_0^2)\,\frac{s-4m_\pi^2}{12m_\pi^2} \begin{pmatrix} \delta_{\ell 0} \\ \delta_{\ell 1}/6 \\ -\delta_{\ell 0}/2 \end{pmatrix} + \sum_{I'=0}^{2} \sum_{\ell'=0}^{1} \fint_{4m_\pi^2}^{110m_\pi^2} K_{\ell I}^{\ell' I'}(s,s')\,\mathrm{Im} f_{\ell'}^{I'}(s')\,ds' + d_\ell^I(s).$$

These equations are valid for $4m_\pi^2 \leq s \leq 68m_\pi^2$ (= 1.15 GeV) and express the real part of the scalar-isoscalar, scalar-isovector and vector-isovector partial waves as integrals on their imaginary parts. The two subtractions are expressed in terms of the scattering lengths a_ℓ^I: a_0^0 and a_0^2. The kernels K are known singular functions. The driving terms $d_\ell^I(s)$ contain the contributions of the partial waves $\ell' \geq 2$ as well as the high-energy contributions [2,3]. For the driving terms we use the parameterization of Basdevant *et al.* [4].

Pions are the quasi-Goldstone bosons of the chiral symmetry of strong interaction, so at low $m_{\pi\pi}$ we use constraints from chiral perturbation theory. For instance the two-loop calculations of the $\pi\pi$ amplitudes using $K_{\ell 4}$ decay constraints lead to: $a_0^0 = 0.219 \pm 0.005 m_\pi^{-1}$, $a_0^2 = -0.042 \pm 0.001 m_\pi^{-1}$ and to the slope parameters of the phase shifts; $b_0^0 = 0.279 \pm 0.011 m_\pi^{-3}$, $b_0^2 = -0.076 \pm 0.002 m_\pi^{-3}$ [5].

2 Applications and outlook

For the scalar-isoscalar phase shifts δ_0^0 we use the unitary three-channel model of Kamiński *et al.* [6] with chiral symmetry constraints on a_0^0, b_0^0 and on $\pi\pi \to K\bar{K}$ and $K\bar{K} \to K\bar{K}$ reactions at the $\pi\pi$ threshold as given by Donoghue *et al.* [7]. For δ_0^2 we use chiral symmetry constraints on a_0^2 and b_0^2 and do a fit to Hoogland A data [8] using the Padé approximant parameterization of Schenk [9]. For δ_1^1 we use the Schenk parameterization with $a_1^1 = 0.035 m_\pi^{-1}$ [10].

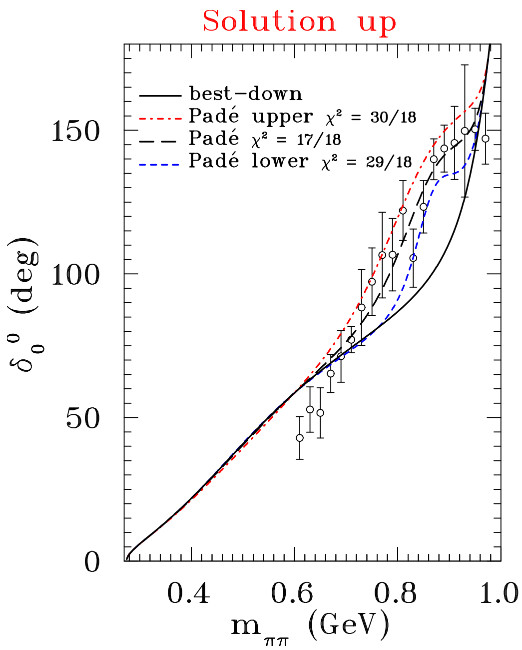

Figure 1: Left: fits to the solution *up*. Right: fits to the solution *down*.

First we built up a three-channel fit to the solution *down* and to Roy's equations. The quality of fit to Roy's equations is judged by a comparison between the exact real part of the partial waves calculated from phase shifts and inelasticities (called input) and the output calculated from Roy's equations. These equations are well satisfied by this fit called "best-down" fit. The input is close to the output with some small deviations above 900 MeV, in particular for the scalar-isotensor wave.

Let us try to solve the *up-down* ambiguity. The solution *up* and *down* differ mainly for $800 \leq m_{\pi\pi} \leq 980$ MeV. We use a Padé approximant with 8 parameters to fit $\tan\delta_0^0$ of the solutions *up* and *down*. The parameters are determined: i) to reproduce the "chiral" values a_0^0, b_0^0 and the δ_0^0 of the "best-down" fit at 500 and 600 MeV, ii) to have a smooth junction to the "best-down" fit close to 970 MeV and iii) to obtain a best fit of the data between 680 and 950 MeV.

Results of different fits with their corresponding χ^2 are shown in Fig. 1. The "Padé lower" and "Padé upper" denote the fits to the data shifted downwards and upwards according to their error bars. In Fig. 2 we check how this "upper" and "lower" fits satisfy Roy's equations. For the S-wave and for $840 \leq m_{\pi\pi} \leq 950$ MeV (left panel) there is no overlap between the "upper" and "lower" input and output bands. Here the solution *up* does not satisfy Roy equation, i.e. it is not compatible with crossing symmetry. On the contrary for the solution *down* (right panel), for $m_{\pi\pi} \leq 950$ MeV, both bands overlap. The other waves satisfy relatively well Roy's equations. The solution *down* is compatible with crossing symmetry.

Let us remark here that recent joint analysis by Kamiński *et al.* [11] of the CERN-Munich, the CERN-Cracow-Munich $\pi^+\pi^-$ data and of the $\pi^0\pi^0$ data of the Brookhaven E852 Collaboration at 18.3 GeV/c [12] eliminates the "up-flat" solution and leads to a solution compatible with solution *down*. Our study here shows that only the solution *down* satisfies crossing symmetry.

Currently we are studying the sensitivity of the driving terms to the parameterization of the resonant $f_2(1270)$ and $\rho_3(1690)$ amplitudes and to the high energy Regge contributions. We shall compare our results to those of Ananthanarayan *et al.* [3].

The present study shows that we can construct a three-channel $\pi\pi$, $K\bar{K}$ and effective $(2\pi)(2\pi)$ model which fulfills unitarity, crossing symmetry and chiral symmetry constraints. This will give

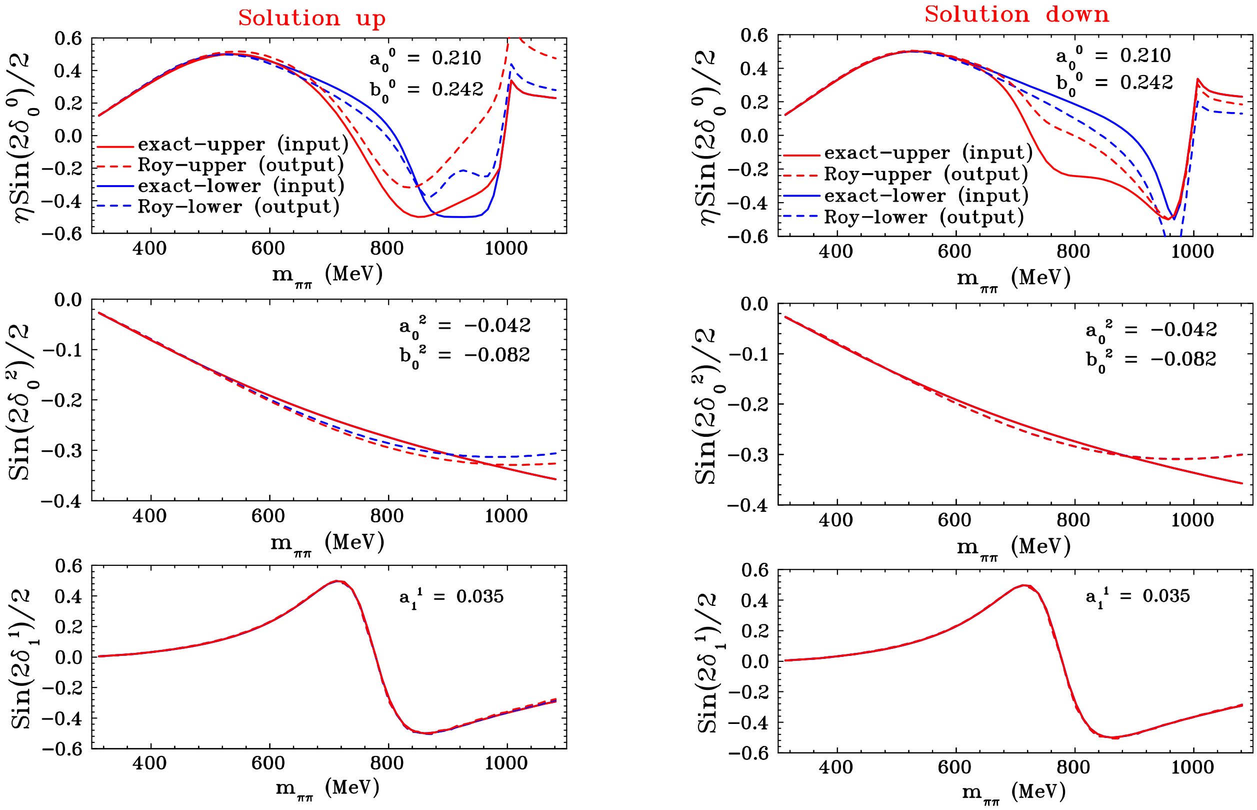

Figure 2: Tests of Roy's equations for solutions *up* (left panel) and *down* (right panel).

more confidence in the parameters of the scalar-isoscalar mesons predicted by the model. This will also allow to check the amplitudes below the $K\bar{K}$ threshold. Let us finally mention that any new precise data on $\pi\pi$ are welcome.

Acknowledgments: The LPNHE is a Unité de Recherche des Universités Paris 6 et Paris 7, associée au CNRS. This work was done in the framework of the IN2P3-Polish laboratories Convention (project No. 99-97).

References

[1] R. Kamiński, L. Leśniak, K. Rybicki, Z. Phys **C74**, 79 (1997); Acta Phys. Polon. **B31**, 895 (2000).

[2] S.M. Roy, Phys. Letters **B36**, 353 (1971).

[3] B. Ananthanarayan, G. Colangelo, J. Gasser and H. Leutwyler, *"Roy equation analysis of $\pi\pi$ scattering"*, hep-ph/0005297, Phys. Rep. in press.

[4] J.-L. Basdevant, C.D. Frogatt and J.L. Petersen, Nucl. Phys. **B72**, 413 (1974).

[5] G. Amoros, J. Bijnens and P. Talavera, Nucl. Phys. **B585**, 293 (2000), hep-ph/0003258.

[6] R. Kamiński, L. Leśniak and B. Loiseau, Eur. Phys. J. **C9**, 141 (1999).

[7] J.F. Donoghue, J. Gasser and H. Leutwyler, Nucl. Phys. **B343**, 341 (1990).

[8] W. Hoogland *et al.*, Nucl. Phys. **B126**, 109 (1977).

[9] A. Schenk, Nucl. Phys. **B363**, 97 (1991).

[10] E. Chell and M.G. Olsson, Phys. Rev. **D48**, 4076 (1993).

[11] R. Kamiński, L. Leśniak and K. Rybicki, *"A joint analysis of the S-wave in the $\pi^+\pi^-$ and $\pi^0\pi^0$ data"*, hep-ph/0109268.

[12] J. Gunter *et al.*, *"A partial wave analysis of the $\pi^0\pi^0$ system produced in π^-p charge exchange collisions"*, hep-ex/0001038.

The DIRAC experiment at CERN: current status and future perspectives

A.M. Rodriguez Fernandez

Facultad de Fisica, Departamento de Fisica de Particulas,
Universidade de Santiago de Compostela, Santiago de Compostela, 15782, Spain

on behalf of the DIRAC Collaboration:

B. Adeva[p], L. Afanasev[l], M. Benayoun[d], Z. Berka[b], V. Brekhovskikh[o], G. Caragheorgheopol[m], T. Cechak[b], M. Chiba[j], S. Constantini[q], S. Constantinescu[m], A. Doudarev[l], D. Dreossi[f], D. Drijard[a], M. Ferro-Luzzi[a], M.V. Gallas[a,p], J. Gerndt[b], R. Giacomich[f], P. Gianotti[e], D. Goldin[q], A. Gorin[o], O. Gortchakov[l], C. Guaraldo[e], M. Hansroul[a], R. Hosek[b], M. Iliescu[e,m], M. Jabitski[l], N. Kalinina[n], V. Karpoukhine[l], J. Kluson[b], M. Kobayashi[g], P. Kokkas[q], V. Komarov[l], A. Koulikov[l], A. Kouptsov[l], V. Krouglov[l], L. Krouglova[l], K.-I. Kuroda[k], A. Lamberto[f], A. Lanaro[a,e], V. Lapshine[o], R. Lednicky[c], P. Leruste[d], P. Levisandri[e], A. Lopez Aguera[p], V. Lucherini[e], T. Maki[i], I. Manuilov[o], L. Montanet[a], J.-L. Narjoux[d], L. Nemenov[a,l], M. Nikitin[l], T. Nunez Pardo[p], K. Okada[h], V. Olchevskii[l], A. Pazos[p], M. Pentia[m], A. Penzo[f], J.-M. Perreau[a], C. Petrascu[e,m], M. Plo[p], T. Ponta[m], D. Pop[m], G.F Rapazzo[f], A. Riazantsev[o], J.M. Rodriguez[p], A. Rodriguez Fernandez[p], V. Rykaline[o], C. Santamarina[p], J. Saborido[p], J. Schacher[r], C. Schuetz[q], A. Sidorov[o], J. Smolik[c], F. Takeutchi[h], A. Tarasov[l], L. Tauscher[q], M.J. Tobar[p], S. Trousov[n], P. Vazquez[p], S. Vlachos[q], V. Yazkov[n], Y. Yoshimura[g], P. Zrelov[l]

[a]*CERN, Geneva, Switzerland;* [b]*Czech Technical University, Prague, Czech Republic;* [c]*Institute of Physics ACSR, Prague, Czech Republic;* [d]*LPNHE des Universites Paris VI/VII, IN2P3-CNRS, France;* [e]*INFN - Laboratori Nazionali di Frascati, Frascati, Italy;* [f]*Trieste University and INFN-Trieste, Italy;* [g]*KEK, Tsukuba, Japan;* [h]*Kyoto Sangyou University, Japan;* [i]*UOEH-Kyushu, Japan;* [j]*Tokyo Metropolitan University, Japan* [k]*Waseda University, Japan;* [l]*JINR Dubna, Russia;* [m]*National Institute for Physics and Nuclear Engineering IFIN-HH, Bucharest, Romania;* [n]*Skobeltsin Institute for Nuclear Physics of Moscow State University Moscow, Russia;* [o]*IHEP Protvino, Russia;* [p]*Santiago de Compostela University, Spain;* [q]*Basel University, Switzerland;* [r]*Bern University, Switzerland*

(Received: 31 October 2001)

The DIRAC experiment [1] at CERN aims to form $\pi^+\pi^-$ atomic states ($A_{2\pi}$) and to measure their lifetime with 10% accuracy. This measurement will enable to improve the precision in the determination of the difference between the S-wave $\pi\pi$ scattering lengths, $\Delta = a_0 - a_2$, from its present value of 20% to 5%. The experimental method is reviewed and some preliminary results from the analysis of 1999 data are presented.

1 Introduction

The study of the low energy pion-pion scattering lies within the domain of non-perturbative QCD and is still an unresolved problem in the context of QCD. However, the approach based on effective chiral lagrangian has been able to provide accurate predictions on the dynamics of light hadron interactions. In particular, Chiral Perturbation Theory (χPT) allows to predict the S-wave $\pi\pi$ scattering lengths at the level of few percent [2]. Available experimental results, on the other side, are much less accurate than theoretical values predictions.

The aim of DIRAC experiment is to determine $|a_0 - a_2|$ through the measurement of the pionium lifetime. This, $\pi^+\pi^-$ atom, is a Coulomb bound state that in the ground state decays predominantly (99.6%) into two neutral pions through strong interaction. The decay probability is proportional to the atom wave function squared, at zero pion separation, and to the square of $\Delta = a_0 - a_2$. Recent

χPT predictions for the scattering lengths lead to a value of the $\pi^+\pi^-$ atom lifetime of 2.9±0.1 fs [3]. A measurement of τ at 10% accuracy will give a precision of 5% on $|a_0 - a_2|$, of the same order of χPT predictions. In this way, DIRAC experiment will submit the current understanding of chiral symmetry breaking of QCD to a crucial test and will provide useful information about the size of the two-flavour quark condensate.

2 Experimental method

Pionium atoms are produced in DIRAC experiment from Coulomb interaction of pions in the final state when their relative distance is comparable with the atom Bohr radius (387 fm). These pions are generated from the interaction of 24 GeV/c protons of the CERN PS accelerator T8 high intensity beam with a fixed target.

After production in the target these relativistic atoms may either decay, get excited or ionised in the target material. The method proposed in DIRAC for detecting $A_{2\pi}$ is based on the observation of the $\pi^+\pi^-$ pairs from the atom breakup within the target. These "atomic pairs" are characterised by their low relative momentum in the centre of mass system (Q < 3 MeV/c) and they will be identified as an excess over a large background of free pairs.

For a given target material and thickness, the ionisation or breakup probability depends on the atom lifetime in a unique way. Therefore, once the breakup probability has been experimentally measured as the ratio between the number of detected atomic pairs, n_A, and the total amount of produced atoms, N_A, the value of τ is deduced by comparison with its calculated dependency.

To accomplish this task the DIRAC apparatus was designed to detect charged pions pairs with very small opening angles and to measure their relative momentum with high precision ~ 1 MeV/c. It consists of a double arm magnetic spectrometer that includes coordinate detectors (microstrip gas chambers, scintillation fibre detector and ionisation hodoscopes), a magnet (bending power of 2.3 Tm) and two telescope arms, each equipped with drift chambers, scintillation hodoscopes, gas Cherenkov counters, preshower and muon detectors.

3 Preliminary experimental results

The DIRAC spectrometer was commissioned at the end of 1998 and since then has been collecting useful data. A preliminary analysis of the data collected in 1999 and 2000 has shown good set-up performances: precise telescopes alignment, accurate time resolution and an excellent momentum resolution. The former quantity has been evaluated by analysing the invariant mass distribution of $p\pi^-$ events, shown in figure 1. The position of the mass peak corresponds to Λ particles reconstructed in DIRAC. The width of the Λ peak, mainly given by the momentum resolution, is found to be $\sigma = 0.43$ MeV/c^2.

Figure 1: Invariant mass for reconstructed $p\pi^-$ pairs showing the Λ peak.

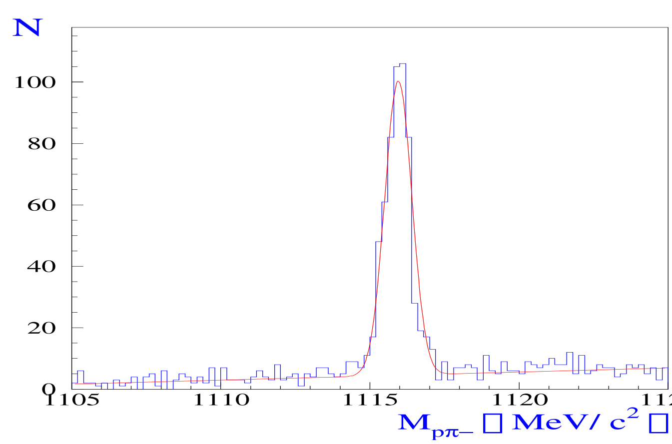

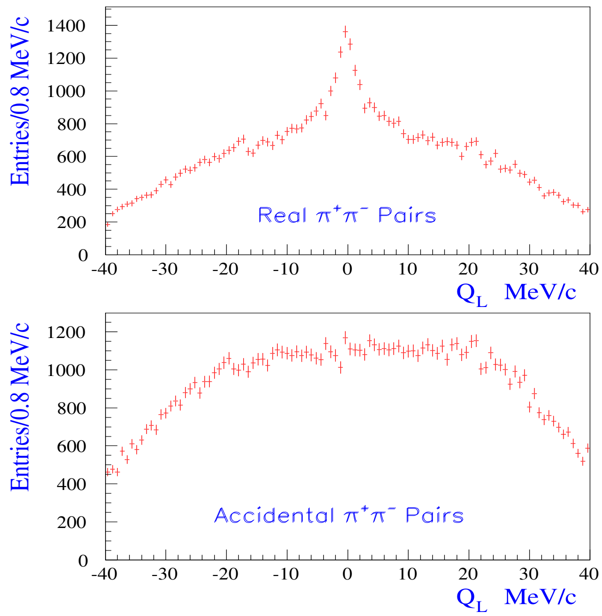

Figure 2: Q_l distribution for $\pi^+\pi^-$ real (top) and accidental pairs (bottom).

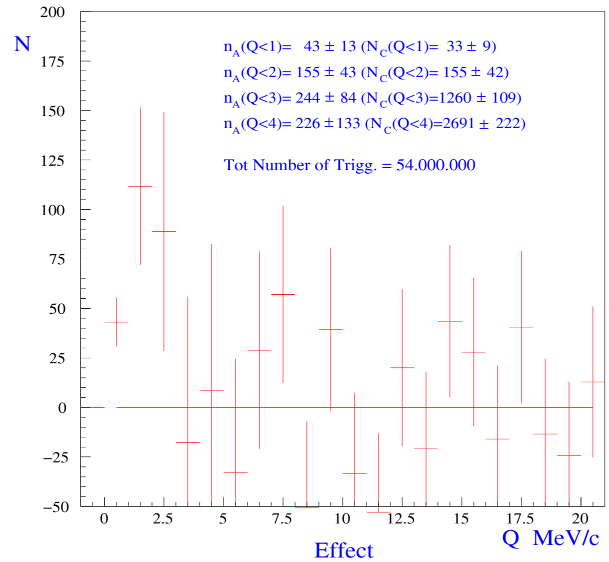

Figure 3: Difference between the experimental Q distribution, $\frac{dN}{dQ}$ and the predicted one for free pairs, $\frac{dN_{free}}{dQ}$.

In figure 2 the distributions of the longitudinal component of the relative momentum are shown for time-correlated (real) and no time-correlated (accidental) events. There is a strong enhancement of $\pi^+\pi^-$ pairs with $|Q_l| < 5\ MeV/c$ for real pairs due to Coulomb interaction in the final state.

The number of observed atomic pairs is obtained through the analysis of the experimental distribution of relative momentum Q for pairs of oppositely charged pions. In the region of very low momentum, Q $< 3\ MeV/c$, this distribution includes both atomic and free pairs. To remove this low-Q background the so called extrapolation method is used. According to this procedure, the distribution of accidental pairs is used to fit the experimental distribution in the region Q $> 3\ MeV/c$, where no atoms are expected, by means of an approximation function that takes into account e.m and strong interactions in the final state. The extrapolation of the approximation function to the region Q $< 3\ MeV/c$ yields the number of free pairs. In figure 3 the distribution obtained after subtracting the predicted Q distribution for free pairs to the experimental Q distribution is shown for data obtained with a Pt target. For Q$< 3\ MeV/c$ there is a clear excess of $\pi^+\pi^-$ pairs that amounts to 244 ± 84 compatible with the expected number of atomic pairs $n_A \sim 240$.

4 Conclusions

The DIRAC experiment is taking data since the end of 1998. The preliminary analysis of the data collected during 1999 has shown the first evidence of a signal associated to atomic pairs coming from the ionisation of $A_{2\pi}$ atoms in a Pt target. At the present, DIRAC experiment is accumulating statistics to achieve its final goal of measuring the pionium lifetime with 10% accuracy at the end of 2002.

References

[1] B. Adeva *et al.*, Proposal to the SPSLC, CERN/SPSLC 95-1 (1995).

[2] G. Colangelo *et al.*, Nucl. Phys. **B603**, 125 (2001).

[3] J. Gasser *et al.*, Phys. Rev. **D64**, 016008 (2001).

The new pionic hydrogen experiment at PSI

D. F. Anagnostopoulos[a], H. Fuhrmann[b], D. Gotta[c], A. Gruber[b], M. Hennebach[c], P. Indelicato[d], Y.-W. Liu[e], B. Manil[d], V. M. Markushin[e], N. Nelms[f], L. M. Simons[e], and J. Zmeskal[b]

[a] *Department of Material Science, University of Ioannina, GR–45110 Ioannina, Greece*
[b] *IMEP, Österreichische Akademie der Wissenschaften, A-1090 Vienna, Austria*
[c] *Institut für Kernphysik, Forschungszentrum Jülich, D-52425 Jülich*
[d] *Laboratoire Kastler–Brossel, Université Pierre et Marie Curie, F–75252 Paris, France*
[e] *Paul–Scherrer–Institut (PSI), CH–5232 Villigen, Switzerland*
[f] *Department of Physics and Astronomy, University of Leicester, Leicester LEI7RH, England*

(Received: 29 October 2001)

The measurement of the hadronic ground–state shift and broadening in pionic hydrogen is resumed at the Paul–Scherrer–Institut (PSI). The final goal of the experiment is to achieve an accuracy of 0.2% for the shift and of 1% for the width of the ground state, which are improvements by factors of about 5 compared to the previous high–resolution measurement.

1 Introduction

A high–precision determination of the πN scattering lengths allows conclusive tests of the methods of HBχPT [1]. Experimentally, the scattering lengths may be obtained either by measuring the ground–state shift ϵ_{1s} and broadening Γ_{1s} in pionic hydrogen or by extrapolating πN scattering data to threshold, e. g. by using results from phase–shift analyses [2,3].

The relations between exotic–atom parameters and isoscalar and isovector scattering lengths are given by Deser–type formulas [4–6]. Furthermore, from Γ_{1s}, which is proportional to the isovector scattering length squared, the pion–nucleon coupling constant is obtained by the Goldberger–Miyazawa–Oehme sum rule [7,8]. The most important quantity to be improved in accuracy is Γ_{1s}.

The new experiment [9] aims at a significant increase in accuracy compared to the previous precison experiments [10]. An important part will be studies for a better understanding of the atomic cascade.

- First goal is to establish a precise value for the shift, which must be proven to be independent of pressure. Such a dependence on the environment may originate from the formation of complex molecular structures like [(πpp)p]ee when the πp system collides with other molecules in the target [11]. Deexcitation from molecular levels could lead to small energy shifts hidden by the line width of the transition.
- Secondly, a more accurate determination of the ground–state width requires a better knowledge of Coulomb deexcitation, a non–radiative deexcitation channel of the pionic–hydrogen atom, where energy is released by accelerating the collision partners. To obtain the pure hadronic contribution, the measured line width has to be corrected for Doppler broadening.

2 Experimental approach

The measurement is based on techniques developed and applied to the precision spectroscopy of X–rays from antiprotonic and pionic atoms together with substantial improvements in background suppression. The cyclotron trap provides a concentrated X-ray source for a focusing low–energy crystal spectrometer. X–rays emitted from the stop volume are reflected by spherically bent silicon or quartz crystals of up to 10 cm diameter. They are detected by a large–area detector built up from an array of Charge–Coupled devices (CCDs) [12].

The measurement of ϵ_{1s} in a wide pressure range will prove or disprove the influence of molecular formation on the decay branches involving the πH Lyman transitions. The pressure is varied in the density range from 3 bar equivalent up to liquid by using a cryogenic target, which is operated at about 1.5 bar absolut pressure. The decrease of X–ray line yields due to the increasing Stark mixing is compensated by the higher stop efficiency of the cyclotron trap for the more dense targets.

The most difficult part is the precise determination of the hadronic broadening. It requires a better knowledge of the Coulomb deexcitation cross section. A detailed investigation of this process will be performed with muonic hydrogen which does not show hadronic effects. Muons are obtained from the decay of slow pions inside the cyclotron trap close to the cryogenic target. The line width in muonic hydrogen will be interpreted in terms of a new dynamical cascade picture involving the velocity of the exotic atom in all stages of the cascade and results from recent calculations for the cross section of the various collision processes [13].

To exploit the detailed studies of the line shape, a better knowledge of the crystal spectrometer response than available up–to–now is required. In the few keV range, narrow X–ray lines for testing the curved Bragg crystals are not available for practical cases. Fluorescence X–rays have large line widths owing to Auger transitions and, in addition, exhibit complicated satellite structures caused by multiple–hole excitation. Therefore, crystal response functions had been obtained from narrow pionic–atom transitions in the previous experiments [10, 14]. However, the limited rates even at high–flux pion channels lead to unacceptable long measuring times for detailed crystal studies.

For that reason, an Electron–Cyclotron–Resonance (ECR) source is being set up. It will be used to produce hydrogen– or helium–like electronic atoms, of which the fluorescence lines are narrow enough for thorough studies of the Bragg crystals without the use of a particle accelerator. The temperature of the plasma is expected not to exceed an equivalent of about 40 meV line width [15]. The magnet of the cyclotron trap itself is used to provide the mirror field for the plasma [16].

3 First results

A first series of measurements took place at the high–intensity pion channel πE5 of PSI. At a target density equivalent to about 4 bar, with a H_2/O_2 gas mixture the πO(6h–5g) calibration line and the πH(3p–1s) transition were measured simultaneously. This method is basically free of systematic errors in the energy calibration due to long–term instability and will be applied in a high-statistics measurement within the next year.

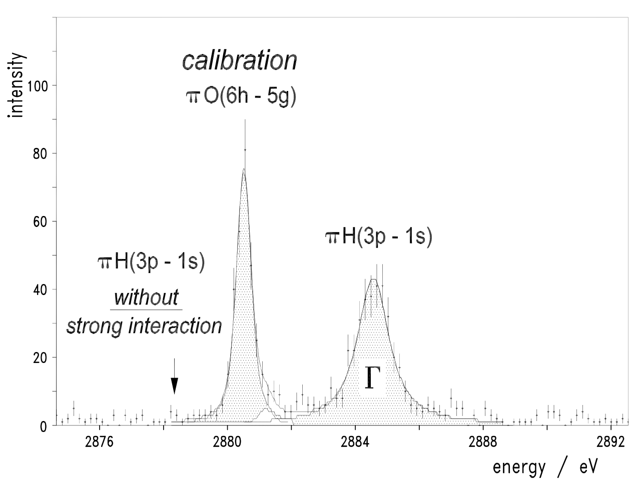

Figure 1: Simultaneously measured reflections of the πH(3p–1s) and the π^{16}O(6–5) transitions.

Table 1: Preliminary results of line shift and broadening for the $\pi H(3p-1s)$ transition obtained at 3 different densities. For the electromagnetic transition energy a value of 2878.808 eV was used as in the analysis of the previous experiment at 15 bar equivalent density [10].

density equivalent	ϵ_{1s} /meV $\pm stat \pm sys$	Γ_{1s} /meV $\pm stat \pm sys$	ref.
3.5 bar	+ 7082 $\pm$ 31 $\pm$ 15	973 $\pm$ 75 $\pm$ 10	this exp.
28bar	+ 7137 $\pm$ 18 $\pm$ 40	969 $\pm$ 26 $\pm$ 10	this exp.
liquid	+ 7095 $\pm$ 25 $\pm$ 25	1052 $\pm$ 58 $\pm$ 10	this exp.
15 bar	+ 7108 $\pm$ 13 $\pm$ 34	969 $\pm$ 45 $\pm$ 10	[10]

At higher densities hydrogen and oxygen have to be measured alternately to prevent the oxygen from freezing. For the first time, pionic hydrogen was measured in the liquid phase.

4 Conclusions and outlook

No pressure dependence of the ground–state shift was observed for pionic hydrogen due to molecular formation. However, evidence for an increase of the line width was found in the liquid phase. This observation, attributed to Coulomb deexciation, will be studied again in the forthcoming beam time.

Later on in the second part, after detailed studies of the Bragg crystals, the investigation of the line widths in muonic hydrogen, where the hadronic effects are absent, will yield more precise information on Coulomb deexcitation. Based on the advanced cascade code a further substantial improvement on the accuracy for the hadronic line width will then be feasible.

References

[1] *Proc. of MENU '99*, Zuoz, Switzerland, 1999, πN newsletter **15** (1999), and references therein.

[2] R. Koch and E. Pietarinen, Nucl. Phys. **A 336**, 331 (1980); R. Koch, Nucl. Phys. **A 480**, 707 (1986).

[3] See e. g. contributions to this workshop by G. C. Oades et al., M. Pavan et al., and M. Sainio.

[4] S. Deser et al., Phys. Rev. **96**, 774 (1954).

[5] G. Rasche and W. S. Woolcock, Nucl. Phys. **A 381**, 405 (1982).

[6] V. E. Lyubovitskij and A. Rusetsky, Phys. Lett. **B 494**, 9 (2000).

[7] M. L. Goldberger, H. Miyazawa, and R. Oehme, Phys. Rev. **99**, 986 (1955).

[8] T. E. O. Ericson, B. Loiseau, and A. W. Thomas, Phys. Scr. **T87**, 71 (2000).

[9] PSI experiment R-98.01:http://pihydrogen.web.psi.ch.

[10] H.-Ch. Schröder et al., Eur. Phys. J. **C 21**, 433 (2001).

[11] S. Jonsell, J. Wallenius, and P. Froelich, Phys. Rev. **A 59**, 3440 (1999).

[12] N. Nelms et al., to be published in Nucl. Instr. Meth. **A**.

[13] V. M. Markushin and T. S. Jensen, contribution to this workshop.

[14] P. Hauser et al., Phys. Rev. **C 58**, R1869 (1998).

[15] D. Hitz et al., Rev. Sci. Instr. **71**, 839 (2000).

[16] S. Biri, L. Simons, and D. Hitz, *proc. of CERIS'99*, CERN, 58 (1999).

Atomic cascade in hadronic atoms

T.S. Jensen[a,b] and V.E. Markushin[a]

[a]*Paul Scherrer Institute, Villigen, Switzerland*
[b]*Institut für Theoretische Physik der Universität Zürich, Switzerland*

(Received: 31 October 2001)

The atomic cascades in hydrogen–like exotic atoms x^-p ($x^- = \mu^-$, π^-, K^-, $\bar{p}$) have been studied with a new detailed kinetics cascade model. By using new results for the differential and total cross sections for the collisional processes, we get a good description of the atomic kinetic energy distributions and cascade times.

1 The extended standard cascade model

The standard cascade model for light exotic atoms, originally introduced by Leon and Bethe [1], provides a fair description of many experimental observables like X-ray yields and absorption fractions. The extended standard cascade model [2] includes all cascade processes of the standard cascade model: the radiative, Auger, and Coulomb deexcitation, Stark mixing, and, in case of hadronic atoms, nuclear absorption. In addition, the change in the kinetic energy distribution of the exotic atoms through the cascade due to acceleration and deceleration mechanisms is taken into account. A significant improvement over earlier calculations is obtained by the use of new results for the collisional processes. In the lower part of the cascade, $n = 2-5$, we use a fully quantum mechanical close–coupling framework (Sect. 2). A semiclassical approach is used for the middle part of the cascade. In the initial stage of the cascade, the collisions are calculated using a classical–trajectory Monte Carlo model (Sect. 3).

2 Quantum mechanical close–coupling framework

The scattering of hydrogen–like exotic atoms in excited states ($n = 2-5$) from hydrogen atoms is calculated in the close–coupling approximation [3–5]. A complete set of differential and total cross sections for the processes

$$(x^-p)_{nl_i} + \mathrm{H} \to (x^-p)_{nl_f} + \mathrm{H} \ , \qquad (x^- = \mu^-, \pi^-, K^-, \bar{p}) \tag{1}$$

has been obtained in a range of kinetic energies relevant for atomic cascade. The shifts and, in case of hadronic atoms, the widths of the ns–states are taken into account ensuring correct threshold behavior of the cross sections. The cross sections for nuclear absorption during collisions via the Stark mixing of the states $l > 0$ with s–states, for example

$$(\pi^-p)_{nl} + \mathrm{H} \to \pi^0 + n + \mathrm{H} \ , \tag{2}$$

are calculated simultaneously. As shown in Refs. [4, 5], transitions to the ns–states and nuclear absorption during collisions in the near–threshold region cannot be calculated reliably in the previously used semiclassical straight–line–trajectory approximation [1]. Apart from these special cases, the semiclassical models provide computationally effective alternatives for calculating the processes (1) and (2), and we use them in the intermediate n–range (for example $n = 6-8$ for π^-p) between the quantum mechanical and fully classical domains.

3 Classical–trajectory Monte Carlo calculation

In the upper part of the atomic cascade, where the x^-p is in a high n state and many nlm substates are involved in the collisions, classical mechanics is expected to give an adequate description. We

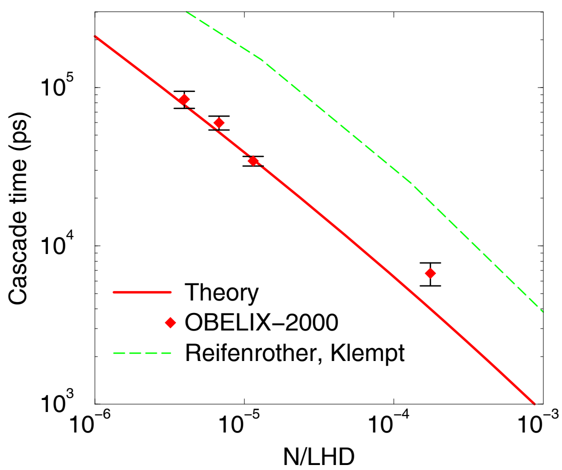

Figure 1: The density dependence of the cascade time in antiprotonic hydrogen. The result of the present cascade calculations is shown in comparison with the result of Ref. [9] and the experimental data [8]. The initial conditions are: $n_i = 30$, the statistical l–distribution , and the kinetic energy given by a Maxwell distribution with $\langle E_i \rangle = 0.5$ eV.

use a classical–trajectory Monte Carlo model to calculate the differential and total cross sections for exotic atoms scattering from hydrogen molecules:

$$(x^- p)_{n_i l_i} + \mathrm{H}_2 \to (x^- p)_{n_f l_f} + X \ , \qquad (X = \mathrm{H}_2,\ \mathrm{H}_2^*,\ \mathrm{H} + \mathrm{H}) \ . \tag{3}$$

The cross sections for the processes (3) are obtained by solving the equations of motion for a large number of collisions with different impact parameters. The system is treated as an effective four–body problem consisting of the x^-, the proton, and the two hydrogen atoms with the electrons kept as fixed charge distributions corresponding to the $1s$ state. The interaction between the particles is given by the electrostatic potentials except for the interaction between the two hydrogen atoms where the Morse potential was used.

Results for muonic hydrogen have been shown in Ref. [5]. Molecular target effects turn out to be very important: transitions with $\Delta n = 2 - 4$ dominate the initial part of the cascade whereas the calculations of scattering on atomic target predict that $\Delta n = 1$ is most likely [6]. The molecular target effect is significant in the other hydrogen–like exotic atoms as well. In all cases examined (μp, $\pi^- p$, $K^- p$, and $\bar{p}p$), we found that, when compared to calculations with atomic target, the Coulomb transitions with large Δn are strongly enhanced in the molecular case.

4 Results

By using the new results for the collisional processes, an improved description of the experimental data has been obtained. In particular, the results of the classical–trajectory calculations for molecular target are essential for explaining the experimental data at low densities in muonic and antiprotonic hydrogen. At low densities (much less than 10^{-3} of liquid hydrogen density) the collisional stage of the cascade ends at high n, whereas the rest of the cascade is purely radiative. In [2] we showed that the observed increase in the kinetic energy of the muonic hydrogen atoms with increasing density reported in Ref. [7] can be explained using the results of the classical–trajectory model, the $\Delta n > 1$ collisional transitions being essential for the initial acceleration of the μp. Additional evidence for large Δn transitions at high n is provided by the measured cascade time in antiprotonic hydrogen [8]. The density dependence of the cascade time in antiprotonic hydrogen is shown in Fig. 1. The theoretical result is in good agreement with the experimental data of Ref. [8], whereas the result of Ref. [9] is inconsistent with the data. The difference in the cascade time between the present calculation and that of Ref. [9] is due to the collisional deexcitation at high n. Though molecular effects of the target were assumed to be responsible for the deexcitation in the initial stages of the cascade in Ref. [9], the estimated cross sections for the "chemical deexcitation" at high n were much smaller than the results of the classical–trajectory model.

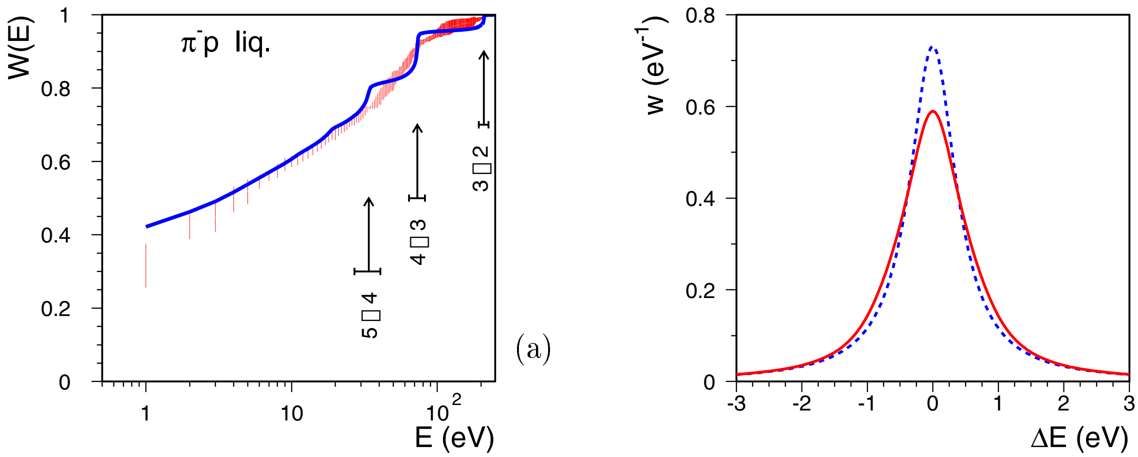

Figure 2: (a) The calculated cumulative energy distribution $W(E)$ of the $\pi^- p$ atom at the instant of nuclear reaction in liquid hydrogen (solid line) in comparison with the data [11]. The kinetic energies corresponding to the Coulomb transitions $n_i \to n_f$ are shown by arrows, with horizontal bars indicating the energy resolution of the measurement. (b) The energy profile of the K_β line in pionic hydrogen at 3 bar with Doppler broadening taken into account (solid line) in comparison with the natural line shape assuming $\Gamma_{1S} = 0.87$ eV (dashed line).

A deep understanding of the kinetic energy evolution during the atomic cascade is crucial for the new pionic hydrogen experiment at PSI [10]. In order to obtain the strong interaction width of the $1s$ state, Doppler corrections to the measured $np \to 1s$ line profile must be taken into account. A reliable cascade model is, therefore, needed to calculate the kinetic energy distribution at the instant of the radiative transition. Cascade calculations at pressures > 1 bar are sensitive to the strength of the Coulomb deexcitation at low n and possible additional absorption mechanisms related to formation of molecular resonances. As discussed in Ref. [2], the experimental results for the absolute X-ray yields and the kinetic energy distributions can be used to adjust the rates for Coulomb deexcitation and absorption at low n. Figure 2a shows the calculated $\pi^- p$ kinetic energy distribution at the instant of absorption in liquid hydrogen compared with the experimental data [11]. The resulting Doppler broadening of the $3p \to 1s$ line at 3 bar is shown in Fig. 2b.

Acknowledgments: We thank P. Hauser, F. Kottmann, L. Simons, D. Taqqu, and R. Pohl for fruitful and stimulating discussions.

References

[1] M. Leon and H.A. Bethe, Phys. Rev. **127**, 636 (1962).
[2] V.E. Markushin and T.S. Jensen, Hyperfine Interactions (in press).
[3] T.S. Jensen and V.E. Markushin, PSI-PR-99-32 (1999), nucl-th/0001009.
[4] T.S. Jensen and V.E. Markushin, Nucl. Phys. A **689**, 537 (2001).
[5] T.S. Jensen and V.E. Markushin, Hyperfine Interactions (in press).
[6] L. Bracci and G. Fiorentini, Nuovo Cimento 43A, 9 (1978).
[7] F. Kottmann *et al.*, Hyperfine Interactions **119**, 3 (1999).
[8] A. Bianconi *et al.*, Phys. Lett. B **487**, 224 (2000).
[9] G. Reifenröther and E. Klempt, Nucl. Phys. A **503**, 885 (1989).
[10] D. Gotta, these proceedings.
[11] A. Badertscher *et al.*, Europhys. Lett. **54**, 313 (2001).

Probing of nucleon mesonic structure by means of quasi-elastic knock-out processes like $p + e \to \pi^+ + e'$

V.G. Neudatchin, I.T. Obukhovsky, and N.P. Yudin

Institute of Nuclear Physics, Moscow State University, Moscow 119899, Russia

(Received: 27 October 2001)

The momentum distributions $\overline{|\Psi_p^{n\pi^+}(\mathbf{k})|^2}$ and $\overline{|\Psi_p^{n\rho^+}(\mathbf{k})|^2}$ of pions and ρ-mesons in the nucleon are extracted from experiment. Perspectives of the quark microscopic theory of mesonic cloud are outlined.

1 Introduction

It is well known that the theoretical description of the pion photoproduction on nucleon encounters the complicated set of problems: a number and a type of used diagrams, their gauge invariance, necessity of inclusion of form factors, taking into account off-shell effects, and so on. But the situation becomes significantly simpler for virtual photons γ^* in the electroproduction process $p + \gamma^* \to n + \pi^+$ at sufficiently high values of the momentum square transfer $Q^2 = -q^2 \gtrsim 1 - 2GeV^2/c^2$. In this case the diagram with the pion pole in the t-channel (the "pion-in-flight" diagram) becomes dominant under the standard conditions of quasielastic knock-out process: $|\mathbf{q}| \gg |\mathbf{k}|$, $q_0 \gg |k_0|$, $k_0 = M_N - E_N(-\mathbf{k})$ (or $W - M_R \gg m_\pi$), where $\{k_0, \mathbf{k}\}$ is the 4-momentum of virtual pion in the nucleon and $W^2 = (p_R + p_{\pi'})^2$ is the mass of final hadron state $R + \pi$ ($R = N$, Δ, N^*, etc.). For the first time the dominance of pion-in-flight diagram in the longitudinal part σ_L of differential cross section (integrated over the azimuthal angles) $d^3\sigma(ep \to e'n\pi^+)/dQ^2dW^2dt = 2\pi\Gamma\,(\epsilon\, d\sigma_L/dt + d\sigma_T/dt)$, $\quad t \approx -\mathbf{k^2}$, was pointed in the paper [1]. Later in Ref. [2] the analysis of the momentum distribution of pions in the nucleon was given in the frame of light cone dynamics. In our works [3,4] the discussion of the knock-out process is given in the laboratory system and just in this frame we find the momentum distribution (MD) of pions (starting from experimental data [1] on σ_L). The similar situation is also for the transverse virtual photon γ_T^* (really the knockout of a vector meson with simultaneous transformation of ρ into the pion). It can provide a valuable information on the properties of vector mesons in nucleon [3]. These facts open a new possibility for the direct investigation of the meson structure of nucleon.

2 Study of the pion and ρ-meson momentum distribution in the nucleon

Our approach to the problem is very similar to the standard methods of nuclear physics, where the process of nucleon knockout has been used for a long time as a mighty tool for investigation of the momentum distribution of nucleons in nuclei. The cross section of quasi-elastic pion knockout from nucleon can be written in the form:

$$\frac{d\sigma_L(\gamma^* p \to n\pi^+)}{d\mathbf{k^2}} = \frac{\alpha\, F_\pi^2(Q^2)}{8|\mathbf{q}^*|W(W^2 - M_N^2)}\,\overline{\left|\frac{M(p \to n + \pi^+)}{t - m_\pi}\right|^2}\,\frac{\mathbf{q}^2}{Q^2}\;4\left[\omega(\mathbf{p}_{\pi'}) - q_0\frac{\mathbf{p}_{\pi'}\cdot\mathbf{q}}{\mathbf{q}^2}\right]^2 ,$$

where asterisk symbols are for values written in the center of mass of the $\gamma^* + p$ collision. The "wave function" (W.F.) of a virtual pion in the nucleon is the following k-dependent factor of σ_L:

$$\overline{\left|\Psi_p^{n\pi^+}(|\mathbf{k}|)\right|^2} = \mathcal{N}^{-1}\,\overline{\left|\frac{M(p \to n + \pi^+)}{k_0 + \omega_\pi(|\mathbf{k}|)}\right|^2} , \qquad \mathcal{N}^{-1} = \frac{4\pi}{(2\pi)^3 2M_N\, 2E_N(|\mathbf{k}|)\, 2\omega_\pi(|\mathbf{k}|)} ,$$

which can be related to the matrix element of the pion creation operator

$$\langle n + \pi^+|a_{\pi^+}^\dagger|p\rangle \sim \frac{M(p \to n\pi^+)}{t - m_\pi} = \frac{\mathcal{N}^{1/2}}{k_0 - \omega_\pi(|\mathbf{k}|)}\,\Psi_p^{n\pi^+}(|\mathbf{k}|) .$$

Recall that for the standard πNN vertex the transition amplitude can be written in the form

$$\overline{|M(p \to n\pi^+)|^2} = 2\mathbf{k}^2 g^2_{\pi NN} F^2_{\pi NN}(\mathbf{k}^2) \ , \qquad F_{\pi NN}(\mathbf{k}^2) = \Lambda^2_\pi/(\Lambda^2_\pi + \mathbf{k}^2) \ .$$

As the normalization of all the above factors is fixed the norm of such W.F. defines a "spectroscopic factor" (S.F.) of the $n + \pi^+$ state in the proton

$$S_p^{n\pi} = \int_0^\infty \overline{\left|\Psi_p^{n\pi^+}(k)\right|^2} k^2\, dk \ ,$$

The pion-baryon structure of nucleon can be described in terms of a set of such spectroscopic factors: $S_p^{\pi n}$, $S_p^{\pi\Delta}$, $S_p^{\pi N^*}$, etc. When the longitudinal cross section is factorizable in the form

$$d\sigma_L(\gamma^* p \to n\pi^+)/d\mathbf{k}^2 \sim \overline{\left|\Psi_p^{n\pi^+}(|\mathbf{k}|)\right|^2} Q^2 F^2_\pi(Q^2) \ , \qquad F_\pi(Q^2) = (1 + Q^2/0.51)^{-1} \ ,$$

(e.g. in terms of the pion-in-flight mechanism) the W.F. and S.F. should be observable values in the coincidence experiments (at fixed Q^2 and M_R). Then one can define (in analogy with the standard definitions in the nuclear cluster physics) the "total number of pions in the nucleon" as a sum $S_\pi = \sum_B S_p^{\pi B}$, where $R \equiv B = N$, Δ, N^*, etc. are all the possible virtual baryons in the nucleon. In Figs. 1 and 2 the longitudinal cross sections calculated on the basis of the above pion-in-flight mechanism (at the value of Λ_π =0.7 and 1.2 GeV) are compared with the old $p(e, e'\pi^+)n$ data [1] at Q^2 =0.7 and 3.3 GeV^2/c^2. One can see that at both high and intermediate Q^2 this mechanism is in a rough agreement with the data if the cut-off parameter Λ_π is not so large ($\approx$0.7 GeV/c), but new more exact data on σ_L at high Q^2 would be desirable.

The pole diagram with the ρ meson as a virtual state in the nucleon provides the main contribution to the transverse cross section $\sigma_T(\gamma^* p \to n\pi)$ at high $Q^2 \gtrsim 2 - 3\,Gev^2/c^2$ (see Fig. 3). However, the spectroscopic factor for the $n + \rho$ channel $S_p^{n\rho}$ cannot be determined from the experiment as the data are only available for too low $\mathbf{k}^2$ as compare with m^2_ρ.

3 Pion-baryon structure of the nucleon in the $^3P_0$ model

Non-diagonal transitions $p \to B + \pi$ for the pion-in-flight mechanism of pion knock out can be considered on the same footing, i.e. on the basis of the field-theory vertex function, but the standard expressions

$$\overline{\left|M(p \to B_i + \pi)\right|^2} = f^2_{\pi NB_i} \frac{4M_N M_{B_i}}{m^2_\pi} 2\mathbf{k}^2 F^2_{\pi NB_i}(\mathbf{k}^2)$$

depend on too many free parameters ($f_{\pi NB_i}$ and $F^2_{\pi NB_i}(\mathbf{k}^2)$ in each channel "i") to be informative for definite predictions of cross sections. The constituent quark model evaluations of the above free

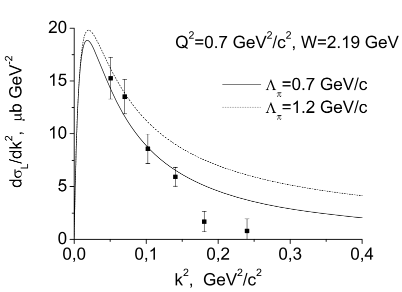

Figure 1: Longitudinal cross section at $Q^2 = 0.7\,\mathrm{GeV}^2/\mathrm{c}^2$. The data are from Ref. [1]

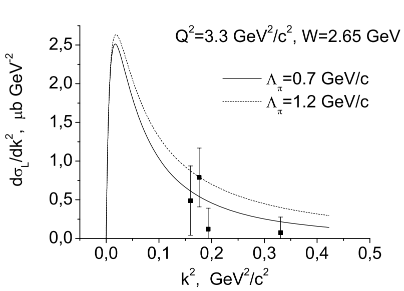

Figure 2: Longitudinal cross section at $Q^2 = 3.3\,\mathrm{GeV}^2/\mathrm{c}^2$.

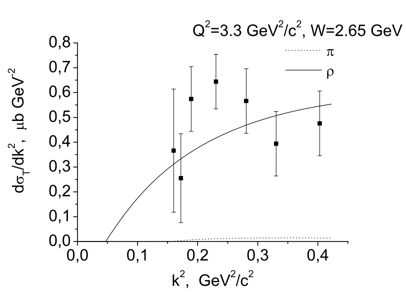

Figure 3: Transverse cross section at $Q^2 = 3.3\,\mathrm{GeV}^2/\mathrm{c}^2$.

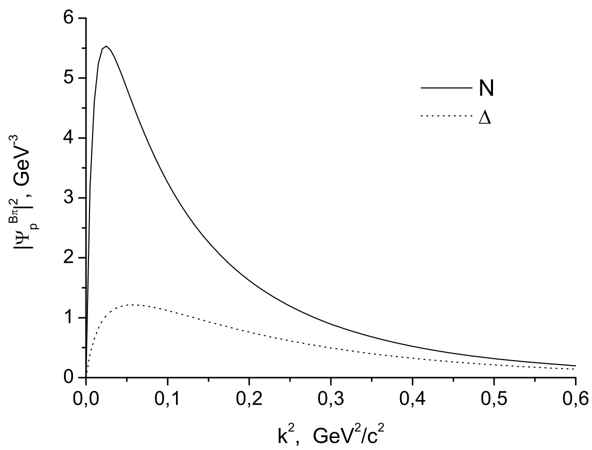

Figure 4: Pion momentum distribution in the nucleon for πB channels $\pi + N$ and $\pi + \Delta$.

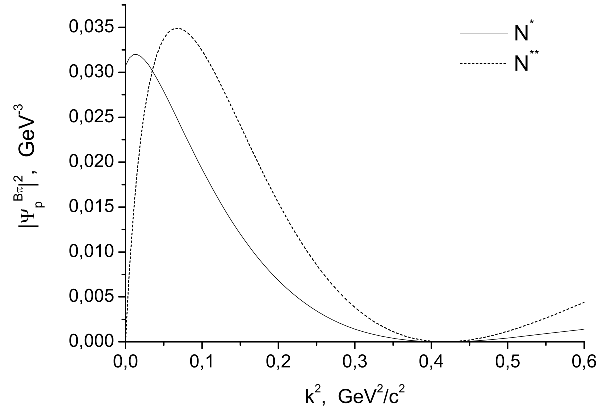

Figure 5: Pion momentum distribution in the nucleon for πB channels $\pi + N^*$ and $\pi + N^{**}$.

parameters would be more effective. For example, the microscopic $^3P_0$ model [5,6] starts from only one free parameter, the amplitude of the vacuum $q\bar{q}$ fluctuation (normalized on the effective πqq coupling constant $f_{\pi qq} = \frac{3}{5} f_{\pi NN}$), but predict all the coupling constants $f_{\pi NB_i}$ and form factors $F_{\pi NB_i}$ of the interest starting from the standard quark-shell-model techniques [4,7]. Parameters of the constituent quark model have already been fixed, and are not free in our approach. All the form factors $F_{\pi NB_i}$ only depend on two quark-shell-model parameters b_N and b_π (quark radii of N and π) fixed earlier. At the standard values $b_N = 0.6\,fm$ and $b_\pi = 0.3\,fm$ we have obtained the predictions for π-B_i wave functions in the nucleon (see Figs. 4 and 5), where $B_i = N,\ \Delta,\ N^* = N_{1/2^-}(1535)$ and $N^{**} = N_{1/2^+}(1440)$. In the used proper normalization of the W.F.'s we are able to determine the S.F.'s for these virtual states in the nucleon [7]. This values could be extracted from coincidence experiments similar to the above cited [1]. Such experiments would be more difficult because of too small predicted cross sections for π+B_i channels, but they will be very informative for understanding the hadron structure in terms of quark and meson degrees of freedom.

Acknowledgments: The authors gratefully acknowledge the contribution of Dr. L.L. Sviridova to the work. The work was supported in part by the Russian Foundation for Basic Research grant No 00-02-16117.

References

[1] B. Brauel, T. Canzler, D. Cords, *et al.*, Z. Phys. C **3**, 101 (1979).

[2] F. Guttner, G. Chanfray, H.P. Pirner, and B. Povh, Nucl. Phys. A**429**, 389 (1984).

[3] V.G. Neudatchin, L.L. Sviridova, and N.P. Yudin, Yadernaya Fizika **62**, 694 (1999).

[4] V.G. Neudatchin, I.T. Obukhovsky, and N.P. Yudin, *Relativistic Nuclear Physics and Quantum Chromodynamics*, Proc. XIV Int. Seminar on High Energy Physics Problems (Editors: A.M. Baldin and V.V. Burov), JINR, Dubna (2000), vol. 1, p. 55.

[5] A. LeYaouanc, Ll. Oliver, O. Pène, and J.-C. Raynal, *Hadron Transitions in the Quark Model.* Gordon and Breach Sci. Publ., N.Y., London, Paris. 1988.

[6] F. Cano, P. Gonzalez, S. Noguera, and B. Desplanques, Nucl. Phys. **A343**, 331 (1996).

[7] I.T. Obukhovsky, contributed paper in this issue, to be published.

A possible quark origin of two-pion emission in $e + N$ and $N + N$ collisions

I.T. Obukhovsky

Institute of Nuclear Physics, Moscow State University, Moscow 119899, Russia

(Received: 27 October 2001)

The constituent quark model has been taken as a starting point for investigation of one- and two-pion emissions. A wide range of observables has been evaluated in the framework of the $^3P_0$ model. Comparison of the results with the data (when it is possible) shows an approximate agreement.

1 Introduction

In recent works of the Moscow [1] and Moscow-Tübingen [2] groups the $^3P_0$ model of pion emission [3, 4] has been extended to the description of mesonic clouds in nucleonic systems. In this model the meson momentum distribution in the cloud replicates the quark momentum distribution in the nucleon or in the overlap region of a two-nucleon system, and thus the standard quark-shell-model technique can be used for evaluation of meson cloud contributions to varied processes. As a result the pion emission amplitudes of interest [e.g. the amplitudes $M(N \to \pi + B)$ of virtual transitions $N \to B + \pi$ for pion quasielastic knockout $N + e \to e' + \pi + B$ with $B = N,\ \Delta,\ N_{1/2^+}(1440)$, etc.] have been calculated by this technique without invoking the Lagrangian field theory coupling constants $f_{\pi NB}$ and vertex form factors $F_{\pi NB}(k^2)$ (mostly unknown). On the same footing the related two-nucleon vertices $N + N \to^2 B + \pi$, actual for quasielastic processes of a similar type (e.g. $d + e \to e' + \pi +^2 B$), have been evaluated.

In reactions $N + e \to e' + \pi + B_i$ ($d + e \to e' + \pi +^2 B$) a pionic decay of the final baryon (dibaryon) leads to a second pion emission $B_i \to N + \pi$ ($^2B \to N + N + \pi$) with a momentum distribution predicted by the $^3P_0$ model as well. However, the predicted cross sections for respective coincidence experiments are too small [1] to be seen over the background. Nevertheless another two-pion processes, e.g. the virtual "σ-meson" (correlated $\pi\pi$ pair) emission, have been considered.

2 One-pion predictions

Table 1 shows the "spectroscopic factors" [1] $S_N^{\pi B} = \int \overline{|\Psi_N^{\pi B}(\mathbf{k})|^2}\, d^3k$ for pion momentum distributions $\Psi_N^{\pi B_i}(\mathbf{k})$ in varied channels $N \to \pi + B_i$, $B_i = N,\ \Delta,\ N^*$, etc.

$$\Psi_p^{\pi B_i}(\mathbf{k}) \sim \frac{M(N \to \pi + B_i)}{E_N(\mathbf{k}) - M_N + \omega_\pi(\mathbf{k})}, \quad \overline{|M(N \to \pi + B_i)|^2} = f_{\pi qq}^2 \frac{4M_N M_B}{m_\pi^2} C_{\pi N B_i}^2 \mathbf{k}^2\, F_{\pi N B_i}(\mathbf{k}^2)\ ,$$

with coefficients $C_{\pi N B_i}^2$ calculated algebraically in the framework of $^3P_0$ model ($f_{\pi qq} = 3/5\, f_{\pi NN}$ is the effective $\pi q\bar{q}$ coupling constant common for all the channels).

The calculated values Γ_{B_i} are realistic ones but they are no more than in a rough agreement with

B_i	N	Δ	$N_{1/2^-}(1535)$	$N_{1/2^+}(1440)$
$C_{\pi N B_i}^2$	2	$\frac{64}{25}$	$\frac{16\omega_\pi(\mathbf{k}^2)}{75\mathbf{k}^2}$	$\frac{2}{27}$
Γ_{B_i}(MeV)	–	63	52	47
$S_p^{B_i\pi}$	0.153	0.065	0.006	0.011

Table 1: Spectroscopic factors $S_p^{B_i\pi}$ and pion decay widths Γ_{B_i} for some baryons.

experimental data. Nevertheless the evaluations made on the basis of $^3P_0$ model have some advantages over the standard phenomenological description. In the model all the form factors $F_{\pi NB_i}(\mathbf{k}^2)$ depend only on two parameters: b and b_π/b, where $b \approx 0.6$ fm and $b_\pi \approx 0.3$ fm are standard free parameters of the constituent quark model (the baryon and pion radius correspondingly). It is interesting that the sum of all the calculated spectroscopic factors $N_\pi = \sum_i S_N^{\pi B_i} = 0.24$, which is said (by analogy with the nuclear cluster physics) to be "a total number of pions in the nucleon", shows and approximate agreement with the "experimental" value $N_\pi = 0.18\pm0.06$ obtained previously [1] by fitting the old pion knock-out data [5].

3 Two-pion predictions

In the recent work [2] the σ-meson formation has been considered in both the nucleon and the NN-system. We start from the $^3P_0$-model effective πqq vertex [2,4,6]

$$H_\alpha^{(3)}(\boldsymbol{\rho}_2', \boldsymbol{\rho}_2) = \frac{f_{\pi qq}}{m_\pi} \frac{e^{2i\mathbf{k}\cdot\boldsymbol{\rho}_2'/3}}{\sqrt{2\omega_\pi}(2\pi)^{3/2}} \hat{O}(\boldsymbol{\rho}_2', \boldsymbol{\rho}_2)\, \tau_{-\alpha}^{(3)}\boldsymbol{\sigma}^{(3)} \cdot \left[\frac{\omega_\pi}{2m_q}\left(\frac{2}{i}\nabla_{\rho_2} + \frac{2}{3}\mathbf{k}\right) + \left(1 + \frac{\omega_\pi}{6m_q}\right)\mathbf{k}\right] ,$$

and an effective $\sigma\pi\pi$ scalar coupling $H_{\pi\pi\sigma} = g_{\pi\pi\sigma}\, \vec{\phi}_\pi \cdot \vec{\phi}_\pi\, \phi_\sigma$ ($g_{\pi\pi\sigma} \approx 2 - 4\ GeV$) with the vertex form factor $F_{\pi\pi\sigma}(q^2)$ of a Gaussian form $\sim exp(-q^2 b_\sigma^2/2)$ (here $\hat{O}$ is a non-local operator related to the pion $q\bar{q}$ wave function and $\boldsymbol{\rho}_2 = (\mathbf{r}_1 + \mathbf{r}_2)/2 - \mathbf{r}_3$ is a relative coordinate). The resulting expression for the σNN coupling constant $g_{\sigma NN} \equiv g_0\, D_N(0)$ with $g_0 = \frac{f_{\pi qq}^2}{m_\pi^2}\frac{g_{\sigma\pi\pi}}{m_q^2 b^3}$ depends only on the loop integral $D_N(k)$ for the triangle diagram in Fig. 1. It has been shown that a realistic value $g_{\sigma NN} \approx$ 5-10 could be only obtained if one takes into account a *coherent superposition* of all the baryon intermediate states B_i^* in the triangle graph: N, $N^*_{1/2^-}$, $N^*_{3/2^-}$, $N^{**}_{1/2^+}$, Δ, $\Delta^*_{1/2^-}$, $\Delta^*_{3/2^-}$, $\Delta^{**}_{3/2^+}$. In the quark shell model these states correspond to the configurations up to $2\hbar\omega$ h.o. s^3, s^2p, sp^2, and $sp^2 - s^2 2s(2d)$ with all the possible values of spin $S = 1/2,\ 3/2$, isospin $T = 1/2,\ 3/2$, and Young tableau $[f_X] = [3],\ [21]$. Summation over these states leads to the following expression,

$$\begin{aligned} D_N(k{=}0) \quad = \quad & \frac{b}{256}\frac{1}{2\pi^2}\mathcal{P}\int_0^\infty q^2 dq\, \frac{e^{-\beta^2 q^2} f_0(q)\, m_\sigma}{\omega_\pi(q/2)\,(m_\sigma - 2\,\omega_\pi(q/2))} \left\{ \frac{5}{4}\, \frac{1 + q^2b^2/12}{m_B - m_N + q^2/8m_B + \omega_\pi(q/2)} \right. \\ & - \frac{m_q^2}{\omega_\pi^2(q/2)}\, \frac{q^2b^2}{2} \left[\frac{1}{q^2/8m_N + \omega_\pi(q/2)} + \frac{4}{m_\Delta - m_N + q^2/8m_N + \omega_\pi(q/2)} \right. \\ & \left.\left. + \frac{5}{288}\, \frac{q^2b^2\,(1 + 3q^2b^2/16)}{m_B - m_N + q^2/8m_N + \omega_\pi(q/2)} \right] \right\} , \qquad \beta^2 = \frac{b^2}{12}\left(1 + \frac{3b_\sigma^2}{2b^2}\right) , \end{aligned}$$

where the function f_0 takes into account all the possible time orderings in the triangle diagram [2] (for simplicity the common mass $m_B = 1500$ MeV is used for all the baryons except Δ and N). However, for realistic values of the free parameters $b = 0.5$ fm, $b_\sigma = 0.2$ fm and $g_{\sigma\pi\pi} = 4$ GeV we obtain a relatively small value $g_{\sigma NN} = 0.433$. It shows that the high-momentum behaviour of vertex form factors $N \to B^* + \pi$, $B^* \to N + \pi$ and $\pi + \pi \to \sigma$ plays an important role in deriving a realistic value of the coupling constant $g_{\sigma NN}$. The standard quark shell model with a characteristic (confinement) scale $b \approx$0.5 - 1 fm predicts too soft vertex form factors, and thus some generalization of the model is needed to incorporate a new scale parameter of about 0.2-0.3 fm (the inverse value of the characteristic chiral scale 0.6 - 1 GeV/c). The following modification of a simple Gaussian form: $e^{-\beta^2q^2} \;\to\; \frac{2}{3}\, e^{-\beta^2q^2} + \frac{1}{3}\, e^{-(\beta/Z)^2q^2}$, with $Z \simeq 2$ was used to imitate a power-like behaviour $\sim \left(\frac{\Lambda^2}{q^2+\Lambda^2}\right)$ of the vertices. At $Z = 1.9$ (which corresponds to $\Lambda = 0.9$ GeV/c) a more realistic value $g_{\sigma NN} = 3.26$ has been obtained.

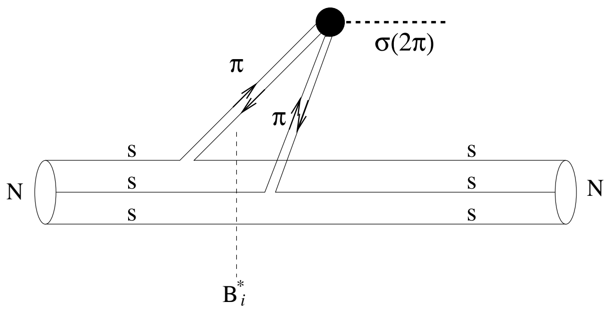

Figure 1: Quark diagram of the $N \to \sigma(\pi\pi) + N$ transition.

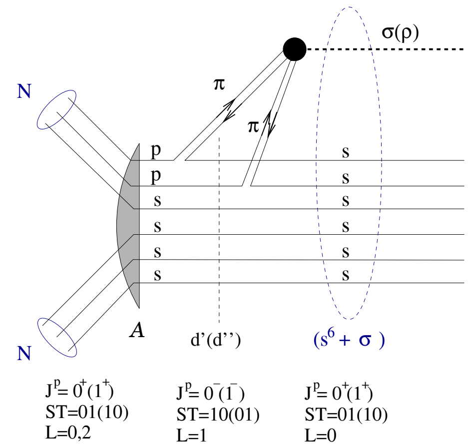

Figure 2: The $N + N \to DB$ transition.

The developed model has been used for the two-nucleon system. A special feature of the above processes in the NN system (see Fig. 2) is that a sum over intermediate dibaryon six-quark states ${}^2B_i^* + \pi$ should be taken into consideration (hand by hand with the sum $\sum_i B_i^* + \pi$ for each nucleon). The quantum numbers of intermediate dibaryons are fixed by the selection rules. In the channel $J^P = 0^+(ST = 01)$ the ${}^2B^*$ has quantum numbers of the so-called d' dibaryon [6] $d' = |s^5p[51]_X L = 1, [321]_{CS} ST = 10, J^P = 0^- >$, while in the "deuteron channel" $J^P = 1^+(ST = 10)$ it has quantum numbers of the d'' dibaryon (a counterpart of the d' for $S \rightleftarrows T$ interchange [2]). The calculated amplitude for the transition $N + N \to {}^2B + \sigma(2\pi)$, where ${}^2B$ is a compact six-quark configuration $s^6[6]_X$ (a "quark core" of a "dressed bag" state $DB = {}^2B + \sigma(2\pi)$), leads to a non-diagonal potential $V_{DB,N+N}$ for two coupled channels (DB and $N+N$). The corresponding coupled-channel model of NN interaction proposed in Ref. [2] on the basis of the above mechanism leads to a very reasonable description of the NN scattering at intermediate energies [2]. The DB admixture in deuteron P_{DB} has been also calculated [2]: $P_{DB} = 3.66\%$. This small value seems to be very important for a high-precision description of the deuteron proprties.

Acknowledgments: The author gratefully acknowledges the contribution to the talk of all the collaborators of the Moscow and Moscow-Tübingen groups: Profs. A. Faessler, V.I. Kukulin, V.G. Neudatchin, N.P. Yudin, and Drs. V.M. Pomerantsev and L.L. Sviridova. The work was supported in part by the Deutsche Forschungsgemeinschaft grant No. Fa-67/20-1 and the Russion Foundation for Basic Research grants No. 01-02-04015 and 00-02-16117.

References

[1] V.G. Neudatchin, I.T. Obukhovsky, and N.P. Yudin, *Relativistic Nuclear Physics and Quantum Chromodynamics*, Proc. XIV Int. Seminar on High Energy Physics Problems (Editors: A.M. Baldin and V.V. Burov), JINR, Dubna (2000), vol. 1, p. 55; I.T. Obukhovsky, V.G. Neudatchin, and N.P. Yudin, contributed paper in this issue, to be published.

[2] V.I. Kukulin, I.T. Obukhovsky, V.N. Pomerantsev, and A. Faessler, Physics of Atomic Nuclei **64**, 1667 (2001).

[3] A. LeYaouanc, Ll. Oliver, O. Pène, and J.-C. Raynal, *Hadron Transitions in the Quark Model.* Gordon and Breach Sci. Publ., N.Y., London, Paris. 1988.

[4] F. Cano, P. Gonzalez, S. Noguera, and B. Desplanques, Nucl. Phys. **A343**, 331 (1996).

[5] B. Brauel, T. Canzler, D. Cords, *et al.*, Z. Phys. C **3**, 101 (1979).

[6] I.T. Obukhovsky, A. Faessler, G. Wagner, and A. Buchmann, Phys. Rev. C **60**, 035207 (1999).

Study of the η-proton interaction via the reaction $pp \to pp\eta$

P. Moskal[a,b], H.-H. Adam[c], A. Budzanowski[d], R. Czyżykiewicz[a], T. Götz[b], D. Grzonka[b], L. Jarczyk[a], A. Khoukaz[c], K. Kilian[b], C. Kolf [b], P. Kowina[b,e], N. Lang[c], T. Lister[c], W. Oelert[b], C. Quentmeier[c], R. Santo[c], G. Schepers[b], T. Sefzick[b], M. Siemaszko[e], J. Smyrski[a], S. Steltenkamp[c], A. Strzałkowski[a], P. Winter[b], M. Wolke[b], P. Wüstner[b], W. Zipper[e]

[a]*Institute of Physics, Jagellonian University, Cracow, Poland*

[b]*IKP & ZEL, Forschungszentrum Jülich, Germany*

[c]*Institut für Kernphysik, Westfälische Wilhelms–Universität, Münster, Germany*

[d]*Institute of Nuclear Physics, Cracow, Poland*

[e]*Institute of Physics, University of Silesia, Katowice, Poland*

(Received: 30 October 2001)

A measurement of the $pp \to pp\eta$ reaction at the excess energy of Q = 15.5 $\pm$ 0.4 MeV has been carried out at the internal beam facility COSY-11 with an integrated luminosity of 811 nb^{-1}. The number of $\sim$24000 identified events permits a precise determination of total ($2.32 \pm 0.05 \pm 0.35\ \mu b$) and differential cross sections. Preliminary investigations show that the angular distribution of the η meson in the center-of-mass system is isotropic. A qualitative analysis of the Dalitz-plot distribution is presented.

1 Introduction

Investigations of the η meson production via the $pp \to pp\eta$ reaction address the question of the strength of the proton-η interaction at low relative momenta of the interacting particles. In the frame of the optical potential model this interaction can be expressed in terms of phase shifts, which in turn are described by the scattering length $a_{\eta N}$ and the effective range of the potential. Usually, the $a_{\eta N}$ is defined as a complex quantity with the imaginary part accounting for the $\eta N \to \pi N$ and $\eta N \to \pi\pi N$ processes. The real part of it is a direct measure of the formation – or non-formation – of an η-nuclear quasi-bound state [1]. At present it is still not known whether the attractive interaction between η meson and nucleons is strong enough to form an η-mesic nucleus or a quasi-bound ηNN state. The values of Re($a_{\eta N}$) range between 0.25 fm and 1.05 fm depending on the analysis method and the studied reaction [2]. According to reference [3], within the present inaccuracy of Re($a_{\eta N}$) the existence of quasi-bound η-mesic light nuclei could be possible. The shape of the energy dependence of the $pd \to {}^3$He$\,\eta$ cross section implies that either the real or imaginary part of the $\eta\,{}^3$He scattering length has to be very large [4], which may be associated with a bound $\eta\,{}^3$He system. Similarly encouraging are results of reference [5], where it is argued that a three-body ηNN resonant state, which may be formed close to the ηd threshold, may evolve into a quasi-bound state for Re($a_{\eta N}$) $\geq$ 0.733 fm. Also the close to threshold enhancement of the total cross section of the $pp \to pp\eta$ reaction [6] was interpreted as being either a Borromean (quasi-bound) – or a resonance ηpp state [7], provided that Re($a_{\eta N}$) $\geq$ 0.7 fm. Contrary, recent calculations performed within a three-body formalism indicate [8] that a formation of a three-body ηNN resonance state is rather not possible, independently of the ηN scattering parameters. Moreover, the authors of reference [9] exclude the possibility of the existence of an ηNN quasi-bound state. However, results of both calculations [8,9], although performed within a three-body formalism, used the assumption of a separability of the two-body ηN and NN interactions, and hence the new quality in the three-body ηNN-interaction is not excluded and deserves experimental investigations.

2 Experimental results

A close to threshold measurement of the $pp \to pp\eta$ reaction allows to study the interaction of the η-meson with the proton. At an excess energy of Q = 15.5 MeV, at which the reported measurement has been performed, the final state particles are in the range of the strong interaction much longer than 10^{-23} s – typical life-time of N* and Δ baryon resonances. Thus their mutual interaction may significantly influence the distributions of their relative momenta.

By means of the COSY-11 detection system [10], using a stochastically cooled proton beam of the cooler synchrotron COSY [11] and a hydrogen cluster target [12], we have performed a high statistics measurement of the $pp \to pp\eta$ reaction at an excess energy of Q = 15.5 MeV. The experiment was based on the four-momentum registration of both outgoing protons, whereas the η meson was identified via the missing mass technique. Figure 1a presents the missing mass spectrum, with the clear signal originating from ∼24000 events of the $pp \to pp\eta$ reaction seen on a flat distribution due to multi-pion production. By means of the simultaneous measurement of elastically scattered protons we were able to monitor not only the luminosity but also the synchrotron beam geometrical dimensions and its position relative to the target [13]. This, and the correction for the mean beam-momentum-changes determined by means of the Schottky-spectrum and the known beam optics, allow us to reproduce exactly the observed missing mass distribution as it is shown by the dashed line in Figure 1a, which is hardly distinguishable from the real data. Figure 1b shows that the full range of the η meson center-of-mass polar scattering angles has been covered by the detection system acceptance. This permitted to determine the angular distribution of the created η meson which, as can be seen in Figure 2a, is completely isotropic within the shown statistical errors. The observed distribution is consistent with the previous measurement performed at an excess energy of Q = 16 MeV at the CELSIUS facility [14]. However, it improves the former statistics by a factor of 80. The determination of the four-momentum vectors for both outgoing protons of each registered event gives the complete information of the ηpp-system allowing for investigations of the ηp and ηpp interactions. Figures 2b and 2c show the Dalitz-plots of the identified $pp\eta$ system corrected for the detection acceptance and the proton-proton interaction. The enhancement from the η-proton interaction at small $m^2_{p\eta}$ is evident. However, one can also easily recognize a difference between Figures 2b and 2c, which originates from various prescriptions of the proton-proton FSI enhancement factors. It is well established that for the close-to-threshold meson production the energy dependence of the total cross section and the distributions of the differential cross section are predominantly determined by the nucleon-nucleon final state interaction [15]. However, when reducing the proton-proton FSI effect to a multiplicative factor, one finds that it depends on the assumed nucleon-nucleon potential and on the produced meson mass [16]. Figures 2b and 2c present the extreme cases in the estimation of the proton-proton FSI effects [17]. Due to these differences a derivation of the ηp or ηpp scattering length from the taken data will require a careful estimation of the model dependence of corrections for the proton-proton FSI.

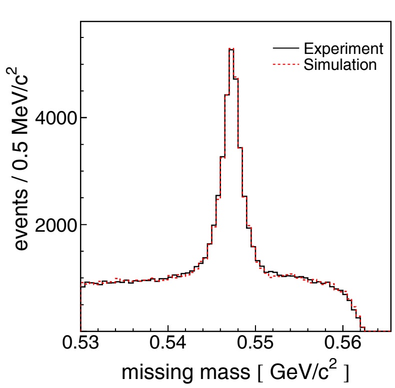

(a)

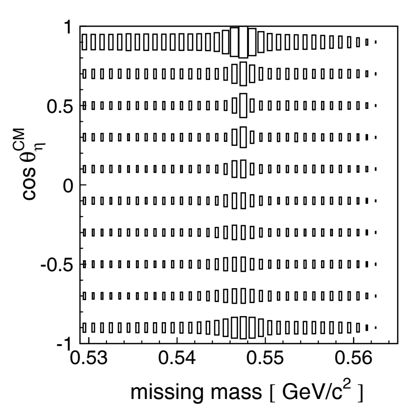

(b)

Figure 1: (a) Missing mass spectrum for the $pp \to ppX$ reaction determined at a beam momentum of 2.0259 GeV/c. The mass resolution amounts to 1 MeV/c^2 (σ). (b) Distribution of the center-of-mass polar angle of the produced system X as a function of the missing mass.

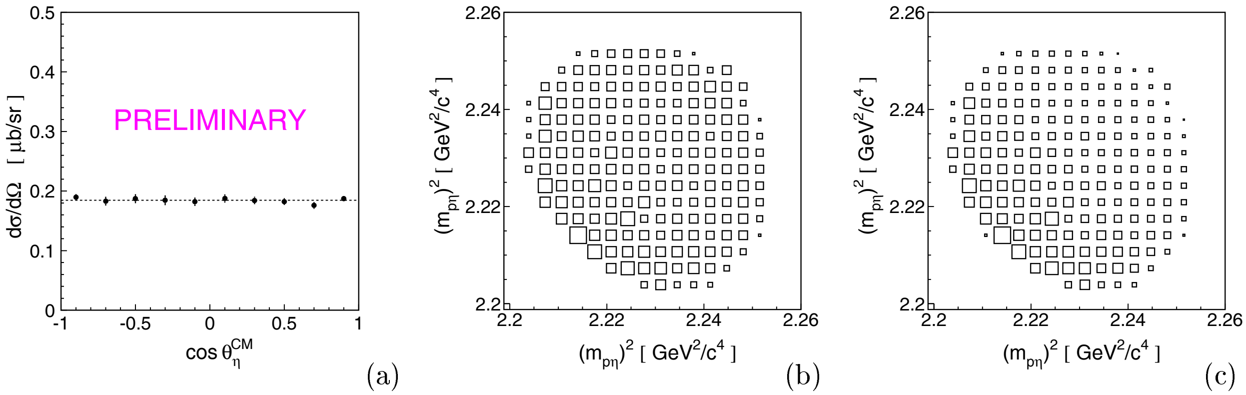

Figure 2: (a) Differential cross section of the $pp \to pp\eta$ reaction as a function of the η meson center-of-mass polar angle. (b) Dalitz-plot distribution corrected for the detection acceptance and the proton-proton FSI. For this plot only events with a mass differing no more than 1 MeV/c^2 from the real η meson mass were taken into account. The proton-proton FSI enhancement factor was calculated as an inverse of the Jost function presented in reference [18]. (c) The same as (b) but the enhancement factor accounting for the proton-proton FSI was calculated as a square of the on-shell proton-proton scattering amplitude derived according to the modified Cini-Fubini-Stanghellini formula including Wong-Noyes Coulomb corrections [17, 19].

Acknowledgments: This work was partly supported by the European Community - Access to Research Infrastructure action of the Improving Human Potential Programme.

References

[1] A. Švarc, S. Ceci, Contribution to N*2000, e-Print Archive: nucl-th/0009024

[2] A. M. Green, S. Wycech, e-Print Archive: nucl-th/0009053.

[3] S. A. Rakityansky *et al*, Phys. Rev. **C 53**, R2043 (1996).

[4] C. Wilkin, Phys. Rev. **C 47**, R938 (1993).

[5] N. V. Shevchenko *et al*, Eur. Phys. J. **A 9** , 143 (2000).

[6] H. Calén *et al*, Phys. Lett. **B 366**, 39 (1996); J. Smyrski *et al*, Phys. Lett. **B 474**, 182 (2000); F. Hibou *et al*, Phys. Lett. **B 438**, 41 (1998); E. Chiavassa *et al*, Phys. Lett. **B 322**, 270 (1994); A. M. Bergdolt *et al*, Phys. Rev. **D 48**, R2969 (1993).

[7] S. Wycech, Acta Phys. Pol. **B 27**, 2981 (1996).

[8] A. Fix, H. Arenhövel, Eur. Phys. J. **A 9**, 119 (2000).

[9] H. Garcilazo, M. T. Peña, Phys. Rev. **C 63**, 021001 (2001).

[10] S. Brauksiepe *et al*, Nucl. Instr.& Meth. **A 376**, 397 (1996).

[11] D. Prasuhn *et al*, Nucl. Instr. & Meth. **A 441**, 167 (2000).

[12] H. Dombrowski *et al*, Nucl. Instr. & Meth. **A 386**, 228 (1997).

[13] P. Moskal *et al*, Nucl. Instr. & Meth **A 466**, 448 (2001).

[14] H. Calén *et al*, Phys. Lett. **B 458**, 190 (1999).

[15] G. Fäldt, C. Wilkin, Phys. Rev. **C 56**, 2067 (1997) and e-Print Archive: nucl-th/0104081; F. Kleefeld, e-Print Archive: nucl-th/0108064; K. Nakayama, e-Print Archive: nucl-th/0108032; A. Sibirtsev, W. Cassing, Eur. Phys. J. **A 2**, 333 (1998); H. Machner, J. Haidenbauer, J. Phys. **G 25**, R231 (1999).

[16] V. Baru *et al*, Phys. Atom. Nucl. **64**, 579 (2001).

[17] P. Moskal *et al*, Phys. Lett. **B 482**, 356 (2000).

[18] J. A. Niskanen, Phys. Lett. **B 456**, 107 (1999).

[19] H. P. Noyes, H. M. Lipinski, Phys. Rev. **C 4**, 995 (1971).

Exclusive measurements of the $pp \to pp\pi^+\pi^-$ reaction

J. Pätzold[1], R. Bilger[1], W. Brodowski[1], H. Calén[2], H. Clement[1], C. Ekström[2], K. Fransson[3], S. Häggström[3], B. Höistad[3], J. Johanson[3], A. Johansson[3], T. Johansson[3], K. Kilian[4], S. Kullander[3], A. Kupść[2], P. Marciniewski[3], A. Mörtsell[3], B. Morosov[5], W. Oelert[4], J. Pätzold[1], R.J.M.Y. Ruber[3], M. Schepkin[6], J. Stepaniak[7], A. Sukhanov[5], P. Sundberg[3], A. Turowiecki[8], G.J. Wagner[1], Z. Wilhelmi[8], J. Zabierowski[9], A. Zernov[5], and J. Zlomanczuk[3]

[1]*Physikalisches Institut, Universität Tübingen, Morgenstelle 14, D-72076 Tübingen, Germany*
[2]*The Svedberg Laboratory, S-751 21 Uppsala, Sweden*
[3]*Department of Radiation Sciences, Uppsala University, S-751 21 Uppsala, Sweden*
[4]*IKP - Forschungszentrum Jülich GmbH, D-52425 Jülich, Germany*
[5]*Joint Institute for Nuclear Research Dubna, 101000 Moscow, Russia*
[6]*Institute for Theoretical and Experimental Physics, 117218 Moscow, Russia*
[7]*Institute for Nuclear Studies, PL-00681 Warsaw, Poland*
[8]*Institute of Experimental Physics, Warsaw University, PL-0061 Warsaw, Poland*
[9]*Institute for Nuclear Studies, PL-90137 Lódz, Poland*

(Received: 8 November 2001)

With the PROMICE/WASA setup at CELSIUS the reaction $pp \to NN\pi\pi$ has been measured in the energy range from 650 to 775 MeV. These data constitute the first exclusive high-statistics measurements on a pure hydrogen target, supplying both differential and integral cross sections. Most of the differential spectra for $pp \to pp\pi^-\pi^+$ are close to phase space predictions (including NN-FSI) identifying the production via $N^*(1440) \to N(\pi\pi)_{I=L=0}$ as the dominant process. However, the measured $M_{\pi^+\pi^-}$-spectrum is strikingly different from phase space simulation pointing to the importance of other processes in this reaction.

1 Introduction

The 2π production in the basic reaction $NN \to NN\pi\pi$ offers a variety of aspects concerning the dynamics of the total system as well as that of its subsystems $\pi\pi, NN, \pi N, \pi\pi N$ and πNN. Apart from small non-resonant chiral contributions the 2π production process is dominated by excitation of one or both participating nucleons. Since a single Δ excitation leads to the emission of only one pion, the lowest order to which the Δ mechanism can contribute is the simultaneous Δ excitation in both nucleons. Since this $\Delta\Delta$ process needs higher energies for its excitation than the excitation of $N^*(1440)$ in one of the participating nucleons, the latter is expected to dominate this reaction at low energies. Hence 2π-production offers the unique possibility to investigate the as of yet rather poorly known Roper resonance in more detail.

Here we report specifically on the $pp \to pp\pi^-\pi^+$ measurement from the 1996 run at $T_p = 750$ MeV with the PROMICE/WASA setup [1] at CELSIUS. This measurement had been carried out to increase substantially the statistics accumulated in 1995 at the same energy, in order to obtain high quality data on differential spectra.

2 Results

Figure 1 shows the energy dependence of the total cross section. Our data have turned out to be an order of magnitude below prior measurements. Those mainly come from inclusive and/or low-statistic measurements. Only the data from [7], which was taken with a spectrometer setup, are in general agreement.

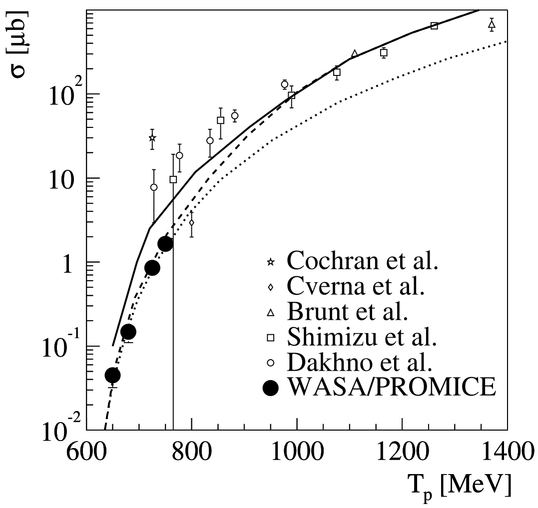

Figure 1: Energy dependence of the total cross section. Results from this work are shown as solid points. The dotted line shows the pure phase space behavior normalized arbitrarily, solid and dashed lines represent theoretical predictions [6] with and without pp FSI, respectively.

In Fig. 2 differential cross section spectra at $T_p = 750\,\mathrm{MeV}$ are shown. The measured spectra (solid points) show significant deviations from phase space distributions (shaded area). To explain the deviations several mechanisms have been introduced in the model calculation. Each mechanism is primarily affecting only one observable.

The proton proton invariant mass system (left upper figure) shows an enhancement towards small invariant masses. This effect can be described by including proton proton final state interaction (pp FSI), shown as dashed line. This effect however does not explain the non-isotropic proton scattering angle distribution (right upper figure). The concave deviation from isotropy observed there is in agreement with heavy meson exchange (σ, ρ) mediating the inelastic pp collision (dotted

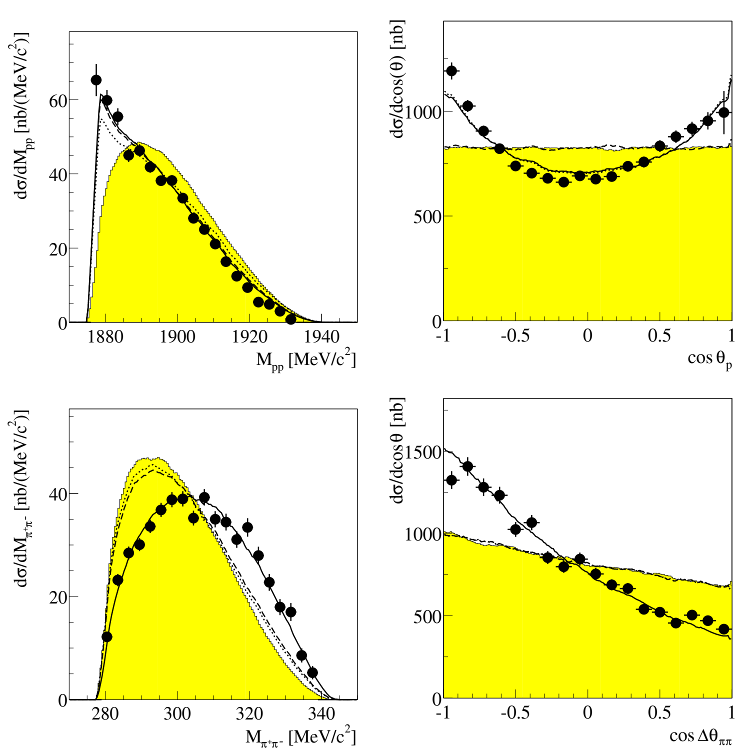

Figure 2: Differential cross sections for invariant mass distribution of M_{pp}, $M_{\pi^+\pi^-}$ (left side) and proton scattering angle θ_p and the opening angle of both pions $\Delta\theta_{\pi\pi}$ (right side). Solid points present the experimental results. The shaded area shows the phase space distribution. The dashed, dotted and solid lines include FSI, FSI & σ-exchange and FSI, σ-exchange & coherent superposition of two $N^*(1440)$ decay channels. (for details see text)

lines). Note, that pion exchange would lead to an convex shape in the angular distribution. The lower figures address the $\pi\pi$ system. The left plot shows the invariant mass spectrum, which is shifted towards higher invariant masses compared to phase space. On the right the opening angle of the two pions in the overall c.m. system is displayed. As has been pointed out in the introduction, the Roper resonance $N^*(1440)$ plays an important role in this reaction. The effects in the $\pi\pi$-system can be described by assuming coherent superposition of N^* decay channel: the direct decay into the sigma channel ($N^* \to p(\pi\pi)_{l=I=0}$) and the decay via the Δ-resonance ($N^* \to \Delta\pi \to p(\pi\pi)_{l=I=0}$). A 20% contribution in amplitude of the latter gives the best description of the data.

3 Outlook

The CELSIUS/WASA detector in Uppsala has been upgraded over the last years [12]. This upgrade was done for measuring rare decays of light neural mesons (π^0, η). In future it will also be used for exclusive measurements of two pion production. The angular coverage of almost 4π steradians and acceptance for neural particles (γs as well as neutrons) opens the opportunity for exclusively measuring the reaction channels $pp \to pp\pi^0\pi^0$, $pp \to pn\pi^+\pi^0$ and $pp \to nn\pi^+\pi^+$. From these results one will expect more information about the details of the reaction mechanism in two pion production and the involved resonances.

Acknowledgments: We are grateful to L. Alvarez-Ruso for intensive fruitful discussions. We acknowledge the continued help of the TSL/ISV personnel and the support by DFG (Graduiertenkolleg), DAAD and BMBF (06 TU 886, 06 TU 987).

References

[1] H. Calén *et al.*, Nucl. Instr. Meth. **A379** (1996) 57.

[2] W. Brodowski *et al.*, Z. Phys. **A355** (1996) 5.

[3] R. Bilger *et al.*, Phys. Rev. Lett. **71** (1993) 42, **72**. (1994) 2972, and **79** (1997) 3849; Phys. Lett. **B420** (1998) 37, **B428** (1998) 18 and **B443** (1998) 77; Phys. Rev. **C58** (1998) 1576.

[4] W. Brodowski, PhD thesis, Univ. Tübingen, July 2000.

[5] F. Belleman *et al.*, Phys. Rev. **C60** (1999) 061002.

[6] L. Alvarez-Ruso, E. Oset, E. Hernández, Nucl. Phys. **A633** (1998) 519, and private communication.

[7] F.H. Cverna *et al.*, Phys. Rev. **C23**, 1698 (1981).

[8] D.R.F. Cochran *et al.* Phys. Rev. **D6**, 3085 (1972).

[9] F. Shimizu *et al.*, Nucl. Phys. **A386**, 571 (1982).

[10] L.G. Dakhno *et al.*, Sov. J. Nucl. Phys. **37**, 540 (1983).

[11] D. C. Brunt *et al.*, Phys. Rev. **187**, 1856 (1969).

[12] H. Calén, these proceedings.

Strangeness production at the time-of-flight spectrometer COSY-TOF

S. Wirth, for the COSY-TOF Collaboration

Physikalisches Institut, Universität Erlangen-Nürnberg, 91058 Erlangen, Germany

(Received: 25 October 2001)

The associated strangeness production in elementary proton induced reactions is studied exclusively at the external COSY beam using the time-of-flight spectrometer TOF. The complete measurement of all primary and decay particle tracks allows the extraction of total and differential cross sections as well as Dalitz plots and invariant mass spectra of the subsystems for the channels $pp \to K^+ \Lambda p$, $K^0 \Sigma^+ p$, $K^+ \Sigma^0 p$ and $K^+ \Sigma^+ n$ from the reaction thresholds up to the COSY-limit of about 3.5 GeV/c.

1 Introduction

The interest in the investigation of the associated strangeness production in elementary reactions like $pp \to KYN$ close to threshold is the insight in the dynamics of the $\bar{s}s$ production. The results should also provide information on the structure of the involved baryons, in the favorable case especially on a possible strangeness content of the nucleon.

Meson exchange models appear to be the most appropriate way to describe strangeness production near the threshold. Here, the questions especially concern the contribution of the various strange and non strange mesons, including the influence of N^* resonances in the production mechanism and the role of the hyperon-nucleon final-state interaction which is known to be of special importance close to threshold.

To come to more conclusive results more precise data are needed especially in the threshold region including different reaction channels. The measurements should concentrate on exclusive data covering the full phase space. Moreover, spin observables are important, in particular the polarization of the hyperon, which can be extracted via the self-analysing weak decay.

Apart from the $\bar{s}s$ creation process itself there are more special topics related to the strangeness production close to threshold. An interesting example is the question of the existence of an exotic $qqqq\bar{q}$ resonance which is proposed in the soliton model and which should show up in the KN subsystem in the $pp \to K\Sigma^+ N$ reactions.

Moreover, the data of the strangeness production in elementary nucleon-nucleon reactions are very useful as an input to explain strangeness production in nucleon-nucleus and nucleus-nucleus systems especially including medium effects.

2 Experiment

The external experiment COSY-TOF is a wide angle, non magnetic system with various start and stop detector components for time-of-flight measurement. The modular apparatus combines high efficiency and acceptance with an energy and momentum resolution of a few percent. The whole detector system together with a tiny liquid hydrogen target is installed inside a vacuum vessel. This ensures a rather precise definition of the interaction point and a strongly reduced contamination from background reactions in air. Figure 1 shows the standard version of the TOF setup with a length of about 3.4 meters.

The outer detector, serving as stop for the time-of-flight consists of several plastic scintillator hodoscopes: basically a huge cylindrical segmented barrel and a circular endcap in the forward direction. The endcap is made up by two separate scintillator hodoscopes, a central one ("quirl") with a diameter of one meter and a ring-like one with an outer diameter of three meters. Both consist of three segmented layers, one of wedge like parts and two of left and right hand spirally formed

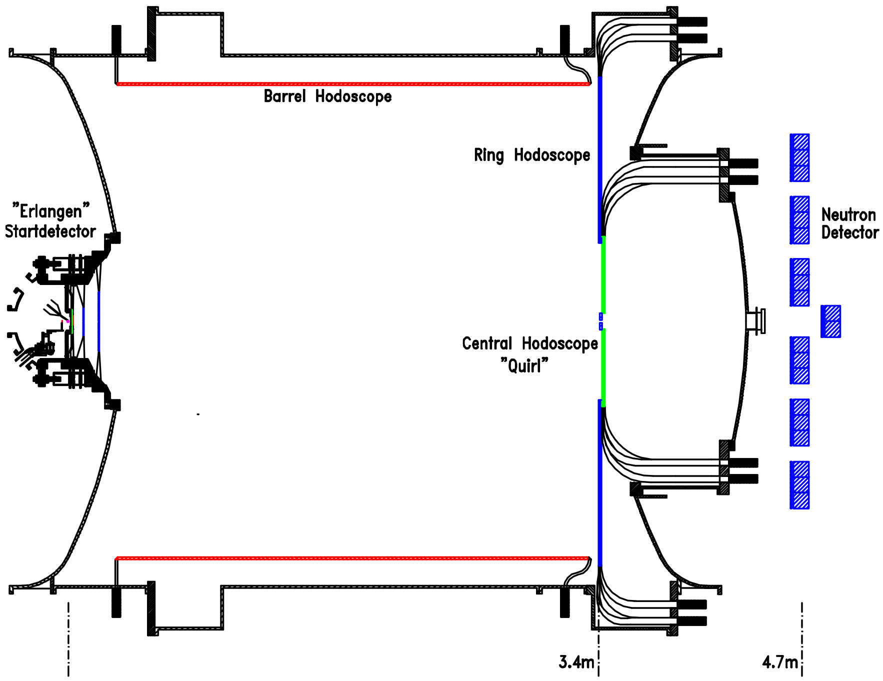

Figure 1: Setup 2000 of the TOF spectrometer

elements. Furthermore, a neutron detector consisting of a large area scintillator wall is installed behind the vessel to measure primary and decay neutrons which appear in the Σ^+ channels.

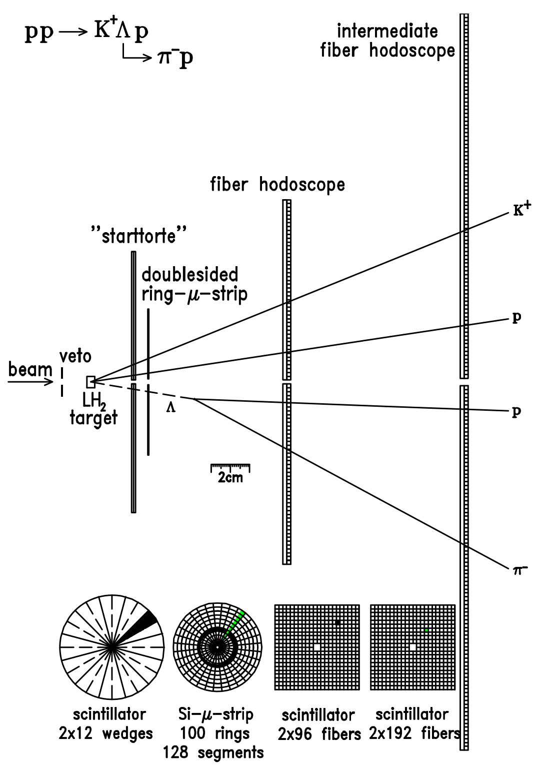

Figure 2: Scheme of the Start detector

The inner detector system as shown in Figure 2 together with a typical $K^+\Lambda p$ event is optimized for strangeness production measurements and consists of the "starttorte", made of two thin segmented layers of plastic scintillators providing the start timing, a double-sided silicon microstrip detector with a highly granulated ring and sector structure, respectively, and two hodoscopes made of scintillating fibers. This system with small beam holes between 2 and 4 mm diameter covers the full angular range of the reaction products and allows the complete reconstruction of the $pp \to KYN$ events including the precise measurement of the delayed decays of the hyperons in $\Lambda \to \pi^- p$, $\Sigma^+ \to \pi^0 p$ or $\pi^+ n$ as well as the K^0-decay into two charged pions, which give unique signatures for the reactions of interest.

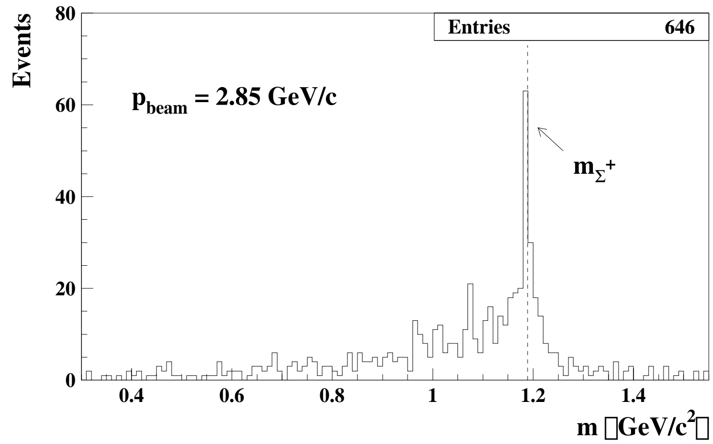

Figure 3: Missing mass of reconstructed $K^0\Sigma^+p$-events

3 Results

In the meantime the $pp \rightarrow K^+\Lambda p$ reaction has been investigated at several beam momenta between 2.5 GeV/c and 3.2 GeV/c. From the Dalitz plots of the data there is especially clear evidence on the $p\Lambda$-final state interaction and also indication for the influence of N^*-resonances coupling to the $K\Lambda$-system. Furthermore, the Λ polarization can be extracted from the angular distribution of its decay products [1]. For the data at 2.75 and 2.85 GeV/c it shows a trend to negative values with increasing transverse Λ momentum.

The reaction $pp \rightarrow K^+\Sigma^0 p$ can be separated from the Λ production by using the additional energy loss information of the various detector systems. This strongly reduces the dominating Λ missing mass peak to a small background in the Σ^0 region allowing a sufficient separation of the Σ^0 events.

As mentioned above, besides the production of the neutral Λ and Σ^0 hyperons the TOF detector for the first time also allows the investigation of the Σ^+ production in the channels $pp \rightarrow K^0\Sigma^+p$ and $pp \rightarrow K^+\Sigma^+n$ in the threshold region. The identification of events of the type $K^0\Sigma^+p$ is done by observing both the delayed decays of the Σ^+ and the K^0. As shown in Figure 3 about 200 events of this type could be extracted for the beam momentum at 2.85 GeV/c, allowing the evaluation of the total cross section of this reaction channel; the preliminary value is 5.9 $\pm$ 1.0 μb.

For the $K^+\Sigma^+n$-channel first events could be reconstructed. Here, in addition to the Σ^+ decay, the primary neutron has to be measured with the scintillator wall behind the TOF detector.

In summary, with the upgraded TOF-detector completed by ring and barrel sections in 2000, a precision study of the hyperon production was performed at beam momenta of 2.95 and 3.2 GeV/c. From this about fifty thousand fully reconstructed Λ events and a few thousand Σ^+ events are expected. Moreover, the hyperon production in neutron proton scattering was successfully tested using a deuterium target. The next step for measurements at COSY-TOF will be the use of a polarized beam.

Acknowledgments: We gratefully acknowledge financial support by the Forschungszentrum Jülich and the German BMBF.

References

[1] TOF-collaboration, R. Bilger *et al.*, Phys. Lett. **B420**, 217 (1998).

Phase-shift analyses of elastic pp scattering at $T_L = 1 \sim 11$ GeV

J. Nagata[a], H. Yoshino[b], and M. Matsuda[c]

[a]*Kyushu International University, Kitakyushu 805-8512, Japan*
[b]*Hiroshima International University, Kurose 724-0695, Japan*
[c]*Hiroshima University, Higashi-Hiroshima 739-8521, Japan*

(Received: 31 October 2001)

The phase-shift solutions in the single-energy analysis of pp scattering in the wide energy region : T_L = 1~11 GeV are given, where the analyses at T_L = 1~2.4 GeV were carried out using the updated database.

A series of polarized-beam experiments of elastic pp scattering has been performed in the incident energy region $T_L = 0.5 \sim 11$ GeV since the late 1970's. Recently, COSY [1,2] and SATURNE II [3] provided a rich amount of data on $d\sigma/d\Omega$, A_y, the spin-correlation (A_{ij}), the spin-transfer (K_{ij}) and even the triple-spin correlation observables (H_{ijk}) in this energy region. In particular, COSY precicely measured A_y at $T_L = 0.437 \sim 2.493$ GeV [2].

We have developed computer-program of the phase-shift analysis (PSA) of elastic NN (pp and np) scattering, which can be used even in multi-GeV region. Both of the S-matrix representations

Table 1: The observables and the corresponding numbers of experimental data used in the single-energy phase-shfit analyses at each energy.

T_L(MeV)	1095	1295	1596	1796	2096	2396
Forward Obs.$^{a)}$	7	7	7	7	7	7
$d\sigma/dt$	98	50	48	35(*7)	37(*8)	83(*8)
P	168	65	51	181(*7)	119(*7)	183(*6)
D_{NN}	14	13	18	12	25	3
D_{LS}	14	16	17	16	19	7
A_{NN}	63	35	36	40	86	63
A_{LL}	61	60	52	55	81	32
A_{SL}	31	43	38	32	50	27
K_{NN}	31	8	9	13	20	8
K_{LS}	7	7	8	8	9	4
H_{NLS}						8
$P+\delta A_{SL}$	22					
$K_{LS}+\alpha K_{SS}+\beta K_{LL}$	7	8	8	4		
$H_{LLN}+\beta K_{LL}$	7	7	7	10		4
$H_{NLS}+\alpha K_{SS}$	6	7	9	8		4
$H_{LNS}+\alpha H_{SNS}+\beta K_{LL}$	6	8	9	6	9	
$K_{NN}+\alpha H_{SLN}+\beta K_{SL}+\gamma H_{NLL}$	6	8	9	10	8	4
Total	499	342	378	477	492	431
No. of free parameters	41	41	41	50	53	53
χ^2	868	388	432	889	782	673

$^{a)}\sigma_t$, σ_r, $\Delta\sigma_T$, $\Delta\sigma_L$, α, ReF_2, ReF_3

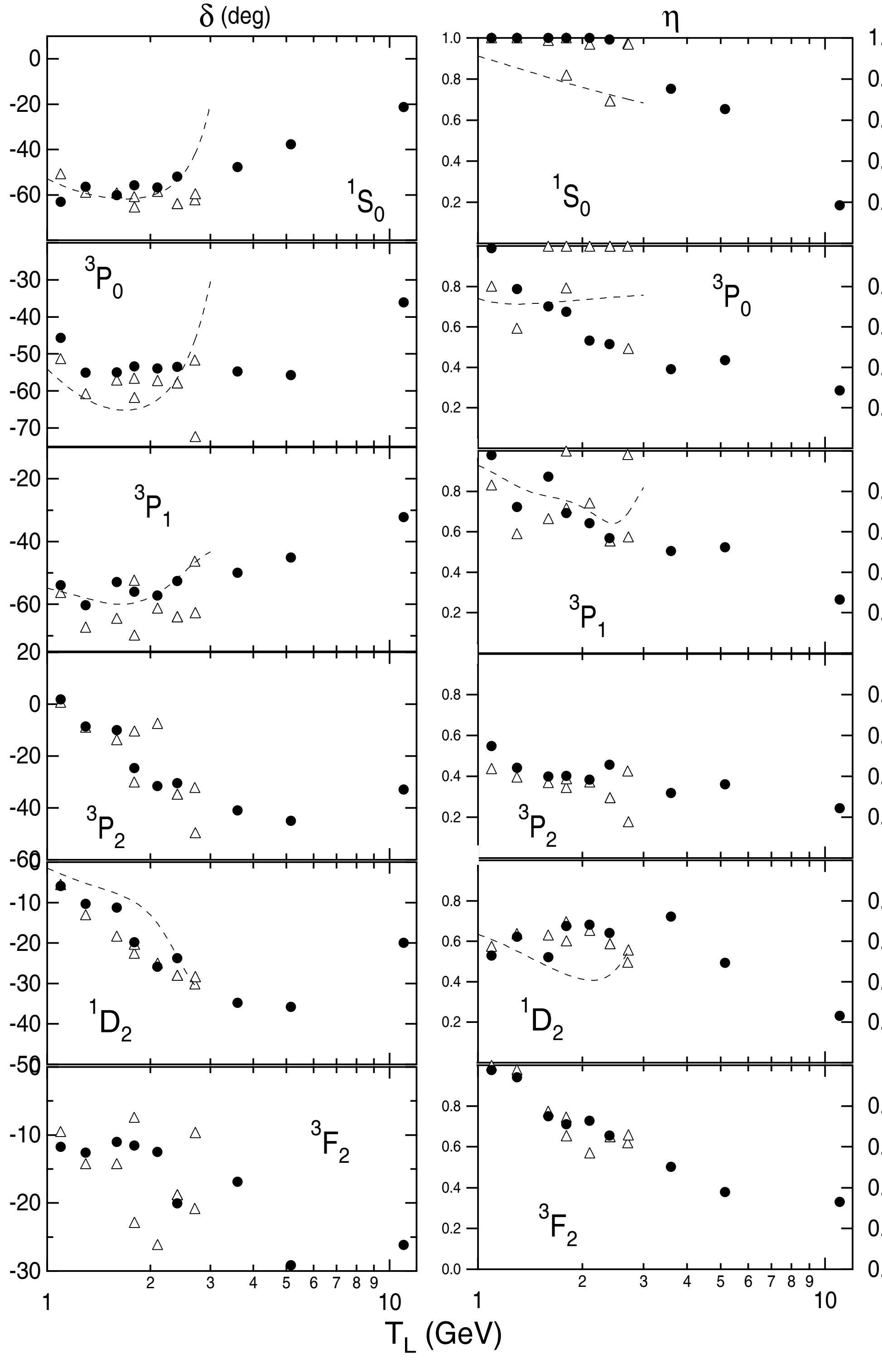

Figure 1: The present solutions for the phase shifts (δ) in degrees and the reflection parameters (η) vs T_L in GeV for comparison with those obtained by other groups. Here, black circles are our solutions, broken lines GWU [9] and triangles Saclay [10] groups, respectively.

defined by the VPI group (VPI-rep.) [4] and by Matsuda and Watari (MW-rep.) [5] can be used to search for the phase-shift solutions in this program. In this report, we present our most recent solutions of the single-energy PSA of elastic *pp* scattering at $T_L = 1 \sim 2.4$ GeV adding the COSY-A_y and SATURNE II data to our database. The numbers and kinds of the experimental data used in the present analyses are given in Table 1, where asterisks(*) represent the pseudo data which are obtained by Cubic-Spline interpolation method [6]. In Figure 1, the present solutions at 1$\sim$2.4 GeV and our previous higher-energy solutions [7,8] are shown together with those given by the GWU [9] and Saclay [10] groups for comparison. In some partial waves, differences among solutions of ours, GWU and Saclay groups are found. The absolute values of the phase shifts start decreasing around at 2 GeV as the incident energy increasing.

A shrinkage of the spin-orbit interaction of elastic *pp* scattering beyond 2 GeV was suggested by Matsuda *et al.* [7] in terms of the PSA of elastic *pp* Scattering at $T_L = 5$ and 11 GeV. They estimated the threshold radius for this dynamical shrinkage as about 0.5 fm, which almost agrees with the bag-radius predicted by the MIT bag model. In order to discuss the shrinkage, the determination of the scattering amplitudes at intermediate energies is obviously important.

Future polarized-spin experiments for spin-correlation parameters planned in Jülich (COSY) will contribute to more detail discussion about the difference of solutions among several groups.

References

[1] D. Albers *et al.*, Phys. Rev. Lett. **78**, 1652 (1997).

[2] M. Altmeier *et al.*, Phys. Rev. Lett. **85**, 1819 (2000).

[3] J. Ball *et al.*, CTU reports (Prague) 4 (2000); CTU reports (Prague) 4 (2000) - corrections; F. Lehar, Private communication, December 2000.

[4] R. A. Arndt and L. D. Roper, Phys. Rev. **D25**, 2011 (1982).

[5] M. Matsuda and W. Watari, Lett. Nuovo Cimento, **6**, 23 (1973).

[6] J. Nagata, M. Matsuda, N. Hiroshige and T. Ueda, Phys. Rev. **C45**, 1432 (1992).

[7] M. Matsuda, J. Nagata, H. Yoshino, K. Harada, S. Ohara, Prog. Theor. Phys. **93**, 1059 (1995).

[8] H. Yoshino, V. Limkaisang, J. Nagata, Y. Yoshino, and M. Matsuda, in *16th International Conference on Few-Body Problems in Physics*, Taipei, 2000, Book of Abstracts, edited by C.-Y Cheung and S.N. Yang, p. 149.

[9] R. A. Arndt, I. I. Strakovsky, and R. L. Workman, Phys. Rev. **C62**, 034005(2000)

[10] J. Bystricky, C. Lechanoine-Leluc, and F. Lehar, Eur. Phys. J. **C4**, 607 (1998).

Threshold $pp \to pp\pi^0$ up to one-loop order in HBχPT

S. Ando[a], T.-S. Park[a], and D.-P. Min[b]

[a]*Department of Physics and Astronomy, University of South Carolina, Columbia, SC 29208, U.S.A.*
[b]*Department of Physics and Center for Theoretical Physics, Seoul National University, Seoul 151-742, South Korea*

(Received: 31 October 2001)

The total cross section for the near-threshold $pp \to pp\pi^0$ reaction is estimated within the framework of heavy-baryon chiral perturbation theory up to next-to-next-to-leading order (*i.e.,* one-loop order), employing the counting rule *à la* Weinberg. We find that the calculated cross section is close to the experimental value and that its cutoff dependence is mild.

1 Introduction

An early estimate of the near-threshold $pp \to pp\pi^0$ reaction was made in 1966 by Koltun and Reitan [1]. These authors calculated the amplitude in DWBA including only long-range operators, *i.e.,* one-body operators and one-pion exchange operators. It was only recently that this theoretical prediction was tested experimentally. Meyer *et al.* [2] in 1990 made a very precise measurement of the total cross section and reported that the experimental value is ~5 times larger than the theoretical value of Koltun and Reitan. This discrepancy has motivated searches for a possible mechanism that increases the cross section. Notably, the heavy-meson (σ, ω, *etc.*) exchange effects [3] and the off-shell enhancement of the πN scattering amplitude [4] were considered as possible enhancement mechanisms. Although these solutions are phenomenologically successful, they rely on models. Meanwhile, there has been growing interest in describing physics of few-nucleon systems from the first principle based on QCD. Heavy-baryon chiral perturbation theory (HBχPT) is a low-energy effective theory of QCD, which is a systematic expansion scheme in powers of Q/Λ_χ, where Q denotes a typical momentum scale or the pion mass m_π, and Λ_χ is the chiral scale $\Lambda_\chi \sim$ 1 GeV. This approach has been extensively applied to one-nucleon processes as well as multi-meson systems, see, *e.g.*, [5]. To extend HBχPT to nuclear systems, Weinberg suggested to separate out nucleon-irreducible diagrams. After constructing the potential and transition operator from the effective Lagrangian, the transition matrix element is obtained in the framework of multiple-scattering theory.

A delicate point in applying HBχPT to $NN \to NN\pi$ is that the typical momentum scale involved is larger than that of an ordinary low energy process; *i.e.,* $Q \sim \sqrt{m_\pi m_N} \gg m_\pi$, where m_N is the nucleon mass. Since $Q/\Lambda_\chi \sim 0.4$, one expects a slow convergence of the chiral series here. Furthermore, the significant cancellation between the leading and sub-leading contributions [7] renders it particularly important to make a systematic evaluation of higher order contributions. We will report here the results of a HBχPT calculation [8] up to one-loop order. We adopt the so-called hybrid approach and the fixed kinematics approximation. Thus the initial and final two-nucleon wavefunctions are calculated using a phenomenological potential and the energy transfer in the pion-production operator is determined by the threshold kinematics.

2 S-wave pion production operator up to one-loop order

The effective Lagrangian is expanded as $\mathcal{L} = \sum \mathcal{L}_{\bar\nu} = \mathcal{L}_0 + \mathcal{L}_1 + \mathcal{L}_2 + \cdots$, where the *chiral index* $\bar\nu$ is given by $\bar\nu = d + n/2 - 2$, with n being the number of nucleons and d the number of derivatives and/or powers of m_π involved in the vertex. $\mathcal{L}_0$, $\mathcal{L}_1$, and $\mathcal{L}_2$ are the leading order (LO), next-

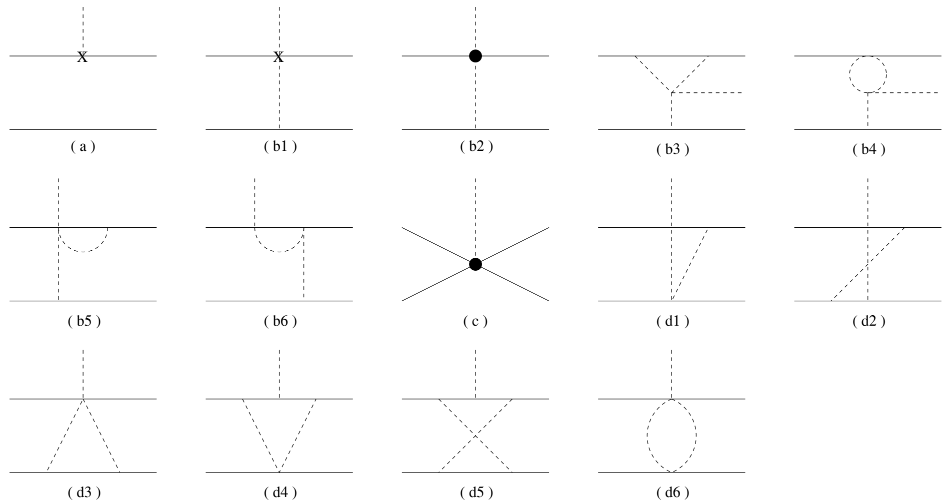

Figure 1: Diagrams for the pion production operator up to one-loop order.

to-leading order (NLO) and next-to-next-to-leading order (NNLO) Lagrangian, respectively, and their explicit expressions are given in [8]. Note that our Lagrangian has pion and nucleon degrees of freedom only; the effect of heavier degrees of freedom, such as the delta isobar, is incorporated in the *low energy constants* (LECs) which are determined by fitting experimental data. The LECs of NLO have been fixed by Bernard *et al.* [9] using πN scattering data. The LECs of NNLO are determined by using resonance saturation with the sigma- and omega-meson exchange.

Weinberg's counting rule [6] dictates that a Feynman diagram with $\nu = 2(1-C) + 2L + \sum_i \bar{\nu}_i$ is of the order of $(Q/\Lambda_\chi)^\nu$, where C (L) is the number of separate pieces (loops). The $\bar{\nu}_i$ denotes the chiral order $\bar{\nu}$ of the ith vertex, and i runs over all the vertices. The Feynman graphs relevant to the process are shown in Fig. 1, where a vertex with $\bar{\nu} = 1$ is marked by an "X", while a vertex with $\bar{\nu} = 2$ by a filled circle.

A remark about the nucleon propagator is in order here. Since the nucleon kinetic energy term, $\vec{p}^2/(2m_N)$, is of the order of m_π (because of $\vec{p}^2 \sim m_\pi m_N$), one may think that it should be included in the leading order nucleon propagator, $1/(p^0 + i\epsilon)$. This is, however, not the case for irreducible loops. The energy component of the loop momentum p^0 picks up pole of the pion propagator, which has the large momentum scale $Q \sim \sqrt{m_\pi m_N}$. As a result, $p^0 \ll \vec{p}^2/(2m_N)$, and thus the kinetic energy term can be treated perturbatively.

3 Numerical results and discussion

In Fig. 2 we plot our results for the total cross section as a function of $\eta = |\vec{q}|_{max}/m_\pi$, where $\vec{q}_{max}$ is the maximum momentum of the out-going pion; we have used the Reid soft-core (RSC) and Hamada-Johnston (HJ) potentials to generate the two-nucleon wavefunctions. Our theoretical predictions with loop corrections included are close to the experimental data. This clearly points out the importance of the one-loop contribution. We note that, since the HJ potential has a hard-core (~ 0.5 fm), the contributions of the zero-range counter term are identically zero with HJ. For the RSC potential, on the other hand, the counter-term contributions do not vanish. The short-range effect may be investigated by modifying the zero-range term and the two-body (2B) operators by introducing a cutoff parameter r_c: $\delta(r) \to \delta(r - r_c)$, $\quad \mathcal{O}_{2B}(r) \to \theta(r - r_c)\mathcal{O}_{2B}(r)$. The corresponding results with the RSC potential are given in Fig. 3. As can be seen in Fig. 3, The results exhibit visible but moderate sensitivity to r_c.

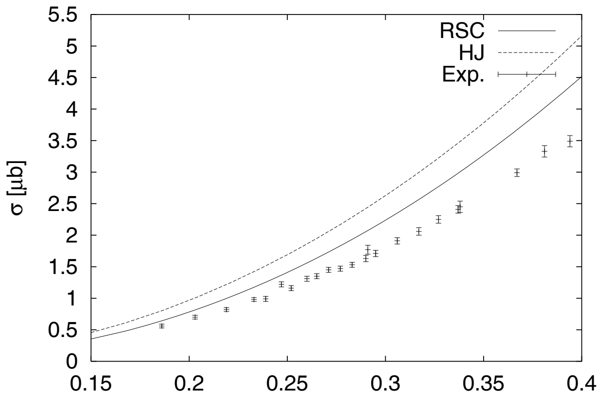

Figure 2: Total cross section for the Reid soft-core (RSC) and Hamada-Johnston (HJ) potential.

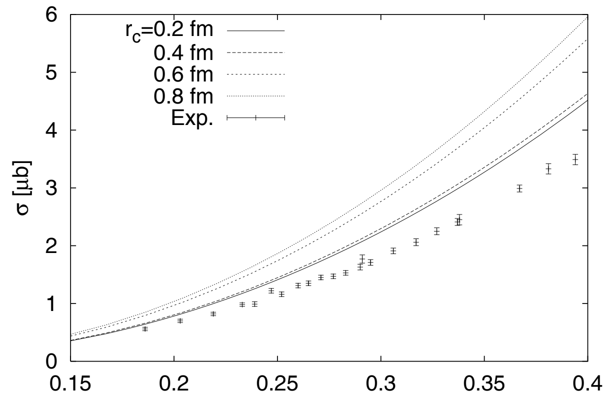

Figure 3: Total cross section for various values of the cutoff r_c with the RSC potential.

A serious question here is the convergence of the perturbation series. One may get some idea about this issue by looking at the breakdown of the transition amplitude into the individual contributions. We give the numbers obtained for the RSC potential and at $|\vec{q}|_{max} = 0.1 m_\pi$; for convenience, we normalize these numbers by the one-body (1B) amplitude corresponding to diagram (a) in Fig. 1. The tree-level 2B (b) diagram gives -0.8, leading to in a substantial cancellation between (a) and (b). The one-loop order 2B diagrams (b2-d6) give $(-1)+(-1.2)=(-2.2)$, where the first (second) term represents the contribution from the *one-particle irreducible* one-pion-exchange (two-pion-exchange) diagrams. Summing up all the contributions leads to -2.0 in units of the 1B amplitude (a). Thus there is no sign of convergence to the order considered.

In summary, we have quantitatively confirmed that the contribution of the one-loop order is quite important. We have also found that there is no strong dependence on the short range interaction. However, the apparently poor HBχPT convergence may indicate that significant contributions from higher-order operators may still be missing in our scheme. Clearly, more work is required including studies of next order terms and the verification of the approximations involved.

Acknowledgments: We are grateful to M. Rho, K. Kubodera, F. Myhrer, T. Sato, B.-Y. Park, and V. Dmitrašinović for useful comments and discussions. This work is supported by National Science Foundation, Grant PHY-9900756 and INT-9730847.

References

[1] D.S. Koltun and A. Reitan, Phys. Rev. **141**, 1413 (1966).

[2] H.O. Meyer *et al.*, Phys. Rev. Lett. **65**, 2846 (1990); Nucl . Phys. **A 539**, 633 (1992).

[3] T.-S. Lee and D.O. Riska, Phys. Rev. Lett. **70**, 2237 (1993); D.O. Riska, talk in this conference.

[4] E. Hernández and E. Oset, Phys. Lett. **B 350**, 158 (1995).

[5] U.-G. Meißner, talk in this conference, `hep-ph/0108133`.

[6] S. Weinberg, Phys. Lett. **B 251**, 288 (1990); Nucl. Phys. **B 363**, 3 (1991); Phys. Lett. **B 295** 114 (1992).

[7] B.-Y. Park, F. Myhrer, J.R. Morones, T. Meissner, and K. Kubodera, Phys. Rev. **C 53**, 1519 (1996); T.D. Cohen, J.L. Friar, G.A. Miller, and U. van Kolck, Phys. Rev. **C 53**, 2661 (1996); T. Sato, T.-S.H. Lee, F. Myhrer, and K. Kubodera, Phys. Rev. **C 56**, 1246 (1997); E. Gedalin, A. Moalem, and L. Razdolskaya, Phys. Rev. **C 60**, 031001 (1999); V. Bernard, N. Kaiser, and U.-G. Meißner, Eur. Phys. J. **A4**, 259 (1999); V. Dmitrašinović, K. Kubodera, F. Myhrer, and T. Sato, Phys. Lett. **B 465**, 43 (1999).

[8] S. Ando, T.-S. Park, and D.-P. Min, Phys. Lett. **B 509**, 253 (2001).

[9] V. Bernard, N. Kaiser, and U.-G. Meißner, Int. J. Mod. Phys. **E 4**, 193 (1995).

Consistency of a large πN sigma term

M.G. Olsson[a] and W.B. Kaufmann[b]

[a]*Department of Physics, University of Wisconsin, Madison, WI 53706, U.S.A.*
[b]*Department of Physics, Arizona State University, Tempe, AZ 85287, U.S.A.*

(Received: 31 October 2001)

We show in several transparent ways why the πN sigma term must be in the 80 to 90 MeV range. Our method is based upon a fixed $t = 2\mu^2$ dispersion sum rule for $\sigma(2\mu^2)$.

1 Introduction

An enduring puzzle in chiral physics is why the πN sigma term is much larger than the "theoretical value" of 25 MeV. More recent experimental data now indicate that the historic value of 55–60 MeV [1] seems to have risen to the 80 to 90 MeV range. This has been a surprise to many and in this talk four straightforward methods are presented showing how this increase has come about. Our methods are based on two simple sum rules which tie the value of the σ-term to scattering in the threshold region [2, 3].

In Figure 1 we depict the low energy πN scattering region. As is well known, the quantity

$$\overline{D}(2\mu^2) \equiv A^{(+)}(\nu = 0,\, t = 2\mu^2) - g^2/M \tag{1}$$

is closely related to $\sigma(2\mu^2)$, the sigma term at $t = 2\mu^2$, by the "on-shell theorem" [4]

$$\sigma(2\mu^2) \simeq F_\pi^2 \overline{D}(2\mu^2) \tag{2}$$

up to a small correction term, probably less than 1 MeV. A dispersion relation for $D^{(+)}(\nu = 0,\, t = 2\mu^2)$ and subtracted at the $t = 2\mu^2$ absorptive threshold $\omega = \mu$ is

$$\overline{D}(2\mu^2) = D^{(+)}(\nu = \nu_T,\, y = 2\mu^2) - I_0 \ , \tag{3}$$

$$I_0 = \frac{2\mu^3(1+r)^2}{\pi} \int_0^\infty \frac{dk(\omega+\mu)}{\omega(\omega+\mu r)(\omega+\mu+2\mu r)} \left[\frac{\mathrm{Im}\, D^{(+)}(\omega, 2\mu^2)}{k} - \lambda_2 \right] \ , \tag{4}$$

where $r = \mu/2M \simeq 0.0744$ and $\nu_T = \mu(1 + r)$.

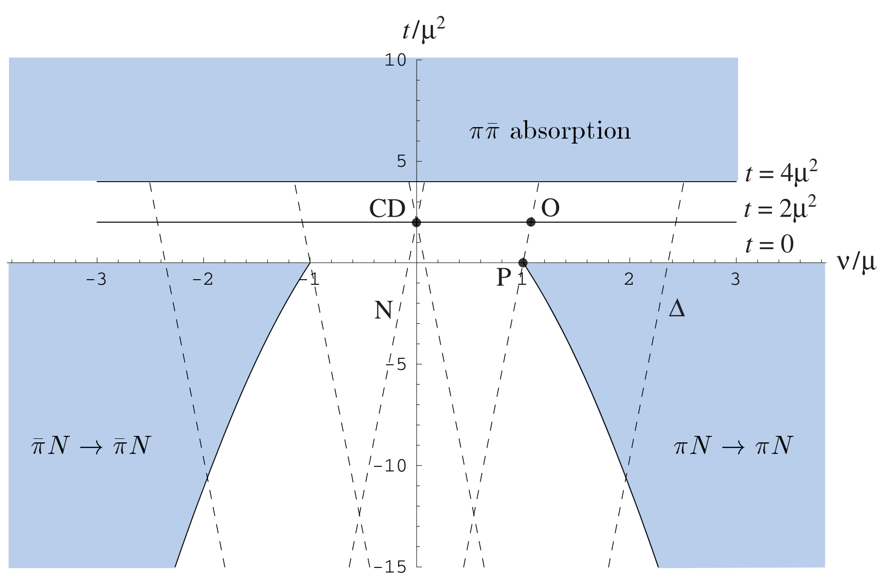

Figure 1: Kinematic region for low energy πN scattering.

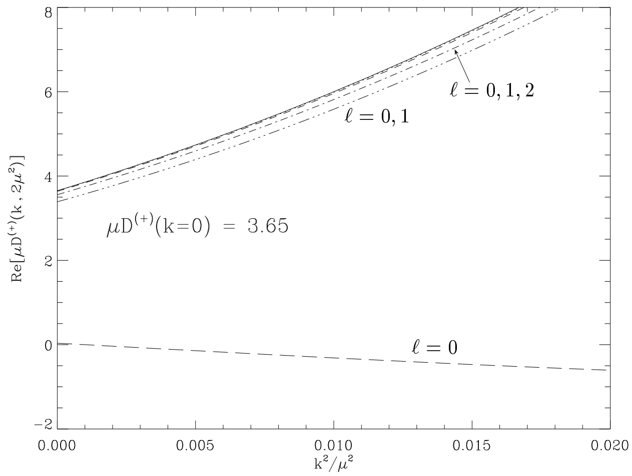

Figure 2: The SM01 prediction for $\mathrm{Re}\, D^{(+)}(k, 2\mu)$ with cumulative partial waves shown. The intercept appears in the sum rules.

2 Evaluation of sum rule #1

First we use the GWU SM01 shift analysis [5] to show in Fig. 2 how $D^{(+)}(\omega^2,\, t = 2\mu^2)$ varies near threshold. The threshold value of

$$D^{(+)}(\nu_T, 2\mu^2) = 3.65 \pm 0.05 \tag{5}$$

is extracted. We show cumulative partial wave contributions illustrating the dominance of p-waves but with a small but significant d and f wave parts. The continuum contribution I_0 is dominated by the (3,3) resonance and is (from SM01)

$$I_0 = 2.25 \pm 0.1\,, \tag{6}$$

giving

$$\sigma_1(2\mu^2) = 81 \pm 8 \text{ MeV}\,. \tag{7}$$

Alternatively, the threshold $D^{(+)}(\nu_T, 2\mu^2)$ amplitude can be evaluated in an "orthognal" way using the threshold data at ($T_\pi < 100$ MeV) alone [6] as discussed earlier [2] to obtain

$$D^{(+)}(\nu_T, 2\mu^2) = 3.69 \pm 0.10\,. \tag{8}$$

Here we supplement the s and p wave scattering lengths of Ref. [6] with the SM01 d and f waves. The resulting sigma term is

$$\sigma_2(2\mu^2) = 85 \pm 15 \text{ MeV}\,. \tag{9}$$

Without the higher partial waves the above result would be about 10 MeV smaller.

3 Evaluation of the second sum rule

A second sum rule was also described [2, 3], in which a $t = 0$ (forward) dispersion relation was subtracted from (3). The result is to express $\sigma(2\mu^2)$ almost entirely in terms of threshold parameters. The continuum is suppressed by an order of magnitude over I_0. The result is

$$\overline{D}(2\mu^2) = \left[D^{(+)}(\nu_T, 2\mu^2) - \nu_T^2 K\right] + \text{small corrections}\,, \tag{10}$$

where

$$K = \lim_{k\to 0} \frac{\mathrm{Re}\, D^{(+)}(\omega, 0) - D^{(+)}(\mu, 0)}{k^2}\,. \tag{11}$$

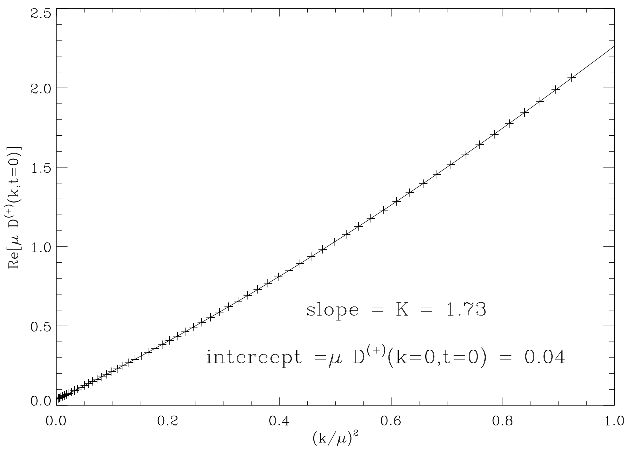

Figure 3: The lab momentum dependence of $D^{(+)}(k,0)$ as found from SM01. The slope at $k = 0$ is K.

Again we evaluate in two ways. First, directly from SM01 we show in Fig. 3 the k dependence (lab momentum) of (11) before the $k = 0$ limit is taken. As seen, the limit is evaluated with no difficulty to give

$$K = 1.73\,, \tag{12}$$

resulting in

$$\sigma_3(2\mu^2) = 85 \text{ MeV}\,. \tag{13}$$

Finally, as shown in [2, 3], we can directly evaluate (10) using the threshold phase shifts of Gashi *et al.* [6]. As before, we add the contribtion to $D^{(+)}(\nu_T, 2\mu^2)$ from higher partial waves. The result is

$$\sigma_4(2\mu^2) = 88 \pm 10 \text{ MeV}\,. \tag{14}$$

This value $\sigma(2\mu^2)$ should be compared with our older result [1] of 71 ± 9 MeV. The final version of Gahsi *et al.* [6] increases this to 78 MeV and the higher partial waves another 10 MeV.

We find excellent consistency for a $\sigma(2\mu)$ in the 80 to 90 MeV range and this is similar to the GWU results presented at this conference. Most of the error given in (14) for σ_4 comes from the crossing even s-wave effective range $C^{(+)}$ [2, 3]. This threshold parameter evalution of σ_4 can be greatly improved by a better determination of $C^{(+)}$. This latter method has some distinct advantages in that a realistic error can be assigned since the threshold parameters are directly related to the low energy data. If the older threshold parameters [1] are used we find $\sigma_4 = 60$ MeV. The impact of modern data is clearly seen.

References

[1] G. Höhler, *Pion-Nucleon Scattering*, Landolt-Börnstein New Series, Group I/9b2, ed. by H. Schopper (Springer, 1983).

[2] M. G. Olsson, Phys. Lett.**B482**, 50 (2000).

[3] W.B. Kaufmann and M.G. Olsson, in prepration.

[4] E.T. Osypowski, Nucl. Phys. **B21**, 615 (1970); T.P. Cheng and R. Dashen, Phys. Rev. Lett. **26**, 594 (1971); L.S. Brown, W. Pardee, and R.D. Peccei, Phys. Rev. **D14**, 2801 (1971).

[5] R.A. Arndt, R.L. Workman and M.M. Pavan, nucl-th/9807287; SAID on-line solution SP99 (http://said.phys.vt.edu/said_branch.html).

[6] A. Gashi *et al.*, hep-ph/0009081.

Covariant meson-exchange model of the $\bar{K}N$ interaction

A.D. Lahiff

TRIUMF, 4004 Wesbrook Mall, Vancouver, B.C., Canada V6T 2A3

(Received: 10 October 2001)

A covariant meson-exchange model of the $\bar{K}N$ interaction within the framework of the Bethe-Salpeter equation is presented. With just one free parameter we are able to get a good description of the available experimental data from below threshold to 300 MeV laboratory momentum.

The construction of nonperturbative models of the $\bar{K}N$ interaction has a long history, dating back to early work such as that of Dalitz, Wong, and Rajasekaran [1]. This model consisted of a coupled-channel Schrödinger equation with static vector meson exchange potentials, and was able to dynamically generate the S-wave $\Lambda(1405)$ resonance. More recent calculations are based on similar ideas, and commonly use a coupled-channel Lippmann-Schwinger equation to iterate a set of potentials to infinite order, with the strengths of the potentials in the various channels constrained by SU(3) symmetry. The strong attraction produced by the $I = 0$ $\bar{K}N \to \bar{K}N$ potential results in the dynamical generation of the $\Lambda(1405)$ resonance as an unstable $\bar{K}N$ bound state. Further resonances, including the $\Lambda(1670)$ and $\Sigma(1620)$, have also been found to be formed dynamically [2,3].

Previous works have in general relied upon non-relativistic formulations, or have made use of the (ladder) Bethe-Salpeter equation [4] but solved it in an approximate way. Here we outline a covariant model of low-energy $\bar{K}N$ scattering based on the 4-dimensional Bethe-Salpeter equation, and present some preliminary results.

The multi-channel Bethe-Salpeter equation for the $\bar{K}N$ system is

$$T_{nm}(q',q;P) = V_{nm}(q',q;P) - \sum_k \frac{i}{(2\pi)^4} \int d^4q'' V_{nk}(q',q'';P) G_k(q'';P) T_{km}(q'',q;P) \ , \qquad (1)$$

where m (n) label the initial (final) states, and k is summed over the included channels (K^-p, $\bar{K}^0n$, $\Lambda\pi^0$, $\Sigma^-\pi^+$, $\Sigma^0\pi^0$, $\Sigma^+\pi^-$, $\Lambda\eta$, and $\Sigma^0\eta$). Also, $P = (\sqrt{s}, \mathbf{0})$ is the total 4-momentum in the center-of-mass (c.m.), while q, q' and q'' are the relative 4-momenta in the initial, final and intermediate states. The two-body propagator $G_k(q;P)$ is given by the product of the appropriate baryon and pseudoscalar meson propagators. The interaction kernels V_{nm} are constructed from the s- and u-channel baryon poles and t-channel vector meson pole diagrams obtained from the usual SU(3)-symmetric BBP, BBV, and PPV interaction Lagrangians [5] (here B, P, and V represent the $J^P = 1/2^+$ baryons, the pseudoscalar mesons, and the vector mesons, respectively). In order to regularize the Bethe-Salpeter equation all the propagators are multipled by form factors, which are given by

$$f_{B_k}(p^2) = \left(\frac{m_{B_k}^2 - \Lambda^2}{p^2 - \Lambda^2 + i\epsilon}\right)^2, \quad f_{P_k}(p^2) = \left(\frac{m_{P_k}^2 - \Lambda^2}{p^2 - \Lambda^2 + i\epsilon}\right)^2, \quad f_{V_k}(t) = \left(\frac{-\Lambda^2}{t - \Lambda^2 + i\epsilon}\right)^2. \qquad (2)$$

We use the same cutoff mass Λ for all particles in order to minimize the number of free parameters.

The method of solution is the same as that described in Ref. [6]. A partial wave decomposition is applied to Eq. (1) which gives a system of coupled 2-dimensional integral equations. The singularities in the relative-energy variables are handled by performing a Wick rotation [7], i.e., the relative-energy integration contour is rotated from the real to the imaginary axis. All of the basic coupling constants in the model are fixed using information from other sources, such as decay widths and

coupling constants		
$g_{\pi\pi\rho}$	6.05	$\Gamma(\rho^0 \to \pi^+\pi^-)$
$g_{NN\rho}$	2.52	$\Gamma(\rho^0 \to e^+e^-)$
$\kappa_{NN\rho}$	3.71	VMD
$g_{NN\omega}$	3.4 $g_{NN\rho}$	$\Gamma(\rho^0 \to e^+e^-)/\Gamma(\omega \to e^+e^-)$
$\kappa_{NN\omega}$	-0.12	VMD
$f_{NN\pi}^2/4\pi$	0.075	nucleon-nucleon data
$F/(F+D)$ ratios		
α_{PV}	0.4	semileptonic hyperon decays
α_V^e	1.0	universality
α_V^m	0.28	relativistic SU(6)
cutoff mass		
Λ	2.42 GeV	

Table 1: Parameters of the model. The basic coupling constants and the $F/(F+D)$ ratios are fixed: the sources of the values used are given in the right-hand column. Also note that we assume ideal $\phi-\omega$ mixing, and take the physical η to be the pure octet state.

vector meson dominance (VMD), and are not left as free parameters. The only adjustable parameter is the cutoff mass, which we fix by fitting to the $\bar{K}N$ data. The values of the basic coupling constants and the cutoff mass are shown in Table 1.

The K^-p cross sections are shown in Figure 1, where we find good agreement with the experimental data. The $Y\eta$ channels give non-negligible contributions, even though the energies we consider are well below the $\Lambda\eta$ and $\Sigma\eta$ thresholds.

We now turn to the threshold behaviour. For the K^-p scattering length we find $a_{K^-p} = -0.54 + i1.2$ fm, which is consistent with the experimental value of $a_{K^-p} = -0.78 \pm 0.18 + i(0.49 \pm 0.37)$ fm obtained in a kaonic hydrogen experiment [9]. The relative strengths of the different channels at threshold are tightly constrained by the threshold branching ratios γ, R_c, and R_n, which are given

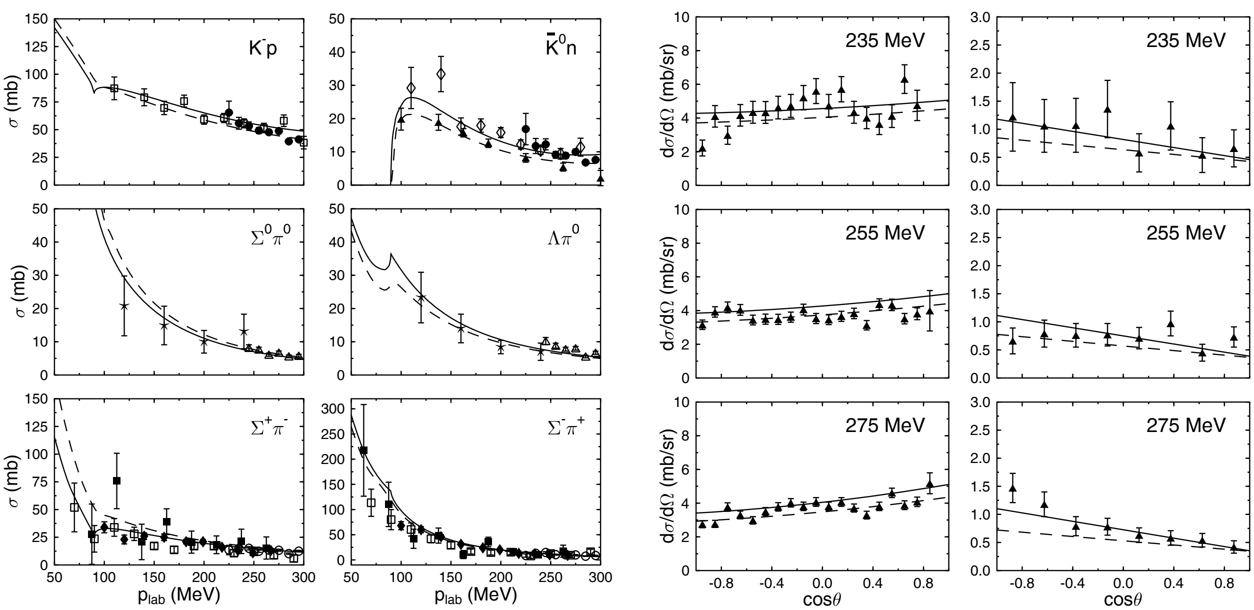

Figure 1: The first two columns show the cross sections for the six final states. The third and fourth columns show the elastic and charge-exchange differential cross sections, respectively, compared to the experimental data of Mast et al. [8]. The solid lines correspond to the full model, while the $Y\eta$ channels were omitted in the calculations giving the dashed lines.

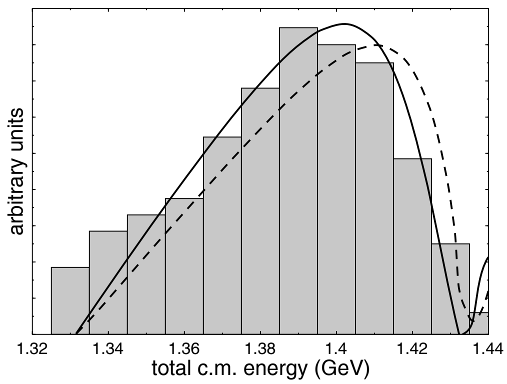

Figure 2: The $\Sigma\pi$ mass distribution compared to the experimental data from Hemingway [13]. The solid line is the result of the full calculation, while the dashed line shows the effect of omitting the $Y\eta$ channels.

in Refs. [10,11] as

$$\gamma = \frac{\Gamma(K^- p \to \Sigma^- \pi^+)}{\Gamma(K^- p \to \Sigma^+ \pi^-)} = 2.36 \pm 0.04 \ , \qquad R_c = \frac{\Gamma(K^- p \to \text{charged})}{\Gamma(K^- p \to \text{all})} = 0.664 \pm 0.011 \ ,$$

$$R_n = \frac{\Gamma(K^- p \to \Lambda \pi^0)}{\Gamma(K^- p \to \text{neutral})} = 0.189 \pm 0.015 \ .$$

Our values for the branching ratios are $\gamma = 2.14$, $R_c = 0.651$, and $R_n = 0.132$, which are in reasonable agreement with the experimental values. As found previously by Oset and Ramos [12], the $Y\eta$ channels (in particular $\Lambda\eta$) give important contributions to the branching ratios. When the $Y\eta$ channels are neglected, R_c and R_n are essentially unchanged, but γ reduces to 1.38.

Finally we consider the energy region below the $\bar{K}N$ threshold, where the $I = 0$ $\Sigma\pi \to \Sigma\pi$ amplitude exhibits the $\Lambda(1405)$ resonance. In Figure 2 we compare the $\Sigma\pi$ mass spectrum of the $\Lambda(1405)$ obtained in our model with experiment, and find good agreement.

To summarize, we have solved the multi-channel Bethe-Salpeter equation for the $\bar{K}N$ system by means of a Wick rotation, and obtained good agreement with the low-energy $\bar{K}N$ experimental data by adjusting a single cutoff mass. Future work will include extending the model to higher energies, and searching for evidence of additional dynamically-generated S- and P-wave hyperon resonances.

Acknowledgment: This work was supported in part by a grant from the Natural Sciences and Engineering Research Council of Canada.

References

[1] R. H. Dalitz, T. C. Wong, and G. Rajasekaran, Phys. Rev. **153**, 1617 (1967).
[2] P. B. Siegel and S. Guertin, PiN Newsletter **15**, 246 (1999).
[3] E. Oset, A. Ramos and C. Bennhold, arXiv:nucl-th/0109006.
[4] E. E. Salpeter and H. A. Bethe, Phys. Rev. **84**, 1232 (1951).
[5] J. J. de Swart, Rev. Mod. Phys. **35**, 916 (1963).
[6] A. D. Lahiff and I. R. Afnan, Phys. Rev. C **60**, 024608 (1999).
[7] G. C. Wick, Phys. Rev. **96**, 1124 (1954).
[8] T. S. Mast *et al.*, Phys. Rev. D **14**, 13 (1976).
[9] M. Iwasaki *et al.*, Phys. Rev. Lett. **78**, 3067 (1997).
[10] R. J. Nowak *et al.*, Nucl. Phys. B **139**, 61 (1978).
[11] D. N. Tovee *et al.*, Nucl. Phys. B **33**, 493 (1971).
[12] E. Oset and A. Ramos, Nucl. Phys. A **635**, 99 (1998).
[13] R. J. Hemingway, Nucl. Phys. B **253**, 742 (1985).

Low-energy K^- optical potentials: deep or shallow?

A. Cieplý[a], E. Friedman[b], A. Gal[b], and J. Mareš[a]

[a]*Nuclear Physics Institute, CZ-25068 Řež, Czech Republic*
[b]*Racah Institute of Physics, The Hebrew University, Jerusalem 91904, Israel*

(Received: 29 October 2001)

The K^- optical potential in the nuclear medium is evaluated self consistently from a free-space K^-N t matrix constructed within a coupled-channel chiral approach. The fit of model parameters gives a good description of the low-energy data *plus* the available K^- atomic data. The resulting optical potential is relatively 'shallow' in contradiction to the potentials obtained from phenomenological analysis. The calculated $(K^-_{\mathrm{stop}}, \pi)$ hypernuclear production rates are very sensitivive to the details of kaonic bound state wave function, which makes the reaction suitable for distinguishing between shallow and deep K^- optical potentials.

1 Introduction

Calculations existing to date for the $\bar{K}$ nucleus interaction at threshold essentially give two different predictions for the depth of the K^- nucleus potential at nuclear matter density. The phenomenological density dependent (DD) [1] and the relativistic mean field (RMF) [2] models, which describe the kaonic atom data very well, produce deep attractive potentials. In contrast, chirally inspired models of the $\bar{K}N$ interaction [3–5] yield relatively shallow attractive potentials while giving worse description of the kaonic atoms. Recently, Baca et al. [6] improved significantly the fit to the atomic data by adding to the optical potential of Ref. [5] a phenomenological '$t\rho$' term. However, this improvement was achieved at the cost of losing the direct connection of the optical potential to the chirally inspired microscopic model of the $\bar{K}N$ interaction.

In this contribution based on our recent work [7] we demonstrate that one can find such parameters of the chirally motivated microscopic model of the $\bar{K}N$ interaction that the low-energy $\bar{K}N$ data plus the K^- atomic data are fitted *simultaneously* without introducing any additional 'non-chiral' terms. The quality of the K^- atomic fit provided by our optical potential is superior to other chirally motivated approaches. Furthermore, we demonstrate that the outcome of K^- initiated reactions at low energy is sensitive to the wavefunction of the kaon inside the nucleus, where different optical potentials produce noticeably different wavefunctions. As an example, we discuss the $(K^-_{\mathrm{stop}}, \pi)$ reaction into specific hypernuclear states.

2 Chiral $\bar{K}N$ amplitude

We follow the chirally motivated model developed by Weise and collaborators [3, 4] for the $\bar{K}N$ scattering and reactions near threshold. The $\Lambda(1405)$ resonance is generated dynamically by solving coupled Lippmann-Schwinger equations for the meson-baryon t-matrix. The channels included in the model are: K^-p, $\bar{K}^0n$, $\pi^0\Lambda$, $\pi^+\Sigma^-$, $\pi^0\Sigma^0$, $\pi^-\Sigma^+$. The $\bar{K}N$ interaction is treated self-consistently [8]. This means that the K^- optical potential constructed from the elementary $\bar{K}N$ amplitudes enters the in-medium propagator through the kaon self selfenergy correction. We included only the kaon and nucleon selfenergies in $\bar{K}N$ sector and neglected the selfenergy corrections in the pion-hyperon channels, for simplicity.

The model was used [7] in χ^2 fits to K^--atomic data and to representative low energy K^-p data. We started from the original parametrization of Refs. [3,4] and refitted the meson-baryon coupling constant f_π and the four inverse range parameters α_i that characterize the range of meson-baryon interaction in the included channels. All parameters turned out to be close to their initial values

Table 1: The fits to K^- atomic data (for notation see text).

model	no Π	$\Pi_{\bar{K}}$	$\Pi_{\bar{K}} + \Pi_N$	RO	RO $+t\rho$	SKE	SKE $+t\rho$	DD	DD + RMF
χ^2/N	16.5	6.72	2.24	4.62	2.73	12.7	2.46	1.28	1.40
$V_{\rm R}$(MeV)	-117	-71	-55	-44	-58	-34	-159	-190	-185
$V_{\rm I}$(MeV)	-67	-85	-60	-54	-23	-62	-95	-55	-60

resulting in a moderate modification of the original model. The details of our fitting procedure can be found in Ref. [7].

The fit to kaonic atoms data includes 65 data points throughout the periodic table. Our results are summarized in Table 1 where we also show the results of similar fits performed with other K^- nuclear optical potentials. The degree of success of those potentials is characterized by the values of χ^2 per data point. We also show the depths of the optical potentials $V_{\rm R}$ (real) and $V_{\rm I}$ (imaginary) at nuclear density $\rho_0 = 0.17$ fm^{-3}. The first three columns show values obtained for the present model in three different cases: 'no Π' - no medium effects beyond Pauli blocking are included; 'Π_K' - the self-consistent calculation including the $\bar{K}$ self energy; and '$\Pi_K + \Pi_N$' - the kaon and nucleon self energies are included. In order to improve the fit to the data for the chiral optical potentials by Ramos and Oset (RO) [5] and by Schaffner-Bielich et al. (SKE) [9], we followed the approach of Ref. [6] and added a phenomenological '$t\rho$' term to the potential. Although our model gives clearly superior description of the data when compared with the other two chiral models, the phenomenological DD model [1] and the combined DD+RMF model [2] give even better χ^2/N.

At zero energy the optical potential is related to the isospin averaged (effective) $\bar{K}N$ threshold scattering amplitude $a_{\rm eff}$ by the standard formula

$$V^{\bar{K}}_{\rm opt} = -(4\pi/2\mu_{KN})\, a_{\rm eff}(\rho)\, \rho \; . \tag{1}$$

The density dependence of $a_{\rm eff}$ observed in Fig. 2 of Ref. [7] indicates that the inclusion of K^- self energy generally leads to a weaker density dependence of the threshold scattering amplitude. This means that the selfconsistent K^- optical potential is well approximated by a '$t\rho$' form (where $t =$const.) over a wide range of densities. A genuine ρ dependence of t appears only at very low densities where the transition from a repulsive free-space interaction to an attractive one in the nuclear medium occurs.

The addition of the pion and hyperon selfenergies to the propagator in non-kaonic channels was found to have only marginal effect on our $\bar{K}N$ amplitude. This fact fully justifies the simplification used in Ref. [7] (and mentioned above) but it contradicts the observations of Ref. [5]. Although we used only a simple local effective pion potential to probe the effect it is hard to believe that a more sophisticated form of the pion selfenergy [5] can make such difference. We have no clear understanding of the discrepancy at the moment.

3 Stopped K^- reactions

Various models of K^- optical potential at threshold can be tested in $(K^-_{\rm stop}, \pi)$ reactions to specific Λ hypernuclear states. We have studied the sensitivity of the capture rates to the choice of the K^- nucleus optical potential within the distorted wave impulse approximation (DWIA) [7, 10]. Here we limit the discussion to the following K^- capture-at-rest reactions on ^{12}C:

$$K^- \;+\; {}^{12}{\rm C} \;\longrightarrow\; \pi^- \;+\; {}^{12}_{\Lambda}{\rm C}\;, \qquad\qquad K^- \;+\; {}^{12}{\rm C} \;\longrightarrow\; \pi^0 \;+\; {}^{12}_{\Lambda}{\rm B}\;. \tag{2}$$

Our results are summarized in Table 2. Different optical potentials, ordered according to their central depth, were tested. The 'chiral' potential corresponds to the relatively shallow potential of

Table 2: Calculated capture rates on ^{12}C per stopped K^- (in units of 10^{-3}) to the summed $p_N \to s_\Lambda$ 1^- excitations in $^{12}_{\Lambda}$C and $^{12}_{\Lambda}$B for various optical potentials.

final $^{A}_{\Lambda}$Z	chiral	effective	fixed	DD
$^{12}_{\Lambda}$C	0.231	0.169	0.089	0.063
$^{12}_{\Lambda}$B	0.119	0.087	0.046	0.032

the present work and the deep potential is represented by the density dependent 'DD' approach [1]. The 'effective' potential was obtained as a best-fit solution for the standard form $V_{\rm opt} = t_{\rm eff}\,\rho$. As these potentials were obtained within *global* fits to the available K^--atomic data, we add another potential of the $t\rho$ form 'fixed' to fit exclusively the carbon data.

The calculated capture rates per K^-, are shown for the production of the 1^- hypernuclear ground states off ^{12}C. It is clear that the deeper the K^- optical potential is, the lower the calculated rate becomes. This pattern is caused by the strong-interaction bound D state generated by all but the 'chiral' potentials. The atomic wavefunction acquires then *extra* nodes within the nucleus, thus causing substantial cancelations in the DWIA amplitude. All the calculated rates shown in Table 2 are much lower than the measured values [11]. Unfortunately, some uncertainties inherent in the calculation (pion distortion, adopted value for in-medium branching ratio) make it difficult to compare the present results with experiment.

4 Conclusions

- Only minor modifications of the parameters involved in the chirally motivated model for the $\bar{K}N$ amplitude are necessary to get good agreement with the atomic data while maintaining the good description of low-energy free space K^-p data. No phenomenological '$t\rho$' term is required in our analysis.
- In our model, the pion and hyperon selfenergies have marginal impact on the $\bar{K}N$ amplitude.
- The optical potential constructed from the 'chiral' $\bar{K}N$ amplitude does not yield as strong attraction as phenomenological potentials do.
- Λ-hypernuclear ground-state production rates calculated for the $(K^-_{\rm stop}, \pi)$ reactions on carbon vary by more than a factor of 3 for the optical potentials adopted in our work.

References

[1] Friedman, E., Gal, A., and Batty, C.J., *Nucl. Phys.* **A579**, 518 (1994).

[2] Friedman, E., Gal, A., Mareš, J., and Cieplý, A., *Phys. Rev. C* **60**, 024314 (1999).

[3] Kaiser, N., Siegel, P.B., and Weise, W., *Nucl. Phys.* **A594**, 325 (1995).

[4] Waas, T., Kaiser, N., and Weise, W., *Phys. Lett. B* **365**, 12 (1996); **379**, 34 (1996).

[5] Ramos, A., and Oset, E., *Nucl. Phys.* **A671**, 481 (2000).

[6] Baca, A., García-Recio, C., and Nieves, J., *Nucl. Phys.* **A673**, 335 (2000).

[7] Cieplý, A., Friedman, E., Gal, A., and Mareš, J., in print *Nucl. Phys.* **A**, preprint nucl-th/0104087.

[8] Lutz, M., *Phys. Lett. B* **426**, 12 (1998).

[9] Schaffner-Bielich, J., Koch, V., and Effenberger, M., *Nucl. Phys.* **A669**, 153 (2000).

[10] Gal, A., and Klieb, L., *Phys. Rev. C* **34**, 956 (1986).

[11] H. Tamura, R.S. Hayano, H. Outa and T. Yamazaki, *Prog. Theor. Phys. Suppl.* **117**, 1 (1994).

New determination of the ηN Scattering length in the K-matrix approach

W. J. Briscoe[a], T. W. Morrison[a], I. I. Strakovsky[a], and A. B. Gridnev[b]

[a] *Center for Nuclear Studies, Department of Physics,*
The George Washington University, Washington, DC 20052, U.S.A.
[b] *Petersburg Nuclear Physics Institute, Gatchina*
St. Petersburg 188350, Russia

(Received: 13 November 2001)

The new data on total and differential cross sections of η pion-production near threshold are analyzed within the multichannel K-matrix approach with effective Lagrangians. The new value for the lower bound for the imaginary part of ηN scattering length $\mathrm{Im}A_{\eta N} \geq 0.172 \pm 0.009$ fm was obtained.Analysis show the good description of the η production data and give $\mathrm{Im}A_{\eta N} = 0.18 \pm 0.03$ fm and $\mathrm{Re}A_{\eta N} = 0.47 \pm 0.09$ fm for the ηN scattering length value.

1 Introduction

The η meson is one of the member of the pseudoscalar meson octet and according to the Goldstone's theorem can be viewed as the massless Goldstone boson. Then, the quark masses are turned on and SU(3) χPT can be used to calculate meson - nucleon scattering lengthes. Because the strange quark mass is considerably bigger than u and d quark masses, the ηN scattering length $A_{\eta N}$ is an important tool for the low energy QCD testing. In addition, the strong attraction in the ηN interaction observed in the most analyses, leads to possibility of the existence of new type of nuclear matter - bound state η-mesic nuclei [4]. To determine the ηN scattering length, the data on cross sections of the η meson production $\pi N \to \eta N$ and $\gamma N \to \eta N$ reactions were studied [2,8]. Previous analyses (see references in [5]) show a large spread for the $A_{\eta N}$ from negative [3] to 1 fm. One of the reasons for that is rather old and conflicting data on η meson production data and πN elastic scattering amplitude. In recent years, progress has been made in this input - the new solution for the πN elastic scattering amplitude SM01 by the GW group (former VPI group), based on the latest experimental data [6] and new data on $\pi N \to \eta N$ reaction [7] appeared. Here, we present the results from analyses of these new data.

To remove the rapid variation of the phase space due to the large η-meson mass versus pion one (Fig. 1), the total cross-section of the η production by pions is shown as a function of the η cm momentum p^*_η. From this picture, we see that data can be described very well by the linear fit (solid line). This means the S-wave dominate the total cross-section in this energy region. From the slope of the best-fit, a restriction on the imaginary part of the ηN elastic scattering amplitude $A_{\eta N}$ can be found. Indeed, using the time reversal invariance and isospin conservation, for isospin $I = 1/2$, we get

$$\mathrm{Im}A_{\eta N} \geq \frac{3p^{*\,2}_\pi}{8\pi p^*_\eta}\,\sigma_{\pi^- p\to\eta n}\ . \tag{1}$$

Following to the recipe by Binnie *et al.* [1], the recent E909 threshold data [7] gives

$$\frac{1}{p^*_\eta}\sigma_{\pi^- p\to\eta n} = 15.2 \pm 0.8\ \mu b/\mathrm{MeV} \qquad \text{and} \qquad \mathrm{Im}A_{\eta N} \geq 0.172 \pm 0.009\ \mathrm{fm}\ , \tag{2}$$

which can be compared with the previous output of Ref. [1],

$$\frac{1}{p^*_\eta}\sigma_{\pi^- p\to\eta n} = 21.2 \pm 1.8\ \mu b/\mathrm{MeV} \qquad \text{and} \qquad \mathrm{Im}A_{\eta N} \geq 0.24 \pm 0.02\ \mathrm{fm}\ . \tag{3}$$

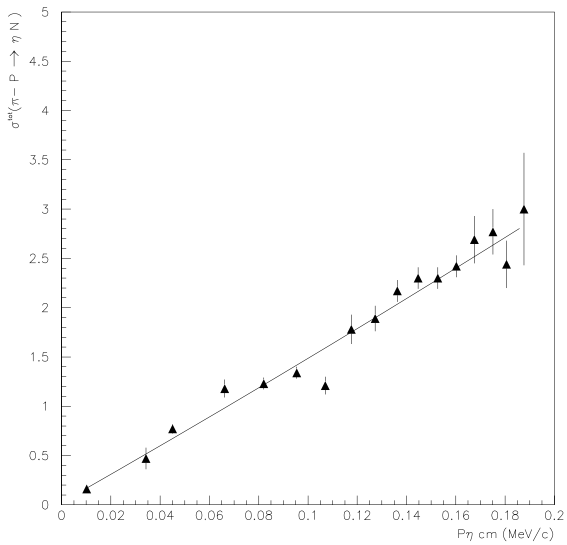

Figure 1: Total cross-section of the $\pi N \to \eta N$ reaction. Experimental data are taken from [7].

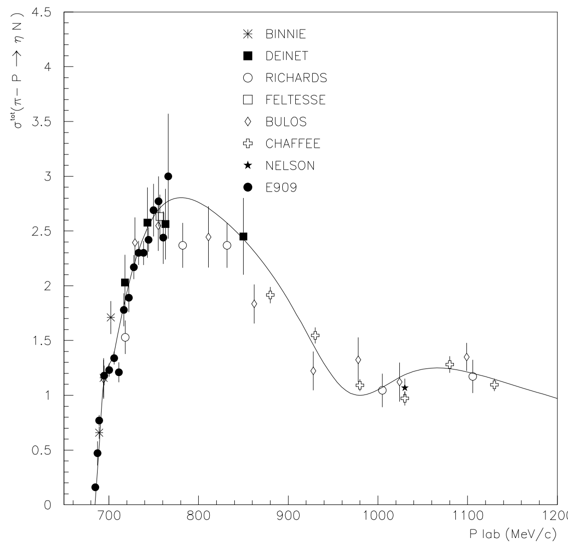

Figure 2: Total cross-section of the $\pi N \to \eta N$ reaction. Experimental data are taken from [7] and [8].

So, the new data leads to significantly smaller value for the lower bound of $\mathrm{Im}A_{\eta N}$ with much better accuracy. It should be noted that $d\sigma/dt$ was measured in [1] and data on $\sigma_{\pi^- p \to \eta n}$ has been obtained assuming the S-wave dominance.

2 Tree-level model for the K-matrix

The detailed description of the multichannel K-matrix approach, which we use in this analysis, can be found in Ref. [9]. Here, we outline the basic assumptions only. It is supposed that the K-matrix, being a solution of the Bethe-Salpeter equation, can be considered as a sum of the tree-level Feynman diagrams with the effective Lagrangians in the vertices. The Lagrangians contain the derivative couplings which corresponds to expansion of the proper vertex functions on the power of invariants. Therefore, we do not use any form factors.

For $P_\pi \leq 1$ GeV/c, there are three dominant channels in the πN interaction: $\pi N \to \pi N$, $\pi N \to \eta N$, and $\pi N \to \pi\pi N$. For the elastic channel, we take into account t-channel diagrams with the scalar-isoscalar (σ-meson) and vector-isovector (ρ-meson) exchange and s and u-channel diagrams with nucleon and all four-star S and P nucleon resonances following to the Particle Data Group (PDG). For the η-production, the resonance and t-channel a_0 exchange are accounted. This mechanism was suggested in [3] in an analogy with the charge πN exchange reaction where the t-channel ρ-exchange dominates. Because, we are interesting in the ηN scattering length, the σ-meson exchange for ηN elastic scattering was included. For the two pion production, we follow the same phenomenological quasi-two-body procedure as in Ref. [9].

The parameters of the model were determined by the best-fit of all S and P πN elastic partial wave amplitudes to single-energy solutions (SES) associated with the recent GW solution SM01 [6]. In the analysis, we covered $P_\pi \leq 1100$ MeV/c range. The data on the total $\pi^- p \to \eta n$ cross sections at the same momentum range are used in the fit as well.

We found that the agreement of our tree-level model for the πN K-matrix with the results of single-energy phase-shift analyses associated with SM01 [6] is good to $P_\pi \leq 1$ GeV/c.

The calculated total η pion-production cross section is shown in Fig. 2 (solid line) together with all experimental data. The good agreement is observed to $P_\pi \sim 1.1$ GeV/c ($\chi^2/dp \sim 1.4$).

We found that including the t-channel graph with a_0-meson exchange leads to considerably better agreement with the data. As a main result of this work, we obtain the following value of the ηN scattering length:

$$A_{\eta N} = [0.47 \pm 0.09 + i(0.18 \pm 0.03)] \text{ fm} . \tag{4}$$

This value of $\mathrm{Re}A_{\eta N}$ is enough to create a bound states of η with nuclei [4]. The essential source of the uncertainties in the real part of $A_{\eta N}$ is the ηN interaction via σ-meson exchange. This process is very important for $\mathrm{Re}A_{\eta N}$ but it's parameters not well defined by the η pion-production data. We hope that the data on the two η production can improve the situation. We also plan to continue an analysis including η photoproduction data.

Acknowledgments: This work was supported in part by the U. S. Department of Energy under Grants DE–FG02–95ER40901 and DE–FG02–99ER41110. I. S. acknowledge a partial support from Jefferson Lab, by the Southeastern Universities Research Association under DOE contract DE–AC05–84ER40150. A. G. acknowledges the hospitality extended by the Center for Nuclear Studies of The George Washington University.

References

[1] D. M. Binnie *et al.*, Phys. Rev. D **8**, 2793 (1973).
[2] B. Krusche *et al.*, Phys. Rev. Lett. **74**, 3736 (1995).
[3] B. L. Birbrair and A. B. Gridnev, Z. Phys. **A354**, 95 (1996).
[4] R. S. Bhalerao and L. C. Liu, Phys. Rev. Lett. **54**, 865 (1985); Q. Haider and L. C. Liu, Phys. Lett. **B172**, 257 (1986).
[5] M. Batinic *et al.*, Physica Scripta, **58**, 15 (1998).
[6] R. A. Arndt, R. L. Workman, I. I. Strakovsky, and M. M. Pavan, in preparation for Phys. Rev. C,
[7] T. W. Morrison, W. J. Briscoe, I. I. Strakovsky, and A. B. Gridnev, Bull. Am. Phys. Soc. **45**, 58 (2000); T. W. Morrison, Ph. D. Thesis, The George Washington University, Dec. 1999 (unpublished).
[8] M. Clajus and B. M. K. Nefkens, πN Newsletter **7**, 76 (1992).
[9] A. B. Gridnev and N. G. Kozlenko, Eur. Phys. J. A **4**, 187 (1999).

Baryons in the nonperturbative string approach

I.M. Narodetskii and M.A. Trusov

ITEP, Moscow, Russia

(Received: 25 October 2001)

We present some piloting calculations of masses and short–range correlation coefficients for the ground states of light and heavy baryons in the framework of the simple approximation within the nonperturbative QCD approach.

The purpose of this talk is to discuss the results of the calculation [1] of the masses and wave functions of the heavy baryons in a simple approximation within the nonperturbative QCD (see [2] and references therein). The starting point of the approach is the Feynman–Schwinger representation for the three quark Green function in QCD in which the role of the time parameter along the trajectory of each quark is played by the Fock–Schwinger proper time. The proper and real times for each quark related via a new quantity that eventually plays the role of the dynamical quark mass. The final result is the derivation [2] of the Effective Hamiltonian (EH). For the ground state baryons without radial and orbital excitations in which case tensor and spin-orbit forces do not contribute perturbatively the EH has the following form

$$H=\sum_{i=1}^{3}\left(\frac{m_i^{(0)2}}{2m_i}+\frac{m_i}{2}\right)+H_0+V\ , \tag{1}$$

where H_0 is the non-relativistic kinetic energy operator and V is the sum of the perturbative one gluon exchange potential V_c and the string potential V_{string}. The latter has been calculated in [3] as the static energy of the three heavy quarks: $V_{\text{string}}(\mathbf{r}_1,\mathbf{r}_2,\mathbf{r}_3)=\sigma R_{\text{min}}$, where R_{min} is the sum of the three distances $|\mathbf{r}_i|$ from the string junction point, which for simplicity is chosen as coinciding with the center–of–mass coordinate.

In Eq. (1) $m_i^{(0)}$ are the current quark masses and m_i are the dynamical quark masses. In contrast to the standard approach of the constituent quark model the dynamical mass m_i is not a free parameter but it is expressed in terms of the current mass $m_i^{(0)}$ defined at the appropriate scale of $\mu\sim 1$ GeV from the condition of the minimum of the baryon mass M_B as function of m_i: $\partial M_B(m_i)/\partial m_i=0$. Technically, this has been done using the einbein (auxiliary fields) approach, which is proven to be rather accurate in various calculations for relativistic systems.

The EH has been already applied to study baryon Regge trajectories [3] and very recently for computation of magnetic moments of light baryons [4]. The essential point of this talk is that it is very reasonable that the same method should also hold for hadrons containing heavy quarks. In what follows we will concentrate on the masses of double heavy baryons. As in [4] we take as the universal parameter the QCD string tension σ fixed in experiment by the meson and baryon Regge slopes. We also include the perturbative Coulomb interaction with the frozen coupling $\alpha_s(1\text{ GeV})=0.4$.

We use the hyper radial approximation (HRA) in the hyper-spherical formalism approach. In the HRA the three quark wave function depends only on the hyper-radius $R^2=\boldsymbol{\rho}^2+\boldsymbol{\lambda}^2$, where $\boldsymbol{\rho}$ and $\boldsymbol{\lambda}$ are the appropriate three-body Jacobi variables. Introducing the reduced function $\chi(R)=R^{5/2}\psi(R)$ and averaging $V=V_c+V_{\text{string}}$ over the six-dimensional sphere one obtains the Schrödinger equation

$$\frac{d^2\chi(R)}{dR^2}+2\mu\left[E_n+\frac{a}{R}-bR-\frac{15}{8\mu R^2}\right]\chi(R)=0\ , \tag{2}$$

where

$$a = \frac{2\alpha_s}{3}\,\frac{16}{3\pi}\sum_{i<j}\sqrt{\frac{\mu_{ij}}{\mu}}\ , \qquad b = \sigma\,\frac{32}{15\pi}\sum_{i<j}\sqrt{\frac{\mu(m_i+m_j)}{m_k(m_1+m_2+m_3)}}\ , \tag{3}$$

with μ_{ij} being the reduced mass of quarks i and j, and μ is an arbitrary parameter with the dimension of mass which drops off in the final expressions. We use the same parameters as in Ref. [5]: $\sigma = 0.17$ GeV, $\alpha_s = 0.4$, $m_q^{(0)} = 0.009$ GeV, $m_s^{(0)} = 0.17$ GeV, $m_c^{(0)} = 1.4$ GeV, and $m_b^{(0)} = 4.8$ GeV.

The dynamical masses m_i and the ground state eigenvalues E_0 calculated using the described above procedure are given for various baryons in Table 1 of Ref. [1]. For the light baryons the values of light quark masses $m_q \sim 450 - 500$ MeV ($q = u, d, s$) qualitatively agree with the results of Ref. [5] obtained from the analysis of the heavy–light ground meson states, but ~ 60 MeV higher than those of Refs. [3], [4]. This difference is due to the different treatment of the Coulomb and spin–spin interactions. The light quark masses are increased by $100 - 150$ MeV when going from the light to heavy baryons. For the heavy quarks (c and b) the variation in the values of their dynamical masses in different baryons is marginal. Note that the masses of the light quarks in baryons are slightly smaller than those in the mesons.

For many applications the quantities $R_{ijk} = \langle\psi_{ijk}|\delta^{(3)}(\mathbf{r}_j - \mathbf{r}_i)|\psi_{ijk}\rangle$ are needed. Note that these quantities depend on the third or 'spectator' quark through the three–quark wave function. To estimate effects related to the baryon wave function we solve Eq. (2) by the variational method using a simple trial function $\chi(R) \sim R^{5/2}e^{-\mu\beta^2R^2}$, where β is the variational parameter. Then $R_{ijk} = \left(2\beta^2\mu_{ij}/\pi\right)^{3/2}$. The results of the variational calculations are given in Table 3 of [1]. Comparing the results with those of Ref. [5] we confirm the inequalities $R_{ijk} < \frac{1}{2}R_{ij}$ and $R_{ijk} > R_{ijl}$, if $m_k \leq m_l$, first suggested in Ref. [6] from the observed mass splitting in mesons and baryons. Here R_{ij} is the corresponding quantity for a meson. In particular, we obtain $R_{ijk}/R_{ij} = 0.44$, 0.40, 0.37, and 0.34 for $ijk = ucd$, scu, ubd, and sbu, respectively. These estimations agree with the results obtained using the non–relativistic quark model or the bag model or QCD sum rules which are typically in the range $0.1 - 0.5$. Note also that if i, j are the light quarks, and the quarks k and l are the heavy then $R_{ijk} \approx R_{ijl}$ (*i.g.* $R_{qqc} \approx R_{qqb}$) in agreement with the limit of the heavy quark effective theory.

Note also that the wave function calculated in HRA show the marginal diquark clustering even in the doubly heavy baryons . E.g. in the qcc baryon $\bar{r}_{qc} = 0.61$ fm while $\bar{r}_{cc} = 0.45$ fm. Likewise $\bar{r}_{qb} = 0.53$ fm and $\bar{r}_{bb} = 0.25$ fm in the qbb baryon. This is principally kinematic effect related to the fact that in the HRA the difference between the various $\bar{r}_{ij}$ in a baryon is due to the factor $\sqrt{1/\mu_{ij}}$ which varies between $\sqrt{2/m_i}$ for $m_i = m_j$ and $\sqrt{1/m_i}$ for $m_i \ll m_j$. For the light baryons $\bar{r}_{qq} \sim 0.7 - 0.8$ fm.

To calculate hadron masses we, as in Ref. [3], first renormalize the string potential: $V_{\rm string} \to V_{\rm string} + \sum_i C_i$, where the constants C_i take into account the residual self-energy (RSE) of quarks. In the present work we treat them phenomenologically. We adjust C_i to reproduce the center-of-gravity for baryons with a given flavor. To this end we consider the spin-averaged masses, such as: $(M_N + M_\Delta)/2$, and $(M_\Lambda + M_\Sigma + 2M_{\Sigma^*})/4$ and analogous combinations for qqc and qqb states. Then we obtain $C_q = 0.34$, $C_s = 0.19$, $C_c \sim C_b \sim 0$.

We keep these parameters fixed to calculate the masses given in Table 1, namely the spin–averaged masses (computed without the spin–spin term) of the lowest double heavy baryons. In this Table we also compare our predictions with the results obtained using the additive non–relativistic quark model with the power-law potential [7], relativistic quasipotential quark model [8], the Feynman–Hellmann theorem [9] and with the predictions obtained in the approximation of double heavy diquark [10].

State	present work	Ref. [7]	Ref. [8]	Ref. [9]	Ref. [10]
$\Xi\{qcc\}$	3.69	3.70	3.71	3.66	3.48
$\Omega\{scc\}$	3.86	3.80	3.76	3.74	3.58
$\Xi\{qcb\}$	6.96	6.99	6.95	7.04	6.82
$\Omega\{scb\}$	7.13	7.07	7.05	7.09	6.92
$\Xi\{qbb\}$	10.16	10.24	10.23	10.24	10.09
$\Omega\{sbb\}$	10.34	10.30	10.32	10.37	10.19

Table 1: Masses of baryons containing two heavy quarks.

In conclusion, we have employed the general formalism for the baryons, which is based on nonperturbative QCD and where the only inputs are the string tension σ, the strong coupling constant α_s and two additive constants, C_q and C_s, the residual self–energies of the light quarks. Using this formalism we have performed the calculations of the spin–averaged masses of baryons with two heavy quarks. One can see from Table 1 that our predictions are especially close to those obtained in Ref. [7] using a variant of the power–law potential adjusted to fit ground state baryons.

Acknowledgments: One of the authors (I.M.N.) thank W.Briscoe and H.Haberzettl for organizing an excellent Conference with a stimulating scientific program. This work was supported in part by RFBR grants Refs. 00-02-16363 and 00-15-96786.

References

[1] I. M. Narodetskii and M. A. Trusov, Yad. Fiz., in press [hep-ph/0104019].

[2] Yu. A. Simonov, in Proc. of the XVII International School of Physics, Lisbon 1999, eds. L.Ferreira *et al.* (World Scientific 2000) p.60.

[3] M. Fabre de la Ripelle and Yu. A. Simonov, Ann. Phys. (N.Y.) **212**, 235 (1991).

[4] B. O. Kerbikov and Yu. A. Simonov, Phys. Rev. D **62**, 093016 (2000).

[5] Yu. S. Kalashnikova and A. Nefediev, Phys. Lett. B **492**, 91 (2000).

[6] D.B.Lichtenberg, Phys. Rev. D **54**, 5887 (1996).

[7] E. Bagan, H. G. Dosch, P. Godzinsky, S. Narison, and J.–M. Richard, Z. Phys. C **64**, 57 (1994).

[8] D. Ebert *et al.*, Z. Phys. C **76**, 111 (1997).

[9] R. Roncaglia, D. B. Lichtenberg, and E. Predazzi, Phys. Rev. D **52**, 1248 (1995).

[10] A. K. Likhoded and A. I. Onishchenko, hep-ph/9912425.

π and $\pi\pi$ decays of excited D mesons

T.A. Lähde and D.O. Riska

Helsinki Institute of Physics, University of Helsinki, PL 64 Helsinki, Finland

(Received: 21 August 2001)

The π and $\pi\pi$ decay widths of the excited charm mesons are calculated using a Hamiltonian model within the framework of the covariant Blankenbecler-Sugar equation. The pion-light constituent quark coupling is described by the chiral pseudovector Lagrangian.

1 Introduction

The pionic decay widths of the excited charm mesons (D mesons) are interesting observables, since they depend straightforwardly on the coupling of pions to light constituent quarks. The D mesons consist of one light (u, d) quark and a heavy charm (c) antiquark, of which it is only the light constituent quark that couples to pions. The coupling of light constituent quarks to pions may be described by the chiral model [1], which includes the pseudovector Lagrangian and, for $\pi\pi$ decay, also a Weinberg-Tomozawa term.

In order to predict the decay widths of the excited D meson states, a model for the radial wavefunctions is needed. Here the interaction between the quarks is modeled as the sum of a screened one-gluon exchange (OGE) and a scalar linear confining interaction. The wavefunctions are obtained as solutions of the covariant Blankenbecler-Sugar equation [2]. These are then used together with the chiral Lagrangian to obtain predictions for the π [3] and $\pi\pi$ [4] decays of the excited D mesons.

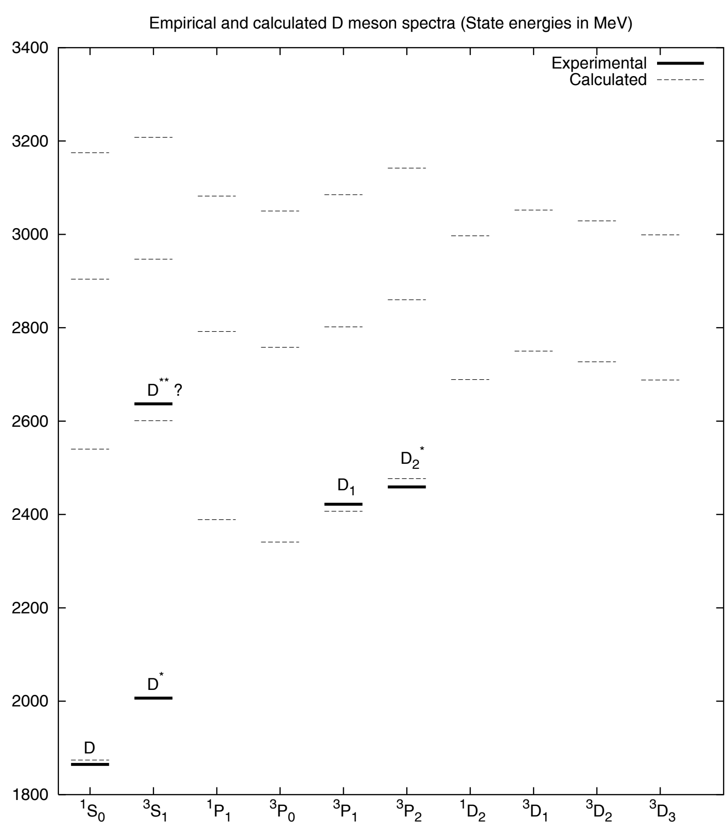

Figure 1: Empirical and calculated spectra of the D meson from ref. [3]. The D^* is an S-wave spin-triplet state which lies almost exactly at threshold for decay to $D\pi$. The decay widths for π decay of the D^* are predicted here along with those of the four $L = 1$ states, which can decay to both $D^*\pi$ and $D\pi$. These states can also decay to $D^*\pi\pi$ and $D\pi\pi$. Note that empirical data is only available for the spin triplet states with $L = 1$ and total angular momentum $J = 1$ and $J = 2$.

2 Single pion decay

The chiral Lagrangian describing the coupling between pions and light constituent quarks may be written as [3]

$$\mathcal{L} = i\frac{g_A^q}{2f_\pi}\bar{\psi}_q\,\gamma_5\gamma_\mu\,\partial_\mu\,\vec{\phi}_\pi\cdot\vec{\tau}\,\psi_q, \tag{1}$$

where g_A^q is the pion-quark axial coupling constant and f_π is the pion decay constant. The Lagrangian (1) gives rise to both axial current and charge single-quark amplitudes which may be obtained as

$$T_P^{1\mathrm{q}} = -i\frac{g_A^q}{2f_\pi}\sqrt{\frac{(E'+m_{\bar{q}})(E+m_{\bar{q}})}{4EE'}}\left(1-\frac{P^2-k^2/4}{3(E'+m_{\bar{q}})(E+m_{\bar{q}})}\right)\vec{\sigma}^q\cdot\vec{k}\,\tau_\pi, \tag{2}$$

$$T_S^{1\mathrm{q}} = i\frac{g_A^q}{2f_\pi}\frac{2m_{\bar{q}}+E+E'}{\sqrt{4EE'(E+m_{\bar{q}})(E'+m_{\bar{q}})}}\,\omega_\pi\,\vec{\sigma}^q\cdot\left(\frac{\vec{p}\,'+\vec{p}}{2}\right)\,\tau_\pi. \tag{3}$$

Here the relativistic momentum-dependent factors arise from the spinors of the light constituent quark. Because of the small mass (450 MeV) of the light constituent quark, these factors should not be dropped, as otherwise large overestimates will result. In the above expression, $\vec{k}$ denotes the momentum of the emitted pion. The quark momentum operator $\vec{P}$ is defined as $(\vec{p}\,'+\vec{p})/2$. In addition to the above single-quark amplitudes, two-quark amplitudes involving excitation of intermediate negative energy quarks by the quark-antiquark interaction have been considered. Especially for the π decays of the $L=1$ states, they are shown to have a large effect.

Using the standard phase-space expressions and wavefunctions for the initial and final D meson states, the π decay widths of these states may be predicted. The predictions for the decays of the D^* agree well with the recent CLEO measurement [5] of the width of the $D^{*\pm}$, which is reported as $96\pm4\pm22$ keV.

Decay	$g_A^q=0.87$	$g_A^q=1.0$
$D^{*\pm}\to D^\pm\pi^0$	29 keV	38 keV
$D^{*\pm}\to D^0\pi^\pm$	64 keV	84 keV
$D^{*0}\to D^0\pi^0$	41 keV	54 keV

Table 1: Numerical results for the D^* widths using $g_A^q=0.87$ and $g_A^q=1.0$. The CLEO measurement concerns the sum of the two decay modes of the $D^{*\pm}$. As of this time, no constraining data exists for the pion decay of the neutral D^* meson.

Predictions for the pion decay widths of the $L=1$ D meson states have also been made in ref. [3]. In case of S-wave decay of these states, it is shown that in order to avoid large overestimates it is important to include also two-quark exchange charge amplitudes associated with excitation of intermediate negative energy quarks by the quark-antiquark interaction. Generally, the predicted widths of the spin triplet states fall somewhat below the empirical values, which suggests that $\pi\pi$ decay may play a role.

3 Two-pion decay

The Lagrangian (1) gives rise to Born terms describing $\pi\pi$ decay of excited D mesons. The model is completed by adding the Weinberg-Tomozawa Lagrangian

$$\mathcal{L}_{\mathrm{WT}} = -\frac{i}{4f_\pi^2}\bar{\psi}_q\,\gamma_\mu\,\vec{\tau}\cdot\vec{\phi}_\pi\times\partial_\mu\vec{\phi}_\pi\,\psi_q. \tag{4}$$

Together, the Lagrangians (1,4) give rise to amplitudes for $\pi\pi$ decay, which are usually expressed in the form $T = \delta_{ab}T^+ + \frac{1}{2}[\tau_b, \tau_a]T^-$, where a, b are isospin indices, and the amplitudes $T^\pm$ are given as $T^\pm = \bar{u}(p')\,(A^\pm - i\gamma \cdot QB^\pm)\,u(p)$. Here Q is defined as the combination $(k_b - k_a)/2$ of the pion four-momenta. The resulting expressions for the sub-amplitudes A, B are obtained as

$$A^+ = \left(\frac{g_A^q}{2f_\pi}\right)^2 4m_q, \tag{5}$$

$$A^- = 0, \tag{6}$$

$$B^+ = -\left(\frac{g_A^q}{2f_\pi}\right)^2 4m_q^2\left[\frac{1}{s-m_q^2} - \frac{1}{u-m_q^2}\right], \tag{7}$$

$$B^- = -\left(\frac{g_A^q}{2f_\pi}\right)^2 \left(2 + 4m_q^2\left[\frac{1}{s-m_q^2} + \frac{1}{u-m_q^2}\right]\right) + \frac{1}{2f_\pi^2}. \tag{8}$$

Computation of the two-pion decay widths of the excited D mesons using the above amplitudes together with the appropriate phase space expressions is shown in ref. [4] to lead to a significant increase of the total widths of the $L = 1$ D meson states, which is also expected from comparison with the analogous strange mesons [6].

D state	π width	$\pi\pi$ width	Total	Exp
D_2^*	15.7	3.05	18.8	25^{+8}_{-7}
D_1	13.6	1.34	14.9	$18.9^{+4.6}_{-3.5}$
D_0^*	27.7	~ 0.1	27.8	–
D_1^*	13.2	8.62	21.8	–

Table 2: Summary of results for π and $\pi\pi$ decay of the $L = 1$ D mesons in MeV, for $g_A^q = 1.0$. Empirical data is only available for the spin triplet D_2^* and D_1 states. The large variations in the $\pi\pi$ widths are due to the large differences in phase space.

In this context it is to be noted that the widths of the D_0^* and the D_1^* are here predicted to be an order of magnitude smaller than previously thought, because of the inclusion of negative energy components into the decay amplitudes; A similar effect has been noted in the calculation of ref. [7]. However, the results are strongly dependent on both the assumed spin-orbit structure of the $L = 1$ states and the composition and coupling structure of the quark-antiquark interaction, and should therefore be viewed as suggestive rather than as definite quantitative predictions.

References

[1] B.R. Holstein, Czech. J. Phys. **49** (1999), eprint hep-ph/9911449.

[2] T.A. Lähde, C.J. Nyfält and D.O. Riska, Nucl. Phys. **A674**, 141 (2000).

[3] K.O.E. Henriksson, T.A. Lähde, C.J. Nyfält and D.O. Riska, Nucl. Phys. **A686**, 355 (2001).

[4] T.A. Lähde and D.O. Riska, Nucl. Phys. **A693/3-4**, 755 (2001).

[5] CLEO Collaboration (S. Ahmed *et al.*), eprint hep-ex/0108013.

[6] D.E. Groom *et al.* (Particle Data Group), Eur. Phys. J. **C15**, 1 (2000).

[7] J.L. Goity and W. Roberts, Phys. Rev. D**60**, 034001 (1999).

Fano theory for hadronic resonances: the rho meson and the pionic continuum

N.E. Ligterink[a,b]

[a]ECT*, Strada delle Tabarelle 286, I-38050 Villazzano (Trento), Italy
[b]Dept. of Physics & Astronomy, University of Pittsburgh, 3941 O'Hara Street, Pittsburgh, USA

(Received: 9 October 2001)

For a model-independent analysis of hadronic scattering data in the resonance region we develop the Fano theory for such systems. We analyze the rho meson. The coupling of a bare rho meson to the two-pion and the four-pion continua is determined from the chiral theory. For a good fit of the two-pion decay of the rho meson with the data the four-pion continuum is necessary and sufficient. Furthermore, this four-pion continuum corresponds with the data of the four-pion decay channel.

The analysis of hadronic resonances is beset with difficulties, not in the least because of the ambiguous generalization of the two parameters, the mass and the width, that characterizes the Breit-Wigner shape of a single, narrow resonance. Resonances in hadronic physics are often wide, especially if they couple directly to the pionic continuum. The continuum can therefore not be considered flat, and the different resonances with overlapping widths interact with each other. On top of that, since the Fermi-Breit-Wigner-Weisskopf analysis is based on perturbation theory it cannot properly handle multiple resonances and competing decay channels at the same energy.

I will adapt a method for analyzing resonances used in atomic theory. It will relate the scattering data to matrix elements of the Hamiltonian. The mass of the resonance can be maintained as a useful characterization, however, the width, in itself, is less significant. In atomic physics the analysis of spectra has been the central issue for over a century. The spectra come in a rich variety, partly because of the tunability of experiments by varying field strengths and beam intensity.

In the sixties, Fano developed [1] an analysis for resonances by writing down general Hamiltonians for such systems. The Hamiltonian can be diagonalised exactly, which gives us direct relations between scattering data and the parameters of this Hamiltonian. In effect it is based on the separation of the problem in two parts: the continuum, characterized by the energy of the asymptotic states in a particular channel, and the resonances, which in the absence of a continuum are discrete eigenstates, such as, for example, the states that would follow from a constituent quark model, or a lattice calculation with heavy quarks, where pions are absent. The continuum should be considered an eigenstate of the decoupled system as well.

The rho meson plays an important role in photon-hadron interactions at intermediate energies. It seems that the photon couples to hadrons mainly via the isovector-vector rho meson, which in its turn, couples to a universal hadronic current via the coupling constant g. We see the rho meson mainly through its decay in two pions. In order to describe the physical rho meson, we assume a discrete state $|\rho\rangle$ at rest, which couples to the two-pion continuum $|\pi\pi(\Delta)\rangle$ with energy Δ. We have the following matrix elements:

$$\langle\rho|H|\rho\rangle = M \quad , \tag{1}$$

$$|\langle\rho|H|\pi\pi(\Delta)\rangle|^2 = \frac{g^2(\Delta^2-4m_\pi^2)^{\frac{3}{2}}\theta(\Delta-2m_\pi)}{48\pi\Delta} = W^2(\Delta) \quad , \tag{2}$$

$$\langle\pi\pi(\Delta')|H|\pi\pi(\Delta)\rangle = \Delta\delta(\Delta-\Delta') \quad , \tag{3}$$

where the coupling function follows from the interaction term $g\vec{\rho}^{\mu}\cdot[\vec{\pi}\times\partial_\mu\vec{\pi}]$ in the chiral Lagrangian, where the vectors are in the isospin space. We also include the next contribution to the physical

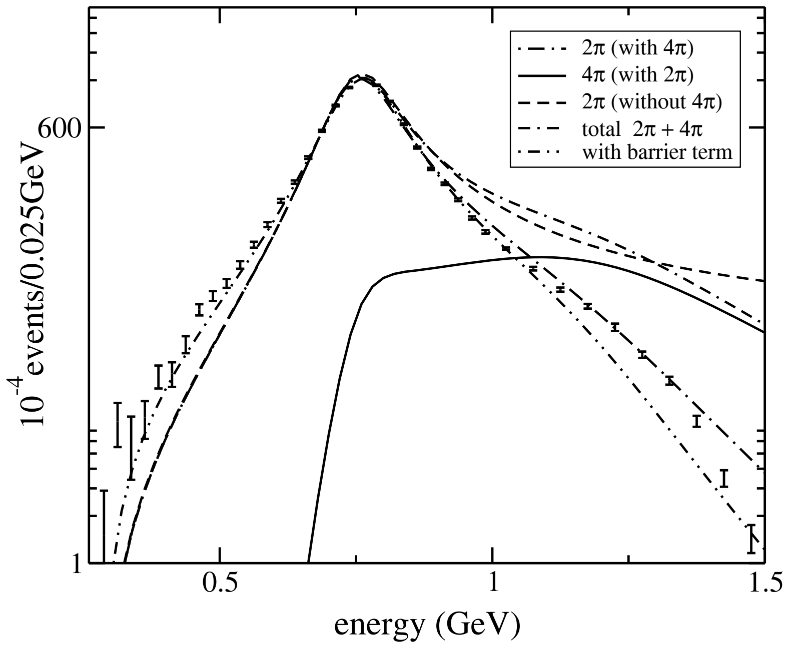

Figure 1: The Fano calculation compared with the τ^- decay data from the CLEO collaboration [3]. There are three cases: the two-pion results without four-pion contributions (long dashed), the results for the two-pion (dot-dashed) and four-pion (solid) continua and their sum (dot-dash-dashed), and the change in the two-pion decay of the latter if an artificial barrier term [3] is introduced, and coupling constants refitted (dot-dot-dashed).

rho, which, considering the possible states in this channel and their energies, must be the four-pion state. From the chiral Lagrangian there are many intermediate states that lead to the four-pion state from the discrete rho, however, all these states are highly virtual, so we can approximate the coupling between the discrete rho and the four-pion state with a single derivative coupling. The additional matrix elements are well-approximated by:

$$|\langle\rho|H|\pi\pi\pi\pi(\Delta)\rangle|^2 = \frac{g_2^2(\Delta^2-16m_\pi^2)^{\frac{9}{2}}\theta(\Delta-4m_\pi)}{M^5\Delta^3} = W_2^2(\Delta) \quad , \tag{4}$$

$$\langle\pi\pi\pi\pi(\Delta')|H|\pi\pi\pi\pi(\Delta)\rangle = \Delta\delta(\Delta-\Delta') \quad . \tag{5}$$

The continuum part of the eigenstate is composite: it contains a two-pion and a four-pion fraction to the ratio W/W_2. We did not allow a direct coupling between them, so they mix given with ratios proportional to the coupling strengths to the discrete state $|\rho\rangle$.

The real parts are made finite by subtracting $c_n(\omega^2-M^2)^n$ terms to the necessary order. We are not really interested in generating series of counterterms at a specific scale, therefore we use on-shell renormalization without much ado, where the scale is fixed by the rho mass.

Inserting this into the Hamiltonian and fitting it to hadronic decay of the τ^- we find a number of results. First, from the fit of the $\pi\pi$ decay of the ρ-meson, we find a coupling constant $g_2 \approx 0.2$ to the four-pion state, which agrees well with the actual four-pion data [4] between threshold (0.558 GeV) and 1.2 GeV. Beyond 1.2 GeV we expect other contributions, which decay to four pions, like $\omega\pi$, to be important. The $\pi\omega$ system has a threshold (921 MeV) close enough to the ρ mass (770 MeV) to yield contributions that do not simply follow the four-pion phase space. However, we leave this to future investigations, where systematically the many decay channels, e.g.: π^6, $\omega\pi$, $\rho\pi^2$ and $a_0\pi$, as predicted by the chiral lagrangian [2] between 900 MeV and 1.5 GeV are to be taken in account. Good exclusive data would yield independent tests on the importance of each of the discrete and the continuum states.

Second, if we consider the pion as an elementary particle, the initial state, as generated by the electroweak process, will be the discrete rho state. There is no direct coupling to the two-pion continuum, as this would lead to large amplitudes for large energies, while the actual two-pion data falls off for large energies. We are unable to get a very good fit for the data near threshold, within the model. We could improve the low-energy fit, if we dress the pions and allow for a direct electroweak-pion-pion coupling, but it would fail for higher energies [5]. There has been several suggestions [5, 6], based on chiral symmetry, how to improve the low-energy results. They all use a direct electroweak-pion-pion coupling, which violates unitarity for large energies, and would lead away from the clear separation of the continuum and the discrete part, where the pions are the asymptotic, but pointlike particles.

Third, the presence of the four-pion continuum changes the two-pion coupling constant. It is interesting to notice that the coupling constants have to be adjusted if additional, non-interacting channels are included. The competition between decay modes generates an effective final-state interaction. Fourth, the real part, after the on-shell renormalization, yields a negligible effect. Since, with on-shell renormalization, the real part vanishes when the energy equals the rho mass, the value of the real part is only small in the neighborhood of this value.

For the problem of the rho meson studied here we did not require the full machinery of the Fano theory. For example, there is only one discrete state in the system. In the case of a neutral rho meson the mixing with the ω meson could be taken into account explictly and unitarily. For the moment it has been more important to show that the two-pion and the four-pion continua describe the rho resonance well, where the four-pion continuum results in two independent observations: its effect on the two-pion decay, and a direct measurement of the four-pion decay of the rho meson. All this can be discussed at the level of *restricted Hamiltonians*. These Hamiltonians contain given states and continua which are expected to dominate the results, in this case a composite continuum consisting of two- and four-pion states in the rho channel, and the bare rho state. The fact that no further approximation is required allows one to draw definite conclusions, whether these states and continua actually dominate the physics in a certain channel and at a certain energy, or other degrees of freedom are deemed necessary. In this case the data between 0.6 GeV and 1.2 GeV is well-described by these degrees of freedom.

The Fano theory allows one to go further in particle numbers and complexity than other methods. Complex states can be build up hierarchically from admixing states in their expected order, similar to angular momentum coupling schemes in atomic physics.

Acknowledgments: I would like to thank Wim Ubachs for pointing me in the right direction on atomic physics, and Wolfram Weise and Rob Timmermans for useful and stimulating discussions. I also would like to thank Evgeni Kolomeitsev for pointing out useful references and reading material.

References

[1] U. Fano, Phys. Rev. **124**, 1866 (1961); S. M. Barnett and P. M. Radmore, *Methods in theoretical quantum optics*, (Oxford Press, Oxford, 1997).
[2] L. Banyai and V. Rittenberg, Phys. Rev. **184**, 1903 (1969).
[3] S. Anderson *et al.* (CLEO), Phys. Rev. D **61**, 112002 (2000).
[4] K. Ackerstaff *et al.* (OPAL), Eur. Phys. J. **C 7** 571 (1999).
[5] F. Klingl, N. Kaiser, and W. Weise, Z. Phys. **A 356**, 193 (1996).
[6] H. B. O'Connell *et al.*, Nucl. Phys. **A 623**, 559 (1997); M. Benayoun *et al.*, Z. Phys. **C 72**, 221 (1996).

Rare kaon decays with the NA48 experiment

M. Contalbrigo

Dipartimento di Fisica dell'Università di Ferrara, Via Paradiso 12, 44100 Ferrara, Italy

(Received: 31 October 2001)

Rare kaon decays provide interesting informations on low-energy dynamic of hadron interactions. Their phenomenology can be used to test the predictions of Chiral Perturbation Theory in the non-perturbative QCD sector. The latest results of NA48 rare kaon decay program based on 1998-1999 data taking will be presented: in particular the results on $K_L \to \pi^0\gamma\gamma$ and $K_S \to \gamma\gamma$ will be discussed. The NA48 future project aiming to search for rare kaon and hyperon decays is also briefly reviewed.

1 The NA48 experiment

The NA48 experiment is designed to measure the direct CP-violation effects in the neutral kaon decays into two pions [1]. It employs two simultaneous neutral kaon beams (a long and a short one) derived from 450 GeV/c protons extracted from the CERN SPS. The protons directed toward the target of the short beam are detected by an array of scintillation counters: the presence (absence) of a proton reconstructed in coincidence with (within ± 2 ns) the event tags the event as K_S (K_L).

The charged decays are measured by a magnetic spectrometer consisting of four drift chambers and a dipole magnet. The spatial resolution is 90 μm and the momentum resolution is $\frac{\sigma_\mathbf{P}}{\mathbf{P}} = \mathbf{0.5\% \oplus 0.009\% \cdot P}$ (P in GeV/c), where $\oplus$ means that the contributions are added in quadrature. A quasi-homogeneous liquid krypton electromagnetic calorimeter of 27 radiation lengths is used to measure the photons from neutral decays. The energy resolution is $\frac{\sigma(\mathbf{E})}{\mathbf{E}} = \frac{\mathbf{3.2\%}}{\sqrt{\mathbf{E}}} \oplus \frac{\mathbf{0.10}}{\mathbf{E}} \oplus \mathbf{0.5\%}$ (E in GeV) and the time resolution is better than 300 ps. The setup is completed by an hadron calorimeter, a muon detector and two hodoscope planes used for triggers. Seven counter rings consisting of plastic scintillators and iron converters detect photons which miss the calorimeter.

2 The NA48 rare decay program

The ϵ' setup described above was employed from 97 to 2001. In 2002 only the short beam will be used, with an about 400 times increased intensity, to study rare processes of K_S mode with high statistic [2]. The present results on K_S decays profit from dedicated runs taken in 99 and 2000, where the future K_S setup was successfully tested. Starting from 2003 two beams of K^+ and K^- will be provided for study direct CP violation effects and rare decays of the charged modes, [2].

The following table summarizes NA48 results based on the 97-99 data taking period, dividing them into three main subjects: tests of Chiral Perturbation Theory (χPT), CP-violating modes, and hyperon decays. The isospin amplitudes of the main $K \to 3\pi$ vertex [3], the $K_L \to \pi^0\gamma\gamma$ and $K_S \to \gamma\gamma$ decays (see next section), and the $K_L \to \gamma^{(*)}\gamma^{(*)}$ processes where the virtual photons convert into lepton pairs [3], lead to significant tests of the χPT predictions. Despite the extremely small branching ratio (about 10^{-12}), the $K_L \to \pi^0 e^+e^-$ decay may be one of the most sensitive probes to direct CP violation, [4]. In order to prove this feature one has to quantify both the CP conserving contribution from $\pi^0\gamma\gamma$ intermediate state and the indirect CP violating component via the related $K_S \to \pi^0 e^+e^-$ mode; moreover one has to study the $K_L \to e^+e^-\gamma\gamma$ background, which turns out to be irreducible when $m_{\gamma\gamma} \sim m_{\pi^0}$. In $K_{L,S} \to \pi^+\pi^-e^+e^-$ decays the lepton pair originates from an indirect CP-violating polarized photon only for K_L mode, [5]. This becomes visible as an asymmetry in the decay rate as a function of the angle between the planes containing the ee and $\pi\pi$ pairs. The sizeable number of hyperon neutral decays, provided by the short beam, can be used to get informations about the hyperon structure related to $SU(3)$ violation [6].

Decay mode	Events	Branching ratio	Parameter	Motivation
$K_L \to 3\pi^0$	$15 \cdot 10^6$		$h = (-6.1 \pm 1.0) \cdot 10^{-3}$	Dalitz quadratic slope
$K_L \to \pi^0\gamma\gamma$	2558	$(1.36 \pm 0.05) \cdot 10^{-6}$	$a_V = -0.46 \pm 0.05$	rate and vector coupling
$K_S \to \gamma\gamma$	149	$(2.58 \pm 0.42) \cdot 10^{-6}$		rate unambig. predicted
$K_L \to e^+e^-\gamma$	6864	$(1.06 \pm 0.05) \cdot 10^{-5}$	$\alpha_K^* = -0.36 \pm 0.06$	γ^* form factor
$K_L \to e^+e^-e^+e^-$	132	$(3.67 \pm 0.40) \cdot 10^{-8}$		γ^* form factor
$K_L \to e^+e^-\mu^+\mu^-$	19			γ^* form factor
$K_S \to \pi^0e^+e^-$	0	$< 1.4 \cdot 10^{-7}$		contribution to $K_L \to \pi^0 ee$
$K_L \to e^+e^-\gamma\gamma$	492	$(6.32 \pm 0.47) \cdot 10^{-7}$		background to $K_L \to \pi^0 ee$
$K_L \to \pi^+\pi^-e^+e^-$	1337	$(3.1 \pm 0.2) \cdot 10^{-7}$	$\mathcal{A}^{ee}_{\pi\pi} = (13.9 \pm 3.4)\%$	CPV γ^* polarization
$K_S \to \pi^+\pi^-e^+e^-$	921	$(4.3 \pm 0.4) \cdot 10^{-5}$	$\mathcal{A}^{ee}_{\pi\pi} = (-0.2 \pm 3.7)\%$	CPV γ^* polarization
$\Xi^0 \to \Lambda\gamma$	497	$(1.9 \pm 0.2) \cdot 10^{-3}$		
$\Xi^0 \to \Sigma^0\gamma$	374	$(3.7 \pm 0.5) \cdot 10^{-3}$		
$\Xi^0 \to \Sigma^+e^-\nu$	60			

3 $K_S \to \gamma\gamma$ and $K_L \to \pi^0\gamma\gamma$ decays

Since there are only neutrals in the final state of $K_S \to \gamma\gamma$ and $K_L \to \pi^0\gamma\gamma$ decays, the amplitude is zero at the leading order in the chiral expansion and there are no counterterms at $\mathcal{O}(p^4)$. Therefore the amplitudes are directly sensitive to the next to leading order of the chiral expansion and finite at that order.

$K_S \to \gamma\gamma$ decay. The NA48 result is based on the two-days test run taken during 99 with an high intensity short beam, Fig. 1. The kaon flux is estimated from the number of $K_S \to 2\pi^0$ and $K_L \to 3\pi^0$ decays. 149 ± 21 candidates are found corresponding to a branching ratio of $(2.58 \pm 0.36_{\rm stat} \pm 0.22_{\rm sys}) \times 10^{-6}$, whereas the χPT predicts a value of 2.3×10^{-6} with an error less than 10 % [7]. The analysis of the 40 times higher statistic collected during the 40-days test run in 2000 will allow more accurate checks of the agreement.

$K_L \to \pi^0\gamma\gamma$ decay. The χPT $\mathcal{O}(p^4)$ description predicts well the diphoton invariant mass ($m_{\gamma\gamma}$) spectrum, but deeply underestimates the decay rate. At $\mathcal{O}(p^6)$ one can reproduce the rate and the $m_{\gamma\gamma}$ spectrum adding the contribution from exchange of heavy mesons like the vector ones (ρ, ω, K^*) [8]. The price is that the calculation becomes dependent from the coupling constant a_V of the vector to the pseudo-scalar mesons, which is unknown [9]. Since the tail of the decay amplitude at low $m_{\gamma\gamma}$ values is sensitive to the a_V value, it provides a way to measure the coupling and fix the ambiguity for the branching ratio calculation. The NA48 result is based on the 98 and 99 ϵ' runs, where the kaon flux is estimated from the number of $K_L \to 2\pi^0$ decays. After the selection criteria, 2558 $K_L \to \pi^0\gamma\gamma$ candidate events are found with the residual background reduced to the small level of 3 %. The residual background from $K_L \to 2\pi^0$ and pile-up events is estimated directly from the data, using the tagged $K_S \to 2\pi^0$ events and the events with out-of-time clusters or with a center-of-gravity of the energy far from the beam axis. The $K_L \to 3\pi^0$ background only

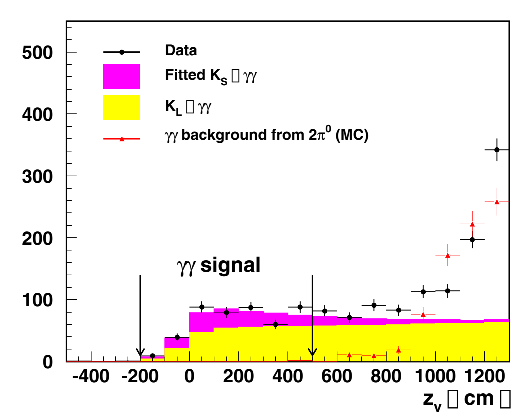

Figure 1: Distribution of the vertex position along the beam axis for the $K_{L,S} \to \gamma\gamma$ candidates. The $K_S \to \gamma\gamma$ branching ratio is measured in the first 5 meters after the target (corresponding to $z_V = 0$) where the $K_S \to 2\pi^0$ background is negligible. The $K_L \to \gamma\gamma$ component is estimated from the measured kaon flux and the known branching ratio.

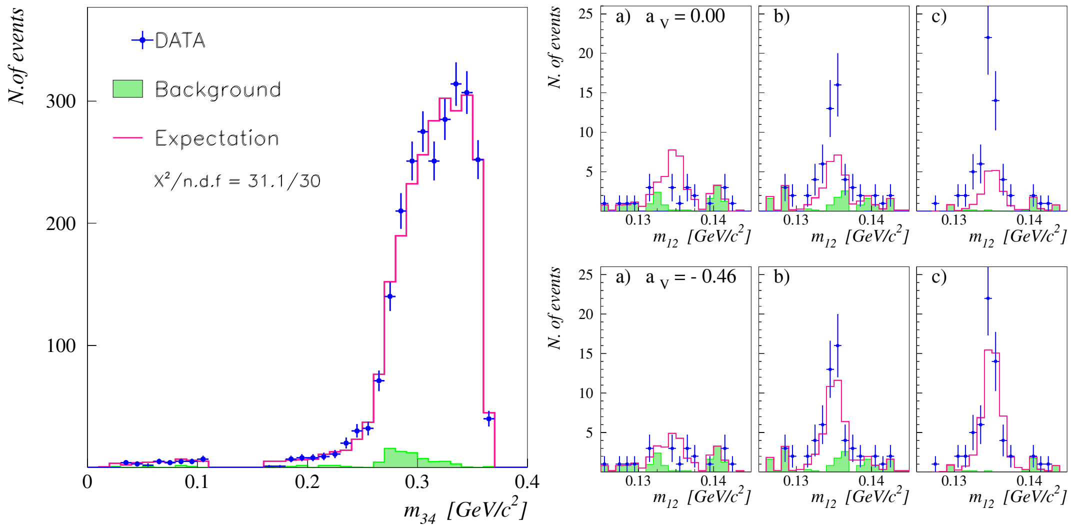

Figure 2: *Left:* $m_{\gamma\gamma}$ distribution of $K_L \to \pi^0\gamma\gamma$ candidates. *Right:* Data vs χPT expectations for no vector coupling (*top*) and fitted a_V (*bottom*). The signal peaking at the π^0-mass is shown in three intervals of the low $m_{\gamma\gamma}$ tail: a) $m_{\gamma\gamma} \in [30 \div 110]$; b) $m_{\gamma\gamma} \in [160 \div 240]$; c) $m_{\gamma\gamma} \in [240 \div 260]$ (all values in MeV/c^2).

is estimated from Monte Carlo simulation, generating a sample of K_L events which is comparable with the number of decays inside the fiducial volume of the experiment.

NA48 data clearly disfavor the case with no vector coupling, as shown in Fig. 2. The vector contribution leads to restore the agreement between the measured $(1.36 \pm 0.03_{\text{stat}} \pm 0.03_{\text{sys}} \pm 0.03_{\text{norm}}) \times 10^{-6}$ and the χPT predicted branching ratio, the latter being close to 1.2×10^{-6} for the fitted value of the vector coupling $a_v = -0.46 \pm 0.03_{\text{stat}} \pm 0.03_{\text{sys}} \pm 0.02_{\text{theo}}$. Since a non-zero vector coupling should give negligible effects on $K_S \to \gamma\gamma$, the $K_L \to \pi^0\gamma\gamma$ result does not affect the χPT expectations for this decay. Most interesting, NA48 result on a_V points to the hypothesis that the CP-violation effects are dominating the $K_L \to \pi^0 e^+ e^-$ mechanism. A useful cross check can be provided by the analysis of the $K_L \to e^+e^-\gamma$ and $K_L \to \mu^+\mu^-\gamma$ decays, because the form factor of the virtual gamma is sensitive to the vector coupling.

4 Conclusions

The NA48 rare decay program is providing interesting physics results in the field of χPT and CP violation in the neutral kaon sector. The program will continue with the 2002 high intensity K_S and hyperon run and with the 2003 charged kaon run.

References

[1] V. Fanti *et al*, *Phys. Lett.* B **465**, 335 (1999)

[2] R. Batley *et al*, CERN-SPSC-P-253-ADD-2; R. Batley *et al*, CERN-SPSC-P-253-ADD-3

[3] A. Lai *et al*, *Phys. Lett.* B **515**, 261 (2001); V. Fanti *et al*, *Phys. Lett.* B **458**, 553 (1999)

[4] J. F. Donoghue *et al*, *Phys. Rev.* D **51**, 2187 (1995); A. Lai *et al*, *Phys. Lett.* B **514**, 253 (2001)

[5] P. Heiliger *et al*, *Phys. Rev.* D **48**, 4146 (1993); A. Lai *et al*, *Phys. Lett.* B **496**, 137 (2000)

[6] V. Fanti *et al*, *Eur. Phys. J. C* **12**, 69 (2000)

[7] J. F. Donoghue, Private Communication; A. Lai *et al*, *Phys. Lett.* B **493**, 29 (2000)

[8] G.D. Barr *et al.*, *Phys. Lett.* B **284**, 440 (1992); A. Alavi-Harati *et al.*, *Phys. Rev. Lett.* **83**, 917 (1999)

[9] G. D'Ambrosio *et al*, *Nucl. Phys.* B **492**, 417 (1997); A.G. Cohen *et al*, *Phys. Lett.* B **304**, 347 (1993)

A new measurement of direct CP violation in the neutral kaon system

R. Fantechi[a], on behalf of the NA48 Collaboration

[a] *INFN - Sezione di Pisa*
Via Vecchia Livornese 1291, I56010, S. Piero a Grado, Italy

(Received: 29 October 2001)

The NA48 collaboration at CERN has recently announced a new measurement of the parameter ε'/ε which describes the direct CP violation contribution to the kaon to two pion decay. The analysis has been done with data from 1998 and 1999 runs, which yielded more than 3 million $K_L \to \pi^0\pi^0$ decays, allowing to reach an accuracy of $\pm 2.6\times 10^{-4}$. As a by-product of the systematic studies, a new measurement of the η mass has been obtained.

1 Introduction

CP violation was first reported in 1964 [1] with the detection of $\mathrm{K_L} \to \pi^+\pi^-$ decays. CP violation can occur via the mixing of CP eigenstates (indirect violation, represented by ε) and also in the decay process, through the interference of final states with different isospins (direct violation, represented by ε'). With three quark families, the CKM matrix [2] for the quark mixing contains a non trivial phase and this can give origin to both types of CP violation. Experimentally, it is convenient to measure the double ratio R related to $\mathrm{Re}(\varepsilon'/\varepsilon)$ by:

$$\mathrm{Re}(\varepsilon'/\varepsilon) \simeq \frac{1}{6}\left\{1 - \frac{\Gamma(\mathrm{K_L} \to \pi^0\pi^0)}{\Gamma(\mathrm{K_S} \to \pi^0\pi^0)} \Big/ \frac{\Gamma(\mathrm{K_L} \to \pi^+\pi^-)}{\Gamma(\mathrm{K_S} \to \pi^+\pi^-)}\right\} = \frac{1}{6}(1-\mathrm{R}) \ .$$

Experiments in the 1970s had shown that the dominant contribution to $K_L \to \pi\pi$ decay was due to indirect CP violation, while theoretical work indicated that direct CP violation in the SM could be large enough to be measurable. A first generation of precise experiments couldn't give a definitive answer about the existence of direct CP violation: NA31 [3] measured $\mathrm{Re}(\varepsilon'/\varepsilon) = (23.0\pm6.5)\times10^{-4}$, while the result of E731 [4], $\mathrm{Re}(\varepsilon'/\varepsilon) = (7.4\pm5.9)\times10^{-4}$, was compatible with no effect. A new generation of more precise experiments reported recently results from a first sample of data, confirming the existence of a direct CP violation component. NA48 [5] reported $\mathrm{Re}(\varepsilon'/\varepsilon) = (18.5\pm7.3)\times10^{-4}$ and KTEV [6] $\mathrm{Re}(\varepsilon'/\varepsilon) = (28.0\pm4.1)\times10^{-4}$.

This paper reports a measurement of $\mathrm{Re}(\varepsilon'/\varepsilon)$ performed by NA48, using data taken in 1998 and 1999, with a statistics seven time larger than the result published in 1997 [5].

2 The method

The measurement of $\mathrm{Re}(\varepsilon'/\varepsilon)$ with the precision of $\simeq 10^{-4}$ requires the collection of several million $\mathrm{K_L}$ and $\mathrm{K_S}$ decays. The design of the experiment as well as the analysis strategy are such as to minimize the systematic biases in the event counting, keeping them symmetric between at least two of the four decay modes. Most systematic errors drop out at first order in the double ratio.

All four modes are collected simultaneously, in order to be insensitive to time variations. Simultaneous $\mathrm{K_L}$ and $\mathrm{K_S}$ beams are produced from the same proton beams to two targets at different distances from the decay fiducial zone. The intensity of the two beams is such to have similar rates for $\mathrm{K_S}$ and $\mathrm{K_L}$ decays. Kaon spectra in the two beams are also about the same. The two beams are almost collinear and point to the centre of the detector. The acceptance for $\mathrm{K_L}$ and $\mathrm{K_S}$ are made almost identical by weighting each $\mathrm{K_L}$ decay by a factor equal to the ratio of $\mathrm{K_S}/\mathrm{K_L}$ decay rates as a function of proper time. Remaining differences are small and are corrected using Monte Carlo simulation.

K_S and K_L are distinguished using a tagging station, where the transit time of the protons directed to the K_S target is recorded and compared with the event time. As this method is used for both charged and neutral channels, only the differences in K_S misidentification probability affects the ratio R.

High resolution detectors perform an efficient background rejection. Residual contamination from unwanted kaon decays is estimated and subtracted. Several indipendent methods are used to evaluate the remaining uncertainties. Analysis is performed in twenty 5 GeV energy bins in the interval from 70 to 170 Gev, where the ratio of energy spectra is flat within a few percent.

3 The beam and the detector

A 450 GeV primary proton beam($\sim 1.5\times 10^{12}$ proton per pulse) from the CERN SPS hits, 126 meters upstream of the decay fiducial region, a Be target with an angle of incidence of 2.4 mrad wrt to the K_L beam axis. The charged component is swept away and the neutral beam is collimated and sent to the decay region, where only K_L survive. Part of the non interacting proton beam is directed onto a bent silicon crystal, where a fraction of the protons are channeled and deflected. This beam is then transported through the tagging station up to the K_S target, located 120 meters downstream of the K_L target and 7.2 mm above the K_L beam line. An anticounter is located at the exit of the K_S collimator and is used to define offline the beginning of the decay region for the K_S beam. Its sharp edge gives the geometrical reference to control the energy scale.

The key elements of the detector are the liquid krypton calorimeter and the magnetic spectrometer. The first is a quasi-homogeneous device with an active volume of $\sim$10 m^3; Cu-Be-Co ribbons define $\sim$13000 2cm$\times$2cm cells, pointing to the centre of the decay region. The calorimeter fully contains electro-magnetic showers with energies up to 100 Gev. The energy resolution is given by $\frac{\sigma(E)}{E} = \frac{3.2\%}{\sqrt{E}} \oplus \frac{9\%}{E} \oplus 0.42\%$ and the response is linear to about 0.1% in the range 5-100 Gev. For energies above 25 Gev, the position resolution is about 1 mm. The calorimeter gives a precise time information for neutral events, used with the tagging station time to distinguish K_L from K_S decays. The time resolution for $2\pi^0$ events is 220 ps.

The magnetic spectrometer is composed of 4 drift chambers located before and after a central dipole magnet. The integral of the magnetic field is 0.883 Tm, corresponding to a transverse momentum kick of 265 Mev/c in the horizontal plane. Each chamber is made up of four sets of two staggered sense wire planes oriented along four directions, to allow reconstruction without ambiguities and minimization of inefficiencies due to wire redundancy. The geometrical accuracy is better than 0.1 mm/m and the average plane efficiency is greater than 99%. High rate operation is guaranteed by the short drift distance (5mm i.e. 100ns). Track positions are reconstructed with a precision of 100 μm per view. The momentum resolution is $\sigma(P)/P \simeq 0.48\% \oplus 0.009\ P[\mathrm{GeV}/c]\ \%$ and the reconstructed mass resolution is 2.5 Mev/c^2. Time resolution of 0.7 ns is achieved on the event time.

A scintillator hodoscope provides the trigger for charged events and it is used offline to reconstruct the charged event time with a precision of $\sim$150 ps. A calorimeter made of iron and scintillator measures hadronic energy, contributing to the total energy trigger. Following the hadron calorimeter there are three walls of muon counters, providing timing information used offline to identify the background from $K_L \to \pi\mu\nu$ decays.

4 The statistics and the result

The result presented here has been obtained using data collected in 1998 and in 1999. The first set consists of 1.1 million $K_L \to \pi^0\pi^0$ collected in 135 days, while in 1999, after a considerable improvement of the DAQ system and in the efficiency and reliability of the detectors, 2.2 million

$K_L \rightarrow \pi^0\pi^0$ were collected in about the same time. The spectrometer magnetic field was regularly inverted to do systematics checks in the charged mode. Several special runs were taken regularly: with K_L only to check the alignment of the spectrometer, with K_S only to monitor tagging and neutral trigger inefficiencies. Checks of the LKr calorimeter performances were made using polyethylene targets exposed to a negative pion beam to produce π^0 and η in precisely defined vertex positions.

The analysis was performed by several independent groups and many checks were done for the stability of the result wrt the selection cuts.

$\pi^+\pi^-$ trigger inefficiency	-3.6	$\pm$ 5.2	Tagging inefficiency	—	$\pm$ 3.0
AKS inefficiency	+1.1	$\pm$ 0.4	Acceptance statistical	+26.7	$\pm$ 4.1
			Acceptance systematic		$\pm$ 4.0
Reconstruction of $\pi^0\pi^0$	—	$\pm$ 5.8	Accidental activity	—	$\pm$ 4.4
Reconstruction of $\pi^+\pi^-$	+2.0	$\pm$ 2.8			
Background to $\pi^0\pi^0$	-5.9	$\pm$ 2.0	Long term variations of K_S /K_L	—	$\pm$ 0.6
Background to $\pi^+\pi^-$	+16.9	$\pm$ 3.0			
Beam scattering	-9.6	$\pm$ 2.0			
Accidental tagging	+8.3	$\pm$ 3.4	**Total**	**+35.9**	**$\pm$ 12.6**

Systematic uncertainties (on R in 10^{-4})

The result for R, averaged over the twenty energy bins and with all corrections applied is R = (0.99098 $\pm$ 0.00101(stat) $\pm$ 0.00126(syst)), which translates in $\mathrm{Re}(\varepsilon'/\varepsilon)$ = (15.0 $\pm$ 1.7(stat) $\pm$ 2.1(syst))$\times$ 10^{-4}. The combined result, including the published 1997 result, is $\mathrm{Re}(\varepsilon'/\varepsilon)$ = (15.3 $\pm$ 2.6)$\times$ 10^{-4}.

5 A new measurement of the eta mass

Among the various checks of the liquid krypton calorimeter systematics using π^0 and η (see above), a study was performed using the decay $\eta \rightarrow 3\pi^0$, computing the η mass with the following method: the vertex position was estimated as the average of the 3 decay vertices of the 3 π^0 mass constraints and this vertex was used to compute the overall mass of the 6 photons. The advantages of this method are the cancellation of the energy and transverse scales and a mass resolution of $\sim$ 1 Mev.

The preliminary result for the η mass measurement is M_η = (547.823 $\pm$ 0.020(stat) $\pm$ 0.055 (syst)) Mev, $1^0/_{00}$ higher than the PDG value.

6 Conclusion

The NA48 experiment has measured the parameter $\mathrm{Re}(\varepsilon'/\varepsilon)$ in good agreement with the 1997 result and found it to be 5.9 sigmas different from zero, thus providing definitive evidence for direct CP violation in the neutral kaon two pion decay.

References

[1] J.H. Christenson *et al.*, Phys. Rev. Lett. **13**, 138 (1964).

[2] M. Kobayashi and K. Maskawa, Prog. Theor. Phys. **49**, 652 (1973).

[3] G. Barr *et al.*, Phys. Lett. **B 317**, 233 (1993).

[4] L.K. Gibbons *et al.*, Phys. Rev. Lett. **70**, 1203 (1993).

[5] V. Fanti *et al.*, Phys. Lett. **B 465**, 335-348 (1999).

[6] A. Alavi-Harati *et al.*, Phys. Rev. Lett. **83**, 22-27 (1999).

New results and future prospects of the spin structure of the nucleon as measured by HERMES

Michael Düren, on behalf of the HERMES Collaboration

II. Physikalisches Institut, Universität Giessen, 35392 Giessen, Germany

(Received: 13 September 2001)

Inclusive and semi-inclusive polarised deep inelastic scattering allows for the determination and separation of the spin contributions of the various quark flavours to the spin of the nucleon. Recent updates of polarised HERMES data are shown. The orbital angular momentum of the quarks is not accessible by inclusive data, however, it can be accessed by measuring GPDs in exclusive processes. To increase the sensitivity to GPDs, HERMES plans to build a large acceptance recoil detector.

1 Introduction

The HERMES experiment at DESY has been build to study the spin and flavour distributions of quarks in nucleons by inclusive and semi-inclusive scattering of 27.5 GeV electrons off free and bounded nucleons. Since 1995, HERMES has been taking data and produced various new and partially surprising results. Highlights are the measurement of the flavour asymmetry of the light quarks sea [1] in semi-inclusive unpolarised deep inelastic scattering (DIS), the measurements of the spin structure functions of proton and neutron in inclusive polarised DIS [2, 3] and the flavour separation of the quark spin distributions in semi-inclusive polarised DIS [4].

The measurements of the quark spin distributions Δq clearly show that only a fraction of the nucleon spin originates in the spin of the quarks. Major pieces of the spin structure of the nucleon are still in the dark. The helicity sum rule

$$\frac{1}{2} = \frac{1}{2}\left(\Delta u + \Delta d + \Delta s\right) + \Delta G + L_q + L_G \tag{1}$$

shows, that the most unknown pieces are the spin distribution of the gluon ΔG and the orbital angular momenta L_q and L_G of quarks and gluons. First measurement of ΔG from HERMES indicates a positive contribution [5], and future precision measurements of this quantity at COMPASS and RHIC are on the way. For years it has not been clear how to access the last missing parts of the nucleon spin, the orbital angular momentum contributions L_q and L_G of quarks and gluons. Only recently, Ji found a convincing way how to access the orbital angular momentum by using the concept of generalised parton distributions (GPDs) in exclusive lepton scattering processes [6].

2 Spin structure functions

A precision measurement of the spin structure function $g_1^d(x)$ of the deuteron has recently been extended to values of small x as shown in Figure 1 (left). The measurement at small values of the Bjorken scaling variable x is of special interest for the discussion about the determination of the Ellis-Jaffe and Bjorken sum rules. It has been argued that there might be a large increase of $g_1(x)$ at small values of x which might increase the values of the first moments [7]. In the x range of the new HERMES data this is obviously not the case [see Figure 1 (left)].

3 Polarised parton distributions

Figure 1 (right) shows the preliminary results of the most recent analysis for the flavour decomposition of the quark polarisation [8]. The up quarks are positively polarised with a polarisation up to 50% at large x, the down quarks are negatively polarised, and the sea quarks are compatible

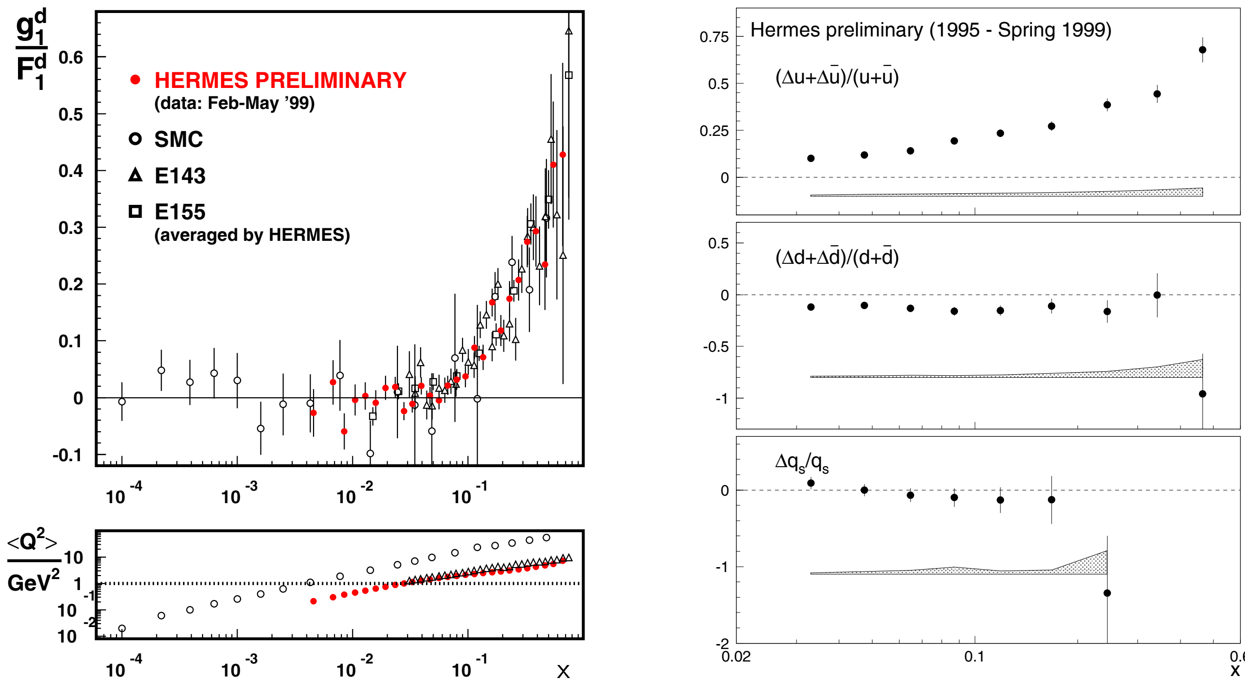

Figure 1: Left: Measurements of the spin structure function g_1/F_1 are shown as a function of the Bjorken scaling variable x. The results of the three data sets displayed are in agreement, even though the mean value of Q^2 is different by a factor of 10 (see left bottom figure). Right: The polarisation of up, down and sea quarks as a function of Bjorken x.

with being unpolarised. The sea polarisation has been extracted in this preliminary result under the assumption that the sea polarisation is the same for all flavours. In the new HERMES data, a RICH detector allows a positive identification of pions and kaons and this will enable HERMES to measure the polarisation of the $\bar{u}$, $\bar{d}$ and strange sea separately. Only then will it be known whether the violation of the Ellis-Jaffe sum rule is due to a violation of the $SU(3)_f$ symmetry or due to a large negative strange sea. In addition, HERMES will be able to investigate whether the polarisation of the up and down sea is the same or not.

4 Generalised parton distributions

As mentioned above, the concept of generalised parton distributions (GPDs) in exclusive lepton scattering processes can be used to access the orbital angular momentum L of quarks and gluons in nucleons. The total angular momentum density $J^q(x)$ of a quark flavour q is obtained according to [6]

$$J^q(x) = \frac{x}{2}\left[H^q(x,0,0) + E^q(x,0,0)\right]. \quad (2)$$

Here, H^q and E^q denote the generalised parton distributions. For details and first experimental results from HERMES see the contributions of B. Seitz and M. Hartig in this volume. GPDs are experimentally accessible by hard exclusive processes. The Feynman diagrams in Figure 2 illustrate why exclusive processes are such a powerful tool. The forward Compton amplitude of the left diagram corresponds to deep inelastic scattering. The handbag diagrams of DVCS (centre) and exclusive meson production (right) generalise the left diagram. In the left diagram, the quark which is picked up from the proton, has to be put back with the identical momentum fraction x. In the DVCS diagram the quark goes back to the proton with a modified momentum $x-\xi$, and in

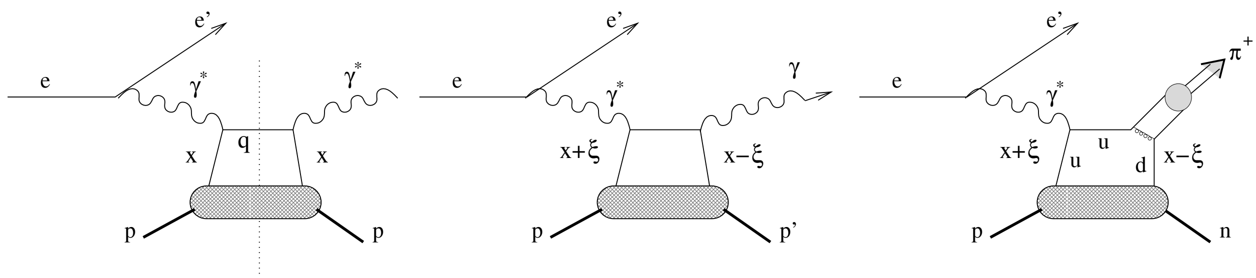

Figure 2: DIS corresponds to the imaginary part of the Compton forward amplitude of the left diagram. A small modification leads to the handbag diagrams for GPDs as measured in DVCS (centre) or exclusive meson production (right).

exclusive meson production it can even change flavour before it goes back to the nucleon. Hence, exclusive processes allow to measure additional information of the quark structure of the nucleon compared to DIS processes. The amplitudes of the diagrams are described by GPDs.

5 A large acceptance recoil detector

HERMES plans to do precision measurements of hard exclusive scattering processes. To improve the capabilities of the detector system to select exclusive events, HERMES plans to build a large acceptance recoil detector [9] which consists of the following parts:

1. a inner silicon detector for the measurement of large angle, low energy recoil protons,
2. a double layer of scintillating fibres to measure charged particles with larger momentum,
3. a superconducting solenoid magnet which delivers the magnetic field as required for the momentum determination, and
4. a detector to measure neutral pions and photons.

Starting data taking in 2004 with this detector, HERMES should be in the position to do first precise measurements of generalised parton distributions, using hard exclusive meson production and deeply virtual Compton processes.

References

[1] HERMES, K. Ackerstaff *et al.*, Phys. Rev. Lett. **81** (1998) 5519.

[2] HERMES, K. Ackerstaff *et al.*, Phys. Lett. **B404** (1997) 383.

[3] HERMES, A. Airapetian *et al.*, Phys. Lett **B442** (1998) 484.

[4] HERMES, K. Ackerstaff *et al.*, Phys. Lett. **B464** (1999) 123.

[5] HERMES, A. Airapetian *et al.*, Phys. Rev. Lett. **84** (2000) 2584.

[6] X. Ji, Phys. Rev. Lett. **78**, (1997) 610, Phys. Rev. **D55** (1997) 7114.

[7] E.g., F.E. Close, Proc. of XXVII Int. Conf. on High Energy Physics, Glasgow, July 20-27, 1994, eds. P.J. Bussey and I.G. Knowles, Vol. 2, p. 669.

[8] T. Lindemann, Proc. of 14th International Spin Physics Symposium (SPIN 2000), Osaka, Japan, Oct 16 - 21, (2000) to be published.

[9] HERMES Collaboration, "A large acceptance recoil detector for HERMES", DESY-PRC 01-01, HERMES 01-017.

Single spin asymmetries in exclusive electroproduction at HERMES

B. Seitz, on behalf of the HERMES Collaboration

Department of Physics, University of Alberta, Edmonton, Alberta T6G 2J1, Canada

(Received: 11 October 2001)

Single Spin Asymmetries in the hard electroproduction of real photons (DVCS) and π^+ mesons have been measured for the first time by HERMES. Sizeable asymmetries for DVCS using a polarized positron beam and an unpolarized hydrogen target have been observed. A large asymmetry using an unpolarized beam and a longitudinal polarized target has been observed in the exclusive electroproduction of π^+ mesons. Measurements of these reactions provide access to the presently unknown Generalized Parton Distributions (GPD) of the nucleon.

1 Introduction

Growing theoretical interest has recently surrounded the nature of the unknown Generalized Parton Distribution (GPD) functions of the nucleon which appear in the factorization scheme of hard exclusive processes. These GPDs are a natural generalization of the well known Parton Density Functions (PDF) in inclusive deep inelastic scattering. Generalized Parton Distributions were introduced in a formalism which provides a unified theoretical description of exclusive reactions in the Bjorken regime.

Most of the recent interest and activity in this field have been triggered by the observation of Ji [1], who showed that the second moment of these GPDs provides an access to the contribution of the spin and orbital angular momentum of the quarks to the nucleon spin (see [2] for a recent overview).

The most promising reaction to study these new distribution functions is the hard exclusive electroproduction of a real photon, known as Deeply Virtual Compton Scattering (DVCS). In addition, the hard exclusive production of pseudoscalar and vector mesons provides another way to access different GPDs.

The HERMES experiment at the HERA storage ring at DESY with its 27.5 GeV polarized positron beam and pure, polarized and unpolarized nucleon targets provides a unique environment to measure these reactions [3].

2 Deeply Virtual Compton Scattering

Deeply Virtual Compton Scattering provides the theoretically cleanest access to GPDs. Experimentally however, there is a second process, Bethe–Heitler (BH) which interferes with DVCS since it leads to an identical final state. This interference can be exploited in order to obtain information on the DVCS amplitudes directly. For that purpose HERMES has measured the beam–spin asymmetry in hard exclusive electroproduction of photons from a hydrogen target [4].

The leading order interference term that depends on the helicity of the incident lepton is

$$(\tau^*_{BH}\tau_{DVCS} + \tau^*_{DVCS}\tau_{BH})_{pol} \propto eP_{beam}\left[-\sin\phi\sqrt{\frac{1+\epsilon}{\epsilon}}Im\tilde{M}^{1,1}\right]. \tag{1}$$

The quantity $\tilde{M}^{1,1}$ is the linear combination of DVCS helicity amplitudes that contributes in the case of polarized beam and unpolarized target. The angle ϕ denotes the angle between the lepton scattering plane and the photon–hadron plane. The $\sin\phi$ moment of the asymmetry of this interference term with respect to the beam polarization provides information on the imaginary part of the DVCS amplitude combination $\tilde{M}^{1,1}$ which is related to GPDs.

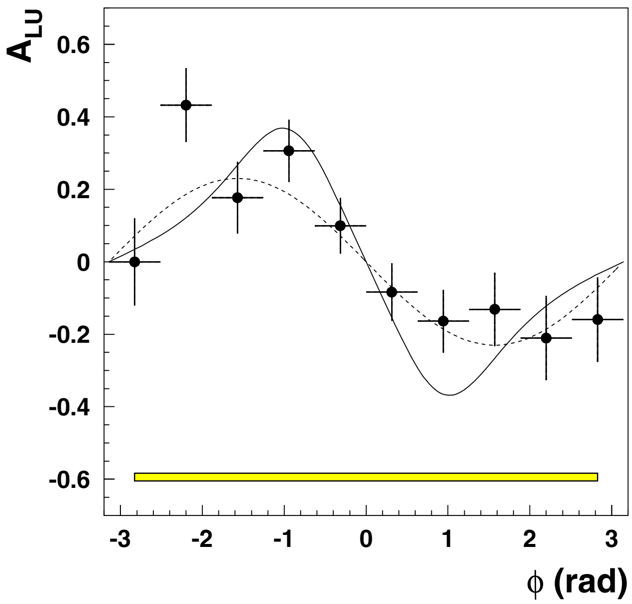

Figure 1: Beam–spin asymmetry A_{LU} for hard electroproduction of photons as a function of the azimuthal angle ϕ. The data correspond to the missing mass region between -1.5 and +1.7 GeV. The dashed curve represents a $\sin\phi$ dependence with an amplitude of 0.23, while the solid curve represents the result of a GPD calculation taken from [5]. The horizontal error bars represent the bin width and the error band below the systematic uncertainty.

DVCS events were identified by selecting events with only one positron track with momentum larger than 3.5 GeV, $Q^2 > 1$ GeV^2, $W^2 > 4$ GeV^2 and only one photon with an energy deposition greater than 0.8 GeV in the calorimeter. Exclusive events were selected via their missing mass. The azimuthal dependence of the measured beam–spin asymmetry A_{LU} defined as

$$A_{LU}(\phi) = \frac{1}{\langle|P_{beam}|\rangle} \frac{N^+(\phi) - N^-(\phi)}{N^+(\phi) + N^-(\phi)} \tag{2}$$

is shown in Fig. 1, where $N^\pm$ represent the luminosity normalized yields of events with corresponding beam helicity states $(+/-)$ and $\langle|P_{beam}|\rangle$ the average magnitude of the beam polarization. The comparison of these data with a simple $\sin\phi$–curve demonstrates that the data have the ϕ–dependence expected from Eq. 1. The GPD–model calculation of [5] computed at the average kinematics of the present experiment has also been displayed. The amplitude yields $A_{LU} = -0.23 \pm 0.04 \pm 0.03$. Another measurement at a much lower energy has confirmed our observations [6] but reporting a smaller single spin asymmetry..

3 Exclusive electroproduction of π^+ mesons

HERMES has furthermore measured the single spin asymmetry with unpolarized beam and longitudinally polarized hydrogen target in the exclusive production of π^+ mesons on the proton. Exclusive events were selected by requiring the missing mass of the reaction $e^+ + \vec{p} \to e^+ + \pi^+ + X$ to correspond to the nucleon mass. In order to take the resolution of the spectrometer into account, a subtraction of π^- mesons fullfilling the same kinematical criteria was performed. The ϕ dependence of the polarized cross section appears most clearly in the cross section asymmetry defined similar to Eq. 2 where P_{beam} gets replaced by the average longitudinal polarization of the target P_{target}.

This cross section asymmetry integrated over x, Q^2 and t is shown in Fig. 2. The data show a large asymmetry in the distribution of the azimuthal angle ϕ and a clear $\sin\phi$ dependence of the cross section. A fit to this dependence yields $A_{UL} = -0.18 \pm 0.05 \pm 0.01$ with a reduced χ^2 of 0.8. The quoted systematic uncertainty contains contributions due to a remaining asymmetry from semi–inclusive events as well as the uncertainty in the background yield and target polarization. Theoretical estimates of the observed asymmetry are not yet available. The asymmetry is

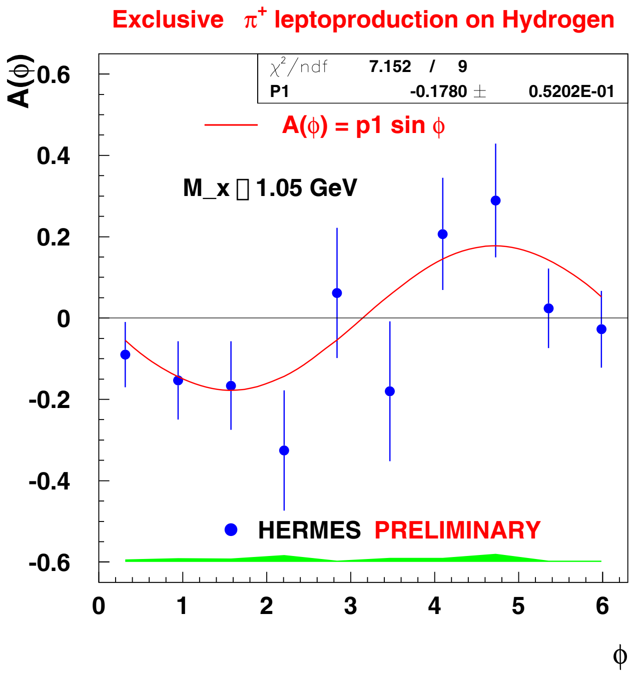

Figure 2: Cross section asymmetry $A_{UL}(\phi)$ averaged over x, Q^2 and t for the reaction $e^+ + \vec{p} \to e^+ + n + \pi^+$. The curve is the best fit to the data by $A(\phi) = A_{UL} \cdot \sin\phi$ where $A_{UL} = -0.18 \pm 0.05$ and the reduced χ^2 of the fit is 0.8. The error band below represents the combined systematic uncertainty.

surprisingly large and its sign is opposite to what can be expected from a transverse polarization component of the target with respect to the virtual photon. It has been suggested that the dominant contribution to the measured asymmetry is of higher twist [7].

4 Conclusion

Single spin asymmetries have been measured for exclusive processes at HERMES. For DVCS an asymmetry using a polarized positron beam and an unpolarized hydrogen target could be extracted. A clear $\sin\phi$ shape is visible and compares favorably with a calculation based on the GPD framework. Furthermore, a $\sin\phi$ asymmetry in the hard exclusive electroproduction of π^+ using a polarized hydrogen target and an unpolarized beam was observed.Presently no quantitative prediction for this asymmetry is available

The present data, in combination with new data expected from future HERMES measurements on a transversely polarized target [8], will provide one of the first tests of QCD factorization theorems for exclusive processes and will give access to GPDs.

References

[1] X. Ji, Phys. Rev. Lett. **78**, 610 (1997); Phys. Rev. **D 55**, 7114 (1997).

[2] K. Goeke, M. V. Polyakov, M. Vanderhaeghen, Prog. Part. Nucl. Phys. **47**, 401 (2001).

[3] See also contributions by M. Düren and M. Hartig in this volume.

[4] HERMES Collaboration, A. Airapetian *et al.*, Phys. Rev. Lett. **87**, 182001 (2001).

[5] N. Kivel *et al.*, Phys. Rev. **D 63**, 114014 (2001).

[6] S. Stepanyan *et al.*, hep–ex/0107043 and PRL in press.

[7] A. V. Belitsky, D. Müller, Phys. Lett. **B 513**, 349 (2001).

[8] W. D. Nowak (for the HERMES Collaboration), Talk given at DIS 2001, Bologna, Italy, 2001.

The FINUDA experiment: status and perspectives

M. Bertani, on behalf of the FINUDA Collaboration

Laboratori Nazionali di Frascati dell'INFN, Via E.Fermi 40, 00044 Frascati, Italy

(Received: 31 October 2001)

FINUDA is a hypernuclear physics experiment that will be carried out at DAΦNE, the e^+e^- ϕ-factory currently in operation at the INFN Frascati Laboratory. The apparatus, which is assembled in the DAΦNE hall, consists of a magnetic spectrometer with high resolution tracking capabilities. In this paper the status of the experiment is presented, together with the main features of the apparatus and of its physics program.

1 Introduction

An hypernucleus is a many-body system composed of conventional (non-strange) nucleons and one or more hyperons (Λ, Σ or Ξ). The presence of the strangeness degree of freedom in a hypernucleus adds a new dimension to the evolving picture of nuclear physics.

The FINUDA Collaboration [1] has a very ambitious program in hypernuclear physics including high statistics and high resolution spectroscopy, study of hypernuclear mesonic and non-mesonic decay modes, search for Σ-hypernuclei and neutron-rich hypernuclear states.

The peculiar idea of the FINUDA experiment is to stop the large flux of slow and monochromatic K^- (127 MeV/c) coming from the main ϕ decay $\Phi \to K^+K^-$ (49%) in thin nuclear targets ($0.1 \div 0.3\,\mathrm{g\,cm^{-2}}$) with minimum straggling. After degradation and nuclear capture Λ-hypernuclei are produced through the reaction

$$K^-_{stop} + \ {}^AZ \to \ {}^A_\Lambda Z + \pi^- \ , \tag{1}$$

and the spectroscopy of hypernuclear states can be performed by measuring the momentum of the isotropically emitted π^-. This feature provides unprecedented momentum resolution, as long as transparent detectors are employed before and after the target.

In the case of Λ hypernucleus formation, the following weak-interaction non mesonic decay modes of the Λ are strongly favored in medium-heavy nuclei,

$$\Lambda + n \to n + n \ , \qquad \Lambda + p \to n + p \ , \tag{2}$$

which are interesting for studying the validity of the empirical $\Delta I = 1/2$ rule.

The FINUDA magnetic spectrometer has the typical cylindrical geometry of collider experiments, therefore it is capable of detecting the π^- from hypernuclear formation, eq. 1, in coincidence with the products of the Λ decay, eq. 2. Up to now, this is a unique capability in the hypernuclear physics panorama.

2 The FINUDA spectrometer

FINUDA is a high resolution spectrometer ($\Delta p/p \simeq 0.3\%$ FWHM)with cylindrical geometry, characterized by a large solid-angle ($\sim 70\%$ of 4π), good triggering capabilities, state-of-the-art tracking, particle identification and neutron detection.

The apparatus, described in detail in [1, 2] and references therein, is sketched in fig. 1 and consists of an inner section surrounding the interaction region (beam pipe, thin scintillator counter barrel, 8-fold nuclear target, silicon microstrip detectors), an external tracker (low-mass planar drift

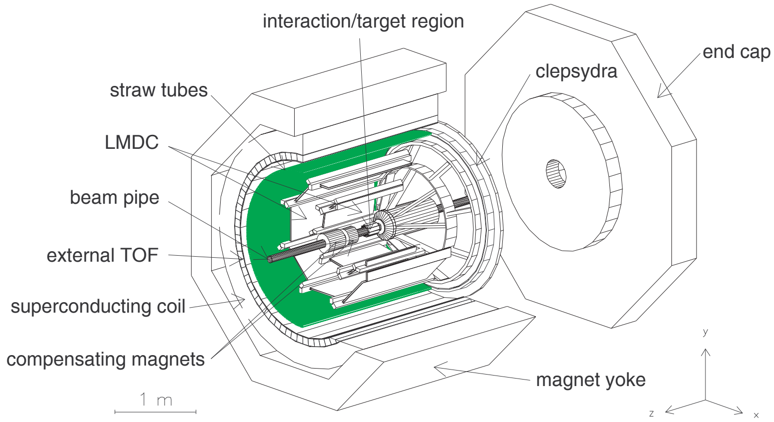

Figure 1: Layout of the FINUDA apparatus.

chambers (LMDC) and a straw tube array detector), an outer scintillator array and a superconducting solenoid providing a maximum magnetic field of 1.1 T. The whole tracking volume (8 m^3) is immersed in a He atmosphere to minimize Multiple Coulombian Scattering. The geometry of the spectrometer, the position of the detectors and the value of the maximum magnetic field have been optimized for maximizing the momentum resolution and acceptance for the prompt π^- from hypernuclear formation (eq. 1). For such π^- (250-280 MeV/c), a momentum resolution of 0.3%(FWHM) is obtained, corresponding to a resolution of 700 KeV in the hypernuclear energy levels.

3 The physics program: expected performances

FINUDA will investigate a wide physics program consisting both of hypernuclear spectroscopy and of hypernuclear decays [1, 3–5]. High statistics p-shell hypernuclear studies are foreseen: ${}^{12}_{\Lambda}C$, ${}^{7}_{\Lambda}Li$, ${}^{9}_{\Lambda}Be$, ${}^{10}_{\Lambda}B$ and the light hypernuclei ${}^{5}_{\Lambda}He$, ${}^{4}_{\Lambda}He$ and ${}^{4}_{\Lambda}H$ will be produced using a ${}^{6}Li$ target.

Fig. 2 (left side) shows the hypernuclear mass spectrum of ${}^{12}_{\Lambda}C$ recently measured by experiment E369 [6] at KEK with an energy resolution of 1.45 MeV (FWHM). An old spectrum form the previous E140 [7] experiment with an energy resolution of 1.9 MeV is superimposed in an arbitrary scale for comparison. This picture shows how the improvement in resolution is essential for the understanding of hypernuclear spectra. The E369 hypernuclear levels have been simulated with the FINUDA Monte Carlo and injected in the reconstruction program to test the physics performances of the apparatus. The result is a very clean spectrum with practically no background (right side of fig. 2): FINUDA with 700 KeV (FWHM) energy resolution may reveal finer splittings in the same hypernuclear spectra. The simulated spectrum corresponds to an integrated luminosity of $5\,\mathrm{pb}^-1$, that is about 2 days at the present DAΦNE luminosity, $3 \times 10^{31}\,\mathrm{cm}^{-2}\mathrm{s}^{-1}$.

Concerning the weak decay studies of hypernuclei, FINUDA has the opportunity of measuring with good accuracy the ratio Γ_n/Γ_p between the p-induced and n-induced hypernuclear weak decay amplitudes (eq. 2) which is related to the validity of the $\Delta I = 1/2$ rule. In fact there are indications [8] that the rule may be violated in the non mesonic decay modes. As it has already been noted, the hypernuclear formation and decay products can be measured in coincidence and within the same apparatus. This double capability of FINUDA spectrometer is up to now unique with respect to existing hypernuclear facilities.

Table 3 shows the expected FINUDA performances in hypernuclear high resolution spectroscopy and weak decay studies for the ${}^{12}_{\Lambda}C$ which is the best known hypernuclear system and can be used as a reference mark. The table refers an integrated luminosity of $50\,\mathrm{pb}^{-1}$, corresponding to about 20 days of data taking at the present DAΦNE luminosity and to a formation rate of the ${}^{12}_{\Lambda}C$ ground state of 10^{-3} per stopped K^-. The comparison with existing measurement (se-

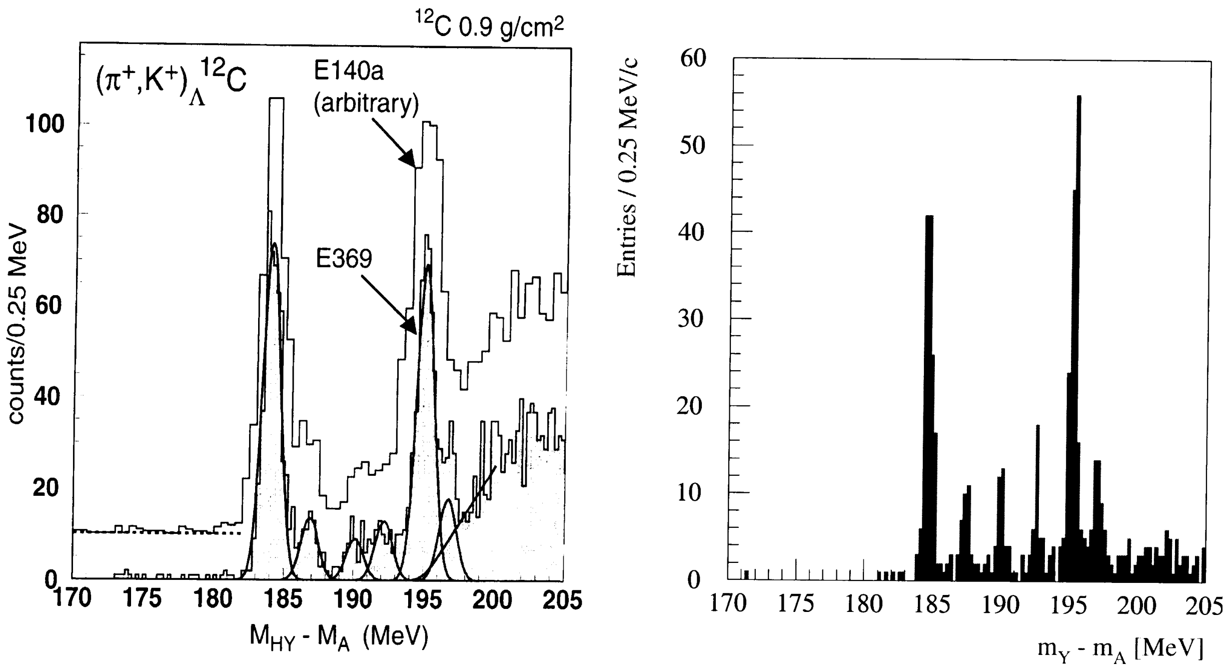

Figure 2: Left (from ref. [6]): hypernuclear mass spectrum of ${}^{12}_{\Lambda}C$ from KEK experiments E369 and previous E140a with energy resolution of 1.45 MeV and 1.9 MeV (FWHM) respectively. Right : FINUDA simulation of the E369 ${}^{12}_{\Lambda}C$ levels reconstructed with an energy resolution of 700 KeV (FWHM).

cond column of tab. 3) shows that, even with a reduced luminosity with respect to DAΦNE and FINUDA projects, FINUDA can in principle significantly lower the statistical error: in some cases the reduction is even of one order of magnitude. In particular the accuracy that will be reached in the Γ_p/Γ_n ratio measurement will hopefully allow to discriminate among different theoretical predictions.

4 Present status and future plans

DAΦNE [9], the e^+e^- Frascati ϕ-factory, has been designed to achieve high luminosity ($1 \div 5 \times 10^{32}\mathrm{cm}^{-2}\mathrm{s}^{-1}$) at the ϕ resonance energy (1.020 GeV) in two opposite interaction regions where the KLOE [10] and the DEAR [11] detectors are currently positioned. FINUDA spectrometer will take the place of DEAR in the second interaction region. DAΦNE commissioning started in 1998 and is now providing collisions to the KLOE and DEAR experiments with a maximum luminosity of about $3 \times 10^{31}\mathrm{cm}^{-2}\mathrm{s}^{-1}$.

FINUDA magnet is in the DAΦNE pit, next to the beam line, since 1998; all the subdetectors are ready and tested since 1999, they have all been installed and tested again inside the superconducting magnet during some machine shutdowns between the end of the year 2000 and August 2001. The roll-in of the apparatus in the second DAΦNE interaction region is scheduled for August 2002, and consequently data taking with colliding beams should finally start.

The FINUDA Collaboration plans to begin data taking using two sets of different nuclear targets, namely 4 ${}^{12}C$ and 4 ${}^{6}Li$ targets. The first set will be a sort of reference mark, being the ${}^{12}_{\Lambda}C$ the best known hypernuclear system, the second set will allow the study of the light hypernuclei ${}^{5}_{\Lambda}He$, ${}^{4}_{\Lambda}He$, and ${}^{4}_{\Lambda}H$ [4].

observable	B.R.(%) $^{12}_{\Lambda}C$ g.s.	collected event	stat. err. (%)
high resolution hypernuclear spectroscopy		11.2×10^3	
$\Gamma_{tot}/\Gamma_\Lambda$	1.25 ± 0.18 [12]	2.2×10^3	~ 2
$\Gamma_{\pi^-}/\Gamma_\Lambda$	$0.14 \pm 0.07 \pm 0.03$ [13]	7.0×10^2	~ 4
Γ_p/Γ_Λ	$0.31 \pm 0.07^{+0.11}_{-0.04}$ [13]		
only p detected		2.2×10^3	~ 2
both p and n detected		1.9×10^2	~ 7
Γ_n/Γ_Λ both n detected		96	~ 10
Γ_n/Γ_p	$1.87 \pm 0.59^{+0.32}_{-1.00}$ [13] $1.33^{+1.12}_{-0.81}$ [12] $0.59^{+0.17}_{-0.14}$ [14]		~ 10

Table 1: Finuda expected performances in hypernuclear spectroscopy and decay studies for $^{12}_{\Lambda}C$, for an integrated luminosity of $50\,\mathrm{pb}^{-1}$.

5 Conclusions

A powerful spectrometer for high quality hypernuclear studies is ready to start taking data at the Frascati DAΦNE ϕ-factory. It is scheduled to be rolled in the machine second interaction region in August 2002. As shown in table 3, even with a reduced luminosity with respect to DAΦNE and FINUDA designs, FINUDA can give world class results in hypernuclear spectroscopy and weak decay measurements thus allowing to discriminate among the different theoretical predictions.

References

[1] The FINUDA Collaboration (M. Agnello *et al.*), *"FINUDA a detector for nuclear physics at DAΦNE"*, LNF-93/021(IR) (1993), *"FINUDA technical report"*, LNF-95/024(IR) (1995).

[2] P. Gianotti the FINUDA Collaboration, Nucl. Phys. A**691**, 483 (2001).

[3] M. Bertani for the FINUDA Collaboration,*"Proceedings of the International Conference on e^+e^- Collisions from ϕ to J/Ψ*, Edited by G.V. Fedotovich and S.I. Redin, BINP, 167 (2000).

[4] A. Feliciello on behalf of the FINUDA Collaboration, Nucl. Phys. A**691**, 170 (2001).

[5] V. Paticchio on behalf of the FINUDA Collaboration, Nucl. Phys. A**691**, 119 (2001).

[6] T. Nagae, Nucl. Phys. A**670**, 269 (2000) .

[7] T. Hasegawa et al, Phys. Rev. C**53**, 1210 (1996).

[8] R.A. Shumacher, Nucl. Phys. Lett. B**547**, 143 (1992), A. Parreno et al, Phys. Rev. B**435**, 1 (1998).

[9] G. Vignola *Workshop on Physics and Detectors for DAΦNE*, ed. G. Pancheri, INFN-LNF, 11 (1991); S. Guiducci *et al.*, *"Status Report on DAFNE"*, presented at PAC2001, Chicago (2001).

[10] KLOE Collaboration, LNF-93/002(IR) (1993), LNF-94/028(IR) (1994).

[11] DEAR Collaboration, LNF-95/055(IR) (1995).

[12] J.J. Szymansky *et al.*,Phys. Rev. C**43**, 849 (1991).

[13] H. Noumi *et al.*, Phys. Rev. C**52**, 2936 (1995).

[14] A. Montwill *et al.*, Nucl. Phys. A **234**, 413 (1974).

A determination of the nucleon tensor charge

Leonard Gamberg[a] and Gary R. Goldstein[b]

[a] *Department of Physics and Astronomy, University of Pennsylvania, Philadelphia, PA, U.S.A.*
[b] *Department of Physics and Astronomy, Tufts University, Medford, MA, U.S.A.*

(Received: 8 November 2001)

Exploiting an approximate phenomenological symmetry of the $J^{PC} = 1^{+-}$ light axial vector mesons and using pole dominance, we calculate the flavor contributions to the nucleon tensor charge. The result depends on the decay constants of the axial vector mesons and their couplings to the nucleons.

1 Introduction

The spin composition of the nucleon has been intensely studied and has produced important and surprising insights, beginning with the revelation that the majority of its spin is carried by quark and gluonic orbital angular momenta and gluon spin rather than by quark helicity [1,2]. In addition, considerable effort has gone into understanding, predicting and measuring the transversity distribution, $h_1(x)$, of the nucleon [3]. *Transversity*, as combinations of helicity states, $|\perp/\top>\sim(|+>\pm|->)$, for the moving nucleon is a variable introduced originally by Moravcsik and Goldstein [4] to reveal an underlying simplicity in nucleon–nucleon spin dependent scattering amplitudes. In their analysis of the chiral odd distributions, Jaffe and Ji [5] related the first moment of the transversity distribution to the flavor contributions of the nucleon tensor charge: $\int_0^1 (\delta q^a(x) - \delta\overline{q}^a(x))\, dx = \delta q^a$ (for flavor index a). This leading twist transversity distribution function, $\delta q^a(x)$, is as fundamental to understanding the spin structure of the nucleon as its helicity counterpart $\Delta q^a(x)$. However, while the latter in principle can be measured in hard scattering processes, the transversity distribution (and thus the tensor charge) decouple at leading twist in deep inelastic scattering since it is chiral odd. Additionally, the non-conservation of the tensor charge makes it difficult to predict. While bounds placed on the leading twist quark distributions through positivity constraints suggest that they satisfy the inequality of Soffer [6], there are no definitive theoretical predictions for the tensor charge. In contrast to the axial vector isovector charge, no sum rule has been written that enables a clear relation between the tensor charge and a low energy measurable quantity. Among the various approaches, from the QCD sum rule to lattice calculations models [7], there appears to be a range of expectations and a disagreement concerning the sign of the down quark contribution. We present a new approach to calculate the tensor charge that exploits the approximate mass degeneracy of the light axial vector mesons ($a_1(1260)$, $b_1(1235)$ and $h_1(1170)$) and uses pole dominance to calculate the tensor charge [8, 9]. Our motivation stems in part from the observation that the tensor charge does not mix with gluons under QCD evolution and therefore behaves as a non-singlet matrix element. In conjunction with the fact that the tensor current is charge conjugation odd (it does not mix quark-antiquark excitations of the vacuum, since the latter is charge conjugation even) suggests that the tensor charge is more amenable to a valence quark model analysis.

2 The tensor charge and pole dominance

The flavor components of the nucleon tensor charge are defined from the forward nucleon matrix element of the tensor current,

$$\langle P, S_T\big|\overline{\psi}\sigma^{\mu\nu}\gamma_5\frac{\lambda^a}{2}\psi\big|P, S_T\rangle = 2\delta q^a(\mu^2)(P^\mu S_T^\nu - P^\nu S_T^\mu) \ . \tag{1}$$

We adopt the model that the nucleon matrix element of the tensor current is dominated by the lowest lying axial vector mesons

$$\langle P, S_T \left| \overline{\psi} \sigma^{\mu\nu} \gamma_5 \frac{\lambda^a}{2} \psi \right| P, S_T \rangle = \lim_{k^2 \to 0} \sum_{\mathcal{M}} \frac{\langle 0 | \overline{\psi} \sigma^{\mu\nu} \gamma_5 \frac{\lambda^a}{2} \psi | \mathcal{M} \rangle \langle \mathcal{M}, P, S_T | P, S_T \rangle}{M_{\mathcal{M}}^2 - k^2} . \tag{2}$$

The summation is over those mesons with quantum numbers, $J^{PC} = 1^{+-}$ that couple to the nucleon via the tensor current; namely the charge conjugation odd axial vector mesons – the isoscalar $h_1(1170)$ and the isovector $b_1(1235)$. To analyze this expression in the limit $k^2 \to 0$ we require the vertex functions for the nucleon coupling to the h_1 and b_1 meson and the corresponding matrix elements of the meson decay amplitudes which are related to the meson to vacuum matrix element via the quark tensor current. The former yield the nucleon coupling constants $g_{\mathcal{M}NN}$ and the latter yield the meson decay constant $f_{\mathcal{M}}$. Taking a hint from the valence interpretation of the tensor charge, we exploit the phenomenological mass symmetry among the lowest lying axial vector mesons that couple to the tensor charge; we adopt the spin-flavor symmetry characterized by an $SU(6) \otimes O(3)$ [10] multiplet structure. Thus, the 1^{+-} h_1 and b_1 mesons fall into a $(35 \otimes L = 1)$ multiplet that contains $J^{PC} = 1^{+-}, 0^{++}, 1^{++}, 2^{++}$ states. This analysis enables us to relate the a_1 meson decay constant measured in $\tau^- \to a_1^- + \nu_\tau$ decay [11], $f_{a_1} = (0.19 \pm 0.03)\mathrm{GeV}^2$, and the $a_1 NN$ coupling constant $g_{a_1 NN} = 7.49 \pm 1.0$ (as determined from a_1 axial vector dominance for longitudinal charge as derived in [12] but using $g_A/g_V = 1.267$ [13]) to the meson decay constants and coupling constants. We find

$$f_{b_1} = \frac{\sqrt{2}}{M_{b_1}} f_{a_1} \ , \qquad g_{b_1 NN} = \frac{5}{3\sqrt{2}} g_{a_1 NN} \ , \tag{3}$$

where the 5/3 appears from the $SU(6)$ factor $(1 + F/D)$ and the $\sqrt{2}$ arises from the $L = 1$ relation between the 1^{++} and 1^{+-} states. Our resulting value of $f_{b_1} \approx 0.21 \pm 0.03$ agrees well with a sum rule determination of 0.18 ± 0.03 [14]. The h_1 couplings are related to the b_1 couplings via $SU(3)$ and the $SU(6)$ F/D value,

$$f_{b_1} = \sqrt{3} f_{h_1} \ , \qquad g_{b_1 NN} = \frac{5}{\sqrt{3}} g_{h_1 NN} \ . \tag{4}$$

For transverse polarized Dirac particles, $S^\mu = (0, S_T)$ these values, in turn, enable us to determine the isovector and isoscalar parts of the tensor charge,

$$\delta q^v = \frac{f_{b_1} g_{b_1 NN} \langle k_\perp^2 \rangle}{\sqrt{2} M_N M_{b_1}^2} \ , \qquad \delta q^s = \frac{f_{h_1} g_{h_1 NN} \langle k_\perp^2 \rangle}{\sqrt{2} M_N M_{h_1}^2} \ , \tag{5}$$

respectively (where, $\delta q^v = (\delta u - \delta d)$, and $\delta q^s = (\delta u + \delta d)$). Transverse momentum appears in these expressions because the tensor couplings involve helicity flips that carry kinematic factors of 3-momentum transfer, as required by rotational invariance. The squared 4-momentum transfer of the external hadrons goes to zero in Eq. (2), but the quark fields carry intrinsic transverse momentum. This intrinsic $k_\perp$ of the quarks in the nucleon is determined from Drell-Yan processes and from heavy vector boson production.

3 Mixing

In relating the $b_1(1235)$ and $h_1(1170)$ couplings in Eq. (4) we assumed that the latter isoscalar was a pure octet element, $h_1(8)$. Experimentally, the higher mass $h_1(1380)$ was seen in the $K + \bar{K} + \pi' s$

decay channel [13,15] while the $h_1(1170)$ was detected in the multi-pion channel [13,16]. This decay pattern indicates that the higher mass state is strangeonium and decouples from the lighter quarks – the well known mixing pattern of the vector meson nonet elements ω and ϕ. If the h_1 states are mixed states of the $SU(3)$ octet $h_1(8)$ and singlet $h_1(1)$ analogously, then it follows that

$$f_{h_1(1170)} = f_{b_1} \ , \qquad g_{h_1(1170)NN} = \frac{3}{5} g_{b_1 NN} \ , \tag{6}$$

with the $h_1(1380)$ not coupling to the nucleon (for $g_{h_1(1)NN} = \sqrt{2} g_{h_1(8)NN}$). These symmetry relations yield the results

$$\delta u(\mu^2) = (0.58 \text{ to } 1.01) \pm 0.20 \ , \qquad \delta d(\mu^2) = -(0.11 \text{ to } 0.20) \pm 0.20 \ . \tag{7}$$

These values are similar to several other model calculations: from the lattice; to QCD sum rules; the bag model; and quark soliton models [7]. The calculation has been carried out at the scale $\mu \approx 1$ GeV, which is set by the nucleon mass as well as being the mean mass of the axial vector meson multiplet. The appropriate evolution to higher scales (wherein the Drell-Yan processes are studied) is determined by the anomalous dimensions of the tensor charge [17] which is straightforward but slowly varying.

It is interesting to observe that the symmetry relations that connect the b_1 couplings to the a_1 couplings in Eq. (3) can be used to relate directly the isovector tensor charge to the axial vector coupling g_A. This is accomplished through the a_1 dominance expression for the isovector longitudinal charges derived in [12],

$$\Delta u - \Delta d = \frac{g_A}{g_V} = \frac{\sqrt{2} f_{a_1} g_{a_1 NN}}{M_{a_1}^2} \ . \tag{8}$$

Hence for δq^v we have

$$\delta u - \delta d = \frac{5}{6} \frac{g_A}{g_V} \frac{M_{a_1}^2}{M_{b_1}^2} \frac{\langle k_\perp^2 \rangle}{M_N M_{b_1}} \ , \tag{9}$$

It is important to realize that this relation can hold at the scale wherein the couplings were specified, the meson masses, but will be altered at higher scales (logarithmically) by the different evolution equations for the Δq and δq charges. To write an analogous expression for the isoscalar charges $(\Delta u + \Delta d)$ would involve the singlet mixing terms and gluon contributions, as Ref. [12] considers. However, given that the tensor charge does not involve gluon contributions (and anomalies), it is expected that the relation between the h_1 and b_1 couplings in the same $SU(3)$ multiplet will lead to a more direct result

$$\delta u + \delta d = \frac{3}{5} \frac{M_{b_1}^2}{M_{h_1}^2} \delta q^v \ , \tag{10}$$

for the ideally mixed singlet-octet $h_1(1170)$. These relations are quite distinct from other predictions.

In conclusion, our axial vector dominance model with $SU(6)_W \otimes O(3)$ coupling relations provide simple formulae for the tensor charges. This simplicity obscures the considerable subtlety of the (non-perturbative) hadronic physics that is summarized in those formulae. We obtain the same order of magnitude as many other calculation schemes. These results support the view that the underlying hadronic physics, while quite difficult to formulate from first principles, is essentially a 1^{+-} meson exchange process. Forthcoming experiments will begin to test this notion.

Acknowledgment: This work is supported in part by Grant No. DE-FG02-92ER40702 from the U.S. Department of Energy.

References

[1] J. Ashman *et al.* Nucl. Phys. **B328**, 1 (1989); B. Adeva *et al.*, Phys. Lett. B **302**, 533 (1993); P.L. Anthony *et al.*, Phys. Rev. Lett. **71**, 959 (1993) ; K. Abe *et al.*, Phys. Rev. Lett. **72**, 25 (1995).

[2] X. Ji, Phys. Rev. Lett **78**, 610 (1997).

[3] V. Barone , A. Drago and P. G. Ratcliffe, arXive: hep-ph/0104283 and references contained therein .

[4] G.R. Goldstein and M.J. Moravcsik, Ann. Phys. (NY) **98**, 128 (1976); Ann. Phys. (NY) **142**, 219 (1982); Ann. Phys. (NY)**195**, 213 (1989).

[5] R. L. Jaffe and X. Ji, Phys. Rev. Lett. **67**, 552 (1991); Nucl. Phys. **B375**, 527 (1992).

[6] J. Soffer, Phys. Rev. Lett. **74**, 1292 (1995); G. R. Goldstein, R. L. Jaffe and X. Ji, Phys. Rev. D **52**, 5006 (1995).

[7] H. He and X. Ji, Phys. Rev. D **52**, 2960 (1995); Phys. Rev. D **54**, 6897 (1996); S. Aoki, *et al.*, Phys. Rev. D **56**, 433 (1997); L. Gamberg, H. Reinhardt and H. Weigel, Phys. Rev. D **58**, 054014 (1998); L. Gamberg, "Structure Functions and Chiral Odd Quark Distributions in the NJL Soliton Model of the Nucleon", Proceedings of Future Transversity Measurements, RIKEN-BNL Workshop (2000).

[8] L. Gamberg and G. R. Goldstein, arXive: hep-ph/0106178.

[9] L. Gamberg and G. R. Goldstein, arXive: hep-ph/0107176, to appear in Phys. Rev. Lett. .

[10] B. Sakita, Phys. Rev. **136**, B1756 (1964); F. Gürsey and L.A. Radicati, Phys. Rev. Lett. **13**, 173 (1964).

[11] W.-S. Tsai, Phys. Rev. D **4**, 2821 (1971).

[12] M. Birkel and H. Fritzsch, Phys. Rev. D **53**, 6195 (1996).

[13] D.E. Groom, *et al.* (Particle Data Group), Eur. Phys. Jour. **C15**, 1 (2000).

[14] V.M. Belyaev and A. Oganesian , Phys. Lett. **B395**, 307 (1997).

[15] A. Abele, *et al.*, Phys. Lett. **B415**, 280 (1997); D. Aston, *et al.*, Phys. Lett. **B201**, 573 (1988).

[16] A. Ando, *et al.*, Phys. Lett. **B291**, 496 (1992); and references contained therein.

[17] X. Artu and M. Mekhfi, Z. Phys. **C45** (1990) 669.

Phenomenological analysis of experimental data on η-photoproduction on protons

E. M. Leikin, E. V. Balandina, and N. P. Yudin

Skobeltsyn Institute of Nuclear Physics, Moscow State University, Moscow, Russia

(Received: 18 September 2001)

The results of linear regression of differential cross sections, Σ-, and T-asymmetries of η-photoproduction on protons in the energy region from threshold up to 1 GeV are presented. Serious contradictions between angular distributions measured in different laboratories are revealed. The energy dependence of regression coefficients may be due to the transition from the energy region of the $S_{11}(1535)$ and $D_{13}(1520)$ to the energy region of the $D_{15}(1675)$ and $F_{15}(1680)$ resonances.

During the past years η-photoproduction on protons has attracted increasingly high interest. This is due not only because this item is a new physical phenomenon different from photoproduction of pions but mainly because η-photoproduction should proceed through the small number of nucleon resonances. Even in energy region up to 1 GeV there will be not too many overlapping resonances that permits to extract reliable information on resonance parameters from experimental data.

Complete phenomenological analysis of experimental data on photoproduction, as a rule, encounters a number of problems, e.g. solving of nonlinear equations, removal of continuous and discrete theoretical ambiguities, elimination of experimental ambiguities, etc. Analysis of experimental data may be naturally divided in two stages [1]. The first is the linear regression which provides the information about the number of partial waves that contribute to the measured experimental characteristics of process and provides information on the resonances concerned. The linearity of the model used ensures that the estimates of regression coefficients are unbiased. The second is to determine the multipole amplitudes.

This paper is confined to the first stage of the analysis. We have analyzed all known experimental data on differential cross sections (angular distributions) of process $\gamma p \to \eta p$ [2–4], and also the data on polarization observables, i.e. angular distributions of asymmetry Σ, measured with linear polarized beam [5] and angular distributions of asymmetry T, measured on a polarized target [6]. The energy independent analyses consist in expanding angular distributions of the observables at definite energy using Legendre polynomials. To find how many terms in this expansion provide the best description of data standard statistical procedures including the Fisher criterion were used. Unlike the energy dependent analysis that is based on parametric models and, generally, gives biased estimates, energy independent analysis relies on nonparametric model that provides unbiased estimates. Expansion of the observables and corresponding statistics are:

$$\frac{k}{q}\frac{d\sigma(\theta)}{d\Omega} = \sum a_n P_n(\cos\theta) \; , \tag{1a}$$

$$\frac{k}{q}\frac{d\sigma}{d\Omega}\frac{1}{\sin^2\theta}\Sigma = \sum b_n P_n(\cos\theta) \; , \tag{1b}$$

$$\frac{k}{q}\frac{d\sigma}{d\Omega}\frac{1}{\sin\theta}T = \sum c_n P_n(\cos\theta) \; . \tag{1c}$$

Multipole decomposition of coefficients $a_n,\ b_n,\ c_n$ up to terms E_{3-} and M_{3-} may be found in [7]. In all cases the best description of experimental data on $d\sigma/d\Omega$ were obtained with three terms of the expansion. The dominance of s-wave, the coefficient a_0, was already pointed out [2,8]. However, the coefficients a_1 and a_2 connected, correspondingly, with the sp- and sd-interferences demonstrate the existence of serious contradictions between the results in [2–4]. This is also displayed by Fig. 1. Since the observables $d\sigma/d\Omega$, Σ, T were measured at different energies and angles to form the statistics with Σ and T we used interpolated values of $d\sigma/d\Omega$. The polarization statistics Σ and T were analyzed with both $d\sigma/d\Omega$ obtained in the same laboratory and $d\sigma/d\Omega$ from another laboratories.

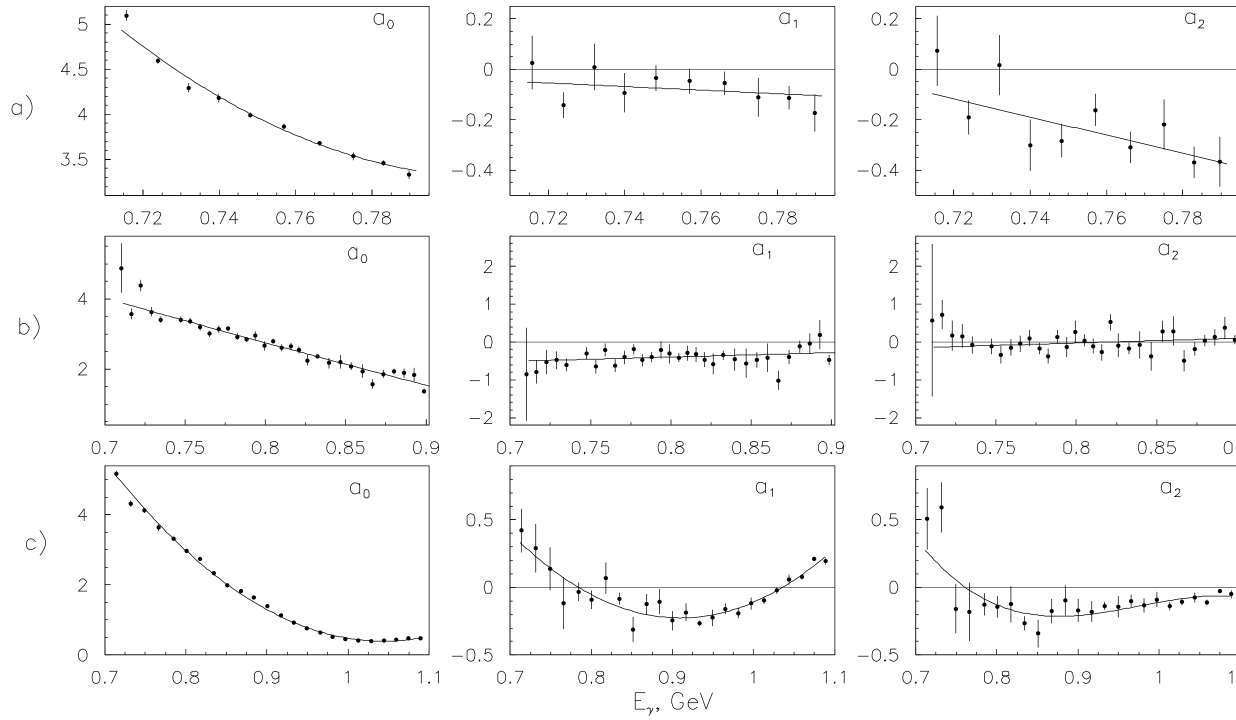

Figure 1: Coefficients a_0, a_1, a_2 in expansion (1a). Data are taken (a) from Ref. [2], (b) from Ref. [3], and (c) from Ref. [4]; lines show the results of the fit.

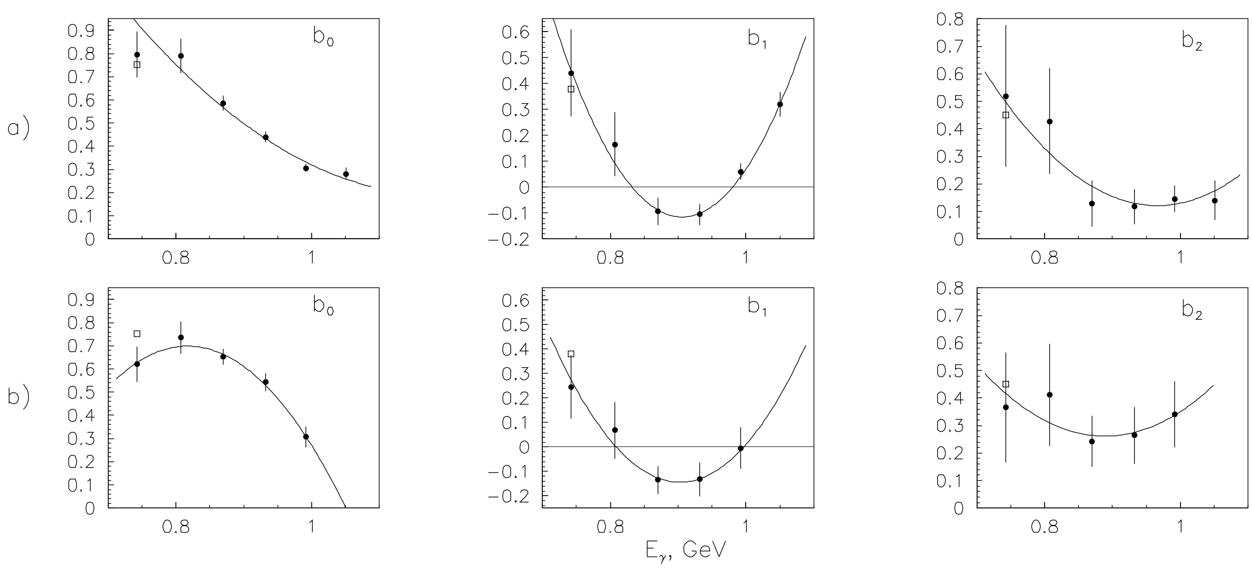

Figure 2: Coefficients b_0, b_1, b_2 in expansion (1b). Data for Σ are taken from Ref. [5]. (a) $d\sigma/d\Omega$ from Ref. [4], (b) $d\sigma/d\Omega$ from Ref. [3]. Square symbols: $d\sigma/d\Omega$ from Ref. [2].

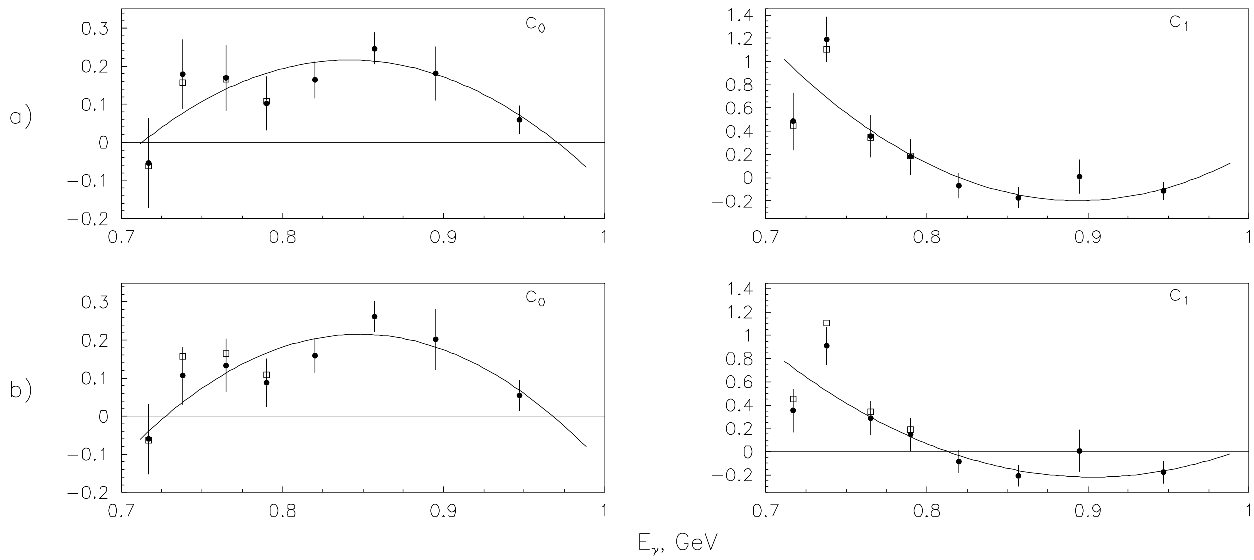

Figure 3: Coefficients $c_0,\ c_1$ in expansion (1c). Data for T are taken from Ref. [6]. (a) $d\sigma/d\Omega$ from Ref. [4], (b) $d\sigma/d\Omega$ from Ref. [3]. Square symbols: $d\sigma/d\Omega$ from Ref. [2].

To get the description of $\Sigma(\theta)$ it was necessary to keep three terms in the expansion. For $T(\theta)$ it was sufficient to keep two terms. The energy dependence of b_n and c_n is shown in Figs. 2 and 3. Contradictions between angular distributions obtained in different laboratories are not reflected in the general behavior of the coefficients b_n and c_n. In other words, these contradictions between $d\sigma/d\Omega$ do not appear in polarization observables.

It seems to be instructive to consider the energy behavior of the coefficients a_1, b_1, b_2 and c_0, c_1. The change of energy dependence of this coefficients at 0.9 GeV might indicate the change of regime of the process. For instance, the decrease of a_1 [4] from the threshold to 0.9 GeV may be due to the damping of the s-wave and to weakening of the sp-interference. The further rise of a_1 may be related to the contribution of higher partial waves. The decrease of b_2 at energies below 0.9 GeV may be related to the resonance $D_{13}(1520)$; the growth of b_2 at energies 0.9–1.1 GeV may be due to influence of the resonances $D_{15}(1675)$ and $F_{15}(1680)$. The interference of d- and f-waves should lead to the shift of angular distribution $\Sigma(\theta)$ to smaller angles in the CM system as really seen in experiment [5]. The behavior of b_1 at energies higher than 0.9 GeV can be attributed to sf-interference and so on.

Thus, the energy dependence of the regression coefficients found in our analysis may be due to the transition from the energy region of the $S_{11}(1535)$ and $D_{13}(1520)$ to the energy region of the $D_{15}(1675)$ and $F_{15}(1680)$.

References

[1] V. F. Grushin *et al.*, Yadernaya Fizika **38**, 1448 (1983).

[2] B. Krusche *et al.*, Phys. Rev. Lett. **74**, 3736 (1995).

[3] L. Soezueer *et al.*., http//gwdac.phys.gwu.edu.

[4] F. Renard *et al.*, hep-ex/0011098.

[5] J. Ajaka *et al.* Phys. Rev. Lett. **81**, 1797 (1998.

[6] A. Bock *et al.*, Phys. Rev. Lett. **81**, 534 (1998).

[7] E. V. Balandina, E. M. Leikin, N. P. Yudin, Preprint NPI MSU – 2001-26/666.

[8] L. Tiator *et al.*, Phys. Rev. C **60**, 35210 (1999)

Bootstrap equations for effective theories and the calculation of the G_T/G_V ratio

A. Vereshagin

University of Bergen, Department of Physics, Bergen, Norway.

(Received: 30 October 2001)

A method is described for dealing with effective theories of hadron scattering. It allows one to reduce the number of independent renormalization prescriptions in those theories and gives a possibility to make numerical predictions. As an illustration, we show the results of comparison with the known data on $\pi\pi$, πK and πN elastic scattering. This work presents a generalization and the further development of our results first discussed at the MENU'99 Symposium [1].

1 Preliminary notes

It is widely believed that to construct the complete theory of strong processes one needs to make two steps:

1. With the help of QCD (which is supposed to be the fundamental theory of strong forces) find the hadronic spectrum (poles of the Green functions) and construct the complete set of asymptotic states.

2. Construct the scattering theory for those (composite) states.

It is not yet clear how to solve the first problem. Is it possible to say anything about the scattering theory of hadrons, having no information on their inner structure? That is how the *effective theory*[1] concept naturally comes to mind.

When constructing a theory of hadron scattering, we are forced to rely upon the Dyson series for the S-matrix, because this is the only known perturbative approach guaranteeing unitarity, causality and Lorentz-invariance of the results (see, e.g., [3]). In the case of effective theory this series can always be presented in the form

$$S_{fi} = \langle f | T_W \exp\left\{ -i \int H_{\text{int}} dx \right\} | i \rangle \,, \tag{1}$$

where T_W stands for Wick's (explicitly covariant) T-product and the Hamiltonian density (in the interaction picture) H_{int} does not contain any noncovariant terms. Imposing any algebraic[2] symmetry requirements on a theory based on the form (1) looks not more difficult than if the Lagrangian picture is used: the S-matrix is covariant and satisfies the symmetry requirements, if H_{int} does.

In contrast, the problem of *dynamical* symmetries looks much more transparent in the Lagrangian picture. And the transition from the Lagrangian picture to the Hamiltonian one looks almost hopeless when one deals with an effective theory. Indeed, in this case one needs to solve an infinite system of constraints arising, in particular, due to the presence of higher powers of time derivatives. However, as shown in [2], one needs only a *finite* number of Lagrangian terms when working to a given order in a *small momentum.* Thus, in the last case one can construct the corresponding Hamiltonian and, hence, avoid problems with unitarity. This program (first realized in [4]) gives us the natural way (*"matching"*) to take into account the dynamical symmetry requirements in the effective theory based on the Hamiltonian. Namely, one needs to compute the amplitude of

[1]Here this term is understood precisely in the same sense as in [2].
[2]Linearly realized, for example isotopic SU_2 (or SU_3).

the process in question, expand it in powers of a small momentum (of the Goldstone particle) up to a given order, and, finally, compare the result with that following from the canonical approach (based on the invariant Lagrangian of the same order) and equate the corresponding constants.

Which fields should be included in the Hamiltonian? To be able to work *not* only in the low energy region, we include the *resonance fields* (like the ρ-meson) as well as the fields of the true asymptotic states (stable with respect to the strong forces, like the π-meson).[3] To avoid model dependence of the results, we reserve the possibility to work with an arbitrary (possibly infinite) number of resonances with arbitrarily high values of spin J and mass M. The only limitation is suggested by experiment: we imply that there is a finite number of resonances with the same mass (though the mass spectrum may be unbounded). To put it another way, we imply the existence of a leading Regge trajectory (in the *real* plane of ReM and J) which, however, is not necessarily linear. According to the phenomenology of strong interactions we do not deal with massless spin $J > \frac{1}{2}$ particles. Also, we assume that the maximal isospin value is $I = 1$ for mesons and $I = \frac{3}{2}$ for baryons.

Thus, we consider the effective hadron scattering theory based on Dyson's series (1) with the Hamiltonian written in the form of an infinite sum of Lorentz-invariant (and SU(2)-invariant) local terms, each one constructed from the fields (and all powers of their derivatives of arbitrary high order) of pions, K-mesons, nucleons and all possible resonances.

2 Essential parameters, self-consistency and the bootstrap equations

It is possible to show that the *essential parameters*[4] of the effective scattering theory are masses (real parts of pole positions) and those (and only those) combinations of coupling constants which are needed to fix the *on-shell* kinematic structure of tree-level vertices. When computing the S-matrix elements one does not need to impose a renormalization condition on each coupling constant appearing in the Hamiltonian: only the essential parameters require fixing of their finite parts.

The central idea of our work is that one cannot take independent renormalization prescriptions even for the essential parameters of the effective scattering theory: certain natural self-consistency requirements impose an infinite number of constraints (bootstrap conditions) on the allowed *physical* values of the essential parameters. Namely, to make it possible to construct the one-loop approximation for the amplitude of a given scattering process (here we only discuss $2 \to 2$ processes), the corresponding *tree-amplitude* $A(s, t, u)$ must satisfy the following two requirements[5]:

1. It must be a *meromorphic function*[6] of the Mandelstam variables s, t, u, with poles and residues fixed by the Feynman rules.

2. This amplitude must be *polynomially bounded*[7] in each independent energy-like variable at zero value of the corresponding momentum transfer.

As explained in [7], these two requirements turn out to be sufficient to derive the exact form of the tree-amplitude. At the same time they lead to an infinite set of equations connecting the tree-amplitude parameters among themselves (*bootstrap equations*). And if we write the Hamiltonian in terms of physical parameters (plus the necessary counterterms — what we can always do), then the

[3]No problem with unitarity occurs in spite of the fact that Dyson's series is based on the Hamiltonian depending on resonance fields (see, e.g. [5]). In fact, this approach is used in the Standard Model of electroweak interactions: for instance, the W-boson is not an asymptotic state.

[4]These are the only parameters that appear in the S-matrix elements, see [3], Chapter 7.

[5]Both of them are trivial if there is a finite number of terms in the Hamiltonian (Lagrangian).

[6]No singularities except poles.

[7]Polynomial boundedness of the meromorphic functions is understood as in complex analysis, see e.g. [6].

tree-amplitude is automatically written in terms of *physical* (experimentally measurable) parameters. All this means that **the bootstrap equations are not affected by the renormalization procedure and can be tested experimentally**.

3 Comparison with experiment

In the cases of $\pi\pi$ and πK elastic scattering (see [7,8]) it has been found that the resulting equations strongly contradict the known data unless two light scalar resonances are taken into account. These are the σ (0^+0^+) and κ $(0^+\frac{1}{2}^+)$ mesons with the following parameters estimated from the bootstrap equations: $m_\sigma \sim 500$ MeV; $\Gamma_\sigma \sim 300$ MeV; $m_\kappa \sim 1$ GeV; $\Gamma_\kappa \sim 500$ MeV.

These parameters are strongly supported by modern data, see, e.g. [7, 9]. It is interesting to note, that, as was shown in [10] (see also [9]), to preserve the unitarity bound for the $\pi\pi$ and πK amplitudes one must take into account both the resonance and the (automatically implied in our approach) background interaction terms.

Perhaps, the most interesting result has been obtained from the analysis of the bootstrap equations for the πN scattering amplitude parameters. It was possible to make the accurate estimate of the ratio $G^T_{NN\rho}\Big/G^V_{NN\rho} = 6(\pm 20\%)$, of tensor/vector $NN\rho$ coupling constants[8]. This value turned out to be in nice agreement with experimental data. As far as we know, such a relation has never been explained in terms of model-independent theoretical arguments.

Besides, with the help of the bootstrap equations we have estimated the values of 40 coefficients in the expansion of the πN amplitude around the crossing symmetry point, first introduced in [12]. The detailed analysis will be published elsewhere.

Acknowledgments: I wish to thank V. Cheianov, P. Osland, F. Sannino, J. Schechter, V. V. Sukhanov, A. N. Vassilev and especially V. Vereshagin for stimulating discussions. This work was supported in part by RFBR (grant 01-02-17152), INTAS (INTAS call 2000, project 587), and by Russian Ministry of Education (programme "Universities of Russia" and grant E00-3.3-208).

References

[1] A. Vereshagin and V. Vereshagin, πN Newsletter, **15**, 288 (1999).
[2] S. Weinberg, Physica A **96**, 327 (1979).
[3] S. Weinberg. *The Quantum Theory of Fields.* Cambridge Univ. Press, Cambridge, 1996. v.1.
[4] J. Gasser and H. Leutwyler, Ann. Phys. (NY), **158**, 142 (1984).
[5] M. Veltman. Physica, 29, 186 (1963).
[6] G. B. Arfken, H. J. Weber. *Mathematical methods for physicists.* (Academic Press, New York, 1995). 4-th edition.
[7] A. Vereshagin and V. Vereshagin, Phys. Rev., **D59**, 016002 (1999).
[8] V. Vereshagin, Phys. Rev., **D55**, 5349 (1997).
[9] V. V. Vereshagin, K. N. Mukhin, and O. O. Patarakin, Phys. Usp., **43**, 315 (2000).
[10] M. Harada, F. Sannino, J. Schechter, Phys. Rev., **D54**, 1991 (1996); D. Black, A. Fariborz, F. Sannino, and J. Schechter, Phys. Rev., **D58**, 054012 (1998); *ibid*, **D59**, 074026 (1999); see also D. Black, A. Fariborz, S. Moussa, S. Nasri, and J. Schechter, Phys. Rev., **D64**, 014031 (2001).
[11] M. M. Nagels *et al.*, Nucl. Phys., **B109**, 1-91 (1976); O. Dumbrajs *et al.*, Nucl. Phys., **B216** 277 (1983).
[12] G. Höhler, H. P. Jacob, and R. Strauss, Nucl. Phys., **B39**, 237 (1972).

[8] For the corresponding experimental data and notations see [11].

9th International Symposium on Meson-Nucleon Physics and the Structure of the Nucleon (MENU2001)

The George Washington University, Washington, DC, July 26–31, 2001

Program

(Numbers in brackets indicate page number of the corresponding paper)

Thursday, 26 July, 2001

Plenary session *Chair: G. Wagner (Tübingen)*

Plenary session *Chair: E. Gibson (California State, Sacramento)*

Plenary session *Chair: B. Loiseau (Paris)*

Plenary session *Chair: W. Kluge (Karlsruhe)*

4:00 pm J. Mueller (Pittsburgh)
η electroproduction with CLAS [59]

4:30 pm M. Sadler (Abilene)
Pion-nucleon charge exchange measurement at low energy [65]

5:00 pm D.-O. Riska (HIP Helsinki)
Short-range contributions in eta-meson production near threshold [68]

5:30 pm *Happy hour*

Friday, 27 July, 2001

Plenary session *Chair: C. Bennhold (GW)*

9:00 am M. Manley (Kent State)
Multichannel analyses of $\bar{K}N$ scattering [74]

9:30 am S. Barrow (Florida State)
Strangeness electro- and photoproduction at CLAS [80]

10:00 am T. Mart (Indonesia)
An isobar model for kaon photo- and electroproduction [86]

10:30 am *Coffee break*

Plenary session *Chair: L. Tiator (Mainz)*

11:00 am A. Lahiff (TRIUMF)
Pion-nucleon scattering in a Bethe–Salpeter approach [92]

11:30 am S. N. Yang (Taipei)
A relativistic meson-exchange model for πN scattering [98]

12:00 pm S. A. Dytman (Pittsburgh)
Recent coupled channel results for baryon spectra and an overview of BRAG [104]

12:30 pm *Lunch break*

Plenary session *Chair: I. Strakovsky (GW)*

2:00 pm M. Pavan (TRIUMF)
The GWU πN partial-wave analysis solution SM01 [110]

2:30 pm J. Stahov (Tuzla)
Calculation of the low-energy πN partial waves based on hyperbolic dispersion relations [116]

3:00 pm P. Piirola (Helsinki)
Resurrecting the KH78/80 pertial-wave analysis [121]

3:20 pm *Coffee break*

Plenary session *Chair: M. G. Olsson (Wisconsin)*

3:50 pm A. Rusetsky (Bern)
Electromagnetic and strong isospin breaking in hadronic amplitudes [127]

4:20 pm G. Oades (Åarhus)
Threshold and subthreshold πN scattering amplitudes; comparison with chiral perturbation theory predictions [133]

4:50 pm M. Sainio (Helsinki)
Pion-nucleon sigma term—a review [138]

5:10 pm S. Kruglov (PNPI Gatchina)
Pion-nucleon scattering in the energy region 300–2000 MeV [144]

5:40 pm *Happy hour*

Saturday, 28 July, 2001

Plenary session *Chair: G. Smith (JLab)*

9:00 am R. A. Arndt (GW)
Analysis of pion electroproduction data [150]

9:30 am H. Egiyan (JLab)
Single π^+ electroproduction in the resonance region using CLAS [154]

10:00 am V. Kouznetsov (Grenoble)
Meson photoproduction and Compton scattering at GRAAL [160]

10:30 am *Coffee break*

Plenary session *Chair: B. Norum (Univ. of Virginia)*

11:00 am R. Beck (Mainz)
New results and future experiments with real photons at MAMI [166]

11:30 am B. S. Zou (Beijing)
Baryon spectroscopy at BEPC [174]

12:00 pm H. Q. Jiang (Beijing)
Theoretical study of N^* from J/ψ decays [180]

12:30 pm *Lunch break*

Plenary session *Chair: D.-O. Riska (HIP Helsinki)*

2:00 pm P. Pedroni (Pavia)
Helicity structure of the γN interaction and the GDH sum rule [186]

2:30 pm B. Y. Oh (Penn State/DESY)
Physics at HERA; some highlights

3:00 pm H. Weigel (Tübingen)
The spin of the proton in effective models [192]

3:30 pm F. Myhrer (South Carolina)
Muon capture on hydrogen [198]

4:00 pm *Coffee break*

Parallel session A1 *Chair: M. Sadler (Abilene)*

4:30 pm T. Inoue (Valencia)
Chiral dynamics and pion-nucleon scattering around N^*(1535) [296]

4:45 pm M. R. Dugger (Arizona State)
η and η' photoproduction from the proton using CLAS

5:00 pm W. T. Chiang (Taipei)
An isobar model study of eta photoproduction and electroproduction [299]

5:15 pm H. Denz (Tübingen)
Pion-proton cross sections in the Coulomb-nuclear interference region [302]

5:30 pm M. Cröni (Tübingen)
Measurement of analyzing powers in πp scattering [305]

5:45 pm *Happy hour*

Parallel session A2 *Chair: R. Beck (Mainz)*

4:30 pm I. Preobrajenski (Mainz)
Helicity dependence of single-pion photoproduction; results from the GDH experiment at MAMI [308]

4:45 pm G. Zeitler (Erlangen-Nürnberg)
First experimental check of the GDH sum rule at ELSA [311]

5:00 pm R. A. Lindgren (Univ. of Virginia)
High precision measurements of the reaction $p(e, e')\pi^0$ near threshold: A test of chiral dynamics [315]

5:15 pm K. Miyagawa (Okayama)
Electromagnetic K^+ production on the deuteron with hyperon polarization [318]

5:30 pm S. Karppi (GW)
Photon- and meson-induced production of pion-delta states: Extraction of properties of baryon resonances in the intermediate state [321]

5:45 pm *Happy hour*

Parallel session A3 *Chair: F. X. Lee (GW)*

4:30 pm L. Zhou (GW)
N^* masses from lattice QCD [325]

4:45 pm X. Liu (GW)
N^* masses from QCD sum rules [328]

5:00 pm W. Detmold (Adelaide)
Quark distributions from lattice QCD [331]

5:15 pm T.-S. Park (South Carolina)
The 'HEP' process in the sun in effective field theory [334]

5:30 pm *Happy hour*

Sunday, 29 July, 2001

5:30 pm *Conference Banquet*
Dinner cruise on the Potomac River on board the passenger vessel 'Odyssey'

Monday, 30 July, 2001

Plenary session *Chair: M. Fuda (SUNY – Buffalo)*

9:00 am C. Roberts (Argonne)
Dyson–Schwinger equations: From charge radii to deep inelastic scattering [204]

9:40 am P. Maris (North Carolina State)
Electromagnetic, weak, and strong interactions of light mesons [213]

10:15 am *Coffee break*

Plenary session *Chair: A. Lahiff (TRIUMF)*

10:45 am M. A. Pichowsky (Indiana)
Dyson–Schwinger studies of baryons [219]

11:20 am B. Metsch (Bonn)
A relativistic quark model of baryons [225]

11:55 am S. Capstick (Florida State)
New positive-parity baryons, and baryon-meson loop effects [232]

12:30 pm *Lunch break*

Parallel session B1 *Chair: M. Sainio (HIP Helsinki)*

2:00 pm M. G. Fuda (SUNY at Buffalo)
A method for calculating meson photoproduction from the nucleon [337]

2:15 pm M. B. Hecht (Argonne)
Neutron electric dipole moment: Constituent-dressing and compositeness [204]

2:30 pm A. Gårdestig (Indiana)
Covariant description of hadron scattering processes [340]

2:45 pm I. Akushevich (JLab)
QED radiative corrections in processes of exclusive pion electroproduction [343]

3:00 pm M. F. M Lutz (GSI)
Relativistic chiral SU(3) symmetry, large N_c sum rules and meson-baryon scattering [346]

3:15 pm E. Pace (Roma)
Baryon form factors with Poincaré covariant current operator

3:30 pm *Coffee break*

Parallel session B2 *Chair: M. Pavan (TRIUMF)*

2:00 pm B. Loiseau (Paris)
Application of Roy's equations to the analysis of $\pi\pi$ experimental data [349]

2:15 pm A. M Rodriguez Fernandez (Santiago de Compostela)
The DIRAC experiment at CERN: Current status and future perspectives [352]

2:30 pm D. Gotta (FZ Jülich)
The new pionic hydrogen experiment at PSI [355]

2:45 pm T. S. Jensen (PSI)
Atomic cascade in hadronic atoms [358]

3:00 pm I. T. Obukhovsky (Moscow State)
The probing of nucleon mesonic structure by means of quasielestic knock-out processes like $p + e \to n + \pi^+ + e'$ [361]

3:15 pm I. T. Obukhovsky (Moscow State)
A possible quark origin of the two-pion emission in processes of quasi-elastic knock-out of the pion [364]

3:30 pm *Coffee break*

Parallel session B3 *Chair: H. Machner (FZ Jülich)*

2:00 pm P. Moskal (Cracow and FZ Jülich)
Study of the eta-proton interaction via the reaction $pp \to pp\eta$ [367]

2:15 pm J. Pätzold (Tübingen)
Exclusive measurements of the $pp \to pp\pi^+\pi^-$ reaction [370]

2:30 pm S. Wirth (Erlangen-Nürnberg)
Strangeness production at the time-of-flight spectrometer COSY-TOF [373]

2:45 pm J. Nagata (Kyushu)
Phase-shift analyses of elastic proton-proton scattering at $T_L = 1 \sim 11\ GeV$ [376]

3:00 pm S. Ando (South Carolina)
Threshold $pp \to pp\pi^0$ up to one-loop accuracy [379]

3:15 pm *Coffee break*

Parallel session C1 *Chair: T. Mart (Indonesia)*

4:00 pm M. G. Olsson (Wisconsin)
Consistency of a large sigma term [382]

4:15 pm A. D. Lahiff (TRIUMF)
Covariant meson-exchange model of the $\bar{K}N$ interaction [385]

4:30 pm A. Cieplý (Řež)
Low-energy K^- optical potentials: deep or shallow? [388]

4:45 pm A. B. Gridnev (PNPI Gatchina)
New determination of the ηN scattering length in the K-matrix [391]

5:00 pm I. M. Narodetskii (ITEP Moscow)
Baryons in the nonperturnative string approach [394]

5:15 pm *Happy hour*

Parallel session C2 *Chair: H. Q. Jiang (IHEP Beijing)*

4:00 pm T. Lähde (Helsinki)
π and $\pi\pi$ decays of excited D mesons [397]

4:15 pm N. E. Ligterink (ECT*)
Fano theory for hadronic resonances [400]

4:30 pm K. S. Nelson (Univ. of Virginia)
A search for matter/anti-matter asymmetry in hyperon decays

4:45 pm B. Norum (Univ. of Virginia)
Physics at a new asymmetrical e^+e^- collider at SLAC at $1.4 < \sqrt{s} < 2.5$ GeV

5:00 pm M. Contalbrigo (Ferrara)
Rare kaon decays with the NA48 experiment [403]

5:15 pm R. Fantechi (INFN Pisa)
A new measurement of direct CP violation in the neutral kaon system [406]

5:30 pm *Happy hour*

Parallel session C3 *Chair: J. Price (UCLA)*

4:00 pm M. Düren (Giessen)
New results and future prospects of the spin structure of the nucleon as measured at HERMES [409]

4:15 pm B. Seitz (Alberta)
Single spin asymmetry in hard exclusive electroproduction of π^+ and real photons at HERMES [412]

4:30 pm M. Hartig (TRIUMF)
Diffractive vector meson production at HERMES

4:45 pm M. Bertani (Frascati)
The FINUDA experiment: Status and perspectives [415]

5:00 pm L. Gamberg (Pennsylvania)
A determination of the nucleon tensor charge [419]

5:15 pm *Happy hour*

Tuesday, 31 July, 2001

Plenary session *Chair: J.R. Comfort (Arizona State)*

9:00 am H. Calén (Uppsala)
The CELSIUS/WASA 4π *detector* [238]

9:30 am H. Machner (FZ Jülich)
Meson production in $p + d$ *reactions* [243]

10:00 am S.D. Reitzner (Ohio)
Charge symmetry breaking in $n + p \to d + \pi^0$ [249]

10:30 am *Coffee break*

Plenary session *Chair: C. Schaerf (Univ. di Roma)*

11:00 am R. De Vita (Genova/JLab)
Spin physics in the resonance region with CLAS [255]

11:30 am M. Battaglieri (Genova/JLab)
Photoproduction of vector mesons on the proton at large momentum transfer [261]

12:00 pm S. Schadmand (Giessen)
Medium modifications of hadrons studied with photonuclear reactions [267]

12:30 pm *Lunch break*

Plenary session *Chair: B.S. Zou (IHEP Beijing)*

2:00 pm M. Maggiora (Torino)
Meson and hyperon production with polarized protons of about 3 GeV [273]

2:30 pm W.R. Gibbs (New Mexico State)
Proton-proton scattering at 90 degrees [280]
and *Fundamental quantities from doubly subtracted forward dispersion relations* [286]

3:10 pm *Coffee break*

3:40 pm B.M.K. Nefkens (UCLA)
Meson-nucleon physics: Past, present and future [289]

List of Registered Participants

Igor Akushevich
NCCU
1910 Cassowary Lane
Apex, NC 27502
USA
aku@jlab.org

Hamoud H. Alharbi
SUNY at Buffalo
131 Pheasant run (right)
Amherst, NY 14228
USA
alharbi@acsu.buffalo.edu

Chris E. Allgower
Indiana University Cyclotron Facility
2401 Milo B. Sampson Lane
Bloomington, IN 47408
USA
allgower@iucf.indiana.edu

Shung-ichi Ando
Dept. of Physics and Astronomy
University of South Carolina
Columbia, SC 29208
USA
sando@nuc003.psc.sc.edu

Richard A. Arndt
Physics Department
VPI & SU
Blacksburg, VA 24060
USA
arndtra@said.phys.vt.edu

Marco A. Battaglieri
Istituto Nazionale di Fisica Nucleare
Via Dodecaneso 33
16146 Genova
Italy
battaglieri@ge.infn.it

Steve P. Barrow
Thomas Jefferson National Lab
T11B
12000 Jefferson Ave.
Newport News, VA 23606
USA
barrow@jlab.org

Adnan Bashir
Edifico C-3, Ciudad Universitaria
Apartado Postal 2-82
Universidad Michoacana
de Sán Nicolas de Hidalgo
Morelia, 58040
Mexico
adnan@itzel.ifm.umich.mx

Reinhard Beck
Institut für Kernphysik
Universität Mainz
Becherweg 45
55099 Mainz
Germany
rbeck@kph.uni-mainz.de

Monica Bertani
INFN
Laboratori Nazionali di Frascati
Via E. Fermi 40
00044 Frascati
Italy
monica.bertani@lnf.infn.it

Raimondo Bertini
Turin University and INFN
Via P. Giuria 1
10125 Torino
Italy
bertini@to.infn.it

Cornelius Bennhold
Department of Physics
The George Washington University
Washington, DC 20052
USA
bennhold@gwu.edu

William J. Briscoe
Department of Physics
The George Washington University
Washington, DC 20052
USA
briscoe@gwu.edu

Hans O. Calén
The Svedberg Laboratory
Uppsala University
Box 533
SE-75121 Uppsala
Sweden
calen@tsl.uu.se

Simon C. Capstick
Department of Physics
Florida State University
Tallahassee, FL 32306-4350
USA
capstick@csit.fsu.edu

Wen-Tai Chiang
Department of Physics
National Taiwan University
Taipei, 10617
Taiwan
wtchiang@phys.ntu.edu.tw

Ales Cieplý
Nuclear Physics Institute
CZ-25068 Řež near Prague
Czech Republic
cieply@ujf.cas.cz

Joseph R. Comfort
Dept. of Physics and Astronomy
Arizona State University
Tempe, AZ 85287-1504
USA
Joseph.Comfort@asu.edu

Marco M. Contalbrigo
University of Ferrara
Via Paradiso 12
44100 Ferrara
Italia
contalbrigo@fe.infn.it

Margit Cröni
Universität Tübingen
Auf der Morgenstelle 14
72070 Tübingen
Germany
croeni@pit.physik.uni-tuebingen.de

Holger A. Denz
Universität Tübingen
Physikalisches Institut
Auf der Morgenstelle 14
72076 Tübingen
Germany
denz@pit.physik.uni-tuebingen.de

William Detmold
Adelaide University
North Terrace
Adelaide, SA 5005
Australia
wdetmold@physics.adelaide.edu.au

Raffaella De Vita
Istituto Nazionale di Fisica Nucleare
Via Dodecaneso 33
16146 Genova
Italy
devita@ge.infn.it

Michael Düren
II. Physikalisches Institut
Universität Giessen
Heinrich-Buff-Ring 16
35392 Giessen
Germany
Michael.Dueren@desy.de

Michael R. Dugger
Dept. of Physics and Astronomy
Arizona State University
Tempe, AZ 85287-1504
USA
dugger@jlab.org

Steven A. Dytman
Physics Department
University of Pittsburgh
Pittsburgh, PA 15260
USA
dytman@pitt.edu

Hovanes Egiyan
Department of Physics
The College of William and Mary
Williamsburg, VA 23187
USA
hovanes@jlab.org

Riccardo R. Fantechi
INFN - Sezione di Pisa
Via Vecchia Livornese 1291
I-56010 S. Piero a Grado (Pisa)
Italy
fantechi@pi.infn.it

Jerry Feldman
Department of Physics
The George Washington University
Washington, DC 20052
USA
feldman@gwu.edu

Alessandro Feliciello
I.N.F.N. – Sezione di Torino
Via P. Giuria 1
I-10125 Torino
Italy
Alessandro.Feliciello@to.infn.it

Michael G. Fuda
Department of Physics
239 Fronczak Hall
University at Buffalo-SUNY
Buffalo, NY 14260
USA
fuda@acsu.buffalo.edu

Leonard P. Gamberg
Dept. of Physics and Astronomy
David Rittenhouse Labs
University of Pennsylvania
209 South 33rd Street
Philadelphia, PA 19104-6396
USA
gamberg@dept.physics.upenn.edu

Anders E. Gårdestig
Nuclear Theory Center
Indiana University
2401 Milo B. Sampson Lane
Bloomington, IN 47408
USA
anders@niobe.iucf.indiana.edu

William R. Gibbs
Dept. of Physics, 3D
New Mexico State University
Las Cruces, NM 88003
USA
gibbs@nmsu.edu

Edward F. Gibson
Physics Department 6041
California State University
at Sacramento
6000 J Street
Sacramento, CA 95819-6041
USA
egibson@csus.edu

Detlev Gotta
Institut für Kernphysik
Forschungszentrum Jülich
52425 Jülich
Germany
d.gotta@fz-juelich.de

Anatoly B. Gridnev
Petersburg Nuclear Physics Institute
Gatchina
St. Petersburg, 188350
Russia
gridnev@mail.pnpi.spb.ru

Helmut Haberzettl
Department of Physics
The George Washington University
Washington, DC 20052
USA
helmut@gwu.edu

Eamon P. Harper
Department of Physics
The George Washington University
Washington, DC 20052
USA
epah@gwu.edu

Matthias Hartig
TRIUMF
4004 Wesbrook Mall
Vancouver, BC V6T 2A3
Canada
matthias.hartig@desy.de

Martin B. Hecht
Physics Division, Bldg 203
Argonne National Laboratory
Argonne, IL 60439-4843
USA
hecht@theory.phy.anl.gov

Christina I. Helminen
Department of Physics
P.O. Box 64
University of Helsinki
00014 Helsinki
Finland
chelmine@pcu.helsinki.fi

Rafael G. Hurtado
Departamento de Física
Universidad Nacional de Colombia,
sede de Bogotá
Ciudad Universitaria
Bogotá
Colombia
rhurtado@ciencias.unal.edu.co

Takashi Inoue
IFIC
Institutos de Investigacion de Paterna
Apdo. 22085
University of Valencia
46071 Valencia
Spain
inoue@ific.uv.es

Thomas Jensen
WHGA/138
Paul Scherrer Institute
5232 Villigen PSI
Switzerland
Thomas.Jensen@psi.ch

Huan Qing Jiang
Institute of High Energy Physics
Chinese Academy of Sciences
P.O. Box 918
Beijing 100039
China
chiang@mail.ihep.ac.cn

Steven C. Karppi
Department of Physics
The George Washington University
Washington, DC 20052
USA
karppi@gwu.edu

Wolfgang Kluge
Universität Karlsruhe
Postfach 3640
76021 Karlsruhe
Germany
wolfgang.kluge@phys.uni-karlsruhe.de

Viatcheslav Kouznetsov
Physics Department
University "Tor Vergata", Rome
Via della Ricerca Scientifica 1
I-00133 Roma
Italy
Slava@roma2.infn.it

Siggi Krewald
Institut für Kernphysik
Forschungszentrum Jülich
52425 Jülich
Germany
s.krewald@fz-juelich.de

Sergei P. Kruglov
PNPI
Meson Physics Group
Petersburg Nuclear Physics Institute
Gatchina
Russia
kruglov@lnpi.spb.su

Alexander E. Kudryavtsev
ITEP
B. Cheremushkinskaya 25
117279 Moscow
Russia
kudryavt@heron.itep.ru

Timo Lähde
Helsinki Institute of Physics
P.O. Box 64
University of Helsinki
00014 Helsinki
Finland
talahde@pcu.helsinki.fi

Andrew D. Lahiff
TRIUMF
4004 Wesbrook Mall
Vancouver, B.C. V6T 2A3
Canada
lahiff@triumf.ca

Jörn Langheinrich
CB-ELSA
Universität Bonn
Adolfstr 9-11
D-53111 Bonn
Germany
langhei@physik.uni-bonn.de

Frank X. Lee
Physics Department
The George Washington University
Washington, DC 20052
USA
fxlee@gwu.edu

Norbert E. Ligterink
ECT*
Villa Tombosi
Strada delle Tabarelle 286
38050 Villazzano (Trento)
Italy
ligterin@ect.it

Richard A. Lindgren
Department of Physics
University of Virginia
Charlottesville, VA 22901
USA
ral5q@virginia.edu

Xinyu Liu
Department of Physics
The George Washington University
Washington, DC 20052
USA
xyliu@gwu.edu

Benoit Loiseau
L.P.T.P.E. (Case 127)
Tour 12 - 3eme etage
Univ. P. & M. Curie
4 Place Jussieu
75252 Paris Cedex 05
France
loiseau@in2p3.fr

Matthias Lutz
GSI
Planck Str. 1
64291 Darmstadt
Germany
m.lutz@gsi.de

Hartmut K. Machner
Institut für Kernphysik
Forschungszentrum Jülich
52425 Jülich
Germany
h.machner@fz-juelich.de

Marco G.M. Maggiora
Department of General Physics
University of Turin
Via P. Giuria 1
10136 Turin
Italy
marco.maggiora@to.infn.it

D. Mark Manley
Department of Physics
Kent State University
Kent, OH 44242-0001
USA
manley@kent.edu

Pieter Maris
Dept. of Physics
North Carolina State University
Box 8202
Raleigh, NC 27695
USA
pmaris@unity.ncsu.edu

Terry Mart
Jurusan Fisika, FMIPA
Universitas Indonesia
Depok, 16424
Indonesia
mart@makara.cso.ui.ac.id

Rudolf O. Meier
Universität Tübingen
Auf der Morgenstelle 14
72076 Tuebingen
Germany
rmeier@pit.physik.uni-tuebingen.de

Ulf-G. Meißner
Institut für Kernphysik (Th)
Forschungszentrum Jülich
52425 Jülich
Germany
u.meissner@fz-juelich.de

Harald Merkel
Institut für Kernphysik / MAMI
Universität Mainz
Becherweg 45
55099 Mainz
Germany
Merkel@Kph.Uni-Mainz.de

Bernard Ch. Metsch
ITKP
Universität Bonn
Nussallee 14-16
D-53115 Bonn
Germany
metsch@itkp.uni-bonn.de

Kazuya Miyagawa
Okayama University of Science
1-1 Ridai-cho
Okayama, 700
Japan
miyagawa@dap.ous.ac.jp

Pawel Moskal
Institut für Kernphysik
Forschungszentrum Jülich
52425 Jülich
Germany
p.moskal@fz-juelich.de

James A. Mueller
Dept. of Physics and Astronomy
University of Pittsburgh
3941 O'Hara Street
Pittsburgh, PA 15260
USA
mueller@pitt.edu

Fred Myhrer
Dept. of Physics and Astronomy
University of South Carolina
Columbia, SC 29208
USA
myhrer@nuc003.psc.sc.edu

Junichi Nagata
Kyushu International University
1-6-1 Hirano
Yahatahigashi-ku
Kitakyushu, 805-8512
Japan
nagata@law.kiu.ac.jp

Ilya M. Narodetskii
ITEP
B. Cheremushkinskaya, 25
Moscow, 117259
Russia
naro@heron.itep.ru

Bernard (Ben) M. Nefkens
Dept. of Physics and Astronomy
UCLA
405 Hilgard Ave
Los Angeles, CA 90095-1547
USA
Nefkens@physics.ucla.edu

Kenneth S. Nelson
Dept. of Physics
University of Virginia
382 McCormick Rd
Charlottesville, VA 22903
USA
kennelso@uvahea.phys.virginia.edu

Blaine E. Norum
Department of Physics
University of Virginia
PO Box 400714
Charlottesville, VA 22904
USA
ben@virginia.edu

Geoffrey C. Oades
Institute of Physics and Astronomy
Aarhus University
Ny Munkegade
DK-8000 Aarhus C
Denmark
gco@ifa.au.dk

Igor I.T. Obukhovsky
Institute of Nuclear Physics
Moscow State University
Vorobievy Gory
Moscow 119899
Russia
obukh@nucl-th.sinp.msu.ru

Benedict Y. Oh
Physics Department
Penn State University
University Park, PA 16802
USA
byo@phys.psu.edu

Martin G. Olsson
Physics Department
University of Wisconsin
1150 University Ave.
Madison, WI 53706
USA
olsson@pheno.physics.wisc.edu

Grant V. O'Rielly
Physics Department
The George Washington University
Washington, DC 20052
USA
orielly@gwu.edu

Eulogio Oset
IFIC
Institutos de Investigacion de Paterna
Apdo. 22085
University of Valencia
46071 Valencia
Spain
oset@condor1.ific.uv.es

Mohamed Ouchrif
DESY, Blg. 66, Zi. 3
Notkestr. 85
D-22603 Hamburg
Germany
ouchrif@mail.desy.de

Emanuele E. Pace
Dipartimento di Fisica
Universitá di Roma "Tor Vergata"
Via della Ricerca Scientifica 1
00133 Roma
Italy
pace@roma2.infn.it

Tae-Sun Park
Dept. of Physics and Astronomy
University of South Carolina
Columbia, SC 29208
USA
tspark@nuc003.psc.sc.edu

Eduard Yakovlevich Paryev
Institute for Nuclear Research
Russian Academy of Sciences
60th Oct. Anniversary Prospect 7a
Moscow, 117312
Russia
Paryev@al20.inr.troitsk.ru

Jens Pätzold
Physikalisches Institut
Universität Tübingen
Auf der Morgenstelle 14
72076 Tübingen
Germany
paetzold@pit.physik.uni-tuebingen.de

Marcello M. Pavan
TRIUMF
4004 Wesbrook Mall
Vancouver, B.C. V6T-2A3
Canada
marcello@triumf.ca

Paolo Pedroni
INFN – Sezione di Pavia
Via Bassi 6
27100 Pavia
Italy
pedroni@pv.infn.it

Michael A. Pichowsky
Nuclear Theory Center
Indiana University
2401 Milo B Sampson Lane
Bloomington, IN 47405
USA
pichowsk@indiana.edu

Pekko Piirola
Department of Physics
University of Helsinki
P.O. Box 64
00014 Helsinki
Finland
Pekko.Piirola@Helsinki.FI

Ilja Preobrajenski
Institut für Kernphysik
Universität Mainz
J.-J.-Becher Weg 45
55099 Mainz
Germany
preobraz@kph.uni-mainz.de

John W. Price
Dept. of Physics and Astronomy
UCLA
Los Angeles, CA 90095-1547
USA
price@physics.ucla.edu

Christoph Reiss
Dipartimento di Fisica
Universita di Trento
Via Sommarive 14
I-38050 Povo (Trento)
Italy
reiss@science.unitn.it

Diane Reitzner
TRIUMF
4004 Westbrook Mall
Vancouver, BC V6T 2A3
Canada
reitzner@triumf.ca

Dan-Olof Riska
Helsinki Institute of Physics
P.O. Box 64
University of Helsinki
00014 Helsinki
Finland
riska@pcu.helsinki.fi

Craig D. Roberts
Physics Division
Argonne National Laboratory
Argonne, IL 60439
USA
cdroberts@anl.gov

Ana Maria A. Rodriguez Fernandez
Departamento de Fisica de particulas
Univ. de Santiago de Compostela
15782 Santiago de Compostela
Spain
ana@fpsunae2.usc.es

Akaki Rusetsky
Institute for Theoretical Physics
University of Bern
Sidlerstrasse 5
3012 Bern
Switzerland
rusetsky@itp.unibe.ch

Michael E. Sadler
Abilene Christian University
ACU Box 27963
Abilene, TX 79601
USA
sadler@physics.acu.edu

Mikko E. Sainio
Helsinki Institute of Physics
P.O. Box 64
00014 Helsinki
Finland
mikko.sainio@helsinki.fi

Susan Schadmand
II. Physikalisches Institut
Universität Giessen
Heinrich-Buff-Ring 16
D-35392 Giessen
Germany
s.schadmand@exp2.physik.uni-giessen.de

Carlo Schaerf
Dipartimento di Fisica
Università di Roma “Tor Vergata”
Via della Ricerca Scientifica 1
00133 Roma
Italy
schaerf@roma2.infn.it

Bjoern Seitz
DESY/HERMES
Notkestrasse 85
22603 Hamburg
Germany
bjoern.seitz@desy.de

Gregory Smith
Jefferson Lab
12000 Jefferson Avenue
Newport News, VA 23606
USA
harris@jlab.org

Daniel I. Sober
Department of Physics
Catholic University of America
Washington, DC 20064
USA
sober@cua.edu

Jugoslav Stahov
University Tuzla
Univerzitetska 8
75000 Tuzla
Bosnia and Herzegovina
stahov@inet.ba

Igor I. Strakovsky
Department of Physics
The George Washington University
Washington, DC 20052
USA
igor@gwu.edu

Lothar Tiator
Institut für Kernphysik
Universität Mainz
J.J. Becherweg 45
55099 Mainz
Germany
tiator@kph.uni-mainz.de

Alexander Vereshagin
Department of Physics
University of Bergen
Allegt. 55
N-5007 Bergen
Norway
alexand@fi.uib.no

Gerhard J. Wagner
Physikalisches Institut
Universität Tübingen
Auf der Morgenstelle 14
72076 Tübingen
Germany
wagner@pit.physik.uni-tuebingen.de

Agung B. Waluyo
Department of Physics
The George Washington University
Washington, DC 20052
USA
waluyoab@gwis2.circ.gwu.edu

Herbert Weigel
Institut für Theoretische Physik
Universität Tübingen
Auf der Morgenstelle 14
72076 Tübingen
Germany
herbert.weigel@uni-tuebingen.de

Stefan Wirth
Physikalisches Institut
Universität Erlangen-Nürnberg
Erwin-Rommel-Str. 1
91058 Erlangen
Germany
wirth@physik.uni-erlangen.de

Ron L. Workman
Department of Physics
The George Washington University
Washington, DC 20052
USA
rworkman@gwu.edu

Shin Nan Yang
Department of Physics
National Taiwan University
Taipei, 10617
Taiwan
snyang@phys.ntu.edu.tw

Farid Zamani
Dept. of Physics
Villanova University
800 Lancaster Ave
Villanova, PA 19085
USA
farid.zamani@villanova.edu

Günter Zeitler
Physikalisches Institut
Universität Erlangen-Nürnberg
91058 Erlangen
Germany
guenter.zeitler@physik.uni-erlangen.de

Leming Zhou
Department of Physics
The George Washington University
Washington, DC 20052
USA
lmzhou@gwu.edu

Bingsong Zou
Institute of High Energy Physics
P.O. Box 918 (4)
Beijing, 100039
P.R. China
zoubs@mail.ihep.ac.cn